

PRINCIPLES OF SUSTAINABLE ENERGY SYSTEMS

THIRD EDITION



Charles F. Kutscher ■ Jana B. Milford ■ Frank Kreith

Principles of Sustainable Energy Systems

Third Edition

MECHANICAL and AEROSPACE ENGINEERING

Efstathios E. Michaelides

Series Editor

Frank Kreith

Founding Series Editor

RECENTLY PUBLISHED TITLES

Handbook of Hydrogen Energy

S.A. Sherif, D. Yogi Goswami, E.K. (Lee) Stefanakos, and Aldo Steinfeld

Fuel Cells: Principles, Design, and Analysis

Shripad, T. Revankar and Pradip Majumdar

Design and Control of Automotive Propulsion Systems

Zongxuan Sun and Guoming (George) Zhu

Energy Efficiency and Renewable Energy Handbook, Second Edition

Edited by D. Yogi Goswami and Frank Kreith

Heating and Cooling of Buildings: Principles and Practice of Energy Efficient Design, Third Edition

T. Agami Reddy, Jan F. Kreider, Peter S. Curtiss, and Ari Rabl

Energy Management and Conservation Handbook, Second Edition

Edited by Frank Kreith and D. Yogi Goswami

Multiphase Flow Handbook, Second Edition

Edited by Efstathios E. Michaelides, Clayton T. Crowe, and John D. Schwarzkopf

Nuclear Engineering Handbook, Second Edition

Edited by Kenneth D. Kok

Energy Efficient Electrical Systems for Buildings

Moncef Krarti

Energy Conversion, Second Edition

Edited by D. Yogi Goswami and Frank Kreith

CRC Handbook of Thermal Engineering, Second Edition

Edited by Frank Kreith and Raj P. Chhabra

Energy, the Environment, and Sustainability

Efstathios E. Michaelides

Principles of Sustainable Energy Systems, Third Edition

Charles F. Kutscher, Jana B. Milford, and Frank Kreith

Principles of Sustainable Energy Systems

Third Edition

**Charles F. Kutscher
Jana B. Milford
Frank Kreith**



CRC Press

Taylor & Francis Group

Boca Raton London New York

CRC Press is an imprint of the
Taylor & Francis Group, an **informa** business

CRC Press
Taylor & Francis Group
6000 Broken Sound Parkway NW, Suite 300
Boca Raton, FL 33487-2742

© 2019 by Taylor & Francis Group, LLC
CRC Press is an imprint of Taylor & Francis Group, an Informa business

No claim to original U.S. Government works

Printed on acid-free paper

International Standard Book Number-13: 978-1-4987-8892-2 (Hardback)

This book contains information obtained from authentic and highly regarded sources. Reasonable efforts have been made to publish reliable data and information, but the author and publisher cannot assume responsibility for the validity of all materials or the consequences of their use. The authors and publishers have attempted to trace the copyright holders of all material reproduced in this publication and apologize to copyright holders if permission to publish in this form has not been obtained. If any copyright material has not been acknowledged please write and let us know so we may rectify in any future reprint.

Except as permitted under U.S. Copyright Law, no part of this book may be reprinted, reproduced, transmitted, or utilized in any form by any electronic, mechanical, or other means, now known or hereafter invented, including photocopying, microfilming, and recording, or in any information storage or retrieval system, without written permission from the publishers.

For permission to photocopy or use material electronically from this work, please access www.copyright.com ([http://www.copyright.com/](http://www.copyright.com)) or contact the Copyright Clearance Center, Inc. (CCC), 222 Rosewood Drive, Danvers, MA 01923, 978-750-8400. CCC is a not-for-profit organization that provides licenses and registration for a variety of users. For organizations that have been granted a photocopy license by the CCC, a separate system of payment has been arranged.

Trademark Notice: Product or corporate names may be trademarks or registered trademarks, and are used only for identification and explanation without intent to infringe.

Visit the Taylor & Francis Web site at
<http://www.taylorandfrancis.com>

and the CRC Press Web site at
<http://www.crcpress.com>

*This book is dedicated to the memory of our colleague, Frank Kreith,
with the hope that it will advance his inspiring vision for
protecting our planet through sustainable energy.*



Taylor & Francis

Taylor & Francis Group

<http://taylorandfrancis.com>

Contents

Foreword	xv
Preface.....	xvii
Acknowledgments	xix
Authors	xxi
Contributors.....	xxiii
1 Introduction to Sustainable Energy.....	1
<i>Contributing Author: Susan Krumdieck</i>	
1.1 Sustainability Principles	2
1.1.1 Energy Crisis: Security Issues.....	3
1.1.2 Sustainable Development	5
1.1.3 Sustainability Principles in Practice.....	6
1.1.4 Challenges for Sustainability Engineering	7
1.2 Carrying Capacity and Exponential Growth.....	7
1.2.1 Population Issue.....	7
1.2.2 Water Issue.....	9
1.2.3 Food Supply Issues	11
1.2.4 Per Capita Energy Use.....	12
1.2.5 Mathematics of Exponential Growth.....	12
1.3 Context for Sustainable Energy.....	15
1.3.1 Historical Energy Development in the United States.....	15
1.3.2 Current Energy Use	17
1.3.3 Future Energy Scenarios for the United States.....	18
1.4 Key Sustainability Considerations	18
1.4.1 The Challenge of Climate Change	18
1.4.2 Energy Economic Efficiency.....	23
1.4.3 Energy Return on Energy Invested.....	23
1.4.4 Cost of Energy Production	25
1.4.5 Other Costs of Energy Development	26
1.5 Energy Efficiency and Conservation.....	28
1.5.1 Energy End-Use Demand Reduction in Buildings	29
1.5.2 Energy End-Use Demand Reduction in Transportation.....	30
1.5.3 Energy Management in Industry and Manufacturing	30
1.6 Conventional Energy	31
1.6.1 Fossil Fuels.....	31
1.6.2 Nuclear Power	31
1.7 Renewable Energy.....	32
1.7.1 Wind Energy.....	33
1.7.2 Solar Photovoltaics.....	34
1.7.3 Solar Thermal	35
1.7.4 Ocean and Geothermal Energy	36
1.7.5 Biomass and Biofuel	38
1.7.6 Hydroelectric Generation	39

1.8	Hydrogen.....	40
1.9	NREL System Advisor Model	42
	Energy Units and Conversion Factors	45
	Problems.....	45
	Discussion Questions	48
	Online Resources.....	50
	References	51
	Suggested Readings.....	53
2	Economics of Energy Generation and Conservation Systems	55
2.1	Unit Cost of Energy	55
2.2	Payback Period	56
2.3	Time Value of Money.....	57
2.4	Inflation	59
2.5	Total Life Cycle Costs	60
2.6	Internal Rate of Return.....	63
2.7	Capital Recovery Factor	66
2.8	Levelized Cost of Energy	68
2.9	Societal and Environmental Costs	71
	Problems.....	73
	References	75
3	Energy Systems Analysis Methodologies	77
3.1	Life Cycle Approach	77
3.2	Process Chain Analysis.....	81
3.3	Input–Output (I/O) Analysis	83
3.4	Embedded Energy	87
3.5	Energy Return on Energy Invested	92
3.5.1	Calculation of EROI	95
3.5.2	EROI and Energy Budgets	96
3.5.3	EROI for a Wind Energy System.....	99
3.6	Greenhouse Gas Accounting.....	101
	Problems.....	103
	References	105
4	Energy Use and Efficiency in Buildings and Industry	107
4.1	Background.....	107
4.2	Energy Audits and Energy Management.....	110
4.3	Buildings	112
4.3.1	Calculations of Heating and Hot Water Loads in Buildings.....	112
4.3.1.1	Calculation of Heat Loss	112
4.3.1.2	Internal Heat Sources in Buildings.....	116
4.3.1.3	Degree-Day Method	116
4.3.1.4	Service Hot Water Load Calculation	120
4.3.2	Cooling Requirements for Buildings	121
4.3.3	Vapor-Compression Cycle	125
4.3.4	Evaporative Cooling	130
4.3.5	Energy Efficiency in Commercial Buildings.....	130
4.3.5.1	Commercial Buildings Case Studies	135

4.3.6	Energy Efficiency in Residential Buildings.....	137
4.3.6.1	Residential Case Study: Net-Zero Habitat for Humanity House.....	145
4.3.7	Zero-Energy Urban Districts.....	146
4.4	Industrial Energy Efficiency.....	148
4.4.1	Background.....	148
4.4.2	Improving Industrial Processes.....	148
4.4.3	Improvements in Industrial Equipment.....	151
	Problems.....	154
	References	156
5	Electricity Supply Systems	159
5.1	Historical Development of the U.S. Electric Power System	159
5.2	Electrical Transmission	160
5.3	The Electric Grid and Electricity Markets	163
5.3.1	Rate Structures	166
5.3.2	Electricity Markets.....	166
5.3.2.1	Energy Market	167
5.3.2.2	Capacity Market	168
5.3.2.3	Ancillary Services Market	169
5.3.2.4	Financial Transmission Rights Market	170
5.4	Grid Operations.....	170
5.5	Integration of Variable Renewable Energy into the Grid	175
5.6	Demand Response and Transactional Controls	184
	Problems.....	187
	References	193
6	Fossil Fuels.....	195
6.1	Fossil Fuel Resources and Extraction.....	195
6.1.1	Coal.....	195
6.1.2	Natural Gas.....	198
6.1.3	Petroleum.....	200
6.2	Fossil Fuel Combustion and Energy Conversion Technologies	203
6.2.1	Heat of Combustion.....	203
6.2.2	Fossil Fuel Use for Heat	204
6.2.3	Electricity Generation from Pulverized Coal	205
6.2.4	Electricity Generation from Natural Gas	208
6.2.5	Integrated Gasification Combined Cycle.....	209
6.3	Air Pollution from Fossil Fuel Combustion	210
6.3.1	Local and Regional Scale Air Pollution	210
6.3.2	Greenhouse Gas Emissions and Climate Change	212
6.3.3	Carbon Capture and Sequestration.....	215
6.3.4	Leaving It in the Ground	217
	Problems.....	217
	References	219
7	Nuclear Energy.....	223
7.1	Introduction	223
7.2	Fission Mechanism	225

7.3	Available Nuclear Resources.....	229
7.3.1	Uranium Resources	229
7.3.2	Plutonium.....	231
7.4	Reactor Types.....	231
7.4.1	Pressurized-Water Reactors (PWRs)	231
7.4.2	Boiling Water Reactors (BWRs).....	232
7.4.3	Heavy Water Cooled and Moderated Reactor	233
7.5	Nuclear Waste Management and Disposal.....	233
7.6	Spent Fuel Storage and Reprocessing	236
7.7	Nuclear Power Plant Accidents.....	237
7.8	Current Status and Cost of Nuclear Technology.....	238
7.9	Next-Generation Nuclear Technologies.....	238
	Discussion Questions	241
	Acknowledgment.....	242
	References	242
8	Wind Energy.....	245
	<i>Contributing Author: Gary E. Pawlas</i>	
8.1	Introduction	245
8.2	Environmental Impact	248
8.2.1	Noise and Visual Impact.....	249
8.2.2	Life Cycle Greenhouse Gas Emissions, Land, and Water Use	250
8.2.3	Bird and Bat Fatalities	250
8.3	Power and Energy of Wind	252
8.4	Coefficient of Performance	254
8.5	Aerodynamics	255
8.6	Wind Characteristics	258
8.6.1	Wind Generation.....	258
8.6.2	Distribution of Wind	259
8.6.3	Wind Speed Increasing with Height.....	261
8.6.4	Log Law Wind Speed Profile	261
8.6.5	Power Law Wind Speed Profile	263
8.6.6	Probability of Observing a Given Wind Speed	265
8.7	Turbine Performance	269
8.7.1	Control Schemes	278
8.8	Levelized Cost of Energy for a Wind Turbine	279
8.9	Wind Farms	284
8.10	Offshore Wind Energy	287
8.11	System Advisor Model for Wind Farm Analysis	292
8.12	Additional Topics for Study.....	298
	Acknowledgment.....	300
	Problems.....	300
	References	303
9	Capturing Solar Energy through Biomass.....	307
	<i>Contributing Authors: Robert C. Brown and Mark M. Wright</i>	
9.1	Biomass Production and Land Use	307
9.1.1	Waste Materials	308

9.1.2	Energy Crops.....	309
9.1.3	Algae.....	311
9.1.4	Land Use for Biomass Production.....	311
9.1.5	Important Properties of Biomass.....	316
9.2	Biomass Process Economics and Technology.....	318
9.2.1	Biomass Process Economics.....	318
9.2.2	Conversion of Biomass to Gaseous Fuels.....	321
9.2.2.1	Biomass to Biogas.....	321
9.2.2.2	Biomass to Synthetic Gas.....	321
9.2.3	Conversion of Biomass to Liquid Fuels.....	326
9.2.3.1	Corn Ethanol.....	327
9.2.3.2	Cellulosic Ethanol.....	328
9.2.3.3	Biomass Fermentation to Alternative Fuels.....	329
9.2.3.4	Biomass to Fischer–Tropsch Liquids.....	330
9.2.3.5	Biomass Pyrolysis Oil to Gasoline and Diesel.....	331
9.2.3.6	Compressed Gases as Transportation Fuel.....	333
9.2.3.7	Modern Concepts in Biofuel Conversion.....	333
9.2.4	Conversion of Biomass to Electricity.....	336
9.2.4.1	Direct Combustion.....	336
9.2.4.2	Combustion Equipment.....	338
9.2.4.3	Biomass Cofiring.....	339
9.2.5	Fossil and Biomass Fuel Properties.....	340
9.3	Use of Biomass in Developing Communities.....	342
9.4	Conclusions.....	344
	Problems.....	345
	References.....	347
10	Fundamentals of Solar Radiation.....	351
	<i>Contributing Author: Jan Kreider</i>	
10.1	Physics of the Sun and Its Energy Transport.....	351
10.2	Thermal Radiation Fundamentals.....	352
10.2.1	Black-Body Radiation.....	353
10.2.2	Radiation Function Tables.....	354
10.2.3	Intensity of Radiation and Shape Factor.....	357
10.2.4	Transmission of Radiation through a Medium.....	360
10.3	Sun–Earth Geometric Relationship.....	361
10.3.1	Solar Time and Angles.....	364
10.3.2	Sun-Path Diagram.....	369
10.3.3	Shadow-Angle Protractor.....	374
10.4	Solar Radiation.....	376
10.4.1	Extraterrestrial Solar Radiation.....	377
10.5	Estimation of Terrestrial Solar Radiation.....	381
10.5.1	Atmospheric Extinction of Solar Radiation.....	381
10.5.2	Solar Radiation on Clear Days.....	383
10.5.3	Solar Radiation on a Tilted Surface.....	384
10.6	TMY Data to Determine Solar Radiation.....	388
10.7	Measurement of Solar Radiation.....	388
10.7.1	Instruments for Measuring Solar Radiation and Sunshine.....	389

10.7.2	Detectors for Solar Radiation Instrumentation	392
10.7.3	Measurement of Sunshine Duration.....	393
10.7.4	Measurement of Spectral Solar Radiation.....	393
10.7.5	National Solar Radiation Database	393
	Problems.....	394
	References	395
11	Photovoltaics.....	397
11.1	Semiconductors	399
11.1.1	p - n Junction	402
11.1.2	Photovoltaic Effect	402
11.2	Analysis of Photovoltaic Cells.....	406
11.2.1	Efficiency of Solar Cells.....	411
11.2.2	Multijunction Solar Cells	411
11.2.3	Design of a Photovoltaic System.....	412
11.3	Manufacture of Solar Cells and Panels.....	415
11.3.1	Single Crystal and Polycrystalline Cells	415
11.3.2	Amorphous Silicon.....	419
11.4	Design for Remote Photovoltaic Applications	420
11.4.1	Estimation of Loads and Load Profiles.....	420
11.4.2	Estimation of Available Solar Radiation.....	422
11.4.3	PV System Sizing	422
11.4.4	Water Pumping Applications.....	424
11.5	Thin-Film PV Technology.....	425
11.6	Multilayer PV Technology	427
11.7	Today's PV Market	434
11.8	Using System Advisor Model (SAM) for PV Performance Estimates	436
	Problems.....	441
	References	444
	Suggested Readings.....	445
12	Solar Thermal Collectors and Systems	447
	<i>Contributing Authors: Jan Kreider and Jeffrey H. Morehouse</i>	
12.1	Radiation Properties of Materials.....	447
12.1.1	Selective Surfaces	449
12.1.2	Reflective Surfaces	449
12.2	Energy Balance for a Flat Plate Collector.....	451
12.3	Experimental Testing of Collectors	453
12.3.1	Testing Standards for Solar Thermal Collectors	454
12.4	Evacuated Tube Collectors.....	456
12.5	Transpired Air Collectors	457
12.6	Concentrating Solar Collectors	460
12.6.1	Line-Focus Concentrators.....	460
12.6.1.1	Parabolic Troughs.....	460
12.6.1.2	Linear Fresnel Collectors.....	463
12.6.2	Point-Focus Concentrators.....	463
12.7	Solar Domestic Hot Water, Space Heating, and Cooling Systems	466
12.7.1	Solar Thermosyphon Water Heating	466

12.7.2	Forced-Circulation Hot Water Systems	470
12.7.3	Liquid-Based Solar Heating Systems for Buildings.....	476
12.7.4	Passive Solar Heating Systems.....	477
12.7.5	Solar Cooling Systems.....	480
12.8	Solar Thermal Power Plants	482
12.8.1	Parabolic Trough-Based Power Plants	482
12.8.2	Power Towers.....	490
12.9	Solar Industrial Process Heat	498
	Problems.....	501
	References	502
13	Ocean, Hydropower, and Geothermal Energy Conversion	505
13.1	Ocean Thermal Energy Conversion	505
13.1.1	Closed-Cycle Ocean Thermal Energy Conversion.....	507
13.1.2	Open-Cycle Ocean Thermal Energy Conversion	511
13.1.3	Direct Contact Evaporation and Condensation.....	513
13.1.4	Comparison of Open- and Closed-Cycle OTEC Systems	514
13.1.5	Cold-Water Pipe and Pumping Requirements	515
13.1.6	Economics	516
13.2	Tidal Energy.....	516
13.3	Wave Energy	523
13.3.1	Deep Water Wave Power.....	523
13.3.2	Wave Power Devices.....	526
13.4	Hydropower.....	528
13.5	Geothermal Energy.....	531
13.5.1	Geothermal Power	531
13.5.1.1	Current Commercial Geothermal Power Technologies.....	534
13.5.1.2	Technology Status	536
13.5.2	Direct Use of Geothermal Energy	537
	Problems.....	537
	References	539
14	Storage Technologies	541
14.1	Overview of Storage Technology.....	541
14.1.1	Applications.....	542
14.1.2	Technology Characterization	542
14.2	Mechanical Technologies.....	544
14.2.1	Pumped Hydroelectric Energy Storage.....	546
14.2.1.1	Turbines	548
14.2.2	Compressed Air Energy Storage	549
14.2.3	Flywheels	550
14.3	Direct Electrical Technologies.....	551
14.3.1	Ultracapacitors.....	551
14.3.2	Superconducting Magnetic Energy Storage.....	551
14.4	Fundamentals of Batteries and Fuel Cells.....	551
14.4.1	Principles of Battery Operation	553
14.4.2	Cell Physics	555
14.5	Rechargeable Batteries	555
14.5.1	Lead-Acid Batteries.....	556

14.5.2	Nickel Metal (Ni-Cd and Ni-MH)	558
14.5.3	Lithium Ion	559
14.5.4	Flow Batteries	560
14.6	Fuel Cells and Hydrogen	562
14.6.1	Principles of Fuel Cell Operation	562
14.6.2	Types of Fuel Cells	563
14.6.3	Generation of Hydrogen	564
14.6.4	Storage and Transport	565
14.6.5	Thermodynamics and Economics	565
14.7	Thermal Energy Storage	566
14.7.1	Sensible Heat	566
14.7.2	Phase Change Heat Storage	567
14.7.3	Thermochemical Storage	568
14.7.4	Applications	570
14.7.5	Thermal Storage for Concentrating Collector Systems	570
14.7.6	Overnight Storage for Buildings and Domestic Hot Water	570
14.8	Virtual Storage in the Electric Transmission Grid	576
	Problems	580
	References	582
15	Transportation	585
15.1	Introduction	585
15.2	Overview of Transportation Systems and Energy Use	586
15.3	Well-to-Wheels Analysis	589
15.4	Biofuels	592
15.5	Hybrid Electric Vehicles	594
15.6	Plug-in Hybrid Electric Vehicles	595
15.7	Combining HEVs or PHEVs with Biofuels	598
15.7.1	Petroleum Requirement	599
15.7.2	Carbon Dioxide Emissions	600
15.8	Future All-Electric System	602
15.9	Natural Gas as a Transportation Fuel	602
15.10	Hydrogen for Transportation	604
	Problems	606
	References	609
	Online Resources	611
Index		613

Foreword

As with the previous editions, this third edition of *Principles of Sustainable Energy Systems* adds enormously, in a clear and comprehensive way, to the foundational understanding of our energy challenges and opportunities. It is clearer today, than ever before, that our global community needs to accelerate the transition to a low-carbon energy economy. This latest edition reflects the recognition that to do so, a better understanding of all energy generation and end use sources and options is required. It is most appropriate that this edition adds very relevant chapters on energy efficiency, fossil and nuclear energy, and expands the text to include integrating variable renewable energy into the existing electricity grid. While support for clean energy alternatives has never been higher, the obstacles to achieving a true energy transformation that appropriately values low-carbon alternatives remain formidable. Additionally, this book examines the practical aspects surrounding the widespread adoption of energy efficiency and renewable energy systems in the context of new technology developments, policies, and evolving global markets.

I can think of no better team to update Professor Kreith's original book than the three authors of the new edition. The team for this edition was led by Dr. Charles F. Kutscher of the National Renewable Energy Laboratory with whom I have worked for many years. The new edition also includes significant contributions from Professor Jana B. Milford, an expert on the environmental effects of energy systems. And as one who has followed and actively engaged in renewable energy research, development, and deployment for more than four decades, I can attest to the fact that Professor Kreith's contributions in this arena were legendary. All three authors bring deep and complementary expertise in renewable energy technology and sustainability assessment.

To those who choose renewable energy and sustainability as an academic field or career path, this text and the insights you gain from it will likely become fundamental to the achievements that await you. But this text is not merely academic; it serves a valuable purpose in its clearheaded look at the energy picture from the ground up, and the environmental, economic, and sustainability benefits that renewable energy systems can provide.

Principles of Sustainable Energy Systems builds on previous editions and combines the expertise earned from decades of practical and scholarly research with the most up-to-date analysis of the energy scene. It provides an important guide for practitioners worldwide. Today, sustainable energy is no longer just a topic discussed at the margins in the energy sector. It is central to it. Its study also provides incredible opportunities for practitioners and decision-makers to create the future that will serve humanity for generations to come.

Dan E. Arvizu

*Director Emeritus, National Renewable Energy Laboratory
Member, National Academy of Engineering*



Taylor & Francis

Taylor & Francis Group

<http://taylorandfrancis.com>

Preface

The world is undergoing rapid transitions on many technological fronts. The fields of communications, artificial intelligence, and medicine are evolving at a breakneck pace. All of these technologies require energy. And no transition is more important to the future of our planet than the wholesale reinvention of our energy system. For two centuries, we have harnessed rich reserves of coal, oil, and natural gas that took nature millions of years to create. Continuing to burn up these finite reserves is not sustainable. More importantly, we now have overwhelming evidence (in the form of studies of past climates, today's most advanced computer models, and myriad scientific measurements underway around the world) that our burning of fossil fuels is rapidly warming the planet, resulting in a wide range of serious social and economic consequences. The unsustainability of fossil fuels makes an energy transition necessary. Climate change makes it urgent.

Numerous studies have concluded that the societal costs of climate change are roughly an order of magnitude greater than the cost of taking measures to reduce it. In other words, the faster we get off fossil fuels, the better. But we should not underestimate the enormous change that is required. There are thousands of coal plants operating around the world, and the largest ones will burn the contents of a mile-long coal train every single day. Add to that all the natural gas consumed by power plants and buildings, and all the gasoline burned by a billion motor vehicles worldwide and you get an idea for the size of the problem. Transitioning to 100% carbon-free energy will require an engineering effort of unprecedented scale.

While renewable energy falls freely on nations around the world, the distributions of the resources vary widely. Different technologies will be favored in different places. The engineering challenge is to rapidly harness these technologies in the most economical way possible. The purpose of this book is to provide engineering students with a fundamental understanding of the economic and technical aspects of the wide range of low-carbon energy technologies.

Since the first edition of this textbook was published in 2010, wind and solar photovoltaic technologies have experienced dramatic decreases in cost and exponential growth in deployment. In 2014, 2015, and 2016, renewable energy sources supplied more than half of the new electricity generation added to the U.S. electric grid, and many countries around the world are experiencing even faster renewable energy growth rates. The energy landscape has changed greatly in the last 7 years.

In this third edition, we have not only updated energy statistics, but we have also expanded our approach to cover the rapidly changing market. In 2010, the amount of renewable electricity on the electric grid was too small to present a problem to utility operators. Today, however, there are times when wind power in Texas or solar power in Hawaii must be curtailed due to overproduction compared to demand. Cost-effectively integrating renewable electricity into the electric grid on a large scale is now a top priority, and so we have added a new chapter ([Chapter 5](#)) that provides the fundamentals of this challenge.

In its studies on addressing climate change, the International Energy Agency has emphasized the importance of energy efficiency measures. Energy efficiency is the lowest-cost means to address climate change, and it reduces the amount of carbon-free energy sources that must be deployed. In particular, according to IEA, "More efficient buildings

support the whole energy system transformation.” Thus, in this third edition we have added a new chapter devoted to efficiency ([Chapter 4](#)), with special emphasis on reducing building energy use. We include in that chapter a discussion of the latest computer tools that are available to identify and analyze energy efficiency opportunities in residential and commercial buildings. We also discuss the important role that cities are playing.

Of course, a complete transition to carbon-free energy cannot occur overnight, and so it’s important for engineers to understand today’s energy system. Thus, we have added a new chapter on fossil fuels ([Chapter 6](#)) that explains these traditional energy sources and their associated technologies, as well as their societal impacts. There is also a new chapter on nuclear power ([Chapter 7](#)). Although uranium is not a renewable energy source like wind, solar, or biomass, nuclear power plants have played an important role in avoiding carbon emissions. There is a lively debate in the scientific community about the role of nuclear power vis-à-vis renewable energy in our transition to a carbon-free energy ecosystem, and there are strong arguments on both sides. While this book emphasizes renewable energy solutions, we believe it’s important for students to gain an understanding of the nuclear power option, especially because so many nuclear power plants are being built in China and other countries.

In addition to providing students with an understanding of these various technologies and their economics, we believe it is also important for them to learn how to use modeling tools to design systems. Thus, we have expanded our use of the System Advisor Model (SAM), developed by the National Renewable Energy Laboratory and Sandia National Laboratories. SAM is a free tool that simplifies the economic and technical analysis of renewable energy systems. SAM is designed to easily access information on weather, solar radiation, and utility rate data for many locations, as well as information on various types of energy equipment. Engineers can use it to determine the detailed performance and cost of different renewable energy technologies. SAM examples appear for solar hot water, wind power, solar photovoltaics, and concentrating solar power. The book website, <https://www.crcpress.com/Principles-of-Sustainable-Energy-Systems-Third-Edition/Kutscher-Milford-Kreith/p/book/9781498788922>, contains tables of useful information and other materials that supplement the text.

We believe there has never been a more exciting or more critical time for engineering students to enter the energy field. There is much work to be done. It is our hope that this book will provide students with the foundation they need to help lead the transition to a twenty-first-century sustainable energy economy that will preserve our planet for generations to come. And beyond addressing climate change, the rewards of that effort will include millions of new jobs created, a more secure electric grid, cleaner air and water, stronger national security, and greater energy access and independence throughout the world.

Charles F. Kutscher
Jana B. Milford
Frank Kreith
Golden and Boulder, Colorado

Acknowledgments

Charles F. Kutscher would like to thank the following people. Dave Roberts provided helpful review comments for [Chapter 4](#), and Michael Deru provided a homework problem. Jennie Jorgenson, Ben Kroposki, and Mark Mehos provided suggestions on [Chapter 5](#). Brian Keyes and Mike Woodhouse made important improvements to [Chapter 11](#). Mike Wagner provided two SAM examples for [Chapter 12](#). Sheri Anstedt provided helpful editorial support. Charles also thanks his many colleagues at the National Renewable Energy Laboratory for providing countless insights into energy efficiency, renewable energy technologies, and the challenge of integrating renewable energy into the electric grid. Finally, he would like to thank Jonathan Plant and Richard Tressider of Taylor & Francis for their able guidance and support in the preparation of all three editions of this book.

In addition to the contributing authors, Frank Kreith would like to thank the coauthors of the previous two editions of the book. First, Dr. Jan Kreider, his former student, and professional colleague who contributed material for the topic of solar thermal conversion, some of which has been retained for this edition. He would like to express his appreciation to Professor Susan Krumdieck of the Canterbury University in New Zealand for helpful discussion on the transition from a system based on nonrenewable fossil fuels to one that relies on sustainable energy sources. He would also like to thank Claire Kallahan, Carisa Merchant, and Beverly Weiler for transcribing his rough draft into a publishable version of several chapters and locating references for the updated and new chapters that have been written for this third edition. Frank would also like to thank his wife Marion for her forbearance and help in many tangible and intangible ways during the preparation of the manuscript for this third edition. Lastly, he thanks his students for providing helpful comments while using the previous editions as their text.

Jana B. Milford sincerely thanks the following individuals for important contributions to the third edition. Azadeh Keshavarzmohammadian worked out solutions to several of the examples and problems in [Chapters 2](#) and [3](#). Patrick Moriarty provided helpful review comments on updates to [Chapter 8](#). Forrest Lacey and Ricardo Piedrahita provided valuable reviews of the new section in [Chapter 9](#) on the use of biomass in developing countries. Susan Krumdieck and Joel Swisher helped identify key areas where updates and additions to the second edition were needed. Jana also thanks the mechanical and environmental engineering students who have taken Sustainable Energy at the University of Colorado Boulder from 2013 to 2017 for their feedback on the previous edition of the book and the insights they gave her on what to keep and what to change for the new edition.



Taylor & Francis

Taylor & Francis Group

<http://taylorandfrancis.com>

Authors

Charles F. Kutscher is a fellow of the Renewable and Sustainable Energy Institute (RASEI), a joint institute between the University of Colorado Boulder (CU-Boulder) and the National Renewable Energy Laboratory (NREL). He served as the director of the Buildings and Thermal Sciences Center at NREL from 2013 until his retirement in 2018. He has worked in the field of renewable energy for over four decades, during which time he has led research investigations on solar heating and cooling, building energy efficiency, solar industrial process heat, geothermal power, and concentrating solar power. He is a fellow of the American Solar Energy Society (ASES) and served as the Society's chair in 2000 and 2001. He was the chair of two major conferences: the SOLAR 2006 National Solar Energy Conference and the 2012 World Renewable Energy Forum. He led the ASES study, *Tackling Climate Change in the U.S.*, which detailed how energy efficiency and six renewable energy technologies could greatly reduce U.S. carbon emissions by 2030. He has served as an adjunct professor at the University of Colorado at Boulder and the Colorado School of Mines. He earned a BS in physics from the State University of New York at Albany, an MS in nuclear engineering from the University of Illinois at Urbana-Champaign, and a PhD in mechanical engineering from the University of Colorado at Boulder. He is a registered professional engineer in California and Colorado.

Jana B. Milford is professor in the Department of Mechanical Engineering and the Environmental Engineering Program at the University of Colorado at Boulder. Her research and teaching interests focus on air quality modeling and data analysis, environmental impacts of energy systems, and environmental law and policy. She has previously worked as a congressional fellow and analyst at the Congressional Office of Technology Assessment, assistant professor in the Department of Civil Engineering at the University of Connecticut, and senior scientist and staff attorney at the Environmental Defense Fund. Professor Milford currently serves as member of the Colorado Air Quality Control Commission, and has previously served as a member of the board of Environmental Studies and Toxicology of the National Academy of Sciences and on the Science Advisory Board of the U.S. Environmental Protection Agency. She holds a B.S. in engineering science from Iowa State University, a M.S. in civil engineering from Carnegie Mellon University, a Ph.D. in engineering and public policy from Carnegie Mellon University, and a J.D. from the University of Colorado School of Law.

Frank Kreith taught at the University of California, Lehigh University, and the University of Colorado, as a professor emeritus of engineering. From 1988 to 2001 he was the American Society of Mechanical Engineers International (ASME) legislative fellow for Energy and Environment at the National Conference of State Legislatures (NCSL) where he provided assistance on energy, transportation, and environmental protection to legislators in all fifty state governments. Prior to joining NCSL in 1988, Kreith was the chief of thermal research at the Solar Energy Research Institute (SERI), currently the National Renewable Energy Laboratory. During his tenure at SERI, he participated in the Presidential Domestic Energy Review, served as an energy advisor to the Governor of Colorado, and was the editor of

the ASME *Journal of Solar Energy Engineering*. He is the author of over a hundred peer-reviewed articles and of textbooks on heat transfer, solar energy, and transportation. He is the recipient of the Charles Greeley Abbot Award from the American Solar Energy Society and the Max Jakob Award from ASME-AIChE, and in 1997, he received the Washington Award for “unselfish and preeminent service in advancing human progress.” In 1998, Kreith was awarded the ASME Medal for research, publications, and public service and in 2004 he was named ASME Honorary Member. In 2005, the ASME established the Frank Kreith Energy Award in recognition of Kreith’s contribution to heat transfer and renewable energy.

Contributors

Robert C. Brown

Department of Mechanical Engineering
Iowa State University
Ames, Iowa

Jan Kreider

K&A, LLC
Boulder, Colorado

Susan Krumdieck

Advanced Energy and Material Systems Lab
and
Department of Mechanical Engineering
University of Canterbury
Christchurch, New Zealand

Jeffrey H. Morehouse

Department of Mechanical Engineering
University of South Carolina
Columbia, South Carolina

Gary E. Pawlas

Department of Mechanical Engineering
University of Colorado
Boulder, Colorado

Mark M. Wright

Department of Mechanical Engineering
Iowa State University
Ames, Iowa



Taylor & Francis

Taylor & Francis Group

<http://taylorandfrancis.com>

1

Introduction to Sustainable Energy

It is evident that the fortunes of the world's human population, for better or for worse, are inextricably interrelated with the use that is made of energy resources.

M. King Hubbert (1969)

The development of human society and our quality of life are inextricably linked to our use of energy. The emergence of coal in the eighteenth century made possible the Industrial Revolution, and widespread electrification in the twentieth century brought with it all manner of labor-saving devices from washing machines to clothes driers to refrigerators. Similarly, the advent of internal combustion engine vehicles in the early 1900s, followed by the airplane, turned us into a highly mobile society. All of this was made possible by fossil fuels. But after a century of growth and technological advances powered by these fuels, we have come to realize that we humans had made a large-scale Faustian bargain.

In exchange for the wonders of these fossil fuels, we are now coming to grips with their serious side effects. Air pollution from the burning of coal and oil has led to a wide range of health problems from childhood asthma to other life-threatening lung diseases. Acid rain has contaminated lakes, and mercury emissions have poisoned fish and so compromised our food supply. And, most importantly, as we have learned over the last several decades, the carbon dioxide (CO₂) emissions emanating from power plant smokestacks and vehicle tailpipes are increasing the infrared radiation-absorbing blanket in our atmosphere, which is heating the Earth and causing it to rapidly depart from the 10,000-year period of steady temperature that allowed human civilization to develop. We are already seeing the effects of global warming, which includes the melting of ice sheets (see [Figure 1.1](#)), rising sea level, and an increase in extreme weather events.

Although measures have been taken to reduce air pollution by cleaning up stack emissions from power plants and capturing tailpipe emissions from cars, these have only been temporary solutions to an energy system that has a fundamental flaw. The burning of fossil fuels is not sustainable. Fossil fuels are the result of millions of years of nature sequestering atmospheric CO₂ in the ground, and we are releasing all that carbon in a timescale of decades. Although it is technically feasible to capture the carbon in fossil fuels and sequester it in the ground again, the fundamental solution to these issues is to convert our unsustainable, carbon-emitting energy sources to sustainable, carbon-free ones. To accomplish that transition, we need to simultaneously reduce our energy needs by using energy much more efficiently and produce the energy from noncarbon sources. This book introduces the knowledge and tools energy professionals and informed citizens will need to lead this twenty-first-century energy transition.

The purpose of this chapter is to give an overview of the principles of sustainability in the context of energy engineering. Section 1.1 gives a historical review of sustainability principles. Section 1.2 presents the critical issues for sustainability: population, water,

**FIGURE 1.1**

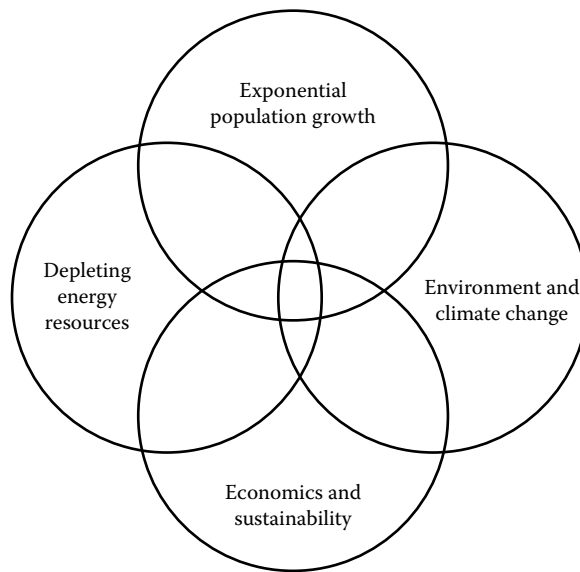
People in front of a melting glacier, Kangerlussuaq, Greenland.

food and growth, and the relationships between these systems and energy use. Section 1.3 presents some context for the complex nature of sustainable energy by looking at the world energy system of the past, present, and future and the urgent challenge of addressing climate change. Section 1.4 explains some of the most important considerations you must understand to effectively deal with sustainability in engineering, including energy return on energy invested (EROI) and the costs of energy. Section 1.5 explains the most cost-effective of all sustainable energy strategies—reducing energy demand by improving efficiency. Section 1.6 gives an overview of conventional fossil and nuclear energy. Section 1.7 reviews the technology, history, current status, and future prospects for renewable resources including geothermal, hydro, wind, solar, biomass, and the ocean. Section 1.8 discusses the issues involved in the concept of a hydrogen economy.

A unique feature of this book is that it makes use of energy design tools developed by the National Renewable Energy Laboratory (NREL). In particular, this book includes numerous detailed examples of the design of renewable energy systems using the freely available System Advisor Model (SAM). An introduction to SAM is presented in Section 1.9, whereas NREL building energy modeling tools are utilized in [Chapter 4](#), “Energy Use and Efficiency in Buildings and Industry.”

1.1 Sustainability Principles

This book focuses mostly on the engineering challenges confronting our efforts to achieve sustainability, but it is important to keep in mind that the development of energy sustainability is taking place in an era when other relevant forces impinge on one another. The energy challenge also involves societal issues such as population growth, resource depletion, and environmental degradation. As shown in [Figure 1.2](#), all of these issues impinge upon the engineering design and economics of a sustainable energy future.

**FIGURE 1.2**

The interrelated nature of engineering, social, and environmental issues. (From Alliance for Water Efficiency and American Council for an Energy-Efficient Economy, May 2011. Addressing the energy-water nexus: A blueprint for action and policy agenda; ASME, ETP. Energy–water nexus—Cross-cutting impacts. [1])

Although this book does not directly cover these other issues, it is important to keep them in mind because, unless the political and social systems support the road map toward a sustainable energy future, social obstacles can impede the implementation of long-term solutions that are technically reasonable as well as economically acceptable. For the reader interested in these social issues, several books in the supplemental reading list at the end of the chapter will provide further background information.

The energy choices made today are among the most important of any choices in human history. Although energy development questions may appear to be mostly technical and economic, there are broader considerations. Sustainability considerations reflect priorities in our society as well as our attitude toward future generations. Development of more renewable energy is not a panacea for all of our energy problems. A sustainable energy future appears feasible only if we develop an overall social and political strategy that includes renewable energy development, combined with energy conservation and efficiency. It requires adopting a lifestyle that reduces energy consumption.

1.1.1 Energy Crisis: Security Issues

The world oil production capacity increased apace with demand for liquid fuels most of the last 100 years. Consider the perspective of people in 1950. At that time, the potential future oil supply would have been much larger than any conceivable demand, oil was abundant and cheap, and few were thinking about global, irreversible environmental impacts. The production of oil in the United States has been controlled at affordable prices by various organizations since 1910. In this context, the decisions made about building roads, dismantling urban trams, underinvestment in rail, and promotion of low-density land use reflect the perception that the oil supply would last forever.

The average price of oil remained below \$3.00 per barrel until 1970. On October 5, 1973, the Yom Kippur War started when Syria and Egypt attacked Israel. The United States and most Western countries showed support for Israel. Several Arab nations, members of the Organization of Petroleum Exporting Countries (OPEC), plus Iran imposed an oil embargo on Western nations and curtailed their production by 5 million barrels per day. There had been no spare production in the United States, the largest oil-producing nation, since 1971, and other non-OPEC producers were able to increase production by only 1 million barrels per day, resulting in an overall 7% decline in world oil supply. By the end of 1974, the price of oil was over \$12 per barrel. OPEC did not increase production again after the crisis, but there was a rapid increase in world supply from other areas like the North Sea, Mexico, and Alaska. Despite the increased supply, the price remained in the new range of \$12.50–\$14.50 per barrel. The Iranian revolution followed shortly after the invasion by Iraq in September 1980 and led to a decrease in production of 6.5 million barrels per day from the two warring nations, representing a further 10% decline in world supply from 1979. This led to a second oil supply shortage with long lines at gas stations and scarcity around the world. By 1981, crude oil prices had more than doubled to \$35 per barrel, and the global economic recession of the early 1980s was the most severe economic crisis since the Great Depression.

In the United States, this series of events caused a serious energy crisis in the 1980s. Electricity demand had grown rapidly since World War II with a building boom and an explosion of new energy uses from conveniences like air conditioning, refrigeration, washing machines, and other appliances. With no spare oil production capacity in the United States, the OPEC Oil Embargo also caused electricity price increases and shortages in some places. The energy crisis generated great interest in alternative energy sources, spurred research and development, and resulted in new standards and regulations on energy efficiency for buildings, appliances, and vehicles. The energy crisis also started a political obsession with energy independence as a national security objective that persists to this day. The realization that all critical activities relied on finite fossil fuels like oil and natural gas influenced thinking about sustainability to extend beyond environmental impacts and to look at the future implications of depletion. Energy engineering emerged as a new field, primarily within mechanical engineering with courses on energy conversion, air pollution, and energy management taught at many major universities.

However, as new oil fields in the North Sea and other non-OPEC nations were developed, world oil production capacity increased again, the oil price declined to a new price range below \$30 per barrel, and it became politically unpopular to worry about energy shortages. In fact, the discussion around fossil fuel use and the development of the resources in remote and higher-risk environments became polarized and framed in terms of the environment versus the economy. Beginning in 2008, the action by U.S. developers to harness shales for oil and natural gas led Middle East producers to overproduce oil in response. These actions, together with a slowdown in the Chinese economy and, in January 2016 an increase in Iranian oil production resulting from the lifting of U.S. sanctions, has led to an oversupply of oil on the world market and a depression of prices, although future oil prices are difficult to predict.

Sustainability in terms of fossil fuel energy supply is often seen as a short-term economics and political issue. There have been 11 recessions in the U.S. economy since World War II. One of them followed the bursting of the dot-com investment bubble, and the rest were preceded by an oil price spike. All of the oil price spikes except the 2007–2008 price run-up have resulted from political conflict causing reduced spare production capacity. The best economic mitigation for the short-term risks of oil supply insecurity is the ability to reduce demand as demonstrated in the previous energy crises. In the long term, there



FIGURE 1.3

The 2017 Chevy Bolt is the first electric vehicle with an electric range of over 200 miles (320 km) (The Environmental Protection Agency range is 238 miles or 381 km) and a retail price (after U.S. federal tax credit) of under \$30,000. (Photo by C. Kutscher.)

is a convergence of downward pressure on energy supplies including the retirement of aging nuclear and coal power plants, decreased coal use, and high cost and environmental risks limiting the development of deep sea oil, tar sands, and shale gas. The ability to use energy more efficiently will be the most cost-effective and timely mitigation for risks to our economy. The need to address the health issues and climate change impacts linked to the burning of fossil fuels and the increasing cost effectiveness of renewable energy technologies, especially solar photovoltaic energy and wind power, are accelerating a transition to these technologies. Although this transition is occurring mostly in the electricity sector in which renewables are beginning to displace coal and natural gas, the development of hybrid and electric vehicles (see [Figure 1.3](#)) will also impact the transportation sector. Because electric vehicles are so simple mechanically, they have low maintenance costs and thus are very appealing to fleet operators, which should help accelerate their market penetration.

1.1.2 Sustainable Development

In 1983, the United Nations set up an independent body headed by Gro Harlem Brundtland, the former prime minister of Norway, entitled the World Commission on Environment and Development. The commission was asked to examine the critical environmental and developmental problems facing the planet and to formulate realistic proposals to solve them. The proposed solution was to make sure that human progress can be sustained, but without bankrupting the resources of future generations. The outcome of this study was an important book entitled *Our Common Future* [2]. The Brundtland commission concluded that worldwide efforts to guard and maintain human progress to meet human needs and

to realize human ambition are unsustainable, both in developed and developing nations, because they rely on ever-increasing use of already overdrawn environmental resources. The commission provided a widely quoted definition of sustainability.

Sustainable development should meet the needs of the present without compromising the ability of future generations to meet their own needs [2].

The commission stated that sustainable global development requires that those who are more affluent adopt lifestyles that can be accommodated by the planet's ecological means, particularly their use of energy. Further, the rapidly growing population increases the pressure on resources. Sustainable development can, therefore, only be achieved if population size and the population growth rate are limited to a point where they no longer exceed the productive potential and maintenance level of the Earth's ecosystems. The commission realized that future economic growth must be less energy intensive than growth in the past. Energy efficiency policy must be the primary vehicle of national energy strategies for sustainable development, but the commission also realized that energy efficiency can only buy time for the world to develop energy paths based on renewable sources and that this goal must be the foundation of any global energy strategy for the twenty-first century.

1.1.3 Sustainability Principles in Practice

Allocation of the use of common resources is an ancient practice that is essential for sustainability. There are villages in the Old World where the same families have farmed the same land and lived in the same homes for over 600 years. All of the people in an area shared grazing areas, forest resources, and water. Management of the *commons* was part of the operation of the village to ensure that users did not overtax resources. In American history, abundant resources were always available for development, and the traditional methods of allocation and management of individual use of common resources were not developed to the same degree as in Europe. During the westward expansion, there was little interest in preserving the environment or protecting resources. However, as resources have become scarce, there has been increasing interest in protecting them. For example, water is an essential resource that is in short supply in the Western United States. Systems have been developed to allocate water to end users and to regulate and limit taking more water than the allocation. Water allocation systems are engineered systems that include monitoring, modeling, and communication between users and the supplier that involves more than just price signals.

Regulations to limit environmental impacts and protect public health are key sustainability principles. As industries grew up around the country, states, counties, and cities have worked with health boards to monitor and regulate pollution discharged into rivers. The 1970s saw a raft of federal environmental legislation in the United States, including the Clean Air Act Amendments of 1970 and the Safe Drinking Water Act (1974), which resulted in great improvements in air and water quality. In 1987, the Montreal Protocol on Substances that Deplete the Ozone Layer was ratified by most of the nations of the world and required corporations to stop producing certain widely used refrigerants and chemicals that were extremely useful and profitable, but which had been shown by scientists to be depleting the Earth's protective ozone layer. Environmental regulation often comes after the problem arises. In most cases, technical remedial processes are developed. Scientists observe and measure the harm being caused by a given practice or pollutant, engineers undertake

research and development of alternative processes, and finally, when the environmental and health issues get sufficiently alarming and the alternative engineering solutions are available at a reasonable cost, the legislation is enacted that requires alteration of the harmful industrial process. This pattern has many examples: banning of the pesticide DDT, lead additive being removed from gasoline, particulate and sulfur dioxide scrubbing being required for coal-fired power plants, and placing catalytic converters on automobiles. Unfortunately, there can be a long lag time between an environmentally harmful practice and when the adverse consequences become apparent. That is the case with climate change caused largely by CO₂ and methane emissions. The worst damages will occur long after the emissions are released.

Corporations usually focus on “the bottom line,” meaning the financial balance sheet. However, major corporations around the world are voluntarily addressing not just the financial benefits of their operations but the social and environmental impacts as well. This is the idea behind triple bottom line accounting, which accounts for the financial, social, and environmental impacts of corporate operations on workers, customers, and people who live near factories or mines. Social and environmental bottom lines are not as easy to quantify as the financial bottom line, so corporations have set out principles for their practices so that they do not exploit resources or people in a way that negatively impacts their well-being. For example, Fair Trade certification has been developed to ensure that suppliers in less developed countries receive a fair price for their goods and labor. Ecological footprint, life cycle assessment, cradle-to-grave, and cradle-to-cradle (zero waste) analyses of goods are techniques that have been developed to quantify the energy and material use and emissions associated with products.

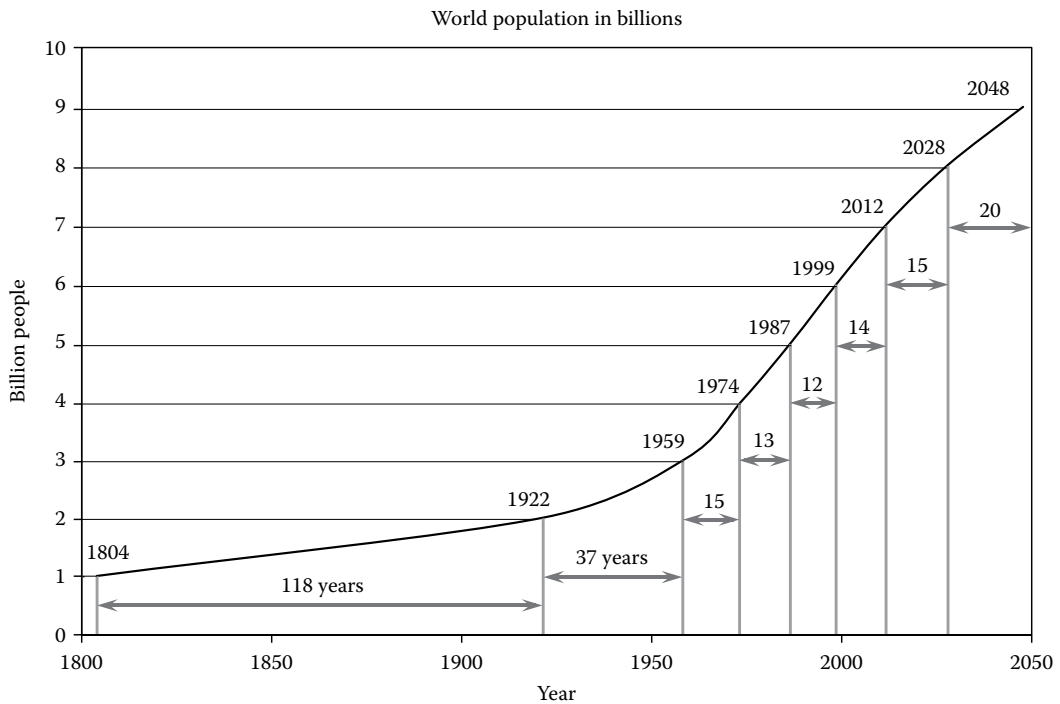
1.1.4 Challenges for Sustainability Engineering

The challenge for engineering professions is to institute sustainability considerations in all projects and operations in much the same way that safety issues are included. Safety engineering requires honesty with employees and the public about the previous safety failures, the potential hazards, and effective risk management measures. Energy engineers will need to similarly be honest with business leaders, policy makers, and the public about the issues of raw material supply security, the potential for alternative technologies, and environmental risks. One challenge is the perceived conflict between economic benefit and sustainability. Again, energy engineers can follow the lead of safety engineers, who are educated to value health and well-being over profit.

1.2 Carrying Capacity and Exponential Growth

1.2.1 Population Issue

World energy use and the associated carbon emissions are clearly linked to world population. As shown in [Figure 1.4](#) [3], the world population started to increase rapidly at the end of the eighteenth century. Note that it took 118 years for the population to double from 1 to 2 billion and only 40 years to double from 3 to 6 billion. The highest population growth rate, 2.06%, occurred in the late 1960s. The world population reached 7 billion in 2011. The United Nations predicts that the world population may reach 8.5 billion by 2030.

**FIGURE 1.4**

Growth of world population. (From Population Division of the Department of Economic and Social Affairs of the United Nations secretariat, March 2009. World population prospects: The 2008 revision. [3])

Current population is a function of the number of people alive last year, minus the number who died, plus the number who were born. The number who die is related to life expectancy, which accounts for the deaths at all ages, including people who die in childhood. A higher life expectancy means more elderly people, but it also means more females are living to childbearing age. Life expectancy is currently around 80 years in Europe, 75 in China, 67 in India, and 50 years in Africa, largely reflecting vastly different childhood mortality. In the United States, the current life expectancy is 75–80 depending on gender. Consider that in 1900, the life expectancy in the United States was 46–48.

The average fertility rate is expressed as the expected number of children a woman would have during her lifetime. The dramatic increase in world population in the last century is largely due to the reduced infant and childhood mortality, an increasing number of fertile women, as well as increased longevity. The rate of population growth has slowed appreciably in countries around the world, but remain higher in Africa, the Middle East, and parts of Southeast Asia than in more developed countries. In the United States, the native-born population decreased for the first time in its history during 2009. In Western countries including Italy, Germany, and Canada, the number of births has dropped to a point at which the population is no longer growing, even though the longevity is very high and the infant mortality is very low. Up-to-date information on population, life expectancy, and fertility rates is available from the United Nations Department of Economic and Social Affairs, Population Division at <https://esa.un.org/unpd/wpp>.

A large body of research (see, for example, Bongaarts, 2003 [4]) has concluded that if women have socially acceptable alternatives to childbearing, they will voluntarily limit

the number of children they have. Education has been shown to be the most effective way to reduce population growth. In locations where girls are given the chance to go to school, the average age of first pregnancy shifts upward. And in places where women have the opportunity for employment, as occurs with increased urbanization, the number of children per woman declines. Adding availability of contraception and social acceptability of small families can bring the population growth rate down to replacement levels.

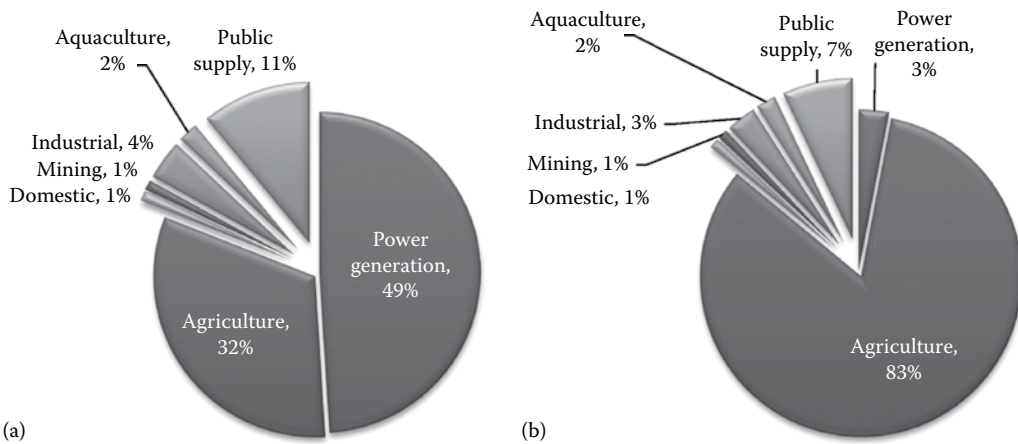
1.2.2 Water Issue

Less than 1% of the water on the planet is suitable for drinking and agriculture; the rest is saltwater, brackish, or frozen. Freshwater refers to rivers and lakes fed by seasonal precipitation. Aquifers are underground freshwater reservoirs in permeable gravels or sand. Unconfined aquifers are replenished by surface precipitation, but confined aquifers like the massive Ogallala aquifer under the Great Plains in the United States actually contain fossil water, deposited over 1 million years ago. The sustainable water consumption in any given location depends on the precipitation rate, storage systems, and the requirements to sustain local ecosystems. Confined aquifers have a finite lifetime for use rather than a sustainable usage rate. In Texas, artesian wells were plentiful in the early twentieth century, but wells must now be pumped and in some places have run dry. A study published in 2012 found that 30% of the Southern Great Plains will have exhausted the groundwater resource within 30 years [5].

The World Health Organization stipulates that the basic requirement for water is that 20 liters per day (L/day) per person be accessible within 1 km of the home. In an industrial society such as the United States, personal water consumption is 10 times as large, somewhere between 200 and 300 L/day for household uses. But if industrial and energy production usage are added, freshwater usage can exceed 5000 L/day on a per capita basis. The World Bank [6] suggests that an indicator of water scarcity is an annual availability of less than 1000 m³ (or 1 million L) per person. By comparing a country's total freshwater resources to this number, a country's water carrying capacity can be determined, that is, how many millions of people the water resources can support. Many countries in the world, especially in the Middle East, already have populations that exceed the country's water carrying capacity.

There are more than 7000 desalination plants in operation worldwide, with 60% located in the Middle East. The levelized cost of water produced by various desalination plants is between \$0.60/m³ for large plants and \$3.00/m³ for small remote plants. The energy requirement varies greatly with the type of process used and is much lower for brackish water than for seawater. Thermal processes like multistage flash desalination use 10–15 kilowatt hours of electricity per cubic meter of water (kWh/m³) while reverse osmosis uses 4–13 kWh/m³ of electricity for seawater and 0.5–2.5 kWh/m³ for brackish water [7]. Desalination is currently an option only in those parts of the world where energy supplies are plentiful and the value of water is extremely high. For example, in Saudi Arabia, the world's largest desalination plant produces 128 million gallons per day (0.5 million m³) of potable water.

It is estimated that around 3% of the electricity demand in the United States (56 billion kWh/year) is for treating and pumping freshwater. California has a large agricultural sector, and a sizable population living far from freshwater sources, resulting in 19% of electricity demand associated with provision of water. The biggest user of freshwater from lakes and rivers is for cooling thermoelectric power plants. Figure 1.5 shows a breakdown of the water withdrawal and consumption according to [1]. (Water withdrawal refers to the sum of water that is consumed without being returned to the source and the water that is

**FIGURE 1.5**

(a) U.S. freshwater withdrawal and (b) U.S. freshwater consumption. (From Alliance for Water Efficiency and American Council for an Energy-Efficient Economy, May 2011. Addressing the energy-water nexus: A blueprint for action and policy agenda; ASME, ETP. Energy–water nexus—Cross-cutting impacts. [1])

TABLE 1.1

Water Consumption for Different Types of Power Plants

Plant Type	Water Consumption per Unit of Electricity (L/MWh _e)
Solar thermal	2600–3800
Nuclear	2600–3000
Subcritical pulverized coal	2000
Supercritical pulverized coal	1700
Integrated gasification combined cycle	1200
Natural gas combined cycle	720

returned.) Power generation and agriculture are the largest sources of water withdrawal, and agriculture is by far the largest consumer of water.

As shown in detail in [Chapter 6](#), thermal power plants operating on a Rankine cycle reject heat in a condenser. The amount of water consumed or withdrawn depends on the kind of cooling system used for the condenser. In coastal locations or where a large river or lake is available and where the water temperature is cool year-round, the withdrawn water is returned to the freshwater body. In hot weather, the freshwater is sprayed over evaporation pads, air is blown through the cooling tower, and the evaporation cools the water stream. In this process, some of the freshwater is consumed and exhausted to the atmosphere. [Table 1.1](#) gives the amount of water consumed by various types of thermal electric power plants. The U.S. average water consumption for thermoelectric power generation was about 23 gal (87 L) per kWh in 2005 for all types of cooling [8]. Water use in electricity generation is an issue of long-term sustainability. ([9] is a good reference on energy and water.) In an extensive report prepared for the U.S. Congress in 2006, the U.S. Department of Energy [10] stated that:

Available surface water supplies have not increased in 20 years, and groundwater tables and supplies are dropping at an alarming rate. New ecological water demands and changing climate could reduce available freshwater supplies even more [10].

As a result, more and more power plants are being air-cooled. Air-cooled condensers require a large heat exchange surface area and considerable fan power to reject heat to the ambient air. Air-cooled plants can suffer significantly reduced performance on hot summer afternoons—the time when electricity is most highly valued. To address this problem, some plants use a combination of air and evaporative cooling during these periods.

Production of biofuels also places pressure on water resources. Ethanol processing from corn requires 3 L of water per L of fuel and anywhere from 10 to 330 L water per L fuel for agriculture depending on irrigation requirements [11]. American petroleum production requires 2–6 L (w) per L crude oil depending on the amount of recycling of produced water as injection fluid. Water consumption and pollution are major issues with the extraction of oil from Canadian tar sands.

1.2.3 Food Supply Issues

To have sustainable development, global food production must be adequate to feed the world's population. Food comes from the sea and the land. It has been estimated that the Earth has 8.2 billion acres (ac) (33 million km²) of potentially arable land. According to a study by the Millennium Institute [12], this acreage is divided according to the levels of productivity shown below:

- World Agricultural Land Endowment:
 - Highly productive—1.1 billion acres
 - Total somewhat productive—2.2 billion acres
 - Total slightly productive—4.9 billion acres
 - Currently productive—3.6 billion acres
 - Potentially productive—8.2 billion acres

In the United States, about 1.5 ac (0.006 km²) of land is used to produce the food for one person per year, but a modest per capita global footprint based on diets with less meat and more grain is estimated to require only 1 ac per capita. At this modest per capita global footprint, the global carrying capacity would be somewhere between 3.6 and 8.2 billion people. In 2015, the United Nations Food and Agriculture Organization estimated that 795 million people were undernourished globally, most of whom live in Asia and Africa [13]. Global limits on food production and water availability indicate that more than 9 or 10 billion people would be an unsustainable global population.

The food supply system in the United States and other industrial countries requires fossil fuel. The current food supply system for the typical American diet requires approximately 2000 L of oil equivalent per year per person and accounts for 19% of the total national energy use, with 14% for production, processing, packaging and storage, and 5% for transportation [14].

Competition between agriculture for food and for biofuels has become an international issue. Corn, soybeans, wheat, and sorghum are the basis of the American food production system. In 2014, the United States produced about 17% of the total world grain supply. Further, about 12% of the domestic corn market is for food: the majority of corn is used for animal feed and ethanol. Biofuel production grew rapidly from 2005 in response to U.S. government mandates and incentives. The consequences of the bioethanol boom have been that the percentage of corn crop used for food in the United States dropped from 13% in 2000 to 11% in 2011, exports dropped from 20% to 13%, and feed for U.S. cattle and chickens plummeted from 60% to 36% of the annual crop. In 2016, ethanol processing consumed

40% of the total U.S. corn crop. According to the U.S. Energy Information Administration, biodiesel expanded from 0.5 million gal in 1999 to 1.6 billion gal in 2016. Despite this growth, biodiesel accounted for a little less than 1% of U.S. highway fuel in 2014 [15].

1.2.4 Per Capita Energy Use

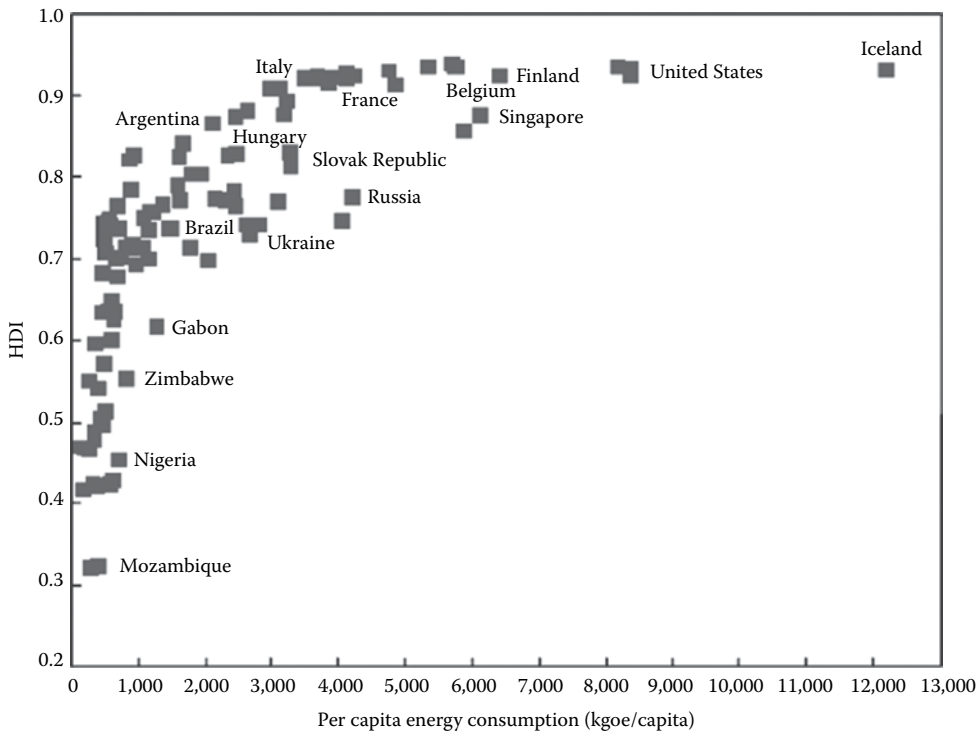
Unlike food and water, the basic level of energy to sustain a given human population is more difficult to specify. The daily energy requirement for a family living a traditional lifestyle on a remote island in Fiji is two coconut husks dried for 2 days in the sun that are used to cook the day's taro in a pit fire and fry the day's fish catch on a simple grill. On the same island, there are homes connected to village electric grids and the island water supply. Their daily energy demand also includes 72 Wh for two small lights for 6 h per day when the village generator functions and a small share of the 20 L of diesel fuel used to run the island water pump for 3 h each day. Also, on the same island, a home built by an Australian has a much different lifestyle with continuous electricity, a refrigerator, TV, lights in every room, and air conditioning. This home supplies its own 11 kWh per day by solar panels, a small wind generator, a large battery bank, and several diesel generators, and compressed natural gas is used for cooking. Although the needs of this house are only about half the average in Australia, they are still vastly different from their neighbors on the island [16]. The standard of living for all of the island residents is roughly similar to the extent that they all have adequate nutrition, access to the same quality of air and water, access to medical treatment and education, and the same life expectancy. Clearly, the energy use of the traditional lifestyle contrasts sharply with that of the Australian lifestyle, which depends heavily on finite resources. Even though about half of the energy for the Australian home is provided by renewable sources, some fossil fuels were consumed in the manufacture of the renewable technologies.

The United Nations proposed a measure of standard of living, termed the Human Development Index, based on various criteria [17]. [Figure 1.6](#) [18] is a plot of energy consumption per capita for various countries as a function of a composite indicator, developed by the United Nations Development Programme, to show countries' relative well-being using the Human Development Index. It is apparent that the United States and Iceland have the highest energy consumption per capita (although Iceland uses 100% renewable energy comprised of geothermal and hydropower), but their human satisfaction level is not much different from other developed countries such as France or Germany, which provide their populations with a good standard of living at much lower energy consumption per capita.

There are large variations in the amount and type of food and the amount of water used according to lifestyle, just as there are wide variations with energy. We can set physiological requirements for food and water; however, it is hard to set such a requirement for energy. In considering the data in [Figure 1.6](#), 1000 kg of oil equivalent (41.9 GJ) can be set as a range for determining the modest energy requirement, or the fossil energy budget plus an allowance for shelter in more extreme climates. This level of energy use may seem draconian in relation to the current U.S. average per capita consumption of over 9000 (377 GJ). However, in quantifying carrying capacity, we are not considering lifestyle; rather, we are considering necessity.

1.2.5 Mathematics of Exponential Growth

Economic growth is a complex phenomenon, which is conventionally measured in terms of year-over-year increases in the value of goods and services produced in a particular

**FIGURE 1.6**

Relationship between Human Development Index and per capita energy use, 1999–2000. (From Goldemberg, J. and Johansson, T.B., eds., 2004. *World Energy Assessment: Energy and the Challenge of Sustainability*, United Nations Development Programme, New York, http://www.undp.org/content/undp/en/home/librarypage/environment-energy/sustainable_energy/world_energy_assessmentoverview2004update.html. [18])

country (i.e., the gross national product). The factors that influence economic growth include increases in capital stock, advances in technology and education, and growth in workforce population. One important limitation of standard economic measures of growth such as change in gross national product is that they fail to capture changes in the distribution of wealth or income across the society. Another important limitation, especially relevant to this textbook, is that they ignore the long-term economic and environmental consequences of depleting natural resources.

For much of the past 150 years, energy use has increased relentlessly along with economic activity, population, and water, food, and land use. An important goal of sustainable energy engineering is to relax the historical linkage between improved quality of life and increased consumption of nonrenewable energy and natural resources. This goal can be accomplished by switching to renewable resources, using technological advances to improve efficiency, and by reducing consumption in the developed world. The importance of taking steps to curtail overconsumption of finite resources is dramatically illustrated using the simple and clear arithmetic of exponential growth.

Suppose the quantity, N , periodically increases from an initial value, N_0 , at a continuous fractional growth rate, r , per unit time, t . The future value of the quantity, $N(t)$, is given by

$$N(t) = N_0(1 + r)^t \quad (1.1)$$

After one period, the quantity will be equal to $N(1) = N_0(1 + r)$, after two periods $N(2) = N_0(1 + r)^2$, and so on. The time it would take for the original quantity to double, or the doubling time, D , is of interest in the studies of growth. Setting $N(t) = 2N_0$ in Equation 1.1 and solving for t gives

$$D = t = \frac{\ln(2)}{\ln(1 + r)} \quad (1.2)$$

For most practical situations, r is small, say less than 10%, and the quantity $\ln(1 + r) \cong r$. Noting that $\ln(2)$ is equal to 0.693, Equation 1.2 simplifies to the rule-of-thumb approximation for doubling time:

$$D \cong \frac{0.7}{r} \quad (1.3)$$

Thus, for a growth rate of 7%, the doubling time would be about 10 years.

Now, suppose that a finite resource would have a total useable quantity, N_T . The initial consumption rate per year is N_0 . If the consumption rate does not change, then the lifetime of the resource, t_L , would be found by $t_L = N_T/N_0$. However, when the consumption rate of the resource is increasing every year with an annual fractional growth rate, r , the lifetime of the resource is given by

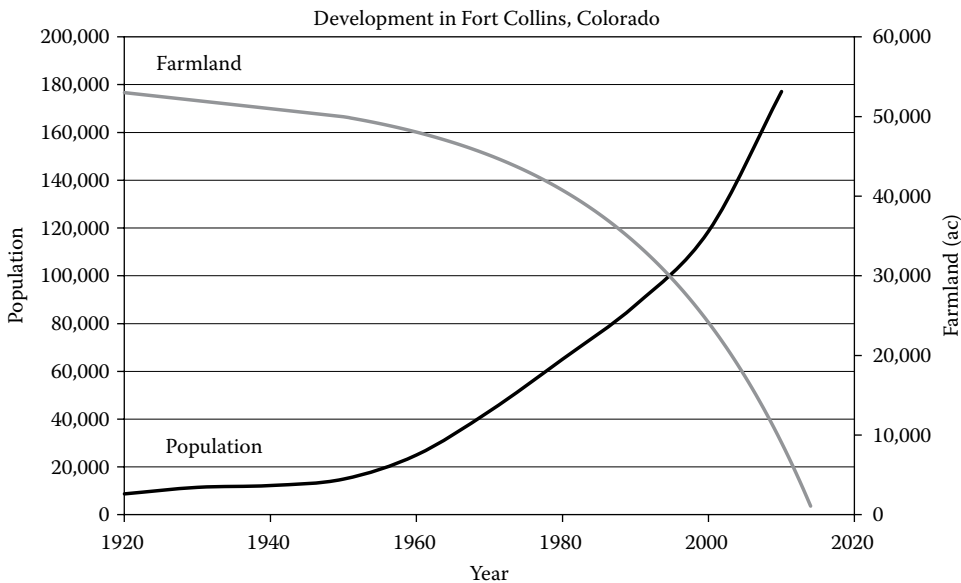
$$t_L = \frac{1}{r} \ln \left(r \frac{N_T}{N_0} + 1 \right) \quad (1.4)$$

Economic value or money is a human construct and not a natural resource, so the supply of money can indeed grow as long as all the participants in the economy continue to agree on its value as a proxy for their goods and labor. However, when we are considering the carrying capacity of a region or the lifetime of a finite resource, we need to be able to perform quantitative analysis to assess the depletion risks and the time frames associated with these issues.

EXAMPLE 1.1: CONTINUOUS GROWTH, FINITE RESOURCES, AND PERCEPTION

In 1950, the city of Fort Collins, Colorado, had a population of 15,000 and occupied 3,750 ac. The city was surrounded by 50,000 ac of prime farmland within a 20 min drive, which grew most of the food sold in the city markets plus grains, fruits, vegetables, and dairy that were transported to the capital city of Denver. Like the rest of the country, Fort Collins was about to experience a prolonged period of population growth at an annual rate of 4.2%. New housing for the population was typical suburban single-family homes, and 158 ac was converted from agriculture to urban use in 1950.

In 1950, people started to wonder: if this current rate of land conversion continued, how long until the farmland was consumed? The answer (50,000/158) is 317 years. No worries! But the next year, 164 ac was developed, and the next year, 171 ac. A professor at Colorado State University used Equation 1.1 and determined that the city seemed to be increasing its land use by 4.2% each year, the same rate as the population growth. If the 3750 ac of urban land in 1950 were to increase apace with population, then Equation 1.4 gives the year that the city would have grown to 53,750 ac and consumed all of the farmland as 63 years later, in 2014, as shown in [Figure 1.7](#). The professor in 1953 would surely have looked at the map and the

**FIGURE 1.7**

Population growth and farmland reduction as a function of time for Fort Collins assuming an annual population growth rate of 4.2%.

farmland around his city and not really been able to picture 118,000 people living there and all of the farmland gone. The mathematical model is clear, but the professor's perception of the issues associated with future growth would likely be limited by his lack of experience with this kind of situation. He might think that something would change in the future to slow the growth or manage the preservation of some of the agricultural productivity.

The professor would have been called an alarmist if he suggested that population and land use were an issue. The mayor would not appreciate the suggestion that population growth could be a problem when it is actually necessary to pay for the new schools, sewer system, and library to meet the needs of previous growth. In 1997, there was still half of the farmland remaining around the city. But in fact, the steady, "healthy" growth rate of the city continues to the present day, and all of the original farmland is now within urban city limits.

Let us say that the professor had argued for more "efficient" urban development and championed regulations to increase the housing density so that the land use per person could be cut in half? If the council had taken this advice, then today a bit less than half of the farmland would still remain. However, if the population growth rate continues unabated into the future, the farmland would still be consumed by 2035. The improved efficiency would have bought 23 years before total consumption of the farmland resource, but it would not have changed the inevitable outcome.

1.3 Context for Sustainable Energy

1.3.1 Historical Energy Development in the United States

The United States has made two major energy transitions in its relatively short history as shown in [Figure 1.8](#) [19]. Before the Civil War, U.S. industry depended on wood, wind, water,

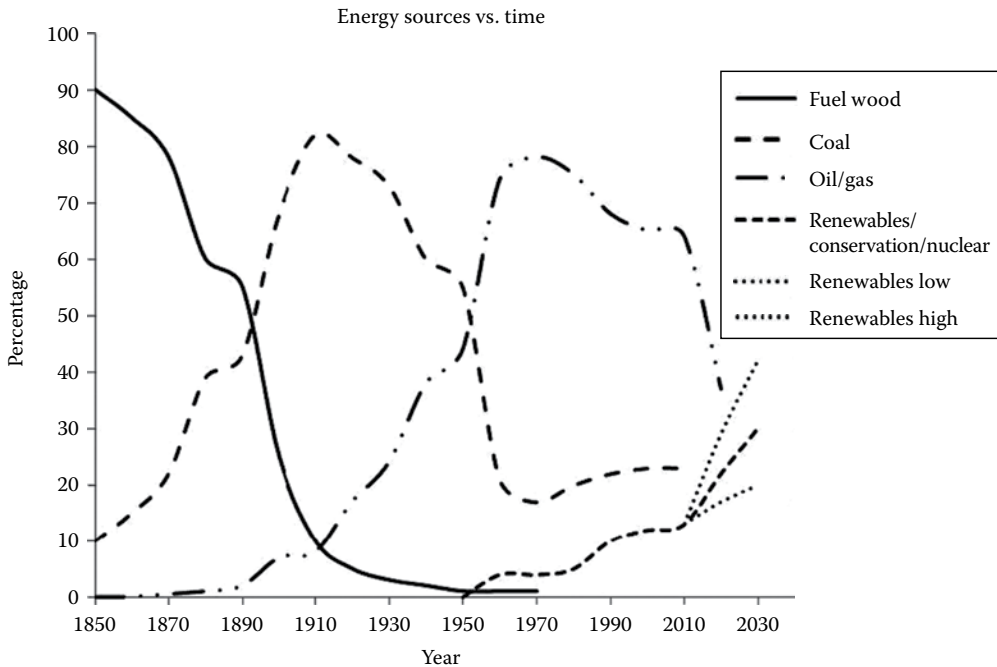
**FIGURE 1.8**

Diagram illustrating energy transitions in share of total energy supplied by wood, coal natural gas, and renewables. (From U.S. Energy Information Administration. History of energy consumption in the United States, 1776–2012, <https://www.eia.gov/todayinenergy/detail.php?id=11951>. [19])

and animals for its heat, energy, and power. Charcoal from hardwoods had been used for processing metals and ceramics since ancient times. The industrial revolution outstripped the wood supply in Europe and contributed to the clearance of forests in North America. In the first energy transition, coal became the major supply for U.S. energy needs between 1885 and the start of World War II in 1941. New steam engines that could pump water and ventilate coal mines stimulated a transition to coal followed by a dramatic increase in total energy consumption. Coal was found to be a vastly superior fuel to wood in both running the new steam engines and high materials processing. However, the air pollution from coal burning in factories and homes, and gasification of coal for lighting, was a serious public health issue in most cities around the turn of the century.

The second transition from coal was not due to a shortage of coal; rather, there were great advantages to using oil and gas. The development of oil and natural gas, and coal-fired power generation that could supply electricity via the grid provided a vast improvement in air quality in cities. Beginning in the 1970s, the United States transitioned from being a net exporter of oil to being an importer. Total U.S. energy production had leveled off and conversion efficiency had improved, but consumption continued to grow. The enormous increase in energy utilization since the end of World War II in 1945 is the result of rebuilding parts of the world devastated by the war, improvement in the living standards of the middle class, and an exponential growth in population. In the 1960s, it was thought that nuclear energy would be the next major energy source of the future. However, the costs of nuclear energy turned out to be much higher than expected, and the anticipated safe long-term waste storage solution did not emerge. In the 1980s, concerns about nuclear plant safety caused public opposition, and excessive cost overruns derailed new nuclear power developments.

U.S. domestic oil production peaked at 9.64 million barrels per day in 1970. Until the 1970s, energy prices remained low, thus putting no damper on ever-increasing demand. The oil crisis caused higher oil prices, but it is important to note that even though market conditions were favorable and policy incentivized oil exploration, the U.S. crude oil increased until 1986 and then declined steadily until it reached a minimum in September 2008. The advent of hydrofracking and horizontal drilling techniques to tap into oil and gas shale reserves led to an increase in natural gas production beginning in 2006, followed by an increase in oil production in late 2008. U.S. crude oil production steadily increased to reach a 45-year high of 9.59 million barrels per day in June 2015, nearly breaking the 1970 record and sharply reducing U.S. oil imports. Production began to decline after that as a result of decreasing oil prices caused in part by OPEC's decision to overproduce oil. At the time of this writing, oil prices—and hence U.S. oil production—are in a state of flux. Although the share of consumer energy provided by coal declined after the surge in energy use in the 1950s, the total amount of coal production increased until 2008, when cheap natural gas from shale increased dramatically and displaced coal.

1.3.2 Current Energy Use

Although tapping into unconventional sources of fossil fuels has spurred periods of increased production subject to international economic conditions, ultimately, the finite reserves of fossil fuels in the Earth will require a transition to other energy sources, namely renewables and nuclear (fission in the near term and likely fusion in the long term). Even though we are not yet running out of oil, the transition to other forms of energy is already occurring. Former Saudi Oil Minister, Sheik Ahmed Zaki Yamani, was famously quoted as saying “The Stone Age didn’t end because we ran out of stones.” The rapid energy transition that is now occurring is driven not by declining fossil fuel reserves but by the growing concern for climate change, as well as by the pollution and health concerns in China (see [Figure 1.9](#)) and India associated with burning coal.



FIGURE 1.9

Surgical masks are a common sight on the streets of Beijing, China, where air pollution from coal-fired power plants is a major health concern.

To get an idea of the scale of the transition from current energy systems to renewable systems, the detailed pattern of energy supply and consumption needs to be examined. It is useful to look at end-use consumption by dividing it into four major sectors: residential, commercial, industrial, and transportation. These sectors consume, respectively, 21.0%, 18.7%, 31.7%, and 28.7% of total U.S. energy, as shown in [Figure 1.10 \[20\]](#). Total U.S. consumption in 2016 was 974 quads, which is about one-fifth of the world's energy use, with fossil fuel accounting for about 81% of the total. The total contribution of renewable energy is now 10.4%—up from 8.2% in 2010. Renewable energy is divided into the following sources: biomass (including wood, waste, and biofuels), 46.8%; hydropower, 24.3%; wind, 20.8%; solar, 5.8%; and geothermal, 2.3%. Because of the significant legacy reliance on fossil fuels, the transition to renewable energy systems represents a very large-scale shift in primary energy supply.

Renewable energy technologies have been incentivized with tax credit policies and state renewable portfolio standards (which require that a certain percentage of electricity be supplied by renewable sources). Although these policy measures have helped give a boost to an emerging industry, recent large increases in the deployment of wind and solar have stemmed from large cost reductions. Wind energy costs have dropped because of the trend toward taller turbine towers that yield higher wind speeds and steadier conditions. Solar photovoltaic modules have dropped in price as a result of Chinese investments in low-cost manufacturing. As both these technologies have seen a jump in deployment, learning curve effects have provided a positive feedback to drive down costs even further. As a result of these low costs, more than half of the new electric-generating capacity added in the U.S. in 2014, 2015, and 2016 has been comprised of wind and solar [\[21\]](#).

The manufacture of renewable energy technologies initially requires some fossil fuel investment with its associated carbon emissions. This impact is accounted for in life cycle assessments. Also, despite the fact that utilities are experienced at handling variations in electric demand, the transition to more wind and solar on the grid means that they must also address variations in energy supply. These and other issues are covered in later chapters.

1.3.3 Future Energy Scenarios for the United States

Future scenarios are typically developed using historical information, interpreting trends, and modeling future behavior under different assumptions. Nearly every nation has a governmental energy-modeling unit dedicated to developing the national energy outlook. The EIA projects natural gas growing and coal decreasing, consistent with recent trends. It also shows the energy from nonhydro renewables doubling by 2040. But EIA reference case projections have greatly underpredicted renewable energy deployment on a consistent basis. And while the decline of coal production is necessary to address climate change, the projected large increase in natural gas consumption has serious climate change implications, especially if fugitive methane emissions associated with natural gas are not aggressively addressed.

1.4 Key Sustainability Considerations

1.4.1 The Challenge of Climate Change

The average surface temperature of the Earth is determined by a heat balance with outer space. Absorbed incoming solar energy is balanced by outgoing infrared radiation (IR).

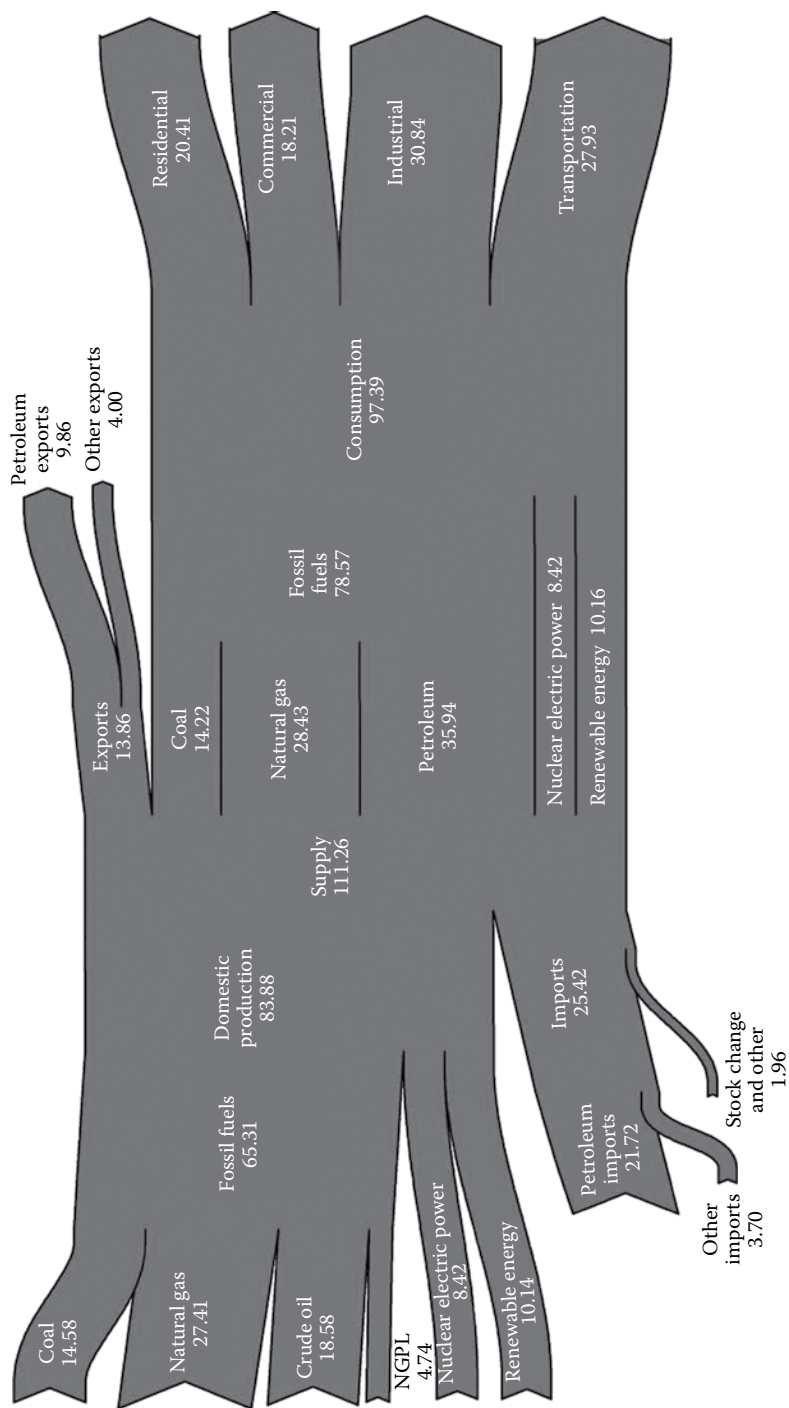


FIGURE 1.10 U.S. primary energy flow in 2016 in quadrillion Btus. (From U.S. Energy Information Administration. U.S. energy flow 2016, https://www.eia.gov/totalenergy/data/monthly/pdf/flow/total_energy.pdf. [20])

The Earth's surface reflectivity, or albedo, plays a role in how much sunlight is absorbed. Deforestation, carbon soot from diesel fuel burning, and melting ice all affect the albedo. The atmosphere also plays a very large role by absorbing some of the solar radiation (aerosols from man-made air pollution play a significant role in reducing the sunlight that makes it through the atmosphere) and by absorbing and reemitting much of the outgoing IR. Gases in the atmosphere that absorb and emit IR are called "greenhouse gases"—a reference to the window glass used in many greenhouses, which absorbs infrared radiation. Thanks to the greenhouse gases that are naturally present in the atmosphere—primarily water vapor, CO₂, and methane—that trap outgoing IR, the Earth is about 15°C warmer than it otherwise would be, thus making the widespread presence of liquid water possible.

However, since we began burning fossil fuels on a large scale in the late nineteenth century, we have increased the CO₂ content of the atmosphere by 45%—or about 30% just since 1958 when the American scientist Charles David Keeling began measuring it with high accuracy atop Mauna Loa in Hawaii. This CO₂ can be correlated with the known amount of fossil fuel burned and has the exact isotopic composition of that contained in fossil fuels. Basic calculations and ever-improving detailed computer models indicate that this has upset the Earth's heat balance. It is estimated that there is now about 0.7 Watts per square meter of the Earth's surface area more solar energy being absorbed than there is IR radiation going out. (This is warming the Earth with an amount of energy equivalent to 5 Hiroshima atom bombs exploding every second.) This warming is manifest in many scientific observations: increasing surface land and sea temperatures, decreasing sea ice volume and land-based ice mass, shifting flora and fauna, and so on. All other possible explanations for the warming have been exhaustively investigated by scientists and eliminated. (For example, accurately measured solar output does not correlate and, in fact, has declined over the last 35 years.) On the other hand, specific observed changes are unique signatures of greenhouse gas warming. These include the temperature distributions in the ocean and the atmosphere, the preferential warming in the Northern Hemisphere and the Arctic, and the divergence of average daytime and nighttime temperatures are all clear.

The main human CO₂ additions to the atmosphere are from burning fossil fuels and from the manufacture of cement, plus forest clearance and soil disturbance. In 2016, the CO₂ emissions from fossil fuels and cement manufacturing were 32.1 ± 1.5 Gt/yr (where Gt refers to billion metric tons). The ocean is estimated to be absorbing 9.5 ± 1.8 Gt/year of CO₂, which is causing acidification effects that, in addition to ocean warming and other man-made impacts, are harming coral reefs and other marine ecosystems. Some forest areas that were previously cleared are being allowed to regenerate and so forests are now believed to be a net absorber of CO₂ at the rate of 7.3 ± 3.4 Gt/yr. Accounting for all these effects, the CO₂ in the atmosphere is increasing at the rate of 15.3 Gt/yr. Thus, roughly half of the CO₂ emitted from fossil fuels and cement manufacturing winds up in the atmosphere. This has led to the current CO₂ atmospheric concentration, which is higher than it has been in 3 million years. The increased energy retention in the Earth system has, to date, resulted in a global average of about a 1°C temperature increase.

It is important to put this seemingly small temperature rise into context. Our species, *Homo sapiens*, has existed for approximately 200,000 years. However, it is only in the last 10,000 years that agriculture and permanent cities developed. This development of civilization coincides with a period of very stable temperature and sea level following the last glacial period. During this time, the global average temperature has stayed within a $\pm 0.5^\circ\text{C}$ band. The global average temperature rise of 1°C already puts us outside that stable temperature band. Continuing business-as-usual potentially means a 6°C rise by 2100. Thus, man-made climate change—caused mostly by the burning of fossil fuels—is rapidly

subjecting us to climates that human civilization has never before experienced. The 1°C change to date has already resulted in increased probability of extreme weather events such as floods, droughts, heat waves, and severe storms. Numerous studies have concluded that the future economic costs of climate change are an order of magnitude greater than the cost of making an energy transition to carbon-free fuels. That is, it is much more cost-effective to prevent further climate change than to clean up the damages if we don't address it.

The 2016 energy-related CO₂ emissions were unchanged from the previous 2 years. This is despite the fact that the global economy grew 3.1%. The fact that global CO₂ emissions did not increase was attributed to the reduction in U.S. coal burning and the associated increase in the use of natural gas and renewable energy for electricity generation. (Note that this is different from the total greenhouse gas impact. Methane levels in the atmosphere have been rising, and it is suspected that the increase in shale gas generation is playing a role in this.)

Each unit of energy produced by fossil fuels results in the emission of CO₂. The energy productions associated with each kilogram of CO₂ emitted for the three fossil fuel products are:

Natural gas	18.3 MJ/kg CO ₂
Gasoline	16.1 MJ/kg CO ₂
Coal (average)	8.2 MJ/kg CO ₂

The issue of climate disturbance from fossil fuel combustion has taken on highly political and social aspects, even though the effects of man-made emissions and land-use changes have long been well understood. Sustainable energy is normally thought of as increasing the renewable energy production, but the most serious risk that must be managed at the current time is reduction of fossil fuel use and the attendant emissions so that climate systems do not become catastrophically destabilized.

According to the Intergovernmental Panel on Climate Change (IPCC) Working Group 3, the decline rate of fossil energy use must be dramatic and sustained to manage the risks of catastrophic global climate change [22]. According to the report, the most cost-effective near-term action is improved energy efficiency in buildings and reduction of coal combustion for power generation.

In June 2016, following the December 2015 COP21 agreement in Paris, the International Energy Agency (IEA) published *Energy Technology Perspectives: Towards Sustainable Urban Energy Systems* [23], in which they provided projections of what must be done to meet carbon reduction goals. The worst-case scenario for climate change is a 6°C global average temperature rise above the preindustrial level; whereas the IPCC target is 2°C to prevent the worst impacts of climate change. (A 2°C increase is by no means “safe,” however, as we are already experiencing a wide range of consequences at today’s 1°C rise.) Limiting temperature rise will likely require the electrification of highly energy-efficient buildings and transportation and a rapid transition to carbon-free electricity generation. IEA has made projections for the future electric generation mix to achieve the 2°C goal. Specifically, they project what must be done between now and 2050 to go from a scenario that would eventually lead to a 6-degree rise (called 6DS) to the target 2-degree rise scenario (2DS). The large-scale shift from fossil fuels to efficiency and carbon-free energy sources reduces potential 2050 world electric power sector emissions from 23 billion tons of CO₂ per year to approximately 2 billion tons per year, which is over an 80% reduction compared to the 2012 world electric power sector emissions of 13 Gt/yr. Table 1.2 [23] shows the percentage of total accumulated carbon emissions reductions attributable to each technology.

TABLE 1.2

Percent Contributions from Various Technologies for Reducing Power Sector CO₂ Emissions between 2016 and 2050 in the IEA 2-Degree Rise Scenario versus the 6-Degree Scenario

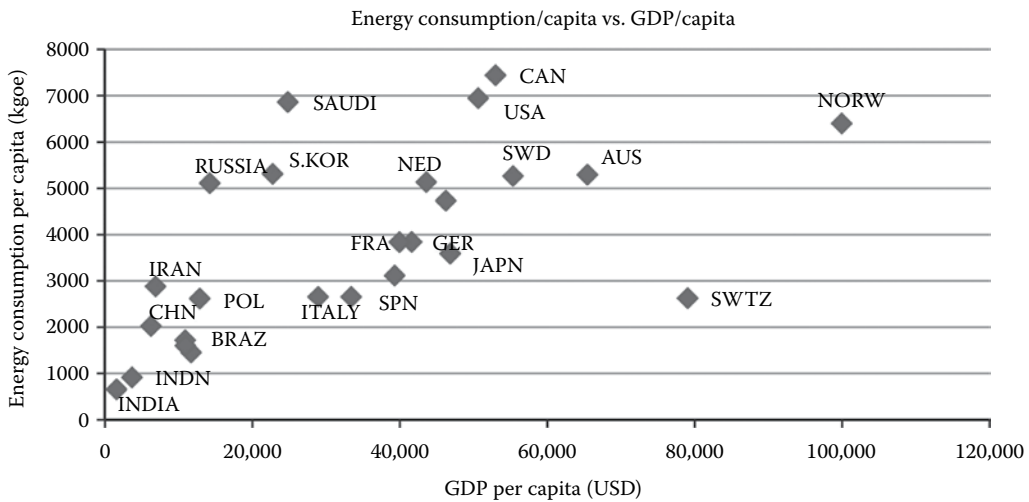
Technology	Percent of Accumulated CO ₂ Emission Reduction
Electricity savings (efficiency)	28
Solar	16
Wind	15
Nuclear	13
Carbon capture and storage (CCS)	12
Biomass	6
Hydropower	5
Other renewables	3
Fuel switching and power plant improvements	2

Source: Data from IEA, 2016. Energy technology perspectives: Towards sustainable urban energy systems, OECD/IEA. www.iea.org/statistics, License: www.iea.org/t&c as modified by Charles F. Kutscher. [23]

Fully 28% of the needed power sector emissions reductions (cumulative from 2016 to 2050) are from electricity savings at the point of use (energy efficiency in the use of electricity, especially in buildings) and 45% is from renewable energy (40% from nonhydro). The efficiency keeps emissions from growing significantly but other measures are needed to drastically reduce them. The remaining 27% is from nuclear and carbon capture and storage, with a very small amount from fuel switching (e.g., switching from coal to natural gas) and power plant efficiency. Thus, nearly three-quarters of the emissions reductions result from the deployment of efficiency and renewables.

In December 2015, 195 countries signed onto the landmark COP21 Paris agreement. (Only Syria and Nicaragua did not join. Syria was engulfed in civil war, and Nicaraguan representatives stated that the agreement was not strong enough.) Each country made individual voluntary pledges to reduce carbon emissions to support the goal of keeping the global average temperature rise below 2°C. One of the hallmarks of the Paris agreement is that it addresses a long-held criticism of previous climate agreements, namely that they excluded developing nations. At the Paris meeting, all of the 195 nations pledged to make reductions. On June 1, 2017, in a major shift of U.S. policy on global warming, President Donald Trump announced that the United States would withdraw from the Paris agreement. However, at the time of this writing, a large number of U.S. corporations and city mayors, along with several states, have announced that they will honor the agreement. In particular, the State of California, which is the world's sixth largest economy, is committed to going well beyond the Paris agreement. Thus, it appears that the United States will continue to make important contributions to this international agreement, albeit not at the federal level.

The transition to an energy economy dominated by renewables will require addressing new issues. For example, high-value wind resources are often located in sparsely inhabited regions requiring investment in upgraded transmission systems to transport the power from the source to where it is needed in industrial parts of the country. The same applies, although to a lesser extent, to good solar radiation sources, many of which are located in parts of the world with limited water resources and some distance from industrial centers and large cities.

**FIGURE 1.11**

Per capita energy consumption versus per capita gross domestic product. (From Ramachandra, T.V. and Ganesh, H., 2015. Energy trajectory in India: Challenges and opportunities for innovation, *Journal of Resources, Energy, and Development* 12(1–2), 1–24, <http://wgbis.ces.iisc.ernet.in/energy/paper/Energy-trajectory-in-India/Introduction.html>. [24])

1.4.2 Energy Economic Efficiency

Energy efficiency is a widely used term in the public realm. In engineering, there are technical meanings: generation efficiency, conversion efficiency, or appliance efficiency. There is also a concept of economic efficiency. Economic efficiency refers to the ratio of resources and energy used to produce goods and services. Economic efficiency always improves profitability and is a necessary part of the strategy for adapting to resource constraints in a prosperous manner.

There is a direct coupling between the wealth of a country and its energy use. The data in Figure 1.11 [24] show the energy consumption per capita as a function of gross domestic product (GDP) for several countries. Although there is a strong positive correlation between energy consumption and wealth, a number of countries have twice the energy economic efficiency as the United States but with the same standard of living.

The low energy economic efficiency of the United States has resulted in an enormous discrepancy in relative energy use with the rest of the world. Table 1.3 [25, 26] shows the percentage shares of world population, world gross domestic product and energy consumption for some of the major countries of the world. The United States, with less than 5% of the world's population, consumes almost a quarter of the total world energy and produces almost one-third of the world's GDP. In contrast, China, with 19% of the world's population, contributes 14% of the GDP, while using 11% of the world's energy.

1.4.3 Energy Return on Energy Invested

Energy transformation systems take natural resources from the environment and produce fuels and electricity for sale in the economy. They initially require an investment in money and materials as well as in energy for manufacture and installation. Once installed, the energy production system will use or consume natural resources and fuel to generate

TABLE 1.3

Percentage Shares of World Population, World GDP, and World Commercial Energy Consumption for Selected Countries

Country	% of World Population 2011 ^a	% of World GDP 2011 ^b	% of World Energy Consumption 2011 ^c
United States	4.5	19	19
Japan	1.8	5.6	4.2
France	0.9	2.8	2.1
Germany	1.2	3.9	2.7
United Kingdom	0.9	2.8	1.7
China	19	14	20
India	17	5.6	4.4

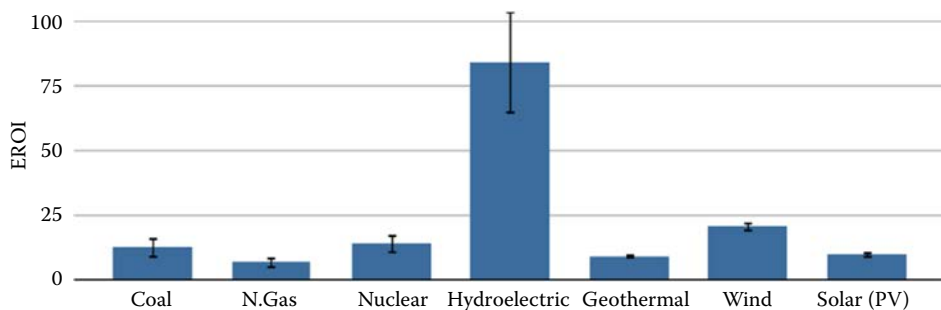
^a World population 2011 was 7.0 billion. Country data from *The World Factbook*. [25]

^b World GDP 2011 was \$79 trillion. Country data from *The World Factbook*. [25]

^c World primary energy consumption 2011 was 12 billion tonnes of oil equivalent. Country data from BP. [26]

electricity, or it will extract and process resources into fuel. During the lifetime of the energy transformation plant, there will also be maintenance and replacement requirements. If we put all of these inputs and outputs in terms of energy, we can compare the consumer energy produced for the market to the energy required either from the economy or parasitic internal use. The main point of examining the EROI is to compare different energy transformation systems in terms of their effectiveness. Also, in calculating an EROI, one must explore the appropriate system boundaries and, in doing so, it is possible to identify potential improvements.

Figure 1.12 gives EROI values of different electric generation systems [27]. The biggest difference between fossil fuel electric generation and renewables is that the fossil EROI is often calculated on an annual basis using annualized values of embedded energy in equipment, whereas the EROI for wind and solar is determined over the generating lifetime. The EROI for coal power generation is in the range of 10. For nuclear power plants, the EROI would depend greatly on the lifetime of the plant and whether the energy needed for the storage of spent fuel and decommissioning is counted. Nuclear power plants are vastly energy intensive to build, but the EROI not counting the uranium processing and waste storage is in the range of 10–15. However, even a small energy requirement for long-term

**FIGURE 1.12**

EROIs for different electricity generation technologies. (From Hall, C.A.S., Lambert, J.G., and Balogh, S.B., 2014. EROI of different fuels and the implications for society, *Energy Policy* 64, 141–152. [27])

safe storage of spent fuel, given the very long storage period, can considerably reduce the lifetime EROI of nuclear power.

EROI is a quantitative means to understand the past, present, and future net flows of energy to the economy for different energy transformation technologies. Even though EROI is valuable for comparing the efficiency of different means of providing marketable energy, it does not take into account the impact of carbon emissions. Although coal-fired electric power generation has a higher EROI than electricity generation by solar photovoltaics (PV) or geothermal power, these renewable technologies have dramatically lower life cycle carbon emissions and thus are among the technologies of choice for limiting global temperature rise. Thus, while EROI can be a useful metric for comparing fossil fuel technologies to each other and renewable technologies to each other, life cycle greenhouse gas emissions or the carbon payback period (discussed in Section 1.7) are more useful for comparing conventional and renewable sources to each other and determining the best path forward to address climate change.

1.4.4 Cost of Energy Production

The capital cost per kilowatt (kW) capacity is a way to compare the cost of building an energy production system to the market value of the energy produced. The investment costs include the capital cost, which is the cost of engineering and building the plant, plus maintenance and cost of fuel. The amount of energy produced for sale depends on the plant capacity and the number of hours per year the plant is generating at capacity, called the utility factor, and the ability of the plant to generate on demand during peak times. A broad perspective of the capital and levelized energy costs of renewables, as well as more traditional energy technologies, has been prepared by Lazard, a well-known financial advisory and asset management firm. The firm provides advice on mergers and acquisitions, as well as asset management services for large institutions and governments. The technology assessments shown here were prepared to advise its customers about investments in energy technologies. The details of the approach taken by Lazard are available in [28], but in subsequent chapters of this book, we will explain how to make such estimates and describe how these estimates depend on assumptions such as the cost of money or the assumed life of the system. The cost figures provided by an impartial investment company will be useful for preliminary estimates, and particularly for making what are called “back-of-the-envelope” calculations. Lazard has estimated ranges of capital costs (i.e., the cost of installing a given technology in \$/kW) and levelized cost of energy (LCOE, in \$/MWh) for conventional and alternative electric-generating systems. A summary of these costs is given in Table 1.4 [28]. They do not include the benefit of subsidies for the alternative sources (e.g., investment and production tax credits). Therefore, actual costs after subsidies for these are lower. These estimates also do not include social and environmental costs, which are much higher for conventional technologies.

Table 1.4 shows costs for community-scale solar PV installations. The cost per megawatt hour (MWh) of utility-scale solar is about 35% lower than community scale, and the cost of residential rooftop PV is about 70% higher than community scale. It is important to note that these estimates are based on current generation technologies for the conventional systems, which are considered mature. It should also be noted that the conventional systems, such as coal, nuclear, and natural gas, can operate continuously, whereas solar and wind are variable. Moreover, the performance of renewable technologies is very dependent on geographic location.

TABLE 1.4

U.S. Capital Costs and Levelized Costs of Energy for Conventional and Renewable Electric Power Plants

	Technology	Capital Cost (\$/kW)	LCOE (\$/MWh)
Conventional	Coal	3000–8400	60–143
	Gas combined-cycle	1000–1300	48–78
	Nuclear	5400–8200	97–136
Renewable	Community PV	2000–2800	78–135
	Land-based wind	1250–1700	32–62
	Biomass direct	2500–4000	77–110
	Geothermal	4250–6400	79–117

Source: Lazard, December 2016. Lazard's levelized cost of energy analysis, Ver. 10.0. [28]

1.4.5 Other Costs of Energy Development

Land has a potential for producing food, fibers, and wood. Table 1.5 shows the lifetime power generation per unit land area for various electric-generating plants [29, 30]. Fossil fuel sources have a great energy density, whereas the renewable sources (except geothermal) are very diffuse and therefore require larger power plant areas. However, fossil fuels and nuclear require mining, and fossil fuels also require pipelines. When these areas are accounted for, the areas needed for coal and natural gas are comparable to that needed for the solar technologies. Directly impacted wind land area is very low because only the wind turbine footprints and permanent service roads have been included, and the land between turbines can be used for agricultural or other purposes.

TABLE 1.5

Average Direct Impact Land Area Used for Different Electric Power Plants per Gigawatt Hour (Gwh) of Electricity Produced over the Plant Lifetime

Technology	Area (m ² /GWh)
Large PV	430 ^a
Concentrating solar	360 ^a
Geothermal	19 ^a
Wind	26 (3000) ^a
Natural gas	45 (620) ^a
Coal (surface mined)	9 (400) ^b
Nuclear	45 (113) ^b

Note: Numbers in parentheses are total land area including area for mining, pipelines, etc., and the total wind farm area in the case of wind.

^a Jordaan, S.M. et al., 2017. Towards accurate accounting of the surface land requirements of natural gas-fired electricity, *Nature Energy*, 2, 804–812. [29]

^b Fthenakis, V. and Kim, H.C., 2009. Land use and electricity generation: A life-cycle analysis, *Renewable and Sustainable Energy Reviews*, 13, 1465–1474. [30]

EXAMPLE 1.2: BACK-OF-THE-ENVELOPE ENERGY CALCULATIONS

The Arizona legislature passed a law requiring that by the year 2025, 15% of all the electric energy generation must come from renewable sources. Calculate the collector area required and estimate land area for this target to be met by solar PV.

Solution

From the Arizona Energy Commission website, we find that in 2009, electricity demand was 30,800 GWh/year and growth to 50,000 GWh/year in 2025 is expected. From the NREL U.S. Solar Radiation Resource Map, the annual average of the solar radiation impinging on a flat plate facing south and inclined at the latitude is 5.5 kWh/m²/day, which is equivalent to about 2×10^3 kWh/m²/year. Assuming a PV efficiency of 17%, the amount of electric power delivered per year is 340 kWh/m². Hence, the collector area is

$$\begin{aligned} A &= \frac{50,000(\text{GWh/year}) \times 0.15 \times 1 \times 10^6 (\text{kWh/GWh})}{340(\text{kWh/year} \times \text{m}^2)} \\ &= \frac{7.5 \times 10^9 \text{kWh/year}}{340(\text{kWh/year} \times \text{m}^2)} = 2.2 \times 10^7 \text{m}^2 \end{aligned}$$

The rule of thumb for PV installation to avoid shading is spacing so the total area is twice the collector area, giving a land requirement of 4.4×10^7 m². The land area of Arizona is 29.5×10^{10} m², hence the required PV power plant area would be 0.015% of the state of Arizona. Using the average capital cost of community PV from Table 1.4 of \$2400/kW and assuming the PV capacity is 170 W/m² (i.e., 17% of 1,000 W/m²), the total capacity is:

$$170 \frac{\text{W}}{\text{m}^2} \times 2.2 \times 10^7 \text{m}^2 = 3.74 \times 10^9 \text{W} = 3.74 \times 10^6 \text{kW}$$

Multiplying this by \$2400/kW gives a cost about \$9 billion.

EXAMPLE 1.3: BACK-OF-THE-ENVELOPE POLICY EVALUATION

On July 17, 2008, former Vice President Al Gore proposed that by 2018, all U.S. electric power generation be carbon-free. Senator John McCain suggested that nuclear power plants be installed to reduce the effects of global warming. In the summer of 1979, at the height of the energy crisis, President Jimmy Carter suggested that Americans conserve energy. Assume that conservation and efficiency could reduce fossil generation demand by 20%. Estimate how many new 8-megawatt (MW) land-based wind turbines (assume an average yearly capacity factor of 40%) would meet Mr. Gore's suggestion. Then, estimate the total costs and land area of these wind turbines assuming that new wind turbines cost about \$1100/kW_e installed. Next, estimate how many 1000-MW nuclear power plants with a 92% capacity factor would be required and what would be the capital cost if nuclear power installation cost is \$8000/kW_e.

Solution

U.S. Electricity Generation from the EIA—*Annual Energy Outlook* gives the following:

Total U.S. electricity generation in 2016: 4.08×10^9 MWh/yr

Fossil-based electricity generation in 2016 (65% of total): 2.652×10^9 MWh/yr

Assuming conservation can reduce the electricity needs by 20%, we are left with 2.122×10^9 MWh/yr of electric energy that must be produced by renewable sources.

Wind power: Given a 40% annual capacity factor, the 8-MW wind turbine would be expected to generate

$$(0.40) \times (8\text{MW}) \times \left(8760 \frac{\text{h}}{\text{year}} \right) = 2.80 \times 10^4 \text{MWh/yr}$$

Dividing this into the total energy needed, we find that 75,800 wind turbines would be needed. Using the wind farm area from [Table 1.5](#) (wherein the energy is based on 30 years of plant operation), the total wind farm area needed would be:

$$3000 \frac{\text{m}^2}{\text{GWh}} \times \frac{2.80 \times 10^4 \text{MWh}}{\text{yr}} \times \frac{1\text{GWh}}{1000\text{MWh}} \times 75,800 \times 30 \text{years} = 1.91 \times 10^{11} \text{m}^2$$

or 47 million acres.

This is 2% of U.S. land area. However, land between the turbines in wind farms can be used for other purposes. The land that cannot otherwise be used (using [Table 1.5](#)) is only 0.87% of this, or a little over 400,000 acres.

At \$1100 per kW for wind turbines, the capital needed for the installation of these farms is:

$$\left(\frac{\$1100}{\text{kW}} \right) \times \left(\frac{1000\text{kW}}{\text{MW}} \right) \times \left(\frac{8\text{MW}}{\text{turbine}} \right) \times (75,700 \text{turbines}) = \$666 \text{billion}$$

Nuclear power: The yearly electric energy produced by one 1000-MW nuclear power plant operating at 92% capacity is:

$$(0.92) \times (1000\text{MW}) \times \left(8760 \frac{\text{h}}{\text{year}} \right) = 8.06 \times 10^6 \frac{\text{MWh}}{\text{year}}$$

Dividing this into the total energy needed, we find that this would require 263 power plants, and at \$8000 per kW for nuclear plants, we determine the capital investment for the construction of these plants:

$$\left(\frac{\$8000}{\text{kW}} \right) \times \left(\frac{1000\text{kW}}{\text{MW}} \right) \times \left(\frac{1000\text{MW}}{\text{plant}} \right) \times (263 \text{plants}) = \$2.1 \text{trillion}$$

Thus, the nuclear power plant cost is about three times the cost of the wind farms. We can see from [Table 1.5](#) that the nuclear plants would occupy only about 13% of the wind farm area, but the land that cannot be used for other purposes would be 73% greater.

Note that the nuclear plants would provide base-load electricity, whereas the wind farms provide varying output, which must be addressed via some combination of storage and controlling the electric demand.

1.5 Energy Efficiency and Conservation

Reducing energy consumption through efficiency and conservation provides the most important and economically strategic projects for transition to a sustainable energy system.

The present per capita energy consumption in the United States is 281 GJ, which is equivalent to about 9 kW per person. The average consumption in Europe is 4.2 kW and the average for the whole world is only 2 kW. According to the World Energy Assessment by the United Nations Development Programme in 2004 (the last year that it was done), a reduction of 25%–35% in primary energy in the industrialized countries is achievable (cost-effectively) over a 20-year period, without sacrificing the level of energy services [18]. The report also concluded that similar reductions of up to 40% are cost-effectively achievable in the transitional economies and more than 45% in developing economies. As a combined result of efficiency improvements and structural changes such as increased recycling, substitution of energy-intensive materials, etc., energy intensity could decline at a rate of 2.5% per year over the next 20 years [18].

1.5.1 Energy End-Use Demand Reduction in Buildings

Buildings (not including those in the industrial sector) account for about 40% of all end-use energy demand in the United States. Buildings use 74% of the electric power and are responsible for nearly 40% of the nation's greenhouse gas emissions. Residential buildings account for about half of the building energy use. Over half of all energy used in residences is for heating and cooling and a further 20% for heating water. Residential air conditioning is a main contributor to the peak demand on the power grid. Peak power is the most expensive to provide as the entire grid must be able to meet the peak load. However, the peaking power plants only run, and thus only earn revenues, during the peak periods, resulting in very low utilization factors for investors. Thus, economic residential energy efficiency and conservation programs focus on reducing space conditioning and water usage. Figure 1.13 shows the average relative effectiveness of a range of residential energy retrofit options (although effectiveness varies with location and building vintage). Windows are the highest source of conductive heat loss as shown in Figure 1.14.

Commercial buildings are demolished and new ones built on a shorter cycle than residential buildings, with around 1% of buildings turned over each year. Heating, ventilating, air

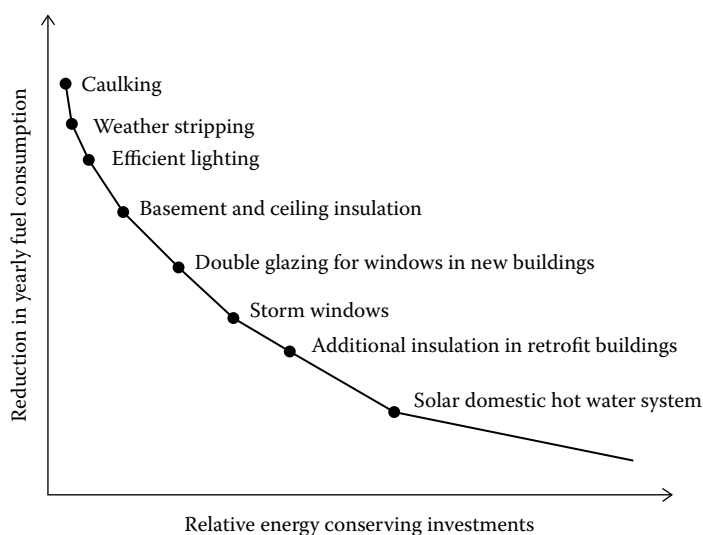
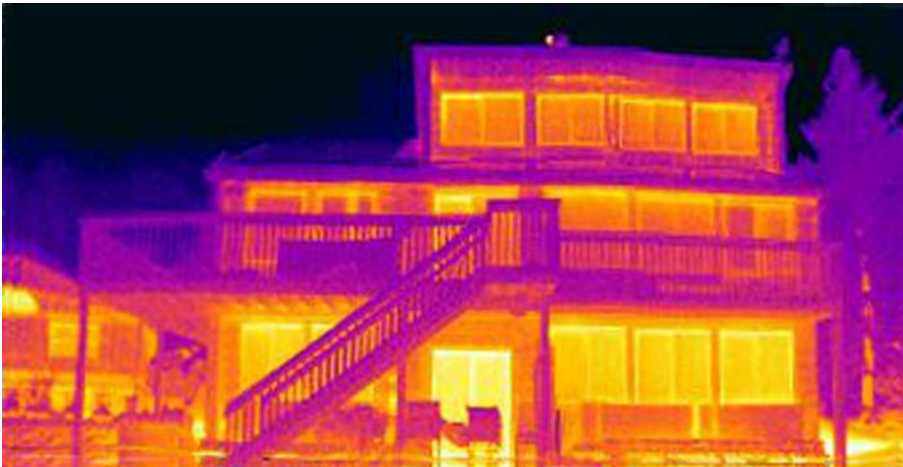


FIGURE 1.13
Relative energy savings of various energy efficiency measures.

**FIGURE 1.14**

An infrared image of a house. The lightest colored windows have the highest heat loss. (Courtesy of John Avenson.)

conditioning, and lighting are major loads in commercial buildings. Professional energy auditing and energy management are required for commercial buildings. Commercial sites such as shopping centers, offices, medical centers, and schools also have a transport impact because they become attractors for travel demand. Thus, the location and the context of commercial buildings are part of the overall U.S. Green Building Council's Leadership in Energy and Environmental Design (LEED) framework. The framework is a building certification that identifies and implements green design, construction, operation, and maintenance measures yet is flexible for each existing or new project. The approach is to consider the building life cycle as well as the surrounding community and environment.

1.5.2 Energy End-Use Demand Reduction in Transportation

Of every 5 dollars spent in the United States, 1 dollar is estimated to be related to transport: fuel, vehicles, road, and parking infrastructure or related services. The U.S. personal transportation system has many features that make it the ideal target for energy demand reduction. Transportation accounts for nearly 30% of total U.S. energy use, with approximately 92% of that energy from petroleum [31]. Cars and light trucks use 58% and large trucks use 23% of the energy consumed in transport [32]. The U.S. Environmental Protection Agency has reported that the average fuel economy of 2015 model-year vehicles reached 24.8 miles per gallon [33].

Various programs can reduce transportation energy use by reducing vehicle miles traveled (VMT). Car-pooling and car-sharing programs address this, as does the acceptance of telecommuting. The trend toward urbanization and walkable communities directly impacts VMT. Increased public transportation, construction of bike paths, and bike-sharing programs are also having an increasing impact.

Transportation is covered in [Chapter 15](#).

1.5.3 Energy Management in Industry and Manufacturing

Industry and the primary production sector are good candidates for energy management projects. The best way for energy engineers to tap into the energy savings in this sector is

to study the best examples of energy management projects that have already been achieved and develop new projects for those companies that do not yet have progressive energy management practices. For example, at 3M, engineering teams are rewarded based on meeting energy-efficiency targets. In 2006, 3M completed more than 185 projects that delivered \$18.2 million in savings. The U.S. Department of Energy has a Better Buildings program [34] and a Better Plants program [35] aimed at reducing energy use in buildings and industry.

Energy efficiency in buildings and industry is covered in [Chapter 4](#).

1.6 Conventional Energy

1.6.1 Fossil Fuels

The production rate of fossil fuels is, from a historical perspective, truly enormous. The amount of fossil fuels in the Earth is finite, and in the first decade of the twenty-first century, there was much discussion of the prospect of “peak oil,” whereby the world production of oil would finally peak and then decline, with attendant economic consequences. However, the application of hydrofracking and directional drilling in shale reserves led to a temporary resurgence in U.S. oil and gas production. Thus, the near-term supply issues with fossil fuels are not so much depletion, as the increased cost associated with pursuing less conventional reserves. The long-term sustainability issues with fossil fuels arise from environmental degradation and, in particular, the need to drastically reduce carbon emissions.

Burning fossil fuels has always presented air pollution issues. Soot from coal and diesel and nitrogen oxides emissions from combustion of coal, petroleum, and natural gas directly cause negative health effects. Combustion science and air pollution engineering have provided great improvements in air quality since the 1970s, but acid precipitation from the sulfur dioxide and the deposition of mercury, arsenic, and radioactive minerals from coal combustion continue to be major environmental issues. The release of mercury into the atmosphere from coal combustion is a serious sustainability issue for humans, agriculture, and wild animals, particularly aquatic predator species like swordfish. The U.S. National Research Council has estimated that the use of fossil fuels costs the U.S. economy \$120 billion/yr mainly because of health costs. And this does not include subsidies or climate change impacts. The decline of coal in the United States is due largely to the low cost of natural gas, and the transition to natural gas reduces or eliminates some of the air pollution issues associated with burning coal.

Fossil fuels are covered in detail in [Chapter 6](#).

1.6.2 Nuclear Power

Nuclear power plants utilize the energy release of nuclear fission, the splitting of U-235 atoms, to generate steam in thermal power cycles. In 2016, there were 442 reactor units in operation in 30 countries contributing about 11% of the world’s electric energy production. The majority of reactors are located in the United States (99 units), France (58 units), Japan (43 units), and Russia (35 units). Nuclear reactors are typically large, base-load power producers—on the order of 1000 MW. Unlike the burning of fossil fuels, energy from nuclear fission does not result in the emission of greenhouse gases. Thus, the construction of nuclear power plants offers a means to produce carbon-free electricity on a large scale, and so nuclear power is a favored technology by many climate scientists.

As one of the potential solutions to climate change, however, nuclear power presents a number of challenges. Nuclear power plant waste presents problems with long-term storage and nuclear proliferation. Although nuclear power generally has a good track record for reliability and safety, accidents can have serious consequences. Most notably, the meltdown of the graphite-moderated reactor in Chernobyl, Ukraine, resulted in the evacuation of the city and caused both short-term and long-term deaths, the exact numbers of which are controversial. And the meltdown of three reactor units in Fukushima, Japan, in March 2011, which resulted from an earthquake and subsequent tsunami, is expected to take decades to clean up.

The biggest challenge facing further nuclear power development, however, is its high initial cost. Large cost overruns have occurred for new plants being built in the United States. Future U.S. plants are estimated to cost as much as \$8000/kW. In addition to the high capital cost, nuclear reactors have experienced high operating costs, causing some plants to be converted to natural gas plants. Some countries totally depend on nuclear power for their future energy needs, but low electricity growth and rapidly falling costs of wind and solar power have put further pressure on the nuclear industry in the United States.

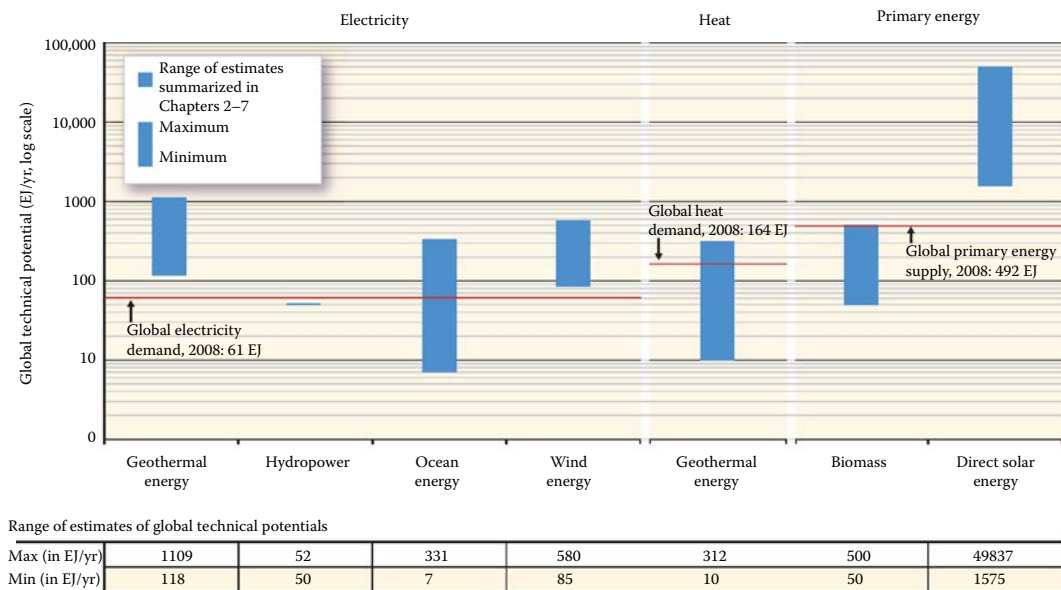
Compared to the carbon-free renewable energy options, nuclear power does maintain the advantage of being able to provide base-load power 24 hours per day with high availability. And the operating nuclear fleet in the United States supplies about 20% of U.S. electricity, thus providing enormous savings in carbon emissions. If one properly accounts for the cost of climate change damage, an argument can be made to keep the existing nuclear plants in the United States operating for as long as is safely possible. However, some countries that have limited renewable sources, such as Japan and South Korea, may depend on nuclear power for most of their future energy needs.

Nuclear power is covered in [Chapter 7](#).

1.7 Renewable Energy

By definition, the term “reserves” does not apply to renewable resources. So, we need to look at the annual potential of each resource. [Figure 1.15](#) from the IPCC Special Report on Renewable Energy [22], summarizes the range of technical resource potentials for each of the renewable energy technologies. The maximum and minimum values of potential, which are derived from different studies, are shown, respectively, as the top and bottom of the bars and are also given numerically in the table at the bottom of the figure. A key observation is that direct solar energy has a technical potential that is one to two orders of magnitude greater than for the other renewable technologies and greatly exceeds the current global primary energy supply. The IPCC defines technical potential as “the amount by which it is possible to reduce greenhouse gas emissions or improve energy efficiency by implementing a technology or practice that has already been demonstrated” [22]. Although it does not explicitly refer to costs, economic considerations may come into play in determining the technical potential.

Renewable energy sources are not completely free of carbon emissions, with some CO₂ emissions occurring in their manufacture and construction. (Nuclear power also has associated emissions resulting from mining, concrete manufacture, and plant construction.) In determining the overall impact of an energy transition on carbon emissions, it is thus valuable to know how the various renewable and nuclear technologies compare in terms

**FIGURE 1.15**

Ranges of global technical potentials of RE sources derived from studies presented in [Chapters 2](#) through [7](#) of Renewable energy sources and climate change mitigation, Special Report of the Intergovernmental Panel on Climate Change (IPCC). Biomass and solar are shown as primary energy due to their multiple uses. Note that the figure is presented in logarithmic scale due to the wide range of assessed data. (From Intergovernmental Panel on Climate Change, Working Group III, 2012. Renewable energy sources and climate change mitigation, Special Report of the Intergovernmental Panel on Climate Change. [22])

of life cycle greenhouse gas emissions, typically expressed as grams of CO₂ equivalent emissions per kWh of energy produced. Renewable energy and nuclear power have very low life cycle emissions compared to the fossil fuel technologies, although there is a range for each technology, depending on what manufacturing techniques are employed and, in the case of renewables, the quality of the resource in which the technology is deployed. For example, the manufacture of thin-film photovoltaic cells generally results in lower greenhouse gas emissions than the manufacture of crystalline silicon PV. Also, a solar PV system will have lower life cycle emissions per kWh produced if deployed in Arizona than in New Jersey. Technologies are also sometimes compared in terms of how long it would take (compared to fossil fuel technologies) to save an amount of carbon emissions equivalent to those created during the manufacture. For most renewable technologies, the carbon payback period is typically about a year or less, but it depends on the conventional fuel mix in the country where the technology was manufactured as well as both the conventional fuel mix that it is replacing and the resource quality in the location where it is deployed.

Of all the renewable technologies, wind and photovoltaics have exhibited the most rapid reduction in cost and market penetration. In the following sections, a brief introduction of each of the renewable energy technologies is provided, with greater detail to follow in the individual chapters.

1.7.1 Wind Energy

Wind energy technology has progressed significantly over the last two decades. Wind turbine towers have gotten taller and taller, thereby reaching stronger and steadier winds. As a result

**FIGURE 1.16**

The 160-MW Horns Rev offshore wind farm in the North Sea. Water vapor streams show how turbine wakes affect downwind turbines. Optimizing wind farm geometries and individual turbine controls to address wake effects and maximize total wind farm output is a major research area for wind energy. (Aeolus Energy Group, used with permission.)

of this and other technology improvements, the levelized costs have come down greatly. In 2016, the levelized cost of wind power was one-quarter what it was in 1990, and levelized costs are now as low as 3 cents per kWh. Wind power is thus already economical at locations with fairly good wind resources. By the end of 2016, there were 81,000 MW of wind installed in the United States—an eightfold increase over 10 years. And there were 486,000 MW installed in the world. Although offshore wind farms are considerably more expensive than land-based systems, they offer the advantage of higher-speed and steadier winds (see [Figure 1.16](#)).

The biggest issue with wind generation is the variability and inability to dispatch electricity on demand. When the wind slows suddenly, a large drop in wind generation can cause instability on the grid. If system operators can harness wind farms over a wider area, the total wind output is much steadier than with a single wind farm. A high level of cooperation among power generators and network operators on the grid is another possible way to manage intermittent generation. Firming capacity can be provided by natural gas turbines, which provide rapid start-up, as well as by hydroelectricity. The addition of energy storage to the grid can help enable larger wind penetrations. Another means for accommodating variable electricity supply is to control the electric demand. So-called demand response measures in buildings can be very effective. These things are described in [Chapter 5](#).

1.7.2 Solar Photovoltaics

Solar photovoltaic modules directly convert solar energy to electricity. They are installed on rooftops or ground-mounted in community solar gardens or in large utility-owned

**FIGURE 1.17**

In a small Brazilian village, each 50-watt PV system can power two fluorescent bulbs, allowing students to study and do homework in the evening. (Roger Taylor, NREL.)

installations. They are typically installed as fixed arrays, but ground-mounted arrays can provide 15% to 20% more energy if oriented in north–south rows that actively track the sun from east to west. Although there are many different PV cell types, crystalline silicon modules dominate the market with over 90% of installations. PV modules are reliable and, unlike thermal power generation, do not require large cooling systems. The solar-to-electric conversion efficiency of modules has increased significantly over the years. Today's commercial PV modules that utilize crystalline silicon have efficiencies in the range of 16% to 22%. Solar PV panels have come down greatly in cost from about \$30 per watt to under 50 cents per watt in the last three decades. As a result of the rapid drop in costs, solar PV growth has soared. By the end of 2016, there was a cumulative total of over 40,000 MW of installed PV in the United States—a twenty-fold increase over 10 years! Also, at the end of 2016, there were 303,000 MW of PV installed in the world [36]. While residential rooftop PV has grown rapidly, utility-scale PV is actually much bigger, owing to its lower cost. Small PV systems are being deployed in developing nations around the world to provide indoor lighting and to charge cell phone batteries (see [Figure 1.17](#)).

1.7.3 Solar Thermal

Concentrating solar power (CSP) uses reflectors to concentrate sunlight onto a fluid-carrying pipe (line-focus technology) or a tower-mounted receiver (power tower technology) to provide the high temperatures needed to produce steam in an efficient Rankine power cycle. CSP is the first solar technology that demonstrated its grid power potential. The Solar Electric Generating Systems (SEGS) parabolic trough power plants in the Mojave Desert have been reliably providing 354 MW of electricity to southern California since the 1980s. Progress in solar thermal power stalled after that time because of a decrease in government incentives and low natural gas prices. However, a resurgence of interest in this technology

**FIGURE 1.18**

The 250-MW Solana parabolic trough power plant with 6 hours of thermal storage in Gila Bend, Arizona, provides electricity for Phoenix. (Courtesy of Atlantica Yield.)

began with the completion of the 64-MW Nevada Solar One trough plant near Las Vegas in 2007. In addition, a feed-in tariff in Spain stimulated the development of a significant number of CSP plants. There were about 5000 MW of CSP installed in the world at the end of 2016, about 1800 MW of which were in the United States [37].

Beginning around 2014, the very low cost of PV modules slowed the development of CSP in the United States. A significant advantage of CSP, however, is that thermal energy offers a cheaper and more efficient storage option than batteries (see [Figure 1.18](#).) Also, fuels such as natural gas or biogas may be used as backup to ensure continuous operation. Thus, CSP offers the ability to dispatch electricity when it is needed. To improve the economic competitiveness of CSP, advanced power towers are being designed to achieve higher temperatures (and thus higher power cycle efficiencies). Also, “peaker plants” are being designed that utilize solar thermal storage in such a way that electricity is sold primarily when rates are at their highest.

Low-temperature solar thermal collectors to heat domestic hot water and provide industrial process heat are well developed. By the end of 2013, an installed capacity of approximately $375 \text{ GW}_{\text{th}}$ of low-temperature solar thermal energy was in operation around the world [38], a vast majority of this being used in China for domestic hot water (see [Figure 1.19](#)). The improvements made in parabolic trough technology for CSP technology could be leveraged to better utilize solar thermal energy for industrial processes.

1.7.4 Ocean and Geothermal Energy

Ocean energy is of two types: thermal and hydrokinetic. An ocean thermal energy conversion (OTEC) plant uses the temperature difference between ocean water at the surface and at depth to drive a Rankine power cycle. This can be done via a closed cycle using ammonia as the working fluid or via an open cycle in which surface water is flashed to vapor in a vacuum chamber. The latter cycle has the benefit of also producing desalinated

**FIGURE 1.19**

China has the most solar hot water systems in the world. Simple rooftop thermosyphon systems like those shown here are the most widely used type.

water. Because of the very low temperature difference involved, OTEC plants operate at very low thermodynamic efficiencies, which makes economic power production difficult. As a result, only small experimental OTEC plants have been built.

Ocean hydrokinetic technologies harness the kinetic energy of moving ocean water associated with tidal flows, wave action, and ocean currents. A wide variety of different technologies have been developed to tap into these various energy sources. Although hydrokinetic projects have been built, this does not yet represent a significant commercial source of world electricity and is under development. Greater effort has been spent on the development of offshore wind.

Geothermal power has been successfully developed around the world. Geothermal heat originates from two sources: residual heat generated in the formation of the planet by gravitational collapse, and heat generated by the decay of radioactive isotopes. Commercially viable geothermal resources occur along spreading or subduction zones between tectonic plates and at volcanic hot spots where magma from the mantle has pushed up toward the surface. Exploitable geothermal resources depend on the presence of water. These hydrothermal resources are key as the water is heated by convection as it flows through cracks in the hot rock zone. High-quality geothermal resources are tapped by drilling into the high-pressure zone and can produce brine at temperatures around 300°C. Steam is produced either directly from the resource or through flashing liquid brine, and this then drives a steam turbine. For resource temperatures below about 175°C, binary-cycle plants are employed (see [Figure 1.20](#)). In this type of plant, an organic fluid such as pentane or isobutane is boiled and used to power a so-called organic Rankine cycle (ORC). An organic Rankine cycle can also be used as a bottoming cycle in a flash steam system where it can extract additional energy from the liquid brine remaining from the flash process. Geothermal power plants are considered base load and are (on average) available more than 90% of the time.

**FIGURE 1.20**

The 30-MW, binary-cycle, geothermal power plant in Mammoth Lakes, California, with large arrays of air-cooled condensers. The plant owner has experimented with systems that evaporatively precool the air on hot summer days. (Courtesy of Ted J. Clutter.)

Because of the limited number of hydrothermal resources suitable for electric power production, there is increased interest in creating reservoirs in hot dry rock. This approach is called enhanced geothermal systems (or EGS, also sometimes referred to as engineered geothermal systems) and can tap into the large amount of the Earth's stored thermal energy at great depth. The EGS technology attempts to drill into the depth of the earth up to 1000 m or more. Injected water is used in a hydrofracking operation to create porosity and establish a water reservoir in the rock. Production wells are then tapped to bring the hot water to the surface and power either a flash system or a binary-cycle plant. EGS has so far been limited to experimental efforts. No commercial system has yet been built and put into operation.

1.7.5 Biomass and Biofuel

According to the IEA, bioenergy accounts for about 10%, or 50 EJ, of the world's primary energy supply [39]. Most of this is used for cooking and heating and in developing countries has serious consequences for human health (as a result of open flames used indoors) and deforestation. Even a small improvement in conversion efficiency for cooking stoves could reduce wood fuel demand and improve indoor air pollution for millions of people. Various efforts are being made to develop better cooking stoves. The Global Alliance for Clean Cookstoves is an organization hosted by the UN Foundation with a mission of getting 100 million households to adopt clean cookstoves by 2020.

Governments of developed countries around the world are viewing the development of liquid biofuels from biomass very favorably. Most ethanol in the United States is made from corn via fermentation. Between 40% and 70% of the U.S. corn crop, depending on weather and market conditions, can be processed into ethanol, which creates a food supply issue. From a climate change standpoint, this is only marginally better than gasoline. Efforts to transition from corn to cellulosic feedstocks such as crop residues, which have a much

lower carbon footprint, have shown good progress but have not yet had a major impact in the marketplace. Ethanol in the United States today is used mainly in a 10% blend with gasoline (E10) to comply with the federal renewable fuel standard.

In 2015, the world annual ethanol production had reached about 25.7 billion gallons, of which 58% was in the United States. Brazil, whose transportation systems relies heavily on ethanol from sugar cane, was second with 28% of the production [40].

Biofuel production depends primarily on agricultural production and therefore on land use. The major feedstocks for ethanol and their production rates in liters per hectare are: sugar cane (6000), beets (5000), and corn (3200). The largest feedstock for biodiesel is oil palms. The high economic value of palm oil has resulted in enormous amounts of forestland in Indonesia being burned to develop oil palm plantations. (Indonesia is the world's sixth largest producer of biodiesel with 6% of the total.) This has caused a significant increase in greenhouse gas emissions and negatively impacted the wildlife through massive habitat destruction.

The proliferation of zero-emission vehicle mandates (i.e., new vehicles are required to have no harmful tailpipe emissions by a certain date, such as 2030) in California and countries around the world has lowered the future prospects for biofuel in passenger cars. However, bio-derived fuels may still play an important future role for ships and planes.

Besides producing biofuels, biomass feedstocks can also be burned to generate electricity. According to Research and Markets [41], in 2016 there were 3600 active biomass power plants producing a total of 51 GW. Although biomass power is generally considered carbon-neutral (CO_2 is absorbed by growing feedstock and then emitted when it is burned), it is possible to gasify the biomass and capture and sequester the carbon. Such a system, called BECCS (BioEnergy with Carbon Capture and Storage), is carbon-negative and could help draw down atmospheric CO_2 .

1.7.6 Hydroelectric Generation

According to the EIA, 10% of U.S. energy consumption was renewable and 25% of that (or 2.5% of the total energy) was hydroelectric power in 2015. In terms of electricity only, hydropower produced 6.1% of the U.S. total, or a little over one-third of renewable electricity. On a worldwide basis, hydropower provided 16.4% of the world's total electricity and 71% of the world's renewable electricity in 2015. There are three types of hydropower: reservoir systems, in which reservoir water is released through turbines in a dam, pumped storage systems, in which water is pumped to a high-elevation reservoir and released during peak electric demand, and run-of-the-river systems, which rely on the kinetic energy of river flow. Hydropower is dominated by the first type of system. However, there is increased interest in pumped storage as a means to control variable wind and PV on the grid. And small run-of-the-river projects are being pursued in many rural areas.

Large-scale hydropower can produce electricity at a very low cost and high EROI. The enormous hydropower public works projects undertaken in the Columbia River Basin during the Great Depression have been credited with allowing the United States to produce large quantities of aluminum at a low cost, which was needed for the manufacture of aircraft during World War II. Hydropower dams have the ability to provide both base-load power and also follow the load when needed. And once built, hydropower is a carbon-free form of energy generation. [Figure 1.21](#) shows a Pacific Northwest dam.

There are a number of drawbacks to large-scale hydropower, however. Large reservoirs can displace human and animal populations and damage the ecosystem, including fish and other aquatic species. The buried vegetation will decompose and release methane,



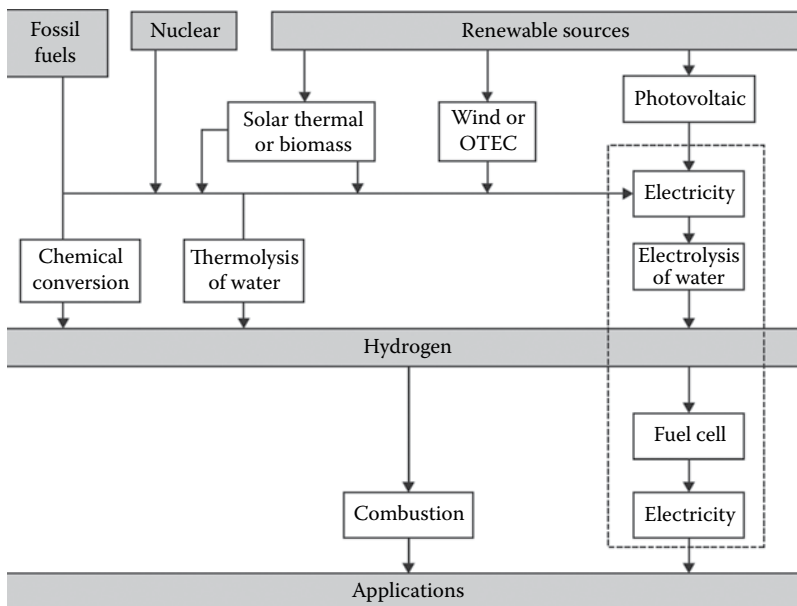
FIGURE 1.21
Bonneville Dam spillway on the Columbia River.

thus contributing to climate change, especially in tropical regions. This consequence must be taken into account when assessing the overall impact of large hydropower on climate change. The creation of a reservoir will increase evaporation of the river water and water salinity, an issue in dry regions. When a river that carries a large amount of silt is dammed, the silt will build up at the bottom of the reservoir over time, thus decreasing the reservoir volume until it is no longer viable.

1.8 Hydrogen

When considering a hydrogen economy, it is important to recognize that hydrogen is an energy carrier, much like electricity, and not an energy source (although, if nuclear fusion technology develops and is implemented, hydrogen is a potential feedstock). However, hydrogen differs from grid electricity because its production does not instantaneously balance demand, that is, hydrogen can be stored more readily than electricity. This ability makes hydrogen attractive as a fuel. It also allows hydrogen-powered vehicles to be refilled in a time frame similar to that of gasoline vehicles, whereas electric battery vehicles require longer charge times.

Figure 1.22 shows the major pathways to produce molecular hydrogen as an energy carrier [42]. The top row of Figure 1.22 shows the primary energy sources: fossil fuels, nuclear materials, and renewable sources. The next three rows show the major processing steps for conversion of the primary energy into hydrogen. Following the hydrogen row are the two methods of using it in energy applications: one is to combust hydrogen to produce

**FIGURE 1.22**

Pathways for hydrogen production and utilization. (From Kreith, F. and West, R.E., 2004. Fallacies of a hydrogen economy: A critical analysis of hydrogen production and utilization, *J. Energy Resources Technol.*, 126(4), 249–257. [42])

heat for various applications, and the other is to generate electricity from hydrogen by means of a fuel cell.

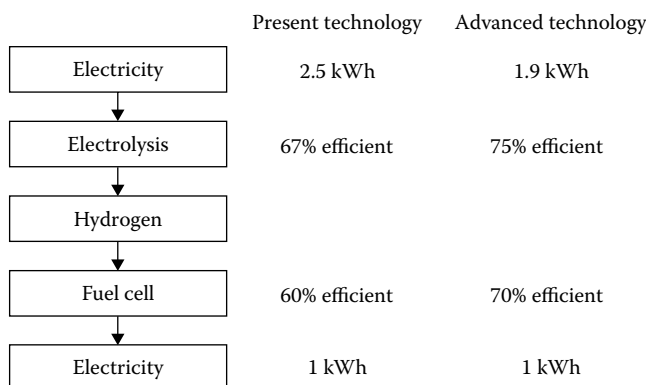
Over 10 million metric tons of molecular hydrogen are used annually in the United States for hydrotreating and hydrocracking in petroleum refineries and to produce ammonia. It is important to note that 95% of the hydrogen produced in the United States is via the steam reformation of natural gas, which contributes to climate change. For a hydrogen economy to address climate change, the hydrogen must be produced by nuclear or renewable energy. Potential pathways are electrolysis from nuclear or renewable electricity or thermolysis of water (breaking down water into hydrogen and oxygen at high temperatures) via nuclear or solar thermal energy.

Water provides a large resource for hydrogen; however, water splitting requires a substantial energy input. As limited by the laws of thermodynamics, energy inputs exceed the energy released by the same hydrogen when used as a fuel. The following reaction describes water splitting into hydrogen and oxygen:



In it, 120 MJ/kg-hydrogen is needed (all gases at 25°C), and the reverse reaction of combining hydrogen and oxygen to give water (all gases at 25°C) ideally yields 120 MJ/kg hydrogen. To evaluate the losses, it is useful to examine the round-trip efficiency of hydrogen production processes quantitatively.

Figure 1.23 shows the round-trip efficiency of electricity to hydrogen via low-temperature water electrolysis and conversion of that hydrogen back to electricity via a fuel cell [43]. These steps are shown in Figure 1.23 with current and targeted efficiencies for the electrolysis and fuel cell steps.

**FIGURE 1.23**

Inefficiencies associated with the generation of electricity via hydrogen that is produced from electrolysis. (From DOE. Fuel cell technologies office multi-year research, development, and demonstration plan, <https://energy.gov/eere/fuelcells/downloads/fuel-cell-technologies-office-multi-year-research-development-and-22>. [43])

With current technology, it would take 2.5 kWh of electricity input to produce 1 kWh of electricity output, and with the most optimistic advanced efficiency, 1.9 kWh would only yield 1 kWh of output. The difference between input and output would be lost, as inefficiencies are involved in each of these sequential steps. Hence, the output of electricity via the hydrogen fuel cell path costs approximately two to three times as much as the electricity input. Thus, the viability of electrolysis is dependent upon the power system having a large number of hours in which the price of electricity is very low or zero (as could happen at high penetrations of wind and solar PV generation).

In summary, a round-trip energy analysis shows that low-temperature electrolysis is energy inefficient compared to using the electric power or heat from any of these sources directly, so hydrogen's inherent ability to store energy and decouple electricity generation from loads drives the value of hydrogen via low-temperature electrolysis. There are processes described in the technical literature that can produce hydrogen from renewable or nuclear sources without using either electrolysis or thermolysis of water [44]. However, these concepts are still in the research phase [44,45].

For passenger vehicles, battery electric technology currently appears to be the front-runner. Nevertheless, multiple automobile companies are pursuing hydrogen fuel cell passenger cars. Decreases in battery costs and the ability of battery electric vehicles to connect directly to the grid have led to more rapid adoption of battery electric vehicles. Hydrogen vehicles will likely be most competitive in market segments where longer ranges or faster charging is desired. These include larger vehicles (including ships and aircraft) and material handling equipment that is operated for multiple shifts. Hydrogen might also be economically competitive against stationary batteries for large-scale grid storage.

1.9 NREL System Advisor Model

An important feature of this book is the utilization of efficiency and renewable energy tools developed by the National Renewable Energy Laboratory (NREL). Foremost among these

tools is the System Advisor Model (SAM) that provides the ability to analyze a variety of renewable energy systems. Estimating the performance and cost of most renewable energy systems is difficult because the availability of the resource, be it wind or solar, varies with time of day, time of year, the local weather, and location. To make realistic estimates of performance and cost, it is necessary to understand and be able to simulate the basic theory of the energy generation system, using local environmental data. SAM calculates the performance and cost of generating electricity or heat, using data for the project's location, installation, operating costs, financing, and physical system specifications. SAM's performance model makes hour-by-hour calculations for various types of renewable systems' thermal or electric output, generating a set of 8760 hourly values that present the system's heat or energy production during a typical year. SAM then uses the hourly performance data to estimate the system's total annual output and capacity factors for practical performance evaluations. Throughout this text, you will find calculations for major technologies based on detailed engineering analysis, as well as calculations using SAM for similar systems. The examples demonstrate the use of the model based on typical performance calculations at a given location using default parameters that are built on the experience with and data from previous installations. In order to use the model properly, however, it is necessary to first understand the engineering basis for the given technology. Then default parameters can be replaced with parameters that are more specific to the system being analyzed.

As of early 2017, SAM provides performance models for the following technologies:

- Photovoltaic systems (flat and concentrating)

- Parabolic trough CSP systems

- Power tower CSP systems

- Dish Stirling CSP systems

- Linear Fresnel CSP systems

- Wind power electric turbines

- Geothermal power

- Biomass power

- Flat-plate collectors for domestic or commercial hot water heating

- A simple model for other technologies, including fossil fuel thermal power plants.

SAM requires information about the location, type of equipment used in the system, various operating parameters related to the resource, geometry of the energy generation system, cost of installation, and operating and fuel costs during its life, as well as economic parameters such as interest and inflation rates. Running the model for wind or solar technologies requires a weather file for the project's location. These files are generally used at hourly resolution for a typical meteorological year (TMY). SAM links to several libraries for weather and solar resource files, including NREL's National Solar Radiation Database, Wind Integration National Dataset (WIND) Toolkit, and Biofuels Atlas. Typical meteorological year files are provided for some other countries besides the United States. Users can also supply their own meteorological data, as text files that follow SAM's weather file format requirements. SAM provides, for each technology, a set of sample files that contain complete sets of sample cost and performance input data. However, for more accurate results users will need to modify the input data as appropriate for the design of the system they are working on.

Finally, SAM displays modeling results in tables and graphs, displaying first-year annual energy production, LCOE, and other performance data of importance for the analysis. A built-in graphic tool displays a set of default graphs and allows for the creation of custom graphs that fit each individual system and requirements. Suppose, for example, the default analysis of a flat-plate solar collector in a specific location uses a default tilt angle of 20° , whereas the collector has a tilt value of 40° . In that case, it is necessary to replace the default value by the actual tilt angle of the installation. If, in the design, there is an option to select the particular tilt angle, users can run SAM for various angles, compare the results, and then select the value most appropriate for their installation. The availability of SAM makes it possible for the designer or operator to quickly assess the effect of changing parameters and avoid the tedious calculations previously associated with inputting the data and carrying out hour-by-hour calculations to obtain the daily, monthly, or yearly performance of the

TABLE 1.6

Energy Conversion Factors

	Btus	Quads	Calories	kWh	MWyr		
Btus	1	10^{-15}	252	2.93×10^{-4}	3.35×10^{-11}		
Quads	10^{15}	1	2.52×10^{17}	2.93×10^{11}	3.35×10^4		
Calories	3.97×10^{-3}	3.97×10^{-18}	1	1.16×10^{-6}	1.33×10^{-13}		
kWh	3413	3.41×10^{-12}	8.60×10^5	1	1.14×10^{-7}		
MWyr	2.99×10^{10}	2.99×10^{-5}	7.53×10^{12}	8.76×10^6	1		
bbbls oil	5.50×10^6	5.50×10^{-9}	1.38×10^9	1612	1.84×10^{-4}		
Tonnes oil	4.04×10^7	4.04×10^{-8}	1.02×10^{10}	1.18×10^4	1.35×10^{-3}		
kg coal	2.78×10^4	2.78×10^{-11}	7×10^6	8.14	9.29×10^{-7}		
Tonnes coal	2.78×10^7	2.78×10^{-8}	7×10^9	8139	9.29×10^{-4}		
MCF gas	10^6	10^{-9}	2.52×10^8	293	3.35×10^{-5}		
Joules	9.48×10^{-4}	9.48×10^{-19}	0.239	2.78×10^{-7}	3.17×10^{-14}		
EJ	9.48×10^{14}	0.948	2.39×10^{17}	2.78×10^{11}	3.17×10^4		
	Btus	Quads	Calories	kWh	MWyr		
	bbbls Oil Equivalent	Tons Oil Equivalent	kg Coal Equivalent	Tons Coal Equivalent	>MCF Gas Equivalent	Joules	EJ
Btus	1.82×10^{-7}	2.48×10^{-8}	3.6×10^{-5}	3.6×10^{-8}	10^{-6}	1055	1.06×10^{-15}
Quads	1.82×10^8	2.48×10^7	3.6×10^{10}	3.6×10^{10}	10^9	1.06×10^{18}	1.06
Calories	7.21×10^{-10}	9.82×10^{-11}	1.43×10^{-7}	1.43×10^{-10}	3.97×10^{-9}	4.19	4.19×10^{-18}
kWh	6.20×10^{-4}	8.45×10^{-5}	0.123	1.23×10^{-4}	3.41×10^{-3}	3.6×10^6	3.6×10^{-12}
MWyr	5435	740	1.08×10^6	1076	2.99×10^4	3.15×10^{13}	3.15×10^{-5}
bbbls oil	1	0.136	198	0.198	5.50	5.80×10^9	5.80×10^9
Tons oil	7.35	1	1455	1.45	40.4	4.26×10^{10}	4.26×10^{-8}
kg coal	5.05×10^{-3}	6.88×10^{-4}	1	0.001	0.0278	2.93×10^7	2.93×10^{-11}
Tons coal	5.05	0.688	1000	1	27.8	2.93×10^{10}	2.93×10^{-8}
MCF gas	0.182	0.0248	36	0.036	1	1.06×10^9	1.06×10^{-9}
Joules	1.72×10^{-10}	2.35×10^{-11}	3.41×10^{-8}	3.41×10^{-11}	9.48×10^{-10}	1	10^{-18}
EJ	1.72×10^8	2.35×10^7	3.41×10^{10}	3.41×10^7	9.48×10^8	10^{18}	1

Note: To convert from the first column units to other units, multiply by the factors shown in the appropriate row (e.g., 1 Btu = 252 cal). MWyr = megawatt-year; bbbls = barrels; tons = metric tons = 1000 kg = 2204.6 lb; MCF = thousand cubic feet; EJ = exajoule = 10^{18} J. Nominal calorific values assumed for coal, oil, and gas.

system. It should be emphasized, however, that using SAM without a thorough knowledge of the basic engineering information associated with the system can lead to serious errors.

SAM is available for free at <https://sam.nrel.gov>. Versions are available for installation on Windows, OS X, and Linux operating systems. NREL and its partners continue to develop SAM, including adding new technology performance models and updating cost and performance estimates, so it is important to keep abreast of the website. In addition to new model releases, the website provides access to legacy versions, which are useful for being able to replicate earlier work. Because of updates, use of later versions to solve problems presented in this book will likely result in modest departures from the solutions shown.

Energy Units and Conversion Factors

In reading the literature pertaining to energy, an overwhelming number of units that are not usually used in conventional engineering calculations are encountered. To assist the reader in handling data from various sources that include unusual units such as barrels of oil equivalent, conversion factors are presented in [Table 1.6](#).

PROBLEMS

- 1.1 The hallways of a three-story building in Denver, Colorado, use 600 lights per floor, and each light is an incandescent bulb rated at 60 W.
 - a. Estimate the amount of energy that could be saved in August by turning the lights on when the sun sets and turning them off when it becomes light.
 - b. Assuming that the power for the lights comes from a 30% efficient coal-fired power plant, estimate the amount of CO_2 that would be saved with this conservation measure. Assume that the chemical composition of the coal is $\text{CH}_{0.8}$ and that coal has a heating value of 29 MJ/kg.
 - c. Prepare a brief report, making recommendations for reasonable conservation measures.
- 1.2 On May 27, 2009, U.S. Senator Lamar Alexander proposed to build 100 new nuclear power plants in 20 years “for a rebirth of industrial America while we figure out renewable electricity.” In his talk, he stated “This would double America’s nuclear plants, which today produce 20% of all of our electricity and 70% of our pollution-free, carbon-free electricity.”

Analyze the proposal of the senator from several perspectives:

 - a. Cost of 100 nuclear power plants
 - b. Need to replace existing nuclear power plants to generate net power output
 - c. Amount of water required for the condensers of the new power plants.
- 1.3 Two different fuels are being considered for a 1-MW (net output) heat engine, which can operate between the highest temperature produced during the burning of the fuels and an atmospheric temperature of 300 K. Fuel A burns at 2500 K, delivering 50 MJ/kg (heating value), and costs \$2.00/kg. Fuel B burns at

1500 K, delivering 40 MJ/kg, and costs \$1.50/kg. Compare the fuel costs per hour of fuel A and fuel B, assuming that the heat engine operates:

- a. At Carnot efficiency
 - b. At 50% of Carnot efficiency.
- 1.4 A solar energy collector produces a maximum temperature of 100°C. The collected energy is used in a cyclic heat engine that operates in a 5°C environment. Estimate the thermal efficiency if the engine operates at 40% of Carnot efficiency. How would the answer change if the collector were redesigned to focus the incoming solar radiation to enhance the maximum temperatures to 400°C?
 - 1.5 Because meat is higher on the food chain than grains, the more calories you get from meat, the more agricultural land you use. Using the arable land area in your state and data from [46] (which concludes that 5.6 GJ metabolized energy is produced annually per hectare for meat and that 41.4 GJ of metabolized energy is produced annually per hectare for grain), estimate
 - a. How many vegetarians could you feed with land available in your state? Determine this as a number (percentage of 2011 population) and percentage of estimated population in 2030.
 - b. Repeat this estimate for the average American diet (the typical American gets two-thirds of their calories from meat and one-third from grain).
 - 1.6 If 10% of your state were covered with PV collectors, estimate the power produced in kWh/day per capita on average. If 10% of the people in your state had to drive 100 km/day to commute to work, how many kWh/day would that consume? Discuss the implications of these two estimates. How many collectors of 3 m × 10 m would be required to produce the energy for commuting with an all-electric car with 60% efficient batteries?
 - 1.7 Assuming that a heat pump has a coefficient of performance equal to 4, how much heat could this device deliver to the interior of a building with 1 kWh of electricity?
 - 1.8 If there were a carbon tax of \$250/ton of CO₂ on fossil fuels, estimate the increase in the price of a barrel of oil.
 - 1.9 In 2009, the administration of President Obama instituted a Cash for Clunkers program. You are to evaluate the effectiveness of the program, which was intended to stimulate the economy and reduce the import of oil. According to the program announcement, an average of \$4000 per car in rebate was offered if a consumer brought in a “clunker” and exchanged it for a new car that would have a fuel efficiency equal to at least 10 mi/gal better than the car they traded. The total amount of money allocated to the program was \$3 billion.
 - a. What reduction in oil import per year, in terms of both barrels of oil and percentage of total import, was achieved by the program?
 - b. Assuming that imported oil cost \$55 per barrel, how long did it take for the savings in import to equal the investment in the program?
 - c. The energy required to build a new car, called the embedded energy in car construction, has been estimated to be 30,500 kWh/car by Argonne National Laboratory [47]. The embedded energy is mostly coal and nuclear, whereas the energy saved by the improved efficiency is mostly imported over the life of the car. Estimate how many years it would take to recoup the energy

invested in the construction of the car by the savings in energy from the improved mileage of the new vehicle.

- d. What reduction in CO_2 generation did the program achieve? Discuss the effectiveness of the program from an energy perspective and what changes in the program you would recommend to make it more effective.
- 1.10 While completing your homework, imagine the study space you are using employs a space heater with a rating of 30 kW, a refrigerator (for snacks) that is rated for 5 kW, and a light fixture with two 100-W bulbs, all operating at a constant rate for the 1.5 h it takes you to finish.
 - a. What is the total power consumed at any given moment?
 - b. How much energy do you consume to complete the task?
 - c. Assume the utility company charges 6.5 cents per unit of energy in part b, how much did it cost you to complete the assignment?
 - d. If you were willing to pay the utility company \$5, what would be the power rating of an additional appliance you could add to your study space?
 - 1.11 In 2009, a group of environmentalists approached the Boulder City Council with a request to deny an application to continue operating the local coal-fired 200-MW power plant to reduce CO_2 emissions. The group suggested that the coal-fired power plant be replaced by a nonpolluting solar plant.
 To evaluate the feasibility of their request, a steel plate is placed in sunlight in Boulder at an angle equal to the latitude. The plate is treated with a coating that has an absorptivity for solar insolation of 0.9 and an emissivity in the long-range spectral range of 0.2.
 - a. If the average insolation between 9 a.m. and 5 p.m. is equal to 400 W/m^2 and the convective heat-transfer coefficient from the top surface of the plate is $8 \text{ W/m}^2 \text{ K}$, estimate the equilibrium temperature of the plate assuming the bottom is insulated and the effective sky temperature is 50 K.
 - b. If you could operate a heat engine between the plate temperature calculated in part (a) and the environment at 10°C , estimate the plate surface area required to generate the power equal to the coal-fired power plant. Then comment on the result and compare it with a PV system of 12% efficiency.
 - 1.12 A large nuclear power plant has a rated capacity of 1 GW. Its actual output is estimated to average about 80% of capacity because of the need for maintenance and imperfect match between supply and demand. Assuming that year-round average residential electricity needs are about 1 kW electric per housing unit and there are three residents per unit, estimate how many power plants would be needed to satisfy the demand of a metropolitan area with a population of 30 million.
 - 1.13 The yearly average solar flux incident on a horizontal surface in the United States is about 180 W/m^2 . The average total energy demand in the United States is approximately 100 quads ($100 \times 10^{18} \text{ J}$) per year. Assuming an average efficiency of PV cells of 14% and a biomass conversion efficiency around 1%, estimate the percentage of land required to provide the energy of the country by these two renewable technologies. (The total land area of the United States is about $9.2 \times 10^6 \text{ km}^2$.)
 - 1.14 Calculate the doubling time for annual percentage increases of 2% and 10%, assuming an exponential growth function.

- 1.15 In 2011, the United Nations announced that the human population reached 7 billion and was increasing at approximately 1.5%. Estimate the doubling time of the human population and then estimate the available land area on Earth per person at the end of the first and the third doubling times. The Earth is approximately two-thirds water and can be approximated as a sphere of 8000 mi in diameter. Then, discuss the implications for these estimates.
- 1.16 Experts claim that there is enough coal left for at least another 400 years at current rates of consumption. Estimate how long the coal would last if its annual usage rate increases by 5% and 10% per year.
- 1.17 The following equation can be used to solve all problems involving exponential growth and decay:

$$N = N_0 e^{kt}$$

where

N is the number in the population after a time t

N_0 is the initial number

k is the growth constant (if *positive*) or the decay constant (if *negative*)

e is the base of the natural logarithms (approximately 2.72)

1. The population for a town was 100,000 in 2011. To estimate future energy needs, calculate the population in 2030, assuming a growth rate of 3% per year.
2. When would the population reach 1,000,000 at this growth rate?
3. If the city placed a limit of 200,000 people for 2030, what would the allowable growth rate be?
4. Suppose someone bought a house in 2000 for \$200,000 and expected to sell it for their retirement in 2011 for \$250,000. What exponential growth rate did they assume?
5. Suppose this person put the house on the market, and the best offer received was \$170,000. What was the exponential decay rate?
6. Explain the collapse in the U.S. housing market a few years ago in terms of the earlier problems (4 and 5).
7. Obtain data from reliable sources for the global population and oil production between 1850 and 2010. Then plot the data and fit an exponential curve to it. What is the growth constant for the two parameters? Is there a physical explanation for the result?

Discussion Questions

Discussion of Sustainability Principles

Propose a "Sustainable Development Act" legislation that would embody the Brundtland definition of sustainable development in regulations on land use, energy development, end-user appliances, or the management and use of some resource. Do some research on a resource management regulation in your area. There are fishing regulations in most areas: many national parks have limits on the number of visitors and how they can

access sensitive areas; regulations may exist for grazing or logging on public lands. Do all of these existing regulations arise because of previously unsustainable exploitation? Do they all involve limits on what people can take so that the resource can continue into the future?

Discussion on Oil Supply, Depletion Effects, and the Economy

Consider the short-term impacts on a small company that uses 9 million barrels of oil per year. Companies must make annual budgets that spell out how much they will spend and expected earnings. During most of 2010, the price of oil had remained below \$80 per barrel. The company's 2011 budget for oil was \$720 million (at a price of \$80), with other planned expenditures on new production equipment worth \$100 million and \$80 million for new workers. Look up the historical price of oil based on U.S. EIA data on a reputable website like www.indexmundi.com, and you will see that the oil price rose to over \$100 per barrel for most of 2011. Was the company able to purchase the new equipment, increase production, or hire new workers? Was oil price an issue? What risk did it pose to the company's operation? The 2007–2008 oil price shock had a negative impact on the company's financial position. What if the company had conducted an energy audit on their oil use and worked with some energy engineers to devise a plan where they could reduce their oil consumption to 7 million barrels in 2011 (22% reduction) at a cost of \$20 million to implement? How would this be a risk management approach? Would the company be able to buy the equipment and hire the new workers if they had implemented this plan? What would happen if the price of oil went back down to \$80 per barrel in 2012? Is it fair to say that energy engineering to reduce the amount of energy used in a business is good risk management and good for the economy?

Discussion on the Solar Energy Flow Rate and Photosynthesis Conversion

Put the zip code of your hometown into the solar database PVWatts viewer from NREL (<http://pvwatts.nrel.gov>) and find the average daily solar insolation per m². The maximum photosynthetic conversion efficiency of plants in direct sunlight is 8%, but the annual average can be assumed around 2%. In Section 1.2.3, a modest estimate of 1 ac per person was used for food production, remembering that we only eat part of the plants. Compare the solar energy flows for food, the ecosystem, and storage as fossil fuels.

Discussion of Energy Content of Corn and Transportation

If the American sport utility vehicle driver rode his bicycle the 225 miles that the tank of E100 would have provided, pedaling at an average power output of 220 W, how many kg of corn would he need to eat to fuel his transportation? Discuss any ideas you have for how market forces would balance the demand for driving low efficiency in the United States with eating tortillas in Costa Rica. Do some research on *green marketing* and *environmental behavior*.

Discussion on CO₂ Emissions

Make a spreadsheet of CO₂ emissions to the year 2100. Start with the current figure of 32.1 Gt/year. Think about different scenarios and try plotting them. Make sure to keep track of the sum total of CO₂ emitted. What year would a 1000 Gt remaining CO₂ budget

(to stay under a 2°C temperature rise relative to preindustrial) be breached if growth in fossil fuel production continues at 3% per year? What if growth were 2% per year? What if an aggressive demand management program were driven by the engineering profession worldwide to stop growth of fossil fuels and maintain consumption at the current level? The first 10% demand reduction would be the most economical and achievable, but a further 10%–20% could be achieved economically in nearly all end uses. Model several different production rate reduction scenarios. What would it take to keep within the emission limits needed to manage the climate risks? Discuss the benefits to people later in the century if there are still economically recoverable fuel resources available.

Discussion of Instability Caused by Growth

Can you think of some examples of civilizations that have faced risks from hitting the limits of population growth? What were the implications? Did any of these civilizations know they were on an unsustainable path? What did they do about it? Most engineers are employed in industry or public service. Can you think of any examples of how engineering work has been influenced by these external factors? Can you think of any ideas of how engineering work could help to manage the risks of growth beyond carrying capacity limits?

Online Resources

The field of sustainable energy is not only very large but also changes so rapidly that a single book is not able to capture information on a real-time basis. The following websites and suggested readings will make it possible for the reader to access developments in the sustainable energy field and keep up to date. The list is not exhaustive, but will provide an entry into useful information and current data.

<http://www.technologyreview.com>—Massachusetts Institute of Technology's publications on current technological advances in computing, internet, communications, energy, materials, biomedicine, and business.

<http://www.nrel.gov>—Publications from NREL that focus on innovations for our nation's future energy. The following are some of the numerous tech subjects:

- Advanced vehicles and fuels
- Basic sciences
- Biomass
- Buildings
- Electric infrastructure systems
- Energy analysis
- Geothermal
- Hydrogen and fuel cells
- Solar
- Wind

<http://www.eere.energy.gov>—DOE efficiency and renewable energy publications focusing on a wide range of programs from biomass and solar energy to building technologies.

<http://cleanenergysector.com>—Profits from the global energy transformation with clean and solar energy technologies.

<http://sciencedaily.com>—Contains current science advancements and articles of the latest science news from Earth to space.

<http://www.sciencedirect.com>—Current science advancements in physical science and engineering.

<http://www.skyfuel.com>—Information from a leader in solar thermal technology.

<http://www.awea.org>—American Wind Energy Association promotes wind energy and has the most up-to-date news on wind power.

<http://www.renewableenergyworld.com>—Global perspective on renewable energy.

<http://www.theoil Drum.com>—Discussion about renewable energy from reputable sources.

<http://www.aceee.org>—Information and news about energy efficiency economy on a federal and state level.

<http://www.withouthotair.com>—A textbook with careful analysis of the options for a sustainable energy system in Great Britain.

<http://www.iea.org>—IEA provides useful information on global energy topics with important up-to-date data.

References

1. Alliance for Water Efficiency and American Council for an Energy-Efficient Economy, May 2011. Addressing the energy-water nexus: A blueprint for action and policy agenda; ASME, ETP. Energy–water nexus—Cross-cutting impacts.
2. Brundtland, G.H., 1987. *Our Common Future*, World Commission on Environment and Development, Oxford University Press, New York.
3. Population Division of the Department of Economic and Social Affairs of the United Nations secretariat, March 2009. World population prospects: The 2008 revision.
4. Bongaarts, J., 2003. Completing the fertility transition in the developing world: The role of educational differences and fertility preferences, *Population Studies* 57(3), 321–335, DOI: 10.1080/0032472032000137835.
5. Scanlon, B., Faunt, C., Longuevergne, L., Reedy, R., Alley, W., McGuire, V., and McMahon, P., June 2012. Groundwater depletion and sustainability of irrigation in the US High Plains and Central Valley, in: *Proceedings of the National Academy of Sciences* 109(24), 9320–9325. www.pnas.org/cgi/doi/10.1073/pnas.1200311109.
6. World Bank, 2003. Development data and statistics, www.worldbank.org/data.
7. Loupasis, S., May 2002. Technical analysis of existing RES desalination schemes—RE driven desalination systems REDDES, Report, Contract # 4.1030/Z/01-081/2001.
8. Kenny, J., Barber, N., Huston, S., Linsey, K., Lovelace, J., and Maupin, A., 2005. Estimated use of water in the United States in 2005, Circular 1344, U.S. Geological Survey, Washington, DC, 38–41.
9. Webber, M.E., 2016. *Thirst for Power: Energy, Water, and Human Survival*. Yale University Press, New Haven and London.
10. U.S. DOE, 2006. Energy demands on water resources, Report to Congress, U.S. Department of Energy, Washington, DC.

11. Wu, M., Mintz, M., Wang, M., and Arora, S., January 2009. *Consumptive Water Use in the Production of Ethanol and Petroleum Gasoline*, Argonne National Laboratory, Argonne, IL.
12. Barney, G.O., Blewett, J., and Barney, K.R., 1993. Global 2000 revisited: What shall we do? The Millennium Institute, Alexandria, VA, p.11.
13. United Nations Food and Agriculture Organization. The state of food insecurity in the world 2015, <http://www.fao.org/3/a-i4646e.pdf>.
14. Pimentel, D., Williamson, S., Alexander, C., Gonzalez-Pagan, O., Kontak, C., and Mulkey, S., 2008. Reducing energy inputs in the US food system, *Human Ecology* 36, 459–471.
15. United States Department of Transportation Bureau of Transportation Statistics. Table 4–5: Fuel consumption by mode of transportation in physical units, https://www.rita.dot.gov/bts/sites/rita.dot.gov/bts/files/publications/national_transportation_statistics/html/table_04_05.html.
16. Krumdieck, S. and Hamm A., 2009. Strategic analysis methodology for energy systems with remote island case study, *Energy Policy* 37(9), 3301–3313.
17. United Nations Development Programme Human Development Reports. About human development, <http://hdr.undp.org/en/humandev/>.
18. Goldemberg, J. and Johansson, T.B., eds., 2004. *World Energy Assessment: Energy and the Challenge of Sustainability*, United Nations Development Programme, New York, http://www.undp.org/content/undp/en/home/librarypage/environment-energy/sustainable_energy/world_energy_assessmentoverview2004update.html.
19. U.S. Energy Information Administration. History of energy consumption in the United States, 1776–2012, <https://www.eia.gov/todayinenergy/detail.php?id=11951>.
20. U.S. Energy Information Administration. U.S. energy flow 2016, https://www.eia.gov/totalenergy/data/monthly/pdf/flow/total_energy.pdf.
21. U.S. Energy Information Administration, January 10, 2017. Renewable generation capacity expected to account for most 2016 capacity additions, <https://www.eia.gov/todayinenergy/detail.php?id=29492>.
22. Intergovernmental Panel on Climate Change, Working Group III, 2012. Renewable energy sources and climate change mitigation, Special Report of the Intergovernmental Panel on Climate Change.
23. International Energy Agency, 2016. Energy technology perspectives: Towards sustainable urban energy systems.
24. Ramachandra, T.V. and Ganesh, H., 2015. Energy trajectory in India: Challenges and opportunities for innovation, *Journal of Resources, Energy, and Development* 12(1–2), 1–24, <http://wgbs.ces.iisc.ernet.in/energy/paper/Energy-trajectory-in-India/Introduction.html>.
25. CIA, May 2, 2012. *The World Factbook*, <https://www.cia.gov/library/publications/the-world-factbook/print/textversion.html>.
26. BP, June 2011. Statistical review of world energy. www.bp.com/statisticalreview.
27. Hall, C.A.S., Lambert, J.G., and Balogh, S.B., 2014. EROI of different fuels and the implications for society, *Energy Policy* 64, 141–152.
28. Lazard, December 2016. Lazard's levelized cost of energy analysis, Ver. 10.0.
29. Jordaan, S.M. et al., 2017. Towards accurate accounting of the surface land requirements of natural gas-fired electricity, *Nature Energy*, 2, 804–812, DOI: 10.1038/s41560-017-0004-0.
30. Fthenakis, V. and Kim, H.C., 2009. Land use and electricity generation: A life-cycle analysis, *Renewable and Sustainable Energy Reviews* 13, 1465–1474.
31. U.S. Energy Information Administration. Energy explained, https://www.eia.gov/Energyexplained/?page=us_energy_transportation.
32. U.S. Energy Information Administration. Use of energy in the United States, https://www.eia.gov/Energyexplained/?page=us_energy_transportation#tab2.
33. U.S. Environmental Protection Agency. Highlights of CO2 and fuel economy trends, <https://www.epa.gov/fueleconomy/trends-report>.
34. U.S. Department of Energy. Better buildings, <https://betterbuildingssolutioncenter.energy.gov>.
35. U.S. Department of Energy. Better plants, <https://energy.gov/eere/amo/better-plants>.

36. Masson, I.G. et al., 2016. Snapshot of global PV markets—The latest survey results on PV markets and policies from the IEA PVPS programme 2016, 32nd European Photovoltaic Solar Energy Conference and Exhibition, Munich, Germany.
37. CSP Plaza, January 18, 2017. Global solar thermal power generation capacity built end of 2016 or added to, Focal Solar, <http://en.cspplaza.com/global-csp-installed-capacity-increased-to-5133-mw-by-the-end-of-2017/>.
38. Mauthner, F., Weiss, W., and Spork-Dur, M., 2015. Solar heat worldwide: Markets and contribution to the energy supply 2013, International Energy Agency Solar Heating & Cooling Programme, Freiburg, Germany.
39. International Energy Agency. Our work on renewables, <https://www.iea.org/topics/renewables/subtopics/bioenergy>.
40. U.S. DOE. Alternative fuels data center, maps and data, <https://www.afdc.energy.gov/data>.
41. Research and Markets, April 6, 2017. Biomass to power report: Industry for electricity generation from solid biomass, *Global Newswire*, <https://globenewswire.com/news-release/2017/04/06/955050/0/en/Biomass-to-Power-Report-Industry-for-Electricity-Generation-from-Solid-Biomass-By-2025-We-Expect-There-to-be-approximately-5-700-Power-Plants-With-a-Capacity-of-About-74-GW.html>.
42. Kreith, F. and West, R.E., 2004. Fallacies of a hydrogen economy: A critical analysis of hydrogen production and utilization, *J. Energy Resources Technol.*, 126(4), 249–257, DOI: 10.1115/1.1834851
43. Energy.gov. DOE fuel cell technologies office multi-year research, development, and demonstration plan, <https://energy.gov/eere/fuelcells/downloads/fuel-cell-technologies-office-multi-year-research-development-and-22>.
44. National Research Council, 2000. *Renewable Power Pathways—A Review of the U.S. Department of Energy's Renewable Energy Programs*, National Research Council, National Academies Press, Washington, DC.
45. National Research Council, National Academy of Engineering, 2000. *The Hydrogen Economy: Opportunities, Costs, Barriers, and R & D Needs Draft*, The National Academies Press, Washington, DC, www.nap.edu.
46. Dale, M., Krumdieck, S., and Bodger, P., 2012. Global energy modeling—A biophysical approach (GEMBA) part 2: Methodology and results, *Ecological Economics*, 73, 158–167.
47. Chandler, D., June 9, 2011. Report: Natural gas can play major role in greenhouse gas reduction, MIT News Office. <http://web.mit.edu/newsoffice/2011/natural-gas-full-report-0609.html>.

Suggested Readings

- Boyle, G., 2004. *Renewable Energy—Power for a Sustainable Future*, Oxford University Press, Oxford, U.K.
- Carson, R., 2002. *Silent Spring* (1963), Houghton Mifflin Harcourt, Boston, MA.
- Heinberg, R., 2005. *The Party's Over—Oil War and the Fate of Industrial Society*, New Society Publishers, Gabriola Island, British Columbia, Canada.
- Hinrichs, R.A. and Kleinbach, M., 2013. *Energy: Its Use and the Environment*, 5th ed., Brooks/Cole, Boston, MA.
- Kreith, F. and West, R.E., 1996. *Handbook of Energy Efficiency*, CRC Press, Boca Raton, FL.
- Metz, B., Davidson, O.R., Bosch, P.R., Dave, R. and Meyer, L.A. (eds.), 2007. *Contribution of Working Group III to the Fourth Assessment Report of the Intergovernmental Panel on Climate Change, 2007—IPCC Fourth Assessment Report (AR4)*, Cambridge University Press, Cambridge.
- Webber, M.E., 2016. *Thirst for Power: Energy, Water, and Human Survival*, Yale University Press, New Haven and London.



Taylor & Francis

Taylor & Francis Group

<http://taylorandfrancis.com>

2

*Economics of Energy Generation and Conservation Systems**

Anyone who believes exponential growth can go on forever in a finite world is either a madman or an economist.

Kenneth Boulding (ca. 1980)

This chapter and the next one present useful analysis tools that engineers should understand. These include a basic process for economic assessment, energy flow analysis, and resource accounting methods for complex energy systems. The objective of economic assessment is to provide useful financial insight and enable a comparison between various energy options. No familiarity with microeconomics is presumed and, given the uncertainty in predicting a future economic environment, one could argue that added complexity may not be warranted. The standard methods presented here are equally applicable to renewable and nonrenewable energy systems, as well as to energy conservation projects. The objectives of energy flow analysis and resource accounting are to conceptualize and compare different energy system investments, to account for resource and external costs, and to identify sustainability issues.

More than 85% of world's commercial energy production is currently from fossil resources. Hydropower is the largest renewable electricity resource and has been well developed in the United States for decades. Other renewables are experiencing rapid growth, but from a small base and with upper limits on capacity near that for hydro. There are plentiful fossil resources, and fossil fuels will continue to be convenient and valuable energy resources for the near future, but fossil resources are exhibiting depletion effects, and the future growth of net energy supply is increasingly unlikely. The approach of sustainable energy engineering is to use quantitative analysis to understand the end use, environmental and social requirements, and resource availability, and then help to make development decisions based on analysis of the dynamics of energy activity systems into the future. This analysis should lead to adaptive design innovations that meet the environmental, social, and economic requirements, manage risks, and provide benefits. This section explores several different ways to understand the energy/social/economic system and the ways that this understanding can inform investment and development decisions.

2.1 Unit Cost of Energy

The source of energy in renewable energy (RE) systems, such as wind turbines and solar collectors is essentially free, but so are oil, coal, and gas in the current economic system

* Sections in this chapter marked with an asterisk may be omitted in an introductory course.

that only requires purchase of mineral rights and a small royalty on mining as the price of access to fossil resources. The costs for energy prospecting, extraction, refining, and generation are largely associated with the equipment purchased and the fuels or electricity used [1]. Neglecting interest charges on capital and operating costs, the unit cost of energy produced by a system, C_s dollars, with initial construction and installation cost, C_0 dollars, over the life of the system, t years, and annual energy production, Q units of energy, is given by

$$C_s = \frac{C_0}{Q \cdot t} \quad (2.1)$$

For example, consider a Solartech 40 W solar PV panel with a list price of \$167 for a 0.38 m² panel (\$440/m²). The panel has a 10-year warranty for 90% of nominal power output and a 25-year warranty for 80% power output. The performance specifications are measured at standard test conditions (25°C, 1000 W/m²) giving conversion efficiency of 10.5%, and the panel is installed in a location where the mean horizontal surface irradiance is 200 W/m². The electricity production can be estimated for a year as $Q = 0.2$ (kW/m²) \times 10.5% \times 8760 (h/year) = 184 (kWh/year/m²). The cost of solar electricity can be estimated by using Equation 2.1:

$$C_s = \frac{440(\$/\text{m}^2)}{184(\text{kWh}/\text{year} \cdot \text{m}^2) \times (0.9 \times 10 \text{ year} + 0.8 \times 15 \text{ year})} = \$0.11/\text{kWh}$$

Note that we use three significant figures when evaluating energy costs, as the methods do not have accuracy to justify fractions of cents. The sensitivity of energy production cost to the technical factors and resource factors can be explored using Equation 2.1. If the solar PV panel were installed in a location with only 100 W/m² mean solar radiation, although the system cost would be the same, the production cost would increase to \$0.22/kWh. If it were possible that research in materials and manufacturing for the solar PV panel could increase efficiency to 20%, reduce cost to \$300/m², and improve lifetime and performance degradation to 90% power output over 30 years, then the production cost would be reduced to just \$0.03/kWh.

2.2 Payback Period

A common method of evaluating the value of an energy generation or conservation system is to determine the time required for the system to payback the initial costs. The payback period (PP) is determined by comparing the total cost of equipment and installation, C_0 , to the annual benefit in either value of net energy produced or net energy saved per year. The value of the energy saved equals the amount of energy saved per year, B_i (kWh/year) times the unit cost of energy, C_s (\$/kWh). Once the yearly value of the net saved energy and the cost of installing a conservation measure are known, the simple PP in years is

$$\text{PP} = \frac{C_0(\$)}{B_i C_s (\$/\text{year})} \quad (2.2)$$

This approach is acceptable for preliminary estimates if the PP is short, say less than 4 years. For a more precise estimate, or for longer horizons, the time value of money, the inflation rate, and the escalation in fuel costs or maintenance costs must be considered.

2.3 Time Value of Money

If money is deposited in a bank, it earns interest. Similarly, when money (capital) is invested in a project or a business that is financed through a purchase of bonds or stock, a certain rate of return on the investment is expected, to compensate the owners of the invested capital for both the opportunity cost of having their money temporarily unavailable for other uses, and also for the risk of loss, since few investments are “sure things.” Conversely, if you borrow money from a bank, you have to pay interest (or dividends) as the cost of the money lent to you. These issues are known as the *time value of money*.

Since it is convenient to conduct economic analyses in a unit of fixed monetary value, a concept known as *present worth* is used. The present worth of a future cash flow or a future payment is the future value of that flow, accounting for the time value of the money. For example, the future value F , of a sum of money P , invested today at an annual interest rate i is

$$F = P(1 + i)^t \quad (2.3)$$

where t is the time interval in years or other time unit corresponding to the time basis of the interest rate i expressed as a fraction. This equation essentially states that an initial sum of money P appreciates by a multiplier factor, $(1 + i)$ each year, disregarding monetary inflation.

Stated alternatively, a future sum of money F has a *present worth* P given by

$$P = \frac{F}{(1 + i)^t} \quad (2.4)$$

This indicates that the present worth of a given amount of money in the future is discounted, in constant dollars, by a factor of $(1 + i)^{-t}$ for each year in the future. In this context, i is generally called the discount rate, but is also referred to as the cost of money or rate of return. Note that this approach assumes that i remains constant over the period of concern. In real life, however, it may well not be constant and constitutes a source of uncertainty.

The present worth factor [PWF(i, t)] is given by

$$\text{PWF}(i, t) = \frac{1}{(1 + i)^t} \quad (2.5)$$

To obtain the present value of a cash flow F that would come t years into the future, it is multiplied by PWF(i, t).

As an example, consider a discount rate of 5% and a cash inflow of \$100, 1 year from now. Using Equation 2.4, the present worth is only \$95. Conversely, if \$95 were invested at 5%

interest today, it would be worth approximately \$100 a year from now. The same approach can be used to evaluate cash flows at any future period.

The present worth concept is the key for a discounted cash flow analysis. Its use permits all calculations to be made in terms of *present discounted money*. Every kind of business or organization has a discount rate that it uses and that reflects the rate of return it expects on investments. Remember, the company could invest capital in making more products and expect a certain rate of return, determined by their experience with past investments. If they instead invest that capital in an energy conservation project, they want to know how that investment compares to other options. The mathematics of the discounted value of money demonstrates why revenues realized in the future are worth less than money earned at the present. For example, \$100 of revenue realized 40 years in the future at an annual discount rate i of 10% has a present worth of only \$1.83 today. This explains why the far future has little influence on conventional business planning and why many businesses shy away from investments in RE systems or conservation measures that have high up-front costs and long-term benefits.

When future cash flows are fixed in size, A , and regularly occur over a specific number of periods, the situation is known as an annuity. For an annuity, the present worth is given by Equation 2.6.

$$P = A \left[\frac{(1+i)^t - 1}{i(1+i)^t} \right] \quad (2.6)$$

For example, assume a cash flow of \$100/year at the end of each year for the next 5 years at a discount rate of 10%. According to Equation 2.6, the present value of the \$500 of inflow is only \$379.

$$P = \$100 \times \frac{(1+0.10)^5 - 1}{0.10(1+0.10)^5} = \$379$$

The present worth is most commonly used to compare different options for investment in different energy management or energy conservation opportunities as illustrated in the following example.

EXAMPLE 2.1

A company has a discount rate of 10% for its investments. The company has two different energy conservation opportunities. Assume that opportunity A generates benefits equal to \$100, \$150, and \$200 at the end of years 1, 2, and 3, respectively. Assume that opportunity B yields benefits of \$225 in year 2 and \$225 in year 3. Over 3 years, both opportunities A and B yield benefits of \$450. However, the timing of the benefits received is different in each case. By using the present worth technique, the two benefit flows can be viewed in terms of today's dollar value.

Solution

Step 1

Compute the PWF using Equation 2.5 for the discount rate of $i = 10\%$

$$\text{PWF}(10,1) = \frac{1}{(1+0.1)^1} = 0.909$$

$$PWF(10,2) = \frac{1}{(1+0.1)^2} = 0.826$$

$$PWF(10,3) = \frac{1}{(1+0.1)^3} = 0.751$$

Step 2

Compute the present worth of each opportunity benefit flow by multiplying the PWF by the annual benefit amount. Note that we use the same significant figures to report results as was given in the cost and benefit estimates.

Year	PWF	Annual Benefit (\$)		Present Worth (\$)	
		A	B	A	B
1	0.909	100	0	91	0
2	0.826	150	225	124	186
3	0.751	200	225	150	169
Total		450	450	365	355

Note that although the total benefits are the same, the present worth for opportunity A is higher because the annual benefits occur sooner. Since opportunity A provides cash sooner, that money can be invested for additional financial return, which is more beneficial for the investor.

2.4 Inflation

The cost and revenues of a project can be expressed either in “current dollars” or “constant dollars.” Actual cash flows observed in the marketplace at a given time are called current dollar cash flows. They are the actual number of dollars required or acquired in the year the cost or the benefit is incurred. The base year is defined as the year around which an analysis is structured. Most commonly, it is the initial period, which may be denoted by 0. In the base year, constant and current dollar cash flows are the same. The future current dollar equivalent, F_t , of a current amount, F_0 dollars, after t years at inflation rate of j per cent per year is

$$F_t = F_0(1+j)^t \quad (2.7)$$

For example, energy savings due to efficiency improvement valued at \$100 in current 2013 dollars, assuming 4% inflation over the next 10 years, will be worth \$148.02 in 2023 dollars. The effect of inflation on the future money is to reduce the value by a factor $(1+j)^{-1}$ per year. Inflation rate in the future will not be constant and will not be known, which constitutes a source of uncertainty in financial analysis. The most common way to deal with inflation risk is to add an extra percentage to the future annual inflation rate.

In practice, it is important to distinguish between real and nominal discount rates. A real discount rate excludes inflation, whereas a nominal value includes inflation:

$$i' = i + j \quad (2.8)$$

where

i' is the nominal discount rate

i is the real discount rate in the absence of inflation

j is the inflation rate

For example, given an inflation rate of 6% and a nominal discount rate of 10%, the real discount rate is 4%. For power generation projects, a typical real discount rate is 3%–4%.

When calculating a present value, it is important to remember that the real discount rate must be used if cash flows are to be in constant dollars, whereas a nominal discount rate is to be used if the cash flow is in current dollars.

If it is necessary to convert a stream of cash flows from current dollars to constant dollars or vice versa, it is useful to refer to an inflation rate index. There are a number of inflation rate indices, for example, the consumer price index (CPI). The CPI measures the average change in prices of goods and services at the retail end. The gross national product (GNP) is the measure of output supplied by U.S. labor and property. Table 2.1 presents the changes in U.S. GNP, as well as the CPIs from 1970 to 2015. Additional information and up-to-date data can be obtained from the U.S. Department of Commerce, which publishes the *Statistical Abstract of the United States* every year (available from <http://www.ntis.gov/products>).

The effect of inflation can be integrated into the present value analysis by using the nominal discount rate:

$$PV[F_0] = \frac{F_t}{(1 + i')^t} \quad (2.9)$$

It should be noted that if all cash flows are inflated at the same rate and are discounted with the appropriate discount rate, then working with either all constant or all current dollars gives the same result for PV, as demonstrated below in Examples 2.2 and 2.3.

2.5 Total Life Cycle Costs

A total life cycle cost (TLCC) analysis should consider all significant dollar costs over the life of a project. These costs are then discounted to a base year value using present value analysis. Any revenue generated from the resale of an investment is also discounted to the base year and subtracted from present value costs. TLCC analysis includes many different costs and must use the appropriate form of the cash flows (current or constant dollars) so that the correct discount rate is applied. If the cash flows are not discounted with the appropriate rate, the analysis will be flawed. The TLCC analysis is normally done to

TABLE 2.1

Selected Inflation Indices

Year	GDP Implicit Price Deflator (2009 = 100) ^a	GNP Implicit Price Deflator (2009 = 100) ^a	Consumer Price Indices (82–84 = 100) ^b	Annual Inflation Rate
1980	44.4	44.3	82.4	13.85
1981	48.5	48.5	90.9	10.35
1982	51.5	51.5	96.5	6.16
1983	53.6	53.5	99.6	3.22
1984	55.5	55.4	103.9	4.30
1985	57.2	57.2	107.6	3.55
1986	58.4	58.3	109.6	1.91
1987	59.9	59.8	113.6	3.66
1988	62.0	61.9	118.3	4.08
1989	64.4	64.3	124	4.83
1990	66.8	66.7	130.7	5.39
1991	69.0	69.0	136.2	4.25
1992	70.6	70.5	140.3	3.03
1993	72.2	72.2	144.5	2.96
1994	73.8	73.7	148.2	2.61
1995	75.3	75.3	152.4	2.81
1996	76.7	76.7	156.9	2.93
1997	78.0	78.0	160.5	2.34
1998	78.9	78.8	163	1.55
1999	80.1	80.0	166.6	2.19
2000	81.9	81.9	172.2	3.38
2001	83.8	83.7	177.1	2.83
2002	85.0	85.0	179.9	1.59
2003	86.7	86.7	184	2.27
2004	89.1	89.1	188.9	2.68
2005	92.0	92.0	195.3	3.39
2006	94.8	94.8	201.6	3.24
2007	97.3	97.3	207.3	2.85
2008	99.2	99.2	215.3	3.85
2009	100.0	100.0	214.5	−0.34
2010	101.2	101.3	218.1	1.64
2011	103.3	103.4	224.9	3.16
2012	105.2	105.3	229.6	2.09
2013	106.9	107.1	233.0	1.48
2014	108.7	108.8	236.7	1.59
2015	109.8	109.9	237.0	0.13

^a Data from <http://www.bea.gov/>^b Data from <http://www.bls.gov/cpi/>

evaluate differences in the costs and the timing of these costs between alternative projects. The formula for calculating the present value of TLCC is

$$\text{TLCC} = \sum_{t=0}^N \frac{C_t}{(1+i')^t} \quad (2.10)$$

where

C_t is the cost in current dollars in period t , including finance charges, operating and maintenance (O&M) costs, and energy costs

N is the analysis period

i' is the nominal discount rate

Since the major costs associated with most conservation and RE technologies are the initial investment costs and O&M costs (including fuel), the formula for TLCC for residential, government, and nonprofit organizations often simplifies to

$$\text{TLCC} = C_0 + \text{PVOM} \quad (2.11)$$

where

C_0 is the initial investment

PVOM is the present value of all O&M costs

$$\text{PVOM} = \sum_{t=0}^N \frac{(\text{O\&M})_t}{(1+i)^t}$$

If the investment is by a for-profit organization, taxes must be included in the calculations as follows:

$$\text{TLCC} = C_0 - (T \times \text{PVDEP}) + \text{PVOM}(1 - T) \quad (2.12)$$

where

T is the income tax rate

PVDEP is the present value of depreciation

EXAMPLE 2.2

A nonprofit organization invests \$10,000 in new double-paned windows and estimates that O&M costs will be \$1300 in the first year for new painting and the windows will have no salvage value. Assuming an annual inflation rate of 3% and a nominal discount rate of 12%, [Table 2.2](#) demonstrates the TLCC evaluation, both in current dollars and in constant dollars. Note that the TLCC is the same, but the discount rate and cash flows are different.

TABLE 2.2

Current and Constant Dollar TLCC Evaluation

Year	Investment	Discounted Investment	Current Dollar O&M Costs	Discounted O&M Costs (w/12% Nominal)	Constant Dollar O&M Costs	Discounted O&M Costs (w/8.74% Real)
0	\$10,000	\$10,000	\$0	\$0	\$0	\$0
1	0	0	\$1339	\$1196	\$1300	\$1196
2	0	0	\$1379	\$1100	\$1300	\$1100
3	0	0	\$1421	\$1011	\$1300	\$1011
4	0	0	\$1463	\$930	\$1300	\$930
5	0	0	\$1507	\$855	\$1300	\$855
NPV		\$10,000		\$5091		\$5091

TLCC = \$15,091.

TABLE 2.3

After-Tax TLCC Evaluation

Year	Investment	Discounted Investment	Depreciation	Discounted Depreciation	O&M Costs	Discounted O&M Costs
0	\$10,000	\$10,000			\$0	\$0
1	0	0	\$4000	\$3571	\$1339	\$1196
2	0	0	\$2400	\$1913	\$1379	\$1100
3	0	0	\$1440	\$1025	\$1421	\$1011
4	0	0	\$864	\$550	\$1463	\$930
5	0	0	\$518	\$294	\$1507	\$855
NPV		\$10,000		\$7353		\$5091

$$\text{TLCC} = \$10,000 - (0.34 \times \$7353) + (\$5091 \times 0.66) = \$10,860.$$

EXAMPLE 2.3

Suppose that the investor of Example 2.2 is a private company in the 34% federal income bracket but pays no state income tax. The initial investment is \$10,000, O&M is \$1300 per year in current dollars in year zero with an inflation rate of 3%, and the nominal discount rate is 12%. The investor uses a “5 year double-declining depreciation schedule” as shown in column 4, and there is no salvage value. The results are shown for each of the steps for evaluating the after-tax TLCC ([Table 2.3](#)).

***2.6 Internal Rate of Return**

The internal rate of return (IRR) analysis is a convenient procedure to compare a variety of investment activities. It is commonly used for accept/reject decisions by comparing the IRR with a minimal acceptable rate, often referred to as the “hurdle rate.” The IRR of an investment that has a series of future cash flows (F_0, F_1, \dots, F_t) is that rate of return on investment that causes the net present value (NPV) of cash flows to equal zero. IRR implicitly assumes reinvestments of any return at the IRR rate and is therefore not recommended for ranking projects. However, it has the advantage of giving an investor a quick comparison of the after-tax return on various financial instruments such as bonds and providing the investor with a quick assessment of energy management project options.

The NPV can be expressed in equation form as

$$\text{NPV} = \sum_{t=0}^N \frac{F_t}{(1+i')^t} \quad (2.13)$$

where

NPV is the net present value of the capital investment

F_t is the net cash flow received at time t in current dollars

i' is the nominal discount rate

**FIGURE 2.1**

Kreith residence, 3 kW Sanyo high-efficiency photovoltaic system. (See also [Figure 11.1](#))

in 2008 (see [Figure 2.1](#)). The cost of the system was \$25,294. The electric utility serving the customer offered a rebate of \$4.50 per Watt in order to meet the RE mandate in the Colorado constitution that requires that 20% of all electric power be from renewable sources by 2020. Moreover, the federal government offered a tax credit capped at \$2000 for the 2008 tax year.

Use the following assumptions:

Price of electricity in year 0: \$0.152 per kWh

Average annual rate of power cost increase: 5% per year (nominal terms)

Tilt: 20°

Azimuth: 180°

Productive life: 20 years

Discount rate (nominal): 6%

Inflation rate: 3%

The system's annual energy output is estimated by inputting the system parameters at the National Renewable Energy Laboratory's PVWatts website: <http://pvwatts.nrel.gov>.

Solution

To find the value of the annual savings, we first multiply the annual energy output by the price of electricity. We assume annual savings start 1 year after the initial investment is made at year 0. Since the cost of electricity will increase 5% per year, we must project the cost of energy for 20 years. The future cost of energy, F_t , is found from Equation 2.7, using a 5% annual increase from the original value. In the first year, $F_1 = 0.152(1 + 0.05)^1 = \0.16 . Then in the second year, as for each successive year, the value of F_t for the previous year becomes the value of F_{t-1} . So in the 20th year, electricity will cost \$0.40 per kWh. Then, the electricity costs for each year are used to calculate annual savings by multiplying by 4207 kWh/year.

The future costs of energy for each of the next 20 years are shown in [Table 2.5](#).

The annual values of electricity produced by the PV system are found by multiplying each year's respective cost of energy by the annual energy output. The results are shown in [Table 2.6](#).

The savings this electricity production represents will be cumulative and must be adjusted for the time value of money. To find the cumulative savings, simply add all of the annual savings values. After 20 years of production, the cumulative savings is

TABLE 2.5

Future Cost of Energy

Year	1	2	3	4	5	6	7	8	9	10
Price/kWh	\$0.15	\$0.16	\$0.17	\$0.18	\$0.18	\$0.19	\$0.20	\$0.21	\$0.22	\$0.24
Year	11	12	13	14	15	16	17	18	19	20
Price/kWh	\$0.25	\$0.26	\$0.27	\$0.29	\$0.30	\$0.32	\$0.33	\$0.35	\$0.37	\$0.38

TABLE 2.6

Value of Electricity Produced

Year	1	2	3	4	5	6	7
kWh	4207	4207	4207	4207	4207	4207	4207
Price/kWh	\$0.16	\$0.17	\$0.18	\$0.18	\$0.19	\$0.20	\$0.21
Annual savings	\$670.55	\$704.08	\$739.29	\$776.25	\$815.06	\$855.82	\$898.61
Year	8	9	10	11	12	13	14
kWh	4207	4207	4207	4207	4207	4207	4207
Price/kWh	\$0.22	\$0.24	\$0.25	\$0.26	\$0.27	\$0.29	\$0.30
Annual savings	\$943.54	\$990.71	\$1040.25	\$1092.26	\$1146.87	\$1204.22	\$1264.43
Year	15	16	17	18	19	20	
kWh	4207	4207	4207	4207	4207	4207	
Price/kWh	\$0.32	\$0.33	\$0.35	\$0.37	\$0.38	\$0.40	
Annual savings	\$1327.65	\$1394.03	\$1463.73	\$1536.92	\$1613.77	\$1696.69	

\$22,813. With future savings in current dollars, the nominal discount rate of 6% is used in Equation 2.4 to adjust the yearly savings back to the NPV of money. After each year's savings are adjusted for the time value of money, they are added together to find the cumulative NPV savings. The cumulative NPV savings of each year is shown in [Table 2.7](#). After 20 years, the total cumulative NPV savings is \$12,219.

After the deduction of the utility's rebate and the federal tax credit, the net capital cost to the customer is $\$25,294 - (\$4.50 \times 3000) - \$2000 = \9794 . After 20 years, assuming a 6% discount rate the customer has made a profit of \$2425. The PP is calculated by comparing the cost of the system to the customer and the value of the energy saved per year. From [Table 2.7](#), we can see that the adjusted cumulative savings (the cost of the energy saved) equals the net cost of the system to the customer between the 15th and 16th years of operation. Therefore, the payback time of the system for the customer with the applied incentive and tax rebate is about 15.5 years. Note that the cost of the system is not paid back to the owner through energy savings without the incentives.

The IRR, found by using Equation 2.14, represents the summation of the discounted cash flows that will equal the initial investment. It is found by iterating on the discount rate until the summation of the yearly discounted cash flows equals zero. The results are shown in [Table 2.8](#), which shows the calculation for a nominal discount rate of 7.81%, representing the IRR.

2.7 Capital Recovery Factor

In many economic analyses, a *series* of annual or monthly sums is invested or used to pay off a loan. The series of equal periodic payments necessary to pay off such a loan is

TABLE 2.7

Annual Adjusted Net Savings

Year	1	2	3	4	5
Annual savings	\$670.55	\$704.08	\$739.25	\$776.25	\$815.06
Cumulative savings	\$1309.17	\$2013.25	\$2752.50	\$3528.75	\$4343.81
Adjusted annual savings	\$632.59	\$626.63	\$620.69	\$614.86	\$609.06
Adjusted cumulative savings	\$1271.21	\$1897.84	\$2518.53	\$3133.39	\$3742.45
Year	6	7	8	9	10
Annual savings	\$855.82	\$898.61	\$943.54	\$990.71	\$1040.25
Cumulative savings	\$5199.63	\$6098.24	\$7041.78	\$8032.49	\$9072.74
Adjusted annual savings	\$603.32	\$597.63	\$591.99	\$586.40	\$580.87
Adjusted cumulative savings	\$4345.77	\$4943.40	\$5535.39	\$6121.79	\$6702.66
Year	11	12	13	14	15
Annual savings	\$1092.26	\$1146.87	\$1204.22	\$1264.43	\$1327.65
Cumulative savings	\$10,165.00	\$11,311.87	\$12,516.09	\$13,780.52	\$15,108.17
Adjusted annual savings	\$575.39	\$569.96	\$564.59	\$559.26	\$553.98
Adjusted cumulative savings	\$7278.05	\$7848.01	\$8412.59	\$8971.85	\$9525.83
Year	16	17	18	19	20
Annual savings	\$1394.03	\$1463.73	\$1536.92	\$1613.77	\$1696.69
Cumulative savings	\$16,502.20	\$17,965.93	\$19,502.85	\$21,116.62	\$22,813.31
Adjusted annual savings	\$548.75	\$543.58	\$538.45	\$533.37	\$529.04
Adjusted cumulative savings	\$10,074.59	\$10,618.17	\$11,156.62	\$11,689.99	\$12,219.02

TABLE 2.8

Yearly Cash Flows for PV System IRR

Year	Net Investment \$	O&M Cost \$/Year	Annual Savings \$/Year	Cash Flow Discounted at 7.81% \$/Year
0	9794	0	-9794	-9794.00
1	0	0	670.55	621.97
2	0	0	704.08	605.76
3	0	0	739.25	589.95
4	0	0	776.25	574.60
5	0	0	815.06	559.62
6	0	0	855.82	545.04
7	0	0	898.61	530.83
8	0	0	943.54	517.00
9	0	0	990.71	503.52
10	0	0	1040.25	490.40
11	0	0	1092.26	477.61
12	0	0	1146.87	465.16
13	0	0	1204.22	453.04
14	0	0	1264.43	441.23
15	0	0	1327.65	429.73
16	0	0	1394.03	418.53
17	0	0	1463.73	407.62
18	0	0	1536.92	397.00
19	0	0	1613.77	386.65
20	0	0	1696.69	377.07
Summation of cash flows discounted at 7.81%				~0

determined as follows. If a uniform payment P_{ann} is invested each year at interest rate i , the present worth of the *sum* of these payments S is

$$S = \frac{P_{ann}}{1+i} + \frac{P_{ann}}{(1+i)^2} + \frac{P_{ann}}{(1+i)^3} + \dots, \quad (2.15)$$

or

$$S = P_{ann} \left[(1+i)^{-1} + (1+i)^{-2} + (1+i)^{-3} + \dots + (1+i)^{-t} \right]$$

The expression in brackets is a geometric series with the first term $P_{ann}/(1+i)$ and ratio $(1+i)^{-1}$. It follows from the expression for the sum of such a series that

$$P_{ann} = S \left[\frac{i}{1 - (1+i)^{-t}} \right] \quad (2.16)$$

where P_{ann} is the annual payment required to achieve a sum S , after t years. It converts equal payments made at the end of each of t consecutive periods to the equivalent amount in the present using an interest or discount rate i . The term in brackets in Equation 2.16 is called the *capital recovery factor* (CRF(i, t)):

$$\text{CRF}(i, t) = \left[\frac{i(1+i)^t}{(1+i)^t - 1} \right] \quad (2.17)$$

Table 2.9 is a summary tabulation of CRFs. The term P_{ann} is the annual or periodic payment on a self-amortizing loan of value S . Each payment is a mix of interest and principal repayment. Early payments are mostly interest because of the large outstanding balance; later payments are primarily principal repayment. Most solar systems owned by private firms or individuals are purchased with self-amortizing loans. This repayment process is also widely used in paying for the loan of a house.

2.8 Levelized Cost of Energy

The levelized cost of energy (LCOE) is widely used for comparing different energy generation technologies. For example, LCOE could be used to compare the cost of electric energy from a renewable source with that from a nuclear generating unit. The LCOE is defined as cost that, if assigned to every unit of energy produced (or saved) by the system over the analysis period, will equal the TLCC when discounted back to the base year. The LCOE is the present value of all the investment costs plus operation and maintenance costs plus fuel costs in each future year per unit power generation, which is also discounted to the present time:

$$\text{LCOE} = \frac{\sum_{t=1}^N \frac{C_t}{(1+i)^t}}{\sum_{t=1}^N \frac{Q_t}{(1+i)^t}} \quad (2.18)$$

TABLE 2.9Capital Recovery Factors (CRF [i, t])

t	Interest Rate, i									
	0%	2%	4%	6%	8%	10%	12%	15%	20%	25%
1	1.00000	1.02000	1.04000	1.06000	1.08000	1.10000	1.12000	1.15000	1.20000	1.25000
2	0.50000	0.51505	0.53020	0.54544	0.56077	0.57619	0.59170	0.16152	0.65455	0.69444
3	0.33333	0.34675	0.36035	0.37411	0.38803	0.40211	0.41635	0.43798	0.47473	0.51230
4	0.25000	0.26262	0.27549	0.28859	0.30192	0.31547	0.32923	0.35027	0.38629	0.42344
5	0.20000	0.21216	0.22463	0.23740	0.25046	0.26380	0.27741	0.29832	0.33438	0.37184
6	0.16667	0.17853	0.19076	0.20336	0.21632	0.22961	0.24323	0.26424	0.30071	0.33882
7	0.14286	0.15451	0.16661	0.17914	0.19207	0.20541	0.21912	0.24036	0.27742	0.31634
8	0.12500	0.13651	0.14853	0.16101	0.17401	0.18744	0.20130	0.22285	0.26061	0.30040
9	0.11111	0.12252	0.13449	0.14702	0.16008	0.17364	0.18768	0.20957	0.24808	0.28876
10	0.10000	0.11133	0.12329	0.13587	0.14903	0.16275	0.17698	0.19925	0.23852	0.28007
11	0.09091	0.10218	0.11415	0.12679	0.14008	0.15396	0.16842	0.19107	0.23110	0.27349
12	0.08333	0.09156	0.10655	0.11928	0.13270	0.14676	0.16144	0.18148	0.22526	0.26845
13	0.07692	0.08812	0.10014	0.11296	0.12652	0.14078	0.15568	0.17911	0.22062	0.26454
14	0.07143	0.08260	0.09467	0.10758	0.12130	0.13575	0.15087	0.17469	0.21689	0.226150
15	0.06667	0.07783	0.08994	0.10296	0.11683	0.13147	0.14682	0.17102	0.21388	0.25912
16	0.06250	0.07365	0.08582	0.09895	0.11298	0.12782	0.14339	0.16795	0.21144	0.25724
17	0.05882	0.06997	0.08220	0.09544	0.10963	0.12466	0.14046	0.16537	0.20944	0.25576
18	0.05556	0.06670	0.07899	0.09236	0.10670	0.12193	0.13794	0.16319	0.20781	0.25459
19	0.05263	0.06378	0.07614	0.08962	0.10413	0.11955	0.13576	0.16134	0.20646	0.25366
20	0.05000	0.06116	0.07358	0.08718	0.10185	0.11746	0.13388	0.15976	0.20536	0.25292
25	0.04000	0.05122	0.06401	0.07823	0.09368	0.11017	0.12750	0.15470	0.20212	0.25095
30	0.03333	0.04465	0.05783	0.07265	0.08883	0.10608	0.12414	0.15230	0.20085	0.25031
40	0.02500	0.03656	0.05052	0.06646	0.08386	0.10226	0.12130	0.15056	0.20014	0.25003
50	0.02000	0.03182	0.04655	0.06344	0.08174	0.10086	0.12042	0.15014	0.20002	0.25000
100	0.01000	0.02320	0.04081	0.06018	0.08004	0.10001	0.12000	0.15000	0.20000	0.25000
∞		0.02000	0.04000	0.06000	0.08000	0.10000	0.12000	0.15000	0.20000	0.25000

Note: For interest rates i from 0% to 25% and for periods of analysis n from 1 to 100 years.

where

Q_t is the electricity generated by the system (kWh) in year t (or the energy savings from conservation measures), calculated by the performance model based on weather data and system performance parameters

N is the analysis period in years

C_t is the after-tax cash flow in the year t , equal to state tax savings + federal tax savings + performance-based incentives – operating costs – debt total payment + energy value in the project cash flow

LCOE can use the real discount rate or the nominal discount rate. Substituting Equation 2.10, we can calculate the LCOE in terms of the total lifecycle cost (TLCC):

$$\text{LCOE} = \frac{\text{TLCC}}{\sum_{t=1}^N \left(Q_t / (1+i)^t \right)} \quad (2.19)$$

Note that, if the system energy output, Q_i (or the energy savings), is constant over the time of analysis, the relation for LCOE simplifies to

$$\text{LCOE} = \left(\frac{\text{TLCC}}{Q} \right) \times \text{CRF} \quad (2.20)$$

where Q is the annual energy output or energy saving in the case of a conservation system. This form of the equation illuminates the term “levelized cost” as the CRF takes the TLCC of the project and distributes it as uniform annual cost over the project lifetime.

Using the data from Example 2.2, and assuming that the system produces 120,000 kWh per year, the uniform capital recovery factor for $i' = 0.12$ and $t = 5$ is 0.277 and, therefore, the nominal LCOE is

$$\text{LCOE} = (\$15,091 / 120,000) \times 0.277 = \$0.0348 / \text{kWh}$$

The next example illustrates the LCOE estimate for a conservation measure.

EXAMPLE 2.6

Calculate the TLCC and LCOE for replacing a 75 W incandescent light bulb with a 40 W fluorescent bulb. Assume that the incandescent bulb operates 6 h per night and needs to be replaced every year at a cost of \$1.00, while the fluorescent bulb lasts for 5 years with an initial cost of \$15. The cost of electricity over this period is \$0.08/kWh. Assume a discount rate of 12%.

Solution

The yearly energy requirement for the incandescent lamp is 164 kWh, while the 5-year discounted O&M cost, that is, the total discounted cost of annual replacement, is

$$\$1 \left[1 + \left(\frac{1}{1.12} \right) + \left(\frac{1}{1.12} \right)^2 + \left(\frac{1}{1.12} \right)^3 + \left(\frac{1}{1.12} \right)^4 \right] = \$4.03$$

The discounted cost of electricity at the end of the first year is

$$\text{Cost of Electricity} = \frac{164 \text{ kWh}}{\text{year}} \times \frac{\$0.08}{\text{kWh}} \times \left(\frac{1}{1.12} \right)^1 = \$11.71$$

The following table shows the discounted cost of electricity after every year and the total discounted cost of electricity assuming that the electricity is paid at the end of each year.

75 W Incandescent Light Bulb						
Year	1	2	3	4	5	Total
Cost of electricity	\$11.71	\$10.46	\$9.34	\$8.34	\$7.44	\$47.29

The TLCC for the incandescent light bulb can now be calculated to be

$$\text{TLCC} = \$4.03 + \$47.29 = \$51.32$$

The 40 W fluorescent bulb will require 87.6 kWh per year. The discounted electric power cost is \$25.26 if the electricity is also paid at the end of each year. The following table shows the same information as the earlier table, but for the fluorescent bulb.

40 W Fluorescent Light Bulb						
Year	1	2	3	4	5	Total
Cost of electricity	\$6.26	\$5.59	\$4.99	\$4.45	\$3.98	\$25.26

Therefore, the TLCC for the fluorescent light bulb is

$$\text{TLCC} = \$15 + \$25.26 = \$40.26$$

Thus, the net 5-year savings is \$11.06 and the CRF from Table 2.9 is 0.277. Hence, the levelized cost of the saved energy is

$$\text{LCOE} = \frac{\$11.06}{76.4 \text{ kWh}} \times 0.277 = \$0.04/\text{kWh}$$

Note that LCOE for an energy conservation measure should be based on the incremental costs and savings for the system over the analysis period.

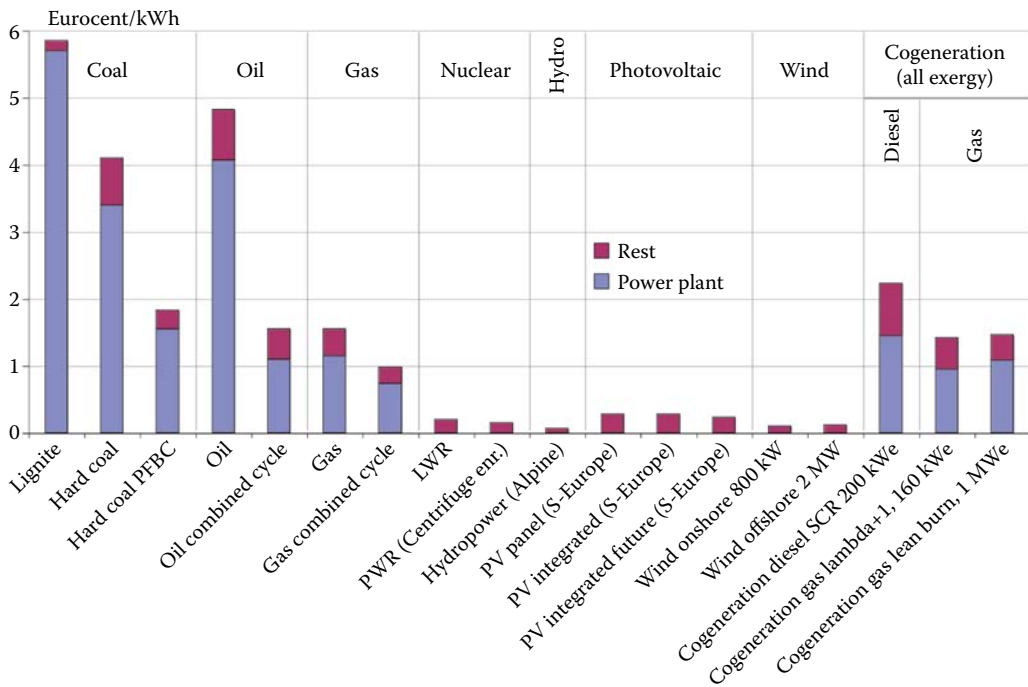
More extensive economic analyses, including taxes, incentives, depreciation, and salvage value, are presented in [2].

2.9 Societal and Environmental Costs

The use of conventional technologies, such as coal-fired power plants, to generate electricity creates environmental degradation and societal costs that are usually considerably higher than those from most renewable technologies. These hidden costs are called *externalities* and are not included in conventional energy economics. Externalities are defined as “an activity of one agent (for example, an individual or an organization, such as a company) that affects the well-being of another agent and occurs outside the market mechanism” [3]. Many different studies have estimated external costs of providing energy. The results vary widely, because they depend on many factors that are difficult to pinpoint. For example, what is the appropriate discount rate for long-term effects? How does one assign a monetary value to items such as human health or life? How does one treat the effects of global warming?

A representative set of external cost estimates for electricity systems is shown in Figure 2.2 [4]. The estimates are from the European Commission’s Externalities of Energy (ExternE) project [5]. The project provides a systematic method for estimating external costs for a range of electricity, heating, and transportation technologies. ExternE focuses on effects of air pollutant emissions, including human health effects and effects on crops, materials, and climate. Results in Figure 2.2 are representative of European electricity systems in the late 1990s. For coal, the external costs are estimated at about 6 cents per kWh. Forty to fifty percent of the costs are from climate change, with the balance mainly from premature mortality associated with particulate air pollution. A methodology for evaluating the economic cost of the environmental impacts of energy generation is presented in [6].

For the United States, a 2010 study by the National Research Council [3] found average external costs of coal-fired electricity generation of 3.2 cents per kWh, accounting only

**FIGURE 2.2**

External costs (€/MWh) of current and more advanced electricity systems associated with emissions from the operation of the power plant and the rest of the fuel-supply chain (EU, 2005). “Rest” is the external cost related to the fuel cycle (1 € = 1.3 US\$ approximately). (Reprinted from IPCC, 2007. *Climate Change 2007: Mitigation. Contribution of Working Group III to the Fourth Assessment Report of the Inter-governmental Panel on Climate Change*, in: Metz, B. et al. (eds.), Cambridge University Press, Cambridge, UK. [4])

for conventional air pollutant effects, not global warming. Across the population of coal-fired power plants in the United States, these costs varied from 0.19 to 12 cents per kWh, depending on control technology and location relative to surrounding population. For comparison, residential electricity prices in the United States in 2010 averaged about 12 cents per kWh [7]. For conventional gasoline-fueled passenger vehicles, the same study [3] estimated that external health costs of air pollution (not considering climate change) average 1.3 cents per mile traveled, with a range from 0.3 to 5 cents per mile. Again, for comparison, at \$3/gallon of gasoline, fuel costs for a car getting 27 miles per gallon would be about 10 cents per mile.

The major societal cost of renewable technologies comes from building the equipment necessary for the energy conversion. Once built, with the exception of biomass, and to a certain degree, hydro reservoirs and noncondensable gases from geothermal, renewable energy technologies do not emit polluting gases into the atmosphere. Burning biomass does not increase the concentration of CO₂ in the atmosphere from fossil sources, because an approximately equivalent amount of CO₂ is absorbed in growing the feedstock. However, upstream processes of harvesting and transporting biomass normally do involve fossil fuel combustion. The key goal for biomass utilization is either to grow the feedstock in a sustainable manner that does not impact food production or to utilize waste products such as wood chips or wood industry wastes from sustainably managed forests.

PROBLEMS

- 2.1 What is the present value of a \$10,000 payment in 2015 if the discount rate is 7%?
- 2.2 Repeat the previous problem in constant dollars for the \$10,000 payment if the inflation rate is 4%/year.
- 2.3 Calculate the annual payments for a solar system whose initial extra cost is \$10,000. Assume that the interest rate is 8% and the mortgage term is 15 years.
- 2.4 Assuming that the price of fuel is \$5.00/GJ and is increasing at a rate of 4%/year while the discount rate is 6%, calculate the equivalent levelized price over 20 years.
- 2.5 A home buyer obtains a mortgage of \$100,000 at an interest rate of 8% over 20 years. Estimate the annual payments to repay this loan.
- 2.6 A rooftop solar hot water heater with collector areas of 8 m² and storage of 640 L is installed in Phoenix, Arizona, on a house that uses 160 L/day of hot water at 60°C. Of the total energy required, 70% is supplied by solar energy (the solar fraction is 70%) and 30% is supplemented with an electric heater. The solar system costs \$3000 for installation, whereas an electric water heater and tank for the same supply costs \$800 for installation. Assuming that the electricity cost is \$0.10/kWh and does not change over time, estimate the simple payback time for the solar hot water heater. The temperature of the water in the main from which it is to be heated is 10°C.
- 2.7 Repeat the previous problem, but assume that the cost of installation is to be repaid at 7% interest over 15 years and that the electricity costs escalate at 10% per year. Compare the NPV of the solar system in Problem 2.6 to that of an electric heating system over a 15-year period, then discuss whether or not the solar system is a good investment relative to the payback time. Also prepare a spreadsheet showing the NPV for each year.
- 2.8 Repeat the previous problem, but assume that the cost of the equipment is reduced from a government grant by 20%.
- 2.9 Compare the capital costs and the levelized costs of operation for a 1000 MW nuclear power plant and a 1000 MW PV system constructed in the Mojave Desert in California. The PV system is to use thin film technology currently available. Neglect the cost of nuclear fuel. Comment on environmental impact and availability of water.
- 2.10 A solar system is to be installed in Phoenix, Arizona. The estimated amounts of energy from the system as a function of collector area are shown in the following tabulation. If the solar system costs \$195/m² and is to be paid off over 25 years at 10% interest, prepare the total cost curve and specify the cost optimal system. Assume that the backup fuel is fuel oil at \$7/GJ and that the fuel price is inflating at 8%/year. The total energy demand for which the solar system is constructed is estimated to be 1000 GJ/year.

Collector Area (m ²)	Energy Delivered (GJ)
100	336
150	444
200	531
250	612

Continued

Collector Area (m ²)	Energy Delivered (GJ)
300	673
400	791
500	856
600	915

- 2.11 Calculate and tabulate the annual cash flows associated with a solar system for a 10-year period of analysis if the initial solar cost is \$6000 and if
- Interest rate = 9%
- Power cost = \$30/year escalating at 10%/year
- Property tax = 0
- Income tax bracket = 32%
- Maintenance = 0.5% of the capital per year (escalating at 10%/year)
- Scrap value = 50% of initial cost
- If the solar system saves \$550/year in conventional fuel (escalating at 10%/year), is it cost-effective? Work the problem in current dollars.
- 2.12 Compute the annual payment of a self-amortizing loan for the solar system with the characteristics tabulated as follows:

Factor	Specification
Expected system lifetime t (year)	20
Effective interest rate (%)	8
Collector area A_c (m ²)	20
Collector cost (\$/m ²)	100
Storage cost (\$/m ²)	6.25
Cost of control system (\$)	100
Miscellaneous costs (e.g., pipes, pumps, motors, heat exchangers) (\$)	$200 + (5A_c)$

- 2.13 If the initial extra cost of a solar system is \$5000, what are the annual payments of a self-amortization loan if the interest rate is 12%, the inflation rate is 4%, and the mortgage term is 15 years?
- 2.14 A factory uses 700 40 W standard fluorescent lamps for its lighting. The lamps are to be replaced by 34 W high-efficiency lamps that can operate on the existing standard ballasts. The standard and high-efficiency fluorescent lamps cost \$1.80 and \$2.50 each, respectively. The factory operates 3000 h/year, and all of the lamps operate during that period. Assuming the unit cost of electricity is 6 cents/kWh and the ballasts consume 10% of the rated power of the lamps, calculate how much energy and money will be saved as a result of switching to the high-efficiency fluorescent lamps. Then, estimate the PP assuming an interest rate of 6% and an inflation rate of 3%. Finally, calculate the levelized cost of the saved energy assuming the lamps last for 2 years.
- 2.15 The hallways of a university are lit by 40 fluorescent lights, each containing two lamps rated at 60 W each. The lights are on all day and night during the year, but the building is only used from 7 a.m. to 7 p.m. 5 days per week during the

year. If the price of electricity is 7 cents/kWh, estimate the amount of energy and money that could be saved by installing two motion sensors that turn off the lights when the building is not being used. Then, estimate the simple payback and the payback with a 6% effective interest rate if the price of a sensor is \$50 and the cost of installation is \$40.

- 2.16 Estimate the levelized cost of electricity in \$/kWh for a new natural gas fired power plant that has an initial capital cost of \$700 million, an expected lifetime of 35 years, and will produce 1.2 billion kWh/year of electricity. Assume there will be no salvage value or decommissioning costs. Total operating costs are \$20 million per year. The power plant developer needs a 12% rate of return to cover financing costs and the expected profit on the investment.

References

1. Rueg, R.T., 1994. Economic methods, in: Kreith, F. and West, R.E. eds., *CRC Handbook of Energy Efficiency*, Chapter 3, CRC Press, Boca Raton, FL.
2. Tester, J.W., Drake, E.M., Golay, M.W., Driscoll, M.J., and Peters, W.A., 2005. *Sustainable Energy: Choosing among Options*, MIT Press, Cambridge, MA.
3. National Research Council Committee on Health, Environmental, and Other External Costs and Benefits of Energy Production and Consumption, 2010. *Hidden Costs of Energy: Unpriced Consequences of Energy Production and Use*. The National Academies Press, Washington, D.C.
4. IPCC, 2007. *Climate Change 2007: Mitigation. Contribution of Working Group III to the Fourth Assessment Report of the Inter-governmental Panel on Climate Change*, in: Metz, B., Davidson, O.R., Bosch, P.R., Dave, R., and Meyer L.A. eds., Cambridge University Press, Cambridge, UK.
5. European Union, 2005. Externalities of energy: Extension of accounting framework and policy applications (Extern E-Pol). Final report of project, http://www.externe.info/externe_2006/expoltec.pdf, last accessed May 20, 2016.
6. Rabl, A. and Spadaro, J.V., 2007. Environmental impacts and cost of energy, in: Kreith, F. and Goswami, D.Y. eds., *CRC Handbook of Energy Efficiency and Renewable Energy*, Chapter 4, CRC Press, Boca Raton, FL.
7. Energy Information Administration, *Electric power monthly: Average price of electricity to ultimate consumers*, https://www.eia.gov/electricity/monthly/epm_table_grapher.cfm?t=epmt_5_3.



Taylor & Francis

Taylor & Francis Group

<http://taylorandfrancis.com>

3

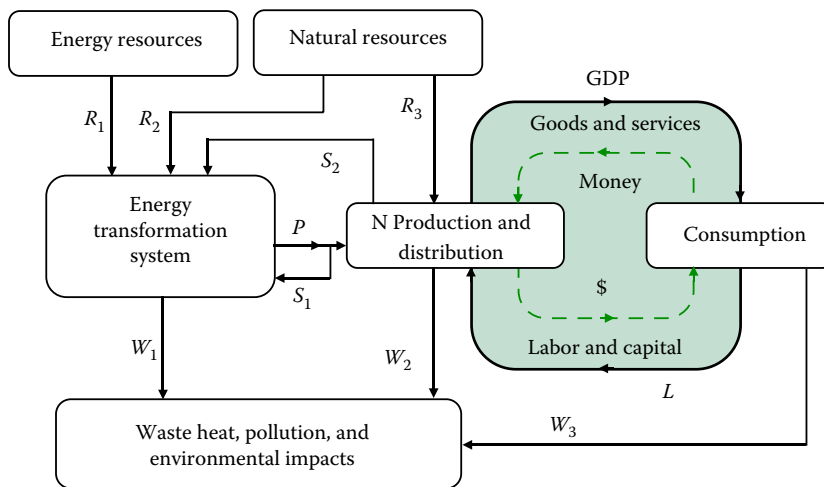
Energy Systems Analysis Methodologies

The objective of energy systems analysis is to understand the energy production and supply system and the relationships to consumer energy and to the economy. Energy systems analysis is necessary to identify and evaluate sustainability issues and potentially beneficial developments. [Figure 3.1](#) demonstrates the flow of energy and the flow of money through the economy. Money, created and circulated in the economy, is not subject to any physical constraints. In contrast, the energy and resources supplied to the economy by energy transformation systems and the associated environmental impact are subject to both technological and resource constraints. For the development of sustainable energy systems, it is important to evaluate the potential of a proposed energy production system to substitute for fossil fuels. It is also important to evaluate the adaptive potential of the end use and the upstream effects of demand. The energy provided to the end user has to be “economical,” meaning that it has to be priced at an acceptable market price, but must also cover the total production cost including any waste disposal or emissions costs.

[Figure 3.1](#) can be used to conceptualize the entire energy system or one particular subsystem. The definitions listed below the figure can be calculated on an annual, unit, or cumulative basis. Some common characterizations of the energy and resource flows are given in [Table 3.1](#). A flow of energy consumed by an energy transformation plant (S_1) can be measured in mass, volume, or the heating value. A flow of capital equipment, (S_2) can be measured in dollars or embedded energy. Production (GDP) can be measured in units of goods or dollars or embedded energy or resources according to the objective of the analysis.

3.1 Life Cycle Approach

[Figure 3.1](#) implies an approach to energy systems analysis that considers the full life cycle of a product or service, starting from raw material extraction and processing through to disposal, reuse, or recycling at the end of the useful life. [Figure 3.2](#) depicts this in a conventional “cradle to grave” format [1]. A life cycle perspective is useful in assessing and comparing economic costs of competing energy technologies or projects and in characterizing their physical attributes, including the use of fossil fuels and other resources and environmental impacts on the biosphere, land, air, and water. Environmental life cycle assessments (LCA) systematically inventory the energy and material requirements that go into producing a product (such as electricity) along with the environmental discharges and wastes requiring disposal, reuse, or recycling. Depending on the scope, LCAs may assess impacts on resource use, air and water quality, climate, or human and ecosystem health. Using a life cycle perspective helps avoid unintended consequences of alternatives that might appear favorable in their direct use phase, but could cause harmful impacts upstream or at the point of disposal. Life cycle approaches are also valuable for helping

**FIGURE 3.1**

Schematic of the flows of energy, resources, goods, and money through the economy. R_i are the flows of primary energy and natural resources, P is the consumer energy produced for sale into the economy, S_1 is the energy (electricity or fuel) needed to run the energy transformation system, and S_2 is the embodied energy in equipment and materials needed to extract and process energy. N is the net energy to the economy, GDP refers to dollar or unit values of products and services, L includes the units of labor and investment or taxes, and W_i are the waste flows.

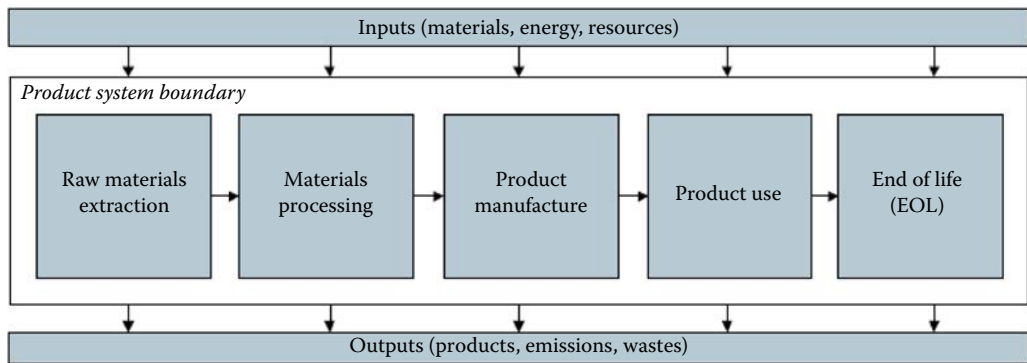
identify opportunities for reducing energy or resource use or minimizing environmental or health impacts.

Some life cycle assessments reach beyond primary inputs and discharges that directly contribute to making, using, or disposing of a product, to include secondary inputs and outputs that contribute to making or doing something in the supply chain that supports the product of interest. For example, an expanded LCA for electricity generation from wind could go beyond accounting for energy and materials required to manufacture and install

TABLE 3.1

Indicators of Energy and Resource Characteristics of the Economy, a Particular Sector, or a Particular Subsystem Using the Structure in [Figure 3.1](#)

Indicator	Parameters	Example
Energy conversion efficiency	$\eta_c = P/R_1$	MWh _e /ton coal
Energy resource intensity	P/R_2	Gal ethanol/gal water
Energy intensity of the economy	P/GDP	kWh/\$
Energy return on energy invested	$\text{EROI} = P/(S_1 + S_2)$	MJ/MJ
Embedded energy	R_1/GDP	MJ/kg steel
Net energy to the economy	$N = P - (S_1 + S_2)$	GWh electricity or GJ fuels
Externality loading of conversion	W_1/P	Ton-CO ₂ /MWh
Lifecycle assessment	$\Sigma R/\text{GDP}$	Resources/unit good or service
External costs	$\Sigma W/\text{GDP}$	Impacts/unit good or service
Impact footprint	W/GDP	Carbon footprint
Levelized cost of energy	$\text{LCOE} = \Sigma S + \Sigma R + W_1$	Annualized investment cost
Energy prosperity	$N/P = 1 - 1/\text{EROI}$	Rate of return on energy

**FIGURE 3.2**

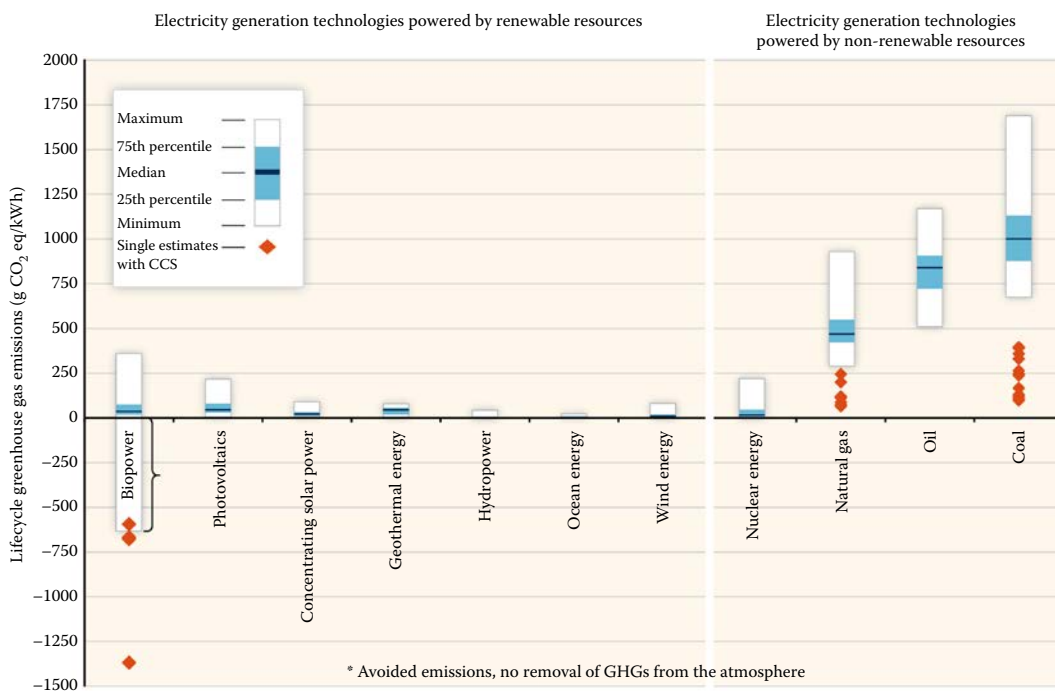
Cradle-to-grave depiction of a product lifecycle. (From U.S. Environmental Protection Agency, April 2003. *Application of Life Cycle Assessment to Nanoscale Technology: Lithium-Ion Batteries for Electric Vehicles*, EPA 744-R-12-001. [1])

a wind turbine and also consider the upstream energy and materials required to construct the equipment needed to manufacture the turbine. Extending in a different direction, “consequential” LCA studies examine how a new product or technology might alter energy and resource flows beyond those associated with its direct use, by displacing or enabling other products or technologies. Because LCA studies could theoretically extend without limit in many directions, analysts must give careful consideration to choosing the study scope and boundaries, and must clearly articulate these choices.

The International Organization for Standardization has developed standards for conducting environmental LCA, which are published as ISO 14040:2006 [2] and 14044:2006 [3]. The standards detail four key steps to LCA: (1) goal definition and scoping, (2) conducting a life cycle inventory of energy and material inputs and outputs, (3) assessment of the impacts associated with the energy and material flows, and (4) interpretation. The standards emphasize careful selection of a functional unit for the assessment, which should be chosen so that two alternative ways of delivering the same function can be compared on equal footing. For electricity generation technologies, MWh of electricity is a common functional unit; for freight shipping, an appropriate unit might be ton-km moved. For studies that will be used to make public statements comparing alternatives, the standards also emphasize the importance of full documentation of the data collection process, setting and adhering to data quality specifications, and peer review of the assessment.

Figure 3.3 shows estimates of life cycle greenhouse gas emissions for a range of electricity generating technologies that were compiled from hundreds of individual LCA studies published in the literature [4]. The central or median estimate for each technology is indicated by the heavy black bar and shows the significant advantage that renewable electricity technologies have over fossil fuels on a life cycle basis. For coal, oil, and natural gas, the majority of emissions come from combustion of the fuel in the power plant. For the renewable technologies, life cycle greenhouse gas emissions are much lower than for fossil fuels but are not zero, due to emissions associated with other stages in the life cycle, including equipment manufacturing, installation, maintenance, and decommissioning.

Material and energy inventories required for LCA can be done using “bottom-up” process chain analysis (PCA) (also known as process flow analysis), or “top-down” input/output modeling (I/O), or a hybrid of the two. These approaches are briefly described in Sections 3.2 and 3.3, respectively. Matthews et al. [5] provide an excellent introduction to life cycle



Count of estimates	222(+4)	124	42	8	28	10	126	125	83(+7)	24	169(+12)
Count of References	52(+0)	26	13	6	11	5	49	32	36(+4)	10	50(+10)

FIGURE 3.3

Estimates of lifecycle GHG emissions (g CO₂eq/kWh) for broad categories of electricity generation technologies, plus some technologies integrated with CCS. Land-use related net changes in carbon stocks (mainly applicable to biopower and hydropower from reservoirs) and land management impacts are excluded; negative estimates for biopower are based on assumptions about avoided emissions from residues and wastes in landfill disposals and co-products. References and methods for the review are reported in Annex II of reference [4]. The number of estimates is greater than the number of references because many studies considered multiple scenarios. Numbers reported in parentheses pertain to additional references and estimates that evaluated technologies with CCS. Distributional information relates to estimates currently available in LCA literature, not necessarily to underlying theoretical or practical extrema, or the true central tendency when considering all deployment conditions. Note 1. “Negative estimates” within the terminology of lifecycle assessments presented in this report refer to avoided emissions. Unlike the case of bioenergy combined with CCS, avoided emissions do not remove GHGs from the atmosphere. (From Sathaye, J. et al., 2011. Renewable energy in the context of sustainable development, in: Edenhofer, O. et al. (eds). *IPCC Special Report on Renewable Energy Sources and Climate Change Mitigation*, Cambridge University Press, Cambridge, UK. [4])

assessment that covers the bottom-up, top-down, and hybrid approaches in more detail. They also provide information on both free and commercial databases and software tools for conducting LCA. As a starting point for LCA studies, the Green Design Institute at Carnegie Mellon provides a free web-based Economic Input–Output Life Cycle Assessment tool that is useful for screening analyses at <http://www.eiolca.net>. The National Renewable Energy Laboratory (NREL) provides a free U.S. Life Cycle Inventory (LCI) database that covers commonly used materials, products, and processes and can be accessed at <http://www.nrel.gov/lci>.

3.2 Process Chain Analysis

Process chain analysis (PCA) is basic tool that can be used for auditing any system or subsystem of a production process or product life cycle. The purpose of process chain analysis is to take account of the energy and resources needed and the waste produced over the different production steps. The PCA approach is used in environmental LCA, embedded energy calculations, supply chain analysis, EROI calculations, and many other types of analysis. PCA can be used to provide conceptual understanding or to calculate specific energy and material flows and costs. In process chain analysis, the production steps are separated, and for each of them, the relevant inputs and outputs are identified and evaluated according to the specific goals of the analysis.

Figure 3.4 shows a schematic of the PCA method. The individual, sequential steps or unit operations in a process are separated out, and all inputs and outputs are identified for each process in the sequence. Inputs and outputs include the product as it is transformed, the utilities, U, services, S, materials, M, and equipment, E, that are required for production, as well as possibly joint products, JP, and other outputs, OO. A PCA can be done for any part of a process chain, for example from natural resources, R, to consumer products, P, or the PCA can be done for the whole life cycle through the steps of consumer end use and disposal.

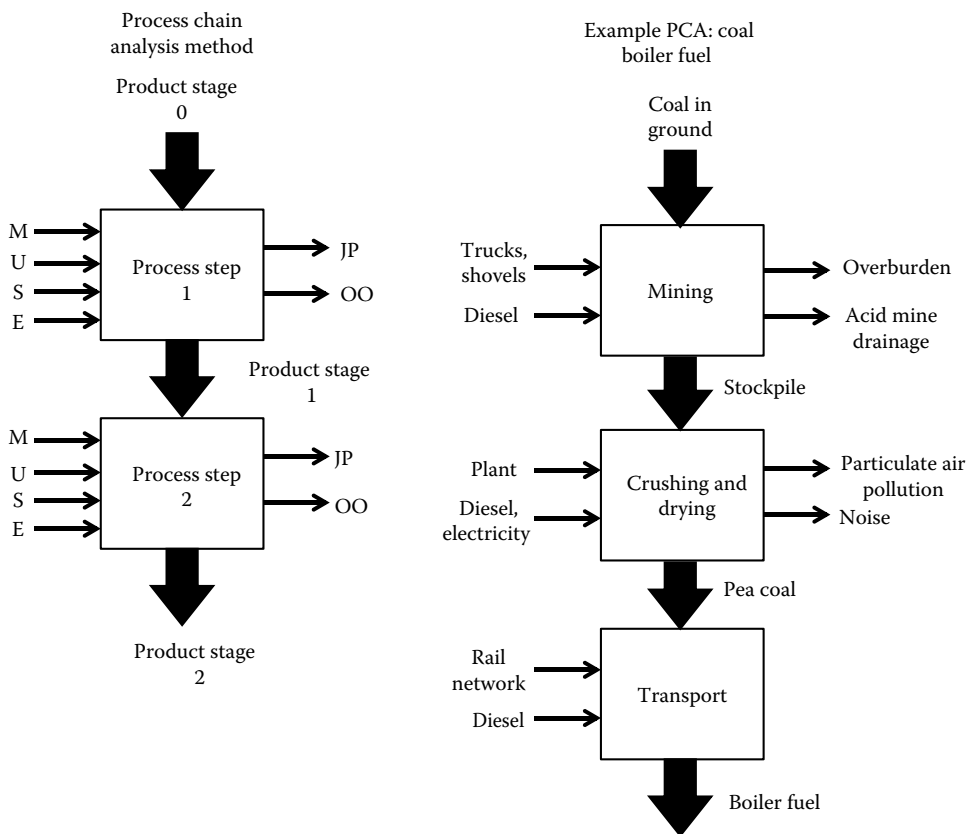


FIGURE 3.4

Illustration of the concept of process chain analysis (PCA) with an example of qualitative assessment of the transformation of coal deposits to delivered pea coal boiler fuel.

The example shown for coal fuel production could be compared to the product chain for an alternative fuel like wood. Depending on the regional locations and the grade of coal, the PCA analysis may be helpful in understanding the energy penalty in gathering wood from a plantation, chipping and drying, and transporting a fuel with nominally half the energy density as coal. If no rail network is available to transport wood regionally, the way there is for coal, more diesel fuel might be needed to transport wood than would be needed for coal. This hypothetical illustrates how even a basic conceptual PCA can help to inform energy system investments and policy.

In PCA applications that take a life cycle approach, such as environmental LCA or net energy assessments such as EROI, the PCA approach depicted in Figure 3.4 is conventionally extended to the point that key inputs and outputs can be expressed as “elementary” flows [5]. Elementary inputs are defined as material or energy entering the system that has been drawn from the environment without previous human transformation (e.g., groundwater from an aquifer or coal in the ground). Elementary outputs are wastes released to the environment that will not undergo subsequent human transformation (e.g., CO₂ emissions). These flows would then be expressed in elementary units of energy or mass of material.

Whether in terms of elementary flows or intermediate products like electricity, evaluating the relevant inputs and outputs for each step of the process can be tedious and complicated if exact figures for a sector or specific product are desired. When PCA is used to evaluate hypothetical systems, assumptions must be made about possible technologies where none actually exists for reference. The results can vary widely depending on the assumptions made. PCA can be used to determine embedded energy for materials and products. Figure 3.5 illustrates a PCA for primary aluminum production [6]. For details of the assumptions and possible pitfalls, the reader is referred to [7]. The NREL LCI database mentioned above and

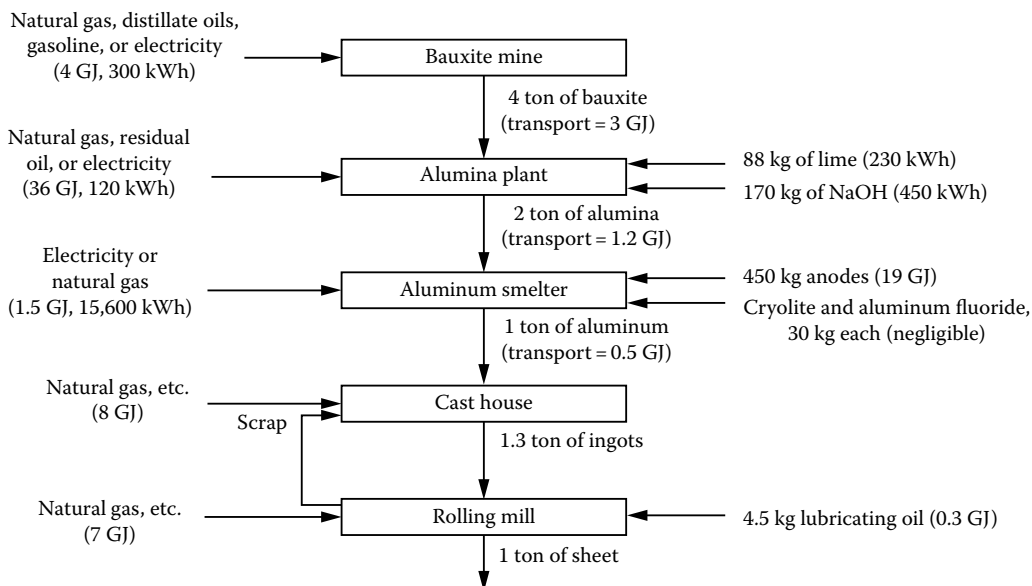


FIGURE 3.5

Quantitative PCA analysis of the energy use in the production of primary aluminum. (From Boercker, S.W., 1978. Energy use in the production of primary aluminum, ORAU/IEA-78-14, Oak Ridge Associated Universities, Oak Ridge, TN. [6])

other databases described in [5] provide PCA data on material and energy requirements for thousands of finished and intermediate products and unit processes. These databases are excellent starting points for assembling PCA data for screening purposes and assessing whether a particular intermediate or unit operation warrants further study.

3.3 Input–Output (I/O) Analysis

Economists use input–output (I/O) analysis of money flowing through the economy to characterize the effect of production in one sector on the production in other sectors. Industries use the products of other industries to produce their own products that are in-turn used by the other industries. In keeping with a life cycle approach to sustainability, it can be critical to account for these supply chain dependencies in considering the resource, energy, and material consequences of alternative products or technologies.

The results of a simple hypothetical input–output analysis can be highly instructive for illustrating the “blow-up” result of the production chain loops between sectors. For example, consider a simple two-sector economy that produces steel and coal. Let’s say it takes 3 tons of coal to make a ton of steel and that the direct steel requirement for the mining, crushing, and transportation of coal is 0.2 tons of steel per ton of coal. Assume the final demand for coal in the economy is 1000 tons and for steel is 10 tons. In order to make the steel for the final demand, along with that for the coal mining, we actually need to produce $10 + (1000)(0.2) = 210$ tons of steel. But, making that extra 200 tons of steel takes 600 tons of coal. Now that extra coal would require another $(600)(0.2) = 120$ tons of steel, which would in turn require an additional $(120)(3) = 360$ tons of coal. This causal loop of internal production demand is shown in Figure 3.6, together with seven rounds of incremental accounting of the internal demand.

A more convenient way to assess the chain of indirect production requirements is to solve the causal loops mathematically. To do this in our two-input case, consider the following:

- The coal production process produces 1 ton of coal for every 0.2 tons of steel as input
- The steel production process produces 1 ton of steel for every 3 tons of coal as input

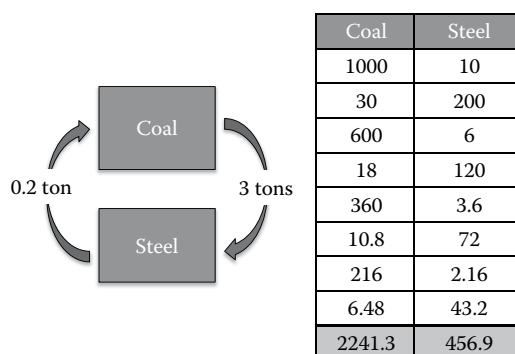


FIGURE 3.6

Causal loop diagram for coal and steel illustrating the “blow-up” effect for the baseline production rates of different sectors in order to produce a unit of output in another sector.

We want to find the total amount of coal and steel needed to produce a net final product of 1000 tons of coal and 10 tons of steel. We define two variables to solve for:

x_1 = total amount of steel in tons that must be produced to achieve the net final product

x_2 = total amount of coal in tons that must be produced to achieve the net final product

The two processes provide us with two linear equations in the two unknowns.

Coal production process:

Amount of coal produced – amount of coal consumed = net coal product

$$x_2 \text{ tons coal} - 3 \text{ tons coal/ton steel} \times x_1 \text{ tons steel} = 1000 \text{ tons coal}$$

or

$$x_2 - 3x_1 = 1000 \quad (3.1)$$

Steel production process:

Amount of steel produced – amount of steel consumed = net steel product

$$x_1 \text{ tons steel} - 0.2 \text{ tons steel/ton coal} \times x_2 \text{ tons coal} = 10 \text{ tons steel}$$

or

$$x_1 - 0.2x_2 = 10 \quad (3.2)$$

Rearranging, the two equations are:

$$-3x_1 + x_2 = 1000 \quad (3.3)$$

$$x_1 - 0.2x_2 = 10 \quad (3.4)$$

To solve these two simple, linear simultaneous equations for the two unknowns, we can use the elimination method. Multiplying the second equation by 3 and adding to the first equation leaves us with a single equation in x_2 only:

$$0.4x_2 = 1030 \quad (3.5)$$

$$x_2 = 2575 \text{ tons coal} \quad (3.6)$$

Inserting the solution for x_2 into either equation and solving for x_1 yields:

$$x_1 = 525 \text{ tons steel} \quad (3.7)$$

For more complex problems, a matrix solution is typically used. Solving this same problem in matrix form [5]:

$$\begin{bmatrix} -3 & 1 \\ 1 & -0.2 \end{bmatrix} \begin{bmatrix} x_1 \\ x_2 \end{bmatrix} = \begin{bmatrix} 1000 \\ 10 \end{bmatrix} \quad (3.8)$$

In generalized matrix notation, this equation has the form $AX = Y$. The square matrix, A , is called the technology matrix. Requirements for steel and coal to produce a specified net output for the economy can be found by replacing the entries in the total demand vector, Y , with the specified amounts, and solving for $X = A^{-1}Y$. In our case, the inverse matrix (which is determined by a method similar to the elimination method used above) is:

$$A^{-1} = \begin{bmatrix} 0.5 & 2.5 \\ 2.5 & 7.5 \end{bmatrix} \quad (3.9)$$

Thus, production of 1000 tons of coal for the economy and 10 tons of steel requires:

$$\begin{bmatrix} x_1 \\ x_2 \end{bmatrix} = \begin{bmatrix} 0.5 & 2.5 \\ 2.5 & 7.5 \end{bmatrix} \begin{bmatrix} 1000 \\ 10 \end{bmatrix} = \begin{bmatrix} 525 \\ 2575 \end{bmatrix} \quad (3.10)$$

Thus, for this illustrative example to produce a net 1000 tons of coal and 10 tons of steel requires a total of 2575 tons of coal from the coal production process and 525 tons of steel from the steel production process. Of the total coal produced, $2575 - 1000 = 1575$ tons goes to making steel. Of the total steel produced, $525 - 10 = 515$ goes to making coal. The cumulative causal loop sequence in [Figure 3.6](#) would eventually converge to these values.

The implications of this analysis are interesting. If we just looked at the unit production requirement for steel we might reason that production of 10 tons of steel requires 30 tons of coal. But when the causal loop analysis is taken to the limit with a final demand vector of $Y = \begin{bmatrix} 0 \\ 10 \end{bmatrix}$ we find that the total amount of steel needed is $x_1 = 25$ tons and the amount of

coal needed is $x_2 = 75$ tons. The supply chain contributions of this simple example are exaggerated because of the numbers chosen. Nevertheless, supply chain effects in the economy are important to consider in assessing sustainability.

Following the approach developed by Wassily Leontief in the 1930s, government agencies around the world use economic input–output analysis to characterize the structure of their national economies. The transactions tables used in these analyses are expressed in monetary terms and have tens to hundreds of sectors, with table elements showing the value of inputs to each sector from every other sector that supplies it. In many countries, the tables are developed directly from industry surveys, with periodic updates. The U.S. Bureau of Economic Analysis publishes I/O tables for the United States at http://www.bea.gov/industry/io_annual.htm. To understand these tables, it is useful to know the standard nomenclature, which can again be illustrated with a hypothetical two-sector example, in which corn is an input to make biofuel and biofuel is used in production of corn. The following example and explanation are adapted from a similar example provided for teaching purposes by the Green Design Institute at Carnegie Mellon University [5].

Assume the two-sector economy produces \$155 billion worth of corn, including \$55 billion used in corn production, \$70 billion used in biofuel production, and \$30 billion sold to consumers. The economy produces \$205 billion worth of biofuel, including \$20 billion used in corn production, \$15 billion used in biofuel production, and \$170 billion sold to consumers. In producing corn, farmers add \$80 billion worth of value through their knowledge, labor, and other inputs; similarly, biofuels manufacturers add \$120 billion worth of value through process engineering, labor, and other inputs. The complete transactions table ([Table 3.2](#)) shows all of these exchanges. For a two-sector economy, the direct requirements matrix ([Table 3.3](#)) is a 2×2 matrix that shows the requirements from

TABLE 3.2

Complete Transactions Table (\$ Billions) for Two-Sector Example
Economic Input–Output Analysis

	Corn	Biofuel	Final Demand	Total Output
Corn	55	70	30	155
Biofuel	20	15	170	205
Value added	80	120		
Total Input	155	205		

TABLE 3.3

Direct Requirements Matrix for
Two-Sector Input–Output Analysis

	Corn	Biofuel
Corn	0.355	0.341
Biofuel	0.129	0.073

each sector needed to produce a unit (i.e., one dollar) of output for each sector, and is obtained by dividing the entries in [Table 3.2](#) by the total output for each commodity. In matrix notation, for an economy with n sectors, the requirements matrix A is an $n \times n$ matrix with elements a_{ij} = the amount of output from sector i required to produce a unit of output from sector j .

The value of input–output analysis is that the requirements matrix can be used to calculate not only the direct purchases required to produce a given product, but also the indirect purchases—that is, the corn used to produce the biofuel used to produce the corn, and back through the causal chain. For a given level of total output, Y , the vector of required production throughout the full supply chain, X , can be calculated as:

$$X = [I + A + AA + AAA + \dots]Y \quad (3.11)$$

where I is the identity matrix. It turns out that the geometric series in the brackets has a simple approximation:

$$[I + A + AA + AAA + \dots] = [I - A]^{-1} \quad (3.12)$$

In input–output analysis nomenclature, the matrix $[I - A]^{-1}$ is called the total requirements matrix. It is shown for our case in [Table 3.4](#).

TABLE 3.4

Total Requirements Matrix for
Two-Sector Input–Output Analysis

	Corn	Biofuel
Corn	1.67	0.62
Biofuel	0.23	1.16

With the total requirements matrix in hand, we can determine how production in each sector would need to change to meet additional demand. For example, assume \$30 billion more biofuel is required due to a new policy promoting biofuels over petroleum-based fuels.

$$\begin{bmatrix} x_1 \\ x_2 \end{bmatrix} = \begin{bmatrix} 1.67 & 0.62 \\ 0.23 & 1.16 \end{bmatrix} \begin{bmatrix} 0 \\ 30 \end{bmatrix} = \begin{bmatrix} 18.5 \\ 34.9 \end{bmatrix} \quad (3.13)$$

The new demand would require total outputs, accounting for the full supply chain, of \$18.5 billion more corn and \$34.9 billion more biofuels. In contrast, direct purchases by the biofuels suppliers to produce \$30 billion more biofuel for the market would be \$10.2 billion in corn and \$2.2 billion in biofuels.

As seen above, I/O analysis can be conducted in terms of material flows, as done in process matrix analysis, or in terms of money, as in economic I/O analysis. I/O analysis can also be conducted in terms of energy requirements or environmental burdens such as greenhouse gas emissions. Building on economic I/O analysis, the embedded energy or life cycle environmental impacts of production can be determined as:

$$E = RX \quad (3.14)$$

where E is the vector of energy or environmental effects, X is the vector of required production (in dollars), and R is a square matrix with diagonal elements that represent the energy use or environmental burden per dollar of production in the sector. Carnegie Mellon University's EIO-LCA uses data from the Manufacturing Energy Consumption Survey (MECS) as a main source of data to estimate energy use for the R -matrix for the sectors in their I/O model [5]. Note that when X is calculated using total requirements, E reflects not only the direct energy use or environmental burdens but also accounts for those carried through the full supply chain.

3.4 Embedded Energy

Embedded (or embodied) energy, as calculated through PCA or I/O analysis, is a quantitative measure of the energy cost associated with the processing or supply chain for a material or product. Embedded energy for a product is calculated by using a PCA of all the materials and energy used in the extraction and manufacture. Energy intensity factors (Btu/\$ or kWh/\$) give the energy required to produce or provide a given product or service and are generally determined through economic analysis by looking at the energy use and activity of whole sectors. By quantifying all the energy and dollars flowing into particular sectors, say the steel industry, it is possible to estimate the amount of energy the steel industry uses in the form of energy embodied in all the inputs it purchases from other sectors. The ratio of all such energies to the dollar value of the steel produced is the energy intensity in Btu/dollar or kWh/dollar of steel production purchases from other sectors. The energy intensity factors in Table 3.5 were calculated for an energy-based input-output model of the U.S. economy in 1977 [7,8], and adapted for 2008 dollars [8]. The ratio of 2008's CPI to 1977's CPI is 3.52 [9]. The CPI is a measure of the price of consumer goods and services. The

TABLE 3.5

Embedded Energy in Various Materials and Commodities

Commodity	1977 Values	1977 Values	Adjusted 2008 Values
	Energy Intensity (Btu/\$)	Energy Intensity (kWh/\$)	Energy Intensity (kWh/\$)
Alum castings	70,000	20.5098	6.6821
Air transport	80,846	23.6877	7.7174
Aircraft	21,288	6.2373	2.0321
Aircraft engines	29,238	8.5667	2.7910
Alum rolling	106,723	31.2696	10.1876
Arch metal work	45,552	13.3466	4.3483
Asbestos product	72,140	21.1368	6.8864
Asphalt	184,121	53.9470	17.5759
Auto repair	22,055	6.4621	2.1053
Banking	9,820	2.8772	0.9374
Bearings	42,638	12.4928	4.0702
Blowers	35,077	10.2775	3.3484
Boatbuilding	23,933	7.0123	2.2846
Brass other cast	50,508	14.7987	4.8214
Bricks	127,994	37.5019	12.2181
Canned fruit, vegetable	40,981	12.0073	3.9120
Carbon products	108,949	31.9218	10.4001
Cement	216,631	63.4723	20.6792
Ceramic tile	63,362	18.5649	6.0484
Chem mineral min	128,720	37.7146	12.2874
Clay products	119,323	34.9613	11.3904
Communications	6,887	2.0179	0.6574
Computing mach	21,306	6.2426	2.0338
Concrete blocks	70,374	20.6194	6.7178
Concrete product	50,789	14.8810	4.8482
Const machinery	34,534	10.1184	3.2966
Conveyers	31,042	9.0952	2.9632
Copper mining	86,570	25.3648	8.2638
Copper rolling	70,649	20.7000	6.7440
Doctors, dentists	8,488	2.4870	0.8103
Eat and drink places	23,620	6.9206	2.2547
Elec h'wares	36,919	10.8172	3.5242
Elec ind apparat	31,648	9.2728	3.0211
Elec meas instr	21,561	6.3173	2.0582
Electric lamps	28,390	8.3182	2.7101
Electrical equip	38,118	11.1685	3.6387
Electronic comp	31,502	9.2300	3.0071
Elevators	33,497	9.8145	3.1976
Engine elec eq	29,349	8.5992	2.8016
Fab metal prod	47,163	13.8186	4.5021
Fab struc steel	49,469	14.4943	4.7222

(Continued)

TABLE 3.5 (Continued)

Embedded Energy in Various Materials and Commodities

Commodity	1977 Values	1977 Values	Adjusted 2008 Values
	Energy Intensity (Btu/\$)	Energy Intensity (kWh/\$)	Energy Intensity (kWh/\$)
Fab wire product	71,355	20.9068	6.8114
Farm machinery	32,417	9.4981	3.0945
Fed govt enterp	16,946	4.9651	1.6176
Feed grains	66,423	19.4618	6.3406
Fertilizers	179,710	52.6546	17.1548
Food prod mach	27,346	8.0123	2.6104
For, grhouse, nurs	47,697	13.9751	4.5531
Forest fish prod	43,390	12.7132	4.1419
General ind mach	28,793	8.4363	2.7485
Glass containers	80,487	23.5825	7.6832
Glass products	58,274	17.0741	5.5627
Guided missiles	14,272	4.1817	1.3624
Gypsum products	99,292	29.0923	9.4783
Hardware	38,859	11.3856	3.7094
Heating equip	33,553	9.8309	3.2029
Hoists, cranes	30,233	8.8582	2.8860
Hospitals	23,123	6.7750	2.2073
Hotels	33,939	9.9440	3.2398
Ind controls	23,412	6.8597	2.2349
Indus furnaces	27,255	7.9856	2.6017
Industrial truck	34,245	10.0337	3.2690
Inorg-org chem	171,572	50.2701	16.3780
Int combust eng	31,345	9.1840	2.9921
Ir. stl forging	75,110	22.0070	7.1699
Iron ore mining	92,650	27.1462	8.8442
Light fixtures	37,594	11.0149	3.5887
Lime	235,675	69.0522	22.4972
Local transport	32,804	9.6115	3.1314
Mach shop prod	27,116	7.9449	2.5884
Man-made fibers	123,386	36.1518	11.7782
Manufactured ice	61,718	18.0832	5.8915
Measuring pumps	29,195	8.5541	2.7869
Meat products	42,456	12.4395	4.0528
Meat, animal prod	46,311	13.5690	4.4208
Medical instr	29,339	8.5962	2.8007
Met cutting tool	23,163	6.7867	2.2111
Met forming tool	28,021	8.2101	2.6748
Met working mach	30,373	8.8992	2.8994
Metal stampings	52,502	15.3829	5.0118
Mineral wool	79,474	23.2857	7.5865
Mining machinery	31,541	9.2414	3.0109
Misc bus service	10,000	2.9300	0.9546

(Continued)

TABLE 3.5 (Continued)

Embedded Energy in Various Materials and Commodities

Commodity	1977 Values	1977 Values	Adjusted 2008 Values
	Energy Intensity (Btu/\$)	Energy Intensity (kWh/\$)	Energy Intensity (kWh/\$)
Misc chem prod	95,178	27.8869	9.0855
Misc leather	32,165	9.4243	3.0704
Misc metal work	65,247	19.1172	6.2284
Misc plastics	63,281	18.5412	6.0407
Misc rubber prod	53,271	15.6083	5.0852
Motor transport	29,196	8.5544	2.7870
Motor veh and parts	35,846	10.5028	3.4218
Motor, bicycles	36,373	10.6572	3.4721
Motors, generator	33,556	9.8318	3.2032
NCNST highways	59,333	17.3844	5.6638
NCST dams, resv	44,509	13.0410	4.2488
NCST elect utility	30,648	8.9798	2.9256
NCST gar, srv, sta	38,198	11.1919	3.6463
NCST gas utility	28,039	8.2154	2.6766
NCST indust. bldg	32,103	9.4061	3.0645
NCST railroads	35,264	10.3323	3.3662
Newspapers	30,902	9.0542	2.9499
Nonclay refract	69,607	20.3947	6.6446
Nonfer casting	61,395	17.9886	5.8607
Nonfer forging	64,560	18.9159	6.1628
Nonfer rolling	81,118	23.7674	7.7434
Nonfer wire	66,253	19.4120	6.3244
Nonferr mining	53,225	15.5948	5.0808
Nonmet min prod	56,700	16.6130	5.4125
Oil bearing crop	23,352	6.8421	2.2291
Oil field mach	30,547	8.9502	2.9160
Optical instr	28,458	8.3381	2.7166
Organic fibers	99,470	29.1444	9.4952
Paint products	75,217	22.0384	7.1801
Paperboard cont	64,427	18.8769	6.1501
Paving	181,838	53.2781	17.3580
Personal service	24,405	7.1506	2.3297
Photographic eq	35,148	10.2983	3.3552
Pipe	37,637	11.0275	3.5928
Pipe line transp	67,173	19.6815	6.4122
Plastics	126,087	36.9432	12.0361
Plumb fittings	36,093	10.5752	3.4454
Plumbing fixture	60,760	17.8025	5.8001
Power trans eq	31,596	9.2575	3.0161
Prim nonfer met	109,365	32.0437	10.4398
Primary aluminum	158,201	46.3525	15.1016

(Continued)

TABLE 3.5 (Continued)

Embedded Energy in Various Materials and Commodities

Commodity	1977 Values	1977 Values	Adjusted 2008 Values
	Energy Intensity (Btu/\$)	Energy Intensity (kWh/\$)	Energy Intensity (kWh/\$)
Primary battery	41,578	12.1822	3.9690
Primary copper	112,850	33.0648	10.7725
Primary lead	130,108	38.1213	12.4199
Primary zinc	137,242	40.2115	13.1009
Pumps, compressors	27,731	8.1251	2.6472
Radio, TV sets	24,898	7.2950	2.3767
Railroad	46,041	13.4899	4.3950
Railroad equip	38,825	11.3756	3.7062
Ready-mix concr	80,909	23.7061	7.7234
Real estate	6,525	1.9118	0.6229
Refrig mach	36,589	10.7205	3.4927
Retail trade	19,433	5.6938	1.8550
R-TV commun eq	18,243	5.3452	1.7414
Scien instr	24,659	7.2250	2.3539
Screw mach prod	44,247	12.9643	4.2237
Semiconductors	29,749	8.7164	2.8398
Sheet metal work	56,289	16.4925	5.3733
Shipbuilding	29,048	8.5110	2.7729
St loc govt entr	31,395	9.1987	2.9969
Steel prod	115,724	33.9068	11.0468
Steel springs	59,220	17.3513	5.6530
Stone product	39,667	11.6223	3.7865
Storage battery	69,024	20.2238	6.5889
Switchgear	25,726	7.5377	2.4558
Syn rubber	143,451	42.0308	13.6936
Tanks	39,964	11.7093	3.8149
Temp controls	32,331	9.4729	3.0863
Textile goods	65,964	19.3273	6.2968
Textile mach	31,319	9.1764	2.9897
Tires	55,977	16.4011	5.3435
Trans services	17,678	5.1796	1.6875
Transformers	42,591	12.4791	4.0657
Transport equip	44,317	12.9848	4.2304
Truck, bus bodies	35,634	10.4407	3.4016
Vegt, misc crops	29,798	8.7307	2.8445
Water transport	11,369	3.3311	1.0853
Water, sanit ser	89,974	26.3621	8.5888
Wholesale trade	18,326	5.3695	1.7494
Wiring devices	40,586	11.8916	3.8743
Wood products	52,030	15.2447	4.9667
X-ray equipment	26,598	7.7931	2.5390

data for 2008 *does not* mean that manufacturing has become more energy/cost productive, rather it shows that the same energy investment produces product value in terms of money that is worth less than 30 years earlier. This is a good illustration of the destructive effects of inflationary economic systems. All producers, whether producing dairy products or ingots of aluminum, must continuously expand their production, and thus their energy and resource consumption, in order to even maintain a particular level of income in real terms. Note that [Table 3.5](#) is included here because it provides a convenient and relatively comprehensive listing for use in example exercises. Researchers and practitioners will want to refer to updated embedded (embodied) energy estimates, such as those found in the life cycle databases listed above and in [\[10\]](#).

3.5 Energy Return on Energy Invested

Energy return on energy invested (EROI) is an important concept for sustainable energy engineers to understand and to communicate to the public and policy makers. In terms of the schematic in [Figure 3.1](#), the EROI is given by the equation [\[7,11\]](#):

$$\text{EROI} = P / (S_1 + S_2) \quad (3.15)$$

where P is the rate of energy production (kWh/analysis period) from the transformation system, S_1 is the conversion energy input (kWh/analysis period), and S_2 is the embodied energy in the various items used by the production system (kWh/analysis period). The EROI can be evaluated for the whole energy system in a given year, or it can be assessed for a particular energy production technology over the useful life of the plant. The only reason for building an energy conversion plant (investing embodied energy in capital equipment, S_2) and operating the plant (investing process energy, S_1) is to produce consumer energy for the market (distributing and selling P). The EROI is a measure of the energy profitability of an energy transformation system. Since the energy invested in the transformation system could not be used by the economy, the EROI is also an indication of the availability of energy to meet demand and to provide the surplus needed for maintenance, replacement, and new manufacturing and construction.

The concept of EROI is simple, but exact calculation can be difficult. Companies are not likely to invest in an energy platform with low EROI because it would be bad business. However, misguided government policy and mandates can provide incentives and subsidies for platforms with poor EROI and end up wasting time and money, reducing the overall EROI of the economy, and increasing the risk exposure to supply security issues.

The main point of evaluating the EROI of a given energy supply system is the same as for financial analysis of different investments. EROI lets us compare different energy transformation platforms and make informed investment decisions. The objective of investing is to realize a profit. In the energy system the “profit” for the society as a whole is the net energy. The net energy yield, N , is given by Equation 3.16:

$$N = P - (S_1 + S_2) = P(1 - 1/\text{EROI}) \quad (3.16)$$

The net energy yield can be assessed for a particular energy conversion system or for the sector as a whole. The net energy yield can be evaluated on a year-by-year basis or over the

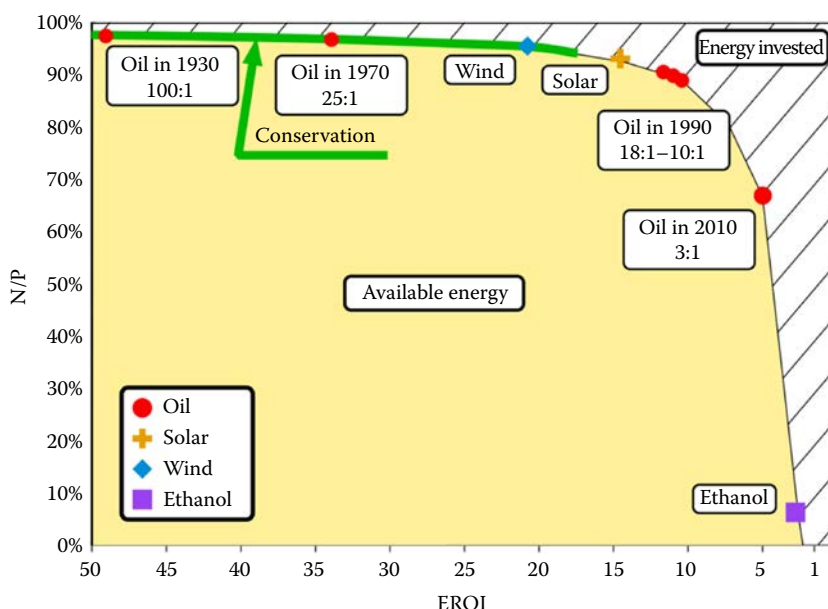
lifetime of the energy conversion plant. On a year-by-year basis, the net energy yield may be negative at the early stage of a power plant, and the point at which the cumulative net energy return reaches zero is also known as the payback period (PP).

In order to understand the importance of EROI and net energy yield for a civilization, we will consider a simple model system of eighteenth-century farming. At this time, more than 85% of all labor would have been engaged in agriculture and primary production. Agriculture was the first energy system developed by people. A preindustrial farm required inputs (S_1) of grains and fodder for animals, plus food for the workers, plus wood for heat and processing. The farm required capital equipment (S_2) such as a plough, farm buildings, a thresher, harnesses, tools, and the equipment for the farmhouse that were also part of the farm system. The production from the farm would be the produce taken to the market to fuel the work of other people and animals in the society or to provide the wood for fuel or the fibers for clothes. A prosperous farm (large EROI) would have high-quality, well-maintained equipment, healthy animals, and wealthy farmers with nice houses. A prosperous farm community would have a town with thriving businesses, civic amenities, schools, police, and so on. A large net “energy” return in the form of plentiful harvest compared to farm inputs means prosperity. A farming community that is not prosperous would have hunger, unemployment, poor civic services, and if the net return is zero, this implies a total failure of the farm economy system because all of the production from the farm was needed just to run the farm.

EROI is the underlying determining factor for prosperity. The astute reader will notice that we have not yet discussed the price of the energy or resources in this discussion. In the areas of primary production such as food, materials, and energy, prosperity is more fundamentally determined by the physical ability to return a positive net product to the economy than by the prices the economy attaches to commodities. In fact, there is an inverse relation between prosperity and price of commodities—scarcity causes price rise for primary goods, but does not result in prosperity as demonstrated in many historical cases, including the energy crisis caused by the OPEC oil embargo.

The implication of low EROI energy investments is demonstrated in [Figure 3.7](#), where the net energy return to the economy as a percentage of the total energy produced, $N/P = 1 - 1/\text{EROI}$, is plotted versus EROI. The ratio N/P is essentially a measure of the prosperity for a society. An N/P of 95% implies that all of the energy and resources used by the energy sector were returned to the economy as useful energy production with a 95% rate of return. An N/P of 50% means that the energy transformation sector consumed half of the resources internally and only returned half to the economy. Inspection of [Figure 3.7](#) shows that once EROI drops below 5, the useful available energy decreases precipitously.

Oil is a good example to consider. We can see that around 1930, EROI was over 80:1 and the surplus energy to the economy was very large. In other words, for 1 Btu invested in finding and producing oil, 80 Btu of oil energy was returned with a rate of return of nearly 99%. By 1956, the EROI had dropped to 25, but the rate of return of 96% was still very favorable. Today, the EROI is below 10 for new oil fields giving a rate of return of 90%. This is still pretty good, but if the liquid fuel sector starts developing tar sands that have an EROI of only 2, then there will still be a rate of return, N/P , of 50%, but this is only half the level of prosperity of conventional oil. This would mean a fuel system based on tar sands would be able to support only half the fuel demand in the economy as conventional oil, even if the tar sand system would have the same production volume as conventional oil. As clearly shown in [Figure 3.7](#), corn ethanol with an EROI less than 2 is not a primary fuel that can provide the same level of prosperity that has been provided historically by oil.

**FIGURE 3.7**

Ratio of net energy to the rate of energy production vs. EROI.

Cross-sector EROI comes into play in electricity generation. Hydroelectricity has the highest EROI of any power generation platform, estimated at over 40 and as high as 100 depending on the site. For example, some hydroelectric facilities can just be built at the natural outlet of a preexisting lake. Most of the hydroelectric dams in the United States were built many decades ago using high EROI diesel fuel (50+) and coal for making the cement and steel (EROI 80+). The water flowing through hydro turbines does not need to be extracted from mines and transported to the power plant, it simply arrives courtesy of weather, geography, and gravity. Areas of the country where hydro generation was built, quickly developed prosperous economies based on plentiful, secure, on-demand electricity. The second highest EROI electricity generation platform is from coal with EROI over 10. Historically, areas of the country with easily extractable coal and navigable waterways also developed prosperous manufacturing and production economies. Today, the energy intensity of primary materials is increasing and the EROI of fuels and electricity is declining. Wind and solar generated electricity have lifetime EROI of 2–60, which is highly dependent on the conversion efficiency, service life, and utilization factor. But manufacture of the wind and solar plant require investment of fossil fuels and energy intensive materials, so renewable energy does not offer an “alternative” to fossil fuels in the way often discussed in the popular media. Reduced fossil fuel use means reduction in net energy to the economy. One way to address this is to invest in renewable energy. But another way to address the situation is to invest in conservation—changing existing energy end-use systems to reduce demand. The EROI for conservation systems has the same definition as for energy production. The “low hanging fruit” conservation investments, such as improving insulation in buildings, have very high lifetime EROI and are also profitable.

3.5.1 Calculation of EROI

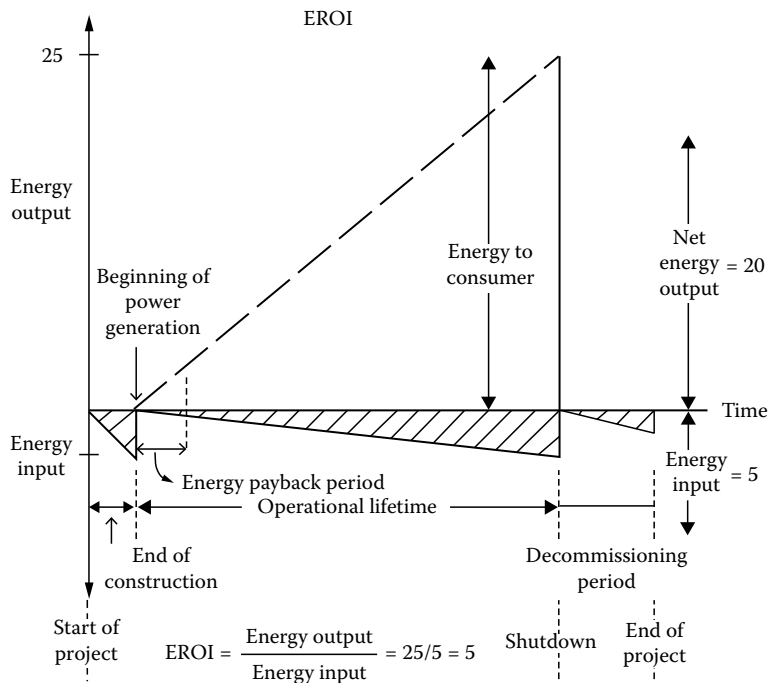
Energy analyses are useful supplements to standard economic procedures based on monetary assessments of costs and benefits for several reasons. All economic analyses require assumptions about the future, such as interest rates, future price of conventional fuels, and inflation rates. Also, assumptions about future government regulation, taxation rates, and political decisions can greatly influence the economic evaluation process. EROI is calculated by putting all inputs and outputs into energetic terms so the evaluation is more straightforward and the result can be interpreted in terms of the general potential for prosperity of the economy.

Researchers and analysts have been increasingly interested in calculating the EROI for different energy platforms. There are different timescales and different assumptions that can be made in the analysis. Determining the embedded energy in the power plant and the exploration and extraction equipment for fossil fuels can be difficult, so back-of-the-envelope calculations using standard embedded energy values for materials and estimates of the weight of the equipment usually provide sufficient accuracy. Another possibility is to use the dollar cost for each item of the energy production system. Then each material input to the entire system is assigned an energy intensity factor from [Table 3.5](#) calculated for the sector that produced the material. The dollar value of the input times its energy intensity is the indirect energy cost of that item. Summing the indirect energy costs for all the items of the system gives the indirect energy cost for the entire energy system. It is also usually necessary to construct a process chain analysis of the energy transformation platform in order to define the energy and materials used for analysis.

In electricity generation from thermal power plants, clarity is needed because the generation is often given in technical data, but the parasitic power uses for pumps and fans represent components of S_1 . If the net power plant output is known, make sure the parasitic losses have been accounted for. In coal and nuclear power plants, the energy content in the fuel is usually not included in S_1 in calculation of EROI, but the consumer energy used to extract and process the fuel should be included. For petroleum, the exploration, drilling, and oil well equipment are included in S_2 , and the thermal energy, pumps, and fans used in refining the petroleum into consumer fuel products is counted in S_1 .

[Figure 3.8](#) illustrates schematically the EROI calculation method for a hypothetical energy transformation system. During the construction phase, 2 units of energy are used to build the system; during its operational life, 2 units of energy are used; finally, 1 unit of energy is used to decommission the system. The energy produced is 25 units and the net energy output for this system is 20 units. Thus, the EROI for this example is 5. In [Figure 3.8](#), the shaded area of energy input during the operational lifetime includes the energy of the fuel input for a fossil or nuclear plant. If this were a renewable that does not require energy to operate and decommission, the EROI would be 12.5.

A key difference between the EROI for fossil or nuclear generating systems and renewable technologies, such as solar or wind, is the fact that the renewable systems depend on a primary energy source that not only varies with time of day and time of year, but also with the location at which the system is deployed. Therefore, the evaluation of the energy produced has to be carried out in considerably more detail for a renewable system than for a fossil or nuclear system. In the following chapters, we will present detailed analytical and experimental methods for estimating the energy output of renewable systems. Here, we will simply specify the capacity factor, U , as well as system lifetime, and multiply the plant capacity by that factor to obtain a time-average value of electricity or heat generation over the lifetime of the system.

**FIGURE 3.8**

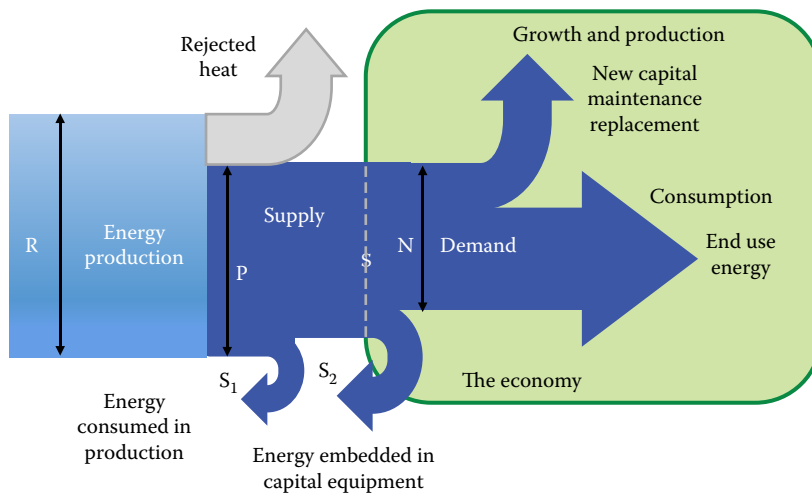
Energy input and output for a renewable energy generation system during its lifetime.

The EROI for conservation measures and waste heat recovery is calculated using the same approach as for energy transformation systems. The energy being wasted or rejected to the environment is treated as a resource like wind or solar, and the energy recovered or saved is treated as the energy production, P .

3.5.2 EROI and Energy Budgets

Energy budgeting is an important tool for planning a sustainable energy future. In an industrial society, a certain amount of energy is necessary to maintain the energy infrastructure, which includes the pipelines and roads for distributing liquid fuel or natural gas, as well as the hydroelectric dams and power plants that generate electricity. The need to maintain a flow of energy requires drilling for oil or digging for coal and uranium in a fossil-based energy system or building wind turbines and solar PV in a sustainable energy structure. In addition, we must also invest some energy in building and maintaining the capital structure necessary for a modern industrial society. This includes items such as the roads and bridges for transportation, and the electricity and buildings to maintain human comfort. An additional amount must be set aside in order to find more energy to replace the amount of energy being used up. All of these items are mandatory expenses for a steady-state energy budget. They are unavoidable expenses related to the energy necessary for a particular industrial society.

The remaining part of the available energy is divided into two parts: The first part is used for basic needs that support the standard of living such as health, shelter, water, and food. The second part is for discretionary uses associated with lifestyle such as entertainment, vacations, and the arts. This latter part can also be used for growth of the

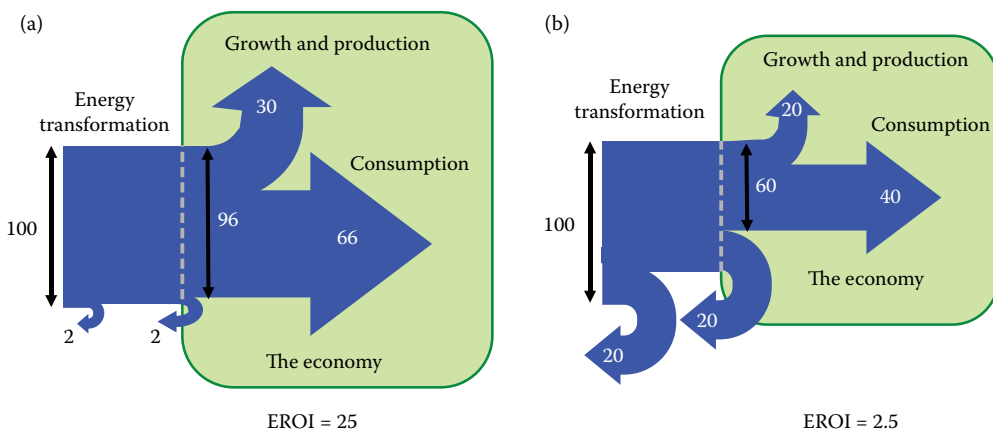
**FIGURE 3.9**

Energy flow diagram depicting the energy budget from extraction and transformation to end use.

economy. Figure 3.9 shows an energy flow diagram that accounts for the energy budget of the system depicted in Figure 3.1.

The energy budget diagram is useful in illustrating the impact on the economy of the trend to low EROI energy resources. Energy budget diagrams for an energy system with $EROI = 25$ and for $EROI = 2.5$ are shown in Figure 3.10a and b. In a simplified fashion, we can divide our energy budget into (a) energy necessary to maintain the energy flows, buildings, roads, and other basic needs, and (b) energy that can be used for discretionary activities. If there is a surplus of energy, we can apply that toward growth and/or prosperity, but the amount is finite and cannot be fully allocated to both simultaneously.

The EROI of oil production has declined over the past 70 years as the most productive resources were initially used and it was necessary to go further from easily accessible

**FIGURE 3.10**

Energy budget diagrams for two energy transformation systems (a) has $EROI = 25$ and supports a larger economy than (b) which has $EROI = 2.5$ even though both have the same energy production.

locations, or to drill deeper for increasingly smaller oil fields as time went on. It is estimated that by 1970, the EROI of oil production had dropped to 25; and in 1990, it was somewhere between 10 and 18. Today, the EROI of new energy oil production is somewhere between 3 and 4 [12]. This decline in the EROI is the result of having used up the most productive sources such as the Spindle Top in Texas, and about half of the Ghawar Field in Saudi Arabia, which were about 1000 feet below the surface. In contrast, the fields in the Gulf of Mexico are more than 20,000 feet below the surface and hold only a fraction of the amount of oil that the Saudi Arabian and Texan oil fields once produced [13].

There are some oil economists who claim that as liquid fuels are becoming scarcer, we can turn to the tar sands of Canada and the oil shale in the United States to replace oil as the liquid fuel. It is true that these resources hold an enormous amount of energy, but the energy and financial cost of extracting useful energy from them is much greater than that of the oil fields of the past. It has been estimated that for extracting oil from tar sands, the EROI is less than 5, while for oil shale it may be as low as 2. This means that an enormous amount of energy needs to be invested for a relatively small amount in return. In addition, extraction of oil from both tar sands and oil shale has a deleterious effect on the ecology, as well as requiring large amounts of water for their energy output.

The EROI of renewable energy sources, which are necessary for a sustainable energy system, varies widely. EROIs for wind reported in the literature through 2012 and standardized for comparison purposes to a lifetime of 25 years and capacity factor of 0.35, range from ~ 30 to 60 [14]. EROI values for solar PV installations, standardized to a lifetime of 25 years, efficiency of 13%, and irradiation of 1700 kWh per m² per year, range from ~ 2 to 5 [14]. On the other hand, the EROI for ethanol from corn is only barely greater than unity, which means that it is not a truly sustainable energy source. It is a somewhat ironic fact that of all the sustainable energy sources, ethanol from corn has received the most substantial financial support from the U.S. government for its production. This is largely a result of politics, since the corn-growing states represent an important political power in the U.S. Congress. The EROI of ethanol from sugar cane in Brazil may be as high as 6–8. Considerable research is going on worldwide to produce ethanol from cellulosic material and algae, but the technology is not sufficiently advanced to make quantitative estimates.

A conclusion to be drawn from these facts is that, as the most productive fossil energy sources are used up, we will have far less energy surplus available for our future basic needs, and particularly for discretionary activities that modern man has come to expect to enjoy ever since the fossil fuel era started 150 years ago. The reality of our times is that the energy investment to produce more energy will increase as the energy return on these investments dwindles. This means that the high-energy lifestyles of Western society will have to adapt to lower energy use. A few years ago, there were some who extolled the potential of a so-called hydrogen economy. However, as shown in [Chapter 1](#), hydrogen is not an energy source. It has to be produced from other forms of energy, such as electricity via hydrolysis or chemical reactions from natural gas. There are no hydrogen energy reservoirs.

The perspective on energy budgeting also has some major implications on the engineering design and optimization of energy production systems. The levelized costs of renewable energy systems ([Table 1.4](#)), as well as the energy return on investment, depend heavily on the assumed lifetime. In fact, since there are no fuel costs associated with any of the renewable systems, the EROI is directly proportional to the lifetime of the system; whereas, for fossil fuel generation, the initial capital investment is relatively small, but the operation requires a continuous flow of energy. This flow of energy has its own EROI associated with it, as illustrated in connection with oil. Consequently, the EROI of the energy fuel will decrease

with time and the cost of the fuel is likely to increase along with increases in exploration and delivery costs. Therefore, for future energy systems using renewable energy sources, the key goal of the engineering design should be the highest possible lifetime, which may, in many instances, be more important for the EROI, as well as, probably, for the levelized costs, than the efficiency of the system.

3.5.3 EROI for a Wind Energy System

A detailed energy analysis for three wind power systems has been made by White and Kulcinski [15], who calculated the EROI, as well as the air pollution emitted. In the time since this paper was published, unit costs of wind equipment have come down and capacity factors have increased, but the paper still provides a useful illustration of the EROI calculation method. The project for which the most detailed information was available was built in 1997 and is located near the city of DePere in Wisconsin and will be referred to as the DePere Wind Project (DPWP). It consists of two Taike 600e turbines that have a combined electric power capacity of 1.2 MWe with a capacity factor of 31% (predicted), and a predicted life for each of the nacelles of 20 years. The other two wind projects were designed for a maximum power of 25 MWe (BR-I) with 73 turbines and 107 MWe (BR-II) with 143 turbines. Their respective predicted capacity factors were 33% and 35%, and the predicted nacelle life was 25 years for both.

Table 3.6 shows the energy requirements to construct the two DePere wind turbines [15]. These requirements are obtained from the cost data shown in column 1, for example, craning cost was \$75,000. Then the energy per dollar in 1977 dollars is obtained from the I/O sector data in Table 3.5, for example, 30,233 Btu/1977\$ for hoists and cranes. But the time at which the craning cost was \$75,000 was 1997, while the I/O tables are for 1977\$. Hence, we must adjust the cost figure for inflation, which for these periods can be obtained from Table 2.1. Conversion from 1997 dollars (the year of construction), to 1977 dollars (the year the I/O tables were developed) was done using the CPI ratio 1977:1997 = 60.6:160.5, obtained from the CPI of the Bureau of Labor Statistics [9]. Multiplying the cost times the price index ratio and the Btu/\$ gives the embodied energy, that is, 8.56×10^8 Btu. A similar analysis for the other items in column 1 yields the total energy input required to make the

TABLE 3.6

Energy Requirements to Construct Two Turbine Wind Farms at DePere, Wisconsin

	1997\$	I/O Sector ^a	Btu/1977\$ ^b	Btu	GJ _{th} /2 Turbines
Craning	75,000	Hoists, cranes	30,233	8.56E+08	903
Labor	25,000	Misc. business services	10,000	9.44E+07	100
Local equipment rental	3000	Construction machinery	34,534	3.91E+07	41
Lodging and food for employees	8000	AVI ^c	28,780	8.69E+07	92
Electrical grounding	12,000	NC, electrical utilities	30,648	1.39E+08	147
Total: 1283 GJ_{th}/2 turbines					

Source: White, S.W. and Kulcinski, G.L., December 1998. Net energy payback and CO₂ emissions from wind-generated electricity in the Midwest, Fusion Technology Institute, University of Wisconsin, Madison, WI, <http://fti.neep.wisc.edu/pdf/fdm1092.pdf>. [15]

^a I/O sector data is from [8].

^b 1997\$ were calculated from the CPI by the scale 1977/1997 = 60.6/160.5 = 0.3776 [9].

^c Sector AVI is an average of the I/O sectors eat and drink places and hotels.

TABLE 3.7

Costs and Energy Requirements for On-Site Construction of the DePere Wind Power Plant

	1997\$	I/O Sector	Btu	GJ
Foundation preparation	73,000	Ready mix concrete	2.23E+09	2353
Transformer (2 at \$10 K per)	20,000	Transformers	3.22E+08	339
Craning	75,000	Hoists, cranes	8.56E+08	903
Labor	25,000	Misc. business services	9.44E+07	100
Local equipment rental	3000	Construction machinery	3.91E+07	41
Lodging and food for employees	8000	AVI	8.69E+07	92
Electrical grounding	12,000	NC, electric utilities	1.39E+08	147
				1282

Source: White, S.W. and Kulcinski, G.L., December 1998. Net energy payback and CO₂ emissions from wind-generated electricity in the Midwest, Fusion Technology Institute, University of Wisconsin, Madison, WI, <http://fti.neep.wisc.edu/pdf/fdm1092.pdf>. [15]

turbines. A similar analysis for the energy embodied in on-site construction is shown in Table 3.7. [15].

The lifetime and annual energy investments in the DPWP are shown in Table 3.8. Using these data, the *total energy input* per installed 1.2 MWe is 13,933 GJ_{th} or 3.89×10^6 kWh_{th}. The power output is 1.2×10^3 kWe $\times 0.31 = 0.372 \times 10^3$ kWe, and for the assumed lifetime

TABLE 3.8

Lifetime and Annual Energy Investments for the DePere Wind Power Plant

Process	Source	Total Energy Per Installed 1.2 MW _e	Annual Energy Per GW _{e,y}
		GJ _{th} /Power Plant	GJ _{th} /GW _{e,y}
<i>Wind turbine (embodied)</i>			
Blades	PCA	154	
Nacelles	PCA	2273	
Inverter	I/O	339	
Wiring	PCA	209	
Tower	PCA	4890	
Foundations	PCA	1925	
Materials total		9790	326
<i>Transportation</i>			
Blades		21	1
Nacelles		257	9
Towers		178	6
Concrete		23	
Control cabinets		0.29	0.01
Transportation totals		480	15
Construction	I/O	1282	43
Maintenance	I/O	1636	55
Decommissioning		641	21
Total required energy		13,933	

of the system of 20 years, the *total power output* is $0.372 \times 10^3 \text{ kWe} \times 20 \text{ year} \times 365 \text{ day/year} \times 24 \text{ h/day} = 65.2 \times 10^6 \text{ kWh}_e$. Hence, $\text{EROI} = 65.2/3.89 = 16.75$.

If the wind farm were located at a place where new transmission lines would have to be built to deliver the power to a user, additional energy input for grid extension could be included. Currently, energy storage is not used with commercial wind farms. If the wind were to be stored, as is often done for remote power installations, then the energy embedded in batteries would need to be included.

The EROI of wind energy has increased as the technology has improved. As noted above, recent published EROI estimates for wind range from ~ 30 to 60. It is therefore not surprising that wind energy has become economically competitive with conventional fossil and nuclear power plants.

3.6 Greenhouse Gas Accounting

As international efforts to combat climate change began to accelerate in the late 1990s, the World Resources Institute and World Business Council for Sustainable Development identified the need for a standard protocol for businesses to perform greenhouse gas accounting. The Corporate Accounting and Reporting Standard they developed (ghgprotocol.org; hereinafter GHG Protocol) was first published in 2001, was revised in 2004, and is now used by most large companies around the world to track and report their GHG emissions and emissions reduction efforts. Companies use GHG accounting to identify opportunities to reduce emissions, fulfill requirements of either voluntary or mandatory reporting programs, support participation in carbon trading markets, and report to the public. The corporate reporting protocol was adopted by the International Standards Organization in 2006 as the basis for ISO 14064-1: Specification with Guidance at the Organizational Level for Quantification and Reporting of Greenhouse Gas Emissions and Removals [16].

The GHG Protocol requires reporting of emissions of the seven greenhouse gases or groups of gases covered by the United Nations Framework Convention on Climate Change (UNFCCC): carbon dioxide (CO_2), methane (CH_4), nitrous oxide (N_2O), hydrofluorocarbons (HFCs), perfluorocarbons (PFCs), sulfur hexafluoride (SF_6), and nitrogen trifluoride (NF_3). Businesses are required to identify the basis for their reporting, as either emissions for operations in which they have an equity share (ownership) or operations under their control. The scope of reporting is split into three tiers:

Scope 1: Direct greenhouse gas emissions coming from sources that are owned or controlled by the company. Such emissions may come from combustion in the company's own furnaces or vehicles, from physical or chemical processing operations such as cement or fertilizer manufacture, or from fugitive emissions such as natural gas or refrigerant leaks.

Scope 2: Indirect emissions from generation of purchased electricity that is used in operations owned or controlled by the company.

Scope 3: Other indirect emissions that occur as a consequence of the company's activities, but not from sources that are owned or controlled by the company. Examples include emissions from extraction or processing of fuel used by the company, emissions associated with the use of the company's products, or from waste disposal.

Companies adhering to the GHG Protocol are required to report Scope 1 and 2 emissions, but tracking and quantifying Scope 3 emissions is optional. Following a revision to the Scope 2 requirements in 2015, companies must report emissions from purchased electricity in two ways: first, using grid-average emissions for their operational locations, and second, using a contract-based approach that accounts for electricity purchases from specific facilities or purchases of electricity generated with specific characteristics, such as from low carbon or renewable energy.

Emissions can be determined through direct measurements of concentrations and flow rates, or more commonly through engineering estimates. In the case of combustion emissions, these are often determined through mass balances and stoichiometry based on purchased quantities of fuel. Emissions can also be estimated using corporate records of operational activities (e.g., vehicle mileage) combined with published emissions factors. The GHG Protocol website includes spreadsheet tools for estimating emissions from stationary sources, mobile sources, air conditioning and refrigeration operations, and from a variety of manufacturing activities.

The GHG Protocol requires companies to report emissions of the seven UNFCCC greenhouse gases separately, and also to report combined emissions on a CO₂-equivalent basis using global warming potentials. The global warming potential (GWP) for a greenhouse gas is essentially the amount of energy that a unit mass of the gas will absorb over a given amount of time, relative to the amount of energy absorbed over the same time period by a unit mass of CO₂. GWP values reflect the fact that greenhouse gases differ in their infrared radiation absorption efficiencies, and in their atmospheric lifetimes. GWP values also reflect differences in the gases' indirect effects. For example, methane oxidation contributes to the formation of ozone, which is also a greenhouse gas. Because GWP depends on changing atmospheric conditions and because GWP calculations depend on evolving scientific understanding of atmospheric chemistry and dynamics, recommended GWP values have changed over time. Many programs and reporting protocols, including the GHG Protocol, use the GWP values estimated by the Intergovernmental Panel on Climate Change (IPCC) integrated over a 100-year time horizon to estimate CO₂-equivalent emissions. Table 3.9 gives selected GWP estimates integrated over both 20-year and 100-year time horizons from

TABLE 3.9

Global Warming Potential (GWP) with/without Inclusion of Climate-Carbon Feedbacks in Response to Emissions of the Indicated Non-CO₂ Gases

	Lifetime (Years)	GWP ₂₀	GWP ₁₀₀
CH ₄	12.4	86/84	34/28
HFC-134a	13.4	3790/3710	1550/1300
CFC-11	45	7020/6900	5350/4660
N ₂ O	121	268/264	298/265
SF ₆	3200	17,783/17,500	26,087/23,500
NF ₃	500	13,000/12,800	17,885/16,100

Source: IPCC, 2014. *Climate Change 2013: The Physical Science Basis. Working Group I Contribution to the Fifth Assessment Report of the Intergovernmental Panel on Climate Change. Chapter 8: Anthropogenic and natural radiative forcing*, Cambridge University Press, United Kingdom, https://www.ipcc.ch/pdf/assessment-report/ar5/wg1/WG1AR5_Chapter08_FINAL.pdf. [17]

Note: Climate-carbon feedbacks are always included for CO₂.

the latest IPCC Assessment (AR5), which was published in 2014 [17]. The table shows values estimated with and without accounting for the feedback effect of changes in the climate on the carbon cycle. The IPCC report recommends using values with climate-carbon feedbacks for consistency in treatment of CO₂ versus the other greenhouse gases. Values for many other greenhouse gases are given in Table 8.A.1 of the IPCC report [17].

PROBLEMS

- 3.1 The complete transactions matrix for a two-sector economy is shown below, with units in \$. Find the output from each sector that would be required to meet \$150 of additional consumer demand from sector 1 and \$200 of additional consumer demand from sector 2, considering supply chain requirements along with direct requirements. Compare the total output requirements across the supply chain with the direct requirements.

In completing this problem, use the following steps:

- Compute the technical requirements matrix
- Compute the Leontief inverse matrix
- Compute the total (including supply chain) output required for each sector to meet the new demand
- Compute the direct (excluding supply chain) output required for each sector to meet the new demand.

	Sector 1	Sector 2	Final (Consumer) Demand	Total Output
Sector 1	300	350	500	1150
Sector 2	200	300	1000	1500
Value added	650	850	1500	
Total input	1150	1500		

- 3.2 Use information from Table 3.5 to make a rough approximation of the energy embedded in the Golden Gate Bridge. The Bridge contains about 390,000 cubic yards of concrete and about 83,000 tons of structural steel (<http://goldengatebridge.org/research/factsGGBDesign.php>). Assume concrete cost about \$100 per cubic yard in 1977 \$ and steel costs about \$300 per ton in 1977 \$. Express your answer in kWh and in barrels of oil equivalent (BOE), where 1 BOE = 1700 kWh.
- 3.3 A new supercritical 200 MW coal-fired power plant operates with an 87% capacity factor and has a 45-year lifetime. The power plant's gross efficiency is 36%. The plant is located at the mine, thus minimizing the costs and energy requirements of transporting coal. Five percent of the total electricity produced by the plant is used internally. Find the EROI for the plant, assuming that the predominant upstream energy requirement is for the coal mining operation. You can neglect the energy embodied in equipment at the plant itself. Use the embedded energy estimate for non-metal mining ("non met. min. prod.") from Table 3.5 to estimate the energy used to mine the coal, assuming coal costs of \$0.65/million Btu in 1977 \$. In computing the denominator for the EROI, you should account for both the electrical energy used internally at the plant and the energy used for coal

mining. Neglect the heat content of the coal itself, as is the convention for EROI calculations for electricity from fossil fuels. Use the following steps and units as you calculate the EROI:

- a. Compute the net electrical energy to the consumer in kWh per year and in Btu per year (ignore transmission losses).
 - b. Compute the coal energy required by the plant in Btu per year and the cost of this coal in 1977 dollars.
 - c. Calculate the embedded energy for producing the coal in Btu per year.
 - d. Calculate the amount of energy consumed by the plant in its internal operations in Btu per year.
 - e. Calculate the EROI.
 - f. How would the EROI change if 25% of the plant's electricity has to be used internally, as might be the case with added carbon capture and sequestration? (Assume the gross capacity remains at 200 MW.)
- 3.4 You are an energy consultant who has been asked to assess the sustainability of a concentrating solar thermal power (CSP) plant with thermal energy storage. The specified plant has a capacity of 250 MW, a capacity factor of 0.50, and an expected lifetime of 30 years. Major inputs to plant construction include \$190 million in machinery (turbine, pumps, etc.); \$400 million in glass products; and \$30 million in cement, all in 2008 \$. The plant uses 15,000 MWh per year of external energy for its operations. Use embedded energy values from [Table 3.5](#) for your calculations.
- a. Based on only the specified inputs, and assuming continuous operation and no deterioration in performance over time, calculate the plant's EROI.
 - b. From a sustainable energy perspective, would you support building the CSP plant based on the EROI you calculated? Explain why or why not, by discussing the significance of the EROI metric and including a brief comparison of your EROI with those from other energy technologies or fuels.
- 3.5 Complete a preliminary GHG emissions report for a small natural food cooperative, accounting for Scope 1 and Scope 2 emissions. The food co-op is housed in a 5000 square foot space. It uses 65,000 kWh of electricity per year for space cooling, refrigeration, lighting, and electronic equipment. Grid electricity in the area has average emissions of 1.8 lb CO₂ per kWh. Space heating needs are met by a natural gas furnace that uses 250 million Btu of NG per year. The co-op owns a fleet of five gasoline-fueled delivery vans with average fuel economy of 7 miles per gallon. Each vehicle is driven 25,000 miles per year. The co-op has an old refrigerator/freezer unit that uses HFC 134a. The co-op manager estimates the freezer is charged with 1 kg of refrigerant every year to make up for leaks. Assume NG has the composition of methane (CH₄) and a heat content (LHV) of 50 MJ kg⁻¹. Assume gasoline has a density of 0.74 kg L⁻¹ and an effective molecular formula of C₇H₁₆. Present results separately for each Scope and each relevant GHG. Also, present results for each scope in terms of CO₂-equivalent emissions. What are some opportunities for the co-op to reduce its GHG emissions?

References

1. U.S. Environmental Protection Agency, April 2003. *Application of Life Cycle Assessment to Nanoscale Technology: Lithium-Ion Batteries for Electric Vehicles*, EPA 744-R-12-001.
2. ISO 14040:2006. Environmental management—Life cycle assessment—Principles and framework, <https://www.iso.org/obp/ui/#iso:std:iso:14040:ed-2:v1:en>.
3. ISO 14044:2006. Environmental management—Life cycle assessment—Requirements and guidelines, <https://www.iso.org/obp/ui/#iso:std:iso:14044:ed-1:v1:en>.
4. Sathaye, J., Lucon, O., Rahman, A., Christensen, J., Denton, F., Fujino, J., Heath, G. et al., 2011. Renewable energy in the context of sustainable development, in: Edenhofer, O., Pichs-Madruga, R., Sokona, Y., Seyboth, K., Matschoss, P., Kadner, S., Zwickel, T. et al. (eds), *IPCC Special Report on Renewable Energy Sources and Climate Change Mitigation*, Cambridge University Press, Cambridge, UK.
5. Matthews, H.S., Hendrickson, C., and Matthews, D.H., 2015. *Life Cycle Assessment: Quantitative Approaches for Decisions That Matter*, <http://www.lcatextbook.com>.
6. Boercker, S.W., 1978. Energy use in the production of primary aluminum, ORAU/IEA-78-14, Oak Ridge Associated Universities, Oak Ridge, TN.
7. Ballard, C.W., Penner, P.S., and Pilati, D.A., November 1978. Net energy analysis—Handbook for combining process and input–output analysis, *Resources and Energy* 1, 267–313.
8. Hannon, B., Casler, D.S., and Blasek, T., 1985. Energy intensity for the U.S. economy—1977, Energy Research Group, University of Illinois Press, Urbana, IL.
9. Bureau of Labor Statistics, 1998. Consumer price index—All urban consumers, March 13, 1998, <http://146.142.4.24/cgi-bin/surveymost?cu>.
10. Ashby, M.F., 2012. *Materials and the Environment: Eco-Informed Material Choice*, Second Edition, Butterworth-Heinemann, Amsterdam.
11. Spreng, D.T., 1988. *Net Energy Analysis and the Energy Requirements of Energy Systems*, Praeger Publishing Company, New York.
12. Cleveland, C.J., 2005. Net energy from oil and gas extraction in the United States, 1954–1997. *Energy* 30, 769–781.
13. Cleveland, C.J., and O'Connor, P., 2010. An assessment of the energy return on investment of oil shale, Western Resource Advocates, <https://westernresourceadvocates.org/publications/assessment-of-energy-roi-of-oil-shale>.
14. Wu, K., Paranjothi, G., Milford, J.B., and Kreith, F., 2016. Transition to sustainability with natural gas from fracking. *Sustainable Energy Technologies and Assessments* 14, 26–34.
15. White, S.W., and Kulcinski, G.L., December 1998. Net energy payback and CO₂ emissions from wind-generated electricity in the Midwest, Fusion Tech Inst., University of Wisconsin, Madison, WI, <http://fti.neep.wisc.edu/pdf/fdm1092.pdf>.
16. ISO 14064-1:2006. Greenhouse gases—Part 1: Specification with guidance at the organization level for quantification and reporting of greenhouse gas emissions and removals, <https://www.iso.org/standard/38381.html>.
17. IPCC, 2014. *Climate Change 2013: The Physical Science Basis. Working Group I Contribution to the Fifth Assessment Report of the Intergovernmental Panel on Climate Change*, Chapter 8: Anthropogenic and natural radiative forcing, Cambridge University Press, United Kingdom, https://www.ipcc.ch/pdf/assessment-report/ar5/wg1/WG1AR5_Chapter08_FINAL.pdf.



Taylor & Francis

Taylor & Francis Group

<http://taylorandfrancis.com>

4

Energy Use and Efficiency in Buildings and Industry

Energy efficiency is one weapon in the arsenal against over-dependence on GHG-emitting fossil fuels. I believe efficiency is the best weapon: cheapest, safest, and most immediately achievable.

Art Rosenfeld*

4.1 Background

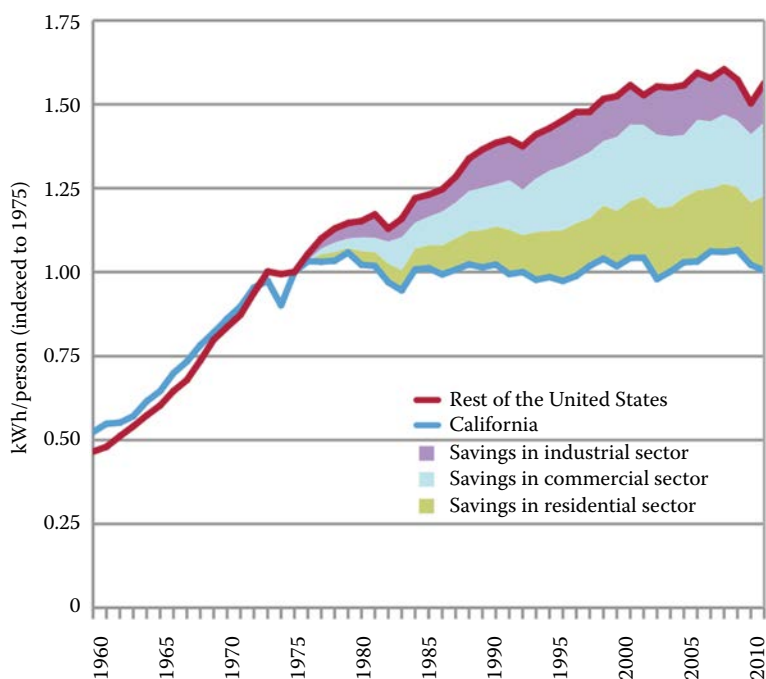
Energy conservation and efficiency have long been considered the low-hanging fruit in our efforts to improve our energy system. Saving energy is generally more cost-effective than generating new energy. In the words of energy futurist Amory Lovins, “negawatts” (i.e., watts of saved power) are better than megawatts. Energy *conservation* means using less energy or getting by with less. This can be done through active choices or interventions, such as actively turning down the lights or thermostat. A problem with conventional “energy conservation” measures is that they depend on human behavior and motivation, and may be considered inconvenient. Increasingly, however, automated systems can take care of these measures for us, setting thermostats back or shutting off lights when a building or room is unoccupied. Energy *efficiency* entails using energy in a more efficient way that has little or no impact on the function or service provided. Thus, the replacement of incandescent bulbs with LED bulbs can reduce energy consumption while providing the same illumination level and quality of light. Or a homeowner might purchase a higher efficiency furnace that provides the same level of heating with less energy required.

In the United States, total energy use (on-site primary fuel use plus the primary fuel used to generate electricity) is divided among the end-use sectors as follows: 40% buildings (split 54 : 46 between residential and commercial), 32% industrial, and 28% transportation [1]. World energy use is more heavily skewed to industrial and is divided as follows: 30% buildings (split 60 : 40 between residential and commercial), 51% industrial, and 20% transportation [2].

Energy efficiency measures are not as conspicuous as big new power plants, and so people often do not appreciate the great strides that have been made. Since the oil embargoes of the 1970s, energy efficiency measures have greatly limited energy growth, even as standards of living have risen.

How much difference have these efficiency measures made? The International Energy Agency analyzed how much energy 11 developed countries in the world would use today if efficiency measures had not been taken. Actual energy use in 2010 was 20% higher than in 1974. But without energy efficiency improvements it would have been 100% higher [3].

* Rosenfeld, H. and Poskanzer, D., 2009. A graph is worth a thousand gigawatt-hours: How California led the United States in energy efficiency. *Innovations* 4(4), 57–79.



Source: EIA, SEDS database (2012)

FIGURE 4.1

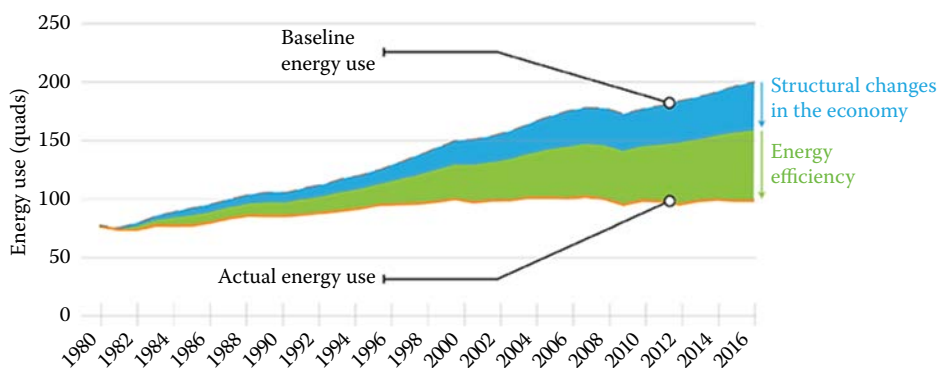
California electricity growth vs. rest of United States. (From NRDC Fact Sheet, July 2013. California's energy efficiency success story: Saving billions of dollars and curbing tons of pollution, FS:13-06-A, <https://www.nrdc.org/sites/default/files/ca-success-story-FS.pdf>. [4])

A classic case in the United States is the state of California, where aggressive measures began in the 1970s to control energy use. As shown in Figure 4.1, California managed to keep per-capita electricity use essentially constant despite increasing use of air conditioning, whereas per capita electricity use increased in the United States as a whole [4].

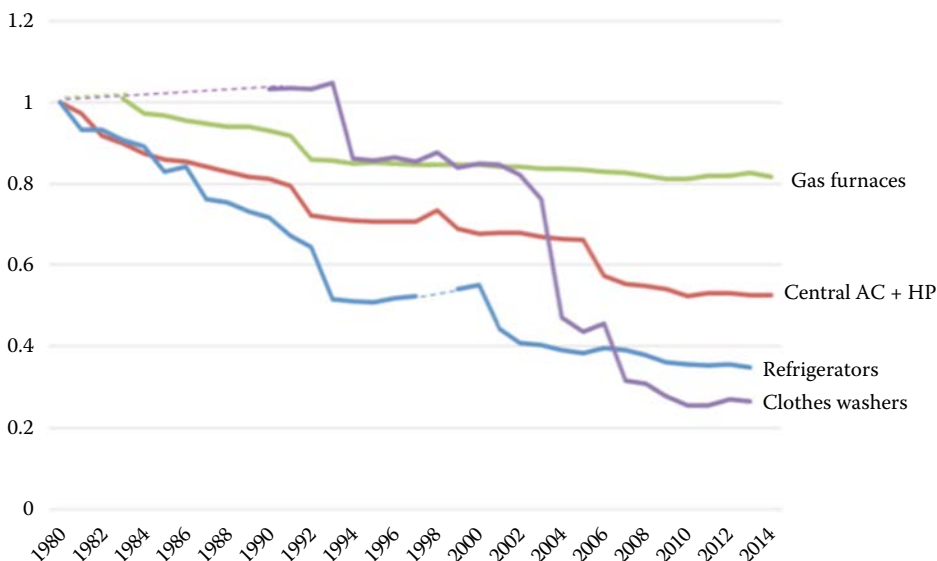
Note that 80% of the electricity savings in California compared to the rest of the country is due to efficiency improvements in residential and commercial buildings. Much of this success is due to utility incentives and state policies that promote aggressive building energy efficiency and federal appliance efficiency standards. Despite these energy efficiency measures (or perhaps, in part, because of them) California ranks as the world's 6th largest economy.

When reviewing historical improvements in energy consumption, a logical question is how much of the change is due to energy efficiency versus structural changes in industry. (Structural change involves shifts in economic production and employment, for example, from agriculture and manufacturing to software and services.) The American Council for an Energy-Efficient Economy (ACEEE) has estimated that approximately 40% of the improvement in total energy use in the United States has been due to structural changes as shown in Figure 4.2 [5]. However, the total energy use in the United States today is 60% less than it would otherwise be if energy efficiency improvements had not been made.

A great success story has been the impact of appliance and equipment efficiency standards in the United States. Figure 4.3 shows the relative improvement of the energy consumption of some new appliances and equipment in the United States from 1980 to 2014 [5].

**FIGURE 4.2**

Total U.S. primary energy use changes due to structural change and energy efficiency. (From Nadel, S., Elliott, N., and Langer T., June 2015. Energy efficiency in the United States: 35 years and counting, ACEEE, Report E1502, ACEEE analysis based on EIA data; updated version at <http://aceee.org/blog/2017/05/doing-more-less-how-us-economy-grows>. [5])

**FIGURE 4.3**

Relative average energy consumption of new appliances sold in the U.S. from 1980 to 2014. (From Nadel, S., Elliott, N., and Langer T., June 2015, Energy efficiency in the United States: 35 years and counting, ACEEE, Report E1502. [5])

These improvements came with no downside. For example, today's refrigerators are lower in cost (in real dollars) and somewhat larger than the ones sold in 1980, despite using about one-quarter of the energy.

To calculate the cost of energy efficiency measures, a common metric used is the cost of conserved energy or CCE. CCE is useful because it allows a direct comparison between the cost of purchasing energy and the cost/benefit of installing efficiency measures. The CCE for an energy efficiency measure (EEM) is equal to the levelized net annual cost divided by the annual energy savings. The net levelized cost is the capital cost (including equipment, installation, and other upfront costs) multiplied by the capital recovery factor, or CRF, which converts a present value to an equivalent constant annual value based on the discount rate. Thus,

$$\text{CCE} = \text{Capital Cost} \times \text{CRF} / \text{Annual Energy Savings} \quad (4.1)$$

where, as we have seen in [Chapter 2](#),

$$\text{CRF} = \frac{i(1+i)^n}{(1+i)^n - 1}$$

where i = the discount rate (e.g., 0.04) and n = number of years

EXAMPLE 4.1

An office lighting upgrade has a net capital cost premium over conventional lighting of \$2,000 but saves 2 kW of electric power during its 5,000 hours per year of operation.

The annual savings = 2 kW \times 5,000 h = 10,000 kWh

Assuming a 15-year lifetime ($n = 15$) and a discount rate of 4% ($i = 0.04$),

$$\text{CRF} = \frac{0.04(1+0.04)^{15}}{(1+0.04)^{15} - 1} = 0.08994$$

$$\text{CCE} = \frac{\$2,000 \times 0.08994}{10,000 \text{ kWh}} = \$0.018/\text{kWh} \text{ or } 1.8\text{¢}/\text{kWh}$$

Thus, in this case, the lighting upgrade has a CCE that is about one fifth the purchased electricity cost (assuming an average cost of 10¢/kWh). Higher electricity costs make the lighting upgrade even more favorable.

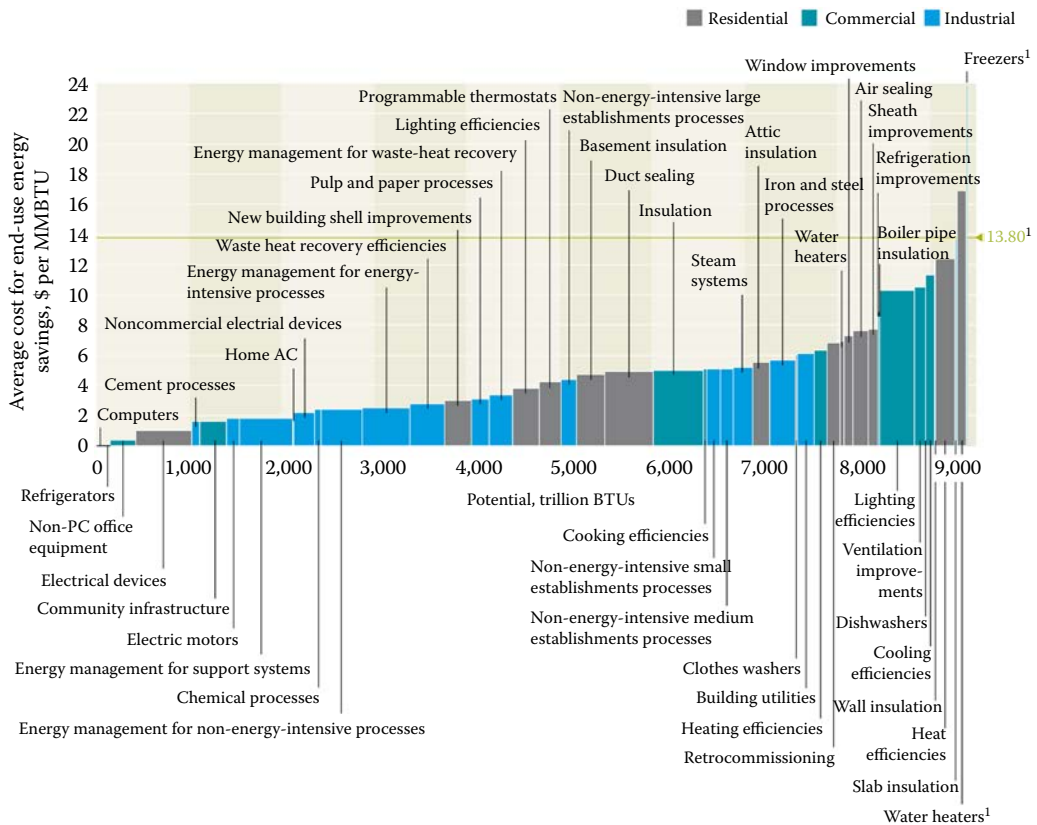
While significant efficiency improvements have already been made, studies indicate that efficiency also has a large potential going forward. Various studies have shown that energy efficiency measures are very cost-effective. Molina estimated that energy efficiency measures have a levelized cost of electricity in the range of 2 to 5 cents per kWh, making it the lowest cost energy option [6]. McKinsey analyzed the costs for a range of energy efficiency measures and their results are shown in [Figure 4.4](#) [7].

While this chapter covers efficiency in buildings and industry, it is important to note that standards for vehicle efficiency are also having a significant impact. Recent international historical and target miles per gallon and kilometers per liter for passenger vehicles are given at the Center for Climate and Energy Solutions [8]. Improved aerodynamics, lighter weight construction materials, low rolling resistance tires, internal combustion engine refinements, and hybrid and electric vehicles are all playing a role in achieving improved vehicle efficiency. The batteries in electric vehicles (EV) may be important for allowing deeper penetration of variable renewables and zero energy buildings on the grid. Transportation is covered in [Chapter 15](#).

4.2 Energy Audits and Energy Management

Achieving high levels of energy efficiency requires a focused, systematic approach. This has spawned the field of Strategic Energy Management, or SEM. SEM programs have become popular in states and utilities across the United States and Canada [9]. A typical SEM plan benchmarks current energy use including an energy audit, develops energy performance

US energy-efficiency supply curve—2020

**FIGURE 4.4**

CCE comparison of different energy efficiency measures. McKinsey & Company, March 2010. Energy efficiency: A compelling global resource, www.mckinsey.com. Copyright 2010 McKinsey & Company. All rights reserved. Reprinted by permission. [7]

goals, evaluates the impact and cost of potential measures, establishes a measurement and verification plan, and schedules multi-year implementation.

An international Energy Management System standard, International Organization of Standardization (ISO) 50001, has been developed to provide an energy management framework for organizations to follow in improving energy efficiency. ISO 50001 is a voluntary standard that provides guidance on the following [10]:

- Energy use and consumption
- Measurement, documentation, and reporting of energy use
- Design and procurement practices for energy-using equipment, systems, and processes
- All variables affecting energy performance that can be monitored and influenced by the organization

Organizations that follow the ISO 50001 management standard and demonstrate continuous improvement in energy efficiency can apply for ISO 50001 certification.

4.3 Buildings

Buildings represent 40% of energy use in the United States and 30% in the world. Energy efficiency improvements opportunities can be divided between commercial and residential buildings. The International Energy Agency gives world energy consumption in petajoules for residential and nonresidential buildings in [11]. Total residential buildings energy use was 88,000 PJ in 2012 with space heating, cooking, and water heating being the three largest users. Total nonresidential building energy use was 31,000 PJ in 2012 with appliances (and other equipment) and space heating being the largest users.

Through much of the world, cooking is a major energy user in homes. There is a worldwide effort to make cooking stoves in the developing world more efficient and safer. Clearly, space heating and water heating are major end uses of building energy throughout the world. Note that while space cooling is a major energy consumer in the United States, it is still not widely used in much of the world. Cooling tends to increase as countries develop economically and so is increasing around the world. Appliances, which include computers and office equipment, are an especially major load in nonresidential buildings.

4.3.1 Calculations of Heating and Hot Water Loads in Buildings

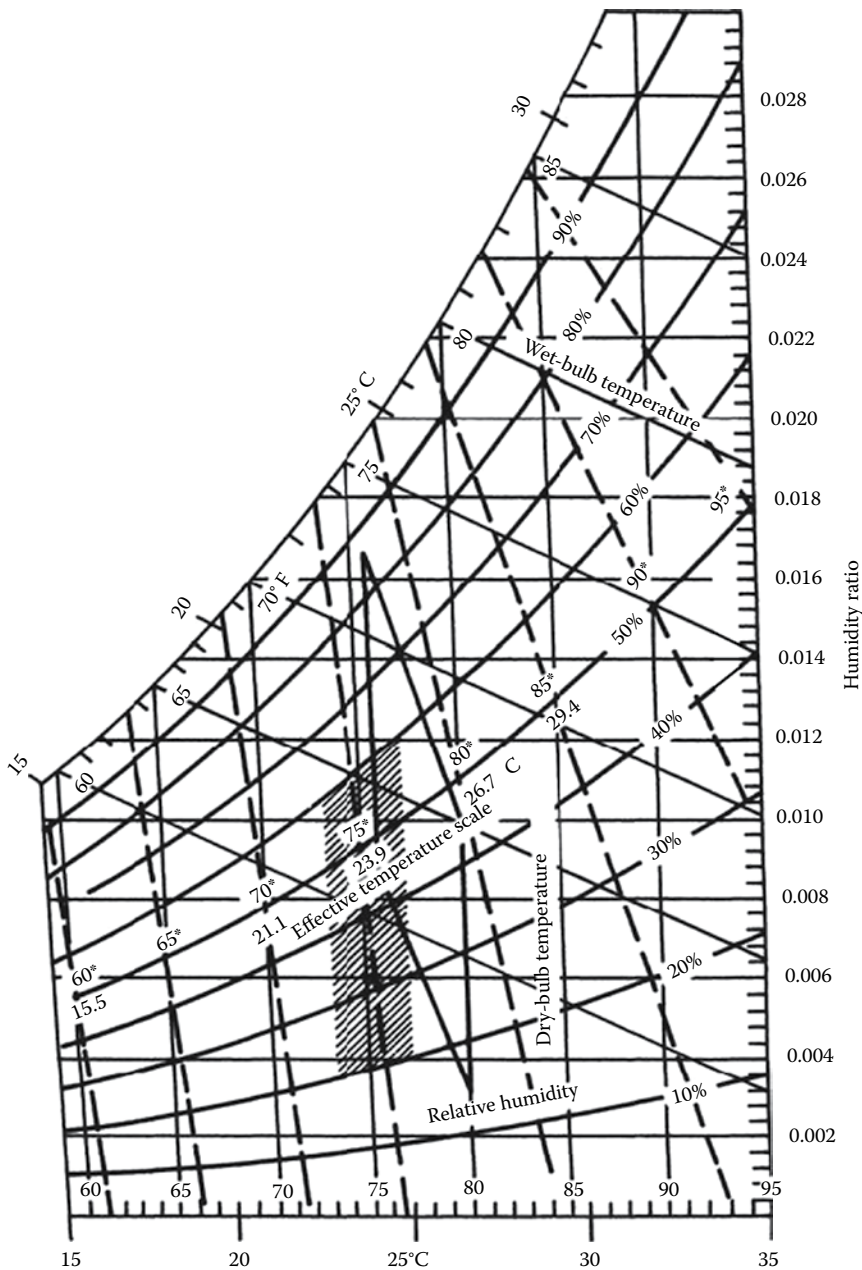
Energy requirements for space heating or service water heating can be calculated from basic conservation of energy principles. For example, the heat required to maintain the interior of a building at a specific temperature is the total of all heat transmission losses from the structure and heat required to warm and humidify the air exchange with the environment by infiltration and ventilation.

Comfort in buildings has long been a subject of investigation by the American Society of Heating, Refrigerating, and Air-Conditioning Engineers (ASHRAE). ASHRAE has developed extensive heat load calculation procedures embodied in the *ASHRAE Handbook of Fundamentals* [12]. The most frequently used load calculation procedures will be summarized in this section; the reader is referred to the ASHRAE handbook for details.

Figure 4.5 shows the combinations of temperature and humidity that are required for human comfort. The shaded area is the standard U.S. comfort level for sedentary persons. Many European countries have human comfort levels from 3°C to 7°C below U.S. levels. If activity of a continuous nature is anticipated, the comfort zone lies to the left of the shaded area; if extra clothing is worn, the comfort zone is displaced similarly.

4.3.1.1 Calculation of Heat Loss

It is outside the scope of this book to describe the details of the heat load calculations for buildings. However, the method is described briefly in this section. For details, one should refer to the *ASHRAE Handbook of Fundamentals* [12] or some other textbook on heating and air conditioning. See also a general heat transfer textbook, such as *Principles of Heat Transfer*, 8th edition, by Frank Kreith and Raj M. Manglik [13]. Table 4.1 lists the components of heat loss calculations of a building.

**FIGURE 4.5**

Psychrometric chart of moist air properties with the range of dry bulb temperature and relative humidity conditions for human comfort.

Complete tables of thermal properties of building materials are on the accompanying website, <http://www.crcpress.com/product/isbn/9781498788922>, and are numbered from Table W.4.1 to Table W.4.11. Transmission heat losses through attics, unheated basements, and the like, are buffered by the thermal resistance of the unheated space. For example, the temperature of an unheated attic lies between that of the heated space and that of

TABLE 4.1

Heating Load Calculations for Buildings

Heating Load Component	Equations	Descriptions/References
Walls, roof, ceilings, glass	$q = U \cdot A(T_i - T_o)$	T_i, T_o are inside and outside air temperatures, respectively. U values of composite section are calculated from the thermal properties of components given in the tables on the accompanying website
Concrete floors on ground	$q_{fe} = F_e P_e (T_i - T_o)$	p_e is the perimeter of the slab. F_e values are given in the tables on the accompanying website
Infiltration and ventilation air	$q_{sensible} = Q \rho_a C_p (T_i - T_o)$ or $= 1200 \cdot Q (T_i - T_o)$ $q_{latent} = Q \rho_a h_{fg} \Delta W$ or $= 2808 \cdot Q \Delta W$	Q is the volume of airflow in m^3/s . ρ_a and C_p are density and specific heat of air h_{fg} is the latent heat of water at room temperature. ΔW is humidity ratio difference between inside and outside air

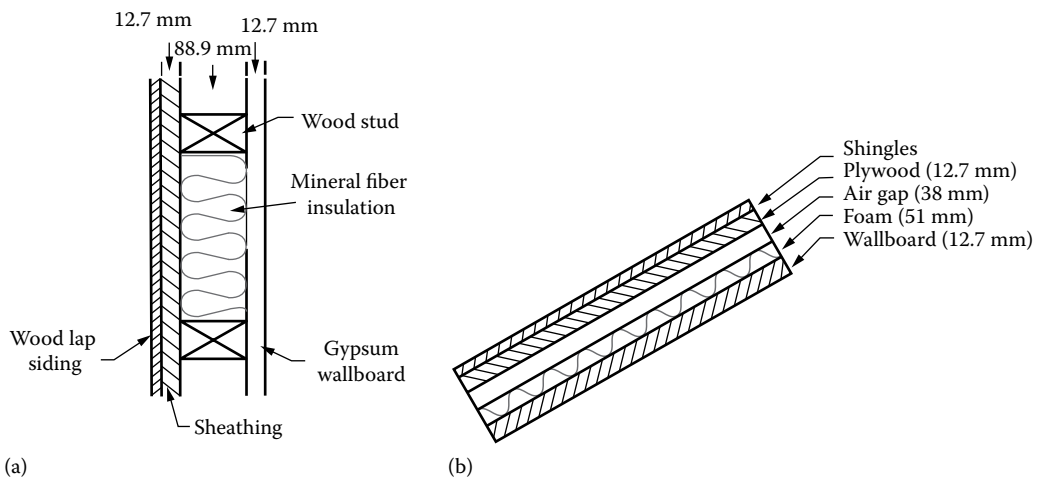
^a Assuming $\rho_a = 1.2 \text{ kg/m}^3$; $h_{fg} = 2340 \text{ J/kg}$, $C_p = 1000 \text{ J/kg}^\circ\text{C}$.

the environment. As a result, the ceiling of a room below an attic is exposed to a smaller temperature difference and consequent lower heat loss than the same ceiling without the attic would be. The effective conductance of thermal buffer spaces can easily be calculated by forming an energy balance on such spaces.

The following example is an illustration of the heat loss calculation method described in this section.

EXAMPLE 4.2

Calculate the heat load on a house for which the wall area is 200 m^2 , the floor area is 600 m^2 , the roof area is 690 m^2 , and the window area totals 100 m^2 . Inside wall height is 3 m . The construction of the wall and the roof is shown in [Figure 4.6](#).

**FIGURE 4.6**

Cross sections of (a) the wall and (b) the roof for Example 4.2.

Solution

The thermal resistance of the wall shown in Figure 4.6 can be found by the electrical resistance analogy as

$$R_{wa} = R_{outside\ air} + R_{wood\ siding} + R_{sheathing} + R_{comb} + R_{wall\ board} + R_{inside\ air}$$

The wood stud and the insulation are in parallel, so as in the case of electrical resistors in parallel, to get the combined resistance we add them in parallel. (The R -value equals $1/UA$. The UA values indicate the heat flow and are additive just like the currents in parallel resistors. Thus, the reciprocals of parallel resistors add.)

The wood stud is a 2 by 4 with an actual depth of 3.5". Its R -value is $4.37\text{ ft}^2\text{F}/(\text{Btu}/\text{h})$. To convert from English to SI units, we multiply by 0.176. Thus, the R -value of the wood stud is $4.37 \times 0.176 = 0.77\text{ m}^2\text{C}/\text{W}$.

The 3.5" of mineral fiber insulation has an R -value of $11.02\text{ ft}^2\text{F}/(\text{Btu}/\text{h}) = 1.94\text{ m}^2\text{C}/\text{W}$.

Assume that the studs occupy 15% of the wall area and the insulation occupies the other 85%. Then

$$\frac{1}{R_{comb}} = \frac{0.15}{0.77} + \frac{0.85}{1.94}$$

or

$$R_{comb} = 1.58\text{ m}^2\text{C}/\text{W}$$

Therefore, the wall thermal resistance, R_{wa} , can be found as

Element	Thermal Resistance ($\text{m}^2\text{C}/\text{W}$)
Outside air (6.7 m/s wind)	0.030
Wood bevel lap siding	0.14
12.7 mm sheathing	0.23
88.9 mm combined wood stud and mineral fiber insulation	1.58
1.7 mm gypsum wallboard	0.079
Inside air (still)	0.12
	$R_{wa} = 2.179$

Therefore

$$U_{wa} = \frac{1}{R_{wa}} = \frac{1}{2.179} = 0.46\text{ W}/\text{m}^2\text{C}.$$

The heat loss through the windows depends on whether they are single- or double-glazed. In this example, single-glazed windows are installed, and a U factor equal to $4.7\text{ W}/\text{m}^2\text{C}$ is used. (If double-glazed windows were installed, the U factor would be $2.4\text{ W}/\text{m}^2\text{C}$.)

The roof is constructed of 12.7 mm gypsum wall board, 51 mm foam insulation board, 38 mm still air, 12.7 mm plywood, and asphalt shingles (wooden beams and roofing paper are neglected for the simplified calculations here). Therefore

$$U_{rf} = \frac{1}{\frac{0.030}{\text{outside air}} + \frac{0.077}{\text{Shingles}} + \frac{0.11}{\text{Plywood}} + \frac{0.17}{\text{Air gap}} + \frac{2.53}{\text{Foam}} + \frac{0.079}{\text{Wallboard}} + \frac{0.1}{\text{inside air}}} = 0.32\text{ W}/\text{m}^2\text{C}$$

If the respective areas and U factors are known, the rate of heat loss per hour for the walls, windows, and roof can be calculated, assuming that floor heat loss is negligible:

$$\begin{aligned}\text{Walls: } q_{wa} &= (200\text{m}^2) \times 0.46\text{ W/m}^2\text{°C} = 92\text{ W/°C} \\ \text{Windows: } q_{wi} &= (100\text{m}^2) \times 4.7\text{ W/m}^2\text{°C} = 470\text{ W/°C} \\ \text{Roof: } q_{rf} &= (690\text{m}^2) \times 0.32\text{ W/m}^2\text{°C} = 220\text{ W/°C} \\ \text{Total} &= 782\text{ W/°C}\end{aligned}$$

If double-glazed windows were used, the total heat loss would be reduced to 552 W/°C.

The infiltration and ventilation rate Q for this building is assumed to be 0.5 air changes per hour (ACH). The sensible and latent heat loads of the infiltration air may be calculated using the equations given in Table 4.1. Therefore

$$Q = 0.5 \times (600\text{m}^2 \times 3\text{m}) = 900\text{m}^3/\text{h} = 0.25\text{m}^3/\text{s}$$

$$q_{\text{sensible}} = 0.25\text{m}^3/\text{s} \times (1.2\text{kg/m}^3)(1000\text{J/kg°C}) = 300\text{ W/°C}.$$

In residential buildings, humidification of the infiltration air is rarely done. Neglecting the latent heat, the total rate of heat loss q_{tot} is the sum of q_{sensible} and q_{tr}

$$q_{\text{tot}} = (782 + 300) = 1082\text{ W/°C}$$

This calculation is simplified for purposes of illustration. Heat losses through the slab surface and edges have been neglected, for example.

More refined methods of calculating energy requirements on buildings do not use the steady-state assumption used earlier [14]. The thermal inertia of buildings may be expressly used as a load-leveling device. If so, the steady-state assumption is not met and the energy capacitance of the structure must be considered for accurate results. Many adobe structures in the U.S. Southwest are built intentionally to use daytime sun absorbed by 1 ft thick walls for nighttime heating, for example.

4.3.1.2 Internal Heat Sources in Buildings

Heat supplied to a building to offset energy losses is derived from both the heating system and internal heat sources. Table 4.2 lists the common sources of internal heat generation for residences. Commercial buildings such as hospitals, computer facilities, or supermarkets will have large internal gains specific to their function. Internal heat gains tend to offset heat losses from a building but will add to the cooling load of an air conditioning system. The magnitude of the reduction in heating system operation will be described in the next section.

4.3.1.3 Degree-Day Method

The preceding analysis of heat loss from buildings expresses the loss on a per-unit temperature difference basis (except for unexposed floor slabs). In order to calculate the peak load and total annual load for a building, appropriate design temperatures must be defined for each. The outdoor design temperature is usually defined statistically, such

TABLE 4.2

Some Common Internal Sensible Heat Gains That Tend to Offset the Heating Requirements of Buildings

Type	Magnitude (W or J/s)
Incandescent lights	Total W
Fluorescent lights	Total W
Electric motors	$746 \times (\text{hp}/\text{efficiency})$
Natural gas stove	$8.28 \times \text{m}^3/\text{h}$
Appliances	Total W
A dog	50–90
People	
Sitting	70
Walking	75
Dancing	90
Working hard	170

Source: From ASHRAE, 1989, 1993, 1997. *ASHRAE Handbook—Fundamentals*, American Society of Heating, Refrigerating and Air-Conditioning Engineers, Atlanta, GA. With permission. [12]

that the actual outdoor temperature will exceed the design temperature 97.5% or 99% of the time over a long period. The design temperature difference (ΔT) is then the interior building temperature minus the outdoor design temperature. The design ΔT is used for rating nonsolar heating systems, but is not useful for the selection of solar thermal energy systems, since they rarely provide 100% of the energy demand of a building at peak conditions.

A more useful index of heating energy demand is the total annual energy requirement for a building. This quantity is somewhat more difficult to calculate than the peak load. It requires knowledge of day-to-day variations in ambient temperature during the heating season and the corresponding building heat load for each day. Building heat loads vary with ambient temperatures, as shown in Figure 4.7. The environmental temperature, T_{nl} , above which no heat need be supplied to the building, is a few degrees below the required interior temperature, T_i , because of internal heat-generation effects.

The no-load temperature at which internal source generation, q_i , just balances transmission and infiltration losses can be determined from the energy balance:

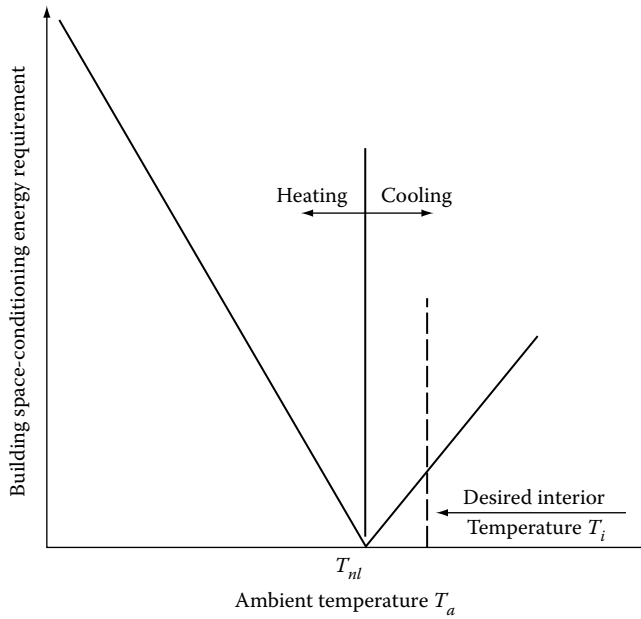
$$q_i = \overline{UA}_B(T_i - T_{nl}) \quad (4.2)$$

where \overline{UA}_B is the overall heat loss coefficient for the building (W/°C). Then,

$$T_{nl} = T_i - \frac{q_i}{\overline{UA}_B} \quad (4.3)$$

The total annual heat load on the building, Q_T , can be expressed as:

$$Q_T = \int_{365 \text{ days}} \overline{UA}_B(T_{nl} - T_a)^+ dt \quad (4.4)$$

**FIGURE 4.7**

Building load profile versus ambient temperature showing no-load temperature, T_{nl} , and desired interior temperature, T_i .

in which all arguments of the integral are functions of time. The superscript $+$ indicates that only positive values are considered. In practice, it is difficult to evaluate this integral; therefore, three simplifying assumptions are made:

1. \overline{UA}_B is independent of time.
2. T_{nl} is independent of time.
3. The integral can be expressed by the sum.

$$\overline{UA}_B \sum_{n=1}^{365} (T_{nl} - \bar{T}_a)_n^+ \quad (4.5)$$

where n is the day number, and the daily average temperature \bar{T}_a can be approximated by $1/2(T_{a,max} + T_{a,min})$, in which $T_{a,max}$ and $T_{a,min}$ are the daily maximum and minimum temperatures, respectively.

The quantity $(T_{nl} - T_a)^+$ is called the *degree-day unit*. For example, if the average ambient temperature for a day is 5°C and the no-load temperature is 20°C , 15°C -days are said to exist for that day. However, if the ambient temperature is 20°C or higher, 0°C -days exist, indicating 0 demand for heating that day. Degree-day totals for monthly $\sum_{month} (T_{nl} - T_a)^+$, and annual periods can be used directly in Equation 4.5 to calculate the monthly and annual heating energy requirements.

In the past, a single value of temperature has been used throughout the United States as a universal degree-day base: 65.0°F or 18.3°C . This practice is now outdated, since many homeowners and commercial building operators have lowered their thermostat settings in response to increased heating fuel costs, thereby lowering T_{nl} . Likewise, warehouses

and factories operate well below the 19°C level. Therefore, a more generalized database of degree-days to several bases (values of T_{nl}) has been created by the U.S. National Weather Service [15].

EXAMPLE 4.3

A building located in Denver, CO, has a heat loss coefficient \overline{UA}_B of 1000 kJ/h°C and internal heat sources of 4440 kJ/h. If the interior temperature is 20°C (68°F), what are the monthly and annual heating energy requirements? A gas furnace with 65% efficiency is used to heat the building.

Solution

In order to determine the monthly degree-day totals, the no-load temperature (degree-day basis) must be evaluated from Equation 4.3.

$$T_{nl} = 20 - \frac{4440}{1000} = 15.6^\circ\text{C} (60^\circ\text{F})$$

The monthly °C-days for Denver are taken from the U.S. NWS and given in Table 4.3. The energy demand is calculated as

$$\text{Energy demand} = \overline{UA}_B \times 24 \frac{\text{h}}{\text{day}} \times ^\circ\text{C-days}$$

The monthly energy demand is given in Table 4.3.

If the annual energy demand of 62.9 GJ is delivered by a 65% efficient gas furnace, then the

$$\text{Average annual purchased energy} = \frac{62.9}{0.65} \text{ GJ} = 96.8 \text{ GJ}$$

TABLE 4.3

Monthly and Annual Energy Demands for Example 4.3

Month	°C-Days	Energy Demand ^a (GJ)
January	518	12.4
February	423	10.2
March	396	9.5
April	214	5.2
May	68	1.6
June	14	0.3
July	0	0
August	0	0
September	26	0.6
October	148	3.6
November	343	8.2
December	472	11.3
	2622	62.9

^a Energy demand equals $\overline{UA}_B \times ^\circ\text{C-days} \times 24 \text{ h/day}$.

4.3.1.4 Service Hot Water Load Calculation

Service hot water loads can be calculated precisely with the knowledge of only a few variables. The data required for calculation of hot water demand are:

Water source temperature (T_s)

Water delivery temperature (T_d)

Volumetric demand rate (Q)

The energy requirement for service water heating q_{hw} is given by:

$$q_{hw}(t) = \rho_w Q(t) c_{pw} [T_d - T_s(t)] \quad (4.6)$$

where

ρ_w is the water density

c_{pw} is the specific heat of water

The demand rate, $Q(t)$, varies in general with time of day and time of year; likewise, the source temperature varies seasonally. Source temperature data are not compiled in a single reference; local water authorities are the source of such temperature data.

Few generalized data exist with which to predict the demand rate Q . Table 4.4 indicates some typical usage rates for several common building types. Process water-heating rates are peculiar to each process and can be ascertained by reference to process specifications.

EXAMPLE 4.4

Calculate the monthly energy required to heat water for a family of four in Nashville, TN. Monthly source temperatures for Nashville are shown in Table 4.5, and the water delivery temperature is 60°C (140°F).

Solution

For a family of four, the demand rate Q may be found using a demand recommended from Table 4.4

$$Q = 4 \times 76 \text{ L/day} \times \frac{1 \text{ m}^3}{1000 \text{ L}} = 0.30 \text{ m}^3/\text{day}$$

TABLE 4.4

Approximate Service Hot Water Demand Rates

Usage Type	Demand per Person	
	L/Day	gal/Day
Retail store	2.8	0.75
Elementary school	5.7	1.5
Multifamily residence	76.0	20.0
Single-family residence	76.0	20.0
Office building	11.0	3.0

TABLE 4.5

Water Heating Energy Demands for Example 4.4

Month	Days/Month	Demand (m ³ /Month)	Source Temperature (°C)	Energy Requirement (GJ/Month)
January	31	9.3	8	2.0
February	28	8.4	8	1.8
March	31	9.3	12	1.9
April	30	9.0	19	1.5
May	31	9.3	17	1.7
June	30	9.0	21	1.5
July	31	9.3	22	1.5
August	31	9.3	24	1.4
September	30	9.0	24	1.4
October	31	9.3	22	1.5
November	30	9.0	14	1.7
December	31	9.3	12	1.9

The density of water can be taken as 1000 kg/m³ and the specific heat as 4.18 kJ/kg°C. Monthly demands are given by

$$\begin{aligned}
 q_m &= (Q \times \text{days/month})(\rho_w c_{pw})[T_d - T_s(t)] \\
 &= (0.30 \times \text{days/month})(1000 \times 4.18)[60 - T_s(t)]
 \end{aligned}$$

The monthly energy demands are tabulated in [Table 4.5](#).

4.3.2 Cooling Requirements for Buildings

The cooling load of a building is the rate at which heat must be removed to maintain the air in a building at a given temperature and humidity. It is usually calculated on the basis of the peak load expected during the cooling season. For a given building, the cooling load depends primarily on:

1. Inside and outside dry-bulb temperatures and relative humidities
2. Solar radiation heat load and wind speed
3. Infiltration and ventilation
4. Internal heat sources.

A method of calculating the cooling load is presented in detail in [\[12\]](#). The steps in calculating the cooling load of a building are as follows:

1. Specify the building characteristics: wall area, type of construction, and surface characteristics; roof area, type of construction, and surface characteristics; window area, setback, and glass type; and building location and orientation.
2. Specify the outside and inside wet- and dry-bulb temperatures.
3. Specify the solar heat load and wind speed.

4. Calculate building cooling load resulting from the following: heat transfer through windows; heat transfer through walls; heat transfer through roof; sensible and latent heat gains resulting from infiltration and ventilation; and sensible and latent heat gains (water vapor) from internal sources, such as people, lights, cooking, etc.

Equations 4.7 through 4.13 may be used to calculate the various cooling loads for a building. Cooling loads resulting from lights, building occupants, and so on, may be estimated from [12]. For unshaded or partially shaded windows, the load is

$$\dot{Q}_{wi} = A_{wi} \left[F_{sh} \bar{\tau}_{b,wi} I_{h,b} \frac{\cos i}{\sin \alpha} + \bar{\tau}_{d,wi} I_{h,d} + \bar{\tau}_{r,wi} I_r + U_{wi} (T_{out} - T_{in}) \right] \quad (4.7)$$

For shaded windows, the load (neglecting sky diffuse and reflected radiations) is

$$\dot{Q}_{wi,sh} = A_{wi,sh} U_{wi} (T_{out} - T_{in}) \quad (4.8)$$

For unshaded walls, the load is

$$\dot{Q}_{wa} = A_{wa} \left[\bar{\alpha}_{s,wa} \left(\gamma_r + I_{h,d} + I_{h,b} \frac{\cos i}{\sin \alpha} \right) + U_{wa} (T_{out} - T_{in}) \right] \quad (4.9)$$

For shaded walls, the load (neglecting sky diffuse and reflected radiations) is

$$\dot{Q}_{wa,sh} = A_{wa,sh} [U_{wa} (T_{out} - T_{in})] \quad (4.10)$$

For the roof, the load is

$$\dot{Q}_{rf} = A_{rf} \left[\bar{\alpha}_{s,rf} \left(I_{h,d} + I_{h,b} \frac{\cos i}{\sin \alpha} \right) + U_{rf} (T_{out} - T_{in}) \right] \quad (4.11)$$

Sensible-cooling load due to infiltration and ventilation is

$$\dot{Q}_i = \dot{m}_a (h_{out} - h_{in}) = \dot{m}_a C p_a (T_{out} - T_{in}) \quad (4.12)$$

Latent load due to infiltration and ventilation is

$$\dot{Q}_w = \dot{m}_a (W_{out} - W_{in}) \lambda_w \quad (4.13)$$

where

\dot{Q}_{wi} is the heat flow through unshaded windows of area A_{wi}

$\dot{Q}_{wi,sh}$ is the heat flow through shaded windows of area $A_{wi,sh}$

\dot{Q}_{wu} is the heat flow through unshaded walls of area A_{wa}

$\dot{Q}_{wu,sh}$ is the heat flow through shaded walls of area $A_{wa,sh}$

\dot{Q}_{rf} is the heat flow through roof of area A_{rf}

\dot{Q}_i is the heat load resulting from infiltration and ventilation

\dot{Q}_w is the latent heat load

$I_{h,b}$ is the beam component of insolation on horizontal surface

$I_{h,d}$ is the diffuse component of insolation on horizontal surface

I_r is the ground-reflected component of insolation

W_{out}, W_{in} is the outside and inside humidity ratios

$U_{wi}, U_{wa'}$ are the overall heat-transfer coefficients for windows, walls, and roofs, including radiation

\dot{m}_a is the net infiltration and ventilation mass flow rate of dry air

Cp_a is the specific heat of air (approximately 1.025 kJ/kg K for moist air)

T_{out} is the outside dry-bulb temperature

T_{in} is the indoor dry-bulb temperature

F_{sh} is the shading factor (1.0 = unshaded, 0.0 = fully shaded)

$\bar{\alpha}_{s,wa}$ is the wall solar absorptance

$\bar{\alpha}_{s,rf}$ is the roof solar absorptance

i is the solar incidence angle on walls, windows, and roof

h_{out}, h_{in} is the outside and inside air enthalpy

α is the solar altitude angle

λ_w is the latent heat of water vapor

$\bar{\tau}_{b,wi}$ is the window transmittance for beam (direct) insolation

$\bar{\tau}_{d,wi}$ is the window transmittance for diffuse insolation

$\bar{\tau}_{r,wi}$ is the window transmittance for ground-reflected insolation

ASHRAE handbooks recommend the use of the cooling load temperature difference method. For more details of the method, refer to [12].

EXAMPLE 4.5

Determine the cooling load for a building in Phoenix, AZ, assuming the north, east, and west walls are shaded and having the specifications tabulated in Table 4.6.

Solution

To determine the cooling load for the building just described, calculate the following factors in the order listed:

1. Solar altitude α at solar noon (from Equation 10.28), noting that $h_s = 0$,

$$\sin \alpha = \sin \delta_s \sin L + \cos \delta_s \cos L \cos h_s = \cos(L - \delta_s) = \cos 15^\circ = 0.966$$

$$\text{Hence } \alpha = \sin^{-1}(0.966) = 74.9^\circ$$

2. For a vertical wall, the wall normal is horizontal. Hence at solar noon, the incident angle, i , is equal to the solar altitude. Thus, for a vertical, south-facing surface, $i = \alpha = 74.9^\circ$ and $\cos i = 0.26$
3. South-facing window load (from Equation 4.7)

$$\begin{aligned} \dot{Q}_{wi} &= 40 \left\{ \left(0.20 \times 0.6 \times 185 \frac{0.26}{0.966} \right) + (0.81 \times 80) + (0.60 \times 70) + [1.09(100 - 75)] \right\} \\ &= 5600 \text{ Btu/h} \end{aligned}$$

TABLE 4.6

Specifications for Example 4.5

Factor	Description or Specification
Building characteristics	
Roof	
Type of roof	Flat, shaded
Area $A_{f,sh}$, ft ²	1700
Walls (painted white)	
Size, north and south, ft	8 × 60 (two)
Size, east and west, ft	8 × 40 (two)
Area A_{wn} , north and south walls, ft ²	480 – A_{wi} = 480 – 40 = 440 (two)
Area A_{we} , east and west walls, ft ²	320 – A_{wi} = 320 – 40 = 280 (two)
Absorptance $\bar{\alpha}_{s,wi}$ of white paint	0.12
Windows	
Size, north and south, ft	4 × 5 (two)
Size, east and west, ft	4 × 5 (two)
Shading factor F_{sh}	0.20
Insolation transmittance	$\bar{\tau}_{b,wi} = 0.6$; $\bar{\tau}_{d,wi} = 0.81$; $\bar{\tau}_{r,wi} = 0.60$
Location and latitude	Phoenix, AZ; 33°N
Date	August 1
Time and local-solar-hour angle H_s	Noon; $H_s = 0$
Solar declination δ_s , deg	17°–55'
Wall surface tilt from horizontal β	90°
Temperature, outside and inside, °F	$T_{out} = 100$; $T_{in} = 75$
Insolation I , Btu/h ft ²	$I_{h,b} = 185$; $I_{h,d} = 80$; $I_r = 70$
U factor for walls, windows, and roof	$U_{wn} = 0.19$; $U_{wi} = 1.09$; $U_f = 0.061$
Infiltration, lbm dry air/h	Neglect
Ventilation, lbm dry air/h	Neglect
Internal loads	Neglect
Latent heat load Q_{wv} , %	30% of wall sensible heat load ^a

^a Approximate rule of thumb for Phoenix, AZ.

4. Shaded-window load (from Equation 4.8) Assuming the north, east, and west walls are all shaded with two 20 ft² windows on each wall

$$\dot{Q}_{wi,sh} = (3 \times 40)[1.09(100 - 75)] = 3270 \text{ Btu/h}$$

5. South-facing wall load (from Equation 4.9)

$$\begin{aligned} \dot{Q}_{wa} &= (480 - 40) \left\{ 0.12 \left[70 + 80 + \left(185 \frac{0.26}{0.966} \right) \right] + 0.19(100 - 75) \right\} \\ &= 12,639 \text{ Btu/h} \end{aligned}$$

6. Shaded-wall load (from Equation 4.10)

$$\dot{Q}_{wa,sh} = [(480 + 320 + 320) - (3 \times 40)][0.19(100 - 75)] = 4750 \text{ Btu/h}$$

7. Roof load (from Equation 4.11)

$$\dot{Q}_{rf} = 1700[\bar{\alpha}_{s,rf} \times 0 + 0.061(100 - 75)] = 2600 \text{ Btu/h}$$

8. Latent heat load (30% of sensible wall load, neglecting solar radiation)

$$\dot{Q}_w = 0.3[(480 + 480 + 320 + 320) - (4 \times 40)][0.19(100 - 75)] = 2050 \text{ Btu/h}$$

9. Infiltration load

$$\dot{Q}_i = 0$$

10. Total cooling load for the building described in the example

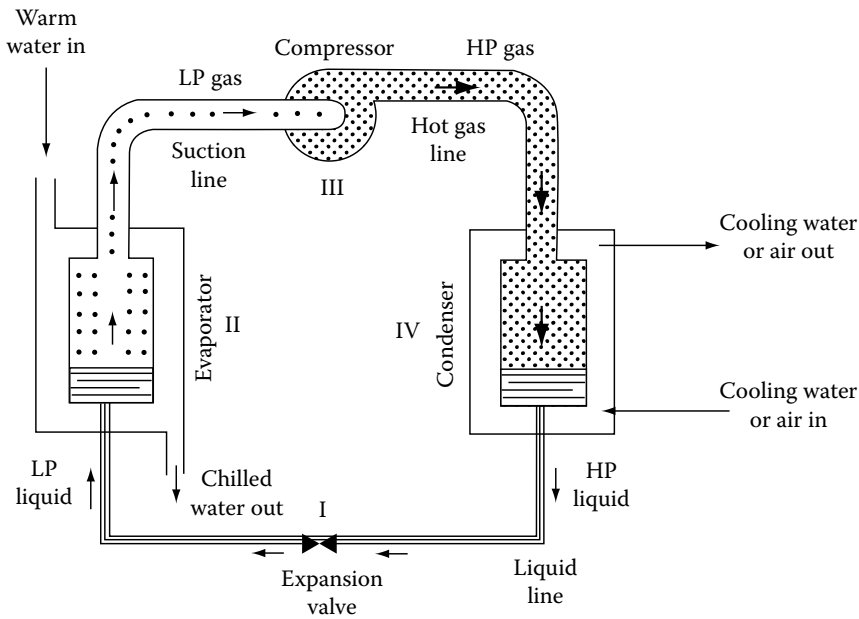
$$\begin{aligned}\dot{Q}_{tot} &= \dot{Q}_{wi} + \dot{Q}_{wi,sh} + \dot{Q}_{wa} + \dot{Q}_{wa,sh} + \dot{Q}_{rf} + \dot{Q}_w + \dot{Q}_i \\ \dot{Q}_{tot} &= 30,900 \text{ Btu/h}\end{aligned}$$

Looking at the various heat loads, it is apparent that the largest heat load comes from the south-facing walls. The heat load from these walls is three times larger than that from the shaded walls, and it would therefore behoove the architect or engineer to consider the options for reducing the heat load through the southern walls. Architectural options such as overhangs could be helpful.

4.3.3 Vapor-Compression Cycle

The two principal methods of lowering air temperature for comfort cooling are refrigeration with actual removal of thermal energy from the air or evaporation cooling of the air with adiabatic vaporization of moisture into it. Refrigeration can be used under any humidity condition of entering air, whereas evaporative cooling can be used only when the entering air has a comparatively low relative humidity.

The most widely used air conditioning method employs a vapor-compression refrigeration cycle. Another method uses an absorption refrigeration cycle similar to that of the gas refrigerator. The vapor-compression refrigeration cycle requires energy input into the compressor, which may be provided as electricity from a photovoltaic (PV) system. Referring to Figure 4.8, the compressor raises the pressure of the refrigerant, which also increases its temperature [16]. The compressed high-temperature refrigerant vapor then transfers thermal energy via a heat exchanger to the ambient environment in the condenser, where it condenses to a high-pressure liquid at a temperature close to, but above, the environmental temperature. The liquid refrigerant is then passed through the expansion valve where its pressure is reduced, resulting in a vapor-liquid mixture at a much lower temperature. The low-temperature refrigerant is then used to cool air or water in the evaporator where the liquid refrigerant evaporates by absorbing heat from the medium being cooled. The cycle

**FIGURE 4.8**

Schematic diagram illustrating the basic refrigeration vapor-compression cycle. (From Goswami, Y. et al., 2000. *Principles of Solar Engineering*, 2nd ed, Taylor & Francis, Philadelphia. [16])

is completed by the vapor returning to the compressor. If water is cooled by the evaporator, the device is usually called a chiller. The chilled water is then used to cool the air in the building.

The operating principle of a vapor-compression refrigeration cycle can be illustrated conveniently with the aid of a pressure-enthalpy diagram, as shown in Figure 4.9. The ordinate is the pressure of the refrigerant in N/m^2 absolute, and the abscissa its enthalpy in kJ/kg . The Roman numerals in Figure 4.9 correspond to the physical locations in the schematic diagram of Figure 4.8.

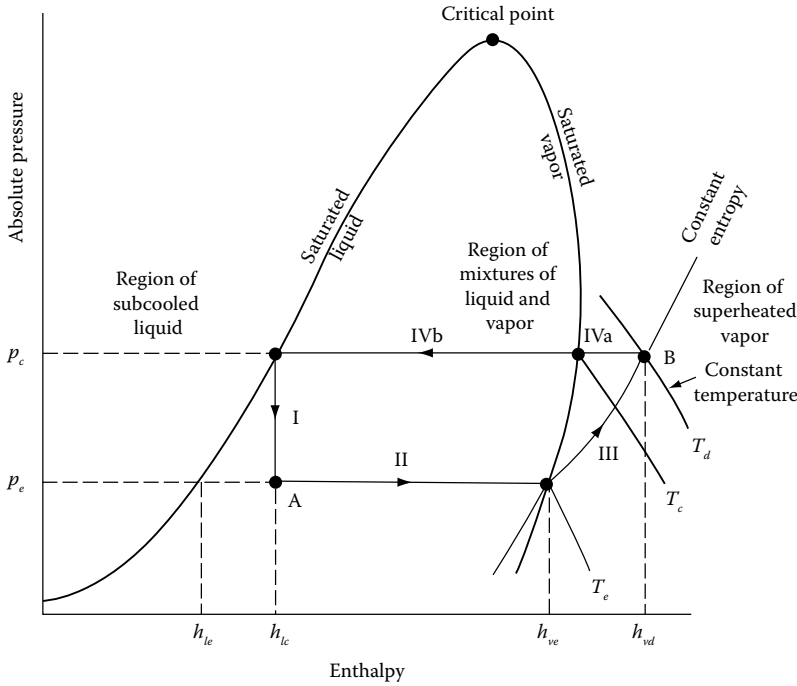
Process I is a throttling process in which hot liquid refrigerant at the condensing pressure, p_c , passes through the expansion valve, where its pressure is reduced to the evaporator pressure, p_e . This is an isenthalpic (constant enthalpy) process, in which the temperature of the refrigerant decreases. In this process, some vapor is produced, and the state of the mixture of liquid refrigerant and vapor entering the evaporator is shown by point A. Since the expansion process is isenthalpic, the following relation holds

$$h_{ve}f + h_{le}(1 - f) = h_{lc} \quad (4.14)$$

where

f is the fraction of mass in vapor state
subscripts v and l refer to vapor and liquid states,
respectively

c and e refer to states corresponding to condenser and evaporator pressures, respectively

**FIGURE 4.9**

Simple refrigeration cycle on a pressure-enthalpy diagram. (From Goswami, Y. et al., 2000. *Principles of Solar Engineering*, 2nd ed., Taylor & Francis, Philadelphia. [16])

and

$$f = \frac{h_{lc} - h_{le}}{h_{ve} - h_{le}} \quad (4.15)$$

Process II represents the vaporization of the remaining liquid. This is the process during which heat is removed from the chiller. Thus, the specific refrigeration effect per kilogram of refrigerant q_r is

$$q_r = h_{ve} - h_{lc} \text{ in kJ/kg (Btu/lb)} \quad (4.16)$$

In the United States, it is still common practice to measure refrigeration in terms of tons. One ton is the amount of cooling produced if 1 ton of ice is melted over a period of 24 h. Since 1 ton = 907.2 kg and the latent heat of fusion of water is 334.9 kJ/kg

$$1 \text{ ton} = \frac{(907.2 \text{ kg}) \times (334.9 \text{ kJ/kg})}{(24 \text{ h}) \times (3,600 \text{ s/h})} = 3.516 \text{ kW} = 12,000 \text{ Btu/h} \quad (4.17)$$

If the desired rate of refrigeration requires a heat-transfer rate of \dot{Q}_r , the rate of mass flow of refrigerant necessary, \dot{m}_r , is

$$\dot{m}_r = \frac{\dot{Q}_r}{(h_{ve} - h_{lc})} \quad (4.18)$$

Process III in Figure 4.9 represents the compression of refrigerant from pressure p_e to p_c . The process requires work input from an external source, which may be obtained from a solar-driven expander-turbine or a solar photovoltaic system. In general, if the heated vapor leaving the compressor is at the condition represented by point B in Figure 4.9, the work of compression W_c is

$$W_c = \dot{m}_r(h_{vd} - h_{ve}) \quad (4.19)$$

In an idealized cycle analysis, the compression process is usually assumed to be isentropic.

Process IV represents the condensation of the refrigerant. Actually, sensible heat is first removed in the subprocess IVa as the vapor is cooled at a constant pressure from T_d to T_c and latent heat is removed at the condensation temperature, T_c corresponding to the saturation pressure, p_c in the condenser. The heat-transfer rate in the condenser \dot{Q}_c is

$$\dot{Q}_c = \dot{m}_r(h_{vd} - h_{lc}) \quad (4.20)$$

This heat must be rejected into the environment, either to cooling water or to the atmosphere if no water is available.

The overall performance of a refrigeration machine is usually expressed as the ratio of the heat transferred in the evaporator, \dot{Q}_r , to the shaft work supplied to the compressor. This ratio is called the *coefficient of performance* (COP), defined by

$$\text{COP} = \frac{\dot{Q}_r}{W_c} = \frac{h_{ve} - h_{lc}}{h_{vd} - h_{ve}} \quad (4.21)$$

The highest COP for any given evaporator and condenser temperatures would be obtained if the system were operating on a reversible Carnot cycle. Under these conditions [17]

$$\text{COP}(\text{Carnot}) = \frac{T_e}{T_d - T_e} \quad (4.22)$$

The earlier cycle has been idealized. In practice, the liquid entering the expansion valve is several degrees below the condensing temperature, while the vapor entering the compressor is several degrees above the evaporation temperature. In addition, pressure drops occur in the suction, discharge, and liquid pipelines, and the compression is not truly isentropic. Finally, the work required to drive the compressor is somewhat larger than W_c provided earlier, because of frictional losses. All of these factors reduce the COP below the maximum and must be taken into account in a realistic engineering design.

EXAMPLE 4.6

Calculate the amount of shaft work to be supplied to a 1-ton (3.52 kW) refrigeration plant operation at evaporator and condenser temperatures of 273 and 309 K, respectively, using Refrigerant 134a (R-134a) as the working fluid. The properties of Refrigerant 134a are tabulated in Table 4.7. Also calculate the COP and the mass flow rate of the refrigerant based on the ideal cycle described earlier.

TABLE 4.7

Properties of Refrigerant 134A for Example 4.6

Temperature (K)	Absolute Pressure (kPa)	Vapor-Specific Volume (m ³ /kg)	Liquid Enthalpy (kJ/kg)	Vapor Enthalpy (kJ/kg)	Vapor Entropy (kJ/kg·K)
Saturated					
273	292.8	0.0689	50.02	247.2	0.919
309	911.7	0.0223	100.25	266.4	0.9053
Superheated					
308.5	900	0.0226	–	266.18	0.9054
313	900	0.0233	–	271.3	0.9217
312.4	1000	0.0202	–	268.0	0.9043
313	1000	0.0203	–	268.7	0.9066

Solution

From the property table, the enthalpies for process 1 are

Saturated vapor at 273 K $h_{ve} = 247.2$ kJ/kg

Saturated liquid at 309 K $h_{lc} = 100.3$ kJ/kg

Saturated liquid at 273 K $h_{le} = 50.0$ kJ/kg

Therefore, from Equation 4.15:

$$f = \frac{100.3 - 50.0}{247.2 - 50.0} = 0.255$$

The mass flow rate of refrigerant, \dot{m}_r , is obtained from Equation 4.18 and the enthalpies given earlier, or

$$\dot{m}_r = \frac{3.52 \text{ kW}}{(247.2 - 100.3) \text{ kJ/kg}} = 0.024 \text{ kg/s}$$

The specific shaft-work input required is:

$$\frac{W_c}{\dot{m}_r} = h_{vd} - h_{ve}$$

The entropy s_e of the saturated vapor entering the compressor at 273 K and 292.8 kPa is 0.919 kJ/kg K. For an isentropic compression, the vapor will have the same entropy at point B and temperature T_d . From the property table, superheated vapor at a pressure of 911.7 kPa has an entropy of 0.919 kJ/kg K at a temperature of 313 K with an enthalpy of 270.8 kJ/kg. Thus, the energy input to the working fluid by the compressor is

$$W_c = 0.024(270.8 - 247.2) = 0.566 \text{ kW}$$

Finally, the heat-transfer rate from the refrigerant to the sink, or cooling water in the condenser, is from Equation 4.20

$$\dot{Q}_c = \dot{m}_r(h_{vd} - h_{lc}) = 0.024(270.8 - 100.3) = 4.09 \text{ kW}$$

The COP of the thermodynamic cycle is

$$\text{COP} = \frac{247.2 - 100.3}{270.8 - 247.2} = 6.2$$

whereas the Carnot COP is 273/36 or 7.6.

Air conditioners are commonly characterized using a metric related to the COP called the energy efficiency ratio, or EER. EER is the ratio of output cooling energy in Btu to the electric energy input in watt-hours. Whereas COP is dimensionless, EER has units of Btu/Wh. EER is related to COP via a simple units conversion, that is, $\text{EER} = 3.41 \times \text{COP}$. Considerable strides have been made to improve the EER and seasonal EER (SEER) of air conditioners. The latest improvements are aimed at using variable-speed compressors. Also, air-conditioning refrigerants have very high global warming potentials (GWPs). For example, the R134a used in the example problem has a GWP of 1,430, that is, it has 1,430 times the global warming potential of carbon dioxide. Just as the Montreal Protocol, originally signed in 1987, led to the phase-out of ozone-depleting refrigerants, there are now many research efforts focused on replacing today's common refrigerants with new ones that have low GWPs.

4.3.4 Evaporative Cooling

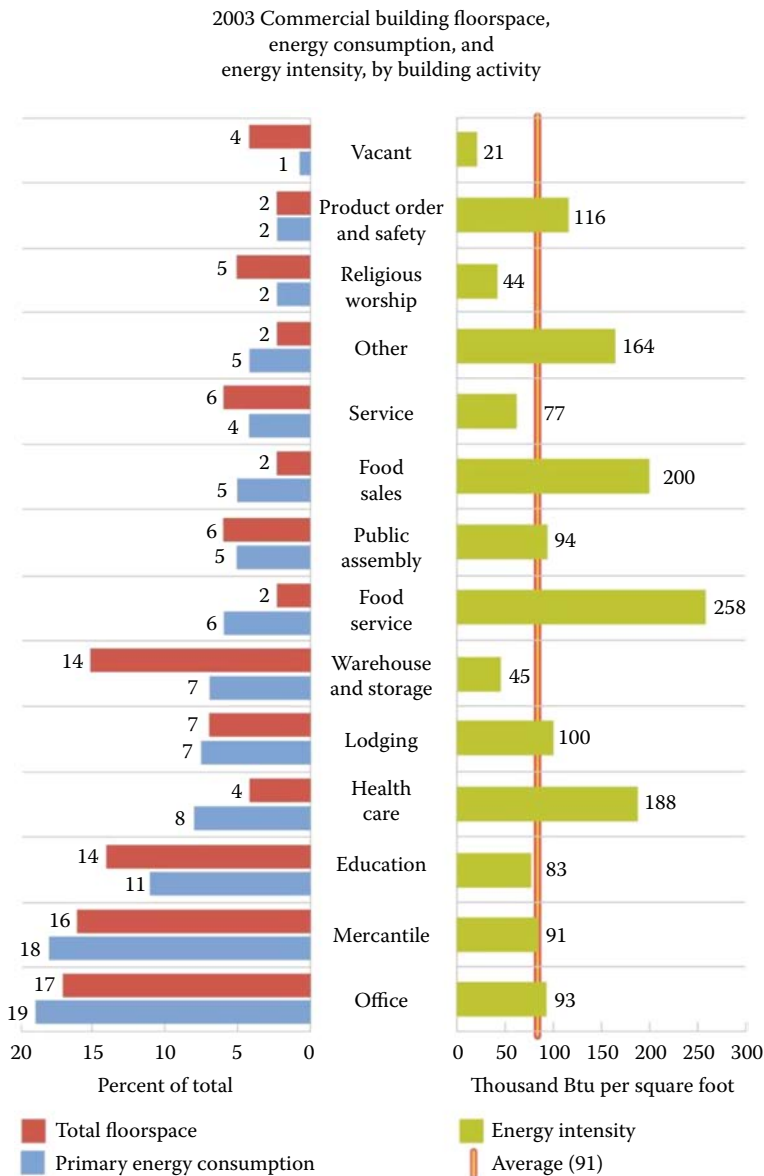
When air with less than 100% relative humidity moves over a water surface, the evaporation of water causes both the air and the water to cool. The lowest temperature that can be reached by this direct evaporative cooling effect is the wet-bulb temperature of the air, which is directly related to the relative humidity, with lower wet-bulb temperature associated with lower relative humidity. Thus, dry air (low relative humidity) has a low wet-bulb temperature and will undergo a large temperature drop with evaporative cooling, whereas humid air (high relative humidity) can only be slightly cooled evaporatively. The wet-bulb temperature for various relative humidity and air temperature conditions can be found via the psychrometric chart available in most thermodynamic texts. Normally, an evaporative cooling process cools the air only part of the way down to the wet-bulb temperature. To achieve the maximum temperature decrease, it is necessary to have a large water surface area in contact with the air, and interior ponds and fountain sprays are often used to provide this air-water contact area.

The use of water sprays and open ponds on roofs provides cooling primarily via evaporation. The hybrid system involving a fan and wetted mat, the “swamp cooler,” is by far the most widely used evaporative cooling technology. Direct, indirect, and combined evaporative cooling system design features are described in [12,17].

4.3.5 Energy Efficiency in Commercial Buildings

Commercial buildings come in a wide variety of types and encompass many activities as shown for the United States in Figure 4.10 [18]. This figure shows the total commercial building floor space, the primary energy consumption, and the energy use intensity (EUI) for various activities. Office buildings, stores, and schools are the largest primary energy users in that order, while food service, sales, and health care have the highest energy use intensities per square foot of floor area.

Commercial building energy uses in the United States by major end uses are shown in Figure 4.11 [19].

**FIGURE 4.10**

Commercial building floor space, energy consumption, and energy use intensity by activity. (From DOE. *Buildings Energy Data Book*, <http://buildingsdatabook.eren.doe.gov>. [18])

We can see that significant gains have been made in reducing heating and lighting loads, as their total energy consumption has gone down despite the growth in building square footage.

Energy-efficient building design starts with a goal for energy use, usually expressed in terms of EUI, which is the annual energy use per square foot of total building floor area, for example, 25,000/ft² per year. Experience has shown that aggressive energy design goals can be achieved if combined design-build teams compete to win the building contract and if the EUI goal is specifically tied to financial incentives.

Energy use in U.S. commercial buildings by major end uses, 2012
trillion British thermal units

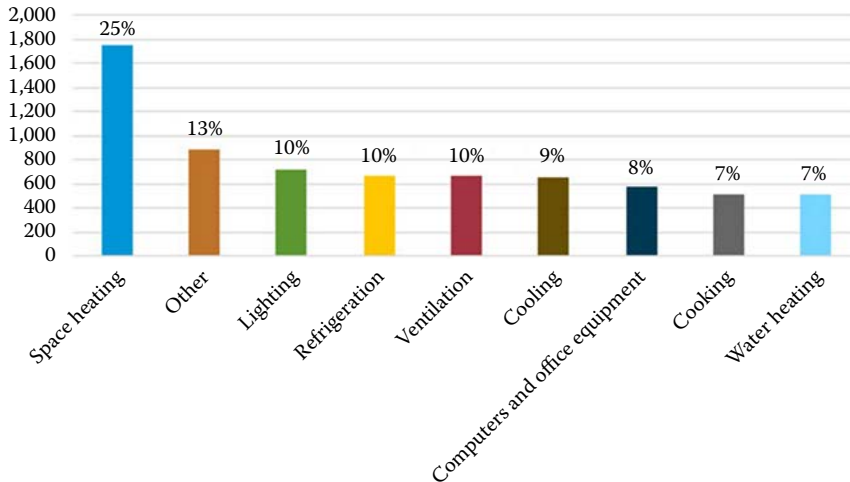


FIGURE 4.11

Energy use in U.S. commercial buildings by major end uses, 2012. (From EIA, 2012. Commercial Buildings Energy Consumption Survey: Energy usage summary, <https://www.eia.gov/consumption/commercial/reports/2012/energyusage>. [19])

In making buildings more efficient, we can focus on building types (for example, supermarkets and hospitals) or end uses (cooling and computing). For building types, the U.S. Department of Energy (DOE) has partnered with the ASHRAE to develop Advanced Energy Design Guides (AEDGs). These cover various building types and provide guidelines for either a 30% or 50% energy reduction compared to code (ASHRAE 90.1) [20]. These are available online at ASHRAE [21]. Fifty percent reductions are more in line with recent practice, and these design guides are available for:

- Grocery stores
- Large hospitals
- Small-to-medium office buildings
- K–12 schools
- Medium- to big-box retail buildings

A variety of energy efficiency measures (EEMs) are considered in minimizing commercial building energy use.

Building Envelope: High levels of envelope insulation, highly-reflective fenestration, and air-tight construction are essential for minimizing heat gain in the summer and heat loss in the winter. The optimum amounts and orientation of glazing and shading elements are essential for minimizing summer heat gain and winter heat loss, providing adequate daylighting and allowing for some passive solar heat gain. (Passive solar heating concepts are described in [Chapter 12](#).) Double- or triple-pane windows reduce convective heat loss. And low emittance (low-e) coatings also reduce radiative heat exchange. Low solar heat

gain factors are especially important in hot, sunny climates and in buildings with high internal heat gain.

Lighting: Highly efficient fluorescent or light-emitting diode (LED) lighting not only reduces the electricity needed for lighting but also reduces air conditioning loads that result from the waste heat associated with inefficient lighting. LED lights are becoming especially popular because of their rapidly falling costs and high efficacy. (Efficacy is the radiant flux of visible light in units of lumens divided by the total energy consumed in watts. Today's LEDs have efficacies comparable to natural daylight—although daylight consumes no electric power—and are still improving.) LEDs (p-n junctions) emit light by electroluminescence, whereby electrons passing through the diode drop to a lower energy state and emit photons of light. Automatic adjusting of lighting levels can save energy by taking advantage of natural daylight—balancing artificial lighting and daylighting. Various means, such as films and reflectors, can be used to reflect and spread daylighting to the building interior. Lighting can also be aimed at product shelves.

Ventilation: Tight construction to minimize infiltration through air leaks in the building envelope has made it more important to address indoor air quality. Commercial buildings require ventilation for the health of occupants. Ventilation is one of the largest contributors to space heating and cooling loads in commercial buildings. Controlled ventilation facilitates minimum air changes that maintain indoor air quality and meet code, thereby minimizing associated heating and cooling loads. Heat recovery devices can be used to preheat or precool incoming ventilation air using the exhaust air stream, and when outdoor conditions are favorable, natural or forced ventilation can displace mechanical cooling (commonly called economizer cooling).

Heating and Cooling Equipment: Variable-speed heat pumps (heat pumps are essentially air conditioners that can also run backwards as a heating system) have a coefficient of performance (COP), which is the ratio of the rate of heating or cooling in Btus per hour divided by the compressor power in using the same units. A heat pump uses mechanical energy (an electrically-driven compressor in a refrigeration cycle) to move heat from a low-temperature source to a high-temperature sink. For an air-source heat pump operating in summer cooling mode, the source is the indoor air and the sink is the outside air. When operating in winter heating mode, the source is the outside air and the sink is the inside air. The smaller the difference between the source and sink temperatures, the higher the efficiency of the heat pump. Using the ground as the heat source and sink instead of outside air yields, on average, a lower delta-T and thus increases the COP. (The ground temperature at depth is close to the average annual air temperature and so is cooler than outdoor air temperature in summer cooling mode and warmer than outdoor air temperature in winter heating mode.)

Research is being done on desiccant-based cooling systems that allow latent heat (moisture) to be removed from indoor air separately from sensible cooling (i.e., lowering the air temperature). In humid climates, moisture is removed by running the air conditioner evaporator coil below the indoor air dew point temperature to cause the moisture to condense out. This requires running the evaporator at a lower temperature than would be needed to sensibly cool the air and often requires "re-heat" for comfort. Both these effects reduce efficiency. In a desiccant cooling system, moisture is removed by passing indoor air through the desiccant. The dried air can then be cooled via evaporative cooling (the same mechanism by which perspiration cools the skin), which requires only a source of water and

a small amount of fan power. (Studies have shown that the water used on-site is similar in volume to the water used for the cooling of central power plants that supply the electricity for conventional air conditioners. See, for example [22].) A separate heat source is needed, however, to “bake out” the desiccant to remove and reject the collected moisture to the outside air. In an all-electric design, a small heat pump powered by PV electricity can be used for desiccant regeneration.

Office Computers and Equipment: Office equipment energy use can be reduced by using central printers and copiers (private documents can be printed out via codes), use of laptops instead of desktop computers, local task LED lighting, and energy-saving power strips. Data centers are becoming major energy users. Capturing the waste heat from servers and using it to provide building space heating can result in considerable energy savings. This has been done using both air and water cooling. There is current research underway on capturing the heat from CPUs by immersing them directly in a dielectric fluid that efficiently carries the heat away and uses it for other purposes. See, for example, Figure 4.12. There is also research to design more heat-tolerant CPUs so that the waste heat is at more useful temperatures [23].

There are clearly many design features to consider in maximizing energy efficiency. Evaluating them properly requires a detailed hour-by-hour energy analysis using typical weather data corresponding to the building site. To make this analysis widely available, DOE has developed OpenStudio [24], a suite of free and open-source software applications that facilitates building energy analysis using DOE’s EnergyPlus calculation engine and a program called Radiance for daylighting calculations. Figure 4.13 shows the flow process for an OpenStudio building model. OpenStudio has a Building Component Library that allows the modeler to drag and drop in a wide range of building components and their associated performance parameters.

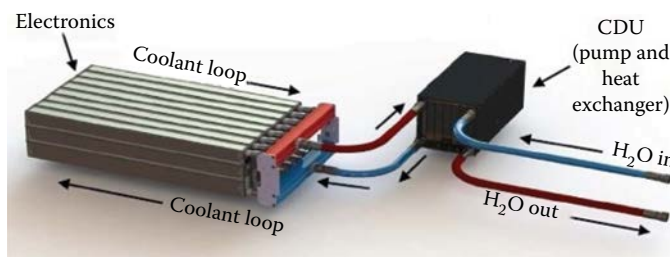


FIGURE 4.12
Product for direct liquid cooling of data center CPUs. (Courtesy of LiquidCool Solutions.)

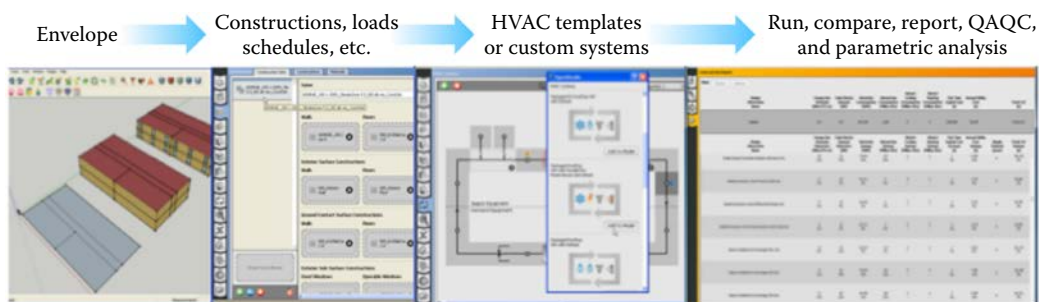
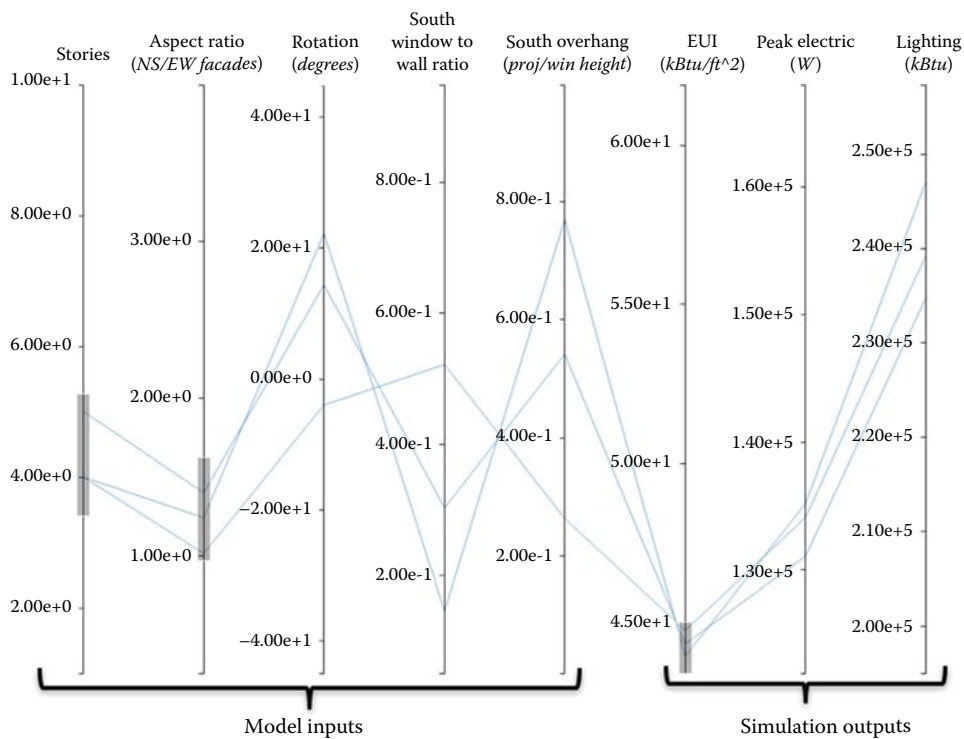


FIGURE 4.13
The OpenStudio flow process for modeling a building. (From Open Studio, <https://www.openstudio.net>. [24])

**FIGURE 4.14**

An example OpenStudio parallel coordinates plot that captures the results of thousands of parametric runs and allows the user to easily investigate the impact that changes in inputs and outputs have on each other. (Courtesy of D. Goldwasser, NREL.)

Once a model is created, parametric runs allow the designer to compare many different options, as shown in Figure 4.14. The five items on the left of the figure (number of stories, building aspect ratio, building rotation, window-to-wall ratio, and south overhang) are building model input parameters. The three items on the right (Energy Use Intensity, peak electric demand, and lighting energy) are outputs of the simulation. After parametric runs are made, the user can adjust the sliders to see how the other parameters (both input design parameters and output values) change. The various gray lines represent the different runs that were made for the parametric analysis. A number of other building energy simulation programs are listed on the DOE Qualified Software List [25].

4.3.5.1 Commercial Buildings Case Studies

An ultimate goal in commercial building efficiency is to achieve net zero (or even positive energy production) status. Different definitions have been used for net-zero energy buildings. According to DOE's recent report, *A Common Definition of Zero Energy Buildings*, a net-zero energy building is "an energy-efficient building where, on a source energy basis, the actual annual delivered energy is less than or equal to the on-site renewable exported energy" [26]. In other words, net zero does not imply a building that used no energy, but rather on whose annual energy use is equal to the annual on-site production of renewable energy. Thus, net-zero buildings directly address climate change. We will consider two case studies: a large office building and a small commercial building that combines retail and some grocery.

The National Renewable Energy Laboratory Research Support Facility: The National Renewable Energy Laboratory (NREL) Research Support Facility (RSF) is the nation's largest net-zero energy office building. A key to accomplishing net-zero energy at the RSF was using a performance-based acquisition process that required a design-build team to meet a specific energy design goal, specifically an annual energy use (including the data center) of 35,000 Btus per square foot per year. Building energy computer modeling was used to analyze the impacts of a variety of energy performance measures that were employed to achieve the design goal, including [27]:

- East–west orientation of 60-foot deep wings with significant south-facing glass that provides passive solar heating in the winter and daylighting throughout the year, the latter aided by LightLouvers™, which reflect daylight deep into the interior
- Radiant heating/cooling in ceilings that eliminates ducting and fan power and operates at an efficient water temperature
- A dedicated outdoor air system that maintains air quality with minimal impact on heating and cooling loads; the system uses evaporative cooling when needed in hot weather
- Automated and manually operable windows for natural ventilation cooling
- High-efficiency lighting with automatic controls to augment daylighting
- Precast wall panels with 2 inches of concrete for thermal mass on the inside and outside surfaces with an internal core of 4 inches of rigid board insulations; the thermal mass allows the building to be cooled in the summer via purging the building with cold nighttime air
- Transpired Solarwall® for preheating building ventilation air in cold weather
- Shading devices and electrochromic glazing to reduce solar heat gain in summer
- Overhead tubular daylighting devices
- Minimal workstation plug loads at only 70 W per station

In addition to the energy-efficiency features, the RSF utilizes a total of 2.5 MW of photovoltaic modules mounted on the RSF roof, the NREL parking garage, and the visitors' parking lot canopy. A wood chip heating plant (utilizing wood chips from bark beetle kill) and data center waste heat augment natural gas used to provide hot water heating. Sufficient excess solar photovoltaic electricity is exported to the grid to make up for the natural gas burned on-site.

Net-Zero Walgreens Store: Robbins et al. [28] describe the development of a net-zero-energy Walgreens store. Walgreens stores present a valuable opportunity because they combine both a retail and small supermarket space in one building and are ubiquitous with 76% of Americans living within 5 miles of a Walgreens. When Walgreens replaced an existing store in Evanston, Illinois, they decided to take advantage of the fact that their corporate engineers are located only 15 miles away and replace it with a state-of-the-art net-zero store. A challenge the engineers faced was to achieve net-zero status while maintaining more glass area than is optimum from an energy standpoint in order to make the store attractive to retail customers. The 15,000 ft² building features include the following [28]:

- R-30 roof and R-20 walls
- 840 roof-mounted PV modules rated at 256 kW

- South-facing rooftop clerestories that admit daylighting with automatic operable windows to allow for natural ventilation during appropriate ambient conditions
- A revolving entrance door to reduce infiltration loads
- Light-redirecting film on high west-facing glass to bounce daylight off the ceiling and deep into the building
- All-LED lights directionally aimed at retail shelves with a lighting density of only 0.89 W/ft² (compared to an ASHRAE Standard 90.1-2016 value for retail spaces of 1.4 W/ft²) [20]
- A ground-source heat pump for heating and cooling using the ground under the parking lot; transcritical CO₂ is used as the working fluid, thus eliminating HCFC refrigerants that have a high global warming potential; the heat pump takes advantage of waste heat from the freezers

As a first-of-a-kind project, Walgreens engineers learned valuable lessons. For example, while CO₂ worked well as a refrigerant, its high pressure required more expensive piping. Measurement and verification (M&V) would have been easier if it had been sufficiently considered early enough in the project and checked at each stage. The building has performed as net zero for many months but not on an annual basis. Nevertheless, its annual operating cost has been less than 20% of the previous store on that site, which was smaller.

4.3.6 Energy Efficiency in Residential Buildings

Residential building on-site energy consumption and end uses vary by housing type (single family attached, single family detached, multifamily), vintage, and region and details are given in the DOE Buildings Energy Data Book [18]. It indicates that space heating is responsible for 45% of on-site energy use, water heating is 18%, and space cooling is 9%. The rest is split among lighting, cooking, electronics, refrigeration, and other uses.

The breakdown is different when one looks at primary energy use. Table 4.8 gives a breakdown of residential building primary (or source) energy uses [29]. Primary energy use, which accounts for fossil fuels used on-site and the fuels used to produce electricity. While space heating represents 45% of on-site energy use (due largely to natural gas furnaces), it represents only 25% of primary energy use because of the fuels consumed in power plants to provide electricity to the buildings.

DOE has evaluated energy savings potentials for both residential and commercial buildings, and these are shown in Figure 4.15 [30].

Roughly 80% of residential building square footage and energy consumption is in single-family buildings, so the DOE's energy savings efforts are currently focused on that market. The following are example areas for energy efficiency improvements in residential buildings [30].

Building Envelope:

- Roof/attic insulation
- Exterior wall insulation
- Air sealing to reduce infiltration to 3-5 ACH measured at a 50 Pa differential pressure during blower door testing; this corresponds to about 0.2 to 0.3 natural air changes per hour

TABLE 4.8

U.S. Residential Buildings Primary Energy Use in 2016

End Use	Quads	Percent
Space heating	5.11	24.9%
Space cooling	2.31	11.2%
Water heating	2.68	13.0%
Refrigeration	1.06	5.2%
Cooking	0.57	2.8%
Clothes dryers	0.68	3.3%
Freezers	0.23	1.1%
Lighting	1.48	7.2%
Clothes washers	0.08	0.4%
Dishwashers	0.29	1.4%
Televisions and related equipment	0.98	4.8%
Computers and related equipment	0.33	1.6%
Furnace fans and boiler pumps	0.35	1.7%
Other uses	4.39	21.4%
Total	20.54	100.0%

Source: From EIA. *Annual Energy Outlook 2015*, <http://www.eia.gov/forecasts/aeo/data/browser/#/?id=4-AEO2015&cases=ref2015&sourcekey=0>. [29]

- For new or retrofit building envelope systems careful consideration must be given to moisture management including interstitial condensation, outside water drainage, and the ability to dry after a wetting event. Moisture is managed through detailing of vapor retarders (selection of proper perm ratings), drainage planes, and weather skins

Equipment:

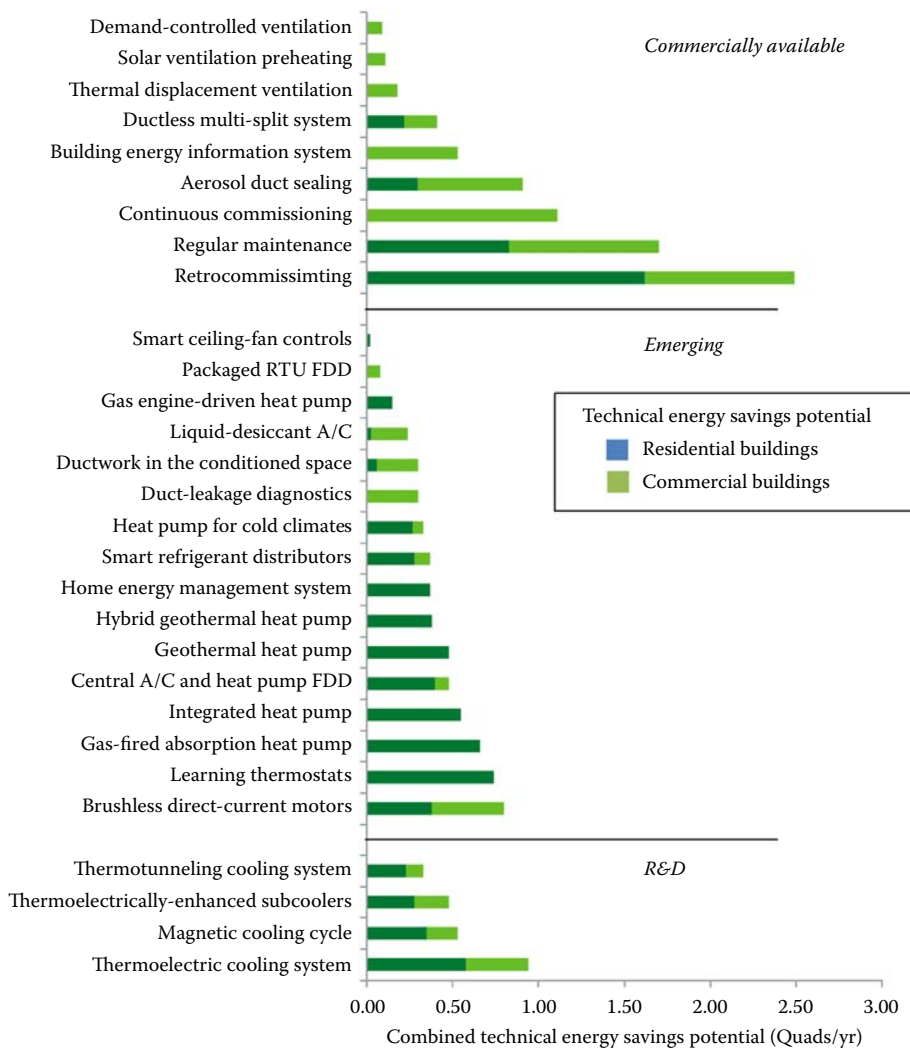
- Higher efficiency air conditioners and air source heat pumps (now available in cold climate models) or ground source for new homes in appropriate climates (multifamily or community scale projects offer the best economics) or high-efficiency, sealed combustion condensing gas furnaces
- Duct sealing and insulation (or moving inside conditioned space)
- Ducted heat pump water heater or tankless gas-fired heater (which eliminate tank heat losses)

Lighting:

- Replace all fixtures with LED
- Controls to turn off lighting based on occupancy

Appliances:

- ENERGY STAR refrigerator, washer, dryer, and dishwasher. (The U.S. Environmental Protection Agency's ENERGY STAR program has identified and promoted energy efficiency in products and buildings since its inception in 1992)

**FIGURE 4.15**

DOE energy savings potentials for residential and commercial buildings. Residential is shown by the bars and commercial by the light bars (From U.S. Department of Energy, October 2012. *Energy Savings Potential and Research, Development & Demonstration Opportunities for Residential Building Heating, Ventilation, and Air Conditioning Systems*, DOE/EE-0850. [30])

Other:

- Smart thermostat (which can be controlled remotely, for example, via Wi-Fi, and generally provides different programming or self-learning options)
- WaterSense-labeled fixtures
- Energy-saving power strips to reduce miscellaneous electrical loads (MELs), also called plug loads
- Energy Star laptop computer

The design of all buildings and the impacts of energy efficiency measures depend strongly on the climate region in which the building is located. This is especially true of residential

buildings, which, unlike many commercial buildings, are impacted more by external weather conditions than by internal human and equipment loads. The International Energy Conservation Code (IECC) classifies 7 different climate regions in the United States as shown in the map of Figure 4.16 [31].

Researchers at NREL have performed detailed computer analysis called ResStock of the single-family residential building stock in the United States using a number of data sources [32]. They considered the impact of climate zone, building vintage, and fuel type to determine the energy savings potentials for various energy efficiency measures. Table 4.9 shows rolled-up results aggregated by region for four different energy efficiency measures:

1. Replacing an electric water heater with a heat pump water heater
2. Replacing single-pane windows with double-pane low-e windows
3. Air sealing to reduce infiltration to 5 ACH as measured using a blower door test operating at an indoor-outdoor pressure differential of 50 Pa (This would be equivalent to about 0.3 natural ACH; the current International Energy Conservation Code calls for 3 or more ACH [depending on climate zone] during a blower door test at 50 Pa pressure difference)
4. Adding attic insulation to achieve a level of R-49

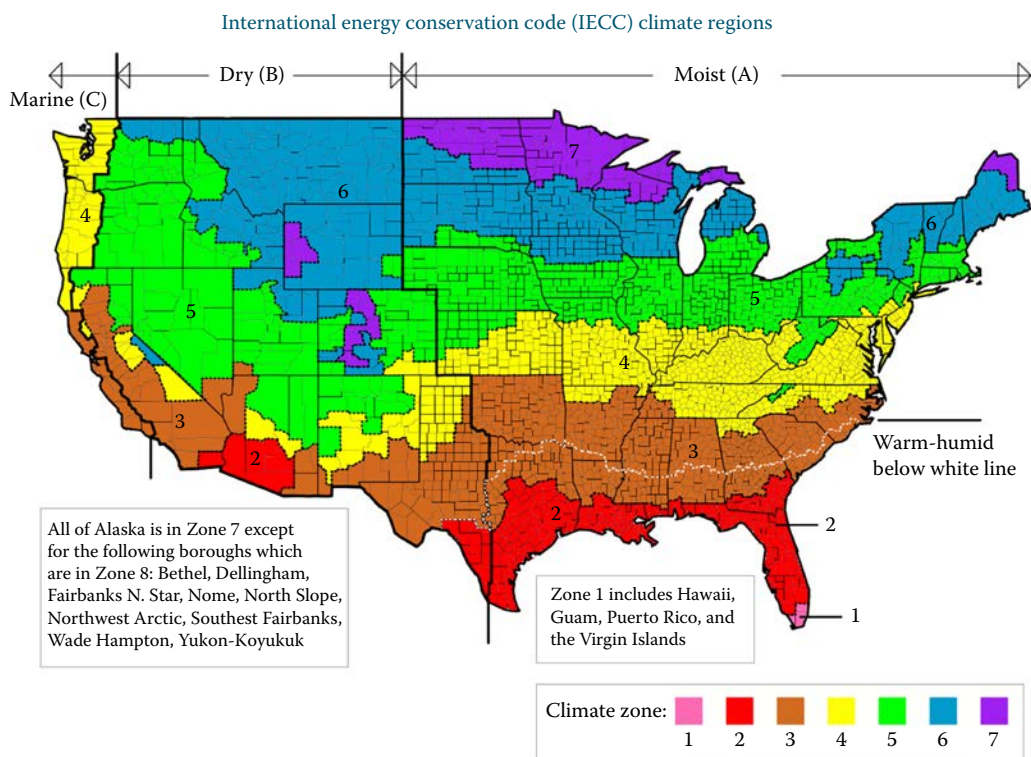


FIGURE 4.16

International Energy Conservation Code climate regions. Republished with permission from Pacific Northwest National Laboratory. (From Pacific Northwest National Laboratory, January 2013. Building science-based climate maps, PNNL-SA-90570. [31])

TABLE 4.9
Primary (or Source) Energy Savings Potential of Four Energy Efficiency Measures for Detached Single-Family Homes in the United States
(Excludes Alaska and Homes with Propane or other Atypical Fuel Types). Darker Cells Indicate Higher Performance. (NREL)

IECC Climate Zone	Baseline Source Energy Consumption [Quads/yr]	Aggregate Energy Savings [Source Quads/yr]				Per House Energy Savings, Upgraded Houses [Source MBtu/yr], (Millions)					
		Heat Pump Water Heater ^a	Windows ^b	Air Sealing ^c	Attic Insulation ^d	Total	Heat Pump Water Heater ^a		Windows ^b	Air Sealing ^c	Attic Insulation ^d
							Water Heater ^a	Water Heater ^a			
1	0.21	0.01	0.01	0.01	0.01	0.04	17.4	0.7	21.9	0.5	0.8
2	2.2	0.12	0.09	0.11	0.06	0.38	18.0	6.9	19.4	4.9	10.4
3	3.31	0.13	0.12	0.13	0.12	0.5	17.5	7.5	15.0	8.3	17.3
4	3.4	0.12	0.09	0.24	0.1	0.55	17.0	6.9	16.4	5.5	15.7
5	4.04	0.07	0.08	0.26	0.11	0.52	16.7	4.5	17.5	4.7	15.4
6	0.89	0.02	0.02	0.04	0.01	0.09	17.3	0.9	19.5	0.9	3.0
7	0.07	0	0	0	0	0	16.3	0.1	22.8	0.1	0.2
Total	14.12	0.47	0.41	0.79	0.41	2.08	27.6		24.7		64.5

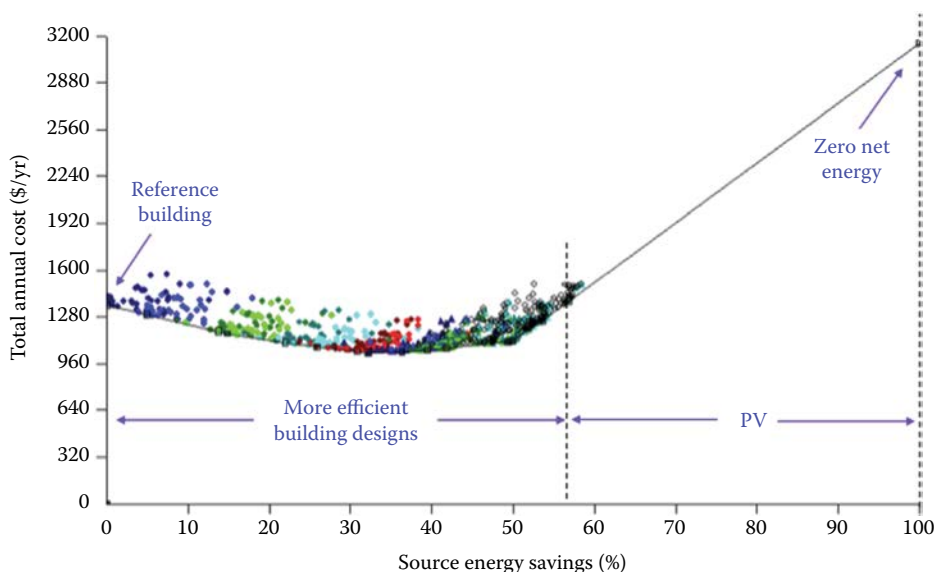
Source: From Wilson, E. et al., January 2017. Electric end-use energy efficiency potential in the U.S. single family housing stock, NREL/TP-5500-65667. [32]

^a Replacing electric tank with heat pump water heater.

^b Single pane to double low-e.

^c To 5 ACH50.

^d To R-49.

**FIGURE 4.17**

Example output from BEopt analysis of the cost and energy savings impact of various combinations of energy efficiency measures. (From Christensen, C. et al., August 2006. BEopt software for building energy optimization: Features and capabilities, NREL/TP-550-39929. [33])

The aggregated energy savings for these four measures in each region are expressed both as aggregated savings in the region in source energy quads per year and as per house energy savings in thousands of Btus of source energy per year [32].

To analyze the value of energy efficiency measures in new and existing homes, NREL has developed a computer model called BEopt, which optimizes various combinations of measures. BEopt accepts as input a full range of energy performance specifications including window area and R-value, air changes, type and efficiency of space conditioning equipment, insulation levels (attic, wall, basement), type and efficiency of water heater (including solar), lighting type and efficiency, appliance efficiencies, equipment schedules, PV arrays (size, efficiency, tilt, and azimuth), and so on. Quantities such as attic or wall insulation are provided in a list of actual thicknesses that can be purchased.

Figure 4.17 shows an example plot of data points representing various combinations of a multitude of example EEMs for a single-family residence. The reference building is whatever you start with before you add additional energy efficiency features, for example, a new home built to code or your existing home. Different combinations of features can achieve the same savings. The y-axis represents total annual cost, which is the sum of energy (utility) costs and total loan costs (mortgage and any additional loan for purchasing the EEMs). As efficiency measures are added, energy savings costs exceed additional loan costs and so the total decreases until it reaches a minimum. In this example, at an energy savings of about 57%, the total cost is equal to the original total cost. This is called the neutral cost point. These savings are achievable at no net cost to the homeowner.

Achieving zero energy (assuming an all-electric home) requires the addition of PV modules, which increases the cost. However, the cost of PV has dropped rapidly. As a result, the straight PV line is moving to the left (the point at which the addition of

PV is less expensive than the marginal cost of additional energy efficiency measures, which reach a point of diminishing returns) and its slope is decreasing. Given the right financial terms, the net-zero point can be reached with little or no increase in total annual cost, which is equivalent to positive cash flow for the building owner from day one.

BEopt is available as a free download at <https://beopt.nrel.gov> [33]. Like OpenStudio, its calculations use the EnergyPlus model.

EXAMPLE 4.7

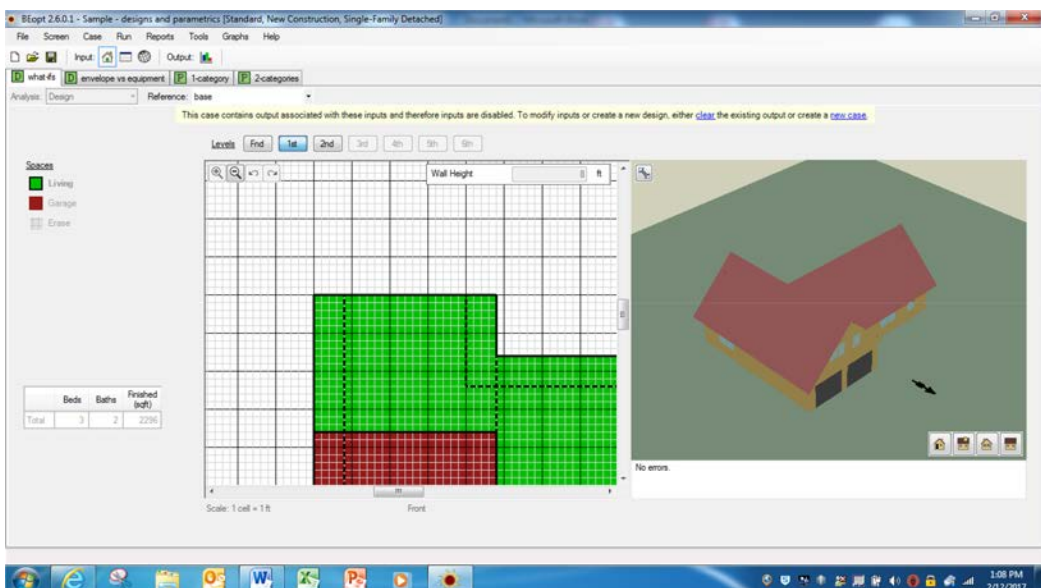
The sample BEopt model “Sample—designs and parametrics” compares a base case single family residence to 5 energy improvement cases involving changes in different components: walls, window type, lighting, AC & furnace, and water heater. Do the following:

- Construct a table showing for each of the 5 improvements the absolute and percent source energy savings and energy-related cost savings relative to the base design
- Identify the design with the maximum energy savings
- Identify the design with the maximum cost savings
- Identify the designs that are not cost-effective (that is, have higher energy related costs than the base design)

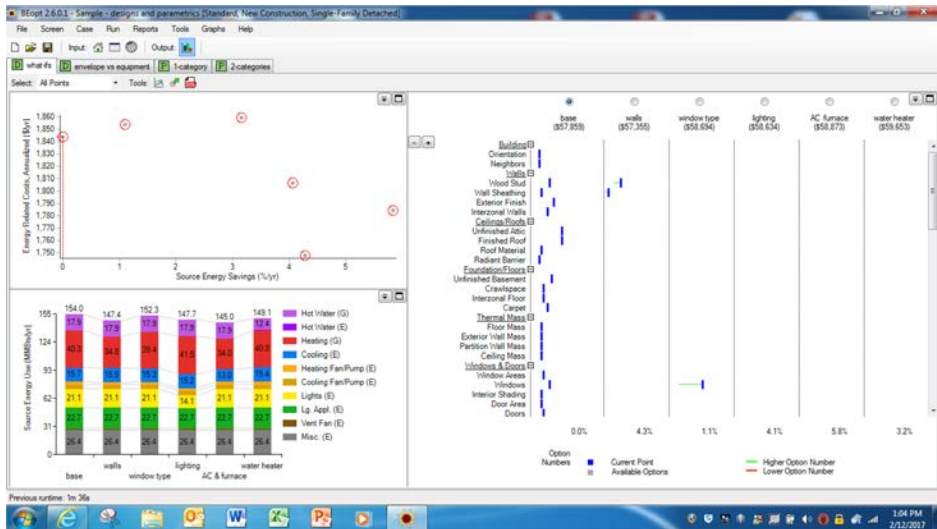
Solution

Do the following steps:

- After downloading BEopt, make sure that the boxes on the main screen are checked for Standard, New Construction, and Single-Family Detached and click OK.
- In the upper left-hand corner choose File-Open Project-Sample—designs and parametrics.BEopt
- Click the what-ifs tab in the upper left-hand corner



4. Click on the small bar chart icon in the Output tab at the top of the screen



5. Click in the check boxes for the various cases modeled at the upper right of the screen. For each case, move your cursor over the blue bars to see what design changes were made. (For example, in the window type case, double-pane windows have been replaced by triple-pane windows.)
- To get the absolute source energy savings compared to the base case for each of the five improvements, refer to the bar chart in the lower left and subtract the source energy use in each case from the base case value. You can get the percent savings from the bottom of the case columns at the right of the screen. To get the cost savings for each case, click in the pull-down menu in the upper left next to Select. For each case selected, the energy cost in \$/yr is in the lower right of the screen. To get the savings for each improvement case, subtract this value from the value for the base case. Calculate the percentage savings by dividing the savings for each improvement case by the base case energy use.

You can also find these values compiled in the BEopt Detailed Report. To download that spreadsheet, click on Reports—Detailed Report at the top of screen and choose What ifs. After you download it, open it and scroll down to the table “Output-Cost/Energy Graph Metrics” near the bottom of the spreadsheet. Note: Energy-Related Costs include utility savings and annualized investment costs for efficiency measures and future replacements. Percentages are of whole-house values, including significant quantities of nonspacing conditioning energy use.

The following table results:

Point	Source Energy Savings [MMBtu/yr]	Source Energy Savings [%/yr]	Energy-Related Cost Savings, Annualized [\$/yr]	Energy-Related Cost Savings %, Annualized [%/yr]
Walls	6.6	4.3%	97	5.2%
Window types	1.7	1.1%	–27	–1.4%
Lighting	6.3	4.1%	55	2.9%
AC & furnace	9.0	5.9%	61	3.3%
Water heater	4.9	3.2%	–14	–0.8%

- b. The design with the maximum energy savings is the AC & furnace case
- c. The design with the maximum cost savings is the walls case
- d. The cases that are not cost-effective are the window type and water heater cases.

4.3.6.1 Residential Case Study: Net-Zero Habitat for Humanity House

Habitat for Humanity volunteers build homes for low-income families. Low-income families pay a comparatively high percentage of their income on energy, so energy efficiency is important to minimize monthly utility bills. In 2008, building scientists from NREL teamed with Habitat for Humanity of Metro Denver to design and build an affordable and replicable zero-energy home in the cold Denver climate. Norton et al. [34] presented a case study on this project. State-of-the-art computer modeling tools were used to design the home.

A summary of the key features of the home taken from the case study is given in Table 4.10 [34].

TABLE 4.10

Summary of NREL-Habitat Zero Energy Home Attributes

Square footage	1.280 ft ²
Number of bedrooms	3
Number of occupants	3
Design heating load	15.000 Btu/h
Walls	Double stud wall Fiberglass batt insulation Nominal R-value = 40 h ft ² F/Btu
Ceiling	2-ft raised heel trusses Blown-in fiberglass insulation Nominal R-value = 60 h ft ² F/Btu
Floor	Fiberglass batt insulation Nominal R-value = 30 h ft ² F/Btu
South windows	Low-e, high SHGC $U = 0.30$ Btu/h ft ² F, SHGC = 0.58
North, west, and east windows	Low-e heat mirror $U = 0.23$ Btu/h ft ² F, SHGC = 0.27
Solar tempered	96 ft ² of south facing windows 3-ft overhangs for summer shading
Water heating	Drainback solar system 96-ft ² collectors with 200-gal storage tank NG tankless water heater for backup
Ventilation	ERV system with electronically computed motors
Space heating	Direct vent ductless NG heater in living room Electric baseboard heaters (750 W each) in bedrooms
Lighting	CFLs throughout the house
Appliances	ENERGY STAR clothes washer and refrigerator
Solar electric	Nominal 4-kW _p DC PV system
Other features	All mechanical equipment is within conditioned space Light-colored roof shingles Increased attic ventilation

Source: Norton, P. et al., June 2008. The NREL/Habitat for Humanity zero energy home: A cold climate case study for affordable zero energy homes, NREL/TP-550-4318. [34]

Note: SHGC = solar heat gain coefficient or the fraction of incident solar radiation admitted through a window, ERV = energy recovery ventilator, NG = natural gas, CFL = compact fluorescent light bulbs.

Although an all-electric home was considered, the cost of PV at that time caused the designers to elect to use some natural gas heating, which allowed them to downsize the PV array. At today's PV prices, a larger PV array powering heat pumps for space and water heating could eliminate the on-site burning of any fossil fuel. This early net-zero home exceeded its goal of zero net source energy and was a net energy producer (thus sending electricity back to the grid) during the first 2 years of operation when it was monitored. The cost per square foot was only 8% higher than for a standard Habitat home, although the home benefitted from lower land costs than is typical. The average utility bill was only \$17 per month, but some credit must be given to the energy-conscious occupants. The authors noted that the economics depends heavily on local net metering tariffs. Denver had rate structures that were less generous for rooftop PV systems than some locations.

4.3.7 Zero-Energy Urban Districts

We have described energy-efficient and zero-energy buildings. To achieve faster carbon emissions reductions we can't just address buildings one at a time. We need to extend these concepts to a multibuilding, or district, scale. Polly et al. [35] provide details on the concept of zero-energy urban districts, some of which we will summarize here. As the authors point out, there is especially a need to use the best building energy design concepts in cities, which are growing rapidly in developing nations. Over half of the world's population currently lives in urban areas. The United Nations is projecting that this number will increase to 66% by mid-century [36]. In 2011, the organization Architecture 2030 estimated that by 2030, 900 billion ft² (836 million m²) of new and rebuilt buildings would be constructed, mostly in the developing world [37]. This is equivalent to three-and-a-half times the total floor area currently existing in the United States.

The need to address climate change is recognized by mayors around the world who are already facing extreme weather events such as record heat waves and rainfall events. According to the Compact of Mayors website, as of March 2018, 7513 cities worldwide, representing nearly 700 million people, have committed to the Compact of Mayors, an agreement to measure and reduce greenhouse gas emissions [38]. In the United States, over 1000 mayors have signed the Mayors' Climate Protection Agreement and vowed to reduce carbon emissions below 1990 levels [39].

The concept of net-zero energy can be extended from buildings to a community scale. In 2009, Carlisle et al. developed definitions for net-zero energy communities [40]. More recently, DOE published source-energy-based definitions for zero-energy campuses and communities [26]. After decades of suburban living in the United States, there is a growing tendency, especially among Millennials, to choose to live in cities where all their needs are within walking distance. Thus, mixed-use developments that combine homes, retail stores, restaurants, recreation, and workplaces into one community are becoming more common, and this provides new energy savings opportunities. Energy can be moved from an internally load-dominated commercial building that needs cooling to a residential one that needs heating. Also, aggregating buildings makes it possible for renewable generation to be shared. And economies-of-scale may be achieved when purchasing large quantities of photovoltaic modules.

The organization EcoDistricts has published a protocol for sustainable urban development, and they state that "the district is the optimal scale to accelerate sustainability—small enough to innovate quickly and big enough to have a meaningful impact" [41]. There are a number of zero-energy districts and communities under

development. For example, the University of California, Davis, has pursued a net-zero energy community in the West Village development [42]. Two Denver projects, the National Western Center and the Sun Valley Neighborhood, are briefly described in [35]. DOE's Better Buildings program has launched a Zero-Energy District Accelerator to assist new projects [43]. Finally, European work on district energy systems can be found in the UN District Energy Initiative [44]).

Table 4.11 from Polly et al. shows design principles for zero-energy districts [35].

TABLE 4.11

Net-Zero Energy District Design Principles

Design Principle	Design Subprinciple
Maximize building efficiency	<p>Orientation: Maximize natural daylighting, take advantage of passive solar design (see Chapter 12)</p> <p>Enclosure: efficiencies currently being implemented in net zero energy building industry (e.g., DOE's Zero Energy Ready Program^a; ASHRAE's 50% Advanced Energy Design Guides^b)</p> <p>Miscellaneous electric loads: Carefully select best-in-class products; develop robust control strategies; verify with ongoing monitoring to minimize miscellaneous electric loads</p> <p>Lighting: 100% LED, controls for occupancy and daylighting variability</p> <p>Heating, ventilation, and air conditioning (HVAC): District-connected systems that maximize thermal energy recovery opportunities from low-grade heat sources across the district. For example, "ambient loops" circulate water that is close to the indoor air temperature and serve as heat source and sink for building heat pumps. Wastewater has been used in ambient loops. These loops can also be connected to the ground.</p>
Maximize solar potential	<p>Arrange buildings in districts to prevent building-to-building shading (shorter buildings to south, ideally)</p> <p>Orient buildings and roof slopes for maximum solar access</p> <p>Minimize other buildings systems that require roof space to provide room for PV modules</p> <p>Reserve all parking lots and garages to be shaded parking with PV</p> <p>To improve potential for off-grid resiliency, maximize rooftop solar</p>
Maximize renewable district thermal energy	Evaluate potential for renewable thermal energy systems and waste heat recovery (e.g., ground-source district heat pump systems, industrial waste heat recovery, wastewater heat recovery)
Maximize load control	Establish controls for building and district system energy demands to accommodate the variable renewable energy supplies (e.g., PV and wind) and to support the district's interaction with the electric grid

Source: From Polly, B. et al., 2016. *Proceedings of the ACEEE Summer Study on Energy Efficiency in Buildings*, ACEEE, Washington, DC. [35]

^a See DOE 2016 [45].

^b See ASHRAE 2018 [21].

4.4 Industrial Energy Efficiency

4.4.1 Background

Industrial energy use falls into the different industry categories shown in Figure 4.18 [46].

Industries also vary in their energy intensity (the ratio of energy consumed to the monetary value of a product) with the cement industry having the highest energy intensity. Figure 4.19 shows relative energy intensities and the energy consumption for different U.S. manufacturing industries (RMI) [47]. U.S. industry has shown a 25% decline in energy intensity since 1980 [5].

Many improvements have been made to decrease energy consumption in industrial processes. One very significant change has been a shift to the simultaneous production of electricity and process heat. This makes use of the heat that is rejected in a power cycle and is typically lost to the environment. This has been called cogeneration and is more commonly referred to today as combined heat and power, or CHP. The U.S. CHP capacity increased from 16,000 MW in 1980 to over 80,000 MW in 2013. [5]. While this means that fossil fuels have been used much more efficiently to simultaneously produce both process heat and electricity, the challenge going forward will be to transition completely off fossil fuels.

The European Union uses an industrial energy efficiency index called ODEX, which is based on tons of oil equivalent per unit of production [48]. The data show an average improvement in efficiency of about 1.4% per year since 2000, although there was some leveling off after the 2008 recession. The chemical industry and transport vehicles have shown the greatest reductions.

4.4.2 Improving Industrial Processes

Today, a key environmental goal in improving energy processes is to reduce greenhouse gas emissions, only one factor of which is energy efficiency. As described by the

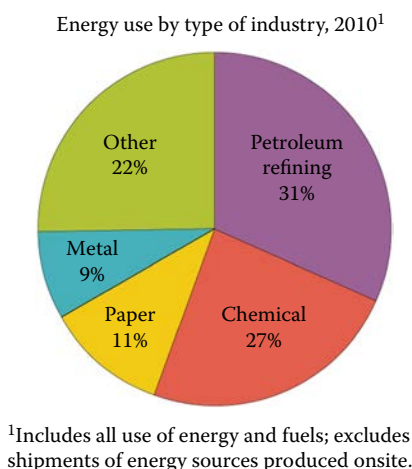
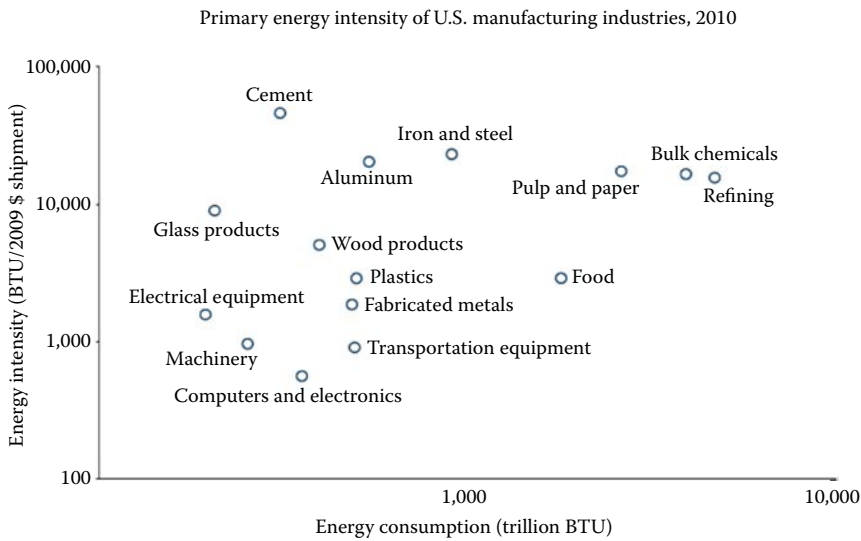


FIGURE 4.18

Energy use by different industry types. (From International Energy Agency, 2010. Manufacturing energy consumption survey 2010: Table 1.2, <http://www.eia.gov/consumption/manufacturing/data/2010/pdf/Table1.2.pdf>. [46])

**FIGURE 4.19**

Primary energy intensities and energy consumptions for different U.S. manufacturing industries in 2010. Rocky Mountain Institute 2011. (From Rocky Mountain Institute, 2011. *Reinventing fire*, <https://www.rmi.org/insights/reinventing-fire/>. [47])

Intergovernmental Panel on Climate Change (IPCC) Working Group III, annual greenhouse gas emissions, G , can be expressed as [49]:

$$G = \frac{G}{E} \times \frac{E}{M} \times \frac{M}{P} \times \frac{P}{S} \times S \quad (4.23)$$

where

G/E = emissions intensity in GHG emissions per unit of energy consumed. This is reduced by switching to lower-carbon or carbon-free sources of energy.

E/M = energy-material intensity or energy consumed per unit of material used. E/M is reduced by adopting energy efficiency measures.

M/P = material-product intensity or the amount of material required to make the product. This is reduced by minimizing scrap or by recycling product.

P/S = product-service intensity or the amount of product needed to provide a service. This can be reduced by making products that last longer or that are more potent so that a smaller quantity of product is needed.

S = the demand for the service or product. This is reduced by directly reducing the product or service demand. Energy *conservation*, as opposed to *efficiency*, (e.g., wearing a sweater as opposed to adding more attic insulation) is an example of direct demand reduction.

The IPCC has examined how each of these categories can be addressed. Examples of each follow.

G/E : Coal and oil supply 40% of world industrial energy. The current breakdown of world industrial energy sources as provided in the IEA World Energy Outlook is given in Table 4.12 [50].

TABLE 4.12

World Energy Demand by Energy Source

Energy Source	World Demand (Mtoe)	Percent of Total
Coal	768	29
Oil	302	11
Gas	557	21
Electricity	711	27
Heating	131	5
Bioenergy	194	7
Other renewables	1	0
Total	2664	100

Source: Based on data from International Energy Agency, *World Energy Outlook 2015*. © OECD/IEA 2016. <https://www.iea.org/publications/freepublications/publication/WEO2015.pdf>. [50]

Fuel switching from oil and coal to natural gas can reduce greenhouse gas emissions provided methane leakage in the entire supply chain is kept to a very low value. Carbon capture and storage (CCS) is also being considered to limit carbon dioxide emissions. In some cases, carbon can be harnessed into a useful product. Ultimately, switching to renewable sources will be needed to drive net carbon emissions to zero. Solar thermal energy can be used for processes requiring temperatures below about 400°C. Renewables can also be used to generate electricity, which can be used to provide very high industrial temperatures.

E/M: While opportunities for improving energy efficiency will vary from one company or industry to another, studies have been done to identify the most cost-effective opportunity areas overall. Hein [51] combined energy savings potential, cost-effectiveness, and popularity of implementation to rank order the best energy efficiency measures for electricity savings. He identified the following measures in order of priority, beginning with the highest: lighting, process, refrigeration, compressed air, controls, variable frequency drives, HVAC equipment upgrades, new construction, motors, and building envelope. For natural gas savings, his recommended measures are: HVAC, process, building envelope, new construction, and refrigeration. Note that many of the items in the industrial list, such as lighting, HVAC, and envelope are also pertinent to commercial and residential buildings.

McKinsey [7] has found that most companies can reduce energy use by 10% to 35%, depending on the size of the investment. In addition to the measures listed by Hein, they recommended greater use of CHP, heat recovery, and improved piping to reduce pumping power.

M/P: Manufacturing processes can be improved to reduce the amount of waste. Scrap materials can be recycled. Recycled materials can, in general, be used in place of new materials. Materials that are damaged can be repurposed. In the construction of the NREL's Research Support Facility, discarded natural gas pipe was used for support structures and bark beetle kill was used for accent wood. Improving packaging can reduce waste. For example, foam boxes have been replaced with simple paper wrap for fast food products.

TABLE 4.13

Eight Kinds of Waste

Sources of Waste	Definition	Example
Overproduction	Producing more energy than needed	Venting steam
Waiting	Energy consumption during stopped process	Laser welding line at 40% power
Transportation	Inefficient transport of energy	Steam and heat leaks in piping
Overspecification	Using more energy than necessary	Furnace operating 100°C higher than necessary
Inventory	Stored goods can waste energy	Crude steel cools in storage and has to be reheated for rolling
Rework/scrap	Need to redo a process product quality is inadequate	Re-drying polymer lines that did not get coagulated in drying process
Inefficient processes	Nonoptimal process design or operation	Excess oxygen in steam boiler
Employee potential	Failure to obtain human input	Employees not involved in developing energy-saving initiatives

Source: McKinsey & Company, March 2010. Energy efficiency: A compelling global resource, www.mckinsey.com. Copyright 2010 McKinsey & Company. All rights reserved. Reprinted by permission. [7]

P/S: Making products more durable is a challenge because many products have planned obsolescence to increase sales. But durability information provided by consumer organizations can impact customer selection and provide an incentive for manufacturers to make more durable products. Making products that are higher strength and require less volume can also serve as a sales tool, for example, stronger laundry detergent.

S: Reducing overall demand is perhaps the most difficult opportunity to address because there may be resistance to changes that are seen as compromising lifestyle. For example, acceptance of smaller homes would reduce the demand for building materials and switching to a vegetarian (or less meat-intensive) diet would reduce emissions associated with beef production, but some people are resistant to these changes. It is possible, however, for government or employers to support or incentivize energy-saving behavior. For example, employer support for telecommuting and video conferencing can reduce the amount of travel.

Achieving significant energy savings and lower emissions requires an energy and waste management program that is tailored to each industry. Lean energy programs are aimed at reducing the various forms of waste. McKinsey [7] has outlined eight forms of waste that industry can reduce through common sense planning and maintenance measures, as shown in Table 4.13.

Opportunities for improvement vary by industrial sector. Examples of improvements that can be made in the major sectors as summarized by the IPCC are given in Table 4.14 [49].

4.4.3 Improvements in Industrial Equipment

Motors, compressed air systems, and refrigeration systems are commonly used industrial equipment that have been the subject of recent energy efficiency case studies.

TABLE 4.14

Example Improvements to Reduce Greenhouse Gas Emissions in Various Industries

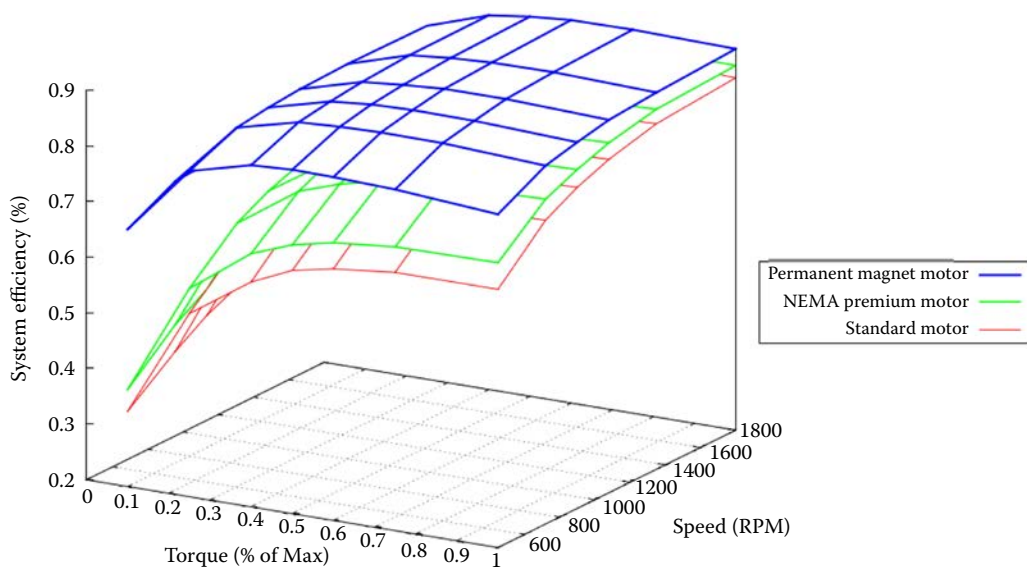
Industry	Example Improvements
Iron and steel	<ul style="list-style-type: none"> • Improved heat recovery from process streams • Recycling of structural steel • Adoption of more realistic structural safety margins for buildings
Cement	<ul style="list-style-type: none"> • Adoption of EPA Energy Performance Indicator score to identify potential improvements • Harvesting of CO₂ • Production of higher-strength, longer-lasting concrete
Chemicals	<ul style="list-style-type: none"> • Generating pure waste streams to enable more recycling • Greater adoption of combined heat and power • Material-conserving plastic packaging
Pulp and paper	<ul style="list-style-type: none"> • Improved heat recovery in drying process • Greater paper recycling • Reduced paper weight and duplex printing
Nonferrous metals (e.g., aluminum)	<ul style="list-style-type: none"> • Adoption of improved electrolysis methods • Minimization and reuse of scrap
Food processing	<ul style="list-style-type: none"> • Less energy-intensive drying techniques, for example, mechanical dewatering • Local sourcing of food • Transition from meat to vegetarian foods
Textiles and leather	<ul style="list-style-type: none"> • More efficient motors and boilers
Mining	<ul style="list-style-type: none"> • Apply latest resource characterization methods to obtain higher quality ore and reduce amount crushing and grinding • Use of more efficient crushing technologies • Great metal recycling

Source: From Intergovernmental Panel on Climate Change (IPCC) Working Group III, 2014. *Climate Change 2014: Mitigation of Climate Change*, Chapter 10, Industry, <http://www.ipcc.ch/report/ar5/wg3/>. [49]

Motors: According to DOE, over 20% of electricity sold in the United States is for electric motors totaling 680 TWh per year. It has been estimated that electric motors consume 45% of world electricity [52]. They thus represent a major opportunity for electricity savings.

When motor speed is plotted against torque, efficiency reaches a peak at the optimum torque and drops off rapidly at lower torque. Thus, to achieve high efficiency, it is important not to oversize a motor. The National Electrical Manufacturers' Association (NEMA) ranks motor efficiencies. High-efficiency motors are given the NEMA Premium performance label. To encourage the use of more efficient motors, Minimum Energy Performance Standards have been developed around the world [53].

To further reduce motor electricity consumption, the Consortium for Energy Efficiency (CEE) Motors and Motor Systems Committee has studied the potential for electronically controlled permanent magnet AC (PMAC) motors. The use of permanent magnets eliminates rotor slip inherent in traditional AC induction motors and hence provides greater efficiency. Coupling PMAC motors with variable-frequency drives (VFDs) makes them especially efficient for fans, pumps, and compressors supplying variable loads. Several case studies of the PMAC motor/drive combination have shown energy savings of 2% to 26% compared to industry-standard induction motors having VFDs [54]. The greatest savings occurred

**FIGURE 4.20**

Efficiencies of three types of fan motors (PMAC, NEMA Premium, and standard) as functions of speed and torque. (From Larsen, W. et al., 2015. *Proceedings of the ACEEE Summer Study on Energy Efficiency in Industry*, ACEEE, Washington, DC. [54]; Sacramento Municipal Utility District, Sacramento, California.)

where reduced speed operation was common. The advantage of PMAC motors was shown in bench tests of fan motors by the Sacramento Municipal Utility District (SMUD). The efficiency of the PMAC motor compared to standard and premium induction motors as functions of speed and torque is shown in [Figure 4.20](#).

Compressed Air Systems: Air compressors of a variety of types are used for various processes throughout industry. The Northeast utility National Grid conducted an energy efficiency study of 41 compressed air systems in their Upstate New York and Massachusetts service area. Opportunities include leak maintenance, use of variable-speed compressors, and better controls. Hessmer et al. [55] provides details on how these opportunities can be addressed.

Refrigeration Systems: Refrigeration systems consist of a compressor, a heat-rejecting condenser, expansion valve, heat-absorbing evaporator, and associated fans to move air over the evaporator and condenser. Two recent case studies aimed at improving refrigeration system efficiency applied a number of energy efficiency measures [56]. Typical measures to improve efficiency include:

- A VFD to drive the compressor
- High-efficiency fan motors with variable-speed drives
- Oversizing of condensers
- Variable condenser pressure control allowing for lower average condenser pressure reducing compressor load during winter months.

PROBLEMS

- 4.1 A home in a cold climate is heated with natural gas, which costs \$8/thousand cubic feet, or \$1.10/therm. It is estimated that raising the attic insulation level from R15 to R40 will cost \$1200 and save 60 therms per year.
 - a. Assuming a 30-year period and a discount rate of 3%, calculate the cost of conserved energy.
 - b. What is the simple payback period for this investment (cost of insulation divided by the annual savings)?
 - c. Comment on why this payback is so long. Why might it still be a worthwhile investment?
- 4.2 Consider the primary energy savings for four energy efficiency measures shown in [Table 4.9](#).
 - a. Air sealing shows similar per house energy savings in climate zones 1, 4, 5, and 7 (see [Figure 4.16](#) for climate zones) but only has significant aggregate energy savings in zones 4 and 5. Why do you think that is the case?
 - b. Replacing an electric hot water heater with a heat pump hot water heater has a high per-house energy savings everywhere but a low aggregate impact in zones 6 and 7 (few homes have electric water heating). Why would that be the case?
 - c. Upgrading single-pane windows to double-pane low-e has much higher per-house energy savings than adding attic insulation to achieve R-49, yet they have the same aggregate energy savings (0.41 Quads/yr.). Speculate on why that would be the case.
- 4.3 An auditorium at sea level is designed to hold an audience of 6,000 people. Outdoor ventilation air is provided at the current ASHRAE minimum guideline of 5 CFM per person. The outdoor temperature is 10°F and the ventilation air is exhausted at a temperature of 70°F.
 - a. Calculate the mass flow rate of air
 - b. Assuming a body heat rate of 225 Btu/hr per person, what is the temperature of the ventilation air as it enters the room?
 - c. Assuming a ventilation heat recovery system reduces the ventilation heating by 80%, how much heat must be supplied to the incoming ventilation air?
- 4.4 The no-load temperature of a building with internal heat sources is given by Equation 4.3. How would this equation be modified to account for heat losses through the surface of an unheated slab, the heat losses being independent of ambient temperature?
- 4.5 An unheated garage is placed on the north wall of a building to act as a thermal buffer zone. If the garage has roof area A_r , window area A_{wi} , door area A_d and wall area A_{wa} , what is effective U value for the north wall of the building if its area is A_n ? The garage floor is well insulated and has negligible heat loss. Express the effective U value in terms of the U values and areas of the several garage surfaces.
- 4.6 What is the annual energy demand for a building in Denver, Colorado, if the peak heat load is 150,000 Btu/h based on a design temperature difference of 75°F? Internal heat sources are estimated to be 20,000 Btu/h, and the design building interior temperature is 70°F.

- 4.7 The table below gives the characteristics of a building in Houston, Texas. Determine the cooling load for July 30 at solar noon. Any information regarding the load not given may be assumed or neglected.

Factor	Description or Specification
Roof:	
Type	Flat, shaded
Area $A_{rf,shr}$ (m^2)	250
U factor (W/m^2K)	$U_{rf} = 0.35$
Walls:	
Type	Vertical, painted white
Orientation, size ($m \times m$)	North, South, 3×10 ; East, West, 3×25
U factor (W/m^2K)	$U_{wa} = 1.08$
Windows:	
Orientation, area (m^2)	North, 8; South, 8; East, 20; West, 25
U factor (W/m^2K)	$U_{wi} = 6.2$
Insolation transmittance	$\bar{\tau}_{b,wi} = 0.60$; $\bar{\tau}_{d,wi} = 0.80$; $\bar{\tau}_{r,wi} = 0.55$
Temperature:	
Inside, outside ($^{\circ}C$)	$T_{in} = 24$; $T_{out} = 37$
Insolation:	
Beam, diffuse, reflected (W/m^2)	$I_{hb} = 580$; $I_{hd} = 250$; $I_r = 200$

- 4.8 An air conditioning system working in a vapor-compression cycle is used to manage the load for the building in Problem 4.7. If the high and low pressure in the cycle are 915 kPa and 290 kPa, respectively, and the efficiency of the compressor is 90%, find the flow rate of Refrigerant 134a (R-134a) used for the equipment and the COP of the cycle.
- 4.9 An industrial condenser unit uses two 500 hp (373 kW) fans that operate in parallel. For 3000 hours per year, the unit operates at half flow and one fan is turned off with the other operating at full power. The plant owner is considering purchasing a variable frequency drive for each fan and running both fans at half flow instead of shutting one fan off. The efficiency of the VFD itself at half load is 98%.
- How much electric energy is saved if VFDs allow both fans to be operated at half flow? (Note: fan power is proportional to flow rate cubed, as one can see from a simple dimensional analysis.)
 - If each VFD costs \$200 per hp and the plant pays 8 cents per kWh for electricity, what is the simple payback period?
- 4.10 A building owner of a small retail store wants to upgrade the 20-year-old HVAC system. The store has two 10-ton rooftop units (RTUs) with an original rated full load energy efficiency ratio (EER) of 8.7 Btu/Wh. The owner is considering two options for replacement: two standard-efficiency RTUs (11.2 EER) or two high-efficiency RTUs (13 EER). As the design engineer, your job is to estimate the energy cost savings of the two replacement options compared to the existing RTUs. Make the following assumptions:
- Estimate the annual energy cost savings of each option.

- b. Determine the simple payback period for the high-efficiency RTUs compared to the standard-efficiency RTUs with no utility incentives and with a utility rebate for using high efficiency of \$350/ton.
 - The performance of the existing RTUs has degraded 1%/year
 - The cost of electricity is \$0.1/kWh and there are no peak demand charges
 - The RTUs operate at an annual equivalent full load hours of 2200 h. (That is, their operation over a year is equivalent to operating a full load of 2200 hours for the year.)
 - The installed cost of the RTUs is \$900/ton for the standard-efficiency RTUs and \$1400/ton for the high-efficiency RTUs

References

1. EIA, August 2016. Monthly energy review, <http://www.eia.gov/totalenergy/data/monthly/>
2. EIA, 2016. World energy outlook, http://www.eia.gov/forecasts/ieo/ieo_tables.cfm
3. The Global Commission on the Economy and Climate, September 2014. The new climate economy report, <http://www.newclimateeconomy.report>
4. NRDC Fact Sheet, July 2013. California's energy efficiency success story: Saving billions of dollars and curbing tons of pollution, FS:13-06-A, <https://www.nrdc.org/sites/default/files/ca-success-story-FS.pdf>
5. Nadel, S., Elliott, N., and Langer, T., June 2015. Energy efficiency in the United States: 35 years and counting, ACEEE, Report E1502, <http://aceee.org/blog/2017/05/doing-more-less-how-us-economy-grows>
6. Molina, M., March 2014. The best value for America's energy dollar: A national review of the cost of utility energy efficiency programs, ACEEE Report No. U1402.
7. McKinsey & Company, March 2010. Energy efficiency: A compelling global resource, www.mckinsey.com
8. Center for Climate and Energy Solutions. Federal vehicle standards, <http://www.c2es.org/federal/executive/vehicle-standards/fuel-economy-comparison>
9. Burgess, J., 2015. The second generation of strategic energy management programs, ACEEE Study on Energy Efficiency in Industry.
10. ISO 50001 – Energy Management, <http://www.iso.org/iso/home/standards/management-standards/iso50001.htm>
11. International Energy Agency, 2015. Energy efficiency marketing report, <https://www.iea.org/publications/freepublications/publication/MediumTermEnergyefficiencyMarketReport2015.pdf>
12. ASHRAE, 1989, 1993, 1997. *ASHRAE Handbook—Fundamentals*, American Society of Heating, Refrigerating and Air-Conditioning Engineers, Atlanta, GA.
13. Kreith, F. and Manglik, R., 2016. *Principles of Heat Transfer*, 8th edn., Cengage Learning, Boston, MA.
14. Klein, S.A. et al., 1975. A method for simulation of solar processes and its applications. *Solar Energy* 17, 29–37.
15. National Weather Service, <http://gis.ncdc.noaa.gov/map/viewer/#app=cdo&cfg=cdo&theme=normals&layers=01&node=gis&extent=-149.3:20.2;-60.1:69.6&custom=normals>
16. Goswami, Y. et al., 2000. *Principles of Solar Engineering*, 2nd edn., Taylor & Francis, Philadelphia, PA.
17. ASHRAE, 1991, 1995. *ASHRAE Handbook—Heating, Ventilating, and Air-Conditioning Applications*, American Society of Heating, Refrigerating and Air-Conditioning Engineers, Atlanta, GA.

18. DOE. Buildings energy data book, <http://buildingsdatabook.eren.doe.gov>
19. EIA, 2012. Commercial buildings energy consumption survey: Energy usage summary, <https://www.eia.gov/consumption/commercial/reports/2012/energyusage/>
20. ASHRAE, 2016. ANSI/ASHRAE/IES Standard 90.1-2016—Energy Standard for Buildings Except Low-Rise Residential Buildings, Atlanta, Georgia.
21. ASHRAE, 2018. Advanced energy design guides, <https://www.ashrae.org/standards-research--technology/advanced-energy-design-guides>
22. Torcellini, P., Long, N., and Judkoff, R., 2003. Consumptive water use for U.S. power production, <https://www.nrel.gov/docs/fy04osti/33905.pdf>
23. NREL, August 2016. NREL + Liquid cool solutions, Fact Sheet, NREL/FS-5C00-66712, <http://www.nrel.gov/docs/fy16osti/66712.pdf>
24. Open Studio, <https://www.openstudio.net>
25. U.S. Department of Energy. Qualified software for calculating commercial building tax deductions, <http://energy.gov/eere/buildings/qualified-software-calculating-commercial-building-tax-deductions>
26. U.S. Department of Energy, 2015. A common definition for zero energy buildings. DOE/EE-1247, <https://energy.gov/eere/buildings/downloads/common-definition-zero-energy-buildings>
27. U.S. Department of Energy, July 2012. Research support facility, DOE/GO-102011-3311.
28. Robbins, J., Skelton, B., and Olden, R., 2015. Revealing net zero, *High Performing Buildings*, Fall 2015, <http://www.hpbmagazine.org/attachments/article/12253/15F-Walgreens-Net-Zero-Store-Evanston-IL.pdf>
29. EIA, 2015. Annual energy outlook, <https://www.eia.gov/outlooks/aeo/data/browser/#/?id=4-AEO2015&cases=ref2015&sourcekey=0>
30. U.S. Department of Energy, October 2012. Energy savings potential and research, development & demonstration opportunities for residential building heating, ventilation, and air conditioning systems, DOE/EE-0850.
31. Pacific Northwest National Laboratory, January 2013. Building science-based climate maps, PNNL-SA-90570.
32. Wilson, E. et al., January 2017. Electric end-use energy efficiency potential in the U.S. single family housing stock, NREL/TP-5500-65667.
33. Christensen, C. et al., August 2006. BEopt software for building energy optimization: Features and capabilities, NREL/TP-550-39929.
34. Norton, P., Christensen, C., Hancock, E., Barker, G., and Reeves, P., June 2008. The NREL/Habitat for Humanity zero energy home: A cold climate case study for affordable zero energy homes, NREL/TP-550-43188.
35. Polly, B., Kutscher, C., Macumber, D., Schott, M., Pless, S., Livingood, B., and Van Geet, O., 2016. From zero energy buildings to zero energy districts. *Proceedings of the ACEEE Summer Study on Energy Efficiency in Buildings ACEEE*, Washington, DC.
36. UN (United Nations), July 10, 2014. World's population increasingly urban with more than half living in urban areas, <http://www.un.org/en/development/desa/news/population/world-urbanization-prospects-2014.html>
37. Architecture 2030, June 2014. Roadmap to zero emissions, http://architecture2030.org/files/roadmap_web.pdf
38. Compact of Mayors, 2016. <https://www.compactofmayors.org>
39. U.S. Conference of Mayors, 2016. <http://www.usmayors.org/climateprotection/list.asp>
40. Carlisle, N., Van Geet, O., and Pless, S., 2009. Definition of a zero net energy community. NREL/TP-7A2-46065, National Renewable Energy Laboratory, Golden, CO, <http://www.nrel.gov/docs/fy10osti/46065.pdf>
41. EcoDistricts, June 2014. The EcoDistricts protocol, <https://ecodistricts.org/get-started/the-ecodistricts-protocol/>
42. Dakin, B. and German, A., 2014. Early performance results from a zero net energy community. *Proceedings of the ACEEE 2014 Summer Study on Energy Efficiency in Buildings*, ACEEE, Washington, DC.

43. Chittum, A., 2014. Going further than an EERS: Danish lessons on maximizing whole energy system efficiency. *Proceedings of the ACEEE 2014 Summer Study on Energy Efficiency in Buildings*, ACEEE, Washington, DC.
44. UN Environment. District energy in cities initiative, <http://www.districtenergyinitiative.org>
45. U.S. Department of Energy, 2016. Guidelines for participating in the DOE zero energy ready home, <https://www.energy.gov/eere/buildings/guidelines-participating-doe-zero-energy-ready-home>
46. International Energy Agency, 2010. Manufacturing energy consumption survey 2010: Table 1.2, <http://www.eia.gov/consumption/manufacturing/data/2010/pdf/Table1.2.pdf>
47. Rocky Mountain Institute, 2011. Reinventing fire, <https://www.rmi.org/insights/reinventing-fire/>
48. European Union, September 2015. Energy efficiency trends and policies in industry, <http://www.odyssee-mure.eu/publications/br/energy-efficiency-in-industry.html>
49. Intergovernmental Panel on Climate Change (IPCC) Working Group III, 2014. Climate change 2014: Mitigation of climate change, Chapter 10, Industry, <http://www.ipcc.ch/report/ar5/wg3/>
50. International Energy Agency. World energy outlook 2015, <https://www.iea.org/publications/freepublications/publication/WEO2015.pdf>
51. Hein, M., 2015. The silver bullet list: Impactful investments in energy efficiency. *Proceedings of the ACEEE Summer Study on Energy Efficiency in Industry*, ACEEE, Washington, DC.
52. Waide, P. and Brunner, C., 2011. Energy-efficiency policy opportunities for electric motor-driven systems, International Energy Agency Working Paper.
53. Delaney, D., 2015. Global motor energy efficiency program. *Proceedings of the ACEEE Summer Study on Energy Efficiency in Industry*, ACEEE, Washington, DC.
54. Larsen, W., Howlett, O., Forsman, K., and Zeller, M., 2015. Exploring the customer benefits of permanent magnet motors: Test results and opportunities for next generation motor programs. *Proceedings of the ACEEE Summer Study on Energy Efficiency in Industry*, ACEEE, Washington, DC.
55. Hessmer, C., Olmested, J., Meserve, S., and Kondapi, R., 2015. Compressed air system energy efficiency upgrades implemented vs. underutilized measures. *Proceedings of the ACEEE Summer Study on Energy Efficiency in Industry*, ACEEE, Washington, DC.
56. Kumpanon, A. and Syed, R., 2015. Industrial refrigeration projects: Challenges and opportunities for energy efficiency. *Proceedings of the ACEEE Summer Study on Energy Efficiency in Industry*, ACEEE, Washington, DC.

5

Electricity Supply Systems

5.1 Historical Development of the U.S. Electric Power System

For virtually every American and citizens of developed nations around the world the impact of electric power on their lives is pervasive. The National Academy of Engineering named electrification the greatest engineering achievement of the twentieth century. The development of the electric grid actually began in the previous century. The first use of generated electricity was a hydropower plant completed in 1868 on the estate of English industrialist William Armstrong. The electricity was used to power early incandescent light bulbs developed by the English inventor John Swan, as well as heat water and run various devices. Thomas Edison made improvements to Swan's light bulbs, and his success spurred him to build the first two public power stations: the Edison Electric Light Station in London and, a few months later, the Pearl Street Station in lower Manhattan. Both employed coal firing to power DC (direct current) electric generators.

The Edison plants generated low-voltage, high-current DC electricity, which required thick copper cables to minimize line losses and allowed for efficient transmission over only short distances on the order of a mile. Power loss in a transmission line is the product of the square of the current, I , being carried and the resistance of the cable, R (which is inversely proportional to the cross-sectional area of the cable): $P = I^2R$. To allow minimal losses when carrying electric current over large distances, it's important to minimize the current. Nikola Tesla and George Westinghouse recognized that by using alternating current (AC) instead of DC, a transformer could be used to achieve lower currents by raising the voltage. (The electric power, which can also be expressed as the product of the current and voltage, $P = VI$, stays approximately constant on each side of a transformer.) In 1885, Westinghouse's employee, William Stanley, built upon European concepts to develop the first reliable transformer that could boost AC electricity to higher voltages, thus achieving the lower currents that would allow efficient, longer distance transmission.

One of the first AC power stations, located near Telluride, Colorado, was completed in 1891. The Ames hydroelectric power plant provided 3000 V to power an ore crusher located 2.6 miles away. Some of the benefits of AC power were demonstrated when Westinghouse and Tesla won the contract to provide electric lighting for the 1893 Chicago World's Fair using AC power. While there was no need to transmit the electricity a great distance, it successfully demonstrated to the public the safe use of alternating current. In 1896, Westinghouse built an 11,000-volt AC transmission line to transmit electricity from a hydropower plant at Niagara Falls to Buffalo, New York, located over 20 miles away [1]. Because of its ability to easily convert to higher voltages for transmitting power over long distances, AC won out over DC. Voltages and distances kept increasing with time.

The electric grid today is over a century old and modernizing the grid is a major national priority in the United States. The infrastructure needs to be upgraded to handle threats from terrorism (both physical and cyber attacks) as well as the increasing threat of extreme weather events associated with climate change (for example, storms, flooding, and heat waves). It must also be reinvented to handle distributed generation sources on the grid and allow for two-way flow of both electricity and information associated with more and more devices communicating with the internet. The addition of variable sources of renewable electricity such as wind and photovoltaics, the interaction with battery electric vehicles, and various measures to control the demand create special challenges and opportunities that will be covered in this chapter.

5.2 Electrical Transmission

Figure 5.1 shows a schematic of a typical AC transmission system [2]. A central generating plant provides 3-phase/3-wire AC electricity at between 11,000 and 25,000 volts for a thermal power plant. Single wind turbines and photovoltaic (PV) arrays typically generate AC power at relatively low levels (480 V–600 V) and then step up the voltage to 34,000 V before increasing the voltage to transmission levels. Power transformers at a transmission substation commonly step the voltage up to as high as 765 kV in North America and even over 1 MV internationally, proportionately decreasing the current. The low current associated with the high transmission voltage results in low transmission losses. These losses are a function of transmission line length and are on the order of 3% of the energy transmitted in the Eastern Interconnection and 5% in the Western Interconnection. After hundreds of miles of primary transmission, step-down transformers at another transmission substation reduce the voltage in the secondary transmission system to provide lower-voltage power to industrial and commercial customers, and to neighborhood transformers mounted on utility poles, which further reduce the voltage for household use.

At the customer level, a range of lower voltages is used depending on the customer class. Commercial and industrial customers typically use three-phase AC power. For a typical household, a three-wire, single-phase power drop provides three lines: +120 V,

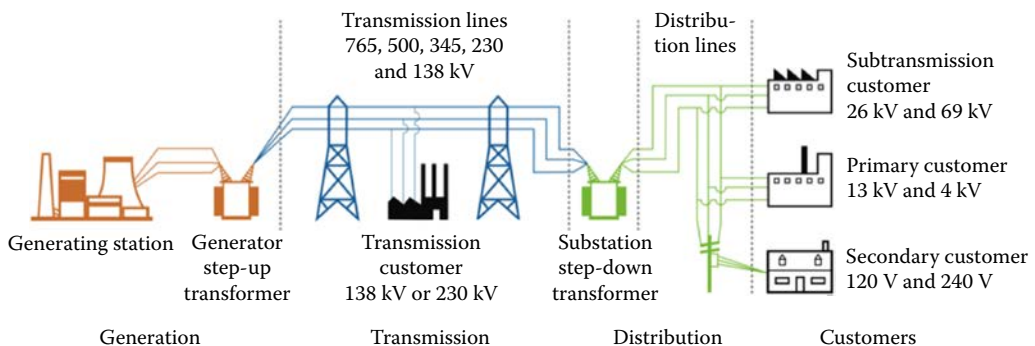


FIGURE 5.1

Diagram of AC electric transmission grid. (From North American Electric Reliability Corporation, August 2013. Understanding the grid. <http://www.nerc.com/news/Documents/Understanding%20the%20Grid%20DEC12.pdf>. Reproduced with permission. [2])

neutral (from the center of the utility pole transformer secondary winding) and -120 V. The 120 V household circuit is between the 120 V lines and neutral, whereas the 240 V circuit is between the +120 V and -120 V lines. The household wiring system also includes a line to ground (connected to the bottom prong in a 3-prong plug). (Ground fault circuit interrupt, or GFCI, electrical outlets used in bathrooms and kitchens sense when current is escaping instead of flowing between a 120 V line and neutral and automatically break the circuit, thus preventing a current leak from passing through a homeowner to ground.)

High ambient temperatures increase the resistance of electric transmission lines. During times of high temperature, air conditioning loads are high, meaning that the hot transmission lines carry more current and so further heat up due to I^2R heating. This can cause lines to sag due to thermal expansion, causing an electric arc to ground through trees. On August 14, 2003, a hot 345-kV transmission line in northern Ohio sagged into tree branches and caused a major cascading blackout that affected 50 million people. Thus, keeping transmission lines cleared of trees is a major maintenance activity for utilities.

AC transmission and distribution system contain both resistive and reactive elements. In resistive elements such as resistive-wire light bulbs, the sinusoidally varying current and voltage are in phase with each other and all the power passing through the element is dissipated as heat (and light). Reactive elements such as generators and motors make use of electromagnetic interactions that can cause current and voltage to be out of phase. Some of the supplied power goes into varying electric and magnetic fields and is not lost to the environment. In the case of capacitors, a changing current builds up the voltage across the capacitor and current leads voltage by 90 degrees. The capacitor alternately charges and discharges, but delivers no net power over a cycle. In the case of an inductor, the changing voltage induces a changing current and current lags voltage. Each of these elements has a reactance measured in ohms that is analogous to a resistance. Capacitive reactance is $1/\omega C$ and capacitive inductance is ωL .

The real power, P , dissipated in resistors is measured in watts (W). The reactive power, Q , does no net work and has units of VARs, which stands for volts-amps-reactive. The apparent power, S , in an AC circuit is VI where V is the root-mean-square voltage and I is the root-mean-square current. It is plotted as a vector on a plot of reactive power, Q , on the y-axis (in VARs) and real power, P , on the x-axis (in watts) as shown in Figure 5.2. (The reactive component, or y-axis, is typically expressed as the imaginary axis. While reactive power is not imaginary, it does no work, and expressing it as an imaginary component of a complex number allows for electrical engineers to harness the calculational efficiency of complex numbers.)

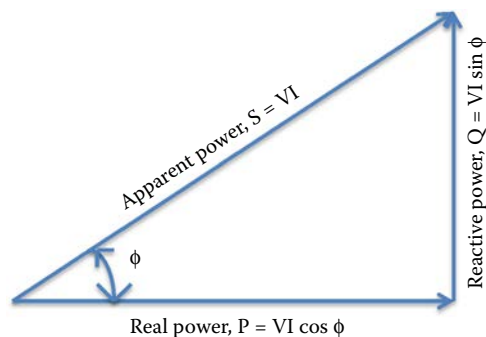


FIGURE 5.2

The power triangle showing apparent power, S , and its two components: real power, P , and reactive power, Q .

The real power is thus the x-component of the apparent power vector or,

$P = VI \cos \phi$ expressed in watts, where ϕ is the phase angle and $\cos \phi$ is the power factor.

The reactive power is the y-component (or “imaginary” component) of the apparent power vector or,

$Q = VI \sin \phi$ expressed in VARs

The apparent power can be expressed in terms of real and reactive power as:

$$S = \sqrt{P^2 + Q^2} \quad (5.1)$$

A utility customer pays only for real power, because that is what is consumed. If loads are all resistive, $\phi = 0$ and $\cos \phi = 1$, and there is no reactive power component. In that case apparent power = real power. If an industrial customer is using large motors or other inductive devices that cause the voltage and current to be out of phase, the power factor is less than 1. The utility needs to send current for the apparent power (both the real and reactive power components), which results in a larger current in the transmission lines and associated equipment than is needed for the real power that is consumed and sold. The utility is not financially compensated for those additional I^2R line losses. Also, the additional current needed to meet reactive loads can cause transformers to overheat. For these reasons, utilities want the power factor to be close to 1. (However, some reactive power is needed to control voltage.) PV inverters provide only real power since they are compensated only for real power production. Current interconnection standards such as IEEE 1547 also do not allow the PV inverters to actively regulate the local voltage. So the addition of PV increases the fraction of reactive power on the grid provided by the utility and decreases the local power factor of the customer. IEEE Standard 1547 is undergoing revisions, which should allow better accommodation of distributed PV into the grid by allowing for local voltage regulation from inverters [3].

As electricity from wind farms and central solar plants become a larger fraction of the grid, the need for new transmission lines to transport the electricity from where the renewable resources are highest to population centers becomes an increasingly important issue.

Transmission line costs are a function of the AC voltage and the distance. Black & Veatch developed a methodology to calculate new transmission and substation capital costs for the Western Electricity Coordinating Council (WECC) [4]. Their baseline per-mile costs as a function of voltage are shown in [Table 5.1](#).

The Black & Veatch report includes various multipliers on these baseline costs to account for different conductor types, tower type, terrain, and so on. These costs are for aboveground transmission. Underground transmission is more aesthetic and better protected from storm damage but costs 3 to 10 times as much and is more expensive to repair. As we build new transmission lines, the need to secure rights of way and the proper permits is an important issue.

Interestingly, more than a century after Tesla and Westinghouse won the AC-DC debate over Edison on the basis of AC being better for transmission, there is increasing interest in utilizing high voltage direct current (HVDC) for very long-range transmission. DC transmission lines do not suffer from the electromagnetic interference and capacitance/inductance effects associated with alternating current. In addition, long-distance HVDC transmission involves fewer conductors (two for bipolar HVDC compared to three for 3-phase AC) that can be spaced closer together, meaning less wire, less robust transmission towers, and narrower rights-of-way. Also, the constant power in DC lines is generally less

TABLE 5.1

Typical Baseline Costs for AC Transmission Lines

Line Voltage (kV)	Single Circuit Cost (\$/mile)	Double Circuit Cost (\$/mile)
230	959,700	1,536,400
345	1,343,800	2,150,300
500	1,919,450	3,071,750

Source: From Black & Veatch, 2014. Capital costs for transmission and substations: Updated recommendations for WECC transmission expansion planning. [4]

TABLE 5.2

Typical Baseline Costs for HVDC Transmission Lines

Line Voltage (kV)	Bi-Pole Cost (\$/mile)
500	1,536,400
600	1,613,200

Source: From Black & Veatch, 2014. Capital costs for transmission and substations: Updated recommendations for WECC transmission expansion planning. [4]

than the peak power in oscillating AC lines, so the conductors do not need to be as thick. Baseline costs for HVDC transmission lines are shown in [Table 5.2](#).

The need to go to high voltage to minimize the current and associated I^2R losses still holds, however. So HVDC transmission requires a method to provide step-up and step-down voltage. HVDC systems use power electronic rectifiers and inverters at each end to convert from AC to DC and back again to AC. Thus, the cost savings associated with the HVDC transmission lines must be weighed against the additional costs of the conversion equipment. Because the added equipment cost for HVDC transmission is fixed independent of mileage, the net advantage of DC over AC occurs for long transmission distances. A study by Argonne National Laboratory [5] concluded that HVDC transmission in the United States is cheaper than AC transmission for distances exceeding about 435 miles.

5.3 The Electric Grid and Electricity Markets

The electric grid in the United States and Canada (and a small part of western Mexico) is divided into different synchronous interconnections as shown in [Figure 5.3](#). There are four separate interconnects: the Western Interconnection, the Eastern Interconnection, the Quebec Interconnection, and the Electric Reliability Council of Texas (ERCOT). Electricity exchanges mostly occur within these four regions, as the generators are synchronized to same frequency within each region. To transfer electricity between these interconnects, the AC electricity must be converted to DC, sent over a DC transmission line, and then converted back to AC to be properly synchronized in the next interconnect.

In 1968, following the 1965 blackout in the Northeast, the Federal Energy Regulatory Commission (FERC) established the National Electric Reliability Corporation, later

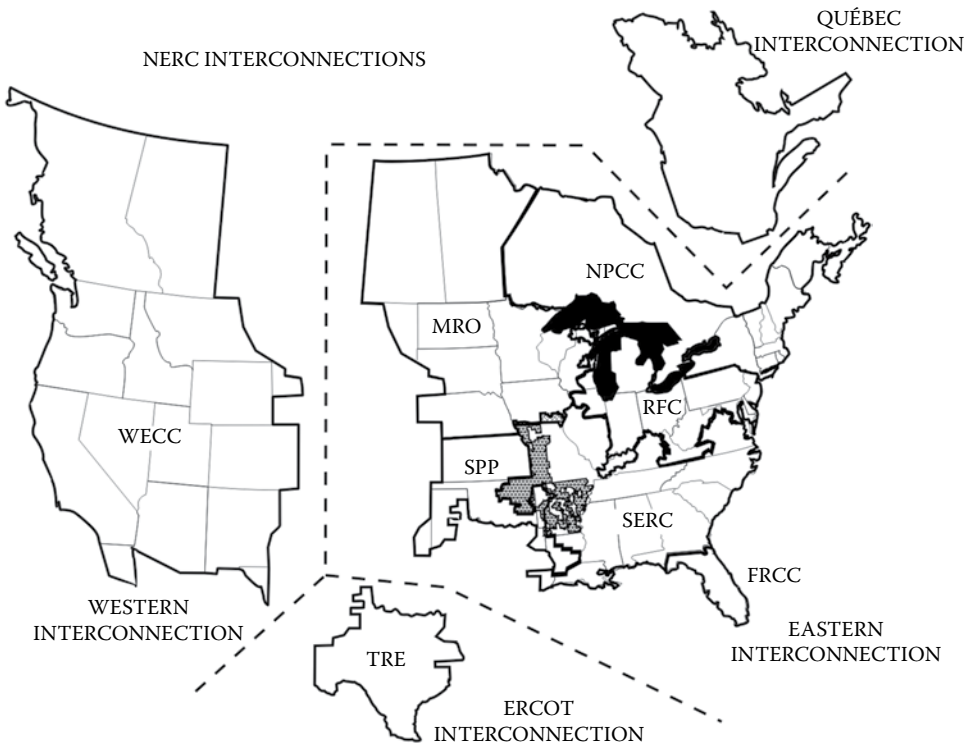


FIGURE 5.3

The four main North American interconnections and the various regions that set reliability standards. (From North American Electric Reliability Corporation, August 2013. Understanding the grid. <http://www.nerc.com/news/Documents/Understanding%20the%20Grid%20DEC12.pdf>. Reproduced with permission. [2])

renamed the North American Electric Reliability Corporation (NERC). This organization subdivided the grid into various regions to ensure reliability and develop operating standards. The Eastern Connect was divided into six regions, whereas ERCOT and the Western Interconnection are each represented by one region. All eight regions are shown in Figure 5.3 [2]. However, in terms of how electricity is actually transmitted, the four main interconnect regions have greater relevance than the reliability regions.

The U.S. electric grid developed in piecemeal fashion over many decades and regions, and thus the electric power markets are complex and vary across the regions. They involve both private and public ownership and are regulated at both the federal and state levels. Utilities are of three types: for-profit investor-owned utilities or IOUs; and two types of nonprofit public-owned utilities: municipal utilities that are operated by a city (also called “munis”); and rural electric coops, which are owned and operate by members in a rural region. All of these utilities fall under the umbrella of “load serving entity” or LSE.

Customers can purchase electricity either from an LSE or, in the case of very large industrial consumers (typically with electricity purchases exceeding 1 MW), directly from the electricity marketplace. This is shown in Figure 5.4 [6]. This shows the purchase of both generated electricity and the electricity savings resulting from demand response (DR) programs.

Most electricity consumed in the United States is purchased through an LSE. Figure 5.5 shows the flow of electricity and the flow of money for two cases: a traditional vertically

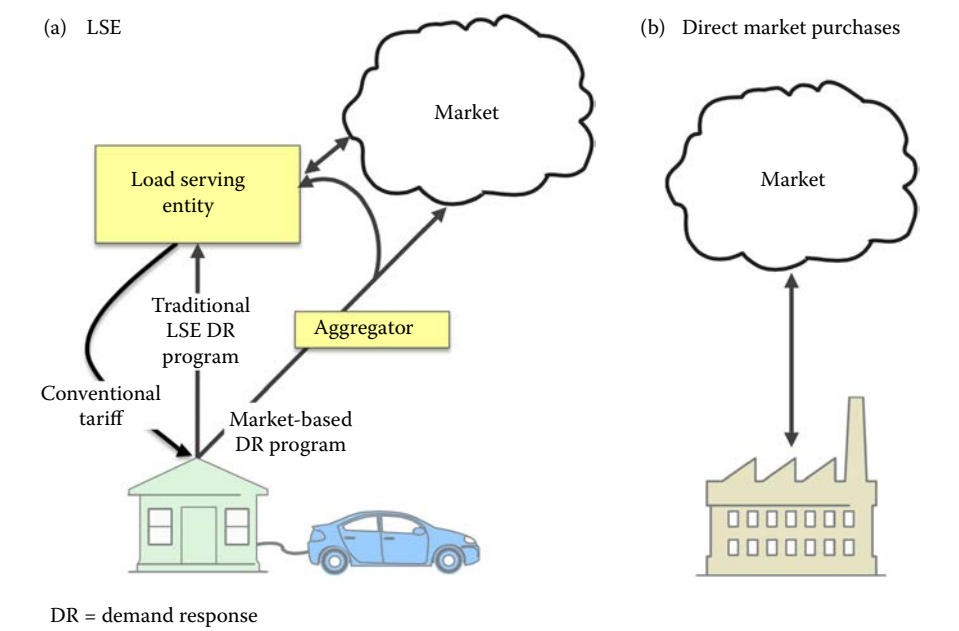


FIGURE 5.4 The purchase of electricity: a) through a load serving entity or b) directly from the electricity market. (From Denholm, P., Eichman, J., and Markel, T., 2015. Summary of market opportunities for electric vehicles and dispatchable load in electrolyzers, NREL/TP-6A20-64172. [6])

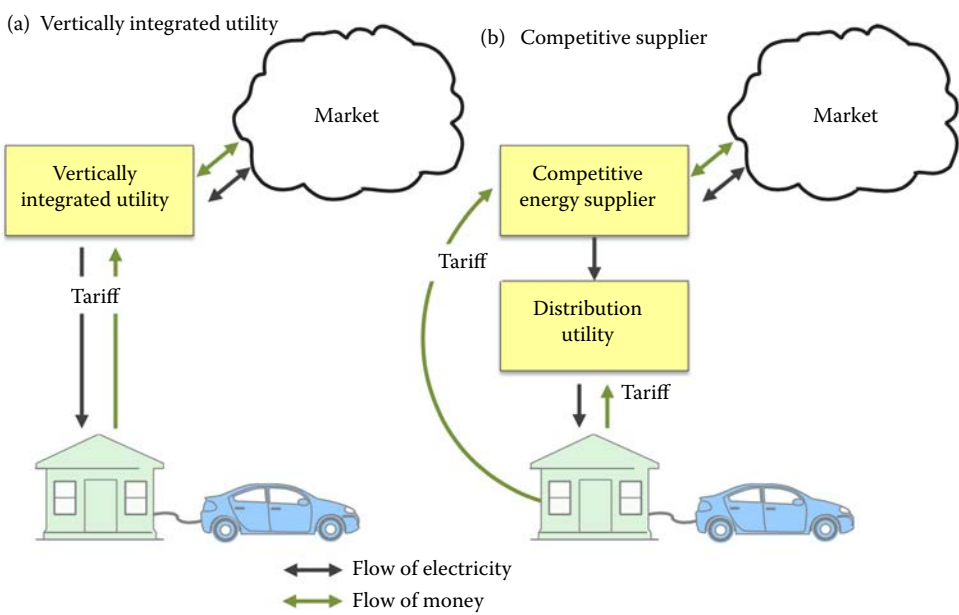


FIGURE 5.5 Electricity sales via an LSE in the case of: a) a vertically integrated utility and b) where customer choice is allowed. (From Denholm, P., Eichman, J., and Markel, T., 2015. Summary of market opportunities for electric vehicles and dispatchable load in electrolyzers, NREL/TP-6A20-64172. [6])

integrated utility that controls generation, transmission, and distribution and—where customer choice is allowed—from a competitive generator. In the latter case, the customer pays both the electricity generator and the utility that provides the local distribution network.

5.3.1 Rate Structures

Residential electricity rates generally consist of a fixed charge and a variable one that is a function of the number of kilowatt-hours consumed. The fixed charge covers things like the generating and transmission equipment capital cost, conversion equipment, electric meter, the labor of the meter reader, and the cost of the record keeping and billing. The cost per kilowatt-hour consumed covers the cost of operating the generator, maintaining the transmission lines, providing the various services needed to ensure reliability, and profit for the utility.

Commercial and industrial customers often have separate energy (kWh) and demand charges (kW). For example, in addition to being charged a certain number of cents per kWh for the total energy consumed in a month, there will be a separate charge for the highest kilowatt demand during a 15-minute period. This incentivizes electric customers to reduce their peak demand. High demands mean that an LSE must have more generating capacity available.

Another way to limit peak demand is to charge different prices for electric energy (kWh) at different times. Time-of-use pricing has a schedule of different charges per kWh for each time of the day and for different days of the week, usually with higher fixed energy prices during defined high-demand periods. A more accurate reflection of reality is real-time pricing, which continually changes in real time to reflect the demand on the LSE. As will be described later in this chapter, time-of-use and real-time pricing structures can encourage consumers to limit peak demand.

5.3.2 Electricity Markets

The electric energy markets shown in [Figures 5.4](#) and [5.5](#) are unique for a number of reasons. Unlike other commodities, electricity cannot be stored cheaply on a large scale. Electricity production constantly changes to exactly meet the instantaneous demand. Also, once electricity enters the power system, the source cannot be identified. For example, a residential consumer can opt to pay for wind power, but the power consumed cannot be directly associated with a wind farm. Finally, electric power is not directed; it simply flows down the path of least resistance.

Wholesale power markets in the United States are of two types: (1) traditional regulated markets and (2) regional markets, or regional transmission organizations (RTOs). In regulated markets, utilities own the power plants and sell the electricity to customers. Prices are set through regulatory control. Traditional markets are common in the Southwest (except California), the Southeast, and the Pacific Northwest. They include all three types of utilities: investor-owned, municipals, and rural electric co-ops. These utilities are often vertically integrated and own all three components: generation, transmission, and distribution. They include large federal systems: the Western Area Power Administration (WAPA) in the Southwest, the Tennessee Valley Authority (TVA) in the Southeast, and the Bonneville Power Administration (BPA) in the Pacific Northwest. These federal organizations work with utilities in their states to market hydropower and provide other services to multi-state regions. Utilities in traditional power markets produce their own electricity and trade electricity with other utilities via bilateral transactions between a seller and a buyer. They determine and build the needed electric capacity, determine the sequence of electric dispatch to balance supply and demand, and plan new transmission.

In other regions of the country, power pools involving multiple utilities developed. This allows for reserve capacity and the costs of new generating capacity to be shared among multiple entities. Approximately two-thirds of the U.S. population is served by these Regional Transmission Organizations or RTOs. Figure 5.6 is a map showing the independent system operators (ISOs) and regional transmission organizations (RTOs) in North America [7].

RTO markets are deregulated, with prices being set in competitive markets. They operate as an auction, whereby electric generating companies submit bids and consumers submit offers.

There are actually four different types of electricity markets:

- Energy
- Capacity
- Ancillary services
- Transmission

These are described in the following sections.

5.3.2.1 Energy Market

The energy market sets the price of electricity on a dollar per megawatt-hour basis. There is a high demand for electricity at a low price and a low demand for electricity at a high price. At an electricity price somewhere in between, the supply matches the demand.

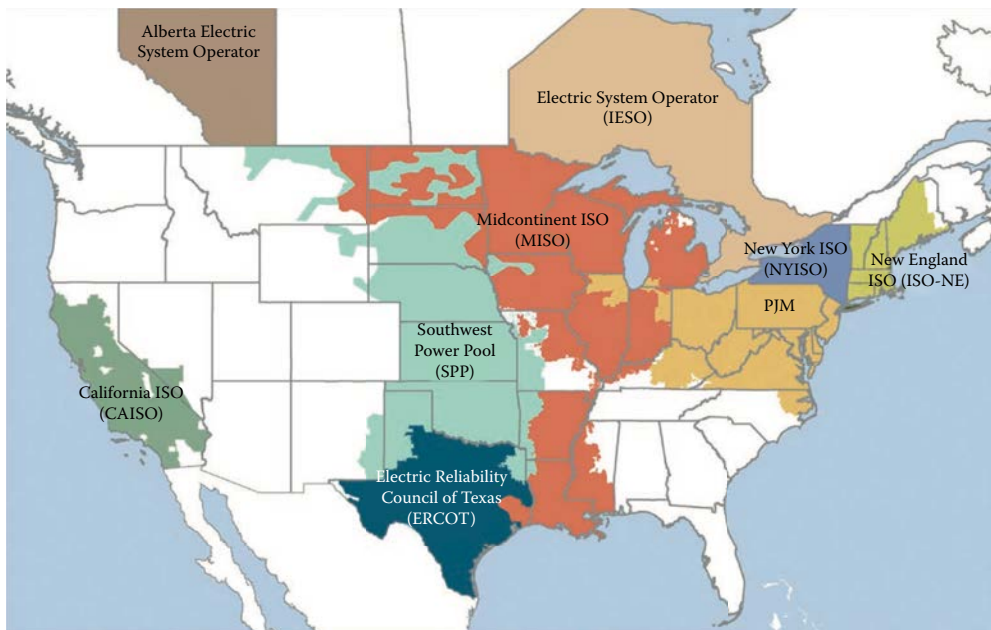


FIGURE 5.6

North American Independent System Operators (ISOs) and Regional Transmission Organizations (RTOs). (From Federal Energy Regulatory Commission, 2012. *Energy Primer: A Handbook of Energy Market Basics*, <https://www.ferc.gov/market-oversight/guide/energy-primer.pdf>. [7])

This is what is referred to as the “market clearing price.” Approximately 95% of energy transactions are done in a day-ahead scheduling market. The rest are real-time prices to reconcile differences between the load that was scheduled the previous day and the actual real-time load.

RTOs use a mechanism called locational marginal price (LMP) to determine the cost needed to serve the next (marginal) MW of load. It is called locational because the price depends both on the area where the electricity is produced and where it is consumed. This cost accounts not only for the costs of different generators in different areas but also the transmission ability between areas. If all consumers cannot be provided by the electricity from the cheapest area due to transmission congestion, areas importing cheaper electricity must pay the higher price for both the cheaper imported electricity and the more expensive local electricity. This added cost above the amount actually going to the generators is called the congestion cost. It is collected to pay investors who purchased financial transmission rights as a hedge against transmission congestion. Financial transmission rights are an example of a financial derivative investment that derives from the electricity commodity market (see Section 5.3.2.3: Ancillary Services Market).

5.3.2.2 Capacity Market

Capacity is the continuous electric power in megawatts (MW) that LSEs can transmit to their customers. Capacity resources are of several types [8]:

- Electric generation (both existing and planned) either generated by the LSE or purchased via a bilateral agreement or on the spot market
- Demand resources, including interruptible loads
- Energy efficiency measures
- Transmission upgrades.

RTOs have various means for attracting new capacity investment and ensuring sufficiency future capacity. In the United States, four RTOs operate a capacity market: PJM, New York ISO, ISO New England, and Midcontinent ISO. These markets assign the needed capacity to meet forecast demand, provide the income to support existing generators, and ensure sufficient reserve margins. Different types of auctions are used to allow generators to bid on providing future capacity. A price cap is used to prevent excessive prices.

RTOs that do not have a capacity market have programs designed to ensure that sufficient capacity is developed. For example, CAISO uses a program established by the California Public Utilities Commission to ensure adequate generation. Load-serving entities are required to contract a year ahead for capacity services that can provide a margin of 15% above the predicted demand [8].

The capacity market has gone through significant change in recent years. The low natural gas prices since the latter half of 2008 have shifted new generation from base load coal plants to natural gas plants with peaking capability. There is also a shift from new generation to demand resources and efficiency measures, thus reducing the need for new generation. Most recently, over two-thirds of new generation has been in wind and solar resources, a trend that is likely to continue due to the decreasing costs of these technologies and state renewable energy requirements.

5.3.2.3 Ancillary Services Market

Ancillary services are various services that ensure that electricity is reliably provided to the load. There are several types of ancillary services including: frequency regulation, operating reserve, voltage control, and black start service. Each of these is described below.

5.3.2.3.1 Frequency Regulation

When demand suddenly exceeds supply, as when a generator goes down, the operating generators will slow, dropping the frequency below the system operating frequency (60 Hz in the United States, 50 Hz in Europe). The opposite situation occurs if demand suddenly drops below the supply. To maintain the operating frequency with a ± 0.5 Hz band, an automatic control signal is continuously provided to special frequency regulation generators to increase or decrease power (referred to as “regulation up” or “regulation down”) to raise or lower the frequency, respectively. Generators that can ramp quickly and provide fine tuning will bid into a special regulation market, and RTOs will award contracts based on the best offer prices and the availabilities of the units. Frequency regulation can also be provided by controlling demand. For example, air conditioner compressors could be temporarily shut off to provide regulation up. It has also been suggested that electric vehicles hooked into the grid could also be programmed to adjust the demand in response to grid frequency changes.

5.3.2.3.2 Operating Reserves

Each RTO will require that there be an operating reserve of contracted power generation assets to handle contingencies. For example, the New York ISO requires that there be an operating reserve capable of providing power equal to 150% of the largest generator on the grid, to allow for that generator to unexpectedly shut down and still have some contingency. There are different types of operating reserve: spinning and non-spinning. Spinning reserves are up and running and synchronized to the grid but are providing less than their rated capacity. They can ramp up within a 10- to 30-minute time window. Non-spinning reserves are not operating but can start up and synchronize quickly and reach full output in 10–30 minutes. As is the case for other ancillary services, RTOs accept bids for operating reserves for the different parts of their operating territory.

5.3.2.3.3 Voltage Control

For a stable grid both the real power must be controlled (to match supply and demand and thus keep frequency steady) and the reactive power must be controlled. The reactive power has a strong impact on the current in transmission lines and hence the voltage drop in those lines, which is proportional to the reactive power being delivered. Thus to ensure that a steady voltage within defined limits (e.g., $\pm 6\%$) is being delivered to the load, a utility must control the reactive power.

AC transmission and distribution lines also contain both inductance and capacitance and so also affect reactive power. Because most reactive industrial loads are inductive, a utility can bring the voltage and current back into phase by using capacitance. Then current can flow back and forth between capacitors and inductors. In terms of reactive power, a synchronous generator acts like a motor in reverse and so also has inductive reactance but of an opposite sign. A utility can control the amount of generator reactive power by adjusting the amount of current through the rotor windings.

Voltage control is thus an ancillary service that involves controlling the reactive power. This service is provided by on-line generators (via current control), capacitor banks, and

devices that have the ability to consume reactive power. Companies providing these voltage control services are paid a monthly service fee.

5.3.2.3.4 Black Start Service

In the case of grid electrical failure, some facilities must be available to start up and generate electricity that is synchronized to the grid (e.g., at ± 0.5 Hz) without the benefit of an outside electricity supply. Natural gas combustion turbines and hydropower turbines are examples of systems that can start during a blackout. Units that can provide this service are paid regardless of whether or not they are used because of the reliability they represent.

5.3.2.4 Financial Transmission Rights Market

If a consumer must pay a higher price for electricity because a transmission line is congested (at its limit) and transmission from a lower-cost generator is thus limited, the additional cost is paid to holders of financial transmission rights (FTRs). (Payments are not made to transmission owners, as this would provide an incentive to create congestion.) FTRs are essentially insurance contracts that provide a hedge against transmission line congestion. They are bought and sold via auctions on various time scales ranging from monthly to long term.

5.4 Grid Operations

In adding new capacity to the grid, a utility must consider the total capital and operating costs of plants [9]. Various plant options can be compared in terms of the levelized cost of electricity, or LCOE, having units of \$/kWh where:

$$\text{LCOE} = \text{Fixed Cost} + \text{Variable O\&M cost} + \text{Fuel cost} \times \text{Heat Rate} \quad (5.2)$$

Where

$$\text{Fixed Cost} = \frac{\text{Capital Cost} \times \text{Capital Recovery Factor} + \text{Fixed Annual O\&M Cost}}{\text{Capacity Factor} \times 8760}$$

and

$$\text{Capital Recovery Factor} = \text{CRF} = \frac{i(1+i)^n}{(1+i)^n - 1}$$

The Capital Cost is the plant construction cost divided by the rated plant capacity and has units of \$/kW. The Fixed Annual O&M Cost depends on plant size and has units of \$/kW per year. The Variable O&M Cost is proportional to the amount of energy produced and has units of \$/kWh. The Heat Rate is the average amount of thermal energy the plant must receive to produce a kilowatt-hour of electricity (i.e., it is inversely proportional to plant efficiency) and has units of Btu/kWh. The fuel cost is then given as \$/Btu.

The numerator consists of annualized costs, so the 8760 hr/yr converts to an hourly cost. The capacity factor is the ratio of the amount of electrical energy produced over a year divided by the electrical energy that would be produced if the plant operated at its

TABLE 5.3

Example Average Values for Calculating LCOE

Plant Type	Capital Cost (\$/kW) ^a	Heat Rate (Btu/kWh) ^b	Fuel Cost (\$/10 ⁶ Btu) ^c	Variable O&M (\$/MWh) ^d	Fixed O&M (\$/kW/yr) ^d
Ultra Supercritical Coal	3,636	8,800	2.16	4.6	42.1
Combined Cycle Gas	978	6,600	2.40	3.50	11
Gas Turbine	1101	10,000	2.40	3.5	17.5

^{a,b,c} EIA November 2016. [10]^d EIA May 2016. [11]

rated plant capacity for every hour of the year. Thus, a capacity factor of 1 would give the minimum leveled cost of electricity. If the plant operated at an average capacity factor of 0.5, its electricity would cost twice as much per unit of fixed costs.

Note that for most renewable energy plants, such as solar, wind, and geothermal, the fuel cost is zero. (Biomass plants do incur a cost for the biomass feedstock.) Thus, these plants are not susceptible to future increases in fuel costs as can occur for natural gas, for example.

Table 5.3 gives some example values for the different parameters for conventional plants [10,11].

EXAMPLE 5.1

In comparing different plants, the LCOE is determined based on a plant's expected capacity factor. The LCOE decreases with increasing capacity factor because more annual energy is produced per investment dollar. Consider the case for three common fossil fuel plants: natural gas combustion turbine, gas combined cycle, and coal. Using the equation for LCOE, calculate the LCOE for each power plant type as a function of capacity factor and plot these on the same graph. For plot a, use a high natural gas cost of \$7 per million Btu. For plot b, use the latest natural gas cost (as of 2016) from Table 5.1. Use the cost of coal and other relevant costs from Table 5.1. In determining the capital recovery factor, assume a plant lifetime of 40 years and a discount rate of 4%.

Calculating the capital recovery factor based on a 40-year lifetime and a 4% discount rate:

$$CRF = \frac{i(1+i)^n}{(1+i)^n - 1}$$

$$CRF = \frac{0.04(1+0.04)^{40}}{(1+0.04)^{40} - 1} = 0.05052$$

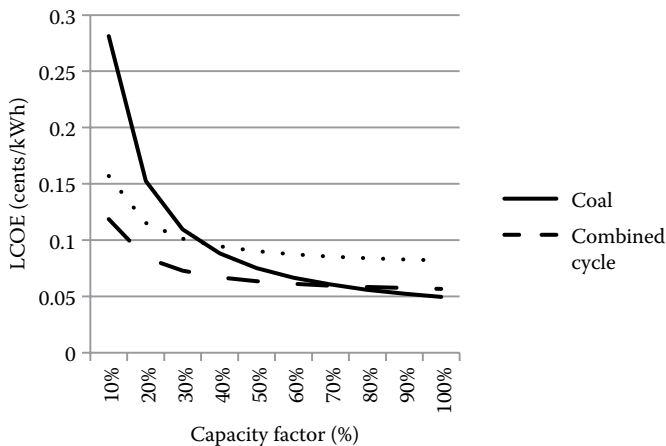
we then calculate the LCOE for a range of capacity factor values using this capital recovery factor and the values from Table 5.1 and repeat the calculations substituting the higher natural gas cost. So, for example, for a capacity factor of 10%, the fixed cost of the coal plant would be:

$$\text{Fixed cost} = \frac{\$3636 \times 0.05052 + \$42.1/\text{kW}/\text{yr}}{0.1 \times 8760 \text{ h}} = \$0.26/\text{kWh}$$

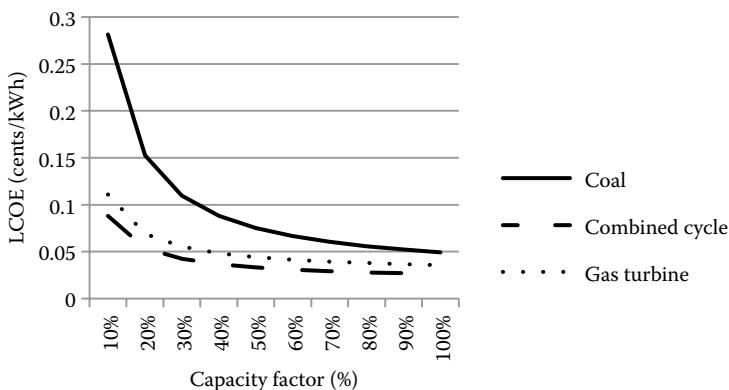
and (converting variable O&M cost from \$/MWh–\$/kWh)

$$\begin{aligned} \text{LCOE} &= \$0.26/\text{kWh} + \$0.0046/\text{kWh} + \$2.16/\text{MMBtu} \times (1\text{MMBtu}/10^6\text{Btu}) \\ &\times 8800\text{Btu}/\text{kWh} = \$0.283/\text{kWh} \end{aligned}$$

The results for a range of capacity factors are plotted below. Note that at the high gas prices, which have often existed, coal plants are the least cost option at high capacity factors. Coal plants have often been run as base load plants with capacity factors over 60%. However, with low natural gas prices, coal plants are not cost-effective even at the highest capacity factors, which is one reason why since 2015, monthly natural gas electric power generation has matched or exceeded coal generation in the United States. At very low capacity factors, simple combustion turbines have traditionally been used as “peakers” to provide electric power during peak summer hours when air conditioning loads are high. The latest EIA cost numbers show that even at low capacity factors combined cycle plants have a lower levelized cost of electricity than combustion turbines. This is because their high efficiency results in a lower capital cost as expressed in dollars per kilowatt. Because combustion turbines have a lower absolute capital cost, however, they require a smaller initial investment.



a. High natural gas costs.



b. Low natural gas costs.

TABLE 5.4

Average Capacity Factors of U.S. Electric Generating Plants in 2015

Plant Type	Capacity Factor (%)
Coal	54.6
Nuclear	92.2
Gas Turbine	6.7
Gas Combined Cycle	56.3
Large Hydropower	35.9
Biomass Combustion	52.9
Geothermal	71.7
Land-Based Wind	32.5
Solar Photovoltaics	28.6
Concentrating Solar Power	23–59 ^a

Source: From EIA. Electric power monthly, https://www.eia.gov/electricity/monthly/epm_table_grapher.php?t=epmt_6_07_a; NREL 2016 Annual technology baseline, <https://www.nrel.gov/analysis/data-tech-baseline.html>. [12,13]

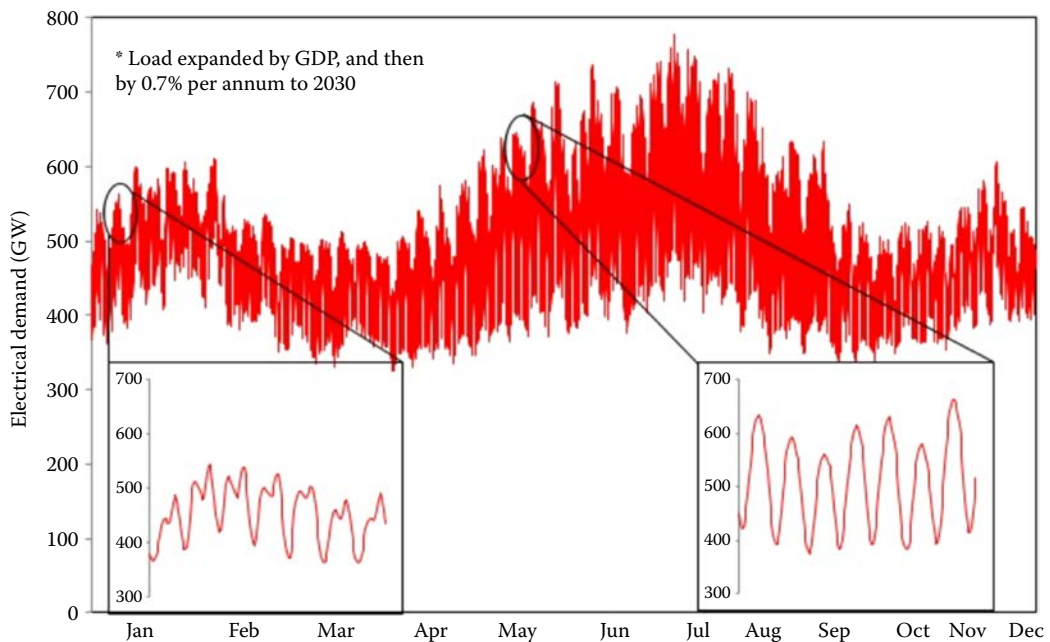
^a 23% with no storage, as high as 59% with 10 hours of storage. [13]

Actual average capacity factors for all the operating electric generating plants in the United States in 2015 are shown in Table 5.4 [12,13]. Note that these are averages across all plants and account for actual operation. So, for example, utilities shifted to burning more natural gas, which left some coal plants idle, thus decreasing the average nationwide coal capacity factor. It is important to also note that the spread of values can be large. For example, a particular plant's capacity factor will be reduced if it experiences operating issues resulting in shutdowns.

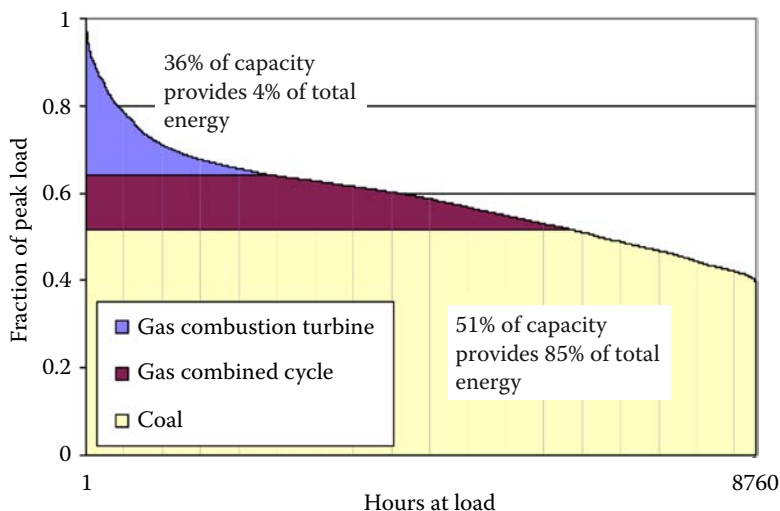
The previous equation for LCOE provides a simple way to compare different plant options. In reality, depreciation; pollution control requirements; tax considerations including government incentives; energy (kWh) vs. peak demand (kW) electricity rates; and loan parameters such as loan period, debt service coverage ratio, and so on, require a more sophisticated calculation. In addition, state renewable portfolio standards may require a utility to deploy more renewable energy. Thus, utilities use sophisticated financial models to compare alternatives for new generation. Any price on carbon dioxide emissions, as currently exists in California, for example, will skew the results more toward renewable options. Finally, when analyzing the addition of a new power plant, a utility needs to understand how that plant will integrate with other plants on the grid. In the case of adding wind and PV on the grid, it requires a detailed resource assessment including hour-ahead and day-ahead forecast modeling.

An example plot of the total U.S. electric load throughout the year is shown in Figure 5.7 [14]. Not shown on this graph is that about a 15% margin of capacity above the peak must be available on a long-term basis to handle unexpected peaks or loss of capacity.

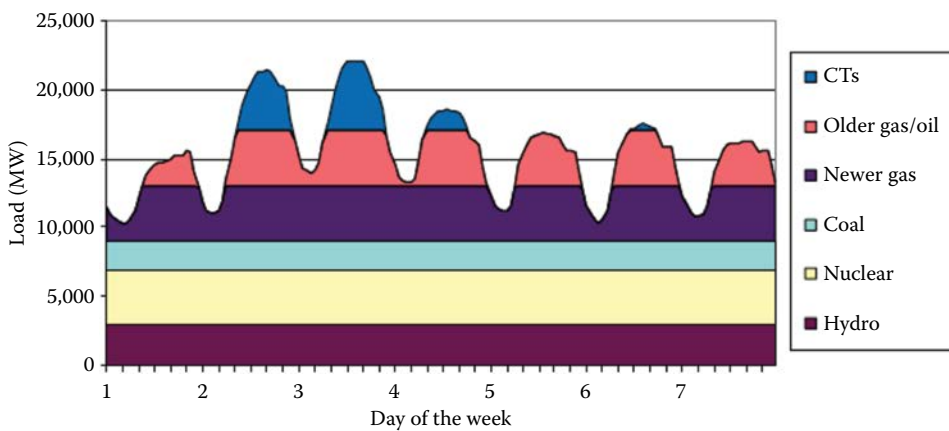
Figure 5.8 [15] shows an example normalized load duration curve for conventional electric generating plants broken into different segments. The bottom area is the region where base load plants operate. These have traditionally been coal, nuclear power plants, and hydropower because they have typically been the cheapest to operate, so it makes sense to use them for more hours. The peak load is provided by combustion gas turbines. They are the most expensive to operate due to lower efficiency, but have the greatest ability to follow rapidly changing loads. In between these two are natural gas combined-cycle plants, which are very efficient and have some load-following capability. (Because of the low natural gas prices since 2015, natural gas plants have been replacing coal plants even as base load.) For

**FIGURE 5.7**

Example plot of U.S. electric load throughout the year. On typical winter days both a morning and early evening peak are common, whereas summer days typically have a late afternoon peak. (From Clack, C.T., 2015. Decarbonizing the U.S. electric sector, presentation, <http://www.slideshare.net/sercuser/decarbonizing-the-us-energy-sector-a-study-in-optimization-and-tradeoffs>. [14])

**FIGURE 5.8**

Example traditional load duration curve showing how many hours per year the load is at a given level and the different dispatch components. The peak load occurs for only a small number of hours per year, whereas the load is at or above a base load value for all 8760 hours per year. (From F. Kreith lecture notes. [15])

**FIGURE 5.9**

Example conventional dispatch stack. (From MCEN Sustainable Energy. Electricity systems, <http://mcensustainableenergy.pbworks.com/w/page/20638049/Electricity%20Systems>. [16])

each plant type, its shaded area represents the total power it delivers over a year. If one extends the area to the right as a horizontal rectangle, the capacity factor is the ratio of the shaded area in the horizontal rectangle to the total area of that rectangle.

Of course, a utility operator must dispatch plants throughout the day as the load changes. Based on operating costs, the utility operator might typically dispatch available hydropower, nuclear, and coal plants in that order to provide the base load. After that would come the most modern and efficient combined-cycle natural gas plants, followed by older combined cycle plants. Finally, to meet those peak loads that occur on certain days, the more expensive to operate combustion gas turbines would be used to follow the load. Figure 5.9 shows how different conventional generators might be dispatched throughout a week [15].

5.5 Integration of Variable Renewable Energy into the Grid

As the electric grid changes to reduce carbon emissions, the emphasis is on energy efficiency to reduce the electricity need and the deployment of renewable energy sources. The two most rapidly growing renewable electricity sources are wind and solar PV. These are sometimes referred to as intermittent resources. However, most experts consider the word “variable” to be more correct. “Intermittent” refers to something that can turn on and off suddenly. In fact, all conventional sources can be subject to intermittency because they will occasionally experience sudden shutdowns. Wind and PV are more correctly considered variable resources, because their output varies with time and the available wind or solar resource as opposed to turning on or off. When wind and PV systems are spread out over a wide area, it is unlikely they will all provide zero output at any given time, but their output will vary with time. (Of course, PV systems without batteries will provide no nighttime electricity.)

Utilities assign a term called “capacity credit” (different from “capacity factor”) to account for the probability that an electric generation technology will be available during peak load periods. The capacity credit of a wind farm or PV installation is the ratio of the capacity

(in megawatts) of the thermal plant that is displaced to the rated output (in megawatts) of the wind or PV, usually expressed as a percentage. It indicates the “firm capacity” that the renewable energy system can supply. Because utility operators have a wide range of different combinations of supplies for meeting electricity demand, capacity credit is viewed from a long-term probabilistic standpoint. Although a wind farm could conceivably have a time when it is not generating any wind power, due to either very low or very high wind speed conditions (wind turbines must shut down at very high wind speeds due to structural limitations), it is not assigned a zero-capacity credit, as that would mean that there is zero probability that the wind farm would be available during peak demand periods [17].

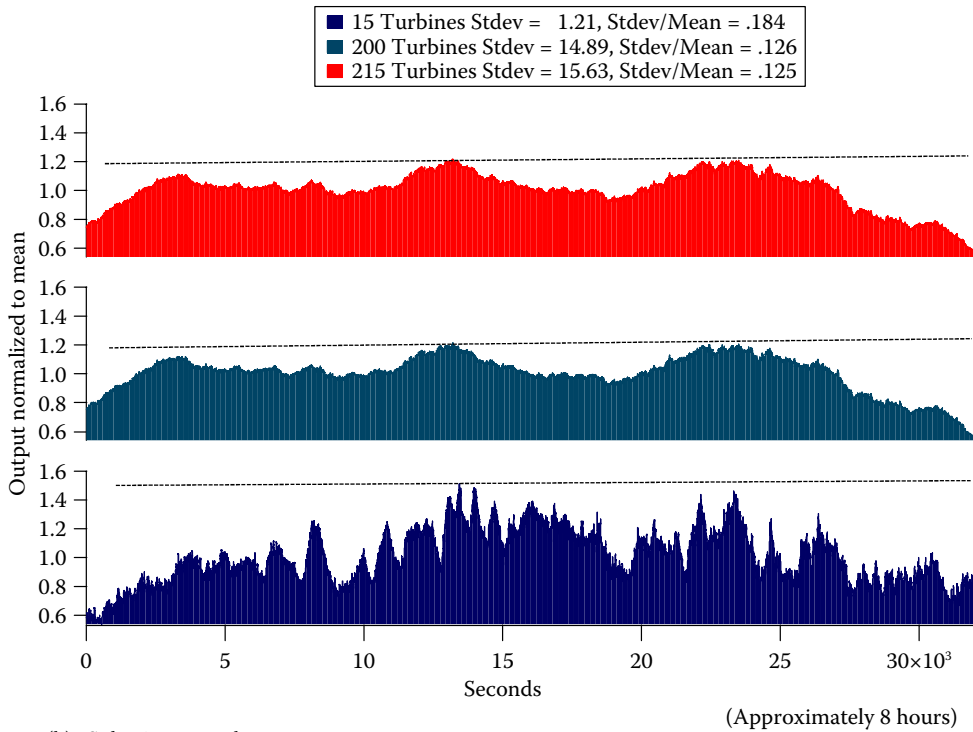
Wind in any one location can be extremely variable. However, while the wind may die down (or scattered clouds may temporarily reduce available sunlight for PV systems), other locations can help carry the load. Thus, expanding an operator’s region to achieve a greater spatial diversity of renewable electricity sources will steady the electric output. Allowing increased interchange of electricity between different utilities provides the same effect. It is especially important for small areas to be able to buy and sell electricity from adjacent areas, because they may have insufficient area to achieve adequate spatial diversity. [Figure 5.10](#) [18] shows how access to greater numbers of wind turbines and PV plants will smooth the total aggregated output.

The dispatch of a power system becomes more complex when renewable sources are brought to bear. [Figure 5.11](#) shows the dispatch of generators on a summer day when more and more PV is added to the grid [19]. This shows the daily load profiles in California for four cases: no PV, 2% PV, 6% PV, and 10% PV. On hot, sunny afternoons, PV output is high and so it coincides well with afternoon air conditioning loads. Thus, adding 2% PV to the grid reduces the peak load that the utility must address with natural gas combustion turbines, which are the highest-cost electricity producers. Note also, however, that the addition of PV has increased the ramp rate for the conventional power that must be dispatched as the solar resource declines at the end of the day.

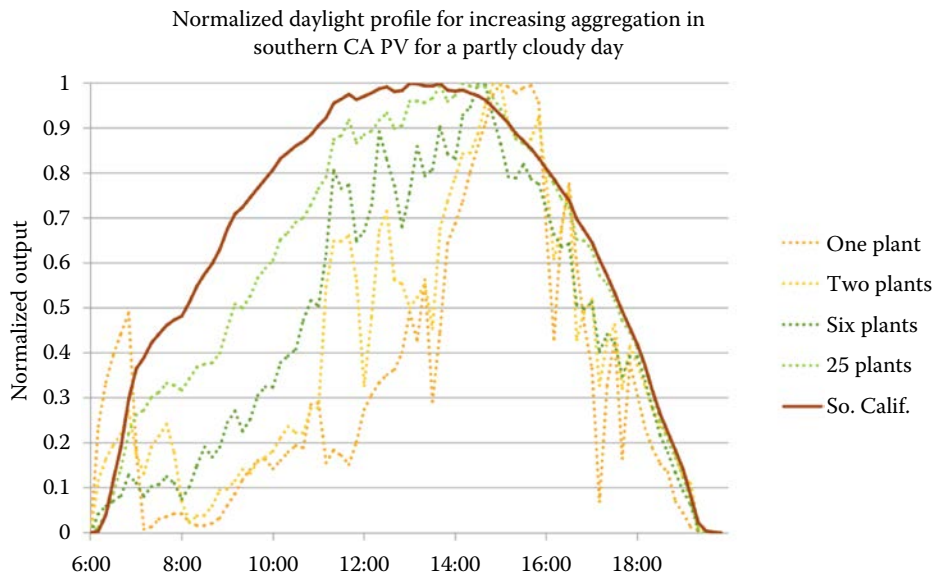
As the PV penetration increases to 6%, it continues to cut into the peak, displacing combustion turbines. As shown by the dashed black line, however, as the PV gets to 10% penetration, we are reaching a point of diminishing returns in reducing the peak load. The peak that the utility must match with conventional energy has shifted to later in the afternoon and evening, at which point the sun is setting and increased PV cannot continue to reduce the peak. Adding more PV will continue to displace conventional fuel on a summer day and thus reduce carbon emissions; however, it will not continue to reduce the peak.

The situation in the swing seasons is different. [Figure 5.12](#) shows the situation for a sunny April day [19]. In this case, PV output is similar to what it is on a summer day. (The number of sunlight hours will be similar to the extent that the spring and summer days are on opposite sides of the summer solstice. If the array is at a tilt angle close to the local latitude, the average incident angle in the spring may be better than that in the summer.) The peak is now in the early evening when people get home from work and so PV doesn’t impact the peak. Also, the total load that the utility must meet is lower. In this case, PV quickly reduces the need for generation from other plants. Note that at just 6% penetration, the wind output is impacted. This shows that the wind power must be curtailed (typically by adjusting the pitch of the turbine blades) so that the electric power supplied matches the lower demand. That’s not good, because it means the cost of the wind farm is not being fully amortized, making wind power effectively more expensive. At 10% penetration, the PV is providing so much electricity on this spring day that the base load coal and nuclear plants need to be curtailed, and these plants are not typically operated at partial loads. The reality in this case is that the PV itself might be curtailed.

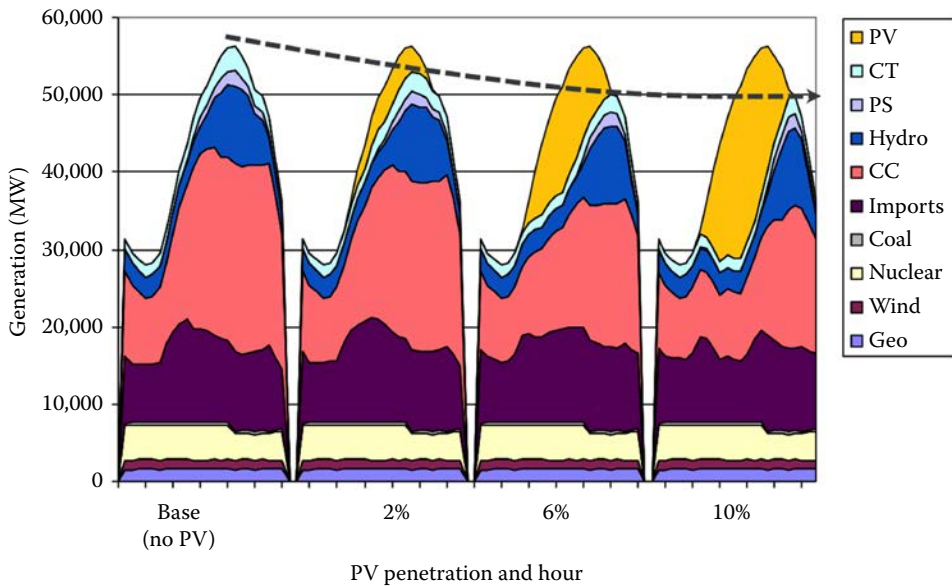
(a) Wind power smoothing with increasing number of turbines



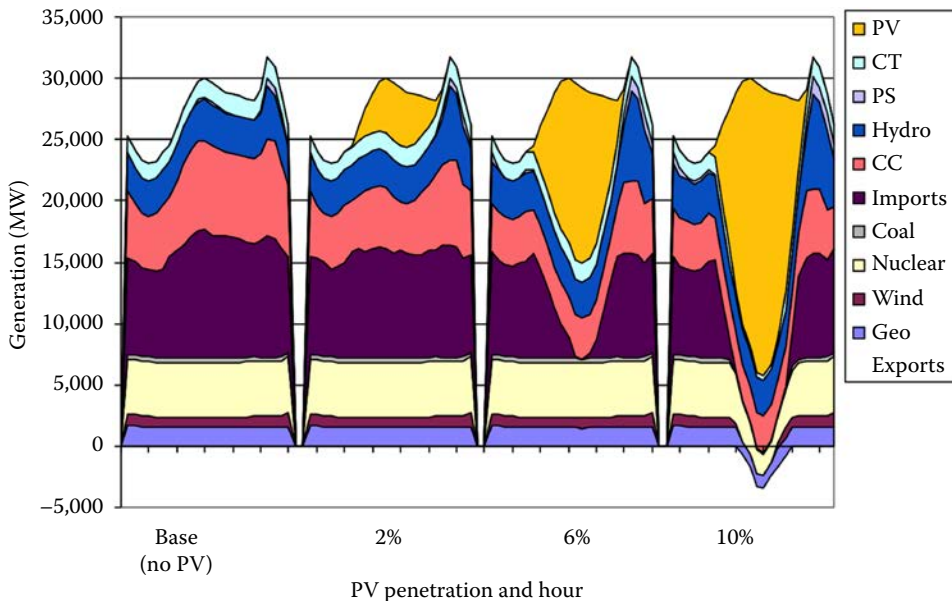
(b) Solar PV smoothing

**FIGURE 5.10**

Smoothing of variable renewable electricity by drawing upon multiple locations: (a) effect of increasing number of wind turbines (NREL wind plant data), and (b) effect of increasing number of PV plants on a partly cloudy day. (From Lew, D. et al., September 2013. *The Western Wind and Solar Integration Study, Phase 2*. NREL/TP-5500-55588. [18])

**FIGURE 5.11**

Impact of adding additional PV to the grid on a typical summer day. (From Denholm, P., and Mehos, M., November 2011. Enabling greater penetration of solar power via the use of CSP with thermal energy storage, NREL/TP-6A20-52978. [19])

**FIGURE 5.12**

Impact of adding additional PV to the grid on a typical spring day. (The negative portion of the graph corresponds to exported electricity.) (From Denholm, P., and Mehos, M., November 2011. Enabling greater penetration of solar power via the use of CSP with thermal energy storage, NREL/TP-6A20-52978. [19])

Curtailement of renewable sources already occurs at times on the electric grid. For example, the CAISO has already had to occasionally curtail wind and solar for short periods in the late winter and early spring. Curtailing wind and PV is undesirable because it increases the effective cost of these sources and it reduces the carbon dioxide emissions reduction benefits of renewable energy. In fact, there is no real physical limit to how much variable renewable energy can be put on the grid. But at high penetration values, curtailment causes renewables to be very expensive unless storage or other measures are taken to increase grid flexibility.

Figure 5.13 shows another way to look at this spring generation problem [19]. A 2013 study looked at the impact on March 31 of adding more and more photovoltaic generation to the California grid each year out to 2030 [20]. The figure shows a family of daily load curves for different years, each progressive year representing additional photovoltaic penetration. As with the previous figure, because this is in the spring, as PV penetration increases the peak shifts to the evening, when PV can no longer contribute to it. (Wind power, on the other hand, might reduce the peak because wind speeds tend to be higher at night in many locations.) Adding PV reduces the remaining need for generation. The large belly in the afternoon means that some generation will need to be curtailed. Note, too, that the ramp rate in the late afternoon becomes very steep. Utilities call these curves “duck curves” because they have the shape of a duck in profile.

Studies have shown that PV can achieve annual energy penetrations of 15%–25% without a large amount of curtailment provided that there is wide spatial diversity of resources and some control and peak shifting occurs on the demand side.

Because wind and PV are variable sources, it is sometimes argued that a large amount of electrical storage must be added to the grid to accommodate them. However, utilities have various means for dealing with the variability of wind and PV. Concentrating solar power (CSP) plants with thermal storage are effective, although they are generally limited to desert regions like the U.S. Southwest. Many regions, especially the Pacific Northwest, utilize

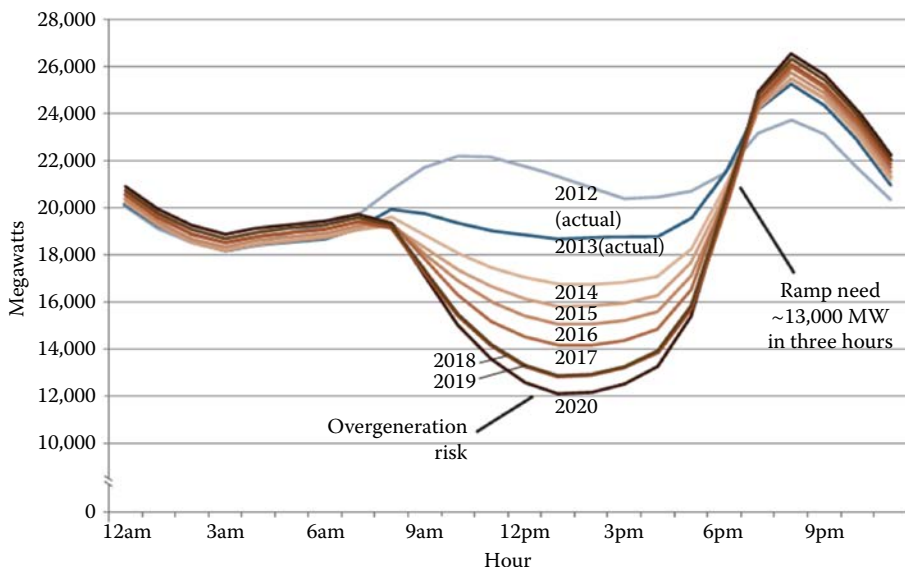


FIGURE 5.13

Utility “duck curves” showing modeled net load for March 31 in California. Where renewable over-generation occurs, the renewable energy must be curtailed, which increases the cost per megawatt-hour. (From California ISO. https://www.caiso.com/Documents/FlexibleResourcesHelpRenewables_FastFacts.pdf. [20])

hydropower, which can provide low-cost base load and yet can also adjust very rapidly to follow a varying load. Denmark produces over 40% of its electricity from wind power and purchases hydropower from Norway when wind speeds drop. Some utilities use pumped-hydro storage, pumping water from a reservoir at low elevation to one at a higher elevation at times of low load and then meeting peak power needs by flowing that water downhill through a turbine. And, of course, because the U.S. electric grid is so interconnected, electricity is continually bought and sold between different operating regions.

To accommodate renewable supply shortages, operators can plan on greater use of natural gas combustion turbines or they can run combined-cycle gas plants at partial load. To effectively address climate change, however, carbon-free strategies must be tapped to accommodate renewable variability. When wind and solar are deployed together, they are generally complementary. That's because the wind resource is generally greater in the winter and at night—the opposite of the solar resource.

At some point, there is not enough flexibility in the grid and some storage is needed to avoid large curtailment costs. A recent study [21] examined how much storage would be needed to achieve 50% grid penetration of PV in California, assuming another 25% of renewable resources exists on the grid. Various changes are needed to achieve these very high PV penetrations to avoid high levels of PV curtailment such as significant electricity exchange with adjacent states and significant penetration of electric vehicles with vehicle-to-grid capability. (Of course, other forms of storage would also support higher penetration.) The study also indicated, however, that a lower penetration of PV coupled with greater wind penetration could result in better economics.

One way to minimize curtailment is to mix PV with dispatchable concentrating solar power containing thermal storage. In Figure 5.14, the percent of solar curtailment is shown as a function of total solar penetration on the grid for three cases: PV with a limited amount of grid flexibility, PV with enhanced flexibility, and a combination of PV and CSP with thermal energy storage. The enhanced flexibility includes variable output from conventional

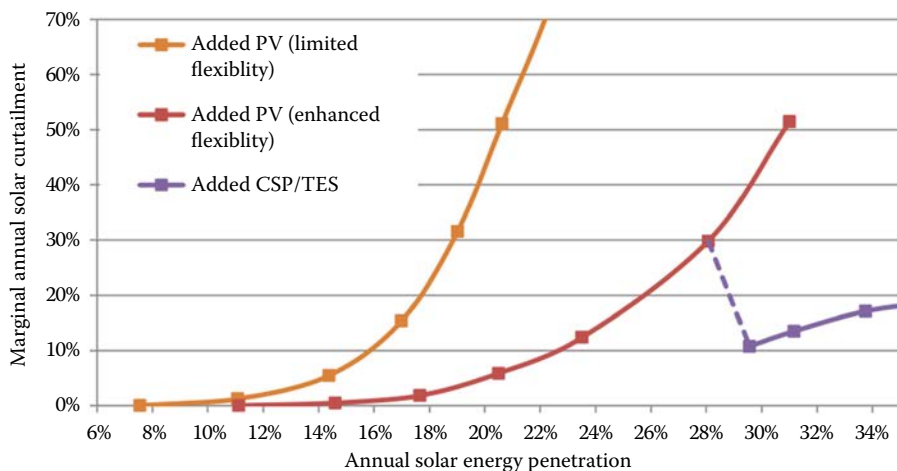


FIGURE 5.14

Comparison of PV only with two assumptions regarding the amount of grid flexibility to the same amount of PV plus CSP with thermal storage (that provides an amount of energy equal to the PV) over a range of different solar energy penetrations. (From Denholm, P., Clark, K., and O'Connell, M., 2016. On the path to SunShot: Emerging issues and challenges in integrating high levels of solar into the electrical generation and transmission system, NREL/TP-6A20-65800, <http://www.nrel.gov/docs/fy16osti/65800.pdf>. [21])

generators, some form of storage, (e.g., stationary battery storage or pumped hydro), greater geographic diversity, and some demand response. The thermal storage of the CSP plants provides additional flexibility regarding when solar electricity is dispatched. This allows greater grid penetration of solar electricity and reduces the amount of solar curtailment.

Numerous utilities have conducted grid integration studies to determine the additional costs of integrating wind energy into the grid. Although variable renewable energy generators save fuel costs (they have zero fuel costs, although they do incur some operating costs), because their resource varies, utilities have calculated what additional costs they might incur, and these are called integration costs. An example of an integration cost is the cost associated with having spinning reserve available for when renewable output drops. These studies have generally shown that even at penetrations as high as 25%–30% of peak power, the integrating renewables adds no more than about a half-cent per kilowatt-hour to the cost of generating electricity.

Figure 5.15 shows the results of an Arizona Public Service study on grid integration costs for varying degrees of wind energy penetration on their grid [22]. The figure shows that at 10% energy penetration, the additional cost is only \$4/MWh or 0.4 cents per kWh. Much of the cost is associated with the uncertainty in day-ahead and hour-ahead forecasting of the wind resource. Accurate forecasting can reduce the amount of spinning reserve that a load serving entity must have and so is a major area of research.

To plan dispatch, RTOs use mathematical models to forecast the load in their service regions. Forecasts are generally done hour ahead, day ahead, week ahead, and longer term.

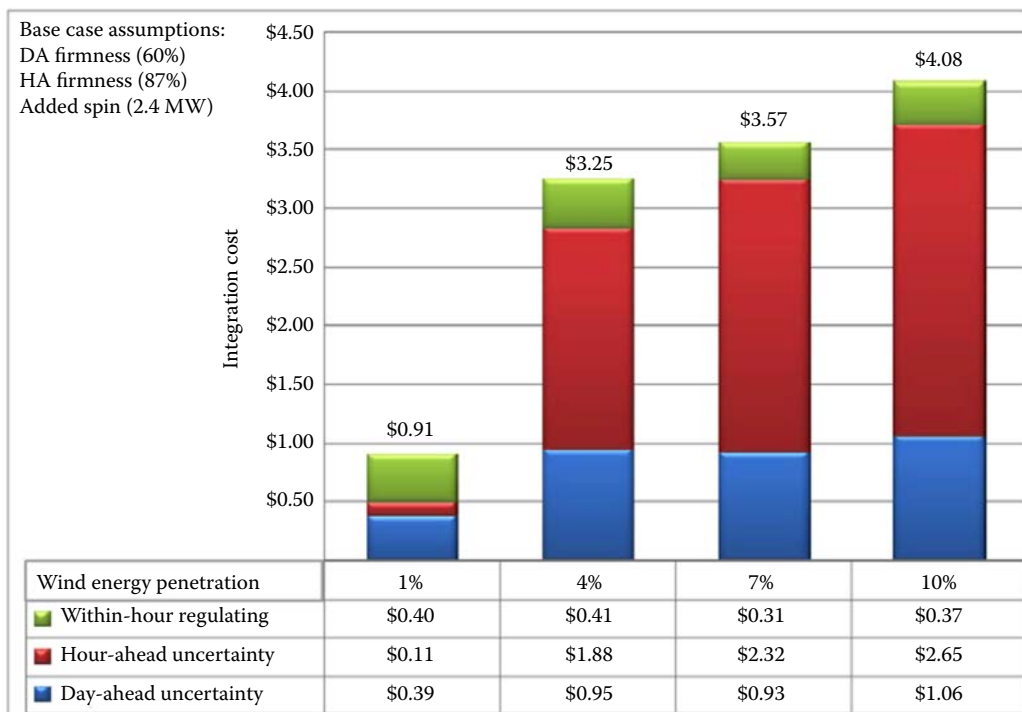


FIGURE 5.15

Arizona Public Service study of the costs (in \$/MWh) of integrating wind power as a function of grid penetration and forecasting ability. (From Acker, T., September 2007. Final report: Arizona public service wind integration cost impact study, Northern Arizona University. [22])

Weather prediction plays the most important role in short-term forecasts. Temperature and humidity are key parameters, temperature being important for both winter heating and summer air conditioning loads, humidity being a factor in the latter. Temperature is also important in determining the performance of thermal power plants. The higher the outdoor temperature, the less efficient the heat rejection and thus the lower the cycle efficiency. This is especially the case for air-cooled power plants. The accuracy of weather forecasts results in an uncertainty of 1%–3% in day-ahead load forecasts [7].

Unlike fossil and nuclear fuels, renewable resources (wind and solar) also require energy resource forecasting in addition to weather forecasting. A utility's ability to utilize renewable energy depends a great deal on how well the availability of the renewable resources can be forecast an hour ahead, a day ahead, and a week ahead. The U.S. National Oceanic and Atmospheric Administration (NOAA) provides the public with information about wind and solar energy resources on these short time scales through the National Weather Service. Wind energy forecasting began in the 1980s and has generally focused on day-ahead forecasting. More recent efforts have looked at much shorter time horizons, from minutes to 6 hours ahead. Forecasts are made of wind speed, direction, and ramp rates (the expected time rate of change of wind speed).

A collaborative effort by NOAA, the U.S. Department of Energy, universities, and private companies is developing improved renewable energy forecasts across a range of time scales, thus making the job of integrating wind power easier and less costly. Forecasting uses a combination of improved numerical weather prediction (NWP) models and enhanced measurement networks. Because wind turbine hub heights keep increasing to reach higher wind speeds, obtaining data at these greater heights and developing models to extrapolate measurements to greater heights have received increasing attention. A research area of special interest has been the prediction of low-level jets that periodically occur in the southern Great Plains of the United States, which is an area with a large wind resource. These jets can greatly increase wind turbine output but also result in a significant vertical wind speed gradient that impacts blade performance [23].

Forecasting solar energy is different from wind forecasting in that it is heavily dependent on cloud cover and movement but can also depend on fog and snow. Solar forecasting employs different techniques depending on the forecast time horizon. Long-term forecasts are accomplished via climate models. Numerical weather prediction models can be used for time horizons shorter than 2 weeks down to as short as an hour, but they lack accuracy below 6 hours because of insufficient resolution to predict individual clouds. For time horizons shorter than 6 hours, forecasts utilize satellite imagery and/or sequences of photographic images of the whole sky. Statistical learning methods can blend results from different models and use the success of previous forecasts to reduce model error. Individual rooftop, or behind the meter (BTM) systems, can be very dependent on local conditions, but, as is the case with the smoothing of the wind resource, aggregation of installations over a wide region reduces overall forecasting error.

Although numerous utilities have done renewable energy integration cost studies like the one shown in [Figure 5.15](#), the accuracy of these studies has been called into question. For one thing, whenever any new generator—renewable or conventional—is brought onto the grid, it can negatively impact operation of the existing generators. And no two plants are alike. Utilities send out automatic generation control (AGC) signals to adjust the outputs of different generators to meet the demand. One coal plant may be able to follow the signal closely, whereas another may not. So, integration costs are not just associated with renewable energy technologies and should be considered to be associated with each individual plant on the grid rather than being viewed by technology type.

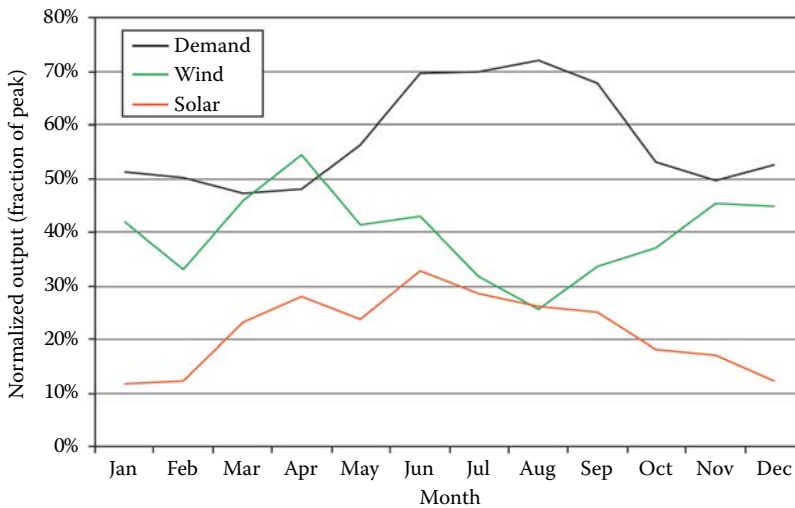
While utilities have often assigned integration costs only to variable renewables, they accrue from any changes in the grid. Thus, the true cost of integrating renewables should be evaluated plant-by-plant and should be considered in the same way as any other changes in the grid mix. Finally, from a societal standpoint, the true grid integration costs for renewables should account for the societal savings associated with the elimination of emissions, including carbon dioxide emissions. One recent study showed the latter are as high as \$220/ton of CO₂ emissions saved [24].

It is important to remember that non-variable sources of renewable energy can also provide power to the electric grid. Combining variable wind and PV power with existing fast-ramping hydropower, steady biomass power, and geothermal power can allow for still higher total renewable energy penetration before one needs to build advanced electrical storage systems such as stationary batteries or compressed air energy storage or additional pumped hydro storage. And, as we have seen, the thermal storage in concentrating solar power plants can also reduce PV curtailment costs. Arizona Public Service built the 250-MW Solana parabolic trough plant with 6 hours of molten salt thermal energy storage that can provide electricity for Phoenix in the evening and morning peak demand periods.

In the United States, non-hydro renewables provided 7.7% of electrical energy or 317 TWh in 2015 [25]. In the world, non-hydro renewable energy represents 7.3% of world electric generating capacity or 5.6% of electrical energy [26]. So there is a lot of room for expansion before the cost of large-scale electrical storage may be warranted for energy supply purposes. At some value of grid penetration by variable wind and PV substantially greater than 25% energy, economics may favor the construction of advanced electric storage systems, so it makes sense to be developing such systems for the future. But before we reach that point, a large amount of renewable and efficiency technologies can be reliably deployed to reduce carbon emissions.

Analysts who have studied how to approach 100% penetration of renewable energy on the electric grid have found that economically achieving the last 20% presents a special challenge [27]. This is due to the difference between spring and summer that we saw earlier; namely, there is a considerable increase in total load from spring to summer but not a commensurate increase in the renewable resource. Figure 5.16 shows this situation for ERCOT. While the peak electricity demand occurs in July and August, peak renewables (wind plus solar) occur in April and May. If one deploys sufficient wind and solar to meet the summer load then they would have to be curtailed in the spring. (This is not a problem for a grid that relies on fossil fuels, because utilities simply burn less fossil fuel in the spring than in the summer.) This suggests the need for a means to store renewable energy over a period of several months. Biomass plants and biofuels are a potential means for addressing this gap without having to over-deploy wind and PV to meet the summer load and curtail them in the spring.

Critics of renewable electricity often point to the variability of renewables (the sun doesn't always shine and the wind doesn't always blow). They argue that renewables are not compatible with a grid that has to provide reliable electricity 99.97% of the time (which corresponds to one day of outage every 10 years). However, this doesn't mean that each power plant must operate with that reliability. Indeed, none do. Rather, it means that the fleet as a whole must meet that standard via a combination of all the electricity sources that grid operators have at their disposal. As we have seen, utilities have a wide range of options available to meet the load requirements. Even base load power does not have to consist of the traditional situation of coal and nuclear plants running at full power 24 hours per day. Steady base load power output can be comprised of a changing mix of many renewable sources—variable sources like wind and PV and steady sources like geothermal, biomass, and concentrating solar power with storage—that working together can meet the demand.

**FIGURE 5.16**

ERCOT profiles of monthly demand and wind and solar outputs. (From Denholm, P., and Hand, M., 2011. *Energy Policy*, 39(3), 1817–1830. [27])

Despite the options that utilities have to integrate renewables, various challenges associated with transitioning to utilities have to be addressed on a variety of levels: building, substation, generating plant, and overall utility. Kroposki [28] has summarized the challenges and potential solutions. These are shown in Table 5.5.

Utilities today are facing multiple challenges: the need to modernize the infrastructure of a century-old grid, the threat of both physical and cyber attacks, and the impact of millions of rooftop solar energy systems adding power to the grid. Forty-three states have net metering laws that, with various stipulations, pay rooftop PV owners retail rates for the power they send back to the grid. Thus, PV owners are essentially using the grid as back-up power for free. Utilities still have to cover the cost of maintaining transmission lines and providing reserve power. They must also deal with all the power quality issues that the PV power injection presents. As suggested in Table 5.5, utilities will have to adopt new business models such as charging for services instead of merely selling electricity as a commodity.

Hawaii is already experiencing these issues. Because fossil fuels must be shipped in, Hawaii has very high electricity rates and so is aggressively adopting renewable energy. The rest of the country is closely watching how Hawaii manages this twenty-first-century energy transition.

5.6 Demand Response and Transactional Controls

Most of the previous discussion has involved the ability of utilities to draw on different sources of electricity supply to meet the changing electric demand. Utilities also have demand side management programs that are focused on the demand side. These programs have traditionally involved energy efficiency measures that tend to reduce total demand and demand response (or DR) measures, which focus more on shaving peak demand.

TABLE 5.5

Summary of Potential Challenges and Solutions for Transitioning to a Grid with a Large Penetration of Variable Renewable Sources

Challenge	Solution
<i>Building</i>	
Addition of PV array to building causes outgoing power to exceed electrical power rating.	Upgrade building service to accommodate maximum expected outgoing power.
Overcurrent protection inadequate	Wiring and circuit breakers may need to be upgraded to accommodate higher peak current
Increased voltage and cycling caused by PV power injection to grid impacts voltage regulation	Advanced inverters at building and improved voltage regulation at substation
PV supply of 100% real power to grid decreases fraction of reactive power and increases cycling of reactive power controls	Advanced inverters can supply some reactive power if needed
<i>Substation</i>	
Substation designed only to provide power out experiences injection of additional power from renewable energy	Reconfigure substations to route power from circuits with excess RE generation to circuits with load to serve
Network protectors prevent inflow of RE power to substation	Advanced inverters can limit output to grid needs or on-site battery storage can accommodate excess power
<i>Generating Stations</i>	
Additional spinning reserve needed to accommodate sudden drops in RE consumes fuel, and the additional runtime increases O&M costs	Improved RE forecasting, adoption of demand response measures and addition of grid electric storage will reduce needed spinning reserve
Generators must maintain frequency synchronization in face of varying RE power injected into grid	Improved generator controls may be needed
<i>Utility/Grid-Level</i>	
Tripping of PV inverters during a low-voltage condition could exacerbate the problem	New inverter standards will allow inverters to ride through low-voltage and low-frequency conditions and will allow some reactive power to be provided for voltage control
Marginal cost of solar and wind is essentially zero and their energy supply suppresses wholesale price and sales of fossil energy, the main income source utilities have to maintain the electric grid	Instead of charging for kilowatt-hour sales, a new utility business model can be based on a service charge for providing reliable, high-quality power that allows distributed energy consumers to use the grid as a storage/backup device

Source: From Kroposki, B., 2016. Energy systems integration, [Chapter 11](#) in: *Integration of Renewable Energy Systems*, ed. Walker, A. et al., ASME Press, New York, 121–136. [28]

Reducing peak demand reduces the cost of transmission and distribution. As more variable renewables enter the grid (64% of new U.S. generating capacity was wind and solar in 2015), utilities have become increasingly interested in changing the load profile to accommodate those renewable supplies. Demand response thus involves both demand reduction and reshaping the load profile. It can also provide ancillary services. Kirby [29] describes the following types of demand response:

1. Price response. Time-of-use pricing (prices set according to a time schedule) and real-time pricing (prices adjust with supply and demand) can shape the demand profile.
2. Peak shaving. Programs focus on reducing peak demand on the highest load days/hours.

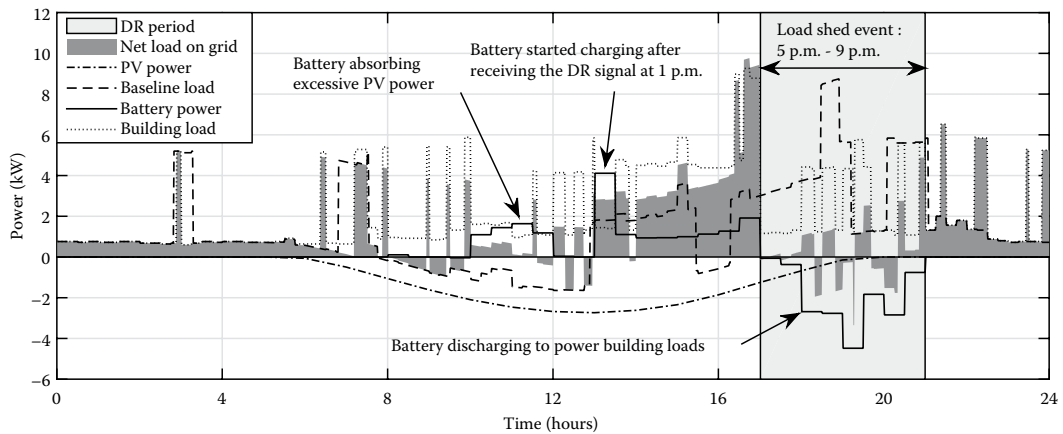
3. Reliability response. This involves rapid change of demand to accommodate power system events like a generator dropping off-line.
4. Regulation response. In this case demand is adjusted to follow the minute-to-minute changes in supply. This and item 3 can have financial value as ancillary services.

The electric grid was developed for one-way transmission of electric power from generating stations to homes and businesses. Local meters on homes have typically recorded electric usage with meter readers coming around periodically to read them. If part of the grid goes down due to a line breakage in an ice storm or a transformer failure, the only way that a utility has had of knowing the specific location of a power failure is through phone calls from affected customers. However, there is now a growing movement to deploy smarter grids that allow two-way communications. According to the U.S. Energy Information Administration, U.S. electric utilities have installed about 65 million smart meters as part of a growing advanced metering infrastructure (AMI), with about 88% of these for residential customers [30]. These meters record electricity usage at a minimum of hourly intervals and provide this data to the utility and the customer at least once a day. Some of the meters can transmit instantaneous data.

Utilities influence demand by sending price signals. Electricity pricing plans can separately price energy sales in cents per kWh of electrical energy and peak demand charges in \$/kW in order to incentivize lower power consumption during peak periods. Utilities often sell specially discounted electricity to industrial customers who agree to have their power curtailed during peak demand periods. In the United States, buildings consume 75% of grid electricity, so measures that control the shape of the load building profile can allow easier penetration of wind and PV on the grid. For example, some utilities have programs for residential customers whereby homeowners can receive a discount by agreeing to allow their air conditioner compressors to be shut off for short periods of time during summer heat waves. Electric hot water heaters and a building's thermal mass can be employed as thermal storage. The defrost operations of supermarket refrigerator cases can be run in such a way as to shift demand times and minimize peak demand charges.

Building equipment manufacturers are developing smart appliances that can time their operation to coincide with lower utility electric rates. So-called "transactional controls" will allow various devices to operate in a manner consistent with getting the best time-of-day or real-time electric prices. For example, a home energy management system could control the various appliances and serve as the point of contact with the utility. (In such a system the utility would monitor the total load profile for the house, avoiding the need for details of how the electricity is used by each appliance, and thus preserving customer privacy.) Beyond buildings, other uses of grid electricity offer opportunities for demand shifting. The water supply and treatment industry consumes a lot of electricity for pumping water, and controlling the times for pumping offer a good opportunity for demand control [31].

Figure 5.17 is a modeled example that shows how a home energy management system responds to a signal received from the utility at 1 p.m. indicating that a load shed event will occur between 5 p.m. and 9 p.m. [32]. To prepare for the event, the building is precooled, and the battery is operated in charging mode only, drawing electricity from rooftop PV and the grid. Then at 5 p.m., the battery is discharged and appliance loads are curtailed. During the 4-hour load shed event, 15.66 kWh of electricity were saved. This savings is composed of

**FIGURE 5.17**

An example of using demand response measures, including PV-charged battery storage, to address an anticipated summer evening load shed event in the Pacific Northwest. (From Jin, X. et al., 2018. *Foresee™: A user-centric home energy management system for energy efficiency and demand response*, *Applied Energy*. [32])

7.90 kWh from the fully discharged battery and 7.76 kWh of reduced building loads. Note in Figure 5.17 how the shaded area representing the net load on the grid is greatly reduced during the 4-hour load shed period.

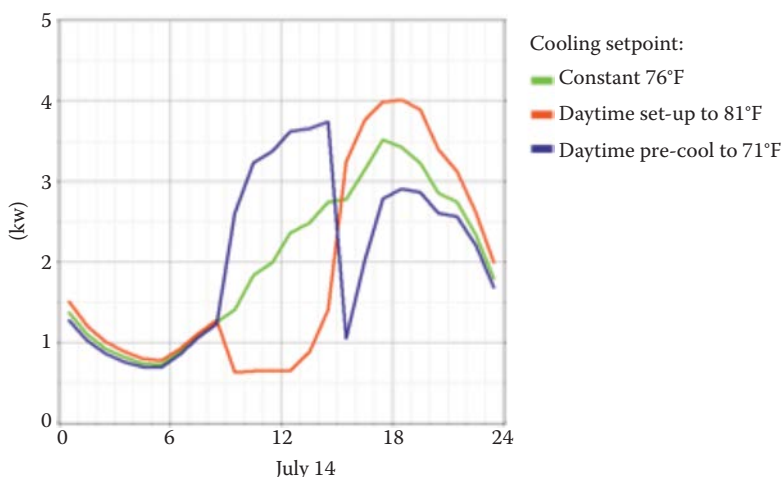
Of course, as the electric grid becomes ever more digitally connected, everything will interact. Actions designed to minimize peak demands will themselves shift that demand. So, for example, if the electricity rate is expected to increase at 3 p.m. on a hot, summer afternoon, smart air conditioners may turn on at full power at 2 p.m. to precool buildings to allow the compressors to shut down at 3 p.m. But if there are enough smart air conditioners doing this at the same time, the utility peak load will actually just shift an hour earlier instead of decreasing in magnitude. Algorithms will be needed to prevent this. In addition to peak shifting, demand response measures can be used to improve the reliability of electricity delivery. Utilities can achieve frequency control by adjusting both the supply and the demand.

The increasing popularity of electric vehicles will drive down the cost of batteries. As these costs drop, more affordable home batteries tied to rooftop PV and electric vehicles will offer an additional opportunity to control demand in a way that could be less complex than smart appliances [33]. Transactional controls can determine at what times those batteries are charged and even when they sell electricity back to the grid, so that both the vehicle/building owner and the utility benefit. The development of electric equipment, storage, and control algorithms to allow the electric grid to operate in an efficient manner that minimizes costs and carbon emissions is an exciting and emerging field.

PROBLEMS

- 5.1 An induction motor has a power factor of 0.82 and draws 800 Watts of apparent power. Calculate the reactive power and the real power, and show these on a power triangle with the correct angles indicated. What is the phase angle difference between the current and the voltage?

- 5.2 A utility is planning to build a 500-mile long 500-kV, 3000-MW transmission line and is considering both double circuit AC and bi-pole DC lines.
- Assuming the lines are going over flat land, using the baseline transmission costs in [Tables 5.1](#) and [5.2](#) and assuming the DC transmission line would require a DC to AC conversion station above and beyond the AC case with a cost of \$460,708,000, calculate the difference in cost between the two transmission methods.
 - Assuming the transmission lines are going over rolling terrain and the terrain cost multiplier for the transmission lines is 1.4, calculate the savings due to DC transmission.
- 5.3 Consider three ways that a residential air conditioner can be operated as shown in the figure, which plots home air conditioner electric power consumption (compressor power plus constant fan power) versus hour of the day.



The three options are:

- Setting the house programmable thermostat to 76°F all day.
- Setting the house thermostat to 81°F until 2 p.m. and then 76°F.
- Setting the house thermostat to 71°F until 3 p.m. and then 76°F.

Option 2, setting the thermostat up to 81°F, might typically be considered the energy-conserving option. However, consider the duck curves of [Figure 5.12](#) and explain why option 3, which takes advantage of the thermal mass of the house, could be a better option for purchasing electric power in the case of large PV penetration scenarios. Why is the 81°F setting the worst one in this case?

- 5.4 As in the case of Example 5.1, consider a utility trying to decide whether to invest in a coal plant. It is anticipated that the coal plant will operate at a capacity factor of 60%. What is the minimum natural gas price at which the coal plant would have a lower levelized cost of electricity than a combined-cycle natural gas plant?
- 5.5 Consider the generation and load profiles in [Figure 5.16](#). To meet the summer load with only wind and solar energy, these generators would have to be large enough that they would not be fully utilized in other months. Propose different

means for meeting the summer load with all renewable energy without having to curtail it in other seasons. Consider not only energy supply alternatives but also how to control the demand.

- 5.6 Consider a case in which generating plants are located in two different areas. Area 1 has a plant that can generate 500 MW and sells it at a cost of \$30/MWh. Area 2 has a plant that can generate 250 MW and must sell it at a higher price of \$40/MWh. A customer in area 2 needs to purchase 300 MWh over a 1-hour period. Assuming there is no transmission constraint between the two areas, the customer in Area 2 would purchase the full 300 MWh from Area 1 and pay \$9000. Now consider the case where the transmission line is limited to a power flow of 250 MW. Purchasing the full 300 MWh over the 1 hour period from Area 1 is not possible because the transmission line is congested. In such a case Area 1 would provide 250 MWh (the limit of the transmission line) and Area 2 would provide the additional 50 MWh.
- Calculate the revenue each of the two generating plants in Area 1 and Area 2 receives with constrained transmission and the total.
 - In the case of constrained transmission, the customer in Area 2 must pay the higher price for all its electricity. Compare the total cost paid by the customer to the cost the generators receive that you calculated in part a. What is the difference, which is called the congestion cost?
 - Show algebraically that the congestion cost is simply the product of the transmitted electricity and the difference in cost between the two areas. Verify this using the numbers in this example. This congestion cost is paid to holders of Financial Transmission Rights (FTRs). (The congestion cost calculated here is an estimate.)

In this example, the customer pays more than the generators receive. But if the customer had purchased an FTR as a hedge against transmission congestion, it could recover that extra expense. The cost of the FTR will depend on auction prices. The customer has a choice to take a chance that congestion will not occur or purchase an FTR as insurance. FTRs are an example of where a primary commodity (kilowatt hours of purchased electricity) generates secondary financial markets that address risk. Financial transmission rights are just one example of the various electricity markets described in Section 5.2.

- 5.7 Market clearing price problem. In an energy market, an RTO or ISO (independent system operator) receives both bids to sell certain amounts of electricity at specific prices from electric generators (the supply) and offers to purchase specific amounts of electricity at various prices from large consumers (the demand). The RTO/ISO must match the supply and demand. It does so by essentially plotting the prices of supply and demand versus the aggregated electricity quantity. It builds up the supply by starting with the lowest generator cost offers and it builds up the demand by starting with the highest consumer offers. When the decreasing supply price and the increasing demand price match (i.e., when the supply and demand curves intersect), that is called the market clearing price (MCP) and the aggregated electric quantity at that price is called the market clearing quantity (MCQ).

Consider two generators, Generator 1 and Generator 2, and two consumers, Consumer 1 and Consumer 2, that bid, respectively, quantities of electricity to sell and buy, at various bid prices. These are shown in the tables below.

Bids to Sell Electricity from Two Generators (Supply Values):

Generator 1

Price (\$/MWh)	Quantity (MWh)
10	200
40	150
60	50

Generator 2

Price (\$/MWh)	Quantity (MWh)
20	100
80	60

Bids to Purchase Electricity from Two Consumers (Demand Values):

Consumer 1

Price (\$/MWh)	Quantity (\$/MWh)
50	100
30	150

Consumer 2

Price (\$/MWh)	Quantity (MWh)
80	50
40	100
20	200

To determine the market clearing price, first stack up the five supply quantities in order of increasing bid starting with the lowest bid and stack up the five demand quantities in order of decreasing bid starting with the highest bid and put them in the tables below.

Aggregated Supply Quantities:

Price (\$/MWh)	Generator Company (1 or 2)	Quantity (MWh)	Aggregated Quantity Range (MWh)
10			
20			
40			
60			
80			

Aggregated Demand Quantities:

Price (\$/MWh)	Consumer (1 or 2)	Quantity (MWh)	Aggregated Range
80			
50			
40			
30			
20			

Now on a plot of price vs. aggregated quantity, plot in stair step fashion the decreasing demand and increasing supply curves. What is the MCP and at what MCQ does it occur?

- 5.8 Frequency regulation service problem. If total generation exceeds demand, frequency will increase above the operating value (60 Hz in the United States). If demand exceeds generation the frequency will decrease. An RTO/ISO must thus have controllable power to provide frequency regulation, which is considered one of the ancillary services. In a regulation market, generators submit bids to an RTO/ISO for the maximum number of megawatts of variable power (regulation capability) they are willing to provide for a particular hour at a particular price. The RTO/ISO then stacks up the various offers to determine the price it will pay.

For the given hour, a generator can bid a block of electricity both into the regulation market and into the energy market. To purchase the regulation, the RTO must pay not only the regulation bid price but, for each MWh of electricity purchased for regulation, it must pay what the generator lost as a result of not selling that MWh into the main energy market. The latter is called the lost opportunity cost, or LOC. It is the difference between the market energy price and the energy bid. (One could think of it as the net profit the generator would have received above its bid price.)

An RTO wants to purchase 20 MW of frequency regulation for a 1-hour period. The table below shows for six different generators, the regulation capability each is bidding (in megawatts) into 1 hour, the regulation bid, the energy bid for that hour, the market price for electricity, and the LOC.

Generator	Regulation Capability (MW)	Regulation Bid (\$/MWh)	Energy Bid (\$/MWh)	Market Price (\$/MWh)	LOC (\$/MWh)	Total Regulation Cost (\$/MWh)
1	10	12	20	40	20	
2	8	7	10	40	30	
3	12	3	20	40	20	
4	6	6	40	40	0	
5	14	5	15	40	25	
6	3	4	15	40	25	

Calculate the total regulation cost in \$/MWh for each generator. Then, in the next table, order the generators from lowest to highest regulation cost.

Generator	Regulation Capability (MW)	Aggregated Capability (MW)	Regulation Cost (\$/MWh)
-----------	----------------------------	----------------------------	--------------------------

The market clearing price is the minimum price needed to meet a sufficient number of bids to provide the power it must purchase for regulation, in this case 20 MW. The 20 MW will be purchased from multiple generators, namely all those who bid to sell regulation power at or below the market clearing price. They will all be paid the regulation market clearing price. Consider that there will be some uncertainty regarding the needed regulation. In this example, if you were the RTO executive, would you consider increasing the market clearing price a bit above the value you obtained? Why?

5.9 LCOE for wind and solar.

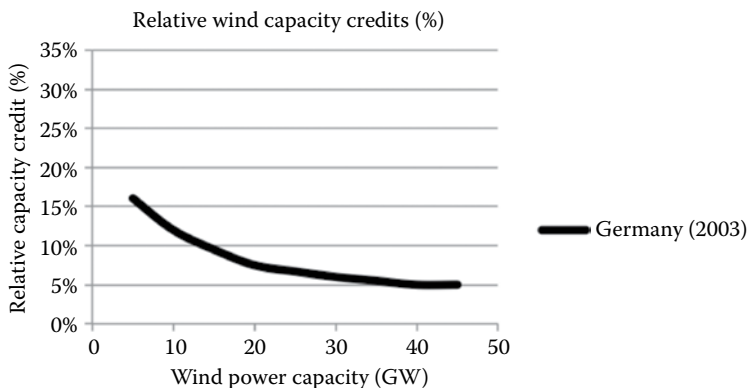
Consider the following costs for combined cycle natural gas and utility-scale wind and photovoltaics systems:

Plant Type	Capital Cost (\$/kW) ¹	Heat Rate (Btu/kWh) ²	Fuel Cost (\$/10 ⁶ Btu) ³	Variable O&M (\$/MWh) ⁴	Fixed O&M (\$/kW/yr) ⁴	Capacity Factor
Combined Cycle	978	6,600	2.40	3.5	11.0	56.3
Wind	1,877	NA	0	0	39.7	32.5
Solar PV	2,671	NA	0	0	23.4	28.6%

Assume a 30-year lifetime and a 4% discount rate, and neglect energy performance degradation with time.

- Calculate the LCOE for each of the three technologies.
- At what natural gas cost would solar PV have a lower LCOE than the combined cycle?
- At what natural gas cost would wind have a lower LCOE than the combined cycle?

5.10 Impact of penetration on wind capacity factor and cost. The figure below shows how wind capacity credit as a percentage of installed wind capacity in Germany decreases with deployed capacity. In Great Britain, wind capacity credit in gigawatts is approximately equal to the square root of the installed capacity in gigawatts.



- Add a plot of relative capacity factor vs. installed capacity for Great Britain on this plot.
- Explain why the curve for Great Britain is higher than the one for Germany. (Hint: consider the geographic orientation of each country.)

References

1. Brown, M.H., and Sedano, R.P., 2004. Electricity transmission: A primer, National Council on Electric Policy, <http://www.raponline.org/wp-content/uploads/2016/05/ncsl-brown-electricity-transmissionprimer-2004-06.pdf>.
2. North American Electric Reliability Corporation, August 2013. Understanding the grid, <http://www.nerc.com/news/Documents/Understanding%20the%20Grid%20DEC12.pdf>. Reproduced with permission.
3. Basso, T., 2014. IEEE 1547 and 2030 standards for distributed energy resources interconnection and interoperability with the electricity grid. NREL/TP-5D00-63157. NREL, Golden, CO.
4. Black & Veatch, 2014. Capital costs for transmission and substations: Updated recommendations for WECC transmission expansion planning, https://www.wecc.biz/Reliability/2014_TEPPC_Transmission_CapCost_Report_B+V.pdf.
5. Argonne National Laboratory, 2007. The design, construction, and operation of long-distance high-voltage electric transmission technologies, ANL/EVS/TM/08-4. Department of Energy National Laboratory, Argonne, IL.
6. Denholm, P., Eichman, J., and Markel, T., 2015. Summary of market opportunities for electric vehicles and dispatchable load in electrolyzers, NREL/TP-6A20-64172.
7. Federal Energy Regulatory Commission, 2012. *Energy Primer: A Handbook of Energy Market Basics*, <https://www.ferc.gov/market-oversight/guide/energy-primer.pdf>.
8. National Energy Technology Laboratory (NETL), 2013. *Power Market Primers*, DOE/NETL-2013/1617.
9. NREL. LCOE calculator documentation, <https://www.nrel.gov/analysis/tech-lcoe-documentation.html>.
10. U.S. Energy Information Administration, November 2016. Capital cost estimates for utility scale electricity generating plants, https://www.eia.gov/analysis/studies/powerplants/capitalcost/pdf/capcost_assumption.pdf.
11. U.S. Energy Information Administration, May 2016. *Monthly Energy Review*, <https://www.eia.gov/totalenergy/data/monthly/previous.php>.
12. EIA. Electric power monthly, https://www.eia.gov/electricity/monthly/epm_table_grapher.php?t=epmt_6_07_a.
13. NREL, 2016. Annual technology baseline, <https://www.nrel.gov/analysis/data-tech-baseline.html>.
14. Clack, C.T., 2015. Decarbonizing the U.S. electric sector, presentation, <http://www.slideshare.net/sercuser/decarbonizing-the-us-energy-sector-a-study-in-optimization-and-tradeoffs>.
15. F. Kreith lecture notes.
16. MCEN Sustainable Energy. Electricity systems, <http://mcensustainableenergy.pbworks.com/w/page/20638049/Electricity%20Systems>
17. Boyle, G., 2009. *Renewable Electricity and the Grid: The Challenge of Variability*, Earthscan, New York, NY.
18. Lew, D. et al., September 2013. *The Western Wind and Solar Integration Study, Phase 2*, NREL/TP-5500-55588. NREL, Golden, CO.
19. Denholm, P., and Mehos, M., November 2011. Enabling greater penetration of solar power via the use of CSP with thermal energy storage, NREL/TP-6A20-52978. NREL, Golden, CO.
20. California ISO. https://www.caiso.com/Documents/FlexibleResourcesHelpRenewables_FastFacts.pdf.
21. Denholm, P., Clark, K., and O'Connell, M., 2016. On the path to SunShot: Emerging issues and challenges in integrating high levels of solar into the electrical generation and transmission system, NREL/TP-6A20-65800, <http://www.nrel.gov/docs/fy16osti/65800.pdf>.
22. Acker, T., September 2007. Final report: Arizona public service wind integration cost impact study, Northern Arizona University.
23. Wilczak, J. et al., October 2015. The wind forecast improvement project, (WFIP), *Bulletin of the American Meteorological Society*.
24. Moore, F.C., and Delavane, D.B., February 2015. *Nature Climate Change*, Vol. 5.

25. DOE, 2015. *Energy Data Book*. U.S. Department of Energy Office of Energy Efficiency and Renewable Energy, <https://www.nrel.gov/docs/fy17osti/66591.pdf>.
26. IEA. *World Energy Outlook 2015*, <https://www.iea.org/publications/freepublications/publication/WEO2015.pdf>.
27. Denholm, P., and Hand, M., 2011. Grid flexibility and storage required to achieve very high penetration of variable renewable electricity, *Energy Policy*, 39(3), 1817–1830.
28. Kroposki, B., 2016. Energy systems integration, Chapter 11, in: *Integration of Renewable Energy Systems*, ed. Walker, A. et al. ASME Press, New York, pp. 121–136.
29. Kirby, B. *Introduction to Bulk Power Systems*, course notes.
30. EIA. Frequently asked questions, <http://www.eia.gov/tools/faqs/faq.cfm?id=108&t=3>.
31. Sparn, B., and Hunsberger, R., November 2015. Opportunities and challenges for water and wastewater industries to provide exchangeable services, Technical Report, NREL/TP-5500-63931.
32. Jin, X. et al., 2018. ForeseeTM: A user-centric home energy management system for energy efficiency and demand response, *Applied Energy* 205, NREL/JA-5500-69073.
33. Jin, X., and Meintz, A., July 2015. Challenges and opportunities for transactive control of electric vehicle supply equipment: A reference guide, Technical Report, NREL/TP-5500-64007.

6

Fossil Fuels

According to the International Energy Agency, global primary energy production in 2012 totaled 13,400 Mtoe [1]. Oil accounted for 31.4% of the total, coal and peat accounted for 29%, natural gas for 21.3%, and nuclear for 4.8%. Only 13.5% of primary energy production came from sources that are or can be renewable: hydropower, biofuels, waste, geothermal, solar, and wind. As discussed in [Chapter 2](#), society depends heavily on fossil fuels because they are convenient and “cheap,” from a market perspective. However, the broader lens of sustainability requires that we reexamine this assumption.

As discussed in [Chapter 1](#), in the United States, coal overtook wood as the largest energy source in around 1890, with oil and gas overtaking coal in around 1960. Combined, coal, petroleum, natural gas, and nuclear energy supplied approximately 90% of primary energy to meet U.S. energy consumption in 2013 [2]. According to U.S. Department of Energy business-as-usual projections, these fuels will still supply 88% of U.S. primary energy consumption in 2040 [2]. Given the dominance of fossil fuel and nuclear energy in current supplies, it is important to understand the prospects for and consequences of continued reliance on these resources, as a prerequisite to examining opportunities to reduce our dependence on them.

6.1 Fossil Fuel Resources and Extraction

6.1.1 Coal

Coal is the most abundant fossil fuel and is widely distributed around the world. Historically, coal has been used for space heating, as fuel for ships and trains, and to provide process heat for steel and other industries. Today, 93% of coal consumption in the United States is for electricity production (see <http://www.eia.gov/coal> for trends).

Coal was formed largely on land in areas of swamps and bogs where vegetation decay was slower than the sedimentation rate. High energy content coal was lithified by being buried by other sediments and exposed to elevated geothermal temperature and pressure. The conditions for coal formation changed over tens of millions of years, so coal is bedded in other geologic sediment layers. Thick coal seams less than 200 ft below the surface are normally extracted in open cast mines. The coal is blasted and fractured in strips, thus the term strip-mining. In the United States, more than 65% of coal is surface mined. Underground coal mines have typically been developed up to 1500 ft deep, but some mines in China reach depths of 3900 ft. Spoil refers to the overburden, top soil and sedimentary layers between coal seams that must be removed and stored. The overburden rate refers to the depth of overburden compared to the coal seam depth. Typical overburden rates exceed 10:1 (10 ft of soil for 1 ft of coal). The blasting and moving of coal can produce dust that is blown and deposited in surrounding areas. Sediment

run-off of coal fines can be a serious water pollution issue. Within the United States, coal is typically transported by rail. Large mines in Wyoming and Montana supply coal to eastern power plants, with transport distances in excess of 1500 miles.

Coal is not a single substance, but has differing composition and is classified by its carbon, volatiles, and heat content. Coal types reflect the degree of chemical processing that has occurred within the coal seam over millions of years at elevated temperatures and pressures. The maturation of coal from the source wood follows the sequence:

wood → peat → lignite → subbituminous → bituminous → anthracite.

The overall effect of the chemical processing is to remove oxygen and hydrogen, so the most “mature” coal types, anthracite and bituminous, have a greater percentage of carbon and a higher heat content than the less mature coals. The highest grade of coal is coking coal that is used in making steel. Hard coal, also called anthracite, has the highest energy content (31 MJ/kg). Brown coal or lignite can have an energy content not much better than wood (14–18 MJ/kg) [3]. Coal composition is characterized by ultimate analysis, which gives the elemental composition of the material on a dry mass basis. DeNevers [4] lists the typical mass-based composition of subbituminous coal from the Powder River Basin: 72.5% C, 6.1% H, 17.2% O, 0.7% N, 0.4% S, 3.1% ash. In addition, coal contains trace amounts of many elements. Some of these elements, like mercury, are of serious concern for air pollution. Coal from the Powder River Basin is relatively low in sulfur compared to coals from other source regions in the United States, which can have sulfur levels as high as 4% [3].

Coal is crushed before use as a fuel. Coal must be burned with excess combustion air in a high temperature combustion chamber with a long fuel residence time. All coal has a mineral content that will remain in the combustion chamber as slag and also be carried out in the combustion gas stream in small particles as fly ash. Fly ash includes silica and other minerals, along with other compounds that are formed or liberated during combustion that condense into the solid phase. Most of the fly ash can be collected in fabric filters or by electrostatic collection onto charged plates called electrostatic precipitation. Both slag and fly ash pose storage and disposal issues. Some fly ash can be used in concrete. As discussed below, coal combustion causes air pollution with serious health and environmental effects.

Coal abundance is categorized at the broadest level by *resources*, defined as the quantity of naturally occurring concentrations or deposits of coal in the Earth’s crust, in such forms and amounts that economic extraction is currently or potentially feasible. Resources may be either known or undiscovered. Coal *reserves* are more narrowly defined, as quantities of unextracted coal that comprise the demonstrated base for future production, including both proved and probable reserves (<http://www.eia.gov/tools/glossary>). Coal reserves are the subset of resources that could be *economically* extracted at the time the determination is made, considering legal and technological constraints, but not requiring that mining facilities be in place to do so. By definition, reserves are relatively well known at a given time, but change over time due to past production and due to changing technology or economics.

The depth of the seam, the amount of overburden, and the quality of the coal limits coal reserves. The United States has the largest coal reserves of any country [5], but China is currently producing the most coal on an annual basis. Worldwide, approximately 7.8 billion metric tons of coal were produced in 2013, with 45.5% of the production in China, 11.6% in the United States, and 7.8% in India [1]. Total coal reserves for the United States are estimated at about 260 billion short tons [5]. Within the United States, the state of Wyoming has the most coal production, accounting for 39% of the country’s total in 2013 [6]. West Virginia and

Kentucky are the next largest coal producers, accounting for 12% and 8% of U.S. production. Wyoming coal is mostly sub-bituminous, with relatively low sulfur content of about 0.4% and heat content of just under 20 MJ/kg [3]. Ninety percent of Wyoming's coal comes from surface mines. Production in West Virginia and Kentucky is more evenly split between underground and surface mines [7].

Coal mining has historically been a hazardous occupation, although deaths and injuries have declined dramatically in some countries, due to improved regulations and safer technology. The U.S. Mine Safety and Health Administration reports that in the United States in the first half of the twentieth century, there were 452 coalmine disasters that each resulted in five or more deaths. Since 1950, there have been 53 such disasters. In 2010, an underground mine explosion at the Upper Big Branch Mine-South, in Raleigh County, West Virginia, resulted in 29 deaths [8]. Total coal mining fatalities in the United States dropped from 242 in 1978, the year after the Federal Mine Safety and Health Act was passed, to 20 in 2013. Over the past decade, the U.S. coal mining fatality rate has averaged approximately 23 deaths per 100,000 workers [9]. For comparison, the overall occupational fatality rate in the United States was 3.3 per 100,000 workers in 2013; the rate in the construction industry was 9.7 per 100,000 [10]. Coalmine safety conditions are much worse in other countries, including China, Turkey, and Ukraine. The International Energy Agency reported in 2009 that between 1985 and 2005, from 5000 to 7000 deaths per year occurred in coal mining operations in China [11]. Due in part to consolidation of the Chinese mining industry and to greater focus on safety, the coalmine fatality rate has subsequently dropped, with about 2000 deaths reported for 2012 [12].

Both surface and underground coal mining can deleteriously affect the environment where mining occurs. Underground mines can lead to subsidence. Mining wastes containing pyrite (FeS_2) cause problems with acid mine drainage. Active strip mines can disturb large areas with excavations, roads, and displaced overburden and soil material (Figure 6.1). To address these disturbances, the Surface Mining Control and Reclamation Act of 1977 requires that mine sites be restored to their previous condition or a condition that supports higher uses. However, in Appalachia, coal mining on steep terrain is done using the mountaintop mining/valley fill method, also known as mountaintop removal.



FIGURE 6.1

Surface mining activity in northwestern Colorado. (Photo by J. Milford.)

Blasting the mountaintop generates large volumes of spoil that cannot be returned to the original location and instead is placed in adjacent valleys. This process permanently reconfigures the terrain, sometimes covering up streams and wetlands in the process.

Methane gas is also formed in coal beds as the sediments are heated by geothermal energy. This gas poses a serious hazard for coal miners. To control this hazard, most underground mines vent methane to the atmosphere, although the methane can be captured and used for energy. Methane can also be released from abandoned mines through fissures, vents, or boreholes. These abandoned mines may also represent opportunities for methane recovery.

6.1.2 Natural Gas

Natural gas is an important fossil fuel for industrial process heat, heating buildings, and electricity production. Natural gas is also used as a chemical feedstock, primarily for production of ammonia, methanol, and hydrogen gas. In 2014 in the United States, a total of about 29.2 trillion MJ was consumed, with about 33% used for power generation, 31% in industry, and 35% in the residential and commercial sectors [13]. In the United States, less than 1% of natural gas is used as a vehicle fuel. Over the past four decades, natural gas has increased its share of primary energy continuously, growing from about 1,000 Mtoe and 16% of primary energy supplies in 1973, to 2,800 Mtoe and 21% of supplies in 2012 [1].

Natural gas is comprised of methane and other light hydrocarbons that are produced from decomposition of organic matter. Thermogenic natural gas was formed over millions of years from buried organic matter processed at high temperature and pressure. Methane is also formed biogenically, as microorganisms decompose waste in anaerobic environments, including wetlands and landfills. Large deposits of natural gas have conventionally been found in relatively porous rock underneath an impervious cap that traps the gas in place. Unconventional deposits are now being developed in tighter source rock, with hydraulic fracturing used to stimulate gas flow.

As delivered to end-users, natural gas is mainly methane, CH_4 . Natural gas wells produce mixtures of methane with water, CO_2 , hydrogen sulfide (H_2S), N_2 , and other volatile light hydrocarbons including ethane, propane, butane, and pentanes. Water and natural gas liquids (the volatile hydrocarbons) are typically removed near the wellhead, using separators and dehydrators. If present in sufficient quantity, the light hydrocarbons are captured and sold as fuel or chemical feedstock. Gas processing plants remove CO_2 , H_2S , and N_2 as unwanted contaminants. Natural gas is commonly transported in pipelines. The United States has more than 300,000 miles of natural gas transmission pipelines that carry gas long distances from supply regions to end-use markets. Pipeline diameters and pressures are stepped down from the transmission system to the distribution system, as gas is conveyed to commercial buildings and residences. International trade in natural gas is much more expensive if it must be liquefied and then transported by ship.

Similar to coal, natural gas and crude oil resources are estimated as the total quantities that might be produced at some time in the future. Portions of the overall resource can be further classified as:

1. Total remaining oil and gas in place
2. Technically recoverable resources, which can be produced based on current technology, industry practice and geologic knowledge
3. Economically recoverable resources, the portion of technically recoverable resources that can be profitably produced, considering both the costs of production and current prices

4. Proved reserves, which are the volumes of oil and natural gas that geologic and engineering data demonstrate with reasonable certainty to be recoverable in future years from known reservoirs under existing economic and operating conditions [14].

Figure 6.2 provides a schematic diagram of the relationship between these categories, showing how the degree of uncertainty in the resource estimate increases from the most restrictive category of proved reserves to the most expansive category of oil and gas in place.

For natural gas in the United States, the technically recoverable resource estimate in 2012 was about 2,300 trillion cubic feet [15], corresponding to more than 80 years' worth of production at the current consumption rate. Reflecting the rapid advance in technology for recovering natural gas from shale and other tight formations, the 2012 estimate of technically recoverable natural gas was more than 70% higher than the 2004 estimate [16].

From 2008 to 2014, natural gas production in the United States increased from 20 trillion cubic feet to 26 trillion cubic feet per year, mostly as a result of horizontal drilling in tight formations that were previously inaccessible [13]. "Unconventional" natural gas formations include shale rock, tight "sands" (sandstone or carbonaceous rock formations), and deep coal seams from which natural gas can be recovered. Natural gas is produced from shale and other tight formations by hydraulic fracturing (fracking) and horizontal drilling (Figure 6.3 [17]). Experts have known for a long time that natural gas and oil deposits exist in deep shale formations, but until recently, these resources were not thought to be economically recoverable. Fracking is the process of creating fissures in underground formations to allow natural gas (or oil) to flow more easily. To create the fractures, fluid is pumped under high pressure into the shale formation. The fluid used is approximately 99% water, with sand added to prop open the fractures, and a small amount of chemical additives. With directional drilling, well bores can be extended horizontally to increase the exposure to the gas formation.

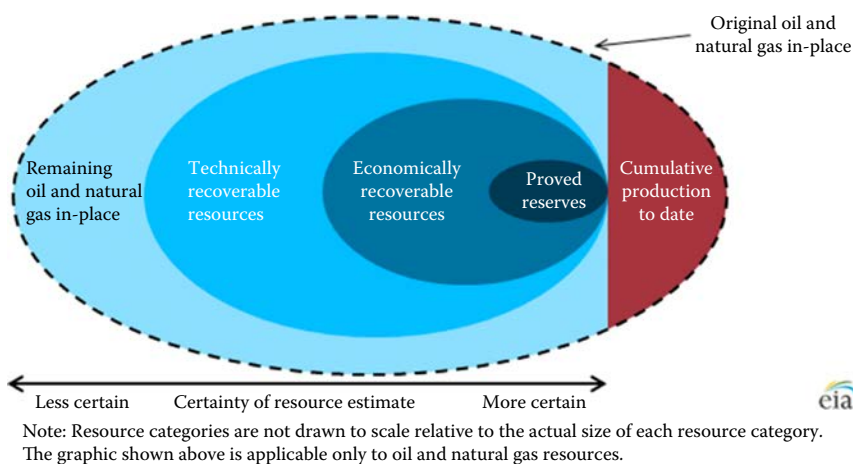
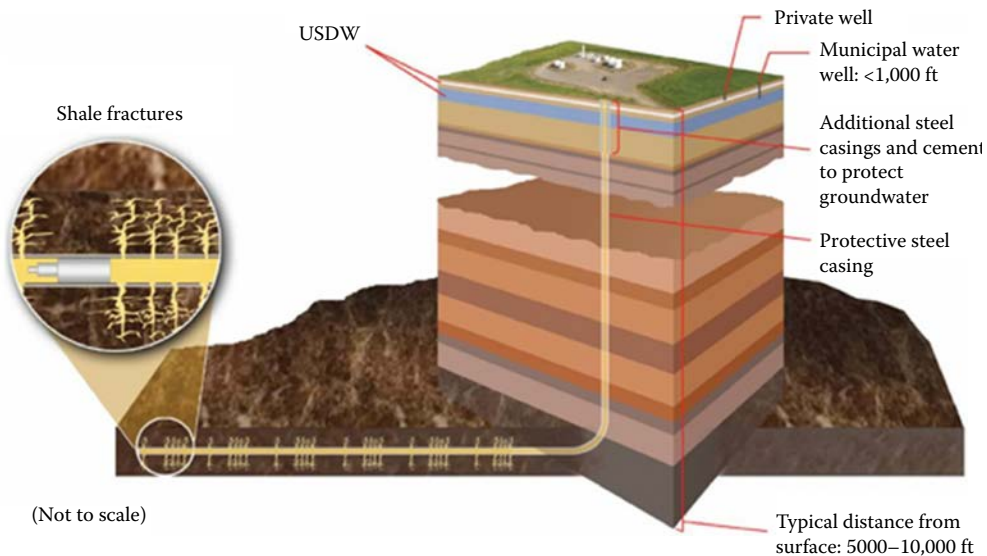


FIGURE 6.2

Schematic representation of oil and natural gas resource categorizations (not to scale). (From EIA, 2015. Oil and natural gas resource categories reflect varying degrees of certainty, *Today in Energy*, <http://www.eia.gov/todayinenergy/detail.cfm?id=17151>. [14])

**FIGURE 6.3**

Schematic of a hydraulically fractured shale gas system (not to scale). (From NETL. On-site research, National Energy Technology Laboratory, U.S. Department of Energy, <http://www.netl.doe.gov/research/on-site-research/research-portfolio/oil--gas-research/ucr>. [17])

The rapid growth of unconventional natural gas production in the United States has lowered natural gas prices and helped shift electricity generation from coal-fired power plants to cleaner, natural gas-fired generation. However, the expansion of natural gas and oil production due to hydraulic fracturing and directional drilling has raised significant environmental concerns. These concerns include contamination of drinking water with methane, spills of toxic drilling fluids, and flow back of produced water with natural salts, heavy metals, hydrocarbons, and radioactive materials [18,19]. There have also been concerns that in some areas, hydraulic fracturing or associated water reinjection can stimulate earthquakes [19,20]. Earthquakes linked to the hydraulic fracturing process itself have been below the threshold associated with structural damage; however, larger earthquakes have apparently been caused by disposal of oil and gas-associated wastewater in deep strata or basement formations [21]. The U.S. Environmental Protection Agency estimates that natural gas and petroleum production account for approximately 30% of U.S. emissions of methane, a potent greenhouse gas [22]. Natural gas production operations also release volatile organic compounds and oxides of nitrogen, which contribute to ground-level ozone formation, and hazardous air pollutants such as benzene and formaldehyde [23]. Although most of the environmental impacts of unconventional gas production can be mitigated through careful engineering, operations, and regulatory oversight [18], in some areas, environmental regulators have been left scrambling to catch up with the rapid growth of the activity.

6.1.3 Petroleum

Petroleum refers to crude oil and natural gas liquids. Petroleum is refined by high temperature catalytic reactions and separation into a wide range of liquid fuels and tar or bitumen. Combustion of liquid fuels requires atomization into a hot combustion chamber,

mixing with air and sufficient residence time to vaporize the liquid and completely burn all of the different chemical components in the fuel. Light fuels such as kerosene are used in jet engines and cook stoves. Petroleum and diesel fuel can produce unburned volatile organic compounds (VOCs), soot and CO if engines are slightly out of tune, not enough air is supplied, or if the mixing and flame residence times are not sufficient. Heavy oil, used engine oil, and diesel are used in boilers with air blast or steam blast atomization.

Petroleum reserves were formed 50 to 200 million years ago by accumulation of biological sediments in coastal waters where low oxygen content slowed decay. These areas with hydrocarbon sediments were then buried under further sedimentation and heated by geothermal energy, causing chemical breakdown of the organic matter. If the matrix rock was porous enough, the lighter organic material could become mobile, and due to its lower density, could migrate upward. Where non-porous sediment layers were folded to form anticlines or where faults caused cap rock traps, the organic material could accumulate into an oil field. If there were no cap rock structure, then the oil, gas, or CO₂ would percolate up through the soils and evolve on the surface.

The productivity of an oil field depends on how porous the resource rock is and how light the hydrocarbons are. Hydrocarbons that have been subjected to the highest temperature for the longest time may be decomposed to CO₂, and the lightest energy deposits of natural gas and oil normally have a significant fraction of CO₂ in the resource that must be separated in production prior to compression. A “sweet” gas or petroleum resource refers to a low CO₂ content.

Crude oil can be refined into a wide range of products, including pure chemicals (e.g., ethylene or propylene) and chemical mixtures. Most crude oil is refined to produce either gasoline or distillate fuel oil, which includes diesel. Gasoline is a mixture of hydrocarbons, comprised of molecules with carbon numbers in the range of C3–C12. The mixture includes straight chain, branched, and cycloalkanes; aromatics; and alkenes. Constituents of diesel fuel are mostly saturated hydrocarbons in the range from C13–C17. Heavy fuel oil is comprised of molecules in the C20 to C45 range. Crude oil often contains sulfur, which is removed or partially removed in the refining process.

As noted above, proved reserves are amounts of oil and gas that have been demonstrated with reasonable certainty to be recoverable under existing economic and operating conditions. Worldwide, proved oil reserves are estimated at about 1.6 trillion barrels. Venezuela and Saudi Arabia lead the world in proved reserves, with 298 billion barrels and 268 billion barrels, respectively [24]. Notably, proved reserves (along with current production numbers) now include significant quantities of oil resources that would have been considered uneconomical to produce a decade ago—from the Canadian tar sands, Venezuelan heavy oil belt, and U.S. shale oil formations. Proved reserves are often much lower than estimates of technically recoverable resources. For example, in the United States, proved reserves in 2012 were estimated at 29 billion barrels of oil, while technically recoverable oil resources (excluding oil shale) were estimated at 238 billion barrels [25]. In 2014, the United States produced about 5.1 billion barrels of oil, leading the world in production [5].

The “low hanging fruit” of petroleum resources is the light sweet crude oil found in highly porous source rock under massive anticline features near the land surface in the Middle East. When drilling first breaches the cap rock of a high-quality oil field, the oil and gas are at very high pressure and can be produced without pumping. Later in the production cycle, oil wells lose pressure, start to produce water mixed with the oil, and require enhanced recovery by injection of natural gas, steam, or CO₂ to continue production. Recent growth in petroleum production in the United States has been spurred by development of light oil found in tight source rock, which is commonly referred to as shale oil. This resource is

developed using similar hydraulic fracturing and horizontal drilling techniques to those used in shale gas production. The lowest grade of petroleum resource currently being exploited is the heavy, viscous hydrocarbons found in the Athabasca “tar” sands of Canada, and the Orinoco oil belt in Venezuela. These deposits are “heavy” because they have not been thermally broken down. Production in the tar sands requires either steam injection to reduce the viscosity of the hydrocarbons in place, before they can be pumped to the surface, or open-pit mining followed by processing of the extracted tar sands with hot water to separate the sand and the bitumen. Bitumen is subsequently upgraded to produce synthetic crude oil. Oil shale is a form of petroleum resource that hasn’t yet been tapped in significant quantities. Oil shale contains kerogen, a solid hydrocarbon substance, which can be converted to liquid oil through thermochemical processing. Possible approaches for producing oil shale include mining the shale, then crushing and heating it in a retort system to liberate the hydrocarbons, or potentially heating it in place. In either case, the process would require significant energy, water, and land disturbance.

In addition to increasingly exploiting heavier, more viscous petroleum resources or resources in less porous deposits, oil and gas development keeps moving to deeper formations and more remote locations. The first offshore oil well was completed in 1938, a mile-and-a-half off the coast of Louisiana, in 14 feet of water [26]. The push into the Gulf of Mexico accelerated in the 1950s, with the introduction of mobile drilling units. By 1957, nearly 450 production platforms were operating off the coasts of Texas and Louisiana, in water depths of up to 100 feet. Advances across numerous technological fronts, from seismology to stronger steel to digital computing, pushed the production limit to 350-foot depths by the late 1960s. In 1979, Shell Oil started production in a Gulf of Mexico oil field under 1000 feet of water. Shell’s production pushed on to 3000-foot water depths in the early 1990s, and then on to astonishing 10,000-foot depths by the early 2000s [26]. In the next few years, the industry is expected to develop significant plays in the Gulf in challenging water depths of 3000 to more than 9000 feet [15]. In 2014, offshore production in the Gulf of Mexico accounted for 16% of total U.S. oil production [27].

In the 1960s, the physical challenges of the offshore environment and pressures to keep costs down compromised safety in the U.S. oil industry, earning offshore oil work a reputation as a high-risk occupation. In 1969, a blowout on an oil platform in the Santa Barbara Channel led to the release of an estimated 80,000 to 100,000 barrels of oil and a slick that covered 800 square miles [26]. Today, that accident is widely credited with helping launch the U.S. environmental movement. Two more disastrous blowouts, including one that killed four people, occurred the following year in the Gulf of Mexico. In the wake of these accidents, the U.S. government finally stepped up its regulation of the industry, and the industry took on voluntary efforts to improve its safety practices. However, accidents and oil spills from wells, pipelines, and tankers remain all too common.

In the United States, two catastrophic oil spills are of particular note. On March 24, 1989, the oil tanker Exxon Valdez struck a reef in Prince William Sound in Alaska. More than 11-million gallons of oil were dumped into the pristine environment, impacting over 1,300 miles of coastline in Alaska. Scientists are still studying the long-term impacts of the disaster on fish, marine mammals, and birds. There are still pockets of crude oil in some locations and damage to the ecosystem continues to be observed. The Exxon Valdez disaster was caused by human error of the tanker captain, but in its wake, the U.S. Congress enacted the Oil Pollution Prevention, Response, Liability, and Compensation Act of 1990, which included requirements for double hulls on oil tankers operating in U.S. waters.

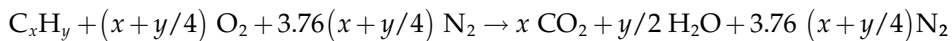
On April 20, 2010, the \$350 million Deepwater Horizon oil drilling rig exploded in the Gulf of Mexico, killing 11 workers. The blowout of BP’s Macondo well released more than 4-million

barrels of crude oil into the Gulf over the course of nearly 5 months [28]. The cause of the BP disaster was not the result of a single human error, but rather of systemic negligence of engineering practice and operations in the oil industry [26]. In July 2015, the U.S. Department of Justice and the states of Alabama, Florida, Louisiana, Mississippi, and Texas announced they had reached a settlement agreement with BP for the company to pay approximately \$18.7 billion in fines and compensation for damage from the spill [29]. The case tragically reiterated the need for the oil industry to adhere to the highest standards of operations and safety, including redundant control and containment systems at all points in the supply process.

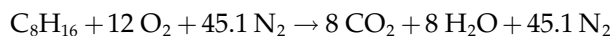
6.2 Fossil Fuel Combustion and Energy Conversion Technologies

6.2.1 Heat of Combustion

Neglecting minor constituents of fuel and air and treating air as 21% O₂ and 79% N₂ by volume, the stoichiometric combustion of hydrocarbon fuels in air can be represented as:



where x is the number of carbon atoms in the hydrocarbon molecule and y is the number of hydrogen atoms. For example, the reaction for the stoichiometric combustion of gasoline in air can be approximated as:



The heat of combustion, or “heating value” of a fuel, is the energy released per unit mass of fuel when it undergoes complete combustion in air. The heat of combustion is numerically equal (but opposite in sign) to the enthalpy of combustion of a fuel, which is the difference between the standard state enthalpy of the products and reactants for combustion of a stoichiometric mixture:

$$\Delta h_C = q_{out} - \Delta h_R = -(h_{products} - h_{reactants}) \quad (6.1)$$

In Equation 6.1, h is the specific enthalpy of the product or reactant mixture at standard state conditions. The combustion process is assumed to be complete. From the first law of thermodynamics, the difference in standard state enthalpies is equal to the heat given off by the reactions, q_{out} , again on a mass basis.

The higher heating value, HHV, is the heat of combustion calculated by assuming that all of the water in the products has condensed to liquid. In contrast, the lower heating value, LHV, is the heat of combustion calculated by assuming that none of the water condenses. The LHV gives a more realistic estimate of heating value for applications where it is not practical to recover the latent heat of condensation, such as in a motor vehicle engine. Heating values are given in Table 6.1 for methane, typical gasoline, and several coal types. The difference between LHV and HHV can be significant, demonstrating the value for energy recovery and efficiency of adding a condensing system where practical. For example, modern gas furnaces for residential applications include a condensing stage to significantly increase their efficiency.

TABLE 6.1

Energy Content of Various Fossil Fuels

Fuel	Heat Content (MJ/kg)
Methane	55 MJ/kg (HHV)
Anthracite coal	~32 MJ/kg (HHV)
Sub-bituminous coal (powder river basin)	~20 MJ/kg (HHV)
Diesel	~45 MJ/kg
Gasoline	~45 MJ/kg

6.2.2 Fossil Fuel Use for Heat

In 2012, the industrial sector accounted for 22% of primary energy use in the United States, and 34% of natural gas consumption. The sector mainly uses primary energy for process heat, and secondarily for space heating. The commercial and residential sectors accounted for 10% of primary energy use, and 28% of natural gas consumption [30]. The commercial and residential sectors use primary energy mainly for space heating, and secondarily for hot water. In 2009, U.S. residences met about half of their space heating needs with natural gas, 35% with electricity, and the balance with fuel oil, liquefied petroleum gas (LPG), or wood [30].

Home furnaces and boilers are rated by Annual Fuel Use Efficiency (AFUE), which is the ratio of the annual heat output compared to the total annual fossil fuel energy they consume. The metric does not account for heat losses in ducts or piping. The U.S. Department of Energy requires a minimum AFUE for residential gas furnaces of 80%. High efficiency systems can achieve 90–98.5% AFUE using a combination of electronic ignition and air flow control, sealed combustion, and a secondary heat exchanger to condense flue gases [31].

Fossil fuels are essential fuels for manufacturing and processing plants. Much of the fuel is burned to produce high temperatures for material processing, including for production of metals, glass, cement, and fertilizer. Once the process is completed, the product needs to be cooled. The industrial process to remove this heat and exhaust it to the environment produces a large thermal resource. The U.S. Environmental Protection Agency (EPA) reports estimates of the technical potential resource from industrial waste heat in the United States at over 150,000 GWh per year [32].

Some industrial facilities can take advantage of cogeneration opportunities to extract process heat and electric power from the same energy source. For example, steam cycle cogeneration plants can be built to route part of the steam from the turbine to use as process heat, without routing it through a condenser. Another approach to utilize waste heat is to run the flue gases from fuel combustion through a heat exchanger to vaporize the working fluid in an organic Rankine cycle (ORC) power generation plant before the heat is exhausted to the environment. The organic Rankine cycle uses a working fluid with a lower boiling point than water, enabling its use at relatively low temperatures. This same technology is already used in geothermal power generation. While the thermal science and the plant technology are mature, developing these waste heat resources requires site-specific analysis and development efforts. These waste heat streams are part of existing production plants and the particular details of the extraction and power plant design and construction must be determined for those specific site conditions. On the other hand, development of industrial waste heat does not require new land or new water resources because these are already being used by the industry for cooling. Most of these industries have sufficient on-site power demand that the power generated can be directly used and does not need to be tied into the grid. Waste heat power plants would not need new environmental assessments and would probably have no public opposition,

as they would be built on existing industrial sites. Due to the relatively low temperatures involved with ORC, the plant efficiencies are often less than half those of coal-fired steam power plants. However, the power is produced at the site where it can be consumed, and it does not need new transport of fuels or wastes.

6.2.3 Electricity Generation from Pulverized Coal

The dominant configuration for existing coal-fired power plants is pulverized coal (PC), where coal is milled to a fine powder and mixed with preheated air before being introduced to the burners. A simplified schematic diagram for a PC power plant is shown in Figure 6.4. PC plants operate on a steam Rankine cycle, shown schematically in Figure 6.5. In this cycle, coal combustion in the boiler (process 1–2) heats water in the tubes that form the boiler walls, producing superheated steam. The superheated steam exits the boiler and enters a multi-stage turbine, where it expands, rotating a shaft that is connected to a generator (process 2–3). The steam exits the turbine and enters the condenser, where it cools and condenses (process 3–4). Feed pumps return the water to the boiler (process 4–1) to continue the cycle. Modern PC plants include multiple heat exchangers to recover heat from the flue gases. Plant equipment also includes an ash handling system, and multiple control devices. As discussed below, almost all coal-fired power plants in the United States have fabric filters or bag houses to control particulate air pollution and most have flue gas desulfurization units to limit sulfur dioxide emissions as well as modified combustion systems or flue gas control devices to reduce emissions of nitrogen oxides.

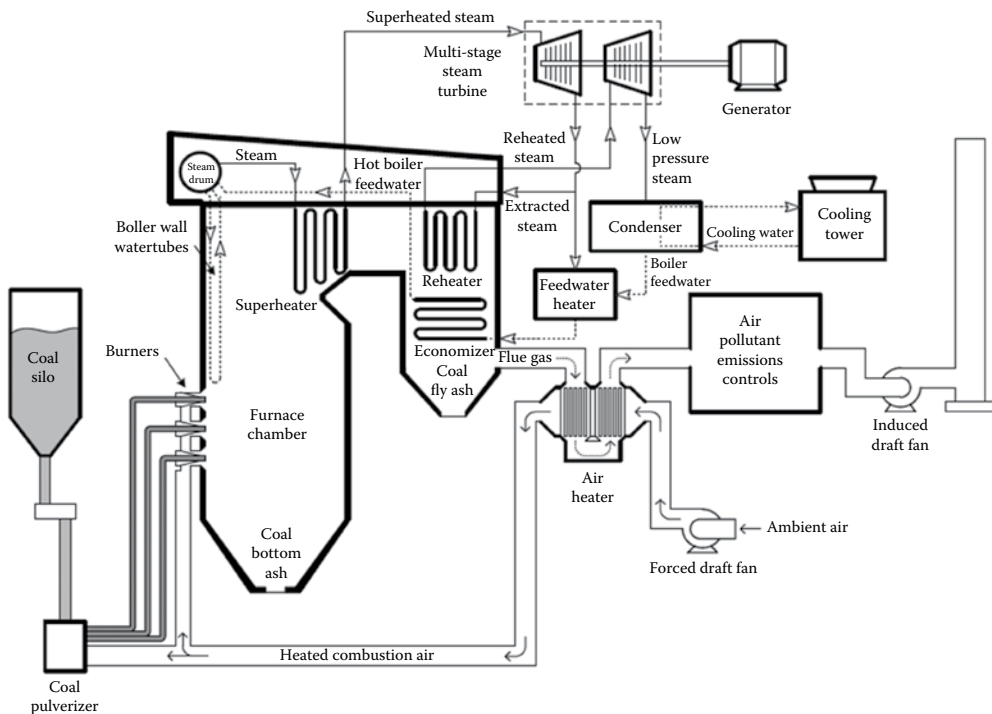
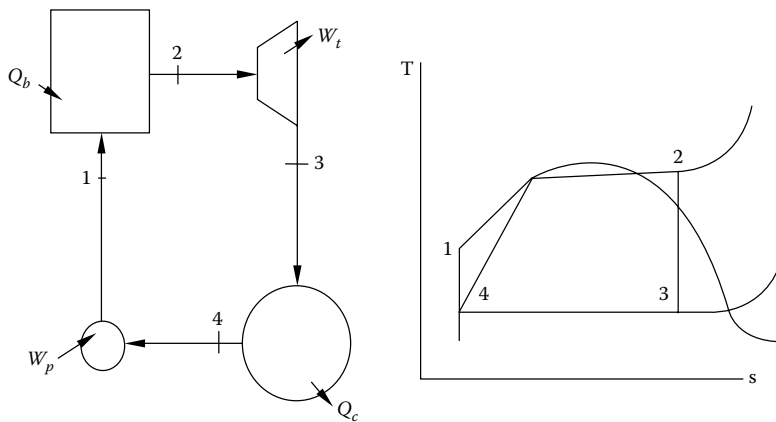


FIGURE 6.4

Simplified schematic diagram for a typical pulverized coal power plant. (From EPA, 2010. *Available and Emerging Technologies for Reducing Greenhouse Gas Emissions from Coal-Fired Electric Generating Units*, U.S. Environmental Protection Agency, Office of Air and Radiation, Research Triangle Park, NC. [33])

**FIGURE 6.5**

Ideal Rankine cycle. (From Wong, K.V., 2012. *Thermodynamics for Engineers*, 2nd edn., CRC Press, Boca Raton, FL, Figure 6.2, p. 6–2. [57])

The product of combustion efficiency, thermal efficiency, and generator efficiency determines the overall efficiency of a coal-fired power plant. Since combustion and generator efficiencies are relatively close to 100%, the thermal efficiency of the actual Rankine cycle implemented at the plant will be the most influential factor. In the United States, heat rate is commonly used as an alternative way to express efficiency, in units of Btu or kJ of heat input per kWh of electricity output. The convention in the United States is to use HHV for power plant efficiency and heat rate calculations. Efficiency values also depend on whether the gross or net output from the plant is considered. Gross output is the total power produced by the facility. Net output is the gross output minus the parasitic load of electricity required to operate the plant, including requirements for pumps, fans, coal and ash handling and pollution control equipment. Operating flue gas desulfurization equipment, for example, commonly requires 1 to 2% of plant output [33]. Table 6.2 shows average heat rate and

TABLE 6.2

Average Efficiencies for Fossil and Nuclear Power Plants in the U.S. in 2013

Fuel Type	Heat Rate (Btu/kWh)	Efficiency
Coal ^a	10,459	32.6%
Petroleum ^b	10,713	31.8%
Natural gas	7,948	42.9%
Nuclear	10,449	32.7%

Source: EIA, 2015. Average operating heat rate for selected energy sources, Energy Information Administration, <http://www.eia.gov/electricity/annual>. [34]

^a Coal includes anthracite, bituminous, subbituminous, and lignite coal. Waste coal and synthetic coal are included starting in 2002.

^b Petroleum includes distillate fuel oil (all diesel and No. 1 and No. 2 fuel oils), residual fuel oil (No. 5 and No. 6 fuel oils) and bunker C fuel oil, jet fuel, kerosene, petroleum coke, and waste oil.

efficiencies for fossil and nuclear power plants in the United States in 2013, calculated by the U.S. EIA based on net electricity output [34].

EXAMPLE 6.1

Consider an ideal Rankine cycle that operates with steam as the working fluid. The steam leaves the boiler and enters the turbine at 600°C and 5 MPa. It enters the condenser at a pressure of 10 kPa. The working fluid enters the pump at 10 kPa as saturated liquid and exits at 5 MPa. The cycle produces 150 MW net power output. Find (a) the thermal efficiency of the cycle and (b) the mass flow rate of steam.

Solution

Figure 6.5 shows a schematic of the cycle and diagrams each process as a function of temperature, T , and entropy, s , indicating which processes are assumed to be isentropic. The T - s diagram also shows how the processes lay out with respect to the vapor dome, indicating the phase of the working fluid as saturated liquid at the pump inlet (state 4), liquid-vapor mixture in the boiler (1–2) and condenser (3–4) and superheated vapor at the turbine inlet (state 2). The cycle is analyzed by applying the first law of thermodynamics to the sequence of four steady flow processes that take the working fluid through the cycle from states 1 through 4. Each thermodynamic state is fixed by specifying two independent properties.

a. The overall thermal efficiency is given by:

$$\eta_{th} = \frac{\dot{W}_{net}}{\dot{Q}_{boiler}} = \frac{\dot{m}_{steam}((h_2 - h_3) - (h_4 - h_1))}{\dot{m}_{steam}(h_2 - h_1)}$$

where:

\dot{W}_{net} = net rate of work output from the cycle

\dot{Q}_{boiler} = net rate of heat input to the cycle

\dot{m}_{steam} = mass flow rate of working fluid

h_i = specific enthalpy of state i

In the following, P_i = pressure at state i , v_i = specific volume at state i , s_i = entropy at state i , and T_i = temperature at state i .

State 4 is the inlet to the pump and exit from the condenser. At state 4, $P_4 = 10$ kPa and the water is saturated liquid. From the steam tables [57], $h_4 = 191.81$ kJ/kg; $v_4 = 0.001010$ m³/kg.

State 1 is the exit from the pump and inlet to the boiler. P_1 is given as 5 MPa. The pump work is:

$$w_{pump,in} = v_4(P_1 - P_4)$$

So, from the first law of thermodynamics:

$$h_1 = h_4 + v_4(P_1 - P_4) = 196.85 \frac{\text{kJ}}{\text{kg}}.$$

State 2 is the boiler outlet and turbine inlet, at which point the steam is superheated with $P_2 = 5$ MPa and $T_2 = 600^\circ\text{C}$. From the steam tables, $h_2 = 3666.9$ kJ/kg and $s_2 = 7.2605$ kJ/kg-K.

State 3 is the turbine exit and condenser inlet. Assuming the turbine is isentropic, $s_3 = s_2$. $P_3 = 10$ kPa, as given. Since the entropy at state 3 is known, using the limiting entropies from the steam tables for pure liquid and pure vapor at $P_3 = 10$ kPa, the quality at that state is found to be 88.2% vapor. The corresponding enthalpy is $h_3 = 2301.64$ kJ/kg.

The overall cycle efficiency is then:

$$\eta_{th} = \frac{(h_2 - h_3) - (h_4 - h_1)}{(h_2 - h_1)} = \frac{((3666.9 - 2301.64) - (196.85 - 191.81))}{(3666.9 - 196.85)} = 0.392$$

- b. The mass flow rate of steam can be calculated from the overall power output of the cycle:

$$\dot{m}_{steam} = \frac{150 \times 10^3 \frac{kJ}{s}}{((3666.9 - 2301.64) - (196.85 - 191.81)) \frac{kJ}{kg}} = 110.3 \frac{kg}{s}$$

Some efficiency improvements at existing coal-fired power plants are likely possible, even without major changes in plant configuration. In 2014, in preparing to propose CO₂ emissions regulations for existing coal-fired power plants in the United States, EPA estimated that on average, existing coal-fired power plants in the United States could reduce their heat rates by about 6% using established, cost-effective measures [35]. Opportunities for improving efficiencies include improved boiler combustion control, optimizing heat exchangers, upgrading motors, pumps, fans and drives to high-efficiency equipment, condenser and turbine upgrades, and improving water quality to reduce scale build-up in boiler tubes.

In new coal-fired power plants, higher efficiencies can be achieved through supercritical or ultra-supercritical operation of the steam cycle. These terms refer to the critical point of water, corresponding to a temperature of 647 K and pressure of 22.1 MPa. While thermal design efficiencies are estimated to range from 33–37% for new subcritical PC plants, supercritical operation at ~850 K and 24 MPa increases the design efficiency range to 39–40%, and ultra-supercritical operation increases the range to 42–45%. These conditions require upgraded boilers and turbines that can withstand high temperatures and pressures. Hundreds of supercritical plants have been built worldwide.

Coal is on the decline in the United States. The U.S. EIA reports plans for six new coal plants to be built between 2014 and 2018, adding a total of 705 MW of peak summer capacity. For the same period, generators reported plans to close 193 coal plants totaling 29,517 MW of capacity. The net change would reduce U.S. coal-fired power plant capacity by about 10% [36].

6.2.4 Electricity Generation from Natural Gas

The most efficient natural gas power plants are combined cycle units, which use a gas power (Brayton) cycle topping a steam turbine (Rankine) cycle. The gas power cycle typically operates with turbine inlet temperatures of about 1700 K, with turbine outlet temperatures of over 770 K. This allows the exhaust from the gas turbine to be used as an energy source for the steam cycle. New natural gas combined cycle (NGCC) power plants advertise design thermal efficiencies of up to 60%. However, if reported on the basis of net electricity output and using the HHV for natural gas, operating efficiencies

above 50% would reflect good performance. In the United States, the overall average efficiency of power production with natural gas is also lowered by the use of relatively inefficient combustion turbines that operate on a simple Brayton cycle, as well as older NGCC units that are less efficient than the state-of-the-art models [37]. Despite their lower efficiency, the simple cycle combustion turbines are valued as peaking units, as they are relatively easy to ramp up and down.

Currently in the United States, as coal-fired power generation capacity is declining, natural gas capacity is increasing. On average, the cost of generation from a new NGCC unit is expected to be less than that from a new coal-fired power plant. U.S. EIA reported in 2015 that generators planned to add 347 new natural gas units with more than 40 GW of capacity between 2014 and 2018. They also planned to retire 153 natural gas units totaling about 7 GW of capacity. The net change would more than offset the planned decrease in coal-fired power plant capacity [36].

6.2.5 Integrated Gasification Combined Cycle

Integrated gasification combined cycle (IGCC) power plants (Figure 6.6) are designed to take advantage of the efficiency gains of combining gas and steam cycles but starting from a solid fuel (coal or biomass) [38]. To accomplish this, the solid fuel is first converted to synthesis gas, which is mostly CO and H₂, by reacting the fuel with air or oxygen at high

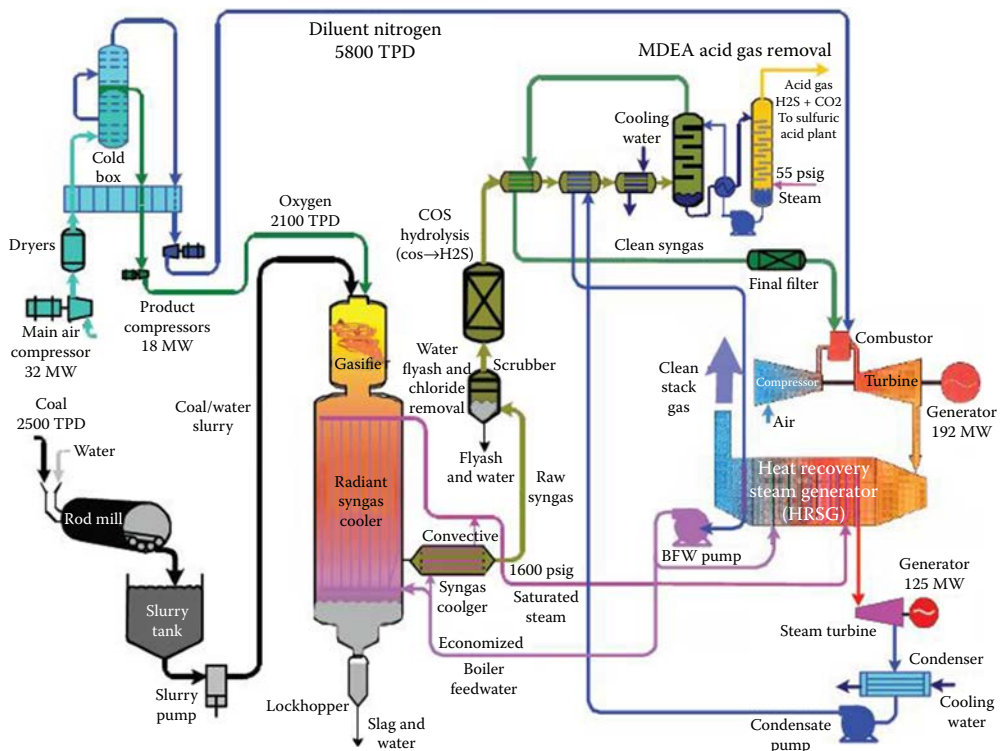


FIGURE 6.6

Simplified process flow diagram for the Tampa Electric IGCC plant. (From NETL, 2015. Simplified process flow diagram for the Tampa Electric IGCC plant, National Energy Technology Laboratory, U.S. Department of Energy, <http://www.netl.doe.gov/research/coal/energy-systems/gasification/gasifiedia/igcc-config>. [38])

temperature and pressure. Reacting with oxygen requires an air separation unit, but avoids diluting the synthesis gas with nitrogen, thus, reducing the costs of gas cleanup. The syngas is cleaned to remove particulate matter, sulfur, and mercury. In some designs, the CO in the syngas is reacted with water in a water-gas shift reactor to produce H₂ and CO₂. The CO₂ can then be captured pre-combustion, when it is present at relatively high concentration and can be captured much more easily than would be the case if the CO₂ were formed from CO in the combustion process. A 2007 MIT study estimated that without CO₂ capture, overall operating efficiencies of IGCC plants processing bituminous coal would approach 40% (based on HHV), on par with a supercritical PC plant [3].

There are several IGCC plants in operation or under construction around the world. Three of the longest running are the Wabash River Coal Gasification Repowering Project near West Terre Haute, Indiana, a 265 MW plant that started up in 1995; Tampa Electric IGCC project in Polk County, Florida, a 250 MW plant that started up in 1996; and the Elcogas IGCC plant in Puertollano, Spain, a 300 MW plant that started up in 1997. MIT [3] reports that the Wabash plant operates at an efficiency of 38.2%. The Edwardsport IGCC station is a 618 MW facility that started commercial operations in 2013. A 582 MW IGCC plant that was scheduled to open in 2016 in Kemper County, Mississippi, will be the first IGCC plant in the United States to capture and sequester carbon. The facility will burn lignite coal. It will use a physical absorption system to capture CO₂, which will be piped from the facility for use in enhanced oil recovery. IGCC plants built to date have benefited from significant government support as demonstration projects. Costs of IGCC are currently not competitive with NGCC or new coal-fired units. However, fees or restrictions on carbon emissions could change the economics, as pre-combustion capture in an IGCC configuration is easier and less expensive than post-combustion capture in a conventional pulverized coal plant.

6.3 Air Pollution from Fossil Fuel Combustion

6.3.1 Local and Regional Scale Air Pollution

From a market perspective, fossil fuels are well recognized for providing “cheap” energy and delivering services that are essential to the functioning of modern society, starting with heat, light, and transportation. However, the use of fossil fuels carries hidden costs that are not apparent in the price we pay for electric power or for gasoline at the pump. These hidden costs sometimes take the form of economically inefficient government subsidies that distort markets and encourage excess consumption. Additionally, unwanted byproducts of fossil fuel production and use can cause significant damage to human health and the environment that are not reflected in market prices. Some of this damage can be prevented through good engineering practices, application of control technology, and remedial actions. However, fossil fuels are extracted and exploited in some areas where requirements to minimize environmental harm are not in place or are not effectively enforced. And even when protective regulations and safety systems are in place, accidental spills and releases can still occur. Most critically, there is currently no established solution to the problem of global warming caused by fossil fuel combustion.

Emissions of air pollutants, including greenhouse gases and other climate forcing aerosols, are arguably the chief environmental concern associated with fossil fuel use. Since the 1970s, significant progress has been made in developing and implementing control technology to reduce emissions of “conventional” air pollutants from fossil fuel combustion systems, covering the range of applications from residential heating to motor

vehicle engines to utility-scale electricity generation. The pollutants that have been widely addressed include particulate matter, carbon monoxide, sulfur oxides, volatile organic compounds, and nitrogen oxides. Nevertheless, significant challenges in reducing emissions of these pollutants remain, especially with older equipment and facilities in less-developed countries. Emissions of mercury from coal-fired power plants are an ongoing global concern. Every state in the United States has issued health advisories banning fishing and consumption of fish due to toxic mercury exposure in at least one lake or river. Mercury bio-accumulates in the fatty tissues and oils in all animals and is never broken down or dispersed. Thus, release of mercury into the atmosphere from coal combustion is a serious sustainability issue for humans, agriculture, and wild animals, particularly aquatic predator species such as tuna, seals, and dolphins. The U.S. EPA adopted stringent limits on mercury emissions from coal-fired power plants in 2012, with compliance required by 2015. However, because atmospheric mercury has a global distribution, health and environmental concerns will persist until action to limit emissions is taken internationally.

Anenberg et al. [39] estimated that the increase in anthropogenic air pollution emissions that has occurred from pre-industrial times up to the year 2000, accounts for 0.7 ± 0.3 million deaths per year from respiratory disease attributable to long-term exposure to ozone air pollution. They also found that the increase in exposure to fine particulate air pollution (suspended particles with aerodynamic diameter less than 2.5 microns, known as $PM_{2.5}$) accounts for 3.5 ± 0.9 million deaths per year from cardiopulmonary disease and $220,000 \pm 80,000$ deaths from lung cancer. The estimated number of excess deaths was greatest in densely populated parts of Europe and Asia, where emissions are also high. Mortality rates (deaths per million people) were also high in the eastern United States.

Anenberg et al. [39] arrived at these estimates by using a global chemistry and transport model to estimate how the increase in anthropogenic emissions since preindustrial times has changed ozone and $PM_{2.5}$ concentrations, then applying concentration-response functions for the specified disease endpoints to estimate the number of excess premature deaths. The concentration-response functions are well established and supported by a very large body of literature on air pollution health effects. Fossil fuel combustion is the dominant source of the anthropogenic emissions contributing to these deaths.

Ground-level ozone is formed in the atmosphere through reactions of volatile organic compounds (VOC) and nitrogen oxides (NO_x) in the presence of sunlight. Major anthropogenic sources of VOC include evaporation of liquid fuels and incomplete combustion of liquid and solid fuels. VOC are also emitted by vegetation, a source category that is considered biogenic, not anthropogenic. Nitrogen oxides are emitted from high temperature combustion sources that convert N_2 in combustion air to NO and NO_2 . Sources of NO_x thus include power plants, motor vehicles, aircraft, industrial process heat, and fuel combustion for cooking and space heating.

Some $PM_{2.5}$ is directly emitted to the atmosphere from abrasive processes including manufacturing, agricultural activities, and road-use wear of tires and vehicles, and from incomplete combustion of liquid or solid fuels, including gasoline, diesel, fuel oil, coal, and biomass. Additional $PM_{2.5}$ is formed in the atmosphere from chemical reactions involving sulfur oxides, nitrogen oxides, ammonia, and carbonaceous compounds. Anthropogenic emissions of sulfur oxides are mainly due to combustion of sulfur-containing fuels, with coal combustion being the largest source.

In many countries around the world, air pollutant emissions from fossil fuel combustion have been regulated with increasing stringency since the 1970s. In the United States, for example, the series of regulations imposed since the 1970 Clean Air Act Amendments were enacted have led to sharp reductions in emissions of SO_2 and NO_x , among other pollutants.

TABLE 6.3

Total Emissions of Sulfur Dioxide from Fossil Fuel Combustion
(Gg/yr)

	China [42]	India [42]	United States [40]
2000	21079	5771	14764
2010	30762	8746	7013

U.S. EPA estimates that total SO₂ emissions in the United States fell by 75% from 1970 to 2010 and that NO_x emissions declined by 45% [40]. Over the same time period, total energy consumption in the United States increased by about 45% [41]. For comparison, Table 6.3 shows how total SO₂ emissions changed from 2000 to 2010 in the United States, China, and India [42].

In the United States, emissions reductions occurred across all sectors of energy use, but reductions in the power sector played a large role, especially for SO₂ and NO_x. EPA reports that in 2013, more than three-quarters of U.S. electricity generation from coal was from facilities with flue gas desulfurization (FGD) units to reduce SO₂ emissions and nearly 60% of generation was from units with advanced post-combustion controls for NO_x [43]. Other units have reduced SO₂ emissions by switching from high to low-sulfur coal and reduced NO_x emissions through combustion modifications. Almost all coal-fired power plants in the United States employ either fabric filters or electrostatic precipitators to reduce PM emissions. In the United States, the Clean Air Act Amendments of 1990 initiated a highly cost-effective “cap and trade” program for reducing power plant emissions. This program capped the total SO₂ emissions that could be released in 1995 and tightened the cap again in 2000. Within the overall cap, individual power plants could buy and sell allowances from each other, so facilities that needed more time to make reductions could buy allowances from other facilities that could reduce emissions relatively cheaply. Exceeding the goals set by the U.S. Congress, the program achieved emissions reductions at a fraction of the cost that had been projected beforehand.

Since the mid-2000s, China has made dramatic progress in reducing the sulfur oxides emissions rates from its expanding fleet of coal-fired power plants [42]. In 2000, only about 1% of Chinese coal-fired power plant capacity was equipped with FGD equipment. By 2010, FGD penetration is reported to have increased to over 80% of capacity. Since about 2007, improvements in enforcement and incentives for compliance have reduced concerns that power plant operators were not consistently operating the FGD units they had installed. Total SO₂ emissions in China increased sharply between 2000 and 2006. They are thought to have declined since then due to the power plant emissions control efforts, although total emissions in 2010 are still higher than they were in 2000. This is partly because the success in reducing emissions from the electric power sector has not been matched in the industrial sector, which now accounts for two-thirds of Chinese SO₂ emissions. In India, emissions of SO₂ and other air pollutants have increased steadily along with energy consumption, as there is little deployment of pollution control equipment in any sector, including electricity generation. Government regulations in India require coal-fired power plants to use control equipment to reduce PM emissions, but not for SO₂ or NO_x [42].

6.3.2 Greenhouse Gas Emissions and Climate Change

For more than 100 years, scientists have understood that carbon dioxide absorbs heat and acts as a greenhouse gas. The concentration of CO₂ in the atmosphere is now greater than 400 ppm, up from a preindustrial level of about 280 ppm. Along with changes in other greenhouse gases and aerosols, this increase is known to have shifted long-standing climate patterns across the

globe. The scientists who observe changes in effects of climate ranging from loss of polar ice to altered growing seasons to seawater chemistry are calling for immediate and deep reductions in CO₂ emissions so that climate systems do not become catastrophically destabilized. The Intergovernmental Panel on Climate Change (IPCC) in its Fifth Assessment Report (2014) described the risks and changes that are likely to happen if the production of fossil fuels and other greenhouse gases is not curtailed [44]. The IPCC has called for an 80% reduction in GHG emissions by 2050 to keep the global temperature increase below catastrophic levels.

The main human CO₂ additions to the atmosphere are from burning fossil fuels and from manufacture of cement, plus forest clearance and soil disturbance. Since 1750, fossil fuel combustion and cement manufacture are estimated to have released 375 Gigatons of carbon (Gt C) to the atmosphere. Deforestation and land use change are estimated to have released an additional 180 Gt C. Of the total released, scientists estimate that 240 Gt C has been retained in the atmosphere. The ocean has absorbed 155 Gt C, which is causing acidification and harming coral reefs and other marine systems. Forests and other terrestrial ecosystems have absorbed the remaining 160 Gt C [45]. The net release to the atmosphere has led to the current CO₂ atmospheric concentration, which has not existed for over 1 million years.

Production of fossil fuels also contributes to emissions of methane, a potent greenhouse gas with 30 or more times as much radiative forcing effect per unit mass as CO₂. Methane has an atmospheric lifetime on the order of a decade, so reducing its emissions could lead to a relatively rapid climate benefit. Based on carbon isotope signatures, which differ between fossil, microbial, and biomass burning sources, the worldwide fossil fuel industry (natural gas, coal, and oil production) is estimated to contribute roughly a quarter of atmospheric methane [46].

Black carbon (BC) aerosol is another potent climate forcing agent that is emitted from fossil fuel combustion. BC absorbs solar radiation at all wavelengths, and also contributes to warming by reducing surface albedo of snow and ice. BC is also a significant component of PM_{2.5} air pollution, discussed above in the context of its health effects. In contrast to BC, some other PM_{2.5} constituents, such as the sulfate aerosol that is produced from SO₂ oxidation, have a cooling effect on climate, because they tend to scatter sunlight (direct effect) and to enhance the cooling properties of clouds (indirect effect). While the overall effect of aerosols on climate change has more uncertainty, it is clear that reducing BC emissions would have benefits for mitigating climate change and reducing health effects. Furthermore, BC has a short atmospheric lifetime (days to weeks) so the atmospheric response to reductions in BC emissions will be faster than the response to reductions in long-lived greenhouse gases. In the United States, about 50% of BC emissions are estimated to be due to fossil fuel combustion, primarily from use of diesel. The balance is mainly due to open biomass burning [47]. Worldwide, open biomass burning and residential fuel combustion are estimated to contribute about two-thirds of black carbon emissions. Emissions from diesel vehicles in the United States are declining due to increasingly stringent control requirements [47].

The increased energy retention in the earth system due to increased atmospheric concentrations of CO₂, methane, and other climate forcing agents has to-date resulted in a global average 0.8°C temperature increase. This seemingly small change in average conditions has already produced an increased risk of occurrence of extreme weather events like floods and droughts, heat waves, and severe storms. Climate modeling indicates that the risk of catastrophic climate change, in particular melting of the Greenland ice sheet and the resulting sea level rise, is very high if the global average temperature increases by 2°C.

The International Energy Agency [48] has identified key elements of a “bridge” strategy to decouple economic growth from energy consumption and set the world on a path to keep the global average temperature increase below 2°C:

- Increasing energy efficiency in the industry, buildings, and transport sectors.
- Reducing the use of the least-efficient coal-fired power plants and not building new ones.
- Increasing investment in renewable energy technologies in the power sector by 50% from 2014 to 2030.
- Gradually phasing out fossil fuel subsidies by 2030.
- Reducing methane emissions from oil and gas production.

While details differ, at a high-level, the elements of the IEA strategy are widely recognized as needed for any global effort to avoid catastrophic climate change.

As discussed in [Chapter 1](#), in Paris, France, on December 12, 2015, more than 190 countries reached an agreement to keep the global temperature increase this century to less than 2°C above preindustrial levels, with the further aim of limiting the increase to below 1.5°C. The Paris Agreement entered into force on October 5, 2016, when it exceeded the threshold of ratification by at least 55 countries representing 55% of global emissions. Parties to the Paris Agreement are obligated to pursue their best efforts to reduce emissions of greenhouse gases and other climate forcing agents. Individual countries submit “Nationally Determined Contributions” that establish their commitments to the global community. The Agreement requires countries to report regularly on their progress and requires the international community to periodically reassess progress and goals. In June 2017, President Donald Trump announced that the United States would withdraw from the Paris agreement. However, many U.S. states, cities, and corporations remain committed to achieving reductions that would match or meet the commitments the United States had made under the Obama Administration.

[Table 6.4](#) shows estimates of greenhouse gas emissions per unit energy for coal, natural gas, and a variety of crude oil products [49,50,51,52]. In each case, the table shows both the direct combustion emissions and estimates of the “upstream” emissions associated with fossil fuel extraction and processing. Upstream greenhouse gas emissions for natural gas are mainly due to methane venting and leaks, which can be further reduced with good engineering practice and regulations. Upstream emissions are also a significant fraction of the total for gasoline and diesel from conventionally produced crude oil, due mainly to

TABLE 6.4

Estimated Greenhouse Gas Emissions Factors for Fossil Fuels (g CO₂-equivalent/MJ).
Upstream Emissions Include Methane as CO₂-e, Where Applicable

	Gasoline from Conventional Crude Oil [49]	Gasoline from Tar Sands [49]		Gasoline from Oil Shale [49]	
		Low	High	Low	High
Upstream	20.5	34.1	57.9	47.7	183.3
Combustion	73.7	73.7	73.7	73.7	73.7
Total	94.2	107.8	131.6	121	256.7

	Diesel from Conventional Crude Oil [49]	Natural Gas [50,51]		Coal [51,52]	
Upstream	16.1	12.7		5.3	
Combustion	77.4	51.1		89.0	
Total	93.5	63.8		94.2	

emissions from oil refining. The upstream contribution increases as petroleum production shifts to unconventional resources such as the tar sands and especially oil shale. Total emissions per unit energy for gasoline could double if oil shale is used.

EXAMPLE 6.2

Estimate the direct combustion emissions of CO₂ per kWh of electricity produced for an average natural gas plant in the U.S., assuming the natural gas is 100% methane, stoichiometric combustion, and using the average heat rate from [Table 6.2](#).

Solution

The average heat rate for natural gas plants is 7948 Btu/kWh and the heat content of methane is 55.5 MJ/kg. The molecular weight of CO₂ is 44 g per mole; that of methane is 16 g per mole. Hence:

$$\frac{7948(\text{Btu/kWh}) \cdot 1055(\text{J/Btu})}{55.5 \cdot 10^6(\text{J/kgCH}_4)} = 0.151 \frac{\text{kg CH}_4}{\text{kWh}}$$

$$0.151 \frac{\text{kg CH}_4}{\text{kWh}} \cdot \frac{1 \text{ mol CO}_2}{\text{mol CH}_4} \cdot \frac{44 \text{ g CO}_2 / \text{mol CO}_2}{16 \text{ g CH}_4 / \text{mol CH}_4} = 0.42 \frac{\text{kg CO}_2}{\text{kWh}}$$

As discussed elsewhere in this book, CO₂ emissions associated with the energy system can be addressed by reducing demand for energy or shifting to low-carbon or carbon-free energy sources. Emissions of methane from energy production can be reduced significantly by avoiding venting, by detecting and fixing leaks, and by upgrading equipment. Although methane is a valuable product, it is often vented off when it is produced in association with oil in areas that lack natural gas pipelines. It is also deliberately vented when wells are cleaned out during completions, liquids unloading, and work overs. The U.S. EPA and individual state regulatory agencies have required the oil and gas industry to reduce or eliminate these emissions. In addition, it is technically feasible to capture CO₂ from large combustion sources and sequester it underground. However, this approach has relatively high costs and energy penalties and limited applicability. The technology to capture and sequester carbon from motor vehicles operating on gasoline or diesel does not exist.

6.3.3 Carbon Capture and Sequestration

Prospects for carbon capture and geological sequestration (CCS) of CO₂ remain uncertain, due to relatively high costs and limited experience with application of the technology in the electricity sector. However, some analysts think application of CCS could be an important element of strategies to reduce CO₂ emissions, particularly in China and other countries where abundant resources and past investments have created strong inertia to move away from use of coal.

Geologic sequestration means capturing CO₂ from a combustion system, then storing it deep underground in structures that will trap the gas. Geological CCS could have application for concentrated CO₂ emissions streams from cement manufacturing, fertilizer production, and electricity generation from coal, natural gas, or biomass. We discuss the main capture alternatives that have been examined for coal, but similar technologies apply to the other source types.

Methods for capturing CO₂ from air-blown pulverized coal-fired power plants are established, but expensive. Post-combustion CO₂ is present in flue gases from coal-fired power plants at concentrations of about 15% (v). These relatively low concentrations make

CO₂ gas separation challenging. CO₂ capture in a relatively dilute flue gas stream would likely be accomplished in a packed absorption tower using chemical absorption with an aqueous amine solution. This approach has been used for decades to separate CO₂ (and H₂S) from natural gas in the oil and gas industry, commonly with monoethanolamine as the solvent. As a second step in the process, CO₂ would be stripped from the solution by using low-pressure steam to elevate the temperature, regenerating the absorbent for future use. In aqueous solution, the amines are weak bases that can react with weak acids (such as CO₂) to form water-soluble salts. Finally, the CO₂ is cooled, dried, and compressed for transport and storage. MIT estimates that a 500 MW subcritical PC plant would require a 37% increase in heat input to maintain level output, if an amine-based CO₂ capture system were added [3]. The solvent regeneration step and CO₂ compression step would require most of the extra energy required for the capture system.

An alternative approach for CO₂ capture from pulverized coal plants involves combusting the coal in oxygen, rather than air. Doing so results in flue gases that are mainly CO₂ and water, without dilution by N₂. Following flue-gas cleanup, CO₂ can be captured directly by compression. However, this oxy-fuel combustion and capture approach requires an air separation unit, which itself imposes a significant energy penalty on plant operations. The MIT study estimates that the energy efficiency of a new supercritical PC plant would be reduced from 38.5% to 30.6% if an oxy-fuel CO₂ capture system were included, due primarily to energy requirements for air separation and CO₂ compression [3].

The last approach that is widely discussed for CO₂ capture from coal-fired power plants is adding CO₂ capture to an IGCC system. In this case, three extra operations have to be added to a standard IGCC configuration. The first is a shift reactor, in which CO from the syngas is reacted with steam over a catalyst, producing CO₂ and H₂O. This allows the CO₂ to be produced prior to the combustion stage so that it isn't diluted with nitrogen. The shift reactor is followed by a CO₂ separation unit. In this case, the CO₂ is more concentrated than it would be in post-combustion flue gases, so it can be separated from the gas stream using a weakly binding physical solvent such as Selexol. The solvent can be regenerated by dropping the pressure, requiring much less energy than needed for amine regeneration in the post-combustion case. After separation, the fuel gas sent to the turbine is mainly H₂, which requires turbine modifications due to its high flame temperature. As with the other capture methods, the last step is compression and drying of the CO₂ to prepare it for transport and storage.

Geologic sequestration essentially means putting CO₂ gas into geologic structures with porous reservoir rocks and non-porous cap rock structures that will trap and permanently hold the gas. The types of formations with these characteristics that we know the most about are depleted oil and gas reservoirs. In enhanced oil recovery processes, CO₂ and methane produced with the oil are compressed and reinjected into the oil field to keep the reservoir pressure up and keep the oil production going. However, there have been a limited number of studies of the long-term storage in such formations. Another challenge with geologic sequestration is that the locations of the possible depleted oil and gas fields are not often near coal-fired power plants. Saline aquifers have been proposed for geologic storage as these formations are more widespread and not considered to be of use as groundwater. The technology to compress CO₂ and transport it via pipelines is known, but the economics are challenging.

The Boundary Dam project in Saskatchewan, Canada, was the first power plant to operate with full-scale carbon capture when it started up in October 2014. This 110 MW (net) unit is designed to use post-combustion amine scrubbing to capture 90% of the CO₂ produced by the facility. The CO₂ will be piped to a nearby oil field for use in enhanced oil recovery.

As noted above, the 580 MW Kemper County, Mississippi, IGCC plant is designed to capture CO₂, again to be used in enhanced oil recovery.

6.3.4 Leaving It in the Ground

According to the IPCC, in order to have a better than even chance of limiting global warming to 2°C above the temperature in preindustrial times, the release of carbon from fossil fuels between 2011 and 2050 would need to be limited to about 860 to 1180 Gt CO₂ [53; Table SPM1]. Meeting this limit would require rapid decarbonization of the global energy system, and/or widespread deployment of CCS systems. The carbon limit mentioned by the IPCC is an order of magnitude less than the carbon contained in global fossil fuel resources, which is estimated to be roughly 11,000 Gt CO₂ [54].

McGlade and Ekins [54] used an integrated assessment model with a bottom-up description of the world energy system to explore how much coal, oil, and gas should be left in the ground between now and 2050 if warming is to be limited to 2°C. The model assumes resources are exploited in the order of increasing cost to satisfy expected demand for energy services in 19 regions around the world, and to meet global constraints on carbon emissions. Of currently estimated *reserves* (the subset of resources that are deemed economical to produce with current technology and economic conditions), they found 33% of oil, 49% of gas, and 82% of coal would need to remain in the ground if the 2°C warming limit is not to be exceeded. They reached this conclusion even though they assumed CCS would become available in 2025. Relaxing the target to limit global warming to 3°C does not change the picture all that much; McGlade and Ekins estimate doing so would increase the total budget for fuels that can be burned by only 30% [54]. McGlade and Ekin's regional assessment suggested that most of the bitumen in the Canadian tar sands and no oil or gas in fields above the Arctic Circle should be exploited [54]. Furthermore, they estimated that if global warming is to be limited to 2°C, the United States would need to leave more than 90% of its coal *reserves* in the ground [54]. As McGlade and Ekins highlight, the pressing question society faces right now about fossil fuels is not whether we're running out of them, but how much more we can afford to use if we want to avoid catastrophic climate change.

PROBLEMS

- 6.1 (Thermodynamics review problem) Examine the effect of steam temperature and pressure on the efficiency of an ideal Rankine cycle. a) Compute the thermal efficiency of a cycle in which superheated steam enters the turbine at 3.5 MPa and 400°C and is condensed at a pressure of 10 kPa. b) Compute the efficiency of a cycle in which the steam enters the turbine at 12.5 MPa and 500°C, and is again condensed at 10 kPa. In both cases assume the compression and expansion are isentropic, and assume the steam exits the condenser as saturated liquid at 10 kPa.
- 6.2 (Thermodynamics review problem) Consider the effect on an ideal Rankine cycle of using a two-stage turbine with steam reheating in between the stages. Compute the thermal efficiency of a reheat cycle for the following conditions. Steam enters the first stage turbine at 12.5 MPa and 500°C, and then is reheated back to 500°C at a pressure of 2 MPa, before entering the second stage turbine. The steam is condensed at 10 kPa and exits the condenser as a saturated liquid. Assume the compression and expansion processes are isentropic.

- 6.3 (Thermodynamics review problem) An ideal Brayton cycle operates with isentropic compression and expansion, with air entering the compressor at 300 K and leaving the combustion chamber at 1000 K. The pressure ratio is 7:1. Use property data for air and compute the thermal efficiency of the cycle.
- 6.4 (Thermodynamics review problem) Determine the thermal efficiency and net power output of an ideal combined cycle power plant, using property data for air in the top cycle and steam properties for the bottom cycle. In the top cycle, air enters the compressor at 300 K at a rate of 300 kg/s and is heated to 1200 K in the combustion chamber. The top cycle has a pressure ratio of 12. The steam in the bottom cycle is heated to 400°C at 8 MPa in a heat exchanger, and after leaving the turbine is condensed at 10 kPa. The combustion gases leave the heat exchanger at 400 K. Assume that all compression and expansion processes are isentropic.
- 6.5 Compute the levelized cost of electricity for a natural gas combustion turbine power plant, assuming the thermal efficiency is 40%, combustor efficiency is 95% and generator efficiency is 95%. The plant is rated at 150 MW and has a capacity factor of 50%. The capital equipment cost is \$165 million and plant lifetime is 20 years. Plant financing is arranged at a nominal interest rate of 8% over a 20-year term. Natural gas is supplied to the plant during the first year at a price of \$5 per thousand cubic feet, with the price expected to escalate at a rate of 2% per year. Other O&M costs are \$10 million per year in the first year, escalating at 2% per year. Neglect tax considerations. Show the calculations and results for the following steps needed to reach the final answer:
- Calculate the annual natural gas requirement for the facility, in units of thousand cubic feet. The average heat content of natural gas is 1.032 MMBtu per Mcf. (Mcf = 1000 cubic feet.)
 - Calculate the annual cost of the natural gas required in the initial year.
 - Calculate the annual payment required to pay back the plant financing in equal payments over 20 years.
 - Calculate the net present value of the 20-year stream of total costs using a nominal discount rate of 10%.
 - Calculate the LCOE.
 - How would the LCOE change if the capacity factor were increased to 75%, all else being equal?
 - How would the LCOE change if the capacity factor were increased to 75% and the natural gas price was \$4 per thousand cubic feet, instead of \$5 per Mcf?
- 6.6 A coal-fired power plant with a steam cycle efficiency of 36% produces 1.8 billion kWh/yr of electricity. Assume the generator is 97% efficient, and the boiler is 95% efficient. Assume the coal has a heating value of 29 MJ/kg and is 75% carbon by mass. Determine:
- The total coal energy content required per year
 - The mass of coal required per year in metric tons
 - The mass of CO₂ emitted per year from the plant
 - The mass of CO₂ emitted per MWh produced in pounds per MWh

- 6.7 In an August 2016 report, the U.S. Energy Information Administration estimated that the levelized cost of electricity for conventional combined cycle natural gas plants entering service in 2022 would be about \$56/MWh and that for utility scale photovoltaics would be about \$74/MWh [55]. Based on these levelized costs, estimate the emissions fee in \$ per metric ton of CO₂-e that would be required to incentivize shifting from natural gas combined cycle electricity generation to utility scale solar PV generation. Assume fees will be imposed on life cycle greenhouse gas emissions of ~600 g CO₂-e/kWh for NGCC and 40 g CO₂-e/kWh for utility-scale PV. How does your estimated emissions fee compare to the U.S. government's social cost of carbon, as published by the U.S. Environmental Protection Agency in 2016?

U.S. EPA, Social Cost of CO₂, 2015–2050 (in 2007 dollars per metric ton CO₂)

Year	Discount Rate and Statistic			
	5% Average	3% Average	2.5% Average	High Impact
(95th pct at 3%)				
2015	\$11	\$36	\$56	\$105
2020	\$12	\$42	\$62	\$123
2025	\$14	\$46	\$68	\$138
2030	\$16	\$50	\$73	\$152
2035	\$18	\$55	\$78	\$168
2040	\$21	\$60	\$84	\$183
2045	\$23	\$64	\$89	\$197
2050	\$26	\$69	\$95	\$212

Source: EPA, 2016. *Technical Support Document: Technical Update of the Social Cost of Carbon for Regulatory Impact Analysis Under Executive Order 12866*, https://www.epa.gov/sites/production/files/2016-12/documents/sc_co2_tsd_august_2016.pdf. [56]

References

1. IEA, 2014. *Key World Energy Statistics*, International Energy Agency, Paris, France.
2. EIA, 2015. *Annual Energy Outlook 2015*, U.S. Energy Information Administration, Washington, DC.
3. Ansolabehere, S. et al., 2007. *The Future of Coal: Options for a Carbon-Constrained World*, Massachusetts Institute of Technology, Cambridge, MA.
4. De Nevers, N., 2000. *Air Pollution Control Engineering*, McGraw-Hill, New York, NY.
5. EIA, 2015. International energy statistics, <http://www.eia.gov/beta/international/>.
6. EIA, 2015. Top coal producing states, 2013, http://www.eia.gov/energyexplained/index.cfm?page=coal_home.
7. NRC, 2010. *Hidden Costs of Energy: Unpriced Consequences of Energy Production and Use*, National Research Council Committee on Health, Environmental, and Other External Costs and Benefits of Energy Production and Consumption, Washington, DC.
8. MSHA, 2015. Historical data on mine disasters in the United States, Mine Safety and Health Administration, <http://www.msha.gov/MSHAINFO/FactSheets/MSHAFCT8.HTM>.
9. MSHA, 2015. Mine safety and health at a glance, Mine Safety and Health Administration, <http://www.msha.gov/MSHAINFO/FactSheets/MSHAFCT10.asp>.

10. BLS, 2015. Census of fatal occupational injuries charts, Bureau of Labor Statistics, <http://www.bls.gov/iif/oshcfoi1.htm>.
11. IEA, 2009. *Cleaner Coal in China*, International Energy Agency, Paris, France.
12. Areddy, J.T., 2012. China coal sector has safety setback. *The Wall Street Journal*.
13. EIA, 2015. U.S. dry natural gas production, Energy Information Administration, <http://www.eia.gov/naturalgas>.
14. EIA, 2015. Oil and natural gas resource categories reflect varying degrees of certainty, *Today in Energy*, <http://www.eia.gov/todayinenergy/detail.cfm?id=17151>.
15. EIA, 2014. *Assumptions to Annual Energy Outlook 2014, Oil and Gas Supply Module*, Energy Information Administration, Washington, DC.
16. EIA, 2006. *Assumptions to Annual Energy Outlook 2006, Oil and Gas Supply Module*, Energy Information Administration, Washington, DC.
17. NETL. On-site research, National Energy Technology Laboratory, U.S. Department of Energy, <http://www.netl.doe.gov/research/on-site-research/research-portfolio/oil-gas-research/ucr>.
18. Small, M.J. et al., 2014. Risks and risk governance in unconventional shale gas development. *Environmental Science & Technology* 48, 8289–8297.
19. Jackson, R.B. et al., 2014. The environmental costs and benefits of fracking. *Annual Review of Environment and Resources* 39, 327–362.
20. Petersen, M.D. et al., 2015. *Incorporating Induced Seismicity in the 2014 United States National Seismic Hazard Model—Results of 2014 Workshop and Sensitivity Studies*, U.S. Geological Survey, Reston, VA.
21. Ellsworth, W.L., 2013. Injection-induced earthquakes. *Science* 341(6142), 1225942.
22. U.S. EPA, 2015. *Inventory of U.S. Greenhouse Gas Emissions and Sinks: 1990–2013*, U.S. Environmental Protection Agency, Washington, DC.
23. Moore, C. et al., 2014. Air impacts of increased natural gas acquisition, processing, and use: A critical review. *Environmental Science & Technology* 48(15), 8349–8359.
24. EIA, 2015. Crude oil proved reserves, Energy Information Administration, <http://www.eia.gov/cfapps/ipdbproject/iedindex3.cfm?tid=5&pid=57&aid=6>.
25. EIA, 2015. Oil and gas supply module, Energy Information Administration, <http://www.eia.gov/forecasts/aeo/assumptions/pdf/oilgas.pdf>.
26. U.S. GPO, 2011. *Deep Water: The Gulf Oil Disaster and the Future of Offshore Drilling*, National Commission on the BP Deepwater Horizon Oil Spill and Offshore Drilling, Washington, DC.
27. EIA, 2015. Crude oil production, Energy Information Administration, http://www.eia.gov/dnav/pet/pet_crd_crpdcn_adc_mbbbl_a.htm.
28. Robertson, C. and Krause, C., August 2, 2010. Gulf spill is largest of its kind, scientists say, *New York Times*.
29. Robertson, C., Perez-Pena, R., and Krause, C., July 2, 2015. BP to pay \$18.7 billion for Deep Water Horizon spill, *New York Times*.
30. EIA, 2015. Energy consumption by sector, Energy Information Administration, <http://www.eia.gov/totalenergy/data/annual/-consumption>.
31. DOE, 2015. Furnaces and boilers, U.S. Department of Energy, <http://energy.gov/energysaver/articles/furnaces-and-boilers>.
32. EPA, 2015. Waste heat to power systems, U.S. Environmental Protection Agency, https://www.epa.gov/sites/production/files/2015-07/documents/waste_heat_to_power_systems.pdf.
33. EPA, 2010. *Available and Emerging Technologies for Reducing Greenhouse Gas Emissions from Coal-Fired Electric Generating Units*. U.S. Environmental Protection Agency, Office of Air and Radiation, Research Triangle Park, NC.
34. EIA, 2015. Average operating heat rate for selected energy sources, Energy Information Administration, <http://www.eia.gov/electricity/annual/>.
35. EPA, 2014. *Carbon Pollution Emission Guidelines for Existing Stationary Sources: Electric Utility Generating Units; Proposed Rule*, U.S. Environmental Protection Agency, 79 FR 34830, Government Printing Office, Washington, DC.

36. EIA, 2015. Planned generating capacity changes, by energy source, Energy Information Administration, <http://www.eia.gov/electricity/annual/>.
37. EIA, 2015. Average tested heat rates by prime mover and energy source, 2007–2013, Energy Information Administration, http://www.eia.gov/electricity/annual/html/epa_08_02.html.
38. NETL, 2015. Simplified process flow diagram for the Tampa Electric IGCC plant, National Energy Technology Laboratory, U.S. Department of Energy, <http://www.netl.doe.gov/research/coal/energy-systems/gasification/gasifiedia/igcc-config>.
39. Anenberg, S.C. et al., 2010. An estimate of the global burden of anthropogenic ozone and fine particulate matter on premature human mortality using atmospheric modeling. *Environmental Health Perspectives* 118(9), 1189–1195.
40. EPA, 2015. National Emissions Inventory (NEI) air pollutant emissions trends data, U.S. Environmental Protection Agency, <http://www.epa.gov/ttnchie1/trends/>.
41. EIA, 2015. Primary energy overview, Energy Information Administration, <http://www.eia.gov/beta/MER/?tbl=T01.01 - /?f=A&start=1949&end=2014&charted=4-6-7-14>.
42. Lu, Z., Zhang, Q., and Streets, D.G., 2011. Sulfur dioxide and primary carbonaceous aerosol emissions in China and India, 1996–2010. *Atmospheric Chemistry and Physics* 11, 9839–9864.
43. EPA, 2015. Summary of coal unit controls, U.S. Environmental Protection Agency, <http://www.epa.gov/airmarkets/progress/datatrends/summary.html-three>.
44. Field, C.B. et al., 2014. *Climate Change 2014: Impacts, Adaptation, and Vulnerability. Part A: Global and Sectoral Aspects*. Contribution of Working Group II to the Fifth Assessment Report of the Intergovernmental Panel on Climate Change, Intergovernmental Panel on Climate Change, Cambridge University Press, Cambridge, UK.
45. Stocker, T.F. et al., 2013. *Climate Change 2013: The Physical Science Basis*. Working Group I Contribution to the Fifth Assessment Report of the Intergovernmental Panel on Climate Change, Intergovernmental Panel on Climate Change, Cambridge University Press, Cambridge, UK.
46. Schwietzke, S.S., Bruhwiler, L., Miller, J.B., Etiope, G., Dlugokencky, E., Englund-Michel, S., Arling, V., Vaughn, B., White, J., and Tans, P., 2016. Upward revision of global fossil fuel methane emissions based on isotope database. *Nature* 538, 88–91.
47. EPA, 2012. *Report to Congress on Black Carbon*. U.S. Environmental Protection Agency, <https://www3.epa.gov/airquality/blackcarbon/2012report/fullreport.pdf>.
48. IEA, 2015. *Energy and Climate Change*, International Energy Agency, Paris, France.
49. Brandt, A.R. and Farrell, A.E., 2007. Scraping the bottom of the barrel: Greenhouse gas emission consequences of a transition to low-quality and synthetic petroleum resources. *Climatic Change* 84, 241–263.
50. Weber, C.L. and Clavin, C., 2012. Life cycle carbon footprint of shale gas: Review of evidence and implications. *Environmental Science & Technology* 46(11), 5688–5695.
51. EPA, 2010. Air Markets Program data for 2010. U.S. Environmental Protection Agency, <http://ampd.ea.gov/ampd/%3E>.
52. Jaramillo, P., Griffin, W.M., and Matthews, H.S., 2007. Comparative life-cycle air emissions of coal, domestic natural gas, LNG, and SNG for electricity generation. *Environmental Science & Technology* 41(17), 6290–6296.
53. Edenhofer, O. et al., 2014. *Climate Change 2014: Mitigation of Climate Change*. Intergovernmental Panel on Climate Change, Working Group III, Cambridge University Press, Cambridge, UK.
54. McGlade, C. and Ekins, P., 2015. The geographical distribution of fossil fuels unused when limiting global warming to 2°C. *Nature* 517, 187–190.
55. EIA, 2017. Levelized cost and levelized avoided cost of new generation resources in the Annual Energy Outlook 2017. Energy Information Agency, https://www.eia.gov/outlooks/aeo/pdf/electricity_generation.pdf.
56. EPA, 2016. *Technical Support Document: Technical Update of the Social Cost of Carbon for Regulatory Impact Analysis under Executive Order 12866*, https://www.epa.gov/sites/production/files/2016-12/documents/sc_co2_tsd_august_2016.pdf.
57. Wong, K.V., 2012. *Thermodynamics for Engineers*, 2nd edn., CRC Press, Boca Raton, FL.



Taylor & Francis

Taylor & Francis Group

<http://taylorandfrancis.com>

Nuclear Energy

7.1 Introduction

The basic process used in today's nuclear power plants is the fission of heavy element nuclei. In this process, a carefully-controlled fission reaction generates heat to produce steam to power conventional turbines for electricity generation. An alternative nuclear reaction, fusion, is the same process by which the sun's radiation is generated. Its mechanism has been under investigation for a long time, but is not likely to reach commercial feasibility for many years to come. This chapter will therefore concentrate on the power derived from fission, which is a commercially available means of generating power that has been developed and employed for many years in several countries. In this type of nuclear reaction, a power source called a nuclear reactor captures the energy from the fission process as heat, which is then transferred to a working fluid that can be used to generate electricity, similar to the Rankine cycle in a coal-fired power plant. The primary fission fuel currently used in a majority of nuclear power plants is Uranium-235 (^{235}U)—an isotope of the element Uranium-238 (^{238}U). Uranium is a widely available element in the Earth's crust, and it occurs naturally as an ore containing about 99% ^{238}U and about 0.7% of the isotope ^{235}U in all natural uranium deposits. When ^{235}U is fissioned in a reactor, it provides about one megawatt day of energy for each gram of ^{235}U that is fissioned.

To understand the nuclear power option, it is necessary to consider the entire nuclear fuel cycle and not only the part of the cycle that occurs in the reactor. The cycle begins with mining of uranium—an ore can be processed or enriched to extract the isotope U^{235} that is used today in a majority of reactors producing electricity.

The enrichment process is the key to the use of uranium as a fuel in a power plant to generate heat for electricity generation. Once the uranium is enriched, it can be made into a form suitable for use in a power plant, usually small pellets that can be formed into fuel rods. After the fission process has been completed, the spent fuel can either be reprocessed or it has to be stored for eventual disposal. Radioactive waste is generated in any of the nuclear power cycles, and it must be safely disposed of. The storage and transportation of fissionable material is an important part of the fuel cycle and constitutes one of the critical steps susceptible to terrorist action.

The first nuclear reactor was Chicago Pile-1 (CP-1), developed under the direction of Enrico Fermi at the University of Chicago. It achieved criticality (continuous fission reaction) on December 2, 1942 [1]. The application of fissionable material for power production began at the end of World War II, when engineers who developed the atomic bomb realized that a controlled nuclear chain reaction could be used as a source of heat for generation of electricity. Electricity production from nuclear energy began in 1954. That year, the first

nuclear power plant generating heat from uranium was connected to the grid in the former USSR [2]. The world's first large-scale nuclear power plant was built in Pennsylvania and began operation in 1957. It was a Pressurized Water Reactor (PWR) capable of producing 231 megawatts of thermal energy and 68 megawatts of electric power. The PWR remains the most widely used nuclear power generation process.

There is worldwide debate on the contribution that nuclear energy will make toward a sustainable energy future. The contribution that nuclear energy will make in a future sustainable energy scenario will vary greatly depending upon the availability and cost of renewable resources. In countries such as Finland, South Korea, or Japan that do not have plentiful sustainable resources, nuclear power will likely be one of the main contributors of energy and power. Finland is currently building the largest nuclear electric power generator on an island near Helsinki [3,4], and Japan has restarted its nuclear power plant after careful safety reevaluation following the Fukushima nuclear disasters in 2011 [5]. On the other hand, for countries such as the United States or Brazil, which have plentiful renewable resources, these sources, rather than nuclear energy, are likely to be the main power source of the future, potentially with nuclear power continuing to provide some base load power.

Nuclear power plants are similar to coal-fired or natural gas power plants, except for the energy source, which is uranium. In 2016, there were 442 reactor units in operation worldwide contributing about 11% of the world's electric energy production [6]. The majority of reactors are located in the United States (99 units), France (58 units), Japan (43 units), and Russia (35 units), as shown in Figure 7.1.

There are at least 66, and possibly more, nuclear plants under construction, mainly in China, Russia, and India, as shown in Figure 7.2 [7].

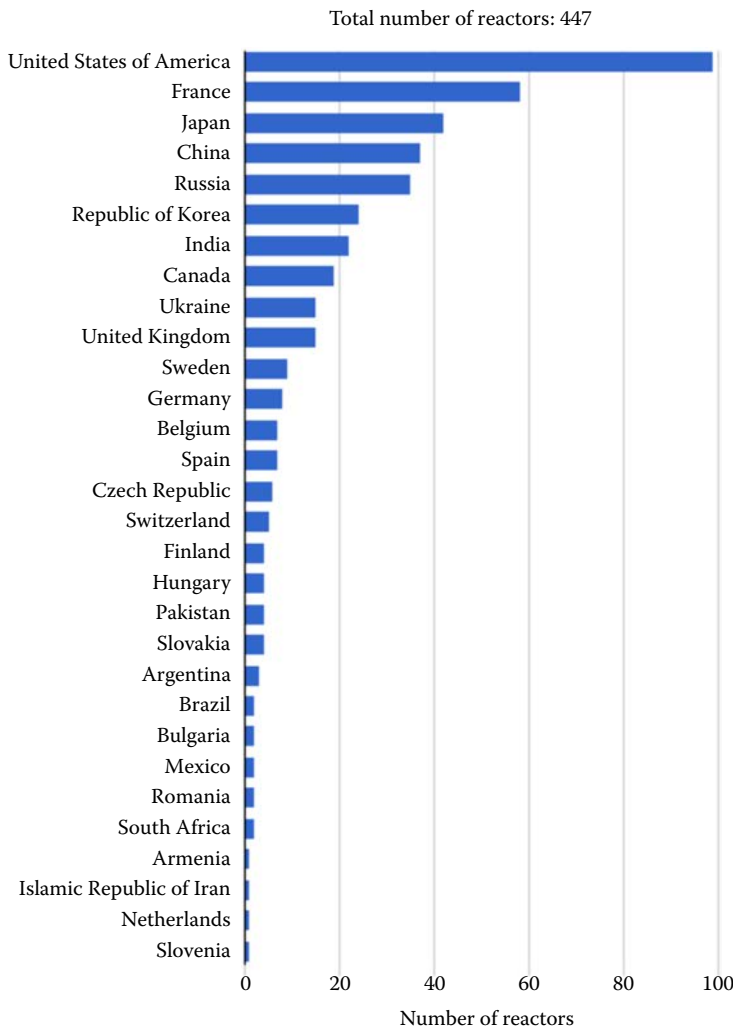
Of the five nuclear plants cited for the United States in Figure 7.2, one of them shown in the photo below (Figure 7.3) is the Tennessee Valley Authority's (TVA) Watts Bar Unit 2, which was connected to the power grid on June 3, 2016, becoming the first nuclear reactor unit in the United States to come online since 1996, when Watts Bar Unit 1 started operations. Watts Bar Unit 2 is undergoing final testing, producing electricity at incremental levels of power, as TVA prepares to start commercial operation later. The new reactor is designed to add 1,150 megawatts of electricity generating capacity to southeastern Tennessee [8].

Watts Bar Unit 2 is the first nuclear plant in the United States to meet new regulations from the U.S. Nuclear Regulatory Commission (NRC) that were established after the 2011 earthquake and tsunami that damaged the Fukushima Daiichi Nuclear Plant in Japan. After the NRC issued an operating license for the unit in October 2015, 193 new fuel assemblies were loaded into the reactor vessel the following month. TVA announced at the end of May 2016 that the reactor achieved its first sustained nuclear fission reaction.

In addition to Watts Bar 2, four other reactors are currently under construction: Vogtle Electric Generating Plant Units 3 and 4 in Georgia and Virgil C. Summer Nuclear Generating Station Units 2 and 3 in South Carolina. Table 7.1 shows the basic elements of these four plants [9].

It is important to note that most of the reactors in operation today are more than 30 years old. Many of them are currently operating under an extension of their original lifetime limit. The age distribution of operating reactors is shown in Figure 7.4 [10].

As a result of the age of these reactors, within the next 10 or 20 years, at least 150 will have to be shut down and replaced. Thus, at least 150 new reactors will have to be built before nuclear energy can make a net increase in contribution for global needs. The cost of construction and the initial energy investment for replacing these old reactors are

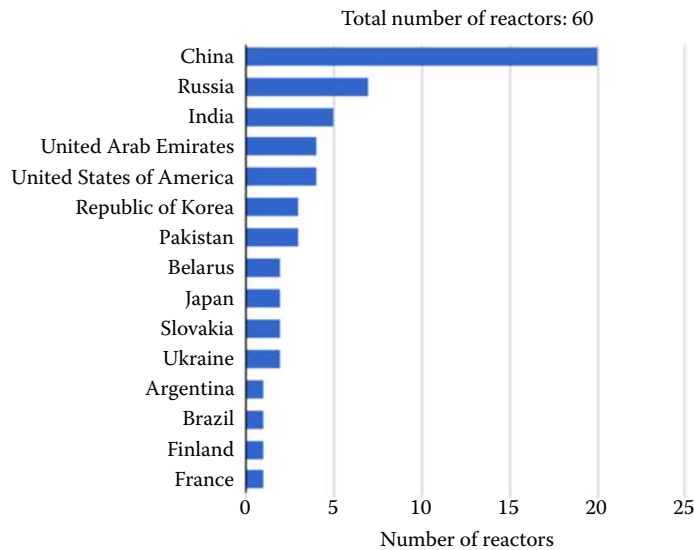
**FIGURE 7.1**

Number of reactors in operation, worldwide, as of April 2016. (From IAEA. Operational reactors by country, <https://www.iaea.org/PRIS/WorldStatistics/OperationalReactorsByCountry.aspx>. [6])

enormous. Because of today's high cost of new nuclear reactors in the United States (see Section 7.8), replacing the old reactors would require a huge initial investment.

7.2 Fission Mechanism

Whereas a conventional power station generates electricity by using the energy released from burning fossil fuels such as coal, a nuclear reactor converts the energy released by controlled nuclear fission into thermal energy for subsequent conversion to electric power. The fission mechanism involves a large fissile atomic nucleus such as Uranium-235

**FIGURE 7.2**

Number of reactors under construction, as of April 2016. (From IAEA. Under construction reactors by country, <https://www.iaea.org/PRIS/WorldStatistics/UnderConstructionReactorsByCountry.aspx>. [7])

or Plutonium-239, absorbing a neutron. In the fission process, the heavy nucleus splits as a result of the impact with a neutron into two or more lighter nuclei called the fission products, releasing kinetic energy, gamma rays, and free neutrons in the process. Some of these neutrons may subsequently be absorbed by other fissile atoms and trigger additional fission events. In fission reactors, the release of these neutrons results in what is known as a chain reaction.

To sustain this chain reaction, and prevent a dangerous runaway, it is controlled by a combination of a moderator that slows the neutrons to increase their capture from one fuel rod to another and thus enhance fission and control rods that move in and out of the reactor

**FIGURE 7.3**

Watts Bar Nuclear Generating Site. Republished with permission from the Tennessee Valley Authority.

TABLE 7.1

US Nuclear Power Reactors Under Construction

Site	Technology	MWe Gross	Proponent/Utility	Construction Start	Loan Guarantee; Start Operation
Vogtle 3, GA	Westinghouse AP1000	1250 (1117 net)	Southern Nuclear Operating Company	March 2013	Has loan guarantee; late 2019
Vogtle 4, GA	Westinghouse AP1000	1250 (1117 net)	Southern Nuclear Operating Company	Nov 2013	Has loan guarantee; mid- 2020
V.C. Summer 2, SC	Westinghouse AP1000	1250 (1117 net)	South Carolina Electric & Gas	March 2013	Shortlist loan guarantee; Apr 2020
V.C. Summer 3, SC	AP1000	1250 (1117 net)	South Carolina Electric & Gas	Nov 2013	Shortlist loan guarantee; Dec 2020
Subtotal under construction: 4 units (5000 MWe gross, 4468 MWe net)					

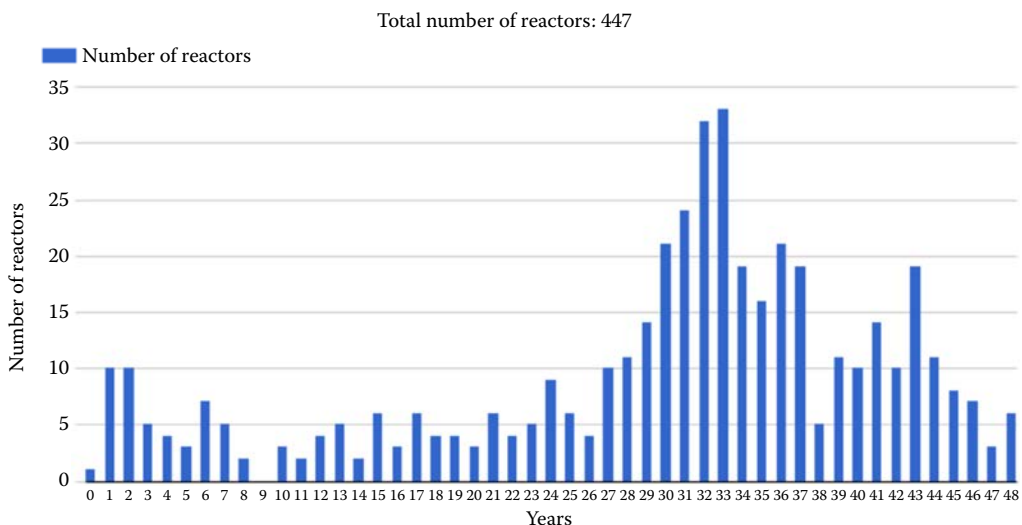
Source: From World Nuclear Association. USA nuclear power, <http://www.world-nuclear.org/information-library/country-profiles/countries-t-z/usa-nuclear-power.aspx>. [9]

Note: On July 31, 2017, South Carolina Electric & Gas and Santee Cooper announced that they were halting construction of the two V.C. Summer reactors due to high costs.

core consisting of boron or other materials that absorb neutrons and thus reduce fission. In a nuclear reactor, safety is assured by automatic and manual systems to shut down the fission reaction when a monitoring device indicates a potentially unsafe condition. Commonly used moderators include regular or light water used in three-quarters of the existing reactors, solid graphite, or heavy water. Water also serves as a coolant and heat transfer medium. Breeder reactors, which operate with fast neutrons, have used liquid metals as a coolant, but none of that type is currently in commercial use.

A reactor core generates heat in three principle ways:

- Kinetic energy of fission products is converted to thermal energy when these nuclei collide with atoms in the vicinity.

**FIGURE 7.4**

Number of nuclear reactors worldwide by age, as of April 2016. (From IAEA. Power Reactor Information System, Operational by age, Vienna, Austria, <https://www.iaea.org/PRIS/WorldStatistics/OperationalByAge.aspx>. [10])

- The reactor absorbs some of the gamma rays produced during fission and converts their energy into heat.
- Heat is produced by the radioactive decay of fission products that have been energized by neutron absorption. This type of heat generation continues even after a reactor is shut down.

The reason nuclear energy is attractive, from technical and environmental perspectives, is because in a nuclear process, 1 kg of uranium releases approximately three million times as much energy as a kilogram of coal burned in conventional combustion. In other words, a nuclear reaction releases 7×10^{13} J/kg of U_{235} compared to 2.4×10^7 J/kg in the burning of coal. Furthermore, the fuel can be reprocessed and used for additional power production.

Protons and neutrons are the basic building blocks of nuclear matter. The sum of the individual masses of each of these subatomic particles that make up a given element will yield a greater mass than the mass of the nucleus. The energy difference is known as the nuclear binding energy, which is the energy necessary to maintain the position of the protons and neutrons. The energy released during fission is the source of nuclear power.

In the fission process, a nucleus splits into two fragments called the fission products, as shown in Figure 7.5 [11]. Each of these is about equal to half the original mass; in addition two or more neutrons are emitted. The sum of the masses of the fission products is slightly less than the original mass, as a result of the release of the binding energy. This difference in mass (about 0.1% of the original mass), has been converted into energy in accordance with Einstein's famous equation, which states that energy and mass are equivalent:

$$E = mc^2 \quad (7.1)$$

where c is the speed of light.

When the emitted neutrons collide with neighboring nuclei, and induce additional fission, a self-sustaining series of nuclear fission reactions, known as a chain reaction, can occur.

The fission of ^{235}U releases two or three neutrons. If these neutrons are absorbed by other ^{235}U nuclei, these neutrons induce more fission reactions and the rate of these reactions increases geometrically, as shown in Figure 7.6 [12].

An example of one of the fission processes that occurs is as follows [13]:

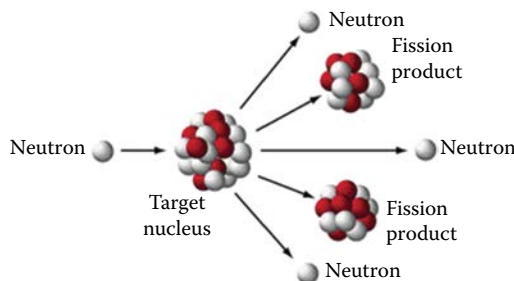
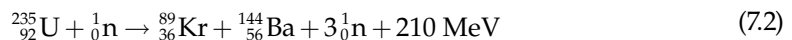


FIGURE 7.5

Typical fission reaction. (From Atomic Archive. Nuclear fission: Basics, <http://www.atomicarchive.com/Fission/Fission1.shtml>. [11])

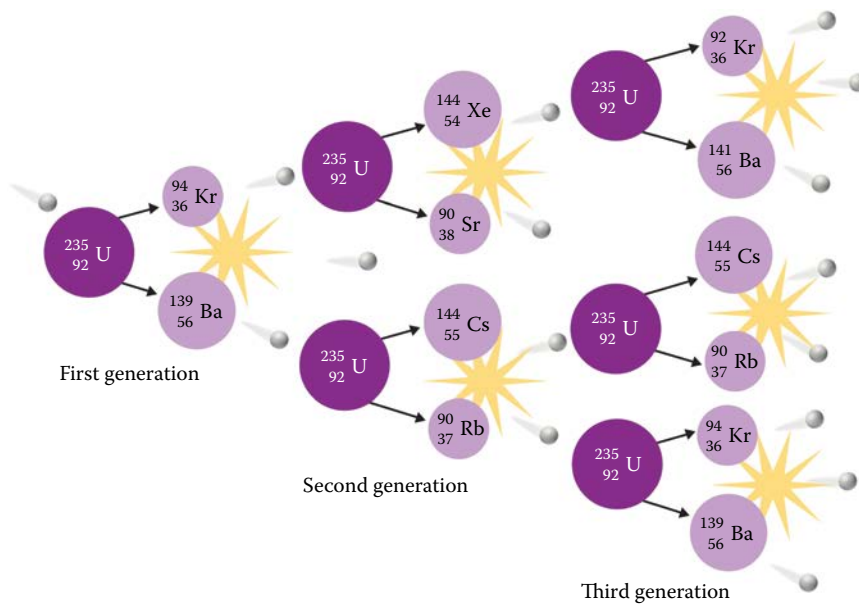


FIGURE 7.6
Schematic of the start of a typical chain reaction. (From Shutterstock Image No. 73672591. [12])

It has been found experimentally that some minimum mass of a fissile isotope is necessary to sustain such a chain reaction. This minimum mass able to support a sustained fission is called the critical mass. The amount of mass required to be critical depends on the purity of the material and its shape.

7.3 Available Nuclear Resources

7.3.1 Uranium Resources

Uranium is a naturally-occurring element in the Earth's crust. Uranium mines operate in more than 20 countries, but half of the world's production comes from mines in six countries: Canada, Australia, Niger, Kazakhstan, Russia, and Namibia.

In conventional mines, the ore is passed through a mill where it is crushed. In the next step, it is ground in water to produce a slurry of fine ore particles. The slurry is leached with sulfuric acid to dissolve the uranium oxide. This leaves the remaining rock and other material undissolved as mine tailings. Recently, however, a different method has been used in mining, called *in situ* leaching. In this process, the mining is accomplished without any major disturbance of the environment. First, groundwater with a lot of oxygen is injected into the ore. The water is then circulated through the mine and uranium is dissolved. The solution with its dissolved uranium is then pumped to the surface for further processing. Both mining methods produce a liquid, which is filtered with the uranium and subsequently separated by means of ion exchange. The filtered and dried product is uranium oxide, which is then placed into drums and sealed. Since the concentrate has a bright yellow color, the product is usually called "yellow cake."

Available resources of uranium are divided into two groups: reasonably assured resources (RAR), and inferred resources (IR). RAR are the uranium in known deposits of sufficient size, grade, and configuration that it could be recovered within reasonable production costs with currently available mining and processing technology. IR are inferred resources whose availability is uncertain. The categories are further divided into various cost classes according to estimated extraction costs. The division of these classes into below \$50/kg, below \$80/kg, and below \$130/kg is widely accepted. According to some experts, RAR for less than \$80/kg uranium are called proven resources. It is estimated that of this type, about 2.6 million tons are available globally. When used in light-water reactors, this corresponds to an energy equivalent of 28 billion tons of hard coal. Table 7.2 shows the deposits of uranium and the various countries in which they are located [14]. If mining costs up to \$130/kg are included, the global uranium sources are increased to 3.3 million tons. The total, irrespective of costs, may be as high as 15 million tons. The amount of energy that can be extracted from these uranium resources depends upon whether or not spent fuel from light-water reactors can be reprocessed. Reprocessing all of the spent fuels from light-water reactors and recycling the uranium and plutonium in mixed oxide (MOX) fuel to operate light-water reactors with 30% MOX and 70% uranium would lead to a cumulative savings of some 600,000 tons of natural uranium in the next 40 years. However, current legislation in the United States forbids reprocessing because it produces plutonium which could be used to make a nuclear bomb.

TABLE 7.2

Known Recoverable Resources of Uranium, 2015

	Tons U	Percentage of World
Australia	1,664,100	29%
Kazakhstan	745,300	13%
Canada	509,000	9%
Russian Fed	507,800	9%
South Africa	322,400	6%
Niger	291,500	5%
Brazil	276,800	5%
China	272,500	5%
Namibia	267,000	5%
Mongolia	141,500	2%
Uzbekistan	130,100	2%
Ukraine	115,800	2%
Botswana	73,500	1%
USA	62,900	1%
Tanzania	58,100	1%
Jordan	47,700	1%
Other	232,400	4%
World total	5,718,400	

Source: From World Nuclear Association. Supply of uranium, <http://www.world-nuclear.org/information-library/nuclear-fuel-cycle/uranium-resources/supply-of-uranium.aspx>. [14]

7.3.2 Plutonium

According to the World Nuclear Association, about one third of the energy produced in nuclear power plants comes from plutonium. Plutonium is created as a by-product in a uranium-type of nuclear type of reactor. Plutonium is recovered by reprocessing of uranium reactor fuel and is recycled as mixed oxide fuel usually called MOX. When a typical 1000 MW_e nuclear power reactor is operating, it contains within its uranium fuel-load several hundred kilograms of plutonium [15].

There are in practice two different kinds of plutonium: reactor-grade and weapons-grade. The first is recovered as a by-product of typical fuel from a nuclear reactor after the fuel has been irradiated or burned for about 3 years. Weapons-grade plutonium requires a specialized plutonium production reactor and cannot be produced in a commercial-type of electric power producing uranium reactor. Plutonium is a valuable energy source when integrated into the nuclear fuel cycle. In a conventional nuclear reactor, one kilogram of the isotope ²³⁹Pu can produce sufficient heat to generate nearly 8 million kilowatt hours of electricity.

Plutonium has a number of isotopes differing in the number of neutrons in the nucleus. All of these isotopes are fissionable with fast neutrons, but only two of them are fissile with slow neutrons, ²³⁹Pu and ²⁴¹Pu. ²³⁹Pu plays a major role in a conventional light-water power reactor. It is formed by neutron capture in ²³⁸U followed by beta decay. It yields much the same amount of energy as the fission of ²³⁵U. A 1000 mega-watt electric light-water reactor produces about 25 tons of used fuel per year containing as much as 290 kg of plutonium. It can be used as a direct substitute for ²³⁵U with ²³⁹Pu being the main fissile part and ²⁴¹Pu contributing a minor amount of energy. In order to extract plutonium for recycling, the used fuel is reprocessed and the recovered plutonium oxide is mixed with uranium oxide to produce MOX which contains about 8% ²³⁹Pu.

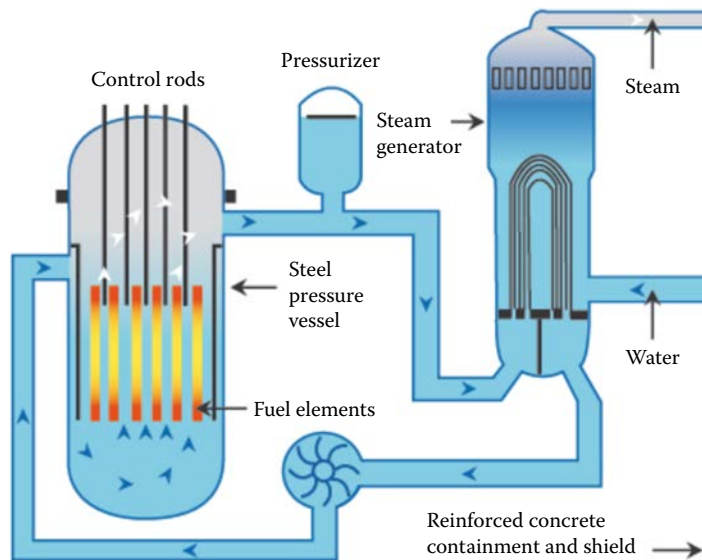
Although not significant in the world's electricity production, the decay heat of the isotope ²³⁸Pu can be used as an electricity source. It produces about 0.56 W/g and is used in some cardiac pacemakers, space satellites, and navigation beacons. Plutonium has also powered some 30 U.S. space vehicles and enabled spacecraft to send back photos of distant planets [16].

7.4 Reactor Types

7.4.1 Pressurized-Water Reactors (PWRs)

The basic element of a PWR generating electricity is shown in Figure 7.7 [17]. It consists of a reactor core contained within a pressure vessel and is cooled by light water under high pressure. The core of the plant contains uranium dioxide fuel pellets enclosed in zircaloy rods that are held together in fuel assemblies. Depending upon the reactor size, there are 200–300 rods in an assembly, and 100–200 fuel assemblies in the reactor core. The rods are arranged vertically and contain as much as 80–100 tons of enriched uranium.

The working fluid in a PWR is pressurized water at 315°C circulated through the steam generators. The steam generator is a typical tubular heat exchanger with the hot water circulating inside the tube. The steam generator separates the reactor cooling water, which is radioactive, from the steam that is taken outside the nuclear reactor to a conventional

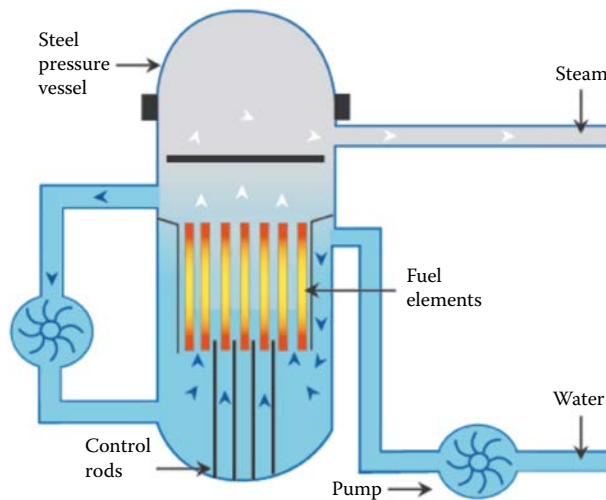
**FIGURE 7.7**

Sketch of a typical PWR power plant. (From World Nuclear Association. Nuclear power reactors, <http://www.world-nuclear.org/information-library/nuclear-fuel-cycle/nuclear-power-reactors/nuclear-power-reactors.aspx>. [17])

turbine. This turbine generates electricity. The pressure vessel contains the reactor core and the steam generators and is located inside the containment structure, which is designed to isolate the radioactive part of the system from the turbine and condenser. The part of the system outside the reactor is an ordinary Rankine cycle steam power plant isolated from the reactor that contains all the radioactive elements in the cycle. The condenser cooling water is usually circulated to a cooling tower, where it is cooled by evaporation. In places where water is scarce, the condenser can also be cooled by air, but this type of design is less efficient. The pressurized water reactor design is widely considered to be the safest type of nuclear power plant and constitutes the largest number of reactors used to generate electricity worldwide. Almost all of the nuclear power plants built since 2008 and those currently under construction are of the PWR type, with sizes ranging up to 1,600 MW_e capacity.

7.4.2 Boiling Water Reactors (BWRs)

A boiling reactor schematic, as shown in Figure 7.8, consists of a reactor core located inside a reactor vessel that is cooled by circulating light water [17]. The BWRs range in size from 400 to 1200 MWe. BWRs are the second largest reactor type used for generating electricity. In a BWR, the cooling water is heated to 285°C in the reactor vessel, and the resulting steam is sent directly to a turbine outside the pressurized container. There is no intermediate loop in a BWR, as there is in the PWR, and the system is therefore somewhat simpler than the PWR because it does not need an intermediate heat exchanger. The steam from the turbine is condensed in a heat exchanger using outside cooling water and then returned into the reactor vessel. The system operates also on a Rankine cycle with the heat source inside the steel pressure vessel, as shown. BWRs depend on careful control of the boiling process to avoid any pockets of steam forming inside the pressurized containers [1].

**FIGURE 7.8**

Sketch of a typical BWR power plant. (From World Nuclear Association. Nuclear power reactors, <http://www.world-nuclear.org/information-library/nuclear-fuel-cycle/nuclear-power-reactors/nuclear-power-reactors.aspx>. [17])

7.4.3 Heavy Water Cooled and Moderated Reactor

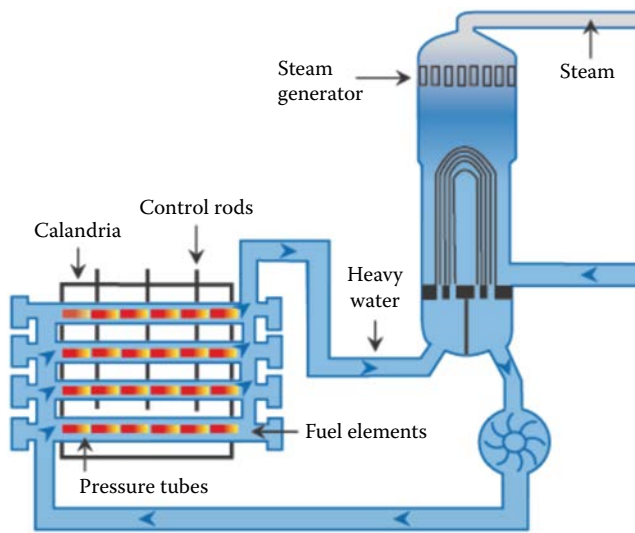
Heavy-water moderated reactors, called the CANDU reactors, were designed and built in Canada. The advantage of the CANDU reactor is that it uses unenriched uranium dioxide, which is held in zirconium alloy cans loaded into horizontal zirconium alloy tubes. Heavy water serves as the moderator as it is pumped through the tubes under high pressure to prevent boiling and cool the fuel. The water is then passed through a steam generator to raise steam from ordinary light water. This design requires additional moderation, which is achieved by immersing the tubes in an unpressurized container called a calandria, a device containing more heavy water. By inserting or withdrawing cadmium rods from the calandria, the nuclear reaction is controlled. The entire assembly is placed inside a concrete shield and containment vessel, as shown in Figure 7.9 [17].

7.5 Nuclear Waste Management and Disposal

There are four types of radioactive waste emanating from the fuel cycle. The first type is the naturally-occurring radioactive materials in the uranium ore during mining. The decay of these materials produces radon, which can be contained by covering the tailings with clay. Technically, these mine tailings are not classified as nuclear waste.

Low Level Waste (LLW) is generated by medical and industrial uses as well as by the nuclear fuel cycle. The radioactivity from such wastes comes from affected paper, clothing, and soils. They are short-lived and are suitable for shallow-land burial. The volume of these materials can be reduced by compacting and incineration prior to their disposal. These wastes make up about 90% of the total waste, but contain only about 1% of its radioactivity.

Intermediate Level Wastes (ILW) are generated during the operation of reactors as well as in the reprocessing of spent fuel and the decommissioning of nuclear power plants. These

**FIGURE 7.9**

Sketch of a typical CANDU reactor power station. (From World Nuclear Association, Nuclear power reactors, <http://www.world-nuclear.org/information-library/nuclear-fuel-cycle/nuclear-power-reactors/nuclear-power-reactors.aspx>. [17])

materials contain higher amounts of radioactivity and are generally made-up of resins, chemical sludges, fuel cladding, and contaminated material from decommissioning. Some of these wastes are processed before disposal by solidifying them in concrete. ILW make up about 7% of the volume and have about 4% of the radioactivity of the total radioactive wastes.

The fourth and largest radioactive waste component is High Level Waste (HLW) generated during the operation of a nuclear reactor. This waste consists of fission product and transuranic elements generated during fission. This material is not only highly radioactive, but also thermally hot so that it must be both shielded and cooled. It contains 95% of the radioactivity produced by nuclear power generation. HLW will eventually have to be disposed in deep geological facilities to allow its decomposition safely over time. Several countries have selected sites for these facilities. But, in the United States, there does not, at this point, exist a High Level Waste depository.

In 1987, Yucca Mountain was designated by the Nuclear Waste Policy Act Amendments to be the long-term storage site for High Level Radioactive Waste. Yucca Mountain is a deep geological storage location located on federal land adjacent to the Nevada Nuclear Test Site, about 130 km northwest of Las Vegas [18]. The project was approved in 2002 by the U.S. Congress, but funding was ended in 2011 for political, not for technical or for safety, reasons according to the Government Accountability Office [19]. Consequently, there are many thousands of tons of spent fuel in temporary storage, mostly at reactor sites in the United States. In countries where spent fuel is reprocessed, the uranium and plutonium are first removed during reprocessing, and then the much smaller volume of remaining HLW is solidified using a vitrification process. In this process, the fission products are mixed in glass materials, vitrified in stainless steel canisters, and finally stored in shielded facilities for later permanent disposal. The disposal process is still one of the unresolved issues regarding the wide-scale use of nuclear power. Table 7.3 presents a summary of current waste management processes adopted by countries throughout the world [20].

TABLE 7.3**Waste Management for Used Fuel and HLW from Nuclear Power Reactors**

Country	Policy	Facilities and Progress Toward Final Repositories
Belgium	Reprocessing	<ul style="list-style-type: none"> Central waste storage at Dessel Underground laboratory established 1984 at Mol Construction of repository to begin about 2035
Canada	Direct Disposal	<ul style="list-style-type: none"> Nuclear Waste Management Organisation set up 2002 Deep geological repository confirmed as policy, retrievable Repository site search from 2009, planned for use 2025
China	Reprocessing	<ul style="list-style-type: none"> Central used fuel storage at LanZhou Repository site selection to be completed by 2020 Underground research laboratory from 2020, disposal from 2050
Finland	Direct Disposal	<ul style="list-style-type: none"> Program start 1983, two used fuel storages in operation Posiva Oy set up 1995 to implement deep geological disposal Underground research laboratory Onkalo under construction Repository planned from this, near Olkiluoto, open in 2020
France	Reprocessing	<ul style="list-style-type: none"> Underground rock laboratories in clay and granite Parliamentary confirmation in 2006 of deep geological disposal, containers to be retrievable and policy “reversible” Bure clay deposit is likely repository site to be licensed 2015, operating 2025
Germany	Reprocessing but moving to direct disposal	<ul style="list-style-type: none"> Repository planning started 1973 Used fuel storage at Ahaus and Gorleben salt dome Geological repository may be operational at Gorleben after 2025
India	Reprocessing	<ul style="list-style-type: none"> Research on deep geological disposal for HLW
Japan	Reprocessing	<ul style="list-style-type: none"> Underground laboratory at Mizunami in granite since 1996 Used fuel and HLW storage facility at Rokkasho since 1995 Used fuel storage under construction at Mutsu, start up 2013 NUMO set up 2000, site selection for deep geological repository under way to 2025, operation from 2035, retrievable
Russia	Reprocessing	<ul style="list-style-type: none"> Underground laboratory in granite or gneiss in Krasnoyarsk region from 2015, may evolve into repository Sites for final repository under investigation on Kola peninsula Pool storage for used VVER-1000 fuel at Zheleznogorsk since 1985 Dry storage for used RBMK and other fuel at Zheleznogorsk from 2012 Various interim storage facilities in operation
South Korea	Direct Disposal, maybe change	<ul style="list-style-type: none"> Waste program confirmed 1998, KRWM set up 2009 Central interim storage planned from 2016
Spain	Direct Disposal	<ul style="list-style-type: none"> ENRESA established 1984, its plan accepted 1999 Central interim storage at Villar de Canas from 2016 (volunteered location) Research on deep geological disposal, decision after 2010
Sweden	Direct Disposal	<ul style="list-style-type: none"> Central used fuel storage facility—CLAB—in operation since 1985 Underground research laboratory at Aspo for HLW repository Osthammar site selected for repository (volunteered location)
Switzerland	Reprocessing	<ul style="list-style-type: none"> Central interim storage for HLW and used fuel at ZZL Wurenlingen since 2001 Smaller used fuel storage at Beznau Underground research laboratory for high-level waste repository at Grimsel since 1983 Deep repository by 2020, containers to be retrievable

(Continued)

TABLE 7.3 (Continued)

Waste Management for Used Fuel and HLW from Nuclear Power Reactors

Country	Policy	Facilities and Progress Toward Final Repositories
United Kingdom	Reprocessing	<ul style="list-style-type: none"> • Low-level waste repository in operation since 1959 • HLW from reprocessing is vitrified and stored at Sellafield • Repository location to be on basis of community agreement • New NDA subsidiary to progress geological disposal
United States	Direct Disposal	<ul style="list-style-type: none"> • DoE responsible for used fuel from 1998, accumulated \$32 billion waste fund • Considerable research and development on repository in welded tuffs at Yucca Mountain, Nevada • The 2002 Congress decision that geological repository be at Yucca Mountain was countered politically in 2009 • Central interim storage for used fuel now likely

Source: From World Nuclear Association. Radioactive waste management, <http://www.world-nuclear.org/information-library/nuclear-fuel-cycle/nuclear-wastes/radioactive-waste-management.aspx>. [20]

Radioactive wastes are produced during any reactor fuel cycle. The cost of managing these wastes must be included in the economics and are a part of the electricity costs. Radioactive materials decay with time, and each radioactive isotope has a half-life, which is the time it takes for half of the material to decay away. Eventually, these materials decay to a stable, nonradioactive form, but this may take a very long time. Hence, the process of managing radioactive waste requires the protection of people from the harmful effects of radiation. The long-lived radioactive materials emit alpha and beta particles. It is relatively easy to shield humans from this type of radiation, but ingesting alpha or beta radiation can be harmful.

7.6 Spent Fuel Storage and Reprocessing

Spent fuel is routinely discharged from operating nuclear reactors. As it is discharged, it is moved to specially designed storage pools of ordinary water, which are an integral part of a nuclear power plant. These storage pools hold fuel from many years of operation, and the heat produced from the spent fuel is removed by circulating cooling water through the pool. The spent fuel capacity of many older reactors is reaching its capacity of on-site storage. At this point, the fuel must be transferred to dry storage, which takes place in large metal or concrete storage facilities. These dry storage facilities can be passively cooled by circulating air around them, but eventually, a final storage for radioactive waste is required.

Reprocessing is the recovery of plutonium from the spent fuel of a nuclear reactor. It extends the amount of energy retrievable from the original uranium by approximately 30%–40%. The process currently used for reprocessing is called PUREX. To reprocess the spent fuel from light-water reactors, the spent fuel is first dissolved in nitric acid and the acid solution is then mixed with an organic solvent consisting of tributyl phosphate in a concrete container. The uranium and plutonium are extracted in this organic phase and the fission products remain in the aqueous phase. Additional processing permits the separation of uranium and plutonium. PUREX has been used successfully for many years by all the countries that reprocess spent fuel.

7.7 Nuclear Power Plant Accidents

The first serious nuclear power plant accident occurred at Three Mile Island, Pennsylvania, in 1979. The accident was the worst in the history of the U.S. commercial power industry. Mechanical problems and human error caused loss of coolant water, which led to a partial nuclear meltdown and the release of some radioactive gases. Orders for new nuclear power plants were cancelled after the accident, and public sentiment shifted to concern about safety and issues of nuclear waste disposal.

On April 26, 1986, a catastrophic accident at the Chernobyl Nuclear Power Plant, Ukraine, involved a massive explosion and fire that released large amounts of radioactive contamination across the USSR and Europe. 350,000 people were evacuated and permanently resettled from the most highly contaminated areas of Belarus and Ukraine. The accident killed 31 plant workers and caused a further 64 deaths from radiation, mostly among emergency and plant workers. Over 300,000 people were relocated and an estimated 400,000 children contracted thyroid cancers [21]. The Chernobyl disaster has been the most devastating nuclear accident, in terms of released radioactivity; about an order of magnitude worse than Fukushima.

On March 11, 2011, a massive 9.0 magnitude earthquake struck 109 miles from Fukushima in the Pacific Ocean. The tsunami that followed breached the safety wall that had been built to protect the nuclear reactors at the Fukushima Daiichi nuclear power plant and flooded the pumps necessary for cooling the reactor rods. The 4.7 GWE (gigawatt electric) Fukushima Daiichi Nuclear Plant consists of six reactor units designed by General Electric [22]. All of the reactors came online between 1970 and 1979, which makes them all more than 30 years old. The reactors were of the boiling water type. The number one reactor was slated to be shut down in 2011, but was granted a 10-year extension by Japanese regulators in 2009, although reactor risks had been foretold earlier.

Three of the units at Fukushima Daiichi Nuclear Power Plant had been shut down prior to the earthquake for maintenance, and the other three reactors shut down automatically after the earthquake, with the remaining decay heat of the fuel rods being cooled with power from emergency generators. The 5.7 m tsunami wall was breached by waves reaching heights of 14 m. The tsunami not only destroyed the primary cooling system, but also disabled the emergency diesel generators that are required to provide power to the pumps used to cool the reactor core in case of primary system failure. In the following 3 weeks, there was evidence of partial nuclear meltdowns in Units 1, 2, and 3, visible explosions believed to be caused by hydrogen gas in Units 1 and 3, and a suspected explosion in Unit 2 that may have damaged the primary containment vessel. Also, due to a loss of water in the pools used to store the spent fuel rods for three of the reactors, some of the rods were uncovered and heated up beyond the safe limit.

Although the events leading up to the nuclear disaster at Fukushima were not the direct result of shortcomings in the nuclear plant operations, they did highlight the vulnerability of nuclear power plants to natural disasters. In response to concerns in the United States about the safety of its own nuclear power plants, the Nuclear Regulatory Commission prepared a report outlining the changes in safety precautions recommended for nuclear power plants [22]. The NRC recommended that nuclear facility operating licenses should be denied unless the operators can demonstrate the ability to deal with a complete loss of power for 8 hours using backup generators, and be able to provide cooling to the radioactive core and spent fuel rods in a water pool for at least 72 hours. The pump failures at Fukushima also caused ignition of tightly packed spent fuel rods stored in cooling water

ponds and caused the water to evaporate after the pumps failed. Spent fuel rods generate heat for many years' time after they are removed from the reactor. This is important for overall safety because the rods in Japan were even less tightly packed than the fuel rods in cooling ponds in the United States. As a precaution to a cooling water accident in the United States, the recommendations from the NRC include requirements for dry storage of the fuel rods after no more than 5 years in a cooling pond. All of these measures will make nuclear reactors safer but also increase the cost of nuclear power in the United States.

7.8 Current Status and Cost of Nuclear Technology

Nuclear power is an important worldwide resource for generating electricity. As shown in this chapter, a large fraction of electric power is generated from nuclear sources worldwide and at least 66 reactors are currently under construction. The global amount of nuclear fuel available is enormous, and many countries are planning their energy future around a nuclear electric generation base. Countries such as Japan, South Korea, and Finland, which have no large sustainable resources, may depend on nuclear sources for their future energy needs. However, in countries such as the United States and Brazil, which have large renewable resources, economic and political considerations will determine the mix of renewable technologies and nuclear power.

But the ability of nuclear reactors to produce electricity without generating greenhouse gases has revitalized interest in nuclear power. Many lessons have been learned from the operation of current power plants that have improved the safety of new designs. This, coupled with the designs to develop new energy sources and a diversity of energy options, has resulted in continuing research and development for a new generation of nuclear plants.

Capital cost estimates by Lazard for new U.S. nuclear plants [23] range from \$5400 to \$8650 per megawatt. Levelized costs of electricity range from \$85 to \$136/MWh. These costs are considerably higher than the current costs of wind and solar photovoltaic power, which are still dropping. Although nuclear power plants provide base load power, operate at high capacity factors (92.2%), and avoid carbon emissions, many observers believe their high cost compared to other carbon-free energy alternatives is the biggest obstacle to growth of the U.S. nuclear industry.

7.9 Next-Generation Nuclear Technologies

The development of nuclear power has undergone four general phases. The initial development of prototype reactor designs (Generation I) occurred in the 1950s and 1960s. Development and deployment of large commercial plants (Generation II) took place in the 1970s and 1980s, when over 100 nuclear power plants were built and deployed in the United States. The development of advanced light-water reactors (Generation III) is an ongoing effort to overcome problems inherent in the large (over 1000 megawatt) nuclear reactors in operation. The fourth phase of nuclear reactor development, known as Generation IV technologies, consists of a number of ideas proposed for more economical and safer nuclear power designs.

Generation II nuclear reactors have effectively demonstrated the viability of nuclear power all over the world. But future development and deployment in the United States faces several challenges that must be overcome for nuclear power to achieve its potential. These challenges include (1) public concerns about safety, (2) high capital cost and complications associated with the construction of new plants, (3) the long time required for construction associated with licensing, (4) concerns about disposal of nuclear waste, and (5) potential for terrorists acquiring material for nuclear weapons. However, since nuclear power plants do not emit pollutants that cause global warming, their increased use in the future is considered by many to be an important part of a low-carbon energy strategy.

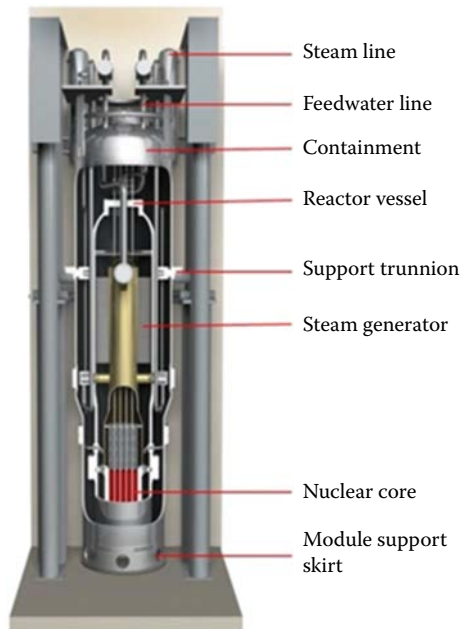
Generation III's key objective is to use modern manufacturing technology with advanced safety systems to develop small (under 300 megawatt electric) or medium-sized light-water power reactors. Medium size is defined as up to seven hundred megawatt electric, according to the IAEA International Atomic Energy Agency. The reason for developing these types of reactors in the United States are: (1) Smaller reactors can be produced in a factory and moved as a single unit to be installed. This would shorten the time of construction and reduce the cost. (2) If larger power stations were needed in the future, they could be made up of multiple small units in accordance with demand. Current large-scale units often produce more electricity than needed and require long transmission lines. (3) Smaller reactors can serve remote areas and thus reduce transmission costs. (4) Smaller reactors can be operated with passive safety systems, which would avoid the possibility of the kind of accidents that concern the public, for example, Three Mile Island.

Several small modular reactor (SMR) designs are currently being developed by private industry with the cooperation of the U.S. Nuclear Regulatory Commission (USNRC). The thermodynamic power cycle of the SMR plants is essentially the same as that described previously in this chapter for large-scale light-water units. Many of the detailed features for the SMRs, however, are proprietary. The SMR designers who have been interacting with the USNRC are mPower, NuScale, and Westinghouse [24,25,26]. They have many features in common and the NuScale design described below is typical. NuScale claims at this time to be the most advanced SMR and the USNRC approved on December 31, 2016, the SMR Commercial-type power plant design. This is the first-ever SMR reactor Design Certification Application (DCA) submitted to NRC, and it is claimed to be an affordable, clean, reliable, scalable, and zero-carbon emitting energy source, which could be deployed worldwide.

Figure 7.10 shows the key features of the NuScale SMR design. It is an integral pressurized light-water reactor based on the MASLWR (Multi-Application Small Light-Water Reactor) design developed at Oregon State University in the early 2000s. It is a natural circulation reactor with the core and helical coil steam generator located in a common reactor vessel placed in a cylindrical steel container. The reactor vessel/containment module is submerged in water in the reactor building safety pool. Thus, in case of an accident, the safety cooling system operates by natural convection without the need of electric power. The entire reactor building is located below ground with the reactor building designed to hold up to 12 SMRs. Each of the reactors has a rated thermal output of 160 MW thermal and electrical output of 50 MW electric. A complete complement of 12 SMRs would thus have a total capacity of approximately 600 MW electric.

The First Commercial 12-module NuScale is planned to be built on the site of the Idaho National Laboratory, and will be owned by the Utah Associated Municipal Power System and run by the Energy Northwest as the nuclear operator.

The development of Generation IV systems is an international effort initiated by the U.S. Department of Energy in 2001, with participation from 13 members: United States, Argentina, Brazil, Canada, China, France, Japan, Russia, South Korea, South Africa,

**FIGURE 7.10**

Key features in the NuScale SMR design. (From NRC. BWXT mPower, <https://www.nrc.gov/reactors/advanced/nuscale.html>. [25])

Switzerland, and the United Kingdom, along with the EU (Euratom), entitled Generation IV International Forum (GIF) [27]. The goal of GIF is to identify the most promising reactor concepts, referred to as the Generation IV technology road map. This effort was further supported by the U.S. Department of Energy that announced \$82 million funding for commercializing advanced reactors in June 2016.

Approximately 100 Generation IV candidate technologies were initially evaluated by GIF, and six of those reactor systems were selected for further evaluation and potential developments:

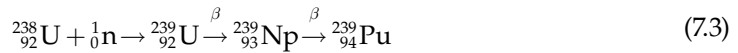
- Very High Temperature Reactor (VHTR)
- Gas-cooled Fast Reactor (GFR)
- Supercritical Water-cooled Reactor (SCWR)
- Sodium-cooled Fast Reactor (SFR)
- Lead-cooled Fast Reactor (LFR)
- Molten Salt Reactor (MSR)

More details about Generation IV reactor concepts can be found in [2] and [27].

The three Generation IV designs called fast reactors are breeders. A breeder can produce enough fuel for its own operation and generate additional fissile material for other reactors. This is achieved primarily by the conversion of the non-fissionable ^{238}U isotope into fissionable plutonium. This process makes much more efficient use of the energy contents of the natural uranium as mined. Current reactors “burn” only ^{235}U , which as mentioned previously, constitutes only 0.7% of natural uranium ore. The main drawback of the breeder

reactor is that it requires fast neutrons and therefore, ordinary water, which acts to slow down the neutrons in a reactor, cannot be used as the working fluid.

The basic equation through which a breeder converts some of the normally non-fissionable isotope of ^{238}U into the fissionable isotope ^{239}Pu occurs in the following steps:



The neutrons captured by the ^{238}U form ^{239}U , which has a half-life of 23 minutes.

The ^{239}U decays into Neptunium-239 by beta decay with a half-life of 2.4 days. The ^{239}Np decays into ^{239}Pu with a half-life of 24,400 years.

The above reaction also occurs in thermal reactors, but is very inefficient due to their design. A typical 1000 MW_e nuclear reactor produces about 200 kilograms of plutonium per year. This is insufficient to replace the fissile material destroyed, whereas, breeders are constructed to maximize the production of plutonium. Breeders use high-energy neutrons, so-called “fast neutrons,” because these fast neutrons have a better chance of being captured by ordinary ^{238}U than by the isotope ^{235}U . When fission is produced with fast neutrons it creates, on average, 2.9 neutrons compared to 2.4 produced per fission event. The breeder design can use 60% of the energy content in natural uranium, compared to 1 or 2% in the LWR. Thus, the breeder has a much higher energy return on energy investment than current LWR designs.

Breeder reactors commercialized in France in the 1970s used liquid sodium as the reactor coolant, and this is still considered the preferred coolant choice. Sodium slows the fission neutrons less than ordinary water or gas. The disadvantage of sodium is that the metal reacts violently with water, and can, at the temperature of the breeder, burn spontaneously in air. Thus, special efforts must be made to prevent leakage of sodium from the cooling system.

In summary, nuclear engineers have proposed many different new concepts for nuclear power plants, and many countries have built and are experimenting with small versions of these ideas. However, none of them has yet reached the point where commercialization appears imminent.

Discussion Questions

1. In the United States, the Price-Anderson Act provides taxpayer-funded insurance in the event of nuclear accidents. Research the estimated costs of the last 3 major nuclear accidents. How do these costs compare to Price-Anderson coverage?
2. Long-term storage of nuclear waste is a challenge for the nuclear industry. Yucca Mountain in Nevada has been proposed as a potential storage site. Research the history of this site and discuss why it has not been utilized. Do you believe it offers a good long-term solution? What other things can be done to address the nuclear waste problem? How are other nations dealing with this problem?
3. There are 99 reactor units operating in the United States. Some environmentalists want them shut down. Determine how much carbon dioxide emissions these

- plants save and how much renewable energy would have to be deployed (assume half solar photovoltaics and half wind power) to save an equivalent amount of emissions and how much this would cost.
4. New nuclear power plants in the United States have proven expensive. Determine the latest cost of a new plant in the United States as well as new plants in China and India. Explain why these costs differ and what might be done to reduce U.S. plant costs.
 5. Another potential issue with nuclear power is proliferation of nuclear weapons material. Discuss how some new reactor designs address this problem.
 6. Research and describe new passive reactor safety mechanisms.

Acknowledgment

The author of this chapter (Frank Kreith) thanks his colleague Ken Kok for providing significant information about many aspects of nuclear energy in his handbook *Nuclear Engineering Handbook, Second Edition*. CRC Press, 2017.

References

1. DOE. *The Manhattan Project*, an interactive history, <https://www.osti.gov/opennet/manhattan-project-history>.
2. Kok, K.D., 2017. *Nuclear Engineering Handbook*, 2nd ed., CRC Press, Boca Raton, FL.
3. Kanter, J., 2009. In Finland, nuclear renaissance runs into trouble, *NYT Energy and Environment*, May 28.
4. Areva. Finland-Olkiluoto 3, <http://www.areva.com/EN/operations-2389/finland--olkiluoto-3.html>.
5. ABC, August 12, 2016. Japan reactor restarts, despite protests, boosting Tokyo's nuclear push, *ABC News*, <http://www.abc.net.au/news/2016-08-12/japan-reactor-restarts-in-post-fukushima-nuclear-push/7729892>.
6. IAEA. Operational reactors by country, Vienna, Austria, <https://www.iaea.org/PRIS/WorldStatistics/OperationalReactorsByCountry.aspx>.
7. IAEA. Under construction reactors by country, Vienna, Austria, <https://www.iaea.org/PRIS/WorldStatistics/UnderConstructionReactorsByCountry.aspx>.
8. EIA, 2016. Today in energy, <https://www.eia.gov/todayinenergy/detail.php?id=26652>.
9. World Nuclear Association. USA nuclear power, <http://www.world-nuclear.org/information-library/country-profiles/countries-t-z/usa-nuclear-power.aspx>.
10. IAEA. Power Reactor Information System. Operational by age, Vienna, Austria, <https://www.iaea.org/PRIS/WorldStatistics/OperationalByAge.aspx>.
11. Atomic Archive. Nuclear fission: Basics, <http://www.atomicarchive.com/Fission/Fission1.shtml>.
12. Shutterstock Image No. 73672591.
13. European Nuclear Society. Nuclear fission, <https://www.euronuclear.org/info/encyclopedia/n/nuclear-fission.htm>.
14. World Nuclear Association. Supply of uranium, <http://www.world-nuclear.org/information-library/nuclear-fuel-cycle/uranium-resources/supply-of-uranium.aspx>.

15. World Nuclear Association. Plutonium, <http://www.world-nuclear.org/information-library/nuclear-fuel-cycle/fuel-recycling/plutonium.aspx>.
16. World Nuclear Association. Nuclear reactors for space, <http://www.world-nuclear.org/information-library/non-power-nuclear-applications/transport/nuclear-reactors-for-space.aspx>.
17. World Nuclear Association. Nuclear power reactors, <http://www.world-nuclear.org/information-library/nuclear-fuel-cycle/nuclear-power-reactors/nuclear-power-reactors.aspx>.
18. DOE, March 2004. Nuclear waste policy act as amended, <https://www.energy.gov/downloads/nuclear-waste-policy-act>.
19. Northey, H., May 10, 2011. GAO: Death of Yucca Mountain caused by political maneuvering, *New York Times*, <https://archive.nytimes.com/www.nytimes.com/gwire/2011/05/10/10greenwire-gao-death-of-yucca-mountain-caused-by-politica-36298.html?pagewanted=all>.
20. World Nuclear Association. Radioactive waste management, <http://www.world-nuclear.org/information-library/nuclear-fuel-cycle/nuclear-wastes/radioactive-waste-management.aspx>.
21. IAEA, 2006. The Chernobyl Forum 2003–2005, Chernobyl's legacy: Health, environmental, and socio-economic impacts and recommendations to the governments of Belarus, the Russian Federation and Ukraine, Austria, <https://www.iaea.org/sites/default/files/chernobyl.pdf>.
22. U.S. Nuclear Regulatory Commission, July 12, 2011. Recommendations for enhancing reactor safety in the 21st century: The near-term task force review of insights from the Fukushima Dai-Ichi accident, <https://www.nrc.gov/docs/ML1118/ML111861807.pdf>.
23. Lazard, December 2016. Levelized cost of energy analysis. V.10.0, <https://www.lazard.com/perspective/levelized-cost-of-energy-analysis-100>.
24. NRC. BWXT mPower, <https://www.nrc.gov/reactors/advanced/mpower.html>.
25. NRC. Design certification application: NuScale, <https://www.nrc.gov/reactors/advanced/nuscale.html>.
26. Westinghouse. Small modular reactor by Westinghouse, <http://www.westinghousenuclear.com/New-Plants/Small-Modular-Reactor>.
27. DOE Nuclear Energy Research Advisory Committee and the Generation IV International Forum, December 2002. A technology roadmap for Generation IV nuclear energy systems, <https://www.gen-4.org/gif/upload/docs/application/pdf/2013-09/genivroadmap2002.pdf>.



Taylor & Francis

Taylor & Francis Group

<http://taylorandfrancis.com>

8

Wind Energy

... As yet, the wind is an untamed, and unharnessed force; and quite possibly one of the greatest discoveries hereafter to be made, will be the taming, and harnessing of the wind.

Abraham Lincoln
Discoveries and Inventions (1858)

8.1 Introduction

Wind power is the fastest growing renewable electricity source in the world. In areas with good land-based resources, wind has reached cost parity with fossil fueled electricity generation. According to the Global Wind Energy Council (GWEC.net), the capacity of installed wind turbines worldwide passed 480 GW in 2016. In the United States, Texas led in installed wind capacity with over 20 GW. Wind provided more than 30% of electricity generation in Iowa in 2015. Turbine designs continue to advance to allow higher hub heights, accessing greater wind resources. Improvements in turbine control systems, wind forecasts, and grid integration are supporting increased grid penetration levels. Although well behind land-based wind in total capacity, offshore installations are expanding rapidly, led by northern European countries including the United Kingdom, Germany, and Denmark.

People have harnessed the energy of the wind for millennia. Wind energy was used to propel boats along the Nile River more than 5000 years ago. Around the beginning of the Common Era, simple windmills were used in China for pumping water. At about the same time, vertical-axis windmills with woven reed sails were used to grind grain in the Middle East. In the seventh century, a vertical-axis windmill was used in Sistan, Afghanistan, to process grain and pump water. People in the Middle East used windmills for food production in the eleventh century; the crusaders brought this idea back to Europe where it spread rapidly. The Dutch refined windmill technology and adapted it for draining lakes and marshes in the Rhine River Delta. American colonists used windmills to grind wheat and corn, and to cut wood at sawmills. Across the United States, windmills were used extensively for pumping water on farms and ranches in the nineteenth and early twentieth centuries.

Professor James Blyth built the first wind turbine (WT) for electricity production in Scotland, successfully generating electricity in 1887 [1,2]. Soon afterward, Charles F. Brush built the world's first automatically operated wind turbine in Cleveland, Ohio, in the winter of 1887–1888 [3]. Like the configuration that dominates today, Brush's turbine was a horizontal-axis wind turbine (HAWT), in which the axis of the rotor was horizontal to the ground. The first megawatt-sized wind turbine to supply electricity through the electric grid was built in 1941 on a hill called Grandpa's Knob, in Vermont (Figure 8.1). Palmer C. Putnam designed the 1.25 MW turbine, which had two 53 m diameter blades.

**FIGURE 8.1**

Smith Putnam wind turbine on Grandpa's Knob in Vermont, circa 1941. The Smith-Putnam machine was rated at 1.25 MW in winds of about 30 miles per hour. It was removed from service in 1945. (https://commons.wikipedia.org/wiki/File:Wind_turbine_1941.jpg.)

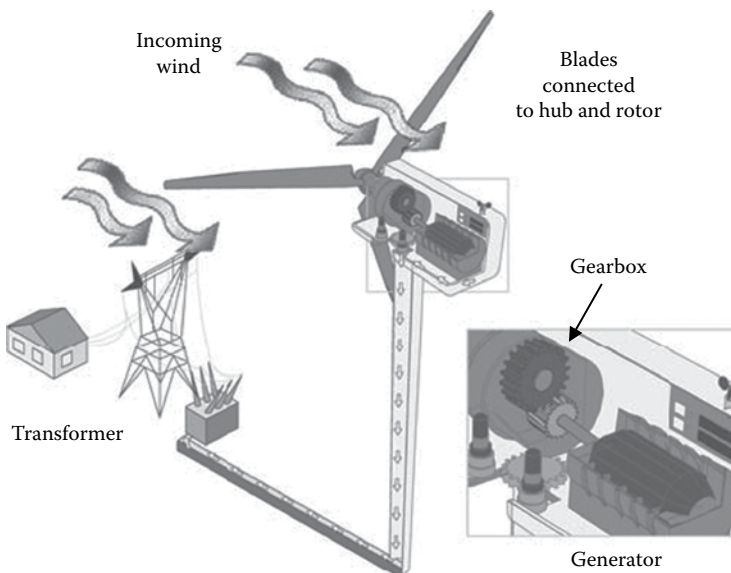
The turbine operated intermittently for 4 years until one of the blades failed [4, 5]. Interest in wind-electric turbines continued into the 1950s, led by Danish engineers, but efforts there were subsequently sidelined by the availability of cheap oil and low energy prices [6]. The picture changed in the 1970s, when oil shortages and interest in alternative energy sources brought wind turbine development to the fore all over the world. For example, Danish manufacturers Kuriant, Vestas, Nordtank, and Bonus began producing 20–30 kW machines, while NASA, at the Lewis (now Glenn) Research Center in Cleveland, Ohio, developed a government research and development program producing the first of the “Mod” series of wind turbines ranging from 0.2 to 2 MW [6].

Much work has occurred over the last three decades leading to optimization of performance and cost in WT design. Currently, the exclusive commercial WT design (e.g., 1 MW and larger) is a horizontal-axis wind turbine, in which the axis of the rotor is horizontal to the ground, as shown in the photograph in Figure 8.2 and schematically in Figure 8.3. Conversely, vertical-axis wind turbines (VAWTs) have blades that spin about a vertical axis, as shown in Figure 8.4. The biggest advantage of this design is that it does not have to be pointed in the direction of the wind. However, HAWTs are generally more efficient. Readers interested in more information on a variety of alternative wind turbine concepts are directed to F.R. Eldridge's *Wind Machines* [7] and V. Nelson's *Wind Energy and Turbines* [8].

Figure 8.5 shows U.S. wind capacity additions and cumulative installed capacity over the period from 2000 to 2015. In 2015, 41% of all electricity generating capacity additions in the United States came from wind, with about 8600 MW added. The investment in new wind projects in the United States between 2005 and 2015 was \$128 billion [9]. At the end of 2015, there were 88,000 wind-related jobs in the United States from development construction, transportation, and manufacturing [9]. Figure 8.6 shows the installed wind capacity in the year 2015 in the top 10 countries with wind energy generation. The leader in installed wind capacity is China, which had a capacity of more than 145 GW in 2015 [10].

**FIGURE 8.2**

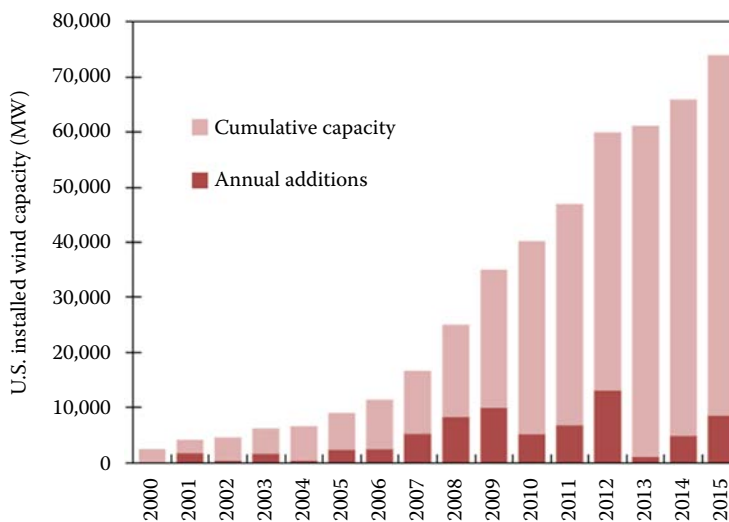
The 2.5 MW Liberty wind turbine (Clipper Windpower) near Medicine Bow, Wyoming. (Courtesy of DOE/NREL, Golden, CO. With permission.)

**FIGURE 8.3**

Schematic of typical wind turbine layout. (From Department of Energy, 2010. How does a wind turbine work? Office of Energy Efficiency & Renewable Energy, http://www1.eere.energy.gov/wind/wind_animation.html. With permission. [54])

**FIGURE 8.4**

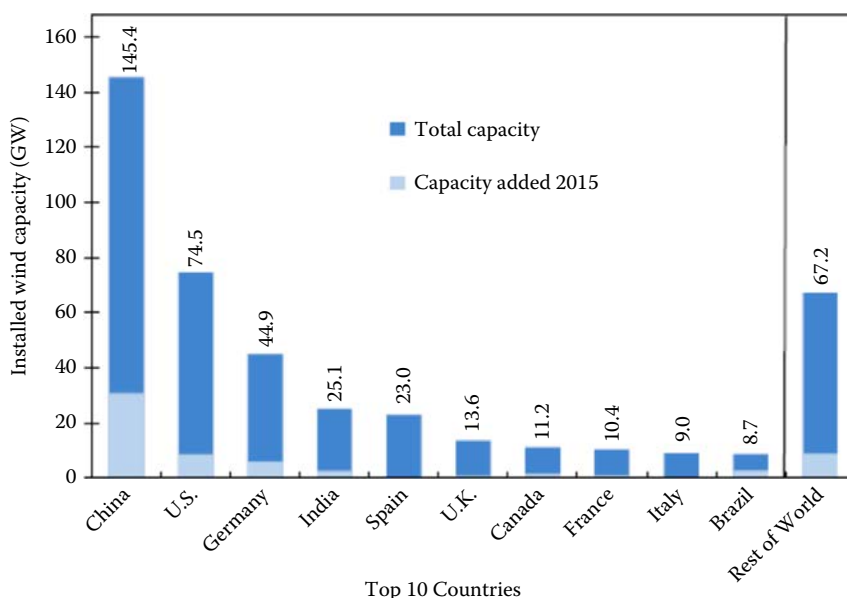
An example of a Darrieus VAWT in Quebec, Canada.

**FIGURE 8.5**

Total U.S. installed wind capacity 2000–2015. (From American Wind Energy Association (AWEA), 2016. U.S. wind industry first quarter 2016 market report; AWEA (2012) annual market report—Year ending 2010, <https://www.awea.org/2016-market-reports>. [9])

8.2 Environmental Impact

The wind industry has historically faced challenges in maintaining strength and reliability as it has developed and as turbine sizes have increased. In addition, the industry has faced concerns about aesthetics, noise, and impacts on birds and bats. On the other hand, wind turbines have significant advantages over other electricity generating technologies in life cycle emissions and water use.

**FIGURE 8.6**

Installed global wind capacity in 2015. (From Global Wind Energy Council, 2016. Global wind report 2015, <http://gwec.net/publications/global-wind-report-2/global-wind-report-2015-annual-market-update>. [10])

8.2.1 Noise and Visual Impact

Noise issues related to wind energy have been reported since the 1980s. Problems were initially found with the mechanical design as well as blade design and operation. For example, the 2-MW MOD-1 turbine developed by NASA in the late 1970s was a two-bladed turbine (61 m rotor diameter) [11]. It operated with the turbine blades downstream of a lattice tower structure. Low-frequency noise was produced as the turbine blades moved in and out of the “tower shadow” caused by wind flowing around and through the lattice tower. Noise of significant magnitude was produced, causing complaints from local residents.

Today, most large commercial WTs have the blades operating upstream of the tower and use a monopole tower. Modern commercial WTs have noise levels of approximately 35–45 dB at 750–1000 ft. In contrast, typical noise or loudness levels in everyday life are given in Table 8.1 [12]. As seen in Table 8.1, the modern turbine (at distances of 750–1000 ft) has a noise level comparable to a library or an average home (40–50 dB). When locating turbines, the distance between residences and WTs needs to be considered. Small WTs can actually have higher noise levels due to higher rates of rotation.

The sound typically heard from a WT comes from the blades. Careful aerodynamic design of the blades, as well as understanding the maximum allowable rotational speed of the blades, has reduced the aerodynamic noise level from previous levels. Similarly, mechanical components have been redesigned to virtually eliminate mechanical noise, leaving blade noise as the predominant noise source, albeit at a low noise level [13].

In Europe, “shadow flicker” created by the shadow of rotating WT blades on residences has occurred due to placing WTs too close to the residences. The resulting flicker can be very annoying. Proper planning and accounting for latitude allow the necessary distance between turbine and residence to be calculated so no turbine shadow falls on the residence [14]. This distance should also take into account the noise level of the operating turbine.

TABLE 8.1

Loudness Levels of Common Noises

Noise Level (dB)	Equivalent Activity
120	Jet plane takeoff, amplified rock music at 4–6 ft, car stereo, band practice
110	Rock music, model airplane
100	Snowmobile, chain saw, pneumatic drill
90	Lawnmower, shop tools, truck traffic, subway
80	Alarm clock, busy street
70	Vacuum cleaner
60	Conversation, dishwasher
50	Average home
40	Quiet library
30	Quiet bedroom

The turbine should be located a sufficient distance away (based on sun angle) to eliminate any shadow flicker or noise concerns.

8.2.2 Life Cycle Greenhouse Gas Emissions, Land, and Water Use

As discussed in previous chapters, an important consideration for any technology is the greenhouse gas emissions for the total fuel cycle. Each phase of the fuel cycle, including resource extraction, facility construction, and facility operation, must be evaluated to quantify and compare emissions from different technologies [15]. As shown in [Chapter 3 \(Figure 3.3\)](#), even when the operations needed to manufacture WTs and build wind farms are included in a greenhouse gas emission analysis, the use of wind power compared to coal or natural gas-fired electricity generation provides significant reductions. In a review of more than 40 studies, Nugent and Sovacool [16] found a median estimate of GHG emissions from wind generation of 12 g CO₂-e per kWh, and a mean estimate of 34 g CO₂-e per kWh. For comparison, life cycle emissions from coal-fired electricity generation are about 1000 g CO₂-e per kWh [17]. Compared to thermal power plants, which require significant water for cooling, wind also has the advantage of very low life cycle water use.

Other environmental impacts from WTs do exist. For example, construction of a wind farm could cause erosion due to the construction and use of roads needed to build the farm (truck and crane traffic, electrical line/equipment installation, etc.), but this impact can be mitigated using standard environmental reclamation techniques. Land occupancy and corresponding disruption of wildlife habitat or interference with other land use are also considerations. Denholm et al. [18] estimated that wind farms in the United States occupy a perimeter area that averages about 35 hectares per MW capacity, although much of that area may be available for other uses. They estimate the area directly occupied by turbine pads, access roads, service buildings, and other infrastructure is about 0.7 hectares per MW during construction and 0.3 hectares per MW during the plant's operating life.

8.2.3 Bird and Bat Fatalities

As can be seen in [Figure 8.7](#), the largest single cause of bird deaths are buildings and/or windows. A study by Erickson et al. [19] provides an annual estimate of the sources of

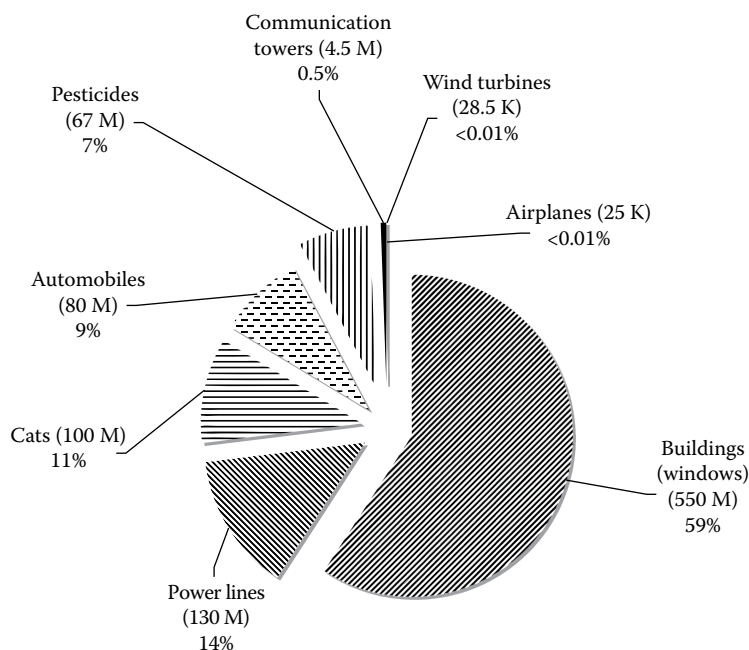


FIGURE 8.7

Most common causes of bird fatalities. Bird deaths are shown in millions (M) or thousands (K) with an annual estimated total near 1 billion birds. (From Erickson, W. et al., 2002. *A Summary and Comparison of Bird Mortality from Anthropogenic Causes with an Emphasis on Collisions*, USDA Forest Service General Technical Report PSW-GTR-191, <https://www.treesearch.fs.fed.us/pubs/32103>. With permission. [19])

bird fatalities in the United States (see Figure 8.7) including deaths from WTs. Bird deaths from WTs are estimated to be much less than 0.0001% of the total number of projected deaths, on the order of 30,000/year. In contrast, bird deaths from cats or buildings are projected to be 3.5 and 19 million times, respectively, more likely than that from WTs. If WTs are sited properly (e.g., away from migratory paths) or even shut down briefly with the help of radar to determine when migratory birds are approaching, the fatalities can be minimized [20]. Increasing the number of wind farms would likely increase the number of deaths, and this topic remains an area of research to minimize the effect on avian mortality.

While bird fatalities occur due to birds being struck by blades or running into towers, bat fatalities may be due to a different cause. Researchers have proposed that decompression may kill bats by barotrauma, due to a rapid reduction in air pressure near rotating turbine blades. Study results showed that, of the bats affected by WTs, “90% of bat fatalities involved internal hemorrhaging consistent with barotrauma, and that direct contact with turbine blades only accounted for about half of the fatalities” [21]. Studies have shown a higher rate of fatalities of bats with WTs than birds. Bird fatalities per turbine ranged from 0.6 to 7.7, whereas bat fatalities ranged from 3.4 to 47.5 per turbine [22]. Research is underway to understand the higher fatality rate as well as ways to stop/minimize bat fatalities and predict and avoid high-risk sites.

8.3 Power and Energy of Wind

Power and energy are common terms that are often misused. Power is the rate at which energy is used or produced. Light bulbs use power; WT's generate power. Units of power are expressed in work (energy) over an amount of time:

$$\text{Power} = \frac{\text{Work}}{\text{Time}} = \frac{\text{Energy}}{\text{Time}} = \frac{\text{N} \cdot \text{m}}{\text{s}} = \frac{\text{J}}{\text{s}} = \text{W} \quad (8.1)$$

WT's are rated in terms of power. Large commercial wind turbines have power ratings in the 1–5 MW range, whereas a WT used for a single home is likely rated in the 3–15 kW range.

Energy, on the other hand, is a measure of how much work can be done by a force. Units of energy are joules, J, the product of force and distance:

$$\text{Energy} = \text{N} \cdot \text{m} = \text{J} \quad (8.2)$$

The link between power and energy comes from the rate of power usage. In other words, energy equals the product of power and time or power is energy divided by time. If a 100-W light bulb is turned on for 24 hours, the energy usage is $100 \text{ W} \times 24 \text{ h} = 2.4 \text{ kWh}$. While turbines are denoted by their rated power production (e.g., 100 kW, 2.5 MW), we pay for electricity based on how much energy we use (e.g., \$0.06 per kWh).

To determine the power contained in the wind moving toward a WT, consider the kinetic energy, KE, of a mass of air, m (in kg), moving at speed, U (in m/s):

$$KE = \frac{1}{2} m U^2 \quad (8.3)$$

$$\text{Unit check: } \text{kg} \left(\frac{\text{m}}{\text{s}} \right)^2 = \frac{\text{kg} \cdot \text{m}^2}{\text{s}^2} = \left(\frac{\text{kg} \cdot \text{m}}{\text{s}^2} \right) \cdot \text{m} = \text{N} \cdot \text{m} = \text{J}$$

Now imagine a horizontal cylinder of air of area A (in m^2) and velocity U , moving toward a WT, as seen in [Figure 8.8](#). Note that the area, A , corresponds to the area swept out by the rotating WT blades. The mass m of the air column is volume V times the density, where ρ represents the air density in kg/m^3 . Mass can then also be expressed as:

$$m = \rho V = \rho A l = \rho A U t \quad (8.4)$$

where

ρ is the air density, kg/m^3

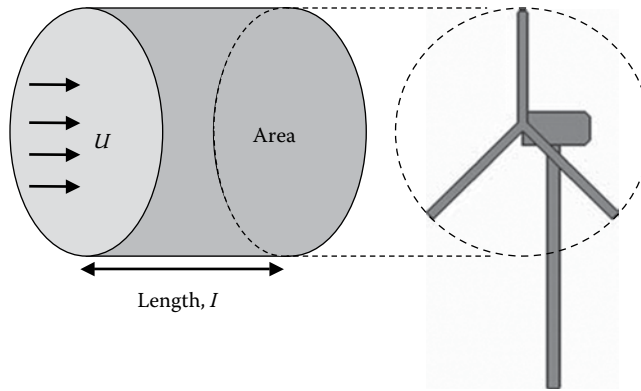
V is the volume, m^3

A is the area, m^2

l is the length, m

U is the wind speed, m/s

t is the time, s

**FIGURE 8.8**

Incoming air column and wind turbine.

The length of the column of air, l , is equal to the distance the wind travels in a given time interval, t , and is found by multiplying the wind speed, U , by the time.

Combining Equation 8.3 with Equation 8.4, the kinetic energy becomes:

$$KE = \frac{1}{2} m U^2 = \frac{1}{2} (\rho A U t) U^2 = \frac{1}{2} \rho A t U^3 \quad (8.5)$$

Dividing the KE by time yields the power of a moving column of air:

$$\text{Power} = \frac{KE}{t} = \frac{1}{2} \rho A U^3 \quad (8.6)$$

In other words, the power in a column of wind is linearly proportional to the air density and area of the air column. Of even more significance, the power is also proportional to the cube of the wind speed. We will see later that a key reason WTs have grown in height over time is to place the WT rotor blades higher in the atmosphere where the wind speed is greater, thus harnessing a much higher kinetic energy output.

To increase power output, the area of the WT blades can be modified to affect the power output. Since the WT power output is linearly proportional to the area, a large-scale commercial WT designer would want to increase the blade length to increase the power output. Since the circular area swept out by the turbine blades is proportional to the blade radius squared (R^2), turbine power is also proportional to the blade radius squared (R^2):

$$\text{Power} = \frac{1}{2} \rho A U^3 = \frac{1}{2} \rho \pi R^2 U^3 \quad (8.7)$$

In summary, longer blade lengths and taller turbines (providing access to higher wind speeds) are options to increasing WT power output. However, this performance increase comes at a price. Longer blades need more sophisticated manufacturing techniques to build blades strong enough to withstand wind gusts and extreme wind speeds (in excess of 100 mph). Taller towers must be strong enough to withstand the forces transmitted from the blades, weight of the nacelle, and other parts while still being cost-effective. Transporting turbine blades from manufacturing facilities to installation sites also becomes more challenging and more costly.

Some applications, for example, remote homes off the electrical grid, require more modest amounts of power. The design challenges here are just as significant: structures (blades, tower, etc.) must be strong enough to withstand wind forces, but also must be light, cost-effective, and reliable.

8.4 Coefficient of Performance

A key performance measure in WT design is the coefficient of performance, C_p , which is a ratio of the aerodynamic power extracted by the WT, P_{aero} , divided by the total power in the wind, P_{wind} , and is calculated as:

$$C_p = \frac{P_{aero}}{P_{wind}} = \frac{P_{aero}}{1/2 \rho A U^3} = \frac{P_{aero}}{1/2 \rho \pi R^2 U^3} \quad (8.8)$$

The theoretical maximum turbine efficiency was derived by Albert Betz in 1920 [23], as well as others [24], and is:

$$C_p = \frac{16}{27} \approx 0.59 = \text{Betz limit} \quad (8.9)$$

In addition, C_p is a function of how fast the tips of the WT blades are rotating compared to the incoming wind. The ratio of the blade's rotational speed divided by the incoming wind speed is known as the tip speed ratio (TSR):

$$\text{Turbine tip speed ratio} = \frac{\Omega R}{U} \quad (8.10)$$

where

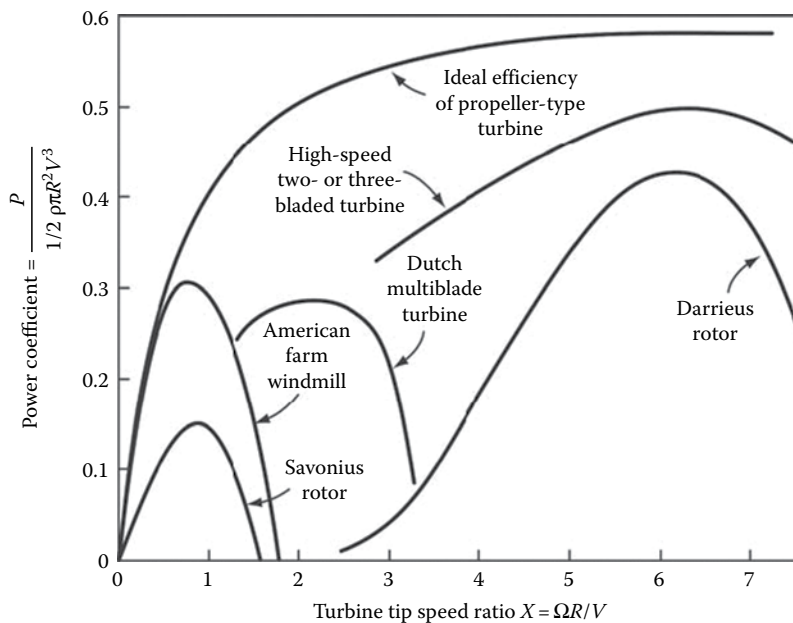
Ω is the turbine blade rotational speed, rad/min

R is the rotor radius, m

U is the wind speed, m/s

In Figure 8.9 [25], the power coefficient is plotted as a function of TSR for different WT configurations. Several key points can be seen in Figure 8.9, starting from the top. The highest line shows how the theoretical maximum power coefficient increases with increasing TSR. The Betz limit value of 0.59 is approached asymptotically as the TSR increases toward a value of seven ($\text{TSR} = 7$). The next highest curve denotes the performance of today's modern high-speed horizontal-axis two- or three-bladed turbines. The maximum theoretical performance coefficient for these turbines is approximately $C_p = 0.5$, whereas the Darrieus vertical-axis rotor has a maximum C_p of approximately 0.40–0.45. Thus, the modern two- and three-bladed HAWTs are approximately 10% more efficient than a Darrieus (VAWT) machine and have the potential to make 10% more energy.

Not only are the large commercial WTs configured horizontally, they are also predominantly three-bladed upwind (blades rotate in front of the tower). Why are HAWTs mainly upwind? The blades on a downwind turbine experience cyclic loading (alternating

**FIGURE 8.9**

Various turbine power coefficients versus TSR. (Note: The figure uses the symbol V for wind speed.) (From Wilson, R.E. and Lissaman, P.B.S., 1974. *Applied Aerodynamics of Wind Power Machines*, Oregon State University, Corvallis, OR, <http://ir.library.oregonstate.edu/jspui/handle/1957/8140>. With permission. [25])

higher forces and lower forces) due to the blades passing behind the tower, which may cause fatigue failure of the blades as well as noise.

8.5 Aerodynamics

Examining the aerodynamics of WT blades helps explain why various WT configurations have such different performance coefficients, C_p [26,27]. Figure 8.10 shows a WT blade rotating (in the plane of the paper) in a clockwise direction. The atmospheric wind, U_w is blowing toward the blade (i.e., into the plane of the paper). A section view of the blade is then taken near the tip of the blade looking in toward the root of the blade (Figure 8.10). The cross-sectional view of the blade airfoil is shown in the right-hand side of the figure. The two airflows acting on the blade are the incoming wind speed, U_w which is perpendicular to the plane of the rotating blades, and the rotational wind speed, $U_{Rot} = \Omega R$, created by the turbine blade rotating at an angular speed, Ω , at the radius of the cross section, R . Note that the side of the airfoil facing the wind (designated the front side) is relatively flat compared to the curved rear side of the airfoil. The leading edge of the airfoil hits the airflow arising from the blade rotation causing the airflow to separate into two streams over the sides of the airfoil. Finally, the trailing edge is where the airflow over the two sides of the airfoil is rejoined.

In Figure 8.11, a blade cross section near the tip of the blade is shown with the resultant forces created by the passing wind, the lift force, F_{Lift} , and the drag force, F_{Drag} . The straight

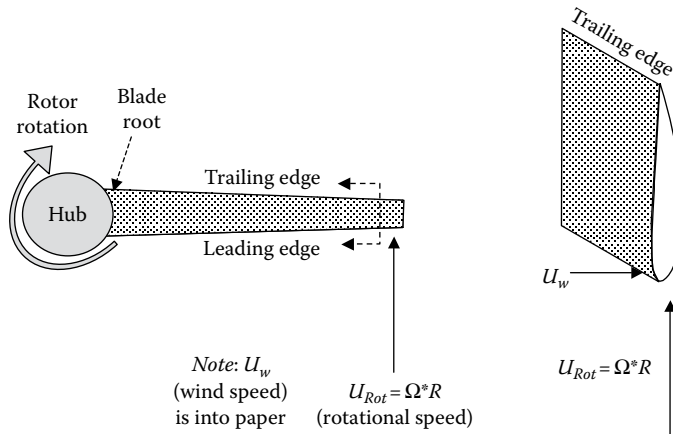


FIGURE 8.10
Rotor blade diagram.

line connecting the front (leading) and rear (trailing) edges of the airfoil is known as the chord line, and the distance between the two points is designated as the chord, c . Also shown are the resultant velocity component, U_{Res} , between the wind speed, U_w , and the wind arising from the blade's rotational speed, U_{Rot} . Finally, the angle between the resultant wind speed, U_{Res} , and the chord line, c , is the angle of attack, α .

Via Bernoulli's law, Equation 8.11, the velocity is highest across the curved (upper) surface of any airfoil (e.g., airplane wing). In addition, Bernoulli's law tells us that the pressure is the lowest where the velocity is the highest. In the case of a WT blade, the pressure is lower over the rear (i.e., upper) surface of the airfoil compared to the front (i.e., lower) airfoil surface.

$$p + \frac{1}{2} \rho U^2 = \text{const.} \quad (8.11)$$

In summary, the lowest pressure is near the leading edge ("nose") of the airfoil, where the wind velocity is the highest, and over the rear (or upper) curved surface. This results in a net force, F_{Lift} , on the airfoil, causing it to be drawn forward, in the direction of the "nose" of the airfoil and hence rotating. By convention, the resultant forces on the airfoil are drawn perpendicular, F_{Lift} , and parallel, F_{Drag} , to the resultant velocity, U_{Res} . The higher the lift force (and conversely the lower the drag force) along a WT blade, the greater the rotational force,

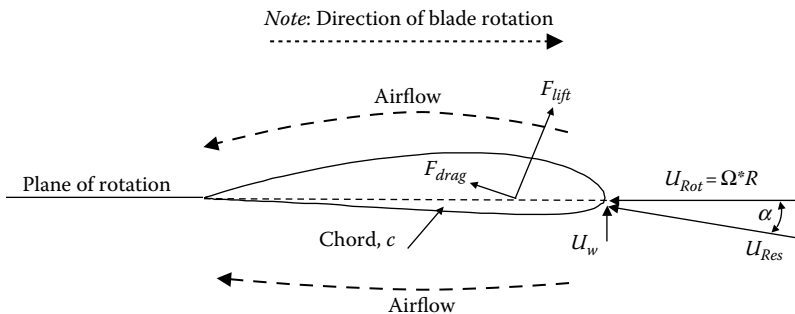


FIGURE 8.11
Lift and drag forces on a blade cross section near the tip.

which means the WT is capturing more of the wind's energy and converting it to electricity. In other words, the higher the lift-to-drag ratio (L/D) is, the more efficient the blade will be at capturing the wind's energy.

Note that it is now possible to better understand the performance of the different WT configurations shown in Figure 8.9. It turns out that a Savonius VAWT has a poor L/D ratio and thus a very low maximum C_p , as shown in Figure 8.9. The American farm windmill and Dutch multiblade turbines have higher L/D ratios and hence higher maximum C_p values. Lastly, machines with high L/D ratios are the Darrieus VAWT rotor and the modern high-speed two- or three-bladed HAWT turbines, with the modern two- and three-bladed turbines having the highest C_p as noted earlier.

WT blades have very complicated shapes that vary along the blade. The shape variation is needed not only to help start the WT rotating but also to operate very efficiently as the wind speed increases. The airfoil is twisted near the blade root to provide the required torque to start the turbine rotating at low wind speeds. Once rotating, the optimized blade profiles in the outer portions of the blade provide the necessary aerodynamic forces to keep the blade rotating at design speeds.

Recall that Figure 8.11 illustrates a cross section of a blade in the outer portion of the blade. Figure 8.12 illustrates the lift and drag forces on a blade cross section near the root of the blade. Note that the blade is twisted, and the chord line now forms an angle θ with the plane of rotation of the blade. This twist angle, θ , is a function of turbine blade radius and has a larger value near the blade root and a decreasing value with increasing blade radius. Because the resultant velocity, U_{Res} , has decreased approaching the blade root, this increases the angle between the chord line and U_{Res} and results in an increased angle of attack.

While the root portion of the blade encounters the same incoming wind speed, U_w , the rotational speed, $U_{Rot} = \Omega R_{Root}$, is lower. This occurs because, although the angular rate of rotation, Ω , is the same along the blade, the radius at the blade root, R_{Root} , is smaller. The resulting lift force, F_{Lift} , per unit area is lower at the blade root compared to the blade tip. However, the direction of the force is better aligned to apply a torque to begin rotating the blades. In addition, the surface area of the blade is considerably larger at the root. This provides sufficient area for the lower magnitude aerodynamic forces to act over, resulting in enough torque to start rotation at low wind speeds. Finally, the larger surface area is needed to accommodate the necessary structural strength to handle the cantilevered loads arising from wind forces on the blade, weight of the blade, and so on.

Figure 8.13 shows the vector diagrams from Figures 8.11 and 8.12 side by side. Assuming a constant wind speed at both the blade root and tip cross sections, we will consider the case where the root cross section is located at a radial location one-fifth of the blade tip cross section. This last assumption means that the rotation speed at the blade root, $U_{Rot-Root}$,

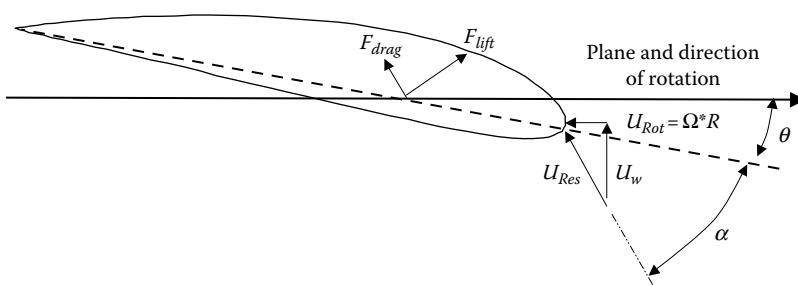
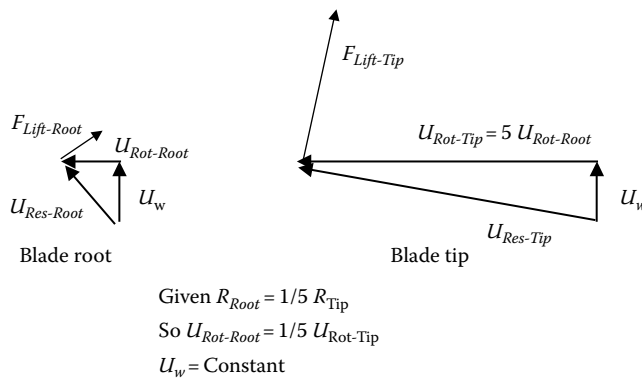


FIGURE 8.12

Lift and drag forces on a blade cross section near the blade root.

**FIGURE 8.13**

Comparison of velocity vector diagrams for blade root and tip cross sections.

is one-fifth the speed at the blade tip, $U_{Rot-Tip}$. Note that $U_{Rot-Root}$ and $U_{Rot-Tip}$ are drawn to scale. The resultant velocity vector at the tip is much larger due to the contribution of the rotational wind speed. This results in a larger lift force per unit area at the tip. At the blade root, the lift force is better aligned to provide a start-up torque. While the blade root lift force is lower per unit area, it is applied over a large surface area. Interestingly, at the tip, the contribution of the wind speed to the resultant velocity is small compared to the contribution from the rotational wind speed when the turbine is at operational conditions.

8.6 Wind Characteristics

8.6.1 Wind Generation

Now we will turn our attention to the atmospheric wind: generation, distribution, characteristics, and so on. The motion of air, otherwise known as wind, is caused by uneven heating of the Earth by solar radiation and the rotation of the Earth. The predominant wind direction varies with latitude and altitude above the Earth's surface, as shown in [Figure 8.14](#) [27,28,29]. Energy is transferred from the equator to the poles via wind. As the wind moves, the Earth's rotation influences the wind direction in two ways. First, Coriolis forces accelerate a particle of air to the right in the Northern Hemisphere (and to the left in the Southern Hemisphere). Second, each air particle has an angular momentum from west to east due to the Earth's rotational direction. As the air particle moves toward the pole, conservation of angular momentum requires its west-to-east velocity component to increase. This effect is pronounced in the midlatitudes, in the region called the westerlies, near the ground [27]. In general, the westerlies are the best-suited region for wind energy applications. In addition, the polar jet stream (7–12 km or 20,000–40,000 ft above sea level) can have a profound impact on the westerlies, moving them north or south, resulting in lower or higher energy production from year to year.

Of course, the most critical part of the atmosphere for a WT is relatively close to the ground. The atmospheric boundary layer (ABL) is the lowest part of the atmosphere and varies from the ground up to 500–2000 m in height depending on the time of day, temperature, and pressure. In the ABL, the mean wind speed varies from zero at or near the ground up to the

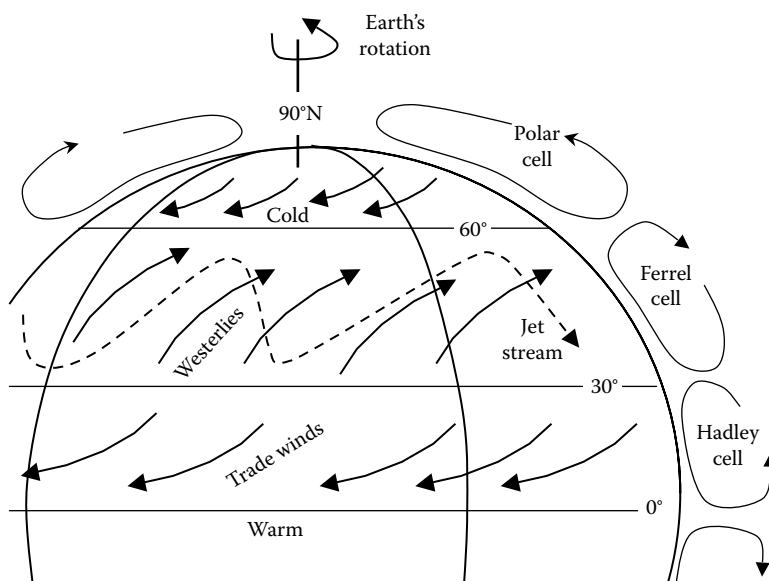


FIGURE 8.14
Wind flow in the Northern Hemisphere.

free stream velocity of the atmosphere at the top of the ABL. In addition, the velocity field exhibits turbulent fluctuations. In other words, each of the three velocity components for an air particle has a mean as well as fluctuating component. The turbulent velocity component can be quite large and by nature is time varying. This results in unanticipated fluctuating forces (high velocity causes high blade loading), which can lead to fatigue failures of WT components such as the blades, gearboxes, and tower. The turbulent portion of the flow field is typically described statistically. Methods of accurately simulating turbulent flow fields for a WT design are an active field of research [30].

8.6.2 Distribution of Wind

Now we transition from a global view of wind to a local area view of the wind resource. The wind resource is the mean wind speed as well as how many hours per year the wind blows at a given speed. A wind farm developer needs high confidence that the wind speeds at a given location are “high” and consistent from year to year. How much of a concern is this? If the average wind speed is only 5% lower than predicted, the maximum possible power will be 14% lower than anticipated! High confidence in the wind resource allows the developer to estimate the probable energy output and compare that to the investment needed to lay out a wind site and purchase or finance, install, and operate the wind farm (consisting of tens of turbines).

Wind resource maps have been developed for the entire world. For example, a U.S. wind resource map is shown in [Figure 8.15](#) [31]. Smaller-scale maps are also available, including each state in the United States [31]. Similar maps are available for other countries.

[Figure 8.15](#) maps the estimated annual average wind speed 80 m above the ground. The 80 m height is a relevant starting point for current commercial installations, but taller turbines are increasingly used. A color version of the map in [Figure 8.15](#) as well as wind maps for 100 m heights and maps at a higher spatial resolution are available from NREL [31]. [Table 8.2](#)

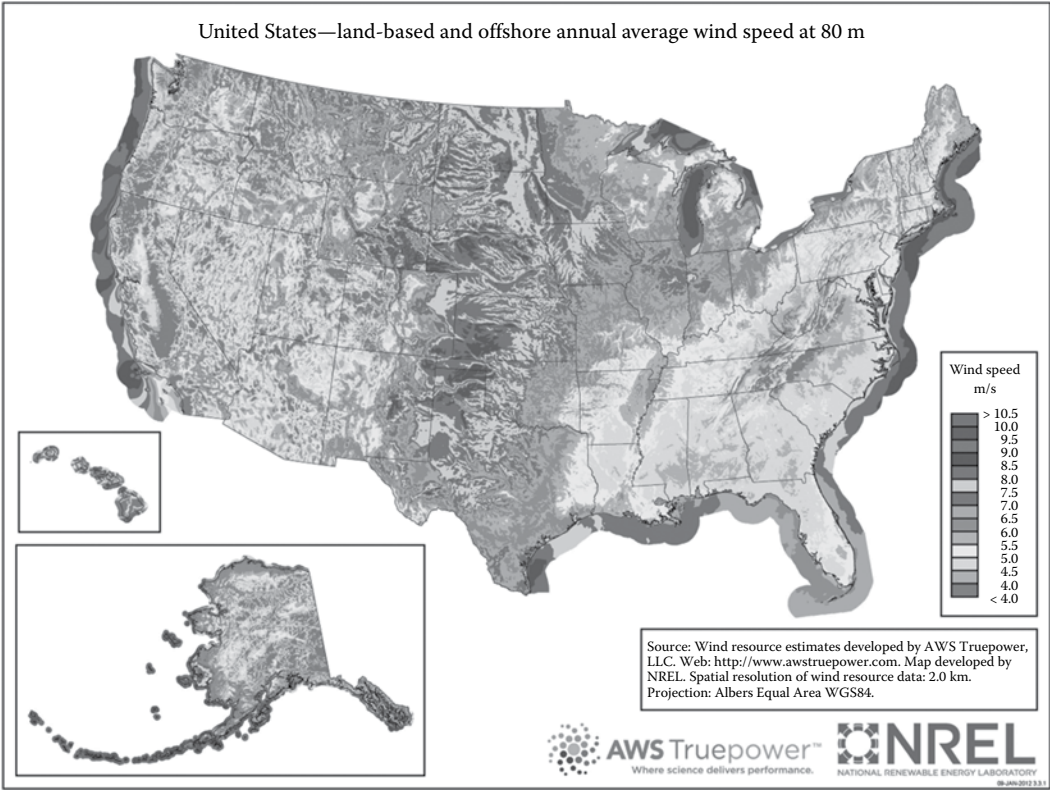


FIGURE 8.15
Wind resource map of the United States. This map shows the annual average wind speed estimates at a height of 80 m. The estimates are model-derived. (Courtesy of U.S. Department of Energy, National Renewable Energy Laboratory, Washington, DC.)

TABLE 8.2
Rating Wind Energy Resource Potential

Wind Power Class	Resource Potential	Wind Power Density at 50 m (W/m ²)	Mean Wind Speed ^a at 50 m (m/s)	Mean Wind Speed ^a at 50 m (mph)
1	Poor	0–200	0.0–5.9	0.0–13.2
2	Marginal	200–300	5.9–6.7	13.2–15.0
3	Fair	300–400	6.7–7.4	15.0–16.6
4	Good	400–500	7.4–7.9	16.6–17.7
5	Excellent	500–600	7.9–8.4	17.7–18.8
6	Outstanding	600–800	8.4–9.3	18.8–20.8
7	Superb	>800	>9.3	>20.8

Source: Enlarged from Wind Powering America, 2009. Wind resource maps, http://www.windpoweringamerica.gov/wind_maps.asp. [32]

^a Wind speeds are based on a Weibull *k* value of 2.0 (Rayleigh).

illustrates the relationship between wind power density (in W per m² swept area) and mean wind speed (in m/s) [32].

Several areas stand out in the U.S. map shown in Figure 8.15. The highest-class wind power (or highest mean wind speeds) regions are offshore along the East and West coasts. The Great Lakes also have high offshore wind power resources. Land-based wind resources are strong across the middle of the country from the Canadian border south into Northern Texas. Correspondingly, states in the middle of the country, including Texas, Iowa, and Wyoming, have been leading locations for wind power development.

Similar regions of high annual wind power can be found in many areas of the country but are not visible at national-scale resolution. This highlights a key point, not surprisingly, that the wind resource is highly dependent on local conditions such as vegetation (forests), terrain (hills, mountains), and water (ponds, rivers, lakes, oceans). Given sufficient resolution, one can search for and decide on a site to locate a WT. Screening-level assessments of annual power output of a turbine may be done using routine meteorological data, adjusted for turbine height. More detailed information would then be gathered to support evaluation for a proposed wind project.

8.6.3 Wind Speed Increasing with Height

Wind resource maps such as Figure 8.15 show, on a large scale, where winds suitable for commercial WTs exist. The next step is to develop a wind speed profile as a function of height. As mentioned earlier, wind speed increases with height and thus power increases with height.

Using local data from airports and weather stations, developers gather the information needed to get site-specific wind speed data. The data are then processed to arrive at an equation expressing the wind speed as a function of height. Two common approaches are the log law and the power law.

8.6.4 Log Law Wind Speed Profile

The log law wind speed profile has a physical basis. It is assumed that the shear stress in the wind is constant with height, the pressure gradient near the Earth's surface is small, and the Earth's rotation is ignored. The height of this constant shear stress layer is 100–200 m and is known as the “surface layer” of the ABL (see, for example, [33]). For a smooth surface, the mixing length, l , of the turbulent wind is given as

$$l = \kappa z \quad (8.12)$$

where

κ is von Karman's constant ($\kappa = 0.4$)

z is the height above the ground

The velocity profile as a function of height can be found to be

$$U(z) = \frac{U^*}{\kappa} \ln \left(\frac{z}{z_0} \right) \quad (8.13)$$

where

$U(z)$ is the wind speed at a height, z

U^* is the friction velocity arising from shear stress

z_0 is the surface roughness length

Values for z_0 are shown in Table 8.3.

There are two unknowns in this equation: U^* and z_0 . Substituting typical values for U^* and z_0 , the shape of the resulting atmospheric velocity profile is illustrated in Figure 8.16 for a neutrally stable atmosphere. One sees a predicted gradual change in wind speed through the first 20 m or so of the ABL and then an exponential growth approaching a steady-state value above 200 m.

There are three stability states of the atmosphere: neutral, stable, and unstable [34]. Neutral stability occurs when there is no change in temperature with height through the ABL due

TABLE 8.3

Surface Roughness for Various Outdoor Surfaces

Terrain Type	Roughness Length, z_0 (m)
Cities, forests	0.7
Suburbs, wooded countryside	0.3
Countryside with trees and hedges	0.1
Open farmland	0.03
Flat grassy plains	0.01
Flat desert, rough sea	0.001

Source: Burton, T. et al., 2001. *Wind Energy Handbook*, Wiley, Chichester, U.K. [34]; Manwell, J.F. et al., 2002. *Wind Energy Explained: Theory, Design and Application*, Wiley, Chichester, U.K. [53]

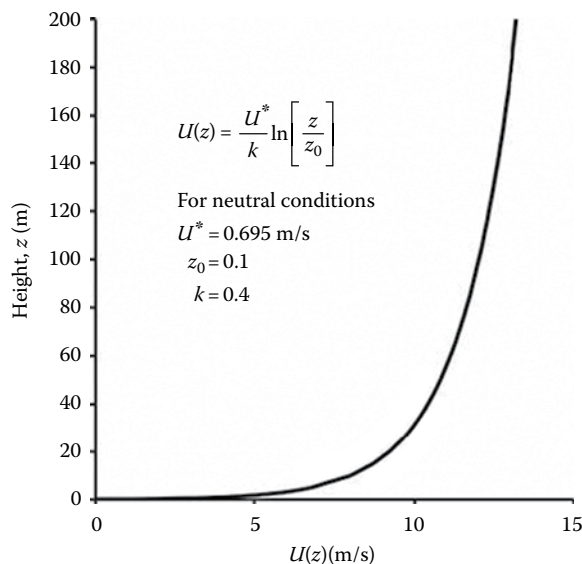


FIGURE 8.16

Log law velocity distribution.

to adiabatic cooling. This state is typically transitional between unstable and stable periods. A stable atmosphere occurs when the air temperature is cold on the ground and increases with altitude. This condition is associated with high wind speeds and results in a steep increase in the wind speed with height (i.e., large wind shear). An unstable atmosphere occurs when the air temperature near the ground is warmer than the temperature at higher altitudes. The air on the ground rises while the colder air above sinks, thereby creating turbulent wind conditions.

If one wants to determine an unknown wind speed at a given height, it can be estimated from a known wind speed at another height using Equation 8.13. This approach is especially valuable because wind speed data are typically known at heights of 50 m or less (reference height); however, turbines operate at much higher heights where wind speed data are unknown. Using this method, wind speeds can be estimated at hub height from data available at lower heights.

So, taking Equation 8.13 at a height z , for the wind speed, $U(z)$, and then dividing it by the same equation for a reference height, z_r , at the reference wind speed, $U(z_r)$, eliminates the unknown friction velocity, U^* , and yields

$$\frac{U(z)}{U(z_r)} = \frac{\ln(z/z_0)}{\ln(z_r/z_0)} \quad (8.14)$$

This equation now has only one unknown, z_0 , the roughness length, which is estimated from Table 8.3. Consider a meteorological tower taking measurements at 40 m ($z_r = 40$ m), measuring a wind speed of $U(z_r) = 7.2$ m/s at z_r , located in a wooded countryside, $z_0 = 0.3$, then the wind speed, $U(z)$, at a hub height of $z = 95$ m is

$$U(z) = 7.2 \cdot \frac{\ln(95/0.3)}{\ln(40/0.3)} = 8.5 \text{ m/s} \quad (8.15)$$

In other words, the wind speed is predicted to increase by approximately 18% from 7.2 to 8.5 m/s if the atmospheric assumptions in the model hold. In this case, the wind power would increase by $(9.7/7.2)^3 = 164\%$. Height does indeed matter when it comes to wind turbines.

8.6.5 Power Law Wind Speed Profile

Another model commonly used in engineering wind studies is the power law profile. It is used to estimate wind speeds given a reference height, z_r , to some desired height, z . The power law profile is used when one does not know the surface roughness, z_0 , and/or stability information (i.e., earlier defined friction velocity, U^*) is unknown. The power law profile is given as

$$U(z) = U(z_r) \cdot \left[\frac{z}{z_r} \right]^\alpha \quad (8.16)$$

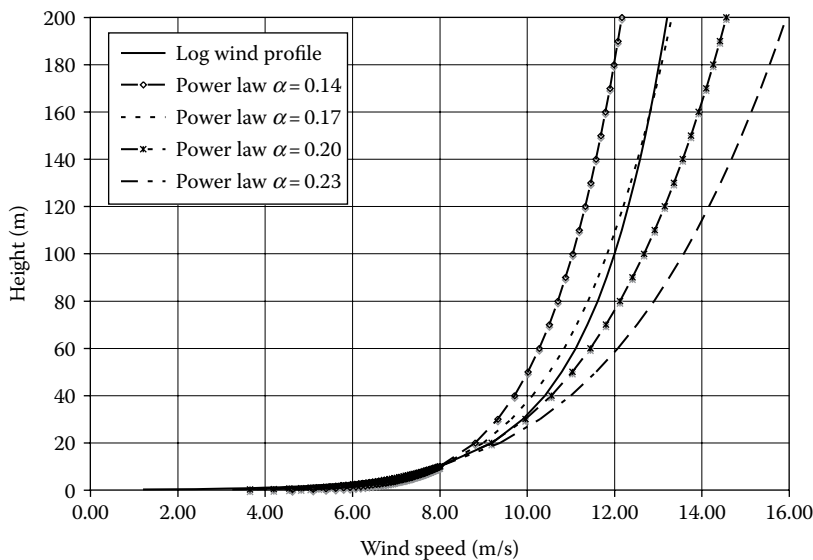
where α is the power law or shear exponent.

Typical values for α are

$$\text{For neutral flows: } \alpha \cong \frac{1}{7} = 0.143$$

$$\text{For unstable flows: } \alpha < 0.1$$

$$\text{For strongly stable flows: } \alpha > 0.3$$

**FIGURE 8.17**

Log law and power law velocity profile comparison.

A comparison between the log law and power law wind speed profiles is shown in [Figure 8.17](#). This figure shows that the wind speed profile of the power law profile for a value of $\alpha = 0.17$ is similar in shape to the log law wind profile plotted earlier for neutral atmospheric conditions. In any case, it should be noted that the value of α is highly dependent on temperature, weather, geographic location (elevation and terrain), and time (of day and season). The power law profile is commonly used in engineering studies due to its simplicity.

[Table 8.4](#) shows the calculated wind speeds for two different values of α at a height of 100 m, which is a typical hub height for modern commercial WTs. The change in predicted power based on these wind speeds is the ratio $(13.6/11)^3 = 1.89$. This indicates that the predicted power can nearly double at 100 m if the value of α increases from 0.14 to 0.23. This has large economic implications. In other words, determining the correct value of α for the power law profile (or using an entirely different method to determine wind speed as a function of height) for a given location and time period is critical when making choices about where to build wind farms. The best option is to gather long-term meteorological data at hub height in a sufficient number of locations at a potential WT site (if doing so is affordable).

Consequently, methods have been developed, and continue to be developed, to choose the best value of α given a set of wind data and environmental wind factors.

TABLE 8.4

Variation in Wind Speed with α
at a Height of 100 m

α	Wind Speed $U(z)$ (m/s)
0.14	11.0
0.23	13.6

8.6.6 Probability of Observing a Given Wind Speed

As has been discussed, the wind speed (and hence power available) varies. The next step is to determine the probability of a given wind speed occurring over a desired time period using a probability distribution function (PDF). A common PDF is the normal or Gaussian PDF, which can be seen in Figure 8.18. Many natural events can be described by a normal PDF, for example, the height distribution of 20-year-old students in the United States. When graphed, this Gaussian PDF yields the commonly known “bell-shaped” curve. For all PDFs, the vertical axis is the observed frequency of a given event within a certain range or magnitude, for example, number of students between the heights of 5'0" and 5'1". The horizontal axis contains the range of all events, for example, 4'0"–6'10". The peak of any PDF curve (where the curve is denoted by $f(x)$) is the mean magnitude of all occurring events.

The area under any section of a PDF curve corresponds to the probability, P , of a range of events occurring. As shown in Figure 8.18, the area represents the probability of having an event occur with a magnitude between a and b . The probability, P , of a range of events occurring is obtained by integrating the PDF, $f(x)$, between the range of the events, a and b .

$$P = \int_a^b f(x) dx \quad (8.17)$$

It should also be noted that integrating the PDF between the limits of $-\infty$ and ∞ yields a value of 1. In other words, the probability of having an event occur of any magnitude between the limits of all events is 100%.

$$P = \int_{-\infty}^{\infty} f(x) dx = 1 \quad (8.18a)$$

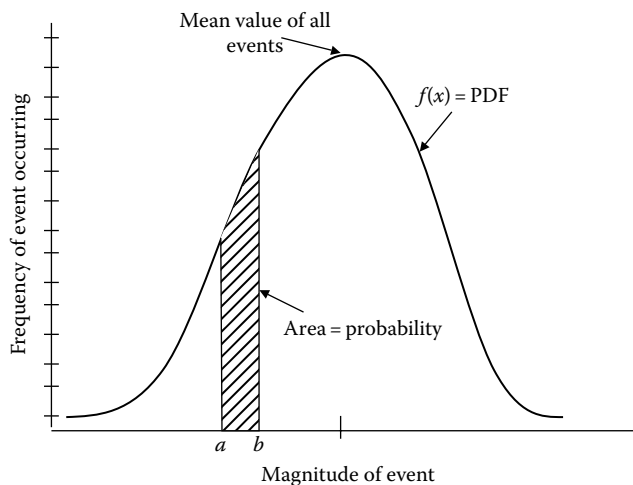


FIGURE 8.18
Illustration of a Gaussian or normal probability density function.

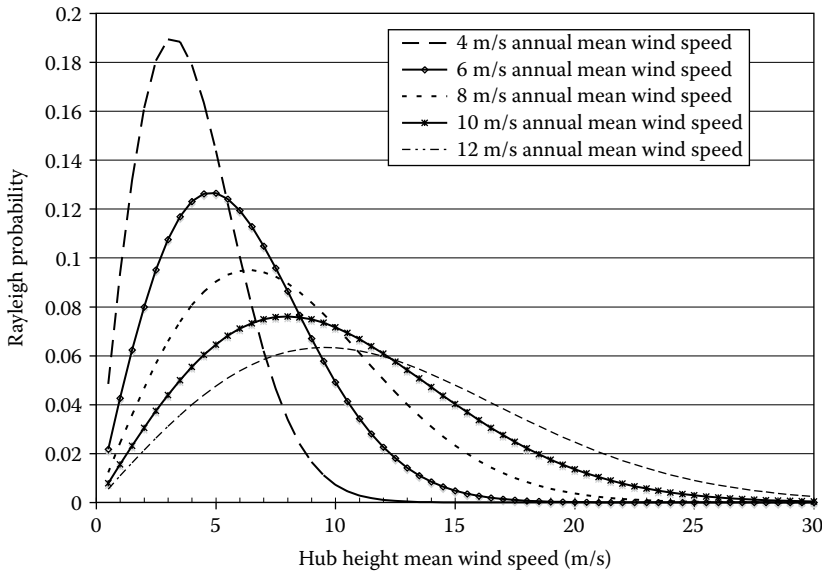


FIGURE 8.19
Rayleigh wind distributions.

Two commonly used PDFs, Weibull and Rayleigh, are used to describe the probability of observing a given wind speed. These distributions are used because they more closely represent the distribution of wind speeds at a given location. These PDFs are NOT symmetric, as is the Gaussian distribution (see [Figure 8.18](#)), but are skewed to the “left” (see [Figure 8.19](#)).

A wind speed distribution skewed to the “left” means that the probability of seeing a lower wind speed is higher than the probability of seeing a higher wind speed (i.e., there is a higher probability of a 3 m/s wind speed than a 25 m/s wind speed at a typical WT site). These PDFs are typically determined at a desired height, for example, hub height. These probability distributions are, of course, only defined for values greater than zero. Integrating the PDF will provide the probability, $P(U)$ of wind speed, U , occurring between two wind speeds, U_a and U_b .

$$P = \int_{U_a}^{U_b} f(U) dU \quad (8.18b)$$

Several other important statistical relationships can be found given a wind speed PDF, $f(U)$, including

$$\text{Mean wind speed: } \bar{U} = \int_0^{\infty} U f(U) dU \quad (8.19)$$

$$\text{Standard deviation: } \sigma = \sqrt{\int_0^{\infty} (U - \bar{U})^2 f(U) dU} \quad (8.20)$$

Lastly, one is likely to want to know the probability (or the percent of time) that the wind will be equal to or less than a given wind speed. For example, what percent of a year will the wind speed be too low for the turbine to operate? This is known as the cumulative distribution function, $C(U)$, and is found by integrating from 0 m/s to a desired wind speed, U m/s:

$$C(U) = \int_0^U f(U) dU \quad (8.21)$$

The Weibull PDF and cumulative distribution function are given by

$$f(U) = \left(\frac{k}{c}\right) \left(\frac{U}{c}\right)^{k-1} \exp\left[-\left(\frac{U}{c}\right)^k\right] \quad (8.22)$$

$$C(U) = 1 - \exp\left[-\left(\frac{U}{c}\right)^k\right] \quad (8.23)$$

where

k is the shape parameter

c is the scale parameter

Both k and c are functions of the mean wind speed, \bar{U} , and the standard deviation of the wind speed, σ . The Rayleigh PDF and cumulative distribution function are given by

$$f(U) = \frac{\pi}{2} \left(\frac{U}{\bar{U}^2}\right) \exp\left[-\frac{\pi}{4} \left(\frac{U}{\bar{U}}\right)^2\right] \quad (8.24)$$

$$C(U) = 1 - \exp\left[-\frac{\pi}{4} \left(\frac{U}{\bar{U}}\right)^2\right] \quad (8.25)$$

The Rayleigh PDF only depends on one parameter, the mean wind speed, \bar{U} , making it much easier to use (but not necessarily more accurate!) Note that the Rayleigh distribution is a special case of the Weibull distribution when $k = 2$ and $c = \bar{U} \left(\frac{4}{\pi}\right)^{1/2}$. An example of the Rayleigh distribution for different annual mean wind speeds is shown in [Figure 8.19](#). [Figure 8.19](#) shows that as the mean speed increases, there is a larger probability of having higher wind speeds at a given site, and hence the annual power production has the potential to be higher.

EXAMPLE 8.1: RAYLEIGH WIND SPEED DISTRIBUTION CALCULATIONS

An analysis of wind speed data (10 min interval average, taken over a 1-year period) has yielded an average speed of $\bar{U} = 6$ m/s for a potential WT site. It has been determined

that a Rayleigh wind speed distribution gives a good fit to the wind data. Recall that the Rayleigh PDF is given by Equation 8.24.

- A. Estimate the number of hours per year that the wind speed will be between $U_B = 10.5$ and $U_A = 9.5$ m/s during the year.

To do this, we will find the probability the wind speed will be in a given range during the year, $P(U_A \leq U \leq U_B)$, and multiply the probability by the number of hours in a year.

$$P(U_A \leq U \leq U_B) = \int_{U_A}^{U_B} f(U) dU = \int_0^{U_B} f(U) dU - \int_0^{U_A} f(U) dU = C(U_B) - C(U_A)$$

$$\text{For a Rayleigh distribution } C(U) = 1 - \exp\left[-\frac{\pi}{4} \left(\frac{U}{\bar{U}}\right)^2\right]$$

So

$$C(U_B) - C(U_A) = \exp\left[-\frac{\pi}{4} \left(\frac{U_B}{\bar{U}}\right)^2\right] - \exp\left[-\frac{\pi}{4} \left(\frac{U_A}{\bar{U}}\right)^2\right] = P(U_A \leq U \leq U_B)$$

Substituting $\bar{U} = 6$ m/s, $U_B = 10.5$ m/s, $U_A = 9.5$ m/s yields

$$P(U_A \leq U \leq U_B) = 0.049$$

In other words, the wind speed will be between U_B and U_A m/s 4.9% of the year. Thus, the total number of hours the wind speed is between u_B and u_A in a year is

$$\frac{\# \text{ h}}{\text{year}} = 0.0494 \cdot \frac{24 \text{ h}}{\text{day}} \cdot \frac{365 \text{ day}}{\text{year}} = 432 \text{ h/year}$$

- B. Estimate the number of hours per year that the wind speed is above 16 m/s. This problem is the same as part A with the wind speed ranges being

$$U_B = \infty \quad \text{and} \quad U_A = 16 \text{ m/s.}$$

$$P(\infty \leq U \leq 16) = \int_{16}^{\infty} P(U) dU = C(\infty) - C(16)$$

$$C(\infty) - C(16) = 1 - \exp[-\infty] - \left[1 - \exp\left[-\frac{\pi}{4} \left(\frac{U_A}{\bar{U}}\right)^2\right]\right] = \exp\left[-\frac{\pi}{4} \left(\frac{U_A}{\bar{U}}\right)^2\right] = 0.0038$$

Thus, the total number of hours the wind speed is greater than 16 m/s (i.e., between $U_B = \infty$ and $U_A = 16$ m/s) in a year is

$$\frac{\# \text{ h}}{\text{year}} = 0.0038 \cdot \frac{24 \text{ h}}{\text{day}} \cdot \frac{365 \text{ day}}{\text{year}} = 33 \text{ h/year}$$

8.7 Turbine Performance

Given a WT site, selected by examining long-term wind speed data, a turbine can be picked and/or designed for the site. In order to do this, detailed engineering work has to be conducted to design the blades, tower, electrical systems, and so on. In this section, we build on Section 8.5 and focus on understanding the basics of the blade aerodynamics to design an efficient WT. Aerodynamics is the study of bodies moving through gases. Its use allows the blade and tower shape to be optimized as well as optimizing blade rotational speed. The goal is to maximize the extraction of power from the incoming wind stream and minimize the effect of wind loads (both steady and unsteady).

The efficiency of a WT is the power it extracts compared to the power contained in the wind flowing through the area of the blades. Figure 8.20 contains a schematic comparing these quantities. Similar power curves are published for commercial turbines based on detailed engineering analysis. Note that the power contained in the wind is always greater than the power extracted by the turbine.

The turbine power curve contains several important points. The turbine does not start producing power until the wind speed reaches the cut-in wind speed. This is the lowest wind speed in which the rotor's aerodynamic power is greater than the sum of equipment loads and mechanical and electrical inefficiencies. The cut-out wind speed is the speed at which additional energy production is less than the cost of structural strength to withstand incremental fatigue damage. Lastly, the rated wind speed is the speed at which the turbine is operating near its peak efficiency. The goal is to operate the WT near or at its maximum efficiency.

Earlier, we saw that the standard measure of a WT's efficiency is known as the power coefficient, C_p , and is defined as

$$C_p = \frac{P_{aero}}{P_{wind}} = \frac{Q\Omega}{1/2\rho AU^3} \quad (8.26)$$

where

Q is the aerodynamic torque

Ω is the rotor rotational speed

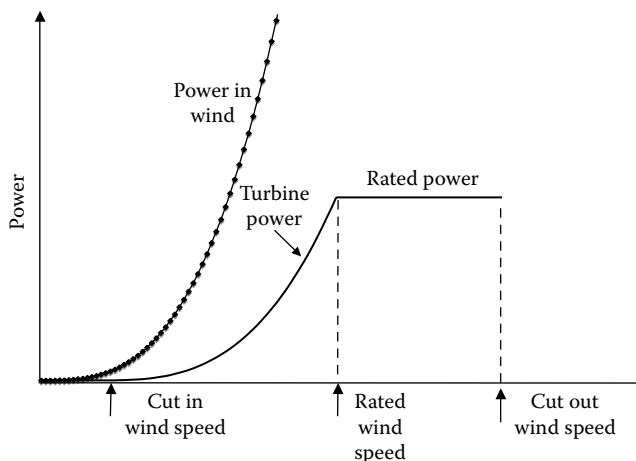


FIGURE 8.20

Wind power and turbine power curves versus wind speed.

A homework problem will show that the maximum theoretical limit of C_p is given by the Betz limit, $C_{p,\max} = C_{p,\text{Betz}} = 16/27 \approx 0.5926$. In other words, the maximum power a WT should be able to extract from the wind is approximately 59% of the power crossing the area swept by the WT blades.

Another heavily used design metric is the TSR, which was defined in Equation 8.10. Design guidelines currently suggest limiting the tip speed to 90 m/s to minimize noise issues.

EXAMPLE 8.2: TIP-SPEED RATIO CALCULATION

What is the TSR for a 90-m-diameter turbine rotating at 15 rpm at a wind speed of 10 m/s?

$$R = \frac{D}{2} = 45 \text{ m} \quad \text{and} \quad U_{\text{wind}} = 10 \text{ m/s}$$

$$\Omega = 15 \text{ rpm} = 15 \frac{\text{rev}}{\text{min}} \cdot 2\pi \frac{\text{rad}}{\text{rev}} \cdot \frac{\text{min}}{60 \text{ s}} = 1.57 \text{ rad/s}$$

$$\text{TSR} = \frac{\Omega R}{U_{\text{wind}}} = \frac{1.57 \text{ rad/s} \cdot 45 \text{ m}}{10 \text{ m/s}} = 7.07$$

Actuator disk theory allows one to find simple relationships for power and thrust. Another more comprehensive theory beyond the scope of this chapter allows one to design the blade shape to optimize power and thrust. This theory, called blade element momentum (BEM) theory, is covered in detail in many of the comprehensive wind energy textbooks (see Burton et al. [34]; Hau [27]).

The first assumption in actuator disk theory is that the area swept by the rotor blades is a permeable disk, shown in Figure 8.21, with an area swept out by the turbine blades. As the wind flows through the disk, momentum (i.e., power and thrust) is extracted.

Figure 8.22 illustrates a top view of an actuator disk (the outlines of a tower and nacelle are omitted). The wind flows from the left to the right. As the wind passes through the actuator disk (area swept by the turbine blades), momentum is extracted and the wind speed is reduced, hence

$$U_{\text{wind}} > U_{\text{disk}} > U_{\text{wake}} \quad (8.27)$$

From the conservation of mass, one can see that as the velocity decreases, the affected area of the column of wind increases (i.e., the mass flow rate remains constant).

Note that the area of the wind column increases after passing through the actuator disk. Additional assumptions are used to develop this theory. Key ones include the following:

- Homogeneous, incompressible, inviscid, and steady-state flow.
- Static pressure far upstream and downstream are equivalent.
- Velocity on either side of the actuator disk is the same.
- Infinite number of blades that are infinitesimally thin.
- Uniform thrust over actuator disk.

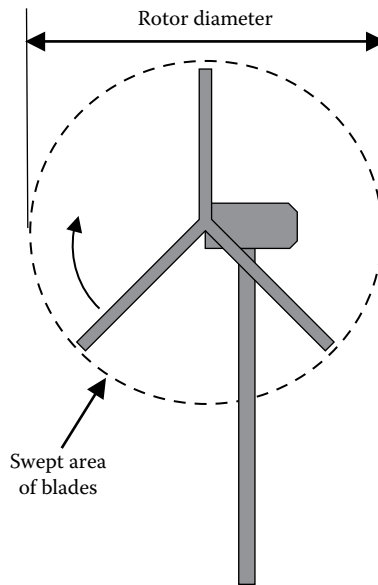


FIGURE 8.21
Actuator disk.

- Nonrotating wake.
- Velocity across the disk is constant.

Bernoulli's theory is valid:

$$P + \frac{1}{2}\rho U^2 = \text{constant} \quad (8.28)$$

More complicated theories such as BEM ease some of these restrictions.

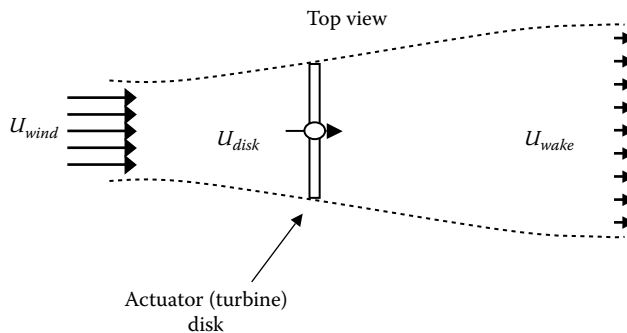
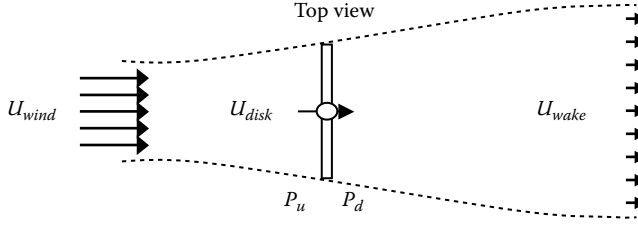


FIGURE 8.22
Actuator disk (top view), showing incoming wind passing through the actuator disk. (Note: Wind speed is denoted by arrow length.)

**FIGURE 8.23**

Actuator disk (top view) with quantities needed for momentum balance. (Note: ρ , air density; A , area of actuator (turbine) disk; P_u , static pressure immediately upstream of disk; P_d , static pressure immediately downstream of disk.)

Next, a momentum balance will be made on the actuator disk (see Figure 8.23) to find the power coefficient, C_p .

Defining x as the wind flow direction and using momentum theory,

$$\sum F_x = (\rho A U_{disk})(U_{wind} - U_{wake}) \quad (8.29)$$

$$A(P_{up} - P_{down}) = (\rho A U_{disk})(U_{wind} - U_{wake}) \quad (8.30)$$

Defining the axial induction factor, a , to be

$$a = \frac{U_{wind} - U_{disk}}{U_{wind}} \quad (8.31)$$

or

$$U_{disk} = (1 - a)U_{wind} \quad (8.32)$$

In other words, the actuator disk induces a reduction in the wind speed at the disk, U_{disk} , compared to the free stream wind speed, U_{wind} .

From the assumptions, one can find

$$U_{wake} = (1 - 2a)U_{wind} \quad (8.33)$$

To find the power coefficient, C_p , we first find the aerodynamic power P_{aero} :

$$P_{aero} = \sum F_{disk} U_{disk} = (2\rho A U_{wind}^2 a(1 - a)) U_{disk} \quad (8.34)$$

$$= (2\rho A U_{wind}^2 a(1 - a)) U_{wind} (1 - a)$$

$$P_{aero} = 2\rho A U_{wind}^3 a(1 - a)^2$$

And substituting P_{aero} into the relationship for C_p (see Equation 8.8),

$$C_p = \frac{P_{aero}}{P_{wind}} = \frac{2\rho A U_{wind}^3 a(1 - a)^2}{1/2\rho A U_{wind}^3} \quad (8.35)$$

Simplifying yields

$$C_p = \frac{P_{aero}}{P_{wind}} = 4a(1-a)^2 \quad (8.36)$$

It is left as a problem to find the Betz limit of $C_{pmax} = 16/27 = 0.59$ from this relationship.

In a similar fashion, a thrust coefficient, C_T , can be found that characterizes the axial thrust on the actuator disk. Summing forces on the disk yields the thrust, T :

$$T = \sum F_{disk} \quad (8.37)$$

$$T = 2\rho AU_{wind}^2 a(1-a) \quad (8.38)$$

Nondimensionalizing the thrust by P_{wind} yields the thrust coefficient

$$C_T = \frac{2\rho AU_{wind}^2 a(1-a)}{1/2\rho AU_{wind}^2} \quad (8.39)$$

and simplifying yields

$$C_T = 4a(1-a) \quad (8.40)$$

The power and thrust coefficients are plotted in [Figure 8.24](#) as functions of the axial induction factor, a . Note that the maximum power and thrust occur at different axial induction factors. The maximum power output of $C_{pmax} = C_{pBetz} = 0.59$ occurs at $a = 1/3$, whereas the maximum nondimensional thrust of 1.0 occurs at a value of $a = 0.5$. When power is maximum at $a = 1/3$, $C_T = 8/9$.

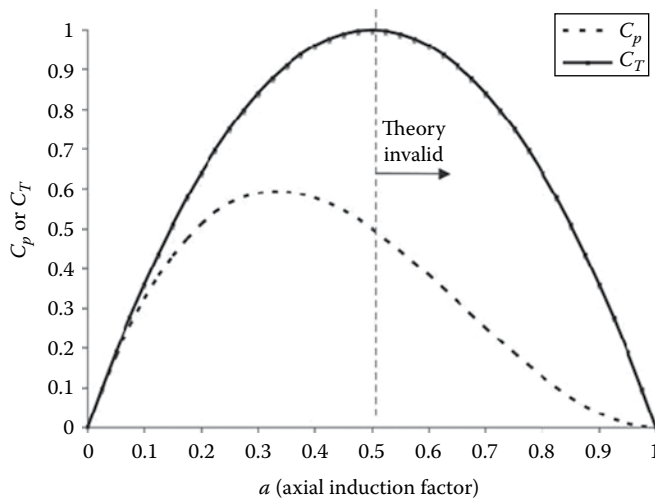


FIGURE 8.24

Power and thrust coefficients versus induction factor showing maximum power coefficient, $C_{p,max}$.

**FIGURE 8.25**

Flow visualization tests conducted in the NASA Ames wind tunnel using smoke emitted from the tips of the turbine helped researchers determine the extent of the wake under a controlled set of conditions. (Courtesy of DOE/NREL, Golden, CO.)

Also note that the axial induction factor theory is not valid for $a > 0.5$. Equation 8.33 shows that the speed of the wake, U_{wake} behind the turbine decreases as the axial induction factor increases from 0.0 to 0.5. At $a = 0.5$, the wake speed equals zero. For values of $a > 0.5$, the wake speed would be negative, violating the assumptions of this simple theory. Figure 8.25 illustrates the wake tip vortex produced by a rotating WT located in a wind tunnel.

Actuator disk theory provides a theoretical limit for the maximum power coefficient of a WT, the Betz limit. In practice, C_p is actually a function of many variables including wind speed, pitch angle, and TSR. Values of C_p are obtained through experiments or numerical modeling.

The aerodynamic power of the wind is determined by rearranging

$$C_p = \frac{P_{aero}}{P_{wind}} \quad (8.41)$$

to yield

$$P_{aero} = C_p P_{wind} = \frac{1}{2} C_p \rho A U_{wind}^3 \quad (8.42)$$

Given C_p and the expected probability of wind distribution, the annual energy production can be estimated. This, in turn, will allow the levelized cost of energy (LCOE) to be calculated as shown in Section 8.8.

EXAMPLE 8.3: DETERMINE ANNUAL ENERGY PRODUCTION

Given a WT with the following parameters, calculate the annual energy production:
 $C_p = C_{p_{\max}} = 0.48$ (C_p value assumed maximum and constant for all wind speeds)

Rated power = 5000 kW = 5.0 MW
 Annual average wind speed = 8.0 m/s
 Rated wind speed = 13.0 m/s
 Cut-out wind speed = 25 m/s
 Rotor radius = 48.0 m
 Area = 7238.2 m²
 Air density = 1.20 kg/m³

The annual energy production for all wind speeds will be illustrated by first calculating the annual energy production at a single wind speed. Then, the methodology will be applied to all wind speeds to arrive at the annual energy production for all wind speeds.

First, determine the power production at a single wind speed, say 10 m/s. Then, a Rayleigh distribution will be calculated to determine the number of hours the wind speed is at 10 m/s. The power and number of hours are then multiplied to determine the yearly energy production for a 10 m/s wind speed.

Power production: For a wind speed of 10 m/s, the power produced for the values shown earlier is

$$P_{aero} = \frac{1}{2} C_p \rho A U_{wind}^3 = \frac{1}{2} (0.48 \cdot 1.2 \cdot 7238.2 \cdot 10^3) = 2084.6 \text{ kW}$$

A plot of the power produced for all wind speeds is shown in [Figure 8.26](#). Note that above the rated wind speed, from 13 m/s up to the cut-out wind speed, the power production is constant at the rated level of 5000 kW.

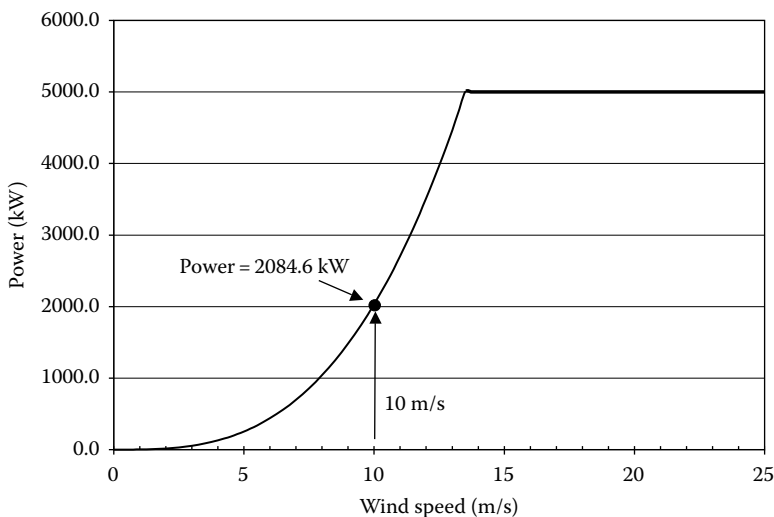


FIGURE 8.26

Power versus wind speed for a 5000-kW turbine with $C_p = C_{p_{\max}} = 0.48$.

Number of hours at 10 m/s: Assuming a Rayleigh PDF with an average wind speed of 8 m/s, the annual probability of a 10 m/s wind, calculated for the interval from 9.5 to 10.5 m/s, is

$$C(10.5) - C(9.5) = \exp\left[-\frac{\pi}{4}\left(\frac{10.5}{8}\right)^2\right] - \exp\left[-\frac{\pi}{4}\left(\frac{9.5}{8}\right)^2\right] = 0.0719 = 7.19\%$$

Thus, in a given year, the number of hours the wind will blow at 10 m/s at this site is the probability times the number of hours in a year

$$0.0719 \cdot \frac{24 \text{ h}}{\text{day}} \cdot \frac{365 \text{ day}}{\text{year}} = 629.8 \text{ h}$$

A plot of the number of hours the wind blows at a given wind speed for all wind speeds is shown in [Figure 8.27](#).

Finally, the annual energy production for this WT, at this site, at a wind speed of 10 m/s is found by multiplying the power production times the number of hours the power is produced, in this case:

$$\text{Annual energy production at 10 m/s} = 2084.6 \text{ kW} \cdot 629.8 \text{ h} = 1312.9 \text{ MWh}$$

In a similar fashion, this is done for all wind speeds up to cut out. The energy production from all wind speeds is then summed to determine the annual energy production estimate. A summary table of the calculations is shown in [Table 8.5](#).

Examination of [Table 8.5](#) shows that the annual energy produced at this site is calculated to be 13,873 MWh. If electricity costs 10 cents/kWh (\$0.10/kWh), the annual value of the energy produced in this example would be

$$\text{Annual value} = 13,873,070 \text{ kWh} \cdot \frac{\$0.10}{\text{kWh}} = \$1.4 \text{ million}$$

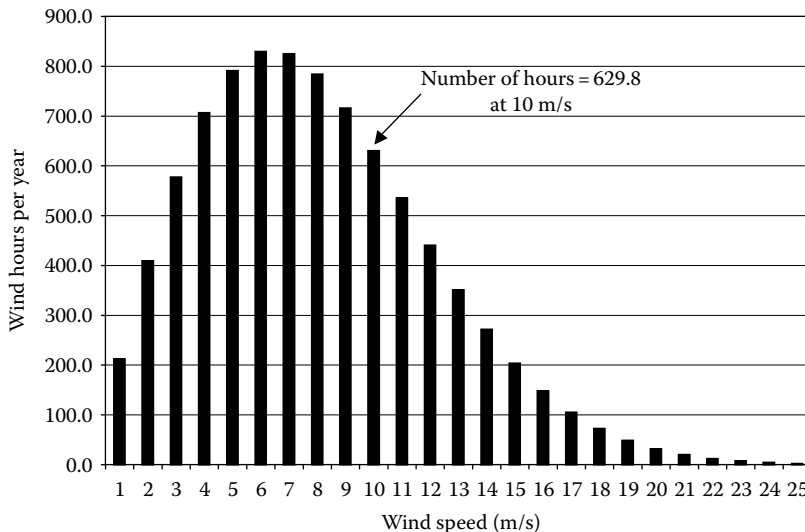


FIGURE 8.27

Number of hours at a given wind speed for a Rayleigh distribution with an annual average wind speed of 8.0 m/s.

TABLE 8.5

Power and Annual Energy Calculation

Wind Speed (m/s)	Power (kW)	Probability (%)	# of Hours/Year	Energy (kWh)
1	2.1	2.42	212.4	442.7
2	16.7	4.67	409.4	6,827.6
3	56.3	6.59	577.6	32,507.8
4	133.4	8.07	706.7	94,283.4
5	260.6	9.03	791.0	206,114.7
6	450.3	9.47	829.3	373,429.3
7	715.0	9.42	824.9	589,808.3
8	1067.3	8.95	784.2	837,017.8
9	1519.7	8.17	716.1	1,088,282.6
10	2084.6	7.19	630.2	1,313,739.7
11	2774.6	6.12	535.7	1,486,478.3
12	3602.2	5.03	440.7	1,587,567.2
13	4579.9	4.01	351.3	1,608,943.1
14	5000.0	3.10	271.6	1,358,130.2
15	5000.0	2.33	203.9	1,019,404.1
16	5000.0	1.70	148.7	743,288.9
17	5000.0	1.20	105.4	526,756.5
18	5000.0	0.83	72.6	362,992.5
19	5000.0	0.56	48.7	243,323.3
20	5000.0	0.36	31.7	158,710.6
21	5000.0	0.23	20.2	100,758.5
22	5000.0	0.14	12.5	62,274.8
23	5000.0	0.09	7.5	37,478.8
24	5000.0	0.05	4.4	21,967.4
25	5000.0	0.03	2.5	12,541.7
Total: 99.76			Total: 13,873,070.1 kWh	

Now, the rationale to build wind farms comprised of dozens of WTs with a similar energy (cash) output can be seen. The wind is literally producing money!

As noted and shown in [Table 8.5](#), the power produced above 13 m/s (rated wind speed) is a constant value of 5000 kW. Control schemes are typically implemented to limit the maximum amount of power produced by a turbine to the rated turbine power (5 MW in this case) at the rated wind speed (13 m/s). Limiting the power production is important from both a structural standpoint and an electrical generation standpoint. In both cases, WT components must be sized to operate under maximum defined loads and thus cannot handle larger loads.

Another measure of a WT's performance is the capacity factor. Because the wind never blows continuously, a turbine will never be able to operate steadily at full power. The capacity factor is the ratio of the energy produced to the theoretical maximum the turbine could produce (i.e., rated power production, 24 hours a day, 7 days a week for a year):

$$\text{Capacity factor} = \frac{\text{Energy generated}}{\text{Rated power} \times (\# \text{ h/year})} = \frac{\text{Energy generated}}{\text{Rated power} \times 8760 \text{ h}}$$

For this example, the capacity factor is found to be

$$\text{Capacity factor} = \frac{13,880 \text{ MWh}}{5 \text{ MW} \times 8760 \text{ h}} = 31.7\%$$

For comparison, typical WT capacity factors are 20%–40% [35].

Finally, the calculations shown in Table 8.5 would typically be done at wind speed increments of 0.10 or 0.25 m/s. Note that slight differences in values between the spreadsheet table and the example calculations are due to round-off errors in the example calculations.

8.7.1 Control Schemes

As a comparison, we will briefly examine the major control schemes currently used in large commercial WTs. In the first case, the rotor speed is held fixed or constant while the blade pitch is variable. In the second case, both the rotor speed and the blade pitch are variable. The fixed rotor speed turbine has a simpler mechanical design, the control scheme is easier to implement, and it also offers advantages by simplifying the electrical power generation. The variable-speed and variable-pitch (VSVP) control scheme is more complicated, both mechanically and electrically. Is the more complicated VSVP turbine worth it from an energy production standpoint?

Figure 8.28 illustrates the power output versus wind speed for both WT control methods. The operating parameters cited in Example 8.3 were also used for Figure 8.28. In addition, the results in Example 8.3 are the same shown here for the VSVP turbine.

The key point is that the VSVP turbine has a higher power output. Two regions can be seen where the VSVP turbine power output is higher than the constant-speed/variable-pitch

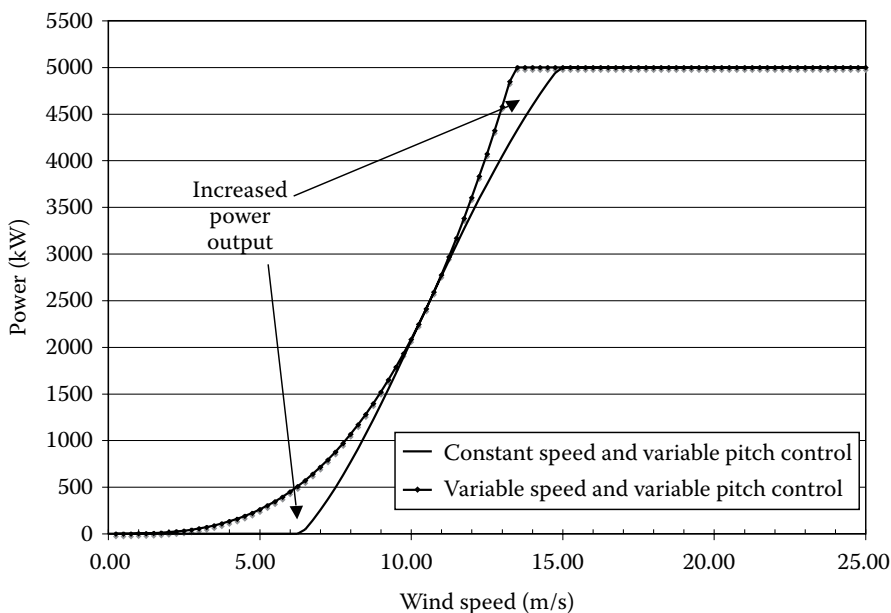


FIGURE 8.28

Power output for constant-speed/variable-pitch and variable-speed and pitch-controlled schemes.

TABLE 8.6

Energy Production and Capacity Factor for VSVP and CSVP Wind Turbines

	CSVP	VSVP	Percent Increase from CSVP to VSVP (%)
Energy (MWh)	12,000	13,880	15.3
Capacity factor	27.5%	31.7%	15.3

(CSVP) turbine. This increased power output will lead to a higher annual energy production and capacity factor. This is because of the ability to operate the VSVP turbine at $C_p = C_{p\max}$ at all wind conditions. The CSVP runs at a variable, C_p . Because the turbine cannot vary rotor speed, it cannot run at $C_p = C_{p\max}$ at all conditions.

Note that both turbines eventually reach a rated power of 5 MW. However, the CSVP reaches the 5 MW turbine rating at a higher wind speed, 15 m/s, whereas the VSVP turbine reaches 5 MW rated power at 13.5 m/s. This is because the CSVP turbine is operating at a lower C_p and thus needs a higher wind speed to reach the higher 5 MW power rating. For the purposes of this illustration, C_p for the CSVP was assumed to be a function of TSR ($\Omega R /$ (wind speed)) and a fixed pitch angle of 0°

$$C_p(\lambda, \beta) = 0.5176 \left(\frac{116}{\lambda_i} - 0.4\beta - 5 \right) e^{-21/\lambda_i} + 0.0068\lambda \quad (8.43)$$

where

$$\lambda = \text{Tip speed ratio} = \frac{\Omega R}{\text{Wind speed}}$$

$$\frac{1}{\lambda_i} = \frac{1}{\lambda + 0.08\beta} - \frac{0.035}{\beta^3 + 1}$$

β is the blade pitch angle.

Examining [Table 8.6](#), we can see that the VSVP-controlled turbine produces over 15% more energy (i.e., 15% more yearly revenue), and thus has a capacity factor 15% higher than the CSVP-controlled turbine. The goal of WT manufacturers is to design and build turbines, such as the VSVP turbine, that produce more power while minimizing the cost to design and build these turbines, to achieve the highest level of performance possible.

8.8 Levelized Cost of Energy for a Wind Turbine

A successful wind turbine design must be strong, reliable, and produce energy at a cost that is competitive with other technologies. Among others, the National Wind Technology Center at the National Renewable Energy Laboratory (NREL) has developed a wind energy electricity cost-estimating tool. The tool focuses on wind turbine configurations that are

currently the most common: three-bladed, upwind, pitch-controlled, variable-speed, and for both land-based and offshore wind turbines [36]. Results are in 2002 dollars, and cost data are based on a mature technical design and mature component production for a 50 MW wind farm installation.

The LCOE of a single WT is found using

$$\text{LCOE} = \frac{(\text{FCR} \cdot \text{ICC})}{\text{AEP}_{\text{net}}} + \text{AOE} \quad (8.44)$$

where

LCOE is the levelized cost of energy (i.e., electricity) (in constant \$) (\$/kWh)

FCR is the fixed charge rate (in constant \$). (Interest rate in %/year expressed as decimal value/year.)

ICC = initial capital cost (\$) = Turbine cost + balance of station

AEP_{net} = Net annual energy production (kWh/year)

= Capacity factor · rated turbine power (kW) · 8766 (h/year)

where

$$\text{Capacity factor} = \frac{\text{Energy capture (kWh)}}{\text{Rated turbine power (kW)} \times 8766 \text{ h/year}}$$

NOTE: The number of hours in a year is typically defined in one of two ways:

1. 24 h/day × 365 day/year = 8760 h/year

or

2. To take into account a leap year every fourth year, 6 h/year is added to account for one-fourth of the leap day: 24 h/day × 365 day/year + 6 h/year = 8766 h/year

The NREL LCOE tool uses the second definition, 8766 h/year, for number of hours in a year.

AOE = annual operating expenses (\$/kWh)

$$\text{AOE} = \text{LLC} + \frac{(\text{O\&M} + \text{LRC})}{\text{AEP}_{\text{net}}} \quad (8.45)$$

where

LLC is the land lease cost (\$/kWh)

O&M is the levelized operation and maintenance cost (\$/year)

LRC is the levelized replacement/overhaul cost (\$/year)

Fixed charge rate (FCR) is the interest rate needed to cover the capital cost, a return on debt and equity, and various other fixed charges.

The initial capital cost (ICC) is the sum of the turbine system cost and the balance of station (BOS) cost: $ICC = \text{turbine system cost} + \text{BOS}$

The components in these systems are:

Turbine system (rotor, drivetrain, nacelle) cost.

Rotor: blades, hub, pitch mechanisms and bearings, spinner, nose cone.

Drivetrain and nacelle: Low-speed shaft, bearings, gearbox, mechanical brake, high-speed coupling, and associated components, generator, variable-speed electronics, yaw drive and bearing, main frame, electrical connections, hydraulic and cooling systems, nacelle cover.

Control, safety system, and condition monitoring.

Tower.

NOTE: Total WT cost = turbine system + control + tower

The total turbine cost is often expressed as a turbine cost per kW (\$/kW) multiplied by the turbine rating (kW).

For example: Given a typical \$1100/kW turbine cost per kW for a 5-MW turbine

$$\text{Total turbine cost} = \$1100 \times 5000 = \$5.5 \text{ million}$$

BOS

Foundation/support structure

Transportation

Roads, civil work

Assembly and installation

Electrical interface/connections, cables, transformers

Engineering permits

Offshore turbines have additional costs

Equipment modifications to handle marine environments

Port and staging equipment

Personal access equipment

Scour protection

Surety bond (to cover decommissioning)

Offshore warranty premium.

Note that, currently, a typical BOS cost for a land-based turbine is approximately \$700,000 per turbine.

LLC, one component of the annual operating expense, are the rental or lease fees charged (e.g., land or ocean bottom lease cost) for the turbine installation.

Operation and maintenance (O&M) is a component of the annual operating expense that is larger than the LLC. The O&M cost normally includes:

Labor, parts, and supplies for scheduled and unscheduled turbine maintenance.

Parts and supplies for equipment and facilities maintenance.

Labor for administration and support.

Levelized replacement/overhaul cost (LRC) distributes the cost of major replacements and overhauls over the life of the WT.

Finally, the AOE includes land or ocean bottom lease cost (LLC), levelized O&M cost, and LRC.

LCOE can then be expanded to show that the annual cost is due to three major components:

$$\text{LCOE} = \frac{(\text{FCR} \times \text{ICC})}{\text{AEP}_{\text{net}}} + \text{AOE} = \text{LLC} + \frac{(\text{FCR} \times \text{ICC})}{\text{AEP}_{\text{net}}} + \frac{(\text{O\&M} + \text{LRC})}{\text{AEP}_{\text{net}}} \quad (8.46)$$

In other words, the LCOE is due to:

1. Costs of leasing land (if land is purchased, this cost is \$0)
2. ICCs to buy/construct all WT parts
3. Ongoing costs due to yearly operations, maintenance, overhauls, and replacements.

Typical values used to calculate LCOE are:

Fixed charge rate (FCR) = 10%–15%

Turbine cost/kW = \$800–1100/kW (for megawatt-size turbines)

Capacity factor = 25%–40%

O&M costs (scheduled maintenance) = \$0.005–\$0.010/kWh

Finally, typical component costs for a megawatt-scale WT are shown in [Figure 8.29](#). [Figure 8.29](#) shows BOS (21%), O&M (19%), and LRC (11%) sum to 51% of the total LCOE cost, whereas the drivetrain (27%) has the largest single cost of the turbine components. The rotor (12%), tower (9%), and control system (1%) sum to only 22% of the total LCOE. When the drivetrain is added to these components, the sum of all WT components is 49% of the total LCOE cost. In summary, installing, maintaining, and overhauling/replacing components is approximately half (51%) of the cost of electricity for a WT, which illustrates the need for an efficient installation method and a well-designed, reliable WT.

EXAMPLE 8.4: LCOE CALCULATION

What is the LCOE for a WT with the following characteristics?

Turbine rating = 5 MW = 5000 kW

CF = capacity factor = 40.00%

TC = turbine cost = \$1100/kW

O&M cost/year = \$87,600/year

FCR = fixed charge rate = 10.00%

BOS = balance of station = \$2,360,000

LRC = levelized replacement costs = \$123,000/year

LLC = land lease costs = \$0/year

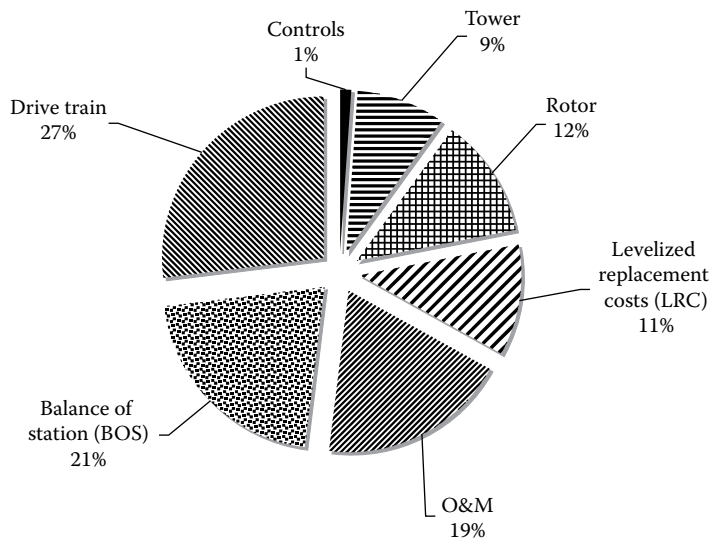


FIGURE 8.29
Individual component costs as a percentage of LCOE for a land-based, megawatt-scale wind turbine.

Answer

$$\begin{aligned} \text{AEP}_{\text{net}} &= \text{Annual energy production, Net (kWh / year)} \\ &= CF \cdot \text{turbine rating} \cdot 8760 = 17,520,000 \end{aligned}$$

$$\begin{aligned} \text{ICC} &= \text{Initial capital cost} = \text{Turbine cost} + \text{Balance of station} \\ &= \text{Rating} \cdot \text{TC} + \text{BOS} = \$7,860,000 \end{aligned}$$

$$\begin{aligned} \text{AOE} &= \text{LLC} + (\text{OM} + \text{LRC}) / \text{AEP}_{\text{net}} = 0 + (87,600 + 123,000) / 17,520,000 \\ &= \$0.012 / \text{kWh} \end{aligned}$$

$$\begin{aligned} \text{LCOE} &= \frac{(\text{FCR} \times \text{ICC})}{\text{AEP}_{\text{net}}} + \text{AOE} = \frac{(0.1 \cdot 7,860,000)}{17,520,000} + 0.012 = 0.045 + 0.012 \\ &= \$0.057 / \text{kWh} \end{aligned}$$

% of total LCOE due to ICC = 79%

% of total LCOE due to AOE = 21%

For this example, 79% of the yearly cost is due to the actual WT and installation of the turbine. The remaining 21% of the yearly cost is a result of expenses needed to keep the turbine running.

This analysis assumes that costs are known for the turbine of interest. If one is planning to design a turbine, the NREL report [36] contains cost relationships for turbine components, for example, estimated cost of a WT blade as a function of length. This allows one to estimate the turbine, control system, tower, BOS, and offshore turbine costs. Knowledge of maintenance costs, replacement costs, and actual WT site information (for capacity factor) allows the COE for a WT at a site to be determined and evaluated for possible commercial development.

8.9 Wind Farms

A wind farm is a group of WTs producing electricity in a single location (see [Figure 8.30](#)). To have a successful wind farm, selecting a proper location is key [37,38]. The most important item is selecting a site with the desired wind resource. The winds must be consistent and have a sufficient speed to generate the desired energy. Wind resource maps (see Section 8.6.2) are a typical starting point. Meteorological data from “met” towers erected by companies interested in a site give a detailed view of the wind resource at a specific site.

Potential impacts of WT farms also need to be considered. As noted earlier, bird/bat activity and avian migration need to be considered to prevent negative effects on the environment. Noise effects can also have an impact in the area local to a proposed wind farm site. In addition, larger questions are also studied, for example: Will the turbines create interference for local air traffic? These additional factors must be weighed in addition to the wind resource when selecting a WT site.

Besides wind resource and environmental effects, other factors that must be considered include land access (lease or purchase, zoning, and permits must be obtained) and sufficient capital to fund the project (approximately \$1 million per megawatt of installed generating capacity) [37]. The wind farm would ideally be located near existing transmission lines to limit the cost (up to \$1 million/mile) of installing large lengths of new transmission lines that drive the BOS costs up. In addition, there has to be a market available and an agreement in place to buy the electric power produced. Assuming that other factors are favorable, based on wind resource and turbine costs, the wind farm developer selects a WT model. Additional steps include checking with the manufacturer for availability and considering a service provider for annual maintenance.

Another consideration is the issue of intermittency. The power output from a single WT can be intermittent because the wind speed can fluctuate. On the other hand, a wind farm,

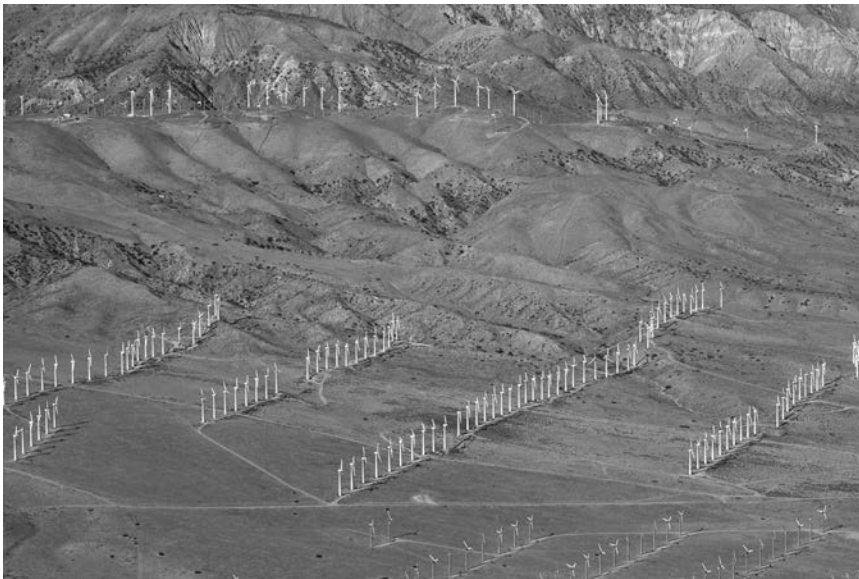
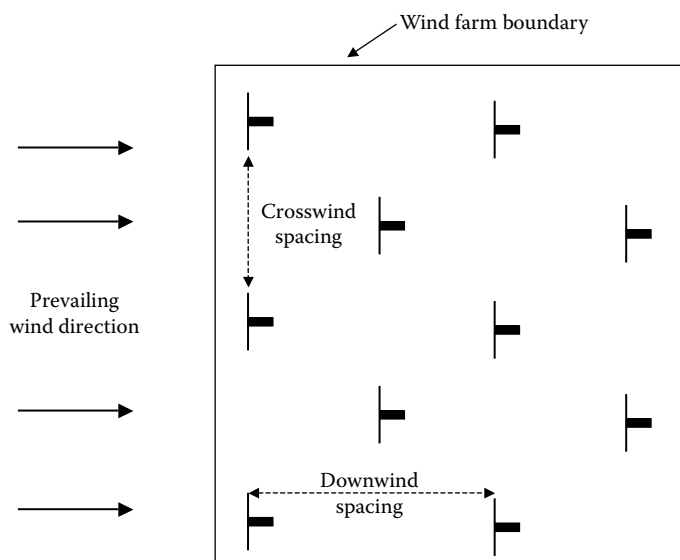


FIGURE 8.30

Wind farm located in Tehachapi, California, operational since the early 1980s. (Courtesy Ian Kluft.)

**FIGURE 8.31**

Schematic (top view) of typical wind farm layout.

with WTs distributed over a large, geographically diverse area, will have less chance of the wind speed being low for all WTs in the wind farm. A study by Archer and Jacobson [39] indicates that when multiple wind farms are interconnected together in an array through the electric transmission grid, the correlation between the wind speeds at the sites decreases, thus producing steadier output. In addition, the benefits of interconnecting wind farms continued to grow as the number of connected wind farms increased.

On the other hand, distributing WTs in a wind farm over a large geographic area drives up BOS costs due to the increased cost of electrical interconnects and the potential need for new transmission lines. Wind farms are typically arranged with a rectangular grid pattern of turbines with each successive row staggered, as shown in Figure 8.31. Turbines are staggered by a specified number of rotor diameters apart, both side to side (crosswind spacing) and between rows (downwind spacing) of turbines. This distance varies with the wind farm owner, site conditions, and wind resource. If only BOS costs are considered, the turbines should be placed closer together. From a power output standpoint, if 100 turbines rated at 2 MW each are to be placed at this site, the total power output could be anticipated to be 200 MW. Unfortunately, this is not the case.

Consider a typical wind farm development scenario. Once transmission, land-use issues, and a power purchase agreement are in place, the wind farm development can proceed. The wind resource estimates from the met tower for a potential site are anticipated to be sufficient for power production; however, wind farms do not always produce the expected power. Several factors could be responsible for this unexpected reduction in power output.

For example, the met tower used to collect data to make the wind resource predictions can only measure wind at one location. The wind resource could change throughout the site depending on terrain such as ridges and hills or on surface features like a forest. As turbines are built farther away from the met tower, the resource prediction becomes less accurate.

Another suspect for producing less-than-expected power is wake effects or array effects. Depending on the locations of the turbines positioned on the site and the direction of the

wind, some turbines can be located downwind of other turbines. As a turbine extracts energy from the wind, the flow downstream becomes slower and more turbulent. This slower, more turbulent flow persisting downwind of a turbine is known as a wake. Turbines built in the wakes of other turbines have a diminished wind resource and do not produce the power levels of the upwind turbines. This will result in the production of less energy, which means a reduced monetary return for investors. Downstream of a WT (perhaps 15 rotor diameters or much more depending on conditions), the wind speed in the wake will begin to approach the free stream velocity, thereby allowing higher energy production by downstream turbines. Unfortunately, increasing the spacing between turbines increases BOS costs (e.g., more construction and materials), resulting in a lower return on investment. Several projects studying wake effects strive to quantify wake losses to better design wind farms.

Wake modeling is an active area of research [40] and detailed treatment is beyond the scope of this textbook. However, a 2009 study by Stovall [41] illustrates the significance of wake interaction effects. Stovall used computational fluid dynamics and large-eddy simulations to examine the overlying boundary layer effects on wake propagation. Two turbines, with 100 m rotor diameters, are modeled as being inline. The incoming wind speed to the upstream turbine is approximately 8–10 m/s. The objective is to determine the effect the wake has on the power output of the downstream turbine compared to power output of the upstream turbine. In this study, the turbines have a downwind spacing of 9 rotor diameters. The power coefficient for the turbines in this simulation is approximately $C_p = 0.50$.

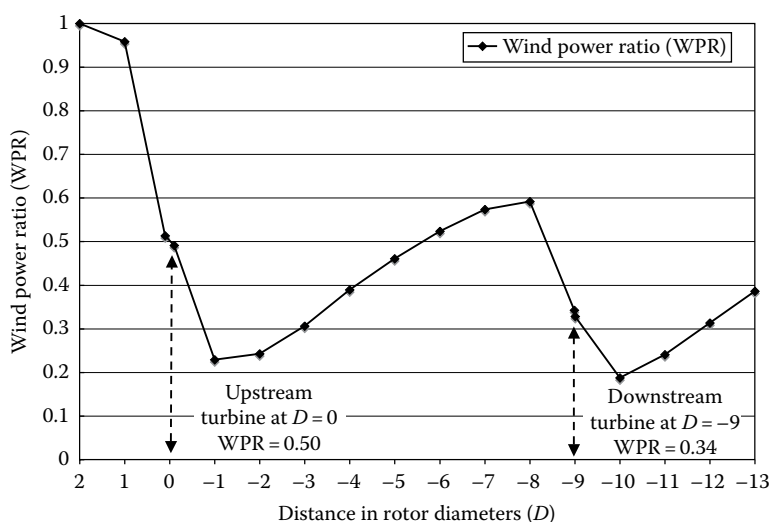
Prior to modeling the power output of the WTs, a simulation of the ABL is created. Once the ABL simulation is validated, turbines are imposed into the domain with the turbine rotors modeled via actuator disks. The actuator disks impose a pressure drop on the flow field proportional to the power extracted by a turbine.

Results from the numerical simulation show the diminished wind resource caused by the wake-forming downstream of a WT. Figure 8.32 illustrates the power in the wind calculated as the area integral of velocity cubed (Equation 8.6). Distances between the turbines are shown in rotor diameters (D). The inlet of the computational domain used in this numerical simulation is located at $D = +2$. The first turbine is located at $D = 0$, whereas the second turbine is located 9 rotor diameters downstream of the first turbine at $D = -9$. All wind power is expressed as a wind power ratio (WPR) of the wind power at a given location divided by the inlet wind power (located at $D = +2$). This results in a $WPR = 1.0$ at the inlet ($D = +2$).

Notice that the nondimensional wind power extracted by the first turbine is half of the wind power at the inlet, yielding a $WPR = 0.50$, as would be expected because the power coefficient is $C_p = 0.50$.

Downstream of the first turbine, the wake is represented by a further reduction in wind power due to turbulent losses. As distance increases downstream of the first turbine, the wake begins to recover (D increases from $-1 \rightarrow -8$) as surrounding higher speed (i.e., higher energy) wind mixes with the wake. The power in the wake, however, does not achieve free stream power levels prior to reaching the second turbine.

Because the incoming power of the wind is lower immediately upstream of the second turbine, the power output of the second turbine should be lower than the power output of the first turbine. Indeed, the WPR of the second turbine in this simulation is $WPR = 0.34$, indicating that the second turbine was only able to extract 34% of the energy available in the incoming stream at $D = +2$. The wake from the first turbine adversely impacts the power output of the second turbine. Another way to view this is that the ratio of

**FIGURE 8.32**

Wind power wake reduction: Local wind power normalized by wind power level at an inlet. (From Stovall T.D., 2009. Simulations of wind turbine wake interactions in OpenFOAM, MS thesis, University of Colorado, Boulder, CO. With permission. [41])

the power extracted by a second turbine (located $9D$ downstream of the first turbine in this study) to the first turbine is approximately 67% (i.e., $0.34/0.50 = 0.67$). In economic terms, the second turbine will only produce 67% of the income of the first turbine in this scenario.

Increasing the spacing between the turbines in the downwind direction reduces the wake effect but increases the BOS costs. A trade-off between these two competing economic factors remains an active area of research. Although the results from the Stovall study match up with experimental data from wind farms, the simulation addresses a relatively simple configuration. The computational resources required for modeling an entire wind farm (dozens of turbines) are significant and remain an area of research for government and industry to develop for optimizing wind farm layouts [42,43]. Significant work still remains to develop a robust, accurate, and fast optimization tool for wind farm wake effects. With such a tool, BOS costs can be optimized simultaneously with turbine location resulting in maximum energy (income) production.

8.10 Offshore Wind Energy

Offshore WT farms (see Figure 8.33) address limits of land-based wind farms such as transmission line access and capacity [44], and space for WTs (more of an issue in higher-density population areas such as Europe), while providing access to a vast wind resource. Significant development still remains for wind farms in water deeper than 30 m. BOS costs can double in an offshore installation compared to land-based installation. Still, the complexity of offshore technology development is more than offset by the need and desire to harness the higher wind resource available offshore (ocean as well as large inland lakes).



FIGURE 8.33
Offshore wind farm. (Courtesy of Hans Hillewaert.)

Offshore wind energy has a number of benefits including:

Better wind resources

- Reduced turbulence resulting in steadier winds
- Higher wind speed resulting in higher energy production
- Higher-capacity factors resulting in better electric load matching

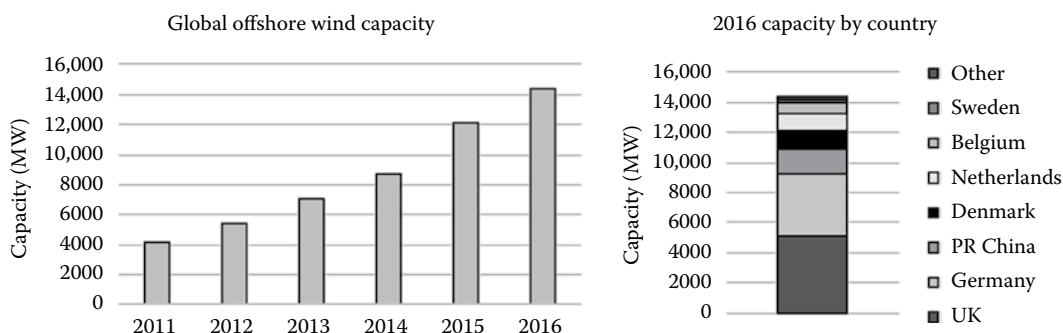
Closer proximity to electric load centers resulting in:

- Lower transmission costs and constraints
- Ability to serve high-cost regions

Avoids land-based size limits:

- Shipping—no land-based roadway limits
- Assembly—sea-based cranes are taller
- Larger machines are more economical

These benefits are significant throughout the world. There are over 12,000 MW of installed offshore wind in the world; approximately 90% of this is off northern Europe. This is shown in [Figure 8.34](#) [45]. In 2016, the first offshore wind farm in the United States was installed—a \$300 million project off the coast of Rhode Island (Block Island Wind Farm) [46]. This 30-MW project consists of five 6-MW turbines on fixed four-legged jacket substructures [47]. World offshore wind capacity is projected to grow to 120,000 MW by 2030 [48]. The cost of offshore wind power has dropped dramatically in recent years: from \$140/MWh in 2012 to \$126/MWh in 2016, with prices forecast to drop to \$100/MWh by 2030 [48].

**FIGURE 8.34**

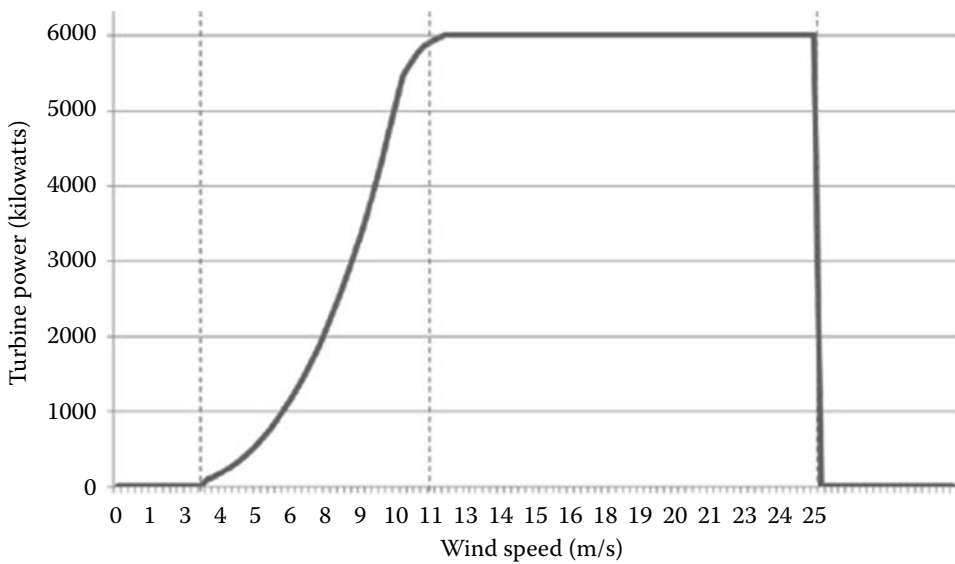
Global cumulative offshore wind capacity in 2016 by country and total global cumulative wind capacity by year from 2011 to 2016. (Data from Global Wind Energy Council. Offshore wind power, <http://www.gwec.net/global-figures/global-offshore/>. [45])

Most of the offshore wind capacity installed or under construction around the world is sited at locations with an ocean depth that is less than 40 m and distances to shore of less than 50 km [47]. However, new projects are advancing beyond these envelopes.

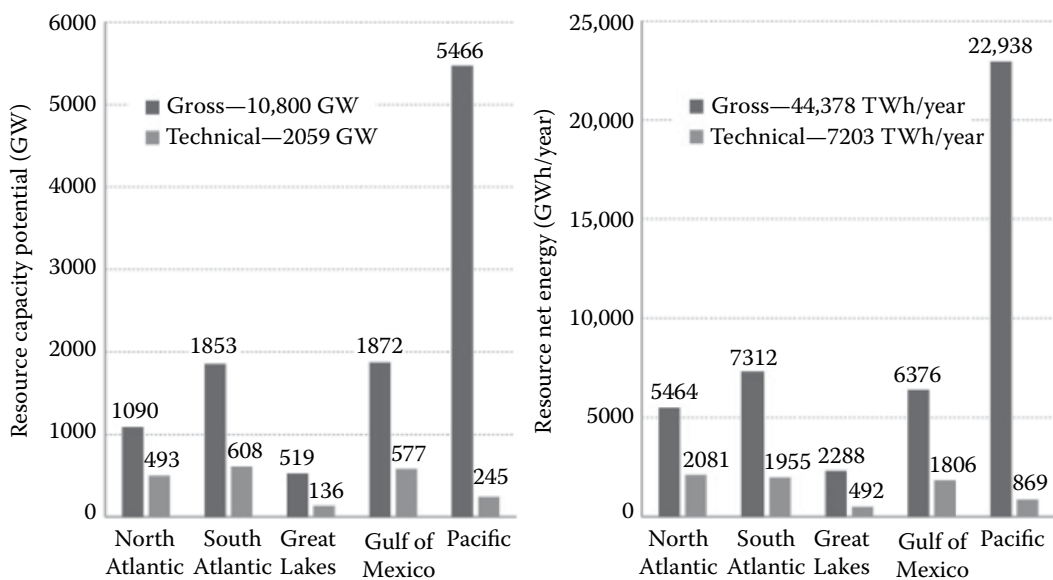
Of the 48 contiguous United States, 28 have a coastal boundary, and these 28 states use three-quarters of the electricity in the United States [49]. Because these coastal load centers are typically located hundreds of miles from land-based wind energy sources, offshore wind power provides a nearby source of energy. Many of these coastal states have relatively modest onshore wind resources, but they have significant resources offshore.

A recent NREL study [50] assessed the potential available offshore wind power as a function of depth and coastal location for the United States. As shown in Figure 8.15, the United States has significant wind resources located off the Atlantic and Pacific Coasts, in the Gulf of Mexico and Great Lakes, and surrounding Hawaii. The study estimated resources assuming a 100 m hub height, with technical potential constrained by currently available technology. Figure 8.35 [50] shows the power curve for a 6 MW offshore turbine that was used as the basis for the assessment. The estimates of technical potential also exclude identified areas with economic or environmental conflicts, although more detailed assessments would be required before development could move forward at specific sites. Losses from wake effects and electrical systems were accounted for in determining net technical potential. Figure 8.36 [50] shows the resulting estimated gross and technical potential for offshore wind by U.S. region. Of the 7203 TWh/yr of technical potential, 22% is at < 30 m depth and an additional 20% at depths between 30 and 60 m. The availability of shallow water sites is more limited in some areas such as California, where only 4% of technical potential is at a depth of < 60 m. With regard to distance offshore, 7% of the U.S. technical potential is located < 3 nautical miles (5.6 km) offshore, 13% between 3 and 12 nautical miles (5.6 and 22.2 km), and 41% between 12 and 50 nautical miles (22.2 and 92.6 km).

Design of substructures to support wind turbines in offshore environments has been a key technical challenge for this industry. Figure 8.37 illustrates six different turbine substructures [51]. The fixed-bottom substructures are used in relatively shallow waters, at depths of up to 60 m. This technology is relatively well established, although innovative

**FIGURE 8.35**

Power curve for a 6 MW wind turbine assumed to be representative of currently available offshore technology. (From Musial, W. et al., September 2016. *2016 Offshore Wind Energy Resource Assessment for the United States*. NREL/TP-5000-66599, National Renewable Energy Laboratory, Golden, CO, <http://www.nrel.gov/docs/fy16osti/66599.pdf>. [50])

**FIGURE 8.36**

Capacity (left) and net energy (right) offshore gross resource (dark shading) and final net technical (light shading) potential estimates for five U.S. offshore wind resource regions. (From Musial, W. et al., September 2016. *2016 Offshore Wind Energy Resource Assessment for the United States*. NREL/TP-5000-66599, National Renewable Energy Laboratory, Golden, CO, <http://www.nrel.gov/docs/fy16osti/66599.pdf>. [50])

**FIGURE 8.37**

Six different substructures for offshore wind turbines. The three on the left are fixed-bottom substructures (monopile, jacket, and inward battered guide); the three on the right are floating substructures (semisubmersible, tension leg platform, and spar). Illustration by Josh Bauer, NREL. (From Gilman, P. et al., 2016. *National Offshore Wind Strategy: Facilitating the Development of the Offshore Wind Industry in the United States*, U.S. Department of Energy and U.S. Department of the Interior, <https://energy.gov/sites/prod/files/2016/09/f33/National-Offshore-Wind-Strategy-report-09082016.pdf>. [51])

designs are still required to accommodate seabed conditions at specific locations. Significant technology challenges exist to develop floating WT that could be deployed for waters deeper than 60 m. Modeling a floating WT is a challenging task because it must include effects from wind and wave interaction with the turbine and floating substructure, a nonstationary and rotating turbine, and a control system, which monitors and controls the turbine for these effects. State-of-the-art research is underway using codes such as NREL's FAST [52].

In addition to design improvements and cost reductions for wind turbine and substructure technology, opportunities for offshore wind energy would benefit from improved engineering solutions for installation of equipment in offshore environments, and for approaches to streamline O&M activities. Another need is for improved resource and site characterization information for offshore locations. Concerns have been raised about the potential impacts of offshore wind installations on migratory birds, marine mammals, and fisheries. Biological surveys have been conducted to characterize the distribution of wildlife in relation to potential offshore wind locations, but empirical information on actual impacts or mitigation methods is limited for this nascent technology. There is also need for better information on impacts of offshore wind farms on human activities and other technologies, including fishing and potential interference with radar systems for air traffic control, weather, and navigation [51].

8.11 System Advisor Model for Wind Farm Analysis

As introduced earlier, the System Advisor Model (SAM) is a numerical performance and economic model designed by NREL to make performance predictions and economic estimates for stand-alone or grid-connected electric power projects in the distributed and central generation markets. For wind projects, the model calculates the cost of generating electricity based on information about the project's desired power output location, wind turbine type, installation, operating costs, and various financial data such as interest rates, incentives, and system specifications. The performance model makes hour-by-hour calculations for the power output of wind systems generating a set of 8760 hourly values that represent the system's electricity production during a typical year.

For wind energy systems, SAM reads weather files provided by Energy Plus. Running the model requires a file of the wind at the project location. SAM comes with a set of sample files that contain complete sets of sample costs and performance input data called default values, but it is the analyst's responsibility to modify the input data as appropriate for the project being evaluated.

To utilize SAM, begin by downloading and installing NREL's free system at <https://sam.nrel.gov>. From the SAM home page, you can create a new utility wind energy project as follows. The following instructions are for the "SAM 2017.1.11" release.

EXAMPLE 8.5: SAM METHOD TO DETERMINE LCOE

Using NREL's SAM software, model a 50 MW utility wind farm using turbines with a nameplate capacity of 2000 kW. Assume a 25-year lifetime, a 10% IRR target, an inflation rate of 2%, an interest rate of 6%, and a 2.3¢/kWh production incentive credit. Run this model for two different locations: southern Wyoming and northern Alabama. How many turbines are needed to build these wind farms? For each location, find the wind farm's capacity factor and LCOE.

Solution

After starting up the SAM program and starting a new "Wind" project for a "PPA (power purchase agreement) single owner (utility)" project, you will see a page with a set of links to parameter sets for Wind Resource, Wind Turbine, etc. on the left-hand side, and an option to select wind resource files on the main portion of the page. SAM allows users to modify turbine cost and performance specifications, financing, government incentives, wind farm layout, etc., allowing them to create a model as simple or complex as needed. For this example, we will only be modifying the model to fit the assumptions in the problem statement while leaving all other options as the default.

The first wind farm location can be selected through the "Wind Resource File" drop-down menu on the "Wind Resource" tab. Start by selecting the "Southern Wyoming flatlands" file from the library. Run the model for this location after setting up the rest of the model parameters. There is no preloaded file for northern Alabama, so for that location you will need to download a file from the NREL Wind Integration National Dataset Toolkit. We will return to that after completing the run for the southern Wyoming location.

Next, select the "Wind Turbine" tab and select the "Vestas V80-2.0" turbine, which has a rated output of 2000 kW and 80 m rotor diameter. [Figure 8.38a](#) shows the power curve from SAM for this turbine.

Now select the "Wind Farm" tab. At the top of the page, choose the option "specify desired farm size." Specify the "Desired farm size" as 50000 kW. Note the resulting number of turbines (25) and system nameplate capacity (50 MW). SAM determines a

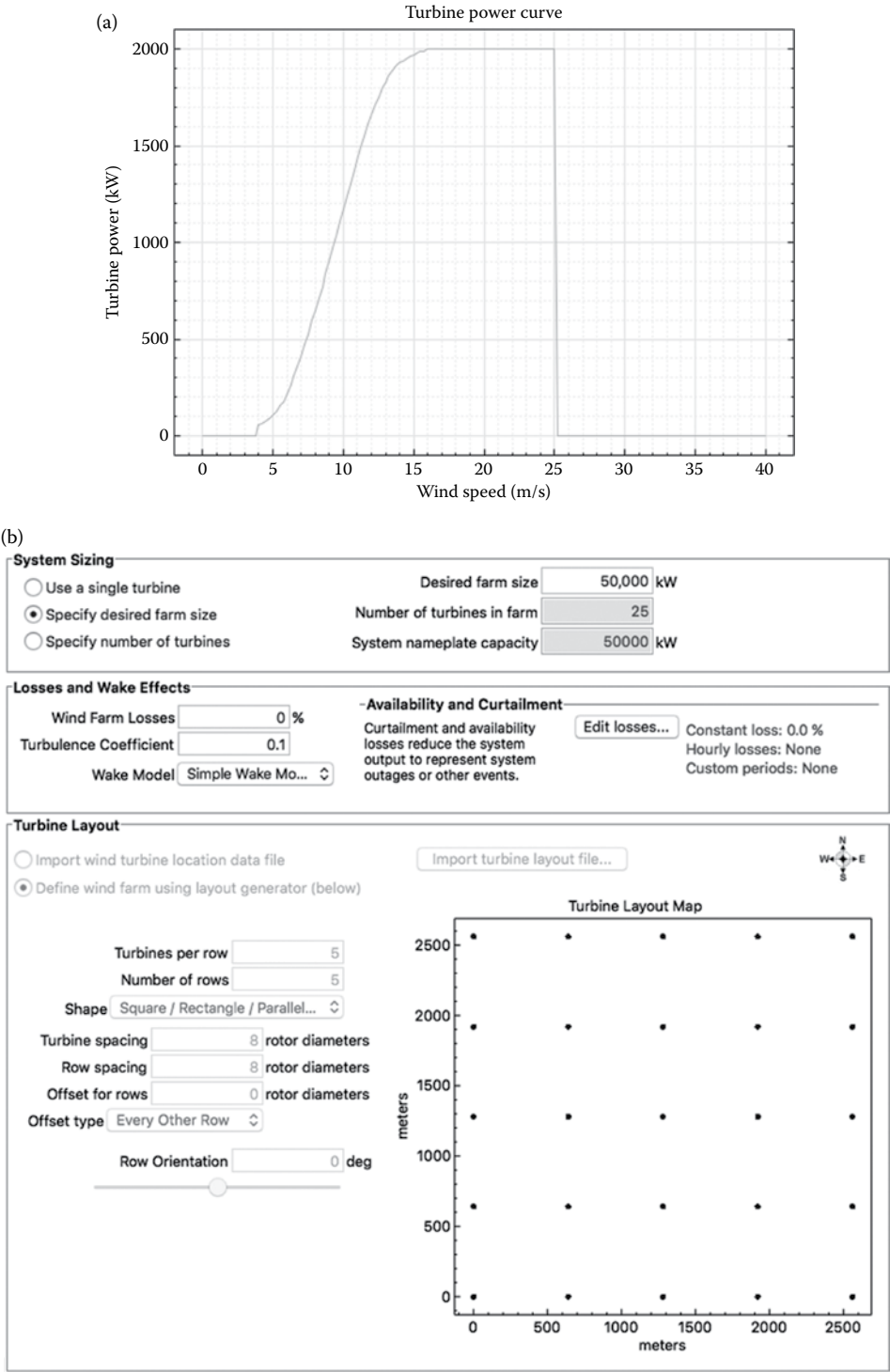


FIGURE 8.38
(a) Power curve for the Vestas V80-2.0 wind turbine from SAM. (b) Wind farm parameters for the 50 MW wind farm example. (Continued)

(c)

Capital Cost Models

Your current wind resource file:

Please ensure that the installation type below matches the resource file you have selected if you plan to estimate any costs.

☒ Land-based installation
☐ Offshore installation

Turbine and/or balance of system (BOS) costs may be able to be estimated for some systems by using the buttons to the left to access various NREL cost models. If your system is not eligible for the cost models available, or you wish to input your own cost data, costs for either category may be entered directly in the "Capital Costs" section below. See Help for details.

Capital Costs

	Cost per kW	Cost per turbine	Fixed Cost	Total
Turbine cost	<input type="text" value="\$1,209.00/kW"/>	<input type="text" value="\$0.00/turbine"/>	<input type="text" value="\$0.00"/>	<input type="text" value="\$60,450,000.00"/>
Balance of System cost	<input type="text" value="\$330.00/kW"/>	<input type="text" value="\$0.00/turbine"/>	<input type="text" value="\$0.00"/>	<input type="text" value="\$16,500,000.00"/>

Wind farm capacity kW Number of turbines

- Sales Tax

Sales tax basis, % of total equipment costs % Sales tax rate %

- Total Cost

Total installed cost

Total installed cost per kW

Operation and Maintenance Costs

	First year cost	Escalation rate (above inflation)
Fixed annual cost	<input type="text" value="0"/> \$/yr	<input type="text" value="0"/> %
Fixed cost by capacity	<input type="text" value="51"/> \$/kW-yr	<input type="text" value="0"/> %
Variable cost by generation	<input type="text" value="0"/> \$/MWh	<input type="text" value="0"/> %

In Value mode, SAM applies both inflation and escalation to the first year cost to calculate out-year costs. In Schedule mode, neither inflation nor escalation applies. See Help for details.

FIGURE 8.38 (Continued)

(c) Equipment and O&M costs for the 50 MW wind farm with Vestas V80-2.0 turbines from SAM. (Continued)

WT farm layout, which is shown in the greyed-out "Turbine Layout" section of this tab (Turbines per row = 5, number of rows = 5, turbine spacing = 8 rotor diameters, row spacing = 8 rotor diameters, offset for rows = 0 diameters, offset type = every other row, row orientation = 0 degrees), see [Figure 8.38b](#).

On the "System Cost" tab, note the turbine cost, BOS costs, and O&M costs, but do not modify them. The costs represented in SAM 2017.1.11 are shown in [Figure 8.38c](#).

The "Lifetime" tab is next and will not be modified in this example. On the "Financial Parameters" tab, select the "Specify IRR target" option, and change the IRR target to 10% and the IRR target year to 25. Select the "Debt percent" option and set the percentage to 50%, with a 20-year tenor (i.e., term), 7% interest rate, \$450,000 closing costs, and 1% up-front fee. Under "Construction financing" (Note: you may need to scroll down the page to see this section), change the "Annual interest rate" on the construction loan (loan 1) to 7%. Keep all other values as defaults. A screen shot of this page from SAM is shown in [Figure 8.38d](#).

The "Time of Delivery Factors" tab is next and will not be modified in this example. Next, select the "Incentives" tab from the left menu. Set the "Federal Investment Tax Credit" to "0" if it is not at that value. Set the "Federal Production Tax" credit to \$0.023/kWh with a 10-year term, escalating at 2.5% per year. Leave all other values as defaults. The relevant portion of this screen is shown in [Figure 8.38e](#).

Solution Mode

☒ Specify IRR target
☐ Specify PPA price

IRR target % IRR target year
 PPA price \$/kWh

Escalation Rate
 PPA price escalation %/year
 Inflation does not apply to the PPA price.

Analysis Parameters

Analysis period years
 Inflation rate %/year
 Real discount rate %/year
 Nominal discount rate %/year

Tax and Insurance Rates

Federal income tax rate %/year
 State income tax rate %/year
 Sales tax % of total direct cost
 Insurance rate (annual) % of installed cost

Property Tax
 Assessed percentage % of installed cost
 Assessed value
 Annual decline %/year
 Property tax rate %/year

Salvage Value

Net salvage value % of installed cost
 End of analysis period value

Project Term Debt

☒ Debt percent % of total cap. cost
☐ DSCR

Tenor years
 Annual interest rate %
 Debt closing costs \$
 Up-front fee % of total debt
 WACC %

☒ Equal payments (standard amortization)
☐ Fixed principal declining interest
 Moratorium years
 Choose "Debt percent" to size the debt manually as a percentage of total installed cost. Choose "DSCR" to size the debt based on cash available for debt service. See Help for details.
 For a project with no debt, set the either the debt percent or the DSCR to zero.
 Be sure to verify that all debt-related costs are appropriate for your analysis: Debt closing costs, up-front fee, and debt service reserve account. Note that debt interest payments are tax deductible, so a project with more debt may have higher net after-tax annual cash flows than a project with less debt.
 The weighted average cost of capital (WACC) is displayed for reference. SAM does not use the value for calculations.

Cost of Acquiring Financing

Financing cost \$

SAM includes the financing cost (and the working capital reserve) in the project's financing cost, which is part of the project's total equity capital reported in the project cash flow. See Help for details.

Construction Financing

Construction Period Debt

Specify the terms of up to five optional short-term construction loans. SAM calculates the total financing cost and adds it to the project's investment cost. The sum of percentages in the Percent of Installed Costs column must equal 100%.

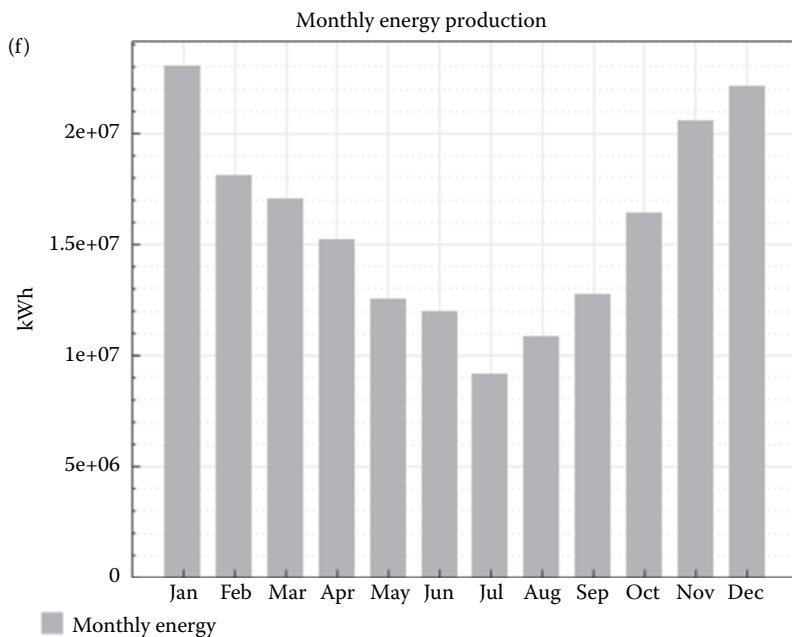
Construction loans	Percent of installed costs	Up-front fee (% of principal)	Months prior to operation	Annual interest rate (%)	Principal (\$)	Interest (\$)	Total construction financing cost
Loan 1	<input type="text" value="100"/>	<input type="text" value="1"/>	<input type="text" value="6"/>	<input type="text" value="7"/>	<input type="text" value="76,950,000.00"/>	<input type="text" value="1,346,625.00"/>	<input type="text" value="2,116,125.00"/>
Loan 2	<input type="text" value="0"/>	<input type="text" value="0"/>	<input type="text" value="0"/>	<input type="text" value="0"/>	<input type="text" value="0.00"/>	<input type="text" value="0.00"/>	<input type="text" value="0.00"/>
Loan 3	<input type="text" value="0"/>	<input type="text" value="0"/>	<input type="text" value="0"/>	<input type="text" value="0"/>	<input type="text" value="0.00"/>	<input type="text" value="0.00"/>	<input type="text" value="0.00"/>
Loan 4	<input type="text" value="0"/>	<input type="text" value="0"/>	<input type="text" value="0"/>	<input type="text" value="0"/>	<input type="text" value="0.00"/>	<input type="text" value="0.00"/>	<input type="text" value="0.00"/>
Loan 5	<input type="text" value="0"/>	<input type="text" value="0"/>	<input type="text" value="0"/>	<input type="text" value="0"/>	<input type="text" value="0.00"/>	<input type="text" value="0.00"/>	<input type="text" value="0.00"/>
Totals:	<input type="text" value="100"/>				<input type="text" value="76,950,000.00"/>	<input type="text" value="1,346,625.00"/>	<input type="text" value="2,116,125.00"/>

(d) Financial model parameters for the 50 MW wind farm example.

(Continued)

(e)

Investment Tax Credit (ITC)				Production Tax Credit (PTC)			
		Reduces Depreciation Basis					
	Amount (\$)	Federal	State		Amount (\$/kWh)	Term (years)	Escalation (%/yr)
Federal	0.00	<input checked="" type="checkbox"/>	<input checked="" type="checkbox"/>	Federal	0.023	10	2.50
State	0.00	<input type="checkbox"/>	<input type="checkbox"/>	State	0	10	2.50
				Inflation does not apply to the PTC amount. In Schedule mode, use nominal (current) dollar values. See Help for details.			
	Percentage (%)	Maximum (\$)					
Federal	0	1e+38	<input checked="" type="checkbox"/>				
State	0	1e+38	<input type="checkbox"/>				

**FIGURE 8.38 (Continued)**

(e) Incentives screen from SAM, with a \$0.023/kWh federal production tax credit. (f) Monthly energy production from the 50 MW wind farm in southern Wyoming. *(Continued)*

Run the simulation by pressing “Simulate” in the lower left corner and review the summary output, hourly time series plots for wind speed and power generation, daily profile plots of wind speed and power generation, and monthly statistics for the same two variables. Figures 8.38f and g show results for the southern Wyoming site.

As a further illustration of SAM’s capabilities, consider the same wind farm size, configuration, and financial parameters in a different location: Decatur, AL. There is no preloaded file for Decatur, so for that location you will need to download a file from the NREL Wind Integration National Dataset Toolkit. To do this, navigate back to the Wind Resources screen, and scroll down to the option for downloading a wind resource file. Click “download.” In the window that pops up, enter Decatur AL as the street address. Select 2010 as the wind data resource year. Click Ok. The system will download a wind resource file for Decatur: 34.61 °N latitude, 86.98 °W longitude. In the next section of the “Wind Resource” tab, check the box to “Use a Wind Resource File Stored on Your Computer.” We are keeping everything else the same in this example, so with the Decatur, AL wind data selected, run the simulation.

As expected, the SAM results indicate that northern AL (see the results in Figure 8.38h) is a less favorable location for a wind farm than southern Wyoming.

(g)

Metric	Value
Annual energy (year 1)	189,177,600 kWh
Capacity factor (year 1)	43.2%
PPA price (year 1)	4.12 ¢/kWh
PPA price escalation	1.00 %/year
Levelized PPA price (nominal)	4.47 ¢/kWh
Levelized PPA price (real)	3.52 ¢/kWh
Levelized COE (nominal)	4.32 ¢/kWh
Levelized COE (real)	3.40 ¢/kWh
Net present value	\$3,071,478
Internal rate of return (IRR)	10.00 %
Year IRR is achieved	10
IRR at end of project	10.00 %
Net capital cost	\$83,367,608
Equity	\$41,684,840
Size of debt	\$41,682,768
Minimum DSCR	0.73

(h)

Metric	Value
Annual energy (year 1)	73,034,720 kWh
Capacity factor (year 1)	16.7%
PPA price (year 1)	14.43 ¢/kWh
PPA price escalation	1.00 %/year
Levelized PPA price (nominal)	15.69 ¢/kWh
Levelized PPA price (real)	12.34 ¢/kWh
Levelized COE (nominal)	15.10 ¢/kWh
Levelized COE (real)	11.88 ¢/kWh
Net present value	\$4,551,028
Internal rate of return (IRR)	10.00 %
Year IRR is achieved	25
IRR at end of project	10.00 %
Net capital cost	\$83,367,608
Equity	\$41,684,840
Size of debt	\$41,682,768
Minimum DSCR	1.55

FIGURE 8.38 (Continued)

(g) Summary financial performance results for the 50 MW wind farm in southern Wyoming. (h) Summary of financial performance results for the 50 MW wind farm in Decatur, AL.

The capacity factor for the Decatur, AL, location is 16.7%, compared with 43.2% for southern Wyoming. The corresponding LCOE values (nominal) for the two locations are 15.1 and 4.3 ¢/kWh.

EXAMPLE 8.6: SAM METHOD TO DETERMINE EFFECT OF WIND TURBINE SPACING

Using NREL's SAM software and the parameters from Example 8.5, determine the effect on annual energy production, capacity factor, and LCOE if the wind turbine spacing is cut in half to reduce land acquisition costs at the "Wind Resource" site of "Southern Wyoming flatlands."

Solution

If you are not continuing from Example 8.5, set up the SAM model as described in Example 8.5 for the "Southern Wyoming flatlands" "Wind Resource." If you are continuing from Example 8.5, make sure the desired "Wind Resource" location is set by selecting the "Wind Resource" tab. In the "Wind Resource File" drop-down menu, select the "Southern Wyoming flatlands" file from the library. Now the desired WT farm layout will be set. In Example 8.5, under the "Wind Farm" tab, the option "specify desired farm size" was chosen and the "Desired farm size" was specified as 50000 kW. This choice resulted in the following default settings being set (see [Figure 8.38b](#), under "Turbine Layout": turbines per row = 5, number of rows = 5, shape = Square/Rectangle/Parallel, turbine spacing = 8 rotor diameters, row spacing = 8 rotor diameters, offset for rows = 0 diameters, offset type = every other row, row orientation = 0 degrees).

For this example, under the "Wind Farm" tab, choose the option "Specify number of turbines" and reduce the spacing between turbines by setting the following options under "Turbine Layout": turbines per row = 5, number of rows = 5, turbine spacing = 4 rotor diameters, row spacing = 4 rotor diameters. Keep all other default values (see [Figure 8.39a](#)). The WT farm now requires approximately 25% of the area of the WT farm in Example 8.5, thereby reducing the land acquisition cost.

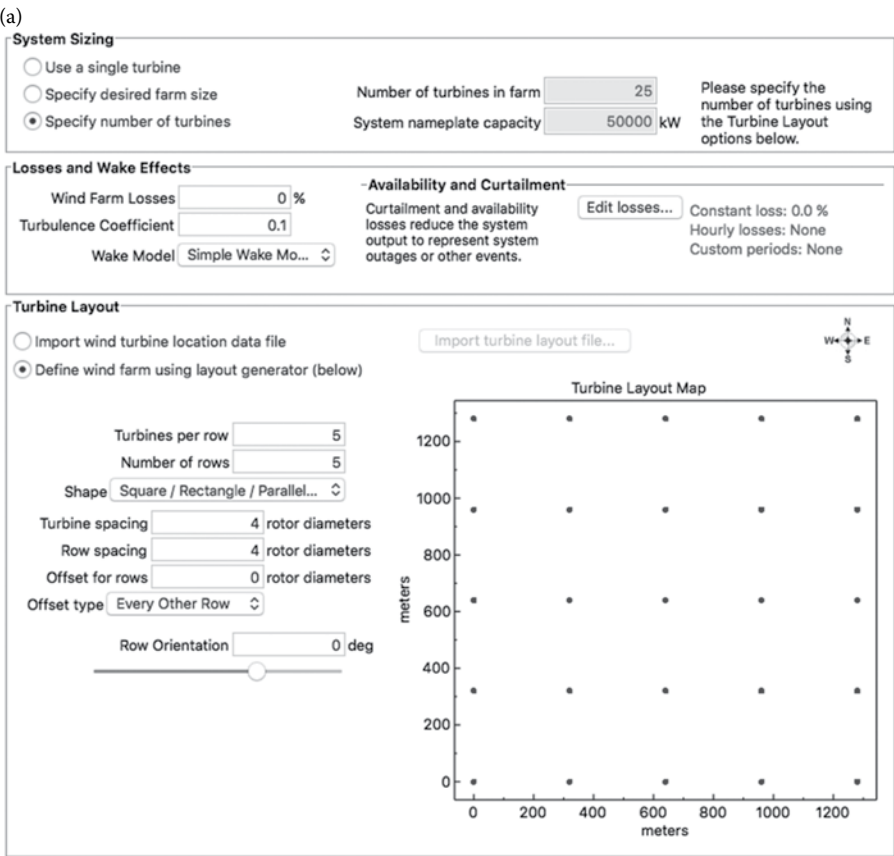
Run the simulation. The results for the reduced turbine spacing are shown in [Figure 8.39b](#).

The annual energy production for the reduced turbine spacing is 182.7 MW, down from 189.2 MW in the baseline case, resulting in a 3.4% loss in first year income. The capacity factor for the reduced turbine spacing is reduced to 41.7%, from 43.2% for the default spacing. The corresponding LCOE values (nominal) for the two cases are 4.56 and 4.3 ¢/kWh.

Now, the lost income over the life of the wind turbine farm due to a reduction in wind turbine spacing can be weighed against the savings in initial land cost, any potential reductions in installation costs, etc. Alternatively, similar studies can be made to improve the performance of the WT farm by determining optimum spacing and orientation of the WT farm to account for the predominant wind direction.

8.12 Additional Topics for Study

A single chapter cannot, of course, completely cover a topic as rich, diverse, and rapidly changing as wind energy. Topics omitted for brevity include (but are not limited to) statistical representation of the wind resource including uncertainty quantification, remote sensing, systems engineering and wind plant control, vibration and fatigue, strength of materials, manufacturing (blades, towers, and nacelles), detailed aerodynamic design,



gearbox, generators, power converters, control systems, connection to the electrical grid, and transmission. Discussion of all these topics and more can be found in wind energy texts such as Burton et al. [34], or Hau [27].

Acknowledgment

Thanks to Tim Stovall for his contributions to Section 8.9.

PROBLEMS

- 8.1 While completing this homework, imagine the study space you are using employs a space heater with a rating of 30 kW, a refrigerator (for snacks) that is rated for 5 kW, and a light fixture with 2100 W bulbs, all operating at a constant rate for the 1.5 h it takes you to finish.
 - a. What is the total power consumed at any given moment?
 - b. How much energy do you consume to complete the task?
 - c. Assume your local power company, XEnergy, charges 6.5 cents per unit of energy in part b, how much did it cost you to complete the assignment?
 - d. If you wanted to pay XEnergy \$5, what would be the power rating of an additional appliance you would need to turn on?
- 8.2 A residential-size WT has a diameter of 1 m. Due to the size, its efficiency is only 25% of the Betz limit. What is the expected power output at a wind speed of 20 miles per hour? Assume the air density is 1.225 kg/m^3 .
- 8.3 You have assembled a modern three-bladed upwind WT with a rotor radius of 5 m at sea level where the density is 1.225 kg/m^3 .
 - a. If the wind is blowing at an average speed of 10 m/s, what is the power of the wind traveling through the swept area of the rotor?
 - b. What is the average actual power produced by a turbine of this type at this wind speed? (*Hint: Find C_p*)

Hint: Find the maximum power coefficient, $C_{p,r}$ based on the following equation for axial induction

$$C_p = 4a(1-a)^2$$

- 8.4 An investor comes to you and tells you that a company wants to invest in a new wind turbine design with the following performance characteristics:
 - 112 m rotor diameter
 - 13 m/s wind speed
 - 2.1 MW
 - 1.223 kg/m^3 air density.

- a. What is the claimed rotor power coefficient, $C_{p'}$, for this turbine design?
- b1. Do you encourage the investor to invest the company's \$1 million? Answer in complete sentence(s).
- b2. Why? Answer in complete sentence(s).
- 8.5 Weibull distribution: From an analysis of wind speed data (hourly interval average, taken over a 1 year period), the Weibull parameters are determined to be $c = 6$ m/s and $k = 1.8$ at a potential WT site.

The Weibull PDF is given by

$$p(U) = \left(\frac{k}{c}\right) \left(\frac{U}{c}\right)^{k-1} \exp\left[-\left(\frac{U}{c}\right)^k\right]$$

- a. Estimate the number of hours per year that the wind speed will be between $u_B = 6.5$ and $u_A = 7.5$ m/s during the year.
- b. Estimate the number of hours per year that the wind speed is above 16 m/s.
- 8.6 Given a WT with the following parameters, calculate the annual energy production assuming a Rayleigh PDF:

$C_p = C_{p\max} = 0.40$ (C_p value assumed maximum and constant for all wind speeds)

Rated power = 3000 kW = 3.0 MW

Annual average wind speed = 7.0 m/s

Rated wind speed = 12.5 m/s

Cut-out wind speed = 25 m/s

Rotor radius = 45.0 m

Area = 6361.73 m²

Air density = 1.20 kg/m³.

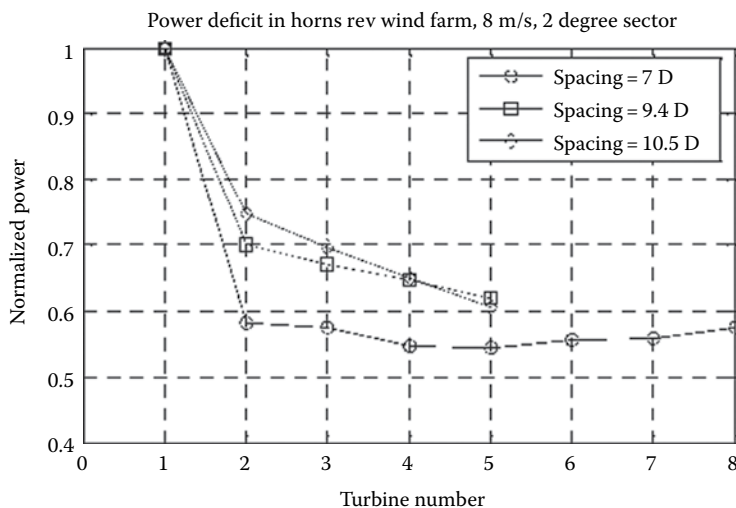
How much (in percent) does the cost of energy increase due to the gearbox replacement?

Wind Speed (m/s)	Power (kW)	Probability (%)	# of Hours/Year	Energy (kWh)
1	1.5			
2	12.2			
3	41.2			
4	97.7			
5	190.9			
6	329.8			
7	523.7			
8	781.7			
9	1113.0			
10	1526.8			
11	2032.2			
12	2638.3			
13	3000.0			
14	3000.0			

Continued

Wind Speed (m/s)	Power (kW)	Probability (%)	# of Hours/Year	Energy (kWh)
15	3000.0			
16	3000.0			
17	3000.0			
18	3000.0			
19	3000.0			
20	3000.0			
21	3000.0			
22	3000.0			
23	3000.0			
24	3000.0			
25	3000.0			
	Total		Total	kWh MWh

- 8.7 a. What is the cost of energy for a turbine with the following assumptions:
- MW rating
 - 31% capacity factor
 - \$1250/kW turbine cost
 - \$91,000 O&M cost/year
 - Fixed charge rate of 9%
 - BOS costs of \$1,999,999
 - Levelized replacement costs of \$135,000/year.
- b. If a gearbox replacement was required every 5 years at a cost of \$600,000, what would the cost of energy be?
- 8.8 Power deficit inside wind farms—Barthelmie et al. [55], present results of modeling the behavior of WT wakes to improve power output predictions. The following figure shows the predicted power deficit in the Danish offshore wind farm Horns Rev.



As an example, if two 2.3 MW turbines are spaced 9.4D apart directly in line with the wind. What is the total power produced?

Front turbine, normalized power is 1.0, power = $1.0 \times 2.3 \text{ MW} = 2.3 \text{ MW}$

Second turbine is “waked,” normalized power is 0.7, waked power = $0.7 \times 2.3 \text{ MW} = 1.61 \text{ MW}$

$$\text{Total power} = 2.3 + 1.61 \text{ MW} = 3.91 \text{ MW}$$

- a. What is the power of three turbines, 9.4D apart, directly in line with the wind?
- b. What is the power of three turbines, 9.4D apart, perpendicular with the wind?

References

1. Nebraska Wind and Solar, 2008. History of wind power, <http://nebraskawindandsolar.com/history.aspx>.
2. Price, T.J., 2005. James Blyth—Britain’s first modern wind power pioneer. *Wind Engineering* 29(3), 191–200.
3. Danish Wind Industry Association (DWIA), 1997. A wind energy pioneer: Charles F. Brush. <http://drømstørre.dk/wp-content/wind/miller/windpower%20web/en/pictures/brush.htm>.
4. Gipe, P., 2003. Smith-Putnam industrial photos, <http://www.wind-works.org/photos/Smith-PutnamPhotos.html>.
5. Renewable Energy Vermont, October 24, 2013. The story of Grandpa’s Knob: How Vermont made wind energy history, *Vermont Biz*, <http://www.vermontbiz.com/news/october/story-grandpa%E2%80%99s-knob-how-vermont-made-wind-energy-history>.
6. Gipe, P., 1995. *Wind Energy Comes of Age*, John Wiley & Sons, Inc., New York.
7. Eldridge, F.R., 1980. *Wind Machines*, 2nd ed., Van Nostrand Reinhold, New York.
8. Nelson, V., 1996. *Wind Energy and Wind Turbines*, Alternative Energy Institute, Canyon, TX.
9. American Wind Energy Association (AWEA), 2016. U.S. wind industry first quarter 2016 market report; <https://www.awea.org/2016-market-reports>.
10. Global Wind Energy Council, 2016. Global wind report 2015, <http://gwec.net/publications/global-wind-report-2/global-wind-report-2015-annual-market-update>.
11. Winds of Change, 2006. American federal projects 1975–1985, <http://www.windsofchange.dk/WOC-usastat.php>.
12. Sengpiel Audio. Decibel table, <http://www.sengpielaudio.com/TableOfSoundPressureLevels.htm>.
13. American Wind Energy Association (AWEA), 2010. Wind power myths vs. facts. <http://www.awea.org/pubs/factsheets/MythsvsFacts-FactSheet.pdf>.
14. Danish Wind Industry Association (DWIA), 1997. Shadow casting from wind turbines, <http://drømstørre.dk/wp-content/wind/miller/windpower%20web/en/tour/env/shadow/index.htm>.
15. San Martin, R.L., 1989. Environmental emissions from energy technology systems: The total fuel cycle, Energy Citations Database, http://www.osti.gov/energycitations/product.biblio.jsp?osti_id=860715.
16. Nugent, D., and Sovacool, B.K., 2014. Assessing the lifecycle greenhouse gas emissions from solar PV and wind energy: A critical meta survey. *Energy Policy* 65, 229–244.

17. Sathaye, J. et al., 2011. Renewable energy in the context of sustainable development, In: Edenhofer, O., Pichs-Madruga, R., Sokona, Y., Seyboth, K., Matschoss, P., Kadner, S., Zwickel, T., Eickemeier, P., Hansen, G., Schlömer, S., and von Stechow, C. (eds), *IPCC Special Report on Renewable Energy Sources and Climate Change Mitigation*, Cambridge University Press, Cambridge, UK.
18. Denholm, P., Hand, M., Jackson, M., and Ong, S., August 2009. *Land-Use Requirements of Modern Wind Power Plants in the US*. NREL/TP-6A2-45834. National Renewable Energy Laboratory, Golden, CO.
19. Erickson, W., Johnson, G., and Young, D. Jr., 2002. *A Summary and Comparison of Bird Mortality from Anthropogenic Causes with an Emphasis on Collisions*. USDA Forest Service General Technical Report PSW-GTR-191, <https://www.treesearch.fs.fed.us/pubs/32103>.
20. Goldenberg, S., 2009. Texas wind farm pioneers radar technology to protect migrating birds, *The Guardian*, <http://www.guardian.co.uk/environment/2009/may/01/wind-farm-bird-radar>.
21. Baerwald, E., D'Amours, G., Klug, B., and Barclay, R., August 2008. Barotrauma is a significant cause of bat fatalities at wind turbines, *Current Biology* 18(16), R695–R696.
22. National Wind Coordinating Committee (NWCC), 2004. Wind turbine interactions with birds and bats: A summary of research results and remaining questions, http://www.nationalwind.org/publications/wildlife/wildlife_factsheet.pdf.
23. Betz, A., 1920. Das maximum der theoretisch möglichen ausnützung des windes durch windmotoren. *Zeitschrift für das gesamte Turbinenwesen* 26, 307–309.
24. van Kuik, G.A.M., 2007. The Lanchester–Betz–Joukowski limit, *Wind Energy* 10, 289–291.
25. Wilson, R.E., and Lissaman, P.B.S., 1974. *Applied Aerodynamics of Wind Power Machines*, Oregon State University, Corvallis, OR, <https://ir.library.oregonstate.edu/jspui/handle/1957/8140>.
26. Stiesdal, H., 1999. The wind turbine: Components and operation, Bonus Energy A/S. Bonus Info Newsletter (autumn).
27. Hau, E., 2006. *Wind Turbines—Fundamentals, Technologies, Application, Economics*, Springer, Berlin, Germany.
28. Frost, W.D., and Asphiden, D., 1994. Characteristics of the wind, Chapter 8 in: Spera, D.A. (ed.), *Wind Turbine Technology*, 467–542, ASME Press, New York.
29. Pidwirny, M., 2006. *Fundamentals of Physical Geography*, 2nd ed., Chap. p. 7, <http://www.physicalgeography.net/fundamentals/7p.html>.
30. Kelley, N.D., and Jonkman, B.J., 2007. Overview of the TurbSim stochastic inflow turbulence simulator version 1.21, National Renewable Energy Laboratory Technical Report, NREL/TP-500-41137, Golden, CO, <http://wind.nrel.gov/designcodes/preprocessors/turbSim/TurbSimOverview.pdf>.
31. National Renewable Energy Laboratory, 2017. *Wind Maps, U.S. 80 m Wind Resource Maps*, <http://www.nrel.gov/gis/wind.html>.
32. Wind Powering America, 2009. Wind resource maps, http://www.windpoweringamerica.gov/wind_maps.asp.
33. Holton, J., 2004. The planetary boundary layer, in: *Dynamic Meteorology*, International Geophysics Series, vol. 88. Chap. 5, 116–139, Elsevier Academic Press, Burlington, MA.
34. Burton, T., Sharpe, D., Jenkins, N., and Bossanyi, E., 2001. *Wind Energy Handbook*, Wiley, Chichester, UK.
35. Renewable Energy Research Laboratory, 2006. Capacity factor, intermittency, and what happens when the wind doesn't blow, U. Massachusetts at Amherst, http://www.ceere.org/rerl/about_wind/RERL_Fact_Sheet_2a_Capacity_Factor.pdf.
36. Fingersh, L., Hand, M., and Laxson, A., 2006. *Wind Turbine Design Cost and Scaling Model*, Technical Report NREL/TP-500-40566, National Renewable Energy Laboratory, Golden, CO, <http://www.nrel.gov/docs/fy07osti/40566.pdf>.
37. American Wind Energy Association (AWEA), 2010. 10 steps in building a wind farm, http://www.awea.org/pubs/factsheets/10stwf_fs.pdf.
38. DOE, 2008. *20% Wind Energy by 2030; Increasing Wind Energy's Contribution to U.S. Electricity Supply*, <https://www.nrel.gov/docs/fy08osti/41869.pdf>.

39. Archer, C.L., and Jacobson, M.Z., 2007. Supplying baseload power and reducing transmission requirements by interconnecting wind farms. *Journal of Applied Meteorology and Climatology* 46(11), 1701–1717.
40. IEA. Wind Task 31 WAKEBENCH, <http://windbench.net/wakebench2>.
41. Stovall, T.D., 2009. Simulations of wind turbine wake interactions in OpenFOAM, MS thesis, University of Colorado, Boulder, CO.
42. Riso, D.T.U., 2003. *Wind Atlas Analysis and Application Program (WAsP)*, DTU Wind Energy, Roskilde, Denmark, www.wasp.dk.
43. National Renewable Energy Laboratory, 2017. Wind-Plant Integrated System Design and Engineering Model (WISDEM), <https://nwtc.nrel.gov/WISDEM>.
44. Piwko, R., Osborn, D., Gramlich, R., Jordan, G., Hawkins, D., and Porter, K., 2005. Wind energy delivery issues: Transmission planning and competitive electricity market operation, *IEEE Power and Energy Magazine* 3(6), 47–56.
45. Global World Energy Council. Offshore wind power. <http://www.gwec.net/global-figures/global-offshore>.
46. Rocky Mountain PBS, 2016. U.S. builds first offshore wind farm, <http://www.pbs.org/newshour/bb/u-s-builds-first-offshore-wind-plant>.
47. Smith, A., Stehly, T., and Musial, W., September 2015. 2014–2015 Offshore Wind Technologies Market Report, NREL/TP-5000-64283, National Renewable Energy Laboratory, Golden, CO, <http://www.nrel.gov/docs/fy15osti/64283.pdf>.
48. Shankleman, J., March, 9, 2017. Wind power blows through nuclear, coal as costs drop at sea, *Bloomberg New Energy Finance*, <https://www.bloomberg.com/news/articles/2017-03-09/wind-power-blows-through-nuclear-coal-as-costs-plunge-at-sea>.
49. EIA, 2006. Electricity. Spread sheet state sales, www.eia.doe.gov/cneaf/electricity/epa/sales_state.xls.
50. Musial, W., Heimiller, D., Beiter, P., Scott, G., and Draxl, C., September, 2016. 2016 Offshore Wind Energy Resource Assessment for the United States, NREL/TP-5000-66599, National Renewable Energy Laboratory, Golden, CO, <http://www.nrel.gov/docs/fy16osti/66599.pdf>.
51. Gilman, P. et al., 2016. *National Offshore Wind Strategy: Facilitating the Development of the Offshore Wind Industry in the United States*, U.S. Department of Energy and U.S. Department of the Interior, <https://energy.gov/sites/prod/files/2016/09/f33/National-Offshore-Wind-Strategy-report-09082016.pdf>.
52. Jonkman, J.M., and Buhl, M.L. Jr., 2007. *Development and Verification of a Fully Coupled Simulator for Offshore Wind Turbines: Preprint*, NREL/CP-500-40979, <http://www.nrel.gov/docs/fy07osti/40979.pdf>.
53. Manwell, J.F. et al., 2002. *Wind Energy Explained, Theory, Design and Application*, Wiley, Chichester, U.K.
54. Department of Energy, 2010. How does a wind turbine work? Office of Energy Efficiency & Renewable Energy, http://www1.eere.energy.gov/wind/wind_animation.html.
55. Barthelmie, R.J. et al., 2007. Modelling and measurements of wakes in large wind farms, *Journal of Physics Conference Series* 75, 012049, *The Science of Making Torque from Wind*, IOP Publishing.



Taylor & Francis

Taylor & Francis Group

<http://taylorandfrancis.com>

Capturing Solar Energy through Biomass

Biorenewable resources, sometimes referred to as biomass, are organic materials of recent biological origin [1]. This definition is deliberately broad with the intent of only excluding fossil fuel resources from the wide variety of organic materials that arise from the biotic environment.

We have the technology to convert biorenewable resources into a variety of gaseous and liquid fuels using both thermal and biological processes. Which process and product we choose depends upon the nature of available biomass feedstock and the target market. Gaseous bioenergy products include biogas from anaerobic digestion and producer gas or synthetic gas (syngas) from thermal gasification; and hydrogen, methane, ammonia, and dimethyl ether (DME) from the upgrading of the primary products of anaerobic digestion or gasification. Liquid bioenergy products are conveniently classified according to the intermediate substrate derived from physically, chemically, or thermally processing biomass: carbohydrates, triglycerides, syngas, and bio-oil/bio-crude.

The majority of carbohydrate conversion processes focus on ethanol production, although we can also produce butanol, isoprenes, furans, and even alkanes. Similarly, refiners convert triglycerides primarily into methyl esters (biodiesel) even though conversion to alkanes via hydrotreating/hydrocracking is receiving increasing industrial attention. Researchers are investigating promising processes to convert syngas into a variety of liquid fuels: Fischer-Tropsch liquids, methanol, ethanol, and methanol-to-gasoline; and to upgrade bio-oil or bio-crude into a range of hydrocarbons such as gasoline, diesel fuel, or aviation (jet) fuel. Finally, we can convert biomass into electricity, which offers an alternative approach to providing energy for transportation.

This chapter provides an introduction to biomass feedstocks, availability, and conversion to valuable energy products. It also includes sections on pressing topics such as land use, environmental impact, and energy efficiency.

9.1 Biomass Production and Land Use

Biomass is a term that encompasses a wide range of materials. Scientists generally classify biorenewable resources as either wastes or dedicated energy crops. A waste is a material that has been traditionally discarded because it has no apparent value or represents a nuisance or even a pollutant to the local environment. Dedicated energy crops are plants grown specifically for the production of bio-based products, that is, for purposes other than food or feed. These resources are typically the product of converting solar energy into organic compounds. The properties of these organic compounds, and the means by which they are formed, are subject to numerous factors.

This section describes the different types of biomass and their properties, the use of land for crop production, and the principles of solar energy conversion. These are important

considerations in order to understand the potential of biorenewable resources for capturing solar energy.

9.1.1 Waste Materials

Categories of waste materials that qualify as biorenewable resources include municipal solid wastes (MSWs), agricultural and forest residues and their by-products, and manure. MSWs are whatever is thrown out in the garbage and clearly include materials that do not qualify as biorenewable resources, such as glass, metal, and plastics. MSW includes food processing waste that is the effluent from a wide variety of industries ranging from breakfast cereal manufacturers to alcohol breweries. Another category of waste product is agricultural residues. Agricultural residues (see [Figure 9.1](#)) are simply that part of a crop discarded by farmers after harvest such as corn stover (husks and stalks), rice hulls, wheat straw, and bagasse (fibrous material remaining after the milling of sugar cane). Modern agriculture continues to heavily employ animals. The recent concentration of animals into giant livestock facilities has led to calls to treat animal wastes in a manner similar to that for human wastes. [Table 9.1](#) shows the potential quantities of agricultural and forest residue available in the United States [2].

Waste materials share few common traits other than the difficulty of characterizing them because of their variable and complex composition. Thus, waste biomass presents special problems to engineers who are tasked with converting this sometimes unpredictable feedstock into reliable power or high-quality fuels and chemicals. The major virtue of waste materials is their low cost. By definition, waste materials have little apparent economic value and can often be acquired for little more than the cost of transporting the material from its point of origin to a processing plant. In fact, it is possible to acquire wastes at a negative cost because of the rising costs for solid waste disposal and sewer discharges and restrictions on landfilling certain kinds of wastes; that is, a biorenewable resource processing plant is

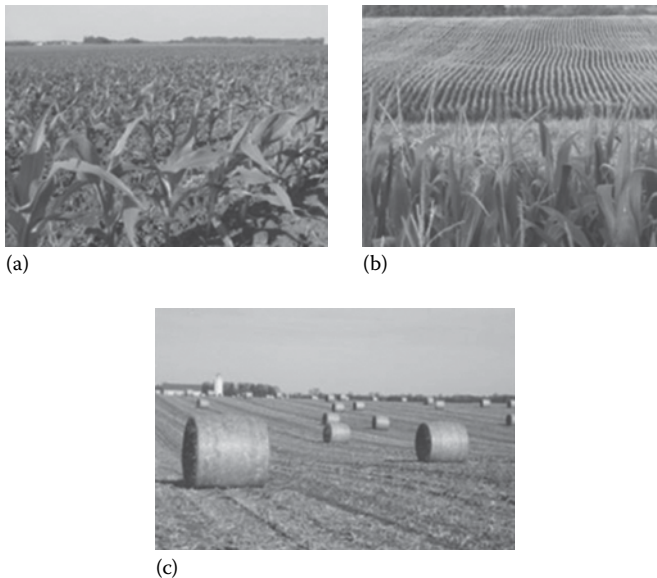


FIGURE 9.1

Corn fields during the early growing season (a), middle growing season (b), and baled corn stover after harvest (c).

TABLE 9.1

Potential Agricultural, Forest, and Process Waste Supply in the United States

	Annual Biomass Supply (million dry Mg/yr)
Logging and other residue	58
Fuel treatments	54
Urban wood residues	43
Wood processing residues	64
Pulping liquor	67
Fuelwood	47
Crop residues	405
Process residues	79

Source: From Perlack, R. et al., 2005. Biomass as feedstock for a bio-energy and bioproducts industry: The technical feasibility of a billion-ton annual supply, Technical Report A357634, Oak Ridge National Laboratory. With permission. [2]

paid by a company seeking to dispose of a waste stream. For this reason, many of the most economically attractive opportunities in biorenewable resources involve waste feedstocks.

Clearly, a waste material that can be used as feedstock for an energy conversion process is no longer a waste material. As demand for these new-found feedstocks increases, those that generate it come to view themselves as suppliers and may demand payment for the one-time waste: a negative feedstock cost becomes a positive cost. Such a situation developed in the California biomass power industry during the 1980s [3]. Concerns about air pollution in California led to restrictions on open-field burning of agricultural residues, a practice designed to control infestations of pests. With no means for getting rid of these residues, an enormous reserve of biomass feedstocks materialized. These feedstocks were so inexpensive that independent power producers recognized that even small, inefficient power plants using these materials as fuel would be profitable. A number of plants were constructed and operated on agricultural residues. Eventually, the feedstock producers had plant operators bidding up the cost of their once nuisance waste material. In the end, many of these plants were closed because of the escalating cost of fuel.

9.1.2 Energy Crops

Energy crops are defined as plants grown specifically as an energy resource. We should note that firewood obtained from cutting down an old-growth forest does not constitute an energy crop. An energy crop is planted and harvested periodically. Harvesting may occur on an annual basis, as with sugar beets or switchgrass, or on a 5–7-year cycle, as with certain strains of fast-growing trees such as hybrid poplar or willow. The cycle of planting and harvesting over a relatively short time period assures that the resource is used in a sustainable fashion; that is, the resource will be available for future generations.

Energy crops contain significant quantities of one or more of four important energy-rich components: oils, sugars, starches, and lignocellulose (fiber). Farmers historically cultivated crops rich in the first three components for food and feed: oils from soybeans and nuts; sugars from sugar beets, sorghum, and sugar cane; and starches from corn and cereal crops. Oil, sugars, and starches are easily metabolized. On the other hand, humans find it hard to digest lignocellulose. Certain domesticated animals with specialized digestive tracts

TABLE 9.2

Typical Woody Biomass Compositions

Component	Weight (%)
Cellulose	44 ± 6
Hemicellulose	28 ± 4
Lignin	20 ± 5

are able to break down the polymeric structure of lignocellulose, and use it as an energy source. From this discussion, it might appear that the best strategy for developing biomass resources is to grow crops rich in oils, sugars, and starches. However, even for “oil crops” or “starch crops,” the largest single constituent is invariably lignocellulose (Table 9.2), which is the structural (fibrous) material of the plant: stems, leaves, and roots. If we harvest oils, sugars, and starches and leave the lignocellulose behind as an agricultural residue rather than used as fuel, we will waste the greatest portion of the biomass crop.

Research has shown that energy yields (joules per km² per year) are usually greatest for plants that are mostly “roots and stems”; in other words, plant resources are directed toward the manufacture of lignocellulose rather than oils, sugars, and starches. As a result, there has been a bias toward the development of energy crops that focus on lignocellulosic biomass, which is reflected in the discussion that follows.

Dedicated energy crops are typically high-fiber crops grown specifically for their high productivity of holocellulose (cellulose and hemicellulose). Harvesting may occur on an annual basis, as with switchgrass, or on a 5–7-year cycle, as with certain strains of fast-growing trees such as hybrid poplar. Lignocellulosic crops are conveniently divided into herbaceous energy crops (HECs) and short rotation woody crops (SRWCs) [4].

Herbaceous crops are plants that have little or no woody tissue. The above-ground growth of these plants usually lives for only a single growing season. However, herbaceous crops include both annuals and perennials. Annuals die at the end of a growing season and must be replanted in the spring. Perennials die back each year in temperate climates but reestablish themselves each spring from rootstock. Both annual and perennial HECs are harvested on at least an annual basis, if not more frequently, with yields averaging 550–1100 Mg/km²/year, with maximum yields between 2000 and 2500 Mg/km²/year in temperate regions [4]. As with trees, yields can be much higher in tropical and subtropical regions.

Herbaceous crops more closely resemble hardwoods in their chemical properties than they do softwoods. Their low lignin content makes them relatively easy to delignify, which improves accessibility of the carbohydrate in the lignocellulose. The hemicellulose contains mostly xylan, which is highly susceptible to acid hydrolysis, compared to the cellulose. As a result, microbes can easily degrade agricultural residues, destroying their processing potential in a matter of days if exposed to the elements. Herbaceous crops have relatively high silica content compared to woody crops, which can present problems during processing.

SRWC is used to describe woody biomass that is fast growing and suitable for use in dedicated feedstock supply systems. Desirable SRWC candidates display rapid juvenile growth, wide site adaptability, and pest and disease resistance. Woody crops grown on a sustainable basis are harvested on a rotation of 3–10 years. Annual SRWC yields range between 500 and 2400 Mg/km²/year.

Woody crops include hardwoods and softwoods. Hardwoods are trees classified as angiosperms, which are also known as flowering plants. Examples include willow, oak,

and poplar. Hardwoods can be regrown from stumps, a process known as coppicing, which reduces their production costs compared to softwoods. Advantages of hardwoods in processing include high density for many species; relative ease of delignification and accessibility of wood carbohydrates; the presence of hemicellulose high in xylan, which can be removed relatively easily; low content of ash, particularly silica, compared to softwoods and herbaceous crops; and high acetyl content compared to most softwoods and herbaceous crops, which is an advantage in the recovery of acetic acid.

Softwoods are trees classified as gymnosperms, which encompass most trees known as evergreens. Examples include pine, spruce, and cedar. Softwoods are generally fast growing, but their carbohydrate is not as accessible for chemical processing as the carbohydrates in hardwood. Since softwoods have considerable value as construction lumber and pulpwood, they are more readily available as waste material in the form of logging and manufacturing residues compared to hardwoods. Logging residues, consisting of a high proportion of branches and tops, contain considerable high-density compression wood, which is not easily delignified. Therefore, logging residues are more suitable as boiler fuel or other thermochemical treatments than as feedstock for chemical or enzymatic processing.

9.1.3 Algae

Algae is a broad term that encompasses several eukaryotic organisms. Eukaryotic organisms are characterized by complex structures enclosed within their cell membranes. Although algae do not share many of the structures that define terrestrial biomass, they are capable of photosynthesis and capturing carbon. Algae's affinity to convert CO₂ into lipids has drawn academic and industrial attention as a means to simultaneously lower carbon emissions and produce biofuels.

Algal biomass uses CO₂ as its carbon source and sunlight as its energy source. About 1.8 kg of CO₂ is fixed for every kg of algal biomass, which contains up to 50% carbon by dry weight. Controlled production of renewable fuels from algae has been proposed in either raceway ponds or photobioreactors. Raceway ponds consist of open, shallow recirculation channels with mechanical flow control and surfaces that enhance light retention. Raceway ponds are inexpensive, but relatively inefficient when compared to photobioreactors. There are various photobioreactor designs with the common goal of maintaining a monoculture of algae that is efficiently exposed to sunlight and carbon dioxide. A common design employs arrays of tubes arranged vertically to minimize land use and oriented north–south to maximize light exposure.

Given that algae do not require fresh water or fertile soils, waste lands have been suggested as potential locations to grow algae. One suggestion is to build algae ponds in the desert Southwest United States, where inexpensive flat land, abundant sunlight, water from alkaline aquifers, and CO₂ from power plants could be combined to generate renewable fuels. Algae's potential for yields of 1.12–9.40 million liters of oil/km²/year promises significant reductions in the land footprint required to produce biofuels.

9.1.4 Land Use for Biomass Production

Global land use is broadly defined by five categories: pasture, crop, forest, urban, and abandoned. Pasture is land devoted primarily to animal grazing; crop lands are areas actively cultivated for food production; forest land contains primarily large trees; urban areas are heavily populated regions; and abandoned lands are territories that formerly fit one of the previous categories but are no longer employed for human activities. Humans,

because of population migrations or land-use change, alter the portions of land devoted to each of these categories over time.

Researchers estimate that 14.5 and 33.2 million km² of global land area were devoted to crops and pasture respectively in 2000 [5]. These land-use groups can coexist within the same region. For example, the U.S. Midwest and parts of the Southeast include regions with more than 70% of the land devoted to crops, and the western sides of the Midwest and Southern U.S. states have a high concentration of land for pasture.

Modern-day farmers devote their production to a small selection of crops depending on socioeconomic factors. Table 9.3 shows a sample of biomass crops grown in various geographical regions and their annual yields [6]. Crops such as corn and sugar cane can serve both food and energy needs due to their high yields of sugar-rich biomass and biomass residue (stover and bagasse respectively).

We can estimate the amount of biomass available in a given region by assuming nominal values for crop productivity and available land-use data using the following equation:

$$\text{Total Biomass} \left[\frac{\text{kg}}{\text{year}} \right] = f \times \text{Crop}_{\text{yield}} \left[\frac{\text{kg}}{\text{km}^2 \times \text{year}} \right] \times \text{Land}_{\text{area}} [\text{km}^2] \quad (9.1)$$

In Equation 9.1, f is a factor that accounts for crop rotations, farmer participation, and land conservation among other considerations that restrict the land use. As an example, Iowa has a total land area of 144,700 km² that is predominantly covered by corn and soybeans. In 2010, farmers planted 37.5% of Iowa land with corn netting an average yield of 165 bushels per acre (1035 Mg/km²). Thus, the total amount of corn grown in Iowa that year was 56.2 million Mg.

Farmers and seed companies have managed to increase crop yields every year for the past couple of decades. Crop yield increases follow the exponential growth formula:

TABLE 9.3

Nominal Annual Yields of Biomass Crops

Biomass Crop	Geographical Location	Annual Yield (Mg/km ²)
Corn: grain	North America	700
Corn: cobs	North America	130
Corn: stover	North America	840
Jerusalem artichoke: tuber	North America	4500
Jerusalem artichoke: sugar	North America	640
Sugar cane: crop	Hawaii	5500
Sugar cane: sugar	Hawaii	720
Sugar cane: bagasse (dry)	Hawaii	720
Sweet sorghum: crop	Midwest U.S.	3800
Sweet sorghum: sugar	Midwest U.S.	530
Sweet sorghum: fiber (dry)	Midwest U.S.	490
Switchgrass	North America	1400
Hybrid poplar	North America	1400
Wheat: grain	Canada	220
Wheat: straw	Canada	600

Source: From Wayman, M., and Parekh, S.R., 1990. *Biotechnology of Biomass Conversion: Fuels and Chemicals from Renewable Resources*, Open University Press, Philadelphia, PA. With permission. [6]

$$\text{Crop}_{\text{yield}}(t) \left[\frac{\text{kg}}{\text{km}^2} \right] = \text{Crop}_{\text{yield},0} e^{kt} \quad (9.2)$$

where k is the growth rate and t is the period of time since the initial value $\text{Crop}_{\text{yield},0}$. Iowa corn yields have increased from an average of 1162 Mg/km² in 1990 to 1533 Mg/km² in 2010. This improvement represents a 1.32% annual growth rate as shown in Equation 9.3:

$$k = \frac{\ln(1533/1162)}{21} = 0.0132 \quad (9.3)$$

The U.S. Department of Agriculture (USDA) maintains a comprehensive database of agricultural statistics (available online for free at <http://quickstats.nass.usda.gov>). The data span several years and include county-level data for crops, demographics, economics, animals and products, and environmental impacts.

EXAMPLE 9.1: BIOMASS COLLECTION AND TRANSPORTATION DISTANCE CALCULATIONS

A facility would like to collect 10,000 metric tons of corn stover per day for 330 days per year into the outskirts of Springfield, Illinois. We can estimate how far, on average, corn stover would need to travel if it is all delivered by truck.

Springfield is centrally located in Sangamon County and surrounded by the counties listed in Table 9.4 [7]. The total amount of stover produced in the area is 6,306,000 tons per year or enough to supply 19,110 tons per day to the facility. However, let us assume that only 70% of the stover is sustainably recoverable ($f = 0.7$). The distance between county seats and Springfield is the travel distance estimated from online mapping tools.

1. The facility has decided to collect the stover from farm gates. They approximated the transport distance by assuming that the facility would need to collect stover from a circular area surrounding the facility. The total area for the seven counties is approximately 10,860 km². The average distance for transport within a circle with this total area is

TABLE 9.4

Counties Surrounding Springfield, IL, and Their County Seats, Distance to Springfield, and 2010 Corn Stover Yields

County	County Seat	Distance to Springfield, IL (km)	Stover Production (Mg/year)	Planted Area (km ²)	County Area (km ²)
Sangamon	Springfield	0	969,347	1000	2271
Menard	Petersburg	38.3	310,667	340	816
Christian	Taylorville	43.1	913,248	927	1854
Cass	Virginia	54.4	351,039	376	995
Morgan	Jacksonville	56.8	580,518	631	1481
Logan	Lincoln	61	838,452	858	1603
Montgomery	Hillsboro	78.2	746,398	761	1839
Macon	Decatur	80.5	749,017	708	1515
Macoupin	Carlinville	83.5	847,035	919	2248

Source: United States Department of Agriculture, 2012. Agricultural statistics database, July 2012, <http://quickstats.nass.usda.gov>. [7]

$$\tau \times \frac{2}{3} \times \sqrt{\frac{\text{Area}}{\pi}} = 50.95 \text{ km} \quad (9.4)$$

where τ is known as the tortuosity factor—a way to account for windings and road degradation in transport networks. Here we assumed that τ is 1.3, and it varies between 1 (straight line) and 1.5 (square grid network).

2. In order to save costs, the facility has convinced farmers to deliver stover to satellite depots in their respective county seats. For this case, the average stover transport distance for the facility is the weighted average of stover transport distance to Springfield (Equation 9.5) for the amount required (Equation 9.6).

$$\text{Distance (ave. km)} = \frac{\sum_{i=0}^n D_i \times S_i}{\sum_{i=0}^n S_i} \quad \forall i \in \text{County Seats} \quad (9.5)$$

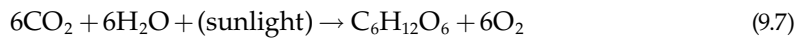
$$\sum_{i=0}^n S_i \leq 10,000 \text{ tons/day} * 330 \text{ days} \quad (9.6)$$

For this case, the seven nearest counties (Sangamon, Menard, Christian, Cass, Morgan, Logan, and Montgomery) can sustainably provide 3,300,000 tons per year to the facility. The average distance that stover would ship from the county seat depots to Springfield is about 45.2 km.

Every year, 5.6 million exajoules (EJ) of solar radiation impacts the top of our planet's atmosphere. This is enough energy to supply the world's energy consumption for several thousand years as the world consumes about 570 EJ per year. Unfortunately, this energy is very diffuse and difficult to convert efficiently. A majority of the energy is unreachable on land surfaces, and only a minuscule amount is converted into biomass.

Only 70% of solar radiation makes it through the planet's atmosphere, and the remaining 30% is absorbed, reradiated, or reflected in the atmosphere—the Earth's surface area is approximately 29.2% land. Furthermore, biomass covers approximately 21% of the Earth's surface. This leaves 6.1% of the solar energy incident on the Earth's surface available for crops.

Biomass captures a small amount of the incident solar irradiation energy via photosynthesis. Equation 9.7 can summarize the overall reaction:



The efficiency depends on the plant's carbon fixation pathway. Plants employ carbon fixation as a biochemical mechanism to capture carbon from airborne CO_2 and convert it to organic forms. Scientists categorize carbon fixation pathways after the carbon chain length of the first carbohydrate formed. C3 and C4 carbon fixation pathways proceed from initial molecules with three and four carbon atoms respectively. The vast majority of plants employ C3 carbon fixation whereas about 3% of known species employ the C4 pathway. Corn, sugar cane, and sorghum are common C4 plants.

Theoretical estimates for solar energy to biomass conversion are 4.6% and 6% for C3 and C4 plants respectively. C3 plants consume energy during carbohydrate synthesis, photorespiration, and respiration. C4 plants employ more energy for carbohydrate synthesis and respiration, but do not suffer from photorespiration energy penalties resulting in higher

TABLE 9.5

Photosynthesis Steps and Efficiencies

Photosynthesis Step	% Total Energy	
Incident solar energy (on leaf surface)	100%	
Energy in photosynthetically active spectrum	48.7%	
Absorbed energy	43.8%	
Photochemically converted energy	37.2%	
Carbon fixation pathway	C3	C4
Energy in synthesized carbohydrates	12.6%	8.5%
Energy available after photorespiration	6.5%	8.5%
Energy available after respiration	4.6%	6.0%

Source: From Zhu, X.G. et al., 2008. *Current Opinion in Biotechnology* 19(2), 153–159. With permission. [8]

overall efficiencies. Table 9.5 summarizes each step involved in converting solar energy at the plant's surface into chemical energy (biomass) [8].

In practice, the most efficient conversion measured in C4 plants is 3.7% of the incident solar energy, and C3 plants managed 2.4% conversion efficiency.

Corn grain and soybeans are C4 and C3 plants grown throughout the U.S. Midwest, where global irradiation on the horizontal surface averages around 4 kWh/m²/day. We can estimate the efficiency of solar energy collection in this region. First, we estimate the amount of solar irradiation in the area:

$$\begin{aligned}
 \text{Iowa irradiation energy} &= 4 \frac{\text{kWh}}{\text{day}} \times 365 \frac{\text{days}}{\text{year}} \times 3600 \frac{\text{s}}{\text{h}} \times 100 \frac{\text{J}}{\text{kW}} \\
 &= 5.25 \times 10^9 \frac{\text{MJ}}{\text{km}^2 \cdot \text{year}}
 \end{aligned} \tag{9.8}$$

Second, we estimate how much biomass grows on a plot of land. Total biomass includes above- and below-ground material. The ratio of below-ground biomass to above ground is known as the root-to-shoot ratio.

$$\frac{\text{Root}}{\text{Shoot}} = \frac{\text{root} + \text{exudates}}{\text{crown or leaves or branches} + \text{trunk or stalk}} \tag{9.9}$$

Corn has a root-to-shoot ratio of about 0.55. Therefore, the total above- and below-ground biomass in land growing corn includes corn grain (700 Mg/km²), corn cobs (130 Mg/km²), corn stover (840 Mg/km²), and root and exudates (918 Mg/km²). Based on an assumed energy value of 17.58 MJ/kg of corn [9], the total corn energy is

$$\text{Corn Energy} \left[\frac{\text{MJ}}{\text{km}^2} \right] = 17.58 \left[\frac{\text{MJ}}{\text{kg}} \right] \times 2,588,000 \left[\frac{\text{kg}}{\text{km}^2} \right] = 45.6 \times 10^6 \left[\frac{\text{MJ}}{\text{km}^2} \right] \tag{9.10}$$

Based on these estimates, corn has an annual solar energy conversion efficiency of 0.62%. Farmers plant corn seeds between April and June, and they harvest in October. Thus, corn has a growth period of about 180 days yielding a 1.25% growing season efficiency.

Although biomass has low solar energy conversion efficiency, they require minimal inputs or maintenance. This low efficiency is sufficient for nature's purposes, but scientists are investigating how to increase it. We could dramatically increase the size of our biomass resource base with incremental improvements in biomass efficiency yielding more food and energy for human use.

9.1.5 Important Properties of Biomass

Scientists need information about plant composition, heating value, bulk density, and production yields to evaluate the potential resource of biomass feedstock. Studies report composition in terms of organic components, proximate analysis, or ultimate analysis. [Table 9.6](#) shows properties of representative fibrous biomass feedstock. Compilations of relevant biomass properties are found in Brown (2003) [1]. Excellent online databases of biomass properties include the U.S. Department of Energy Biomass Feedstock Composition and Property Database and the ECN Phyllis database.

Organic component reports describe types and quantities of biomass compounds including proteins, oils, sugars, starches, and lignocellulose (fiber). These components vary widely among plant parts. For example, corn grain is mostly starch (72 wt.%) with a relatively small amount of fiber (13 wt.%) while corn stover, that part of the crop left on the field, is mostly fiber (84 wt.%) with very little starch content. Often the fiber, which is a polymeric composite of cellulose, hemicellulose, and lignin, is reported in terms of these three constituents. Biochemical and thermochemical process design requires knowledge of the organic components because they influence the final product composition.

Proximate analysis is important in developing thermochemical conversion processes for biomass. Proximate analysis reports the yields (% mass basis) of various products obtained upon heating the material under controlled conditions; these products include moisture, volatile matter, fixed carbon, and ash. Since moisture content of biomass is so variable and can be easily determined by gravimetric methods (weighing, heating at 100°C, and reweighing), the proximate analysis of biomass is commonly reported on a

TABLE 9.6

Physical and Thermochemical Properties of Selected Biomass

	Feedstock	Corn Stover	Herbaceous Crop	Woody Crop
Organic composition (wt-%)	Cellulose	53	45	50
	Hemicellulose	15	30	23
	Lignin	16	15	22
	Other	16	10	5
Elemental analysis (dry wt-%)	C	44	47	48
	H	5.6	5.8	5.9
	O	43	42	44
	N	0.6	0.7	0.5
	Ash	6.8	4.5	1.6
Proximate analysis (dry wt-%)	Volatile matter	75	81	82
	Fixed C	19	15	16
	Ash	6	4	1.3
HHV (MJ/kg)		17.7	18.7	19.4
Bulk density (kg/m ³)		160–300	160–300	280–480
Yield (Mg/ha)		8,400	14,000	14,000

dry basis. Volatile matter is that fraction of biomass that decomposes and escapes as gases upon heating a sample at moderate temperatures (about 400°C) in an inert (nonoxidizing) environment. Knowledge of volatile matter is important in designing burners and gasifiers for biomass. The remaining fraction is a mixture of solid carbon (fixed carbon) and mineral matter (ash), which can be distinguished by further heating the sample in the presence of oxygen: the carbon is converted to carbon dioxide leaving only the ash.

Ultimate analysis is simply the (major) elemental composition of the biomass on a gravimetric basis: carbon, hydrogen, oxygen, nitrogen, sulfur, and chlorine along with moisture and ash. Sometimes this information is presented on a dry, ash-free (daf) basis. Compared to fossil fuels, biomass has relatively high oxygen content (typically 40–45 wt.%), which detracts from its heating value and represents new challenges in converting these compounds into substitutes for the hydrocarbons that currently dominate our economy. In many instances, a generic molecular formula based on one mole of carbon is convenient for performing mass balances on a process. For example, cellulose and starch have the generic molecular formula $\text{CH}_{1.7}\text{O}_{0.83}$, hemicellulose can be represented by $\text{CH}_{1.6}\text{O}_{0.87}$ and wood is $\text{CH}_{1.4}\text{O}_{0.66}$ [10].

Efficient processing facilities keep close track of energy use. They usually employ heating value as a measure of energy content. Heating value is the net enthalpy released upon the reaction of a particular fuel with oxygen under isothermal conditions (the starting and ending temperatures are the same). If water vapor formed during reaction condenses at the end of the process, the latent enthalpy of condensation contributes to what is known as the higher heating value (HHV). Otherwise, the latent enthalpy does not contribute and the lower heating value (LHV) prevails. These measurements are typically performed in a bomb calorimeter and yield the HHV for the fuel. Heating values of biomass are conveniently estimated from the percent of carbon in the biomass on a dry basis using the empirical relationship [10]:

$$\text{HHV (dry)} \left[\frac{\text{MJ}}{\text{kg}} \right] = 0.4571(\% \text{ C on dry basis}) - 2.70 \quad (9.11)$$

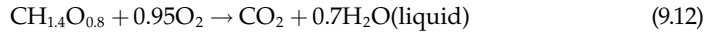
For estimating purposes, assuming an HHV of 18 MJ/kg is a good approximation for many kinds of (dry) biomass. Enthalpies of formation are very useful in thermodynamic calculations, but these data are rarely tabulated for biomass because of the wide variability in its composition. However, if HHV for a biomass fuel has been determined in a bomb calorimeter, its enthalpy of formation can be determined by summing the enthalpies of formation of the products of combustion and subtracting the HHV from this sum.

Biomass transport properties such as bulk density and volumetric energy content are important for transport and storage applications. Bulk density is determined by weighing a known volume of biomass that is packed or baled in the form anticipated for its transportation or use. Clearly, solid logs will have higher bulk density than the same wood chipped. Bulk density will be an important determinant of transportation costs and the size of fuel storage and handling equipment. Volumetric energy content is also important. Volumetric energy content, which is simply the enthalpy content of fuel per unit volume, is calculated by multiplying the HHV of a fuel by its bulk density.

Biomass energy projects need knowledge of appropriate biomass properties to be successful. These include knowledge of the types and quantities of biomass grown in a given area, which depend on many factors including plant variety, crop management (fertilization and pest control), soil type, landscape, climate, weather, and water drainage. Thus, each project will require site-specific information obtained through discussions with state extension agents and local agronomists in combination with field trials in advance of detailed manufacturing plant design.

EXAMPLE 9.2: ENTHALPY OF FORMATION CALCULATIONS FOR SWITCHGRASS

Assume that a sample of switchgrass has an elemental analysis that gives a generic molecular formula of $\text{CH}_{1.4}\text{O}_{0.8}$ (molecular weight of 26.2 kg/kmol) and its HHV is measured to be 18.1 MJ/kg. The complete combustion of one kilomole of switchgrass can be represented by



The enthalpy of reaction, ΔH_R , is calculated from the various enthalpies of formation, h_f° (note: molecular elements like O_2 have an h_f° equal to zero):

$$\begin{aligned} \Delta H_R &= h_{f,\text{CO}_2}^\circ + 0.7h_{f,\text{H}_2\text{O}(\text{liquid})}^\circ - (h_{f,\text{CH}_{1.4}\text{O}_{0.8}}^\circ + 0.95h_{f,\text{O}_2}^\circ) \\ &= -18.1 \left[\frac{\text{MJ}}{\text{kg}} \right] \times 26.2 \left[\frac{\text{kg}}{\text{kmol}} \right] \\ &= -393.5 \left[\frac{\text{MJ}}{\text{kmol}} \right] + 0.7 \times \left(-285.8 \left[\frac{\text{MJ}}{\text{kmol}} \right] \right) - (h_{f,\text{CH}_{1.4}\text{O}_{0.8}}^\circ + 0) \end{aligned} \quad (9.13)$$

Solving for the enthalpy of formation for $\text{CH}_{1.4}\text{O}_{0.8}$ yields

$$h_{f,\text{CH}_{1.4}\text{O}_{0.8}}^\circ = -119.3 \left[\frac{\text{MJ}}{\text{kmol}} \right] \quad (9.14)$$

This value can be used in various thermodynamic calculations for this switchgrass sample, whether gasification to hydrogen or hydrolysis to fermentable sugars. Heat of formation data is available from most engineering thermodynamic textbooks such as Moran et al. (2010) [11].

9.2 Biomass Process Economics and Technology

There are many ways to convert biomass into valuable chemicals, fuels, and electricity. This section will discuss biomass conversion technologies for gaseous and liquid fuel production as well as power generation. Gaseous fuels include biogas from anaerobic digestion and synthetic gas from gasification, and liquid fuels encompass a wide range of products such as ethanol, gasoline, diesel, and Fischer–Tropsch liquids. Combinations of these technologies can improve the overall conversion efficiency, and we will show how to compare these technologies from an energy efficiency perspective.

9.2.1 Biomass Process Economics

Conversion costs are a major factor that determines whether a technology becomes a commercial success. Conversion costs can be grouped into three major categories: capital, operating, and feedstock costs.

Capital costs include equipment purchasing and installation costs as well as interests from financial loans. They are difficult to estimate. The accuracy for most analyses ranges between +100% and –30% (meaning that the project could be twice as expensive or 30%

cheaper). The accuracy can be improved with detailed engineering analysis and/or cost databases.

Operating costs consist of all expenses required to maintain the operation of a given facility such as labor, maintenance, and utilities. Operating costs include both fixed and variable cost components. Fixed costs, like labor and maintenance, are independent of the plant throughput capacity. On the other hand, variable costs are typically related to the amount of feedstock input. For example, a facility would have higher heating costs from drying increasing quantities of biomass.

Finally, feedstock costs are the costs of purchasing and delivering biomass to the facility. Facilities may choose to pay a fixed, plant-gate cost in which case the supplier carries the burden of delivering the feedstock. However, delivery costs are an important factor in how much a biorefinery pays for biomass.

The summation of these cost components allows us to estimate the cost of a biomass product. These are typically reported on a normalized basis such as Equation 9.15:

$$\text{Fuel Cost} \left[\frac{\$}{\text{unit output}} \right] = \frac{\text{Capital} + \text{Operating} + \text{Feedstock}}{\text{Product Output}} \quad (9.15)$$

Fuel costs typically depend on the scale of operation. Large-scale facilities can optimize their operations in order to take advantage of economies-of-scale. The impact of economies-of-scale is greatest for capital costs, and research has shown a strong relationship between the plant capacity and unit capital costs. This relationship is captured by the power law:

$$\text{Capital Cost} = \text{Capital Cost}_0 \times \left(\frac{\text{Capacity}}{\text{Capacity}_0} \right)^n \quad (9.16)$$

where

n is the scale factor

the index 0 indicates the base or known value (cost or capacity)

Typical values for the scale factor are 0.63 for biochemical facilities and 0.7 for thermochemical plants. The higher value is due to the larger capital investment required for most thermochemical projects. Economies-of-scale allow us to estimate the costs of scaling up a facility. For example, if a 40-million gallon per year (MMGPY) ethanol plant costs \$46.7 million, the cost for an equivalent 200-MMGPY facility is

$$\text{Capital Cost}_{200\text{MMGPY}} = \$46.7 \times 10^6 \times \left(\frac{200 \times 10^6}{40 \times 10^6} \right)^{0.63} = \$128.7 \text{ million} \quad (9.17)$$

In this case, per unit capital costs decrease from \$1.17 per gallon of annual capacity to \$0.64. This shows the potential cost reductions from scaling-up operations. In reality, these benefits are not fully realized because of diseconomies of scale. In other words, additional considerations become important at different plant capacities. However, several industries have successfully scaled refineries from a few thousand barrels per day of capacity to over 400,000 barrels per day and benefit from dramatic reductions in per unit costs.

Most operating costs scale linearly with capacity ($m = 1$). However, large facilities can also reduce their per unit operating costs with labor management and equipment maintenance strategies. Thus, operating costs are sometimes scaled with a 0.9 scale factor.

Feedstock costs for biorefinery are notable for their diseconomies-of-scale—their per unit costs increase with capacity. Unlike fossil fuels that travel from a single source (coal mine or oil well) to a facility, biomass must be collected from a wide area. The larger the facility, the further away it must seek feedstock. This relationship can be captured simply using a scale factor greater than 1 ($p \approx 1.5$).

From these relationships, we can roughly estimate the costs of scaling-up a known technology using Equation 9.18:

$$\text{Fuel Cost}_M = C_0 \times \left(\frac{\text{Capacity}}{\text{Capacity}_0} \right)^n + O_0 \times \left(\frac{\text{Capacity}}{\text{Capacity}_0} \right)^m + F_0 \times \left(\frac{\text{Capacity}}{\text{Capacity}_0} \right)^p \quad (9.18)$$

where C , O , and F stand for capital, operating, and feedstock costs. Per unit costs in units of \$/gal can be calculated by dividing total costs by the biorefinery output capacity.

Inflation should be taken into account when comparing estimates published in different years. There are several indices available to account for inflation: consumer price index (CPI), chemical engineering plant cost index, and the Marshall and Swift index. The CPI is maintained by the U.S. government Bureau of Labor Statistics and is a general measure of the time value of money. The other indices are more relevant for industrial estimates, but are not publicly available. The CPI is available at <http://www.bls.gov/cpi>.^{*} Table 9.7 shows the CPI values for 2006–2010.

Adjusting for inflation, the \$46.7 million corn ethanol facility estimate, developed in 2006, would be more expensive. Based on the annual average CPI value for the years 2006 and 2010, the cost would be

$$\$46.7 \times 10^6 \times \frac{218.06}{201.6} = \$50.5 \times 10^6 \quad (9.19)$$

The previous approach is suitable for quick comparisons of biorefineries operating at different scales. However, it would not help us determine the costs for a new facility. To determine the costs of a new biorefinery, we would need detailed process and cost data of the unit operations. These data can be acquired from process modeling tools and cost databases such as Aspen Plus™ and Aspen Process Economic Analyzer™.

The following sections include brief descriptions of mature biorefinery technologies and their costs. This information can help us conduct comparisons such as the one described here.

TABLE 9.7

Consumer Price Index Factors
for 2006–2010

Year	CPI Factor
2006	201.60
2007	207.34
2008	215.30
2009	214.54
2010	218.06

^{*} Direct link: <ftp://ftp.bls.gov/pub/special.requests/cpi/cpi.ai.txt>

9.2.2 Conversion of Biomass to Gaseous Fuels

There are two main approaches to converting biomass into gaseous fuels: anaerobic digestion and gasification. Both of these processes generate a combustible gas suitable for power generation applications. Anaerobic digestion gas is commonly known as biogas, and biomass gasification products are called synthetic gas (syngas) or producer gas depending on the gas composition. The key difference between biogas and syngas is that syngas is better suited for liquid fuel production. Therefore, biomass gasification is a pathway to both power generation and liquid fuel synthesis.

9.2.2.1 Biomass to Biogas

Anaerobic digestion is the decomposition of waste to gaseous products by bacteria in an oxygen-free environment. Bacteria decompose organic wastes into a mixture of methane, carbon dioxide, and trace gases. Although bacteria can convert a wide range of waste materials, their productivity is sensitive to feedstock properties such as moisture and ash content. Anaerobic digestion yields vary from 23 to over 250 m³/Mg (wet basis) with a methane content of 55%–75% by volume. The thermodynamic efficiency of this process is about 60%.

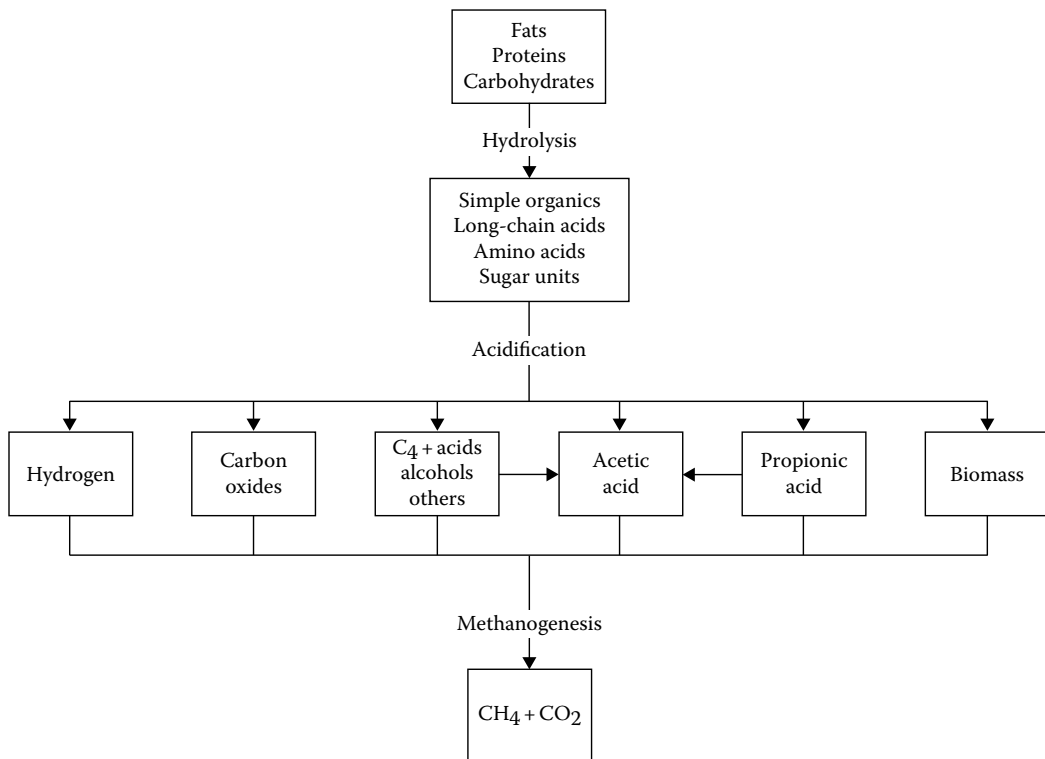
Biogas with a high methane content can substitute for natural gas in many applications. Clean biogas is suitable for engine generator sets, small gas turbines, and some kinds of fuel cells. Biogas contaminants, sulfur in particular, must be removed before use in some equipment.

The biological processes within an anaerobic digester that lead to biogas, as summarized in [Figure 9.2](#), are relatively complicated [12]. They involve a series of steps through which several bacteria species break down proteins, carbohydrates, and fats into simple acids, alcohols, and gaseous compounds. Anaerobic digester systems, on the other hand, are simple as shown in [Figure 9.3](#). These systems are typically operated as either batch or steady flow units although semi-batch operation is also an option. The effluents from these systems are biogas and sludge. The biogas may undergo scrubbing to remove hydrogen sulfide that would otherwise yield the pollutant sulfur dioxide.

Anaerobic digester designs include batch, plug-flow, and continuously stirred tank, upflow, and two-tank reactors. The batch reactor is a single vessel design in which all steps of the digestion process take place. Advanced reactors aim to improve waste contact with active bacteria and/or to separate and control the environments for acid-forming and methane-forming bacteria. Modifying multiple variables can optimize anaerobic digestion: waste pretreatment, heating, mixing, nutrient addition, specialized bacteria addition, and pH among others.

9.2.2.2 Biomass to Synthetic Gas

Gasification is the high-temperature (750°C–850°C) conversion of solid, carbonaceous fuels into flammable gas mixtures consisting of carbon monoxide (CO), hydrogen (H₂), methane (CH₄), nitrogen (N₂), carbon dioxide (CO₂), and smaller quantities of higher hydrocarbons. When the gas mixture has a high nitrogen content, it is known as producer gas; otherwise, it is known as synthetic gas. The overall process is endothermic and requires either the simultaneous burning of part of the fuel or the delivery of an external heat source to drive the process [13]. Gasification converts over 90% of biomass feed into gas with the remaining material ending as solid char and ash, or viscous tar in some applications. Typical biomass-to-syngas efficiencies range between 70% and 90%.

**FIGURE 9.2**

Microbial phases in anaerobic digestion. (Adapted from Klass, D.L., 1998b. *Biomass for Renewable Energy, Fuels, and Chemicals*, Academic Press, San Diego, CA, p. 356. [12])

Figure 9.4 illustrates the steps involved in gasification: heating and drying, pyrolysis, gas–solid reactions that consume char, and gas-phase reactions that adjust the final composition. Solid particles are initially heated and dried at temperatures below 100°C. Pyrolysis takes place as the particle temperature reaches 600°C; pyrolysis produces the intermediate products of char, gases, and condensable vapors (including water, methanol, acids, and heavy hydrocarbons). At high enough temperatures (above 1000°C), it is possible to convert over 95% of the feed carbon with char-consuming reactions. Gas-phase reactions achieve equilibrium in high-temperature gasification; however, gasification is sometimes conducted at low temperatures (approximately 850°C) yielding nonequilibrium products (mostly tars and light hydrocarbons).

EXAMPLE 9.3: THE ROLE OF CARBON CONVERSION IN GASIFICATION

Carbon conversion is a key measure of gasification efficiency. Commercial high-temperature gasifiers can achieve carbon conversions of over 97%. Low-temperature gasifiers commonly employed with biomass operate at lower carbon conversion rates of 90%–95%. Solid residue from the gasifier contains most of the unconverted carbon otherwise known as char. Even though char material yields are low (10 wt.%), char energy content can be high. This example illustrates how much energy can remain unconverted in the relatively small fractions of char and tar.

Based on Table 9.8, we can calculate the percentage of biomass energy remaining as char and tar:

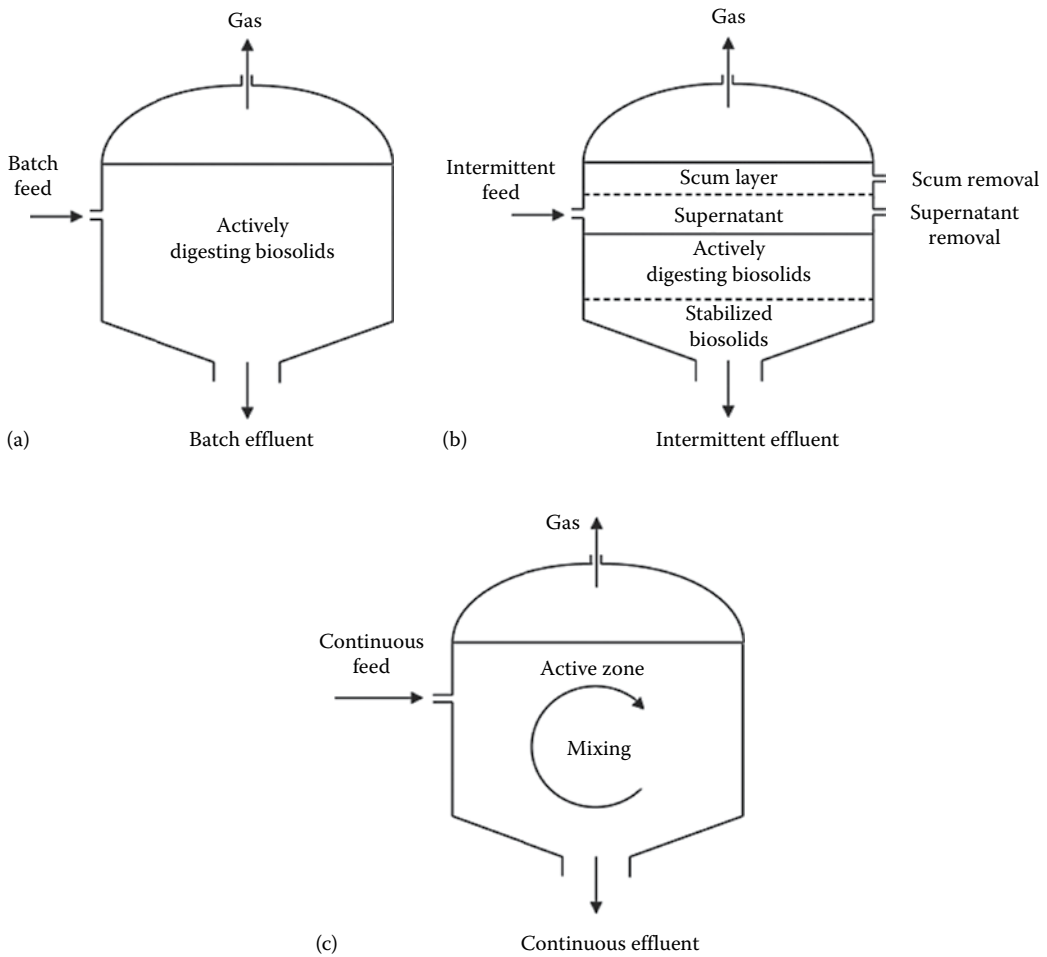


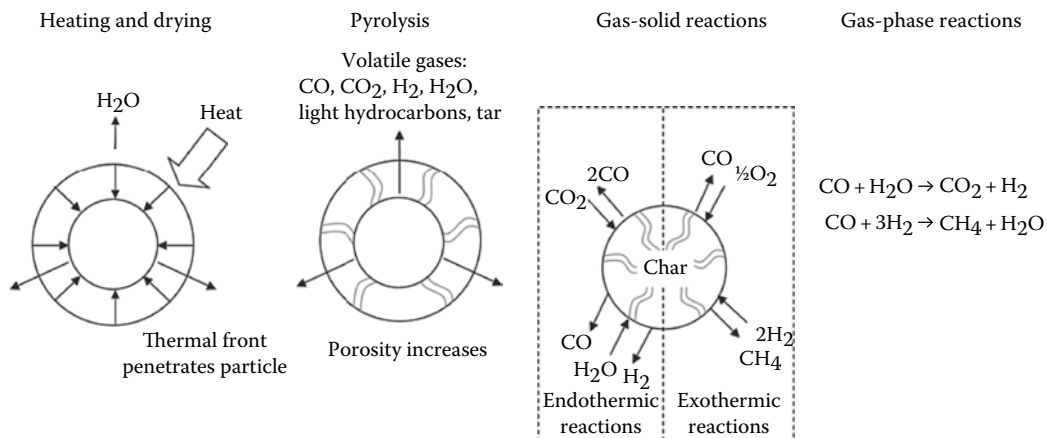
FIGURE 9.3
Types of anaerobic digesters. (a) Batch fed, (b) intermittently fed, and (c) continuously stirred and fed.

$$\text{Char}_{\text{Energy}} \left[\frac{\text{MJ}}{\text{MJ}_{\text{Biomass}}} \right] = \frac{0.12 [\text{kg/kg}] * 22.7 [\text{MJ/kg}]}{17.4 [\text{MJ/kg}]} = 15.6\% \quad (9.20)$$

$$\text{Tar}_{\text{Energy}} \left[\frac{\text{MJ}}{\text{MJ}_{\text{Biomass}}} \right] = \frac{0.07 [\text{kg/kg}] * 12.1 [\text{MJ/kg}]}{17.4 [\text{MJ/kg}]} = 4.87\% \quad (9.21)$$

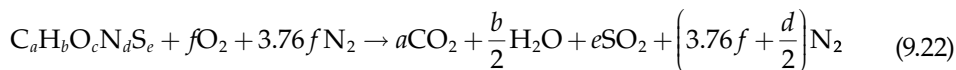
These results show that 20.5% of the biomass energy remains unconverted as char and tar after low-temperature gasification. Higher conversion rates are possible by recirculating the char into the gasifier, and some of the tar energy can be recovered by combustion downstream from the gasifier.

Gasification requires an oxygen source for exothermic processes that help with drying, pyrolysis, and endothermic gas-phase reactions. Air, pure oxygen, and steam are the main oxygen sources employed in gasification. Air gasification dilutes the gasification

**FIGURE 9.4**

Processes of thermal gasification.

gas (producer gas) with nitrogen lowering the product's energy density. Thus, there are advantages in using oxygen or steam despite the additional costs. Oxygen requirement is an important process parameter that can be estimated using combustion equations. The stoichiometric requirement for complete combustion can be calculated using the combustion formula:



For full combustion, the moles of oxygen required are f :

$$f = a + \frac{b}{4} + e - \frac{c}{2} \quad (9.23)$$

For example, the moles of oxygen required to fully combust coal are

$$\text{Coal composition} = CH_{0.739}O_{0.091}N_{0.014}S_{0.003} \quad (9.24)$$

$$f = 1 + \frac{0.739}{4} + 0.003 - \frac{0.091}{2} = 1.14 \text{ moles of } O_2 \quad (9.25)$$

We can calculate the stoichiometric oxygen requirement on a mass basis using

$$\frac{1.14 \text{ moles of } O_2}{\text{mole of Coal}} \frac{32.0 \text{ g of } O_2}{\text{mole of } O_2} \frac{\text{mole of Coal}}{14.49 \text{ g of Coal}} = 2.52 \frac{\text{g of } O_2}{\text{g of Coal}} \quad (9.26)$$

Therefore, a kilogram of coal with this composition consumes 2.52 kg of oxygen for full combustion. Note that it is common practice to burn fuel with about 25% excess oxygen than the stoichiometric amount. We can convert the oxygen requirement into an equivalent amount of air. Since air is 23.2 wt.% oxygen, the total amount of air needed for complete combustion of this fuel is 10.87 kg (oxygen required/0.232). However, gasification requires

TABLE 9.8
Biomass Gasification Product Distribution and Energy Content

Compound	Yield (wt.%)	Energy Content (MJ/kg)
Biomass	—	17.4
Syngas	81	17.1
Char	12	22.7
Tar	7	12.1

that oxygen levels remain below 25% of the stoichiometric amount for full combustion. Therefore, gasification of this coal feedstock would require less than 0.63 kg of oxygen (2.72 kg of air) per kilogram of coal.

There are four main types of gasifiers: updraft (countercurrent), downdraft (cocurrent), fluidized bed, and entrained flow [14]. These are illustrated in Figure 9.5, and their performance characteristics are summarized in Table 9.9. The most common types of gasifiers are variations of the entrained flow and fluidized bed designs [15].

The entrained flow gasifier is a highly efficient reactor. This reactor was developed for steam-oxygen gasification of coal at temperatures of 1200–1500°C. These high temperatures assure excellent char conversion (approaching 99%) and low tar production and convert the ash to molten slag, which drains from the bottom of the reactor. The technology is attractive for advanced coal power plants but has not been widely explored for biomass because of the expense of finely dividing biomass, the difficulty of reaching high temperatures with biomass, and the presence of alkali in biomass, which leads to severe ash sintering. Despite

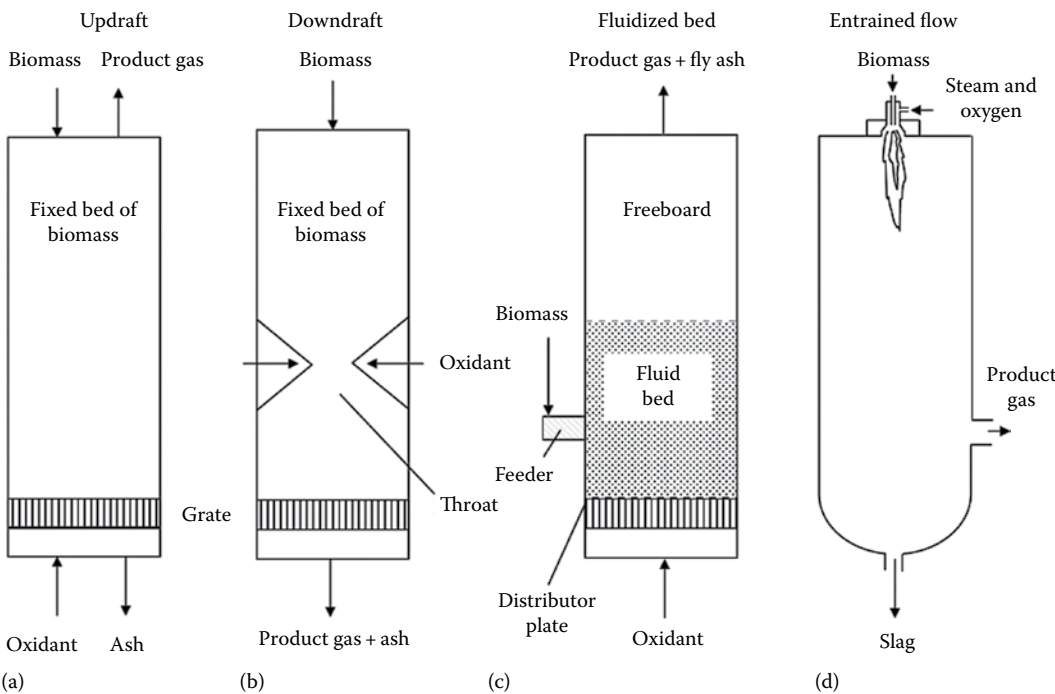


FIGURE 9.5
Common types of biomass gasifiers: (a) updraft, (b) downdraft, (c) fluidized bed, and (d) entrained flow.

TABLE 9.9

Producer Gas Composition from Various Kinds of Gasifiers

Gasifier Type	Gaseous Constituents (vol.% dry)					HHV (MJ/m ³)	Gas Quality	
	H ₂	CO	CO ₂	CH ₄	N ₂		Tars	Dust
Air-blown updraft	11	24	9	3	53	5.5	High (≈ 10 g/m ³)	Low
Air-blown downdraft	17	21	13	1	48	5.7	Low (≈ 1 g/m ³)	Medium
Air-blown fluidized bed	9	14	20	7	50	5.4	Medium (≈ 10 g/m ³)	High
Oxygen-blown downdraft	32	48	15	2	3	10.4	Low (≈ 1 g/m ³)	Low
Indirectly heated fluidized bed	31	48	0	21	0	17.4	Medium (≈ 10 g/m ³)	High

these difficulties, entrained flow reactors are being considered for gasification of pretreated biomass (such as torrefied biomass and pyrolysis liquids) [16].

Torrefied biomass is the product of heating biomass to between 200°C and 350°C—a process known as torrefaction. At these temperatures, biomass undergoes drying and minor loss of volatile content. The remaining product has a closer resemblance to coal: high energy density and improved grindability. It is also hydrophobic, which improves its storage properties by reducing water-related degradation. Torrefaction has attracted recent interest as an approach to introduce biomass into coal-based facilities.

Fluid bed gasifiers are markedly different from entrained flow designs. In a fluidized bed gasifier, gas streams from the bottom of the reactor through a bed of particulate material (typically sand) to form a turbulent mixture of gas and solids. Feed is added at a small enough rate to maintain a low concentration in the bed. Typically a fluidized gasifier operates in the range of 700°C–850°C. By injecting fuel in the base of the bed, much of the tar can be cracked within the fluidized bed. However, a large insulated space above the bed, known as the freeboard, is usually included to promote additional tar cracking as well as more complete conversion of char. However, further conditioning is required to protect downstream equipment. Fluidized beds are attractive for biomass gasification because of their feedstock flexibility and ability to scale.

9.2.3 Conversion of Biomass to Liquid Fuels

Almost 25% of energy consumption in the United States goes toward transportation. Approximately half of this amount comes from imported petroleum. Thus, development of transportation fuels from biorenewable resources (biofuels) is a priority if decreased dependence on foreign sources of energy is to be achieved.

There are two major platforms for biofuel production: biochemical and thermochemical. The biochemical platform employs microorganisms to convert primarily sugars into mostly alcohols, and it is best known for the corn- or sugarcane-to-ethanol process. The thermochemical platform relies on heat and catalysts (precious metals) to synthesize a wide range of compounds that include alcohols and hydrocarbons; this technology builds upon research from the coal, gas, and petroleum industries.

This section will discuss how to convert biomass into transportation fuels (biofuels) via the biochemical and thermochemical platforms. We will discuss the overall efficiencies, the various products generated, and overall process costs.

9.2.3.1 Corn Ethanol

Ethanol is the dominant biofuel with global production exceeding 50 billion liters. The majority of this ethanol comes from Brazilian sugarcane and U.S. corn grain. Microbes convert these sugar-rich crops into alcohols with relative ease and at low cost. Two major types of corn-to-ethanol facilities have been operated in the United States: dry-grind and wet-milling.

Dry-grind plants, shown in [Figure 9.6](#), grind the whole kernel while wet-milling plants soak the grain with water and acid to separate the corn germ, fiber, gluten, and starch components before mechanical grinding [17]. The capital investment for dry-grind is less than that for a comparably sized wet-milling plant. However, the higher value of its by-products, greater product flexibility, and simpler ethanol production can make a wet-milling plant a more profitable investment.

Dry-grind ethanol takes place in four major steps: pretreatment, cooking, fermentation, and distillation. Pretreatment consists of grinding the corn kernel into flour “meal,” which is mixed with water, enzymes, and ammonia. This mixture (“mash”) is then “cooked” to reduce bacteria levels. After cooling, the mash is sent to the fermenter where it remains for 40 h or more. The beer resulting from fermentation consists of a mixture of ethanol and stillage. Energy-intensive distillation of the beer is necessary to separate the stillage and water content from the ethanol and achieve maximum concentrations of 95%. This is followed by further purification to 100% ethanol using molecular sieves.

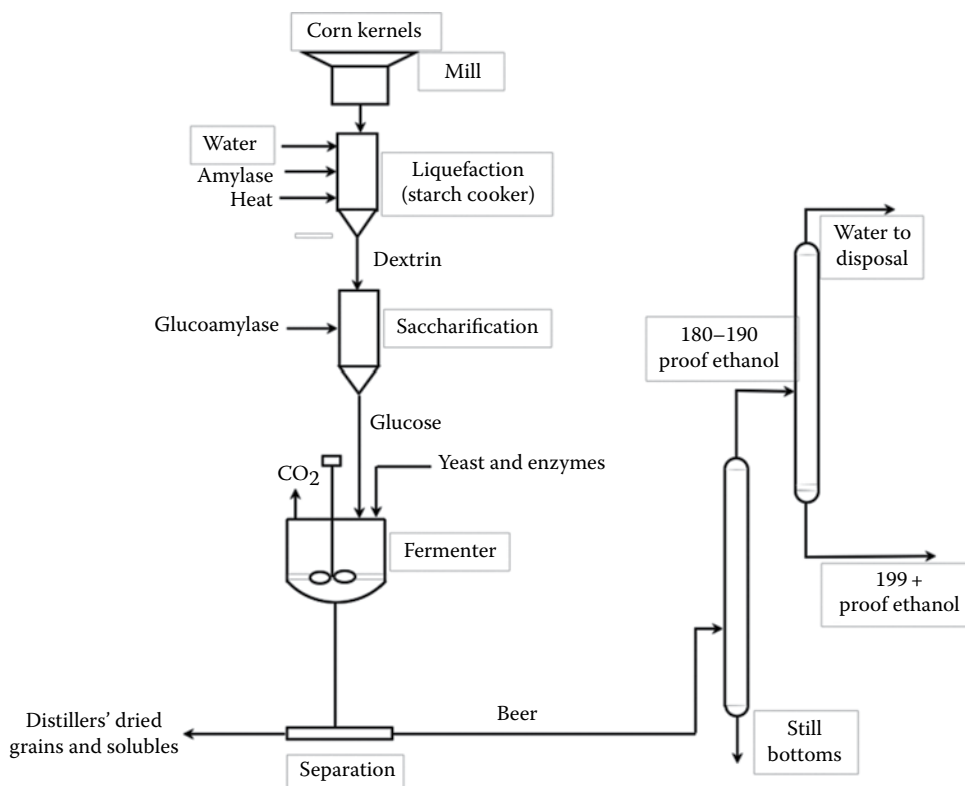


FIGURE 9.6

Dry-grind corn to ethanol.

TABLE 9.10

Ethanol Yields from Various Biorenewable Resources

Feedstock	Yield (L/Mg)
Apples	64
Barley	330
Cellulose	259
Corn	355–370
Grapes	63
Jerusalem artichoke	83
Molasses	280–288
Oats	265
Potatoes	96
Rice (rough)	332
Rye	329
Sorghum (sweet)	44–86
Sugar beets	88
Sugarcane	160–187
Sweet potatoes	125–143
Wheat	355

Source: From Klass, D.L., 1998c. *Biomass for Renewable Energy, Fuels, and Chemicals*, Academic Press, San Diego, CA, p. 416. With permission. [15]

A modern dry-grind plant will produce over 2.7 gal of ethanol per bushel of corn processed. Yields of coproducts per bushel of corn are 7.7–8.2 kg (17–18 lb) of dry distillers grain with solubles and 7.3–7.7 kg (16–17 lb) of carbon dioxide evolved from fermentation, the latter of which can be sold to the carbonated beverage industry. As a rule of thumb, the three products are produced in approximately equal weight per bushel. Table 9.10 shows ethanol yields for various feedstocks [15].

Costs for ethanol from corn grain have been developed by the USDA [18] for the dry mill process. Capital costs for a 40 MMGPY ethanol plant were estimated at \$46.7 million with fuel production costs of \$1.03 per gallon (2006).

9.2.3.2 Cellulosic Ethanol

Much of the carbohydrate in plant materials is structural polysaccharides, providing shape and strength to the plant. This structural material, known as lignocellulose, is a composite of cellulose fibers embedded in a cross-linked lignin–hemicellulose matrix [19]. Depolymerization to basic plant components is difficult because lignocellulose is resistant to both chemical and biological attacks [20]. However, depolymerization is necessary for microbes to efficiently convert cellulosic biomass into alcohols.

Cellulose to ethanol consists of four steps: pretreatment, enzymatic hydrolysis, fermentation, and distillation [17]. Of these, pretreatment is the most costly step, accounting for about 33% of the total processing costs [21]. An important goal of all pretreatments is to increase the surface area of lignocellulosic material, making the polysaccharides more susceptible to hydrolysis. Thus, comminution, or size reduction, is an integral part of all pretreatments.

Enzymatic hydrolysis was developed to better utilize both cellulose and hemicellulose from lignocellulosic materials. Three basic methods for hydrolyzing structural polysaccharides in plant cell walls to fermentable sugars are available: concentrated acid hydrolysis, dilute acid hydrolysis, and enzymatic hydrolysis [20,6]. The two acid processes hydrolyze both hemicellulose and cellulose with very little pretreatment beyond comminution of the lignocellulosic material to particles of about 1 mm size. The enzymatic process must be preceded by extensive pretreatment to separate the cellulose, hemicellulose, and lignin fractions.

Although thermodynamic efficiencies for conversion of carbohydrates to ethanol can be calculated, it is more typical to report the volumetric yield of ethanol per unit mass of feedstock. The yield of ethanol from energy crops varies considerably. Among sugar crops, sweet sorghum yields 80 L/ton, sugar beets yield 90–100 L/ton, and sugar cane yields 75 L/ton. Among starch and inulin crops, the ethanol yield is 350–400 L/ton of corn, 400 L/ton of wheat, and 90 L/ton of Jerusalem artichoke. Among lignocellulosic crops, the potential ethanol yield is 400 L/ton of hybrid poplar, 450 L/ton for corn stover, 510 L/ton for corn cobs, and 490 L/ton for wheat straw.

Researchers at the National Renewable Energy Laboratory (NREL) [22] developed a design report showing capital costs of \$114 million and operating costs of \$1.07 per gallon (2000) of ethanol for a 69-MMGPY cellulosic ethanol plant.

EXAMPLE 9.4: CELLULOSIC ETHANOL ENERGY RETURN ON INVESTMENT CALCULATIONS

There is growing interest in calculating the Energy Return on Investment (EROI) of biofuel technologies and ethanol in particular [23]. The process of estimating EROI can be summarized into three steps: identifying system inputs and outputs, calculating energy transfer quantities, and determining the EROI following a systematic approach.

1. System Identification: The cellulosic ethanol system involves inputs of fuel, electricity, fertilizer, and herbicides. The primary output is ethanol, but excess heat can be considered a coproduct. Energy inputs/costs can be distributed among coproducts using different methods.
2. Energy Transfer: The life cycle analysis literature includes reports of energy input/output in biofuel systems. Hall et al. [23] reported the values shown in Table 9.11 for cellulosic ethanol production. These values are based on converting switchgrass to ethanol. This process employs a portion of the switchgrass feed to provide process heat and electricity.
3. EROI Calculations: In addition to ethanol, the biorefinery supporting Table 9.11 generates 4.79 MJ/L of excess electricity, which displaces three times the amount of energy in the form of fuel input (based on fuel-to-power efficiency of $\approx 33\%$). Thus, the authors concluded that cellulosic ethanol has an energy output of 21.2 MJ/L of ethanol plus 3×4.79 or 14.4 MJ/L for a total of 35.6 MJ/L. The net EROI is therefore 35.7 MJ/L of ethanol.

EROI calculations are subject to numerous assumptions and methodologies. Differences in energy input/output values and calculation methods explain some of the large differences in reported EROI estimates.

9.2.3.3 Biomass Fermentation to Alternative Fuels

Ethanol has several limitations as a transportation fuel, including its affinity for water, which prevents it from being fully compatible with the existing fuel infrastructure, and its

TABLE 9.11

Cellulosic Ethanol Energy Input/Output

Input (MJ/L Ethanol)	Value
Agriculture: fuel	0.19
Agriculture: electricity	0.00
Fertilizer	0.33
Pesticides/herbicides	0.10
Feedstock transport	0.29
Biorefinery: fuel	0
Biorefinery: electricity	0
Ethanol distribution	≈0.00
Biorefinery: coproducts	0
Total direct	0.91
Indirect	0.13
Total input	1.04

Source: From Hall, C.A.S. et al., 2011. *Sustainability* 3(12), 2413–2432. With permission. [23]

low volumetric heating value, which is only two-thirds that of gasoline. For this reason, fermentations that produce metabolites other than ethanol have been proposed. Alternative fermentations could produce hydrophobic molecules that are less oxidized than ethanol including higher alcohols (most prominently butanol), fatty acids, fatty alcohols, esters, alkanes, alkenes, and isoprenes.

Alternative biochemical biofuels could address the energetic and fuel compatibility challenges faced by ethanol. Metabolic engineering, reactor design, and hybrid approaches are some of the approaches employed by researchers to identify and improve microbes' selectivity and performance for biofuel production.

9.2.3.4 Biomass to Fischer–Tropsch Liquids

Fischer–Tropsch liquids from biomass have antecedents in the coal-to-liquids industry. Germany extensively developed the Fischer–Tropsch process during World War II when it was denied access to petroleum-rich regions of the world. Likewise, when South Africa faced a world oil embargo during their era of apartheid, they employed Fischer–Tropsch technology to sustain its national economy. A comprehensive bibliography of Fischer–Tropsch literature can be found on the internet [24].

Fischer–Tropsch catalysis produces a large variety of hydrocarbons including light hydrocarbon gases, paraffinic waxes, and alcohols according to the generalized reaction shown in Equation 9.27:



Fischer–Tropsch liquids composition depends on the process selectivity. Process selectivity is affected by various factors including catalyst and feed gas properties. The Anderson–Schulz–Flory (ASF) distribution (Equation 9.28) describes the probability of hydrocarbon chain growth where the molar yield for a carbon chain can be calculated using the following equation [25]:

$$C_n = \alpha^{n-1}(1 - \alpha) \quad (9.28)$$

where α is the chain growth probability of a hydrocarbon of length n . Light hydrocarbons (mostly methane) can be fed into a gas turbine to provide power. Fischer–Tropsch liquids can be separated into various products in a process similar to petroleum distillation. Product distribution is a function of temperature, pressure, feed gas composition (H_2/CO), catalyst type, and composition [26]. Depending on the types and quantities of Fischer–Tropsch products desired, either low-(200°C–240°C) or high-temperature (300°C–350°C) synthesis at pressures ranging between 10 and 40 bar is used. For example, high gasoline yield can be achieved using high process temperatures and an iron catalyst. Fischer–Tropsch synthesis requires careful control of the H_2/CO ratio to satisfy the stoichiometry of the synthesis reactions as well as avoid deposition of carbon on the catalysts (coking). The optimal H_2/CO ratio for the production of naphtha and diesel range fuels sold in Western markets is 2:1.

Swanson et al. developed an analysis of Fischer–Tropsch liquid fuels from biomass [27]. Their estimates of a 2000 Mg per day corn stover facility found capital costs of \$498–\$606 million with minimum fuel selling prices of \$4.27 and \$4.83 per gallon of gasoline equivalent depending on whether the process was based on a fluid bed or entrained flow gasifier.

9.2.3.5 Biomass Pyrolysis Oil to Gasoline and Diesel

Pyrolysis is the thermal decomposition of organic compounds in the absence of oxygen [28]. The resulting product streams depend on the rate and duration of heating. Liquid yields exceeding 70% are possible under conditions of fast pyrolysis, which is characterized by rapid heating rates (up to 1000°C/s), moderate reactor temperatures (450°C–600°C), short vapor residence times (<0.5 s), and rapid cooling at the end of the process. Rapid cooling is essential if high-molecular-weight liquids are to be condensed rather than further decomposed to low-molecular-weight gases.

Pyrolysis liquid, also known as bio-oil, is a low-viscosity, dark-brown fluid with up to 15%–20% water, which contrasts with the black, tarry liquid resulting from slow pyrolysis [29]. Fast pyrolysis liquid is a complicated mixture of organic compounds arising from thermal degradation of carbohydrate and lignin polymers in biomass [30]. The liquid is highly oxygenated, approximating the elemental composition of the feedstock, which makes it highly unstable. The HHV of pyrolysis liquids ranges between 17 and 20 MJ/kg with liquid densities of about 1280 kg/m³. Assuming conversion of 72% of the biomass feedstock to liquid on a weight basis, yields of pyrolysis oil are about 135 gal/ton.

EXAMPLE 9.5: ENERGY CONTENT IN PYROLYSIS OILS

Producing bio-oils with a high energy content is one of the main challenges for biomass pyrolysis. Bio-oil material yields can exceed 70 wt.% but suffer from high moisture content. In this example, we calculate the energy conversion efficiency for a typical pyrolysis experiment.

Based on Table 9.12, we can estimate the biomass to bio-oil energy efficiency using Equation 9.29:

$$\text{Efficiency}_{\text{Bio-oil}} = \frac{0.65[\text{kg/kg}] * 16.5[\text{MJ/kg}]}{15.8[\text{MJ/kg}]} = 68.0\% \quad (9.29)$$

Production of pyrolysis oils and its coproducts involves several steps [31] that are illustrated in Figure 9.7. Lignocellulosic feedstock, such as wood or agricultural residues,

TABLE 9.12

Pyrolysis Mass and Energy Yield Values for Problem Set

Component	Yield (wt.%)	Energy Density (MJ/kg)
Biomass	–	15.8
Pyrolysis oil	65	16.5
Pyrolysis gas	21	5.7
Pyrolysis char	14	27.5

is milled to a fine powder to promote rapid reaction. The particles are augured into the pyrolysis reactor where they are rapidly heated and converted into condensable vapors, liquid aerosols, noncondensable gases, and charcoal. These products are transported out of the reactor into a cyclone operating above the condensation point of pyrolysis vapors where the charcoal is removed. Vapors and gases are transported to a quench vessel where a spray of pyrolysis liquid cools vapors sufficiently for them to condense. The noncondensable gases, which include flammable carbon monoxide, hydrogen, and methane, are burned in air to provide heat for the pyrolysis reactor. The condensable liquids consist of a mixture of hundreds of organic compounds commonly known as bio-oil.

Bio-oil can be upgraded using conventional oil refinery processes. The most common of these processes are hydrotreatment and hydrocracking. Hydrotreatment can remove most of the bio-oil impurities such as nitrogen, alkali metals, and oxygen carried over from the original biomass. The purpose of hydrocracking is to break down heavy hydrocarbons with long carbon chain lengths into compounds within the naphtha and diesel range (7–20 carbon atoms). Bio-oil contains organic compounds with molecular weights in the hundreds. These compounds can be cracked into lighter hydrocarbons increasing the yield of naphtha and diesel range fuels.

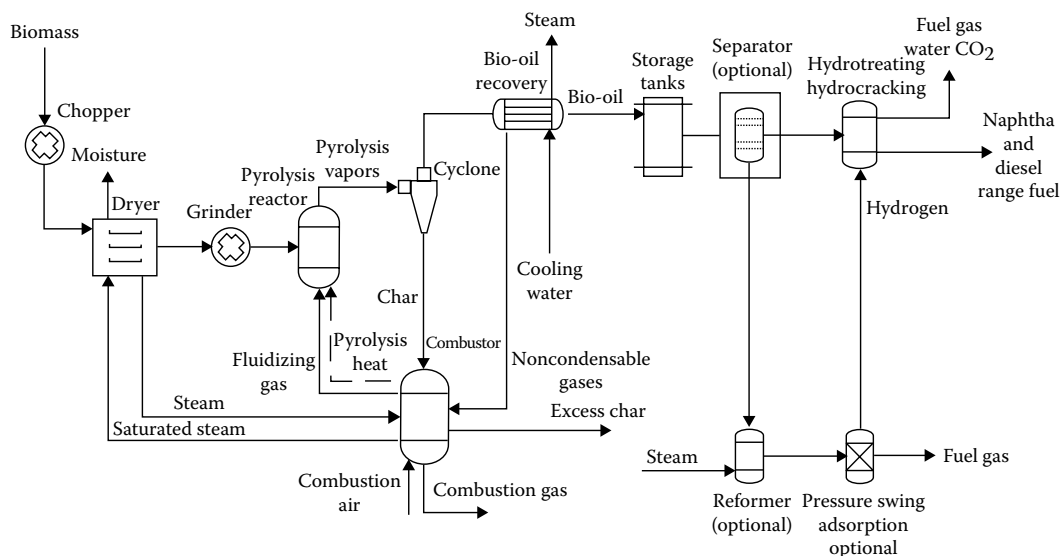


FIGURE 9.7

Biomass fast pyrolysis and bio-oil hydrotreating/hydrocracking to gasoline and diesel.

Gasoline and diesel from corn stover fast pyrolysis followed by bio-oil upgrading could cost between \$2.00 and \$3.10/gal for a 2000 Mg/day biorefinery [31]. This facility would generate 35.4 million gallons per year.

9.2.3.6 Compressed Gases as Transportation Fuel

The ideal transportation fuel is a stable liquid at ambient temperature and pressure that can be readily vaporized and burned within an engine. However, some gaseous compounds are potential transportation fuels by increasing their density through compression. Among these gaseous transportation fuels are hydrogen, methane, ammonia, and DME.

Hydrogen can be manufactured from syngas via the water–gas shift reaction. This moderately exothermic reaction is best performed at relatively low temperatures in one or more stages with the aid of catalysts. Biomass to hydrogen processes face the same fuel delivery challenges as hydrogen from fossil sources in addition to the increased costs associated with using biomass.

Methane can be the main product of gasification under conditions known as hydrogasification [13]:



Although methane is more easily pressurized or liquefied than hydrogen, its density is still too low to be an attractive transportation fuel except in some urban mass transit applications [32].

Ammonia is produced by the Haber process at 200 bar and 500°C [33]:



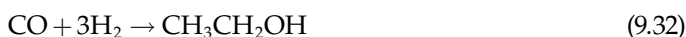
As a widely employed agricultural fertilizer, the United States already has in place production, storage, and distribution infrastructure for its use.

DME, like liquefied petroleum gas, is a nontoxic, flammable gas at ambient conditions that is easily stored as a liquid under modest pressures [34]. It can be produced from syngas and can substitute for diesel after minor engine modifications.

9.2.3.7 Modern Concepts in Biofuel Conversion

There are a wide range of technologies under development that could have a dramatic impact on how we convert biomass to transportation fuels. These technologies include syngas to alcohols, lipid to fuels, hydrothermal processing (HTP), catalytic methylated furan synthesis, and compressed gases.

Syngas affords us with the possibility of generating many different types of alcohols. Efforts in Germany during World War II to develop alternative motor fuels discovered that iron-based catalysts could yield appreciable quantities of water-soluble alcohols from syngas, especially ethanol [35]. The overall conversion can be described by Equation 9.32:

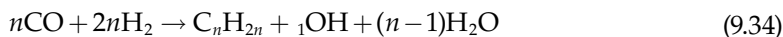


These early efforts yielded liquids containing as much as 45%–60% alcohols of which 60%–70% was ethanol. Working at pressures of around 50 bar and temperatures in the range of 220°C–370°C, researchers have developed catalysts with selectivity to alcohols of over 95%, but production of pure ethanol has been elusive. Researchers have proposed several alternative approaches: direct carbonylation of methanol and syngas fermentation.

Methanol, which can be synthesized from syngas, is readily converted into ethanol with direct carbonylation (Equation 9.33). Direct carbonylation of methanol has the advantage of yielding ethanol without coproduct water, which would eliminate energy-intensive distillations. However, the cost-effectiveness of this approach to ethanol synthesis has not been proven.



Methanol can not only be converted into ethanol, but it can also be converted to alcohols with a wide range of carbon chain lengths. The overall reaction (Equation 9.34) can be described by the conversion of CO and H into a mixture of alcohols and water as the main by-product.



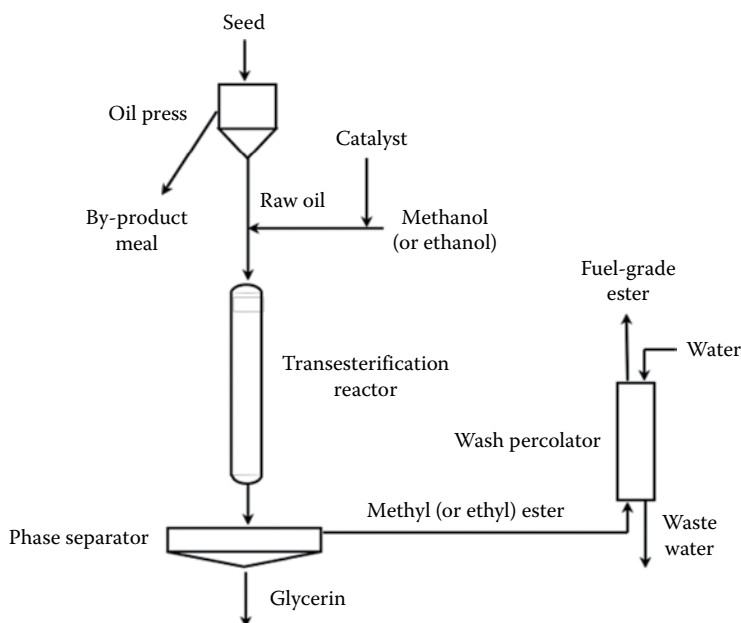
where n ranges between 1 and 8 [36]. Methanol synthesis is favored at low temperatures and high pressures, and higher alcohols are produced as the temperature is increased. Process conditions for high-temperature, high-pressure synthesis catalysts range between 300°C and 425°C, and 12.5 and 30 MPa using modified methanol catalysts.

In 2007, NREL researchers suggested that ethanol and mixed-alcohol synthesis could be cost competitive with corn ethanol by 2012 [37]. Their estimates show capital costs of \$137 million and operating costs of \$1.01 per gallon for a 72.6-MMGPY mixed-alcohol biomass plant.

Syngas fermentation is a hybrid thermochemical and biochemical biofuel synthesis approach. In this process, microorganisms consume the CO, CO₂, and H₂ in syngas to form a variety of products including carboxylic acids, alcohols, and esters [38]. The advantages of this approach include ambient temperature and pressure operating conditions, and improved resistance to contaminants such as sulfur. The disadvantages include product inhibition and mass transfer limitations.

Lipids are a large group of hydrophobic, fat-soluble compounds produced by plants and animals for high-density energy storage. Triglycerides of fatty acids, commonly known as fats and oils depending upon their melting points, are among the most familiar form of lipids and have been widely used in recent years for the production of diesel fuel substitutes. The solution to this problem is to convert the triglycerides into methyl esters or ethyl esters of the fatty acids, known as biodiesel, and the by-product 1,2,3-propanetriol (glycerol).

A wide variety of plant species produce triglycerides in commercially significant quantities, most of it occurring in seeds [18]. Average oil yields range from 15,000 L/km² for cottonseed to 81,400 L/km² for peanut oil although intensive cultivation might double these numbers. Soybeans are responsible for more than 50% of world production of oilseed, representing 48–82 million bbl/year. The average oil yield for soybeans is 38,300 L/km² [18]. A higher yielding crop is oil palm, already grown in plantations for vegetable oil production [39].

**FIGURE 9.8**

Conversion of triglycerides to methyl (or ethyl) esters and glycerol (biodiesel synthesis).

Although oil palm yields are 10 times higher than soybeans, some environmentalists are concerned that its cultivation for fuel production will encourage rainforest destruction. However, several oil seed crops have been identified that could be grown on waste land or even saline soils, which reduces concerns about competition for food crops and rainforest destruction. These alternative oil seed crops include jatropha, Chinese tallow tree, and salicornia [40,41].

Triglycerides can be converted into transportation fuels via transesterification [42]. The process, described in Figure 9.8, has been commercialized for the production of biodiesel. Although biodiesel can substitute for diesel fuel, it has some shortcomings. Fatty acid methyl esters found in biodiesel are subject to microbial or oxidative attack, making them unsuitable in applications requiring long-term fuel storage. Low-temperature performance of biodiesel is sometimes problematic.

For these reasons, hydrogenation is being evaluated as a replacement for transesterification in the production of lipid-based biofuels [42]. Hydrogenation includes a number of reactions: large molecules are broken into smaller molecules; carbon-carbon double bonds are converted into more stable single bonds; molecular structures are rearranged; and undesirable atoms such as sulfur, nitrogen, and oxygen are removed from the hydrogenated compounds. In the case of lipids, hydrogenation yields alkanes, which are highly desirable fuel molecules.

Finally, lipid-rich microalgae might be grown in brackish water or even in seawater [43]. Algae can produce as much as 60% of their body weight as lipids when deprived of key nutrients such as silicon for diatoms or nitrogen for green algae. They employ relatively low substrate concentrations, on the order of 10–40 g/L. However, algae require the proper combination of brackish water, CO₂, and sunlight, which could limit the number of sites where this process would be profitable. Berkeley researchers have estimated that biofuels from algae would require break-even oil prices of \$332/barrel [44].

TABLE 9.13

Capital and Operating Costs of Biomass to Transportation Fuel Pathways

	Grain Ethanol	Cellulosic Ethanol	Butanol	Methanol	Fischer— Tropsch Liquids	Gasoline from Bio-Oil
Publication Date	2006	2005	2000	2002	2010	2010
Plant size (MM L/year)	151	190	136	330	158	134
Capital cost (MM \$/year)	46.7	294	110	224	606	\$287
Operating and feedstock cost (MM \$/year)	41.3	76.0	68.4	60.6	145	\$123
Fuel cost (\$/L)	\$0.27	\$0.40	\$0.50	\$0.18	\$1.13	\$0.82
Fuel cost (\$/lge ^a)	\$0.44	\$0.65	\$0.55	\$1.13	\$0.34	\$0.82

^a Liters of gasoline equivalent.

Researchers have pursued hydrothermal biomass processing as an alternative to producing a variety of biofuels [45]. HTP describes the thermal treatment of wet biomass to produce carbohydrate, liquid hydrocarbons, or gaseous products depending upon the reaction conditions [46,47]. HTP liquids are commonly referred to as bio-crude. Bio-crude contains a wide range of organic compounds including hydrocarbons. Unlike pyrolysis oil, bio-crude contains a much smaller amount of oxygenated organic compounds. Unfortunately, HTP requires severe operating conditions: temperatures of 200°C–600°C and pressures of 5–40 MPa to prevent water from boiling. The metallurgy required for this process has so far limited adoption of this technology.

Destructive distillation of wood is one of several routes to produce methylated furans [48]. Methylated furans have heating values and octane numbers comparable to gasoline making them potential transportation fuel [49]. 2,5-Dimethyl furan in particular has received interest because new catalytic synthesis routes from sugars have been developed [50,51]. Furfural can be methylated by reaction with methanol over zeolite catalyst to yield methyl furan, dimethyl furan, trimethyl furan, and tetramethyl furan [49,52].

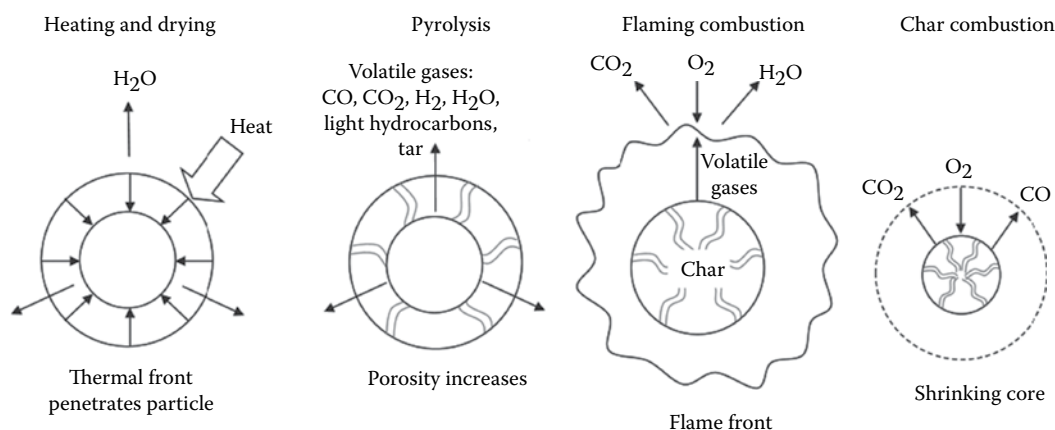
Table 9.13 summarizes the costs for common biofuel conversion processes. These costs are on different bases, but they can be easily compared by scaling the plant capacity and adjusting for inflation.

9.2.4 Conversion of Biomass to Electricity

We can convert the chemical energy in biomass into electric power by a number of different routes. Direct combustion of biomass releases heat that can be used in Stirling engines or Rankine steam power cycles. Fast pyrolysis and thermal gasification, described in earlier sections, yield bio-oil and syngas, respectively, which are suitable for firing in gas turbines or even fuel cells.

9.2.4.1 Direct Combustion

Combustion is the rapid oxidation of fuel to obtain energy in the form of heat. Since biomass fuels are primarily composed of carbon, hydrogen, and oxygen, the main oxidation products are carbon dioxide and water although fuel-bound nitrogen and sulfur can be significant sources of sulfur oxide and nitrogen oxide emissions. Depending on the heating value and

**FIGURE 9.9**

Processes of solid-fuel combustion.

moisture content of the fuel, the amount of air used to burn the fuel, and the construction of the furnace, flame temperatures can exceed 1650°C.

Solid-fuel combustion consists of four steps, illustrated in [Figure 9.9](#): heating and drying, pyrolysis, flaming combustion, and char combustion [53]. Heating and drying of the fuel particle is normally not accompanied by chemical reaction. Water is driven from the fuel particle as the thermal front advances into the interior of the particle. As long as water remains, the temperature of the particle does not raise high enough to initiate pyrolysis, the second step in solid-fuel combustion.

Pyrolysis is a complex series of thermally driven chemical reactions that decompose organic compounds in the fuel [54]. Pyrolysis proceeds at relatively low temperatures, which depend on the type of plant material. Hemicellulose begins to pyrolyze at temperatures between 150°C and 300°C, cellulose pyrolyzes between 275°C and 350°C, and lignin pyrolysis is initiated between 250°C and 500°C.

The resulting decomposition yields a large variety of volatile organic and inorganic compounds, the types and amounts dependent on the fuel and the heating rate of the fuel. Pyrolysis products include carbon monoxide (CO), carbon dioxide (CO₂), methane (CH₄), and high-molecular-weight compounds that condense to a tarry liquid if cooled before they are able to burn. Fine droplets of these condensable compounds represent much of the smoke associated with smoldering fires. Pyrolysis follows the thermal front through the particle, releasing volatile compounds and leaving behind pores that penetrate to the surface of the particle.

Both the volatile gases and the char resulting from pyrolysis can be oxidized if sufficient oxygen is available to them. Oxidation of the volatile gases above the solid fuel results in flaming combustion. The ultimate products of volatile combustion are CO₂ and H₂O although a variety of intermediate chemical compounds can exist in the flame, including CO, condensable organic compounds, and long chains of carbon known as soot. Indeed, hot glowing soot is responsible for the familiar orange color of wood fires.

Combustion intermediates will be consumed in the flame if sufficient temperature, turbulence, and time are allowed. High combustion temperature assures that chemical reactions will proceed at high rates. Turbulent or vigorous mixing of air with the fuel makes certain that every fuel molecule comes into contact with oxygen molecules. Long residence times for fuel in a combustor allow the fuel to be completely consumed. In the

absence of good combustion conditions, a variety of noxious organic compounds can survive the combustion process including CO, soot, polycyclic aromatic hydrocarbons, and the particularly toxic families of chlorinated hydrocarbons known as furans and dioxins. In some cases, a poorly operated combustor can produce pollutants from relatively benign fuel molecules.

Both CO and CO₂ can form at or near the surface of burning char [53]:



These gases escape the immediate vicinity of the char particle where CO is oxidized to CO₂ if sufficient oxygen and temperature are available; otherwise, it appears in the flue gas as a pollutant.

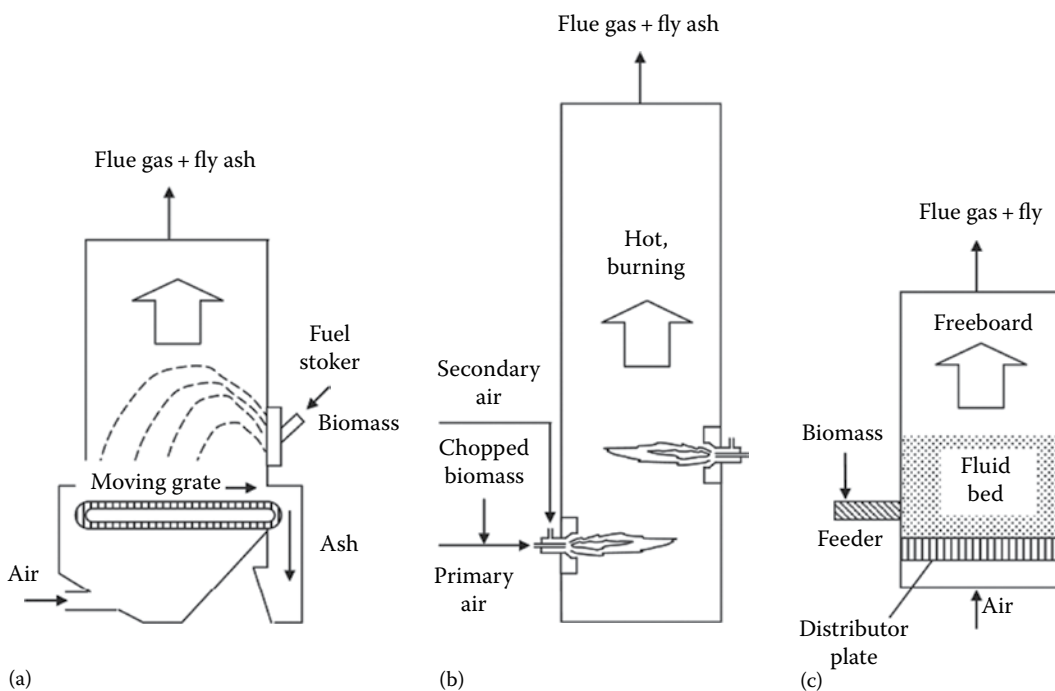
The next step in the combustion of solid fuels is solid–gas reactions of char, also known as glowing combustion, familiar as red-hot embers in a fire. Char is primarily carbon with a small amount of mineral matter interspersed. Char oxidation is controlled by mass transfer of oxygen to the char surface rather than by chemical kinetics, which is very fast at the elevated temperatures of combustion. Depending on the porosity and reactivity of the char and the combustion temperature, oxygen may react with char at the surface of the particle or it may penetrate into the pores before oxidizing char inside the particle. The former situation results in a steadily shrinking core of char whereas the latter situation produces a constant-diameter particle of increasing porosity.

9.2.4.2 Combustion Equipment

A combustor is a device that converts the chemical energy of fuels into high-temperature exhaust gases. Heat from the high-temperature gases can be employed in a variety of applications, including space heating, drying, and power generation. However, with the exception of kilns used by the cement industry, most solid-fuel combustors today are designed to produce either low-pressure steam for process heat or high-pressure steam for power generation. Combustors integrated with steam-raising equipment are called boilers. In some boiler designs, distinct sections exist for combustion, high-temperature heat transfer, and moderate-temperature heat transfer: these are called the furnace, radiative, and convective sections of the boiler, respectively. In other designs, no clear separation between the processes of combustion and heat transfer exists.

Solid-fuel combustors, illustrated in Figure 9.10, can generally be categorized as grate-fired systems, suspension burners, or fluidized beds [55]. Grate-fired systems were the first burner systems to be developed, evolving during the late nineteenth century and early twentieth century into a variety of automated systems. The most common system is the spreader-stoker, consisting of a fuel feeder that mechanically or pneumatically flings fuel onto a moving grate where the fuel burns. Much of the ash falls off the end of the moving grate, although some fly ash appears in the flue gas. Grate systems rarely achieve combustion efficiencies exceeding 90%.

Suspension burners suspend the fuel as fine powder in a stream of vertically rising air. The fuel burns in a fireball and radiates heat to tubes that contain water to be converted into steam. Suspension burners, also known as pulverized coal boilers, have dominated

**FIGURE 9.10**

Common types of combustors: (a) grate-fired, (b) suspension, and (c) fluidized.

the U.S. power industry since World War II because of their high volumetric heat release rates and their ability to achieve combustion efficiencies, often exceeding 99%. However, they are not well suited to burning coarse particles of biomass fuel, and they are notorious generators of nitrogen oxides. Biomass is fed from a bunker through pulverizers designed to reduce fuel particle size enough to burn in suspension. The fuel particles are suspended in the primary airflow and fed to the furnace section of the boiler through burner ports where it burns as a rising fireball. Secondary air injected into the boiler helps complete the combustion process. Heat is absorbed by steam tubes arrayed in banks of heat exchangers (waterwall, superheaters, and economizer) before exiting through a bag house designed to capture ash released from the fuel. Steam produced in the boiler is part of a Rankine power cycle.

Fluidized bed combustors are a recent innovation in boiler design. Air injected into the bottom of the boiler suspends a bed of sand or other granular refractory material producing a turbulent mixture of air and sand. The high rates of heat and mass transfer in this environment are ideal for efficiently burning a variety of fuels. Furthermore, the large thermal mass of the sand bed allows the unit to be operated as low as 850°C, which lowers the emission of nitrogen compounds. A commercial market for fluidized bed boilers developed during the 1980s, especially for industrial applications.

9.2.4.3 Biomass Cofiring

As an alternative to completely replacing coal with biomass fuel in a boiler, mixtures of biomass and coal can be burned together in a process known as cofiring [56]. Cofiring

offers several advantages for industrial boilers. Industries that generate large quantities of biomass wastes, such as lumber mills or pulp and paper companies, can use cofiring as an alternative to costly landfilling of wastes.

The best wood-fired power plants, which are typically 20–100 MW_e in capacity, have heat rates exceeding 12,500 Btu/kWh. In contrast, large, coal-fired power plants have heat rates of only 10,250 Btu/kWh. The relatively low thermodynamic efficiency of steam power plants at the sizes of relevance to biomass power systems may ultimately limit the use of direct combustion to convert biomass fuels to useful energy.

9.2.5 Fossil and Biomass Fuel Properties

Fossil-based transportation fuels include gasoline, diesel, and jet fuel. Gasoline is intended for spark-ignition (Otto cycle) engines; thus, it is relatively volatile but resistant to autoignition during compression. Diesel fuel is intended for use in compression-ignition (diesel cycle) engines; thus, it is less volatile compared to gasoline and more susceptible to autoignition during compression. Jet fuel is designed for use in gas turbine (Brayton cycle) engines, which are not limited by autoignition characteristics but otherwise have very strict fuel specifications for reasons of safety and engine durability (aviation for example). Biomass can be converted into gasoline, diesel, and jet fuel as well as alternative fuels such as alcohols, DME, and Fischer–Tropsch liquids.

Combinations of biochemical and thermochemical technologies could generate biofuels that meet or even exceed the combustion properties of conventional fuels. Table 9.14 [57–60] shows key properties of various fossil- and biomass-derived transportation fuels. These properties help identify biofuel substitutes for conventional fuels.

Transportation fuels are characterized by several properties based on broadly recognized standards and their combustion behavior. Specific gravity is a measure of the fuel's density. Kinematic viscosity describes the fuel's ability to flow at a given temperature—a high fuel viscosity could be detrimental to fuel delivery to an engine. Boiling point range and flash point temperature are important because they are key factors during engine start-up. Flash point is the lowest temperature at which enough fuel vaporizes and mixes with air to form a combustible gas. Below this temperature, the fuel would fail to ignite even when exposed to a spark. Flash point differs slightly from the autoignition temperature: autoignition occurs when the fuel combusts without a spark or ignition source.

The octane number is an important transportation fuel figure of merit. The octane number indicates the tendency of a fuel to undergo premature detonation within the combustion cylinder of an internal combustion engine. The higher the octane number, the less likely a fuel will detonate until exposed to an ignition source (electrical spark). Premature denotation is responsible for the phenomenon known as engine knock, which reduces fuel economy and can damage an engine. Various systems of octane rating have been developed, including research octane and motor octane numbers. Federal regulation in the United States requires gasoline sold commercially to be rated using an average of the research and motor octane numbers. Gasoline rated as “regular” has a commercial octane number of about 87 while premium grade is 93.

These properties specify the potential uses for any type of transportation fuels. Therefore, biofuel development requires careful consideration of these properties. An extended discussion of this topic is beyond the scope of this chapter, but readers are encouraged to consult engine and combustion texts on this matter.

TABLE 9.14
Comparison of Ignition and Combustion Properties of Transportation Fuels

Fuel Type	Fossil Fuel-Derived			Biomass-derived						
	Gasoline	No. 2 diesel Fuel		Methanol	Ethanol	Methyl Ester (From Soybean Oil)	Fischer-Tropsch A	Hydrogen	Methane	Dimethyl Ether
Specific gravity ^a	0.72–0.78	0.85		0.796	0.794	0.886	0.770	0.071 (liq)	0.422 (liq)	0.660
Kinematic viscosity at 20°C–25°C (mm ² /s)	0.8	2.5		0.75	1.51	3.9	2.08	105 [61]	16.5 [61]	0.227
Boiling point range (°C)	30–225	210–235		65	78	339	164–352	–253	–162	–24.9
Flash point (°C)	–43	52		11	13	188	58.5	–184	–	
Autoignition temperature (°C)	370	254		464	423	–	–	566–582	540	235
Octane no. (research)	91–100	–		109	109	–	–	>130	>120	–
Octane no. (motor)	82–92	–		89	90	–	–	–	–	–
Cetane no.	<15	37–56		<15	<15	55	74.6	–	–	>55
Heat of vaporization (kJ/kg)	380	375		1185	920	–	–	447	509	402 [62]
Lower heating value (MJ/kg)	43.5	45		20.1	27	37	43.9	120	49.5	28.88

^a Measured at 16°C except for liquefied gases, which are saturated liquids at their respective boiling points.

9.3 Use of Biomass in Developing Communities

The discussion above has focused on conversion of biomass to liquid or gaseous biofuels, or biofuel combustion to produce electricity. Up to the present, however, by far the largest use of biomass energy worldwide is direct combustion for cooking and residential heating, often in open fires or rudimentary stoves. The International Energy Agency reports that in 2014, about 10% of primary energy use worldwide was biomass or waste, mainly used by households in low-income countries [61]. In many parts of the world, this use of biomass is unsustainable, due to growing populations or energy demand putting increasing pressure on limited biomass resources, heavy time burdens involved in gathering fuels, and the very heavy health burdens associated with chronic exposure to biomass smoke. In 2016, the World Health Organization (WHO) estimated that 3 billion people worldwide rely on burning crop residue, wood, dung, or charcoal to meet household energy needs [62]. The WHO characterizes household air pollution from solid fuels combustion as the “most important environmental health risk factor” worldwide. These burdens were recognized by the United Nations in the sustainable development goals the organization adopted in 2015. The UN’s Sustainable Development Goal #7 is to provide universal access to “affordable, reliable, sustainable, modern energy by 2030” (sustainabledevelopment.un.org). Efforts to reduce reliance on inefficient solid fuel stoves have been underway for several decades, but with inadequate progress. WHO’s 2016 assessment found that on a global basis, population growth has largely offset progress made in reducing the fraction of households that burn solid fuels to meet cooking and heating needs. Major international initiatives that are currently underway to convert households to cleaner fuels include the United Nations-led Sustainable Energy for All (SE4All) program (<http://www.se4all.org>); the Global Alliance for Clean Cookstoves, hosted by the UN Foundation (<http://cleancookstoves.org>); and the Climate and Clean Air Coalition based out of the United Nations Environment Program (<http://www.ccacoalition.org>).

Use of solid biomass for cooking is especially common in Africa and Southeast Asia. For example, in Africa, excluding the Mediterranean region, an estimated 85% of household cooking is done over biomass fires or stoves [62]. In many places, cooking is done over traditional three-stone fires such as the set-up shown in Figure 9.11. Use of biomass or other self-gathered solid fuels is most prevalent in rural areas, but is not limited to them. In colder



FIGURE 9.11

Traditional three-stone fire set-up for biomass cooking in Ghana (left); Philips forced-draft gasifier stove designed as a high-efficiency, low-emissions replacement and sold internationally (center); and a Gyapa wood stove that is locally made in Ghana and features a ceramic insert to retain heat. (Photos courtesy of REACCTING [Research of Emissions, Air quality, Climate, and Cooking Technologies in Northern Ghana].)

climates in low-income countries such as northern Pakistan and northern China, solid fuels are also widely used to provide heat. Burning unprocessed coal for heat remains common in Korea and China [63]. Less information is currently available on household combustion of solid fuels for heating than for cooking. While surveys have been conducted in a few low-income countries, more information is needed to understand the prevalence of in-home solid fuel combustion for heating [62].

WHO estimates that household air pollution from solid fuel combustion caused more than 4 million premature deaths in 2012 [62]. The diseases linked to these deaths include chronic obstructive pulmonary disease and lung cancer in adults, especially women, and pneumonia in children under the age of five. Chronic exposure to smoke from household fuel combustion is associated with a wide range of other diseases, including cataracts and blindness [64].

Uncontrolled incomplete combustion of biomass fuels emits hundreds of pollutants, including carbon monoxide, oxygenated organics, free radicals, and hydrocarbons. Studies of exposure to household air pollution from incomplete combustion commonly use carbon monoxide and particulate matter (PM) as primary exposure metrics. More precisely, scientists and regulators widely reference the mass concentration of Inhalable particulate matter less than 10 microns in aerodynamic diameter (PM_{10}) or the concentration of fine particulate matter less than 2.5 microns in diameter ($PM_{2.5}$) as proxies for the mixture of chemicals found in condensed phase air pollution. The $PM_{2.5}$ size range is considered more dangerous, because the smaller particles can penetrate deep into the alveolar region of the lungs. To protect human health, WHO has set an air quality guideline for $PM_{2.5}$ concentrations to be kept below $10 \mu\text{g m}^{-3}$ on an annual average basis and below $25 \mu\text{g m}^{-3}$ over a 24-hour averaging period [65]. Demonstrating the severity of the problem, some studies of household pollution in kitchen areas where unvented solid-fuel combustion was taking place have reported average $PM_{2.5}$ concentrations above $500 \mu\text{g m}^{-3}$ [66].

In addition to producing pollution that harms human health, household solid fuel combustion is estimated to produce 25% of global emissions of black carbon, which is the light-absorbing component of PM [62]. Black carbon, along with methane, is one of the main short-lived climate forcing pollutants. Black carbon has an atmospheric lifetime on the order of a week—not years or decades like CO_2 or N_2O —so reducing BC presents a good near-term opportunity for mitigating climate change. Lacey et al. [67] used a global atmospheric chemistry and transport model linked to a reduced-form radiative forcing model to estimate the country-specific net surface temperature response to changing out solid fuel cookstoves. Their analysis considered not only BC, but also methane and organic carbon (OC) from incomplete combustion, net CO_2 emissions from unsustainable biomass harvesting, and sulfate aerosol formed from SO_2 emissions from coal. Whether the cook stove interventions in each country would have a net warming or net cooling effect was not clear in advance, because OC and sulfate aerosols are reflective and have a cooling effect in the atmosphere. Nevertheless, Lacey et al. found that for almost all of the countries they examined, changing out cook stoves would have a beneficial climate effect (reducing global warming) in addition to delivering significant health benefits [67].

Sustainably harvested biomass is considered to be a renewable energy resource. On the other hand, biomass used for household fuel combustion in much of the world is not sustainably managed. Deforestation or forest degradation is a centuries-old problem that is partially attributable to biomass fuel use. In a recent global assessment, Bailis et al. [68] estimated that 22%–30% of wood fuel supplies in tropical countries is harvested unsustainably. The African countries of Eritrea, Ethiopia, Kenya, Uganda, Rwanda, and Burundi, and the Asian countries of Pakistan, Nepal, Bhutan, Indonesia, and Bangladesh

all had significant areas where more than half of wood fuel was not sustainably harvested [68]. In other areas, high rates of deforestation due to agricultural expansion constrain wood fuel availability. Significant environmental consequences of deforestation include habitat loss, soil erosion, and flooding, as well as net CO₂ emissions from reduced carbon sequestration in the biosphere. Moreover, in many areas today people who gather their own biomass for cooking or heating are relegated to walking long distances and spending hours a day to gather fuel because nearby supplies have been depleted. The WHO has found that some children spend more than 30 hours a week gathering biomass [62]. In many countries the task of gathering biomass falls primarily to girls, and is a significant impediment to their gaining an education [62].

Options for addressing the problems caused by household combustion of biofuels and other solid fuels include switching to cleaner heat sources, such as electricity, pipeline natural gas, biogas, or liquefied petroleum gas; use of improved biomass stoves with higher combustion efficiency and lower emissions, such as those shown in [Figure 9.11](#); and/or use of stoves with chimneys to move emissions away from occupied areas. Reducing the cost of these alternatives is a key challenge, as many people who use biofuels in a rudimentary stove or fire do so because they cannot afford alternatives. Rural and remote communities often lack the infrastructure to transmit electricity or supply gas by pipeline. Programs to develop and deploy more efficient biomass stoves have often been stymied because new stoves did not meet local expectations for cooking time, fuel costs or fuel preparation requirements, ease of installation and repair, robustness, and durability. More efficient stove designs that use fans may not work in areas lacking access to electric power. Studies that have tried to distribute improved stoves have often found that emissions reductions, efficiency, and performance are variable and that improvements seen in the lab are not replicated in actual use. Recipients of new stoves have often been found to use them to supplement rather than to replace their traditional stoves, a practice known as “stacking.” In colder climates, another issue is that heat given off by cooking stoves is relied upon for space heating, so replacement stoves not designed for that dual purpose are unsatisfactory. In a recent review of studies designed to assess the effectiveness of low-emission stoves, Bruce et al. [69] found that providing these stoves was often not enough to achieve air quality guidelines, due to stove stacking, the presence of other combustion sources in the home, and contributions from outdoor sources. They recommend taking a multi-pronged approach to reducing household air pollution that goes beyond stove replacement, and placing greater emphasis on improving access to clean fuels.

9.4 Conclusions

In developed countries, economic and political concerns have renewed interest in biomass development as a domestic source of clean and renewable fuels and chemicals. Initial efforts have unfortunately competed with food crops for low-cost sugars. A sustainable biomass industry will have to provide food to the world's growing population before supporting future energy needs. Thus, researchers are investigating how to convert crop residues and dedicated energy crops into valuable fuels and chemicals. These feedstocks could provide a bridge from first- to second-generation biofuels and beyond.

First-generation biofuels based on grain ethanol and soy diesel will continue to be important sources of alternative transportation fuels for several years because significant

investment has been made in their infrastructure and continuing political support of government incentives. However, significant expansion of the biofuel industry will require alternatives to corn and soybean crops as feedstocks. These possibilities include both lignocellulose and lipids from alternative crops.

Each of the biofuel and bioenergy options considered in this chapter has its advantages and disadvantages in terms of market, opportunities, environmental benefits, and process economics. Accordingly, no single biofuel is likely to dominate transportation in the same manner as currently exists for petroleum-based gasoline and diesel. Niche markets and regional considerations will heavily influence the best choice of fuel for specific applications. Finally, increased research efforts could raise new possibilities that change the outlook for biofuels.

Although biochemical processing dominates current-generation biofuels, thermochemical processing is likely to play an important role in advanced biofuels because of its technical maturity and potential to efficiently produce hydrocarbon fuels. However, it is too early to designate winners and losers among the many biofuel options. What is certain is that biofuels will evolve as a result of several forces including new technologies, market demand, environmental concerns, and government policies.

PROBLEMS

- 9.1 Wisconsin produced 13,260,000 bushels (25.4 kg per bushel) of oats on 195,000 ac (4046.85 m² per acre) of land. What is the corresponding yield of oat residue in tonnes per km² assuming a residue to grain ratio of 2:1?
- 9.2 Use the USDA Quick Stats service (<http://quickstats.nass.usda.gov/>) to compare the 2009 oat yields between New York and California. What additional land would California require to meet the same amount of oat production as New York?
- 9.3 We can estimate future crop yields using the exponential growth formula

$$\text{Yield}(t) = \text{Yield}_0 e^{kt} \quad (9.36)$$

where k is the growth rate and t is the period of time since the initial value Yield_0 . Collect the required data from Quick Stats to calculate the rate at which corn yields have increased in Minnesota between 1990 and 2009. Given this growth rate, what is the predicted 2020 corn yield for Minnesota?

- 9.4 The U.S. total land area is almost 9,307,800 km². Thirty percent of the land is forestland. How much above-ground biomass is available in the U.S. forestland assuming a 15,240 Mg/km² biomass density? How much land would we need to grow an equivalent amount of biomass with fast-growing trees (hybrid poplar), or energy crops (switchgrass)?
- 9.5 A common assumption for biorefinery capacities is 2000 Mg/day of feedstock input capacity. What is the land area required to grow this quantity of biomass from corn stover with land availability (f) of 40%? How does this compare to switchgrass?
- 9.6 Given the enthalpy of formation for food waste to be -394.7 MJ/kmol, use the combustion reaction from Equation 9.11 to calculate its HHV (assume that the molecular formula is the same as switchgrass). Repeat this calculation for redwood (assume an enthalpy of formation of -50.7 MJ/kmol).
- 9.7 Solar irradiation in parts of California exceeds 9 kWh/m²/day (32 million MJ/km²/day). What are theoretical maximum C3 and C4 biomass energy yields

assuming a 150-day crop growth period? In Florida, solar irradiation is about $3.5 \text{ kWh/m}^2/\text{day}$; what would the theoretical maximum yield be if the crop had a maturity period of 180 days?

- 9.8 How many people can Hawaii feed? Different diets require different energy inputs. Since meat is higher in the food chain than grains, the more calories you get from meat, the more agricultural land you use. About 1 GJ metabolizable energy is produced annually/hectare for meat and 30 GJ metabolizable energy produced annually/hectare for grain.

Hawaii has about 1.3 million acres of zoned agricultural lands and forests. In that, 675,000 ac are designated as prime agricultural lands of importance to the State of Hawaii of which less than 200,000 ac are under cultivation [70].

Assuming all 675,000 ac of prime agricultural land is used for food production, and the average daily energy requirement for a human is about 2000 kilocalories/day (kcal/day), answer the following questions:

How many vegetarians could Hawaii feed? Determine this as an absolute number, percent of 2010 population, and percent of estimated 2030 population.

How many typical Americans could Hawaii feed? (The typical American gets two-thirds of their calories from meat and one-third from grain)? Again, determine this as an absolute number, percent of 2010 population, and percent of estimated 2030 population.

Clearly state all assumptions made and sources of information used. Show your calculations. Take care to convert units as needed (acre-to-hectare and kcal/day-to-GJ for example). Note that 1 food Calorie (with a capital "C") = 1 kcal. Here is an excellent unit conversion website: <http://www.onlineconversion.com>.

- 9.9 A gasifier can convert 1 kg of wood (19.5 MJ/kg) into 1.5 m^3 of syngas (5.2 MJ/m^3). If we define energy conversion efficiency as the ratio of syngas energy to biomass energy, what is the energy conversion efficiency of wood to syngas?
- 9.10 A lactating cow can produce more than 60 kg of manure (about 7 MJ/kg on a dry basis) per day. What is the energy efficiency of converting cow manure to biogas if it yields 25 m^3 per Mg with the methane content of 55% (35 MJ/m^3)?
- 9.11 Gasification uses an oxygen-to-fuel ratio that is 25% of the required oxygen for complete combustion. What is the amount of oxygen required to gasify 1 kg of wood ($\text{CH}_{1.4}\text{O}_{0.66}$)?
- 9.12 Steam gasification employs steam as the oxygen carrier. How much steam would be needed to gasify 1 kg of wood ($\text{CH}_{1.4}\text{O}_{0.66}$)?
- 9.13 How much air is needed to fully combust fuel oil ($\text{CH}_{1.67}\text{O}_{0.006}\text{N}_{0.005}\text{S}_{0.002}$) if 25% excess air is required?
- 9.14 Calculate the energy conversion efficiency of biomass to gasification products assuming the yields and energy contents from Table 9.8.
- 9.15 In 2005, California had almost 440 MW of coal power-generating capacity. What amount of biomass would be required to produce the same amount of electricity? Assume a biomass heating value of 17 MJ/kg , a biomass-to-syngas thermal efficiency of 85%, and a syngas-to-electricity efficiency of 38%.
- 9.16 Assuming a chain growth probability of 0.8, calculate the mole yields for hydrocarbons with 1–24 carbon atoms using the ASF distribution. How does this distribution compare to that of a 0.9 chain growth probability.

- 9.17 Calculate the heat of reaction for ethanol (heat of formation -277.7 MJ/kmol) synthesis with the mixed-alcohol process and with the methanol (heat of formation -238.4 MJ/kmol) conversion process.
- 9.18 Assuming nominal annual yields of 700,000, 5,500,000, and 3,800,000 kg/km² for corn grain, sugar cane, and sweet sorghum respectively, which conversion pathway is the most productive use of land? Use conversion yield values given in ethanol section and units of L/km².
- 9.19 A group proposes a 2000 barrel-per-day ethanol output biorefinery using Jerusalem artichokes. What is the daily feedstock requirement for this biorefinery? What is the minimum amount of land required to grow the feedstock ($f = 100\%$)?
- 9.20 If the yield of bio-oil to liquid fuels (gasoline- and diesel-like fuels) is 42 wt.%, what is the overall energy efficiency? Use the values in Table 9.12 for energy content and product yields. First, calculate the biomass to liquid fuel yield based on the biomass to bio-oil and bio-oil to liquid fuel yields. Finally, assume a liquid fuel energy density of 41.2 MJ/kg and calculate the energy efficiency.
- 9.21 How many liters of bio-oil can be generated with Iowa's 2009 corn stover yield? Use appropriate data from Quick Stats, a 65 wt.% yield of bio-oil from corn stover, and a bio-oil density of 1201.9 kg/m³.
- 9.22 Using an ethanol fuel content of 21.2 MJ/L and TTW efficiency of 3.08 MJ per km, calculate the theoretical travel distance (units of km per km² of land) for an E-85 vehicle powered by corn grain ethanol. How does this number compare to sugar cane ethanol and cellulosic ethanol? Employ appropriate assumptions for crop yields and process conversion efficiency.
- 9.23 Assuming a 10% improvement in the production of H₂ from coal, what is the new WTW efficiency for a H₂ ICE and what is the reduction in CO₂ emissions per kilometer?

References

1. Brown, R.C., 2003. *Biorenewable Resources: Engineering New Products from Agriculture*, Iowa State Press, A Blackwell Publishing Company, Ames, IA, pp. 59–75.
2. Perlack, R., Wright, L., Turhollow, A., Graham, R., Stokes, B., and Erbach, D., 2005. Biomass as feedstock for a bioenergy and bioproducts industry: The technical feasibility of a billion-ton annual supply, Technical Report A357634, Oak Ridge National Laboratory.
3. Morris, G., 2003. The status of biomass power generation in California, July 31, 2003, Technical Report NREL/SR-510-35114, National Renewable Energy Laboratory.
4. Wright, L.L., and Hohenstein, W.G., 1994. Dedicated feedstock supply systems: Their current status in the USA, *Biomass and Bioenergy* 6(3), 159–241.
5. Field, C.B., Campbell, J.E., and Lobell, D.B., 2008. Biomass energy: The scale of the potential resource, *Trends in Ecology & Evolution* 23(2), 65–72.
6. Wayman, M., and Parekh, S.R., 1990. *Biotechnology of Biomass Conversion: Fuels and Chemicals from Renewable Resources*, Open University Press, Philadelphia, PA.
7. United States Department of Agriculture, 2012. Agricultural statistics database, July 2012, <http://quickstats.nass.usda.gov>.

8. Zhu, X.G. et al., 2008. What is the maximum efficiency with which photosynthesis can convert solar energy into biomass? *Current Opinion in Biotechnology* 19(2), 153–159.
9. Jenkins, B.M., Baxter, L.L., and Miles, T.R., 1998. Combustion properties of biomass, *Fuel Processing Technology* 54(1–3), 17–46.
10. Klass, D.L., 1998a *Biomass for Renewable Energy, Fuels, and Chemicals*, Academic Press, San Diego, CA, pp. 72–90.
11. Moran, M.J., Shapiro, H.N., Boettner, D.D., and Bailey, M., 2010. *Fundamentals of Engineering Thermodynamics*, Wiley, New York.
12. Klass, D.L., 1998b. *Biomass for Renewable Energy, Fuels, and Chemicals*, Academic Press, San Diego, CA, p. 356.
13. Reed, T.B., 1981. *Biomass Gasification: Principles and Technology*, Noyes Data Corp., Park Ridge, NJ.
14. Bridgwater, A.V., 1995. The technical and economic feasibility of biomass gasification for power generation, *Fuel* 74(5), 631–653.
15. Klass, D.L., 1998c. *Biomass for Renewable Energy, Fuels, and Chemicals*, Academic Press, San Diego, CA, p. 416.
16. Henrich, E., and Weirich, F., 2004. Pressurized entrained flow gasifiers for biomass, *Environmental Engineering Science* 21(1), 53–64.
17. Bailey, B.K., 1996. Performance of ethanol as a transportation fuel, in: Wyman, C. (ed.), *Handbook on Bioethanol*, vol. 1, Taylor and Francis, Washington, DC, pp. 37–58.
18. Kwiakowski, J.R., McAloon, A.J., Taylor, F., and Johnston, D.B., 2006. Modeling the process and costs of fuel ethanol production by the corn dry-grind process, *Industrial Crops & Products* 23(3), 288–296.
19. Rowell, R.M., Young, R.A., and Rowell, J.K., 1997. *Paper and Composites from Agro-Based Resources*, CRC Press, Boca Raton, FL.
20. Schell, D.J., McMillian, J.D., and Philippidis, G.P., 1992. Ethanol from lignocellulosic biomass, *Advances in Solar Energy* 7, 373–448.
21. Lynd, L.R., 1996. Overview and evaluation of fuel ethanol from cellulosic biomass: Technology, economics, the environment and policy, *Annual Reviews in Energy and the Environment* 21(1), 403–465.
22. Aden, A., Ruth, M., Ibsen, K., Jechura, J., Neeves, K., Sheehan, J., Wallace, B., Montague, L., and Slayton, A., 2002. Lignocellulosic biomass to ethanol process design and economics utilizing co-current dilute acid prehydrolysis and enzymatic hydrolysis for corn stover, Technical Report NREL//TP-510-32438, National Renewable Energy Laboratory.
23. Hall, C.A.S., Dale, B.E., and Pimentel, D., 2011. Seeking to understand the reasons for different energy return on investment (eroi) estimates for biofuels, *Sustainability* 3(12), 2413–2432.
24. Anon., 2005. Fischer–Tropsch archive, <http://www.fischer-tropsch.org>.
25. Schulz, H., 1999. Short history and present trends of Fischer–Tropsch synthesis, *Applied Catalysis A, General* 186(1–2), 3–12.
26. Tijmensen, M.J.A., Faaij, A.P.C., Hamelinck, C.N., and van Hardeveld, M.R.M., 2002. Exploration of the possibilities for production of Fischer Tropsch liquids and power via biomass gasification, *Biomass and Bioenergy* 23(2), 129–152.
27. Swanson, R.M., Platon, A., Satrio, J.A., and Brown, R.C., 2010. Techno-economic analysis of biomass-to-liquids production based on gasification, *Fuel* 89, S11–S19.
28. Bridgwater, A.V., and Peacocke, G.V.C., 2000. Fast pyrolysis processes for biomass, *Renewable and Sustainable Energy Reviews* 4(1), 1–73.
29. Czernik, S., and Bridgwater, A.V., 2004. Overview of applications of biomass fast pyrolysis oil. *Energy and Fuels* 18(2), 590–598.
30. Piskorz, J., and Scott, D.S., 1987. The composition of oils obtained by the fast pyrolysis of different woods, American Chemical Society, Division of Fuel Chemistry, *Preprint Paper*, 32(2).
31. Wright, M.M., Dugaard, D.E., Satrio, J.A., and Brown, R.C., 2010. Techno-economic analysis of biomass fast pyrolysis to transportation fuels, *Fuel* 89(Supplement 1(0)), S2–S10, ISSN 0016-2361, <http://www.sciencedirect.com/science/article/pii/S0016236110003765>.

32. Vieira de Carvalho, A.J., 1982. Natural gas and other alternative fuels for transportation purposes, *Energy* 10(2), 187–215.
33. Satterfield, C.N., 1991. *Heterogeneous Catalysis in Industrial Practice*, McGraw-Hill Book Co., New York.
34. Sorenson, S.C., 2001. Dimethyl ether in diesel engines: Progress and perspectives, *Journal of Engineering for Gas Turbines and Power* 123, 652.
35. Klass, D.L., 1998d. *Biomass for Renewable Energy, Fuels, and Chemicals*, Academic Press, San Diego, CA, pp. 274–276.
36. Forzatti, P., Tronconi, E., and Pasquon, I., 1991. Higher alcohol synthesis, *Catalysis Reviews* 33(1), 109–168.
37. Phillips, S., Aden, A., Jechura, J., Dayton, D., and Eggeman, T., 2007. Thermochemical ethanol via indirect gasification and mixed alcohol synthesis of lignocellulosic biomass, Technical Report NREL//TP-510-41168, National Renewable Energy Laboratory.
38. Brown, R.C., 2007. Hybrid thermochemical/biological processing, *Applied Biochemistry and Biotechnology* 137(1), 947–956.
39. Openshaw, K., 2000. A review of *Jatropha curcas*: An oil plant of unfulfilled promise, *Biomass and Bioenergy* 19(1), 1–15.
40. Glenn, E.P., O'Leary, J.W., Watson, M.C., Thompson, T.L., and Kuehl, R.O., 1991. *Salicornia bigelovii* torr.: An oilseed halophyte for seawater irrigation, *Science* 251(4997), 1065–1067.
41. Kumar, A., and Sharma, S., 2008. An evaluation of multipurpose oil seed crop for industrial uses (*Jatropha curcas* l.): A review. *Industrial Crops & Products* 28(1), 1–10.
42. Kram, J.W., 2013. Aviation Alternatives, *Biodiesel Magazine*, Grand Forks, ND58203, <https://www.biodieselmagazine.com/articles/3071/aviation-alternatives>.
43. Klass, D.L., 1998e. *Biomass for Renewable Energy, Fuels, and Chemicals*, Academic Press, San Diego, CA, pp. 341–344.
44. Lundquist, T.J., Woertz, I.C., Quinn, N.W.T., and Benemann, J.R., 2010. A realistic technology and engineering assessment of algae biofuel production, in: *Energy Biosciences Institute*, Berkeley, CA, p. 1.
45. Peterson, A.A., Vogel, F., Lachance, R.P., Fröling, M., Antal Jr., M.J., and Tester, J.W., 2008. Thermochemical biofuel production in hydrothermal media: A review of sub-and supercritical water technologies, *Energy & Environmental Science* 1(1), 32–65.
46. Elliott, D.C., Beckman, D., Bridgwater, A.V., Diebold, J.P., Gevert, S.B., and Solantausta, Y., 1991. Developments in direct thermochemical liquefaction of biomass: 1983–1990, *Energy & Fuels* 5(3), 399–410.
47. Elliott, D.C., Neuenschwander, G.G., Hart, T.R., Butner, R.S., Zacher, A.H., Engelhard, M.H., Young, J.S., and McCready, D.E., 2004. Chemical processing in high-pressure aqueous environments. 7. Process development for catalytic gasification of wet biomass feedstocks, *Industrial and Engineering Chemistry Research* 43(9), 1999–2004.
48. Moreau, C., Naceur Belgacem, M., and Gandini, A., 2004. Recent catalytic advances in the chemistry of substituted furans from carbohydrates and in the ensuing polymers, *Topics in Catalysis* 27(1–4), 11–30.
49. Carlson, T.R., Vispute, T.P., and Huber, G.W., 2008. Green gasoline by catalytic fast pyrolysis of solid biomass derived compounds, *ChemSusChem* 1(5), 397.
50. Roman-Leshkov, Y., Barrett, C.J., Liu, Z.Y., and Dumesic, J.A., 2007. Production of dimethylfuran for liquid fuels from biomass-derived carbohydrates, *Nature* 447, 982–985.
51. Zhao, H., Holladay, J.E., Brown, H., and Zhang, Z.C., 2007. Metal chlorides in ionic liquid solvents convert sugars to 5-hydroxymethylfurfural, *Science* 316(5831), 1597.
52. Diebold, J.P., and Evans, R.J., 1988. U.S. Patent No. 4, 764, 627. Washington, DC: U.S. Patent and Trademark Office.
53. Tillman, D.A., 1991. *The Combustion of Solid Fuels and Wastes*, Academic Press, San Diego, CA.
54. Bain, R.L., Overend, R.P., and Craig, K.R., 1998. Biomass-fired power generation. *Fuel Processing Technology* 54(1–3), 1–16.

55. Kumar, J.V., and Pratt, B.C., 1996. Compositional analysis of some renewable biofuels, *American Laboratory* 28(8), 15–20.
56. Sami, M., Annamalai, K., and Wooldridge, M., 2001. Cofiring of coal and biomass fuel blends, *Progress in Energy and Combustion Science* 27(2), 171–214.
57. Borman, G.L., and Ragland, K.W., 1998. *Combustion Engineering*, McGraw-Hill Company, New York.
58. Laboratory National Renewable Energy Laboratory. Alternative fuels, general table of fuel properties, [http://www.eere.energy.gov/afdc/altfuel/fuelsdo5\(p\)roperties.html](http://www.eere.energy.gov/afdc/altfuel/fuelsdo5(p)roperties.html).
59. MacKenzie, J.J., and Avery, W.H., 1996. Ammonia fuel: The key to hydrogen-based transportation, in: *Energy Conversion Engineering Conference, IECEC 96*, vol. 3.
60. Teng, H., McCandless, J.C., and Schneyer, J.B., 2001. Thermochemical characteristics of dimethyl ether-an alternative fuel for compression-ignition engines [r], SAE technical paper, 2001-01-0154.
61. International Energy Agency, 2016. *Key Energy Statistics, 2016*, <https://www.iea.org/publications/freepublications/publication/KeyWorld2016.pdf>.
62. World Health Organization, 2016. *Burning Opportunity: Clean Household Energy for Health, Sustainable Development, and Wellbeing of Women and Children*, Geneva, Switzerland.
63. Archer-Nicholls, S. et al., 2016. The regional impacts of cooking and heating emissions on ambient air quality and disease burden in China, *Environmental Science & Technology* 50, 9416–9423. DOI:10.1021/acs.est.6b02533
64. Pokhrel, A.K., Smith, K.R., Khalakdina, A., Deuja, A., Bates, M.N., 2005. Case-control study of indoor cooking smoke exposure and cataract in Nepal and India. *International Journal of Epidemiology* 34, 702–708.
65. World Health Organization, 2006. *WHO Air Quality Guidelines Global Update 2005: Particulate Matter, Ozone, Nitrogen Dioxide and Sulfur Dioxide*, EUR/05/5046029, Copenhagen.
66. Clark, M.L. et al., 2013. Health and household air pollution from solid fuel use: the need for improved exposure assessment, *Environmental Health Perspectives* 121, 1120–1128.
67. Lacey, F.G., Henze, D.K., Lee, C.J., van Donkelaar, A., Martin, R.V., 2017. Transient climate and ambient health impacts due to national solid fuel cookstove emissions, *Proceedings of the National Academy of Sciences of the United States of America* 114, 1269–1274. DOI:10.1073/pnas.1612430114
68. Bailis, R., Drigo, R., Ghilardi, A., Masera, O., 2015. The carbon footprint of traditional woodfuels, *Nature Climate Change* 5, 266–272.
69. Bruce, N., Pope, D., Rehfuess, E., Balakrishnan, K., Adair-Rohani, H., Dora, C., 2015. WHO indoor air quality guidelines on household fuel combustion: Strategy implications of new evidence on interventions and exposure-risk functions, *Atmospheric Environment* 106, 451–457.
70. Turano, B., Ogoshi, R., and Uehara, G., 2009. Can biofuels from non-food sources end the food versus fuel debate? Hawaii Energy Policy Forum, <http://www.hawaiienergypolicyforum.blogspot.com>.

10

Fundamentals of Solar Radiation

Having been admonished by the Holy Office [the Inquisition] entirely to abandon the false option that the Sun was the center of the universe and immovable, and that the Earth was not the center of the same and that it moved ... I abjure ...

Galileo

10.1 Physics of the Sun and Its Energy Transport

The nature of energy generation in the sun is still an unanswered question. Spectral measurements have confirmed the presence of nearly all the known elements in the sun. However, 80% of the sun is hydrogen and 19% helium. Therefore, the remaining 100-plus observed elements make up only a tiny fraction of the composition of the sun. It is generally accepted that a hydrogen-to-helium thermonuclear reaction is the source of the sun's energy. Yet because such a reaction has not been duplicated in the laboratory, it is unclear precisely what the reaction mechanism is, what role the turbulent flows in the sun play, and how solar prominences and sunspots are created.

The nature of the energy-creation process is of no importance to terrestrial users of the sun's radiation. Of interest is the amount of energy, its spectral and temporal distribution, and its variation with time of day and year. These matters are the main subject of this chapter.

The sun is a 13.9×10^5 km diameter sphere comprised of many layers of gases, which are progressively hotter toward its center. The outermost layer, from which energy is radiated into the solar system, is approximately at an equivalent blackbody temperature of 5760 K (10,400°R). The center of the sun, however, may be at 20×10^6 K. The rate of energy emission from the sun is 3.8×10^{23} kW, which results from the conversion of 4.3×10^9 g/s (4.7×10^6 ton/s) of mass to energy. Of this total, only a tiny fraction, approximately 1.7×10^{14} kW, is intercepted by the Earth, which is located about 150 million km from the sun (Figure 10.1).

Solar energy is the world's most abundant permanent source of energy. The amount of solar energy intercepted by the planet Earth is 5000 times greater than the sum of all other inputs (terrestrial, nuclear, geothermal, and gravitational energies, and lunar gravitational energy). Of this amount, 30% is reflected to space, 47% is converted to low-temperature heat and reradiated to space, and 23% powers the evaporation/precipitation cycle of the bio-sphere. Less than 0.5% is represented in the kinetic energy of the wind and waves and in photosynthetic storage in plants.

Total terrestrial radiation is only about one-third of the extraterrestrial total during a year, and 70% of that falls on the oceans. However, the remaining 1.5×10^{17} kWh that falls

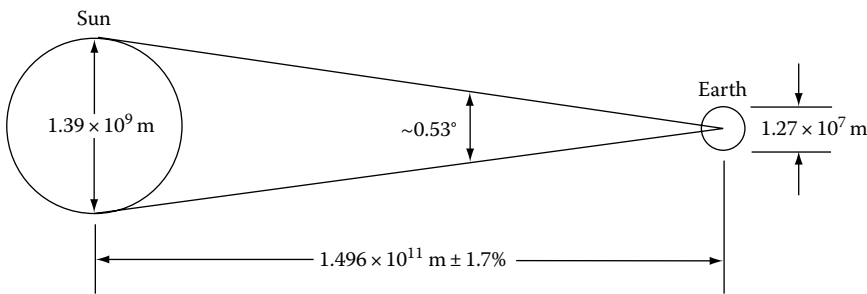


FIGURE 10.1
Relationship between the sun and the Earth.

on land is a prodigious amount of energy—about 6000 times the total energy usage of the United States in 2000. However, only a small fraction of this total can be used because of physical and socioeconomic constraints, as described in [Chapter 1](#).

10.2 Thermal Radiation Fundamentals

The material presented in this section has been selected from textbooks on heat transfer and radiation [1–4]. It provides the background needed to understand the nature of solar radiation for the engineering analysis of solar energy systems.

To begin with, all radiation travels at the speed of light, which is equal to the product of the wavelength and the frequency of radiation. The speed of light in a medium equals the speed of light in a vacuum divided by the refractive index of the medium through which it travels:

$$c = \lambda \nu = \frac{c_0}{n} \quad (10.1)$$

where

λ is the wavelength (m) (or μm , $1 \mu\text{m} = 10^{-6} \text{ m}$)

ν is the frequency (s^{-1})

c is the speed of light in a medium (m/s)

c_0 is the speed of light in a vacuum (m/s)

n is the index of refraction of the medium

Thermal radiation is one kind of electromagnetic energy, and all bodies emit thermal radiation by virtue of their temperature. When a body is heated, its atoms, molecules, or electrons are raised to higher levels of activity called excited states. However, they tend to return to lower energy states, and in this process, energy is emitted in the form of electromagnetic waves. Changes in energy states result from rearrangements in the electronic, rotational, and vibrational states of atoms and molecules. Since these rearrangements involve different amounts of energy changes and these energy changes are related to the frequency, the radiation emitted by a body is distributed over a range

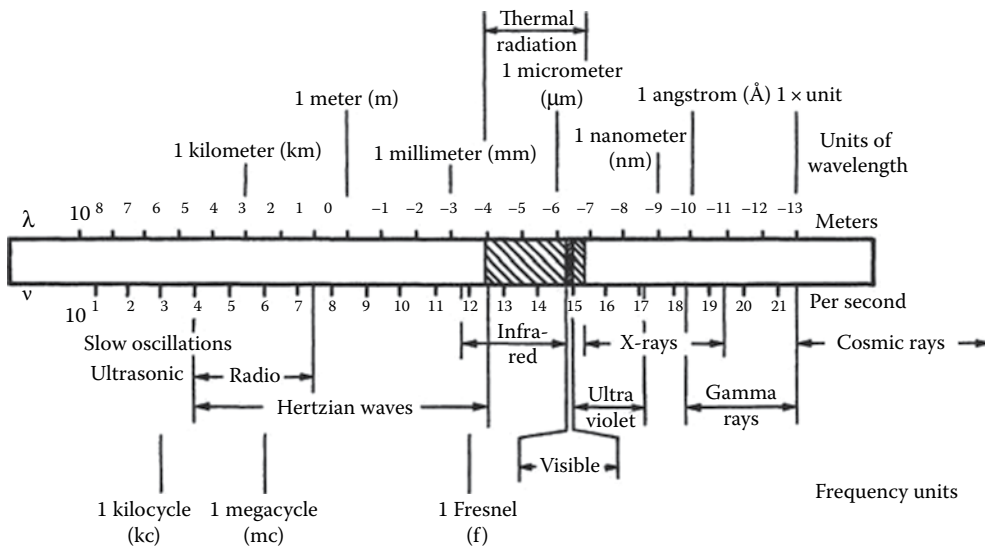


FIGURE 10.2
Electromagnetic radiation spectrum.

of wavelengths. A portion of the electromagnetic spectrum is shown in Figure 10.2. The wavelengths associated with the various mechanisms are not sharply defined; thermal radiation is usually considered to fall within the band from about 0.1 to 100 μm , whereas solar radiation has most of its energy between 0.1 and 3 μm .

For some problems in solar energy engineering, the classical electromagnetic wave theory is not suitable. In such cases, for example, in photovoltaic or photochemical processes, it is necessary to treat the energy transport from the point of view of quantum mechanics. In this view, energy is transported by particles or *photons*, which are treated as energy units or quanta rather than waves. The energy of a photon, E_p , of frequency ν_p is

$$E_p = h\nu_p \quad (10.2)$$

where h is the Planck's constant ($6.625 \times 10^{-34} \text{ J} \cdot \text{s}$).

10.2.1 Black-Body Radiation

The energy density of the radiation emitted at a given wavelength (monochromatic) by a perfect radiator, usually called a black body, is given according to the following relation:

$$E_{b\lambda} = \frac{C_1}{(e^{C_2/\lambda T} - 1)\lambda^5 n^2} \quad (10.3)$$

where

$$C_1 = 3.74 \times 10^8 \text{ W } \mu\text{m}^4/\text{m}^2 \text{ (} 1.19 \times 10^8 \text{ Btu } \mu\text{m}^4/\text{h ft}^2\text{)}$$

$$C_2 = 1.44 \times 10^4 \text{ } \mu\text{m K (} 2.59 \times 10^4 \text{ } \mu\text{m } ^\circ\text{R)}$$

n = refractive index of the medium = 1.0 for vacuum; n is taken to be approximately equal to 1 for air

The quantity $E_{b\lambda}$ has the units of $\text{W/m}^2 \mu\text{m}$ ($\text{Btu/h ft}^2 \mu\text{m}$) and is called the monochromatic emissive power of a black body, defined as the energy emitted by a perfect radiator per unit wavelength at the specified wavelength per unit area and per unit time at the temperature T .

The total energy emitted by a black body, E_b , can be obtained by integration over all wavelengths. This yields the Stefan–Boltzmann law:

$$E_b = \int_0^{\infty} E_{b\lambda} d\lambda = \sigma T^4 \quad (10.4)$$

where

σ is the Stefan–Boltzmann constant = $5.67 \times 10^{-8} \text{ W/m}^2 \text{ K}^4$ ($0.1714 \times 10^{-8} \text{ Btu/h ft}^2 \text{ R}^4$)

T is the absolute temperature (K) (or $R = 460 + ^\circ\text{F}$)

The concept of a black body, although no such body actually exists in nature, is very convenient in engineering because its radiation properties can readily be related to those of real bodies.

10.2.2 Radiation Function Tables

Engineering calculations of radiative transfer are facilitated by the use of radiation function tables, which present the results of Planck's law in a more convenient form than Equation 10.3. A plot of the monochromatic emissive power of a black body as a function of wavelength as the temperature is increased is given in [Figure 10.3](#). The emissive power shows a maximum at a particular wavelength.

These peaks, or infection points, are uniquely related to the body temperature. By differentiating Planck's distribution law (Equation 10.3) and equating to zero, the wavelength corresponding to the maximum value of $E_{b\lambda}$ can be shown to occur when

$$\lambda_{\max} T = 2897.8 \mu\text{m K} (5215.6 \mu\text{m R}) \quad (10.5)$$

Frequently, one needs to know the amount of energy emitted by a black body within a specified range of wavelengths. This type of calculation can be performed easily with the aid of the radiation functions mentioned previously. To construct the appropriate radiation functions in dimensionless form, note that the ratio of the black-body radiation emitted between 0 and λ and between 0 and ∞ can be made a function of the single variable (λT) by using Equation 10.3 as shown (for $n = 1$) in the following equation:

$$\frac{E_{b,0-\lambda}}{E_{b,0-\infty}} = \frac{\int_0^{\lambda} E_{b\lambda} d\lambda}{\sigma T^4} = \int_0^{\lambda T} \frac{C_1 d(\lambda T)}{\sigma (\lambda T)^5 (e^{C_2/\lambda T} - 1)} \quad (10.6)$$

The earlier relation is plotted in [Figure 10.4](#), and the results are also shown in tabular form in [Table 10.1](#).

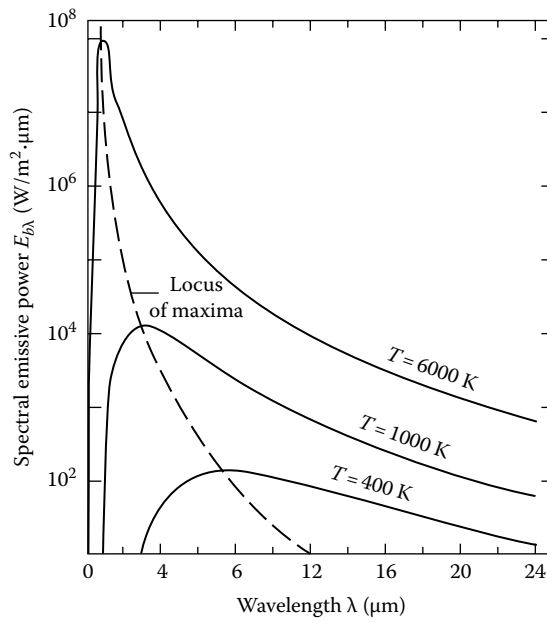


FIGURE 10.3
Spectral distribution of black-body radiation.

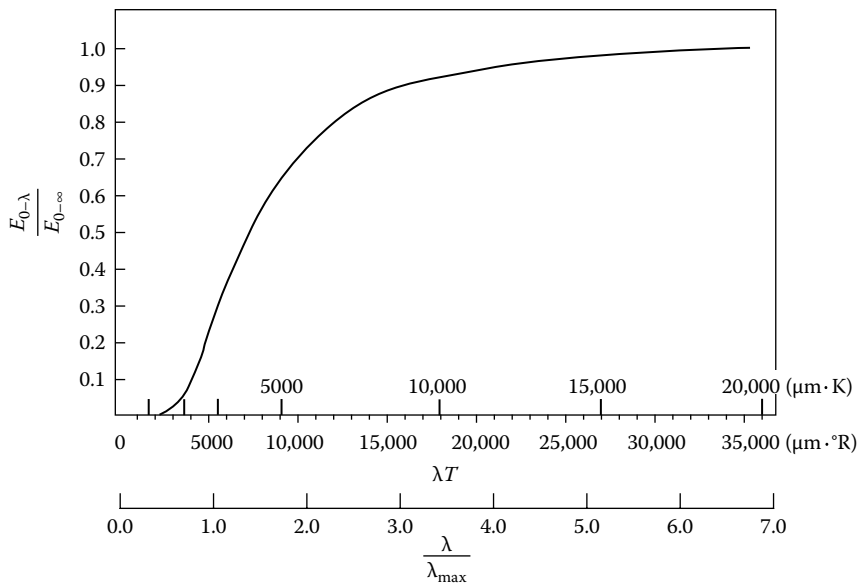


FIGURE 10.4
Fraction of total emissive power in spectral region between $\lambda = 0$ and λ as a function of λT and λ/λ_{\max} .

TABLE 10.1Thermal Radiation Functions^a

λ/λ_{\max}	$E_{b\lambda}/E_{b\lambda_{\max}}$	$E_{b\lambda,0-\lambda}/\sigma T^4$
0.00	0.0000	0.0000
0.20	0.0000	0.0000
0.30	0.0038	0.0001
0.40	0.0565	0.0015
0.50	0.2217	0.0101
0.60	0.4664	0.0325
0.70	0.7042	0.0712
0.80	0.8776	0.1236
0.90	0.9725	0.1849
1.00	1.0000	0.2501
1.10	0.9791	0.3153
1.20	0.9277	0.3782
1.30	0.8600	0.4370
1.40	0.7854	0.4911
1.50	0.7103	0.5403
1.60	0.6382	0.5846
1.70	0.5710	0.6243
1.80	0.5098	0.6598
1.90	0.4546	0.6915
2.00	0.4054	0.7197
2.10	0.3616	0.7449
2.20	0.3229	0.7674
2.30	0.2887	0.7875
2.40	0.2585	0.8054
2.50	0.2318	0.8215
2.60	0.2083	0.8360
2.70	0.1875	0.8490
2.80	0.1691	0.8607
2.90	0.1528	0.8713
3.00	0.1384	0.8809
3.10	0.1255	0.8895
3.20	0.1141	0.8974
3.30	0.1038	0.9045
3.40	0.0947	0.9111
3.50	0.0865	0.9170
3.60	0.0792	0.9225
3.70	0.0726	0.9275
3.80	0.0667	0.9320
3.90	0.0613	0.9362
4.00	0.0565	0.9401
4.20	0.0482	0.9470
4.40	0.0413	0.9528
4.60	0.0356	0.9579
4.80	0.0308	0.9622

(Continued)

TABLE 10.1 (Continued)Thermal Radiation Functions^a

λ/λ_{\max}	$E_{b\lambda}/E_{b\lambda,\max}$	$E_{b\lambda,0-\lambda}/\sigma T^4$
5.00	0.0268	0.9660
6.00	0.0142	0.9790
7.00	0.0082	0.9861
8.00	0.0050	0.9904
9.00	0.0033	0.9930
10.00	0.0022	0.9948
20.00	0.0002	0.9993
40.00	0.0000	0.9999
50.00	0.0000	1.0000

^a λ = wavelength in μm . λ_{\max} = wavelength at $E_{b\lambda,\max}$ in $\mu\text{m} = 2898/T$. $E_{b\lambda}$ = monochromatic emissive power in $\text{W}/\text{m}^2 \cdot \mu\text{m}$
 $= 374.15 \times 10^6 / \lambda^5 [\exp(14,387.9/\lambda T) - 1]$, $E_{b\lambda,\max}$ = maximum monochromatic emissive power in
 $\text{W}/\text{m}^2 \cdot \mu\text{m}$
 $= 12.865 \times 10^{-12} T^5$,

$$E_{b\lambda,0-\lambda} = \int_0^{\lambda} E_{b\lambda'} d\lambda'$$

$$\sigma T^4 = E_{b\lambda,0-\infty} = 5.670 \times 10^{-8} T^4 \text{ W}/\text{m}^2$$

 T = absolute temperature in K.

In Table 10.1, the first column is the ratio of λ to λ_{\max} from Equation 10.5, and the third column the ratio of $E_{b,0-\lambda}$ to σT^4 from Equation 10.6. For use on a computer, Equation 10.6 can be approximated by the following polynomials:

$$\nu \leq 2: \frac{E_{b,0-\lambda}}{\sigma T^4} = \frac{15}{\pi^4} \sum_{m=1,2,\dots} \frac{E^{-m\nu}}{m^4} \{[(m\nu + 3)m\nu + 6]m\nu + 6\} \quad (10.7a)$$

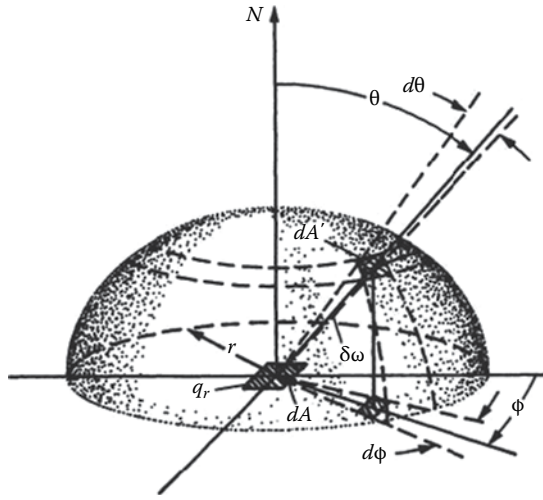
and

$$\nu \geq 2: \frac{E_{b,0-\lambda}}{\sigma T^4} = \frac{15}{1 - \pi^4} \nu^3 \left(\frac{1}{3} - \frac{\nu}{8} - \frac{\nu^2}{60} - \frac{\nu^4}{5,040} + \frac{\nu^6}{272,160} - \frac{\nu^8}{13,305,600} \right) \quad (10.7b)$$

where $\nu = C_2/\lambda T$.

10.2.3 Intensity of Radiation and Shape Factor

The emissive power of a surface gives the total radiation emitted in all directions. To determine the radiation emitted in a given direction, we must define another quantity, the radiation intensity I . As given in Equation 10.8, this quantity is defined as the radiant energy, dE , passing through an imaginary plane in space per unit area, dA' , per unit time and per unit solid angle, $d\omega$, perpendicular to the plane, as shown in Figure 10.5. I is defined by the relation

**FIGURE 10.5**

Schematic diagram illustrating radiation intensity and flux. N is the normal to the surface, θ is the angle between the beam direction and the surface normal, and ϕ is the angle of the projection of the beam onto the surface in the plane of the surface.

$$I = \lim_{\substack{dA' \rightarrow 0 \\ d\omega \rightarrow 0}} = \frac{dE}{dA' d\omega} \quad (10.8)$$

Radiation intensity has both magnitude and direction. It can be related to the radiation flux, defined as the radiant energy passing through an imaginary plane per unit area per unit time in all directions.

Note that, whereas for the intensity, the area dA' is perpendicular to the direction of the radiation, for the flux, the area dA is at the base in the center of a hemisphere through which all of the radiation passes. Recalling that the definition for the solid angle between dA' and dA is $d\omega = dA'/r^2$, the radiation flux q_r emanating from dA can be obtained by integrating the intensity over the hemisphere. As shown in Figure 10.5, the unit projected area for I is $dA \cos \theta$ and the differential area dA' on the hemisphere is $r^2 \sin \theta d\theta d\phi$; thus

$$q_r = \int_0^{2\pi} \int_0^{\pi/2} I \cos \theta \sin \theta d\theta d\phi \quad (10.9)$$

If the area dA is located on a surface, the emissive power E can also be obtained from Equation 10.9. For the special case of a diffuse surface, for which I is the same in all directions, Equation 10.9 gives

$$q_r = \pi I \quad (10.10)$$

Since all black surfaces are diffuse,

$$E_b = \pi I_b \quad (10.11)$$

Equation 10.11 can, of course, also be written for monochromatic radiation as

$$E_{b\lambda} = \pi I_{b\lambda} \quad (10.12)$$

In the evaluation of the rate of radiation heat transfer between two surfaces, not only their temperatures and their radiation properties but also their geometric configurations and relationships play a part. The influence of geometry in radiation heat transfer can be expressed in terms of the *radiation shape factor* between any two surfaces 1 and 2 defined as follows:

F_{1-2} = fraction of radiation leaving surface 1 that reaches surface 2

F_{2-1} = fraction of radiation leaving surface 2 that reaches surface 1

In general, F_{m-n} = fraction of radiation leaving surface “ m ” that reaches surface “ n .” If both surfaces are black, the energy leaving surface “ m ” and arriving at surface “ n ” is $E_{bm}A_mF_{m-n}$ and the energy leaving surface “ n ” and arriving at “ m ” is $E_{bn}A_nF_{n-m}$. If both surfaces absorb all the incident energy, the net rate of exchange $q_{m\leftrightarrow n}$ will be

$$q_{m\leftrightarrow n} = E_{bm}A_mF_{m-n} - E_{bn}A_nF_{n-m} \quad (10.13)$$

If both surfaces are at the same temperature, $E_{bm} = E_{bn}$ and the net exchange is zero $q_{m\leftrightarrow n} = 0$. This shows that the geometric radiation shape factor must obey the reciprocity relation

$$A_mF_{m-n} = A_nF_{n-m} \quad (10.14)$$

The net rate of heat transfer can therefore be written in two equivalent forms:

$$q_{m\leftrightarrow n} = A_mF_{m-n}(E_{bm} - E_{bn}) = A_nF_{n-m}(E_{bm} - E_{bn}) \quad (10.15)$$

The evaluation of geometric shape factors is in general quite involved. For a majority of solar energy applications, however, only a few special cases are of interest. One of these is a small convex object of area A_1 surrounded by a large enclosure A_2 . Since all radiation leaving A_1 is intercepted by A_2 , $F_{1-2} = 1$ and $F_{2-1} = A_1/A_2$.

Another case is the exchange of radiation between two large parallel surfaces. If the two surfaces are near each other, almost all of the radiation leaving A_1 reaches A_2 and vice versa. Thus, $F_{1-2} = F_{2-1} = 1.0$, according to the definition of the shape factor. A third case of importance is the exchange between a small surface ΔA_1 and a portion of space A_2 , for example, the exchange between a flat-plate solar collector tilted at an angle β from the horizontal and the sky it can see. For this situation, we refer to the definition of radiation flux (see [Figure 10.5](#)). The portion of the radiation emitted by ΔA_1 that is intercepted by the surrounding hemisphere depends on the angle of tilt. When the surface is horizontal, $F_{1-2} = 1$; when it is vertical, $F_{1-2} = 1/2$ ($\beta = 90^\circ$). For intermediate values, it can be shown that [4]

$$F_{1-2} = \frac{1}{2}(1 + \cos \beta) = \cos^2 \left(\frac{\beta}{2} \right) \quad (10.16)$$

If the diffuse sky radiation is uniformly distributed and assumed to be black, then a small black area A_1 receives radiation at the rate

$$A_1 F_{1-sky} E_{sky} = \frac{A_1}{2} (1 + \cos \beta) \sigma T_{sky}^4 \quad (10.17)$$

whereas the net radiation heat transfer is given by

$$q_{sky \leftrightarrow 1} = A_1 F_{1-sky} \sigma (T_{sky}^4 - T_1^4) \quad (10.18)$$

If the receiving area is gray with an absorptance $\bar{\alpha}$ equal to the emittance $\bar{\epsilon}$, the net exchange is given by

$$q_{sky \leftrightarrow 1} = A_1 F_{1-sky} \bar{\alpha} \sigma (T_{sky}^4 - T_1^4) \quad (10.19)$$

10.2.4 Transmission of Radiation through a Medium

When radiation passes through a transparent medium such as glass or the atmosphere, the decrease in intensity can be described by Beer's law, which assumes that the attenuation is proportional to the local intensity in the medium. If $I_\lambda(x)$ is monochromatic intensity after the radiation has traveled a distance x , the law is expressed by the equation

$$-dI_\lambda(x) = I_\lambda(x) K_\lambda dx \quad (10.20)$$

where K_λ is the monochromatic extinction coefficient assumed to be a constant of the medium. If the transparent medium is a slab of thickness L and the intensity at $x = 0$ is designated by the symbol $I_{\lambda,0}$, the monochromatic transmittance τ_λ is equal to the ratio of the intensity at $x = L$ to $I_{\lambda,0}$. An expression for $I_\lambda(L)$ can be obtained by integrating Equation 10.20 between 0 and L , which gives

$$\ln \frac{I_\lambda(L)}{I_{\lambda,0}} = -K_\lambda L \quad \text{or} \quad I_\lambda(L) = I_{\lambda,0} e^{-K_\lambda L} \quad (10.21)$$

Then

$$\tau_\lambda = \frac{I_\lambda(L)}{I_{\lambda,0}} = e^{-K_\lambda L} \quad (10.22)$$

The extinction coefficient K_λ is a complex property of the medium since it combines the effects of absorption, emission, and scattering by the molecules and particles that make up the medium. Fortunately, for materials such as glass and plastics with known compositions, this coefficient can be determined accurately. Transmission of radiation through such materials is discussed further in [Chapter 12](#). In this chapter, we are concerned about the transmission of solar radiation through the atmosphere. The atmosphere consists of the molecules of gases in it, such as N_2 , O_2 , CO_2 , H_2O , etc., and aerosols such as dust particles, water droplets, and ice crystals. The extinction processes of the atmosphere consist of (a) absorption and

emission by the molecules and aerosols, (b) scattering by the molecules, and (c) scattering by aerosols. Estimates of atmospheric transmittance can be made using an empirical approach [5] to develop an average extinction coefficient for use in Equation 10.22. More details on the transmission of solar energy through the atmosphere are covered in Section 10.5.1.

10.3 Sun–Earth Geometric Relationship

Figure 10.6 shows the annual orbit of the Earth around the sun. The distance between the Earth and the sun changes throughout the year, the minimum being 1.471×10^{11} m at

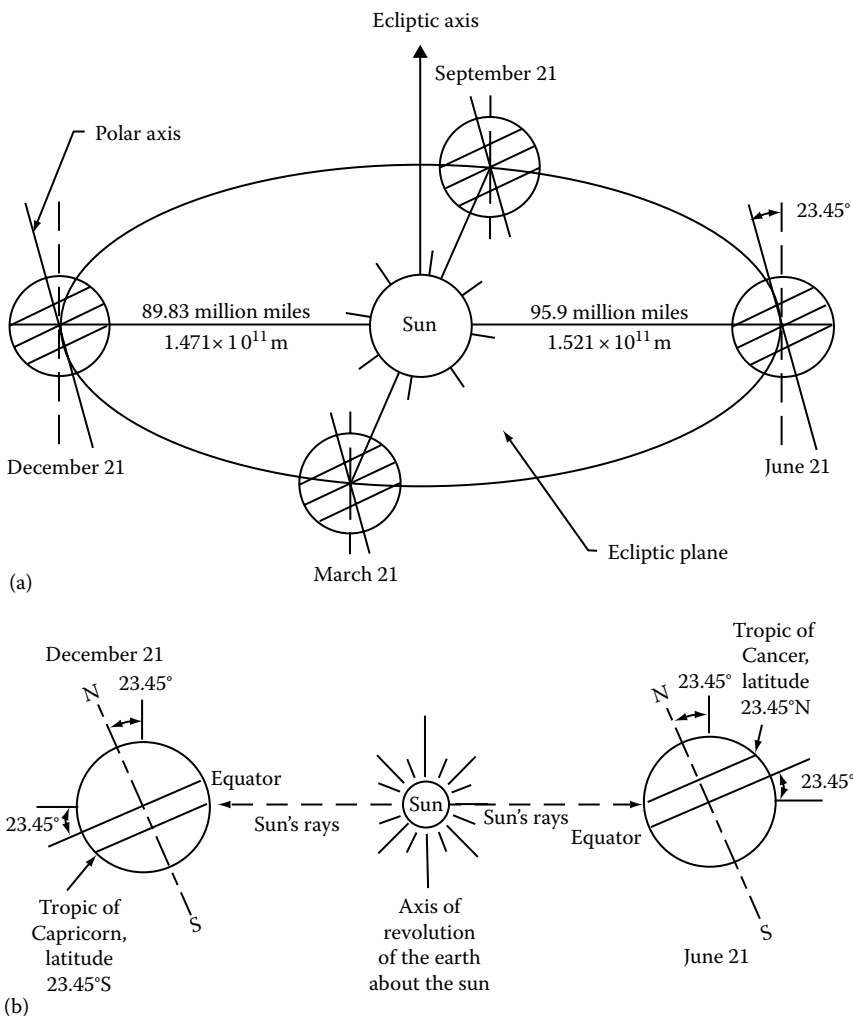


FIGURE 10.6

(a) Motion of the Earth about the sun. (b) Location of tropics. Note that the sun is so far from the Earth that all the rays of the sun may usually be considered as parallel to one another when they reach the Earth (but there are exceptions, as in the case of concentrating optics).

winter solstice (December 21) and the maximum being 1.521×10^{11} m at summer solstice (June 21). The year-round average Earth–sun distance is 1.496×10^{11} m. The amount of solar radiation intercepted by the Earth, therefore, varies throughout the year, the maximum being on December 21 and the minimum on June 21.

The axis of the Earth's daily rotation around itself is at an angle of 23.45° to the axis of its ecliptic orbital plane around the sun. This tilt is the major cause of the seasonal variation of the solar radiation available at any location on the Earth. The angle between the Earth–sun line (through their centers) and the plane through the equator is called the *solar declination*, δ_s . The declination varies between -23.45° on December 21 to $+23.45^\circ$ on June 21. Stated another way, the declination has the same numerical value as the latitude at which the sun is directly overhead at solar noon on a given day. The tropics of Cancer (23.45°N) and Capricorn (23.45°S) are at the extreme latitudes where the sun is overhead at least once a year, as shown in Figure 10.6. The Arctic and Antarctic circles are defined as those latitudes above which the sun does not rise above the horizon plane at least once per year. They are located, respectively, at $66\frac{1}{2}^\circ\text{N}$ and $66\frac{1}{2}^\circ\text{S}$. Declinations north of the equator (summer in the northern hemisphere) are positive; those south, negative. The solar declination may be estimated by the following relation*:

$$\delta_s = 23.45^\circ \sin \left[\frac{360(284 + n)}{365} \right] \quad (10.23)$$

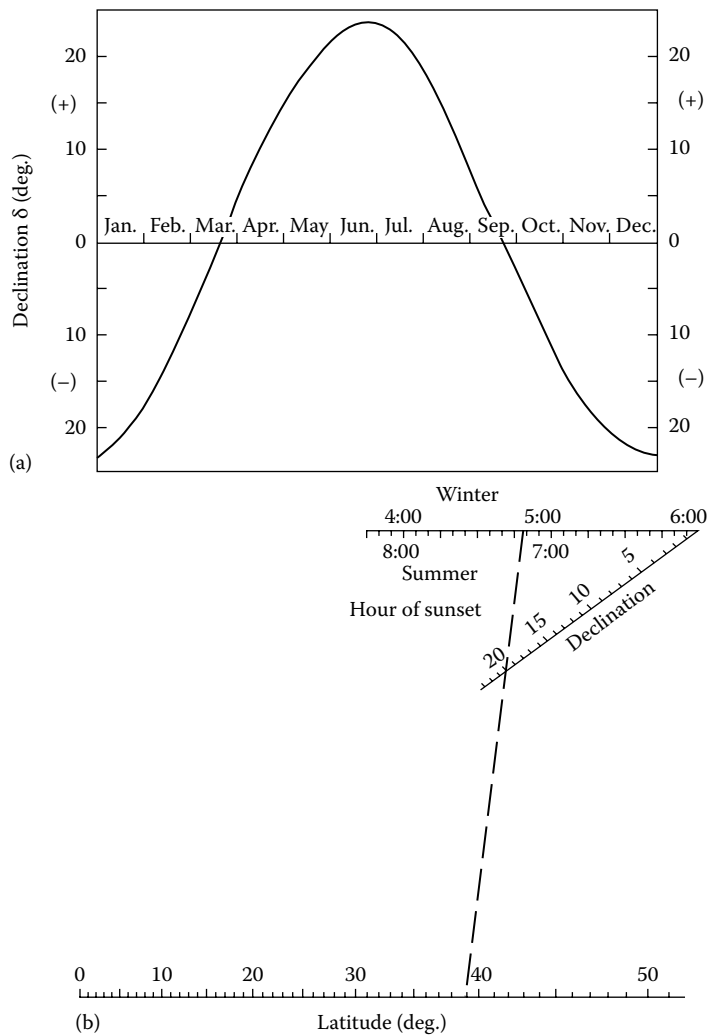
where n is the day number during a year with January 1 being $n = 1$. Approximate values of declination may also be obtained from Figure 10.7. For most calculations, the declination may be considered constant during any given day. A summary table of solar ephemeris can be found in Table W.10.1 on the website for the book, <http://www.crcpress.com/product/isbn/9781498788922>.

For the purposes of this book, the Ptolemaic view of the sun's motion provides a simplification to the analysis that follows. It is convenient to assume the Earth to be fixed and to describe the sun's apparent motion in a coordinate system fixed to the Earth with its origin at the site of interest. Figure 10.8 shows an apparent path of the sun to an observer. The position of the sun can be described at any time by two angles, the altitude and azimuth angles, as shown in Figure 10.8. The *solar altitude angle*, α , is the angle between a line collinear with the sun's rays and the horizontal plane. The *solar azimuth angle*, a_s , is the angle between a due south line and the projection of the site to sun line on the horizontal plane. The sign convention used for azimuth angle is positive west of south and negative east of south. The *solar zenith angle*, z , is the angle between the site to sun line and the vertical at the site:

$$z = 90^\circ - \alpha \quad (10.24)$$

The solar altitude and azimuth angles are not fundamental angles. Hence, they must be related to the fundamental angular quantities *hour angle*, *latitude*, and *declination*. The three angles are shown in Figure 10.9 [6]. The solar hour angle h_s is based on the nominal time of 24 h required for the sun to move 360° around the Earth or 15° per hour. Therefore, h_s , in degrees, can be expressed as a function of the hours or minutes, respectively, from solar noon as follows:

* A more accurate relation is $\sin \delta_s = \sin(23.45^\circ) \sin[360(284 + n)/365]^\circ$. Because the error is small, Equation 10.23 is generally used.

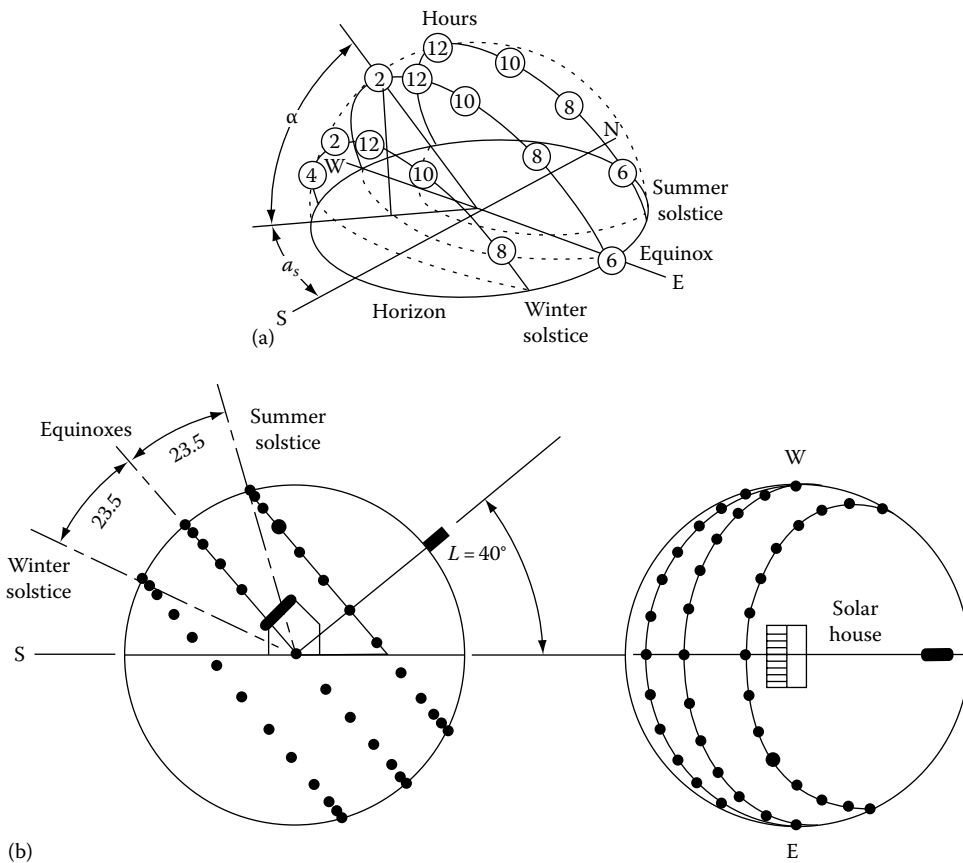
**FIGURE 10.7**

(a) Graph to determine the solar declination. (b) Sunset nomograph example. Example (b) shows determination of sunset time for summer (7:08 p.m.) and winter (4:52 p.m.) when the latitude is 39°N and the solar declination angle is 20°.

$$\begin{aligned}
 h_s &= \frac{15^\circ}{\text{hour}} \times \text{hours from local solar noon} \\
 &= \frac{\text{Minutes from local solar noon}}{4 \text{ min/degree}}
 \end{aligned}
 \tag{10.25}$$

Again, values when the sun is east of due south, that is, morning values, are negative, and values west of due south are positive.

The latitude angle L is the angle between the line from the center of the Earth to the site and the equatorial plane. The latitude may be read from an atlas and is considered positive north of the equator and negative south of the equator.

**FIGURE 10.8**

Sun paths for the summer solstice (6/21), the equinoxes (3/21 and 9/21), and the winter solstice (12/21) for a site at 40°N: (a) isometric view; (b) elevation and plan views.

10.3.1 Solar Time and Angles

The sun angles are obtained from the local solar time, which differs from the local standard time (LST). The relationship between the local solar time and the LST is

$$\text{Solar time} = \text{LST} + \text{ET} + (l_{st} - l_{local}) \cdot 4 \text{ min/degree} \quad (10.26)$$

where

ET is the equation of time, which is a correction factor that accounts for the irregularity of the speed of Earth's motion around the sun

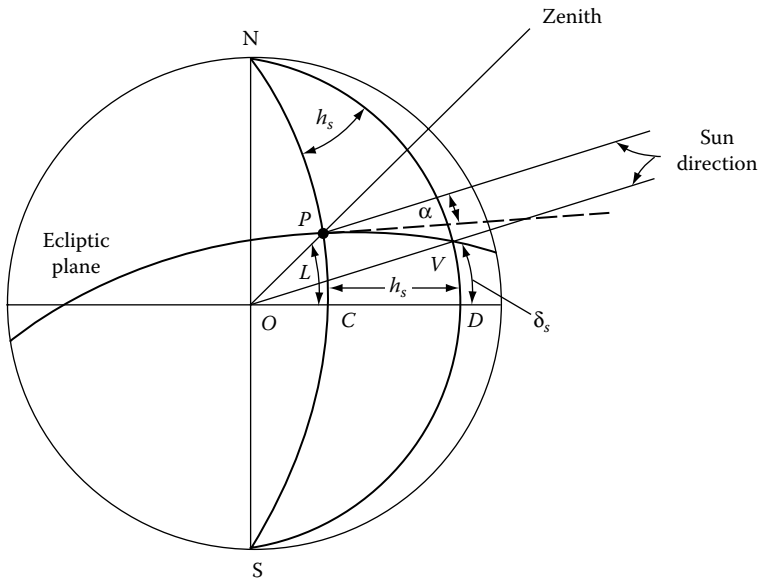
l_{st} is the standard time meridian

l_{local} is the local longitude

ET may be estimated from Table W.10.1 or calculated from the following empirical equation:

$$\text{ET}(\text{min}) = 9.87 \sin 2B - 7.53 \cos B - 1.5 \sin B \quad (10.27)$$

where $B = 360(n - 81)/364^\circ$.

**FIGURE 10.9**

Definition of solar hour angle h_s (CND), solar declination δ_s (VOD), and latitude L (POC); p , site of interest. (Modified from Kreider, J.F. and Kreith, F., 1982. *Solar Heating and Cooling*, Hemisphere Publishing Corp., Washington, DC. [6])

The solar altitude angle, α , can be found from the application of the law of cosines to the geometry of Figure 10.9 and can be simplified as

$$\sin \alpha = \sin L \sin \delta_s + \cos L \cos \delta_s \cos h_s \quad (10.28)$$

Using a similar technique, the solar azimuth angle, a_s , can be found as

$$\sin a_s = \frac{\cos \delta_s \sin h_s}{\cos \alpha} \quad (10.29)$$

where

α is the altitude of the sun (angular elevation above the horizon)

L is the latitude of the observer

δ_s is the declination of the sun

h_s is the hour angle of sun (angular distance from the meridian of the observer)

a_s is the azimuth of the sun (measured eastward from north)

At local solar noon, $h_s = 0$; therefore, $\alpha = 90 - |L - \delta_s|$, and $a_s = 0$.

In calculating the solar azimuth angle from Equation 10.29, a problem occurs whenever the absolute value of a_s is greater than 90° . A computational device usually calculates the angle as less than 90° since $\sin a_s = \sin(180 - a_s)$. The problem can be solved in the following way:

For $L > \delta_s$, the solar times when the sun is due east (t_E) or due west (t_W) can be calculated by t_E or $t_W = 12:00 \text{ Noon} \pm \cos^{-1}[\tan \delta_s / \tan L]^\circ (15^\circ/\text{h})$ (–for t_E , + for t_W).

For solar times earlier than t_E or later than t_W , the sun would be north (south in the southern hemisphere) of the east–west line and the absolute value of a_s would be greater than 90° . Then, a_s may be calculated as $a_s = \pm(180^\circ - |a_s|)$.

For $L \leq \delta_s$, the sun remains north (south in the southern hemisphere) of the east–west line and the true value of a_s is greater than 90° .

Sunrise and *sunset* times can be estimated by finding the hour angle for $\alpha = 0$. Substituting $\alpha = 0$ in Equation 10.28 gives the hour angles for sunrise (h_{sr}) and sunset (h_{ss}) as

$$h_{ss} \text{ or } h_{sr} = \pm \cos^{-1}[-\tan L \cdot \tan \delta_s] \quad (10.30)$$

It should be emphasized that Equation 10.30 is based on the center of the sun at the horizon. In practice, sunrise and sunset are defined as the times when the upper limb of the sun is on the horizon. Because the radius of the sun is $16'$, the sunrise would occur when $\alpha = -16'$. Also, at lower solar elevations, the sun will appear on the horizon when it is actually $34'$ below the horizon. Therefore, for apparent sunrise or sunset, $\alpha = -50'$.

EXAMPLE 10.1

Find the solar altitude and azimuth angles at solar noon in Gainesville, Florida, on February 1. Also find the sunrise and sunset times in Gainesville on that day.

Solution

For Gainesville,

$$\text{Latitude } L = 29^\circ + 41' \text{N or } 29.7^\circ \text{N}$$

$$\text{Longitude } l_{\text{local}} = 82^\circ + 16' \text{W or } 82.3^\circ \text{W}$$

On February 1, day number, $n = 32$. Therefore, from Equation 10.23, the declination is

$$\delta_s = 23.45 \sin \left[\frac{360(284 + 32)}{365} \right] = -17.5^\circ$$

At solar noon, $h_s = 0$. Therefore,

$$\begin{aligned} \sin \alpha &= \cos L \cos \delta_s \cosh_s \sin \alpha = \cos L \cos \delta_s \cosh_s + \sin L \sin \delta_s \\ &= \cos(29.7^\circ) \cos(-17.5^\circ) \cos(0) + \sin(29.7^\circ) \sin(-17.5^\circ) \end{aligned}$$

or $\alpha = 42.8^\circ$

$$\sin a_s = \frac{\cos(-17.5^\circ) \sin(0)}{\cos(42.8^\circ)} = 0$$

or $a_s = 0$

At solar noon, α can also be found as

$$\begin{aligned} \alpha &= 90 - |L - \delta_s|^\circ \\ &= 90 - |29.7 + 17.5| = 42.8^\circ \end{aligned}$$

$$\begin{aligned}
 h_{ss} \text{ or } h_{sr} &= \pm \cos^{-1} [-\tan L \cdot \tan \delta_s] \\
 &= \pm \cos^{-1} [-\tan(29.7^\circ) \cdot \tan(17.5^\circ)] = \pm 79.65
 \end{aligned}$$

$$\begin{aligned}
 \text{Time from solar noon} &= \pm(79.65^\circ)(4 \text{ min/degree}) \\
 &= \pm 319 \text{ min or } \pm (5 \text{ h } 19 \text{ min}) \\
 \text{Sunrise time} &= 12:00 \text{ noon} - (5 \text{ h } 19 \text{ min}) \\
 &= 6 \text{ h } 41 \text{ min a.m. (solar time)} \\
 \text{Sunset time} &= 12:00 \text{ noon} + (5 \text{ h } 19 \text{ min}) \\
 &= 5 \text{ h } 19 \text{ min p.m. (solar time)}
 \end{aligned}$$

To convert these times to local times, we need to find ET:

$$\begin{aligned}
 \text{ET} &= (9.87 \sin 2B - 7.53 \cos B - 1.5 \sin B) \text{ min} \\
 B &= \frac{360}{364}(n - 81) = \frac{360}{364}(32 - 81) = -48.46^\circ
 \end{aligned}$$

Therefore,

$$\begin{aligned}
 \text{ET} &= -13.67 \text{ min} \\
 \text{LST} &= \text{solar time} - \text{ET} - 4(l_{st} - l_{local})
 \end{aligned}$$

Gainesville, Florida, is in the eastern standard time (EST) zone, where $l_{st} = 75^\circ\text{W}$. Therefore,

$$\begin{aligned}
 \text{LST} &= \text{Solar time} - (-13.67 \text{ min}) - 4(75 - 82.27) \text{ min} \\
 &= \text{Solar time} + 42.75 \text{ min}
 \end{aligned}$$

Therefore,

$$\text{Sunrise time} = 6:41 \text{ a.m.} + 43 \text{ min} = 7:24 \text{ a.m. EST,}$$

and

$$\text{Sunrise time} = 5:19 \text{ p.m.} + 43 \text{ min} = 6:02 \text{ p.m. EST.}$$

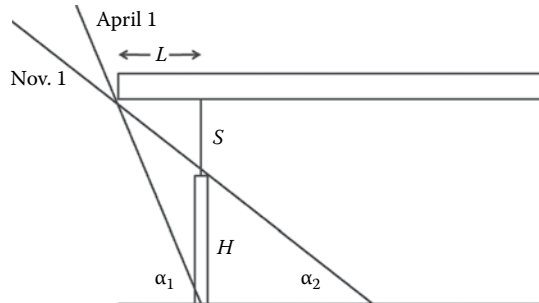
NOTE: Since the sunrise and sunset times are calculated when the center of the sun is at the horizon, they differ from the apparent times. If we use $\alpha = -50'$, the apparent sunrise and sunset times would be 7:20 a.m. EST and 6:06 p.m. EST, respectively.

Knowledge of the solar angles is helpful in the design of passive solar buildings, especially the placement of windows for solar access and the roof overhang for shading the walls and windows at certain times of the year. The following example illustrates this point.

EXAMPLE 10.2

Find the roof overhang L of a south-facing window of height $H = 1 \text{ m}$, such that the window is completely shaded at solar noon on April 1 and not shaded at all at noon

on November 1. Assume that the roof extends far beyond the window on either side. Location: Gainesville, Florida. Also find the overhang if $S = 1.3$ m.



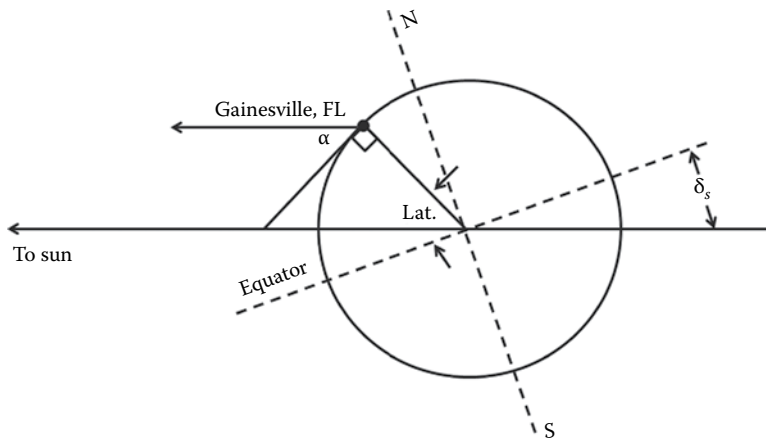
Solution

From the geometry of the figure, we can derive the following two equations with four unknowns, L , S , α_1 , and α_2 :

$$L = \frac{S}{\tan \alpha_2}$$

$$L = \frac{(S + H)}{\tan \alpha_1}$$

From the following figure, it can be determined that $\alpha + |\text{Lat.} - \delta_s| = 90^\circ$ from simple geometry. Therefore, α_1 and α_2 are dependent on the seasonal declination angle δ_s and the latitude of Gainesville, Florida, which is 29.68° from Example 10.1.



To find the declination angle δ_s on April 1, $n = 91$, we use Equation 10.23:

$$n = 91.$$

$$\delta_s = 23.45^\circ \sin \left[\frac{360(284 + 91)}{365} \right] = 4.02^\circ$$

Therefore, at solar noon,

$$\alpha_1 = 90 - |29.68 - 4.02| = 64.34^\circ$$

On November 1, $n = 305$ and

$$\delta_s = 23.45^\circ \sin \left[\frac{360(284 + 305)}{365} \right]^\circ = -15.4^\circ$$

Therefore,

$$\alpha_2 = 90 - |29.68 + 15.4| = 44.9^\circ$$

$$L = \frac{H}{\tan \alpha_1 - \tan \alpha_2} = \frac{1}{\tan(64.34^\circ) - \tan(44.9^\circ)} = 0.92 \text{ m}$$

$$S = L \tan \alpha_2 = 0.92 \times \tan(44.9^\circ) = 0.92 \text{ m}$$

If $S = 1.3 \text{ m}$, then

$$L = \frac{1.3}{\tan 44.9^\circ} = 1.3 \text{ m}$$

Also

$$L = \frac{2.3}{\tan 64.34^\circ} = 1.1 \text{ m}$$

Therefore, $1.1 \text{ m} \leq L \leq 1.3 \text{ m}$.

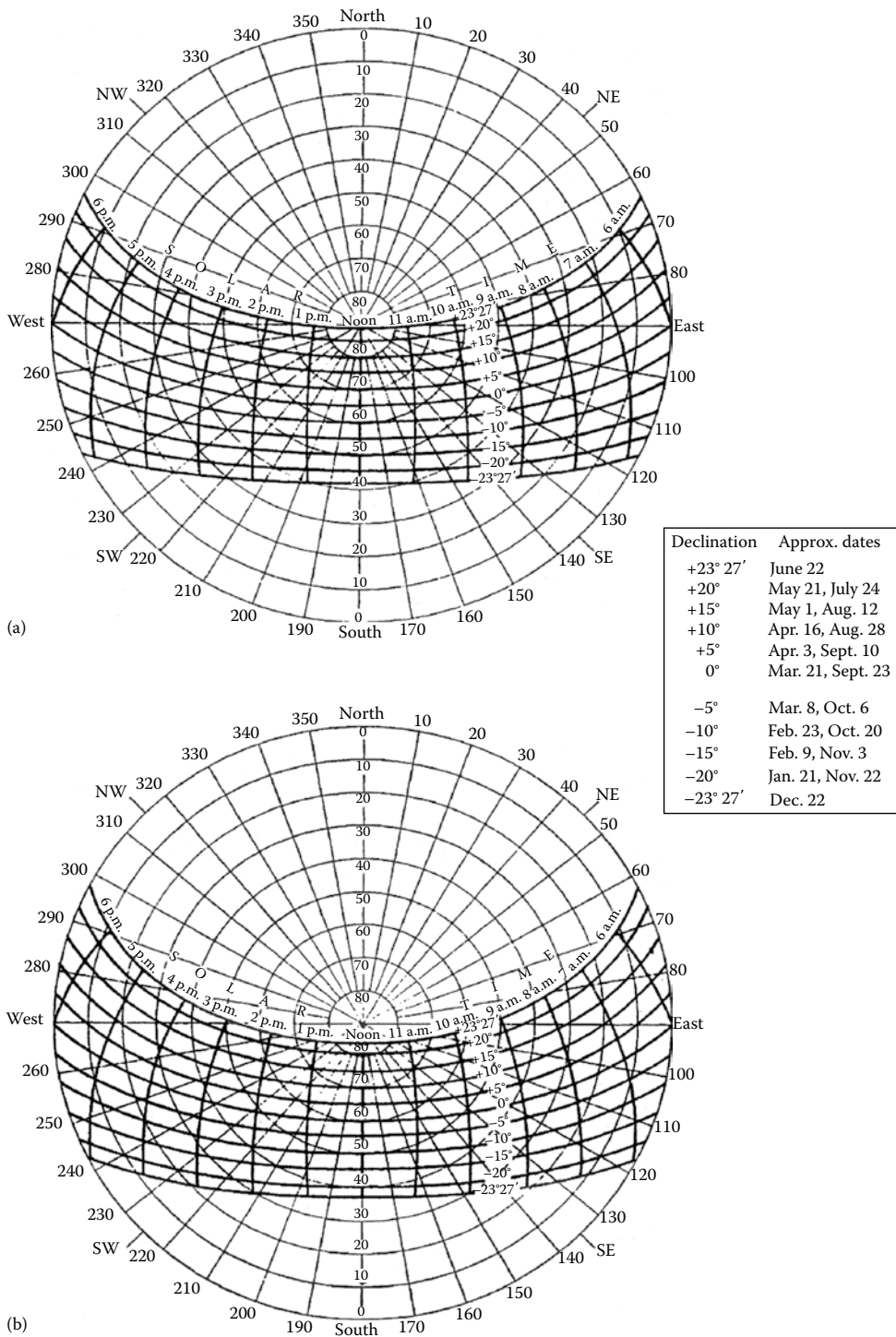
10.3.2 Sun-Path Diagram

The projection of the sun's path on the horizontal plane is called a *sun-path diagram*. Such diagrams are very useful in determining shading phenomena associated with solar collectors, windows, and shading devices. As shown earlier, the solar angles (α , a_s) depend upon the hour angle, declination, and latitude. Since only two of these variables can be plotted on a two-dimensional graph, the usual method is to prepare a different sun-path diagram for each latitude with variations of hour angle and declination shown for a full year. Sun-path diagrams for different latitudes are shown in [Figure 10.10](#) [7].

From Equations 10.28 and 10.29, it can be seen that the altitude and azimuth of the sun are functions of the latitude of the observer, the time of day (hour angle), and the date (declination).

[Figure 10.10a](#) through [f](#) provides a series of charts, one for each 5° of latitude (except 5° , 15° , 75° , and 85°) giving the altitude and azimuth of the sun as a function of the true solar time and the declination of the sun in a form originally suggested by Hand. Linear interpolation for intermediate latitudes will give results within the accuracy to which the charts can be read.

On these charts, a point corresponding to the projected position of the sun is determined from the heavy lines corresponding to declination and solar time.

**FIGURE 10.10**

Description of method for calculating true solar time, together with accompanying meteorological charts, for computing solar altitude and azimuth angles. (a) chart, 25°N latitude; (b) chart, 30°N latitude. (Continued)

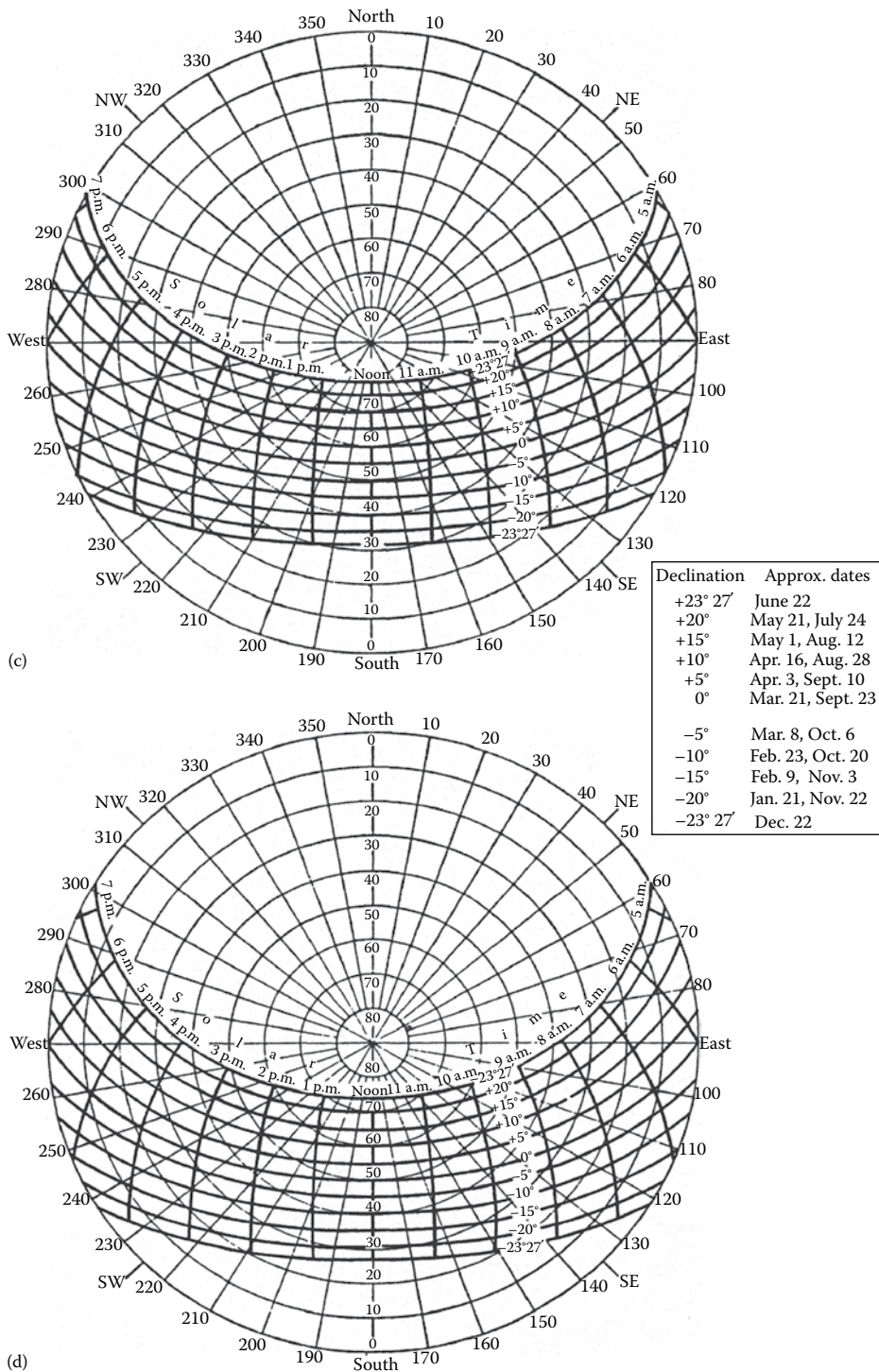
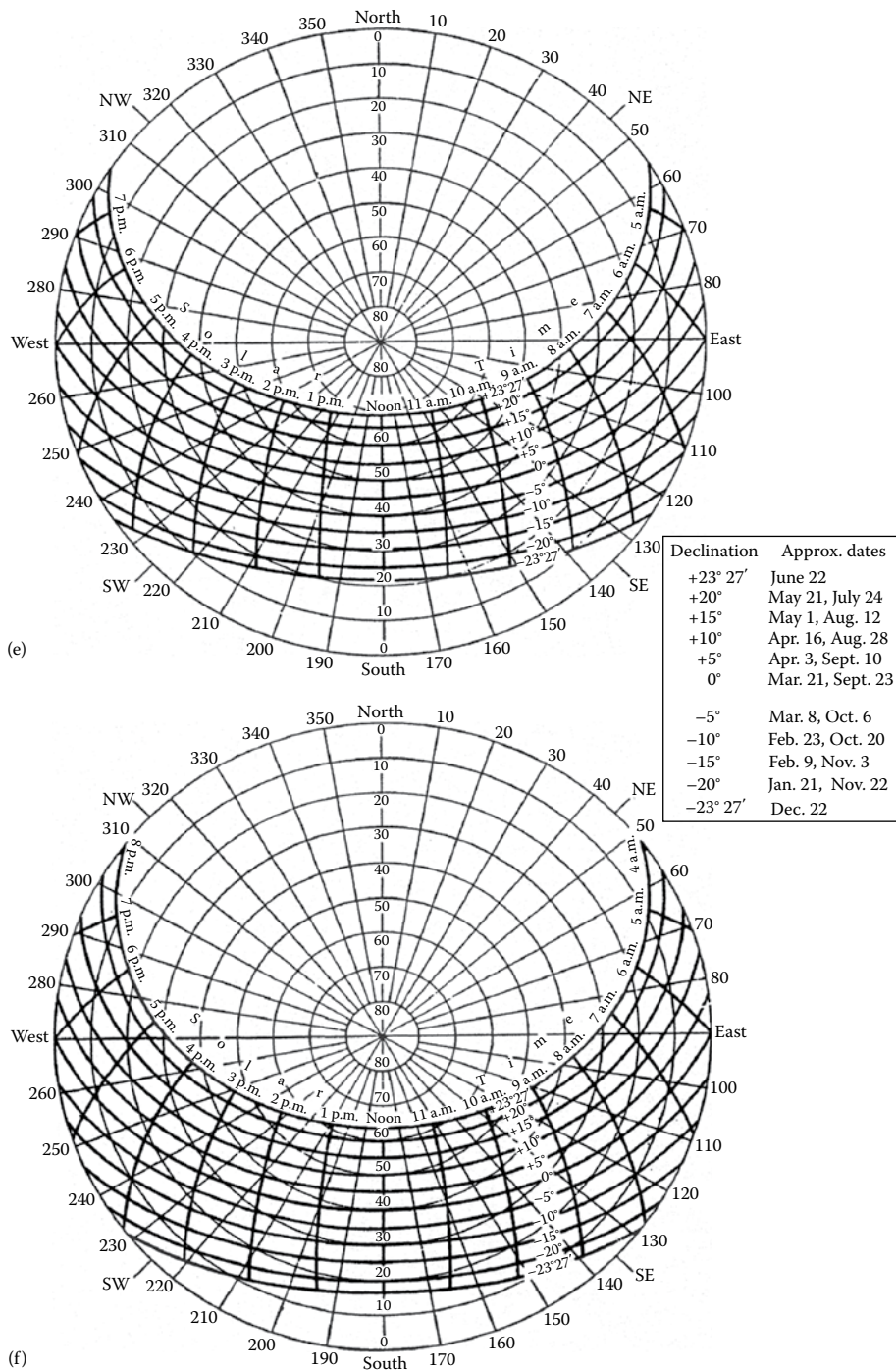


FIGURE 10.10 (Continued)

Description of method for calculating true solar time, together with accompanying meteorological charts, for computing solar altitude and azimuth angles. (c) chart, 35°N latitude; (d) chart, 40°N latitude. (Continued)

**FIGURE 10.10 (Continued)**

Description of method for calculating true solar time, together with accompanying meteorological charts, for computing solar altitude and azimuth angles. (e) chart, 45°N latitude; (f) chart, 50°N latitude. (Reproduced from List, R.J., 1949. *Smithsonian Meteorological Tables*, 6th ed., Smithsonian Institution Press, Washington, DC, pp. 442–443. [7])

To find the solar altitude and azimuth

1. Select the chart or charts appropriate to the latitude.
2. Find the solar declination δ corresponding to the date.
3. Determine the *true solar time* as follows:
 - a. To the *LST* (zone time), add 4° for each degree of longitude the station is east of the standard meridian or subtract 4° for each degree west of the standard meridian to get the *local mean solar time*.
 - b. To the *local mean solar time*, add algebraically the equation of time; the sum is the required *true solar time*.
4. Read the required altitude and azimuth at the point determined by the declination and the true solar time. Interpolate linearly between two charts for intermediate latitudes.

It should be emphasized that the solar altitude determined from these charts is the true geometric position of the center of the sun. At low solar elevations, terrestrial refraction may considerably alter the apparent position of the sun. Under average atmospheric refraction, the sun will appear on the horizon when it actually is about 34° below the horizon; the effect of refraction decreases rapidly with increasing solar elevation. Since sunset or sunrise is defined as the time when the upper limb of the sun appears on the horizon, and the semidiameter of the sun is $16'$, sunset or sunrise occurs under average atmospheric refraction when the sun is $50'$ below the horizon. In polar regions especially, unusual atmospheric refraction can make considerable variation in the time of sunset or sunrise.

The 90°N chart is included for interpolation purposes; the azimuths lose their directional significance at the pole.

Altitude and azimuth in southern latitudes: To compute solar altitude and azimuth for southern latitudes, change the sign of the solar declination and proceed as earlier. The resulting azimuths will indicate angular distance from *south* (measured eastward) rather than from north.

Sun-path diagrams for a given latitude are used by entering them with appropriate values of declination δ_s and hour angle h_s . The point at the intersection of the corresponding δ_s and h_s lines represents the instantaneous location of the sun. The solar altitude can then be read from the concentric circles in the diagram, and the azimuth, from the scale around the circumference of the diagram. Sun path diagrams can be found on the internet [8].

EXAMPLE 10.3

Using Figure 10.10b, determine the solar altitude and azimuth for March 8 at 10 a.m. for a site at 30°N . Compare the results to those calculated from the basic equations (Equations 10.28 and 10.29).

Solution

On March 8, the solar declination is -5° ; therefore the -5° sun path is used. The intersection of the 10 a.m. line and the -5° declination line in the diagram represents the sun's location.

The sun's position lies midway between the 40° and 50° altitude circles, say at 45° , and midway between the -40° and -50° azimuth radial lines (marked on the chart as 150°

and 140° SE using the convention of measuring angles clockwise from the north as 0°, or approximately -45° . So $\alpha \cong 45^\circ$ and $a_s \cong -45^\circ$. Equations 10.28 and 10.29 give precise values for α and a_s :

$$\begin{aligned}\sin \alpha &= \sin(30^\circ)\sin(-5^\circ) + \cos(30^\circ)\cos(-5^\circ)\cos(-30^\circ) \\ \alpha &= 44.7^\circ\end{aligned}$$

$$\begin{aligned}\sin a_s &= \frac{\cos(-5^\circ)\sin(-30^\circ)}{\cos(44.7^\circ)} \\ a_s &= -44.5^\circ\end{aligned}$$

Therefore, the calculated values are within $\pm 0.5^\circ$ (1%) of those read from the sun-path diagram.

10.3.3 Shadow-Angle Protractor

The shadow-angle protractor used in shading calculations is a plot of solar altitude angles, projected onto a given plane, versus solar azimuth angle. The projected altitude angle is usually called the *profile angle* γ . It is termed as the angle between the normal to a surface and the projection of the sun's rays on a vertical plane normal to the same surface. The profile angle is shown in Figure 10.11a with the corresponding solar altitude angle. The profile angle, which is always used in sizing shading devices, is given by

$$\tan \gamma = \sec a \tan \alpha \quad (10.31)$$

where a is the solar azimuth angle with respect to the wall normal.

Figure 10.11b shows the shadow-angle protractor to the same scale as the sun-path diagrams in Figure 10.10d. It is used by plotting the limiting values of profile angle γ and azimuth angle a , which will start to cause shading of a particular point. The shadow-angle protractor is usually traced onto a transparent sheet so that the shadow map constructed on it can be placed over the pertinent sun-path diagram to indicate the times of day and months of the year during which shading will take place. The use of the shadow-angle protractor is best illustrated by an example.

EXAMPLE 10.4

A solar building with a south-facing collector is sited to the north-northwest of an existing building. Prepare a shadow map showing what months of the year and what part of the day point C at the base of the solar collector will be shaded. Plan and elevation views are shown in Figure 10.12. Latitude = 40°N .

Solution

The limiting profile angle for shading is 40° and the limiting azimuth angles are -45° and $+10^\circ$, as shown in Figure 10.12. These values are plotted on the shadow-angle protractor (Figure 10.13a). The shadow map, when superimposed on the sun-path diagram (Figure 10.13b), shows that point C will be shaded during the following times of day for the periods shown:

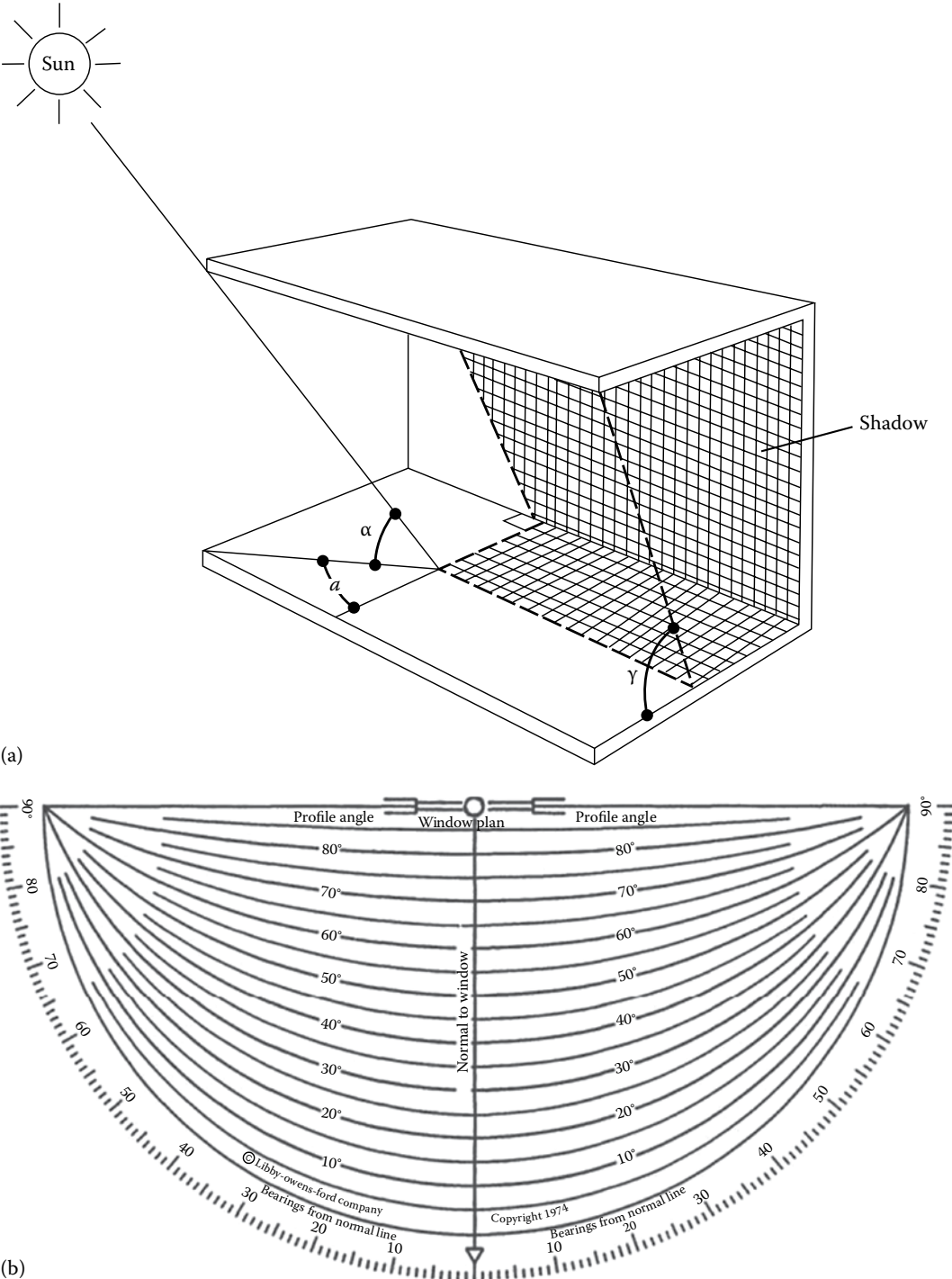
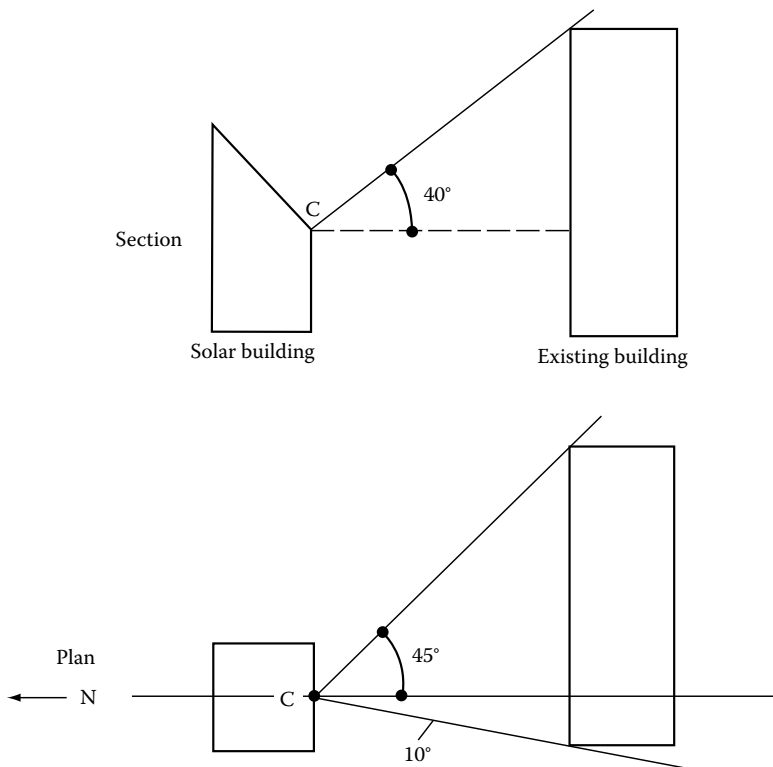


FIGURE 10.11
(a) Sketch showing the profile angle γ and the corresponding solar altitude angle α for a window shading device;
(b) the shadow-angle protractor. (Courtesy of Libby-Owens-Ford Glass Co., Toledo, OH.)

**FIGURE 10.12**

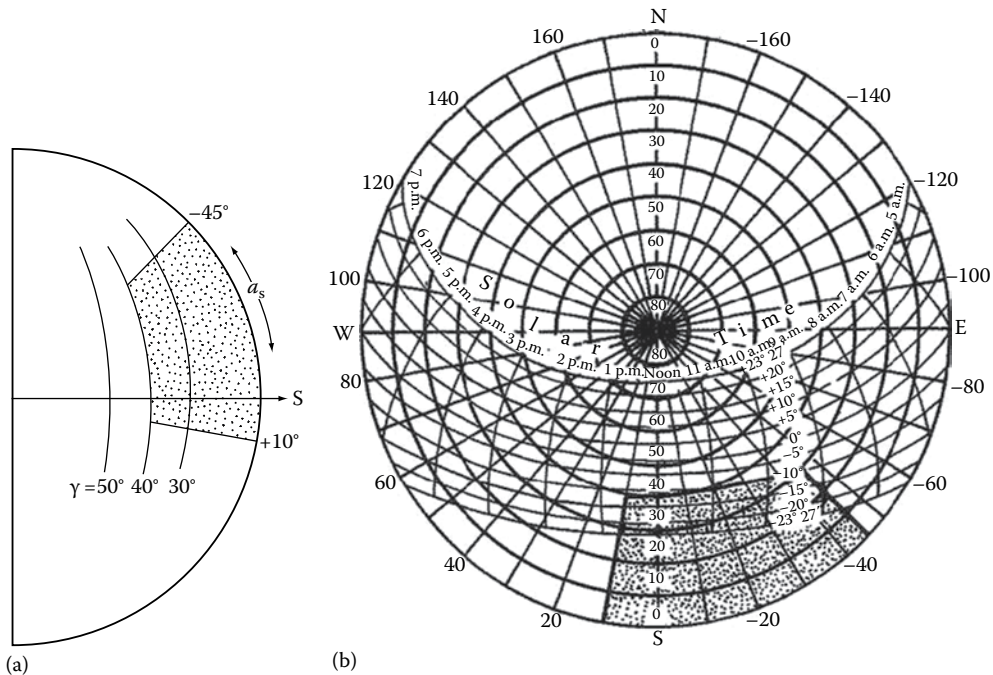
Plan and elevation views of proposed solar building and existing building, which may shade solar collector at point C.

Declination	Date	Time of Day
$-23^{\circ}27'$	December 22	8:45 a.m.–12:40 p.m.
-20°	January 21, November 22	8:55 a.m.–12:35 p.m.
-15°	February 9, November 3	9:10 a.m.–12:30 p.m.

In summary, during the period from November 3 to February 9, point C will be shaded between 3 and 4 h. It will be shown later that this represents about a 50% loss in collector performance for point C, which would be unacceptable for a collector to be used for heating a building in winter.

10.4 Solar Radiation

Detailed information about solar radiation availability at any location is essential for the design and economic evaluation of a solar energy system. Long-term measured data of solar radiation are available for a large number of locations in the United States and other parts of the world. Where long-term measured data are not available, various models based on available climatic data can be used to estimate the solar energy availability. Solar energy

**FIGURE 10.13**

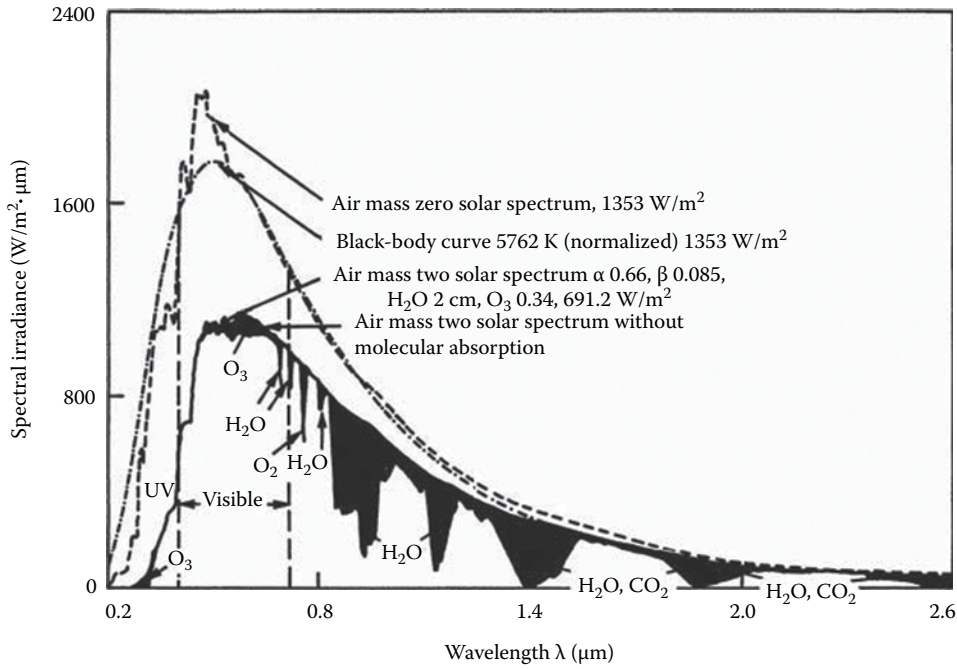
(a) Shadow map constructed for Example 10.4; (b) shadow map superimposed on sun-path diagram. The degrees on the circumference in this version are shown as increasing or decreasing from south.

is in the form of electromagnetic radiation with the wavelengths ranging from about $0.3 \mu\text{m}$ (10^{-6} m) to over $3 \mu\text{m}$, which correspond to ultraviolet (less than $0.4 \mu\text{m}$), visible (0.4 and $0.7 \mu\text{m}$), and infrared (over $0.7 \mu\text{m}$). Most of this energy is concentrated in the visible and the near-infrared wavelength range (see Figure 10.14). The incident solar radiation, sometimes called *insolation*, is measured as irradiance, or the energy per unit time per unit area (or power per unit area). The units most often used are Watts per square meter (W/m^2), British thermal units per hour per square foot ($\text{Btu}/\text{h ft}^2$), and Langley's per minute (calories per square centimeter per minute, $\text{cal}/\text{cm}^2 \text{ min}$).

10.4.1 Extraterrestrial Solar Radiation

The average amount of solar radiation falling on a surface normal to the rays of the sun outside the atmosphere of the Earth (extraterrestrial) at mean Earth–sun distance (D_0) is called the *solar constant*, I_0 . Measurements by NASA indicated the value of the solar constant to be $1353 \text{ W}/\text{m}^2$ ($\pm 1.6\%$), $429 \text{ Btu}/\text{h ft}^2$ or $1.94 \text{ cal}/\text{cm}^2 \text{ min}$ (Langley's/min). This value was revised upward by Frohlich et al. [9] to $1377 \text{ W}/\text{m}^2$ or $437.1 \text{ Btu}/\text{h ft}^2$ or $1.974 \text{ Langley's/min}$, which was the value used in compiling SOLMET data in the United States [10,11]. At present, there is no consensus on the value of the solar constant. However, considering that the difference between the two values is about 1.7% and the uncertainties in estimation of terrestrial solar radiation are 10% or higher, either value may be used. A value of $1367 \text{ W}/\text{m}^2$ is also used by many references.

The variation in seasonal solar radiation availability at the surface of the Earth can be understood from the geometry of the relative movement of the Earth around the sun.

**FIGURE 10.14**

Extraterrestrial solar radiation spectral distribution. Also shown are equivalent black-body and atmosphere-attenuated spectra.

Since the Earth's orbit is elliptical, the Earth–sun distance varies during a year, the variation being $\pm 1.7\%$ from the average. Therefore, the extraterrestrial radiation, I , also varies by the inverse square law as follows:

$$I = I_0 \left(\frac{D_0}{D} \right)^2 \quad (10.32)$$

where

D is the distance between the sun and the Earth

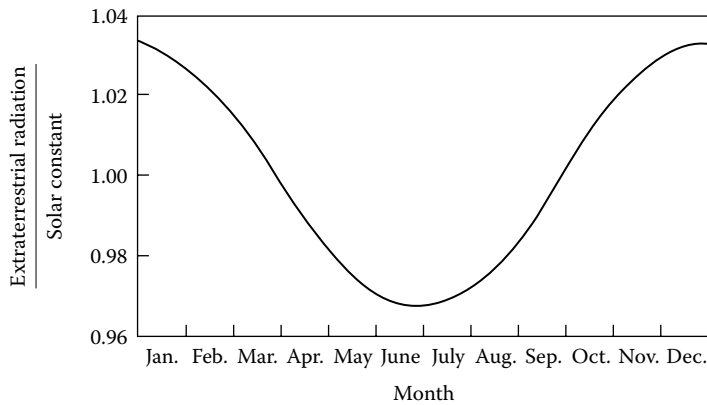
D_0 is the yearly mean Earth–sun distance (1.496×10^{11} m)

The $(D_0/D)^2$ factor may be approximated as [12]

$$\begin{aligned} \left(\frac{D_0}{D} \right)^2 &= 1.00011 + 0.034221 \cos(x) + 0.00128 \sin(x) \\ &\quad + 0.000719 \cos(2x) + 0.000077 \sin(2x) \end{aligned} \quad (10.33)$$

where

$$x = \frac{360(n-1)}{365^\circ} \quad (10.34)$$

**FIGURE 10.15**

Effect of the time of year on the ratio of extraterrestrial radiation to the nominal solar constant.

and n = day number (starting from January 1 as 1). The following approximate relationship may also be used without much loss of accuracy:

$$I = I_0 \left[1 + 0.034 \cos \left(\frac{360n}{365.25} \right)^\circ \right] \quad (10.35)$$

Figure 10.15 also shows the relationship of the extraterrestrial solar radiation to the solar constant. For many solar energy applications, such as photovoltaics and photocatalysis, it is necessary to examine the distribution of energy within the solar spectrum. Figure 10.15 shows the spectral irradiance at the mean Earth–sun distance for a solar constant of 1353 W/m^2 as a function of wavelength according to the standard spectrum data published by NASA in 1971. The data are also presented in Table 10.2 [13,14], and their use is illustrated in the following example.

EXAMPLE 10.5

Calculate the fraction of solar radiation within the visible part of the spectrum, that is, between 0.40 and $0.70 \mu\text{m}$.

Solution

The first column in Table 10.2 gives the wavelength. The second column gives the averaged solar spectral irradiance in a band centered at the wavelength in the first column. The fourth column, $D\lambda$, gives the percentage of solar total radiation at wavelengths shorter than the value of λ in the first column. At a value of $0.40 \mu\text{m}$, 8.7% of the total radiation occurs at shorter wavelengths. At a wavelength of 0.70 , 46.88% of the radiation occurs at shorter wavelength. Consequently, 38% of the total radiation lies within the band between 0.40 and $0.70 \mu\text{m}$, and the total energy received outside the Earth's atmosphere within that spectral range is 517 W/m^2 (163 Btu/h ft^2).

TABLE 10.2
Extraterrestrial Solar Irradiance^a

λ (μm)	E_{λ}^b ($\text{W/m}^2 \cdot \mu\text{m}$)	E_{λ}^b ($\text{Btu/h} \cdot \text{ft}^2 \cdot \mu\text{m}$)	D_{λ}^c (%)	λ (μm)	E_{λ} ($\text{W/m}^2 \cdot \mu\text{m}$)	E_{λ} ($\text{Btu/h} \cdot \text{ft}^2 \cdot \mu\text{m}$)	D_{λ} (%)	λ (μm)	E_{λ} ($\text{W/m}^2 \cdot \mu\text{m}$)	E_{λ} ($\text{Btu/h} \cdot \text{ft}^2 \cdot \mu\text{m}$)	D_{λ} (%)
0.12	0.007	0.002	1×10^{-4}	0.43	1639	520	12.47	0.90	891	283	63.37
0.14	0.03	0.010	5×10^{-4}	0.44	1810	574	13.73	1.00	748	237	69.49
0.16	0.23	0.073	6×10^{-4}	0.45	2006	636	15.14	1.2	485	154	78.40
0.18	1.25	0.397	1.6×10^{-3}	0.46	2066	655	16.65	1.4	337	107	84.33
0.20	10.7	3.39	8.1×10^{-3}	0.47	2033	645	18.17	1.6	245	77.7	88.61
0.22	57.5	18.2	0.05	0.48	2074	658	19.68	1.8	159	50.4	91.59
0.23	66.7	21.2	0.10	0.49	1950	619	21.15	2.0	103	32.7	93.49
0.24	63.0	20.0	0.14	0.50	1942	616	22.60	2.2	79	25.1	94.83
0.25	70.9	22.5	0.19	0.51	1882	597	24.01	2.4	62	19.7	95.86
0.26	130	41.2	0.27	0.52	1833	581	25.38	2.6	48	15.2	96.67
0.27	232	73.6	0.41	0.53	1842	584	26.74	2.8	39	12.4	97.31
0.28	222	70.4	0.56	0.54	1783	566	28.08	3.0	31	9.83	97.83
0.29	482	153	0.81	0.55	1725	547	29.38	3.2	22.6	7.17	98.22
0.30	514	163	1.21	0.56	1695	538	30.65	3.4	16.6	5.27	98.50
0.31	689	219	1.66	0.57	1712	543	31.91	3.6	13.5	4.28	98.72
0.32	830	263	2.22	0.58	1715	544	33.18	3.8	11.1	3.52	98.91
0.33	1059	336	2.93	0.59	1700	539	34.44	4.0	9.5	3.01	99.06
0.34	1074	341	3.72	0.60	1666	528	35.68	4.5	5.9	1.87	99.34
0.35	1093	347	4.52	0.62	1602	508	38.10	5.0	3.8	1.21	99.51
0.36	1068	339	5.32	0.64	1544	490	40.42	6.0	1.8	0.57	99.72
0.37	1181	375	6.15	0.66	1486	471	42.66	7.0	1.0	0.32	99.82
0.38	1120	355	7.00	0.68	1427	453	44.81	8.0	0.59	0.19	99.88
0.39	1098	348	7.82	0.70	1369	434	46.88	10.0	0.24	0.076	99.94
0.41	1751	555	9.92	0.75	1235	392	51.69	20.0	0.0015	0.005	99.99
0.42	1747	554	11.22	0.80	1109	352	56.02	50.0	0.0004	0.0001	100.00

Source: Adapted from Iqbal, M., 1979. *Solar Energy*, 23, 169 [13]; Thekaekara, M.P., 1973. *Solar Energy*, 14, 109–127. [14]

^a Solar constant = 429 Btu/h ft² = 1353 W/m².

^b E_{λ} is the solar spectral irradiance averaged over a small bandwidth centered at λ .

^c D_{λ} is the percentage of the solar radiation associated with wavelengths shorter than λ .

10.5 Estimation of Terrestrial Solar Radiation

As extraterrestrial solar radiation, I , passes through the atmosphere, a part of it is reflected back into space, a part is absorbed by air and water vapor, and some gets scattered by molecules of air, water vapor, aerosols, and dust particles (Figure 10.16). The part of solar radiation that reaches the surface of the Earth with essentially no change in direction is called *direct* or *beam radiation*. The scattered diffuse radiation reaching the surface from the sky is called the *sky diffuse radiation*.

Although extraterrestrial radiation can be predicted with certainty (the effect of sunspots, which may cause up to 0.5% variation, is neglected), radiation levels on the Earth are subject to considerable uncertainty resulting from local climatic interactions. The most useful solar radiation data are based on long-term (30 years or more) measured average values at a location, which unfortunately are not available for most locations in the world. For such locations, an estimation method (theoretical model) based on some measured climatic parameters may be used. This chapter describes several ways of estimating terrestrial solar radiation; all have large uncertainties (as much as $\pm 30\%$) associated with them.

10.5.1 Atmospheric Extinction of Solar Radiation

As solar radiation I travels through the atmosphere, it is attenuated due to absorption and scattering. If K is the local extinction coefficient of the atmosphere, the beam solar radiation at the surface of the Earth can be written according to Beer's law, Equation 10.21 as

$$I_{b,N} = Ie^{-\int K dx} \quad (10.36)$$

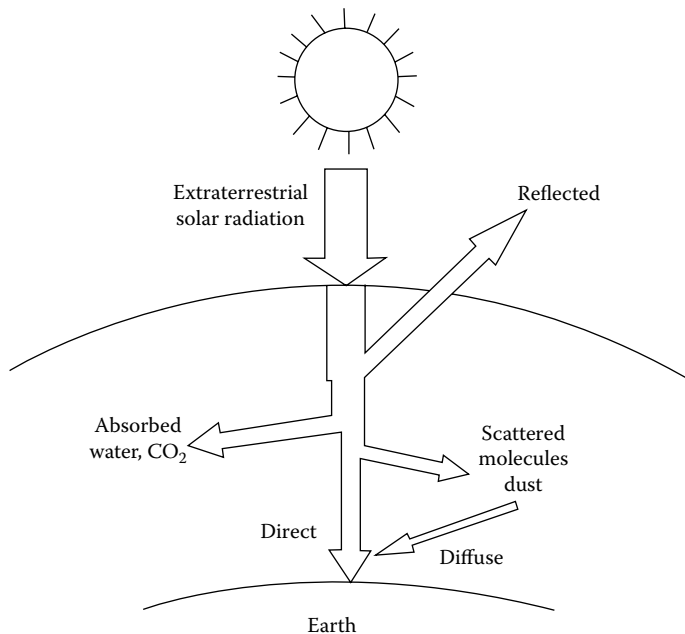


FIGURE 10.16

Attenuation of solar radiation as it passes through the atmosphere.

where

$I_{b,N}$ is the instantaneous beam solar radiation per unit area normal to the sun's rays
 x is the length of travel through the atmosphere

If L_o is the vertical thickness of the atmosphere and

$$\int_0^{L_o} K dx = k \quad (10.37)$$

the beam normal solar radiation for a solar zenith angle of z will be

$$I_{b,N} = Ie^{-k \sec z} = Ie^{-k/\sin \alpha} = Ie^{-km} \quad (10.38)$$

where m is a dimensionless path length of sunlight through the atmosphere, sometimes called the *air mass ratio* (Figure 10.17). When solar altitude angle is 90° (sun is overhead), $m = 1$.

Threlkeld and Jordan [5] estimated values of k (also known as optical depth) for average atmospheric conditions at sea level with a moderately dusty atmosphere and the amount of precipitable water vapor equal to the average value for the United States for each month. These values are given in Table 10.3 [5,15].

To account for the differences in local conditions from the average sea-level conditions, Equation 10.39 is modified by a parameter called clearness number C_n , introduced by Threlkeld and Jordan [5]:

$$I_{b,N} = C_n Ie^{-k/\sin \alpha} \quad (10.39)$$

Note that $C_n = 1$ in clear-sky conditions.

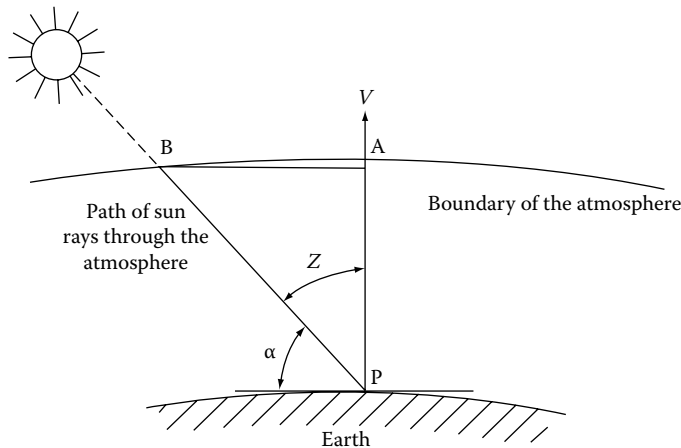


FIGURE 10.17

Air mass definition: air mass $m = BP/AP = \sec \alpha$, where α is the altitude angle. The atmosphere is idealized as a constant thickness layer.

TABLE 10.3

Average Values of Atmospheric Optical Depth (k) and Sky Diffuse Factor (C) for 21st Day of Each Month, for Average Atmospheric Conditions at Sea Level for the United States

Month	1	2	3	4	5	6	7	8	9	10	11	12
k	0.142	0.144	0.156	0.180	0.196	0.205	0.207	0.201	0.177	0.160	0.149	0.142
C	0.058	0.060	0.071	0.097	0.121	0.134	0.136	0.122	0.092	0.073	0.063	0.057

Source: Threlkeld, J.L. and Jordan, R.C., 1958. *Transactions of ASHRAE*, 64, 45. [5]; Islam, M.R., 1994. *RERIC International Energy Journal*, 16(2), 103–113. [15]

10.5.2 Solar Radiation on Clear Days

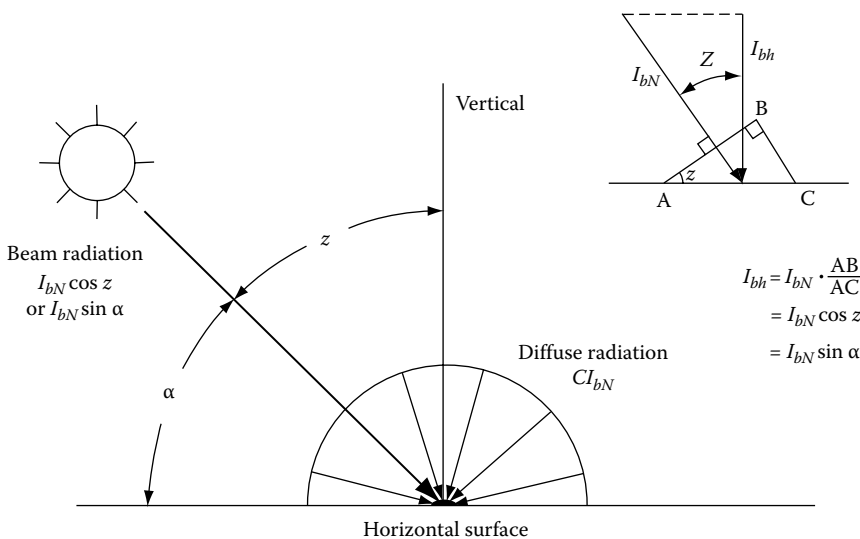
Total instantaneous solar radiation on a horizontal surface (see Figure 10.18), I_h , is the sum of the beam or direct radiation, $I_{b,h}$, and the sky diffuse radiation $I_{d,h}$:

$$I_h = I_{b,h} + I_{d,h} \quad (10.40)$$

According to the Threlkeld and Jordan model [5], the sky diffuse radiation on a clear day is proportional to the beam normal solar radiation and can be estimated by using an empirical sky diffuse factor C . Therefore, I_h can be estimated as

$$\begin{aligned} I_h &= I_{b,N} \cos z + CI_{b,N} \\ &= I_{b,N} \sin \alpha + CI_{b,N} \\ &= C_n I_e^{-k/\sin \alpha} (C + \sin \alpha) \end{aligned} \quad (10.41)$$

Values of C are given in Table 10.3.

**FIGURE 10.18**

Solar radiation on a horizontal surface.

10.5.3 Solar Radiation on a Tilted Surface

Solar radiation on an arbitrary tilted surface having a tilt angle of β from the horizontal and an azimuth angle of a_w (assumed + west of south), as shown in [Figure 10.19](#), is the sum of components consisting of beam ($I_{b,c}$), sky diffuse ($I_{d,c}$), and ground-reflected solar radiation ($I_{r,c}$):

$$I_c = I_{b,c} + I_{d,c} + I_{r,c} \quad (10.42)$$

If i is the *angle of incidence* of the beam radiation on the tilted surface, it is simple to show that the instantaneous beam radiation on the surface per unit area is

$$I_{b,c} = I_{b,N} \cos i \quad (10.43)$$

From the geometry in [Figure 10.19](#), it can be shown that the angle of incidence i for the surface (angle between the normal to the surface and a line collinear with the sun's rays) is related to the solar angles as

$$\cos i = \cos \alpha \cos(a_s - a_w) \sin \beta + \sin \alpha \cos \beta \quad (10.44)$$

The diffuse radiation on the surface ($I_{d,c}$) can be obtained by multiplying the sky diffuse radiation on a horizontal surface by the view factor between the sky and the surface*:

$$\begin{aligned} I_{d,c} &= I_{d,h} \frac{(1 + \cos \beta)}{2} \\ &= C I_{b,N} \frac{(1 + \cos \beta)}{2} \\ &= C I_{b,N} \cos^2 \left(\frac{\beta}{2} \right) \end{aligned} \quad (10.45)$$

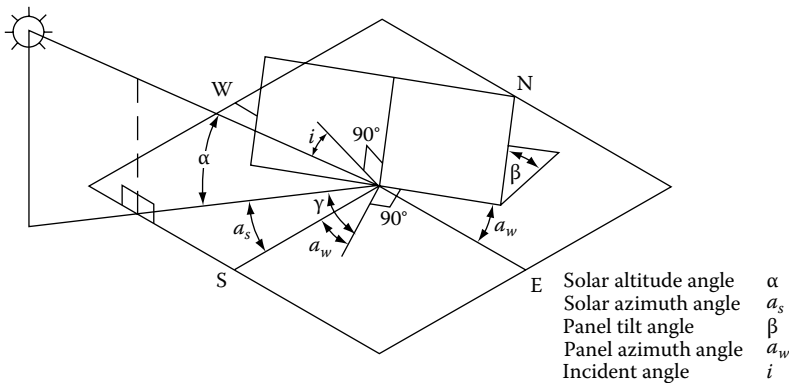


FIGURE 10.19

Definitions of solar angles for a tilted surface. *Note:* α , solar altitude angle; a_s , solar azimuth angle; β , panel tilt angle; a_w , panel azimuth angle; i , incident angle.

* The surface has been assumed infinitely large for this view factor. See Section 10.2.3.

The ground-reflected solar radiation can be found from the total solar radiation incident on a horizontal surface and the ground reflectance ρ as

$$I_{r,c} = I_h \rho \quad (10.46)$$

The part of $I_{r,c}$ intercepted by the tilted surface can be found by multiplying the ground-reflected radiation by the view factor between the surface* and the ground:

$$\begin{aligned} I_{r,c} &= \rho I_h \frac{(1 - \cos \beta)}{2} = \rho I_h \sin^2 \left(\frac{\beta}{2} \right) \\ &= \rho I_{b,N} (\sin \alpha + C) \sin^2 \left(\frac{\beta}{2} \right) \end{aligned} \quad (10.47)$$

For ordinary ground or grass, ρ is approximately 0.2, and for snow-covered ground, it can be taken as approximately 0.8.

EXAMPLE 10.6

Find the instantaneous solar radiation at 12:00 noon EST on a solar collector surface ($\beta = 30^\circ$, $a_w = +10^\circ$) on February 1 in Gainesville, Florida.

Solution

From Example 10.1, for February 1

$$n = 32, \quad \delta_s = -17.5^\circ, \text{ and } ET = -13.7 \text{ min}$$

For finding the values of solar radiation on the collector, we will need to calculate angles α , a_s , h_s , and i .

$$\begin{aligned} \text{Solar time} &= \text{LST} + ET + 4(I_{st} - I_{local}) \\ &= 12:00 - 13.7 \text{ min} + 4(75^\circ - 82.27^\circ) \\ &= 11:17.2 \text{ a.m.}, \\ h_s &= \frac{\text{Minutes from solar noon}}{4 \text{ min/degree}} \\ &= \frac{-42.8}{4} = -10.7^\circ \text{ (before noon)} \end{aligned}$$

From Equation 10.28,

$$\alpha = \sin^{-1}(\sin(29.68^\circ)\sin(-17.5^\circ) + \cos(29.68^\circ)\cos(-17.5^\circ)\cos(-10.7^\circ)) = 41.7^\circ$$

From Equation 10.29,

$$\begin{aligned} a_s &= \sin^{-1} \left[\frac{(\cos(-17.5^\circ)\sin(-10.7^\circ))}{\cos(41.7^\circ)} \right] \\ &= -13.7^\circ \end{aligned}$$

Angle of incidence i for the solar collector is given by Equation 10.44:

$$\cos i = \cos(41.7^\circ)\cos(-13.7^\circ - 10^\circ)\sin(30^\circ) + \sin(41.7^\circ)\cos(30^\circ) \quad i = 23.4^\circ$$

* The tilted surface and the ground in front of it have been assumed to be infinitely large for this view factor.

To calculate the solar radiation using Equations 10.42, 10.43, 10.45, and 10.47, we need to find $I_{b,N}$ and I .

Extraterrestrial solar radiation

$$\begin{aligned} I &= I_0 \left[1 + 0.034 \cos \left(\frac{360n}{365.25} \right)^\circ \right] \\ &= 1353 \text{ W/m}^2 \left[1 + 0.034 \cos \left(\frac{360 \times 32}{365.25} \right) \right] \\ &= 1392 \text{ W/m}^2 \end{aligned}$$

(Find k from Table 10.3 and assume C_n is 1)

$$\begin{aligned} I_{b,N} &= C_n I e^{-k/\sin \alpha} \\ &= 1392 e^{-0.144/\sin(41.7^\circ)} \\ &= 1121 \text{ W/m}^2 \text{ or } 355 \text{ Btu/h ft}^2 \end{aligned}$$

Beam radiation on the collector (Equation 10.43)

$$\begin{aligned} I_{b,c} &= I_{b,N} \cos i \\ &= (1121) \cos(23.4^\circ) \\ &= 1029 \text{ W/m}^2 \text{ or } 326 \text{ Btu/h ft}^2 \end{aligned}$$

Sky diffuse radiation on the collector (Equation 10.45)

$$\begin{aligned} I_{d,c} &= C I_{b,N} \cos^2 \left(\frac{\beta}{2} \right) \\ &= (0.060)(1121) \cos^2 \left(\frac{30}{2} \right) \end{aligned}$$

(Find C from Table 10.3.)

$$63 \text{ W/m}^2 \text{ or } 20 \text{ Btu/h ft}^2$$

Ground-reflected radiation on the collector (Equation 10.47)

$$I_{r,c} = \rho I_{b,N} (\sin \alpha + C) \sin^2 \left(\frac{\beta}{2} \right)$$

Assume

$$\begin{aligned} \rho &= 0.2 \\ I_{r,c} &= (0.2)(1121)(\sin 41.7^\circ + 0.060) \sin^2(15^\circ) \\ &= 11 \text{ W/m}^2 \text{ or } 3.5 \text{ Btu/h ft}^2 \end{aligned}$$

Total insolation on the collector

$$I_c = 1029 + 63 + 11 = 1103 \text{ W/m}^2 \text{ or } 350 \text{ Btu/h ft}^2$$

A convenient website that will provide the same information obtained in the preceding example can be found online at Build It Solar [16]. The online calculator model requires merely inputting the latitude, collector tilt, collector azimuth, altitude of location, the month, and the day. With this information, the program provides the direct, diffuse, and total radiation perpendicular to the sun in the third, fourth, and fifth columns. The sixth column provides the total radiation on a horizontal surface. The seventh column gives the incident angle of the sun on the collector. The 9th, 10th, and 11th columns give the direct, diffuse, and total radiation falling on the collector surface. From this program, the radiation falling on the collector at noon is 1037 W/m^2 , which is about 4% less than the value obtained by the empirical procedure outlined in the book. The printout from the model for the day is shown in Table 10.4 with the radiation values in $\text{Btu/h}\cdot\text{ft}^2$.

TABLE 10.4
Solar Radiation Output for Example 10.6 Using the Online Calculator

Solar radiation on collector for day of 2/1										
Collector area	1 (ft ²)									
Collector azimuth	0 (degree) measured from south + is to east									
Collect tilt	40 (degree) measured from horizontal									
Latitude	30 (degree)									
Altitude	0 (ft) above sea level									
Sun rise	6.7 (h) sunrise in solar time									
	Sun						Collector			
Time (h)	Az.	Elev.	Dir. Normal	Diffuse	Total	Horiz. Tot.	Incid. Ang.	Direct.	Diffuse	Total
4	88.9	−34.1	0	0	0	0	90	0	0	0
5	82	−21.2	0	0	0	0	90	0	0	0
6	75.1	−8.4	0	0	0	0	87	0	0	0
7	67.7	3.9	47	3	50	6	73	14	2	16
8	59.2	15.5	228	13	241	74	59	119	12	131
9	48.8	26	280	16	297	139	44	201	15	216
10	35.6	34.8	302	18	320	190	30	262	16	278
11	19.1	40.8	312	18	330	222	16	300	16	316
12	0	42.9	315	18	333	233	7	312	16	329
13	−19.1	40.8	312	18	330	222	16	300	16	316
14	−35.6	34.8	302	18	320	190	30	262	16	278
15	−48.8	26	280	16	297	139	44	201	15	216
16	−59.2	15.5	228	13	241	74	59	119	12	131
17	−67.7	3.9	47	3	50	6	73	14	2	16
18	−75.1	−8.4	0	0	0	0	87	0	0	0
19	−82	−12.2	0	0	0	0	90	0	0	0
20	−88.9	−34.1	0	0	0	0	90	0	0	0
Day total			2653	156	2809	1496		2102	138	2240
Angles in degrees										
Radiations in Btu/h										
Day total in Btu/day										
1 Btu/h ft ² = 3.152 W/m ²										

10.6 TMY Data to Determine Solar Radiation

Sandia National Laboratories prepared a data set summarizing long-term weather and solar data in 1978. This was updated by NREL and released for use by building designers and solar thermal modelers as the Typical Meteorological Year version 3 (TMY3) data set in 2007. A user's manual for the data set is available from NREL's website [17]. The following example demonstrates the use of the TMY3 data to obtain the insolation on a solar collector.

EXAMPLE 10.7

Using typical meteorological data (TMY3), find the total insolation and beam insolation on a south-facing solar collector tilted at an angle of 25° in Miami, Florida, for January 1. Also find the average total insolation per day for the entire month of January. Assume a ground reflectance of $\rho = 0.2$. Use site information for the Miami International Airport.

Solution

TMY3 data can be accessed via the NREL website on the National Solar Radiation Data Base page [18]. Under "The Data," select "In alphabetical order by state and city." This will link you to a list of all sites for which TMY3 data have been collected. Scroll down to Florida and select site number 722020 for the Miami International Airport. The TMY3 data can be downloaded as a CSV file format that can be read by most spreadsheet programs.

We will only need three separate columns from the TMY3 table: DNI, DHI, and GHI. DNI is *direct normal irradiance* and is the amount of beam radiation received on a surface normal to the sun. DHI is *diffuse horizontal irradiance* and is the amount of sky diffuse radiation received on a horizontal surface. GHI is *global horizontal irradiance* and is the total amount of radiation received on a horizontal surface. DNI, DHI, and GHI correspond to $I_{b,N}$, $I_{d,h}$, and I_h respectively as used in the text (see Table 10.5).

To find the total insolation for January 1, you must sum the hourly values of I_c . Using Equation 10.42, I_c is the sum of $I_{b,c}$, $I_{d,c}$, and $I_{r,c}$ at each hour during the day. Table 10.5 shows how this can be approached using a spreadsheet [17]. Summing the I_c column, the total insolation for January 1 is $4544 \text{ Wh/m}^2 \cdot \text{day}$ ($16,800 \text{ kJ/m}^2 \cdot \text{day}$). Summing the $I_{b,c}$ column, the total beam insolation is $2899 \text{ Wh/m}^2 \cdot \text{day}$. Repeating this problem for the entire month of January, the total monthly insolation is $133,522 \text{ Wh/m}^2$, with a daily average of $4,307 \text{ Wh/m}^2 \cdot \text{day}$.

10.7 Measurement of Solar Radiation

Solar radiation measurements of importance to most engineering applications, especially thermal applications, include total (integrated over all wavelengths) direct or beam and sky diffuse values of solar radiation on instantaneous, hourly, daily, and monthly bases. Some applications such as photovoltaics, photochemical, and daylighting require knowledge of spectral (wavelength specific) or band (over a wavelength range, e.g., ultraviolet, visible, infrared) values of solar radiation. This section describes some of the instrumentation used to measure solar radiation and sunshine, and some sources of long-term measured data for different parts of the world. Also described briefly in this section is the method of satellite-based measurements.

TABLE 10.5

Calculation Solar Insolation for January 1 in Miami, Florida, Using TMY3 Data

Time	DNI	DHI	GHI	h_s	α	a_s	i	$I_{b,c}$	$I_{d,c}$	$I_{r,c}$	I_c
h	W/m ²	W/m ²	W/m ²	°	°	°	°	W/m ²	W/m ²	W/m ²	W/m ²
1	0	0	0	−165.00	−76.1	−81.7	149.9	0.0	0.0	0.0	0.0
2	0	0	0	−150.00	−62.6	−89.4	143.4	0.0	0.0	0.0	0.0
3	0	0	0	−135.00	−49.1	−84.0	131.0	0.0	0.0	0.0	0.0
4	0	0	0	−120.00	−35.8	−79.2	117.7	0.0	0.0	0.0	0.0
5	0	0	0	−105.00	−22.6	−74.4	104.1	0.0	0.0	0.0	0.0
6	0	0	0	−90.00	−9.8	−69.1	90.3	0.0	0.0	0.0	0.0
7	0	0	0	−75.00	2.5	−62.9	76.5	0.0	0.0	0.0	0.0
8	262	18	39	−60.00	14.1	−55.3	62.9	119.2	17.2	0.4	136.7
9	694	38	218	−45.00	24.6	−45.7	49.8	447.9	36.2	2.0	486.2
10	768	65	394	−30.00	33.2	−33.4	37.7	608.0	62.0	3.7	673.6
11	747	125	540	−15.00	39.1	−17.9	27.9	660.1	119.1	5.1	784.3
12	230	265	411	0.00	41.2	0.0	23.8	210.4	252.6	3.9	466.9
13	324	290	503	15.00	39.1	17.9	27.9	286.3	276.4	4.7	567.4
14	517	192	514	30.00	33.2	33.4	37.7	409.3	183.0	4.8	597.1
15	107	339	396	45.00	24.6	45.7	49.8	69.1	323.1	3.7	395.9
16	117	265	313	60.00	14.1	55.3	62.9	53.2	252.6	2.9	308.7
17	152	81	116	75.00	2.5	62.9	76.5	35.4	77.2	1.1	113.7
18	22	14	16	90.00	−9.8	69.1	90.3	−0.1	13.3	0.1	13.4
19	0	0	0	105.00	−22.6	74.4	104.1	0.0	0.0	0.0	0.0
20	0	0	0	120.00	−35.8	79.2	117.7	0.0	0.0	0.0	0.0
21	0	0	0	135.00	−49.1	84.0	131.0	0.0	0.0	0.0	0.0
22	0	0	0	150.00	−62.6	89.4	143.4	0.0	0.0	0.0	0.0
23	0	0	0	165.00	−76.1	81.7	149.9	0.0	0.0	0.0	0.0

Source: Wilcox, S. and Marion, W., April/May 2008. User's Manual for TMY3 Data Sets, Technical Report NREL/TP-581-43156, National Renewable Energy Laboratory, Golden, CO. [17]

See Figure 10.19.

L , latitude = 25.817° (from top line of spreadsheet).

h_s , hour angle (from Equation 10.25; for simplicity in this example, solar time is approximated as local time).

α , solar altitude (from Equation 10.28).

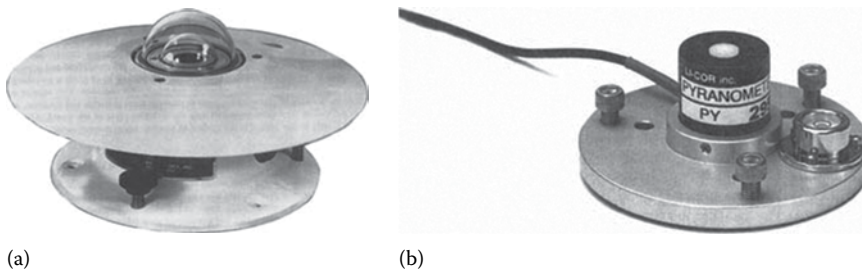
a_s , solar azimuth (from Equation 10.29).

i , incidence angle of sun on collector (from Equation 10.44).

β , tilt angle of collector from horizontal, 25°

10.7.1 Instruments for Measuring Solar Radiation and Sunshine

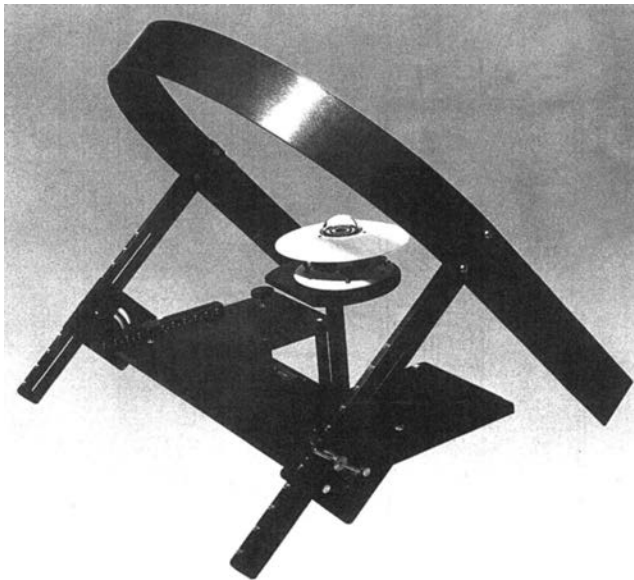
There are two basic types of instruments used to measure solar radiation, *pyranometer* and *pyrheliometer*. A pyranometer has a hemispherical view of the surroundings and therefore is used to measure total, direct, and diffuse, solar radiation on a surface. A pyrheliometer, on the other hand, has a restricted view (about 5°) and is, therefore, often used to measure the direct or beam solar radiation by pointing it toward the sun. Pyranometers are also used to measure the sky diffuse radiation by using a shadow band to block the direct sun view. A detailed discussion of the instrumentation and calibration standards is given by Iqbal [19] and Zerlaut [20].

**FIGURE 10.20**

Typical commercially available pyranometers with (a) thermal detector and (b) photovoltaic detector.

A pyranometer consists of a flat sensor/detector (described later) with an unobstructed hemispherical view, which allows it to convert and correlate the total radiation incident on the sensor to a measurable signal. The pyranometers using thermal detectors for measurements can exhibit serious errors at tilt angles from the horizontal due to free convection. These errors are minimized by enclosing the detector in double hemispherical high-transmission glass domes. The second dome minimizes the error due to infrared radiative exchange between the sensor and the sky. A desiccator is usually provided to eliminate the effect due to condensation on the sensor or the dome. Figure 10.20 shows pictures of typical commercially available precision pyranometers.

A pyranometer can be used to measure the sky diffuse radiation by fitting a shade ring to it, as shown in Figure 10.21, in order to block the beam radiation throughout the day. The position of the shade ring is adjusted periodically as the declination changes. Since the shade ring obstructs some diffuse radiation from the pyranometer, correction factors must be applied.

**FIGURE 10.21**

A pyranometer with a shade ring to measure sky diffuse radiation.

Geometric correction factors (GCFs) that account for the part of the sky obstructed by the shade ring can be easily calculated. However, a GCF assumes isotropic sky, which results in errors because of the circumsolar anisotropy. Eppley Corp. recommends additional correction factors to account for anisotropy as +7% for clear sky, +4% for partly cloudy condition, and +3% for cloudy sky. Mujahid and Turner [21] determined that these correction factors gave less than 3% errors on partly cloudy days but gave errors of −11% for clear-sky conditions and +6% on overcast days. They suggested correction factors due to anisotropy as tabulated in Table 10.6, which reduce the errors to less than $\pm 3\%$ [22]. It must be remembered that these correction factors are in addition to the GCFs. Recently, a sun occulting disk has been employed for shading the direct sun.

Beam or direct solar radiation is usually measured with an instrument called a pyrheliometer. Basically, a pyrheliometer places the detector at the base of a long tube. This geometry restricts the sky view of the detector to a small angle of about 5° . When the tube points toward the sun, the detector measures the beam solar radiation and a small part of the diffuse solar radiation within the view angle. Figure 10.22 shows the geometry of a pyrheliometer sky occulting tube.

In this figure, the opening half angle

$$\theta_o = \tan^{-1} \frac{R}{L} \quad (10.48)$$

The slope angle

$$\theta_p = \tan^{-1} \left[\frac{(R-r)}{L} \right] \quad (10.49)$$

The limit half angle

$$\theta = \tan^{-1} \left[\frac{(R+r)}{L} \right] \quad (10.50)$$

The field of view is $2\theta_o$. The World Meteorological Organization (WMO) recommends the opening half angle θ_o to be 2.5° [20] and the slope angle θ_p to be 1° .

Continuous tracking of the sun is required for the accuracy of the measurements. This is obtained by employing a tracking mechanism with two motors, one for altitude and the other for azimuthal tracking. Another problem is that the view angle of a pyrheliometer is significantly greater than the angle subtended by the solar disk (about 0.5°). Therefore,

TABLE 10.6

Shading Band Correction Factors due to Anisotropy

Solar Altitude Angle	k_r									
	0.0	0.1	0.2	0.3	0.4	0.5	0.6	0.7	0.8	0.9
$<20^\circ$	0.0	0.0	0.0	0.0	0.015	0.06	0.14	0.23	0.24	0.24
$20^\circ\text{--}40^\circ$	0.0	0.0	0.0	0.0	0.006	0.05	0.125	0.205	0.225	0.225
$40^\circ\text{--}60^\circ$	0.0	0.0	0.0	0.0	0.003	0.045	0.115	0.175	0.205	0.205
$60^\circ+$	0.0	0.0	0.0	0.0	0.0	0.035	0.09	0.135	0.17	0.17

Source: Gautier, C., Diak, G., and Masse, S., 1980. *Journal of Applied Meteorology* 19(8), 1005. [22]

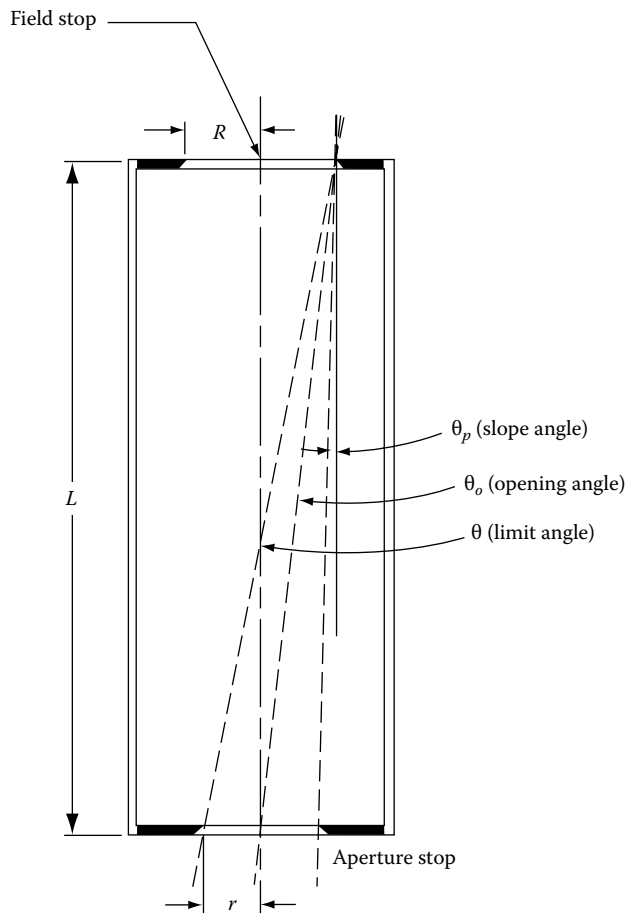


FIGURE 10.22
Geometry of a pyrheliometer sky occulting tube.

the measurements using a pyrheliometer include the beam and the circumsolar radiation. These measurements may present a problem in using the data for central receiver systems that use only direct beam radiation. However, this is not a significant problem for parabolic trough concentrators that in most cases have field of view on the order of 5° .

10.7.2 Detectors for Solar Radiation Instrumentation

Solar radiation detectors are of four basic types [19,20]: thermomechanical, calorimetric, thermoelectric, and photoelectric. Of these, thermoelectric and photoelectric are the most common detectors in use today.

A *thermoelectric detector* uses a thermopile that consists of a series of thermocouple junctions. The thermopile generates a voltage proportional to the temperature difference between the hot and cold junctions, which, in turn, is proportional to the incident solar radiation.

Photovoltaic detectors normally use silicon solar cells measuring the short circuit current. Such detectors have the advantage of being simple in construction. Because heat transfer is

not a consideration, they do not require clear domes or other convection suppressing devices. They are also insensitive to tilt as the output is not affected by natural convection. One of the principal problems with photovoltaic detectors is their spectral selectivity. Radiation with wavelengths greater than the band gap of the photovoltaic detector cannot be measured. Silicon has a band gap of 1.07 eV corresponding to a wavelength of 1.1 μm . A significant portion of the infrared part of solar radiation has wavelengths greater than 1.1 μm . Therefore, photovoltaic detectors are insensitive to changes in the infrared part of solar radiation.

10.7.3 Measurement of Sunshine Duration

The time duration of bright sunshine data is available at many more locations in the world than the solar radiation. That is why a number of researchers have used these data to estimate the available solar radiation. Two instruments are widely used to measure the sunshine duration. The device used by the U.S. NWS is called a *sunshine switch*. It is composed of two photovoltaic cells—one shaded, the other not. During daylight, a potential difference is created between the two cells, which in turn operates the recorder. The intensity level required to activate the device is that just sufficient to cast a shadow. The other device commonly used to measure the sunshine duration is called the *Campbell–Stokes sunshine recorder*. It uses a solid clear glass sphere as a lens to concentrate the solar beam on the opposite side of the sphere. A strip of standard treated paper marked with time graduations is mounted on the opposite side of the sphere where the solar beam is concentrated. Whenever the solar radiation is above a threshold, the concentrated beam burns the paper. The length of the burned part of the strip gives the duration of bright sunshine. The problems associated with the Campbell–Stokes sunshine recorder include the uncertainties of the interpretation of burned portions of the paper, especially on partly cloudy days, and the dependence on the ambient humidity.

10.7.4 Measurement of Spectral Solar Radiation

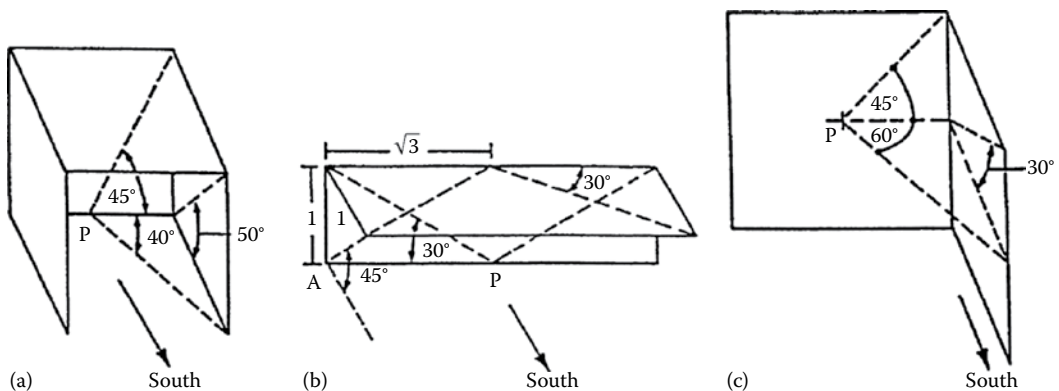
Spectral solar radiation measurements are made with spectroradiometers. Full spectrum scanning is difficult, requires constant attention during operation, and is therefore expensive. Zerlaut [20] has described a number of solar spectroradiometers. These instruments consist basically of a monochromator, a detector–chopper assembly, an integrating sphere, and a signal conditioning/computer package. They have the capability of measuring solar radiation in the wavelength spectrum of 280–2500 nm.

10.7.5 National Solar Radiation Database

Using the System Advisor Model and other tools for predicting the performance of solar energy systems requires detailed solar energy data representative of many locations. NREL has compiled the National Solar Radiation Database (<https://nsrdb.nrel.gov>). The NSRDB [23,24] is a complete collection of hourly and half-hourly values of the three most common measurements of solar radiation—global horizontal, direct normal, and diffuse horizontal irradiance—and meteorological data. These data have been collected at a sufficient number of locations and temporal and spatial scales to accurately represent regional solar radiation climates. Although it was originally focused on the United States, it contains an increasing number of international locations. Data sets can be accessed at <https://nsrdb.nrel.gov/data-sets>. But more commonly, solar energy system designers will use SAM or other tools and specify a location that will pull the NSRDB data.

PROBLEMS

- 10.1 Calculate the declination, the zenith angle, and the azimuth angle of the sun for New York City (latitude 40.77°N) on October 1 at 2:00 p.m. solar time.
- 10.2 A solar energy system in Gainesville, Florida, requires two rows of collectors facing south and tilted at a fixed 30° angle. Find the minimum normalized distance at which the second row should be placed behind the first row for no shading at noon at winter solstice. What percentage of the second row is shaded on the same day at 9:00 a.m. solar time?
- 10.3 Find the sunrise and sunset times for a location of your choice on September 1.
- 10.4 Construct a table of hourly sun angles for the 15th day of each month for a location of your choice. Also show the sunrise and sunset times for those days.
- 10.5 Referring to [Figure 10.19](#), prove Equation 10.44 for the angle of incidence. (*Hint:* Use direction cosines of the sun-ray vector and a vector normal to the tilted surface to find the angle between them. Dot product of two unit vectors gives the cosine of the angle between them.)
- 10.6 Determine the following for a south-facing surface at 30° slope in Gainesville, Florida (latitude = 29.68°N , longitude = 82.27°W), on September 21 at noon solar time:
 - a. Zenith angle
 - b. Angle of incidence
 - c. Beam radiation
 - d. Diffuse radiation
 - e. Reflected radiation
 - f. Total radiation
 - g. Local time
- 10.7 Show that the hourly averaged, extraterrestrial radiation for a given hour is the same, to within 1%, as instantaneous radiation at the hour's midpoint.
- 10.8 Prepare shadow maps for point P on the sun-path diagrams for 35°N and 40°N for the following three geometries shown in a, b, and c. Determine the hours of shading that occur each month.



- 10.9 Repeat Problem 10.8c if the surface containing point P faces due west instead of due south for a 40°N location.
- 10.10 Calculate the incidence angle at noon and 9 a.m. on a fixed flat-plate collector located at 40°N latitude and tilted 70° up from the horizontal. Find i for June 21 and December 21.
- 10.11 a. If the surface in Problem 10.10 faces $\text{S } 45^\circ \text{ E}$, what are the incidence angles?
b. If the collector in Problem 10.10 has a cylindrical surface, what are the incidence angles on June 21 and December 21?
- 10.12 Using a one-term Fourier cosine series, develop an empirical equation for solar declination as a function of day number counted from January 1 (see [Figure 10.7](#)). Note that maximum declination of 23.45 degrees occurs on June 21, which is day number 172.
- 10.13 Derive an equation for the lines of constant declination in a sun-path diagram, for example, [Figure 10.10d](#). Check your equation by plotting a few declination lines on a piece of polar coordinate graph paper.
- 10.14 Derive Equation 10.31 relating profile angle γ to azimuth angle α and altitude angle α .
- 10.15 Based on Equation 10.44, what value of β would result in the annual minimum value of the incidence angle i ? Note that this tilt angle would result in maximum collection of beam radiation on a fixed, flat, south-facing surface. *Hint:* Use a double integration procedure.
- 10.16 At what time does the sun set in Calcutta (23°N) on May 1 and December 1?
- 10.17 What is the true solar time in Sheridan, Wyoming (107°W), at 10:00 a.m. Mountain Daylight Time on June 10? What is the true solar time at 10:00 a.m. Mountain Standard Time on January 10?
- 10.18 Derive an expression for the minimum allowable distance between east–west rows of solar collectors that will assure no shading of one row by the row immediately to the south. Use the law of sines and express the result in terms of the collector tilt and face length and the controlling value of the solar profile angle.

References

1. Howell, J.R., Siegel, R., and Menguc, M.P., 2010. *Thermal Radiation Heat Transfer*, McGraw-Hill Book Co., New York.
2. Kreith, F., 1962. *Radiation Heat Transfer for Spacecraft and Solar Power Plant Design*, International Textbook Co., Scranton, PA.
3. Kreith, F., Mangelik, R.M., and Bohn, S., 2011. *Principles of Heat Transfer*, 7th ed., Cengage Publishing Co., St. Paul, MN.
4. Sparrow, E.M. and Cess, R.D., 1978. *Radiation Heat Transfer*, Wadsworth Publ. Co., Belmont, CA.
5. Threlkeld, J.L. and Jordan, R.C., 1958. Direct radiation available on clear days, *Transactions of ASHRAE*, 64, 45.
6. Kreider, J.F. and Kreith, F., 1982. *Solar Heating and Cooling*, Hemisphere Publishing Corp., Washington, DC.

7. List, R.J., 1949. *Smithsonian Meteorological Tables*, 6th ed., Smithsonian Institution Press, Washington, DC, pp. 442–443.
8. University of Oregon. *Solar Radiation Monitoring Laboratory*, <http://solardat.uoregon.edu/SoftwareTools.html>.
9. Frohlich, C. et al., 1973. The third international comparison of pyrheliometers and a comparison of radiometric scales, *Solar Energy* 14, 157–166.
10. Quinlan, F.T. (ed.), 1977. *SOLMET Vol. 1: Hourly Solar Radiation Surface Meteorological Observations*, NOAA, Asheville, NC.
11. Quinlan, F.T. (ed.), 1979. *SOLMET Vol. 2: Hourly Solar Radiation Surface Meteorological Observations*, NOAA, Asheville, NC.
12. Kimura, K. and Stephenson, D.G., 1969. Solar radiation on cloudy days, *Transactions of ASHRAE* 75, 227–234.
13. Iqbal, M., 1979. Correlation of average diffuse and beam radiation with hours of bright sunshine, *Solar Energy*, 23, 169.
14. Thekaekara, M.P., 1973. Solar energy outside the Earth's atmosphere, *Solar Energy* 14, 109–127.
15. Islam, M.R., 1994. *RE RIC International Energy Journal*, 16(2), 103–113.
16. Build It Solar. Solar radiation on collection program, <http://www.builditsolar.com/Tools/RadOnCol/radoncol.htm>.
17. Wilcox, S. and Marion, W., April/May 2008. *User's Manual for TMY3 Data Sets*, Technical Report NREL/TP-581-43156, National Renewable Energy Laboratory, Golden, CO.
18. NREL. *National Solar Radiation Data Base*, http://rredc.nrel.gov/solar/old_data/nsrdb/1991-2010.
19. Iqbal, M., 1983. *An Introduction to Solar Radiation*, Academic Press, New York.
20. Zerlaut, G., 1989. Solar radiation instrumentation, in: Roland L.H. (ed.), *Solar Resources*, MIT Press, Cambridge, MA, pp. 173–308.
21. Mujahid, A. and Turner, W.D., 1979. Diffuse sky measurement and model, ASME Pap. No. 79-WA/Sol-5.
22. Gautier, C., Diak, G., and Masse, S., 1980. A simple physical model to estimate incident solar radiation at the surface from GOES satellite data, *Journal of Applied Meteorology* 19(8), 1005.
23. Maxwell, E.L., 1998. METSTAT—The solar radiation model used in the production of the national solar radiation data base (NSRDB), *Solar Energy* 62, 263–279.
24. NSRDB, 1992. *Volume 1: User's Manual: National Solar Radiation Data Base (1961–1990), Version 1.0*, National Renewable Energy Laboratory, Golden, CO.

11

*Photovoltaics**

I'd put my money on the sun and solar energy. What a source of power! I hope we don't have to wait until oil and coal run out before we tackle that. I wish I had more years left.

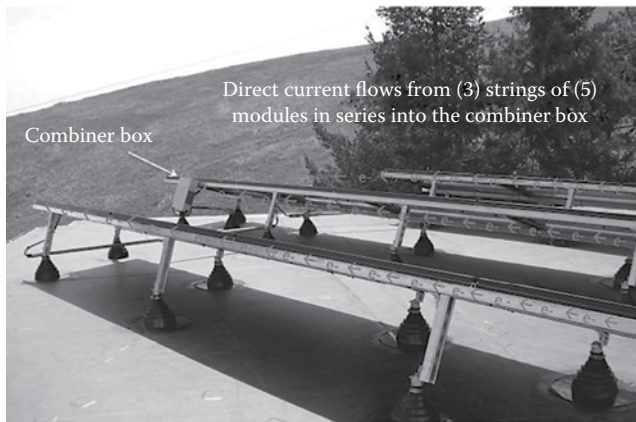
Thomas Edison

Photovoltaic conversion is the direct conversion of sunlight into electricity with no intervening heat engine. Photovoltaic devices are solid-state devices; therefore, they are rugged and simple in design and require very little maintenance. Perhaps the biggest advantage of solar photovoltaic devices is that they can be constructed as stand-alone systems to give outputs from microwatts to megawatts. That is why they have been used as the power sources for calculators, watches, water pumping, remote buildings, communications, satellites and space vehicles, and even megawatt-scale power plants. Photovoltaic panels can even be made to form components of building skin, such as roof shingles and wall panels. With such a vast array of applications, the demand for photovoltaics is increasing every year. According to the International Energy Agency, the market for photovoltaic solar cells has grown exponentially, increasing from 227 MW in 2000 to 20,500 MW in 2010 and 76,000 MW in 2016. Total world installed capacity is now just over 300,000 MW. The global market created \$113 billion in revenue in 2015 [1]. An example of a photovoltaic residential rooftop system is shown in Figure 11.1.

In the early days of solar cells in the 1960s and 1970s, more energy was required to produce a cell than it could ever deliver during its lifetime. Since then, dramatic improvements have taken place in the efficiencies and manufacturing methods. The energy payback periods for installed systems have been reduced to about 1 to 3 years, depending on the module type and the location of use [2], while panel lifetimes were increased to over 25 years. The price of photovoltaic modules has come down to under \$0.50 per peak watt over the last two decades.

Historically, the photoelectric effect was first noted by Becquerel in 1839 when light was incident on an electrode in an electrolyte solution [3]. Adams and Day first observed the effect in solids in 1877 while working with selenium. Early work was done with selenium and copper oxide by pioneers such as Schottky, Lange, and Grandahl. In 1954, researchers at RCA and Bell Laboratories reported achieving efficiencies of about 6% by using devices made of *p*- and *n*-type semiconductors. The space race between the United States and the Soviet Union resulted in dramatic improvements in photovoltaic devices. Bube [4] gives a review of the early developments in photovoltaic conversion.

* Sections in this chapter marked with an asterisk may be omitted in an introductory course.



Combiner box
600 V Fuses protect each of the (3) strings of (5) modules
after the fuses the (3) circuits are combined in parallel
The combined circuit is then brought to the DC disconnect in the garage

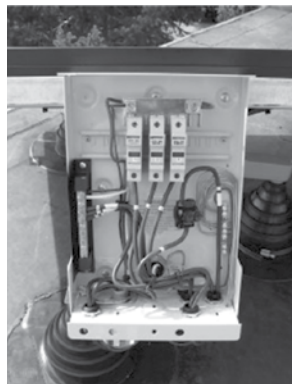


FIGURE 11.1

Kreith residence, 3 kW Sanyo high-efficiency photovoltaic system. (Courtesy of Chris Klinga, Lighthouse Solar, Boulder, CO. With permission.)

11.1 Semiconductors

A basic understanding of the atomic structure is quite helpful in understanding the behavior of semiconductors and their use as the photovoltaic energy conversion devices. Any fundamental book on physics or chemistry generally gives adequate background for basic understanding. Bube [4] presents an in-depth treatment of a number of topics in semiconductor physics.

For any atom, the electrons arrange themselves in orbitals around the nucleus so as to result in the minimum amount of energy. Table 11.1 shows the distribution of the electrons in various orbitals in light elements [5]. In elements that have electrons in multiple orbitals, the innermost electrons are more strongly bound to the positively charged nucleus and, therefore, require the maximum amount of externally imparted energy to overcome the attraction of the nucleus and become free. Electrons in the outermost orbitals are partially shielded from the nucleus by the inner electrons, are less bound to the atom, and provide the means for neighboring atoms to interact. In some cases, atoms may transfer electrons in order to fill an outermost orbital, resulting in positively and negatively charged ions that become attached by the force of attraction of the charges, thus forming *ionic bonds*. In other cases, atoms may share electrons to fill the outermost orbital forming what is known as a *covalent bond*.

As atoms are brought together, the outermost electron states, or orbitals, overlap and mix to create energy bands that are no longer isolated around individual atoms but, rather, are extended throughout the bulk of the material. The highest filled band of these states, at $T = 0$, is called the *valence band*. The band of states above the valence band, empty at $T = 0$, is called the *conduction band*. The difference in the energy of an electron in the top of the valence band and the bottom of the conduction band is called the *band gap* or the forbidden gap.

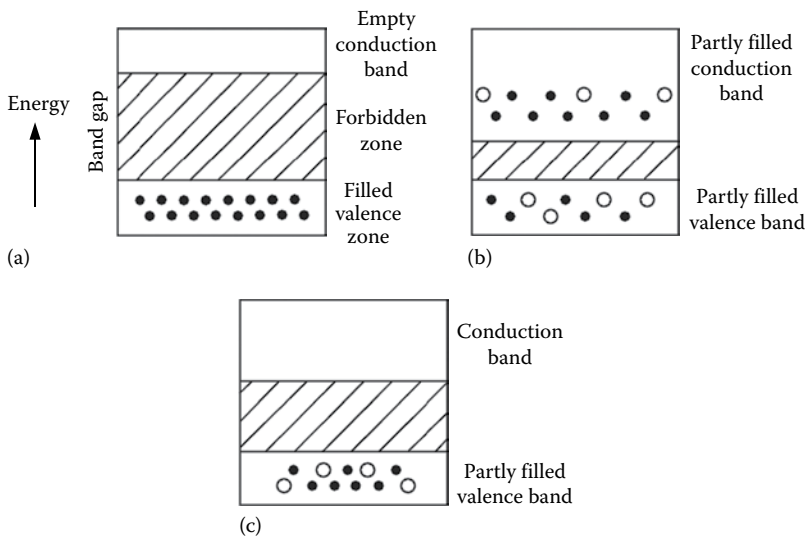
The band gap of a material plays a large role in determining the material's electrical conductivity. Of note, a full band cannot support the flow of electricity. Consequently, materials with high band gaps (>3 eV) tend to be insulators at room temperature because there is not enough thermal energy to excite a significant number of electrons from the filled valence band into the conduction band, where they can participate in the flow of electricity. As the band gap is reduced, the number of electrons that can be thermally excited into the conduction band increases, as does the electrical conductivity of the material. These materials with improved conductivity are called semiconductors (see Figure 11.2) and tend to have band gaps of 1–2 eV and, perhaps most importantly for photovoltaic devices, align well with the energy of photons in the solar spectrum. Materials with overlapping conduction and valence bands do not have a characteristic band gap, require no thermal energy to generate a large population of mobile electrons, conduct electricity with relative ease, and are known as metals.

Pure semiconductors, as discussed above, are called *intrinsic semiconductors*, while semiconductors doped with very small amounts of impurities are called *extrinsic semiconductors*. If the dopant atom has more electrons than the intrinsic atom it is replacing, the extra electrons tend to be very loosely bound and can be easily excited into the conduction band, even at room temperature. This results in a material with a controllable number of free electrons in the conduction band and is called an *n*-type semiconductor (*n* indicating the negative charge of the electron). For example, each silicon atom contributes four electrons to the valence band. Atoms of pure silicon arrange themselves in such a way that, to form a stable structure, each atom shares two electrons with each neighboring atom

TABLE 11.1
Electronic Structure of Atoms

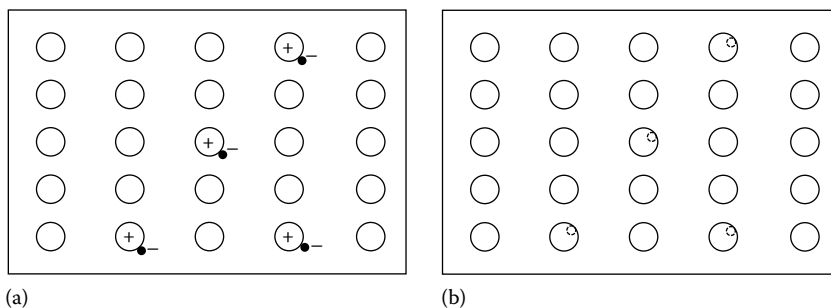
Principal Quantum Number n				1	2		3		4		5
Azimuthal Quantum Number l				0	0	1	0	1	2	0	1
Letter Designation of State				1s	2s	2p	3s	3p	3d	4s	4p
Z	Symbol	Element	V_i (V)								
1	H	Hydrogen	13.60	1							
2	He	Helium	24.58	2							
3	Li	Lithium	5.39	Helium core	1						
4	Be	Beryllium	9.32		2						
5	B	Boron	8.30		2	1					
6	C	Carbon	11.26		2	2					
7	N	Nitrogen	14.54		2	3					
8	O	Oxygen	13.61		2	4					
9	F	Fluorine	17.42		2	5					
10	Ne	Neon	21.56		2	6					
11	Na	Sodium	5.14	Neon core			1				
12	Mg	Magnesium	7.64				2				
13	Al	Aluminum	5.98				2	1			
14	Si	Silicon	8.15				2				
15	P	Phosphorus	10.55				2	3			
16	S	Sulfur	10.36				2	4			
17	Cl	Chlorine	13.01				2	5			
18	A	Argon	15.76				2	6			
19	K	Potassium	4.34	Argon core					1		
20	Ca	Calcium	6.11						2		
21	Sc	Scandium	6.56						1	2	
22	Ti	Titanium	6.83						2	2	
23	V	Vanadium	6.74						3	2	
24	Cr	Chromium	6.76						5	1	
25	Mn	Manganese	7.43						5	2	
26	Fe	Iron	7.90						6	2	
27	Co	Cobalt	7.86						7	2	
28	Ni	Nickel	7.63						8	2	
29	Cu	Copper	7.72						10	1	
30	Zu	Zinc	9.39					10	2		
31	Ga	Gallium	6.00					10	2	1	
32	Ge	Germanium	7.88					10	2	2	
33	As	Arsenic	9.81					10	2	3	
34	Se	Selenium	9.75					10	2	4	
35	Br	Bromine	11.84					10	2	5	
36	Kr	Krypton	14.00					10	2	6	

Source: From Moore, C.E., 1952. *Atomic Energy Levels*, Vol. 2, National Bureau of Standards Circular 467, U.S. Government Printing Office, Washington, DC. With permission. [5]

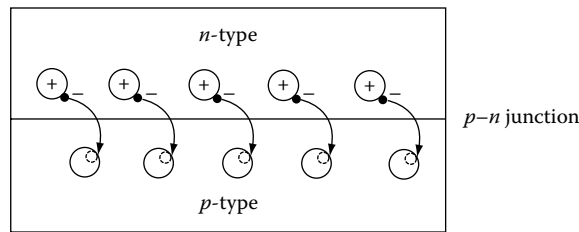
**FIGURE 11.2**

Electrical conduction is described in terms of allowed and forbidden energy bands. Band gap for insulators (a) is the highest, followed by metals (b) and semiconductors (c), respectively.

with covalent bands. If phosphorous, which has five valence electrons (one more than Si), is introduced as an impurity in silicon, the doped material seems to have excess electrons even though it is electrically neutral. Such a doped material is called *n*-type silicon. If, on the other hand, silicon is doped with boron, which has three valence electrons (one less than Si), there seems to be a positive hole (missing electron) in the structure, even though the doped material is electrically neutral. Such material is called *p*-type silicon (*p* denoting the positive charge of the hole). (See Figure 11.3.) Thus, *n*- and *p*-type semiconductors make it easier to increase, and control, the number of electrons and holes in the semiconductor because the energy required to create partially filled bands is now related to the energy level of the impurity electron state which is typically much less than the band gap energy. The ability to control the conductivity and type (*p* or *n*) of semiconductors capable of absorbing solar radiation is the foundation of modern photovoltaic devices.

**FIGURE 11.3**

Representation of *n*- and *p*-type semiconductors: (a) *n*-type showing “excess” electrons as dots; (b) *p*-type showing “excess” positive holes as \circ .

**FIGURE 11.4**

"Excess" electrons from *n* material jump to fill "excess" holes on the *p*-side of a *p-n* junction, leaving the *n*-side of the junction positively charged and the *p*-side negatively charged.

11.1.1 *p-n* Junction

As explained earlier, an *n*-type material has some impurity atoms with more electrons than the rest of the semiconductor atoms. On the other hand, a *p*-type material has some impurity atoms with fewer electrons than the rest of the semiconductor atoms. The scenario where a *p*- and an *n*-type of material are joined together, as shown in Figure 11.4, is called a *p-n* junction. As soon as the two materials are joined, the "excess" electrons from the *n* layer diffuse to fill the "holes" in the *p* layer. Therefore, close to the junction, the material has positive charges on the *n*-side and negative charges on the *p*-side. Eventually equilibrium is established where the negative charges on the *p*-side restrict the movement of additional electrons from the *n*-side to the *p*-side and a potential barrier, or built-in junction, is established at the interface.

The net result of this built-in potential barrier is that the flow of electrons is impeded in one direction but not to other. If a positive voltage is applied to the *p*-side of the junction, relative to the *n*-side, the barrier created by the transfer of electrons is reduced and current will flow more freely. This condition is known as forward bias. Conversely, if a negative voltage is applied to the *p*-side of the junction, relative to the *n*-side, the built in potential barrier is increased and current will flow less freely. This condition is known as reverse bias. This asymmetrical behavior to current flow is a key building block in many semiconductor devices, and the underlying device is known as a diode. As will be shown below, the general electrical behavior of the diode shows up in the current-voltage relationship for photovoltaic cells.

11.1.2 Photovoltaic Effect

When a photon of light is absorbed by a valence electron of an atom, the energy of the electron is increased by the amount of energy of the photon. If the energy of the photon is equal to or greater than the band gap of the semiconductor, the electron with excess energy will jump into the conduction band where it can move freely. If, however, the photon energy is less than the band gap, the electron will not have sufficient energy to jump into the conduction band and the photon will typically pass through the material. If the absorbed photon had more energy than the band gap, the excess energy over the band gap is typically lost as heat and the electron quickly moves to the bottom of the conduction band. This thermalization process represents energy that will not be captured by the flow of electricity and, consequently, can result in a significant reduction in the conversion efficiency of photovoltaic devices. The design and development of multi-junction devices with multiple band gaps, described below, is the primary approach used to reduce this loss mechanism.

As explained in [Chapter 10](#), energy contained in a single photon E_p is given by

$$E_p = h\nu \quad (11.1)$$

where

h is Planck's constant (6.625×10^{-34} J-s)

ν is the frequency, which is related to the wavelength λ and the speed of light c by

$$\nu = \frac{c}{\lambda}$$

Therefore,

$$E_p = \frac{hc}{\lambda}. \quad (11.2)$$

For silicon, which has a band gap of 1.11 eV, the following example shows that photons of wavelength 1.12 μm or less can be absorbed and contribute to the flow of photo-generated current. This wavelength range represents a major part of the solar radiation spectrum, making Si a suitable material for use in a photovoltaic device. [Table 11.2 \[6\]](#) lists other candidate semiconductor materials for photovoltaic cells along with their band gaps.

EXAMPLE 11.1

Calculate the longest wavelength of light capable of forming an electron-hole pair in silicon.

Solution

The band gap energy of silicon is 1.11 eV. From Equation 11.2, we can write

$$\lambda = \frac{hc}{E_p} = \frac{hc}{BG}$$

where BG is the band gap energy in Joules.

For $c = 3 \times 10^8$ m/s, $h = 6.625 \times 10^{-34}$ J-s, and $1 \text{ eV} = 1.6 \times 10^{-19}$ J, the earlier equation gives the required wavelength as

$$\lambda = \frac{(6.625 \times 10^{-34} \text{ J-s})(3 \times 10^8 \text{ m/s})}{(1.11 \text{ eV})(1.6 \times 10^{-19} \text{ J/eV})} = 1.12 \mu\text{m}$$

As photons are absorbed within the semiconductor, electrons are excited to the conduction band, leaving an empty hole state behind. This electron-hole pair can diffuse to the p - n junction where it encounters the built-in potential of the p - n junction. This potential will drive the photo-excited electrons from the p -side to the n -side and, the photo-excited holes from the n -side to the p -side. This results in a photovoltage across the p - n junction and this phenomenon is known as the photovoltaic effect. If the photovoltaic device is placed in a circuit, as in [Figure 11.5](#), the photogenerated current will flow and the optical power of the incident light source will have been converted to electrical power within the circuit. Ideally, all the photoexcited carriers will participate in the flow of electricity but there are material- and device-related loss mechanisms that ultimately reduce the conversion efficiency.

TABLE 11.2

Energy Gap for Some Candidate Materials for Photovoltaic Cells

Material	Band Gap (eV)
Si	1.11
SiC	2.60
CdAs ₂	1.00
CdTe	1.44
CdSe	1.74
CdS	2.42
CdSnO ₄	2.90
GaAs	1.40
GaP	2.24
Cu ₂ S	1.80
CuO	2.00
Cu ₂ Se	1.40
CuInS ₂	1.01
CuInTe ₂	0.90
InP	1.27
In ₂ Te ₃	1.20
In ₂ O ₃	2.80
Zn ₃ P ₂	1.60
ZnTe	2.20
ZnSe	2.60
AlP	2.43
AlSb	1.63
As ₂ Se ₃	1.60
Sb ₂ Se ₃	1.20
Ge	0.67
Se	1.60

Source: From Garg, H.P., 1987. *Advances in Solar Energy Technology*, Vol. 3, D. Reidel Publishing Company, Dordrecht, the Netherlands. With permission. [6]

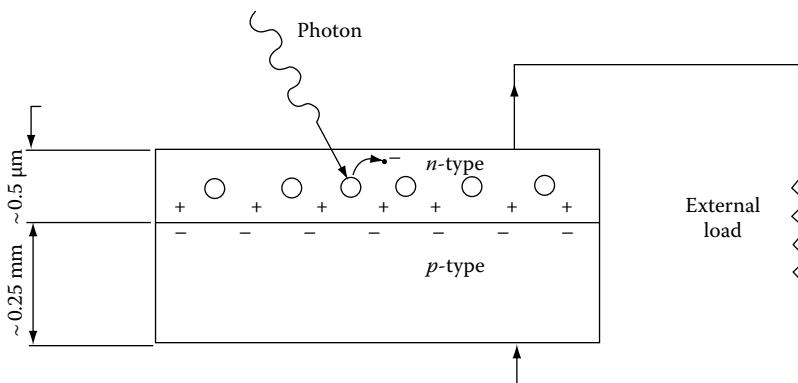


FIGURE 11.5
Schematic of a photovoltaic device.

EXAMPLE 11.2

A monochromatic red laser beam emitting $1 \times 10^{-3} \text{ W}$ at a wavelength of 638 nm is incident on a silicon solar cell. Find

- The number of photons per second incident on the cell
- The maximum possible efficiency of conversion of this laser beam to electricity

Solution

- The laser beam irradiance (I_p), or power, is equal to the energy of all the photons in it per second. If the number of photons per second is N_{ph} , then

$$I_p = N_{ph} \cdot E_p$$

$$1 \times 10^{-3} \text{ W} = N_{ph} \cdot E_p$$

$$E_p = \frac{hc}{\lambda}$$

$$= \frac{(6.625 \times 10^{-34} \text{ J}\cdot\text{s}) \cdot 3 \times 10^8 \text{ m/s}}{638 \times 10^{-9} \text{ m}}$$

$$= 3.12 \times 10^{-19} \text{ J/photon}$$

$$\therefore N_{ph} = \frac{1 \times 10^{-3} \text{ J/s}}{3.12 \times 10^{-19} \text{ J/photon}} = 3.21 \times 10^{15} \text{ photons/s}$$

- Assuming that each photon is able to generate one electron-hole pair, a total number of N_{ph} electron-hole pairs per second will be generated. Therefore, the maximum possible efficiency is

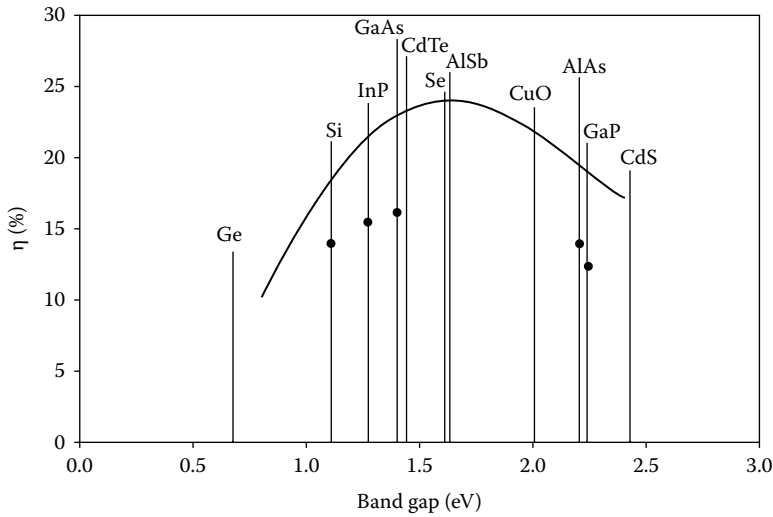
$$\eta_{max} = \frac{(N_{ph}) \cdot (BG)}{(N_{ph}) \cdot E_p} = \frac{BG}{E_p}$$

$$= \frac{1.11 \times 1.6 \times 10^{-19} \text{ J}}{3.12 \times 10^{-19} \text{ J}} = 0.569 \quad \text{or} \quad 56.9\%$$

From the earlier examples, it is clear that for a silicon solar cell, none of the photons of the sunlight with wavelengths greater than 1.12 μm will produce any electricity. However, photons of sunlight with a wavelength of 1.12 μm may be converted to electricity at a maximum efficiency of 100%, while photons at shorter wavelengths will be converted at lower efficiencies. The overall maximum efficiency of a cell can be found by integrating the efficiency at each wavelength over the entire solar spectrum:

$$\eta = \frac{\int \eta_{\lambda} I_{\lambda} d\lambda}{\int I_{\lambda} d\lambda} \quad (11.3)$$

In addition, other factors such as probability of electron–hole recombination reduce the theoretical maximum achievable efficiency of a solar cell. [Figure 11.6](#) shows a comparison of the maximum energy conversion of cells using different materials as well as the optimum band gap for space solar cells, which is on the order of 1.5 eV.

**FIGURE 11.6**

The maximum solar energy conversion efficiency as a function of the energy gap of the semiconductor. The curve has been calculated for an ideal junction outside the atmosphere.

11.2 Analysis of Photovoltaic Cells

This section presents an electrical analysis of photovoltaic cells, which will be useful in the design of photovoltaic devices for various applications. The physics leading to the expressions for the number density of electrons and holes in n and p materials at a temperature T will not be presented here. For such details, the reader is referred to Angrist [3] and Bube [4]. It would suffice to point out here that the net current generated by a photovoltaic cell is a combination of several, often competing, currents that are a function of the incident light intensity and the potential change, or voltage, across the p-n junction. One such current is a light-induced recombination current J_r , which originates from the injection of carriers across the p-n junction, and is given by

$$J_r = J_o \exp\left(\frac{e_o V}{kT}\right) \quad (11.4)$$

where

e_o is the charge of an electron = 1.602×10^{-19} C or J/V

k is Boltzmann's constant = 1.381×10^{-23} J/K

J_o is called the dark, or reverse saturation, current density.

In the dark, the photovoltaic cell behaves like a diode, where current flows easily in one direction but not in the other. The following J-V relationship represents the electrical behavior of an idealized diode.

$$J_j = J_r - J_o = J_o \left[\exp\left(\frac{e_o V}{kT}\right) - 1 \right] \quad (11.5)$$

where V is the applied voltage across the p - n junction and J_o is the reverse saturation current density. In “forward bias”, the applied voltage is positive with respect to the p -type side of the junction, resulting in a reduced potential barrier at the junction, and the flow of electrons from the n -type side to the p -type side of the junction and holes from the p -type side to the n -type side. In “reverse bias”, the applied voltage is negative with respect to the p -type side, the junction potential is increased, and current is restricted to relatively small levels controlled by tunneling and recombination. As we will see below, this “dark” is current opposite in direction to the flow of light-generated current and represents a loss mechanism for the photovoltaic cell.

In the light, photo-excited electrons in the p -type material, and photo-excited holes in the n -type material are driven across the p - n junction resulting in a light-generated current component that is proportional to the incident light intensity. Because the current generated in a photovoltaic device is proportional to the area of the cell (A), it is appropriate to analyze current in terms of the current density J (current per unit area) instead of the current (I). The relationship between the two is

$$I = J \cdot A \quad (11.6)$$

The flow of electrons and holes associated with this light-generated current results in a reduction of the built-in potential drop across the p - n junction or, in other words, a “forward bias condition.” Establishing the convention that the light-generated current is positive, and noting that the voltage driven dark current is opposite in direction results in the following expression for the photovoltaic cell J - V relationship

$$J_L = J_s - J_j = J_s - J_o \left[\exp \left(\frac{e_o V}{kT} \right) - 1 \right] \quad (11.7)$$

where J_s is the short circuit current density.

Referring to [Figure 11.7](#), it is clear that the current generated in the cell has two parallel paths: one through the junction and the other through the external resistance, R_L . [Figure 11.7](#) shows an equivalent circuit of a photovoltaic cell.

For short circuit, $V = 0$ and $J_L = J_s$.

For open circuit, $J_L = 0$ and $V = V_{oc}$ which gives

$$0 = J_s - J_o \left[\exp \left(\frac{e_o V_{oc}}{kT} \right) - 1 \right] \quad (11.8)$$

or

$$V_{oc} = \frac{kT}{e_o} \ln \left(\frac{J_s}{J_o} + 1 \right)$$

[Figure 11.8](#) shows a typical current-voltage (I - V) performance curve of a solar cell. The power output is the product of the load current and voltage and is a function of the load resistance

$$\begin{aligned} P_L &= A J_L V = I_L V \\ &= I_L^2 R_L \end{aligned} \quad (11.9)$$

where A is the area of the cell.

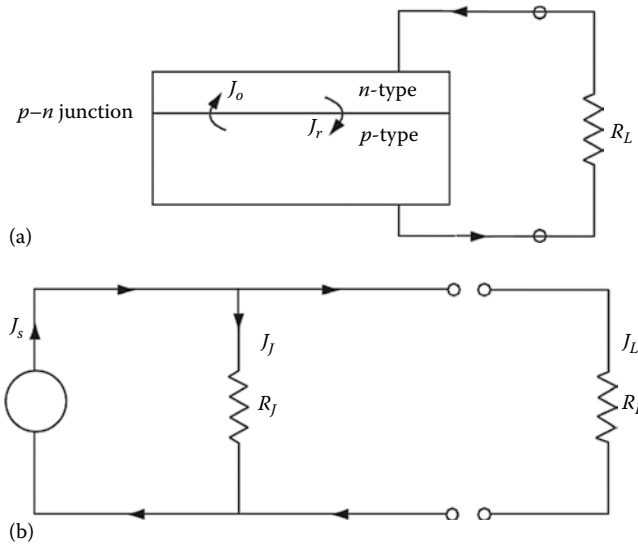


FIGURE 11.7
Equivalent circuit of a photovoltaic cell. (a) p - n junction. (b) Electrical circuit.

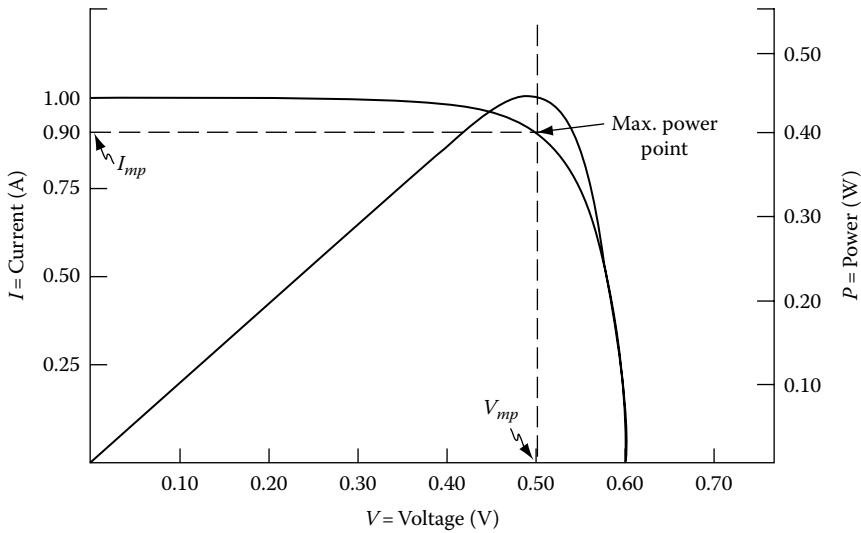


FIGURE 11.8
Typical current, voltage, and power characteristics of a solar cell.

The power output exhibits a maximum. To find the condition for the maximum power output (P_{max}), differentiate P with respect to V and equate it to zero:

$$\exp\left(\frac{e_0 V_m}{kT}\right) \left(1 + \frac{e_0 V_m}{kT}\right) = 1 + \frac{J_s}{J_o} \quad (11.10)$$

where V_m stands for voltage at maximum power. The current at maximum power condition $J_{L,m}$ and the maximum power P_{max} can be found from Equations 11.7 and 11.9, respectively.

$$J_{L,m} = J_s - J_o \left[\exp \left(\frac{e_o V_m}{kT} \right) - 1 \right] \quad (11.11)$$

Combining Equation 11.10 and 11.11, $J_{L,m}$ is found to be

$$J_{L,m} = \frac{e_o V_m / kT}{1 + (e_o V_m / kT)} (J_s + J_o) \quad (11.12)$$

$$P_{max} = \frac{e_o V_m^2 / kT}{1 + (e_o V_m / kT)} (J_s + J_o) \cdot A \quad (11.13)$$

Figure 11.9 shows the effect of illumination intensity and the load resistance on the performance of a silicon cell. Temperature also affects the performance in such a way that the voltage and thus the power output decrease with increasing temperature.

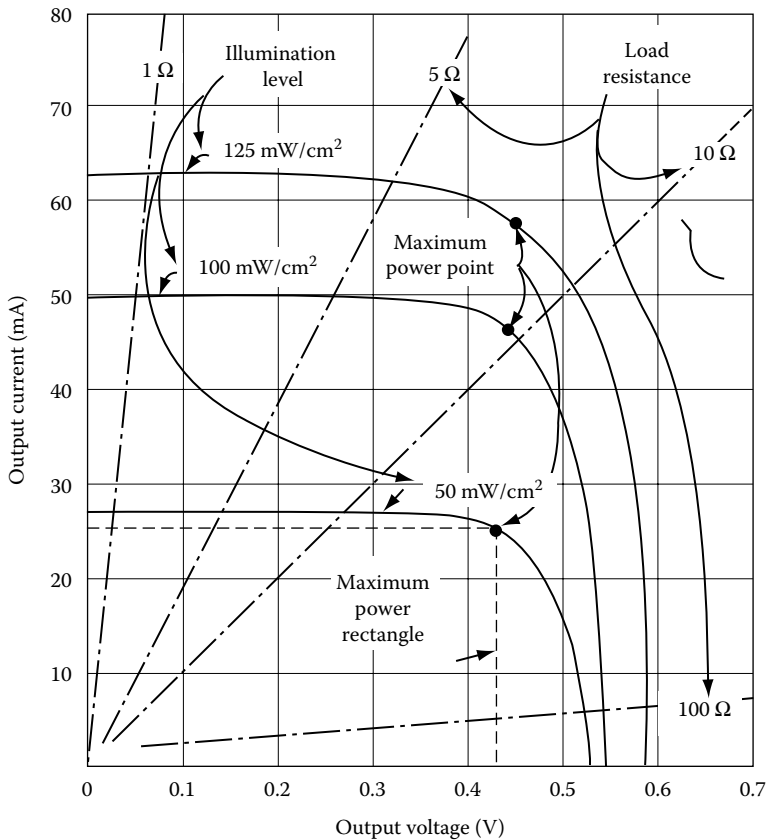


FIGURE 11.9

Typical current-voltage characteristics of a silicon cell showing the effects of illumination level and load resistance.

EXAMPLE 11.3

The dark saturation current density for a silicon solar cell at 40°C is $1.8 \times 10^{-8} \text{ A/m}^2$ and the short circuit current density is 200 A/m^2 when exposed to solar radiation of 900 W/m^2 . Calculate

- Open circuit voltage
- Voltage at maximum power
- Current density at maximum power
- Maximum power
- Maximum efficiency
- The cell area required for an output of 25 W

Solution

Given

$$J_o = 1.8 \times 10^{-8} \text{ A/m}^2$$

$$J_s = 200 \text{ A/m}^2$$

and

$$T = 40^\circ\text{C} = 313 \text{ K}$$

- Using Equation 11.8,

$$V_{oc} = \frac{kT}{e_o} \ln \left(\frac{J_s}{J_o} + 1 \right)$$

Since (e_o/kT) will be needed for other parts of the problem solution, it will be evaluated separately:

$$\frac{e_o}{kT} = \frac{1.602 \times 10^{-19} \text{ J/V}}{(1.381 \times 10^{-23} \text{ J/K})(313 \text{ K})} = 37.06 \text{ V}^{-1}$$

Therefore,

$$V_{oc} = \frac{1}{37.06} \ln \left(\frac{200}{1.8 \times 10^{-8}} + 1 \right) = 0.624 \text{ V}$$

- Voltage at maximum power condition can be found from Equation 11.10 by an iterative or trial-and-error solution:

$$\exp(37.06 V_m)(1 + 37.06 V_m) = 1 + \frac{200}{1.8 \times 10^{-8}}$$

or $V_m = 0.542 \text{ V}$

- Current density at maximum power can be found from Equation 11.12:

$$\begin{aligned} J_{L,m} &= \frac{e_o V_m / kT}{1 + (e_o V_m / kT)} (J_s + J_o) \\ &= \frac{(37.06) \cdot (0.542)}{1 + (37.06) \cdot (0.542)} (200 + 1.8 \times 10^{-8}) \text{ A/m}^2 \\ &= 190.5 \text{ A/m}^2 \end{aligned}$$

d. From Equation 11.13, the maximum power is

$$\begin{aligned} P_{max} &= V_m \cdot J_m \cdot A \\ \frac{P_{max}}{A} &= (0.542 \text{ V}) \cdot (190.5 \text{ A/m}^2) \\ &= 103.25 \text{ W/m}^2 \end{aligned}$$

e. The maximum efficiency is

$$\eta_{max} = \frac{103.25 \text{ W/m}^2}{900 \text{ W/m}^2} = 11.5\%$$

f. Cell area required

$$\begin{aligned} A &= \frac{P_{out}}{P_{max}/A} = \frac{25 \text{ W}}{103.25 \text{ W/m}^2} \\ &= 24.2 \text{ cm}^2 \end{aligned}$$

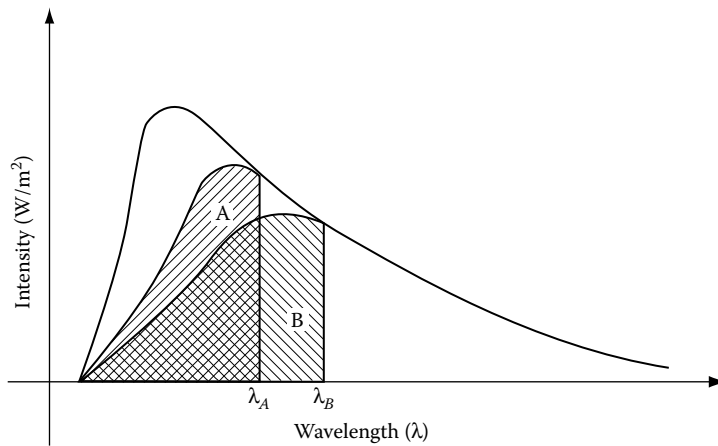
11.2.1 Efficiency of Solar Cells

Theoretical limitation on the efficiency of a single-layer solar cell can be calculated using Equation 11.3. These efficiency limitations and the practical efficiencies of some of the cells are shown in [Figure 11.6](#). Some of the reasons for the actual efficiency being lower than the theoretical limitation are

1. Reflection of light from the surface of the cell. This can be minimized by the use of an antireflection (AR) coating. For example, AR coating can reduce the reflection from a Si cell from 30% from an untreated cell to 3%.
2. Shading of the cell due to current collecting electrical contacts. This can be minimized by reducing the area of the contacts and/or making them transparent; however, both of these methods will increase the resistance of the cell to current flow.
3. Internal electrical resistance of the cell.
4. Recombination of electrons and holes before they can contribute to the current.

11.2.2 Multijunction Solar Cells

The limits imposed on single-layer solar cells due to band gap can be partially overcome by using multiple layers of solar cells stacked on top of each other, with each layer having a band gap higher than the layer below it. For example ([Figure 11.10](#)), if the top layer is made from a cell of material A (band gap corresponding to λ_A), solar radiation with wavelengths less than λ_A would be absorbed to give an output equal to the hatched area A [7]. The solar radiation with wavelength greater than λ_A would pass through A and be converted by the bottom layer cell B (band gap corresponding to λ_B) to give an output equal to the hatched area B. The total output and therefore the efficiency of this tandem cell would be higher than the output and the efficiency of each single cell individually because of a reduction in the thermalization losses discussed above. Theoretically, the conversion efficiency will

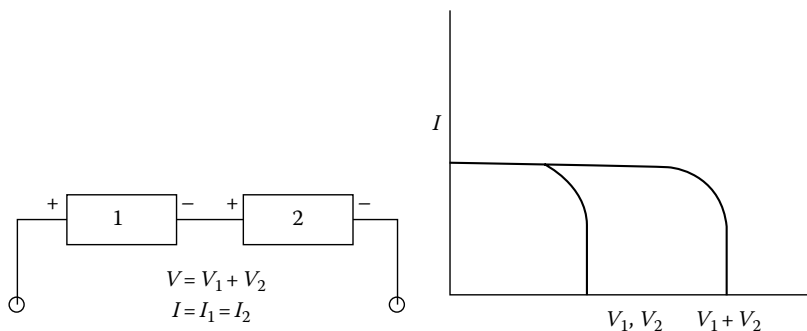
**FIGURE 11.10**

Energy conversion from a two-layered stacked cell. (From Goswami, Y. et al., 2000. *Principles of Solar Engineering*, 2nd ed., Taylor & Francis, Philadelphia, PA. With permission. [7])

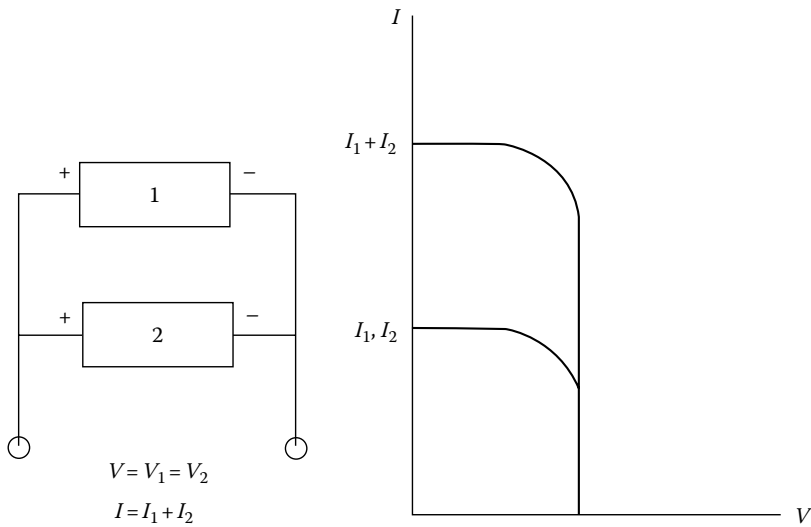
continue to increase with the number of solar cells within the multijunction device. In practice, additional cells create additional complexity and additional cost that make this approach more suitable for applications that are less sensitive to cost relative to other properties (e.g., satellites), or system designs aimed at minimizing the photovoltaic device area (e.g., concentrators).

11.2.3 Design of a Photovoltaic System

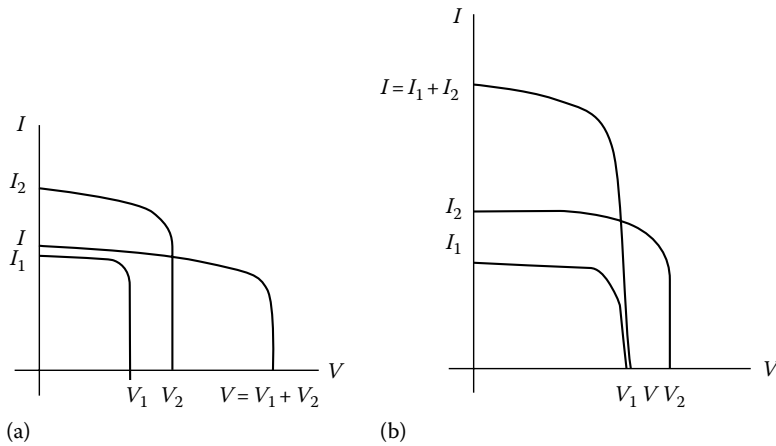
Solar cells may be connected in series, parallel, or both to obtain the required voltage and current. When similar cells or devices are connected in series, the output voltages and current are as shown in Figure 11.11. A parallel connection results in the addition of currents, as shown in Figure 11.12. If the photovoltaic devices have dissimilar characteristics, the output characteristics will be as shown in Figure 11.13. Cells are connected to form modules, modules are connected to form panels, and panels are connected to form arrays. Principles shown in Figures 11.11 and 11.12 apply to all of these connections.

**FIGURE 11.11**

Characteristics of two similar cells connected in series.

**FIGURE 11.12**

Characteristics of two similar cells connected in parallel.

**FIGURE 11.13**

Characteristics of two dissimilar cells connected in (a) series and (b) parallel.

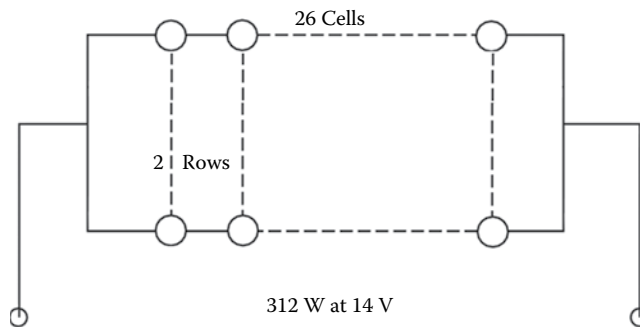
EXAMPLE 11.4

An application requires 300 W at 14 V. Design a PV panel using solar cells from Example 11.3 each with an area of 25 cm².

Solution

Assuming that the cell will be operated at maximum power conditions, the voltage and current from each cell are

$$V_m = 0.542 \text{ V}, \quad I_m = \left(190.5 \frac{\text{A}}{\text{m}^2} \right) (0.0576 \text{ m}^2) = 10.97 \text{ A}$$

**FIGURE 11.14**

Connection of cells in rows and columns for Example 11.4.

$$\text{Power/cell} = 0.542 \text{ V} \times 10.97 \text{ A} = 5.95 \text{ W/cell} \approx 6 \text{ W/cell}$$

$$\text{Number of cells required} = \frac{300 \text{ W}}{6 \text{ W/cell}} = 50 \text{ cells}$$

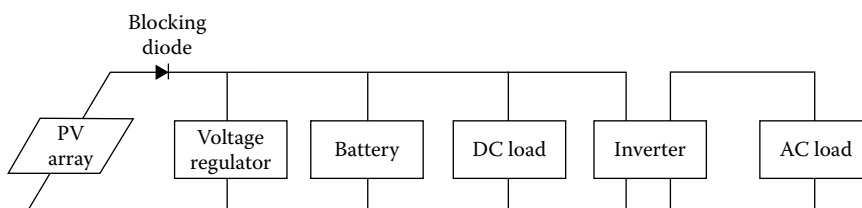
$$\text{Number of cells in series} = \frac{\text{System voltage}}{\text{Voltage/cell}} = \frac{14 \text{ V}}{0.542 \text{ V}} \approx 26$$

$$\text{Number of rows of 26 cells connected in parallel} = \frac{50}{26} = 1.92 \approx 2$$

Since the number of rows must be a whole number, we may increase the number to 2 rows, which will give 312 W output (Figure 11.14).

A blocking diode is used in series with a module or an array to prevent the current from flowing backward (for example, from the battery to the cells under dark conditions). A bypass diode is used in parallel with a module in an array to bypass the module if it is shaded. A photovoltaic system may be connected to a DC or an AC load, as shown in Figure 11.15.

The nameplate rating for a PV system is in terms of the DC output. When the load requires an AC current, an inverter is required between the DC output and the AC load as shown in Figure 11.15. The inverter is a source of energy loss that decreases the net output of a PV system. There are a number of different inverters available, and the selection of the appropriate inverter for a given application depends on the requirements of the load, particularly the waveform, and on whether the system is grid-connected or stand-alone.

**FIGURE 11.15**

Schematic of a PV system.

TABLE 11.3

Inverter Characteristics

Parameter	Square Wave	Modified Sine Wave	Pulse Width Modulated	Sine Wave ^a
Output power range (W)	Up to 1,000,000	Up to 5000	Up to 20,000	Up to 500,000
Surge capacity (multiple of rated output power)	Up to 20 times	Up to 4 times	Up to 2.5 times	Up to 4 times
Typical efficiency over output range	70%–98%	>90%	>90%	>90%
Harmonic distortion	Up to 40%	>5%	<5%	<5%

Source: Messenger, R.A. and Ventre, J., 2010. *Photovoltaic Systems Engineering*, 3rd ed., CRC Press, Boca Raton, FL [8]; Data from Sandia National Laboratories, 1991. *Maintenance and Operation of Stand-Alone Photovoltaic Systems*, Albuquerque, NM, <http://www-satcon.com/> (Information on Satcon PV Inverters. With permission. [9])

^a Multilevel H-bridge or similar technology to yield utility-grade sine wave output.

Table 11.3 summarizes currently available types of inverters [8,9]. The performance of inverters is usually stated in terms of the rated power output, the surge capacity, the efficiency, and the harmonic distortion. Some loads have significant starting currents, and it is therefore important to provide adequate surge current capacity in the inverter to avoid overheating.

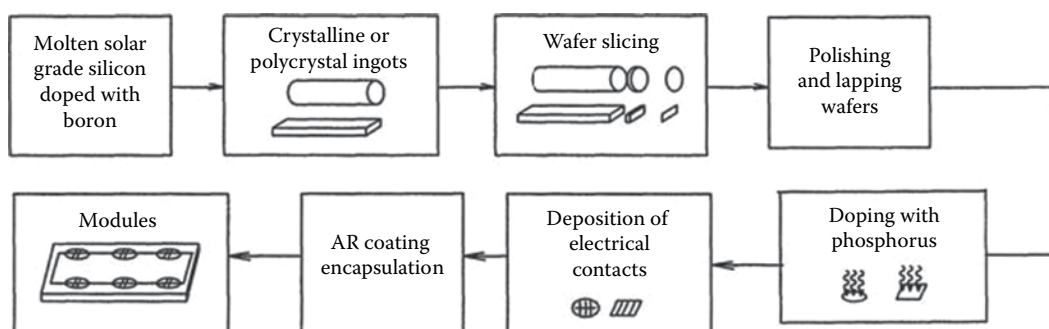
In selecting the appropriate inverter, some general observations are helpful. The square-wave inverter is the least expensive and is relatively efficient. It also has the best surge capacity, but suffers from harmonic distortion. The modified sine converter is fairly efficient but more complicated and expensive. The pulse-width modulated inverter is the most expensive, has the highest efficiency, and minimal distortion. The pure sine inverter has the least distortion and has the highest efficiency. Specifications of the losses incurred by an inverter for an AC load are included in the PV watts calculation illustrated later in the chapter. Detailed information about inverter construction and selection can be found in Messenger and Ventre [8].

*11.3 Manufacture of Solar Cells and Panels

Manufacture of crystalline silicon solar cells is an outgrowth of the manufacturing methods used for microprocessors. A major difference is that silicon used in microprocessors is ultra pure, which is not needed for photovoltaic cells. Therefore, a major source of feedstock for silicon solar cells has been the waste material from the microelectronics industry. Solar cells are also manufactured as polycrystalline and thin films. Some of the common methods of manufacture of silicon solar cells are provided in the following text.

11.3.1 Single Crystal and Polycrystalline Cells

Single-crystal silicon cells are produced by a series of processes: (1) growing crystalline ingots of *p*-silicon, (2) slicing wafers from the ingots, (3) polishing and cleaning the surface, (4) doping with *n* material to form the *p*–*n* junction, (5) deposition of electrical contacts, (6) application of AR coating, and (7) encapsulation. Figure 11.16 illustrates the process.

**FIGURE 11.16**

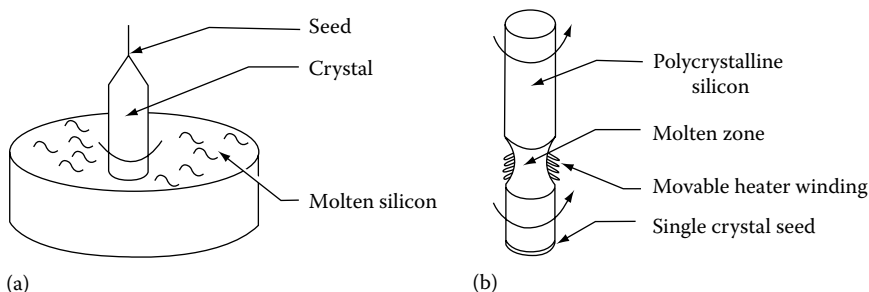
Series of processes for the manufacture of crystalline L polycrystalline cells.

The *Czochralski* method (Figure 11.17a) is the most common method of growing single-crystal ingots. A seed crystal is dipped in molten silicon doped with a *p*-material (boron) and drawn upward under tightly controlled conditions of linear and rotational speed, and temperature. This process produces cylindrical ingots of typically 10 cm diameter, although ingots of 20 cm diameter and more than 1 m long can be produced for other applications. An alternative method is called the *float zone* method (Figure 11.17b). In this method, a polycrystalline ingot is placed on top of a seed crystal and the interface is melted by a heating coil around it. The ingot is moved linearly and rotationally, under controlled conditions. This process has the potential to reduce the cell cost.

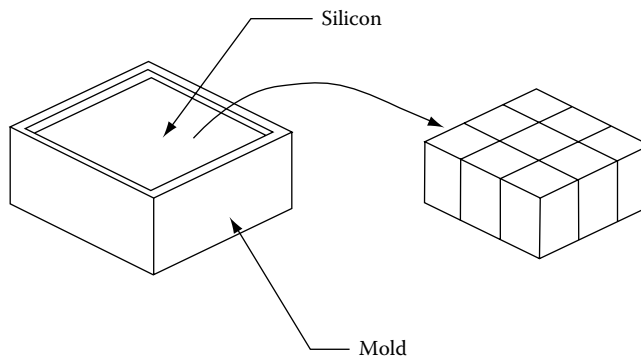
Polycrystalline ingots are produced by casting silicon in a mold of preferred shape (rectangular), as shown in Figure 11.18. Molten silicon is cooled slowly in a mold along one direction in order to orient the crystal structures and grain boundaries in a preferred direction. In order to achieve efficiencies of greater than 10%, grain sizes greater than 0.5 mm are needed, and the grain boundaries must be oriented perpendicular to the wafer. Ingots as large as $400 \times 40 \times 40$ can be produced by this method.

Ingots are sliced into wafers by internal diameter saws with slurry-based cutting elements or multiwire saws impregnated with diamond abrasive particles. Both of these methods result in high wastage of valuable crystalline silicon.

Alternative methods that reduce wastage are those that grow polycrystalline *thin films*. Some of the thin-film production methods include dendritic web growth (Figure 11.19), edge-defined film-fed growth (EFG) (Figure 11.20), ribbon against drop method, supported web method, and ramp-assisted foil casting technique (RAFT) (Figure 11.21).

**FIGURE 11.17**

Crystalline silicon ingot production methods: (a) *Czochralski* method and (b) *float zone* method.

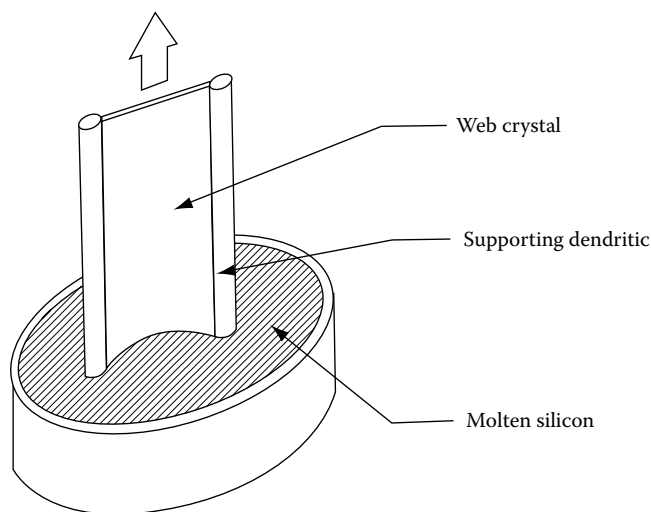
**FIGURE 11.18**

Polycrystalline ingot production.

A p - n junction is formed in the cell by diffusing a small amount of n material (phosphorous) in the top layer of a p -silicon wafer. The most common method is diffusion of phosphorous in the vapor phase. In this case, the backside of the wafer must be covered to prevent the diffusion of vapors from that side. An alternate method is to deposit a solid layer of the dopant material on the top surfaces followed by high-temperature (800°C – 900°C) diffusion.

Electrical contacts are attached to the top surface of the cell in a grid pattern to cover no more than 10% of the cell surface, and a solid metallic contact is made on the back. The front grid pattern is made by either vacuum metal vapor deposition through a mask, by electroplating, or by screen printing. [Figure 11.22](#) shows how cells are connected to form modules.

AR coatings of materials such as silicon dioxide (SiO_2), titanium dioxide (TiO_2), and tantalum pentoxide (Ta_2O_5) can be deposited on the cell surface to reduce reflection from more than 30% for untreated Si to less than 3%. Silicon nitride is the most common AR coating for conventional solar cells in mass production. AR coatings are deposited by

**FIGURE 11.19**

Thin-film production by dendritic web growth.

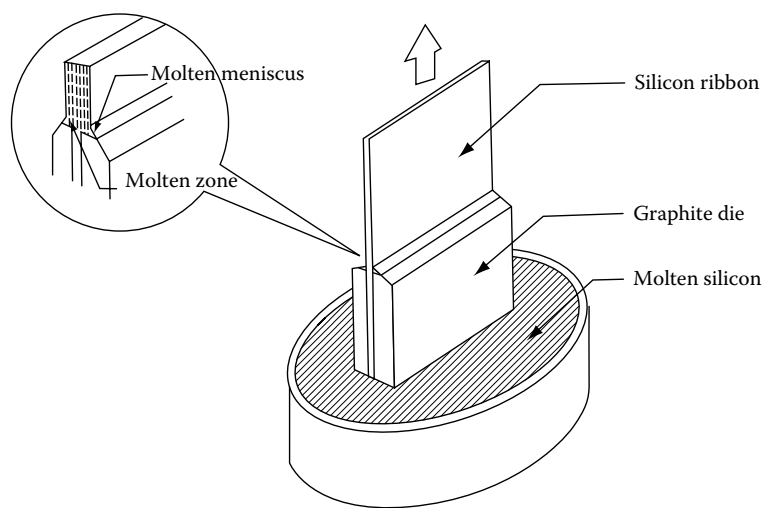


FIGURE 11.20
Thin-film production by edge-defined film-fed growth (EFG).

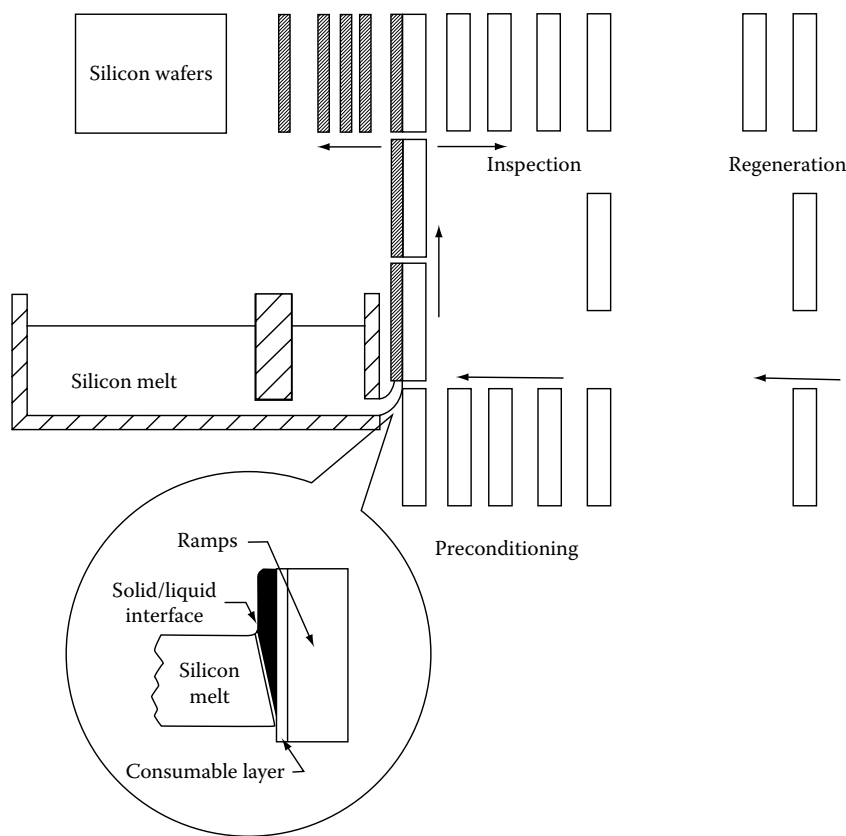
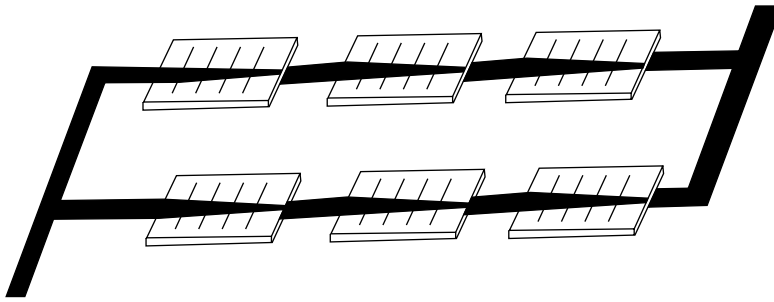


FIGURE 11.21
Schematic of RAFT processing.

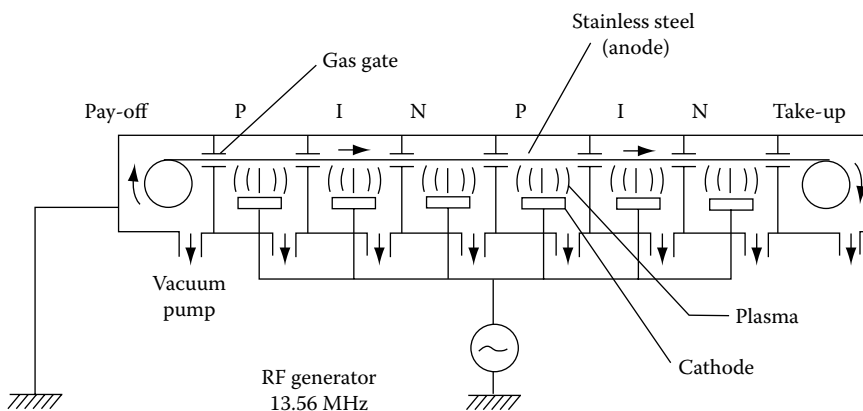
**FIGURE 11.22**

Assembly of solar cells to form a module.

vacuum plasma enhanced chemical vapor deposition (PECVD), sputtering, or chemical spraying. Finally, the cells are encapsulated in a transparent material to protect them from the environment. Encapsulants usually consist of a layer of either polyvinyl butyral or ethylene vinyl acetate and are placed on both sides of the solar cell. A top layer of low iron glass and a bottom layer of another sheet of glass or backsheet completes the process of assembling solar cells into modules.

11.3.2 Amorphous Silicon

Amorphous silicon (*a*-Si) cells are made as thin films of *a*-Si:H alloy doped with phosphorous and boron to make *n* and *p* layers, respectively. The atomic structure of an *a*-Si cell does not have any preferred orientation. The cells are manufactured by depositing a thin layer of *a*-Si on a substrate (glass, metal, or plastic) from glow discharge, sputtering, or chemical vapor deposition (CVD) methods. The most common method is by an RF glow discharge decomposition of silane (SiH_4) on a substrate heated to a temperature of 200°C – 300°C . To produce *p*-silicon, diborane (B_2H_6) vapor is introduced with the silane vapor. Similarly, phosphine (PH_3) is used to produce *n*-silicon. The cell consists of an *n*-layer, an intermediate undoped *a*-Si layer, and a *p*-layer on a substrate. The cell thickness is about $1\ \mu\text{m}$. The manufacturing process can be automated to produce rolls of solar cells from rolls of substrate. Figure 11.23 shows an example of roll-to-roll *a*-Si cell manufacturing equipment

**FIGURE 11.23**

A schematic diagram of a roll-to-roll plasma CVD machine.

using a plasma CVD method. This machine can be used to make multifunction or tandem cells by introducing the appropriate materials at different points in the machine.

11.4 Design for Remote Photovoltaic Applications

Photovoltaic power may be ideal for a remote application requiring a few watts to hundreds of kilowatts of electrical power. Even where a conventional electrical grid is available, for some applications, where uninterruptible or emergency standby power is necessary, photovoltaic power would be appropriate. Some examples of remote PV applications include water pumping for potable water supply and irrigation, power for remote houses, street lighting, battery charging, telephone and radio communication relay stations, and weather stations. Examples of some other applications include electrical utility switching stations, peak electrical utility power where environmental quality is a concern, data acquisition systems, and specialty applications such as ventilation fans and vaccine refrigeration.

The design of a PV system is based on some basic considerations for the application:

1. Which is more important, the daily energy output or the power (average or peak)?
2. Is a backup energy source needed and/or available?
3. Is energy storage important? What type—battery, pumped water, etc.?
4. Is the power needed as AC or DC? What voltage?

There are three basic steps in the design of a PV system:

1. Estimation of load and load profile
2. Estimation of available solar radiation
3. Design of PV system, including area of PV panels, selection of other components, and electrical system schematic

Each of these steps will be explained in the following examples. These examples are based on Peng and Yang [2] and Post and Risser [10].

11.4.1 Estimation of Loads and Load Profiles

Precise estimation of loads and their timings (load profile) are important for PV systems since the system is sized as the minimum required to satisfy the demand over a day. For example, if power is needed for five different appliances requiring 200, 300, 500, 1000, and 1500 W, respectively, so that only one appliance is on at any one time and each appliance is on for an average of 1 h a day, the PV system would be sized based on 1500 W peak power and 3500 Wh of daily energy requirement. The multiple loads on a PV system are intentionally staggered to use the smallest possible system, since the capital costs of a PV system are the most important as opposed to the energy costs in a conventional fuel-based system.

EXAMPLE 11.5: DAILY LOAD CALCULATIONS

How much energy per day is used by a remote weather station given the following load characteristics?

Load	Load Power (W)	Run Time (h/day)
Charge controller	2.0	8
Data gathering	4.0	3
Modem (standby)	1.5	22.5
Modem (send/receive)	30.0	1.5

Solution

$$\begin{aligned}\text{Daily energy} &= (2.0\text{ W})(8\text{ h}) + (4.0\text{ W})(3\text{ h}) + (1.5\text{ W})(22.5\text{ h}) \\ &\quad + (30.0\text{ W})(1.5\text{ h}) = 106.75\text{ Wh}\end{aligned}$$

Daily energy use is about 107 Wh/day.

EXAMPLE 11.6: LOAD CALCULATIONS

An owner of a remote cabin wants to install a PV power system. The loads in the home are described as follows. Assume that water pump and bathroom fan are DC and all others are AC. Find the daily and weekly peak and average energy use estimates. The system used is a 24 V DC system with an inverter.

Lights	4 23 W compact fluorescent bulbs	On at night for 5 h
Lights	6 13 W compact fluorescent bulbs	2 h each (daytime)
Stereo	110 W (amplifier), 15 W (other)	On for 8 h per week
Water pump	55 W (3.75 A start current)	Runs for 2 per day
Computer	250 W (monitor included)	On for 1½ h daily (weekend nights only)
Bathroom fan	40 W (3.5 A start current)	On for 1 h per day
Microwave	550 W (AC)–1000 W surge	On for 30 min per day

Solution

Loads need to be broken down according to (1) run time, (2) peak power, (3) night or day use, and (4) AC or DC loads. The load profile is as follows:

Load Name Description	Power (W)		Run Time (h)		Energy (Wh)	
	Average	Peak	Day	Week	Day	Week
Lights (AC)	(4) (23)	(4) (23)	5.0	35	460	3220
Lights (AC)	(6) (13)	(6) (13)	2.0	14	156	1092
Stereo (AC)	(1) (125)	(1) (125)	—	8	—	1000
Pump (DC)	(1) (55)	(3.75 A) (24 V)	2.0	14	110	770
Computer (AC)	(1) (250)	(1) (250)	1.5	3	—	750
Fan (DC)	(1) (40)	(3.5 A) (24 V)	1.0	7	40	280
Microwave (AC)	(1) (550)	(1) (1000)	0.5	3.5	275	1925

Average DC load: $[770 + 280]/7 = 150$ Wh/day.

Average AC load: $[3220 + 1092 + 1000 + 750 + 1925]/7 = 1141$ Wh/day.

Peak DC load: $\max [(3.5)(24) + 55]; [(3.75)(24) + 40] = 139$ W.

Peak AC load: $(1000) + \max [(4)(23); (6)(13)] + 250 + 125 = 1467$ W.

It can be assumed that the pump and fan will not start precisely at the same instant and that the night- and daylighting loads will not be on simultaneously.

11.4.2 Estimation of Available Solar Radiation

Methods of estimation of available solar radiation are described in [Chapter 10](#). Websites such as the National Solar Radiation Data Base [11] are useful resources for accurate approximations. For designing a PV system, a decision is made whether the PV panel will be operated as tracking the sun or will be fixed at a certain tilt and azimuth angle. For fixed panels, a tilt angle of latitude $+15^\circ$ works best for winter and latitude -15° for summer. To keep the panel fixed year-round, an angle equal to the latitude provides the maximum yearly energy (see [Figure 11.24](#)).

11.4.3 PV System Sizing

If meeting the load at all times is not critical, PV systems are usually sized based on the average values of energy and power needed, available solar radiation, and component efficiencies. This is known as the *heuristic approach*. It is important to note that a system designed by this approach will not give the best design but may provide a good start for a detailed design. A detailed design accounts for the changes in the efficiencies of the components depending on the load and the solar radiation availability and whether the system is operating in a PV-to-load, PV-to-storage, or storage-to-load mode.

EXAMPLE 11.7: HEURISTIC APPROACH TO PV-SYSTEM SIZING

A PV system using 50 W, 12 V panels with Trojan T-105 6 V, 125 Ah batteries is needed to power a home in Farmington, New Mexico, with a daily load of 1700 Wh. System voltage is 24 V. Assuming an average of 5 daylight hours in the winter, specify the collector and storage values for the system using the heuristic approach.

Solution

Load = 1700 Wh/day

Daylight hours = 5 h/day

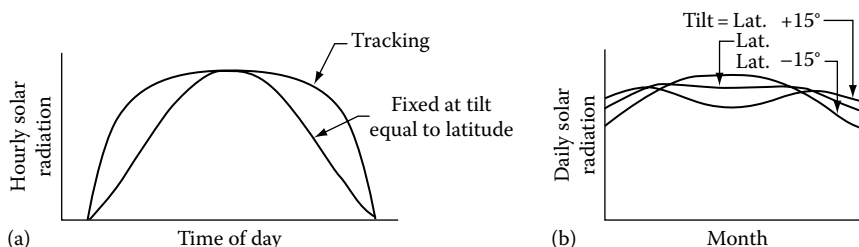


FIGURE 11.24

Solar radiation on panels at different tilt angles: (a) hourly and (b) monthly.

Average panel output = 50 W

$$\text{Number of panels} = \frac{1700 \text{ Wh/day}}{(5 \text{ h/day})(50 \text{ W/panel})} = 6.8, \text{ round off to 7 panels}$$

Since the system voltage is 24 V, but each panel produces only 12 V, an even number of panels will be needed. Therefore, the number of panels = 8.

Farmington, New Mexico, is a very sunny location, so 3 days of storage are sufficient. Assuming a battery efficiency of 75% and a maximum depth of discharge of 70%,

$$\text{Storage} = (1700)(3)/(0.75 \times 0.7) = 9714 \text{ Wh}$$

$$\begin{aligned} \text{Number of batteries} &= (9714 \text{ Wh})/(125 \text{ Ah} \times 6 \text{ V}) \\ &= 13 \text{ (rounded off to the next whole number)} \end{aligned}$$

Since the system voltage is 24 V, and each battery provides 6 V, the number of batteries is increased to 16. In a detailed design, the efficiencies of battery storage, inverter, and the balance of system (BOS) must be accounted for. The following example shows how these efficiencies increase the energy requirements of the PV panel.

EXAMPLE 11.8: SYSTEM OPERATING EFFICIENCY

Using the cabin electrical system from Example 11.6, calculate the overall system efficiency for each operating mode possible for the system. Estimate the amount of energy required per day for the system. When load timing (day or night), assume half of the load runs during the day and half runs at night. The inverter used has a component efficiency of 91%, the battery efficiency is 76%, and the distribution system efficiency is 96%.

Solution

From the example, the loads are

Average DC load: 150 Wh/day
Average AC load: 1141 Wh/day

The various system efficiencies are

PV to load (DC):	0.96 (day, DC)
Battery to load (DC):	(0.76) (0.96) = 0.73 (night, DC)
PV to load (AC):	(0.96) (0.91) = 0.874 (day, AC)
Battery to load (AC):	(0.76) (0.91) (0.96) = 0.664 (night, AC)

Expected day and night loads are

Day (DC):	(0.5) (110) + (0.5) (40) = 75 Wh/day
Night (DC):	(0.5) (110) + (0.5) (40) = 75 Wh/day
Day (AC):	(156) + (0.5) (1000 + 750)/7 + (0.5) (275) = 418.5 Wh/day
Night (AC):	(460) + (0.5) (1000 + 750)/7 + (0.5) (275) = 722.5 Wh/day

Without considering system efficiency, the daily energy requirement is

$$E_{\text{day}} = (150) + (1141) = 1291 \text{ Wh/day}$$

The expected daily energy requirement is

$$E_{day} = \frac{75}{0.96} + \frac{75}{0.73} + \frac{418.5}{0.874} + \frac{722.5}{0.664}$$

$$E_{day} = 1725 \text{ Wh/day}$$

The actual energy requirement is 34% higher than that obtained in the approximate calculation in Example 11.6.

11.4.4 Water Pumping Applications

Water pumping for drinking water or irrigation at remote locations is an important application of PV. For a simple schematic shown in [Figure 11.25](#), the power needed to pump water at a volumetric rate \dot{V} is given by $\rho \dot{V} g H / \eta_p$ where ρ is the density of water, g is the acceleration due to gravity, H is the head loss the pump must overcome, and η_p is the pump efficiency. The static head H_s is $(A + B)$. In the case that the water level is drawn down, the static head would be $(A + B + C)$. The pump must work against the total head H , which includes the static head, the frictional losses in the pipe and fittings, and the dynamic head:

$$H = H_s + H_f + \frac{v^2}{2g} \quad (11.14)$$

where

H_f is the frictional head loss in the pipe and the bends

v is the velocity of the water at the pipe outlet

The pump efficiency η_p is a function of the load (head and flow rate) and is available as a characteristic curve from the manufacturer. There are two basic types of pumps: centrifugal

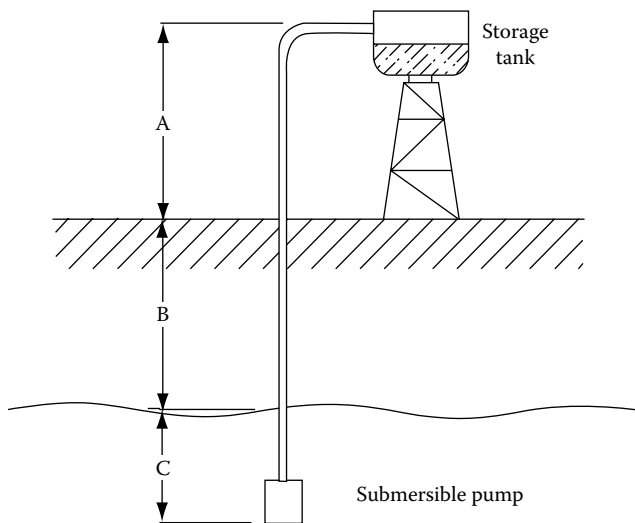


FIGURE 11.25

Water pumping using a submersible pump.

and positive displacement. These pumps can be driven by AC or DC motors. DC motors are preferable for the PV applications, because they can be directly coupled to the PV array output. Centrifugal pumps with submersible motors are the optimum for PV applications because of their efficiency, reliability, and economy. However, for deep wells, Jack pumps may be necessary. Jack pumps are the piston type of positive displacement pumps that move chunks of water with each stroke. They require very large currents; therefore, they are connected through batteries.

11.5 Thin-Film PV Technology

Monocrystalline and multicrystalline PV dominate the PV market. They represent over 90% of PV shipments worldwide [12]. Advances continue to be made, however, in thin film PV technologies. Because they are thinner and often flexible, they offer a wide range of applications including building-integrated photovoltaics and portable power systems as well as rooftop and utility-scale applications.

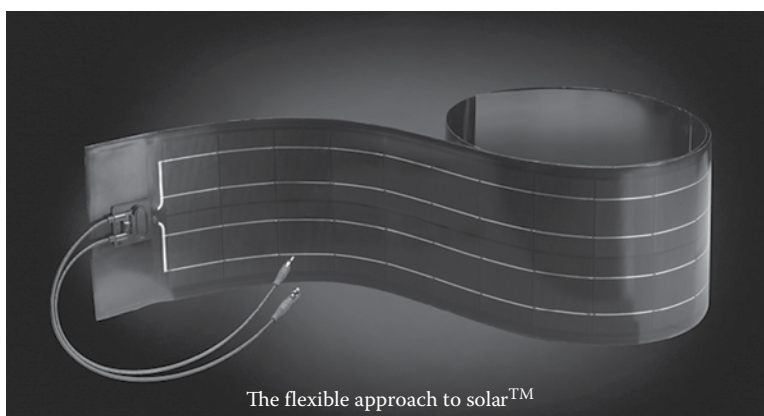
Thin-film PV cells require multiple layers of precisely deposited thin films. An important criterion for the production of thin-film PV in a continuous process, such as a roller coater, is the percentage of the output that has an acceptable efficiency. The three primary thin-film PV technologies currently on the market are amorphous silicon (*a-Si*), cadmium telluride (*CdTe*), and copper indium gallium diselenide (*CIGS*). Each of these technologies has advantages and disadvantages, and the differences between these technologies are described briefly in the following text.

Amorphous silicon PV technology utilizes a widely available material, but the cells have a relatively low efficiency. Amorphous silicon cells have a maximum theoretical efficiency of 28%. An amorphous silicon cell prepared within a laboratory environment at the NREL achieved an efficiency of 13.6%. Small research cells that set records in a laboratory environment are called “champion cells.” However, commercial production efficiencies for amorphous silicon typically only range from 6% to 10%. Furthermore, the capital equipment costs for manufacturing thin-film amorphous silicon are generally higher than that for other thin-film technologies.

Cadmium telluride (CdTe) thin-film PV modules have made impressive advances.

CdTe cells have a maximum theoretical efficiency of 28%. CdTe champion cells produced by First Solar have achieved efficiencies as high as 22.1% [13]. Commercially, the production efficiencies for CdTe PV modules range from 13 to 18%. One U.S. manufacturer of CdTe modules, First Solar, often appears in the list of the top 10 global PV producers. CdTe thin films have the advantages of low material costs and handling requirements associated with the manufacturing process. However, current production processes are limited to glass substrates, which are more limited in their applications than flexible films that can be used in buildings/integrated photovoltaic products, and can often be used to replace conventional building materials in some parts of a building.

Copper indium diselenide (CIS) and gallium-alloyed CIS (CIGS) photovoltaic products are commercially developed, and as many as 10 different deposition methods for growing the thin CIS/CIGS absorber layers are being pursued. CIS/CIGS PV modules have the best efficiency characteristics of the three technologies. A champion cell achieved an efficiency of 22.3%. CIS/CIGS technology utilizes less raw material than the other two technologies and, therefore, achieves lower film thicknesses. Moreover, CIS/CIGS films have highlighted

**FIGURE 11.26**

Thin-film flexible photovoltaic CIGS module. (Courtesy of SoloPower, Inc., San Jose, CA. With permission.)

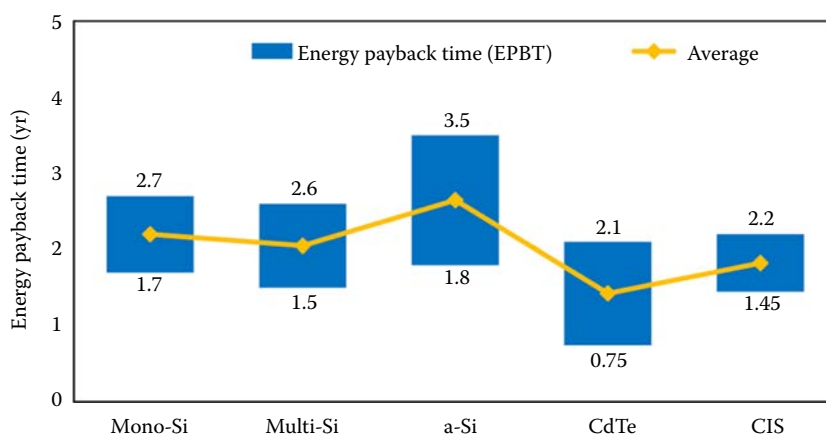
absorption capabilities. This technology appears to combine the highest solar conversion radiation efficiency with low manufacturing costs and the potential of being mass-produced with flexible substrates (see [Figure 11.26](#)).

The production of CIGS solar cells requires deposition of molybdenum, copper, indium, gallium, selenium, a junction layer (e.g., cadmium sulfide or zinc sulfide), and a transparent conductive oxide (TCO) onto a substrate. These manufacturing techniques are very demanding in accuracy, and a variety of different processes are under development. All current CIGS processes use sputtering during the molybdenum and TCO deposition steps. But the other CIGS compounds can be deposited with different technologies, including thermal evaporation, electrochemical plating, nanoparticle printing, or sputtering. The details of these technologies are under active development, and their eventual success will determine the cell efficiencies and cost achievable. A brief description of each of the four major deposition technologies is given as follows.

Sputtering: Sputtering is used extensively in the semiconductor industry to deposit thin films of various materials. The technology is a physical vapor deposition (PVD) method that deposits thin films by ejecting (called “sputtering”) material from a “target” that is a source that then deposits onto a substrate such as a silicon wafer. Sputtering is used for high-volume and high-production manufacturing and has been proven effective in industrial-scale processes of coating glass and plasma display production. In this process, ions or reactive gases dislodge atoms from a solid plate of elements, which are deposited on an adjacent substrate. Targets in the PV industry are made up of materials such as CIS/CIGS and are attached to a reusable black back-plate installed within the PVD system.

Thermal evaporation: This is a commonly used CIS/CIGS deposition technique. For this process, elements are heated in a vacuum and the resulting condensing vapor transfers these elements onto a substrate. Materials for this process are easy to obtain and use, but the process is often inefficient as far as material utilization is concerned, and it is difficult to control for the uniformity of deposition on large areas. Hence, the percent of spoilage can be large, although recent developments may improve this. The thermal evaporation process is also costly.

Electrochemical plating: In this process, a base metal is covered with a thin film of CIS/CIGS or Cd/Te by submersing the substrate in a chemical solution through which an electric current flows. Although electrochemical plating has a high material utilization, the process

**FIGURE 11.27**

Energy payback times for the different types of PV systems. (From Peng, L. and Yang, H., 2013. *Renewable and Sustainable Energy Reviews*, 19, 255–274. [2])

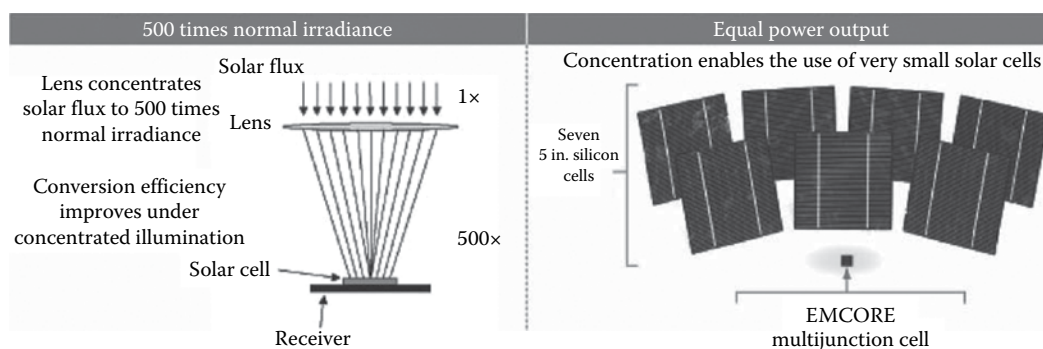
may be slow and often results in nonuniform coverage. Hence, costly disposal of waste by-products from the process may be necessary.

Nanoparticle printing: This process is not yet in commercial production and poses considerable challenges for high-production operation. Ink-based technologies that can be deposited by low-cost inkjet or screen printing approaches have the potential for low cost with adequate resolution for PV applications. Using nanoparticulate precursors as the base for the ink may permit a degree of control in the composition process needed to meet electrical and stability requirements. Ink-depositing processes “print” CIS/CIGS semiconductor ink on a conductive foil substrate. The inks currently used for the CIGS absorber layer consist of oxides or selenide nanoparticles of the metals copper, indium, and gallium dispersed as a colloidal suspension in a solvent. The nanoparticles are intended to form a solid layer of CIGS. The majority of flexible substrates in use today are metal foils, but using polymer fibers such as polyimide that allow for high-speed roll-to-roll processing is gaining in acceptance.

Thin film PV generally has a better EROI and energy payback than silicon technologies. Figure 11.27 shows ranges of payback periods from different studies for various installed PV systems [2]. These are all based on an annual solar radiation of 1700 kWh/m²/yr. CdTe also has the lowest average greenhouse gas emissions rate of 25 g-CO₂-eq/kWh. The other PV systems have GHG emissions, in increasing order as follows: 30 for CIS/CIGS, 35 for multicrystalline silicon, 36 for amorphous silicon, and 38 for monocrystalline silicon.

11.6 Multilayer PV Technology

Advances in photovoltaic energy conversion have been summarized by Dan E. Arvizu [14]. As noted previously, the efficiency of a single-gap solar cell is limited as a result of its inability to efficiently convert the full range of energy of the photons emanating from the sun. Photons with energy below the band gap of the cell material either pass through the cell or are converted to heat within the material. For photons with energy above the

**FIGURE 11.28**

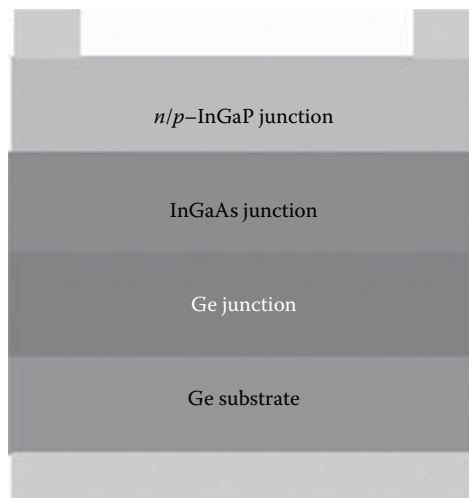
Schematic of multijunction solar cell with Fresnel concentrating lens arrangement. (From SolAero Technologies, Corp. <https://solaerotech.com/solaerotech/>. With permission. [15])

band gap, only the energy necessary to generate the hole–electron pair is utilized while the remainder merely generates heat. The limitations of a single band gap solar cell can be overcome, however, by utilizing multiple junctions with several band gaps that can utilize a much broader range of photon energies from the sun. In the construction of multilayer cells, the layers are optically in series with the highest band gap material at the top. The first junction receives all of the spectrum where photons above the band gap of the first junction are absorbed. Photons below the band gap of the first layer pass through it to the second layer and are absorbed there. This is repeated for the two layers, and the third layer then absorbs as much of the remaining photons as possible. As many as five layers seem feasible.

Multijunction photovoltaic cells use several layers of epitaxially deposited films. Epitaxy is the method of depositing a monocrystalline film on a monocrystalline substrate with the deposited film called the epitaxial layer. Triple-junction high-efficiency solar cells for terrestrial photovoltaic applications have been commercialized by a number of companies, including SolAero Technologies (formerly EMCORE) [15]. The cells are currently much more expensive than single band gap photovoltaic cells, but they can be combined with various types of concentrating devices that can capture solar radiation over a large area and then redirect it onto a small, high-efficiency solar cell. Figure 11.28 shows such a concentrating scheme with solar energy passing through a Fresnel lens that directs the radiation to a small, three-layer cell [15]. A typical example of a three-layer cell is EMCORE T1000 that has achieved an efficiency better than 39% at a solar radiation concentration ratio of 503.

The physical cell structure is shown in Figure 11.29 [15]. It consists of an outer layer of antireflective coating that provides a low reflectance over wavelength in the range from 0.3 to 1.8 μm . The next three layers are an indium gallium phosphorous junction, followed by an indium gallium arsenide layer, and a Ge junction on a Ge substrate. The quantum efficiency of this type of three-layer cell is shown in Figure 11.30 as a function of wavelength [15], and the overall efficiency is shown as a function of concentration in Figure 11.31 [15]. It can be seen from the data in Figure 11.31 that the efficiency increases from 31.4% at 1 \times concentration to 39% at 503 \times concentration, where the peak occurs, and then decreases to about 33% at 1150 \times concentration. Typical current vs. voltage curves (I – V curves) at varying concentration levels and 25°C are shown in Figure 11.32 [15].

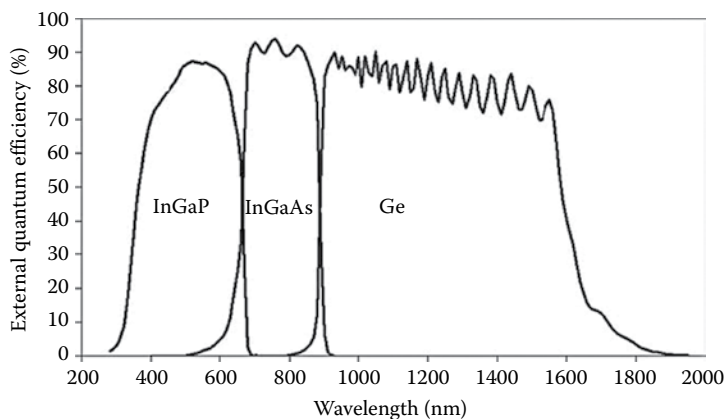
There are a number of methods available for concentrating sunlight. Figure 11.33 shows a photo and a schematic of a PV concentration system using two reflections that direct the solar beam into a refractive rod that guides the radiation toward a triple-layer

**FIGURE 11.29**

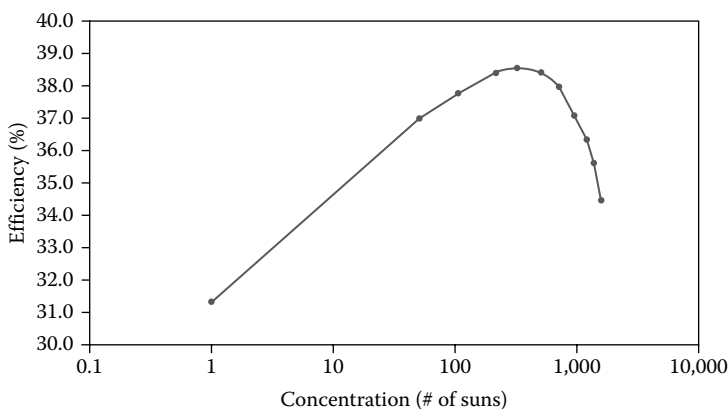
Physical cell structure. (From SolAero Technologies, Corp. <https://solaerotech.com/solaerotech/>. With permission. [15])

high-efficiency PV cell. This arrangement can achieve a concentration of 650 with a dual-axis tracker according to Masia [16]. Another arrangement (Figure 11.34a) with only one reflection and a secondary refractive (Figure 11.34b) lens to guide the radiation toward the PV cell is shown in the photo with a novel dual-axis tracker developed at the University of Colorado (Figure 11.34c). This arrangement may be able to achieve a concentration as high as 1000.

The optimum concentration ratio is determined by economic, rather than optical, considerations. For a cell such as EMCORE T1000, the external dimensions are 12.58 mm × 12.58 mm while the total active area is only 108 mm² with a total cell thickness is 0.16 mm. The conversion efficiency of the design developed at the University of Colorado

**FIGURE 11.30**

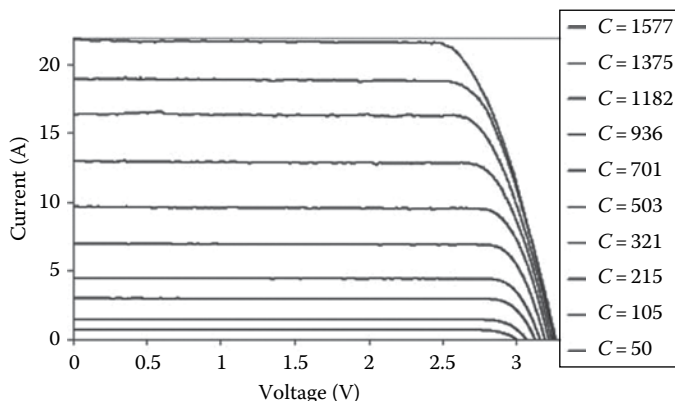
Quantum efficiency as a function of wavelength. (From SolAero Technologies, Corp. <https://solaerotech.com/solaerotech/>. With permission. [15])

**FIGURE 11.31**

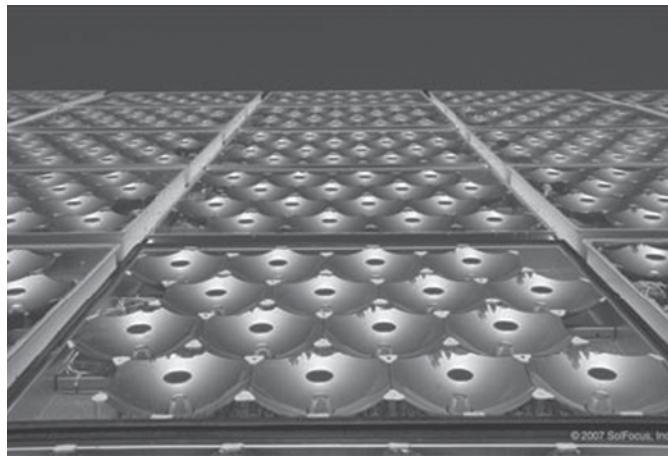
Overall cell efficiency as a function of concentration. (From SolAero Technologies, Corp. <https://solaerotech.com/solaerotech/>. With permission. [15])

can be improved by a finned heat pipe dissipation technique with the heat pipe attached to the bottom of the Ge substrate to avoid shading from the sun. Cooling of such a device is important because the efficiency decreases at about 0.06% per °C increase in operating temperature.

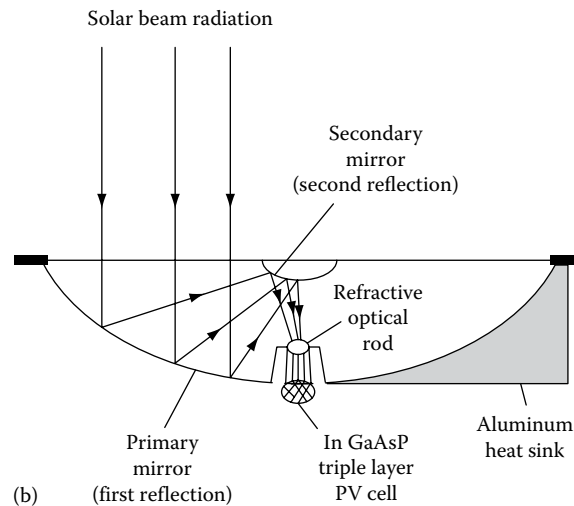
Improvements in multijunction photovoltaic cells are continuing. As of early 2017, the highest efficiency obtained on a multijunction concentrator cell was 46%, obtained at the Fraunhofer Institute. Details of all of these triple cells, their manufacturing methodology, and costs are still privileged information. The cost of three-layer cells is still high and justifies the use of highly accurate CPC design with concentration ratios as high as 1000. But as shown in Figure 11.35 preliminary estimates of cell cost as a function of production by EMCORE indicate that cell cost is likely to decrease and concentrations beyond 500 suns may become counterproductive. Furthermore, since cell efficiency decreases with increase

**FIGURE 11.32**

Typical I - V curves at varying concentration levels, 25°C. (From SolAero Technologies, Corp. <https://solaerotech.com/solaerotech/>. With permission. [15])



(a)



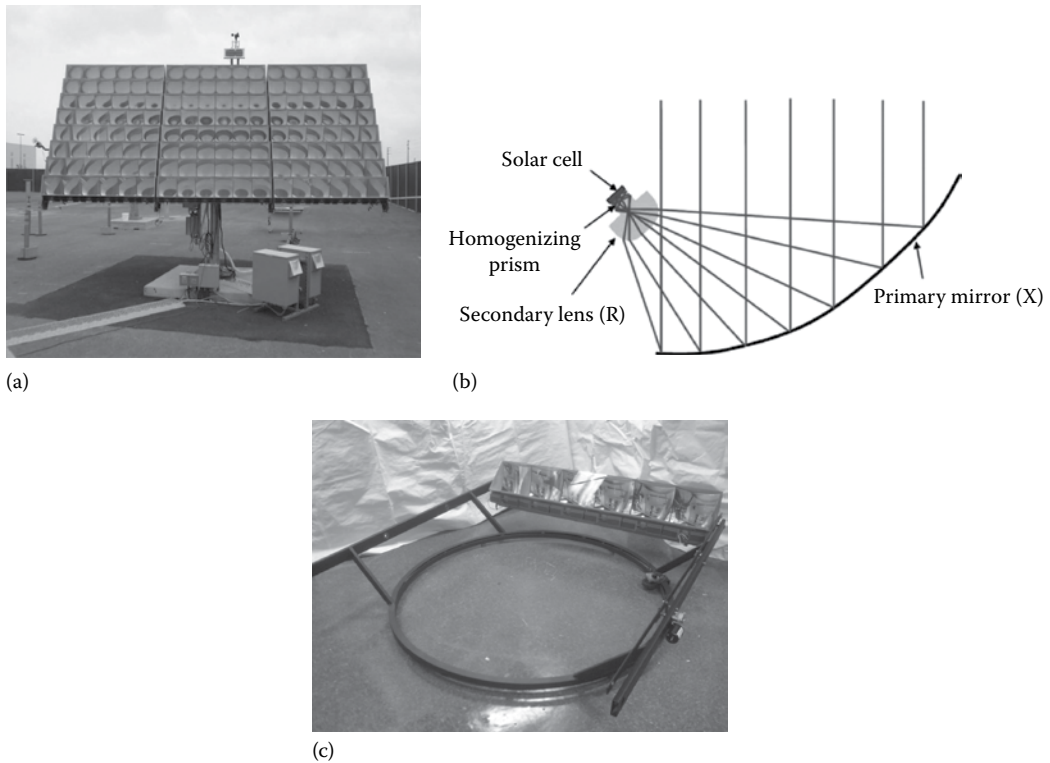
(b)

FIGURE 11.33

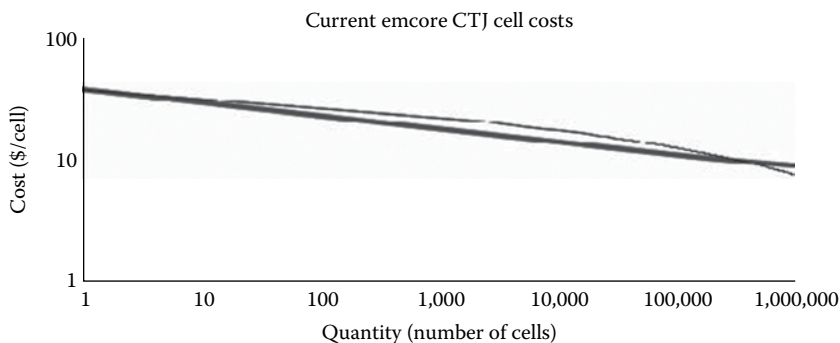
Dual-reflection-single-refraction PV concentrator system. (a) Photograph of SolFocus module. (b) Schematic of optical arrangement. (Courtesy of SolFocus, Inc., Mountain View, CA. With permission.)

in cell temperature by 0.06% per °C, cooling may be important. Since higher concentration will also result in higher heat flux on the cell, cooling becomes more difficult for CPC high-concentration designs. Because of the high cost of these cells, they are primarily used for space-based applications where achieving the highest efficiencies is important and where the cell costs are minor compared to the launch costs.

Figure 11.36 shows the highest research cell efficiencies obtained for all the various PV technologies [13]. This includes the technologies we have discussed, as well as emerging technologies such as dye-sensitized and perovskite cells. (For a recent description of the various emerging cell concepts see “The future of low-cost solar cells” by M. Jacoby [17]) Figure 11.36 clearly shows the progress that has been made in improving cell efficiencies. These research cells are indicative of what may be possible with a given technology, but

**FIGURE 11.34**

Dual-axis rooftop tracker for Boeing high-concentration PV system developed at the University of Colorado, Boulder, CO. (a) Solar array mounted on conventional pedestal. (Courtesy of Adam Plesniak, Guy Martins, John Hall, Andy Messina and other members of the Boeing CPV Engineering Team.) (b) Ray trace pattern of the off-axis SMS3D nonimaging optical system in the Boeing CPV design. (Courtesy of Pablo Benitez, Professor, Universidad Polytechnic de Madrid and Light Prescription Innovators, LLC, Altadena, CA.) (c) Advanced dual-axis tracker with four of the six string Boeing high-concentration modules installed. Tracker was developed by Senior Design Teams at the University of Colorado, Boulder, CO, Dr. Frank Kreith, faculty advisor. (Photo courtesy of Kane Chinnel and Nate Bailey. With permission.)

**FIGURE 11.35**

Multilayer cell costs as a function of production quantity. (Courtesy of EMCORE representative, Personal communication, Albuquerque, NM. With permission.)

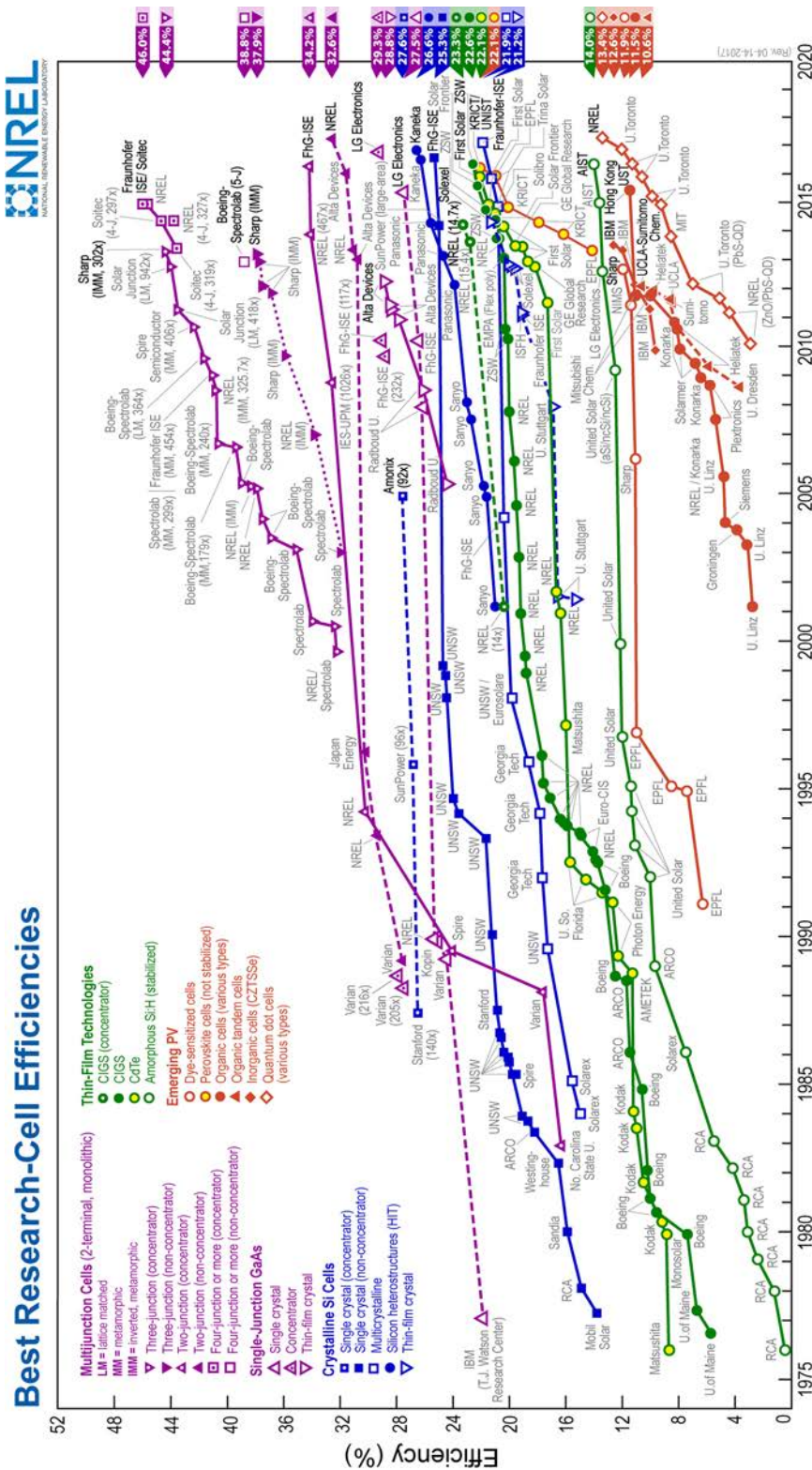


FIGURE 11.36

Best research cell efficiencies for the various PV technologies from 1976 to 2017. (From NREL. Efficiency Chart, <https://www.nrel.gov/pv/assets/images/efficiency-chart.png> [13])

they are not commercial products and are not cost-effective. However, they represent a goal that mass production facilities aim to achieve.

11.7 Today's PV Market

Due to the reduction in the price of Chinese silicon PV modules, learning curves associated with deployment, and some cases of oversupply, the price of PV panels has dropped dramatically in recent years—over 80% between 2008 and 2016—as shown in Figure 11.37 [18]. The experience (or learning) curve shown in the figure indicates a 26.5% drop in price with every doubling of cumulative installed capacity. Module costs are now under 40 cents per Watt.

Because of the rapid drop in prices, PV installations have grown rapidly around the world. The world-installed capacity of PV is now over 300,000 MW—on a par with wind capacity. And the long-term potential of solar PV is very attractive. Deng et al. [19] estimate the high-scenario potential for solar PV electricity at 2800 EJ/yr, or about 3 times that of land-based and offshore wind combined. Utility-scale PV systems in the United States are approaching \$1 per Watt and power purchase agreements have been signed for as low as \$30–\$50/MWh (or 3–5 cents per kWh) [20].

PV panel prices have dropped so low that now more attention is being paid to so-called “soft costs,” especially in the case of residential rooftop systems. These are the non-hardware costs as shown in Table 11.4 [21]. Studies have shown that soft costs in Germany, where the PV market is very established, are considerably lower than in the United States. So soft costs decrease as the market matures. Also, because modules represent a smaller percentage of total PV system cost, reducing their cost further does not have as great an

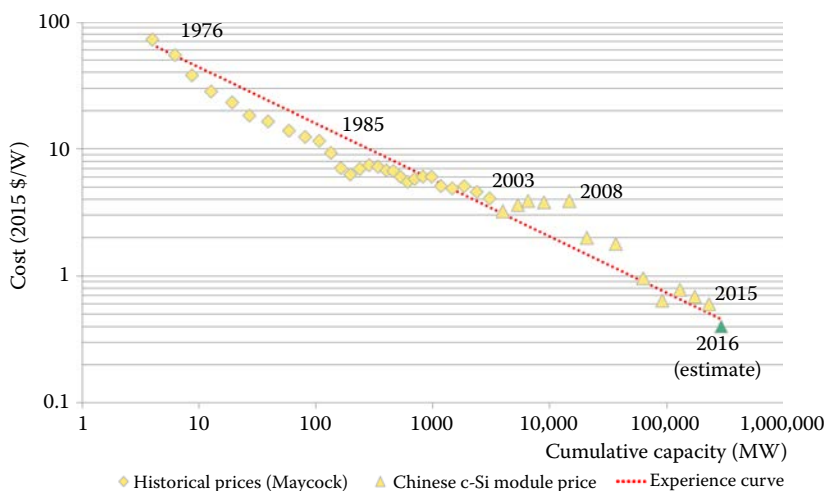


FIGURE 11.37

Price of solar PV modules versus cumulative global capacity. (From Bloomberg New Energy Finance, 2017. *Sustainable Energy in America Factbook*, <https://about.bnef.com/blog/sustainable-energy-america-2017-factbook>. [18])

TABLE 11.4

“Soft Cost” Items as a Percent of Total Installed Cost
for a U.S. Residential Rooftop PV System

Item	Percent of Total Installed Cost
Permit fee	2
Interconnection	2
Sales tax	5
Transaction costs	6
Installer/Developer profit	9
Indirect corporate costs	9
Customer acquisition	9
Installation labor	11
Supply chain costs	12
Total	64

Source: DOE. Soft costs 101: The key to achieving cheaper solar energy. <https://energy.gov/eere/articles/soft-costs-101-key-achieving-cheaper-solar-energy>. [21]

impact on the total cost. A ten percent improvement in module efficiency, however, results in a significant reduction in solar energy cost, so improvements in cell efficiency remain a prime research interest.

Although there are off-grid homes powered by PV with backup from batteries, the vast majority of PV homes are grid-connected. While there is growing interest in having some battery back-up, PV homes with or without batteries are effectively using the electric grid as storage. Because batteries are expensive, excess electricity generated by rooftop PV is sold back to the grid. Many states in the United States allow net metering, whereby electricity going back to the grid is credited at the same price the customer pays. In other words when electricity goes back to the grid, the electric meter runs backward.

Utilities argue that when rooftop PV owners use the grid for storage, they are obtaining a service that gives them a reliable electricity supply at night and—even if they have some battery back-up—during long cloudy periods. If an ice storm takes down a power line, the utility pays to fix it. Therefore, the utility argues that rooftop PV owners should not receive the same price for the electricity they send out as for the electricity they receive. The counter argument is that for many summer-peaking utilities, rooftop PV systems help reduce peak loads on hot summer afternoons. As PV penetration increases, however, and peaks shift later, PV become less effective, as was explained in [Chapter 5](#), Section 5.5.

In addition, regulated utilities generally cannot make money on the customer side of the meter. They prefer central PV systems that they can own and sell electricity from as they have for a century with thermal power plants. As a result, there has been pressure in many states to revise net metering laws or charge fees to rooftop PV owners. As these issues are debated, it’s important to remember that there is value in reducing carbon emissions. Thus, an aggressive effort to address climate change should embrace both rooftop and central PV systems.

Because the boom in PV sales has only occurred in the last decade and the expected lifetime of modules is 20 to 30 years or longer, recycling problems are not yet widely established. The European Union and the State of California already have regulations impacting this, however [22].

11.8 Using System Advisor Model (SAM) for PV Performance Estimates

The System Advisor Model (SAM) provided three different models for analyzing the performance of PV systems: PVWatts, a SAM detailed model, and a concentrating PV model. These models all handle both performance and cost calculations. For most PV systems, the first two models are of most interest. PVWatts is simple to use and is excellent for initial design. The SAM detailed model uses data from actual commercial PV panels and inverters and allows greater detail in system specification. It is best used for final calculations of a system with known, specific components. Both models perform hour-by-hour simulations that provide estimated monthly and annual energy production in kilowatts. Users select a location and choose either to use default values or they can input their own system parameters for size, electricity costs, array type, tilt angle, and azimuth angle. The program uses an extensive library of weather and solar radiation data for many locations. From these data, the calculator determines the irradiation on the PV array and the average cell temperature for each hour of the year. The DC energy output for each hour is calculated from the PV system DC rating and the incident solar radiation, and then corrected for the PV cell temperatures. The AC energy for each hour is then calculated by multiplying the DC energy output by the overall DC to AC derate factor, including the inverter efficiency as a function of load. Hourly values of the AC energy are then summed to calculate monthly and annual AC energy production. The SAM model is available for free download at <https://sam.nrel.gov>.

The following example demonstrates the use of the SAM PVWatts model to calculate the performance of a residential PV system. The same approach can be used to estimate the output of utility-scale PV applications.

EXAMPLE 11.9

Using the PVWatts online software, estimate the incident solar radiation and AC energy output for a 4 kW solar PV panel in Phoenix, Arizona, annually and during the month of October. Note that the 4 kW electric rating is for the DC output. Assume a DC-to-AC derate factor of 0.77, a south-facing array at a tilt of 20°. What tilt angle will achieve the maximum annual energy output for this location?

Estimate the levelized cost of electric power for the system. Assume that the cost of the module is 0.65 \$/W. The real discount rate is 5.5%, the inflation rate is 2.5%, and the lifespan of the system is 30 years.

Solution

We will analyze this system using SAM, which can be accessed through <https://sam.nrel.gov>. (Note: SAM is frequently updated. The instructions that follow are for version 2017.1.17 and may change.)

After downloading SAM from the website, to start a PV project:

1. Start SAM.
2. Click **Start a New Project**
3. Choose **Photovoltaics (PVWatts) – Residential (Distributed)** and click OK in the lower right.
4. Click **Location and Resource** on the left and search for and choose USA AZ Phoenix (TMY2)

SAM 2017.1.17 / Users/ckutsche/Documents/SAM Projects/Phoenix PV Example-PVWatts.sam

File Add untitled Help

PVWatts, Residential

Location and Resource

System Design

System Costs

Lifetime

Financial Parameters

Incentives

Electricity Rates

Electric Load

Download a weather file from the NREL NSRDB

Download... Click Download and type a street address or latitude and longitude to download a weather file from the NREL NSRDB for United States and some international locations. SAM adds the downloaded file to the solar resource library so it will appear in the list below.

[NSRDB Map](#)

Choose a weather file from the solar resource library

Click a name in the list to choose a file from the library. Type a few letters of the name in the search box to filter the list. If your location is not in the library, try downloading a file (see above).

Search for: Name

Name	Station ID	Latitude	Longitude	Time zone	Elevation
USA AZ Page Muni (amos) (TMY3)	723710	36.933	-111.45	-7	1304
USA AZ Phoenix (TMY2)	23183	33.4333	-112.017	-7	339
USA AZ Phoenix Sky Harbor Intl Ap (TMY3)	722780	33.45	-111.983	-7	337
USA AZ Prescott (TMY2)	23184	34.65	-112.433	-7	1531
USA AZ Prescott Love Field (TMY3)	723723	34.65	-112.417	-7	1537
USA AZ Safford (amos) (TMY3)	722747	32.817	-109.683	-7	950

City Phoenix Time zone GMT -7 Latitude 33.4333 °N

State AZ Elevation 339 m Longitude -112.017 °E

Country USA Data Source TMY2 Station ID 23183

Data file /Users/ckutsche/Desktop/SAM.app/Contents/solar_resource/USA AZ Phoenix (TMY2).csv

Annual Weather Data Summary

Global horizontal 5.80 kWh/m²/day Average temperature 22.5 °C

Direct normal (beam) 6.90 kWh/m²/day Average wind speed 3.0 m/s

Diffuse horizontal 1.55 kWh/m²/day [Visit SAM weather data website](#)

Use a specific weather file on disk

☐ Browse...

Check the box and click Browse to choose a weather file stored on your computer without adding it to the solar resource library. Supported solar weather file formats are SAM CSV, TMY2, TMY3, and EPW.

Simulate > Parameters Stochastic P50 / P90 Macros

5. Choose **System Design** on the left and next to System Nameplate Size enter 4 kWdc. Note that the model assumes a DC to AC ratio of 1.2 and chooses the size of the inverter accordingly. Next to **Tilt** enter 20 degrees and next to **Azimuth** enter 180 degrees.

File Add untitled Help

PVWatts, Residential

Location and Resource

System Design

System Costs

Lifetime

Financial Parameters

Incentives

Electricity Rates

Electric Load

System Parameters

System nameplate size 4 kWdc

Module type Standard

DC to AC ratio 1.2

Rated inverter size 3.33 kWac

Inverter efficiency 96 %

Orientation

Azimuth 180 Tilt 20 degrees

Array type Fixed open rack

Ground coverage ratio 0.4

Losses

Soiling 2 % Connections 0.5 %

Shading 0 % Light-induced degradation 1.5 %

Snow 0 % Nameplate 1 %

Mismatch 2 % Age 0 %

Wiring 2 % Availability 3 %

☐ User-specified total system losses 20.95 %

Total system losses 11.42 %

Shading

Edit shading losses Edit shading... Open 3D shade calculator...

Curtailment and Availability

Curtailment and availability losses reduce the system output to represent system outages or other events. Edit losses... Constant loss: 0.0 % Hourly losses: None Custom periods: None

Battery Bank

☐ Enable battery

Battery capacity 10 kWh Battery chemistry Lithium Ion

Battery power 3 kW Battery dispatch Peak Shaving (look a...

Simulate > Parameters Stochastic P50 / P90 Macros

6. Choose **System Costs** on the left and enter a module cost of 0.65 \$/Wdc. Leave the other costs at their default values.

PVWatts, Residential

Location and Resource
System Design
System Costs
Lifetime
Financial Parameters
Incentives
Electricity Rates
Electric Load

Direct Capital Costs

	Units	Value	Unit Cost	Total Cost
Module	1 units	4.0 kWdc/unit	0.65 \$/Wdc	\$ 2,600.00
Inverter	1 units	3.3 kWac/unit	0.21 \$/Wdc	\$ 840.00
Battery bank	0.0 kWh dc	500.00 \$/kWh dc		\$ 0.00
Balance of system equipment	0.00	0.36 \$/Wdc		\$ 1,440.00
Installation labor	0.00	0.30 \$/Wdc		\$ 1,200.00
Installer margin and overhead	0.00	1.25 \$/Wdc		\$ 5,000.00
Subtotal				\$ 11,080.00
Contingency				\$ 0.00
Total direct cost				\$ 11,080.00

Indirect Capital Costs

	% of direct cost	\$/Wdc	\$
Permitting and environmental studies	0	0.10	\$ 400.00
Engineering and developer overhead	0	0.00	\$ 0.00
Grid interconnection	0	0.00	\$ 0.00
Land Costs			
Land purchase	0	0.00	\$ 0.00
Land prep. & transmission	0	0.00	\$ 0.00
Sales Tax			
Sales tax basis, percent of direct cost	52 %	Sales tax rate	5.0 %
			\$ 288.08
Total indirect cost			\$ 688.08

Total Installed Cost

	Value
Total installed cost	\$ 11,768.08
Total installed cost per capacity	\$ 2.94/Wdc

Operation and Maintenance Costs

	First year cost	Escalation rate (above inflation)
Fixed annual cost	0 \$/yr	0 %
Fixed cost by capacity	20 \$/kW-yr	0 %
Variable cost by generation	0 \$/MWh	0 %

In Value mode, SAM applies both inflation and escalation to the first year cost to calculate out-year costs. In Schedule mode, neither inflation nor escalation applies. See Help for details.

Simulate >

Parameters
PS0 / PS90
Stochastic
Macros

7. Choose **Lifetime** on the left and enter a degradation rate of 0.7% per year.
8. Choose **Financial Parameters** on the left. Check the box for a Standard Loan at the top. Enter values for:
- Debt fraction: 100%
 - Loan term: 30 years
 - Loan rate: 5%/year
 - Analysis period: 30 years
 - Inflation rate: 2.5%/year
 - Real discount rate: 5.5%/year
- Leave the other values as defaults

File Add untitled Help

PVWatts, Residential

Location and Resource
System Design
System Costs
Lifetime
Financial Parameters
Incentives
Electricity Rates
Electric Load

Residential Loan Type
☒ Standard loan Standard loan interest payments are not tax deductible.
☐ Mortgage Mortgage interest payments are tax deductible.

Loan Parameters
 Debt fraction 100 % Net capital cost \$ 11,768.08 The weighted average cost of capital (WACC) is displayed for reference. SAM does not use the value for calculations.
 Loan term 30 years Debt \$ 11,768.08
 Loan rate 5 %/year WACC 3.35 % For a project with no debt, set the debt fraction to zero.

Analysis Parameters
 Analysis period 30 years Inflation rate 2.5 %/year
 Real discount rate 5.5 %/year
 Nominal discount rate 8.14 %/year

Tax and Insurance Rates
 Federal income tax rate 28 %/year
 State income tax rate 7 %/year
 Sales tax 5 % of total direct cost
 Insurance rate (annual) 0.5 % of installed cost

Property Tax
 Assessed percentage 100 % of installed cost
 Assessed value \$ 11,768.08
 Annual decline 0 %/year
 Property tax rate 2 %/year

Salvage Value
 Net salvage value 0 % of installed cost End of analysis period value \$ 0

Simulate > Parametric Stochastic P50 / P90 Macros

9. Choose **Electricity Rates** on the left. Click in the **Search for rates** box at the top. A new screen will come up.
10. In the box next to **Filter type** Arizona. Choose Arizona Public Service from the list. Then on the right choose **Residential Service Standard (E12)** the first time it appears. Click the box **Download and apply utility rate** at the lower right.

File Add untitled Help

PVWatts, Residential

Location and Resource
System Design
System Costs
Lifetime
Financial Parameters
Incentives
Electricity Rates
Electric Load

OpenEI U.S. Utility Rate Database
 Download rate structures for electric utility companies included in the OpenEI Utility Rate Database. After downloading a rate structure, compare the inputs below with a copy of the rate sheet to verify that the information is correct.
 Search for rates...
[Go to OpenEI Utility Rate Database website](#)

Save / Load Rate Data
 Save rate to file... Load rate from file...

Monthly Accounting of Excess Generation
☒ Monthly total excess rolled over to next month bill in kWh rate for kWh rolled over at end of year 0.02789 \$/kWh
☐ Monthly total excess credited to next month bill in \$ at sell rate(s)
☐ Cumulative hourly (subhourly) excess credited to current month bill in \$ at sell rate(s) ☐ Use hourly (subhourly) sell rates instead of TOU sell rate
☐ Cumulative hourly (subhourly) excess credited to next month bill in \$ at sell rate(s) Hourly (subhourly) sell rates Edit data... \$/kWh
☐ All generation sold at sell rate(s) and all load purchased at buy rate(s)

Fixed Charge
 Fixed monthly charge 16.68 \$

Minimum Charges
 Monthly minimum charge 0 \$
 Annual minimum charge 0 \$

Annual Escalation
 Electricity bill escalation rate 0 %/yr
 In Value mode, enter a rate in real terms because SAM applies both escalation and inflation to the total first-year electricity bill to calculate the annual electricity bill in later years. In Schedule mode, enter rate in nominal terms because inflation does not apply. See Help for details.

Description and Applicability
 The description and applicability information is for your reference. SAM does not use it in calculations. The information is from the U.S. Utility Rate Database, but may not correspond to the actual energy charge and demand charge data from the database. The description fields are editable, so you can change them to suit your needs.

Description
 Name Arizona Public Service Co
 Schedule Residential TOU ET2
 Source https://www.aps.com/library/rates/et-2.pdf
 Start date empty empty
 URI empty
 This rate schedule is applicable to all Standard Offer and Direct Access electric service required for residential purposes in individual private dwellings and in individually metered apartments when such service is supplied at one site through one point of delivery and measured through one meter.
 Description

Simulate > Parametric Stochastic P50 / P90 Macros

OpenEI Utility Rate Database

Zip code: Search by zip code

Filter: Arizona 13 filtered.

Available rate schedules: Residential Only

☐ Show Active Only

Filter:

Arizona Electric Pwr Coop Inc
 Arizona Power Authority
 Arizona Public Service Co
 City of Fredonia, Arizona (Utility Company)
 City of Mesa, Arizona (Utility Company)
 City of Safford, Arizona (Utility Company)
 City of Williams - AZ, Arizona (Utility Company)
 Columbus Electric Coop, Inc (Arizona)
 Dixie Escalante R E A, Inc (Arizona)
 Garkane Energy Coop, Inc (Arizona)
 Town of Thatcher, Arizona (Utility Company)
 Town of Wickenburg, Arizona (Utility Company)
 Arizona Corporation Commission

Residential Bundled & Adjustments No Tax TOU ; Time Adv 7PM-Noon (E-1)
 Residential Service TOU Combined Advantage 7PM-Noon (ECT-2) (5748ae4a682bea07def0d1ba)
 Residential Service Standard (E-12) (5748ae4a682bea07def0d1ba)
 Residential Service TOU Time Advantage 7PM-Noon (ET-2) (5748ae4a682bea07def0d1ba)
 Residential Service Standard (E-12) (588136e2682bea5a54b4c2ee)
 Residential Service TOU Time Advantage 7PM-Noon (ET-2) (588136e2682bea5a54b4c2ee)

Name: Arizona Public Service Co: Residential Service Standard (E-1)
 Description: Fixed monthly charge= 0.285*30
 Start: 2016-05-02
 End: 2016-05-30
 GUID: 5748ae4a682bea07def0d1ba

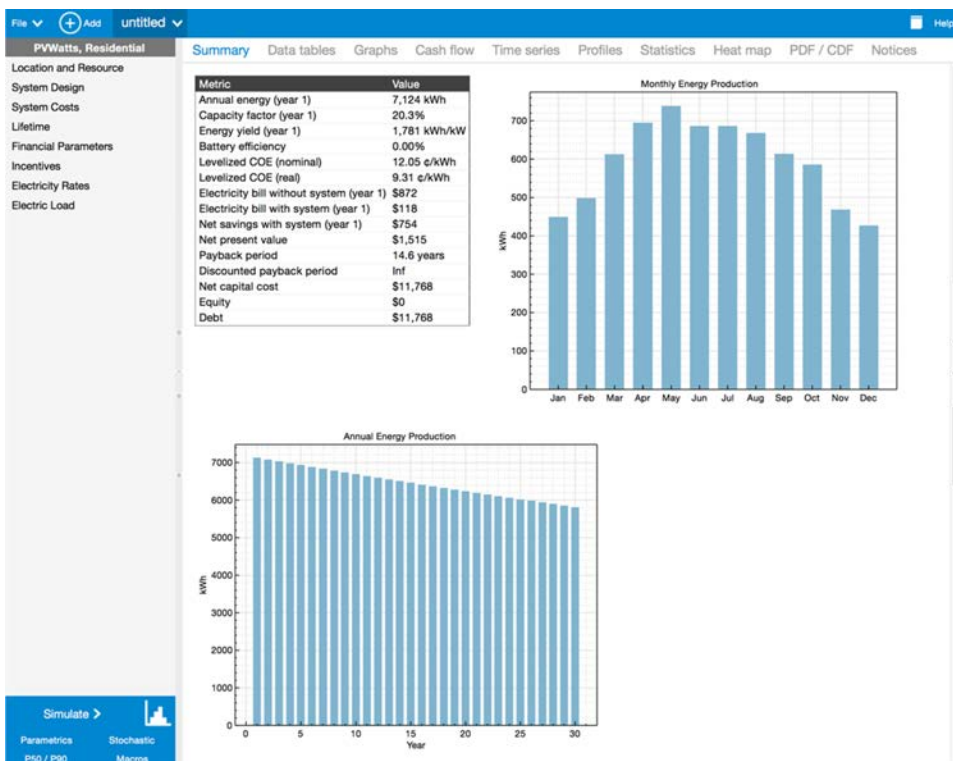
Show all 3884 utilities

Ready.

[Go to rate page on OpenEI.org...](#)
[Rate JSON data page...](#)

Download and apply utility rate Close

11. Click **Simulate** at the lower left.



The results screen shows the monthly and annual energy production. (If you scroll down you will also see a cash flow graph and a graph showing the production and load for each month.) this shows an annual energy production of 6910 kWh, and October output of 570 kWh, a simple payback period of 14.8 years, and a capacity factor in year 1 of 19.7% (i.e., the average power output is 19.7% of the design power output).

PROBLEMS

- 11.1 Find the wavelength of radiation whose photons have energy equal to the band gap of GaAs.
- 11.2 What is the theoretical maximum efficiency of conversion if blue light of wavelength $0.45\ \mu\text{m}$ is incident on a GaAs solar cell?
- 11.3 Find the theoretical maximum overall efficiency of GaAs solar cells in space.
- 11.4 The reverse saturation current I_o of a silicon cell at 40°C is $1.8 \times 10^{-7}\ \text{A}$. The short circuit current when exposed to sunlight is 5 A. From this information, compute
 - a. Open circuit voltage.
 - b. Maximum power output of the cell.
 - c. The number of $4 \times 4\ \text{cm}$ cells needed to supply 100 W at 12 V. How must the cells be arranged?
- 11.5 At what efficiency is a photovoltaic array running if insolation on the collector is $650\ \text{W}/\text{m}^2$, the total collector area is $10\ \text{m}^2$, the voltage across the array is 50 V, and the current being delivered is 15 A?
- 11.6 If a PV array has a maximum power output of 10 W under an insolation level of $600\ \text{W}/\text{m}^2$, what must the insolation be to achieve a power output of 17 W? Would you expect the open circuit voltage to increase or decrease? Would you expect the short circuit current to increase or decrease?
- 11.7 A PV battery system has an end-to-end efficiency of 77%. The system is used to run an all-AC load that is run only at night. The charge controller efficiency is 96% and the inverter efficiency is 85%. How much energy will need to be gathered by the PV array if the load is 120 W running for 4 h per night?
- 11.8 If the average output of the PV system in Problem 11.7 is 200 W, the load is changed to run during the day, how much PV output energy is needed for the same load conditions? Assume that the battery bank is at 100% charge and that input efficiency is equal to output efficiency.
- 11.9 For the system in Problem 11.7, how many hours of sunlight are needed to ensure that the battery bank is at 100% charge at the end of the day assuming the same load?
- 11.10–11.14 The owner of a small cabin would like to convert her home to PV power. She has the following equipment and associated run times:

Household Equipment	Power (W)	Run Time (day) (h)	Run Time (night) (h)
Lighting (DC)	25	2	4
Stereo (AC)	40	3	2
Refrigerator (DC)	125	3 ^a	3 ^a

Continued

Household Equipment	Power (W)	Run Time (day) (h)	Run Time (night) (h)
Water pump (DC)	400	1.5 ^b	0.5 ^b
Alarm clock (DC)	8	12	12
Computer (AC)	250	3	0
Printer (AC)	175	0.25	0
Outdoor safety lights (DC)	48	0 ^c	8 ^c
Answering machine (AC)	7	12	12
Coffee pot (AC)	1200	0.25	0

^a The refrigerator is assumed to run 25% of the time.

^b It can be assumed that the pump and fan will not start precisely at the same instant.

^c It is assumed that the night- and daylighting loads will not be on simultaneously.

- 11.10 a. What is the homeowner's daily energy requirement as measured from the load?
- b. If she replaces her alarm clock with a wind-up clock, how much energy per day will she avoid using?
- c. What would you suggest she do to cut back her daily load?
- 11.11 How many 50 W panels will the owner require assuming battery storage is 75% efficient and all loads are DC (no inverter)?
- a. For a stationary system "seeing" 5 h of sunlight per day?
- b. For a tracking system "seeing" 8 h of sunlight per day?
- 11.12 For the loads listed:
- a. What size inverter (peak watts) should she purchase?
- b. If the inverter is 88% efficient, how much more daily energy is required from the PV array as compared to an all-DC system?
- 11.13 The homeowner decides to hire you to design a system for her. She has arranged with a local solar supplier for the following equipment. Specify the system and provide a line diagram.

PV panels	42 W, nominal 12 V
Batteries	125 Ah, 6 V, end-to-end efficiency = 72%
Charge controller	95% efficient, 12 V
Inverter	90% efficient, sizes of 500, 1000, 2000, and 4000 W available, 12 V input

- 11.14 Redesign the system in Problem 11.13 with the following equipment:

PV panels	51 W, nominal 12 V
Batteries	200 Ah, 12 V, end-to-end efficiency = 78%
Charge controller	97% efficient, 24 V
Inverter	91% efficient, sizes of 500, 1200, 2500, and 5000 W available, 24 V input

- 11.15 A flashing beacon is mounted on a navigation buoy in the shipping channel at a port at 30° N latitude. The load consists of a single lamp operating 1.0 s on and 3.6 s off during the hours of darkness. Hours of darkness vary from 9.8 h in July to 13.0 h in December. The lamp draws 2 A at 12 V when lighted. A flasher controls the lamp and draws 0.22 A when the lamp is on. There is a surge current of 0.39 A each time the flasher turns on. This current flows approximately 1/10th of the time the flasher is on. The design has 14 days of battery capacity. Provision has to be made to disconnect the load if the battery voltage drops below 11 V.

The available module has a rated voltage of 17.2 V at 25°C (15 V at 55°C) and 2.3 A at 1 kW/m². The available battery has a rated capacity of 105 Ah at 12 V. Assume that maximum depth of discharge is 0%. Design the PV system.

- 11.16 Design a PV system for the following application: A refrigerator/freezer unit for vaccine storage in a remote island of Roatan, Honduras (16°N latitude, 86°W longitude, temperature, range 15°C–30°C).

Two compressors—one each for refrigerator and freezer

Each compressor draws 5 A at 12 V

Compressors Remain on for	Summer (h/day)	Winter (h/day)
Refrigerator	9	5
Freezer	7	4

Design the PV system using the panels and the batteries described in Problem 11.15.

- 11.17 A homeowner in Santa Fe, New Mexico, is interested in having a solar PV system installed at his house. He would like the system to be able to cover all of his annual energy needs. The following is a table from his utility provider showing the monthly energy use in the household. His roof with solar access is facing due east at a 20° pitch with no shading. In addition, the local electric company is offering a rebate on residential solar installations of \$2.00 per installed Watt, as well as a renewable energy credit rebate based on predicted system performance. The REC rebate is \$2.50/W, which is then multiplied by the system performance. Since the installation is east facing, the predicted performance efficiency is 83% (with a system facing due south having a performance efficiency of 100%).

Consumption

	kWh
January	400
February	400
March	600
April	600
May	800
June	1000
July	1000
August	900
September	800
October	600
November	600
December	400

- a. Design a system that will offset 100% of the home's consumption.
- b. Assuming \$0.10/W electricity expense with a 5% annual inflationary rate increase, and a \$7.50/W installed cost, what will the payback be for this system after the rebate from the utility provider?
- c. How do you wire the solar panel? Specifically, how many cells would you need and how would you wire them (series versus parallel) if the solar panel is to have a working voltage of 24.46 V and an amperage of 7.6 A? Assume the individual cells produce 98 V and 3.8 A.

Resources

The SMA string sizing program can be found at <https://www.sma.de/en/service/downloads.html>.

PV Watts can be found at <http://pvwatts.nrel.gov>.

- 11.18 A village in Antigua (17°N, 61°W, 15°C–30°C temperature, range), West Indies, requires 5000 gal of water per day for community water supply. Assuming a year-round average insolation of 8 kWh/day, design the system using the following components:

PV panels: Solarex panels 17.5 V and 3.6 A at 1000 W/m² and 25°C

Pump: Grundfos multistage pump input 105 V DC, 9 A, 30% efficiency

- 11.19 Prepare a preliminary design for a solar PV system to provide 1 kW of stand-alone 24 h/day power to a travel trailer. Make a schematic diagram of the overall system, a cost estimate, a cell array design, and a battery storage. Then discuss the assumptions you made for your design.

References

1. Renewables Now, July 21, 2016. PV market revenues to see CAGR of 9.5% through 2020, frost & sullivan says, <https://renewablesnow.com/news/pv-market-revenues-to-see-cagr-of-9-5-through-2020-frost-sullivan-says-533535>.
2. Peng, L. and Yang, H., 2013. Review on life cycle assessment of energy payback and greenhouse gas emissions of solar photovoltaic systems, *Renewable and Sustainable Energy Reviews* 19, 255–274.
3. Angrist, S.W., 1976. *Direct Energy Conversion*, 3rd ed., Allyn & Bacon, Boston, MA.
4. Bube, R.H., 1960. *Photoconductivity of Solids*, John Wiley & Sons, New York.
5. Moore, C.E., 1952. *Atomic Energy Levels*, Vol. 2, National Bureau of Standards Circular 467, U.S. Government Printing Office, Washington, DC.
6. Garg, H.P., 1987. *Advances in Solar Energy Technology*, Vol. 3, D. Reidel Publishing Company, Dordrecht, the Netherlands.
7. Goswami, Y. et al., 2000. *Principles of Solar Engineering*, 2nd ed., Taylor & Francis, Philadelphia, PA.
8. Messenger, R.A. and Ventre, J., 2010. *Photovoltaic Systems Engineering*, 3rd ed., CRC Press, Boca Raton, FL.
9. Sandia National Laboratories, 1991. *Maintenance and Operation of Stand-Alone Photovoltaic Systems*, Albuquerque, NM, <http://www.satcon.com>.
10. Post, H.N. and Risser, V.V., 1995. *Stand-Alone Photovoltaic Systems—A Handbook of Recommended Design Practices*, Sandia National Laboratory Report SAND-87-7023, Sandia National Laboratories, Albuquerque, NM.

11. NREL. National solar radiation data base, http://rredc.nrel.gov/solar/old_data/nsrdb/1991-2010.
12. PV Insider, March 23, 2015. Share of thin film module production to remain at 7% through 2019, <http://analysis.newenergyupdate.com/pv-insider/thin-film-pv/share-thin-film-module-production-remain-7-through-2019>.
13. NREL. Efficiency chart, <https://www.nrel.gov/pv/assets/images/efficiency-chart.png>.
14. Arvizu, D.E., 2009. Let the solar revolution begin, *Solar Today* March, 23(2), 24–27.
15. SolAero Technologies, Corp. <https://solaerotech.com/solaerotech/>.
16. Masia, S., 2010. Concentrating photovoltaics, *Solar Today*, January/February, 24(1), 42.
17. Jacoby, M., May 2016. The future of low-cost solar cells, *Chemical and Engineering News*, 94, 18.
18. Bloomberg New Energy Finance, 2017. *Sustainable Energy in America Factbook*, <https://about.bnef.com/blog/sustainable-energy-america-2017-factbook>.
19. Deng, Y. et al., 2015. Quantifying a realistic, worldwide wind and solar electricity supply, *Global Environmental Change* 31, 239–252.
20. Bolinger, M. and Seel, J., 2015. Utility-scale solar, LBNL-1006037.
21. DOE. Soft costs 101: The key to achieving cheaper solar energy. <https://energy.gov/eere/articles/soft-costs-101-key-achieving-cheaper-solar-energy>.
22. Renewable Energy World, June 1, 2016. Solar PV module recycling: Why it's important, <http://www.renewableenergyworld.com/articles/2016/06/solar-pv-module-recycling-why-it-s-important.html>.

Suggested Readings

- Crossley, P.A., Noel, G.T., and Wolf, M., 1968. Review and evaluation of past solar cell development efforts, RCA Astro-Electronics Division Report, AED R-3346, Contract NASW-1427, NASA, Washington, DC.
- Florida Solar Energy Center, 1991. *Photovoltaic System Design*, FSEC-GP-31-86, Florida Solar Energy Center, Cocoa Beach, FL.
- Jayarama Reddy, P., 2009. Cell efficiencies, in: *Science and Technology of Photovoltaics*, 2nd ed., CRC Press, Boca Raton, FL.
- Jayarama Reddy, P., 2010. *Science and Technology of Photovoltaics*, 2nd ed., CRC Press, Boca Raton, FL. (This is a good basic textbook on the science and technology of solar photovoltaics.)
- Kurtz, S., 2009. Opportunities and challenges for development of a mature concentrating photovoltaic power industry, NREL, NREL/TP-520-43208, revised November 2009.
- Lasnier, F. and Ang, T.G., 1990. *Photovoltaic Engineering Handbook*, Hilger Publishing, New York.
- Markvart, T., ed. 2000. *Solar Electricity*, 2nd ed., John Wiley & Sons, Chichester, U.K. (This is a good general purpose, lower-level introduction.)
- Masters, G.M., 2001. *Renewable and Efficient Electric Power Systems*, John Wiley & Sons, Chichester, U.K. (This is a comprehensive textbook for distributed electric power systems with a solutions manual for instructors.)
- Nelson, J., 2003. Properties of semiconductor materials, in: *The Physics of Solar Cells*, Imperial College Press, London, U.K., 2003. (This book emphasizes solar cell operation with an in-depth coverage of solar cells, including quantum effects.)
- Raugei, M., Bargigli, S., and Ulgaiani, S., 2007. Energy and life cycle assessment of the thin film CdTe photovoltaic modules, http://www.abound.com/pdf/NREL_PV_Embodied_Energy.pdf.



Taylor & Francis

Taylor & Francis Group

<http://taylorandfrancis.com>

12

Solar Thermal Collectors and Systems

We are star stuff harvesting sunlight.

Carl Sagan

The basic principle of solar thermal collection is that when solar radiation strikes a surface, part of it is absorbed, thereby increasing the temperature of the surface. The efficiency of that surface as a solar collector depends not only on the absorption efficiency, but also on how the thermal and radiation losses to the surroundings are minimized and how the energy from the collector is removed for useful purposes. Various solar thermal collectors range from unglazed flat-plate-type solar collectors operating at about 5–10°C above the ambient, to central receivers collectors operating at above 1000°C. [Table 12.1](#) lists various types of solar thermal collectors and their typical temperature and concentration ranges.

This chapter analyzes the thermal and optical performance of several solar-thermal collectors. They range from non-concentrating, flat plate types (see [Figure 12.1](#)) to compound-curvature, and continuously tracking types with concentration ratios up to 1000 or more. Applications of the energy conversion by solar thermal collectors are described in this chapter for building hot water, for electric power and for process heat. The next section describes some fundamental radiation properties of materials, knowledge of which helps in the design and analysis of solar thermal collectors.

12.1 Radiation Properties of Materials

When radiation strikes a body, a part of it is reflected, a part is absorbed, and if the material is transparent, a part is transmitted, as shown in [Figure 12.2](#). The fraction of the incident radiation reflected is defined as the reflectance ρ , the fraction absorbed as the absorptance α , and the fraction transmitted as the transmittance τ . According to the first law of thermodynamics, these three components must add up to unity, or

$$\alpha + \tau + \rho = 1 \quad (12.1)$$

Opaque bodies do not transmit any radiation and $\tau = 0$.

The reflection of radiation can be *specular* or *diffuse*. When the angle of incidence is equal to the angle of reflection, the reflection is called specular; when the reflected radiation is uniformly distributed into all directions, it is called diffuse. No real surface is either purely specular or purely diffuse, but a highly polished surface approaches specular reflection, whereas a rough surface reflects diffusely.

TABLE 12.1

Types of Solar Thermal Collectors and Their Typical Temperature Range above Ambient

Type of Collector	Concentration Ratio	Typical Working Temperature Range (°C)
Flat plate collector	1	≤70
Evacuated tube collector	1.5–2	60–120
Parabolic trough collector	10–50	150–350
Parabolic dish collector	200–500	250–700
Central receiver	500–>3000	500–>1000

Another important radiative property is called emittance, ϵ , which is the ratio of the radiative emissive power of a real surface to that of an ideal “black” surface.

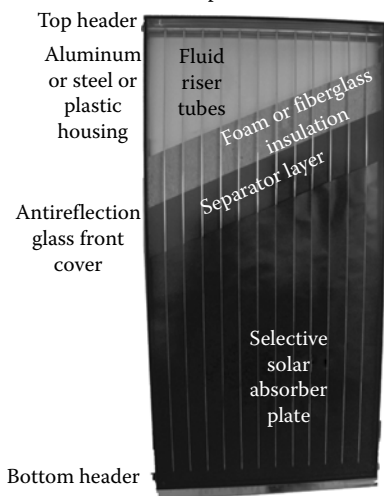
All of the radiative properties of materials, α , τ , ρ , and ϵ can be functions of the wavelength and direction. In fact, such dependence is used in the design of solar energy devices and systems. For example, selective absorbers are used for solar collectors and passive heating systems, and glazing materials for daylighting and solar collectors.

The monochromatic directional emittance of a surface, $\epsilon_\lambda(\theta, \phi)$, in a direction signified by an azimuth angle ϕ and a polar angle θ , is

$$\epsilon_\lambda(\theta, \phi) = \frac{I_\lambda(\theta, \phi)}{I_{b\lambda}} \quad (12.2)$$

The total directional emittance $\epsilon(\theta, \phi)$ over all the wavelengths or the monochromatic hemispherical emittance ϵ_λ can be obtained by the integration of $\epsilon_\lambda(\theta, \phi)$ over all the

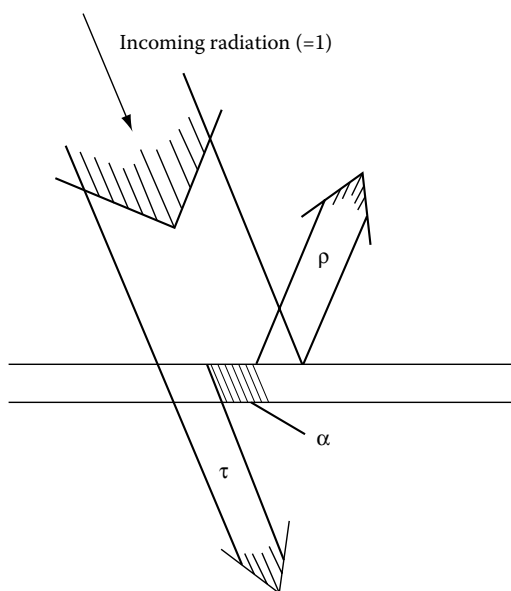
(a) SunMaxx M-2 flat-plate solar collector



(b)

**FIGURE 12.1**

(a) Photo of an active flat plate solar collector. (From Barry Butler, PhD, Butler Sun Solutions, Inc., Solana Beach, CA. With permission.) (b) Photo of an active flat plate solar collector on Kreith's residence.

**FIGURE 12.2**

Schematic representation of transmittance τ , absorptance α , reflectance ρ .

wavelengths or the entire hemispherical space, respectively. The overall emittance, ε , is found by integrating the hemispherical emittance over all the wavelengths.

$$\varepsilon = \frac{1}{\sigma T^4} \int_0^{\infty} \varepsilon_{\lambda} E_{b\lambda} d\lambda \quad (12.3)$$

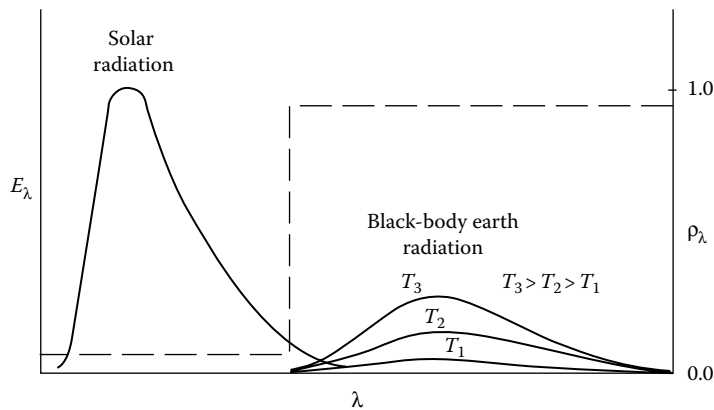
Observe that both ε_{λ} and ε are properties of the surface.

12.1.1 Selective Surfaces

Two types of special surfaces of great importance in solar collector systems are selective and reflecting surfaces. Selective surfaces combine a high absorptance for solar radiation with a low emittance for the temperature range in which the surface emits radiation. This combination of surface characteristics is possible because 98% of the energy in incoming solar radiation is contained within wavelengths below $3 \mu\text{m}$, whereas 99% of the radiation emitted by black or gray surfaces at 400 K is at wavelengths longer than $3 \mu\text{m}$. The dotted line in [Figure 12.3](#) illustrates the spectral reflectance of an ideal, selective semi-gray surface having a uniform reflectance of 0.05 below $3 \mu\text{m}$, but 0.95 above $3 \mu\text{m}$. Real surfaces do not approach this performance. [Table 12.2](#) lists properties of some selective coatings [1].

12.1.2 Reflective Surfaces

Concentrating solar collectors require the use of reflecting surfaces with high specular reflectance in the solar spectrum or refracting devices with high transmittance in the solar spectrum. Reflecting surfaces are usually highly polished metals or metal coatings on suitable substrates. With opaque substrates, the reflective coatings must always

**FIGURE 12.3**

Illustrations of the spectral reflectance characteristics of an ideal selective surface. Shows radiation from ideal surfaces at different temperatures and solar radiation.

be front-surfaced, for example, chrome plating on copper or polished aluminum. If a transparent substrate is used, however, the coating may be front- or back-surfaced. In any back-surfaced reflector, the radiation must pass through the substrate twice and the transmittance of the material becomes very important. Table 12.3 presents typical values of the normal specular reflectance of new surfaces for beam solar radiation.

The purpose of an absorber of a flat plate collector is to absorb as much of the incident solar radiation as possible, re-emit as little as possible, and allow efficient transfer of heat to a working fluid. The materials used for absorber plates include copper, aluminum, stainless steel, galvanized steel, plastics, and rubbers. Copper seems to be the most common material

TABLE 12.2

Properties of Some Selective Plated Coating Systems

Coating ^a	Substrate	$\bar{\alpha}_s$	$\bar{\epsilon}_i$	Durability	
				Breakdown Temperature (°F)	Humidity-Degradation MIL STD 810B
Black nickel on nickel	Steel	0.95	0.07	>550	Variable
Black chrome on nickel	Steel	0.95	0.09	>800	No effect
Black chrome	Steel	0.91	0.07	>800	Completely rusted
	Copper	0.95	0.14	600	Little effect
	Galvanized steel	0.95	0.16	>800	Complete removal
Black copper	Copper	0.88	0.15	600	Complete removal
Iron oxide	Steel	0.85	0.08	800	Little effect
Manganese oxide	Aluminum	0.70	0.08		
Organic overcoat on iron oxide	Steel	0.90	0.16		Little effect
Organic overcoat on black chrome	Steel	0.94	0.20		Little effect

Source: From U.S. Dept. of Commerce, 1975. Optical coatings for flat plate solar collectors, NTIS No. PN-252-383, Honeywell, Inc., Morristown, NJ. [1]

^a Black nickel coating plated over a nickel-steel substrate has the best selective properties ($\bar{\alpha}_s = 0.95$, $\bar{\epsilon}_i = 0.07$), but these degraded significantly during humidity tests. Black chrome plated on a nickel-steel substrate also had very good selective properties ($\bar{\alpha}_s = 0.95$, $\bar{\epsilon}_i = 0.09$) and also showed high resistance to humidity.

TABLE 12.3

Specular Reflectance Values for Solar Reflector Materials

Material	ρ
Silver (unstable as front surface mirror)	0.94 ± 0.02
Gold	0.76 ± 0.03
Aluminized acrylic, second surface	0.86
Anodized aluminum	0.82 ± 0.05
Various aluminum surfaces range	0.82–0.92
Copper	0.75
Back-silvered water-white plate glass	0.88
Aluminized type-C Mylar (from Mylar side)	0.76

used for absorber plates and their tubes because of its high thermal conductivity and high corrosion resistance. However, copper is quite expensive. For low-temperature applications (up to about 50°C or 120°F) a plastic material called ethylene propylene diene monomer (trade names EPDM, HCP, etc.) can be used to provide inexpensive absorber material. To compensate for the low thermal conductivity, adequate thickness is needed to provide sufficient heat transfer.

In order to increase the absorption of solar radiation and to reduce the emission from the absorber, the metallic absorber surfaces are painted or coated with flat black paint or a selective coating.

12.2 Energy Balance for a Flat Plate Collector

The thermal performance of any type of solar thermal collector can be evaluated by an energy balance that determines the portion of the incoming radiation that is delivered as useful energy to the working fluid [2].

The energy collected, Q_{coll} , can be expressed as:

$$Q_{coll} = Q_{in} - Q_{out} \quad (12.4)$$

where

$$Q_{in} = \tau \alpha I_c A_c \quad (12.5)$$

Thus, the energy absorbed is the incident solar radiation on the collector area, I_c , multiplied by the transmittance of any glass or plastic covers (which are employed to reduce heat loss to the ambient) and the absorptance of the absorber plate.

$$Q_{out} = U_L A_c (T_p - T_{amb}) \quad (12.6)$$

where T_p is the average absorber plate temperature. This assumes that the heat loss from a flat plate collector occurs mainly by convection to the outside air and that the back of the collector is highly insulated (although any such heat loss would be included in actual

collector efficiency measurements). U_L is the overall convective heat loss coefficient and depends on the number of transparent covers, or glazings. Calculating the value of U_L is covered in solar energy texts and this is important when designing a solar collector. Generally, however, commercially available collectors have measured performance values that can be used to determine annual performance.

The energy collected is just the difference between the absorbed solar radiation and the heat loss to the environment, or

$$Q_{coll} = \tau \alpha I_c A - U_L A_c (T_p - T_{amb}) \quad (12.7)$$

Because the average plate temperature is difficult to measure and control, the collected heat is usually expressed in terms of the more easily measured and controlled inlet fluid temperature, T_{in} . To change from the average plate temperature to the inlet fluid temperature the energy term is multiplied by the heat removal factor, F_R , which is the ratio of the actual energy collected to the energy that would be collected if the collector plate were at the inlet fluid temperature.

Thus,

$$Q_{coll} = F_R \tau \alpha I_c A_c - F_R U_L A_c (T_{f,i} - T_{amb}) \quad (12.8)$$

The efficiency of the collector, η_c , is just the energy collected divided by the solar radiation incident on the collector area, or

$$\eta_c = \frac{Q_{coll}}{I_c A_c} = F_R \tau \alpha - F_R U_L \frac{(T_{f,i} - T_{amb})}{I_c} \quad (12.9)$$

Thus, the efficiency of a flat plate collector can be plotted as a straight line vs. $(T_{f,i} - T_{amb})/I_c$ as shown in Figure 12.4 [3]. The y-intercept, or $F_R \tau \alpha$, is the product of F_R and the optical

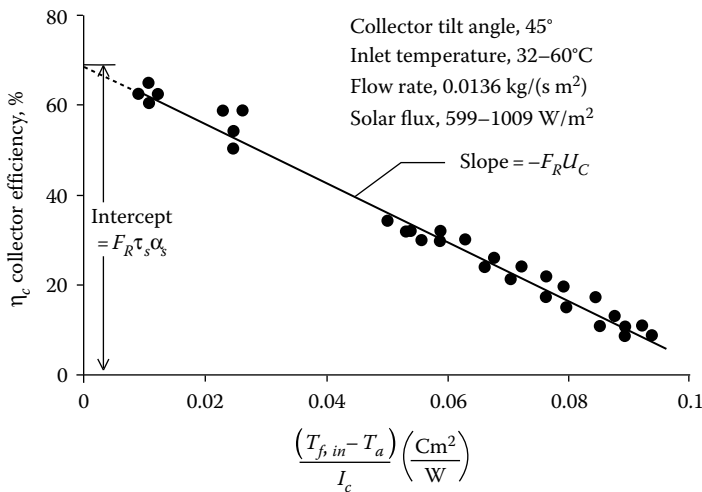


FIGURE 12.4

Experimental thermal efficiency curve for a double-glazed flat plate liquid-type solar collector. (From Goswami, Y. et al., 2000. *Principles of Solar Engineering*, 2nd ed., Taylor & Francis, Philadelphia, PA. With permission. [3])

efficiency. (The optical efficiency is simply $\tau\alpha$ and is the efficiency when there is no heat loss. Although the y-intercept, $F_R\tau\alpha$, is sometimes referred to as the optical efficiency because it is at the zero point on the heat loss axis, in actuality the average plate temperature is higher than the ambient temperature so there is a small amount of heat loss.) The slope of the line is $-F_RU_L$. This is just the convective heat loss coefficient, but corrected with F_R to account for the fact that the abscissa contains the inlet fluid temperature and not the plate temperature. Equation 12.9 is commonly called the Hottel-Whillier-Bliss equation in honor of the three solar energy researchers who developed it.

Flat plate collectors are generally used for applications where air or water needs to be heated to temperatures up to about 50–60°C (or roughly 120–140°F). Thus they can be used for domestic water heating, space heating, crop drying, and low-temperature industrial process heat. Unglazed flat plate collectors are often used to heat swimming pools.

12.3 Experimental Testing of Collectors

The performance of solar thermal systems depends largely on the performance of solar collectors. Therefore, experimental measurement of thermal performance of solar collectors by standard methods is important and necessary. The experimentally determined performance data are needed for design purposes and for determining the commercial value of the collectors. The thermal performance of a solar collector is determined by establishing an efficiency curve from the measured instantaneous efficiencies for a combination of values of incident solar radiation, ambient temperature, and inlet fluid temperature [4]. An instantaneous efficiency of a collector under steady-state conditions can be established by measuring the mass flow rate of the heat-transfer fluid, its temperature rise across the collector ($T_e - T_i$), and the incident solar radiation intensity (I_c) as

$$\eta_c = \frac{q_u}{A_c I_c} = \frac{\dot{m} C_p (T_{f,e} - T_{f,i})}{A_c I_c} \quad (12.10)$$

The efficiency, η_c , of a collector under steady state can then also be written according to the Hottel-Whillier-Bliss equation (Equation 12.9).

Figure 12.4 shows experimental data for a typical flat plate collector [3]. Since τ and α can be measured independently, a thermal performance curve of a flat plate collector allows us to establish the value of F_R and U_L also.

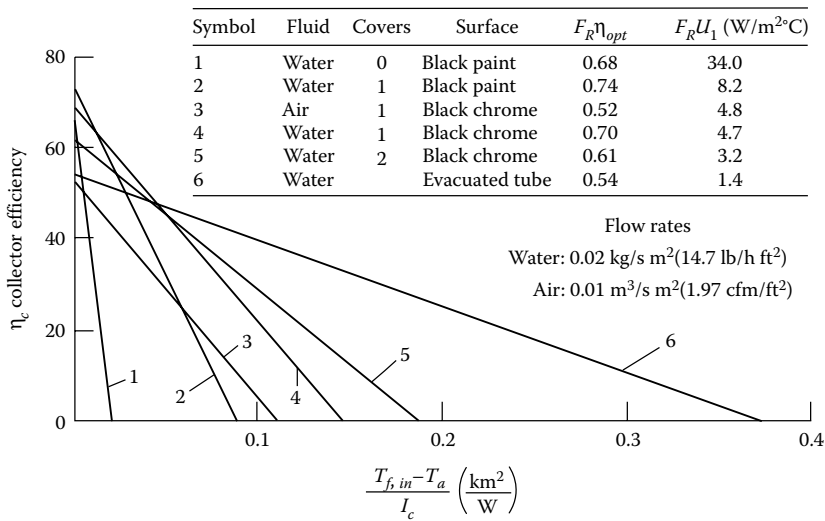
Figure 12.5 shows typical performance curves of various glazed and unglazed non-tracking solar collectors.

The product $\tau\alpha$ will change with the angle of incidence. Since flat plate collectors are normally fixed, the angle of incidence changes throughout the day. A relationship can be written between the actual or effective $(\tau\alpha)$ and $(\tau\alpha)_n$ for normal incidence as

$$(\tau\alpha) = (\tau\alpha)_n K_{\tau\alpha} \quad (12.11)$$

where

$(\tau\alpha)_n$ is the value of the product for normal angle of incidence and
 $K_{\tau\alpha}$ is called the incidence angle modifier

**FIGURE 12.5**

Typical performance curves for various non-tracking solar collectors.

Therefore, the thermal performance of a flat plate collector may be written as

$$\eta_c = F_R \left[K_{\tau\alpha} (\tau\alpha)_n - U_L \frac{(T_{f,i} - T_a)}{I_c} \right] \quad (12.12)$$

Thermal performance of collectors is usually found experimentally for normal angles of incidence in which case $K_{\tau\alpha} = 1.0$. The incidence angle modifier is then measured separately. It has been established that $K_{\tau\alpha}$ is of the form

$$K_{\tau\alpha} = 1 - b \left(\frac{1}{\cos i} - 1 \right) \quad (12.13)$$

where

b is a constant

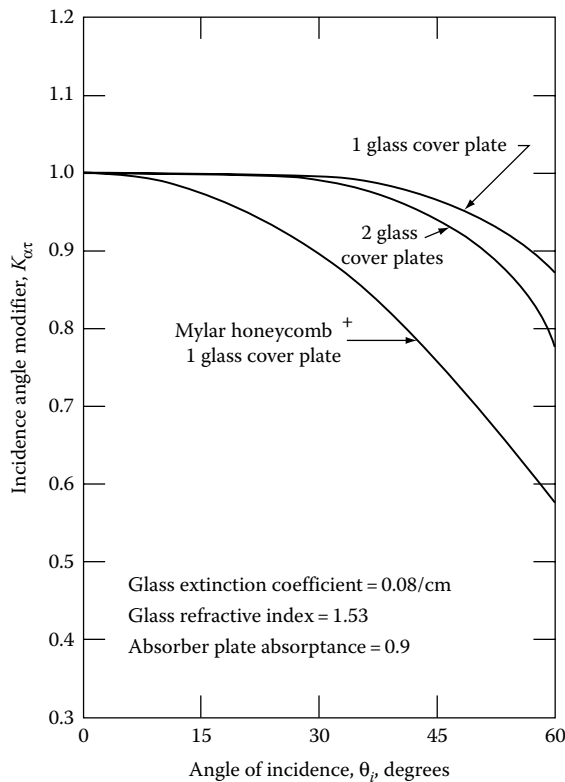
i is the angle of incidence

Figure 12.6 shows the effect of incidence angle on $K_{\tau\alpha}$ for flat plate collectors [4].

12.3.1 Testing Standards for Solar Thermal Collectors

Standard testing procedures adopted by regulating agencies in various countries establish ways of comparing the thermal performance of various collectors under the same conditions. In the United States, the thermal performance standards established by the American Society of Heating, Refrigerating and Air-Conditioning Engineers (ASHRAE) have been accepted for thermal performance tests of solar thermal collectors. Similar standards have been used in a number of countries. The standards established by ASHRAE include:

- ASHRAE Standard 93-77, "Methods of testing to determine the thermal performance of solar collectors," specifies the procedures for determining the time constant, thermal performance, and the incidence angle modifier of solar thermal

**FIGURE 12.6**

Incidence angle modifiers for three flat plate solar collectors. (From ASHRAE. *Standard 93-77: Methods of Testing to Determine the Thermal Performance of Solar Collectors*, Atlanta, GA, <https://www.ashrae.org/technical-resources/standards-and-guidelines>. With permission. [4])

collectors using a liquid or air as a working fluid [4]. Figure 12.7 shows a schematic of a standard testing configuration for thermal performance testing. The tests are conducted under quasi-steady-state conditions.

- ASHRAE Standard 96–80, “Methods of testing to determine the thermal performance of unglazed solar collectors” [5].

ASHRAE 93–77 specifies that a curve for incidence angle modifier be established by determining the efficiencies of a collector for average angles of incidence of 0°, 30°, 45°, and 60° while maintaining T_i at $\pm 1^\circ\text{C}$ of the ambient temperature. Since $(T_{i,i} - T_a) \rightarrow 0$, the incidence angle modifier according to Equation 12.13 is

$$K_{\tau\alpha} = \frac{\eta_c}{F_R(\tau\alpha)_n} \quad (12.14)$$

The denominator is the y intercept of the efficiency curve as shown in Figure 12.4.

In order to avoid transient effects, the performance of a collector is measured and integrated over at least the time constant of the collector. The time constant is measured by operating the collector under steady or quasi-steady conditions with a solar flux of at least 790 W/m^2 and then abruptly cutting the incident flux to zero, while continuing to measure the fluid inlet

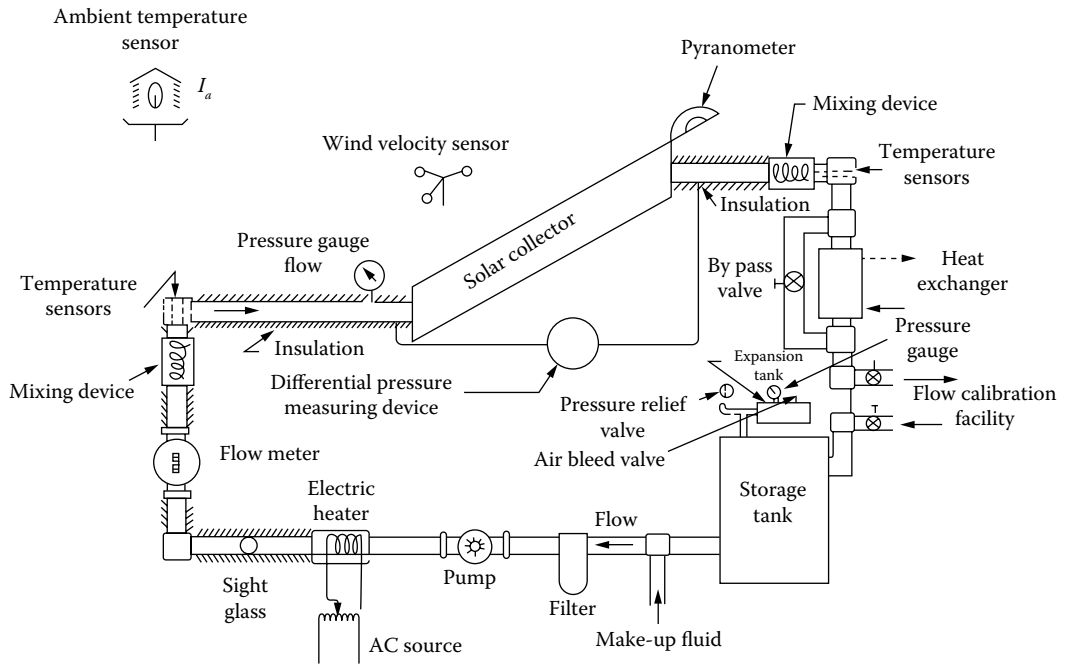


FIGURE 12.7

A testing configuration for a liquid-type solar collector. (From ASHRAE. *Standard 93-77: Methods of Testing to Determine the Thermal Performance of Solar Collectors*, Atlanta, GA, <https://www.ashrae.org/technical-resources/standards-and-guidelines>. With permission. [4])

($T_{f,i}$) and exit ($T_{f,e}$) temperatures. The fluid inlet temperature is maintained within $\pm 1^\circ\text{C}$ of the ambient temperature. The time constant is then determined as the time required to achieve

$$\frac{T_{f,e} - T_{f,i}}{T_{f,e,initial} - T_{f,i}} = 0.30 \quad (12.15)$$

For determining the thermal performance of a collector, ASHRAE Standard 93-77 specifies test conditions to obtain at least four data points for the efficiency curve [4]. The test conditions include:

1. Near normal incidence ($i \leq 5^\circ$) angle tests close to solar noon time
2. At least four tests for each $T_{f,i}$, two before and two after solar noon
3. At least four different values of $T_{f,i}$ to obtain different values of $\Delta T/I_o$, preferably to obtain ΔT at 10%, 30%, 50% and 70% of stagnation temperature rise under the given conditions of solar intensity and ambient conditions.

12.4 Evacuated Tube Collectors

Although flat plate collectors can heat water close to the boiling point, they are inefficient at such high temperatures due to high convective heat losses. Hence, they are usually

operated at temperatures below 60°C. Higher operating temperatures can be achieved in two ways: concentrating the solar energy to reduce the area for heat loss or using a vacuum to reduce the heat loss. Evacuated collectors are made in tubular form to withstand the pressure differential between ambient air and the vacuum. Various designs have been used for evacuated tube collectors. Absorbers made of metal and glass have been used inside the tubes. In all these designs, reflectors are used behind the tubes to reflect back any solar energy passing between the absorbers, so they have a small amount of concentration.

Evacuated tube collectors have been used to achieve the higher operating temperatures needed to power absorption chillers. The fact that evacuated tube collectors have a flatter efficiency curve than flat plates means that they also have higher efficiency in lower solar radiation conditions. The x -axis of the efficiency curve is $\Delta T/I$, so the x -value is large for either a high value of ΔT (i.e., a high operating temperature) or a low value of I . Thus evacuated tube collectors can be superior to flat plates even for heating domestic hot water in locations with only moderate solar radiation.

The efficiency curve of an evacuated tube collector is shown as curve 6 in [Figure 12.5](#).

12.5 Transpired Air Collectors

Flat plate collectors can be used to heat water (or a water/antifreeze mixture) or air. A special type of flat plate air collector is the transpired collector. This concept is used to heat ambient air, either as a preheater for building ventilation air or for crop drying or other dehydration applications. [Figure 12.8](#) shows a transpired wall system in which the air is drawn through a flat perforated absorber plate by a building ventilation fan. In a conventional air collector, recirculated air flows along the solar absorber plate and a transparent glazing is used to reduce heat loss to the outside air. Heat transfer from a plate to air blowing alongside it is relatively poor. The transpired design draws air through numerous holes or slits in the

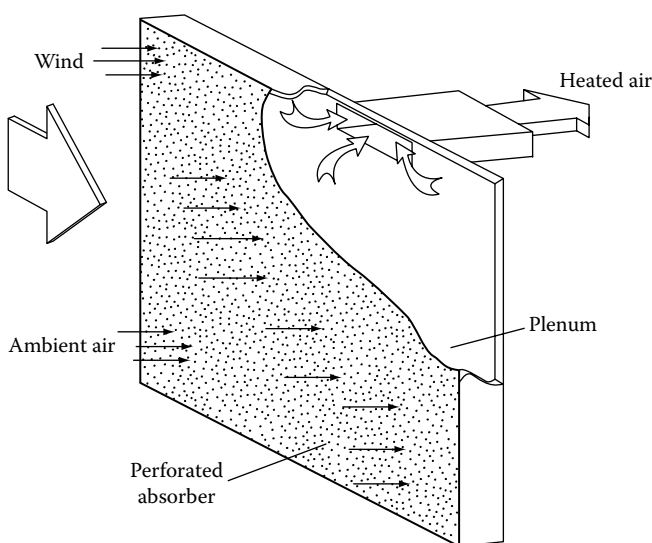


FIGURE 12.8

Unglazed transpired solar collector for air preheating.

absorber plate. Because the objective is to heat ambient air, no glazing is used. The outside air is drawn through the openings and the suction prevents convective heat loss to the ambient. Thus heat transfer rates are high, and the lack of a glazing both reduces cost and increases the amount of solar energy reaching the absorber.

Kutscher and Christensen [6] presented a thermal analysis of this system. From a heat balance on the transpired unglazed collector, the useful heat collected is

$$q_u = I_c A_c a_s - U_c A_c (T_{out} - T_a) \quad (12.16)$$

The overall heat loss coefficient, U_c , which is due to radiative and convective losses, is given as

$$U_c = \frac{h_r}{\varepsilon_{hx}} + h_c \quad (12.17)$$

where

ε_{hx} is absorber heat-exchanger effectiveness

h_r is a linearized radiative heat-transfer coefficient

h_c is the convective heat loss coefficient

The heat-exchanger effectiveness for air flowing through the absorber plate is defined as

$$\varepsilon_{hx} = \frac{T_{out} - T_a}{T_p - T_a} \quad (12.18)$$

where T_p is collector plate temperature. The forced convective heat loss coefficient due to a wind velocity of U_∞ is given as

$$h_c = 0.82 \frac{U_\infty \nu c_p}{H V_0} \quad (12.19)$$

where

ν is the kinematic viscosity of air in m^2/s

c_p the specific heat of the air in $\text{J}/\text{Kg K}$

V_0 the suction velocity in m/s

H is the height of the collector in m

The convective heat loss is associated with the boundary layer of warm air that blows off the downstream end of the collector. Because the suction keeps this thermal boundary layer extremely thin, the convective heat loss for a large wall is negligibly small if proper design criteria are met.

Radiation heat loss occurs both to the sky and to the ground. Assuming the absorber is gray and diffuse with an emissivity, ε_c , the radiative loss coefficient, h_r , is

$$h_r = \varepsilon_c \sigma \frac{(T_p^4 - F_{cs} T_{sky}^4 - F_{cg} T_{gnd}^4)}{T_p - T_a} \quad (12.20)$$

where F_{cs} and F_{cg} are the view factors between the collector and the sky, and collector and the ground, respectively. For a vertical wall with infinite ground in front of it, both F_{cs} and F_{cg} will be 0.5. Using the earlier equations, Kutscher and Christensen [6] showed that the predicted performance matches the measured performances well. Figure 12.9 shows their predicted thermal performances.

Analysis and measurements have shown that at sufficient suction rates, there is virtually no convective loss from a large wall even in windy conditions. The only heat loss is by radiation, and this is small because the absorber typically operates as a preheater at temperatures of only about 10–20°C above ambient. (For higher temperature applications, a selective surface can be used to reduce radiative loss.) Properly designed, these collectors can operate at efficiencies of well over 70% for higher suction flow rates.

Research at NREL [7] concluded that high performance can be achieved by maintaining both sufficient suction velocity and uniform flow. Suction velocity should be no less than 0.02 m/s and preferably greater than 0.04 m/s. Pressure drop across the wall should be at least 25 Pa to prevent very low flow or even outflow effects over portions of the wall subject to local drops in pressure due to the wind. Providing this pressure drop means the use of low wall porosity, typically less than 1%. Flow uniformity is affected by three things: the distance between a point on the wall and the inlet air duct to the building; thermal stack (buoyancy) effect in the plenum between the collector and the building wall; and the Bernoulli effect by which acceleration of the plenum air as it moves upward (due to

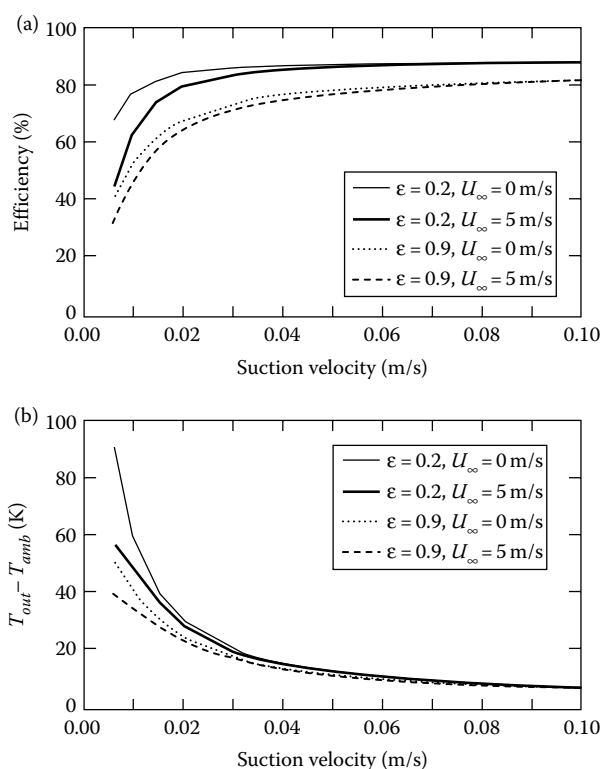


FIGURE 12.9

Predicted thermal performance of unglazed transpired collector. (a) Efficiency vs. suction velocity and (b) temperature rise vs. suction velocity. (From Kutscher, C.F., and Christensen, C.B., 1992. Unglazed transpired solar collectors, in: *Advances in Solar Energy*, vol. 7, ed. K. Boer, 283–307. With permission. [6])

the addition of air), which causes a static pressure drop with height. These three effects can be approximately balanced with the proper choice of plenum depth. The choice of a sufficiently low porosity (to increase pressure drop across the wall) will help ensure uniform flow. In a wall designed and built by NREL with an inlet at the top center of the wall, a horizontal constant velocity header (having a variable cross-sectional area) was used to ensure left-to-right flow uniformity.

Transpired collector walls typically have dampers that prevent inlet air from being heated by the wall in warm weather conditions. In this case, the wall self-cools by natural convection due to the stack effect, and the wall shades the building.

12.6 Concentrating Solar Collectors

To achieve high efficiency at the higher temperatures needed for producing process steam or generating electricity, high concentration of the solar energy is needed. This minimizes the area for heat loss. A wide variety of concentrating solar collector designs has been pursued over the years. These generally fall into two categories: line focus, in which the solar energy is focused onto a fluid-carrying pipe, and point-focus, whereby the solar energy is focused onto a small receiver.

12.6.1 Line-Focus Concentrators

Solar energy can be focused onto a pipe using either reflective or refractive optics. Today, most commercial designs use reflectors. These are of two types: (1) parabolic troughs and (2) linear Fresnel.

12.6.1.1 Parabolic Troughs

Parabolic troughs are the older and, by far, more widely used technology. [Figure 12.10](#) shows a photo of a SkyTrough parabolic trough collector. Line-focus concentrators achieve high temperatures by using a high degree of concentration to reduce the heat transfer area. Because the solar radiation must be highly concentrated, only direct normal irradiance, I_{DN} , is utilized. Hence these concentrators work best in dry, desert-type environments having very clear skies.

The geometric relations for a parabolic trough solar concentrator are shown schematically in [Figure 12.11](#). (Note this figure does not show the cylindrical evacuated tube that surrounds the absorber tube in high-temperature troughs.)

The surface of the reflector/concentrator has a parabolic cross section so that all rays of sunlight parallel to its axis are reflected from the surface to a focal line. The basic geometric relation that defines the parabolic shape for a point source is

$$y = \frac{x^2}{4f} \quad (12.21)$$

where f is the focal length of the concentrator. If D is the width of the concentrator aperture and d the absorber tube diameter, then the concentrator rim angle, ϕ , is

$$\tan\left(\frac{\phi}{2}\right) = \frac{D}{4f} \quad (12.22)$$

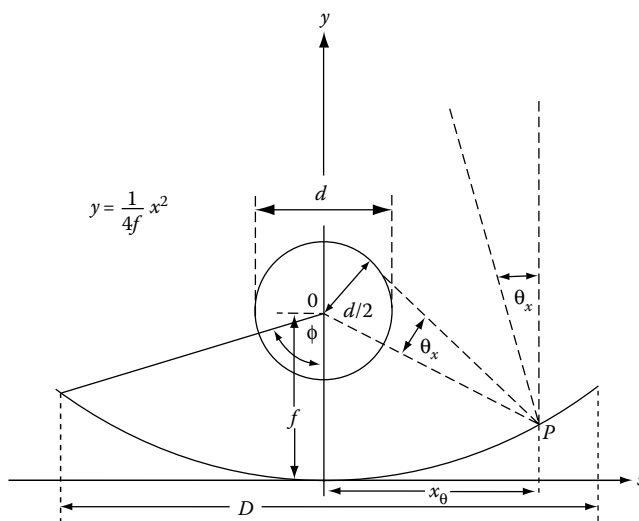
**FIGURE 12.10**

SkyTrough parabolic trough collector near Golden, Colorado, viewed by Professor Frank Kreith (right) and National Institute of Standards and Technology researcher, Dr. Isaac Garaway (left). (Courtesy of CU Engineering, 2009, Casey A. Cass, photographer.)

and the concentration ratio (based on the heat loss area), C , is

$$C = \frac{D}{\pi d} \quad (12.23)$$

In practice, parabolic troughs use concentrators with rim angles between 70° and 110° , as this range provides a balance between optical and structural requirements of the concentrator.

**FIGURE 12.11**

Geometric relations for a parabolic trough solar concentrator (evacuated cylindrical glass envelope not shown).

In addition to the optical error introduced by the finite specularity of the reflective surface, a number of other optical errors contribute to widening of the reflected beam at the receiver, such as concentrator slope error, tracking error, and receiver mislocation errors. Generally, these errors can be characterized by Gaussian distributions, so the total amount of beam spreading can be calculated as the root mean square (rms) value of all the optical errors.

For producing the high temperatures needed for efficient electricity generation, heat loss is also reduced by using a highly selective surface on the absorber tube and by enclosing the steel absorber tube within a high-vacuum Pyrex envelope. Because these collectors operate at much higher temperatures than flat plates or even evacuated tubes, they are subject to radiation heat loss. Hence rather than their efficiency curves being flat, they curve downward. (Radiation heat loss is nonlinear and increases with temperature to the fourth power.)

Parabolic trough efficiency curves are often shown with an additional term containing $(\Delta T)^2$ to capture the curvature. This only works for one ambient temperature, however. If two identical troughs operate at the same ΔT above ambient, the one at the higher temperature will have a greater heat loss and so be less efficient. Thus, the efficiency of these high-temperature collectors is best represented by the operating temperature, rather than the ΔT relative to ambient. NREL measured the efficiency of a SkyTrough parabolic trough collector module manufactured by SkyFuel and found the following equation best fit the efficiency [8]:

$$\eta_c = -1.26 \times 10^{-6} x^3 + 3.02 \times 10^{-5} x^2 - 6.24 \times 10^{-4} x + 0.773 \quad (12.24)$$

Here η_c is the collector efficiency and $x = (T_{htf} - 25)/I^{0.33}$, where T_{htf} is the average temperature of the heat transfer fluid in the collector module and I is the direct normal irradiance. (Here, 25°C is used as a constant reference point because the receiver heat loss was separately measured in a laboratory at an ambient temperature of 25°C. At an operating temperature of 25°C, there was no heat loss to the ambient and so the y-intercept when plotted this way corresponds to the optical efficiency.) The resulting efficiency plot is shown in Figure 12.12 [8].

Note that dividing the abscissa by $I^{0.33}$ allows all the different radiation curves to collapse onto a single curve. (The actual exponent is experimentally derived for each collector tested, but will generally be close to 0.33.) Note that the efficiency equation does not contain ambient temperature and is valid over a range of ambient temperatures.

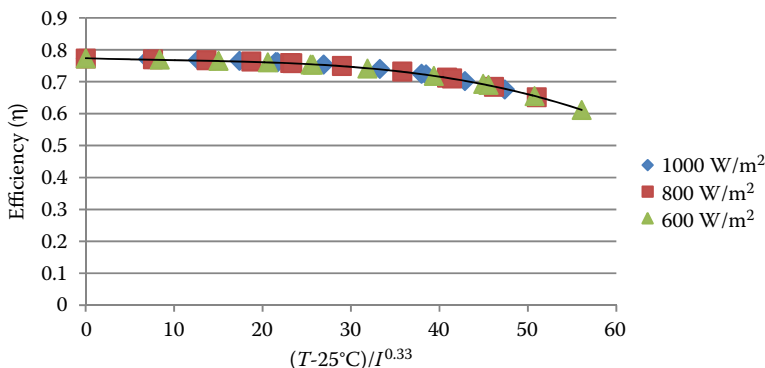


FIGURE 12.12

Efficiency plot for the SkyTrough collector. (From Kutscher, C., Burkholder, F., and Stynes, J.K., February 2012. *Journal of Solar Energy Engineering*, 134(1). [8])

The optical efficiency for this collector is 0.77. For a parabolic trough, the optical efficiency is the product of not just transmittance and absorptance, but of four factors, listed below in the order they occur for incoming solar radiation:

ρ = the reflectivity of the parabolic reflector mirror

τ = the transmittance of the glass enclosing the absorber tube

γ = the intercept factor, or the fraction of the reflected solar radiation that strikes the absorber tube

α = the absorptance of the absorber tube

Whereas ρ , τ , and α are optical properties of the materials used, γ depends on the collector geometry. Parabolic trough collectors are generally designed to have a very high intercept factor, on the order of 0.99. This means that the reflector shape must be a very accurate parabola with very little slope error. The larger the diameter of the absorber pipe, the easier it is to achieve a high intercept factor. Also, the pumping power for the heat transfer fluid flowing through the absorber pipe varies inversely with pipe diameter to the fifth power. Thus larger diameters reduce parasitic pumping power. On the other hand, a larger pipe is more expensive and means a lower concentration ratio and a greater area for heat loss, so this is a design tradeoff.

At low temperatures, a parabolic trough may have a lower efficiency than a flat plate (especially an unglazed one) due to the optical losses associated with the reflector, the glass tube, and the intercept. But its lower heat loss results in an extremely flat (albeit curving) efficiency curve and so it maintains good efficiency at high temperatures.

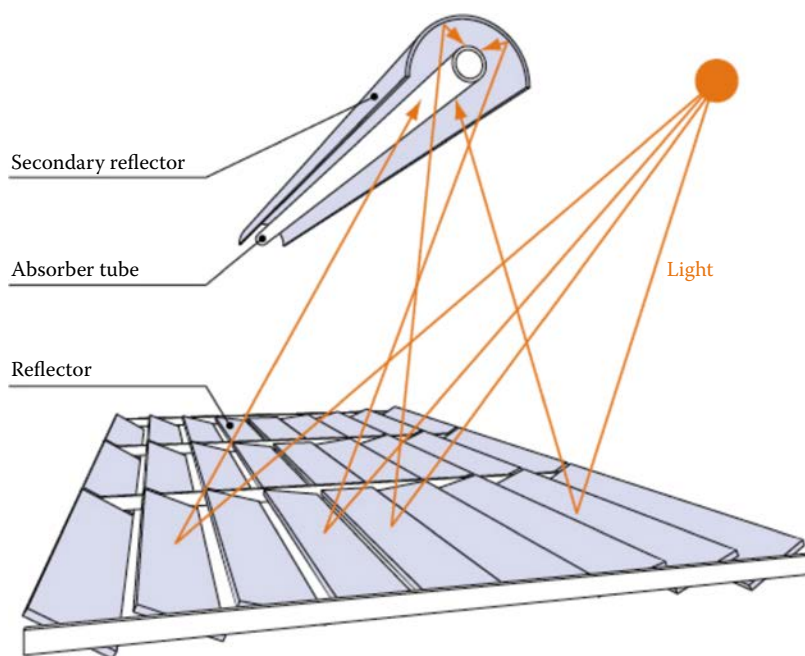
12.6.1.2 Linear Fresnel Collectors

In most commercially successful parabolic trough collector designs, the receiver moves with the tracking parabolic mirror. In the linear Fresnel design, the parabolic mirror is broken up into a number of tracking, ground-mounted segments that reflect the solar energy onto a fixed horizontal receiver tube mounted at a height above the ground. (See [Figure 12.13](#).) This design means that wind loads on the reflectors are reduced, thus resulting in structural savings. Also, linear Fresnel collector systems offer higher ground cover ratio than trough systems. On the other hand, the combination of a fixed receiver and ground-mounted reflectors means that linear Fresnel systems have lower overall optical efficiency than troughs because of the reflection angles (cosine losses).

Commercial parabolic trough systems have been limited to an operating temperature of 390°C, which is the limit of suitable heat transfer oils. There is interest in going to higher temperatures by using molten salt in place of the oil. However, the moving receiver tubes in parabolic trough collectors usually entail the use of ball joints, and ball joints (to date) are not compatible with molten salt. Because linear Fresnel systems have stationary receivers, they may lend themselves more readily to the use of molten salt. More information on linear Fresnel collectors can be found in Zhu et al. [9].

12.6.2 Point-Focus Concentrators

The efficiency of thermodynamic power cycles depends strongly on the operating temperature. By focusing sunlight onto a small receiver instead of a long pipe, higher concentration ratios and their associated smaller heat loss areas allow higher temperature

**FIGURE 12.13**

Linear Fresnel collector. (Courtesy of Andreas Poullikkas.)

to be achieved. These high-temperature concentrators can be divided into two basic types: parabolic dishes and power towers, or central receivers. Parabolic dishes use a collection of mirrors formed into a two-dimensional parabolic shape [10]. They track the sun in two axes and always point directly at the sun. For the generation of electricity, these dishes employ a thermodynamic power cycle engine at the focal point. Both Brayton turbines and Stirling cycle engines have been employed. The most successful ones to date were developed by Stirling Energy Systems with the help of Sandia National Laboratories. The 1.5-MW Maricopa installation near Phoenix consisted of 60 25-kW dishes employing Stirling engines with hydrogen as the working fluid. Although the dishes performed well, the company was unable to compete with low-cost photovoltaics.

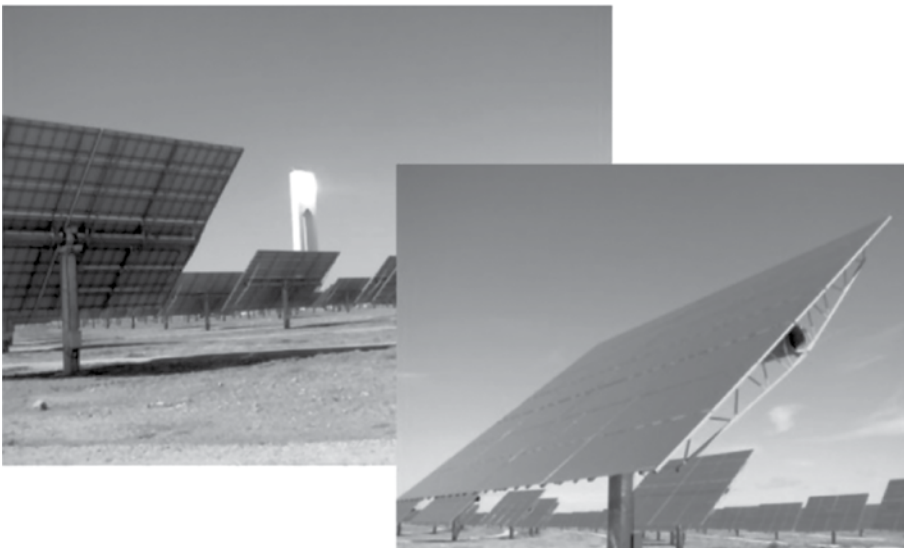
All concentrating solar power technologies have faced increasing competition from lower-cost photovoltaic systems. The main advantage of CSP systems compared to PV is that they can utilize thermal energy storage, which has a high round-trip efficiency and is currently much less expensive than battery storage. Matching thermal energy storage to a multitude of parabolic dish receiver engines is not straightforward. As a result, the CSP industry has focused its future on line-focus and power tower technologies with a recent trend toward the latter due to higher operating temperatures and thus higher power-cycle efficiencies.

Power towers (see Figure 12.14) consist of a large array of mirrors called heliostats (Figure 12.15) that track the sun in two axes and reflect the solar radiation onto a receiver located atop a tall tower [3]. (Beam-down designs have also been developed in which the heliostats focus sunlight onto a mirror that reflects the energy down to a ground-mounted receiver, but tower-mounted receiver designs continue to dominate the marketplace.) The heliostats aim not directly at the sun but at the bisected angle between the sun-Earth line and the line between the heliostat and a particular target point on the receiver. (Heliostats

**FIGURE 12.14**

Gemasolar, a 19.9 MW solar power tower plant in Fuentes de Andalucía, Sevilla, Spain, has 15 hours of molten salt storage and is capable of providing base load electricity 24 hours per day. (Photo by Charles F. Kutscher.)

Heliostats

**FIGURE 12.15**

Power tower heliostats.

are individually aimed to achieve a uniform flux profile on the receiver.) A large power tower may have over 100,000 computer-controlled heliostats.

A key design decision is the size of the heliostat. Larger heliostats require a smaller number of tracking mechanisms and associated electronics but require more structure to handle higher wind loads. As electronic controllers have dropped in cost, the trend has been to design power towers with a larger number of smaller heliostats. The receiver on the tower can contain either water or molten salt as the working fluid. The latter is more compatible with the use of molten salt thermal storage. All the existing power tower systems in the world are used to produce electrical power and are explained in more detail in Section 12.8.

12.7 Solar Domestic Hot Water, Space Heating, and Cooling Systems

Solar water-heating systems represent the most common application of solar energy at the present time. Small systems are used for domestic hot water applications while larger systems are used in industrial process heat applications. There are basically two types of water-heating systems: *natural circulation* or passive solar system (thermosyphon) and *forced circulation* or active solar system. Natural circulation solar water heaters are simple in design and low in cost. Their application is usually limited to nonfreezing climates. Forced-circulation water heaters are used in freezing climates and for commercial and industrial process heat.

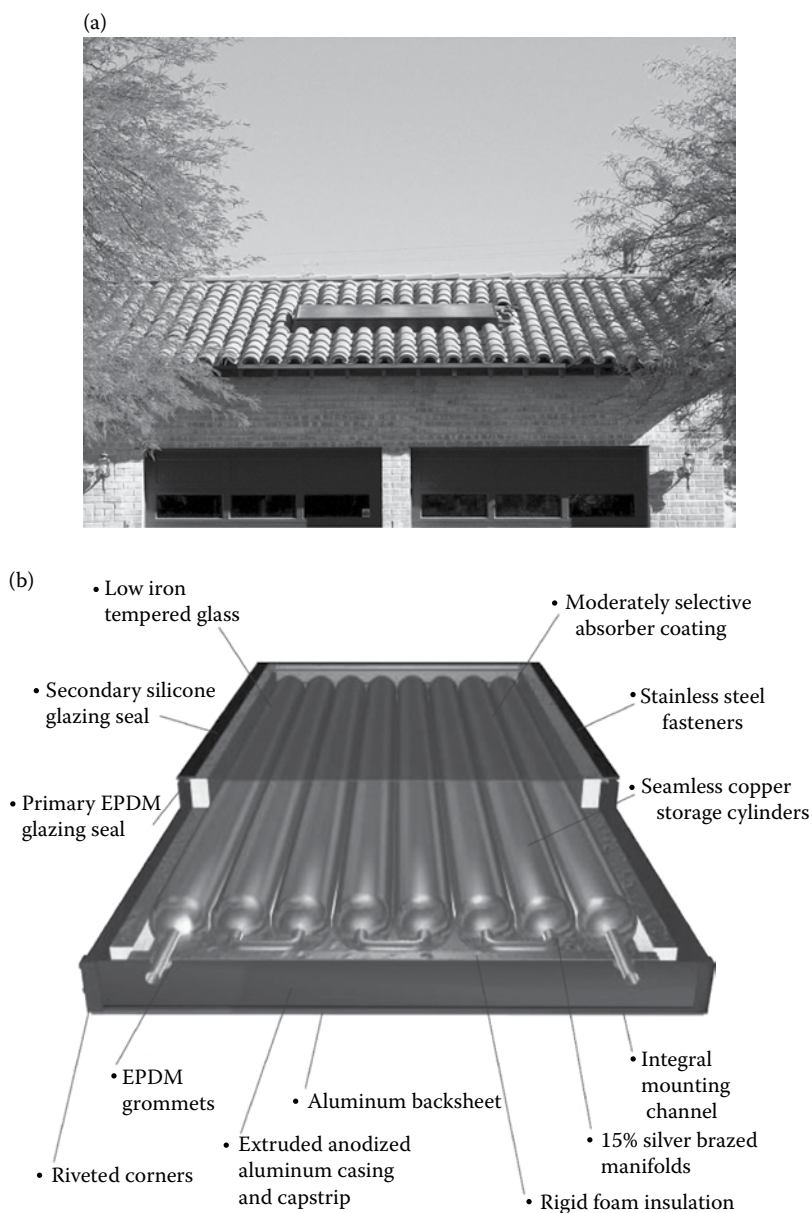
12.7.1 Solar Thermosyphon Water Heating

Solar hot water heating systems are composed of a collector and a storage tank. A passive solar collector with integrated storage is shown in [Figure 12.16](#). When the flow between the collector and the tank is by natural circulation, these passive solar hot water systems are referred to as thermosyphon systems. This ability of thermosyphon systems to heat water without an externally powered pump has spurred its use in both regions where power is unavailable and where power is very expensive and freezing is not a problem.

The natural tendency of a less dense fluid to rise above a more dense fluid can be used in a simple solar water heater to cause fluid motion through a collector. The density difference is created within the solar collector where heat is added to increase the temperature and decrease the density of the liquid. This collection concept is called a thermosyphon, and [Figure 12.17](#) schematically illustrates the major components of such a system [11].

The flow pressure drop in the fluid loop (ΔP_{FLOW}) must equal the buoyant force pressure difference ($\Delta P_{\text{BUOYANT}}$) caused by the different densities in the “hot” and “cold” legs (i.e., the left and right sides of [Figure 12.17](#)) of the fluid loop:

$$\begin{aligned}\Delta P_{\text{FLOW}} &= \Delta P_{\text{BUOYANT}} \\ &= \rho_{\text{stor}} g H - \left[\int_0^L \rho(x) g dx + \rho_{\text{out}} g (H - L) \right]\end{aligned}\tag{12.25}$$

**FIGURE 12.16**

Passive solar collector with integrated storage. (Courtesy of SunEarth, Inc., Fontana, CA.) (a) Photograph of installed module on residence in Arizona. (b) Schematic of CopperHeart integral collector-storage system.

where

H is the height of the water level in the tank and L is the height of the collector (see [Figure 12.17](#))

$\rho(x)$ is the local fluid density in the collector

ρ_{stor} is the tank fluid density

ρ_{out} is the collector outlet fluid density (the latter two densities are assumed uniform)

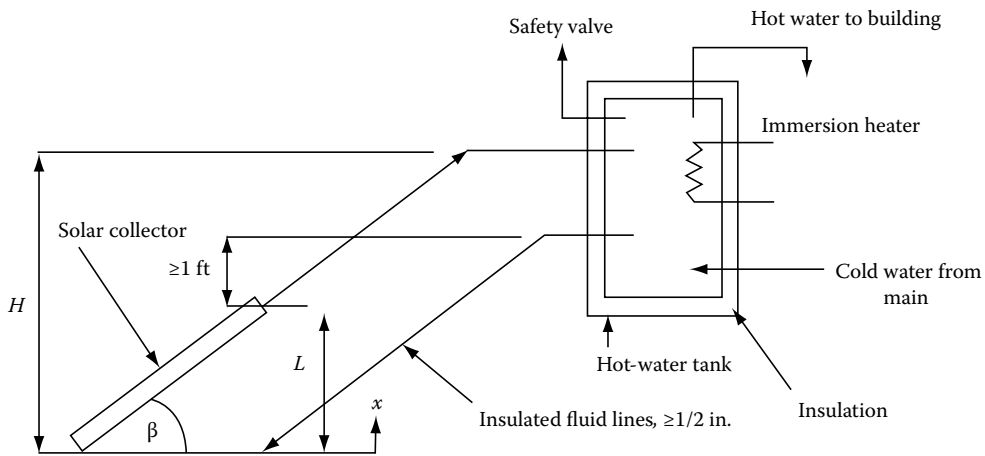


FIGURE 12.17

Schematic diagram of thermosyphon loop used in a natural circulation, service water-heating system. (From Kreith, F., and West, R., 2007. *CRC Handbook of Energy Efficiency and Renewable Energy*, CRC Press, Boca Raton, FL. With permission. [11])

The flow pressure term ΔP_{FLOW} is related to the flow loop system head loss, which is in turn directly connected to pipe friction and fitting losses and the loop flow rate:

$$\Delta P_{\text{FLOW}} = \oint_{\text{LOOP}} \rho dh_L \quad (12.26)$$

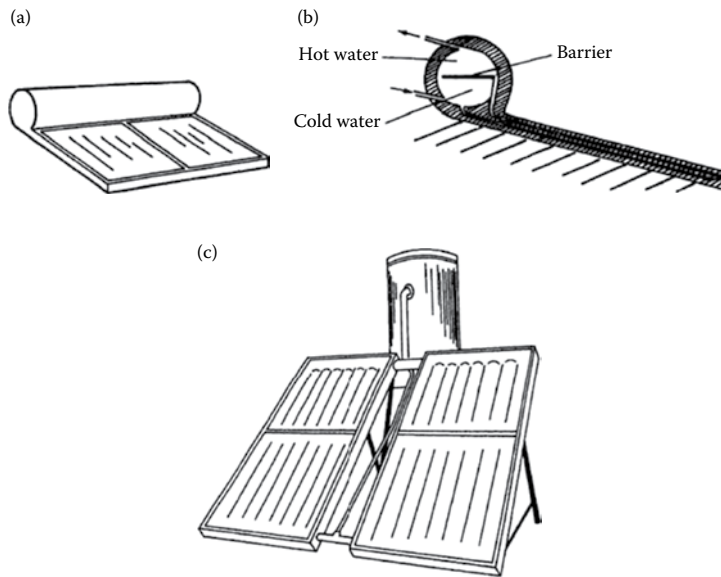
where $h_L = KV^2$, with K being the sum of the component loss “velocity” factors (see any fluid mechanics text) and V the flow velocity.

Since the driving force in a thermosyphon system is only a small density difference and not a pump, larger-than-normal plumbing fixtures must be used to reduce pipe friction losses. In general, one pipe size larger than would be used with a pump system is satisfactory. Under no circumstances should piping smaller than ½ in. (12 mm) national pipe thread (NPT) be used. Most commercial thermosyphons use 1 in. (25 mm) NPT pipe. The flow rate through a thermosyphon system is about 1 gal/ft² h (40 L/m² h) in bright sun, based on collector area.

Since the hot water system loads vary little during a year, the best angle to tilt the collector at is the local latitude. The temperature difference between the collector inlet water and the collector outlet water is usually 15–20°F (8–11°C) during the middle of a sunny day. After sunset, a thermosyphon system can reverse its flow direction and lose heat to the environment during the night. To avoid reverse flow, the top header of the absorber should be at least 1 ft. (30 cm) below the cold leg fitting on the storage tank, as shown.

To provide heat during long cloudy periods, an electrical immersion heater can be used as a backup for the solar system. The immersion heater is located near the top of the tank to enhance stratification so that the heated fluid is at the required delivery temperature at the delivery point. Tank stratification is desirable in a thermosyphon to maintain flow rates as high as possible. Insulation must be applied over the entire tank surface to control heat loss. Figure 12.18 illustrates two common thermosyphon system designs [11].

Several features inherent in the thermosyphon design limit its utility. If it is to be operated in a freezing climate, a nonfreezing fluid must be used, which in turn requires a heat exchanger between the collector and the potable water storage. (If potable water is not required, the collector can be drained during cold periods instead.) Heat exchangers

**FIGURE 12.18**

Passive solar water heaters: (a) compact model using combined collector and storage, (b) section view of the compact model, and (c) tank and collector assembly. (From Kreith, F., and West, R., 2007. *CRC Handbook of Energy Efficiency and Renewable Energy*, CRC Press, Boca Raton, FL. With permission. [11])

of either the shell-and-tube type or the immersion-coil type require higher flow rates for efficient operation than a thermosyphon can provide. Therefore, the thermosyphon is generally limited to nonfreezing climates. A further restriction on thermosyphon use is the requirement for an elevated tank. In many cases, structural or architectural constraints prohibit raised-tank locations. In residences, collectors are normally mounted on the roof, and tanks mounted above the high point of the collector can easily become the highest point in a building. Practical considerations often do not permit this application.

EXAMPLE 12.1

Determine the “pressure difference” available for a thermosyphon system with 1 m high collector and 2 m high hot and cold legs. The water temperature input to the collector is 25°C, and the collector output temperature is 35°C. If the overall system loss velocity factor (K) is 15.6, estimate the system flow velocity.

Solution

Equation 12.25 is used to calculate the pressure difference, with the water densities being found from the temperatures (in steam tables):

$$\rho_{stor}(25^{\circ}\text{C}) = 997.009 \text{ kg/m}^3; \quad \rho_{out}(35^{\circ}) = 994.036 \text{ kg/m}^3;$$

$$\rho_{coll,ave.}(30^{\circ}\text{C}) = 996.016 \text{ kg/m}^3 \text{ (Note: average collector temperature used in integral)}$$

and with $H = 2$ and $L = 1$ m

$$\begin{aligned} \Delta P_{BUOYANT} &= (997.009) 9.81(2) - [(996.016) 9.81(1) + (994.036) 9.81(1)] \\ &= 38.9 \text{ N/m}^2(\text{Pa}) \end{aligned}$$

The system flow velocity is estimated from the system K value given and the pressure difference calculated earlier. Taking the average density of the water around the loop (at 30°C), and substituting into Equation 12.26:

$$\Delta P_{\text{BUOYANT}} = (\rho_{\text{loop,ave.}})(h_L)_{\text{loop}} = (\rho_{\text{loop,ave.}})KV^2$$

$$V^2 = \frac{38.9}{(996.016)(15.6)}$$

$$V = 0.05 \text{ m/s}$$

12.7.2 Forced-Circulation Hot Water Systems

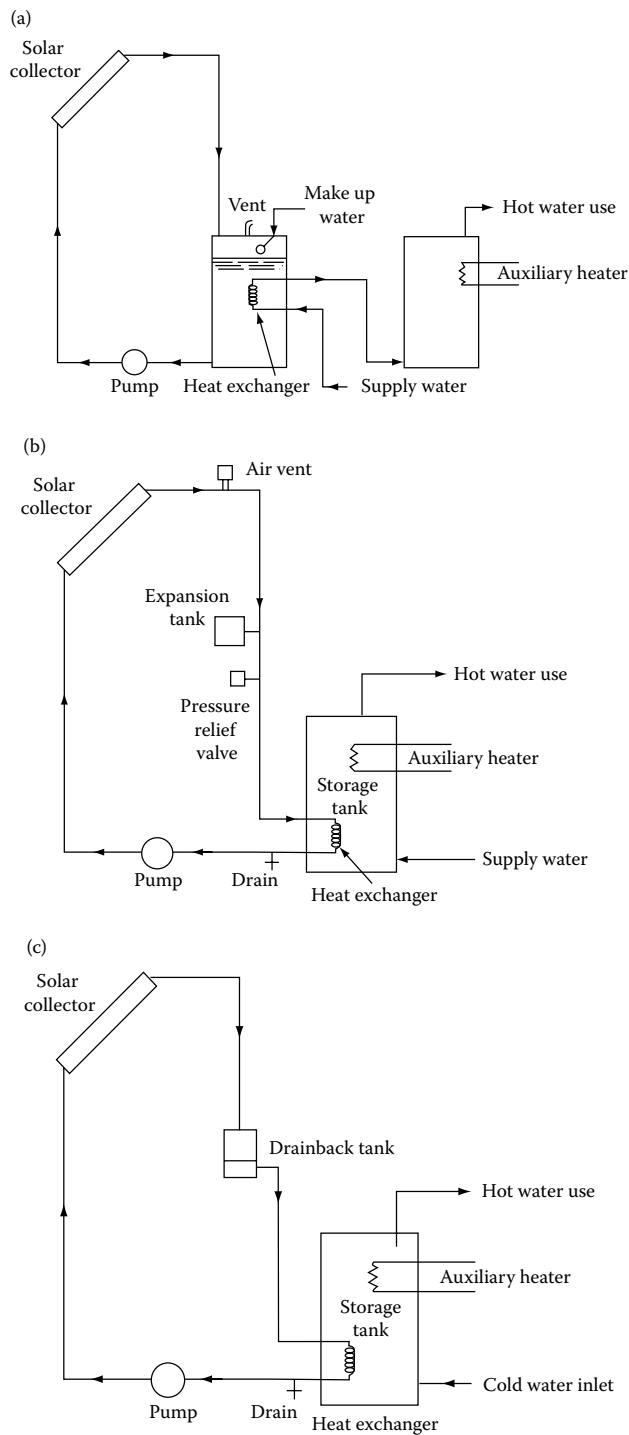
If a thermosyphon system cannot be used for climatic, structural, or architectural reasons, a forced-circulation system is required. Figure 12.19 shows three configurations of forced-circulation systems: (1) open loop, (2) closed loop, and (3) closed loop with drainback [12]. In an open-loop system (Figure 12.19a) the solar loop is at atmospheric pressure; therefore, the collectors are empty when they are not providing useful heat. A disadvantage of this system is the high pumping power required to pump the water to the collectors every time the collectors become hot. In a pressurized closed-loop system (Figure 12.19b) the loop remains filled at all times and the pump has to overcome only the resistance of the pipes.

In order to accommodate the thermal expansion of water from heating, a small (about 2 gal capacity) expansion tank and a pressure relief valve are provided in the solar loop. Because water always stays in the collectors of this system, antifreeze (propylene glycol or ethylene glycol) is required for locations where freezing conditions can occur. During stagnation conditions (in summer), the temperature in the collector can become very high, causing the pressure in the loop to increase. This can cause leaks in the loop unless some fluid is allowed to escape through a pressure relief valve. Whether as a result of leaks or of draining, air enters the loop, causing the pumps to run dry. This disadvantage can be overcome in a closed-loop drainback system that is not pressurized (Figure 12.19c). In this system, when the pump shuts off, the water in the collectors drains back into a small holding tank while the air in the holding tank goes up to fill the collectors. The holding tank can be located where freezing does not occur, but still at a high level to reduce pumping power. In all three configurations, a differential controller measures the temperature difference between the solar collector and the storage. It turns the circulation pump on when the difference is more than a set limit (usually 5°C) and turns it off when the difference goes below a set limit (usually 2°C). Alternatively, a photovoltaic (PV) panel and a DC pump may be used. The PV panel will turn on the pump only when solar radiation is above a minimum level. Therefore, the differential controller and the temperature sensors may be eliminated.

For temperatures of up to about 60°C, required for many industrial process heat applications, forced-circulation flat plate collector water-heating systems described earlier can be used. For higher temperatures, evacuated tube collectors or concentrating collectors must be used.

EXAMPLE 12.2

Determine the performance of a flat plate solar hot water system in Boulder, Colorado, using the SAM program. Assume the cost of the collector is \$300.00 per square meter, the storage tank cost is \$1200.00, and the installation and balance of system costs are \$2500.00 and \$1000.00, respectively. Except for the parameters specified, use the default values in the program. Assume that the average daily hot water usage is 200 kg/day and the

**FIGURE 12.19**

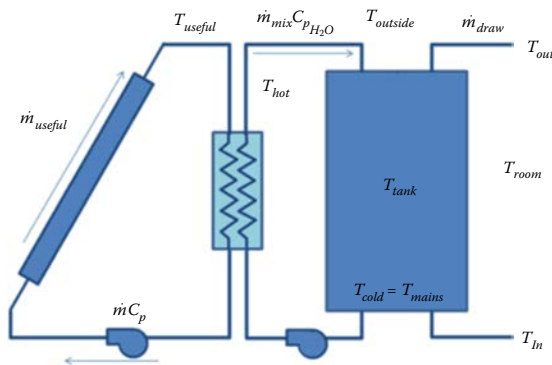
Typical configurations of solar water-heating systems: (a) open-loop system, (b) closed-loop system, and (c) closed-loop drainback system. (Adapted from Goswami, D.Y., 1986. *Alternative Energy in Agriculture*, vol. 1, CRC Press, Boca Raton, FL. [12])

collector area is 3 square meters with a tilt angle of 30° and an azimuth of 180° (south). The parameters in the Hottel-Whillier-Bliss equation (Equation 12.9) are: $F_R \tau \alpha = 0.72$, and $F_R U_L = 3.7$ (W/m²C), and the incident angle modifier is 0.10. Assume the heat exchanger effectiveness is 0.8 and the auxiliary temperature in the electric water tank is set at 50°C . Assume a standard loan with 100% debt fraction, 30-year life, 7% interest rate, 5% real discount rate, 2.5%/yr inflation rate, a 30-year loan term, and a 30-year analysis period.

Solution

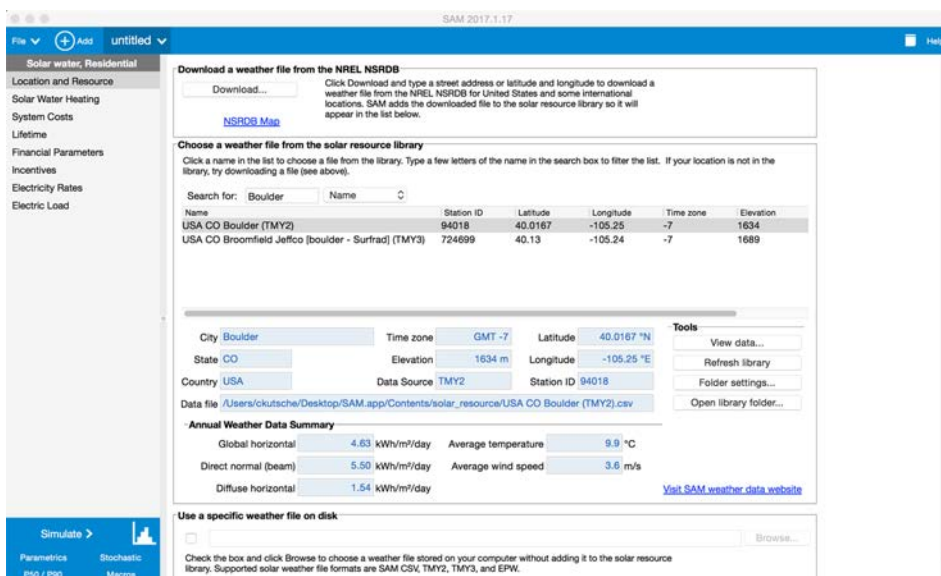
We will analyze this system using SAM, which can be downloaded at <https://sam.nrel.gov/>. (Note: SAM is frequently updated. The instructions that follow are for version 2017.1.17 and may change slightly.)

SAM models a solar hot water system applicable to freezing climates that has a heat exchanger between an antifreeze/water solar collector loop and water storage:



After downloading SAM from the website, to start a solar water heating project:

1. Start SAM.
2. Click **Start a New Project**
3. Choose **Solar water heating**, then **Residential**, then click OK.
4. The collector is located in Boulder, CO, so search for Boulder, CO in the weather file section under the Location and Resource tab.



- Under the “Solar Water Heating” tab, set the Hot Water Draw to 200 kg/day. Under System choose 1 collector with a tilt of 30° and an azimuth of 180°. Under Collector, click “Enter user-defined parameters” and change the collector values to area = 3 m², FRt_a = 0.72 and FRUL = 3.7, and set the incident angle modifier to 0.1. Set the heat exchange effectiveness on the same page to 0.8 and the outlet set temperature to 50°C.

SAM 2017.1.17

Solar water, Residential

Hot Water Draw

Hourly hot water draw profile kg/hr Scale draw profile to average daily usage ☒

Total annual hot water draw kg/year Average daily hot water usage kg/day

System

Tilt deg Diffuse sky model

Azimuth deg Irradiance inputs

Total system flow rate kg/s Albedo 0.1

Working fluid Total system collector area m²

Number of collectors Rated system size kW

Shading Shading losses Open 3D shade calculator...

Curtailment and Availability Edit losses... Constant loss: 0.0 % Hourly losses: None Custom periods: None

Collector

☒ Enter user-defined parameters ☐ Choose from library

User-defined collector

Collector area m²

FRt_a

FRUL W/m².C

Incidence angle modifier

Test fluid

Test flow kg/s

Search for: Name

Name	SRCC Number	Type	Area	IAM	FRt _a
Heliodyne Inc. Gobi 408 001	2007027C	Glazed Flat...	2.99	-0.06	0.73
Heliodyne Inc. Gobi 406 001	2007027B	Glazed Flat...	2.5	-0.06	0.726
Heliodyne Inc. Gobi 336 001	2007027A	Glazed Flat...	2.49	-0.06	0.725
Heliodyne Inc. Gobi 406 002	1981085G	Glazed Flat...	2.5	0.09	0.719
Heliodyne Inc. Gobi 410 002	1981085D	Glazed Flat...	3.73	0.09	0.719
Heliodyne Inc. Gobi 408 002	1981085C	Glazed Flat...	3	0.09	0.719
Heliodyne Inc. Gobi 404 001	2007027E	Glazed Flat...	1.52	-0.06	0.713
Heliodyne Inc. Gobi 410 013	2007026D	Glazed Flat...	3.73	-0.04	0.711
Heliodyne Inc. Gobi 408 013	2007026C	Glazed Flat...	2.99	-0.04	0.707
Heliodyne Inc. Gobi 408 013	2007026R	Glazed Flat...	2.99	-0.04	0.704

Solar Tank and Heat Exchanger

Solar tank volume m³ Heat exchanger effectiveness 0.1

Solar tank height to diameter ratio Outlet set temperature C

Solar tank heat loss coefficient (U value) W/m².C Mechanical room temperature C

Solar tank maximum water temperature C

Piping and Pumping

Total piping length in system m Pump power W

Pipe diameter m Pump efficiency 0.1

Pipe insulation conductivity W/m.C

Pipe insulation thickness m

Advanced

Use custom mains profile ☐ Use custom set temperatures ☐

Hourly custom mains profile C Hourly custom set temperatures C

Simulate Parameters Stochastic P50 / P90 Macros

- Under System Costs, enter a collector cost of \$300.00 per square meter, a storage tank cost of \$1200.00, and installation and balance of system costs of \$1000.00 and \$2500.00, respectively (some of these may be the default values).

SAM 2017.1.17

File Add untitled Help

Solar water, Residential

Location and Resource
Solar Water Heating
System Costs
Lifetime
Financial Parameters
Incentives
Electricity Rates
Electric Load

Direct Capital Costs

Number of Collectors	1	Collector cost	300.00 \$/m2	\$ 900.00
		Storage cost	1200.00 \$/m3	\$ 360.00
		Balance of system		\$ 1,000.00
		Installation cost		\$ 2,500.00
		Contingency	0 %	\$ 0.00
		Total direct cost		\$ 4,760.00

Indirect Capital Costs

	% of Direct Cost	Non-fixed Cost	Fixed Cost	Total
Engineer, Procure, Construct	0 %	\$ 0.00	\$ 0.00	\$ 0.00
Project, Land, Miscellaneous	0 %	\$ 0.00	\$ 0.00	\$ 0.00
Sales tax of	5 %	applies to	100 % of direct cost	\$ 238.00
				Total indirect cost \$ 238.00

Total Installed Costs

Total Installed Cost excludes financing costs (if any, see Financing Page)	Total installed cost \$ 4,998.00
	Total installed cost per capacity (\$/Wt) \$ 2.74

Operation and Maintenance Costs

	First year cost	Escalation rate (above inflation)
Fixed annual cost	0 \$/yr	0 %
Fixed cost by capacity	50 \$/kW-yr	0 %
Variable cost by generation	0 \$/MWh	0 %

In Value mode, SAM applies both inflation and escalation to the first year cost to calculate out-year costs. In Schedule mode, neither inflation nor escalation applies. See Help for details.

Simulate > Parametrics Stochastic P50 / P90 Macros

7. Under Financial Parameters, choose a standard loan with 100% debt fraction, 30-year loan period, 7% interest rate, 5% real discount rate, 2.5%/yr inflation rate, and a 30-year analysis period.

SAM 2017.1.17

File Add untitled Help

Solar water, Residential

Location and Resource
Solar Water Heating
System Costs
Lifetime
Financial Parameters
Incentives
Electricity Rates
Electric Load

Residential Loan Type

☒ Standard loan Standard loan interest payments are not tax deductible.
☐ Mortgage Mortgage interest payments are tax deductible.

Loan Parameters

Debt fraction	100 %	Net capital cost	\$ 4,998.00	The weighted average cost of capital (WACC) is displayed for reference. SAM does not use the value for calculations. For a project with no debt, set the debt fraction to zero.
Loan term	30 years	Debt	\$ 4,998.00	
Loan rate	7 %/year	WACC	4.69 %	

Analysis Parameters

Analysis period	30 years	Inflation rate	2.5 %/year
		Real discount rate	5 %/year
		Nominal discount rate	7.62 %/year

Tax and Insurance Rates

Federal income tax rate	28 %/year	Property Tax	Assessed percentage	100 % of installed cost
State income tax rate	7 %/year		Assessed value	\$ 4,998.00
Sales tax	5 % of total direct cost		Annual decline	0 %/year
Insurance rate (annual)	1 % of installed cost		Property tax rate	1 %/year

Salvage Value

Net salvage value	5 % of installed cost	End of analysis period value	\$ 250
-------------------	-----------------------	------------------------------	--------

Simulate > Parametrics Stochastic P50 / P90 Macros

8. Under Electricity Rates, click the Search for rates button and search for Boulder zip code 80301. Choose Public Service Co of Colorado and click on Residential-Service (Schedule R) the first time it appears. Then click Download and apply utility rate.

OpenEI Utility Rate Database

Zip code: 80301 Search by zip code

Filter:

Public Service Co of Colorado

Available rate schedules: Residential Only

☐ Show Active Only

Filter:

Rate RD - Residential (55fc809b682bea28da63f9d8)
 R (55fc80d9682bea28da642d56)
 Residential Service (Schedule R) (55fc8123682bea28da646c12)
 Residential Demand Service (Schedule RD) (55fc81bf682bea28da64e9b4)
 Residential Time Of Use (Schedule R-TOU). Pilot program (55fc81bf682bea28da64e9b4)
 RESIDENTIAL TIME OF USE SERVICE (55fc81bf682bea28da64e9b4)

Name: Public Service Co of Colorado: Residential Service (Schedule R)
 Description: Applicable to Residential service. Energy charges include
 Start: 2015-03-31
 End: 2015-09-29
 GUID: 55fc8123682bea28da646c12

Show all 1 utilities

[Go to rate page on OpenEI.org...](#)
[Rate JSON data page...](#)

Ready. Download and apply utility rate Close

9. We will use the typical electric load data that is the default in SAM. Click Simulate at the bottom of the screen to run the calculations and get results. The table of results appears as follows:

Metric	Value
Annual energy saved (year 1)	2,055 kWh
Solar fraction (year 1)	0.66
Aux with solar (year 1)	965.5 kWh
Aux without solar (year 1)	3,118.9 kWh
Capacity factor (year 1)	12.8%
Levelized COE (nominal)	24.15 ¢/kWh
Levelized COE (real)	18.33 ¢/kWh
Electricity bill without system (year 1)	\$1,064
Electricity bill with system (year 1)	\$825
Net savings with system (year 1)	\$240
Net present value	\$-2,191
Payback period	29.8 years
Discounted payback period	NaN
Net capital cost	\$4,998
Equity	\$0
Debt	\$4,998

Note that the accuracy of solar performance predictions is generally no better than 10% and the number of significant figures in the computed solutions is not realistic. In this example, the system barely pays for itself over the 30-year lifetime of the system. Note that the installation cost assumed here of \$2500 is a little more than half of the total system cost. A do-it-yourself system would obtain a better payback. Also, installation cost would likely be less of a factor in a large multi-family system. In a market with high electricity prices, such as Hawaii, the economics would also look more favorable. The next table is from a run of the same SAM model but using the Honolulu airport weather file and the Residential R single-phase electric rate for the Hawaiian Electric Company.

Metric	Value
Annual energy saved (year 1)	1,564 kWh
Solar fraction (year 1)	0.85
Aux with solar (year 1)	173.9 kWh
Aux without solar (year 1)	1,844.6 kWh
Capacity factor (year 1)	9.8%
Levelized COE (nominal)	31.73 ¢/kWh
Levelized COE (real)	24.09 ¢/kWh
Electricity bill without system (year 1)	\$3,147
Electricity bill with system (year 1)	\$2,631
Net savings with system (year 1)	\$516
Net present value	\$1,953
Payback period	9.2 years
Discounted payback period	13.5 years
Net capital cost	\$4,998
Equity	\$0
Debt	\$4,998

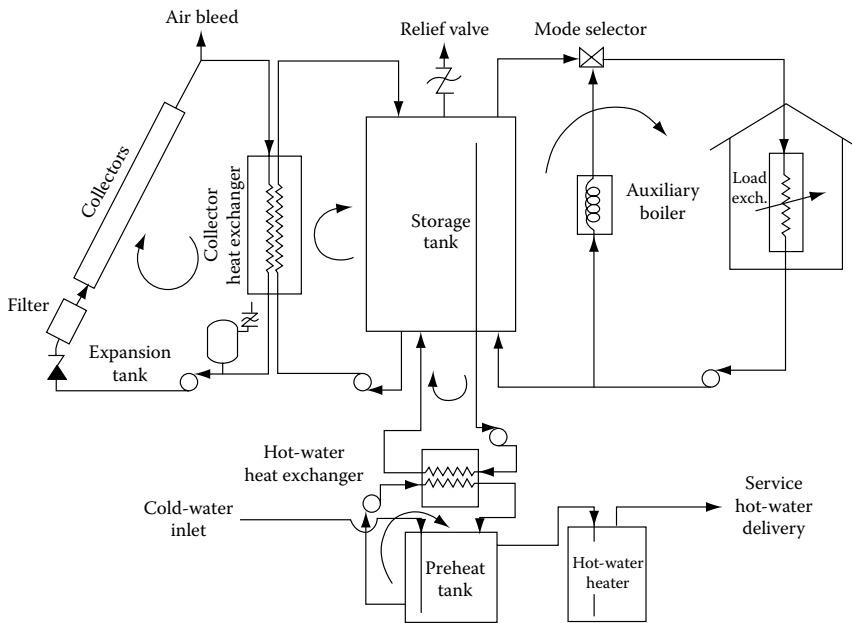
12.7.3 Liquid-Based Solar Heating Systems for Buildings

Solar space-heating systems can be classified as active or passive depending on the method utilized for heat transfer. A system that uses pumps and/or blowers for fluid flow in order to transfer heat is called an active system. On the other hand, a system that utilizes natural phenomena for heat transfer is called a passive system. Passive solar heating systems are described later in this chapter. In this section, configurations, design methods, and control strategies for active solar heating systems are described.

Figure 12.20 is a schematic diagram of a typical solar space heating system. The system consists of three fluid loops—collector, storage, and load. In addition, most space-heating systems are integrated with a domestic water-heating system to improve the yearlong solar load factor.

Since space heating is a relatively low-temperature use of solar energy, a thermodynamic match of collector to task indicates that an efficient flat plate collector or low-concentration solar collector is the thermal device of choice.

The collector fluid loop contains fluid manifolds, the collectors, the collector pump, and heat exchanger, an expansion tank, and other subsidiary components. A collector heat exchanger and antifreeze in the collector loop are normally used in all solar space heating

**FIGURE 12.20**

Typical solar thermal system for space heating and hot water heating showing fluid transport loops and pumps.

systems, since the existence of a significant heating demand implies the existence of some subfreezing weather.

The storage loop contains the storage tank and pump as well as the tube side of the collector heat exchanger. To capitalize on whatever stratification may exist in the storage tank, fluid entering the collector heat exchanger is generally removed from the bottom of storage. This strategy ensures that the lowest temperature fluid available in the collector loop is introduced at the collector inlet for high efficiency. The energy delivery-to-load loop contains the load device, baseboard heaters or fin-and-tube coils, and the backup system with a flow control (mode selector) valve.

The best solar collector orientation is such that the average solar incidence angle is smallest during the heating season. For tracking collectors, this objective is automatically realized. For fixed collectors in the northern hemisphere, the best orientation is due south (due north in the southern hemisphere), tilted up from the horizon at an angle of about 15° greater than the local latitude.

Although due south is the optimum azimuthal orientation for collectors in the northern hemisphere, variations of 20° east or west have little effect on annual energy delivery. Off-south orientations greater than 20° may be required in some cases because of obstacles in the path of the sun. Also, for aesthetic purposes collectors are often mounted at the roof angle, and a small loss of performance is accepted.

12.7.4 Passive Solar Heating Systems

Passive solar heating systems contain the five basic components:

1. Collector \rightarrow windows, walls, and floors
2. Storage \rightarrow walls and floors, large interior masses (often these are integrated with the collector absorption function)

3. Distribution system → radiation, free convection, simple circulation fans
4. Controls → movable window insulation, vents both to other inside spaces or to ambient
5. Backup system → any nonsolar heating system

The design of passive systems requires the strategic placement of windows, storage masses, and the occupied spaces themselves. The fundamental principles of solar radiation geometry and availability are instrumental in the proper location and sizing of the system's "collectors" (windows). Storage devices are usually more massive than those used in active systems and are frequently an integral part of the collection and distribution system.

A commonly used method of cataloging the various passive system concepts is to distinguish three general categories: direct, indirect, and isolated gain. Most of the physical configurations of passive heating systems are seen to fit within one of these three categories.

For direct gain (Figure 12.21), sunlight enters the heated space and is converted to heat at absorbing surfaces [11]. This heat is then distributed throughout the space and to the various enclosing surfaces and room contents.

For indirect gain category systems, sunlight is absorbed and stored by a mass interposed between the glazing and the conditioned space. The conditioned space is partially enclosed and bounded by this thermal storage mass, so a natural thermal coupling is achieved. Examples of the indirect approach are the thermal storage wall, the thermal storage roof, and the northerly room of an attached sunspace.

In the thermal storage wall (Figure 12.22), sunlight penetrates the glazing and is absorbed and converted to heat at a wall surface interposed between the glazing and the heated space [11]. The wall is usually masonry (mass or Trombe wall) or containers filled with water (water wall), although it might contain phase-change material. The attached sunspace (Figure 12.23) is actually a two-zone combination of direct gain and thermal storage wall [11]. Sunlight enters and heats a direct gain southerly "sunspace" and also heats a mass wall separating the northerly-buffered space, which is heated indirectly. The sunspace is frequently used as a greenhouse, in which case the system is called an attached greenhouse.

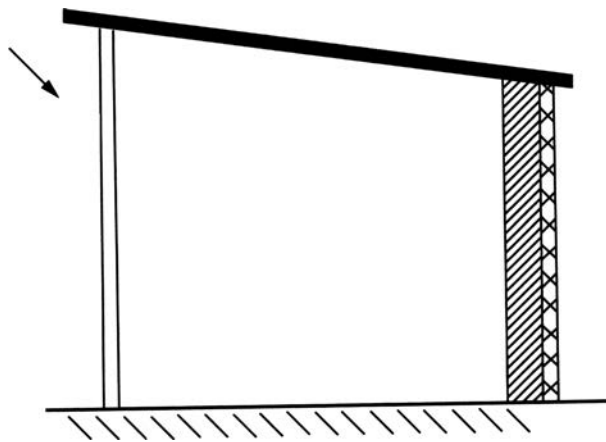
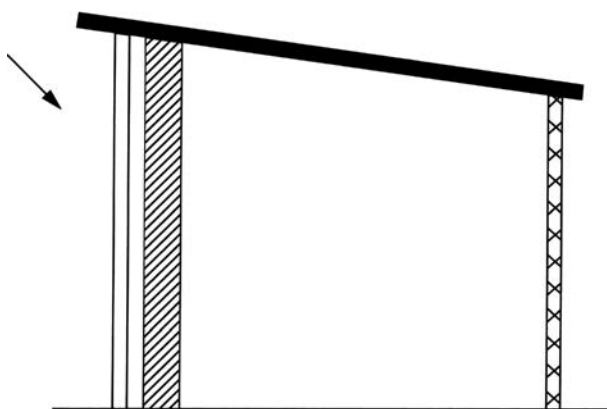


FIGURE 12.21

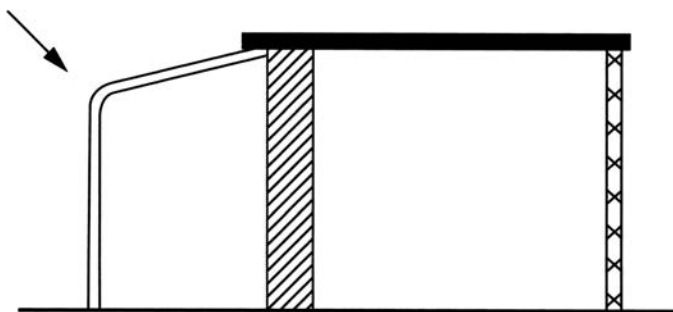
Direct gain. (From Kreith, F., and West, R., 2007. *CRC Handbook of Energy Efficiency and Renewable Energy*, CRC Press, Boca Raton, FL. With permission. [11])

**FIGURE 12.22**

Thermal storage wall. (From Kreith, F., and West, R., 2007. *CRC Handbook of Energy Efficiency and Renewable Energy*, CRC Press, Boca Raton, FL. With permission. [11])

The isolated gain category concept is an indirect system except that there is a distinct thermal separation (by means of either insulation or physical separation) between the thermal storage and the heated space. The convective (thermosyphon) loop, as depicted in [Figure 12.19](#), is in this category and, while often used to heat domestic water, can also be used for building heating, often with air as the working fluid. It is most akin to conventional active systems in that there is a separate collector and separate thermal storage. The thermal storage wall, thermal storage roof, and attached sunspace approaches can also be made into isolated systems by insulating between the thermal storage and the heated space.

Passive solar buildings rose to popularity in sunny regions in the 1970s. Since then, building envelopes have improved greatly. Windows have much higher R-values, roofs and walls are highly insulated, and air leaks are minimized and verified via blower door tests. Although lighting systems have become much more efficient and produce less internal heat, the proliferation of computers, entertainment systems, and other electronic devices has further reduced building heating loads. For many tight homes today, the hot water heating load can be greater than the space heating load. All these things have resulted in less need to take advantage of passive solar heat. In addition, the rapid decrease in photovoltaic (PV) module costs is allowing building owners to cost-effectively convert solar energy striking a building into electricity that can run heat pumps and other devices. Today when someone

**FIGURE 12.23**

Attached sunspace. (From Kreith, F., and West, R., 2007. *CRC Handbook of Energy Efficiency and Renewable Energy*, CRC Press, Boca Raton, FL. With permission. [11])

refers to a “solar home” they are typically referring to a home with rooftop PV. Finally, builders have generally not adopted passive solar designs on a large scale because they can compromise preferred views and it can be a challenge to achieve the proper orientations in a large community.

As a result of these changes, passive solar design features today are more typically included as a part of good overall building design. In performing OpenStudio simulations of commercial buildings or BEopt models of residential buildings, designers can adjust parameters such as the building aspect ratio, the ratio of window to wall area for each wall, and the amount of thermal mass contained in a building. Good design practice generally calls, for example, for a building to be longer in the east–west direction. In cold climates, window area on the north wall is minimized, and south wall window area is favored. Shading devices can be employed on the east, west, and south walls.

There are still passive solar home designs that make maximum use of solar heat. Proper design of a passive home includes sufficient internal thermal mass to minimize temperature swings and proper orientation. It is also important that the design avoid overheating, for example, in September when the sun is low in the sky and outdoor temperatures can still be high. More information on the design of passive solar homes can be obtained from the Passive House Institute of the United States, which provides design software [13]. A passive house design can be certified by the International Passive House Association [14].

12.7.5 Solar Cooling Systems

There are three mechanisms that can utilize solar heat to provide space cooling: a Rankine cycle engine, an absorption chiller, and a desiccant cycle. Achieving high efficiency in a Rankine cycle requires the high temperatures associated with tracking, concentrating solar collectors, and these are not typically deployed on building roofs. Thus absorption chillers and desiccant systems have more typically been used.

In an absorption system, the refrigerant is evaporated or distilled from a less volatile liquid absorbent, the vapor is condensed in a water- or air-cooled condenser, and the resulting liquid is passed through a pressure-reducing valve to the cooling section of the unit. There, it cools the water as it evaporates, and the resulting vapor flows into a vessel, where it is reabsorbed into the absorbing liquid and pumped back to the heated generator. The heat required to evaporate the refrigerant in the generator can be supplied directly from solar energy, as shown in [Figure 12.24](#).

Absorption air conditioning is compatible with solar energy since a large fraction of the energy required is thermal energy at temperatures that high-performance flat plate or evacuated tube solar collectors such as previously described can provide. Absorption refrigeration differs from vapor-compression air conditioning only in the method of compressing the refrigerant. The combination of absorber and generator replaces the compressor. By this means, the refrigerant vapor entering the condenser is compressed without the large input of high-grade shaft work that the vapor-compression air conditioning demands.

Desiccant cooling systems use a desiccant to dry air, which can then be evaporatively cooled. Solar heat can then be used to bake the moisture back out of the desiccant. Liquid desiccants like lithium chloride or lithium bromide are most commonly used. A schematic of a liquid desiccant cooling system is shown in [Figure 12.25](#). Air is brought in contact with concentrated desiccant in a countercurrent flow in a dehumidifier. The dehumidifier may be a spray column or packed bed. The packing provides a very large area for heat and mass transfer between the air and the desiccant. After dehumidification, the air is sensibly cooled before entering the conditioned space. The dilute desiccant exiting the dehumidifier

12.8 Solar Thermal Power Plants

High concentration solar collectors (parabolic trough, linear Fresnel, and power towers) can provide the high temperatures needed to power conventional Rankine steam power cycles. Table 12.4 shows the number of solar power plants in the world that are either operating or under construction. Clearly parabolic trough and power tower systems are the dominant solar power generation technologies, and we describe their operation in this section. Recently, there has been more commercial interest in power towers because their higher operating temperatures promise a lower levelized cost of energy.

12.8.1 Parabolic Trough-Based Power Plants

Luz Corporation developed components and commercialized parabolic trough solar thermal power by constructing a series of hybrid solar power plants from 1984 to 1991. Starting with their first 14 MW_e solar electric generating station (SEGS I) in Southern California, Luz added a series of SEGS power plants with a total generating capacity of 354 MW_e. Figure 12.26 shows a schematic of the SEGS VIII and IX plants [15]. Table 12.5 provides information about the solar field, power block, and other general information about the SEGS plants. All of these plants use solar energy to heat the working fluid and natural gas as the auxiliary fuel to achieve the desired temperature. On average, 75% of the energy is obtained from the sun and 25% from natural gas. With power plant electrical conversion efficiencies of the order of 40% and the solar field efficiencies of 40%–50%, overall efficiencies for solar-to-electricity conversion of order of 15% are being achieved by these plants.

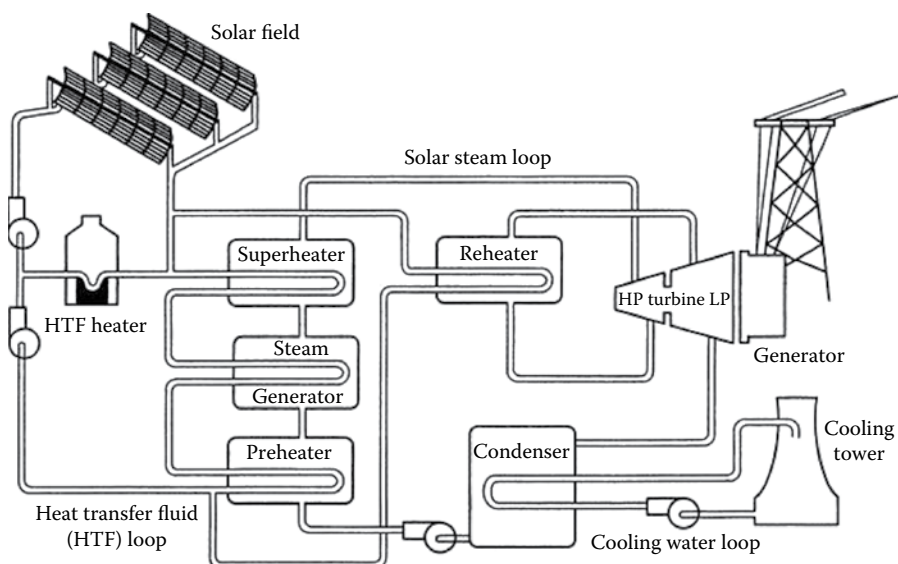
Luz went bankrupt due largely to problems associated with financial incentives. The first large-scale parabolic trough power plant in the United States since SEGS was the Nevada Solar One plant built in 2007. That plant has a nominal capacity of 64 MW and a maximum capacity of 75 MW. The project required an investment of \$266 million, and electricity production is estimated to be 134 million kWh/year [16]. The time of construction for the plant was about 16 months, and it occupies approximately 400 acres (1.6 km²), while the solar collectors cover about 1.2 km². Nevada Solar One uses 760 parabolic troughs that concentrate solar radiation onto evacuated receivers that heat the heat-transfer fluid to 391°C (735°F) [17].

Like the SEGS plants, Nevada Solar One does not have a significant thermal storage system. However, many parabolic trough plants have been built throughout the world with molten salt storage. A feed-in tariff resulted in a large number of 50-MW parabolic trough plants in Spain with 7.5 hours of thermal storage. In 2013, the Spanish company Acciona built the 250-MW Solana plant in Arizona, which has 6 hours of storage and provides electricity to Phoenix. This is shown in Figure 12.27.

TABLE 12.4
World Solar Power Plants

Type	Number of Plants	Capacity (MWe)
Parabolic trough	84	4900
Power tower	15	1030
Linear Fresnel	9	165

Source: SolarPACES.

**FIGURE 12.26**

Flow of heat-transfer fluid through the SEGS VIII and IX plants (Adapted from de Laquil, P. et al., 1993. *Solar Thermal Electric Technology in Renewable Energy*, Island Press, Washington, DC. [15])

EXAMPLE 12.3

The parabolic trough solar collector, whose efficiency was given in Equation 12.25, is to be used for electric power production. Assume that the average operating temperature of the trough field is 50°C lower than the boiler temperature, the average direct radiation in the plane of the collectors is 600 W/m^2 , and the efficiency of the power generation unit equals one-half of the Carnot efficiency, and determine:

- The temperature at which the solar trough power generation system achieves its highest efficiency.
- The levelized cost of energy from this trough generation system assuming a life of 25 years, an effective discount rate of 3%, and assuming that the total installed system cost is $\$600$ per m^2 of collector aperture area. This includes the cost of the installed solar collector field, as well as the power block and balance of system (turbine, cooling tower, power transformers/interconnection, etc.).

Solution

According to thermodynamic principles, the conversion of thermal energy into electric energy increases in efficiency as the temperature of the thermal source increases. But Equation 12.25 shows that the efficiency of the collector decreases with increasing operating temperature. In order to obtain the optimum operating temperature, both of these relations need to be taken into account.

If we assume the ambient temperature (for determining the power cycle efficiency) is 20°C , the electric power output, P , is equal to

$$P = I\eta_c \times 0.5 \left(\frac{\Delta T_a}{T_h} \right) = I[Eq\ 12.25] \times 0.5 \left(\frac{T_h - 293}{T_h} \right)$$

where in Equation 12-24 $x = (T_{htf} - 25)/I^{0.33} = (T_h - 50 - 25)/(600)^{0.33}$.

TABLE 12.5
Important Characteristics of SEGS I to SEGS IX Plants

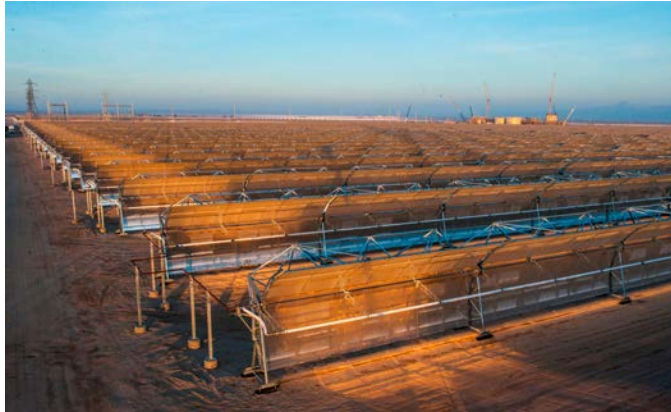
	Units	I	II	III	IV	V	VI	VII	VIII	IX
<i>Power</i>										
Turbine-generator output	Gross MW _e	14.7	33	33	33	33	33	33	88	88
Output to utility	Net MW _e	13.8	30	30	30	30	30	30	80	80
Turbine generator set										
Solar steam conditions										
Inlet pressure	Bar	35.3	27.2	43.5	43.5	43.5	100	100	100	100
Reheat pressure	Bar	0	0	0	0	0	17.2	17.2	17.2	17.2
Inlet temperature	°C	415	360	327	327	327	371	371	371	371
Reheat temperature	°C	N/A	N/A	N/A	N/A	N/A	371	371	371	371
<i>Gas mode steam conditions^a</i>										
Inlet pressure	Bar	0	105	105	105	105	100	100	100	100
Reheat pressure	Bar	0	0	0	0	0	17.2	17.2	17.2	17.2
Inlet temperature	°C	0	510	510	510	510	510	510	371	371
Reheat temperature	°C	N/A	N/A	N/A	N/A	N/A	371	371	371	371
Electrical conversion efficiency										
Solar mode ^b	Percent	31.5	29.4	30.6	30.6	30.6	37.5	37.5	37.6	37.6
Gas mode ^c	Percent	0	37.3	37.3	37.3	37.3	39.5	39.5	37.6	37.6
<i>Solar field</i>										
Solar collector assemblies										
LS 1 (128 m ²)		560	536	0	0	0	0	0	0	0
LS 2 (235 m ²)		0	0	0	0	32	0	184	852	888
LS 3 (545 m ²)		0	0	0	0	32	0	184	852	888
Number of mirror segments										
Field aperture area		41,600	96,464	117,600	117,600	126,208	96,000	89,216	190,848	198,912
Field inlet temperature	m ²	89,960	190,338	230,300	230,300	250,560	188,000	194,280	464,340	483,960

(Continued)

TABLE 12.5 (Continued)
Important Characteristics of SEGS I to SEGS IX Plants

	Units	I	II	III	IV	V	VI	VII	VIII	IX
Field outlet temperature	°C	240	231	248	248	248	293	293	293	293
Annual thermal efficiency	°C	307	321	349	349	349	390	390	390	390
Peak optical efficiency	Percent	35	43	43	43	43	42	43	53	50
System thermal losses	Percent of peak	71	71	73	73	73	76	76	80	80
System thermal losses	Percent of peak	71	71	73	73	73	76	76	80	80
		17	12	14	14	14	15	15	15	15
<i>Heat transfer fluid type</i>										
Inventory		Esso 500	VP-1	VP-1	VP-1	VP-1	VP-1	VP-1	VP-1	VP-1
Thermal storage capacity	m ³	3,213	416	403	403	461	416	416	1,289	1,289
	MWh _t	110	0	0	0	0	0	0	0	0
<i>General</i>										
Annual power outlet	Net MWh/year	30,100	80,500	91,311	91,311	99,182	90,850	92,646	252,842	256, 125
Annual power use	10 ⁹ m ³ /year	4.76	9.46	9.63	9.63	10.53	8.1	8.1	24.8	25.2

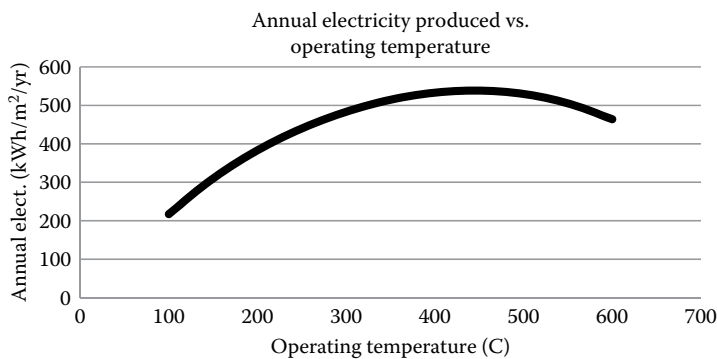
^a Gas superheating contributes 18% of turbine inlet energy.
^b Generator gross electrical output divided by solar field thermal input.
^c Generator gross electrical output divided by thermal input from gas-fired boiler or HTF-heater.

**FIGURE 12.27**

The 250-MW Solana parabolic trough power plant with 6 hours of thermal storage in Gila Bend, Arizona, provides electricity for Phoenix. (Courtesy of Atlantica Yield.)

P is shown in the table and plot below as a function of operating temperature. To estimate the annual power in $\text{kWh}/\text{m}^2/\text{yr}$, we can multiply the power by the number of daylight hours during the year, which is assumed to be 12 hours per day.

Operating Temperature ($^{\circ}\text{C}$)	Collector Efficiency	50% of Carnot	P (W/m^2)	P-annual ($\text{kWh}/\text{m}^2/\text{y}$)
100	0.771	0.11	49.6	217
150	0.769	0.15	70.9	310
200	0.766	0.19	87.5	383
250	0.761	0.22	100.4	440
300	0.753	0.24	110.4	483
350	0.739	0.26	117.5	514
400	0.718	0.28	121.7	533
450	0.689	0.30	122.9	538
500	0.649	0.31	120.9	530
550	0.597	0.32	115.4	505
600	0.531	0.33	105.9	464



We observe that the peak annual electric generation occurs at about 450°C . The annual electricity generation at the optimum operating temperature, as shown in the last column, is approximately $538 \text{ kWh}/\text{m}^2/\text{year}$.

To estimate the LCOE, we neglect annual operation and maintenance costs. The levelized cost of energy delivered by the system over 25 years is

$$\text{LCOE} = \left(\frac{\text{TLCC}}{Q} \right) \times \text{CRF} = \left[\frac{600 \text{ \$/m}^2}{538 \text{ kWh/m}^2} \right] \times 0.064 = \$0.071/\text{kWh}$$

Although this simple analysis has indicated an optimum operating temperature of 450°C, existing trough plants are limited to a maximum operating temperature of about 390°C, due to limitations of the heat transfer oil. Note also that we did not account in this example for heat losses from piping, parasitic pumping power, operation and maintenance costs, and other expenses.

The following example illustrates how SAM can be used to provide a more detailed analysis of the performance of a parabolic trough power system.

EXAMPLE 12.4

The SAM Physical Trough model uses a combination of first-principles heat transfer, thermodynamics, and fluids models with semi-empirical relationships to predict the performance of parabolic trough systems. The model is useful for investigating the sensitivity of system productivity to design or operating parameters. This example will show how to use SAM for a parametric analysis.

Parabolic trough systems utilizing organic heat transfer oil are known to accumulate over time pure hydrogen gas in the annular space between the hot absorber tube and the glass envelope. When the oil temperature approaches its thermal instability point, the hydrocarbon molecules shed hydrogen that is small enough to permeate the steel wall and pass into the annulus. Hydrogen—even at low pressure—transports heat effectively between surfaces with differing temperatures.

Evaluate the annual energy production of a solar trough power system located in Daggett, California, with varying accumulations of annular hydrogen. The solar field aperture area is fixed at 877,000 m². The receiver (heat collection element) is chosen to be the Schott PTR80 (which has a pipe diameter of 80 mm), and several variants of the receiver are to be considered.

SAM models different variations of collector performance. By default, SAM models three receiver variations: variation 1 represents “good as new” receivers that perform as well as they did when first installed, variation 2 represents receivers that have lost their vacuum seal and are infiltrated by air, and variation 3 represents receivers whose glass envelope is broken and missing, and whose absorber tube is exposed directly to ambient conditions.

For this example, we consider a fourth variation in which hydrogen has entered the annulus in substantial quantities. The fourth variant assumes 20% of the field (as specified by the variant weighting fraction) is contaminated with hydrogen while the rest of the field has “good as new” receivers. Variation 4 matches variation 1 in all parameters with the exception of hydrogen annulus pressure. Assume all other input values are left at their default values. Use the Parametrics option to consider how Variation 4 Annulus Pressure affects Annual Energy (kWh) for a range of pressures, beginning with 0.0001 torr (note: 1 atm = 760 torr) and increasing in order of magnitude to 100 torr. (i.e., 0.0001, 0.001, 0.01...100). Plot annual energy as a function of Variation 4 annulus pressure on a logarithmic x-axis scale. What proportion of energy is lost at 0.1 torr compared to 0.0001 torr?

Solution

1. Start SAM
2. Click **Start a new project**

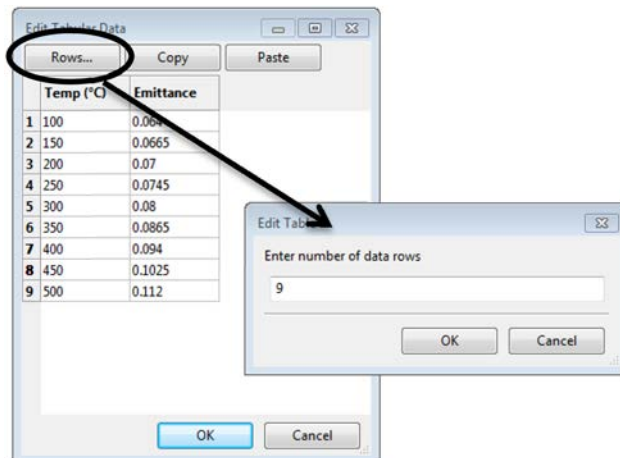
3. Select **CSP parabolic trough (physical)** as the technology model, and **PPA single owner (utility)** as the financial model. Click **Ok**.
4. Navigate to the Location and Resource page, and select **USA CA Daggett (TMY2)** as the solar resource file.
5. Navigate to the **Solar Field** page and click **Option 2** to specify the aperture area of the solar field. Enter 877,000 m² as the value.
6. Navigate to the **Receivers (HCEs)** page. Overwrite the values in Variation 4 under Receiver Type 1 to match the values in Variation 1.

Parameters and Variations

	Variation 1	Variation 2	Variation 3	Variation 4*
Variant weighting fraction*	0.785	0.01	0.005	0.2
Absorber Parameters:				
Absorber absorptance	0.963	0.963	0.8	0.963
Absorber emittance	Table...	Value Table 0.65	Value Table 0.65	Table Table...
Envelope Parameters:				
Envelope absorptance	0.02	0.02	0	0.02
Envelope emittance	0.86	0.86	1	0.86
Envelope transmittance	0.964	0.964	1	0.964
	<input type="checkbox"/> Broken Glass	<input type="checkbox"/> Broken Glass	<input checked="" type="checkbox"/> Broken Glass	<input type="checkbox"/> Broken Glass
Gas Parameters:				
Annulus gas type	Hydrogen	Air	Air	Hydrogen
Annulus pressure (torr)	0.0001	750	750	0.0001
Heat Loss at Design:				
Estimated avg. heat loss (W/m)	190	1270	1500	0
Optical Effects:				
Bellows shadowing	0.935	0.935	0.935	0.935
Dirt on receiver	0.98	0.98	1	0.98

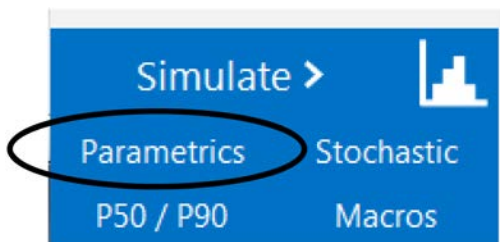
* The variant weighting fractions and Variation 4 inputs are not part of the library.

Make sure that the contents of the Absorber emittance table are copied from Variation 1 to Variation 4, and that the number of rows is equal to 9.



7. It was specified that 20% of the good-as-new receivers (Variation 1) are compromised with high-hydrogen (Variation 4), so change the **Variant weighting fraction** of Variation 1 to 0.785 and Variation 4 to 0.2. (Because Variations 2 and 3 together comprise 0.015 of the collector field, the Variation 1 weighting factor is $1 - 0.2 - 0.015 = 0.785$).

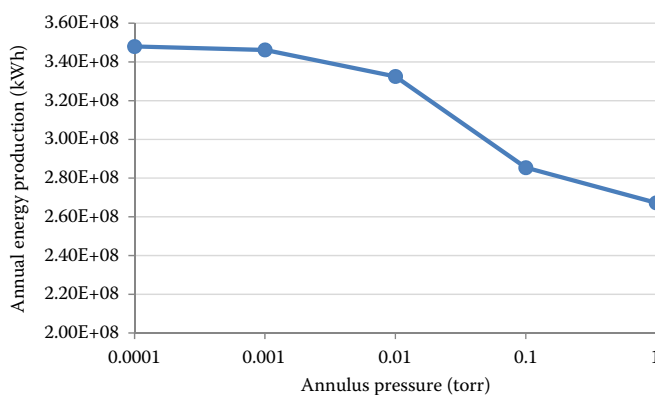
8. Navigate to the Parametrics window.



9. Click **Inputs...** and in the dialog, search for **Variation 4 Annulus Pressure (torr)**, or alternately, expand the **Physical trough Receiver Type 1** tree and check the item of that name. Click **Ok**.
10. Click **Outputs...** and in the dialog, search for **Annual Energy (kWh)**, or alternately, expand the **Net_E_Calc** tree and check the item of that name. Click **Ok**.
11. The requirements for the annulus pressures to consider result in the following set: (0.0001, 0.001, 0.01, 0.1, 1) which requires seven entries in the parametrics table. Change the **Number of runs** to 5, and enter the values in the table.

Quick setup...		Inputs...	Outputs...	Run simulations >	Number of runs: 5
	Variation 4 Annulus Pressure (torr)	Annual Energy (kWh)			
1	0.0001				
2	0.001				
3	0.01				
4	0.1				
5	1				

12. Click **Run simulations >** and allow SAM to calculate the results. The annual energy as a function of annulus pressure is plotted below.



As annulus pressure increases, the annual production from the facility decreases. The reduction in output from 0.0001 torr to 0.1 torr is approximately 18%. As annulus pressure increases, the heat loss from the compromised receivers increases due to the enhanced rate of heat transfer associated with increasing hydrogen thermal conductivity. At pressures above 1 torr, the conductivity approaches a limit, and annual energy production levels off at

about a 25% reduction. Hydrogen contamination of evacuated receivers is a major issue affecting the long-term performance of parabolic trough power plants, and efforts are underway to prevent it.

12.8.2 Power Towers

Figure 12.28 is a schematic diagram of a power tower system [18]. A heat-transfer fluid is pumped through a riser to the receiver where it is heated and then via a downcomer to the thermal storage unit and/or a heat engine, which is usually located on the ground near the tower. Typical optical concentration factors range from 200 to 1000, and plant sizes from 10 to 200 MW_e are typical for new systems. The heat flux impinging on the receiver can be between 300 and 1000 kW/m² and allows the working fluid to achieve temperatures up to 1000°C.

Two types of receiver configurations have been considered for power towers. The cavity receiver consists of an insulated enclosure within which a heat absorbing structure is located. Radiation enters through the aperture, is subjected to multiple reflections, and thus enhances the effective absorptivity of the cavity. Radiation losses can occur only through the aperture and the absorbing area of the receiver can be enlarged without substantially increasing the radiation losses. However, convective losses increase as a result of a larger heated area and cavity receivers tend to be large and heavy. Moreover, the aperture size restricts the field of view and spillage can be considerable. In a plain or flat plate receiver, the aperture of a cavity is replaced by a flat heat-exchanging surface. The back side can be insulated, but overall losses are appreciable.

The external receiver consists of a cylinder with a tubular structure containing a working fluid passing through the pipes on the outside of a cylinder. It can receive solar radiation from all directions and is relatively simple and lightweight because no enclosure is required. The design can accommodate heat flux densities as high as 850 kW/m² with molten salt and the tower needs to be only about 70% as tall as the tower for a cavity receiver, which reduces the cost appreciably. The disadvantage of an external receiver is that the reflected fraction of incident radiation is lost, and the temperature of the molten salt heat-transfer

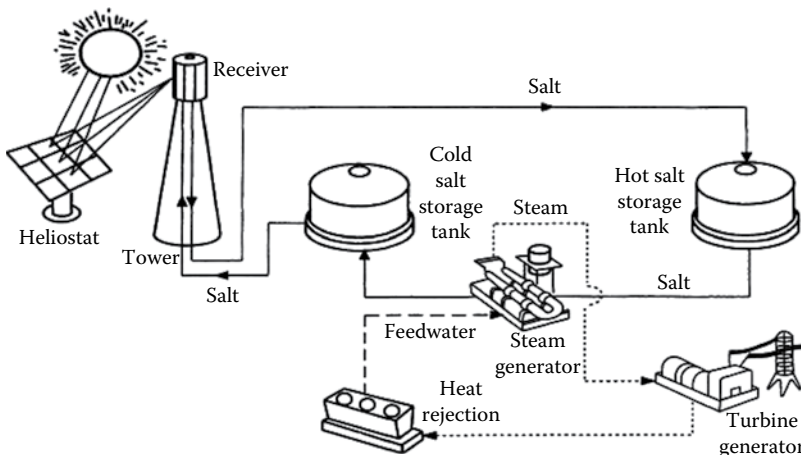


FIGURE 12.28

Schematic of Solar Two central-receiver plant configuration. (Adapted from Hebrank, W.H., 1975. Tenter frame drying, *Am. Dyestuff Rep.*, 63, 34. [18])

fluid must be maintained above a certain limit to avoid freezing. This is accomplished, as shown in [Figure 12.28](#), by having hot and cold storage tanks.

In any high-temperature concentrating system, the receiver is the focal point of the design. Because radiation and convection losses are proportional to the area of the receiver, it should be as small as possible, which requires high concentration. But the receiver must also be large enough to intercept and absorb a large fraction of the solar radiation directed toward it by the heliostats and transfer the heat from the sun to a working fluid. If the designer specifies a more perfect optical system to reduce the receiver size, this will increase the cost of the heliostats and may complicate the thermal design.

The efficiency of the receiver, η_{thr} equals $[1 - (\text{thermal loss/solar input})]$, and it is given by the following equation:

$$\eta_{th} = 1 - \frac{A_{receiver} [\varepsilon \sigma (T^4 - T_a^4) + c(T - T_a)^{1.25}]}{G_b A_{collector} \eta_{col} \eta_{int} \alpha} \quad (12.27)$$

or

$$\eta_{th} = 1 - \frac{\sigma (T^4 - T_a^4) + (c/\varepsilon)(T - T_a)^{1.25}}{G_b C \eta_{col} \eta_{int}} \quad (12.28)$$

where

$$C = \frac{\alpha A_{collector}}{\varepsilon A_{receiver}} = C_g \frac{\alpha}{\varepsilon}$$

T is the receiver operating temperature (K)

T_a is the ambient temperature (K)

ε is the emissivity of the receiver at the temperature T

σ is the Stefan–Boltzmann constant, $5.67 \times 10^{-8} \text{ W/m}^2 \text{ K}^4$

c is a temperature-independent convective loss coefficient, typically between 1 and $25 \text{ W/m}^2 \text{ K}^{1.25}$

G_b is the solar beam radiation, W/m^2

Also, α is the absorptivity for direct beam solar radiation (G_b) and η_{col} is the collector efficiency, which includes reflectivity (typically 0.85–0.95), cosine of angle of incidence effects (typically 0.7–0.9), and a factor to account for shading of mirror surfaces or blocking of reflected sunlight (typically 0.9–1.0). It is conventional to use the actual mirrored area of the heliostats for $A_{collector}$. The fraction of reflected light that is intercepted by the receiver is η_{int} , representing scattering and spillage losses. We see that the geometric concentration, C , plays an important role in suppressing the effects of thermal losses.

Current power tower designs use either steam or molten salt in the receiver. In a steam receiver, water is boiled and superheated in the receiver before being sent to a steam turbine. Towers using direct steam receivers have steam conditions ranging from saturated steam at 250°C to superheated steam at over 550°C [10]. Direct steam towers offer the advantage of using conventional boiler design and have low pumping power. In April 2009, Abengoa Solar began commercial operation of a 20-MW solar power tower plant at the Solucar Platform, near Seville, Spain. PS20 features a higher-efficiency cavity receiver, improved control systems, and a better thermal energy storage system than the first tower, PS10. The

**FIGURE 12.29**

Photograph of two direct steam Spanish central receiver systems. (Courtesy of Clifford Ho, Sandia National Laboratories.)

second system brought the power capacity to 20 MW, double that of the original PS10 tower. A photograph of both of these is shown in [Figure 12.29](#).

BrightSource built the 390-MW Ivanpah project in California, which consists of three separate power towers and more than 170,000 15 m^2 heliostats, which were built in an on-site automated factory. [Figure 12.30](#) shows photos of the large Ivanpah project [10].

Because of the increasingly stiff competition from low-cost photovoltaic modules, the concentrating solar power industry has been shifting away from direct steam systems to take advantage of the fact that CSP plants can utilize relatively low-cost thermal storage. This allows CSP not only to provide electricity when the sun isn't shining but also to sell electricity into the most lucrative electricity markets. While a steam receiver can be coupled to thermal storage, it is much easier to couple thermal storage with a molten salt receiver. As with the case of parabolic trough plants with storage, power tower plants use molten nitrate

**FIGURE 12.30**

Ivanpah direct steam power towers (From Mehos, M. et al., May 2016. On the path to SunShot: Advancing concentrating solar power technology, performance, and dispatchability, NREL/TP-5500-65688. [10])

salts as the storage media. But, unlike current commercial trough plants, which utilize oil as the heat transfer fluid in the receivers and must use heat exchangers to transfer the heat to molten salt storage, a power tower with a molten salt receiver uses molten salt as both the working fluid in the receiver and the storage media. This allows higher receiver operating temperatures and thus higher power cycle efficiencies. Higher temperatures also allow for a smaller storage volume for the same heat storage capacity.

The first power tower plant to use a molten salt receiver was the 10 MW Solar Two plant, which operated in California in 1999. Solar Two demonstrated advanced molten salt technology at a scale sufficient to allow commercialization of the technology. The plant operated successfully with solar energy collected efficiently over a broad range of operating conditions and showed that low-cost thermal energy storage systems can operate reliably and efficiently.

Today's typical molten salt power tower pumps the salt at about 290°C from "cold" storage tanks to the receiver, where it is heated by concentrated sunlight to a temperature of over 550°C and supplied to a hot tank. At times when it is economically desirable to provide electricity to the grid, the hot molten salt from the hot storage tanks is pumped through a heat exchanger where it boils and superheats water to produce steam at temperatures of up to 540°C and pressures of 100–150 bars for powering a steam turbine, which turns an electric generator as in a conventional thermal power plant. The exiting molten salt at lower temperature then returns to the "cold" tanks to repeat the process.

Note that in this design the thermal storage can operate independently of the heliostat field and the receiver. The hot molten salt can be harnessed to produce steam and electricity when the sun isn't shining (when clouds pass overhead or at night) or whenever the price of electricity is high enough to make electric dispatch financially attractive. Storage can be sized to allow a CSP plant to operate as a base load power plant 24 hours per day in the summer. For example, the 20-MWe Gemasolar plant in Spain has 15 hours of storage and can run constantly most of the year. More recently, the 110-MWe Crescent Dunes plants building by Solar Reserve in Tonopah, Nevada has 10 hours of molten salt storage. But while plants with such large storage systems can operate almost as base load plants, dispatching electricity over such a long, continuous time period may not be the most cost-effective option. Selling electricity into 4- to 6-hour periods when electricity is at the highest price can provide a greater return on investment. As competition from photovoltaics has become stiffer, such "peaker" CSP plants are being considered.

Power towers can achieve high annual capacity factors by using thermal storage. [Table 12.6](#) lists the current world's power tower plants that are either operating or under construction. There are 15 plants totaling over 1 GW in capacity. About a half-dozen more plants are planned in China, Chile, Australia, and South Africa. Details about all the concentrating solar power plants in the world can be found at: <http://www.nrel.gov/csp/solarpaces>.

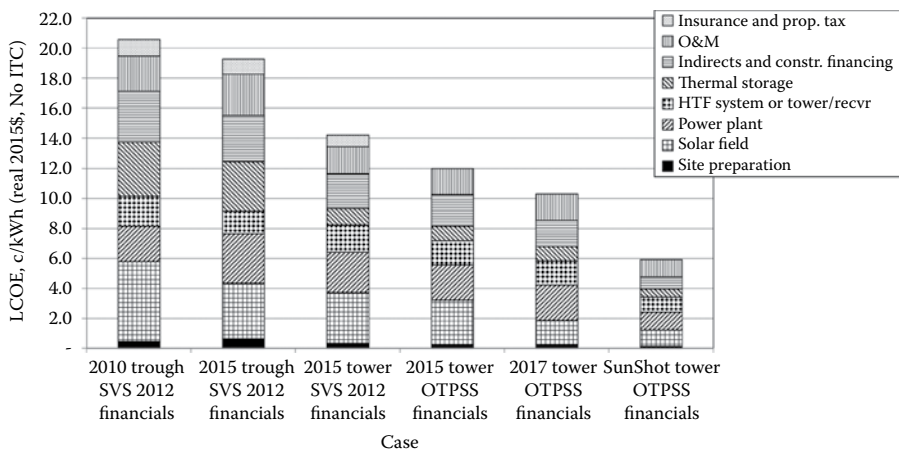
[Figure 12.31](#) shows the levelized cost of electricity and the various cost components for current and target solar power tower plants. The goal of the U.S. Department of Energy program is to achieve a levelized cost of electricity of 6 cents per kWh without a 30% investment tax credit (ITC). Note that this table shows storage sizes of 10–14 hours for the lowest LCOE cases. As pointed out earlier, however, LCOE does not tell the whole story. A plant's return on investment is determined not only by the cost of the energy it produces but also on what price that energy can be sold for. As a result, the CSP industry is looking at developing peaker plants that sell electricity into the highest-price peak markets. That is the subject of the next example. More details about dispatch strategies and [Figure 12.31](#) can be found in Mehos et al. [8].

TABLE 12.6

Solar Power Tower Plants

Name	Capacity (MWe)	Status	Storage (hrs)	Country	Year
Lake cargelligo	3	Operational	0	Australia	2011
Jemalong	1	Under construction	3	Australia	2016
Atacama-1	110	Under construction	17.5	Chile	2017
Supcon solar project	50	Under construction	6	China	2018
Dahan power plant	1	Operational	1	China	2012
Acme solar tower	2.5	Operational	0	India	2011
Ashalim 1	121	Under construction	0	Israel	2017
NOOR III	150	Under construction	7.5	Morocco	2018
Khi solar one	50	Operational	2	South Africa	2016
Gemasolar	20	Operational	15	Spain	2011
PS10	10	Operational	1	Spain	2007
PS20	20	Operational	1	Spain	2009
Sierra SunTower	5	Operational	0	USA	2009
Ivanpah	377	Operational	0	USA	2014
Crescent dunes	110	Operational	10	USA	2015

Source: SolarPACES.

**FIGURE 12.31**

Levelized costs of electricity for current and target concentrating solar power plants (From Mehos, M. et al., May 2016. On the path to SunShot: Advancing concentrating solar power technology, performance, and dispatchability, NREL/TP-5500-65688. [10])

EXAMPLE 12.5

Molten Salt Power Tower systems utilize direct thermal storage, which can be dispatched to generate electricity during times of the day when market prices or demand are elevated. The ability to generate during peak times of the day provides significant value and/or profit for grid operators and plant owners, respectively. Solar power plants with storage can sell electricity into the peak periods that were shown in the “duck curves” in [Chapter 5](#).

Power tower facilities are capable of selectively dispatching during peak times, given a sufficiently “smart” operation policy that reserves enough stored energy to meet demand. In this example we will use SAM to compare the performance of a molten salt power tower plant with single-owner (utility) financing that operates with optimized

dispatch and one that operates without. In both cases, assume that there are two “time of delivery” factor categories. The first category has a price multiplier of 0.5, and the second has a price multiplier of 2. The second category includes 3 hours from 7–10 a.m. and 4 hours from 6–10 p.m. and is applied uniformly for each month of the year and for both weekdays and weekends. All other times are covered by the first category. Specify a power purchase agreement (PPA) price of 0.10 \$/kWh_e, and a fixed debt percentage of 50%. Compare the annual electricity generation and profitability (internal rate of return) for both cases. Also, use SAM’s heat map plots of total electric power to the grid to qualitatively contrast the generation profiles.

Solution

1. Start SAM.
2. Create a new case, and select **CSP power tower molten salt** as the technology model and **PPA single owner (utility)** as the financial model.
3. Navigate to the **Time of Delivery Factors** page. Use the mouse to click and drag across all of the cells in the **TOD Schedules and Factors—Weekday Schedule** table, and once all are selected, type ‘1’ on your keyboard. All numbers in the schedule should change to 1. Select the time windows specified above, and type ‘2’. Repeat for the **Weekend Schedule** table. The result should appear as follows:

TOD Schedules and Factors

☐ Use library values

PPA price multiplier

Period 1: 0.5

Period 2: 2

Period 3: 1

Period 4: 1

Period 5: 1

Period 6: 1

Period 7: 1

Period 8: 1

Period 9: 1

PPA price multipliers, or TOD factors, apply to the PPA price according to the weekday and weekend schedules.

TOD factor data in SAM's library may not be applicable to your project. Be sure that your assumptions are consistent with the requirements described in the appropriate solicitation documents.

Weekday Schedule

	12am	1am	2am	3am	4am	5am	6am	7am	8am	9am	10am	11am	12pm	1pm	2pm	3pm	4pm	5pm	6pm	7pm	8pm	9pm	10pm	11pm
Jan	1	1	1	1	1	1	1	1	2	2	2	1	1	1	1	1	1	1	2	2	2	1	1	
Feb	1	1	1	1	1	1	1	1	2	2	2	1	1	1	1	1	1	1	2	2	2	1	1	
Mar	1	1	1	1	1	1	1	1	2	2	2	1	1	1	1	1	1	1	2	2	2	1	1	
Apr	1	1	1	1	1	1	1	1	2	2	2	1	1	1	1	1	1	1	2	2	2	1	1	
May	1	1	1	1	1	1	1	1	2	2	2	1	1	1	1	1	1	1	2	2	2	1	1	
Jun	1	1	1	1	1	1	1	1	2	2	2	1	1	1	1	1	1	1	2	2	2	1	1	
Jul	1	1	1	1	1	1	1	1	2	2	2	1	1	1	1	1	1	1	2	2	2	1	1	
Aug	1	1	1	1	1	1	1	1	2	2	2	1	1	1	1	1	1	1	2	2	2	1	1	
Sep	1	1	1	1	1	1	1	1	2	2	2	1	1	1	1	1	1	1	2	2	2	1	1	
Oct	1	1	1	1	1	1	1	1	2	2	2	1	1	1	1	1	1	1	2	2	2	1	1	
Nov	1	1	1	1	1	1	1	1	2	2	2	1	1	1	1	1	1	1	2	2	2	1	1	
Dec	1	1	1	1	1	1	1	1	2	2	2	1	1	1	1	1	1	1	2	2	2	1	1	

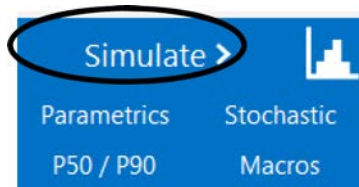
Weekend Schedule

	12am	1am	2am	3am	4am	5am	6am	7am	8am	9am	10am	11am	12pm	1pm	2pm	3pm	4pm	5pm	6pm	7pm	8pm	9pm	10pm	11pm
Jan	1	1	1	1	1	1	1	2	2	2	1	1	1	1	1	1	1	1	2	2	2	1	1	
Feb	1	1	1	1	1	1	1	2	2	2	1	1	1	1	1	1	1	1	2	2	2	1	1	
Mar	1	1	1	1	1	1	1	2	2	2	1	1	1	1	1	1	1	1	2	2	2	1	1	
Apr	1	1	1	1	1	1	1	2	2	2	1	1	1	1	1	1	1	1	2	2	2	1	1	
May	1	1	1	1	1	1	1	2	2	2	1	1	1	1	1	1	1	1	2	2	2	1	1	
Jun	1	1	1	1	1	1	1	2	2	2	1	1	1	1	1	1	1	1	2	2	2	1	1	
Jul	1	1	1	1	1	1	1	2	2	2	1	1	1	1	1	1	1	1	2	2	2	1	1	
Aug	1	1	1	1	1	1	1	2	2	2	1	1	1	1	1	1	1	1	2	2	2	1	1	
Sep	1	1	1	1	1	1	1	2	2	2	1	1	1	1	1	1	1	1	2	2	2	1	1	
Oct	1	1	1	1	1	1	1	2	2	2	1	1	1	1	1	1	1	1	2	2	2	1	1	
Nov	1	1	1	1	1	1	1	2	2	2	1	1	1	1	1	1	1	1	2	2	2	1	1	
Dec	1	1	1	1	1	1	1	2	2	2	1	1	1	1	1	1	1	1	2	2	2	1	1	

4. Set the **PPA price multiplier** to 0.5 for Period 1 and 2 for Period 2. Uncheck the **Use library values** option.

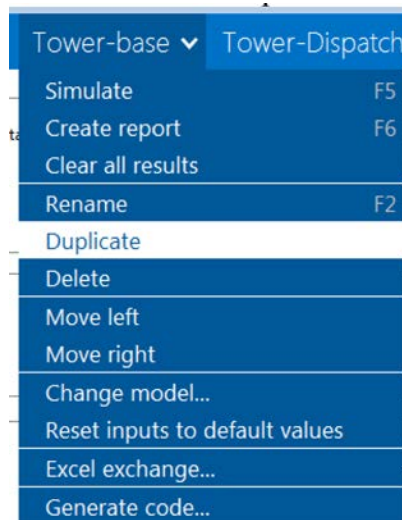
SAM is now configured to weight revenue from electricity sales generated during the specified time windows according to the PPA price multiplier values.

5. Navigate to the **System Control** page and ensure that the **Enable dispatch optimization** checkbox is *disabled* for the first simulation.
6. Navigate to the **Financial Parameters** page, and change the **Solution mode** to **Specify PPA price**, then change the specified **PPA price** to 0.1 \$/kWh.
7. On the same page under **Project Term Debt**, select **Debt percent**, and set it to 50% of total capital cost. Note that if this step is not taken, the internal rate of return calculations will fail and return 'NaN'.
8. Click **Simulate**.



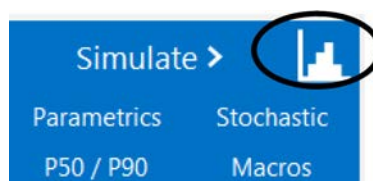
The simulation will proceed without dispatch optimization. Once the simulation is complete, proceed as follows:

9. Under the case dropdown menu, click **Duplicate**.



A new case has been created for the dispatch optimization analysis.

10. In the new case file, navigate to the **System Control** page, then check the **Enable dispatch optimization** checkbox.
11. Click **Simulate** to run the new case. Note that the simulation time for this option is significantly longer than the previous analysis, and may require 5–10 minutes, depending on computer performance.
12. The problem requests a comparison of IRR and Annual energy generation. This information can be retrieved on the Results Summary page in the Metrics table.



The results for the unoptimized case are shown at **left**, and the optimized case is shown at **right**.

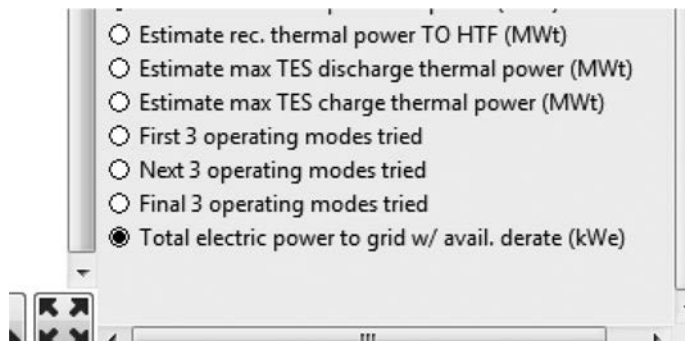
Metric	Value	Metric	Value
Annual energy (year 1)	565,705,984 kWh	Annual energy (year 1)	570,709,440 kWh
Capacity factor (year 1)	62.4%	Capacity factor (year 1)	62.9%
Annual Water Usage	96,838 m ³	Annual Water Usage	97,505 m ³
PPA price (year 1)	10.00 ¢/kWh	PPA price (year 1)	10.00 ¢/kWh
PPA price escalation	1.00 %/year	PPA price escalation	1.00 %/year
Levelized PPA price (nominal)	10.83 ¢/kWh	Levelized PPA price (nominal)	13.17 ¢/kWh
Levelized PPA price (real)	8.52 ¢/kWh	Levelized PPA price (real)	10.36 ¢/kWh
Levelized COE (nominal)	10.39 ¢/kWh	Levelized COE (nominal)	11.26 ¢/kWh
Levelized COE (real)	8.17 ¢/kWh	Levelized COE (real)	8.86 ¢/kWh
Net present value	\$26,330,390	Net present value	\$115,108,080
Internal rate of return (IRR)	8.16 %	Internal rate of return (IRR)	15.73 %
Year IRR is achieved	20	Year IRR is achieved	20
IRR at end of project	10.33 %	IRR at end of project	16.52 %
Net capital cost	\$776,013,248	Net capital cost	\$776,022,400
Equity	\$388,078,976	Equity	\$388,083,552
Size of debt	\$387,934,272	Size of debt	\$387,938,848
Minimum DSCR	1.14	Minimum DSCR	1.47

The results indicate that annual energy is 565.7 GWh for the unoptimized case and 570.7 GWh for the optimized case, representing a 0.9% improvement. The internal rate of return is 8.2% versus 15.7%, respectively, which indicates a near doubling of investment return based solely on the operational scheme, as the design parameters and costs are consistent across both cases.

The problem also requests a qualitative comparison using SAM's heat map plots. To create these plots, navigate to the results page, then click **Heat map**.

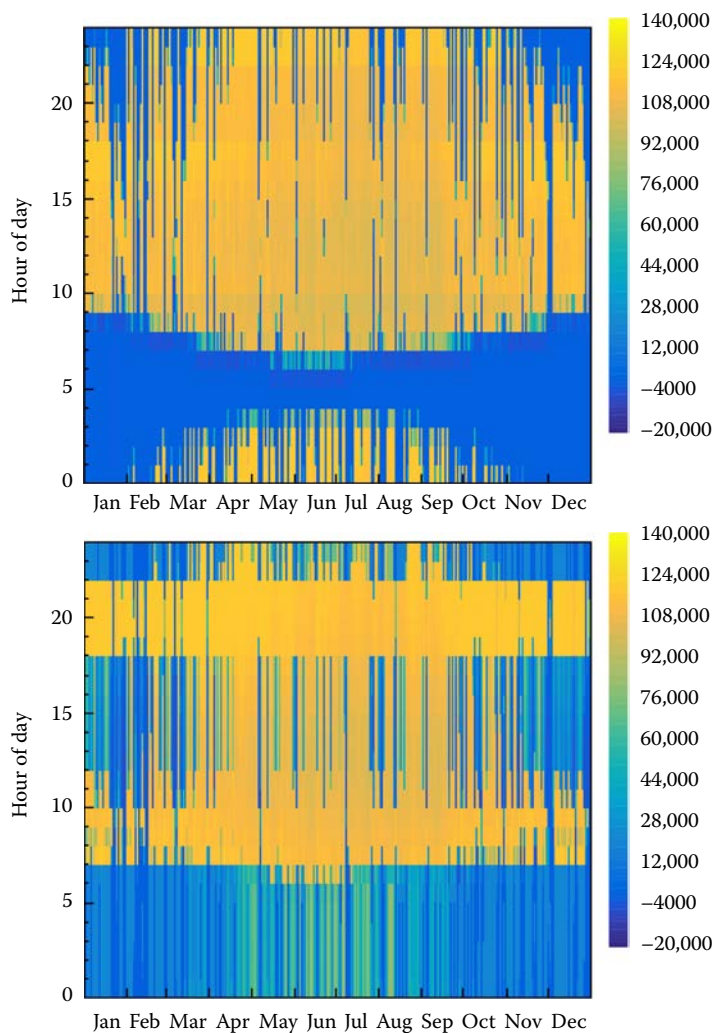
Summary Data tables Graphs Cash flow Time series Profiles Statistics **Heat map** PDF / CDF Notices

Select the Total electric power to grid w/ avail. derate (kWe) output.



The heat map plots show the electrical production by hour (y-axis) for each day of the year (x-axis). Heat map results are shown below for the unoptimized case (**top**) and the optimized case (**bottom**). It is evident from these plots that the optimized plant operation schedule is

capable of consistently delivering power during high-value time periods throughout the year, whereas the unoptimized operation schedule does not consistently provide value. Furthermore, it is evident that the optimized plant can produce power during nighttime or early morning hours long after the solar field has stopped producing thermal energy.



12.9 Solar Industrial Process Heat

About one-third of the energy consumed in the United States is for industrial use and it is over half worldwide [19]. To achieve zero-carbon emissions, we must replace fossil fuels with renewable sources in the industrial process heat sector. Solar energy, biomass, and geothermal energy all represent renewable sources of thermal energy. There is particular interest in the use of solar thermal technology. Solar thermal energy collector systems used to generate power face increasing competition from solar photovoltaic systems. While they offer the advantage of thermal energy storage, only a portion of the energy gets converted to

electricity due to thermodynamic power cycle efficiencies. In the case of industrial process heat, however, all of the thermal energy provided by the collector system can be utilized. Thus for direct thermal applications, solar thermal collectors are more efficient than PV. And, compared to installing solar thermal collectors on individual buildings, a large field of solar collectors used to produce thermal energy for industrial processes benefits from the economy of scale. Depending on the process temperature, either flat plate collectors or line-focus collectors are typically used.

Solar industrial process heat systems received attention in the United States in the early 1980s. The U.S. Department of Energy sponsored a number of demonstration projects, and the Solar Energy Research Institute produced a 450-page design handbook based on the experiences gained [20]. Interest in solar industrial process heat waned, however, due to competition from low natural gas prices. Today, a number of factors have led to a renewed interest in solar IPH. There is now international concern about reducing carbon emissions. Also, solar thermal collector technology has improved significantly over the past three-and-a-half decades. In particular, parabolic trough collectors have experienced many improvements as a result of competition in the concentrating solar power industry and associated government research efforts. The IEA SHIP database [21] gives information on over 200 solar industrial process heat installations around the world. The vast majority of these have collector areas of less than 1000 m².

Table 12.7 shows the different solar thermal technologies for addressing process heat at different temperature ranges [22].

Figure 12.32 shows the annual energy use for various steam temperature ranges in the U.S. industry [23].

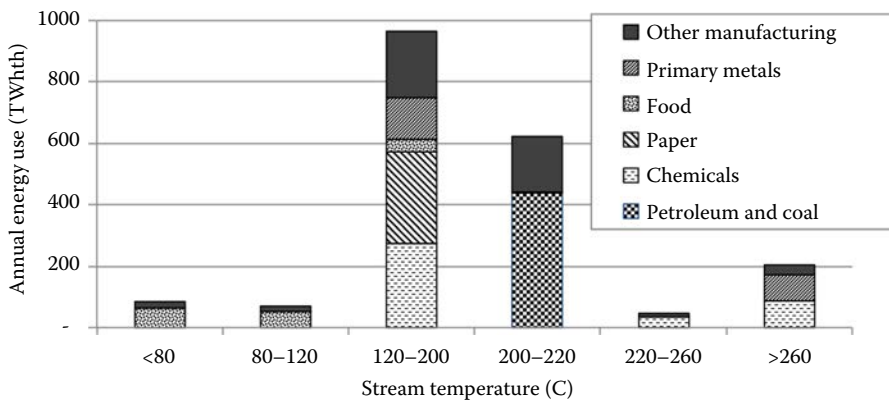
Comparing Table 12.7 and Figure 12.32, Kurup and Turchi [22] concluded that the temperature range of 120 to 220°C is an ideal target range for solar IPH using parabolic trough and linear Fresnel collector technologies.

TABLE 12.7

Solar Thermal Technologies for Different Temperature Ranges

Temperature Range*	Solar Collector Type	HTF of Choice	Applications/ Comments
<80°C	Flat plate Non-tracking compound parabolic Solar pond	Water	Hot water Space heating
80–200°C	Parabolic trough Linear Fresnel	Water/steam	Hot water or steam for IPH
200–300°C	Parabolic trough Linear Fresnel	Mineral oil	Direct heat or steam for IPH Vacuum-jacket receivers become necessary to minimize heat loss
300–400°C	Parabolic trough Linear Fresnel	Synthetic oil	Direct heat or steam for IPH
400–550°C	Parabolic trough Linear Fresnel	Steam or Molten salt	Electric power
>550°C	Heliostat/central receiver Parabolic dish	Steam or Molten salt	Electric power

Source: From Kurup, P., and Turchi, C., 2015. Initial investigation into the potential of the CSP industrial process heat for the southwest United States, NREL/TP-6A20-64709. [22]

**FIGURE 12.32**

U.S. IPH energy use for steam generation for industries using natural gas. Adapted from data published in a Cornell Energy Institute report by Fox, D.B., Sutter, D., and Tester, J.W., 2011. The thermal spectrum of low-temperature energy use in the United States, *Energy & Environmental Science* 4 (10), no. 10. [23]

Of course, effective use of concentrating solar collectors requires locations where the direct normal irradiance (DNI) resource is high. Ideally, the best locations for solar IPH are industrialized areas with high DNI. In the United States, California ranks third in industrial gas use behind Texas and Louisiana. California's Central Valley has a good combination of DNI resource and industrial demand for steam in the temperature range of interest. Figure 12.33 shows a photo of the parabolic trough system installed in 2008 by

**FIGURE 12.33**

The 5065-m² parabolic trough array used to heat cooking oil at Frito Lay's SunChips plant in Modesto, California, which was built by Abengoa Solar in 2008. The California Central Valley has a good combination of solar resource and process need that is suited to that resource. (Courtesy of Ken May.)

Abengoa Solar at the Frito-Lay plant in Modesto, California. It uses 5,065 m² of troughs to provide 2.4 MW of thermal energy at temperatures of up to 249°C. Pressurized hot water is used to heat cooking oil used in the production of (appropriately enough) Frito-Lay's SunChips snack product.

PROBLEMS

- 12.1 The graph in [Figure 12.4](#) gives the results of an ASHRAE standard performance test for a double-glazed flat plate collector. If the transmittance for the glass is 0.90 and the absorptance of the surface of the collector plate is 0.92, determine
- The collector heat-removal factor F_R
 - The overall heat loss conductance of the collector U_c in W/m² K
 - The rate at which the collector can deliver useful energy in W/m² K

When the insolation incident on the collector per unit area is 600 W/m² K, the ambient temperature is 5°C, and inlet water is at 15°C.

The maximum flow rate through the collector, with cold water entering at a temperature of 15°C, which will give an outlet temperature of at least 60°C if this collector is to be used to supply heat to a hot water tank.

- 12.2 What is the operating temperature for an evacuated tube collector operating at 50% efficiency if the insolation is 800 W/m²? Use data from [Figure 12.5](#).
- 12.3 A solar electric engine operating between 5°C and 95°C has an efficiency equal to one-half the Carnot efficiency. This engine is to drive a 4 kW pump. If the collector has an efficiency of 50%, calculate the area needed for operation in Egypt, where the insolation averages about 2800 kJ/m² h during the day. State any additional assumptions.
- 12.4 Consider a solar-driven irrigation pump. Parabolic trough collectors are used to heat the water in the collectors to 423 K, which then vaporizes an organic working fluid that powers the pump-turbine. Calculate the surface area needed to power a 50 hp pump capable of delivering up to 38,000 L/min of water at noon in Albuquerque, New Mexico. Use the collector efficiency given in Equation 12.24 and assume the ORC engine operates at 60% of Carnot efficiency. Also assume a direct normal irradiance of 740 W/m² and a heat rejection temperature of 305 K.
- 12.5 Write a closed-form expression for the work output of a solar-powered heat engine if the energy delivery of the solar collector at high temperature is given approximately by the expression

$$q_u = (\tau\alpha)_{eff} I_c - \frac{\sigma\epsilon\bar{T}_f^4}{CR}$$

(convection and conduction losses are neglected) where \bar{T}_f is the average fluid temperature and CR is the CR. Two heat engines are to be evaluated:

1. Carnot cycle

$$\text{Cycle efficiency } \eta_c = 1 - \frac{T_\infty}{T_f},$$

2. Brayton cycle

$$\text{Cycle efficiency } \eta_B = 1 - \frac{C_B T_\infty}{T_f} C_B \geq 1,$$

where

$$C_B = (r_p)^{(k-1)/k}$$

r_p is the compressor pressure ratio

is the specific heat ratio of the working fluid

Write an equation with \bar{T}_f as the independent variable that, when solved, will specify the value of \bar{T}_f to be used for maximum work output as a function of CR, surface emittance and $(\tau\alpha)_{eff}$ product, insolation level, and C_B . Optional: solve the equation derived previously for CR = 100, $\varepsilon = 0.5$, and $(\tau\alpha)_{eff} = 0.70$, at an insolation level of 1 kW/m². What is the efficiency of a solar-powered Carnot cycle and a Brayton cycle for which $C_B = 2$?

- 12.6 Explain how window placement in a building could be defined as (a) a passive solar feature, (b) an energy conservation measure, and (c) both of these.
- 12.7 List the issues that must be addressed to perform a conceptual design of a 50 MW power tower in Nevada.
- 12.8 It has been estimated that a 400 MW expansion of the existing SEGS solar plant in California would cost \$2.4 billion. Estimate the expected capital costs of the generation facility in dollars/kW capacity and the minimum cost of electricity per kWh generated by the addition, if they are operated at full capacity for 6 h/day and have a lifetime of 30 years.
- 12.9 Using SAM, estimate the levelized cost for a 50 MW_e parabolic trough solar power plant in Boulder City, Nevada, using the physical trough model and a Variation 1 trough (good as new receivers). Also determine the thermal energy delivered to the power block during July and estimate the surface area required for the installation. Assume an inflation rate of 2% and look up the discount rate in the *Wall Street Journal* at the time of this assignment.
- 12.10 Using SAM, estimate the levelized cost for a central receiver solar power plant with 10 h of storage in Phoenix, Arizona. Assume that the receiver is of external design and that heat rejection in the condenser is with a wet cooling tower configuration. Comment on the availability of cooling water and state all of your assumptions.

References

1. U.S. Dept. of Commerce, 1975. Optical coatings for flat plate solar collectors, NTIS No. PN-252-383, Honeywell, Inc., Morristown, NJ.
2. Solar Energy Research Institute, 1988. *Engineering Principles and Concepts for Active Solar Systems*, Hemisphere Publishing, Washington, DC.

3. Goswami, Y. et al., 2000. *Principles of Solar Engineering*, 2nd ed., Taylor & Francis, Philadelphia, PA.
4. ASHRAE. Standard 93-77: *Methods of Testing to Determine the Thermal Performance of Solar Collectors*, Atlanta, GA, <https://www.ashrae.org/technical-resources/standards-and-guidelines>.
5. ASHRAE. Standard 96-80: *Methods of Testing to Determine the Thermal Performance of Unglazed Solar Collectors*, Atlanta, GA, <https://www.ashrae.org/technical-resources/standards-and-guidelines>.
6. Kutscher, C.F., and Christensen, C.B., 1992. Unglazed transpired solar collectors, In: Boer, K. (ed.), *Advances in Solar Energy*, vol. 7, pp. 283–307.
7. Kutscher, C.F., 1996. Transpired solar collector systems: A major advance in solar heating systems, in: *Proceedings of the 19th World Energy Engineering Congress, November 6–8, 1996*, Atlanta, GA.
8. Kutscher, C., Burkholder, F., and Stynes, J.K., February 2012. Generation of a parabolic trough collector efficiency curve from separate measurements of outdoor optical efficiency and indoor receiver heat loss, *Journal of Solar Energy Engineering*, 134(1), DOI: 10.1115/1.4005247.
9. Zhu, G., Wendelin, T., Wagner, M., and Kutscher, C., 2013. History, current state, and future of linear Fresnel collectors, *Solar Energy*, 103, 639–652.
10. Mehos, M. et al., May 2016. On the path to SunShot: Advancing concentrating solar power technology, performance, and dispatchability, NREL/TP-5500-65688.
11. Kreith, F., and West, R., 2007. *CRC Handbook of Energy Efficiency and Renewable Energy*, CRC Press, Boca Raton, FL.
12. Goswami, D.Y., 1986. *Alternative Energy in Agriculture*, vol. 1, CRC Press, Boca Raton, FL.
13. Passive House Institute U.S. WUFI Passive 3.0, <http://www.phius.org/software-technical-resources/wufi-passive-and-other-modeling-tools/wufi-passive-3-0>.
14. International Passive House Association. Certification, https://www.passivehouse-international.org/index.php?page_id=183.
15. de Laquil, P. et al., 1993. *Solar Thermal Electric Technology in Renewable Energy*, Island Press, Washington, DC.
16. Acciona. Nevada Solar One, <http://acciona.us/projects/energy/concentrating-solar-power/nevada-solar-one>.
17. Acciona. <http://www.acciona.us/projects/energy/concentrating-solar-power/nevada-solar-one/>.
18. Hebrank, W.H., 1975. Tenter frame drying, *Am. Dyestuff Rep.* 63, 34.
19. NAS. How we use energy, <http://needtoknow.nas.edu/energy/energy-use/industry>.
20. Kutscher, C. et al., 1982. *Design Approaches for Solar Industrial Process Heat Systems*, NREL, <https://www.nrel.gov/docs/legosti/old/1356.pdf>.
21. SHIP Plants. Collector areas by project, <http://ship-plants.info/reports/areas/overview>.
22. Kurup, P., and Turchi, C., 2015. Initial investigation into the potential of the CSP industrial process heat for the southwest United States, NREL/TP-6A20-64709.
23. Fox, D.B., Sutter, D., and Tester, J.W., September 27, 2011. The thermal spectrum of low-temperature energy use in the United States, *Energy & Environmental Science* 4(10), 3731–3740, DOI: 10.1039/C1EE01722E.



Taylor & Francis

Taylor & Francis Group

<http://taylorandfrancis.com>

13

Ocean, Hydropower, and Geothermal Energy Conversion

The offshore ocean area under U.S. jurisdiction is larger than our land mass, and teems with ... energy sources.

Tom Allen

13.1 Ocean Thermal Energy Conversion

The oceans contain a great deal of energy but the conversion of this energy into a useful form such as electricity or heat requires advanced technology that is still under development. However, many demonstration prototypes have been designed and built. Valuable information is being obtained from the operation of these plants, and the results should lead to the development of large-scale units that are expected to become economically competitive in the future.

The key conversion technologies of ocean energy are:

1. Ocean thermal energy conversion
2. Tidal energy
3. Wave power

The basic elements of these technologies will be presented in this chapter.

Oceans cover 71% of the Earth's surface and receive the majority of the solar energy incident upon the Earth. In semitropical and tropical oceans, the available temperature difference between the surface, which is warmed by the sun, and the temperature at the lower depths (ΔT_0) is sufficient to operate a Rankine-type power plant using fluids such as ammonia. Since the temperature difference is available 24 h/day virtually throughout the year, ocean thermal energy conversion (OTEC) has vast potential for implementation in many parts of the world. If the energy in a band $\pm 10^\circ$ latitude near the equator could be extracted with an energy efficiency of 0.5% of the incident solar energy, more than 7×10^5 MW power could be generated.

The main drawback of an OTEC system is that the overall thermal efficiency of the plant is low, and therefore large seawater pumps and large heat exchangers are required to produce adequate power. The maximum efficiency of any type of thermal power plant is the Carnot cycle efficiency, η_c , which for a typical OTEC plant is equal to

$$\eta_c = \frac{T_h - T_c}{T_h} = \frac{\Delta T_0}{T_h} \quad (13.1)$$

where

T_h is the hot surface water absolute temperature (about 298 K)

T_c is the absolute temperature of the cold water from below (about 278 K)

Thus, the Carnot efficiency is only about 6.7%. This ideal efficiency does not allow for parasitic losses or the temperature differences between the seawater and the working fluid required for evaporation and condensation. A rough rule of thumb is that about 25% of ΔT_0 needs to be allowed for the evaporation, and 25% for the condensing process, leaving only about half of the total temperature difference for the power turbine. For an 80% overall efficiency of the turbine generator, the gross power output efficiency would therefore only be about 3%. Parasitic load takes another 30% or so of the overall thermal efficiency, leaving a net power delivery efficiency of only about 2%–3%.

Figure 13.1 illustrates the four ocean thermal plant types that have been suggested: land-based (or shallow-water), shelf-mounted, floating, and moored plant types relative to the continent/ocean floor profile. The greatest number of potential sites exists for the floating plant with a suspended cold water pipe (CWP). Shelf-mounted or land-based plant types reduce electricity and water transportation cost, as well as the ocean dynamics/plant operation problems. Except for the CWP, the design and construction of floating and moored types are within current state-of-the-art technology. If longer pipes are required, they increase costs and reduce the number of potential sites.

Disadvantages of the floating moored plant types are related to electricity and water transportation and the effect of ocean dynamics on plant operation. For example, efficient transportation of electricity (by cable) and/or freshwater (by pipeline or barge) from a plant far offshore may be difficult. An example of the effect of ocean dynamics on plant design and operation is related to the evaporator. The evaporator produces steam as a result of

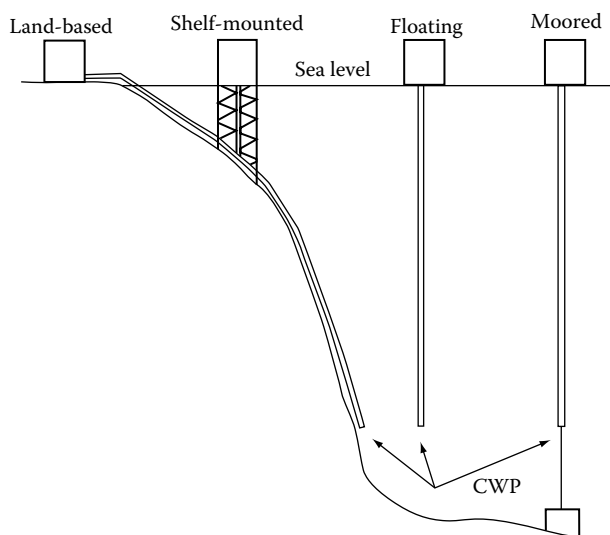


FIGURE 13.1

Basic OTEC plant configurations with cold water pipe (CWP).

the difference between the operating pressure and the saturation pressure of the warm seawater. Since this difference corresponds to only about 0.1 m of water, it is critical that the warm seawater supply pressure remain essentially constant, in spite of the wave action and platform motion, which may be difficult to achieve.

There are two basic technical approaches to producing power from the ocean thermal resources. Both are based on the Rankine thermodynamic cycle; one uses a closed system with a pressurized working fluid (typically ammonia or a fluorocarbon), and the second is an open system using the seawater itself as the working fluid. The concept of a closed-cycle OTEC (CC-OTEC) system was originally proposed by D'Arsonval [1] in 1881, and in 1930, his student, Claude [2], demonstrated the operation of an open-cycle OTEC (OC-OTEC) plant off the coast of Cuba.

13.1.1 Closed-Cycle Ocean Thermal Energy Conversion

Figure 13.2 is a schematic diagram of a closed-cycle ocean thermal conversion system. Warm surface water is used in the boiler to evaporate a working fluid; the sensible heat liberated by the seawater is the maximum heat input, P_0 , for the cycle:

$$P_0 = \rho c Q \Delta T_0 \quad (13.2)$$

where

ρ is the density of seawater in kg/m^3

c is the specific heat of seawater in J/kg K

Q is the flow rate in m^3/s

The vapor produced in the boiler passes through a turbine to the condenser and the expansion process generates power for electrical generation. The condenser heat sink uses

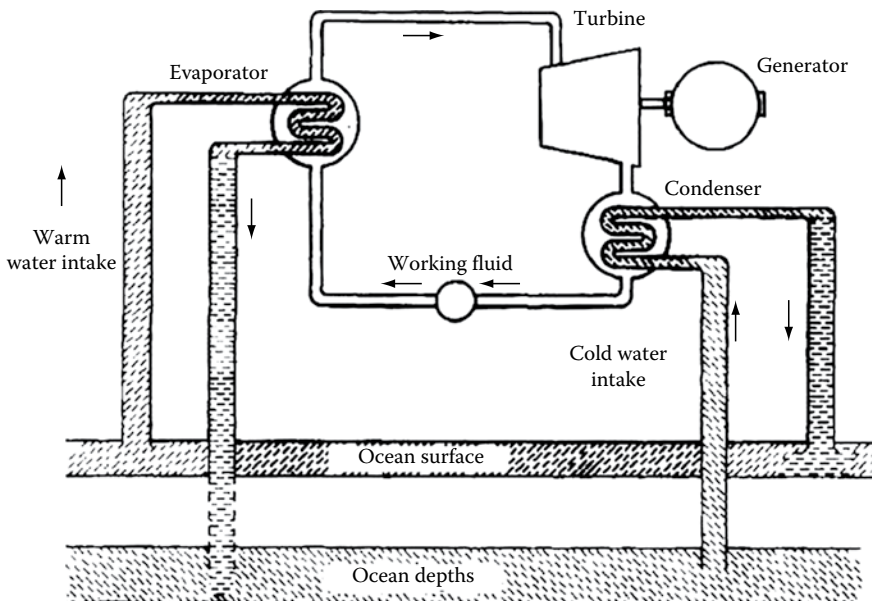


FIGURE 13.2
Schematic diagram of CC-OTEC.

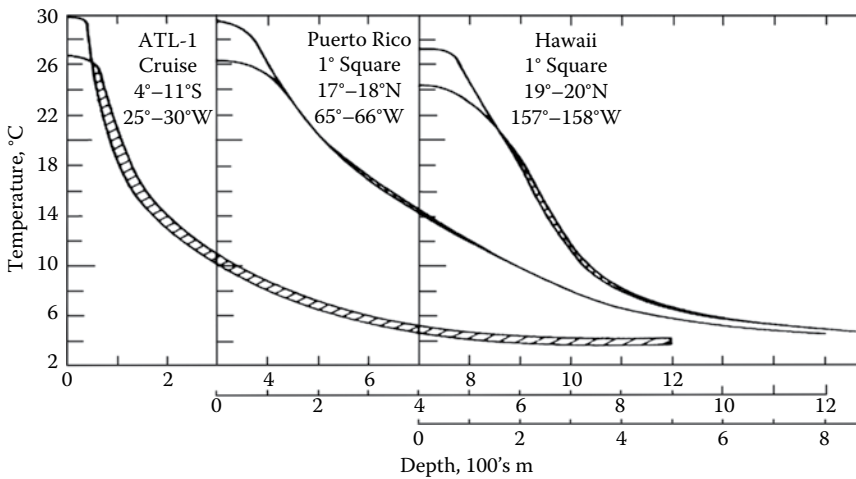


FIGURE 13.3

Temperature profiles vs. depth for Hawaii, Puerto Rico, and Recife, Brazil (ATL-1). (According to Dugger, G. et al., 1981. Ocean thermal energy conversion, in: Kreider, J.F. and Kreith, F. eds., *Solar Energy Handbook*, McGraw-Hill, New York, Chapter 19. With permission. [3])

cold water obtained at a depth of about 1000 m. Obviously, a long section of pipe and substantial pumping power are required for the condensation process.

The mechanical features of the closed cycle are very similar to a refrigeration cycle. Except for preventing bio-fouling of the heat exchanger and the CWP, the technology is currently available. It should also be noted that a CC-OTEC system can also be used to produce potable water [3].

Figure 13.3 shows typical temperature versus depth profiles near Hawaii, Puerto Rico, and Recife, Brazil (designated ATL-1), and Table 13.1 presents seasonal variations in ΔT_0 for the same three sites [3]. The sites near Puerto Rico and Hawaii are of particular interest to the United States, because for these islands, all of the fuel needs to be imported. If movable or so-called grazing plants were to be installed, they would seek out the highest ΔT based on historical plots of monthly surface temperature contours, as well as daily information from satellites, which would indicate the optimum path for the platform on which the OTEC plant is based. A mini OTEC plant, shown in Figure 13.4, operated off of Keahole Point, Hawaii, in 1977 and generated 50 kW (gross) and 10 kW (net) from a temperature difference of 21.2°C (38.2°F). The system contained all the essential components required to build a full-scale CC-OTEC plant. It used a titanium plate-type heat exchanger and the plant was mounted on a barge moored by a single anchor, which incorporated a 24 in. OD polyethylene CWP as an integral member of the moor. A flexible rubber hose connected the top of the CWP to a moon pool in the center of the barge.

EXAMPLE 13.1

Estimate the size of heat exchanger and the cold water flow rate required for a 10 MW CC-OTEC plant.

Assume that the cold water comes from a depth of 1000 m at a temperature T_{wc} of 5°C, while the hot water temperature, T_{wh} , is 25°C. Assume that the evaporator as well as the condenser operate at an effective temperature difference of ΔT of 4 K, with an overall heat transfer coefficient U of 6000 W/m² K. Use the Carnot efficiency for the power plant as an approximation.

TABLE 13.1Monthly Values of ΔT_0 and Power P_{net} (Percentage of Design Value) for Selected Sites

Month	ATL-1		Puerto Rico		Hawaii	
	ΔT_0 (°C)	P_{net} (%)	ΔT_0 (°C)	P_{net} (%)	ΔT_0 (°C)	P_{net} (%)
January	23.5	96	21.3	88	20.6	90
February	24.3	104	20.9	84	20.1	85
March	25.2	115	20.9	84	20.0	84
April	25.2	115	21.2	87	20.6	90
May	24.2	103	22.2	99	21.3	99
June	24.4	105	22.6	104	21.3	99
July	23.6	97	23.0	108	22.4	112
August	24.3	104	23.0	108	22.7	116
September	22.4	84	23.6	116	22.7	116
October	23.3	94	23.9	119	22.5	114
November	22.6	86	23.3	112	21.5	101
December	23.3	94	22.3	100	20.7	92
Average	23.9	99.8	22.3	100.7	21.4	99.8
$P_{net, avg, rel}$	100		83.7		74.2	

For details on the power, see Dugger et al. [3].

SolutionThe rate of heat transfer to the working fluid in the evaporator of area A is approximately

$$q_{in} = UA\Delta T$$

The rate of enthalpy increase of the water is

$$\dot{q}_{in} = \dot{Q}\rho c(T_h - T_c) = \dot{Q}\rho c[(T_{wh} - \Delta T) - (T_{wc} + \Delta T)] = \dot{Q}\rho c(T_{wh} - T_{wc} - 2\Delta T)$$

where

 ρ is the density (1.0 kg/m³) c is the specific heat (4.2×10^3 J/kg K)The Carnot efficiency η_c of the energy conversion process is

$$\eta_c = \frac{T_h - T_c}{T_h} = \frac{T_{wh} - T_{wc} - 2\Delta T}{T_{wh} - \Delta T} = \frac{12}{294} = 0.04$$

The power output, P_0 , is given by

$$P_0 = \frac{\dot{Q}\rho c(T_{wh} - T_{wc} - 2\Delta T)^2}{(T_{wh} - \Delta T)}$$

and the water flow rate by

$$\begin{aligned} \dot{Q} &= \frac{P_0(T_{wh} - \Delta T)}{\rho c(T_{wh} - T_{wc} - 2\Delta T)^2} = \frac{P_0}{\rho c \eta_c} \\ &= \frac{10 \times 10^3 \text{ J/s } 294 \text{ K}}{10^3 \text{ kg/m}^3 \times 4.2 \times 10^3 \text{ (J/kg)} \times (12 \text{ K})^2} \\ &= 4.86 \text{ m}^3/\text{s} \end{aligned}$$

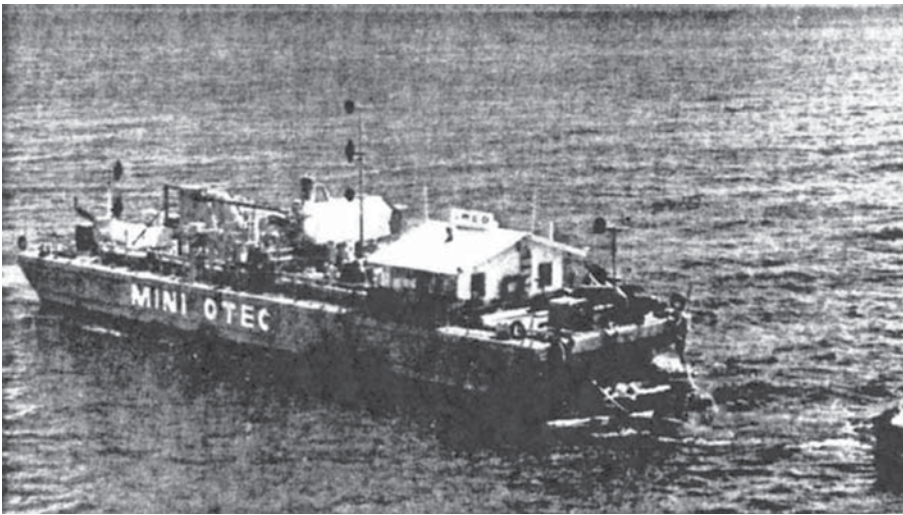
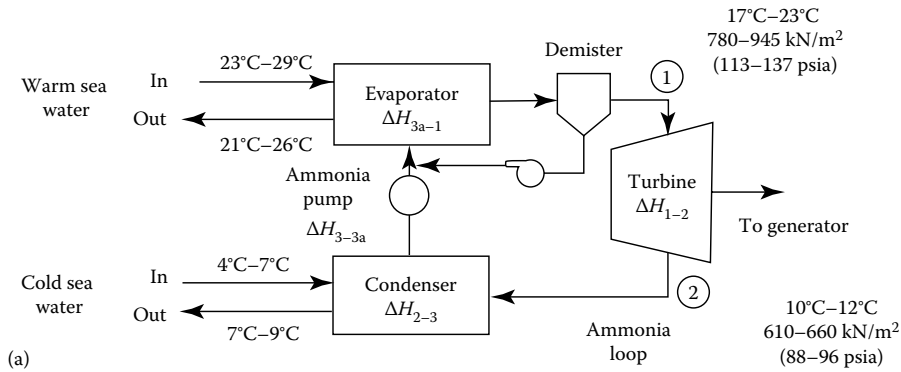


FIGURE 13.4

(a) Simplified diagram for typical closed-cycle OTEC plant using ammonia as the working fluid and (b) photo of the closed-cycle plant operated in 1979 off Hawaii. (According to Dugger, G. et al., 1981. Ocean thermal energy conversion, in: Kreider, J.F. and Kreith, F. eds., *Solar Energy Handbook*, McGraw-Hill, New York, Chapter 19. With permission. [3])

This is a very large flow rate. If the CWP were 1 m in diameter, the water velocity V would be

$$V = \frac{4Q}{\pi d^2} = \frac{4 \times 4.86}{\pi 1^2} = 6.2 \text{ m/s}$$

For a rate of heat transfer, q , the heat exchanger area is

$$\begin{aligned} A &= \frac{q}{U\Delta T} = \frac{\dot{Q}\rho c(T_{wh} - T_{wc} - 2\Delta T)}{U\Delta T} \\ &= \frac{P_0}{U\Delta T\eta_c} \\ &= \frac{10 \times 10^6 \text{ W}}{6,000(\text{W/m}^2 \text{ K})(4\text{ K}) \times 0.041} \\ &= 10,162 \text{ m}^2 \end{aligned}$$

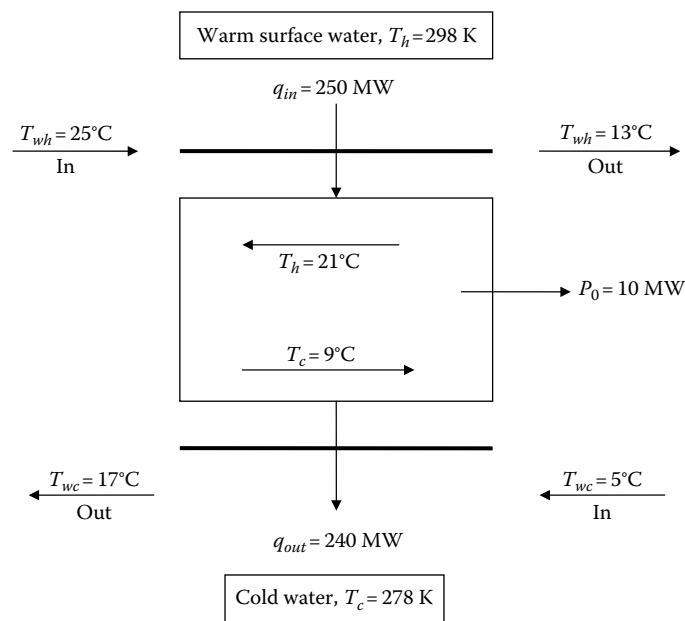


FIGURE 13.5
Schematic diagram for the solution of Example 13.1.

This is a huge and expensive heat exchanger surface area.
The heat transfer and power-generation processes are shown schematically in [Figure 13.5](#).

13.1.2 Open-Cycle Ocean Thermal Energy Conversion

OC-OTEC systems can generate electricity and/or freshwater using the temperature difference between surface and deep ocean seawater without the need of an expensive heat exchanger [4]. It is an attractive concept due to the vast amount of ocean energy available and the minimal eco-logical impact. OC-OTEC is ideally suited for locations that have a need for alternative electricity and freshwater, and are also close to an ocean thermal resource. [Table 13.2](#) provides information about potentially suitable OC-OTEC sites in the United States.

TABLE 13.2
Oceanographic Data for Potential OC-OTEC Sites in the United States

Site	Latitude (°N)	Longitude (°W)	Water Depth (m)	Distance from Shore (km)	Temperature Differential ^a (°C)
Puerto Rico	18.0	65.8	1000	3.1	22.3
Miami	25.4	79.9	740 ^b	28.4	21.2
Key West	24.2	81.3	914 ^b	60.0	21.5
Tampa	27.8	85.2	1000	281.6	20.9
New Orleans	28.8	88.8	1000	80.5	20.8
Island of Hawaii	19.9	156.1	1000	2.3	21.4

^a Average.
^b Maximum depth at location.

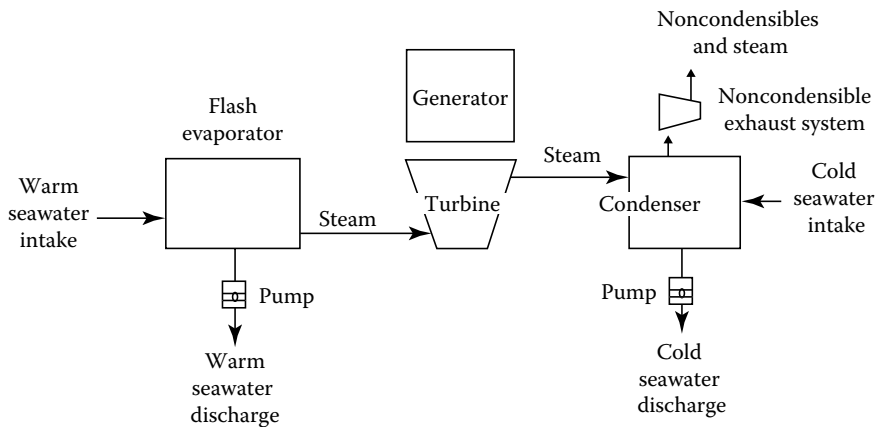
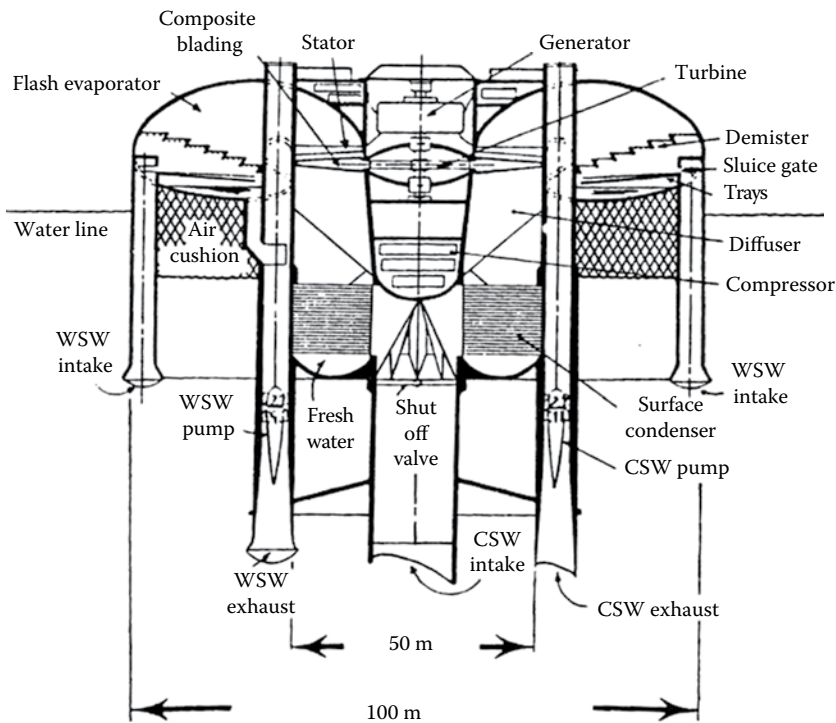


FIGURE 13.6
Conceptual schematic of open-cycle OTEC system.

The OC-OTEC concept is shown schematically in [Figure 13.6](#). Warm (25°C typical) surface seawater is introduced into the evaporator, which operates at a pressure slightly below the saturation pressure corresponding to the warm seawater temperature. A small percentage ($\approx 0.5\%$) of the seawater flashes to produce steam, which is expanded through a turbine connected to an electrical generator. Most of the steam is condensed in a direct contact condenser supplied with cold (typically 5°C) seawater from depths of approximately 1000 m. A surface condenser is used only if freshwater production is desired, whereas a more efficient direct-contact condenser is used for electricity production. The remaining steam and noncondensable gases (released from the seawater in the evaporator and direct-contact condenser, and from possible leaks in the containment structure) are removed from the condenser by the noncondensable exhaust system. Variations of the basic cycle shown in [Figure 13.6](#) include multiple stages of (evaporator, turbine, condenser) seawater pre-deaeration, and a combination of freshwater and direct-contact condenser with freshwater to seawater heat exchanger.

In an OC-OTEC system, seawater itself is used as the working fluid. A 100-MW electric open-cycle system was proposed some time ago by Westinghouse. The Westinghouse design proposed turbines with 140 ft tip diameter that were to operate at 225 rpm and deliver up to 100 MW of electric power under optimum conditions. The hull in this design is located around the vertical axis turbine in an integrated design. An open channel evaporator is located axis-symmetrically around the turbine with warm seawater entering the evaporator through a peripheral submerged sluice. Vapor flashes from the warm water flow along a bent path toward the turbine blade, while the spent vapor leaving the turbine rotor is condensed in a surface condenser centrally located underneath the turbine. More recently, it has been proposed to utilize a direct-contact condenser, which increases the efficiency of the system [5]. The warm seawater leaving the evaporator and the cold seawater leaving the condenser are rejected into the ocean through a common pipe. Depending upon whether the condenser is a surface condenser or a direct-contact condenser, seawater distillation is possible with this approach. [Figure 13.7](#) illustrates schematically such a dual-purpose system [6]. A detailed description of the OC-OTEC system using a falling jet evaporator and direct-contact condenser, a more advanced version of the Westinghouse concept, has been developed at the Solar Energy Research Institute and is described in Bharathan et al. [5].

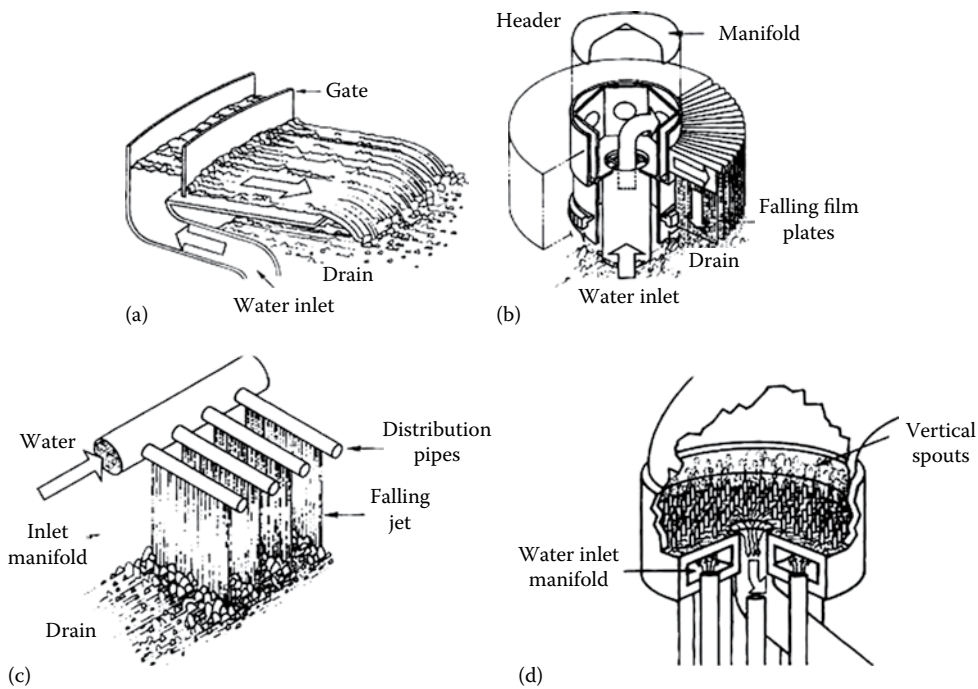
**FIGURE 13.7**

Schematic of OC-OTEC for power and freshwater production. 100 MW, OC-OTEC plant cross-section (as proposed by Westinghouse). (From Rabas, T.J. et al., March 1979. OTEC 100-MWe alternate power systems study. Report by Westinghouse Electric Corp to U.S. DOE under contract EG/77/C/05/1473. With permission. [6])

13.1.3 Direct Contact Evaporation and Condensation

The mechanism by which steam is generated in an OC-OTEC system is called direct contact or “flash” evaporation. This process occurs when warm seawater is introduced into the evaporator at a pressure below the vapor pressure corresponding to the liquid inlet temperature, and steam is produced by the combined action of boiling and surface evaporation. Flash evaporation is usually quite violent as a result of the explosive growth of vapor bubbles from nucleation sites in the liquid. The growth of these bubbles shatters the liquid continuum and yields a wide range of droplet sizes. Because of the irregular geometry of the interface, it is practically impossible to define or measure the surface area from which evaporation takes place. Heat transfer in flash evaporation can therefore not be described in terms of a conventional heat transfer coefficient. To quantify the process and present experimental data, another parameter is used “the effectiveness ϵ .” The effectiveness of flash evaporation is defined as the ratio of the temperature difference between the inlet and outlet liquid streams to the temperature difference between the inlet stream and the vapor temperature corresponding to the chamber saturation pressure. This definition is similar to the effectiveness of a conventional heat exchanger, since it is the ratio of the temperature difference actually achieved to the maximum temperature difference thermodynamically available.

Several evaporator options have been proposed and analyzed for OC-OTEC. They include open channel flow, falling films, falling jets, and spout evaporators. These are shown schematically in Figure 13.8. Based upon extensive experiments at the SERI test

**FIGURE 13.8**

Contending direct-contact heat exchanger geometries for OC-OTEC: (a) open channel flow, (b) falling films, (c) falling jets, and (d) vertical spouts.

facility [7], the single-spout evaporator was found to be the most suitable configuration. The effectiveness measured in experiments with and without screens placed above the pipe outlet varied between 0.9 and 0.97 with a liquid-side pressure drop of 0.7 m (spout height + kinetic energy loss).

OTEC direct-contact condensation is more complicated than for conventional steam turbine applications, because ocean water contains a large amount of noncondensable gases that may come out of solution and the need to reduce parasitic power to a minimum. Based on extensive experiments, it was found that packed columns with structured packing are the best technology for OC-OTEC. The analysis for these configurations is presented in Kreith and Bharathan [4]. The most effective configuration was found to be an initial cocurrent condenser, followed by a countercurrent section in which noncondensable gases can be removed.

13.1.4 Comparison of Open- and Closed-Cycle OTEC Systems

For a given temperature difference potential, the OC-OTEC system is thermodynamically superior to the closed-cycle system because a larger portion of the temperature difference between the hot and the cold water is available to produce net power [5]. This is because of the direct-contact heat transfer mode of the evaporator and condenser, as used in the open-cycle system. The steam in the vacuum chamber can attain the temperature of the warm water discharged from the evaporator. At the same time, the exhaust steam from the turbine can be condensed at a temperature approaching the condenser cold water exit temperature.

In a closed-cycle system, the working fluid passing through the turbine is separated from the warm and cold waters by a solid wall. Hence, in both the evaporator and the

condenser, a temperature drop is necessary first to transfer the heat from the water through the wall to produce the vapor in the boiler, and then another temperature drop is required to condense the vapor of the working fluid at the outlet from the turbine by cold seawater. Consequently, the heat exchangers for CC-OTEC plants require very large surface areas to minimize the thermodynamically required temperature losses. These exchange surfaces are continuously exposed to corrosion and biofouling in the harsh ocean environment. On the other hand, the turbine in a CC-OTEC system is relatively small and is available as an “off-the-shelf” item. But, because of the low pressure in which the turbine must operate in the open-cycle system, the turbine is very large, and so far, no full-scale turbines for plants 1 MW and greater have been designed and operated.

Any ocean thermal energy conversion system faces the enormous challenge of producing net power with a temperature difference on the order of 20°C. Since the Carnot efficiency of such a plant is only on the order of 6% or 7%, any successful ocean energy conversion system must use as much of the temperature potential as possible and, at the same time, reduce parasitic losses to a minimum. The major parasitic losses in ocean thermal systems are the pumping power required to bring the cold water from a depth of about 1000 m to the surface, the power required to remove noncondensable gases in the open-cycle system, and the degradation of the available thermal energy by temperature drops due to fouling and corrosion across the heat transfer surfaces of a closed-cycle system.

13.1.5 Cold-Water Pipe and Pumping Requirements

The cost of the CWP is the dominant feature in the overall cost for an OTEC system [8]. This pipe is subject to stresses that include drag from ocean current, oscillating forces due to vortex shedding, and possibly forces due to the drift and motion of the platform. Moreover, the weight of the pipe is substantial, and it is not clear whether it should be made of a rigid or flexible material such as polythane. There may also be problems in assembling and positioning the pipe because of its enormous length. A premature failure of the CWP could be a financial blow to the entire OTEC system.

To transport the large quantities of cold and hot water necessary to operate an OTEC system requires a good deal of pumping power. This power will have to be supplied from the gross power output of the OTEC system, and constitutes a loss in net energy. The frictional loss in pumping the water through the CWP can be reduced by increasing the pipe diameter, but this will increase the cost and weight of the pipe. It can also lead to instabilities that could prematurely destroy the cold water support. It should also be noted that the power output estimated in the example below is based on the efficiency of a Carnot engine, whereas a real turbine is less efficient and thereby reduces the net power output.

EXAMPLE 13.2: PUMPING POWER REQUIREMENTS

Estimate the power required to move water from a depth of 1000 m for a 10 MW OTEC system described in the previous example. Assume that the diameter of the pipe is 1 m.

Solution

The average water velocity is

$$\bar{u} = \frac{\dot{Q}}{A} = \frac{4.86 \text{ (m}^3\text{/s)}}{\pi 0.5^2 \text{ m}^2} = 6.2 \text{ m/s}$$

Hence, the Reynolds number is

$$\text{Re}_D = \frac{uD}{\nu} = \frac{6.2 \text{ (m/s)} \cdot 1 \text{ m}}{1 \times 10^{-6} \text{ m}^2/\text{s}} = 6.1 \times 10^6$$

The flow is turbulent and the friction factor can be estimated from an empirical relation such as the one given below [9]

$$f = \frac{0.184}{\text{Re}_D^{0.2}} = \frac{0.184}{(6.1 \times 10^6)^{0.2}} = 0.0081$$

The head loss in the pipe thus equals

$$\Delta H = \frac{2fLu^2}{Dg} = \frac{2 \times 0.0081 \times 10^3 \text{ m} \times 6.2^2 \text{ m}^2/\text{s}^2}{1.0 \text{ m} \times 9.8 \text{ m/s}^2} = 62.8 \text{ m}$$

Hence, the pumping power required is

$$\begin{aligned} P_{\text{pump}} &= \rho \dot{Q} g \Delta H = 1 \times 10^3 \text{ kg/m}^3 \times 4.86 \text{ m}^3/\text{s} \times 9.8 \text{ m/s}^2 \times 62.8 \text{ m} \\ &= 3 \times 10^6 \text{ kW} = 3 \text{ MW} \end{aligned}$$

The pumping power requirements could be reduced substantially by using a 2 m diameter pipe.

13.1.6 Economics

Cost estimates have been performed for both open and closed cycle systems [8]. By and large, they have indicated similar results; however, since no large system has ever been built, detailed absolute cost estimates are unreliable. The main conclusions of one of the most detailed investigations are shown in Figures 13.9 and 13.10 [8]. Figure 13.9 shows the capital costs of OC-OTEC plants optimized for power production for a single-stage direct-contact condenser, a double-stage direct-contact condenser, and a single-stage surface condenser. For all three of these configurations, it can be seen that the capital cost decreases rapidly as net power output increases and levels off at net power above 20 MW electric. These results clearly indicate that in order for OTEC to be economically viable, extremely large plants would be necessary. For such large plants, the initial investment is large and this has, so far, discouraged investment in this technology. Figure 13.10 shows the fractional costs in percentage for the various parts of the OTEC system. These estimates indicate that the largest costs associated with an OTEC plant are the discharge and CWP, with the CWP costing approximately 40% of the total at a net power output of 20 MW electric, while the discharge pipe would require about half that amount.

A summary of the status of OTEC can be found Twidell and Weir [10]. For the most up-to-date news regarding OTEC, visit www.otecnews.org.

13.2 Tidal Energy

Tidal energy has a long history. Small tidal mills were used for grinding corn in Europe in the Middle Ages, but more recently, using tidal energy on a large scale to generate electricity

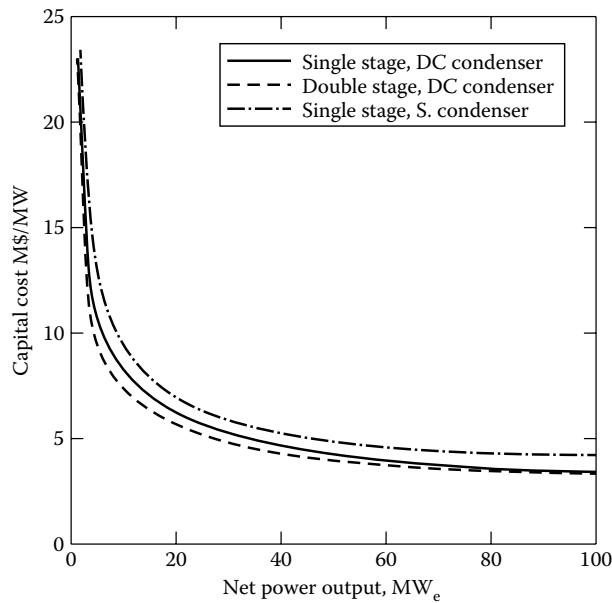


FIGURE 13.9 Capital cost estimates for three types of OC-OTEC plants vs. net power output optimized for power generation (\$1983). (From Block, D.L., and Valenzuela, J.A., May 1985. Thermoeconomic optimization of OC-OTEC electricity and water production plants, SERI/STR-251-2603, U.S. Department of Energy, Washington, DC. With permission. [8])

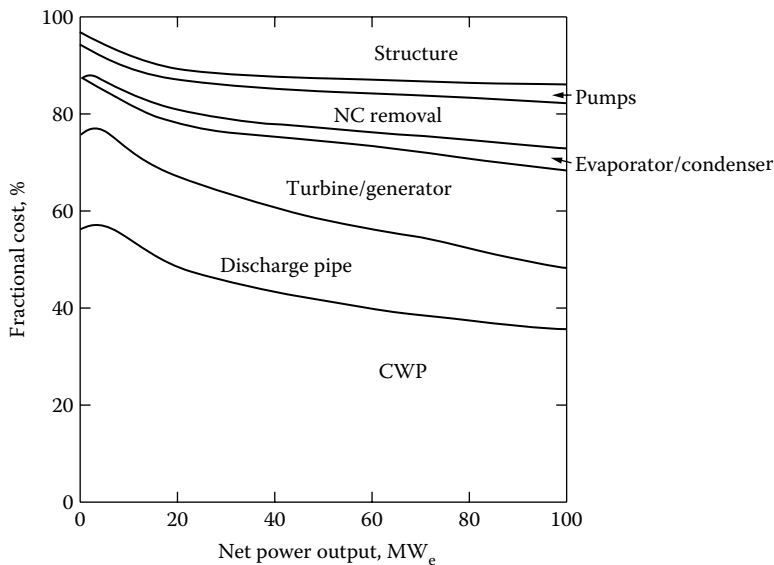


FIGURE 13.10 Fractional component cost of single-stage, direct-contact condenser plant optimized for power output. (From Block, D.L., and Valenzuela, J.A., May 1985. Thermoeconomic optimization of OC-OTEC electricity and water production plants, SERI/STR-251-2603, U.S. Department of Energy, Washington, DC. With permission. [8])

has been proposed for many parts of the world. Tidal energy can be harnessed by building large barrages—essentially long low dams—across the inlet of suitable estuaries. When the tides come in to the shore, they can be trapped by means of sluices in reservoirs, called tidal basins, behind these barrages. When the tide ebbs, the water behind the barrage can be let out via a turbine somewhat similar to a hydroelectric power plant. However, it is important to distinguish tidal power from hydropower. The former is the result of the interaction of the gravitational pull of the moon and the sun on the oceans, while the latter is derived from the hydrological climate cycle powered by solar energy. A simplified analysis of the Earth–moon interaction that produces the tidal behavior is presented in Elliott [11].

Tidal energy technology relies on the twice-daily tides with the concomitant upstream flows and downstream ebbs in estuaries [12]. To extract energy from the rise and fall of the tides, barrages are built across the inlet to the tidal basin, and turbines are located in water passages inside the barrages. The potential energy in the difference in water levels across the barrage due to the tidal motion is converted to kinetic energy as fast-moving water passes through the turbine. The rotational kinetic energy of the blades of the turbine can then be used to drive a generator to produce electricity. The average power output from a tidal system is roughly proportional to the square of the difference in water level between high and low tides. A tidal range of at least 5 m is considered the minimum for viable power generation. Sometimes tidal flows can be increased in height using the effect of concentration, as shown schematically [11] in the Severn Estuary near Cardiff, Wales (Figure 13.11).

Although many tidal systems have been proposed, the only major tidal power plant that has been constructed and operated is the La Rance Tidal Power Plant in France (Figure 13.12) [13]. The barrage for the plant was built in the 1960s near St. Maillot. A dam, 330 m long, was built in front of a 22 km² basin at a location where the tidal range was 8 m. The plant consists of 24 bulb-type turbine generators, 5.35 m in diameter, rated at 10 MW each. Power

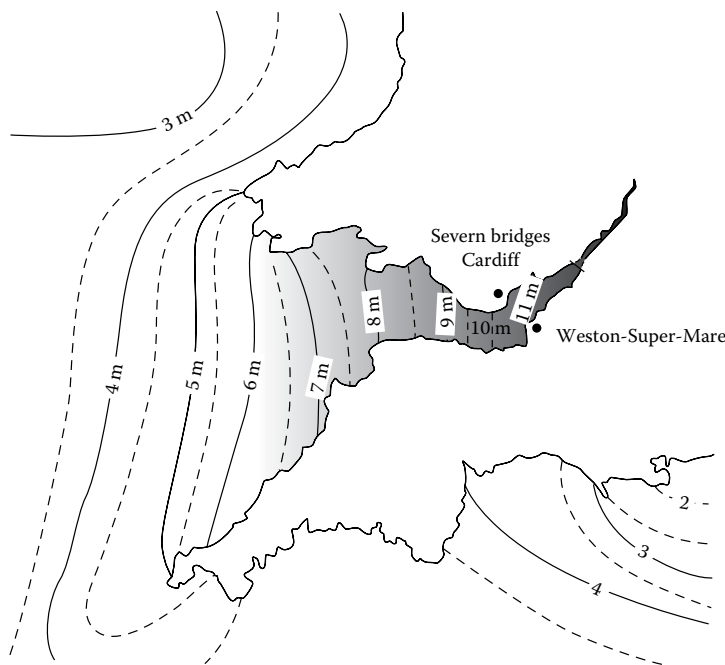


FIGURE 13.11

The effects of concentration of tidal flow in the Severn Estuary (tidal ranges in meters).

**FIGURE 13.12**

A view of La Rance tidal scheme. (a) Aerial photo of La Rance Tidal Power Plant, (b) photo of La Rance showing dam, and (c) turbine wheel. (Courtesy of Renewable Energy UK. La Rance Tidal Power Plant, <http://www.reuk.co.uk/La-Rance-Tidal-Power-Plant.htm>. [13])

can be generated irrespective of whether the tide is going in or out. The plant has now been in operation for 50 years, during which time 25 billion kilowatt hours of electricity has been generated without major incident or mechanical breakdown.

To estimate the amount of power output from a tidal barrage, assume that in front of the barrage is an infinite ocean, whereas behind it, a rectangular basin delineates the volume into which the water flows. The volume has a surface area A , and the range between high and low tide is H , as shown in Figure 13.13.

The incoming tide flows freely into the basin, but when the tide goes out, the water is held in the basin by closing the sluice gates at a level H above the level of the ocean. Given a rectangular basin, the center of gravity of the mass of water in the basin will be at a height $H/2$ above the sea level. The total volume in the basin will thus be AH and its mass will be ρAH . All of the water stored in the basin could now be made to flow through a turbine from the high to the low water level. The maximum potential energy E available per tide, assuming all the water passes through a height $H/2$, is therefore

$$E = \rho AHg \left(\frac{H}{2} \right) \quad (13.3)$$

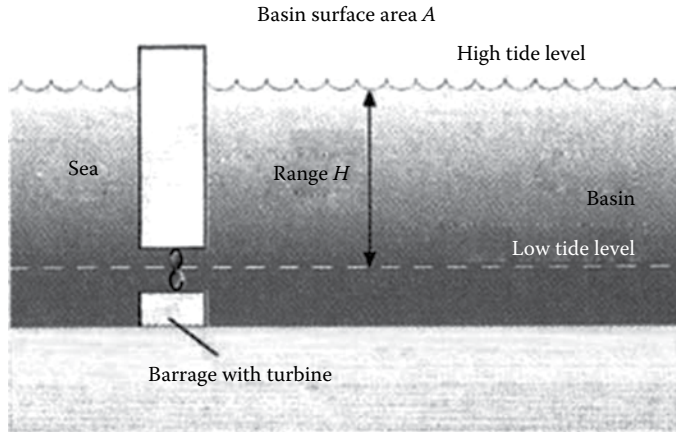


FIGURE 13.13
Nomenclature for tidal power analysis.

where g is the gravitational attraction. The main periods of tides are diurnal at about 24 h and semidiurnal at about 12 h 25 min [11].

If the basin is allowed to fill again with the next incoming tide and the cycle repeats with a period t , the average potential energy, P , that could be extracted becomes

$$P = \frac{\rho A H^2 g}{2t} \quad (13.4)$$

For example, if $A = 10 \text{ km}^2$, $H = 5 \text{ m}$, $t = 12 \text{ h } 25 \text{ min}$, $P = 26.6 \text{ MW}$.

However, the difference between high and low tidal levels, H , varies throughout the year from a maximum H_{\max} in the spring, to a minimum, H_{\min} , for the neap tides. As shown in Twidell and Weir [10], this variation in H can be accounted for by using a mean range for all the tides, \bar{H} . The mean power production per month, \bar{P} , then becomes

$$\bar{P} \sim \frac{\rho A g}{2g} \left(\frac{H_{\max}^2 + H_{\min}^2}{2} \right) \quad (13.5)$$

For example, if $H_{\max} = 5 \text{ m}$, $H_{\min} = 2.5 \text{ m}$, $A = 10 \text{ km}^2$, $\rho = 1030 \text{ kg/m}^3$, and $t = 12 \text{ h } 25 \text{ min}$ ($4.47 \times 10^4 \text{ s}$), then $\bar{P} \cong 16.1 \text{ MW}$.

Tidal power availability is dependent on local conditions, and there are many potential sites for tidal barrages around the world, as shown in Table 13.3, with an estimated total potential of the order of 300 TW hours per year [11]. The total energy dissipated from tides globally is approximately 3000 GW, of which approximately a third is in accessible locations. The realistically recoverable resource has been placed at one-tenth of this amount, or 100 GW, due to practical limitations such as access to major tides [14].

There are essentially three ways to generate power from a tidal system as described in Elliott [11]. The most common method is called ebb generation, in which the incoming tide passes through the sluice gate in the barrage, and the water is trapped in the tidal basin by closing the sluices. The head of water in the basin can then be passed back through the turbine during the outgoing ebb tide, as shown in Figure 13.14.

TABLE 13.3

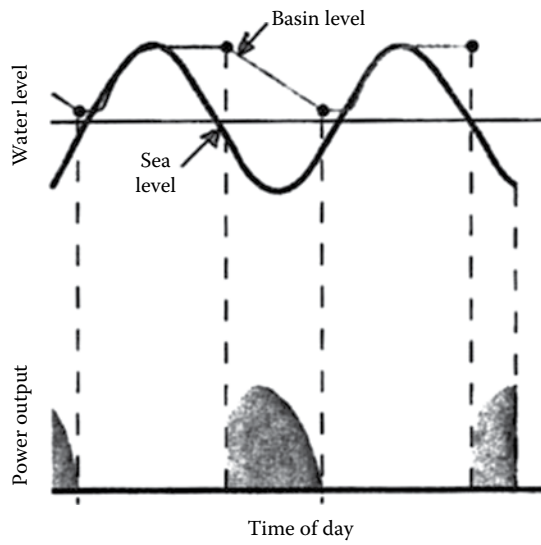
Some World Locations for Potential Tidal Power Projects

Country	Mean Tidal Range (m)	Basin Area (km ²)	Installed Capacity (MW)	Approx. Annual Output (TWh per year)	Annual Plant Load Factor (%)
Argentina					
San José	5.8	778	5,040	9.4	21
Golfo Nuevo	37	2,376	6,570	168	29
Rio Deseado	36	73	180	0.45	28
Santa Cruz	7.5	222	2,420	6.1	29
Rio Gallegos	7.5	177	1,900	4.8	29
Australia					
Secure Bay	7.0	140	1,480	2.9	22
Walcott Inlet	7.0	260	2,800	5.4	22
Canada					
Cobequid	12.4	240	5,338	14.0	30
Cumberland	10.9	90	1,400	3.4	28
Shepody	10.0	115	1,800	4.8	30
India					
Gulf of Kachchh (Kutch)	5.0	170	900	1.6	22
Gulf of Cambay (Khambhat)	7.0	1,970	7,000	15.0	24
Korea (Rep)					
Garolim	4.7	100	400	0.836	24
Cheonsu	4.5	—	—	1.2	—
Mexico					
Rio Colorado	6–7	—	—	54	—
United States					
Passamaquoddy	5.5	—	—	—	—
Knik Arm	7.5	—	2,900	7.4	29
Turnagain Arm	7.5	—	6,500	16.6	29
Russian Federation					
Mezeh	6.7	2,640	15,000	45	34
Tugur ^a	6.8	1,080	7,800	16.2	24
Penzhinsk	11.4	20,530	87,400	190	25

Source: Adapted from World Energy Council. <http://worldenergy.org>; Elliot, D., 2004. Tidal power, in Boyle, G. (ed.), *Renewable Energy*, 2nd ed., Oxford University Press, New York, Chapter 6, pp. 196–243. With permission. [11]

^a 7000 MW variant also studied.

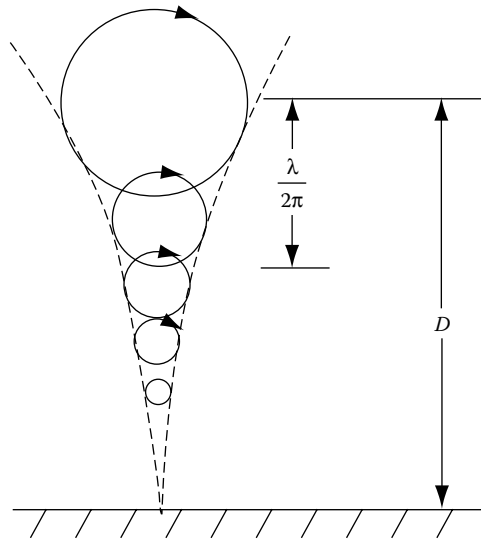
The cost of energy from a tidal system will depend on several factors such as location, capital cost, interest rate, turbine performance, length of time for amortization, and difference in water height between high and low tides. The last factor is particularly important because, as shown by Equation 13.5, the power output from a tidal system is a function of the square of the tidal ebb. If amortized over a life of 50 years, the cost of power from the La Rance tidal system is one of the lowest of any renewable energy schemes (see Figure 13.15 [15]).

**FIGURE 13.14**

Schematic diagram of water levels and power outputs for an ebb generation scheme.

**FIGURE 13.15**

La Rance tidal power station. (From Khaligh, A., and Onar, O.C., 2010. *Energy Harvesting*, CRC Press, Boca Raton, FL, [Figure 3.6](#). [15])

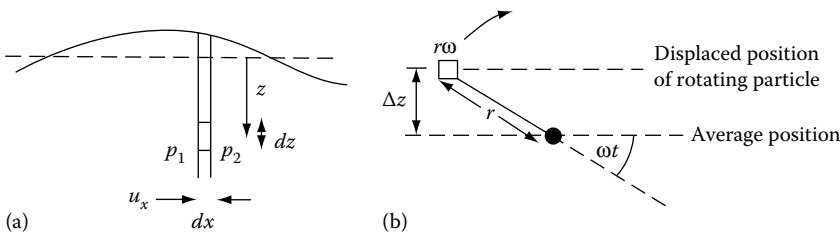
**FIGURE 13.17**

Motion of a particle in deep water waves. The motion is circular with an angular speed ω (rad/s) and a radius a (m).

Since most devices proposed for energy extraction are designed for deep water waves, it may be assumed that the two dominant forces are the result of gravity and circular motion, as shown in Figure 13.17. An average wave for power generation has a wavelength ~ 100 m, an amplitude ~ 3 m, and behaves as a deep water wave of depth greater than ~ 30 m with a circular motion of water particles as illustrated in Figure 13.17. The circles approximate the motion of a particle in a deep water wave. This circular motion has an angular velocity, ω (rad/s), and an amplitude, a (m), that decreases exponentially with depth, D , and becomes negligible when $D > (\lambda/2)$. It should be noted that there is no net motion of water in deep water waves, and an object suspended in water will move in circles, as shown in Figure 13.18.

To calculate the power that can be extracted from deep water waves, we shall simplify the rigorous mathematical treatment. It shows that for a surface wave of amplitude a and wave number k , the radius r of particle motion below the surface is

$$r = ae^{kz} \quad (13.6)$$

**FIGURE 13.18**

Local pressure fluctuation in a deep water wave: (a) pressure in the wave and (b) local displacement of water particle.

where

$$k = 2\pi/\lambda$$

z is the distance below the surface, as shown in [Figure 13.18](#)

The vertical displacement from the average position as a function of time t is

$$\Delta z = r \sin \omega t = ae^{kz} \sin \omega t \quad (13.7)$$

and the horizontal velocity component, u_x , is

$$u_x = r\omega \sin \omega t = \omega ae^{kz} \sin \omega t \quad (13.8)$$

Then, P^1 , the power in the wave at x per unit width of wave-front is given by

$$P^1 = \int_{z=-\infty}^{z=0} (p_1 - p_2) u_x dz \quad (13.9)$$

where $(p_1 - p_2)$ is the pressure difference experienced by the element of height dz in the horizontal direction. This pressure difference is equal to the change in potential energy of particles rotating in the circular paths, or

$$p_1 - p_2 = \rho g \Delta z = \rho g a e^{kz} \sin \omega t \quad (13.10)$$

Hence, substituting the above relation in Equation 13.9, yields

$$P^1 = \int_{z=-\infty}^{z=0} (\rho g a e^{kz} \sin \omega t)(\omega a e^{kz} \sin \omega t) dz = \rho g a^2 \omega \int_{z=-\infty}^{z=0} e^{2kz} \sin^2 \omega t dz \quad (13.11)$$

Since the time average over many periods of $\sin^2 \omega t$ can be shown to equal $\frac{1}{2}$

$$P^1 = \left(\frac{\rho g a^2 \omega}{2} \right) \int_{z=-\infty}^{z=0} e^{2kz} dz = \left(\frac{\rho g a^2 \omega}{2} \right) \left(\frac{1}{2k} \right) \quad (13.12)$$

Introduce the definition of the phase velocity of a wave, c , given by

$$c = \left(\frac{\omega}{k} \right) = \left(\frac{gT}{2\pi} \right) = \left(\frac{g\lambda}{2\pi} \right) \quad (13.13)$$

where T is the period of a sinusoidal wave given by

$$T = \frac{2\pi}{\omega} = 2\pi \left(\frac{\lambda}{2\pi g} \right)^{1/2} \quad (13.14)$$

With these equations, the power in watts is

$$P' = \left(\frac{\rho g a^2 \omega}{2} \right) \left(\frac{1}{2} \right) \left(\frac{gT}{2\pi} \right) = \frac{\rho g a^2 T}{8\pi}, \quad (13.15)$$

or, as a function of the wavelength, it has the form

$$P' = \left(\frac{\rho g a^2}{8\pi} \right) \left(\frac{2\pi\lambda}{g} \right)^{1/2} \quad (13.16)$$

We can see that waves of great height and long wavelength are important parameters for effective wave power production.

13.3.2 Wave Power Devices

Wave power generation has not yet reached the same state of development as wind power, but there have been many proposals for capturing energy from waves, and quite a few prototypes have been built, tested, and put into operation. So far, however, there have been no large-scale wave energy systems built and operated over any length of time. Consequently, it is not possible to decide which of the various devices have the greatest promise for eventual deployment. This section will therefore restrict itself to describing a few typical devices that have been built and operated.

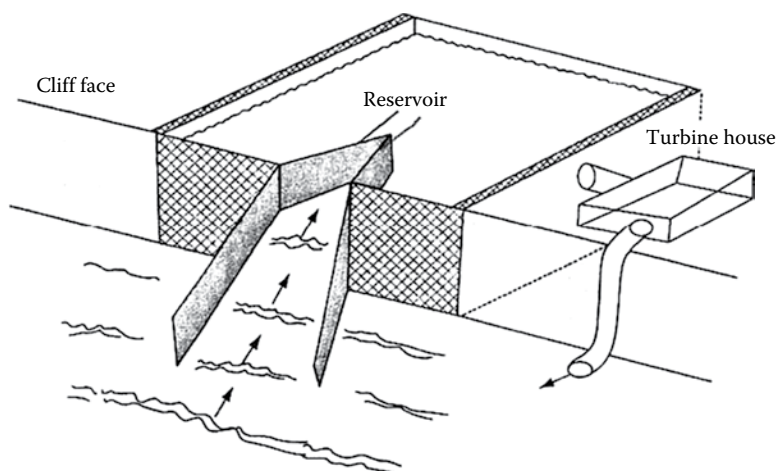
Wave Capture Systems are relatively simple. When waves break over a sea wall or dam near the seashore, water is impounded at a height above the average sea level and can be captured in a reservoir. The water from the reservoir can then be returned to the ocean through a conventional low head turbine attached to a generator, similar to a tidal system described in Section 13.2. The flow pattern of a wave capture system, however, is less regular than that of a tidal system.

A 350 kW wave capture system was built and operated successfully in Norway in 1985. A schematic diagram of the system, which was called Tapchan, is shown in [Figure 13.19 \[18\]](#). In this system, waves were funneled through a tapered channel so that larger waves were able to flow over the walls immediately, while the smaller waves increased in height as they moved up in the channel.

A site for a successful wave capture system should have the following characteristics:

1. Deep water close to shore.
2. A tidal range of less than 1 m.
3. A convenient site for constructing the reservoir, preferably a natural gully in a rock formation near shore.
4. Continuous waves with large amounts of energy.

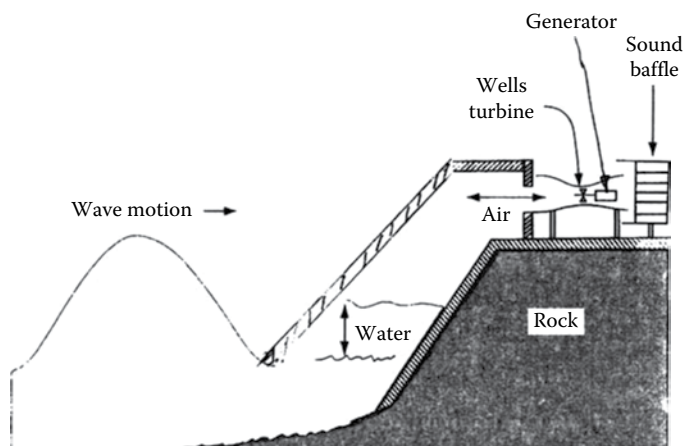
Although these types of wave capture systems are conceptually very simple, they suffer in general from a low head, which requires a large amount of water flow for a respectable energy output. On the other hand, the Tapchan concept has very few moving parts, its maintenance costs are low, and its reliability is high. Moreover, the storage reservoir helps to smooth the electrical output.

**FIGURE 13.19**

Schematic diagram of the Tapchan wave capture system in Norway. (From Hawaii Department of Business, 2002. Feasibility of developing wave power as a renewable energy resource for Hawaii, <https://energy.hawaii.gov/wp-content/uploads/2011/10/Feasibility-of-Developing-Wave-Power-as-a-Renewable-Energy-Resource-for-Hawaii.pdf>. [18])

Oscillating water column (OWC) systems are simple and robust and have been deployed in a number of countries. They probably represent the most common form of wave energy conversion. A successful OWC system, called the Limpet, was constructed in the year 2000 at the Scottish island Islay [19].

A schematic diagram of this onshore wave power system demonstrating its operation is shown in Figure 13.20. Air is compressed and decompressed by the oscillating water column, and this causes air to be forced through a Wells turbine located above. The Wells turbine is capable of rotating in the same direction, regardless of the direction of the air flow. Thus, it generates power irrespective of the direction of movement of the water column. The water column rises with each incoming wave and compresses the air above, which is thus

**FIGURE 13.20**

Schematic diagram of an onshore wave power system using an oscillating water column similar to Limpet.

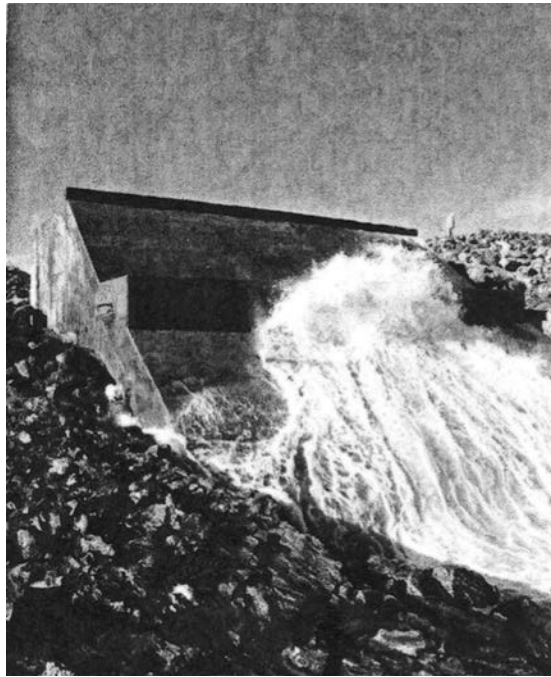


FIGURE 13.21
Photograph of Limpet.

forced to flow through the turbine. As the water column goes down, air is drawn in the opposite direction through the Wells turbine, which generates electricity via a generator. The waves are captured by a reinforced concrete wall set into an excavated rock face on the shore. The existing Limpet system, shown in [Figure 13.21](#), has a capacity of 500 kW, and has been successful in generating electricity for the grid on the island for several years. The electricity is exported to the utility grid within the Scottish Administration's Renewable Obligation Program.











13.4 Hydropower

There are three types of hydropower generation technologies: impoundment with a dam, diversion of run-of-the river, and pumped storage. The first two types are described in this section, whereas pumped storage is discussed in the chapter on storage since it is not a net generation technology. In 2015, hydropower plants generated almost 17% of the world's total electricity and 70% of all renewable electricity. In the United States, hydropower has grown from 56 GW of installed capacity in 1970 to 102 GW in 2011, which generates 6.1% of U.S. electric energy. The 10 largest hydroelectric producers in 2014 are listed in [Table 13.4](#) [20].

It is expected that hydropower generation will continue to increase, mostly in developing countries, where many potentially unused sites still exist. Hydropower is produced in 150 countries, with the Asia-Pacific Region generating 1/3 of the global hydropower. China is

TABLE 13.4

Ten of the Largest Hydroelectric Producers

Country	Annual Hydroelectric Production (TWh)	Installed Capacity (GW)	Capacity Factor	% of Total Production
 China	1064	311	0.37	18.7%
 Canada	383	76	0.59	58.3%
 Brazil	373	89	0.56	63.2%
 United States	282	102	0.42	6.5%
 Russia	177	51	0.42	16.7%
 India	132	40	0.43	10.2%
 Norway	129	31	0.49	96.0%
 Japan	87	50	0.37	8.4%
 Venezuela	87	15	0.67	68.3%
 France	69	25	0.46	12.2%

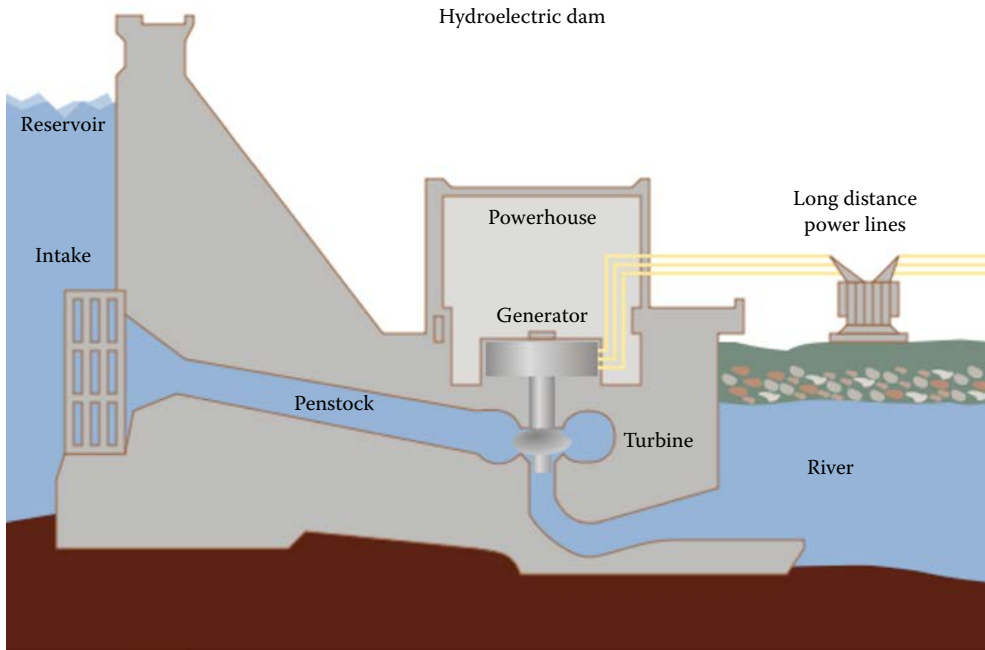
Source: International Energy Agency (IEA), 2015. Key world energy statistics, http://dx.doi.org/10.1787/key_eng_stat-2015-en. [20]

the largest hydroelectricity producer, with 920 TWh of production, representing almost 17% of its electricity use.

Conventional hydroelectric power plants use the potential energy of dammed water to drive a water turbine and generator, as shown in [Figure 13.22](#). The power extracted from the water depends on the difference in height between the top of the source and the water outflow, and the rate of volume of water passing through the penstock.

**FIGURE 13.22**

The Three Gorges Dam on the Yangtze River, China. It is the world's largest power producing facility of any kind. (From Shutterstock. With permission.)

**FIGURE 13.23**

Schematic diagram of a hydroelectricity power plant. (Tennessee Valley Authority)

Figure 13.23 shows the connection between the reservoir, penstock, water turbine, and the generator in more detail. Water released from the reservoir through the penstock drives the turbine, which is connected by a shaft to the generator that delivers power to the grid.

The electric power production from a hydroelectric station is approximately equal to:

$$P = \rho h V g \eta \quad (13.17)$$

where P is the power output in watts, ρ the density of water, h the difference in height between the top of the reservoir and the turbine, usually called the head, in meters. V is the flow rate of water in cubic meters per second, g is acceleration due to gravity (9.8 m/s^2), and η is the efficiency of the generation process.

Hydropower is a flexible source of electricity because the output can be ramped up and down quickly to adapt to changing energy demands. Hydro turbines have a startup time of a few minutes and power generation can decrease quickly when there is a surplus generation. Hydropower is, therefore, not generally used to produce base load power, but rather to serve as a backup for nonhydro generators. The major advantage of hydropower is its ability to meet peak power demand when the cost of energy is high. The average cost of electricity from hydro stations larger than 10 megawatts is \$0.03 to \$0.05 per kilowatt hour in the United States.

The U.S. Department of Energy defines large hydropower facilities as those having a capacity greater than 30 megawatts, small hydropower as projects that generate less than 30 megawatts, and micro hydropower as plants having capacities of less than 100 kilowatts. Micro hydro facilities can provide inexpensive power to isolated communities or buildings. Micro hydro systems can also complement photovoltaic energy systems because in many areas, water flow is highest in the winter when solar energy is at a minimum.

Since hydroelectric dams do not burn fossil fuels, they do not produce carbon emissions during operation. Some CO₂ is generated and other pollutants are emitted during construction. Disadvantages of hydropower are associated with the submersion of extensive areas upstream of the dams, sometimes destroying productive land and biologically rich areas. Damming interrupts the flow of rivers, can harm local ecosystems, and often involves displacing people and wildlife. The decomposition of flooded vegetation releases methane, a strong greenhouse gas. In developing Southeast Asian countries, plans for new hydroelectric dams are pitting the region's need for electricity against its need for food, such as rice and fish, which depends on the river's free-flowing waters.

There are also problems associated with variability in water flow, especially resulting from global warming. There are also certain risks associated with the construction of dams that are not properly engineered and can fail. There have been failures in dams that have resulted in floods and deaths, as for example, the Vajont Dam in Italy, in 1963.

EXAMPLE 13.3: POWER PRODUCED BY A HYDROELECTRIC FACILITY

Determine the energy delivered per month of a hydroelectric system that has a flow rate of 20 kg of water per second, and an available vertical drop of 5 meters. Assume that the energy conversion efficiency of the turbine is 80% solution.

Solution

The energy change of the water per second is:

$$20 \text{ kg/second} * 9.8 \text{ meters/second}^2 * 5 \text{ meters} = 980 \text{ Joules}$$

$$\text{The electric power available is equal to } 980 \text{ J/second} * 0.8 = 780 \text{ Watts.}$$

If this power is available 24 hours/day and 30 days/month, the electrical energy delivered is:

$$\text{Energy} = 780 \text{ W} * 24 \text{ hours/day} * 30 \text{ days/month} = 560 \text{ KW hours/month.}$$

13.5 Geothermal Energy

Geothermal energy can be defined as heat that originates within the Earth. This heat occurs from a combination of two sources: the original heat produced from the formation of the Earth by gravitational collapse and the heat produced by the radioactive decay of various isotopes. Because the thermal conductivity of rock is so low, it is taking many billions of years for the Earth to cool. Geothermal energy can be used for generating electricity if it is at a temperature greater than about 110°C. At lower temperatures, it can be used for district heating or a wide range of low-temperature direct-use applications [21].

13.5.1 Geothermal Power

Geothermal resources can be divided into four types: hydrothermal resources consisting of some combination of hot water and steam in permeable rock; EGS (Enhanced Geothermal Systems), which involve the creation of an artificial hydrothermal reservoir in deep, hot dry rock; geopressured brines; and magma. Geopressured resources are deep, pressurized brines such as exist along the U.S. Gulf Coast and produce natural gas, which has a higher

economic value than geothermal energy. Only one experiment has been performed to tap the geothermal energy in geopressured brine. Magma is the very hot molten rock that exists in volcanic regions; utilizing it presents materials challenges due to the very high temperatures.

Except for geothermal (or ground-source) heat pumps, which utilize the heat naturally contained in shallow soil (which is a function of the local climate), all existing commercial uses of geothermal energy make use of hydrothermal resources that are located relatively close to the surface and do not entail very high drilling costs. The hot geothermal fluid is used for direct heating applications such as spas, greenhouses, district heating, and for the generation of electricity.

The Geothermal Energy Association has summarized the results of a USGS probabilistic study on the U.S. potential for geothermal electric power, and this is shown in Table 13.5 [22]. GEA also refers to an MIT estimate that achieving 100,000 MW of electric power from EGS is achievable in a 15- to 50-year time frame.

Clearly to achieve very large potential, EGS systems must eventually be developed. This involves deep drilling to reach hot rock that is typically dry and low in permeability. Because of the low thermal conductivity of rock, to extract its heat it is necessary to create permeability and inject water, that is, create an artificial hydrothermal reservoir. This is done with hydraulic fracturing. One concept involves a central injection well surrounded by three production wells. The challenge is to fracture the rock in a way that the injected water communicates with enough rock in the field (as opposed to a short-circuit fracture between the injection well and a production well) but is not lost to the surrounding terrain. (Lost circulation is water that is injected but does not reach production wells, wasting both water and pumping power.) Because of the deep wells that are typically needed to achieve a sufficient temperature for electricity production and the challenges associated with creating an artificial reservoir, EGS technology is in the research phase. Despite the technical and economic challenges, it represents a very large potential for producing base load electric power.

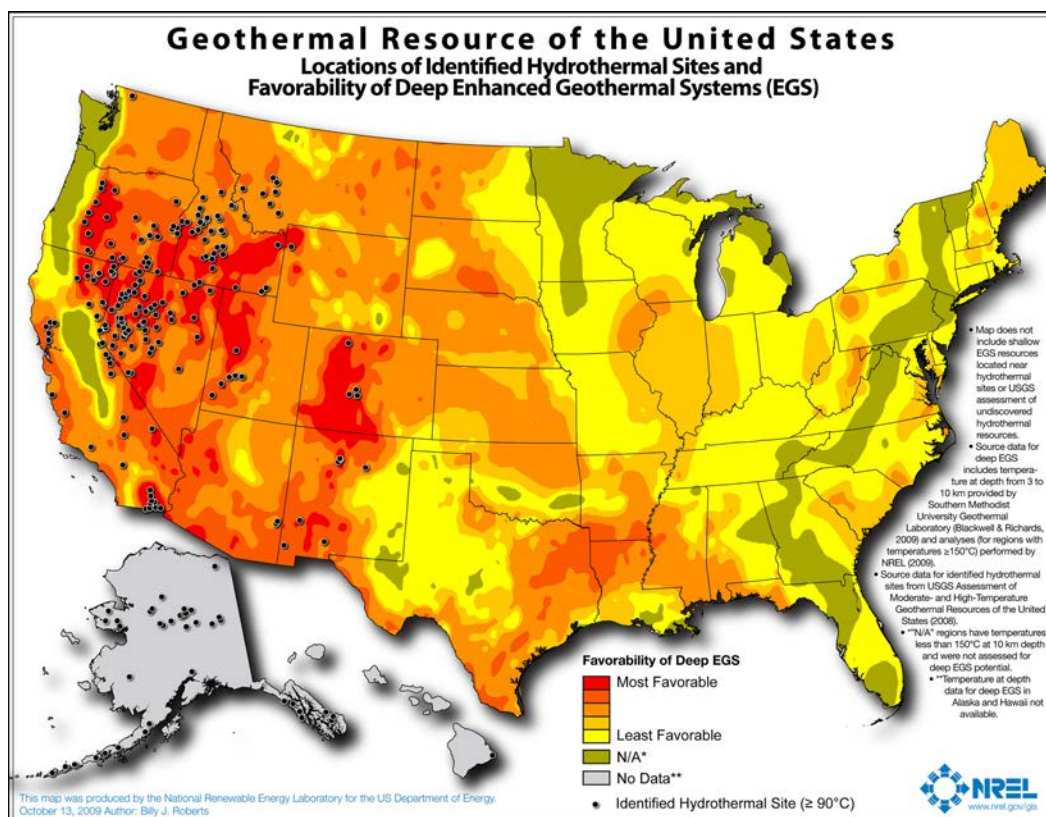
A map of U.S. geothermal resources showing actual production sites and favorable regions for EGS is shown in Figure 13.24 [23]. Details on the various geothermal resources in the United States can be found at the NREL Geothermal Prospector [24]. The dots represent identified hydrothermal sites, and the darkest regions represent the most favorable deep EGS resources [23].

TABLE 13.5

Geothermal Power Potential in Western U.S.

Category	Potential MWe (% Probability)	Description
Identified Geothermal Systems	3,675 (95%) to 16,457 (5%)	The resource is either liquid or vapor dominated and has moderate to high temperature. The resource is either producing, confirmed, or potential.
Undiscovered Geothermal Resources	7,917 (95%) to 73,286 (5%)	Based on mapping potential via regression analysis.
Enhanced Geothermal Systems	345,100 (95%) to 727,900 (5%)	Resource probability in regions characterized by high temperatures but low permeability and lack of water in rock formations.

Source: Geothermal Energy Association. Potential use, <http://geo-energy.org/PotentialUse.aspx>. [22]

**FIGURE 13.24**

Geothermal resources map of the United States.

Although geothermal energy has been used for direct heating purposes since ancient times, its use for the generation of electricity began only in the twentieth century. The first experiments to make use of geothermal energy to generate electricity occurred in Larderello, Tuscany, Italy, in 1904. A 250-kW_e geothermal power plant began operation there in 1913.

Currently, geothermal energy is used to generate a total of about 13,300 MW of electricity in 24 countries [25]. The United States is the largest user with about 2,700 MW of current operating capacity. A list of the world's geothermal power plants can be found online at the Global Energy Observatory [26].

Most of the geothermal power in the United States is generated in California and Nevada with California accounting for the majority of installed capacity. A considerable amount of this power is generated at The Geysers in Northern California, which has hosted a number of commercial geothermal power plants since the first one was built there in 1960. The Geysers, like Larderello, is a rare resource because its wells produce virtually pure dry superheated steam. Although its peak capacity reached about 2,000 MW in the late 1980s, its production was down to 634 MW net in 2016 (at 90% availability) due to the decline in steam pressure with time and plant retirements [27].

Although steam plants tend to release some gases from the geothermal fluid, amounts are usually small, and there are suitable means for mitigating most of these releases. Thus,

geothermal energy tends to be quite clean. In fact, Lake County, which is the location of The Geysers geothermal power plants, has been reported to be the only county in California to be in compliance with all of California's air quality regulations.

While geothermal energy is very clean, it is not immediately renewable like solar and wind energy. Like the energy of the sun, the energy within the Earth is immense and has a lifetime measured in billions of years. However, unlike the use of sunlight, tapping into local sources of the Earth's heat can result in a temporary decrease in the local amount of energy available. Reinjecting geothermal fluid that remains after steam is extracted helps preserve the fluid volume of the reservoir. However, even with reinjection, the heat content of the reservoir gradually declines.

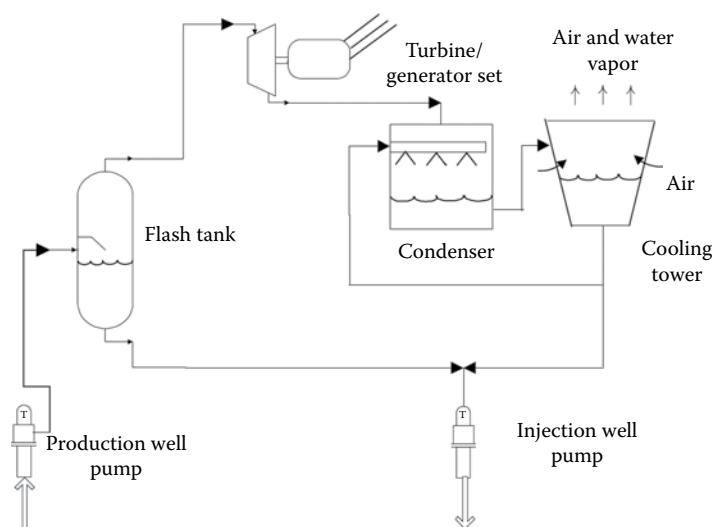
The recovery period for a geothermal resource depends on how it is used. One study [28] indicated that the recovery period is approximately 30 years for geothermal heat pumps, about 100–200 years for district heating, and several hundred years for electricity generation. Resources tapped for electricity generation could provide energy for 50 years or more, if properly managed, but plant equipment typically reaches the end of its useful life before the resource is depleted. Continuous long-term use of geothermal energy for electricity generation would require the periodic construction of new plants at new sites, while previously used reservoirs recover. Augmenting a geothermal power plant with concentrating solar power can increase the power production capability of a declining geothermal resource.

While geothermal is not as renewable as solar and wind, it has a number of important advantages. Geothermal electric power plants operate 24 hours per day and can, therefore, produce base-load electricity. Geothermal plants are not vulnerable to weather effects, except that cycle efficiencies (and hence plant output) tend to be higher in the winter (when heat is rejected to a lower sink temperature) than in the summer. (This is especially true for binary plants that are air-cooled.) Geothermal plants are also extremely reliable and typically operate more than 95% of the time, with some plants at over 99%. This compares to availabilities of 60% to 70% for coal and nuclear plants.

Geothermal plants are sometimes located in areas of high scenic value, where the appearance of the plant is important. Fortunately, geothermal power plants take up little land space, and, with careful design, they can easily blend into the surrounding environment. Wet cooling towers at plants can produce plumes of water vapor, which some people find unsightly. In such cases, air-cooled condensers can be used. A good example of an aesthetic geothermal power plant is the 35-MW binary-cycle plant located near the scenic Mammoth Lakes ski area in northern California. The plant uses air cooling, has a low profile, is painted in colors that match the natural landscape, and is surrounded by trees. As a result, passing motorists on the nearby highway don't even notice it.

13.5.1.1 Current Commercial Geothermal Power Technologies

The current power plants for generating electricity from hydrothermal resources can be divided into two general types: steam and binary. Steam plants are generally considered the most cost-effective technology when the resource temperature is above about 175°C. In these plants, steam is expanded through a turbine as in conventional power plants to generate electricity. For geothermal resources rich in steam (such as at The Geysers), the steam can be used directly. Because such sites are rare, it is much more common for hot water from a geothermal resource to be flashed to steam by spraying it into a tank where

**FIGURE 13.25**

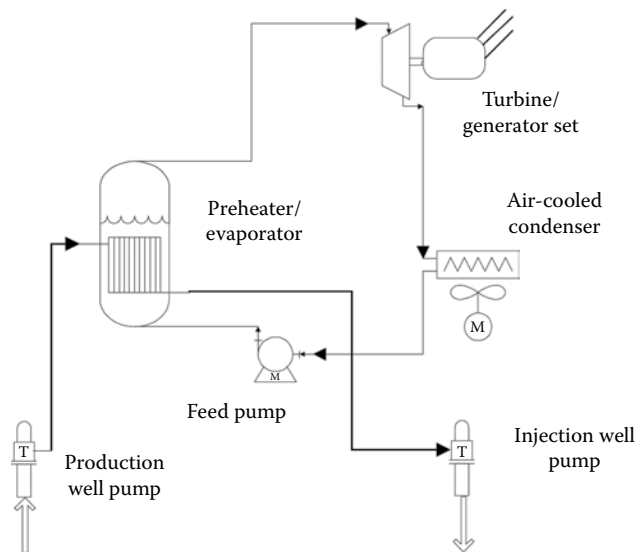
Geothermal single-stage flash plant. (From Kutscher, C.F., 2000. The status and future of geothermal electric power. Presented at the American Solar Energy Society (ASES) Conference, Madison, Wisconsin, June 16-21, NREL/CP-550-28204. [21])

its pressure is decreased. This can occur in either a single- or dual-stage process, with the latter costing more to construct but achieving higher output. A schematic of a single-stage flash plant is shown in [Figure 13.25](#) [21].

For lower-quality resource temperatures below about 175°C, flash plants lose their efficiency. It is more efficient to transfer heat from the geothermal fluid to a volatile working fluid (typically a hydrocarbon such as isobutane or normal pentane) that vaporizes and is passed through a turbine. Such plants are called “binary” because a secondary fluid is used in the actual power cycle. These plants tend to have higher equipment costs than flash plants. Because they transfer heat from the geothermal fluid and return all that fluid to the ground, they do not have condensed steam available as cooling water. Thus, they must use a separate water source or air-cooled condensers. Because all of the geothermal fluid is returned to the reservoir, binary-cycle plants do not require mitigation of gaseous releases, and reservoir fluid volume is maintained. Because larger binary plants are typically comprised of small modules, maintenance can be done on one module at a time, thus minimizing the impact on plant output. A schematic of a typical binary plant is shown in [Figure 13.26](#) [21].

The U.S. Energy Information Administration gives the average capital cost of U.S. geothermal plants as \$4640/KW for binary cycle technology and \$6641 for dual-flash technology [29]. Lazard [30] does not distinguish geothermal plant types in their cost analysis. They give a range for the capital cost of new U.S. geothermal power plants as \$4250-\$6400/kW. They also give a range for the unsubsidized levelized cost of electricity for new U.S. plants as: \$79/MWh (\$49/MWh capital cost + \$30/MWh O&M cost) to \$117/MWh (\$77/MWh capital cost + \$40/MWh O&M cost).

These costs are for plants of 5 MW size or larger, which represent the vast majority of existing plants. For small plants under 5 MW in size, the cost per kW goes up significantly because of a loss in equipment economies of scale, and because the fixed costs associated with exploring a site and drilling wells are divided by a smaller number of kilowatts.

**FIGURE 13.26**

Binary-cycle geothermal power plant. (From Kutscher, C.F., 2000. The status and future of geothermal electric power. Presented at the American Solar Energy Society (ASES) Conference, Madison, Wisconsin, June 16-21, NREL/CP-550-28204. [21])

(Although a small plant requires a smaller diameter well, as well diameter decreases, the well power output drops much more rapidly than the drilling cost.) In addition, there are some minimum fixed O&M costs associated with operating a plant that also become significant when divided by a smaller plant capacity.

Despite their higher energy costs, small-scale plants can offer some potential advantages. Skid-mounted units can be built in the factory and shipped anywhere in the world. Because they are modular, a plant owner can start with a small investment and add additional modules later. Small plants can be designed to operate automatically. Their economics can become attractive in regions where low-cost shallow wells are available and where the exit brine from the plant can be used for direct heating applications. Small plants may be suited for microgrid applications in developing nations where the competition is imported diesel fuel [31].

13.5.1.2 Technology Status

Between 1980 and 1990, about 900 MWe of geothermal electric capacity were installed in the United States. Most of these plants were built in California and Nevada under power purchase agreements that guaranteed prices of more than 10 cents per kWh. Today, these price guarantees have expired, and plants must sell their power at competitive rates. With the loss of government market incentives, the advent of low-cost electricity from natural gas power plants, and the decline in electricity load growth, geothermal power plant construction in the United States declined greatly in the 1990s. Geothermal electricity costs, in the range of 6 to 11 cents per kWh after subsidies, have a difficult time competing against the lower-cost electricity from natural gas power plants, although they achieve higher capacity credits than wind and PV. Some new U.S. geothermal power plants were built between 2000 and 2014, as a result of both tax incentives and state

renewable portfolio standards, with name plate capacity 2800 to 3500 MW. Actual power output did not grow commensurately, however, due to resource decline, especially at the largest set of plants, The Geysers.

To address the reservoir depletion problem, projects were developed to inject reclaimed wastewater into the steam reservoir. Pipelines were built from Lake County and the City of Santa Rosa that combined carry a total of about 17 million gallons per day to The Geysers. These projects have not only helped to prolong the lifetime of the geothermal resource, but they also provide a solution to wastewater disposal problems.

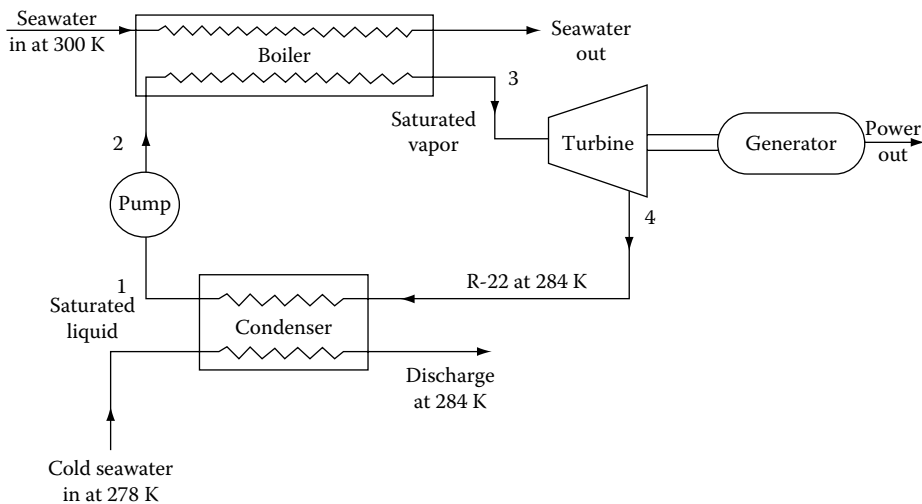
As a result of the difficult economic conditions for geothermal energy in the United States, the industry has focused on opportunities in other countries. According to the Geothermal Energy Association (GEA), 18 new geothermal power plants came online around the world in 2015, adding 313 MW of new electric capacity. GEA indicates that over 4,000 MW are under development in Indonesia.

13.5.2 Direct Use of Geothermal Energy

Most direct uses of geothermal energy tap resources at temperatures below about 150°C. Common uses are for spas, space heating, greenhouse heating, aquaculture, and industrial heating. According to Lund and Boyd [32] there were 70,329 MW_{th} of geothermal direct use worldwide in 2015, of which 49,898 was for geothermal heat pumps. (Geothermal heat pumps are probably more properly called ground-source heat pumps, as they can take advantage of the steady ground temperature at shallow depths in virtually any location, as opposed to those special locations where deep geothermal heat is manifested near the surface.) Lund and Boyd break down the direct uses by application and country. Snyder et al. [33] updated the database of operating direct use applications in the United States and found only about 500 MW_{th}, predominantly for aquaculture, heating, and resorts/pools. They provide a breakdown of both thermal supply and number of installations as a function of application.

PROBLEMS

- 13.1 A 100 MW ocean thermal gradient power plant is to be designed for a location where the ocean surface temperature is 300 K (80°F) and water at a lower depth is available at 278 K (40°F). If the heat exchangers are sized to operate a power plant using R-22 as the working fluid between 294 and 284 K (70°F and 50°F), calculate the flow rates of R-22 and water required, assuming that the condenser heat exchangers have an overall conductance of 1000 W/m² · K (176 Btu/h · ft² °F) and an effectiveness of 100%. Also, calculate the plant efficiency and the surface area of the condenser. The saturation pressure of R-22 at 294 K is 9.38×10^5 N · m⁻² (136.1 psia), the enthalpy is 256.8 kJ/kg (110.4 Btu/lb_m), and the entropy is 0.900 kJ/kg · K (0.215 Btu/lb_m°R). The enthalpy of the saturated liquid at 284 K is 56.45 kJ/kg (24.27 Btu/lb) and the heat of vaporization is 197.0 kJ/kg (85.68 Btu/lb_m). The saturation pressure at 284 K is 6.81×10^5 N · m⁻² (98.73 psia), while the entropy at 284 K of the saturated liquid is 0.217 kJ/kg K (0.0519 Btu/lb_m°R). Assume efficiencies for the pump and turbine are 80% and 90%, respectively. The specific volume of the saturated R-22 liquid at 284 K is 0.000799 m³/kg (0.0128 ft³/lb). A schematic diagram of the system is shown as follows:



- 13.2 If the sea power plant described in the previous problem is to deliver power at \$8/10⁶ Btu, estimate the maximum permissible cost of the condenser and evaporator heat-exchanger surface in dollars per square foot, assuming a 20-year life, 10% discount rate, and 7% yearly fuel inflation.
- 13.3 Explain in your own words the manner in which the Pelamis wave power device operates. Note that the motion at the hinges produces hydraulic power that is fed into electric generators. A motion picture of the operation of the Pelamis can be viewed online [34].
- 13.4 Estimate the period and phase velocity of a deep water wave of 100 m wavelength.
- 13.5 Using the phase velocity calculated in the previous problem, estimate the power in a deep water wave of 1.5 m amplitude and 100 m wavelength.
- 13.6 Estimate the mean tidal power produced by a plant with area of 10 km², a maximum range of 5 m, and a minimum range of 2.5 m (an average range of 3.7 m).
- 13.7 The air-cooled 30-MW Mammoth Lakes Geothermal Power Plant in California has a resource temperature of 339°F. Assume that the plant design ambient temperature is 60°F and that the plant operates at 50% of the Carnot efficiency.
 - a. On a hot summer afternoon when the ambient temperature is 95°F, what is the percent decrease in power output compared to the design condition?
 - b. Assume the wet-bulb temperature of the air is 55°F and that you can use spray nozzles to evaporatively cool the 95°F outdoor air 80% of the way to the wet-bulb temperature. What is the percent increase in plant power output compared to using the 95°F air directly?

The next two problems are open-ended with no solutions:

- 13.8 It has recently been proposed that ocean thermal energy conversion could be used to produce ammonia, a chemical currently manufactured from natural gas at a total energy consumption of about 2.5% of the U.S. natural gas consumption. Since the manufacture of ammonia could be accomplished anywhere, the plant could be located in a favorable location, for example, off the coast of Brazil, where the difference in temperature between the upper layer of the ocean and

the layer at the 600 m depth is approximately 20 K. Using an OTEC power plant of 500 MWe capacity, estimate the number of tons of ammonia that could be produced per year. For a price of \$165/ton of ammonia, estimate the time required to regain the capital investment in the OTEC production plant and compare your estimate with the claim that the capital could be repaid in 2.5 years.

- 13.9 Aluminum sells today at approximately \$1850/ton. The production of aluminum is one of the most energy-intensive processes in the metallurgical industry, and it has recently been proposed that an OTEC plant could be used for the production of aluminum. Metallurgical estimates indicate that approximately 18 kWh of energy is required in the refining process for each kilogram of aluminum produced. Assuming a plant load factor of 85%, calculate the size of an OTEC plant required to produce 250,000 ton/year of aluminum, if there is a temperature gradient similar to that in the previous problem. Then calculate the time required to repay an investment cost in the plant and compare your results with the estimate of 3 years obtained in the literature.

References

1. D'Arsonval, A., 1891. Utilisation des forces naturelles, Avenir de l'électricité, *Revue Scientifique* 17, 370–372.
2. Claude, G., 1930. Power from tropical seas, *Mechanical Engineering* 52, 1039–1044.
3. Dugger, G., Neff, F., and Snyder, J.E., 1981. Ocean thermal energy conversion, in: Kreider, J.F. and Kreith, F. eds., *Solar Energy Handbook*, McGraw-Hill, New York, Chapter 19.
4. Kreith, F., and Bharathan, D., 1988. Heat transfer research for ocean thermal energy conversion, *Journal of Heat Transfer* 110, 5–22.
5. Bharathan, D., Kreith, F., and Owens, W.L., 1987. An overview of heat and mass transfer in open-cycle OTEC systems, in: Mari, Y. and Yang, W.J. eds., *Proceedings of the ASME/JSM Thermal Engineering Joint Conference*, Honolulu, HI, vol. 2, pp. 301–314.
6. Rabas, T.J. et al., March 1979. OTEC 100-MWe alternate power systems study. Report by Westinghouse Electric Corp to U.S. DOE under contract EG/77/C/05/1473.
7. Kreith, F., 1981. An overview of SERI solar thermal research facilities, *Heat Transfer Engineering* 2, 3–4.
8. Block, D.L., and Valenzuela, J.A., May 1985. Thermoeconomic optimization of OC-OTEC electricity and water production plants, SERI/STR-251-2603, U.S. Department of Energy, Washington, DC.
9. Kreith, F., and Manglik, R.M., 2018. *Principles of Heat Transfer*, 8th ed., Cengage Learning, Boston, MA.
10. Twidell, J., and Weir, T., 2006. *Renewable Energy Resources*, 2nd ed., Taylor & Francis, Oxon, U.K., Chapter 13.
11. Elliott, D., 2004. Tidal power, in: Boyle, G. (ed.), *Renewable Energy*, 2nd ed., Oxford University Press, Inc., New York, Chapter 6, pp. 196–243.
12. Baker, A.C., 1991. *Tidal Power*, Peter Peregrinus, London, U.K.
13. Renewable Energy UK. La Rance Tidal Power Plant, <http://www.reuk.co.uk/La-Rance-Tidal-Power-Plant.htm>.
14. Jackson, T., 1992. Renewable energy: Summary paper for the renewable energy series, *Energy Policy* 20(9), 861–83.
15. Khaligh, A., and Onar, O.C., 2010. *Energy Harvesting*, CRC Press, Boca Raton, FL, Figure 3.6.

16. Twidell, J., and Weir, T., 2006. *Renewable Energy Resources*, 2nd ed., Taylor & Francis, Oxon, U.K., Chapter 12.
17. Coulson, C.A., and Jeffrey, A., 1977. *Waves*, Longman, London, U.K.
18. Hawaii Department of Business, 2002. Feasibility of developing wave power as a renewable energy resource for Hawaii, <https://energy.hawaii.gov/wp-content/uploads/2011/10/Feasibility-of-Developing-Wave-Power-as-a-Renewable-Energy-Resource-for-Hawaii.pdf>.
19. Queen's University of Belfast, 2002. *Islay Limpet Wave Power Plant*, https://cordis.europa.eu/docs/publications/6662/66628981-6_en.pdf.
20. International Energy Agency (IEA), 2015. Key world energy statistics, http://dx.doi.org/10.1787/key_energ_stat-2015-en.
21. Kutscher, C.F., 2000. The status and future of geothermal electric power, *Presented at the American Solar Energy Society (ASES) Conference*, Madison, Wisconsin, June 16-21, NREL/CP-550-28204.
22. Geothermal Energy Association. Potential use, <http://geo-energy.org/PotentialUse.aspx>.
23. NREL. Dynamic maps, GIS data, and analysis tools, <http://www.nrel.gov/gis/geothermal.html>.
24. NREL. *Geothermal Prospector*, <https://maps.nrel.gov/geothermal-prospector>.
25. Geothermal Energy Association, 2016. Annual U.S. & global geothermal power production report, <http://geo-energy.org/reports.aspx>.
26. Global Energy Observatory. Current list of geothermal power plants, <http://globalenergyobservatory.org/list.php?db=PowerPlants&type=Geothermal>.
27. Calpine Corporation. Geysers by the numbers, <http://geysers.com/The-Geysers/Geysers-By-The-Numbers>.
28. Rybach, L., Megel, T., and Eugster, W.J., October 1999. How renewable are geothermal resources? *Geothermal Resources Council Transactions* 23, 17–20.
29. EIA, November 2016. *Capital Cost Estimates for Utility Scale Electricity Generating Plants*, https://www.eia.gov/analysis/studies/powerplants/capitalcost/pdf/capcost_assumption.pdf.
30. Lazard, December 2016. Levelized cost of energy analysis, <https://www.lazard.com/perspective/levelized-cost-of-energy-analysis-100>.
31. Vimmerstedt, L., November 1998. Opportunities for small geothermal projects: Rural power for Latin America, the Caribbean, and the Philippines, NREL/TP-210-25107, National Renewable Energy Laboratory.
32. Lund, J., and Boyd, T., 2015. Direct utilization of geothermal energy 2015 worldwide review, in: *Proceedings of the World Geothermal Congress*, Melbourne, Australia, 19–25 April.
33. Snyder, D., Beckers, K., and Young, K., 2017. Update on geothermal direct-use installations in the United States, in: *Proceedings of the 42nd Workshop on Geothermal Reservoir Engineering*, Stanford University, Stanford, California, February 13–15, SGP-TR-212.
34. Ahlqvist, J., June 26, 2009. Pelamis at Aguçadoura, YouTube Video, <http://www.youtube.com/watch?v=JYzocwUfpNg>.

14

Storage Technologies

There must surely come a time when heat and power will be stored in unlimited quantities... all gathered by natural forces.

Thomas A. Edison, 1910

14.1 Overview of Storage Technology

Energy storage will play a critical role in any future renewable energy system. There are two principal reasons why energy storage will be of increasing importance to renewable energy:

- Many of the most significant renewable energy sources like solar and wind are variable in nature
- The transportation system, including cars, buses, ships, and planes, requires energy to be carried by the vehicles. Whether as liquid fuels, hydrogen for fuel cells, or batteries for electric vehicles, some type of energy storage will be needed.

Energy can be stored in many forms: as mechanical energy in rotating, compressed, or elevated substances; as thermal or electrical energy that can be released as needed; or as electrical charges ready to travel from positive to negative poles as demanded. Storage technologies that can absorb and release electricity have great value because electricity can be converted easily into mechanical or thermal energy. Electricity is also the output of the most promising renewable energy technologies: wind turbines, solar thermal power plants, and photovoltaic cells. There are, however, some applications that can benefit from thermal or mechanical storage technology. For example, thermal energy storage (TES) is needed for the continuous operation of solar thermal power plants and overnight heat storage is used for heating or cooling of buildings.

The storage methods treated in this chapter can accept and deliver energy in three ways: electrical, mechanical, and thermal. When energy is stored electrically or mechanically, it can be converted to either of the other two forms quite efficiently. For example, electricity can drive a motor with only about 5% energy loss or can provide heat with a resistive heater with virtually no loss at all. The quality of TES depends mostly on its temperature. The efficiency of conversion of thermal energy into power is limited by thermodynamic considerations. The theoretical maximum quantity of useful work, W_{\max} (mechanical energy) that can be extracted from a given quantity of heat, Q , is

$$W_{\max} = \frac{T_1 - T_2}{T_1} Q \quad (14.1)$$

where

T_1 is the absolute temperature of the stored heat

T_2 is the ambient absolute temperature

Any energy-storage technology must be carefully chosen to accept and produce a form of energy consistent with both the energy source and the final application. Storage technologies that accept and/or produce thermal energy should only be used with heat energy sources or heat applications. Mechanical and electrical technologies are more versatile, but electrical storage technologies are more convenient than mechanical ones because electricity can be easily transmitted [1].

14.1.1 Applications

Table 14.1 presents an overview of the most important energy storage technologies. In this table, each technology is classified by its relevance to one of the following four categories.

Utility shaping: For this application, large capacity storage devices are required to respond to varying electricity demands. Examples would be a solar thermal power plant, which delivers energy generated during the day to a thermal storage device for use at nighttime, or a wind turbine that compresses air during high winds to power a gas turbine when the wind stops.

Power quality: Storage technologies to smooth power delivery during short periods such as outages or switching events must be capable of providing large changes in power output over very short periods. Ultra-capacitors and batteries are in this category.

Distributed grid technology: Storage devices for distributed grid technologies must be able to generate energy and storage at customer locations rather than at a central utility power station. Technologies in this category include batteries for photovoltaic power installed on the roof of a building. Other systems include solar thermal or geothermal power that can be implemented on a distributed scale. The required power generation is small compared to utility shaping. They require capacities in the 1–50 kWh range, while utility shaping requires capacities in the 1000 MWh range.

Transportation technologies: The devices that can be used for storage in automobiles and trucks include all types of batteries. Examples are hybrid electric vehicles such as the basic Prius, and plug-in electric vehicles such as the Volt and the later types of Prius. Large fleets of plug-in-hybrid-electric vehicles (PHEVs) and electric vehicles (EVs) could also help in utility shaping by utilizing off-peak power to charge the batteries and feeding the grid system from the batteries during peak demand.

The physical modes of energy storage may involve one or more mechanical, thermal, or electromagnetic forms. An energy storage technology may require both a storage reservoir and a converter and transmission system for moving the power to and from the reservoir to its destination and use. A pumped hydro system, for example, contains both elements using potential energy to store and a turbine to deliver the energy. A molten salt thermal system for a power tower, on the other hand, requires only one reservoir for storing and delivering energy.

14.1.2 Technology Characterization

Every energy storage technology can be characterized essentially by three important parameters: self-discharge time, storage size, and efficiency. Within a category, the final

TABLE 14.1

Overview of Energy Storage Methods and Their Applications

	Utility Shaping	Power Quality	Distributed Grid	Transportation
<i>Direct electric</i>				
Ultracapacitors		✓		✓
SMES		✓		
<i>Electrochemical</i>				
Batteries				
Lead acid	✓	✓	✓	
Lithium-ion	✓	✓	✓	✓
Nickel-cadmium	✓	✓		
Nickel-metal hydride				✓
Zebra				✓
Sodium-sulfur	✓	✓		✓
Flow batteries				
Vanadium redox	✓			
Polysulfide bromide	✓			
Zinc bromide	✓			
Electrolytic hydrogen				✓
<i>Mechanical</i>				
Pumped hydro	✓			
Compressed air	✓			
Flywheels		✓		✓
<i>Direct thermal</i>				
Sensible heat				
Liquids			✓	
Solids			✓	
Latent heat				
Phase change	✓		✓	
Hydration–dehydration	✓			
Chemical reaction	✓		✓	
<i>Thermochemical</i>				
Biomass solids	✓		✓	
Ethanol	✓			✓
Biodiesel				✓
Syngas	✓			✓

selection of a specific storage technology can be made by the consideration of cycle life, specific energy, specific power, energy density, and power density.

Self-discharge time (SDT) is the time required for a fully charged, self-standing storage device to reach a certain depth of discharge (DOD). DOD can be described as a percentage of the storage device's useful capacity. For example, 80% DOD means that 20% of the device's energy capacity is left. It should be noted that the relation between SDT and DOD is, in general, not linear and must therefore be measured. SDTs vary greatly from a few minutes to weeks, as, for example, in battery or thermal storage.

Storage size describes the intrinsic scale of the technology. It is the most difficult to define of the three parameters. Some technologies have a fairly large storage size but cannot provide small-scale energy storage. Storage size is often called energy storage capacity and is measured in kWh or Btu.

Efficiency is the ratio of the energy output from the device to the energy input. As for energy density and specific energy, the system boundaries must be carefully specified when determining efficiency. It is also important to note the form of energy required at the input and output interconnections and to include the entire system necessary to attach these interconnections. For example, if the system is used to store energy from a utility wind farm, then both the input and output will be AC electricity. However, when comparing a battery with a fuel cell, it is necessary to include the efficiency of an AC-to-DC rectifier for the battery, whereas an AC-powered hydrogen power generation system is required for the fuel cell. DC-to-AC converters are associated with both. Efficiency is also related to the SDT. For example, if the discharge of a thermal storage system occurs much later than charging, the apparent efficiency will be lower because a significant amount of the thermal energy may be lost if the interim between charge and discharge is large.

Cycle life is the number of consecutive charge/discharge cycles that a storage system can undergo while maintaining the system's specifications. Cycle life specifications are made against a selected DOD, depending on the application of the storage device. For example, a battery used in a hybrid electric vehicle may consume only 10%–20% of the energy stored during most of the discharge cycle. The advantage of a thermal storage system is that it can undergo many charge/discharge cycles without significant waste.

Specific energy is a measure of how heavy the system is. It is measured in units of energy per mass and here we will represent this quantity in terms of MJ/kg or kWh/kg. The higher the specific energy, the lighter the device. For transportation applications, a high specific energy is necessary, whereas for utility application, specific energy is relatively unimportant.

Energy density is how much space the system occupies. It is measured in units of energy per volume, MJ/L or kWh/m³.

Storage energy modes depend on the end-use application, but the magnitude of the power load and the time scale are important. [Figure 14.1](#) shows the energy storage technology characteristics of the various storage technologies to be discussed in this chapter according to size and discharge time. For example, to provide electric power for short power outages requiring a large power flux for a short period of time, such as seconds or minutes, capacitors and flywheels are well suited. On the other hand, when large amounts of electric or thermal energy are needed for periods of hours or longer, pumped hydropower, compressed air storage, or thermal storage are appropriate technologies. Distributed grid, automotive, and building applications require a moderate discharge time and a moderate unit size. [Figure 14.2](#) shows the fields of application in terms of discharge time and power rating.

14.2 Mechanical Technologies

Pumped hydroelectric and compressed air energy storage are the two mechanical storage technologies that are currently available for large-scale and long-term utility size storage, as shown in [Figure 14.2](#). Flywheels are only useful for very short time storage.

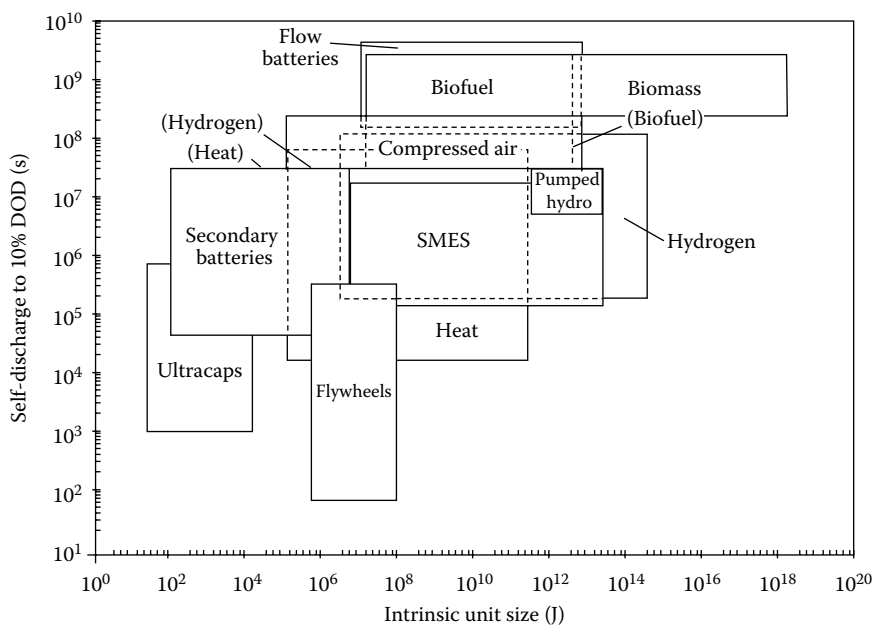


FIGURE 14.1 Self-discharge time to 10% DOD in seconds versus intrinsic unit size in Joules. Not all hidden lines are shown.

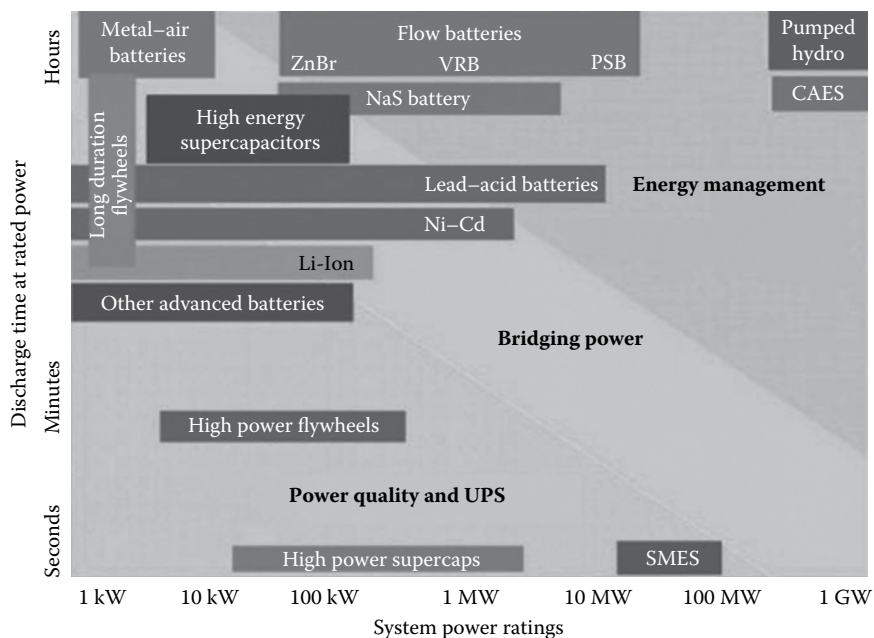


FIGURE 14.2 Discharge time versus power rating for various energy storage methods. (From Electricity Storage Association, 2003. Technology comparisons | Ratings, www.esa.org. With permission [27].)

14.2.1 Pumped Hydroelectric Energy Storage

Pumped hydroelectric energy storage (PHES) is a mature technology that has been deployed for over a century. Examples as early as the 1890s exist in Italy and Switzerland. PHES uses electricity to pump water uphill into a reservoir where it can be stored. The energy can be recaptured when the water is released and runs back downhill through a turbine. These storage systems allow management of water as well as energy resources. PHES systems are very efficient and, with modern turbine technologies, they can approach 80%–85% round-trip efficiencies.

Figure 14.3 is a schematic diagram of a PHES installation at Raccoon Mountain, which is operated by the Tennessee Valley Authority [2]. The Raccoon Mountain pumped storage plant is widely cited as an example of excellent engineering for PHES. The plant, which was completed in 1978, has a generating capacity of about 1600 MW and can run for 22 h to supply about 35,000 MWh of electricity.

The power and capacity of a PHES system is a function of the hydraulic head, the water flow rate, and the efficiency of the pump and the turbine. The head is given by the upper elevation to which the water is pumped and the lower elevation at which the turbine is located. The flow rate can be regulated by valve action. The maximum flow that can be obtained is limited by the reservoir size. The maximum flow rate is dictated by the reservoir size divided by the desired storage time to yield the available flow per unit time, minus a 15% reserve operating condition.

Given the hydraulic head, an upper bound on flow rate and an efficiency of the plant, the power-generating capacity of a pumped hydroelectric installation is given by the equation below:

$$P = QH\rho g\eta \quad (14.2)$$

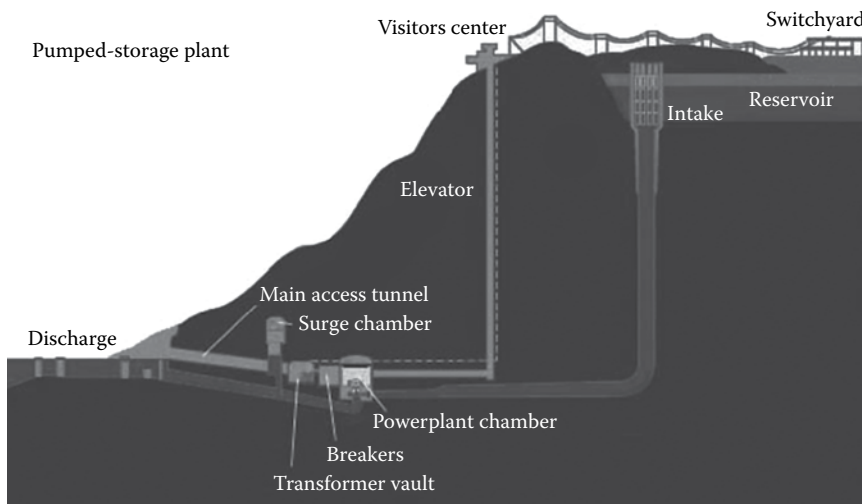


FIGURE 14.3

Schematic of the Raccoon Mountain pumped-storage plant. (From Tennessee Valley Authority. The mountaintop marvel, www.tva.gov/heritage/mountaintop/index.htm [2].)

where

P is the generated output power in Watts (W)

H is the height differential in meters (m)

Q is the fluid flow rate in cubic meters per second (m^3/s)

ρ is the fluid density in kilogram per cubic meter (kg/m^3), about $1000 \text{ kg}/\text{m}^3$ for water

g is the gravitational constant ($9.81 \text{ m}/\text{s}^2$ on Earth)

η is the overall efficiency

Given the power capacity of the plant, the limiting value of the upper or lower reservoir dictates the energy capacity. Potential energy generation in kWh is calculated by power output times the operating time. Figure 14.4 shows the power as a function of flow rate and head in engineering units [3].

EXAMPLE 14.1

Calculate the power generated by a PHES with a potential hydraulic height differential between reservoirs of 100 m and a volumetric flow rate of $1000 \text{ m}^3/\text{s}$ through a hydraulic turbine with an efficiency of 0.8.

Solution

We use Equation 14.2, $P = QH\rho g\eta$. By substituting the appropriate values to find that $P = 1000 \text{ m}^3/\text{s} \times 100 \text{ m} \times 1000 \text{ kg}/\text{m}^3 \times 9.81 \text{ m}/\text{s}^2 \times 0.8 = 784,800,000 \text{ W} = 785 \text{ MWe}$

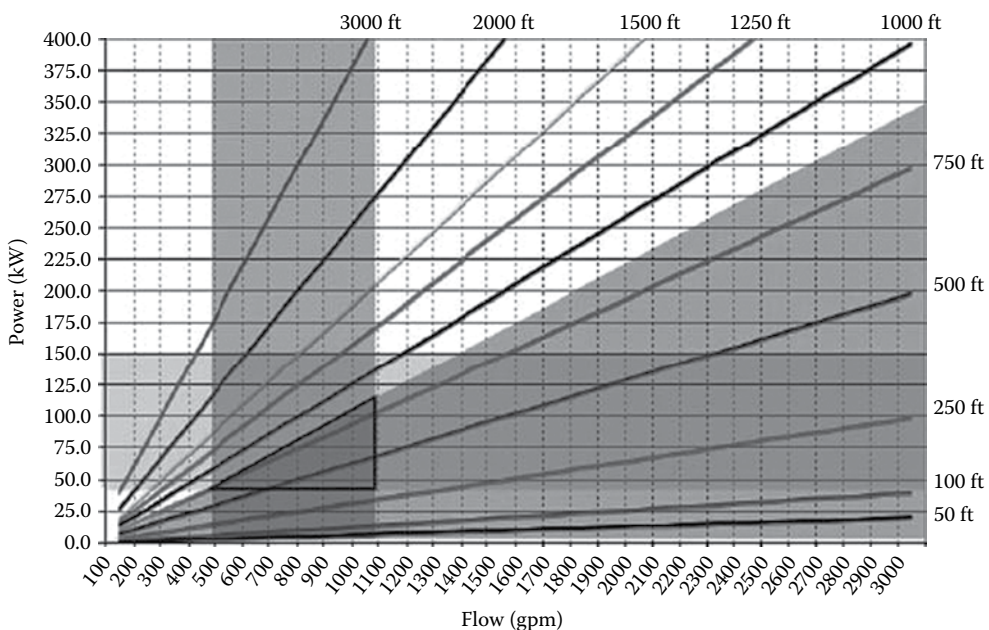


FIGURE 14.4

Pumped hydro turbine power output as a function of flow rate for various hydraulic heads, efficiency = 70%. *gpm*, gallons per minute. (From Levine, J.G., 2007. Pumped hydroelectric energy storage and spatial diversity of wind resources as methods of improving utilization of renewable energy sources, Thesis, University of Colorado, Boulder, CO. With permission [3].)

14.2.1.1 Turbines

Hydro turbines have in the past been used mostly for hydropower generation from large dams. Hydropower produces about 20% of the world's electricity in 150 countries. The technology has evolved for more than 100 years and the literature of hydroelectric power generation can be used as a guide for designing pumped storage facilities.

Conventional hydraulic turbines are either impulse or reaction machines (see [Figure 14.5](#)). Impulse turbines, often called Pelton turbines, convert the potential energy of a fluid into kinetic energy by expansion in a stationary nozzle to form a jet, which is then directed toward buckets attached to a rotating wheel to create shaft work that can be extracted. Reaction turbines are of the Francis or Kaplan type and utilize both hydraulic pressure and kinetic energy to create rotating shaft work. Each of the turbines has a specific operating range in terms of hydraulic head and power output. The choice of which turbine to use depends on the appropriate characteristics.

Pelton wheels were used in the early days of hydropower. They have a lower efficiency at low hydraulic head in comparison to reaction machines. Pelton wheels are still used, however, for high head resources (about 200 m) and small power outputs (less than 5 MW).

Francis turbines use a set of fixed veins that guide the fluid to the buckets that make up the turbine runner and are mounted on a central shaft. Francis turbines have a large operating range with heads from 40 to 500 m and unit sizes from 10 to up to 1000 MWe. Kaplan turbines are similar to Francis turbines, but the turbine blade angle can be adjusted to improve performance under different flow conditions. They work well at low heads, less than 10 m to about 100 m, with power outputs of the order of 200 MWe.

Once built, hydro power installations have operated successfully for more than a century. It is therefore expected that pumped storage facilities will also have a long life. The main drawback of pumped storage is the limited availability of suitable sites. According to Schoenung et al. [4]:

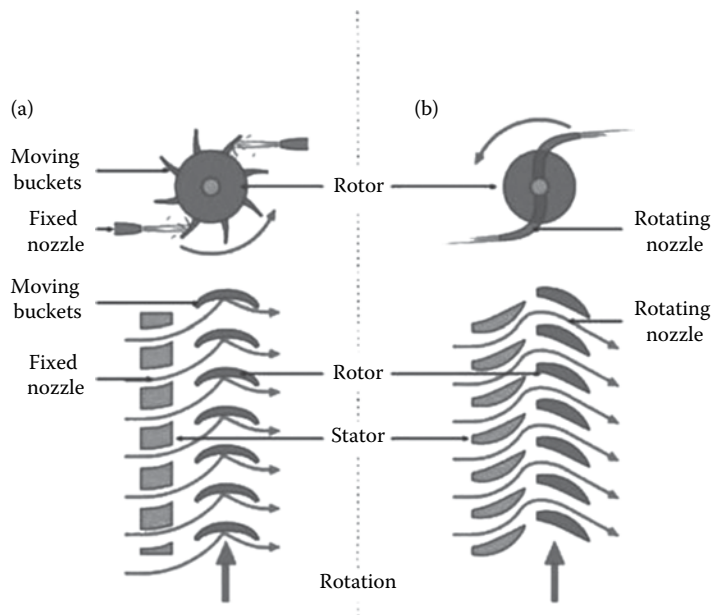


FIGURE 14.5
Schematic diagram of (a) impulse and (b) reaction turbines.

There have been a number of studies that have indicated that the availability of storage can be a key element in the successful operation of a robust electric power system. Pumped hydro-storage systems are therefore in widespread use worldwide. In 1996, more than 300 systems with capacities ranging from about 20 MWe to more than 2000 MWe were operating.

14.2.2 Compressed Air Energy Storage

The compressed air energy storage (CAES) system is a hybrid thermodynamic storage mechanism that requires natural gas as an intermediate component. Figure 14.6 schematically shows side by side the operation of both a gas turbine and a CAES system.

The operation of a CAES system can be demonstrated by comparing these two thermodynamic systems. In a gas turbine power plant, atmospheric pressure air passes through a compressor, is then delivered to a combustion chamber where fuel is injected and the high-pressure (hp) air is heated. The hp heated gas from the combustion chamber then passes through the blades of a turbine whose rotating shaft is connected to an electricity generator. The air from the turbine is exhausted at approximately atmospheric pressure. Approximately two-thirds of the energy generated by the turbine is used to drive the compressor, whereas the remaining one-third is converted to generate electric power.

The components in a CAES system are similar to those in a gas turbine, but clutches are added in order that the compressor and the turbine may be connected separately to the generator, which also has to work as a motor. In addition, provision is made to store the hp

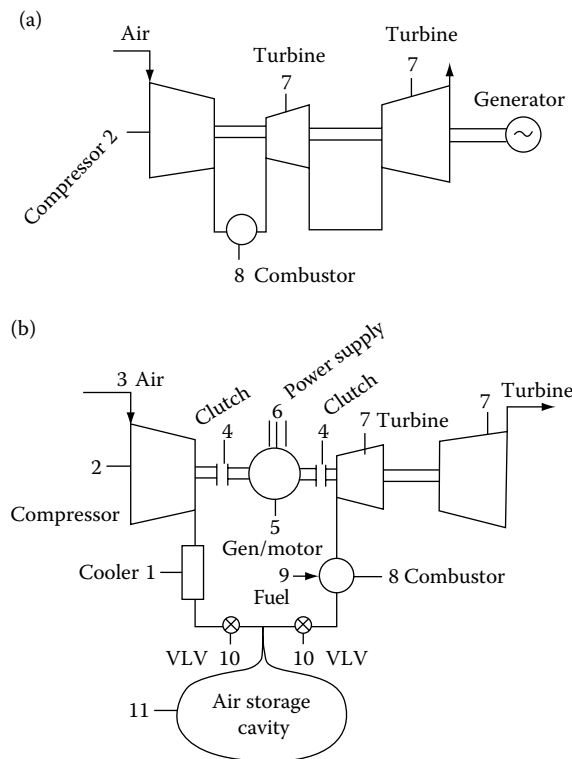


FIGURE 14.6 Comparison of (a) gas turbine and (b) compressed air storage system.

air from the compressor in a suitable cavity. The air from the cavity is heated in a combustor similarly to the gas turbine power plant, but the timing of discharging the stored hp air can be controlled. Since compression and expansion of the air can take place at different times, the entire output from the turbine is available to generate electricity as needed. In other words, compressed air can be placed in the cavity where it is stored until power is needed. This arrangement is of utmost utility for renewable energy systems such as wind turbines that do not operate continuously. But by using any excess power when available to compress and store energy, the compressed air in the cavity becomes available when winds die down but electricity is needed.

Creation of the cavity for a CAES system can be done by leeching existing salt domes, actual excavation in hard rock, or utilizing existing aquifers, if suitable domed caprock is available. Detailed descriptions of these technologies are available in Kreith and Krumdieck [5]. The main advantage of a CAES system is that NG heat input per unit power is less than that for a conventional gas turbine.

There are two existing CAES systems that have been designed and operated for many years. One is located in Huntorf, Germany [6] and the other one is in McIntosh, Alabama [7,8]. The experience gained from these existing CAES systems will be valuable in the design and operation of future compressed air storage, but no specific new CAES systems are being constructed at this time. Detailed derivations for the efficiency of a VAES system can be found in [9].

14.2.3 Flywheels

Flywheels have been used for a long time for short-term energy storage. Modern flywheel energy storage systems consist of a massive rotating cylinder on a shaft that is supported on a stator by magnetically levitated bearings that reduce bearing wear and increase system life. By operating a flywheel system in a vacuum environment, drag can be drastically reduced. To complete the system, the flywheel is connected to a motor/generator that is mounted on the stator that, through power electronics, can interact with the utility grid.

The amount of energy stored in a rotating flywheel is given by

$$E = \frac{I\omega^2}{2}, \quad (14.3)$$

where

I is the flywheel's moment of inertia in kg/m²

ω is its angular velocity in 1/s

E is in joules

In order to obtain a high specific energy for flywheels, the flywheel speed is increased, since the energy stored increases with the square of the velocity, whereas the specific energy only increases in direct proportion with its mass.

Some of the advantages of flywheels are their low maintenance requirements, long cycle life (better than 10,000 cycles), and long lifetime (in excess of 20 years). High-speed and low-mass flywheels, which are the modern approach to flywheel storage, are made from composites such as carbon fiber. Flywheels can have an energy efficiency of better than 90%, but their energy storage capacity is limited to a short period. Their low energy density and specific energy limit them to voltage regulation and uninterruptible power supply (UPS) capability.

14.3 Direct Electrical Technologies

14.3.1 Ultracapacitors

An ordinary capacitor stores energy in the electric field between two oppositely charged conductors with a dielectric between them. The dielectric prevents arcing between the plates and permits the plates to hold more charge, thus increasing the maximum potential energy storage. The ultra-capacitor, also known as super capacitor, differs from the traditional capacitor in that it uses an extremely thin electrolyte instead of a dielectric. This electrolyte is only a few Angstroms thick, thereby making it possible to increase the energy density of the device. The electrolyte can be made either of an organic or an aqueous material. The aqueous design can operate over a larger temperature range but has a smaller energy density than the organic design. The electrodes are usually made of a porous carbon that increases their surface area as well as the energy density, compared to a traditional capacitor.

Ultracapacitors can effectively equalize voltage variation quickly, which makes them useful for power quality management and for regulating the voltage in automobiles during regular driving. Ultracapacitors can also work in tandem with batteries to relieve peak power needs. They also exhibit very high cycle life of greater than 500,000 cycles and a life span of more than 10 years. The main limitation of ultracapacitors is their ability to maintain charge voltage over any significant period, losing up to 10% of the charge per day.

14.3.2 Superconducting Magnetic Energy Storage

Superconducting magnetic energy storage (SMES) systems can store and discharge energy at high rates. They store energy in the magnetic field created by direct current in a coil of cryogenically cooled, superconducting material. The advantage of a cryogenically cooled, superconducting material over copper is that it reduces electrical resistance to nearly zero. SMES recharge quickly and can repeat the charge-discharge sequence thousands of times without degrading the magnet. They can also achieve full power rather quickly, within 100 ms. Theoretically, a coil of around 150–500 m radius would be able to support a load of 18,000 GJ at 1000 MW, depending on the peak field and the ratio of the coil's height and diameter. Since no conversion of energy to other forms is involved (e.g., mechanical), the energy is stored directly and round-trip efficiency is expected to be very high. It is believed that mature, commercialized SMES can operate with round-trip efficiency as high as 97% and are a superb technology for providing reactive power on demand. The downside of SMES is the need to cool the coil to cryogenic temperatures, which requires a cryogenic refrigeration system and uses a large amount of energy [10].

14.4 Fundamentals of Batteries and Fuel Cells

Both batteries and fuel cells date back to the early 1800s. Alexander Volta described an electrochemical cell in a letter to the British Royal Society in 1800. This invention and the development of the telegraph in the 1830s led to the deployment and manufacture of batteries, which provided the electric energy for the telegraph, as well as for other inventions. The fuel cell was first demonstrated by Sir William Grove in 1839, but it was not until recently that significant progress toward practical applications occurred.

The operation of batteries and fuel cells are based on similar electrochemical principles and processes. However, batteries are devices for the storage of energy directly, whereas fuel cells are continuous energy converters that by themselves have no inherent storage capability and need hydrogen or some other energy source to operate. The operation of a typical battery is shown schematically in [Figure 14.7](#).

The battery has a fixed amount of chemicals that spontaneously produce a flow of electrons if a conducting path is connected to its terminals. Fuel cells require a continuous external supply of chemical reactants or hydrogen and the products are eliminated continuously. The operation of the fuel cells is dependent on a supply of hydrogen, which can be stored externally. Hence, the combination of stored hydrogen and a fuel cell that produces electricity can be considered a storage system, which will be considered later on.

The reactions in both batteries and fuel cells are oxidation-reduction reactions. Both contain electron pairs in contact with an electrolyte, which is the charge-carrying medium, as shown in [Figure 14.7](#). The oxidation reaction takes place at the negative electrode called the *anode* whereas the reduction occurs at the positive electrode called the *cathode*. The anode delivers electrons to the external circuit, which flow from the negative to the positive electrode. However, the conventional current flows in the opposite direction from high to low potential. The electrolyte is usually a liquid solution through which positively charged ions pass from the anode to the cathode. At the cathode, electrons from the external load are neutralized by reacting with positive ions from the electrolyte.

Batteries designed for a single discharge cycle, such as flashlight batteries, are called primary cells, whereas those that can be recharged are called secondary cells. Fuel cells, on the other hand, utilize hydrogen to provide a continuous supply of direct current. There are many different types of batteries and fuel cells available and we will consider the most important of these in the following sections.

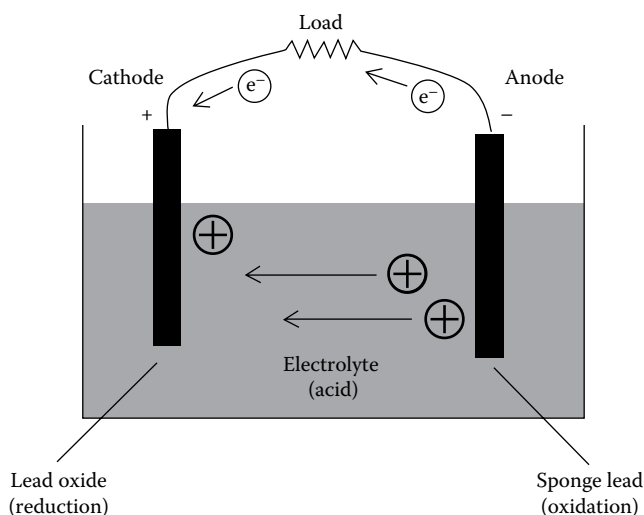


FIGURE 14.7
Schematic diagram of a battery.

14.4.1 Principles of Battery Operation

Batteries find a variety of applications today from tiny button cells in wrist watches to ignition batteries in automobiles and, finally, to large storage batteries in utility power supplies. At present, batteries are considered for storing energy from renewable sources such as solar and wind in order to provide a continuous supply of energy. Batteries are devices for storing an electric charge and automatically delivering an electric current flow on demand. A battery system consists of one or more cells connected in series to provide an open-circuit voltage or electromotive force (EMF). The exact value of the EMF depends on the specific cell reactants used. The operation of the battery can be visualized by means of a simple conceptual model shown in [Figure 14.8](#).

When current is drawn from a battery, the voltage drops below its EMF across the terminals, largely due to the internal voltage drop associated with the battery's internal resistance. As shown in [Figure 14.8](#), the terminal voltage in this model is the difference between the EMF (E) and the potential drop across the internal resistance, R_i :

$$V = E - IR_i \quad (14.4)$$

and the current, I , is

$$I = \frac{E}{R_i + R_o} \quad (14.5)$$

The following example illustrates the simplified model for a conventional lead-acid battery.

EXAMPLE 14.2

Estimate the internal and external resistances for a lead-acid battery with an EMF of 12.7 V. When delivering a current of 50 A through an external resistance of $3\ \Omega$, the voltage measured in operation is 11.1 V. Draw the voltage versus current characteristics.

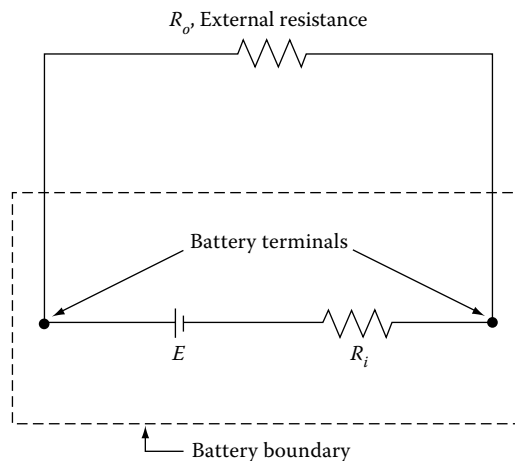


FIGURE 14.8
Simplified battery model.

Solution

From Equations 14.4 and 14.5, we obtain the internal and external resistances as shown below:

$$R_i = \frac{E - V}{I} = \frac{(12.7 \text{ V} - 11.1 \text{ V})}{50 \text{ A}} = 0.032 \Omega$$

$$R_o = \frac{E}{I} - R_i = \frac{12.7}{50} - 0.032 = 0.222 \Omega$$

The current flow through a 3Ω external resistance is

$$I = \frac{E}{R_i + R_o} = \frac{12.7}{0.032 + 3} = 3.825 \text{ A}$$

and the voltage is

$$V = IR_o = (3.825 \text{ A})(3 \Omega) = 11.5 \text{ V}$$

The voltage versus current characteristics for the simplified model are shown in [Figure 14.9](#).

The linear model is useful, but represents real battery characteristics only qualitatively. Real batteries can provide current and power to a wide range of resistances with little voltage drop, but only for short periods of time. The linear model fails for longer periods of time, and when large currents are drawn because it does not account for the finite amount of stored chemical energy and the rate of reaction limits of real batteries. In real batteries, the terminal voltage and power output drop drastically as the chemicals of the cell are consumed.

For utility scale electric power storage and automotive propulsion, secondary cells offer great opportunities. In secondary cells, the reactions are approximately internally reversible and with an external current source, the internal battery reactions may be reversed during a process called charging. For example, in a solar thermal power plant, the batteries can be charged during periods of sunshine and the energy stored in the battery can then be

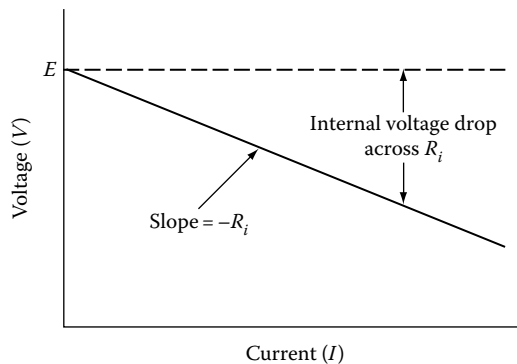


FIGURE 14.9
Current versus voltage characteristics for simplified battery in problem solution.

used for power applications when the sun goes down. In an electric car, the battery can be charged at night and used to power the vehicle in the day.

14.4.2 Cell Physics

When the current is small, the voltage is close to the cell EMF and the power output is small. To analyze the cell physics, assume that the chemical reaction in the battery consumes reactants at an electrode at the rate n_c mol per second. The electrons released in the reaction flow from the electrode through the external load at a rate proportional to the rate of reaction, jn_c , where j is the number of moles of electrons released per mole of reactant. Thus, jn_c is the rate of flow of electrons from the cell in moles of electrons per second. Since there are 6.023×10^{23} electrons per gram-mole and each electron has a charge of 1.602×10^{-19} Coulomb (C), the product is $96,488 \times 10^4$ C/g-mol. The charge transported by a gram-mole of electrons is a constant named in honor of the pioneer of electrochemistry, Michael Faraday, Faraday's constant, F ,

$$F = (6.023 \times 10^{23})(1.602 \times 10^{-19}) = 96,488 \times 10^4 \text{ C/g-mol}$$

With this model, the electric current from a cell, I , can be related to the reaction rate in the cell according to

$$I = jn_c F \quad (14.6)$$

and the instantaneous power, P , delivered by the cell is

$$P = jn_c FV \quad (14.7)$$

It can be seen that the cell electrode, the electrolyte material and the nature and rate of chemical reaction control the maximum cell voltage, cell current, and maximum power output. It is also apparent that the amount of consumable reactants in the battery sets a limit to the battery capacity.

14.5 Rechargeable Batteries

Rechargeable storage batteries offer great opportunities for storing electric power and many different types of batteries are under extensive research at the present time. Although the method of operation for all, except so-called flow batteries, is similar, many different materials and assemblies are being tried. Since at this time it is not clear which battery or groups of batteries will eventually achieve marketability, we will here simply discuss the method of operation of rechargeable batteries and then list the pros and cons of the various types with their potential applications. [Figure 14.10](#) shows ranges of operation for different battery types as specific energy versus specific power [11].

Lead-acid batteries have been the workhorse for electric storage for many decades, but they are too heavy and need to be recharged too often for many current applications, especially in the field of transportation. As a result, a worldwide effort is underway to improve and develop new batteries that can meet the demands of various industries including electric utilities and electric automobiles. The field of batteries is changing rapidly and new batteries are constantly entering the market. At this time, it is impossible to pick

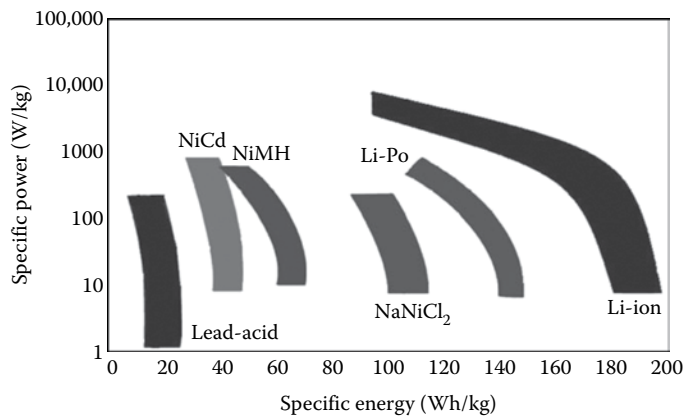


FIGURE 14.10

Approximate operating characteristics of different batteries in terms of specific energy and specific power. (Modified from de Guilbert, A., 2009. Batteries and supercapacitors cells for the fully electric vehicle, Saft Groupe SA, Brussels, https://www.smart-systems-integration.org/public/electric-vehicle/battery-workshop-documents/presentations/Anne%20de%20Guibert%20Saft.pdf/at_download/file [11].)

winners and losers; therefore, the following merely outlines the potential applications, as well as advantages and disadvantages of various typical batteries that are vying for a market share of the future. Only the lead-acid battery will be discussed in detail in order to demonstrate the basic method of operation of rechargeable batteries.

14.5.1 Lead-Acid Batteries

In order to illustrate the operation of the charging cycle of a secondary battery, we will analyze the operation of a common lead-acid battery shown in Figure 14.11 in some detail.

For such a battery, each cell consists of a porous sponge lead anode and a lead-dioxide cathode, which is usually in the form of a plate. The two electrodes are separated by porous

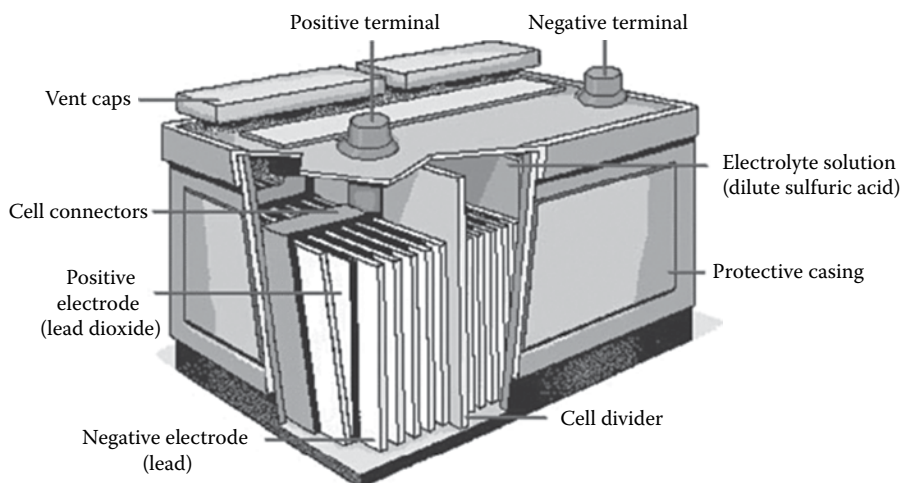


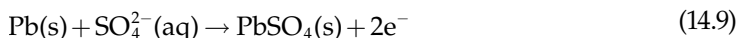
FIGURE 14.11

Schematic diagram of a conventional lead-acid battery.

membranes in a sulfuric acid solution. The aqueous electrolyte contains positive hydrogen ion and negative sulfate ions, resulting from disassociation of the sulfuric acid in solution as shown by the chemical reaction below:

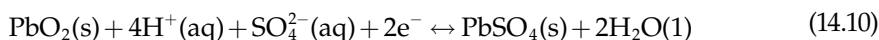


As the lead is converted to lead sulfate at the anode, it releases two electrons to the external load as shown below:



Hence, 2 mol of electrons are produced for each mole of sulfate ions and sponge lead reacted, or $j = 2$ for this battery.

In the reduction reaction at the cathode, lead dioxide, using hydrogen and sulfate ions from the electrolyte and electrons from the external circuit, is converted to lead sulfate, as shown by the chemical reaction below:



We observe that the sulfate radical, that is, the sulfuric acid, is consumed at both electrodes and that hydrogen ions combine with oxygen from the cathode material to form water that remains in the cell. The water that is formed as the battery discharges makes the sulfuric acid electrolyte more dilute, as can be seen from the net cell reaction below. The net cell reaction, obtained as the sum of the electrode and electrolyte reactions, is



In this and all other rechargeable battery chemistries, left-to-right indicates a battery discharging process and right-to-left indicates recharging. When any of the reactant is depleted, the battery ceases to function. However, the battery can be charged by applying an external power source. This reverses the electron flow and the above reactions are also reversed, as water is consumed to produce sulfate and hydrogen ions from the lead sulfate on the electrodes. Thus, the battery regains its charge and upon demand can again produce electric current.

There are three types of lead-acid batteries on the market: the wet cell, the sealed gel cell, and the sealed absorbed glass mat (AGM). Each of them has certain advantages and disadvantages. The wet cell has a liquid electrolyte, which must be replaced periodically to replenish hydrogen and oxygen escaping during the charge cycle. The sealed gel cell has a silica component added to the electrolyte to stiffen it. The AGM uses a fiberglass-like separator to hold the electrolyte in close proximity to the electrodes. This increases the efficiency. For both the gel and the AGM configuration, the risk of hydrogen explosion is reduced and corrosion is lessened. However, these two types require a slower charging rate. Both the gel cell and the AGM batteries are sealed and pressurized so the oxygen and hydrogen produced during charging are recombined into water.

The advantages of the lead-acid battery technology are low cost and high power density. However, its application for utility storage is very limited because of its short cycle life. A typical installation survives only a maximum of 1500 deep cycles. Therefore, lead-acid batteries have not found much use in commercial and large-scale energy-management

application. The largest existing facility is a 140 GJ system in Chino, California, built in 1988 [10]. Because of the low specific energy at only 0.8 MJ/kg, lead-acid batteries are not a viable storage option for electric vehicles.

14.5.2 Nickel Metal (Ni-Cd and Ni-MH)

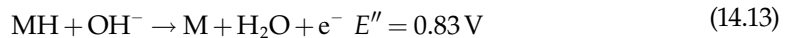
Description: The nickel cadmium battery is the precursor to the nickel metal hydride battery, but Ni-Cd batteries are losing popularity due to the toxicity of cadmium. Nickel metal-hydride (Ni-MH) batteries operate similar to other secondary batteries. The cathode in a Ni-MH battery uses a hydrogen absorbing alloy whereas cadmium is used in a Ni-Cd battery. During cell discharge, hydrogen ions flow from the anode to the cathode through the separator.

Structure: The cathode of a Ni-MH battery is composed of nickel oxyhydroxide. The anode is generally an alloy of nickel, cobalt, manganese, and/or aluminum combined with a mixture of rare Earth metals. The electrolyte is an alkaline, generally potassium hydroxide.

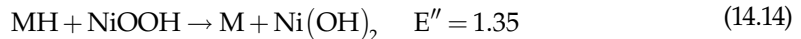
During discharge, the nickel oxyhydroxide is reduced to nickel hydroxide.



And the metal hydride MH is oxidized to the metal alloy M.



The overall reaction on discharge is



The process is reversed during charging.

Advantages of Ni-MH versus Ni-Cd

- Higher energy density than standard Ni-Cd (30–80 Wh/kg).
- Periodic deep discharge cycling is required less often.
- Much more environmentally friendly than Ni-Cd. Ni-MH is easily recyclable.
- Long shelf life.

Disadvantages

- Service life limited with repeated deep cycling. More prevalent with high load currents.
- Low discharge current when compared to Li-ion batteries (0.2 C–0.5 C recommended).
- High self-discharge.
- Requires full discharge to prevent memory effect where the capacitance and the voltage drop until the battery is charged to its correct voltage and then discharged fully.

General uses

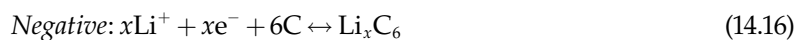
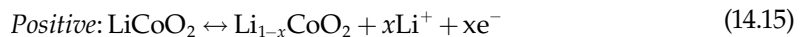
- Small electronics
- Hybrid electric and electric cars
- Wireless communications

14.5.3 Lithium Ion

Pure lithium batteries are primary batteries and cannot be recharged due to the instability of lithium. Li-ion batteries are secondary batteries and use lithium compounds instead of pure metallic lithium for their anode. Li-ion batteries, similar to other rechargeable batteries have three primary functional components, the anode, the cathode, and the electrolyte. Lithium ions move from the anode to the cathode during discharging and the opposite way during charging. Most Li-ion batteries use a liquid organic electrolyte, but lithium polymer (Li-Po) batteries use a solid polymer composite that makes them easier to manufacture and more durable. Research on how to increase the power output of Li-ion batteries by decreasing the internal resistance of the battery is currently in progress. Li-ion batteries can be discharged at a continuous rate of 5–20 C with peak currents reaching 40 C. Li-Po batteries can achieve similar rates.

Structure: The cathode is normally made of a metal oxide such as lithium cobalt oxide (LiCoO_2) or lithium manganese oxide (LiMn_2O_4) attached to a current collector made of aluminum foil. The anode is generally made from layered graphitic carbon with a copper current collector. The electrolyte is a lithium salt such as LiPF_6 , LiBF_4 , or LiClO_4 . These salts are dissolved in an organic solvent. In Li-Po batteries, the electrolyte is a composite of a gelled polymer and one of the lithium salts.

The chemical reactions for a typical Li-ion battery are shown below [12].



Note that the C in the above equations stands for a very carbon-rich negative material such as graphite. The above equations are written in units of moles, using x as a coefficient.

Advantages of Li-ion batteries compared to Ni-MH

- Higher energy densities than other battery types (130–200 Wh/kg) compared to Ni-MH, (30–80 Wh/kg).
- Generally much lighter.
- Low maintenance (Ni-MH have “memory” effects and have to be fully cycled occasionally).
- Low self-discharge rate—typically 5% per month.

Disadvantages of Li-ion batteries

- Shelf life—the battery's capacity will slowly decay over time regardless of the number of charge/discharge cycles. Depending on conditions, the battery can lose anywhere from 6% to 40% of its capacity over 1 year. (If stored at 40% charge level and 25°C, the battery will lose 4% of its capacity after 1 year.)
- Requires a protective circuit to make sure it is not overcharged or over-discharged as this degrades the battery by causing deposits of material that can short the battery (over-discharge), or cause excessive heat (overcharge).
- If damaged, combustion of the electrolyte, anode, and cathode can occur due to the interaction of lithium and the water vapor in the air.
- Currently is expensive to manufacture although expected to become cheaper as the technology matures.

General uses

- Electric/hybrid cars
- Cell phones and laptops

14.5.4 Flow Batteries

Description: Flow batteries are a novel type of secondary battery in which charged electrolytes are passed through a cell, producing electric charge (see [Figure 14.12](#)). The vanadium redox (VR) battery is the most common type of flow battery. The VR battery uses an electrolyte created from electrolytically dissolving vanadium pentoxide (V_2O_5) in sulfuric acid (H_2SO_4). The battery consists of two tanks of electrolyte and a membrane connected to a load, as shown in [Figure 14.12](#).

Charging the electrolyte causes the cathode to produce VO^{2+} ions and the anode to produce V^{2+} . During discharge, the charged electrolyte is pumped across a membrane,

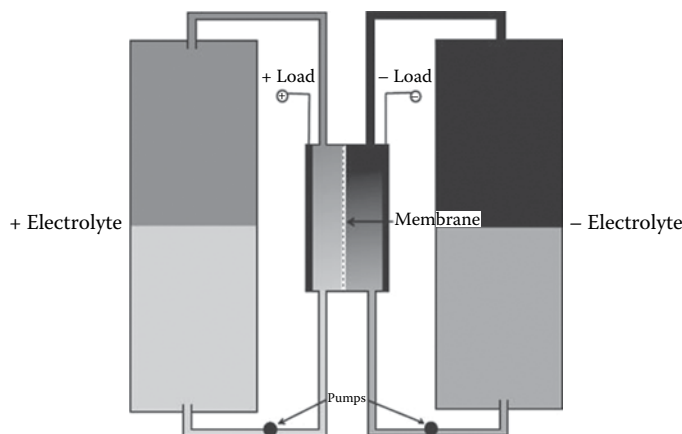
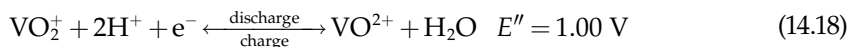


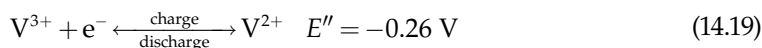
FIGURE 14.12
Schematic diagram of a typical flow battery.

creating VO_2^+ on the positive tank side and V^{3+} on the negative tank side. This produces an open circuit voltage. Since the chemical structure of the electrolyte does not undergo a change, this battery is very stable.

At the positive electrode



At the negative electrode



The potential generated by the cathode and anode combine to create the overall potential for the battery.

Advantages

- Very environmentally friendly—the vanadium electrolyte does not break down and can theoretically last forever thus reducing the waste to near zero for the whole system. Vanadium is a non-toxic element so catastrophic failure of containment is not an issue.
- Capable of very large energy storage. Only limiting factor is how large the electrolyte tanks are. Can reach MWh range (<http://www.vrb.unsw.edu.au>).
- Capable of very fast change in power.
- Can be fully charged/discharged without degradation.
- High cycle life (>10,000) after which only the membrane needs to be replaced.
- Very low self-discharge rate—electrolytes are stable at charged levels.
- Cost/kWh decreases as storage size increases.
- Possibility of instant recharge by replacing electrolyte.
- Already scaled to industrial size (<http://www.vrb.unsw.edu.au>).
- High efficiency (between 80% and 90% in larger installations).

Disadvantages

- Energy density only 10–20 Wh/kg and 15–25 Wh/L. Second generation V/Br batteries can achieve 35–50 Wh/kg with higher concentrations of vanadium in the solution.
- System is complex in larger storage sizes.

Uses

- Load leveling
- Off-peak production storage for renewable energy
- Possible electric car applications (fill up like gasoline, but no burning of fuel, simply recharged at the station)

14.6 Fuel Cells and Hydrogen

Electricity generation from hydrogen requires a fuel cell as an intermediate step, as discussed in [Chapter 1](#). Details of the principles of operation of the fuel cell and the use of hydrogen as a storage medium are discussed below [13].

14.6.1 Principles of Fuel Cell Operation

The operation of a fuel cell is shown schematically in [Figure 14.13](#). A fuel cell consists, like a battery, of two electrodes separated by an electrolyte, which transmits ions but is impervious to electrons. In a fuel cell, hydrogen, or another reducing agent, is supplied to the negative electrode, while oxygen (or air) goes to the positive electrode. A catalyst on the porous anode promotes dissociation of hydrogen molecules into hydrogen ions and electrons. The H^+ ions migrate through the electrolyte to the cathode where they react with electrons supplied through the external circuit and with oxygen to form water.

Although a fuel cell converts chemical energy into electricity directly, without an intermediate combustion cycle, it does not approach its theoretical efficiency of 100% in practice. Similar to batteries, fuel cells have an efficiency on the order of 40% in practice, but this efficiency is independent of the amount of power generated. Since the efficiency of an assembly of fuel cells is approximately equal to that of a single cell, there are no economies of scale. Therefore, fuel cells are promising for small, localized plants in the range of 1–100 kW capacity. Since fuel cells also reject heat, they can operate as a cogeneration system and could supply a building with both electricity and heat.

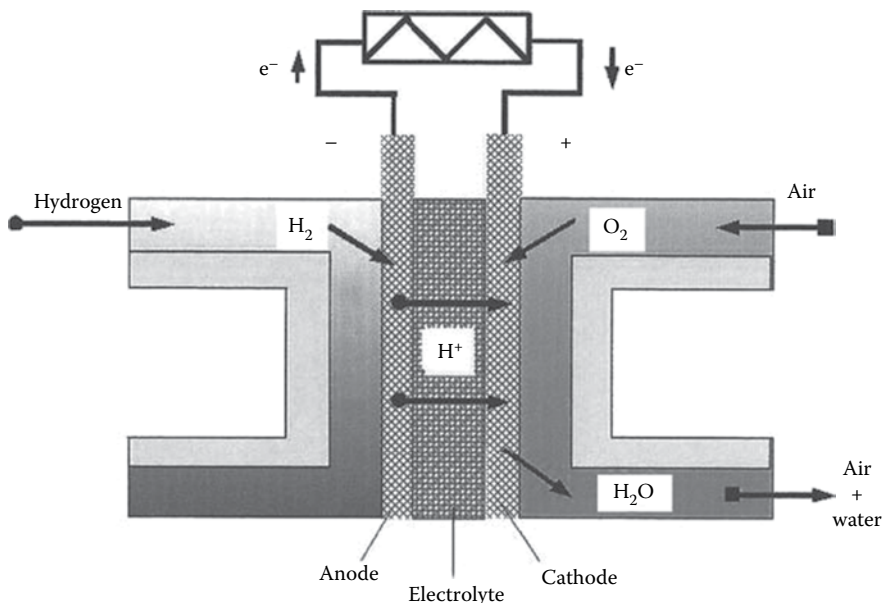


FIGURE 14.13

Schematic diagram of fuel cell operation.

14.6.2 Types of Fuel Cells

There are six principal types of fuel cells, as shown in [Table 14.2](#).

- Proton exchange membrane fuel cell (PEMFC)
- Direct methanol fuel cell (DMFC)
- Molten carbonate fuel cell (MCFC)
- Alkaline fuel cell (AFC)
- Phosphoric acid fuel cell (PAFC)
- Solid oxide fuel cell (SOFC)

The above types of fuel cells differ in operating temperatures, efficiency, and cost. Their operating characteristics and some potential applications are summarized in [Table 14.2](#).

PEMFC cells operate at relatively low temperatures (about 80°C), have a high power density, and can change rapidly to meet varying power demand or a fast startup. These features make PEMFC the favorite for automobile transportation. The membrane of a PEMFC is made of thin perfluorosulfonic acid sheets, which acts as an electrolyte and allows the passage of hydrogen ions only. The membrane is coated on both sides with highly dispersed metal alloy particles (currently mostly platinum) that act as catalysts.

DMFC cells also use a polymer membrane as an electrolyte. The most attractive feature of DMFCs is that they can use liquid methanol as a fuel. The anode of a DMFC can draw hydrogen from liquid methanol and thus eliminates the use of a fuel reformer.

MCFC cells use a molten carbonate salt as the electrolyte. They are flexible in their fuel supply and can use coal-derived gases, methane, or NG as fuel. The efficiency of these fuel cells is about 60%, but if operating as a cogeneration unit that uses the waste heat, the efficiency overall can be even higher.

PAFC cells use an anode and a cathode of finely dispersed platinum catalyst on carbon and a silicon-carbide structure that contains phosphoric acid as electrolyte.

AFC cells are commercially available. They operate at low temperatures, below 100°C, and are used in submarines and for space power applications.

TABLE 14.2

Operating Characteristics of Fuel Cells

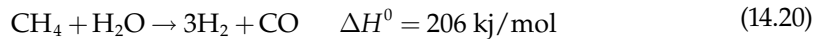
	PEMFC	DMFC	MCFC	AFC	PAFC	SOFC
Electrolyte	Ion exchange membrane	Polymer membrane	Immobilized liquid molten carbonate	Immobilized liquid phosphoric acid	Potassium hydroxide	Ceramic
Operating temperature (°C)	80	60–130	650	200	60–90	800–1000
Efficiency (%)	40–60	40	45–60	35–40	45–60	50–65
Typical electrical power	Up to 250 kW	<10 kW	>1 MW	>50 kW	Up to 20 kW	>200 kW
Possible applications	Vehicles	Portables	Power stations	Small power stations	Submarines, spacecraft	Power stations

SOFC cells work at high temperatures (between 800°C and 1000°C) and utilize a solid ceramic electrolyte such as zirconium oxide stabilized with yttrium oxide instead of a liquid. The efficiency of these cells can reach as high as 60% and they have the potential of being used for large-scale energy storage or generating electricity industrially. They can also be used for cogeneration systems.

The major challenges for widespread application of fuel cells are their cost, durability, and the need for a continuous and inexpensive supply of hydrogen.

14.6.3 Generation of Hydrogen

There are currently two different methods used for commercial production of hydrogen. The most widely used is NG reforming. In this process, called steam methane reforming, NG is mixed with steam and the resulting mixture is introduced into a catalytic reforming reactor where it is passed through a nickel catalyst and converted at about 900°C into CO and H₂ according to the reaction



The other method is electrolysis, where an electric current is passed through water to separate the hydrogen from the oxygen. Today, most commercial water electrolyzers use an alkaline electrolyte system, as shown in Figure 14.14.

In such an electrolytic cell, the following simplified reaction takes place:

In the electrolyte

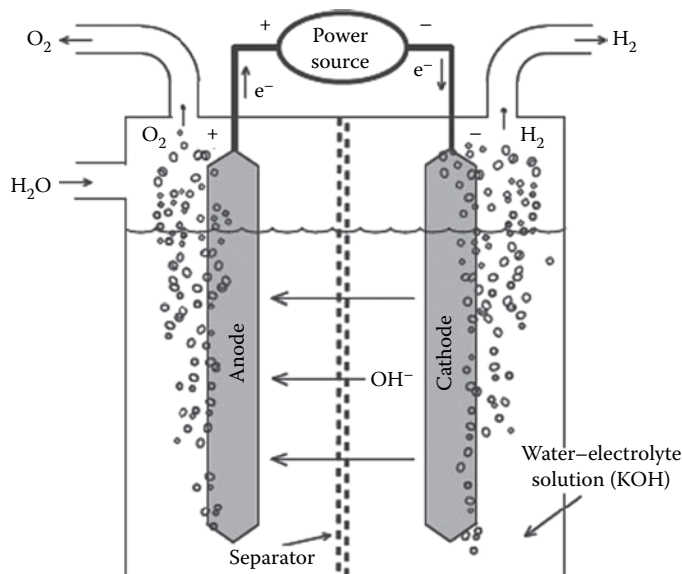


FIGURE 14.14
Schematic diagram of hydrogen generation by electrolysis.

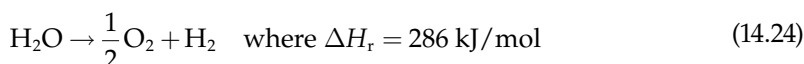
At the cathode



At the anode



The overall reaction is



According to Bossel et al. [14], the estimated cost of hydrogen production by NG reforming or coal gasification is about \$1/kg, whereas the cost via a renewable technology, such as electrolysis with electricity from wind, is between \$6 and \$7/kg. The energy content of 1 kg of H_2 approximately equals the energy content of 1 gal of gasoline.

14.6.4 Storage and Transport

Once the hydrogen is generated, it can be stored and subsequently combusted to provide heat or work, or it can be used to generate electricity with a fuel cell. Gaseous hydrogen has a low specific density and for storage purposes it must be compressed or cryogenically liquefied. If hydrogen is compressed adiabatically to a pressure of 350 bar, a value often assumed suitable for automotive technologies, it consumes about 12% of its higher heating value (HHV). The loss can be reduced appreciably; however, if the compression approaches an isothermal process. If the hydrogen is stored as a liquid at cryogenic temperatures, the process takes about 40% of the HHV with current technology. Moreover, liquid storage is not feasible for automotive applications because mandatory boil-off from the storage container cannot be safely released in closed spaces such as garages or tunnels.

One technology for storing hydrogen consists of bonding it into metal hydrides using an absorption process. The energy penalty of this type of storage, which requires only a pressure of about 30 bar, may be less. However, the density of the metal hydride can be between 20 and 100 times the density of the hydrogen stored [15]. Carbon nanotubes have also received attention as a potential hydrogen storage medium, but neither of the above processes has been fully developed and commercialized.

14.6.5 Thermodynamics and Economics

As an energy carrier, hydrogen should be compared with the only other widespread and viable alternative: electricity. Once generated and compressed, hydrogen could flow through large pipelines with a loss of approximately 0.8%/100 km [1,14], while the energy loss experienced with high voltage DC (long distance) electric transmission lines is of the order of 0.6%/100 km [1,15]. Hence, the losses incurred in transmission of energy by hydrogen and electricity are of the same order of magnitude. However, the cost of building a transmission system for hydrogen has been estimated to be on the order of half a trillion

dollars, and unless this up-front expenditure is made, transmission of hydrogen would have to be accomplished by truck, which would incur enormous expenses and energy penalties. Moreover, as shown by Kreith and West [16], the extraction of electricity from hydrogen is associated with irreversible losses. Electrolysis of water to make hydrogen is commercially available at about 70% efficiency. The sequence of steps required of generating electricity for producing hydrogen and then using a fuel cell to generate electricity again was shown in Chapter 1 (Figure 1.23). Compressing hydrogen to a pressure of 350 bar for transporting it is estimated to be about 88% efficient. And, finally, conversion back into electricity with a fuel cell has an efficiency of approximately 60%, although the theoretical limit is somewhat higher. Taken together, generating power for electrolysis, compression, and generation of electricity in the fuel cell results in, at most, an overall efficiency of only about 50%, compared to the amount of electricity that could have been obtained from the original source. Hence, from a thermodynamic as well as from an economic perspective, the use of hydrogen as a storage and transmission system appears to be inferior to the use of electricity directly. It should also be noted that this loss of energy is the result of basic thermodynamic considerations and would occur irrespective of whether the original generation of electricity came from renewable sources, nuclear power, or fossil fuels. In addition, because two units of electricity are required to produce one unit of useful power at the end use, the amount of CO₂ generation/kW electricity would be double via the hydrogen path compared to any other electric power system.

14.7 Thermal Energy Storage

Solar thermal storage is a well-established technology and the principles of design and operation in tanks or in the ground are extensively described in standard textbooks on heat transfer [17]. For solar thermal heat and power, thermal storage is important in applications such as storing heat overnight for buildings, seasonal heat storage for large-scale heating and/or cooling projects (called seasonal storage), and for storage in solar thermal power plants such as solar troughs or central receivers. Solar storage can also be dispersed through the overall system as, for example, in the thermal mass of a building—an art that has been practiced for centuries. A particularly good example is the Mesa Verde buildings in Colorado, where heat is stored in rock walls, which form a part of the structures.

14.7.1 Sensible Heat

Thermal energy can be stored as sensible heat, as latent heat, or in reversible thermochemical reactions. The sensible heat, ΔQ , gained or lost per unit mass by a material changing temperature from T_1 to T_2 is

$$\Delta Q = \int_{T_1}^{T_2} \rho c_p dT \quad (14.25)$$

Although both the density, ρ , and the specific heat, c_p , vary with temperature, the variations are usually small enough to use average values for engineering calculations. Equation 14.25 then simplifies so that $\Delta Q = c_p \Delta T$ per unit mass, or $\rho c_p \Delta T$ per unit volume. Commonly used

figures of merit are $\$/c_p$ for relative media costs, ρc_p for volumetric heat capacity, using the lowest value of ρ at the highest expected operating temperature for relative container size.

Table 14.3 shows the characteristics of some plentiful and economically competitive solid and liquid materials for sensible heat storage. Rocks, bricks, and cement are excellent candidates for overnight thermal storage in buildings. Among liquids, water is clearly superior for temperatures below 100°C, whereas oils, molten salts, or liquid metals are used for solar thermal power applications such as parabolic troughs or central receivers.

Solids and liquid sensible heat storage materials can be combined in various ways. Rock beds and water tanks have been used in hybrid storage systems for space heating, whereas rocks and oils have been used in single vessels for solar thermal power applications to improve stratification. This approach could reduce the cost compared to relatively expensive dual tank liquid storage systems where two vessels are necessary, as shown in Figure 14.15. However, experiences with single tank storage to achieve stratification have not been reliable, and for solar thermal power applications, dual tank storage is preferred.

14.7.2 Phase Change Heat Storage

Latent heat is the thermal energy released or absorbed by a material undergoing a phase transition, such as solid to liquid (melting), or liquid to gas (vaporization). Materials that have a high heat release or absorption during phase change are of interest for thermal storage. Latent heat storage material should have a large heat of transition, high density,

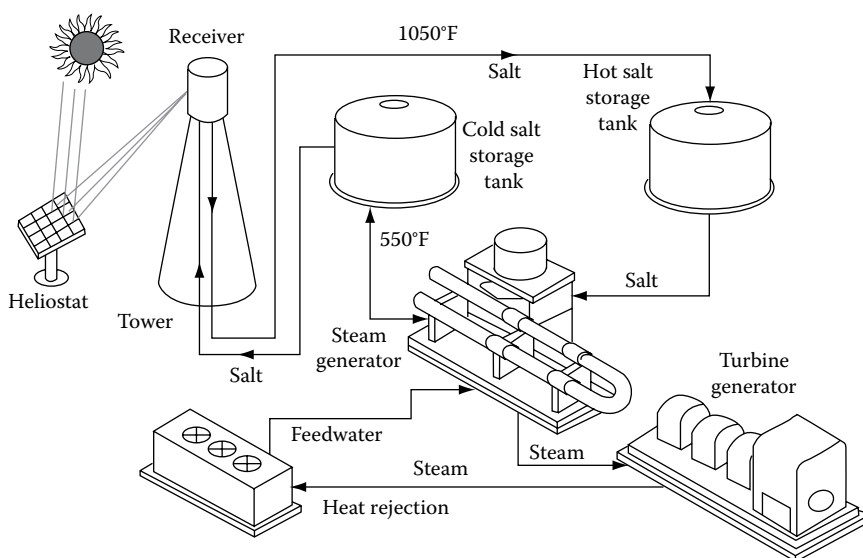
TABLE 14.3

Physical Properties of Some Sensible Heat Storage Materials

Storage medium	Temperature Range (°C)	Density (ρ) (kg/m ³)	Specific Heat (c), (J/kg K)	Energy Density (ρc) (kWh/m ³ K)	Thermal Conductivity (W/m K)
Water	0–100	1000	4190	1.16	0.63 at 38°C
Water (10 bar)	0–180	881	4190	1.03	—
50% ethylene glycol-50% water	0–100	1075	3480	0.98	—
Dowtherm A [®] (Dow Chemical, Co., Midland, Michigan)	12–260	867	2200	0.53	0.122 at 260°C
Therminol 66 [®] (Monsanto Co., St. Louis, Missouri)	9–343	750	2100	0.44	0.106 at 343°C
Draw salt (50 NaNO ₃ -50 KNO ₃) ^a	220–540	1733	1550	0.75	0.57
Molten salt (53 KNO ₃ /40 NaNO ₃ /7NaNO ₃) ^a	142–540	1680	1560	0.72	0.61
Liquid sodium	100–760	750	1260	0.26	67.5
Cast iron	m.p. (1150–1300)	7200	540	1.08	42.0
Taconite	—	3200	800	0.71	—
Aluminum	m.p. 660	2700	920	0.69	200
Fireclay	—	2100–2600	1000	0.65	1.0–1.5
Rock	—	1600	880	0.39	—

Note: m.p. = melting point.

^a Composition in percent by weight.

**FIGURE 14.15**

Two-tank storage for central receiver system.

appropriate transition temperature, low toxicity, and no gradation with multiple phase change. Materials attractive for storage are paraffin waxes and salt hydrates.

The advantage of using phase change material for storage is that a large amount of heat can be stored in small volumes and the temperature of the material remains constant during phase change. The problem with phase change heat transfer is to find materials that have appropriate temperatures during phase change, and also the design of heat exchangers that transfer heat to or from the material during phase change is exceedingly difficult. Table 14.4 shows the material properties of several common TES materials that may potentially be useful for latent heat storage. The engineering design of latent heat storage systems is beyond the scope of this book.

14.7.3 Thermochemical Storage

Thermochemical energy is stored as the bond energy of a chemical compound. In thermochemical energy storage, molecular bonds are broken during a reversible chemical reaction and are catalyzed by an increase in temperature. After thermochemical separation occurs, the constituents are stored apart until the combination reaction is desired. Recombination of the bonds between atoms releases the stored thermochemical energy.

Reversible chemical reactions with reactants and products which can be easily stored as liquids and/or solids are of interest for thermochemical energy storage. Reactions that produce two distinct phases such as a solid and a gas are desirable since the separation of products to prevent back reaction is facilitated. Table 14.5 shows several common thermochemical storage reactions and their standard enthalpy change (ΔH^0) in kJ and their turning temperature (T') in K.

The turning temperature, T' , in Table 14.5 is defined as the temperature at which the equilibrium constant is unity and is calculated using the ratio of the standard enthalpy change and the standard entropy change for the reaction. At this temperature, the

TABLE 14.4

Physical Properties of Latent Heat Storage Materials or PCMs

Storage medium	Melting Point (°C)	Latent Heat (kJ/kg)	Specific Heat (kJ/kg °C)		Density (kg/m ³)		Energy Density (kWh/m ³ K)	Thermal Conductivity (W/m K)
			Solid	Liquid	Solid	Liquid		
LiClO ₃ ·3H ₂ O	8.1	253	—	—	1720	1530	108	—
Na ₂ SO ₄ ·10H ₂ O (Glauber's salt)	32.4	25.1	1.76	3.32	1460	1330	92.7	2.25
Na ₂ S ₂ O ₃ ·5H ₂ O	48	200	1.47	2.39	1730	1665	92.5	0.57
NaCH ₃ COO·3H ₂ O	58	180	1.90	2.50	1450	1280	64	0.5
Ba(OH ₂)·6H ₂ O	90	163	1.56	3.68	1636	1550	70	0.611
LiNO ₃	252	530	2.02	2.041	2310	1776	261	1.35
LiCO ₃ /K ₂ CO ₃ , (35:65) ^a	505	345	1.34	1.76	2265	1960	188	—
LiCO ₃ /K ₂ CO ₃ / Na ₂ CO ₃ (32:35:33) ^a	397	277	1.68	1.63	2300	2140	165	—
<i>n</i> -Tetradecane	5.5	228	—	—	825	771	48	0.150
<i>n</i> -Octadecane	28	244	2.16	—	814	774	52.5	0.150
HDPE (cross-linked)	126	180	2.88	2.51	960	90	45	0.361
Steric acid	70	203	—	2.35	941	347	48	0.172 ℓ

Note: ℓ = liquid.^a Composition in percent by weight.

reactants and products will be present in approximately equal quantities. When $T > T'$, the endothermic storage reaction is favored, meaning heat is necessary for and absorbed during the reaction. Conversely, for $T < T'$, the exothermic reaction dominates, meaning that heat is produced in the reaction.

The primary advantages of thermochemical storage include the high energy density and the long-term, low-temperature, storage capability. However, the thermochemical process is very complex and the thermochemical materials are often expensive and can be hazardous. There is considerable research activity in the field of thermochemical reactions for energy storage, but no large-scale commercial applications exist to date.

TABLE 14.5

Thermochemical Storage Reactions

Reaction	ΔH° (kJ)	T' (K)
NH ₄ F(s) \leftrightarrow NH ₃ (g) + HF(g)	149.3	499
Mg(OH) ₂ (s) \leftrightarrow MgO(s) + H ₂ O(g)	81.1	531
MgCO ₃ (s) \leftrightarrow MgO(s) + CO ₂ (g)	100.6	670
NH ₄ HSO ₄ (l) \leftrightarrow NH ₃ (g) + H ₂ O(g) + SO ₃ (g)	337.0	740
Ca(OH) ₂ (s) \leftrightarrow CaO(s) + H ₂ O(g)	109.3	752
BaO ₂ (s) \leftrightarrow BaO(s) + $\frac{1}{2}$ O ₂ (g)	80.8	1000
LiOH(l) \leftrightarrow $\frac{1}{2}$ Li ₂ O(s) + $\frac{1}{2}$ H ₂ O(g)	56.7	1000
MgSO ₄ \leftrightarrow MgO(s) + SO ₃ (g)	287.6	1470

Source: Wyman, C. et al., 1980. *Solar Energy* 24(6), 517–540 [18].

14.7.4 Applications

Many factors contribute to choosing an appropriate storage method and material for each TES application. [Table 14.6](#) lists several TES options for solar thermal power and their appropriate storage materials [18]. In the table, PCM stands for phase change material, HX means heat exchanger, and VHT means very high temperature.

14.7.5 Thermal Storage for Concentrating Collector Systems

A very important application of thermal storage is in high-temperature concentrator systems such as central receivers or parabolic troughs. Steam is generated in the solar receiver when the sun is up and either passes through the turbine, or, when excess heat is available, it is stored in a tank. The size of the tank will determine the number of hours that the system can operate when the sun is down. For a typical system of this type, steam is raised in the receiver at 40 bar and 250°C, and condensed at 0.6 bar and 5°C. After the steam is condensed, it is returned to the solar receiver as in any typical Rankine cycle. The drawback of this approach is that steam storage requires a large volume, which limits the length of time the turbine can operate when the sun is down.

A significant application of thermal storage is the two-tank storage system shown in [Figure 14.15](#) that was used in the Solar 2 central receiver. In this approach, a single heat transfer fluid is used in the receiver and for storage. This approach eliminates the need for expensive heat exchangers and the degradation in the availability of the energy that occurs during heat transfer from one fluid to another. The fluid most commonly proposed for use in this kind of application is a molten salt, although other heat transfer fluids such as oils or liquid metals are being considered.

When molten salts are used as the heat transfer fluid, care must be taken to avoid freezing anywhere in the system. Molten salts freeze at a temperature between 120°C and 200°C (250°F–430°F). Thus, the Rankine cycle has to operate between a high temperature achievable in the receiver and a cold temperature that does not drop below the freezing point of the salt. The design of a typical two-tank direct system with approximate temperatures is shown in [Figure 14.15](#). The temperature of the molten salt is raised in the receiver to about 565°C and then passed to the hot salt storage tank. From this tank, salt is extracted to a heat exchanger, which raises the steam for a Rankine cycle power plant, and then returned to the cold salt storage tank at about 290°C. The working fluid is then recirculated to the receiver in a virtually closed loop. A normal Rankine cycle is used for the generation of electricity. The length of time that the system can operate once the sun is down depends on the size of the storage tanks. The advantage of this approach is the simplicity of design, and the disadvantage is that a large amount of heat transfer fluid is needed for the plant to operate.

In systems where the heat transfer fluid is very expensive or cannot be used for some reason as the storage fluid, a two-tank indirect system is used. The two-tank indirect system functions the same way as the two-tank direct system, except that different fluids are used in the receiver heating loop and the storage. Therefore, the heat from the working fluid must be transferred to the storage fluid via a heat exchanger, which the fluid enters at high temperature and leaves at low temperature. Storage fluid from the high temperature tank is then used to generate steam, as in the direct system.

14.7.6 Overnight Storage for Buildings and Domestic Hot Water

TES for domestic hot water or for overnight heating of buildings has been mentioned in previous chapters. These applications require storing a liquid, almost always water, in

TABLE 14.6

Options for TES in Solar Power Production

TES Options for Solar Thermal Power	Temperature (°C)	Storage Medium	Type
<i>Small power plants and water pumps</i>			
	100	Water in thermocline tank or two tanks	Sensible
Organic Rankine	300	Petroleum oil in the thermocline tank	Sensible
Steam Rankine with organic fluid receiver	375	Synthetic oil with trickle charge	Sensible
<i>Dish mounted engine generators (buffer storage only)</i>			
Organic Rankine	400	Bulk PCM with indirect HX	Latent
Stirling and air Brayton	800	Bulk PCM with indirect HX	Latent
Advanced air Brayton	1370	Graphite	Sensible
		Graphite Encapsulated PCM	Latent
<i>Larger power plants (typically 3–8 h storage)</i>			
Steam Rankine with organic fluid receiver	300	Petroleum oil in thermocline tank or two tanks, evaporation only	Sensible
	300	Petroleum oil/rocks (dual medium) in thermocline tank	Sensible
Steam Rankine with water-steam receiver		Petroleum oil in thermocline tanks, evaporation only	Sensible
		Petroleum oil/rocks (dual medium) in thermocline tank	Sensible
		Encapsulated PCM with evaporative HX	Latent
		Bulk PCM with indirect HX	Latent
		Bulk PCM with direct HX	Latent
		Pressurized water above ground or underground	Latent
	540	Molten draw salt in thermocline tank or two tanks, superheat	Sensible
		Air/rocks	Sensible
		Bulk PCM with direct HX, evaporation stage	Latent
		Solid or liquid decomposition, evaporation stage	Thermochemical
Steam Rankine with molten draw salt receiver	540	Molten draw salt in thermocline tank or two tanks	Sensible
Steam Rankine with liquid metal receiver	540	Liquid sodium in one tank, mixed, buffer only	Sensible
		Liquid sodium in two tanks Air/rocks	Sensible
Brayton with gas-cooled receiver	800	Refractory or cast-iron	Sensible
		Bulk PCM with indirect HX Solid or liquid decomposition	Thermochemical
Brayton with liquid-cooled receiver	800	VHT molten salt in two tanks	Sensible
		VHT molten salt/refractory (dual medium) in thermocline tank	Sensible
	1100	Bulk glassy slag, liquid and solid bead storage, direct HX	Sensible and Latent

Note: TES, Thermal energy storage; PCM, phase change material; HX, heat exchange; VHT, very high temperature.

a tank. A schematic diagram typical of such systems with electric backup is shown in [Figure 14.16](#). Insulation of the storage tank is a simple heat transfer problem treated in standard textbooks. The properties of insulation materials are given in [Table 14.7](#) [19].

The annual average insolation on a surface tilted at an angle equal to the latitude in the midlatitudes of the United States is about 23,000 kJ/m² per day (2030 Btu/ft² per day). If the average collection efficiency is 30%, 6900 kJ/m² per day (610 Btu/ft² per day) is delivered by the collector system. The service hot-water demand can be taken as 76 L/day (20 gal/day) per person. If the tap water has a temperature of 283 K (50°F), and the hot water 333 K (140°F), about 210 kJ/L (750 Btu/gal) is required for hot water heating. For a delivery of 230 L/day (60 gal/day) for a family of three, 48.3 MJ/day (46,000 Btu/day) is needed. If the collector delivers 6900 kJ/m², a collector with a size of approximately 7 m² is needed. This collector is about one-tenth the size of a collector required for heating a typical building in the midlatitudes. A rule of thumb is that 1 m² of collector is required for each 30 L of hot water to be delivered. The storage tank should be large enough to hold about a 2-day supply of hot water, or about 500 L for a family of three.

Thermal storage tanks must be insulated to control heat loss. If a storage tank is located within a structure, any losses from the tank tend to offset the active heating demands of the building. However, such storage loss is uncontrolled and may cause overheating in the summer.

The amount of thermal storage used in a solar-heating system is limited by the law of diminishing returns. Although larger storage results in larger annual energy delivery, the increase at the margin is small and hence not cost-effective. Seasonal storage is, therefore, usually uneconomic, although it can be realized in a technical sense. Experience has shown that liquid storage amounts of 50–75 kgH₂O/m² (10–15 lb/ft²) are the best compromise between storage tank cost and useful energy delivery.

Since solar energy heating systems operate at temperatures relatively close to the temperatures of the spaces to be heated, storage must be capable of delivering and receiving thermal energy at relatively small temperature differences. The designer must consider the magnitude of these driving forces in sizing heat exchangers, pumps, and air-blowers. The

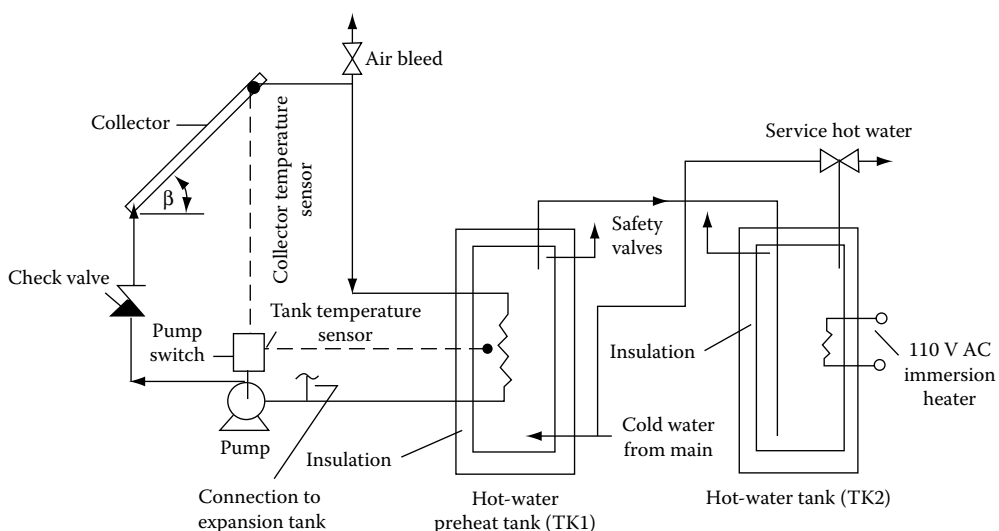


FIGURE 14.16
Schematic diagram of solar heating system with storage.

TABLE 14.7

Thermal Properties of Some Insulating and Building Materials

Material	Average Temperature (°F)	k [Btu/(h·ft·°F)]	c [Btu/(lb _m ·°F)]	ρ (lb _m /ft ³)	α (ft ² /h)
<i>Insulating materials</i>					
Asbestos	32	0.087	0.25	36	~0.01
	392	0.12	—	36	~0.01
Cork	86	0.025	0.04	10	~0.006
Cotton fabric	200	0.046	—	—	—
Diatomaceous earth, powdered	100	0.030	0.21	14	~0.01
	300	0.036	—	—	—
Molded pipe covering	400	0.051	—	26	—
	1600	0.088	—	—	—
<i>Glass wool</i>					
Fine	20	0.022	—	—	—
	100	0.031	—	1.5	—
	200	0.043	—	—	—
Packed	20	0.016	—	—	—
	100	0.022	—	—	—
Hair felt	100	0.027	—	8.2	—
Kaolin insulating brick	932	0.15	—	8.2	—
	2102	0.26	—	—	—
Kaolin insulating firebrick	392	0.05	—	19	—
	1400	0.11	—	—	—
Magnesia, 85%	32	0.032	—	17	—
	200	0.037	—	17	—
Rock wool	20	0.017	—	8	—
	200	0.030	—	—	—
Rubber	32	0.087	0.48	75	0.0024
<i>Building materials</i>					
<i>Brick</i>					
Fire clay	392	0.58	0.20	144	0.02
	1832	0.95	—	—	—
Masonry	70	0.38	0.20	106	0.018
Zircornia	392	0.84	—	304	—
	1832	1.13	—	—	—
Chrome brick	392	0.82	—	246	—
	1832	0.96	—	—	—
<i>Concrete</i>					
Stone	~70	0.54	0.20	144	0.019
	10% moisture	~70	—	140	~0.025
Glass, window	~70	~0.45	0.2	170	0.013
Limestone, dry	70	0.40	0.22	105	0.017
<i>Sand</i>					
Dry	68	0.20	—	95	—
	10% water	68	—	100	—

(Continued)

TABLE 14.7 (Continued)

Thermal Properties of Some Insulating and Building Materials

Material	Average Temperature (°F)	k [Btu/(h·ft·°F)]	c [Btu/(lb _m ·°F)]	ρ (lb _m /ft ³)	α (ft ² /h)
Soil					
Dry	70	~0.20	0.44	—	~0.01
Wet	70	~0.15	—	—	~0.03
Wood					
Oak \perp to grain ^a	70	0.12	0.57	51	0.0041
to grain	70	0.20	0.57	51	0.0069
Pine \perp to grain ^a	70	0.06	0.67	31	0.0029
to grain	70	0.14	0.67	31	0.0067
Ice	32	1.28	0.46	57	0.048

Source: Kreith, F., 1973. *Principles of Heat Transfer*, Intext, New York [19].

^a \perp , perpendicular; ||, parallel.

designer must also consider the nonrecoverable heat losses from storage—even though storage temperatures are relatively low, surface areas of storage units may be large and heat losses therefore appreciable.

Other mechanical components in solar heating systems include pumps, heat exchangers, air bleed valves, pressure release valves, and expansion tanks. Heat exchangers in solar systems are selected based on economic criteria. The best trade-off of energy delivery increase with increasing heat-exchanger size usually results from use of an exchanger with effectiveness in the range of 0.6–0.8. Counterflow heat exchangers are required for this level of effectiveness.

Achievement of the required effectiveness level may dictate fairly high flow rates in the storage tank side of the collector heat exchanger. Flows up to twice that in the collector side can improve exchanger performance significantly in many cases. Since the storage side loop is physically short and has a small pressure drop, increased flow in this loop increases pump energy requirements by a negligible amount. Typical solar heat-exchanger sizes range from 0.05 to 0.10 m² of heat-exchanger surface per square meter of net collector area.

In hydronic heating systems, it is essential that all air be pumped from the system. To facilitate this process, air bleed valves located at the high points in a system are used. These are opened during system fill and later if air should collect. Air bleeds are required at points of low velocity in piping systems where air may collect because the local fluid velocity is too low for entrainment.

Control strategies and hardware used in current solar system designs are quite simple and are similar in several respects to those used in conventional systems. The single fundamental difference lies in the requirement for differential temperature measurement instead of simple temperature sensing. In the space heating system shown in Figure 14.16, two temperature signals determine which of three modes is used. The signals used are the collector-storage differential and room temperature. The collector-storage difference is sensed by two thermistors or thermocouples, the difference being determined by a solid-state comparator, which is a part of the control device. Room temperature is sensed by a conventional dual-contact thermostat.

The control system operates as follows. If the first room thermostat contact closes, the mode selector valve and distribution pump are activated in an attempt to deliver the

thermal demand from solar-thermal storage. If room temperature continues to drop, indicating inadequate solar availability, the mode selector diverts flow through the backup system instead of the solar system, and the backup is activated until the load is satisfied.

The collector-storage control subsystem operates independently of the heating subsystem described above. If collector temperature, usually sensed by a thermistor thermally bonded to the absorber plate, exceeds the temperature in the bottom of the storage tank by 5°C – 10°C (9°F – 18°F), the collector pump and heat-exchanger pump (if present) are activated and continue to run until the collector and storage temperature are within about 1°C – 2°C (2°F – 4°F) of each other. At this point, it is no longer worthwhile to attempt to collect energy, and the pumps are turned off. The collector-storage subsystem also has a high-temperature cutout that turns the collector loop pump off when the storage temperature exceeds a set limit.

A heating load device transfers heat from the solar storage to the air in the space. Therefore, a liquid-to-air heat exchanger is sized based on the energy demand of a building. Several generic types of load devices are in common use:

1. Forced-air systems—tube-and-fin coil located in the main distribution duct of a building or zone of a building (see [Figure 14.17](#)).
2. Baseboard convection systems—tube-and-fin coils located near the floor on external walls. These operate by natural convection from the convectors to the room air.
3. Heated floors or ceilings—water coils. These transfer heat to large thermal masses that in turn radiate or convect into the space. This heating method is usually called radiant heating.

Each load device requires fluid at a different temperature in order to operate under design load conditions, as shown in [Figure 14.18](#). Since baseboard heaters are small in heat-transfer area and rely on the relatively ineffectual mechanism of natural convection, they require the highest fluid temperature. Forced-air systems involve the more efficient forced-convection heat-transfer mode and, hence, are operable at lower fluid temperatures (see [Figure 14.18](#)). Radiant heating can use very large heat-transfer areas and is, therefore, operable at relatively low temperatures.

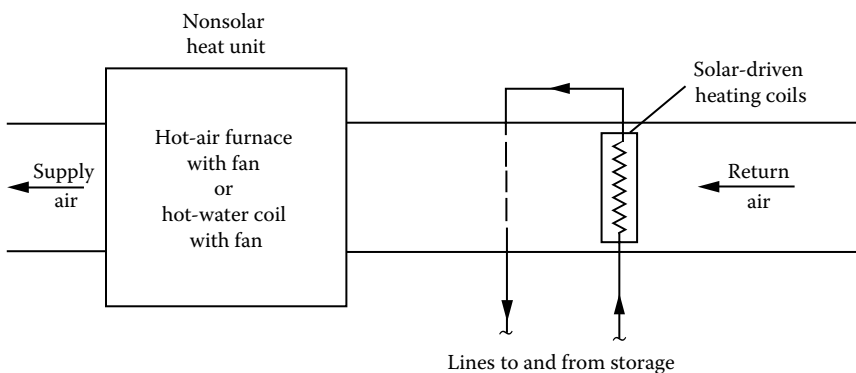
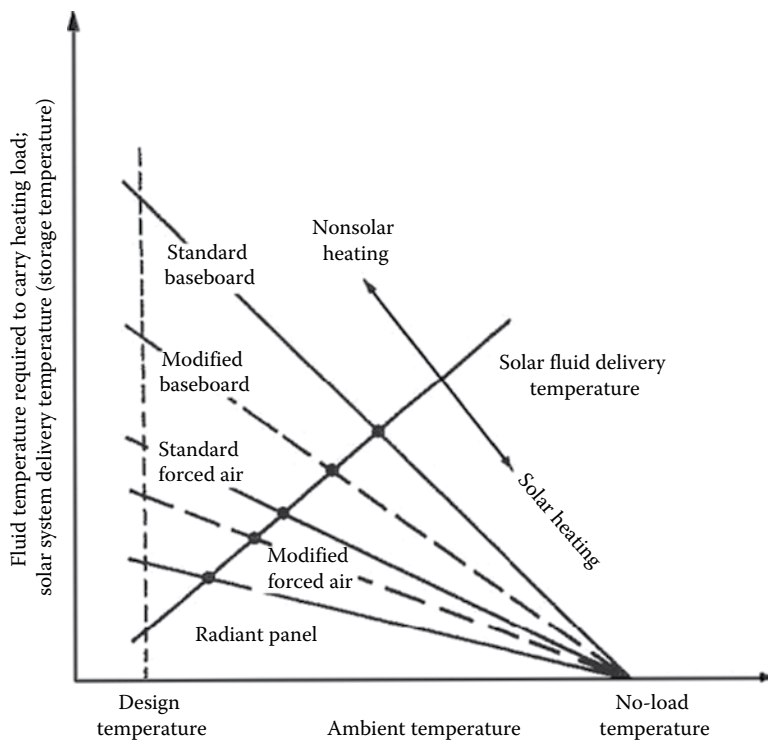


FIGURE 14.17

Forced-air heating system load device location upstream of nonsolar heat exchanger or furnace.

**FIGURE 14.18**

Heating load diagram for baseboard, forced-air, and radiant systems. Modified baseboard and forced-air systems are oversized in order to carry heating demands at lower temperature. Balance points are indicated by large dots at intersections.

In [Figure 14.18](#), the intersection of the solar fluid temperature line and the load line for a specific configuration is called the *balance point*. At ambient temperatures below the balance point, solar energy cannot provide the entire demand, and some backup is required; above the balance point solar capacity is sufficient to carry the entire load. Note that the load lines are specific to a given building. The solar fluid temperature line is not fixed for a building but depends on solar collector and storage size as well as local solar radiation levels. The line shown in [Figure 14.18](#) is, therefore, an average line.

It is possible to modify load devices to lower the balance point, as shown in [Figure 14.18](#). For example, a forced-air tube-and-fin exchanger can be enlarged by adding one or more additional rows of tubes. This increased heat-transfer area will permit the same energy delivery at a lower fluid temperature. The law of diminishing returns is evident as increasing effectiveness returns progressively less energy.

14.8 Virtual Storage in the Electric Transmission Grid

Although it is generally recognized that solar and wind resources in the United States greatly exceed the electricity demand in the country, the variability of wind and solar irradiation is an obstacle to employing these abundant energy resources. However, energy

storage and load matching to offset the variability of wind and solar resources can be used to address this obstacle. If there were an adequate electric distribution and transmission network, it would be possible to transmit excess energy generated by wind and/or solar in one part of the country to another part where the renewable resources cannot meet the load. This potential of using the grid for combined energy transmission/storage is called *virtual storage capacity*. It was analyzed in a seminal paper entitled “Renewable Energy Load Matching for Continental U.S.” by Short and Diakov [20]. Their analysis was somewhat idealized, in that it did not consider transmission constraints, economics, and siting issues, and selected sites only on the basis of their ability to contribute energy and electric capacity. More recent studies have analyzed the problem in more detail. For example, MacDonald et al. [21] examine cost-constrained optimal renewables penetration across the United States in scenarios without additional physical storage but including the build-out of high-voltage direct current (HVDC) transmission lines. We present Short and Diakov’s analysis and results here as it provides a relatively simple introduction to the concept and indicates the potential of this virtual storage technology.

Short and Diakov used two different models; one was based on a quadratic objective function and the other was a linear program with the constraint that the load was met [20]. For the latter approach, wind and solar sites were selected by the model to minimize the dispatchable generation (G_t) along with curtailment (C_t) of excess wind and solar generation and round-trip losses in a pumped hydro-storage system. These losses were taken as the difference between electric input to storage and the electricity removed from storage as determined by the round-trip efficiency (eff). Curtailments of wind and solar output occur when the energy production exceeds the local demand at any given time, as for example by wind turbines late at night when winds are high and loads are low. The optimization criteria of the model asked that the sum of the power from conventional sources plus the curtailment from solar and wind plus the storage energy losses be minimized every hour. In equation form, the objective function

$$\sum_t [G_t + C_t + (1 - eff) * Sch_t] \quad (14.26)$$

is to be minimized and subject to the following five conditions:

$$l_t + C_t = \sum_i W_i * w_{it} + \sum_j P_j * p_{jt} + G_t + (Sdc_t - Sch_t) \quad \text{for all } t \quad (14.27)$$

$$Sdc_t \leq sCAP \quad \text{for all } t \quad (14.28)$$

$$Sch_t \leq sCAP \quad \text{for all } t \quad (14.29)$$

$$0 \leq E_0 + \sum_{t' < t} [eff * Sch_{t'} - Sdc_{t'}] \leq sRES \quad \text{for all } t \quad (14.30)$$

$$eff * \sum_t Sch_t = \sum_t Sdc_t \quad (14.31)$$

where $sCAP$ is the storage charge and discharge rate cap, $sRES$ is the storage reservoir size, Sdc_t is the energy delivered from storage, Sch_t is the energy used to charge storage at

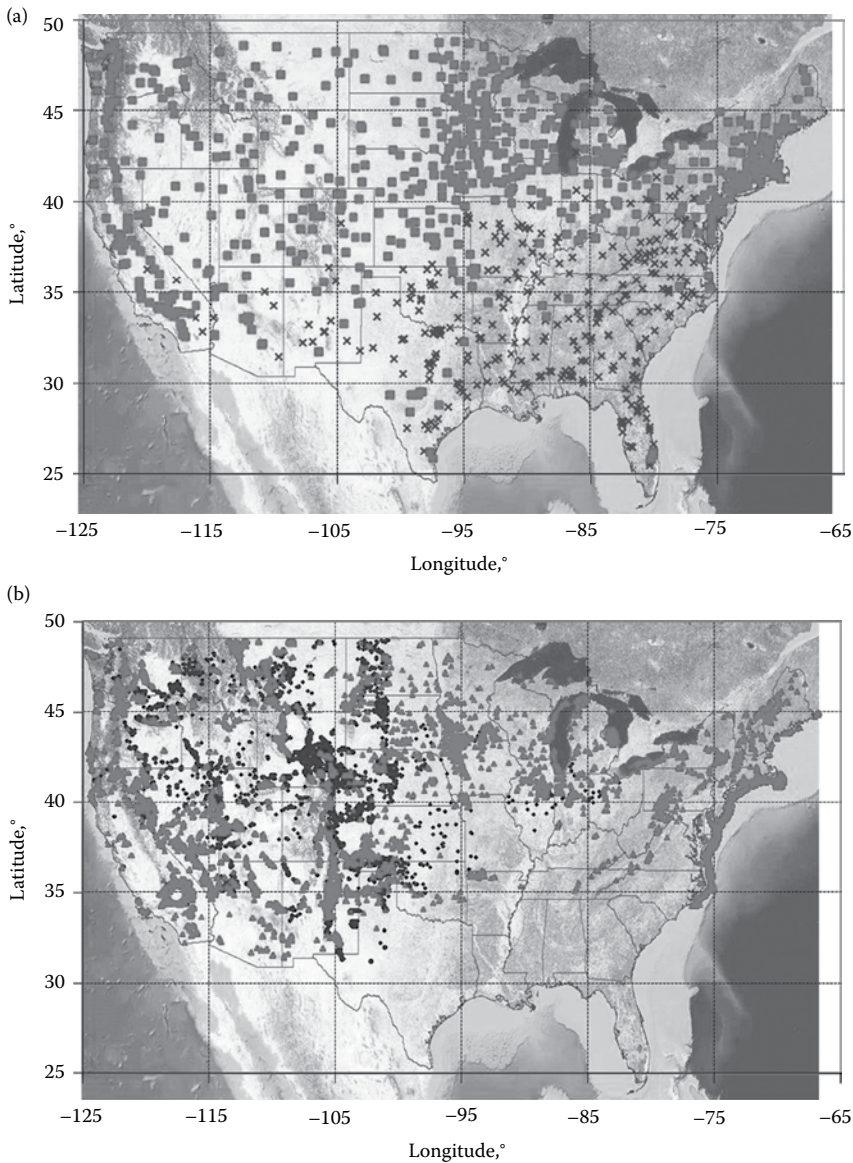


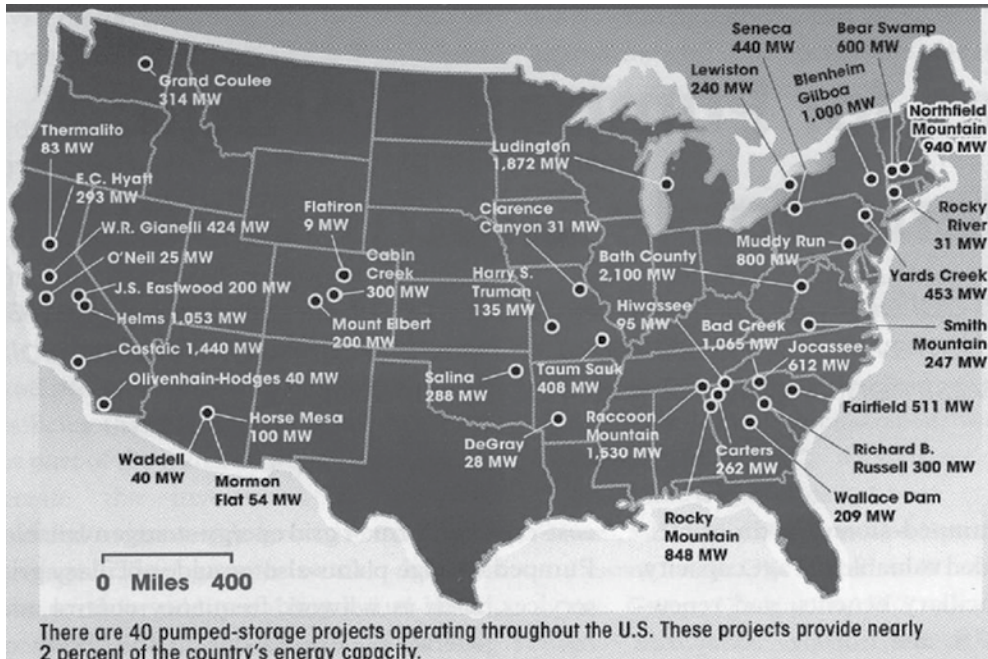
FIGURE 14.19

Optimum locations for (a) PV and (b) wind to provide 80% of electric load in the United States. The symbol “x” in (a) and the darkest dots in (b) indicate sites that were available within the model but not selected. (Courtesy of Victor Diakov, NREL.)

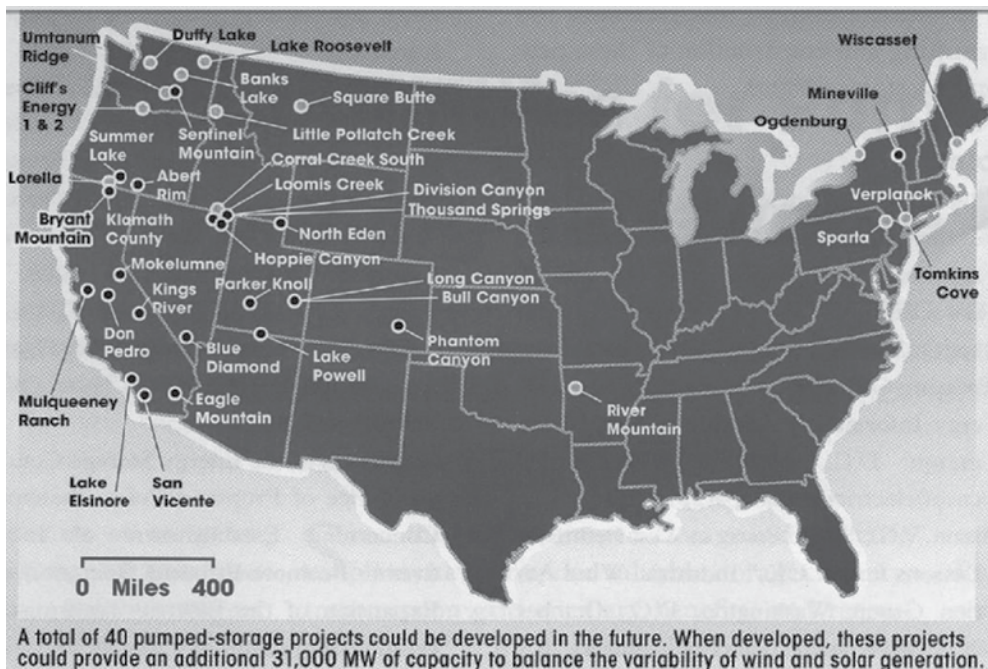
time t , W_i is the action of the maximum potential built capacity at wind site i , w_{it} is the input generation that could be produced at hour t by wind resource at site i , P_j is the fraction of the maximum potential built capacity at the PV site j , and p_{jt} is the input generation that could be produced at hour t by the PV resource at site j .

Using wind and PV data from [22–24], the model assumed that any of these renewable resources could be utilized at full or fractional capacity and the model selected the optimal resource set to match the electric load as close as possible. But recognizing that wind and

(a)



(b)

**FIGURE 14.20**

(a) Locations of existing pumped storage sites. (b) Locations of potentially available pumped storage sites. (Prepared by MWH for the USACE HDC, August 2009.)

PV are variable and alone cannot meet all the load, the model asked what the maximum fraction was that wind and PV could meet with the support of some dispatchable generation from storage or gas turbines. The results of this analysis showed that, without any storage and no curtailment ($C_t = Sch_t = 0$ for all t), wind and PV can meet up to 50% of loads in the Western United States. For the no-storage case, it is beneficial to build more wind than PV because PV cannot meet any of the load after sundown. However, when storage is available and curtailments are allowed, the optimal mix has about 75% as much PV capacity as the wind, with the PV energy contributing 32% of the electricity produced from wind. Assuming that the current hydro pumped storage capacity can be doubled to 40 GW, as much as 83% of the load can be met with wind and PV sources according to the model. This compares to an energy availability factor for nuclear power plants of 81% in 2010 according to the International Atomic Energy Agency [25]. At the same time, there are locations and times when PV and/or wind produce more energy than can be used or stored and production must be curtailed. However, according to the model, less than 10% of the renewable energy potential through the year has to be curtailed, that is, dissipated because there is no suitable load, but that percentage can be reduced by increasing the pumped storage capacity or adding compressed air storage when natural gas or a biogas source is available. A big advantage of the PV/wind combination over any fossil or nuclear scenario is that the generation facilities require virtually no water. This analysis shows that solar and wind can contribute close to a base-load generation electric system provided a robust transmission system was available. Figure 14.19 shows the renewable source locations for the high (83%) load matching scenario and Figure 14.20 shows the locations of existing and potentially available pumped storage sites.

In a follow-up paper, Short and Diakov found that without energy storage, but with curtailment of the renewable sources incorporated, then 80% of the peak load in the Western United States could be met and only 20% would have to be provided from storage and/or dispatchables such as natural gas turbines [26]. These results show that with a robust and efficient electric transmission system, renewable wind and PV could go a long way toward meeting base-load requirements with relatively little additional dispatchable generation.

PROBLEMS

- 14.1 A hydrogen/oxygen fuel cell stack produces 100 kW of DC power at an efficiency of 60% with water vapor as the product. Determine the hydrogen mass flow rate in g/s and the required cell voltage.
- 14.2 Derive an expression for the electric energy generation per unit of air volume stored in a cavity for a CAES system. Assume that there are two expansion stages and express the work output as the sum of the output from the two stages. The system operates with a constant cavern pressure, such as a hard rock cavern with a hydraulic compensation.
- 14.3 Supposing you own some land next to a 50 MW wind farm located on Colorado's Front Range. Your land has a fantastic cliff/ridgeline with an elevation difference of 250 m. As an opportunist, you decide to evaluate whether or not you can make money by building an energy storage system on your land that interfaces with the wind farm. Your plan is to capture excess energy from the wind farm or buy energy from the wind farm when electricity prices are low, and sell that energy back to the grid when electricity prices are high (assume that the utility that owns the grid will grant you a fair contract). You find that a good power rating

for your storage system is 50% of the rated wind farm output, or 25 MW. Also, your storage system should be able to generate electricity at rated power for 8 h.

The first step in this problem is to evaluate the technical design of candidate energy storage systems

- a. Pumped hydroelectric. Determine the flow rate and reservoir size needed to accomplish the required power output and energy capacity. Pumped hydroelectric plants generally run at 80%–90% generating efficiency, depending on the size of the machinery. Suggest a reasonable surface area and depth for your two reservoirs. (Hey, wait! You like to fish and plan to stock one of your reservoirs with some northern pike. You cannot leave them high and dry when the plant cycles).
- b. Pulley and weight. You cannot kick the feeling that a simpler energy storage system is possible. What if you use a weight and a pulley that stores energy as the weight is lifted (using an electric motor) and energy is released when the weight falls (with an electric generator). You need to dig a shaft. Find the value of weight you would use, and the depth and diameter of the shaft. Is this viable?
- c. Propose a new energy storage method. Be creative. Examples may be large springs, thermal storage, steam cycles, batteries, etc. Perform a simple analysis to size the system, and say whether or not your creative idea is viable.

The second step is to evaluate the financial aspects of installing and operating your energy storage system to determine whether you could make money.

- a. Pumped hydroelectric costs about \$500 per kW to install your turbomachinery and penstocks, plus \$2 per cubic yard to build reservoirs. Calculate the initial capital cost of your pumped hydroelectric system.
- b. You buy energy from the wind farm at \$0.035/kWh between the hours of 10:00 pm and 8:00 am to charge your storage, and sell energy between 1:00 pm and 9:00 pm back to the grid at \$0.1/kWh. Select a reasonable simple payback period that would motivate you to invest in energy storage. Calculate the maximum capital cost expenditure on your energy storage system that would allow this payback period.
- c. Would you decide to build an energy storage system? Why or why not?

- 14.4 It has been proposed that the United States should strive toward a hydrogen economy. At present, the United States uses about 100 quads (10^{17} Btu) of energy per year. Suppose that 10% should be produced with hydrogen fuel cells. The hydrogen is to be made by electrolysis of water in central stations located strategically. The electric power for electrolysis is to be supplied by nuclear power plants with a thermodynamic efficiency of 33% and a capacity factor of 0.90. Each plant should be of 500 MW capacity and operate on a simple Rankine cycle.

Estimate

- The number of plants required.
- The amount of cooling water needed for the condensers (assuming evaporative cooling—2400 kJ cooling for each liter of cooling water).
- The amount of water needed for electrolysis assuming 1500 kJ are used by the fuel cell (i.e., only 750 kJ of energy is provided to the end user for each liter of water fed into the process).

- The total initial capital investment (if the cost of a nuclear plant is estimated at \$6000 per kW and that of a fuel cell at \$2100 per kW).
 - Comment on the viability of using hydrogen as an energy carrier on a global scale/niche application.
- 14.5 a. Design a compressed air energy storage system for a wind turbine you analyzed previously. Assume that a cavity in an abandoned salt mine is available adjacent to the wind turbine. Use all the power above 5 kW to drive a compressor, which can compress ambient air. Assume that NG is available for heating the air entering the compressor.
- b. Repeat part 1, but assume that the wind turbine is located near a landfill where low Btu gas can be obtained for free. Compare this option with the design in part a, where the gas has to be purchased at \$5 per 1000 standard ft³.
- 14.6 Derive an expression for the linear battery model power output as a function of the internal-to-external resistance ratio. Nondimensionalize the power output by dividing it by E^2/R_i . Tabulate the dimensional power function with a spreadsheet and then plot it. At what point is the maximum nondimensional power achieved?
- 14.7 Design a battery electric storage system for a power plant with 20 MW peak power delivery for a duration of 4 h and estimate the minimum number of batteries and the current during peak operation. Assume that the plant will use 600 A/h batteries, operating at 400 V DC.
- 14.8 A hydrogen/oxygen fuel cell operates with a voltage of 0.7 V with water vapor production. Calculate the kW/h of work per kg-mol of hydrogen and determine the cell efficiency.
- 14.9 You are asked to estimate the amount of heat that can be stored overnight in a solar-heated building, which has a storage space of 6 m³. The solar system uses water with antifreeze in the collector and there are two options for storing the heat overnight. One option is to use water with an allowable temperature change of 30°C. The other is to use a Glauber salt, which undergoes a phase change at approximately 30°C with a heat of fusion of 329 kJ/L. In both instances, a heat exchanger will be necessary in order to meet building code. Discuss the advantages and disadvantages of the two options.
- 14.10 A neighborhood fuel cell power plant is to be designed for an electric power output of 2000 kW with liquid–water product. Estimate the flow rates of hydrogen and oxygen during peak power production, assuming an 80% efficient power conditioner is used to convert DC to AC power and the fuel cell efficiency is 55%. What is the plant heat rate?

References

1. Hammerschlag, R., Pratt, R., and Schaber, C.P., 2004. Energy storage, in: Kreith, F. and Goswami, D.Y., eds., *Handbook of Energy Efficiency and Renewable Energy*, CRC Press, Boca Raton, FL.
2. Tennessee Valley Authority. The mountaintop marvel, www.tva.gov/heritage/mountaintop/index.htm.

3. Levine, J.G., 2007. Pumped hydroelectric energy storage and spatial diversity of wind resources as methods of improving utilization of renewable energy sources, Thesis, University of Colorado, Boulder, CO.
4. Schoenung, S., Eyer, J.M., Iannucci, J.J., and Horgan, S.A., 1996. Energy storage for a competitive power market, *Annual Review of Energy and the Environment* 21, 347–370.
5. Kreith, F. and Krumdieck, S., 2014. *Principles of Sustainable Energy*, Second Edition, CRC Press, Boca Raton, FL.
6. Crotogino, F., Mohmeyer, K.-U., and Scharf, R., 2001. Huntorf CAES: More than 20 years of successful operation, in: Solution Mining Research Institute Meeting, Orlando, FL.
7. Van der Linden, S., December 2006. Bulk energy storage potential in the USA, Current developments and future prospects. *Energy* 31, 3446–3457.
8. Davis, L. and Schainker, R., 2006. Compressed air energy storage (CAES): Alabama electric cooperative McIntosh plant—Overview and operational history, in: *Electricity Storage Association Meeting 2006: Energy Storage in Action*, Energy Storage Association, Knoxville, TN.
9. Succar, S., September 2008. Baseload power production from wind turbine arrays coupled to compressed air energy storage, PhD thesis, Princeton University, Princeton, NJ.
10. EPRI-DOE, 2003. *Handbook of Energy Storage for Transmission and Distribution Applications*, EPRI/DOE, Palo Alto, CA/Washington, DC.
11. de Guilbert, A., 2009. Batteries and supercapacitors cells for the fully electric vehicle, Saft Groupe SA, Brussels, https://www.smart-systems-integration.org/public/electric-vehicle/battery-workshop-documents/presentations/Anne%20de%20Guibert%20Saft.pdf/at_download/file.
12. GP Batteries, 2000. *Lithium Ion Technical Handbook*, https://web.archive.org/web/20120323234351/http://www.gpbatteries.com/html/pdf/Li-ion_handbook.pdf.
13. Gupta, R.G., ed., 2008. *Hydrogen Fuel—Production, Transport, and Storage*, CRC Press, Boca Raton, FL.
14. Bossel, U. et al., 2003. *The Future of Hydrogen Economy: Bright or Bleak*, Oberrohrdorf, Switzerland.
15. Rabinwitz, M., 2000. Power systems of the future, Parts 1–3, *IEEE Power Engineering Review* 20(135), 5–16, 10–15, 21–24.
16. Kreith, F. and West, R.E., 2004. Fallacies of a hydrogen economy: A critical analysis of hydrogen production, *Journal of Energy Resources Technology* 126, 249.
17. Kreith, F. and Bohn, M.S., 2001. *Principles of Heat Transfer*, 7th ed., Brooks/Cole Pacific Grove, CA.
18. Wyman, C., Castle, J., and Kreith, F., 1980. A review of collector and energy storage technology for intermediate temperature applications, *Solar Energy* 24(6), 517–540.
19. Kreith, F., 1973. *Principles of Heat Transfer*, Intext, New York.
20. Short, W. and Diakov, V., November 2011. Renewable energy load matching for continental U.S., in: *Proceedings of the ASME 2011 International Mechanical Engineering Congress & Exposition*.
21. MacDonald, A.E., Clack, C.T.M., Alexander, A., Dunbar, A., Wilczak, J., and Xie, Y., 2016. Future cost-competitive electricity systems and their impact on US CO₂ emissions, *Nature Climate Change* 6, 526–531, DOI: 10.1038/NCLIMATE2921.
22. Potter, C.W., Lew, D., McCaa, J., Cheng, S., Eichelberger, S., and Gritmit, E., 2008. Creating the dataset for the western wind and solar integration study (U.S.A.), *Wind Engineering* 32(4), 325–338.
23. EnerNex Corp, February 2011. Eastern wind integration and transmission study, Subcontract report NREL/SR-5500-47-86.
24. Wilcox, S. et al., July 2007. Completing production of the updated National Solar Radiation Database for the United States, NREL Rep. CP-581-41511.
25. European Nuclear Society, May 2012. Nuclear power plants, world-wide, <http://www.euronuclear.org/info/encyclopedia/n/nuclear-power-plant-world-wide.htm>.
26. Short, W. and Diakov, V., 2012. Matching western U.S. electric consumption with wind and solar resources, *Wind Energy*, DOI: 10.1002/we.1513
27. Electricity Storage Association, 2003. Technology comparisons | Ratings, www.esa.org.



Taylor & Francis

Taylor & Francis Group

<http://taylorandfrancis.com>

15

Transportation

15.1 Introduction

A viable transportation system is a crucial part of a sustainable energy future. Sustainable transportation is a complex interdisciplinary topic, which really deserves a book (or books) unto itself. As Schiller et al. [1] have written in introducing their book, “sustainable transportation aims at promoting better and healthier ways of meeting individual and community needs while reducing the social and environmental impacts of current mobility practices.” They note that technical factors, such as improved vehicle efficiency or traffic flow management, are only part of the solution. Transportation and land-use planning, policy, economics, and citizen involvement are also critical dimensions. This chapter focuses on alternative motorized vehicle technologies and fuels used for personal mobility, as they are most closely tied to the other topics covered in this book. We provide only a brief introduction to the broader dimensions of sustainable transportation and suggest additional reading for interested readers.

Gasoline and diesel are not only very convenient fuels for ground transportation, but also have a high energy density that permits storage in a relatively small volume—an important asset for automobiles. For example, these liquid fuels have a volumetric specific energy content of about 10,000 kWh/m³, compared to hydrogen compressed to 700 bar at about 1300 kWh/m³. However, known petroleum resources worldwide are being consumed rapidly, and future availability of these resources is bound to decline. At present, more than 90% of the fuel used for ground transportation in the United States is petroleum-based, with about 5% from biofuel and the balance from natural gas and electricity [2]. The cost of gasoline is an ongoing concern to average citizens, and the emission from current transportation systems is a major component of CO₂ pollution that produces global warming.

For several decades, oil experts have offered numerous forecasts of the date when global oil production will reach a peak. [Figure 15.1](#) illustrates what those projections looked like around the turn of the twenty-first century, according to various estimates [3,4]. Since then, as discussed in [Chapter 6](#), new oil fields have been discovered and fracking has accessed additional oil in shale. Over the same time period, there has been increasing recognition of the need to limit future oil production and use, even before resources run out, in order to mitigate climate change and the environmental impacts of drilling in sensitive areas. Whether motivated by the finite nature of the oil resource or by environmental impacts of fossil fuel production and combustion, moving to a transportation system with reduced reliance on petroleum resources is an imperative for a sustainable energy future.

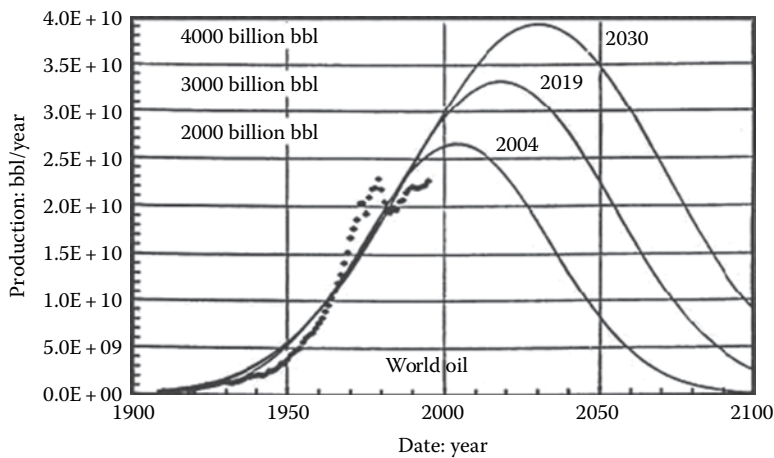


FIGURE 15.1

Oil production vs. time for various recoverable amounts of petroleum. (From Bartlett, A.A., 2000. *Mathematical Geology* 32(1), 1–17. With permission. [3])

15.2 Overview of Transportation Systems and Energy Use

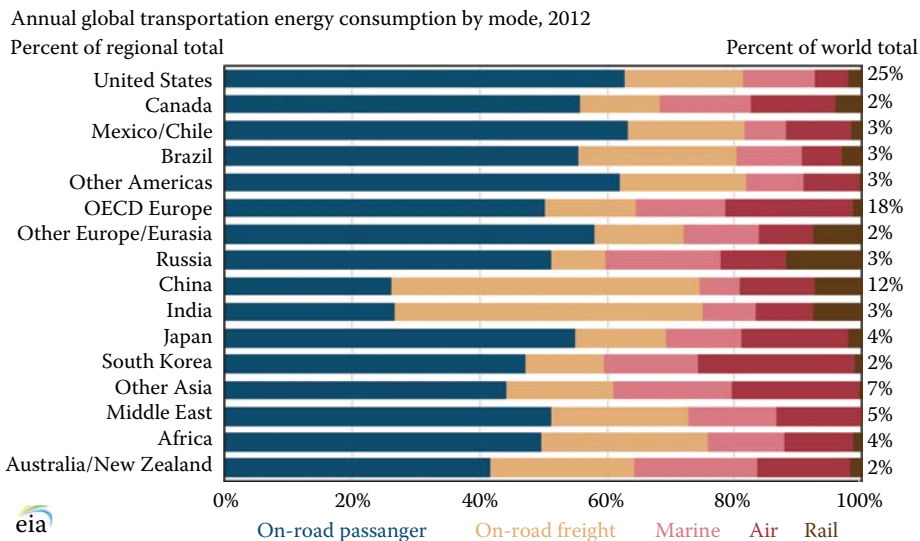
In the late 1990s, Canada's Centre for Sustainable Transportation adopted the following definition of a sustainable transportation system, which has been widely quoted [1]:

A sustainable transportation system is one that:

- Allows the basic access needs of individuals and societies to be met safely and in a manner consistent with human and ecosystem health, and with equity within and between generations.
- Is affordable, operates efficiently, offers choice of transport mode, and supports a vibrant economy.
- Limits emissions and waste within the planet's ability to absorb them, minimizes consumption of non-renewable resources, limits consumption of renewable resources to the sustainable yield level, reuses and recycles its components, and minimizes the use of land and the production of noise.

This definition highlights some of the factors of sustainability that go beyond efficient use of fuels and that are widespread problems with existing transportation systems:

- Need for equitable service to support basic access requirements (e.g., to get to grocery stores, schools, or places of employment) within cities or across countries.
- Noise and pollution associated with transportation facilities.
- Congestion and excessive time demands for meeting transportation needs.
- Safety risks of vehicle accidents.
- Large land footprint for roads, parking, airports, and supporting facilities.
- Disturbance of wildlife and ecosystems.

**FIGURE 15.2**

Transportation energy consumption by mode for countries or regions around the world. (Adapted from Energy Information Administration, November 19, 2015. *Today in energy: Passenger travel accounts for most of world transportation energy use*, www.eia.gov/todayinenergy/detail.cfm?id=23832. [5])

Transportation systems are comprised of the infrastructure, vehicles and equipment, and fuels needed to move goods and provide mobility to people. The requirements for transportation systems to provide personal mobility are closely linked to land-use and economic development patterns through two-way interactions. The form of urban development significantly affects transportation needs, while the transportation infrastructure plays a large role in shaping development patterns. Furthermore, economic growth and globalization have sharply increased freight transport over recent decades, including transport by pipeline, truck, rail, and ship. The relatively low market cost of long-distance shipping and international disparities in production costs have led to remarkably complex and far reaching supply chains for many products [1].

Figure 15.2 shows transportation energy consumption by mode, separated by country or region [5]. Global energy use for transportation totaled just over 100 quadrillion Btu (~100 EJ) of energy in 2012, with about two-thirds of the total used for passenger travel [5]. The United States accounts for about 25% of world energy demand for transportation. In the United States, more than 60% of transportation energy is used for on-road passenger travel. In contrast, the bulk of China's energy demand for transportation is used to move freight [5]. Per capita energy use for transportation differs widely around the world, with consumption rates in North America exceeding those in Africa by more than a factor of ten. In the United States, in 2013, there were more than 800 vehicles for every 1000 people, compared to 590 in Western Europe and 35 in Africa.

In the United States, energy use for highway transportation (including passenger vehicles and trucks for moving goods) almost doubled from 15.4 quadrillion Btu in 1970 to 29 quads in 2007, then declined to 26.2 quadrillion Btu in 2013 [6]. In 2013, there were nearly 220 million personal cars and trucks in the United States. These vehicles were cumulatively driven over 2.4 trillion miles, consuming 13.6 quadrillion Btu of energy [6]. In 2013, the average daily commute time in the United States was 25.5 minutes [6].

On the freight side, more than 11 billion tons of freight were shipped in the United States in 2013, with about 70% carried by truck, 14% by rail, 5% by water, and less than 0.1% by air. When distance is factored in to the statistics (expressed in terms of ton-miles or metric ton-kilometers), the fraction transported by rail increases to about 40%, as rail is more heavily used for longer distances. Average shipment distance within the United States was 630 miles (1010 km) in 2013, up from 472 miles (755 km) in 1997 [6]. Moving freight by truck across long distances is at least four times more energy-intensive than by rail. Innovative engineering solutions are needed for many of the complex infrastructure and policy issues associated with shifting more freight to rail [7].

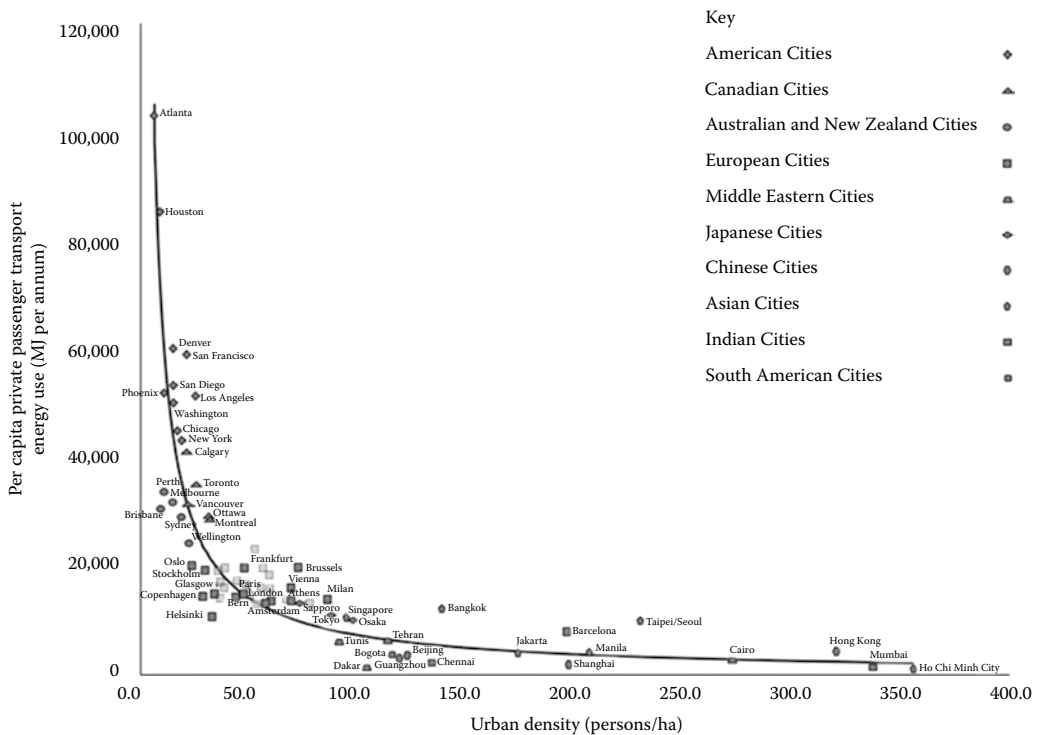
Over short time horizons, engineers and planners look to improving efficiency of vehicles and traffic patterns, modifying supply chains for freight, and adopting programs to shift passengers and freight to more efficient modes as mechanisms to reduce energy and environmental impacts of transportation. Longer planning horizons offer the possibility of greater improvements in vehicle efficiency, introduction of alternative fuels and vehicle technologies, and the potential for restructuring urban development and transportation infrastructure to reduce travel demand.

Mass transportation offers the potential to reduce the total energy consumption for the transportation sector. However, with current occupancy rates, the U.S.-average energy intensity of transit buses and rail, that is, the energy spent per passenger mile traveled, is similar to the energy intensity of automobiles [6]. Transit energy efficiency is highly variable across the country, however. The per-passenger intensity of transit is highest for areas with low density, including metropolitan areas with urban sprawl, where it is difficult to reach outlying areas by a mass transit network. Light rail and other advanced transit developments are capital-intensive and must be carried out in a coordinated way with long-term planning of urban forms that integrate high density and high-intensity developments along the transit corridors.

In the 1980s, Newman and Kenworthy demonstrated the exponential relationship between energy consumption for personal transportation and residential density of cities. These researchers have continued to update their analysis with data from around the world and continue to see the same general trend, as shown in [Figure 15.3](#) [8]. Among the cities surveyed, urban densities range from less than 10 people per hectare in Atlanta and Houston to more than 300 people per hectare in Hong Kong and Mumbai. Corresponding energy use for transportation ranges from more than 100,000 MJ per person per year in Atlanta to less than 5000 MJ per person-year in Hong Kong. Greater urban density and mixed-use development can shorten required travel distances for work, school and shopping, thus promoting walking and bicycling. Higher urban densities can also facilitate the provision and use of faster and more efficient modes of public transit.

Availability and use of public transit also vary widely in cities around the world. Of the 44 cities surveyed by Newman and Kenworthy [8], Prague was the leader in the rate of public transit use with more than 5000 passenger-kilometers per person during 2005–2006. For comparison, that same year, New York City's rate of transit usage was about 1400 passenger-km per person, and Chicago's was about 750 passenger-km per person. In addition to high residential density, high rates of transit use are promoted by having concentrated employment opportunities, limited and expensive parking, and transit systems that compete with private vehicles in terms of shortening commute times. A variety of rapid transit technologies have emerged in recent years, including advanced rail, tramway, and bus rapid transit. Having reserved or restricted right-of-way for these systems is critical for their ability to successfully compete for ridership.

Personal transport accomplished via walking or cycling is conventionally measured in terms of the number or fraction of trips made, rather than their total distance. In their 44-city

**FIGURE 15.3**

Car use per capita reflected in annual energy use, versus urban density. Data are for 1995. (Reproduced from Newman, P., and Kenworthy, J., 2015. *The End of Automobile Dependence: How Cities are Moving Beyond Car-Based Planning*, Island Press, Washington, DC. With permission. [8])

survey, Newman and Kenworthy [8] report that Zurich is the leader in non-motorized travel, with 52% of daily trips taken by non-motorized modes. New York City leads among the U.S. cities surveyed, with 22% of trips via bicycle or walking. Copenhagen is widely recognized as one of the most bicycle-friendly cities in the world. Along with high density and mixed-use development, cities can encourage commuting by bicycle by providing separated bikeways; through bicycle-friendly management of motorized traffic, including signalization and speed control; integrating bicycling with public transit; and providing for adequate bicycle parking.

While the trend toward promoting non-motorized travel is growing, U.S. Census surveys indicate that on average across the United States, progress has been slow in shifting work trips out of private vehicles (Table 15.1 [6]). Working at home and bicycling have increased since 1990, but the percentages of commuters who carpool or walk to work have declined [6].

15.3 Well-to-Wheels Analysis

Vehicle technology is changing rapidly, with new engine and drivetrain configurations, fuels, energy storage systems, and hybrid configurations coming into the market and more advanced designs on display at auto shows. Rather than simply looking at the efficiency of an engine or a given fuel, a more comprehensive way to determine overall efficiency when

TABLE 15.1

Means of Transportation to Work in the United States

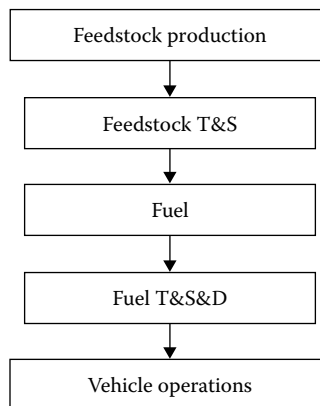
	1990 Millions of Workers (%)	2013 Millions of Workers (%)
Private Vehicle Total	99.6 (86.5)	120.4 (86.1)
Alone	84.2 (73.2)	106.7 (76.3)
Car Pool	15.4 (13.4)	13.6 (9.8)
Public Transportation	6.1 (5.3)	7.2 (5.1)
Walking	4.5 (3.9)	3.9 (2.8)
Bicycling	0.47 (0.4)	0.80 (0.6)
Work at Home	3.4 (3.0)	6.0 (4.3)
Total Workers	115.1 (100)	139.8 (100)

Source: Davis, S.C., Diegel, S.W., Boundy, R.G., 2015. *Transportation Energy Data Book*, Ed. 34, ORNL-6991, Oak Ridge National Laboratory, Oak Ridge, TN. [6]

Note: Data for 1990 from the U.S. Bureau of the Census. Data for 2013 from the 2009–2013 American Community Survey, U.S. Bureau of the Census.

evaluating the potential of any new fuel for ground transportation is to use what is called a *well-to-wheels analysis*. The approach to a well-to-wheels analysis, which is a subset of life cycle assessment (LCA), is shown schematically in Figure 15.4 [9,10]. The well-to-wheels approach for a fuel cycle includes several sequential steps: feedstock production; feedstock transportation and storage; fuel production; transportation, storage, and distribution of fuel; and finally vehicle operation. This approach is essential for a fair comparison of different options because each step entails losses. For example, whereas a fuel cell has a much higher efficiency than an internal combustion (IC) engine, it depends for its operation on a supply of hydrogen, which must be produced by several steps from other sources. Moreover, there is no widespread infrastructure for transporting and storing hydrogen, and this step in the overall well-to-wheels analysis has large losses and contributes to much larger energy requirements compared to a gasoline or electrically-driven vehicle.

Argonne National Laboratory's GREET (Greenhouse Gases, Regulated Emissions, and Energy Use in Transportation) model is a publicly available spreadsheet-based tool that enables users to perform their own life cycle assessments of various vehicle and fuel

**FIGURE 15.4**

Steps in a well-to-wheel analysis for ground transportation vehicles.

combinations [11]. GREET includes a well-to-wheels fuel cycle model in addition to a vehicle cycle model that extends through the vehicle's end-of-life material recovery or disposal. Impacts that can be estimated using GREET include energy use, greenhouse gases, other air pollutant emissions, and water use. The well-to-wheels model has recently been extended to cover heavy-duty vehicles [12]. The model can be downloaded for free from the ANL website at www.greet.es.anl.gov.

Figure 15.5 presents recent results from the GREET model, showing cradle-to-grave greenhouse gas emissions estimates for a range of vehicle technology and fuel combinations [13]. Estimates are shown for midsize passenger vehicles and include both well-to-wheels fuel cycle emissions and vehicle production cycle emissions. Solid black lines at the top represent current emissions; lines midway down show emissions that can be achieved by efficiency improvements that apply across vehicle types, including reducing weight and improving powertrain efficiency. The arrows and corresponding lowest bars show reductions that might be achievable in the next 10 to 15 years through the use of biofuels and low-carbon electricity. The results of the GREET analysis suggest that crosscutting efficiency improvements could reduce emissions from diesel and gasoline ICE by roughly 20%. Combining these crosscutting improvements with renewable H₂ or electricity generation could lead to fuel cell electric vehicles (FCEV) and battery electric vehicles (BEV) with cradle-to-grave emissions of 50 g CO₂e per mile, which is about 10% of the emissions from current gasoline vehicles.

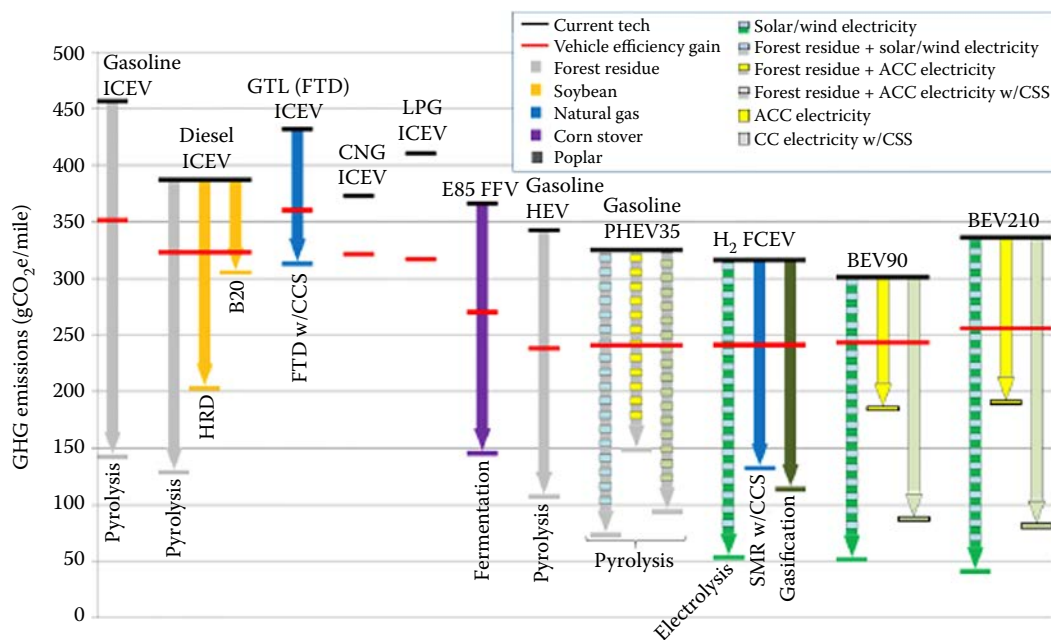


FIGURE 15.5

Potential cradle-to-grave greenhouse gas reductions. (ICEV = internal combustion engine vehicle; FFV = flexible fuel vehicle; HEV = hybrid electric vehicle; PHEV = plug-in hybrid electric vehicle; FCEV = fuel cell vehicle; BEV = battery electric vehicle; HRD = hydroprocessed renewable diesel; B20 = 20% biodiesel; GTL-FTD = gas-to-liquid Fischer-Tropsch diesel; SMR = steam methane reforming; ACC = advanced combined cycle) (Adapted from Elgowainy, A. et al., 2016. Cradle-to-grave lifecycle analysis of U.S. light duty vehicle-fuel pathways: a greenhouse gas emissions and economic assessment of current (2015) and future (2025–2030) technologies, ANL/ESD-16/7, Energy Systems Division, Argonne National Laboratory, U.S. Department of Energy. [13])

15.4 Biofuels

Alternative fuels available to supplement oil are shown together with their feedstocks in [Table 15.2](#) [14]. Inspection of the table shows that biodiesel, electricity, ethanol, and hydrogen (via electricity) are among the fuels potentially independent of a fossil fuel resource such as oil or natural gas. The potential of producing liquid fuel from biomass has been treated in [Chapter 9](#). There is yet no firm engineering picture of how biomass could provide a substantial part of the future transportation fuel, particularly because new conversion processes would be needed such as ethanol produced from switch grass, corn stover or other cellulosic materials, or diesel from algae. The reason for this is that ethanol produced by traditional methods from corn kernels has only an energy return on energy invested (EROI) on the order of 1.25, whereas the EROI for cellulosic ethanol is somewhere between 1 and 6 [15]. Diesel from algae may be even better. However, even cellulosic ethanol might not be able to replace oil, because growing it requires a large land area and the production of large amounts of ethanol could compete with food production.

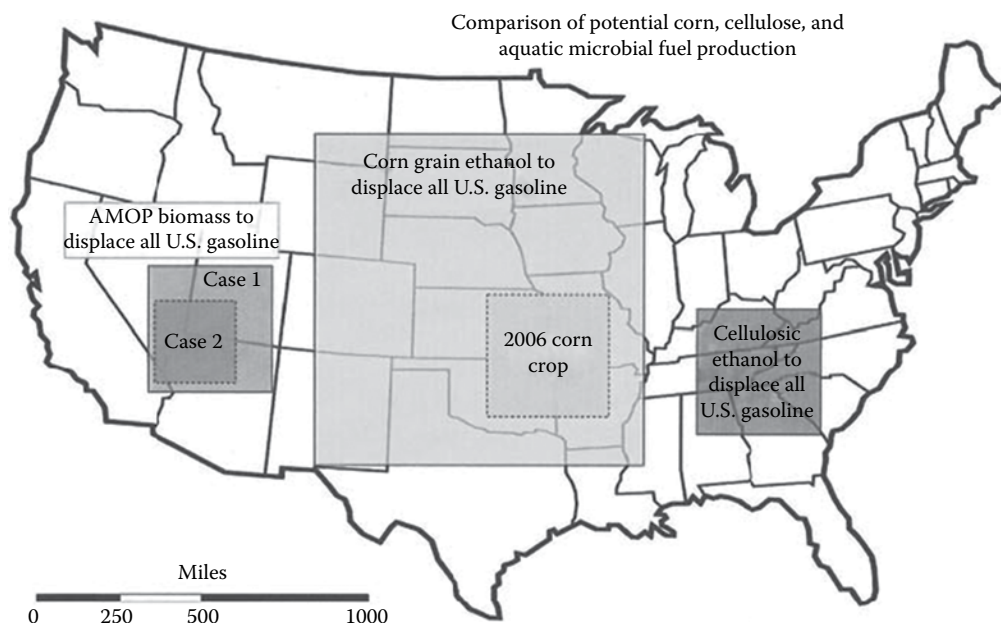
It has been proposed [16] to use biofuels derived from aquatic microbial oxygenic photoautotrophs (AMOPs), including algae, cyanobacteria, and diatoms. Dismukes et al. [16] have shown that AMOPs are inherently more efficient solar collectors, use less or no land, can be converted to liquid fuels using simpler technologies than cellulose, and offer secondary uses that fossil fuels do not provide. AMOPs have a 6- to 12-fold energy advantage over terrestrial plants because of their inherently higher solar energy conversion efficiency, which is claimed to be between 3% and 9%. [Figure 15.6](#) compares the area needed for three different biomass sources [16]. The data are for corn grain, switchgrass, mixed prairie grasses, and AMOPs. Each box superimposed on the map of the United States represents the area needed to produce a sufficient amount of biomass to generate enough liquid fuel to displace all the gasoline used in the United States in the year 2007. The two boxes for AMOPs are for 30% and 70% conversion efficiency. The overall solar energy conversion to biofuels works out to about 0.05% for solar-to-ethanol from corn grain and roughly 0.5% from switchgrass-to-ethanol. Comparatively, this value is about 0.5%–1% for AMOPs-to-ethanol or biodiesel.

An even more favorable assessment for the potential of algae to produce biodiesel is presented in Christi [17]. According to this study, microalgae may be a source of biodiesel that has the potential to displace fossil fuel. According to Christi, microalgae grow extremely rapidly and are exceedingly rich in oil. Some microalgae double their biomass every day,

TABLE 15.2

Feedstocks for Alternative Fuels

Fuel	Feedstock
Propane (LPG)	Natural gas (NG), petroleum
Compressed NG	NG
Hydrogen	NG or (water + electricity)
FT diesel	NG, coal, or algae
Methanol (M85)	NG or coal
Ethanol (E85)	Corn, sugarcane, or cellulosic biomass
Electricity	NG, coal, uranium, or renewables

**FIGURE 15.6**

Relative land area requirement for various liquid fuel biosources. (From Dismukes, C. et al., 2008. *Current Opinions in Biotechnology* 19, 235–240. With permission. [16])

and the oil content of microalgae can exceed 80% by weight. Table 15.3 shows a comparison of some sources of biodiesel that could meet 50% of all of the transportation needs in the United States [17]. According to estimates, only a small percentage of U.S. cropping areas would be necessary to supply 50% of the entire transport fuel needs in the United States [17]. However, no full-scale commercial algae biodiesel production facility has been built and operated for a sufficient time to make reliable predictions regarding the future of algae for a sustainable transportation system.

TABLE 15.3

Comparison of Some Sources of Biodiesel

Crop	Oil Yield (L/ha)	Land Area Needed (Mha) ^a	Percent of Existing U.S. Cropping Area ^a
Corn	172	1540	846
Soybean	446	594	326
Canola	1,190	223	122
Oil palm	5,950	45	24
Microalgae ^b	136,900	2	1.1
Microalgae ^c	58,700	4.5	2.5

Source: From Christi, Y., 2007. *Biotechnology Advances* 25, 294–306. With permission. [17]

^a For meeting 50% of all transport fuel needs of the United States.

^b 70% oil (by weight) in biomass.

^c 30% oil (by weight) in biomass.

15.5 Hybrid Electric Vehicles

A proven approach to reducing dependence on petroleum fuel is to increase the fuel economy of motor vehicles. This can be achieved by reducing vehicle weight and rolling resistance, improving vehicle aerodynamics, using more efficient vehicle accessories, and improving drivetrain efficiency [18]. Hybrid electric vehicles (HEVs) that are already widely available on the market can offer significant fuel economy improvements, taking advantage of the improved battery technology that was discussed in [Chapter 14](#). As shown in [Figure 15.5](#), Argonne National Laboratory's recent assessment indicates that for comparable performance, HEV technology can reduce lifecycle GHG emissions by 25% compared to a conventional gasoline-powered vehicle [13].

An HEV is powered by the combination of a battery pack and electric motor—like that of an electric vehicle—and a power generation unit (PGU), which is normally an IC engine. Unlike electric vehicles, however, HEV batteries can be recharged by an onboard PGU, which can be fueled by existing fuel infrastructure.

HEVs can be configured in a parallel or a series design. The parallel design enables the HEV to be powered by both the PGU and the motor, either simultaneously or separately. The series design uses the PGU to generate electricity, which recharges the HEV battery pack and produces power via an electric motor. The key element of either design is that the battery pack, as well as the PGU, can be much smaller than those of a typical electric vehicle or a vehicle powered by an IC engine because the IC engine can be operated at its maximum efficiency nearly all the time.

Some currently available HEVs, such as the Toyota Prius, use a parallel power split configuration. As shown in [Figure 15.7](#), a parallel HEV has two propulsion paths: one from the PGU and one from the motor, while a computer controls the output of each. A parallel configuration HEV has a direct mechanical connection between the PGU and the wheels, as in a conventional vehicle, but also has an electric motor that can drive the wheels. For example, a parallel vehicle could use the electric motor for highway cruising and the power from the IC engine for accelerating. The power produced by the PGU also drives the generator, which in turn can charge the battery as needed. The system to transfer electricity

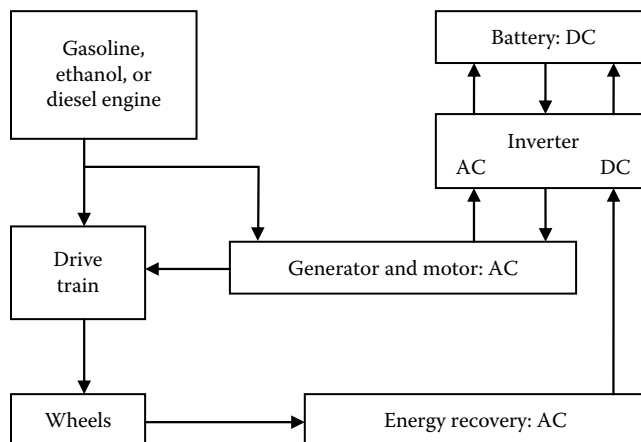


FIGURE 15.7
Schematic of a hybrid electric vehicle.

from the generator to the battery pack is exactly like that of an EV, with alternating current converted to direct current by the inverter. HEV parallel designs also use a regenerative braking feature that converts energy stored in the inertia of the moving vehicle into electric power during deceleration.

Energy savings and incremental costs of owning an HEV depend on many factors, such as the overall car design, cost of fuel, and the cost and efficiency of the batteries. Comparative vehicle costs are obscured in the retail market by differences in vehicle features, car manufacturers' pricing strategies, and government purchase incentives. Real-world fuel economy improvements depend on design tradeoffs, operating environment, and driving style. Given these confounding factors, modeling and simulation studies are useful in providing for more consistent comparisons, matching vehicle size, performance specifications, and accessory features while comparing different drive trains or fuels.

Argonne National Laboratories [13] compared costs as well as greenhouse gas emissions of current and future light duty vehicles with different drivetrain technology and fuel combinations. For a basic mid-size passenger car, they estimated that an HEV with 36.5 miles per gallon (mpg) fuel economy would cost about \$6000 more than an otherwise equivalent gasoline vehicle with fuel economy of 26.2 mpg. Accounting for an HEV's higher expected resale value, the net vehicle cost difference in present value terms is estimated to be about \$5000. Whether HEV fuel savings over time make up for the extra cost of the vehicle depends on the price of gasoline, the expected period of ownership, annual vehicle mileage, and the purchaser's discount rate. For a simple example comparison, we might assume that fuel costs \$2.50 per gallon, that the vehicle is to be driven 10,000 miles per year, that operating costs other than fuel are equal between the HEV and conventional gasoline vehicle, and that the purchaser's discount rate is 5%. Given the difference in fuel economy of the two vehicles, annual fuel savings with the HEV would be 108 gallons per year, or \$270 per year in fuel costs. The present value of the fuel savings over 10 years is calculated using the formula for the present value of an annuity (Equation 2.6), as:

$$NPV_{fuel} = \$270 \left\{ \frac{(1 + .05)^{10} - 1}{.05(1 + .05)^{10}} \right\} = \$2080 \quad (15.1)$$

Thus these fuel savings alone do not suffice to cover the added vehicle cost for the purchaser in this scenario. Of course, other factors come into play in purchasing cars, including styling, driving performance, and, for many HEV owners, the satisfaction they feel in driving a relatively efficient low emissions vehicle.

15.6 Plug-in Hybrid Electric Vehicles

The plug-in hybrid electric vehicles (PHEVs) that have recently become available in the market offer the advantage of even lower emissions, without requiring either new technology or new fuel distribution infrastructure. Like hybrids, PHEVs have a battery and an IC engine for power, but PHEVs have larger battery capacity and a plug-in charger with which the battery can be recharged whenever the car is parked near a 120 or 240 V outlet. The so-called PHEV40 can travel approximately the first 40 mi on grid-supplied electric

power when fully charged. When that charge is depleted, the gas or diesel motor kicks in and the vehicle operates like a conventional hybrid. Because most commuter trips are less than 40 mi, even in the United States, it is estimated that a PHEV could reduce gasoline usage by 50% or more for many drivers. Moreover, using electric energy is cheaper and cleaner than using gasoline in automobile-type ground transportation.

An important feature of PHEVs is that their batteries can be charged at night when utilities have excess power available. Utilities have taken notice of the potential energy charging and storage capabilities of PHEVs because off-peak charging would help utilities to use low-cost base load generation more fully. Furthermore, more advanced vehicle-to-grid (V2G) concepts would allow utilities to buy back energy from the batteries of vehicle owners during peak demand periods and thus make a fleet of PHEVs into a large, distributed storage-generation network. The arrangement would also enable renewable energy storage by charging PHEVs using solar- or wind-generated excess capacity. As mentioned in the chapter on energy storage, lithium-ion and lithium-polymer batteries have the potential to store large charges in a lightweight package, which would make the HEVs even more attractive than the technology that uses nickel-metal hydride (Ni-MH) batteries.

The efficiency of a PHEV depends on the number of miles the vehicle travels on liquid fuel and electricity, respectively, as well as on the efficiency of the prime movers according to the equation

$$\eta_{\text{PHEV}} = \frac{\text{Energy to wheels}}{\text{Energy from primary source}} = f_1\eta_1\eta_2 + f_2\eta_3\eta_4 \quad (15.2)$$

where

η_1 is the efficiency from the primary energy source to electricity

η_2 is the efficiency of transmitting energy to the wheels

f_1 is the fraction of energy supplied by electricity

f_2 is the fraction of energy supplied by fuel $= (1 - f_1)$

η_3 is the well-to-wheel efficiency

η_4 is the tank-to-wheel efficiency

PHEVs can be designed with different all-electric ranges. The range is commonly indicated by a number specifying the distance in miles that a PHEV can travel on batteries alone. Thus, a PHEV20 can travel 20 mi on fully charged batteries without using the gasoline engine. The Electric Power Research Institute (EPRI) [19] has estimated that on average, one-third of the annual mileage of a PHEV20 would be supplied by electricity and two-thirds by gasoline. The percentage depends, of course, on the vehicle design and the capacity of the batteries on the vehicle. A PHEV60 can travel 60 mi on batteries alone, and the percentage of electric miles will be greater as will be the battery capacity and weight. For comparison, Toyota's 2017 plug-in hybrid Prius Prime sold in the United States has a 22-mile all-electric range, while Chevrolet's 2017 Volt has a 53-mile all-electric range.

The Argonne study mentioned above estimated that a PHEV35 that gets 35 mpg in charge-sustaining (CS) mode and requires 342 Wh per mile of electricity in charge depleting (CD) mode would cost about \$17,000 more than an otherwise equivalent mid-size gasoline vehicle [13]. With advances in battery technology and expanded production experience, they anticipate the incremental cost could be cut in half over the next 10 to 15 years. A few thousand dollars of the up-front cost difference might be covered by the discounted difference in resale value. For a vehicle driven 5000 miles per year on \$0.10/kWh electricity

and 5000 miles per year on \$2.50/gallon gasoline, annual fuel costs would be about \$528 per year, about \$426 per year less than needed for the conventional gasoline vehicle. With a 5% discount rate the discounted fuel savings would amount to \$3290 over a 10-year vehicle life. As in the HEV case above, this is a simplified example, and actual costs of vehicle ownership will vary along with other factors that influence vehicle purchases. In the United States, federal and state tax credits and other incentives are available to spur PHEV adoption, with the intent of lowering manufacturing costs through increased production experience and economies of scale, and in order to reduce environmental externalities.

Another question to be asked in the utilization of PHEVs is whether or not the existing electricity system of the United States could handle the charging of the batteries in a PHEV-based ground transportation system. This question was answered by an analysis in Himelich and Kreith [20]. This analysis clearly showed that with a normal commuting scenario, which was based upon statistical information from a major city, if charging occurred during off-peak hours, no additional generating capacity or transmission requirements would be needed to charge a significant portion of the automotive fleet with PHEVs in the system, as illustrated in Figure 15.8. The analysis also showed that the off-peak charging scenario would also add to the profit of the electric utilities.

Another result of the analysis was that, although the amount of CO₂ emitted by the electric utility will increase from PHEV charging, if this is compared to the corresponding reduction in tailpipe emission to assess the overall environmental impact, the generation/PHEV transportation system would substantially decrease CO₂ emission even if the current mix of coal, nuclear, and renewable generation facilities were unchanged [20]. This result can be explained, however, because the average efficiency of the electric power system is on the order of 43%, whereas the average efficiency of IC engines is only on the order of 22%. Consequently, the net emission of CO₂ would be reduced by a hybrid system consisting of PHEVs and electric charging during off-peak hours. Moreover, the utility generation profile would be evened out, and this could also contribute to reducing CO₂ emissions, as well as the cost of producing electricity. Although not yet put into

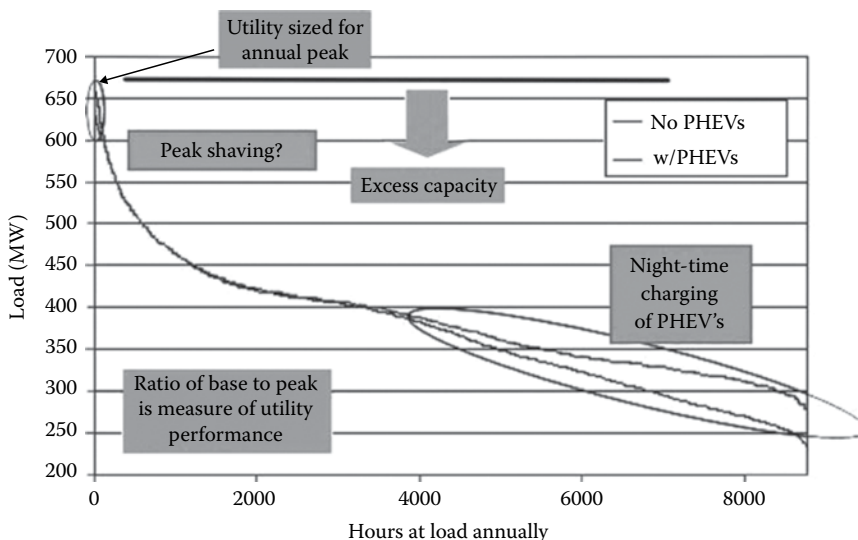


FIGURE 15.8

PHEV impact on utilities' load profile. (Courtesy of National Renewable Energy Laboratory, Golden, CO.)

practice, it is believed that the availability of electric storage in the batteries of a fleet of PHEVs could also be used to reduce the peak demand on electric utilities by utilizing the vehicle's batteries as a distributed storage system. Details of such an arrangement would have to be worked out by differential charges, incentives, and taxation arranged between utilities and owners of PHEVs.

A cautionary note in the expectation of future ground transportation systems, is that introducing new vehicle technology into the fleet takes time [21]. In a study of prospects for converting the U.S. vehicle fleet to advanced technology, Kreith and West [21] assumed a rate of new vehicle sales of 7% of the fleet per year and a retirement rate of 5% per year, resulting in a net increase in total vehicles of 2% per year. This increase was in accordance with historical rates of increase between 1966 and 2003. Based upon the existing mileage for IC engines, HEVs, and PHEVs, it was estimated that *even if all new cars were HEVs or PHEVs*, after 10 years, the annual gasoline savings as a percentage of the gasoline usage by an all-gasoline fleet in the same year would only be about 30% for the HEVs and 38% for the PHEVs. These relatively small reductions in the gasoline use are due to the fact that despite the introduction of more efficient vehicles, it takes time to replace the existing fleet of cars, and the positive effects will not be realized for some years.

15.7 Combining HEVs or PHEVs with Biofuels

In the previous section, we considered the prospect of using batteries combined with traditional engines to reduce the petroleum consumption in the transportation system. However, the scenario used for this analysis can also be extended to determine the combination of PHEVs with biofuels, particularly ethanol made from corn or cellulosic biomass. The example assessment that follows is similar to that done to create [Figure 15.5 \[13\]](#), but is simplified for teaching purposes.

A scenario for a sustainable transportation system based on fuel from biomass has been presented in [22]. In this analysis, the following four vehicle types combined with various fuel options have been considered. The expected mixture in an economy based largely on ethanol would be 85% ethanol and 15% gasoline (E85), which could be used in Flex Fuel automobiles. Currently, the United States is mostly using E10, a mixture of 90% gasoline and 10% ethanol, with ethanol produced from corn for pollution abatement. The fuel types compared in this analysis are gasoline only, E10 with ethanol made from either corn or cellulosic materials, and E85 with ethanol from either corn or cellulosic materials. The four vehicle combinations are a conventional SI engine, an HEV similar to the Toyota Prius, a PHEV20, and a PHEV30. The analysis was based upon average 2009 performance for the U.S. light vehicle fleet at approximately 20 mpg, for an HEV at 45 mpg, and for a PHEV20 at 65 mpg, according to [19]. For ethanol/gasoline-blended fuels, it was assumed that the gasoline and ethanol are utilized with the same efficiency. That is, the mileage per unit of fuel energy is the same for gasoline and ethanol.

Based on the earlier assumption, the following parameters were calculated:

1. The miles per gallon of fuel, including the gasoline used to make ethanol (mpg).
2. The petroleum required to drive a particular distance for a case vehicle as a percentage of the petroleum required to drive the same distance by a gasoline-fueled SI vehicle.

3. The carbon dioxide emission rate for case vehicles as a percentage of that for SI gasoline-only.

Based upon the earlier assumption, one can calculate the miles per gallon of fuel by the following equation:

Miles per gallon of fuel:

$$\begin{aligned} MF_{ij} &= (\text{mi/gal gas}) \\ &\times \left[(\text{gal gas/gal fuel}) + (1 - \text{gal gas/gal fuel}) \times \frac{(\text{energy, LHV/gal ethanol})}{(\text{LHV/gal gasoline})} \right] \\ &= MGO_i \times [FG_j + (1 - FG_j) \times (\text{LHV ratio})] \end{aligned} \quad (15.3)$$

where

MF_{ij} is the miles per gallon of fuel for vehicle type i and fuel type j

MGO_i is miles per gallon gasoline-only for vehicle i

FG_j is volume fraction of gasoline in fuel type

$(1 - FG_j)$ is the volume fraction of ethanol in fuel type j

the ratio of lower heating values (LHVs) is LHV ratio = $(\text{LHV/gal ethanol})/(\text{LHV/gal gasoline}) = 0.6625$

The index i indicates the vehicle type and the index j denotes the volume fraction of gasoline in an ethanol–gasoline blend as follows: for gasoline only, $FG_1 = 1$; for E10 (i.e., 10 vol% ethanol and 90 vol% gasoline), $FG_2 = 0.90$; and for E85 (85 vol% ethanol, 15 vol% gasoline), $FG_3 = 0.15$. Other ethanol concentrations could be used.

The miles per gallon of gasoline in the fuel, including the petroleum-based fuels used in the making of the ethanol in the fuel (by counting the energy of all petroleum-based fuels as gasoline), is given by

Miles per gallon of gasoline in fuel:

$$\begin{aligned} MG_{ijk} &= \frac{MF_{ij}}{[FG_j + (1 - FG_j) \times (0.6625) \times (\text{MJ gasoline used in making 1 gal ethanol}) / (\text{MJ/gal ethanol})]} \\ &= \frac{MF_{ij}}{FG_j + (1 - FG_j) \times (0.6625) \times R_k} \end{aligned} \quad (15.4)$$

where R_k denotes the gallons of gasoline used to make 1 gal of ethanol from process k . For corn-based ethanol ($k = 1$), $R_1 = 0.06$, while for cellulosic-based ethanol ($k = 2$), $R_2 = 0.08$, according to Farrell et al. [23].

15.7.1 Petroleum Requirement

The petroleum required to produce an ethanol–gasoline blend, including the petroleum used to make the ethanol, is expressed as a percentage of the petroleum required for the same miles traveled by the same vehicle type using gasoline-only. For a gasoline-only-fueled vehicle of any type, this percentage is 100%.

A general equation for the percentage petroleum requirement is

$$\text{Petroleum requirement, \%} = 100 \times \frac{(\text{MGO}_i)}{(\text{MG}_{ijk})} \quad (15.5)$$

15.7.2 Carbon Dioxide Emissions

The CO₂ emissions, including those from making the ethanol and generating the electricity used from the grid by the vehicle, are expressed as a percentage of the emissions produced by the same type of vehicle fueled by gasoline-only traveling the same number of miles.

$$\begin{aligned} &= 100 \times \left\{ [\text{FE}_m \times (\text{kWh}/\text{mi}) \times (\text{g-carbon}/\text{kWh})] + [(1/\text{MGO}_i) \times (1 - \text{FE}_m) \right. \\ &\quad \times [\text{FG}_j \times (\text{g-carbon}/\text{MJ gasoline}) \times (\text{MJ}/\text{gal gasoline})] + (1 - \text{FG}_j) [(\text{MJ}/\text{gal ethanol}) \\ &\quad \times (\text{g-carbon}/\text{MJ ethanol})] \left. \right\} / [(\text{g-carbon}/\text{MJ gasoline used}) \times (\text{MJ}/\text{gal gasoline}) / (\text{MGO}_i)] \end{aligned} \quad (15.6)$$

where FE_m is the fraction of the miles driven by electricity from the grid for a plug-in hybrid vehicle. For any non-PHEV, $m = 0$, and $\text{FE}_0 = 0$; for a PHEV20, $m = 1$, and $\text{FE}_1 = 0.327$ [19]; and for a PHEV30, $m = 2$, and $\text{FE}_2 = 0.50$ estimated by analogy with PHEV20.

According to Reference [19], the kWh/mi from the grid = 0.2853, the g-carbon emitted/kWh = 157 (146 average for all electricity generation [24] divided by 0.93, the average transmission efficiency), the g-carbon emitted/MJ gasoline = 94 [19], the MJ/gal gasoline = 121, and the MJ/gal ethanol = 80.2.

So,

$$\begin{aligned} \text{CO}_2 \text{ production as \% of that for a gasoline-only vehicle} &= 100 \times \{ \text{FE}_m \times (0.2853) \times (157) \\ &\quad + (1/\text{MF}_{ij}) \times (1 - \text{FE}_m) \times [\text{FG}_j \times (94) \times 121 + (1 - \text{FG}_j) \times \text{CE}_k \times (80.2)] \} / [(94) \times (121)/21] \end{aligned} \quad (15.7)$$

Where CE_k the g-carbon emitted/MJ ethanol, where for $k = 1$ (corn), $\text{CE}_1 = 87$, and for $k = 2$ (cellulosics), $\text{CE}_2 = 11$.

EXAMPLE 15.1

Calculate the CO₂ production ratio relative to an IC vehicle for a PHEV30, E85 vehicle using ethanol from cellulosic material.

Solution

The relevant variables are

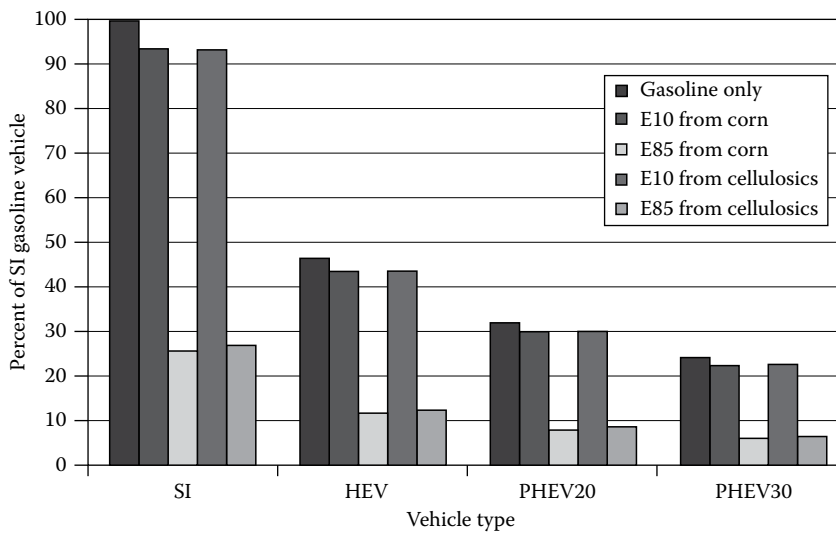
$$\text{FE}_m = 0.5$$

$$\text{MF}_{ij} = 85 \times (0.15 + 0.85 \times 0.6625) = 60.61$$

$$\text{CE}_k = 11$$

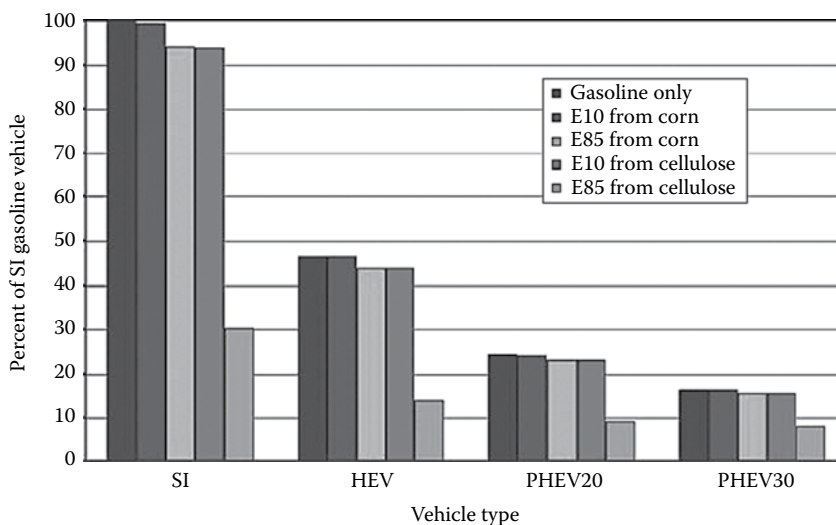
Using these parameters, the CO₂ production, as a % for that of gasoline-only vehicle is

$$\begin{aligned} &= 100 \times \{ (0.5 \times 0.2853 \times 157) + (1/60.61) \\ &\quad \times 0.5 [0.15 \times 94 \times 121 + 0.85 \times 11 \times 80.2] \} / (94 \times 121/21) \\ &= 4.13 + 2.60 + 1.14 = 7.87\% \end{aligned}$$

**FIGURE 15.9**

Petroleum requirement as a percentage of that for SI gasoline vehicle. (From Kreith, F., and West, R.E., 2006. *ASME Journal of Energy Resources Technology* 128(9), 236–243. With permission. [21])

Using the results of the earlier equation, the key conclusions of the analysis are shown in Figures 15.9 and 15.10. Figure 15.9 shows the gasoline requirement of any of the 20 cases considered as a percentage of that for an SI gasoline fleet [21]. It can be seen that the gasoline consumption for a PHEV20 using E10 is about 30% of that for the gasoline fleet, whereas it decreases to about 8.8% for a fuel consisting of 85% ethanol from cellulosic with 15% from gasoline (E85 cellulosic). The potential reduction in CO₂ emission shown in Figure 15.10 is equally impressive. The CO₂ emission of a PHEV20 with E85 cellulosic is only about 10% of that for the SI fleet. Since, at present, emission from automobile

**FIGURE 15.10**

Carbon dioxide emissions as a percentage of emissions for SI gasoline vehicle.

engines is responsible for almost one-third of the total CO₂ emissions of the country, it is apparent that with the existing technology, substantial reduction in CO₂ generation could be achieved by using PHEVs, particularly if the fuel were to be manufactured from cellulosic material.

15.8 Future All-Electric System

The next step in the development of a more sustainable transportation system could be widespread adoption of all-electric vehicles. All-electric cars were mandated in California about 30 years ago as part of an effort to reduce air pollution. Initially automakers embraced the idea, but it is likely that the acceptance by Detroit was the result of the mandate that required that at least 2% of all the cars sold in California by any one automaker had to be zero-emission vehicles. The only zero-emission vehicle available at the time was the electric car, and the mandate therefore required selling a certain number of all-electric vehicles. Battery technology at the time was not yet ready for commercialization, and in addition, there was little infrastructure available for charging vehicle batteries on the road. As a result, the mandate failed to achieve its objective, and as soon as the mandate was lifted, automakers ceased to make electric vehicles. In the meantime, however, battery technology has evolved to where one can envision an all-electric ground transportation system.

It is not currently possible to assess the future of electric vehicles. However, several all-electric vehicles are now on the market, and significant resources are being devoted to research into advanced batteries and other technologies to lower EV costs. In July 2009, President Barack Obama announced a program with \$2.4 billion in federal grants to develop next-generation vehicles and batteries in the United States. In Germany, one of the political party members proposed a €5000 (\$7050) subsidy for people who buy electric cars. In July 2009, Japan's Nissan Motor Company unveiled the LEAF, an electric car with a currently advertised range of up to 107 mi (170 km) on a single battery charge. It went into mass production for a global market in 2012. Mitsubishi Motor Company launched its own electric vehicle program in June 2009. Tesla Motors, Inc., introduced its all-electric Roadster in 2008, followed in 2012 by the Model S, a full-sized sedan with greater than a 200 mile range. *Forbes Magazine* has reported that nearly 190,000 electric or plug-in hybrid vehicles were sold in China in 2015, with production led by the Chinese manufacturer BYD Auto Co [25]. Chevrolet launched the 200-mile range BOLT for the 2017 model year, with a \$37,500 manufacturer's suggested retail price. Tesla Motors was to begin production of its 215-mile range Model 3 in 2017, with a base price of \$35,000. This summary is a snapshot at the time of preparing this text. However, developments in the EV arena are evolving quickly. The reader is encouraged to follow developments in the current literature, including via the websites in the Online Resources section. As shown in Figure 15.5, decarbonization of the electricity system is key to having EVs deliver very low life cycle GHG emissions.

15.9 Natural Gas as a Transportation Fuel

Several countries around the world make extensive use of natural gas as a transportation fuel. While natural gas vans, trucks, and buses are fairly common in the United States, the

fuel has received little attention from the U.S. automobile industry for use in passenger vehicles. In 2001, President George W. Bush proposed the Freedom CAR initiative to replace gasoline with hydrogen, which at that time was largely produced from natural gas. More than a billion dollars was provided for R&D as well as generous tax incentives. However, the efficiency of a natural gas/hydrogen vehicle based on a well-to-wheel analysis is less than that of hybrid SI/natural gas vehicle, and the construction of a hydrogen distribution system would be extremely expensive. Thus the hydrogen via natural gas effort for transportation was terminated in 2010. More recently, however, the increase in natural gas supplies created by advances in hydraulic fracturing and directional drilling technology in the United States has raised the question of whether natural gas itself should be more widely used as a transportation fuel.

Compressed natural gas (CNG) is viewed as a relatively inexpensive fuel for vehicle applications, requiring little modification to IC vehicle technology apart from the fuel tank and refueling system. CNG is especially advantageous for larger vehicles that can accommodate a larger and heavier fuel tank, and for high-mileage vehicles that can recover higher upfront costs through fuel cost savings. A basic infrastructure for distributing natural gas exists, and if CNG were to be used to fuel automobiles, the only major addition at gas stations that have a natural gas outlet would be a compressor to increase the gas pressure above that in the natural gas automobile tank.

Natural gas vehicles have been in use for trucks and other large vehicles in many parts of the world for some time, as shown in Table 15.4 [26]. In the United States, Honda offered a passenger-sized CNG car from 1998 to 2015, but ended production after the 2015 model year. The most recent model carried a CNG fuel tank with 7.8 gasoline gallon equivalents (gge) of storage at a pressure of 3,600 psi. The car has a range of 218 miles on a full tank of CNG based upon EPA mileage ratings. A 7.8 gge tank at 3,600 psi is equivalent to 30 gal in volume, a significant increase in tank volume compared to a gasoline vehicle. CNG tanks are also relatively heavy, as needed to withstand the high pressure. The official list price for the Honda CX-CNG 2012 model was \$25,490, with a fuel efficiency claimed to be 36 mpg (highway), whereas the list price for the SI Honda Civic DX 2012 model was only \$15,805 with an official performance at 39 mpg.

TABLE 15.4
Number of NGV-Powered Vehicles in Top 10 NGV Countries and the United States

Country	Number of Vehicles
1. Iran	2,859,386
2. Pakistan	2,850,500
3. Argentina	1,900,000
4. Brazil	1,694,278
5. India	1,100,000
6. China	1,000,000
7. Italy	779,090
8. Ukraine	390,000
9. Columbia	348,247
10. Thailand	300,581
17. United States	112,000

Source: NGV America. About NGVs, https://www.ngvc.org/about_ngv. [26]

Elgowainy et al. [13] estimate that a current mid-size CNG vehicle would have a cost premium of about \$4700 over an equivalent gasoline vehicle, assuming high volume production. Although ICE can take advantage of higher compression ratios with CNG than gasoline to improve engine efficiency, the greater weight of CNG vehicles would likely wash out this advantage, so fuel economy is expected to be comparable. Relative fuel costs between CNG and gasoline vehicles are difficult to predict, due to variations in the ratio of natural gas and oil prices. A study published in 2013 [18] quoted U.S. transportation fuel prices in the last quarter of 2011 as \$3.37/gal for gasoline and \$2.13/gge for CNG. They concluded that vehicle purchasers with relatively high annual mileage and access to alternative fuel tax credits or other subsidies could make an economic case for switching to CNG. However, with the recent drop in oil prices the CNG fuel cost advantage has been reduced [13].

Determining the comparative life cycle GHG emissions of CNG versus gasoline or diesel vehicles is also challenging. Figure 15.5 shows Argonne National Laboratory's estimate that current CNG vehicles would reduce life cycle GHG emissions by about 20%, compared to gasoline vehicles with similar performance. However, Alvarez et al. [27] have shown that such comparisons turn on two critical factors that require careful consideration. First, the comparison between GHG emissions for CNG versus gasoline vehicles is sensitive to assumptions about how much methane is leaked across the well-to-wheels supply chain. The results shown in Figure 15.5 assume that across the supply chain, about 1.16% of natural gas production is leaked to the atmosphere as methane [13; Table 14]; this is a relatively low value compared to estimates made in other recent studies [28] but could be achievable in the future through careful equipment and system design and regulation. The second factor that complicates the comparison is the fact that methane is a much more potent GHG than CO₂, but also has a much shorter atmospheric lifetime. As Alvarez et al. explain, "[d]etermining whether a unit emission of CH₄ is worse for the climate than a unit of CO₂ depends on the time frame considered. Because accelerated rates of warming mean ecosystems and humans have less time to adapt, increased CH₄ emissions due to substitution of natural gas for coal and oil may produce undesirable climate outcomes in the near-term" [27]. ANL used a global warming potential (GWP) for methane of 30, neglecting the even higher potency that methane emissions have compared to CO₂ when a shorter time horizon is considered. Alvarez et al. conclude that unless methane leakage is strictly controlled, switching from gasoline or diesel to natural gas for transportation could exacerbate climate change in the short term [27].

Looking beyond fossil fuels, a number of renewable sources for natural gas or biomethane are available. Biomethane can be produced from any organic matter. It is produced incidentally in landfills, but it can also be produced, as discussed in Chapter 9, in anaerobic digesters or through pyrolysis from sewage, industrial, animal, or crop wastes or from specific energy crops. The biomethane from landfills used in NGVs reduces greenhouse gases by 90% according to the California Air Resources Board. After biomethane is produced, it can be injected into natural gas pipeline systems and sold to CNG station operators. A 5% or 10% blend of biomethane with natural gas would improve CNG vehicles' potential for helping to reduce global warming.

15.10 Hydrogen for Transportation

Hydrogen was touted as a potential transportation fuel after former President George W. Bush said in his 2001 inaugural address that "a child born today will be driving a

pollution-free vehicle ... powered by hydrogen.” This appeared to be welcome news. However, to analyze whether or not hydrogen is a sustainable technology for transportation, one must take into account all the steps necessary to make the hydrogen from a primary fuel source, get it into the fuel tank, and then power the wheels via a prime mover and a drive train. In other words, one must perform a well-to-wheels analysis, as shown in [Figure 15.4](#). There is a loss in each step, and to obtain the overall efficiency, one must multiply the efficiencies of all the steps.

Fuel cell electric vehicles (FCEV) are similar to battery electric vehicles except that the electric motor is driven by electricity produced on board in a fuel cell system. As described in [Chapter 14](#), fuel cells are similar to batteries, but with hydrogen supplied at the anode and air at the cathode. Current FCEV use polymer-electrolyte membrane/proton-exchange membrane (PEM) fuel cells, with operating temperatures of about 80°C. Hydrogen is stored on-board FCEV as a compressed gas, in carbon fiber-reinforced composite tanks with a typical storage pressure of 10,000 psi. A mid-size FCEV sedan with a 300-mile range requires storage of about 5.6 kg of hydrogen [\[18\]](#). FCEV typically utilize regenerative braking systems like those in hybrid electric vehicles, but with a larger battery to support initial operation as the fuel cell warms up. As discussed in [Chapter 14](#), steam reforming of methane (natural gas) is a well-established process for producing H₂ for industrial needs and could be expanded to supply FCEVs. In comparison, production of H₂ using electrolysis is relatively expensive, but holds the future potential of using electricity from a renewable source such as wind.

Using natural gas as the primary energy source, a well-to-wheel analysis [\[29\]](#) found that a hybrid spark ignition (SI) car operating on natural gas would have a well-to-wheel efficiency of 32%; a hydrogen-powered fuel cell car with hydrogen made by steam reforming of natural gas would have a well-to-wheel efficiency of 22%; and a hydrogen fuel cell car with hydrogen made by electrolysis with 63% efficiency using electricity from a natural gas–combined cycle power plant would have a well-to-wheel efficiency of 12%, as shown in [Table 15.5](#). The estimates in [Table 15.5](#) assume a fuel cell stack efficiency at a peak load of 44.5%, a part load efficiency factor of 1.1, and a transmission efficiency of 90% (for details, see [\[10\]](#)).

The 2016 Argonne National Laboratory study referenced above [\[13\]](#) estimates that a mid-size FCEV would currently cost about \$16,500 more than an equivalent gasoline vehicle, with a prospect that the cost premium could be halved in the next 15 years. ANL estimates that dispensed fuel costs for H₂ would be about \$4.90/gge, with potential for cost reductions if production and distribution systems are expanded. The Argonne study [\[13\]](#) suggests that current FCEV using H₂ from methane steam reforming could have cradle-to-grave GHG emissions of about 320 g CO₂-e per mile ([Figure 15.5](#)), which is not much better than a gasoline-fueled HEV. Note that because these GHG emissions are due in part to methane

TABLE 15.5

Well-to-Wheel Efficiency of Fuel-Cell Vehicle with
Hydrogen Produced by Electrolysis

NG feedstock production efficiency	95%
Conversion efficiency (NG to electricity)	55%
Electrolysis efficiency (electricity to H ₂)	63%
Storage and transmission	97%
Compression efficiency	87%
Overall efficiency of fuel production	28%
Total fuel cell well-to-wheel efficiency: (0.28 × 445 × 1.1 × 0.9)	12%

used in H_2 production, the estimate is subject to the complicating factors mentioned above for CNG: uncertainty about methane leak rates and sensitivity of the CO_2 -equivalence calculation to the climate response time-horizon. In the future, GHG emissions could be reduced by capturing and sequestering the CO_2 that is coproduced with H_2 in steam methane reforming; producing H_2 from biomass (possibly also with CCS); or by using electrolysis with a low or zero-carbon electricity source.

In addition to the relatively low overall efficiency of a hydrogen transportation system, as well as the high cost compared to other options, it should also be noted that it requires expensive new infrastructure for transport, distribution, and storage of the hydrogen. A study of the comparative costs of fuel distribution systems conducted at Argonne National Laboratory in 2001 estimated that to support a year 2030 market penetration of 40% hydrogen vehicles with a mileage of 2.5 times that of average conventional vehicles (i.e., about 55 mpg), hydrogen distribution infrastructure would minimally cost \$320 billion, but could be as high as \$600 billion [30]. Thus, in addition to the need to bring down vehicle costs and to develop less costly methods to produce hydrogen with low greenhouse gas emissions, the cost and challenge of deploying the needed refueling infrastructure is a major obstacle to developing hydrogen-based transportation systems [18].

PROBLEMS

- 15.1 Assume a hydrogen car uses 2.5 kWh/km. Compare this performance with that of a typical U.S. car that is able to get 22 mpg of gasoline.
- 15.2 From the information supplied in the following text, estimate the percentage of the total land area in the lower 48 U.S. states that would have to be used to replace all of the gasoline currently used for transportation with ethanol obtained from switchgrass. Do the same for the arable land in the lower 48 U.S. states.

Data:

Estimated ethanol productivity ~ 1000 gallons ethanol per hectare per year (based on switchgrass as the crop) [31].

1.5 gallons ethanol are required to obtain the same energy as 1-gallon gasoline, based on their respective LHVs.

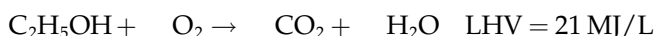
U.S. gasoline consumption in 2008 was 138×10^9 gal/year (information obtained from EIA [32]).

U.S. total land area (lower 48) = 1.92×10^9 ac (information obtained from CIA [33]).

U.S. arable land area (suitable for crops) = 0.45×10^9 ac (information obtained from CIA [33]).

1 ha = 2.47 ac.

- 15.3 Estimate the net amount of CO_2 produced in g per MJ from using corn-based ethanol as a biofuel, and compare it to the amount of CO_2 produced in g per MJ from burning gasoline.
 - a. The combustion of ethanol goes according to the following equation:



where LHV = lower heating value, the symbol "L" designates liter. The density of ethanol at 16°C is 780 g/L. Based on the combustion stoichiometry,

calculate the amount of CO_2 released to the atmosphere per MJ of ethanol burned.

- b. Assume the growth of corn and conversion of the corn into ethanol produce 87 g CO_2 /(MJ of ethanol) from the fossil fuels required. In addition, 35 g of CO_2 /(MJ of ethanol) is produced during the fermentation of corn sugar into ethanol. However, each atom of carbon in the corn sugar, and thus each atom of carbon in the CO_2 released by fermentation of the sugar, originally came from an atom of carbon dioxide in the atmosphere. Therefore, the CO_2 from the fermentation is “carbon neutral,” that is, the amount of CO_2 released by the fermentation is balanced by CO_2 removed from the atmosphere in making the corn sugar. [Note: The same is true for the fermentation of any biomass.] Likewise, each atom of C in the CO_2 produced by combustion of ethanol is also carbon neutral. Using this information calculate the net amount of CO_2 released per MJ of ethanol made from corn. The net amount is the amount by which the production and combustion of ethanol increase the amount of CO_2 in the atmosphere.
 - c. Gasoline is a mixture of many compounds of carbon and hydrogen, but may be represented by the formula C_8H_{16} , with an LHV of 32.8 MJ/L (L = liter). Calculate the CO_2 emissions from combusting gasoline in g CO_2 /MJ (LHV) with gasoline as fuel.
 - d. Estimate the total CO_2 emissions [g CO_2 /MJ (LHV)] from “well-to-wheel” by including “well-to-tank” emissions with gasoline as a fuel. The well-to-tank energy efficiency for gasoline is approximately 90% ($100 \times (\text{MJ energy to tank})/(\text{MJ energy of petroleum “in the well”})$). Assume that the ratio of CO_2 emissions from tank-to-wheel is also 90% of the total CO_2 emissions.
- 15.4 A truck engine consumes diesel at a rate of 30 L/h and delivers 65 kW of power to the wheels. If the fuel has a heating value of 43.5 MJ/kg and a density of 800 kg/m³, determine
 1. The thermal efficiency of the engine
 2. The waste heat rejected by the engine
 - 15.5 An automobile storage battery with an open circuit voltage of 12.8 V is rated at 260 A/h. If the internal resistance of the battery is 0.2 Ω , estimate the maximum duration of current flow and its value through an external resistance of 1.8 Ω .
 - 15.6 Estimate the mass of hydrogen required to fuel a hydrogen powered vehicle for one year, assuming the vehicle operates 2 hours per day with output power requirements of 170 hp, and that the fuel cell delivers power at 60% efficiency.
 - 15.7 Explain the difference in operation between HEVs with parallel and series designs.
 - 15.8 Estimate the annual CO_2 emissions and fuel cost implications of shifting from a full-size car with a gasoline internal combustion engine (ICE) to a similarly sized battery electric vehicle (BEV) that is charged with electricity from an average natural gas power plant. Assume the vehicle will be driven 12,000 miles per year. Assume the ICEV has fuel economy of 32 miles per gallon, and that gasoline has a density of 0.74 kg L⁻¹, energy content of 45 MJ kg⁻¹ and direct CO_2 emissions of 74 g CO_2 MJ⁻¹. Assume the BEV uses 0.17 kWh mi⁻¹, and that the natural gas power plant emits 0.42 kg CO_2 kWh⁻¹. Gasoline costs \$2 per gallon and electricity costs \$.09 per kWh. How do the fuel cost savings of the

BEV compare to the external cost benefits of reduced CO₂ emissions, using the U.S. government's estimate of the social cost of carbon? For the comparison, assume a mid-range estimate of about \$50 per metric ton of CO₂. What sources of greenhouse gas emissions that are relevant to BEV and ICEV life cycles have been left out of this comparison?

**EXTRA CREDIT PROBLEMS SUPPLIED BY ROBERT KENNEDY, MEMBER,
ASME ENERGY COMMITTEE**

- 15.9 Suppose you own and operate a good modern turbo-diesel automobile in Southern California. Unlike all your neighbors, your job is not so far away, plus you telecommute whenever you can, so you burn only 1 gal per day on average. Nevertheless, you are thinking of "going greener" by switching to an all-electric car, charging at night. In fact, "even greener," you are considering installing your own PV panels. You wonder when you should make these bets, if any.

According to the Bureau of Labor Statistics

1. The long-term trend (40 years, from 1973 to 2012) for price inflation for #2 diesel is 7.2% *per annum* (nominal dollars).
2. The long-term trend (40 years, from 1973 to 2012) for price inflation for grid electricity is 2.2% *per annum* (nominal dollars).

(For comparison, note that the prevailing Consumer Price Index is reckoned to be about 3%. YMMV.)

Assume an initial price of \$4 per gal and an energy content of 135,000 Btu/gal (37 MJ/L).

Assume an initial fuel efficiency of 35 MPG (combined city + hwy). (Note: Per Kreith in this textbook, the "well-to-wheel" efficiency of a modern automobile with a turbo-diesel is about 33%, the best there is.)

Assume an initial residential off-peak rate of 10¢ per kWh, and peak daytime rate of 30¢ per kWh.

Assume 20% loss each way (in/out) for in-car battery storage, otherwise perfect drive train efficiency but zero regeneration.

Use NREL's solar map to get average full-sun-hours per day at your location, with flat plate tilted at latitude, southern azimuth, no seasonal bias. [Hint: it's 6.25 h/day.]

Assume an initial capital cost of \$3.00 per DC-watt, 40 year economic life, with a capital cost reduction curve for installed PV capacity of 1% (relative, compounded) per month.

Assume basic conversion efficiency of sunlight-to-DC-electric technology improves by +1% (absolute, i.e., 100 basis points) each year.

Assume no OpEx for the PV system.

Find in terms of cents per km.

1. Forecast the date at which specific motive energy from off-peak grid electricity will cross over to become nominally cheaper than that from a diesel engine.
2. Forecast the date at which specific motive energy from peak grid electricity will cross over to become nominally cheaper than that from a diesel engine.

3. Forecast the date at which specific motive energy from photovoltaic electricity will cross over to become nominally cheaper than that from a diesel engine.

Approach to Solution

- Step 1. Calculate the effective energy consumption for travel via present method, which is 2.53 MJ/km. Effective cost, present method and day, is 7.1¢ per km.
- Step 2. Prepare a baseline series for the delivered cost of diesel-fueled travel, escalated over the next 50 years [nominal cents/km].
- Step 3. Prepare a second series for the delivered cost of off-peak electric-fired travel, escalated over the next 50 years [nominal cents/km].
- Step 4. See how many years from now when the terms in the first two series become equal. ANSWER (1).
- Step 5. Modify the second series to a third series (simple) for the delivered cost of peak electric-fired travel, escalated over the next 50 years [nominal cents/km].
- Step 6. See how many years from now when the terms in the first and third series become equal. ANSWER (2).
- Step 7. Prepare a fourth series for the delivered cost of solar electric-fired travel, escalated over the next 50 years [nominal cents/km].
 - 7A. Calculate the PV system capacity required now to provide 2.23 GJ of daily DC solar electricity input to the electric car [watts].
 - 7B. Calculate the CapEx, then calculate the daily capital recovery charge to amortize CapEx over the 40-year life, using the methods presented in this chapter [cents/day].
 - 7C. Divide by 56.3 km daily travel to get [cents/km].
 - 7D. Apply the two improvement curves (conversion eff. and CapEx redux) to generate the fourth series over the next 50 years to forecast the trend in [nominal or “then-year” cents/km].
 - 7E. See how many years from now when the terms in the first and fourth series become equal. ANSWER (3).

References

1. Schiller, P.L., Bruun, E.C., and Kenworthy, J.R., 2010. *An Introduction to Sustainable Transportation: Policy, Planning and Implementation*, Earthscan, London and Washington, DC.
2. Energy Information Administration. Energy use for transportation, http://www.eia.gov/Energyexplained/?page=us_energy_transportation.
3. Bartlett, A.A., 2000. An analysis of U.S. and world oil production patterns using Hubbert-style curves, *Mathematical Geology* 32(1), 1–17. DOI:10.1023/A:1007587132700.
4. Kreith, F., 1999. Ground transportation for the 21st century, in: *National Conference of State Legislatures*, Denver, CO and ASME Press, New York.
5. Energy Information Administration, November 19, 2015. Today in energy: Passenger travel accounts for most of world transportation energy use, www.eia.gov/todayinenergy/detail.cfm?id=23832.

6. Davis, S.C., Diegel, S.W., Boundy, R.G., 2015. *Transportation Energy Data Book*, Ed. 34, ORNL-6991, Oak Ridge National Laboratory, Oak Ridge, TN.
7. Davis, S., and Diegel, S., 2004. *Transportation Energy Data Book*, Oak Ridge National Laboratory/ U.S. Department of Energy, Oak Ridge, TN.
8. Newman, P., and Kenworthy, J., 2015. *The End of Automobile Dependence: How Cities are Moving Beyond Car-Based Planning*, Island Press, Washington, DC.
9. Kreith, F., and West, R.E., 2003. Gauging efficiency: Well-to-wheel, *Mechanical Engineering Power*, 20–23.
10. Kreith, F., West, R.E., and Isler, B.E., 2002. Efficiency of advanced ground transportation technologies, *Journal of Energy Resources Technology* 24, 173–179.
11. Argonne National Laboratory, 2016. GREET: Life-cycle model user guide, Center for Transportation Research, Energy Systems Division, Argonne National Laboratory, U.S. Department of Energy.
12. Cai, H., Burnham, A., Wang, M., Hang, W., and Vyas, A., 2015. The GREET model expansion for well-to-wheels analysis of heavy duty vehicles, ANL/ESD-15/9, Energy Systems Division, Argonne National Laboratory, U.S. Department of Energy.
13. Elgowainy, A. et al., 2016. Cradle-to-grave lifecycle analysis of U.S. light duty vehicle-fuel pathways: A greenhouse gas emissions and economic assessment of current (2015) and future (2025–2030) technologies, ANL/ESD-16/7, Energy Systems Division, Argonne National Laboratory, U.S. Department of Energy.
14. Kreith, F., West, R.E., and Isler, B., 2002. Legislative and technical perspectives for advanced ground transportation system, *Transportation Quarterly* 96(1), 51–73.
15. Hammerschlag, R., 2006. Ethanol's energy return on investment: A survey of the literature 1990–present, *Environmental Science and Technology* 40, 1744–1750.
16. Dismukes, C. et al., 2008. Aquatic phototrophs: Efficient alternatives to land-based crops for biofuels. *Current Opinions in Biotechnology* 19, 235–240.
17. Christi, Y., 2007. Biodiesel from microalgae, *Biotechnology Advances* 25, 294–306.
18. National Research Council, 2013. *Transitions to Alternative Vehicles and Fuels*, National Academies, Washington, DC.
19. EPRI, 2004. Advanced batteries for electric drive vehicles: A technology and cost-effectiveness assessment for battery electric vehicles, power assist hybrid electric vehicles and plug-in hybrid electric vehicles, EPRI Tech Report 1009299, EPRI, Palo Alto, CA.
20. Himelich, J.B., and Kreith, F., 2008. Potential benefits of plug-in hybrid electric vehicles for consumers and electric power utilities, in: *Proceedings of ASME 2008 IMEC*, October 31–November 6, Boston, MA.
21. Kreith, F., and West, R.E., 2006. A vision for a secure transportation system without hydrogen or oil, *ASME Journal of Energy Resources Technology* 128(9), 236–243.
22. Kreith, F., and West, R.E., 2008. A scenario for a secure transportation system based on fuel from biomass, *Journal of Solar Energy Engineering* 130, 1–6.
23. Farrell, A.E., Plevin, R.J., Turner, B.T., Jones, A.D., O'Hare, M., and Kammen, D.M., 2006. Ethanol can contribute to energy and environmental goals, *Science* 311, 506–508.
24. EIA, 2007. Annual energy outlook, www.eia.gov/fuelelectric/electricityinfocard2005.
25. De Feijter, T., May 18, 2016. 10 new electric cars from China, *Forbes*.
26. NGV America. About NGVs, https://www.ngvc.org/about_ngv.
27. Alvarez, R.A., Pacala, S.W., Winebrake, J.J., Chameides, W.L., and Hamburg, S.P., 2012. Greater focus needed on methane leakage from natural gas infrastructure, *PNAS*, 109, 6435–6440, www.pnas.org/cgi/doi/10.1073/pnas.1202407109.
28. Brandt, A.R., Heath, G.A., Kort, E.A., O'Sullivan, F., Petron, G., Jordaan, S.M., Tans, P., Wilcox, J., and Gopstein, A.M., 2014. Methane leaks from North American natural gas systems, *Science* 343, 743–745.
29. Kreith, F., and West, R.E., 2004. Fallacies of a hydrogen economy: A critical analysis of hydrogen production and utilization, *Journal of Energy Resources Technology* 126, 249–257.

30. Mince, M., 2001. Infrastructure requirement of advanced technology vehicles, in: *NCSL/TRB Transportation Technology and Policy Symposium*, Argonne National Laboratory, Argonne, IL.
31. Schmer, M.R. et al., 2008. Net energy of cellulosic ethanol from switchgrass, *PNAS* 105(2), 464–496, www.pnas.org/cgi/content/full/105/2/464.
32. EIA. Petroleum, <https://www.eia.gov/petroleum>.
33. CIA. *The World Factbook*, <https://www.cia.gov/library/publications/the-world-factbook>.

Online Resources

<https://www.nrel.gov/transportation>. NREL's transportation research site.

<https://www.nrel.gov/bioenerg/>. NREL's biofuels research site.

<https://greet.es.anl.gov>. Argonne National Laboratory's GREET model for vehicle and fuel life cycle assessment.

<http://cta.ornl.gov/data/index.shtml>. Oak Ridge National Laboratory's Annual Transportation Energy Data Book.

<http://www.iea.org/topics/transport>. International Energy Agency transportation data portal.



Taylor & Francis

Taylor & Francis Group

<http://taylorandfrancis.com>

Index

A

Abengoa Solar, 491, 501
absorbed glass mat (AGM) batteries, 557
absorber plates, 450–451
accidents, nuclear power plants, 237–238
Acciona company, 482
AC/DC debate, 159–163
A Common Definition of Zero Energy Buildings, 135
actuator disk theory, 270–274
Advanced Energy Design Guides (AEDGs), 132
aerodynamics, wind energy, 255–258
agricultural competition, 11–12
air pollution
 carbon capture and sequestration, 215–217
 climate change, 212–215
 fossil fuels, 31
 greenhouse gas emissions, 212–215
 household, 342–344
 leaving it in the ground, 217
 local and regional scale air pollution, 210–212
algae, 311, 335; *see also* aquatic microbial
 oxygenic photoautotrophs
alkaline fuel cell (AFC), 563
all-electric system (future), 602
Ames hydroelectric plant, 159
amorphous silicon PV technology, 425
ancillary services market
 black start service, 170
 electricity markets, 169–170
 financial transmission rights market, 170
 frequency regulation, 169
 operating reserves, 169
 voltage control, 169–170
Anderson–Schulz–Flory (ASF) distribution, 330
angle of incidence, 384
Annual Fuel Use Efficiency (AFUE), 204
anodes, 552
appliances, residential, 138
applications
 remote design, photovoltaics, 420–425
 storage energy modes, 544
 storage technology, 542
 thermal energy storage, 570
aquatic microbial oxygenic photoautotrophs
 (AMOPs), 592–593

aquifers, 9
Architecture 2030 organization, 146
Arctic Circle, 217
Argonne National Laboratory (ANL), 590,
 594–596, 604–606
Armstrong, William, 159
artesian wells, 9
ASHRAE standards, 112, 123, 454–455
Aspen Plus, 320
Aspen Process Economic Analyzer, 320
Athabasca “tar sands,” 202
Atlanta urban density, 588
atmospheric boundary layer (ABL), 258–259,
 261–262
atmospheric extinction of solar radiation,
 381–383
automatic generation control (AGC), 182
availability, nuclear resources, 229–231
available solar radiation estimation, 422
axial induction factor, 272–274

B

“back-of-the-envelope” calculations, 25–28
balance point, 576
band gap, 399
baseboard convection systems, 575
batteries
 charging, impact on electricity system,
 597–598
 energy storage applications, 542
 flow batteries, 560–561
 lead-acid batteries, 556–558
 lithium ion, 559–560
 nickel metal type, 558–559
 vanadium redox (VR) type, 560–561
batteries and fuel cells
 battery operation, 553–555
 cell physics, 555
 fundamentals, 551–553
 rechargeable batteries, 560–561
battery electric vehicles (BEV), 591
Beer’s law, 360
BEopt models, 142–143, 480
Bernoulli’s law and theory, 256, 271

- Better Buildings program, [31](#), [147](#)
 - Better Plants program, [31](#)
 - Betz, Albert, [254](#)
 - Betz limit, [274](#)
 - BioEnergy with Carbon Capture and Storage (BECCS), [39](#)
 - biofuels
 - conversion, modern concepts, [333–336](#)
 - production, [11](#)
 - transportation, [592–593](#)
 - Biofuels Atlas, [43](#)
 - biomass
 - cofiring, conversion to electricity, [339–340](#)
 - conclusions, [344–345](#)
 - cooking with, [342–343](#)
 - developing communities, use of, [342–344](#)
 - overview, [307](#)
 - process economics and technology, [318–342](#)
 - production and land use, [307–318](#)
 - properties of, [316–318](#)
 - renewable energy, [38–39](#)
 - transport properties, [317](#)
 - biomass, conversions to
 - alternative fuels, [329–330](#)
 - biogas, [321](#)
 - electricity, [336–340](#)
 - Fischer–Tropsch liquids, [330–331](#)
 - gaseous fuels, [321](#)
 - liquid fuels, [329–336](#)
 - pyrolysis oil to gasoline and diesel, [331–333](#)
 - synthetic gas, [321–326](#)
 - Biomass Feedstock Composition and Property Database, [316](#)
 - biomass process economics and technology
 - biomass to electricity, conversion, [336–340](#)
 - biomass to liquid fuels, [326–336](#)
 - conversion of biomass to gaseous fuels, [321–326](#)
 - fossil and biomass fuel properties, [340–341](#)
 - overview, [318](#)
 - process economics, [318–320](#)
 - biomass production and land use
 - algae, [311](#)
 - biomass properties, [316–318](#)
 - energy crops, [309–311](#)
 - land use, [311–316](#)
 - overview, [307](#)
 - waste materials, [308–309](#)
 - biomethane, [318–342](#)
 - bird and bat fatalities, [250–251](#)
 - black-body radiation, [353–354](#)
 - black carbon, [213](#), [343](#)
 - black start service, [170](#)
 - Black & Vetch methodology, [162](#)
 - blade element momentum (BEM) theory, [270–274](#)
 - blocking diode, [414](#)
 - Block Island Wind Farm, [288](#)
 - Blyth, James, [245](#)
 - boiling water reactors (BWRs), [232](#)
 - Bolt vehicle, [602](#)
 - Boltzmann’s constant, [406](#)
 - Bonneville Power Administration (BPA), [166](#)
 - Boundary Dam project, [216](#)
 - BP’s Macondo well, [202–203](#)
 - Brayton cycle, [208](#), [340](#)
 - breeder reactors, [227](#), [240–241](#)
 - Brightsource company, [492](#)
 - Brundtland commission, [5–6](#)
 - Brush, Charles F., [245](#)
 - buildings
 - commercial buildings, energy efficiency, [130–137](#)
 - cooling requirements, [121–125](#)
 - envelope, [132](#), [137–138](#)
 - evaporative cooling, [130](#)
 - heating and hot water load calculations, [112–121](#)
 - overnight storage, [570](#), [572–576](#)
 - residential buildings, [137–146](#)
 - Build It Solar, [387](#)
 - Bush (George W.) administration, [603](#)
 - BYD Auto Co. (China), [602](#)
 - bypass diode, [414](#)
- C**
- cadmium telluride (CdTe) modules, [425](#)
 - Campbell–Stokes sunshine recorder, [393](#)
 - CANDU reactors, [233](#)
 - capacity, electricity markets, [168](#)
 - “capacity credit,” [175–176](#)
 - capital recovery factor (CRF)
 - economics, energy generation and conservation systems, [66–68](#)
 - energy use and efficiency, [109–110](#)
 - levelized cost of energy, [70](#)
 - carbon capture and sequestration (CCS), [215–217](#)
 - carbon capture and storage (CCS), [150](#)
 - carbon dioxide (CO₂) emissions
 - climate change, [20–21](#)
 - combining HEVs/PHEVs with biofuels, [600–602](#)
 - electric vehicles/biofuel combination, [600–602](#)
 - sustainable energy, [49–50](#)

- carbon nanotubes, 565
- Carnot cycle and efficiency, 505–506, 508–509, 515
- carrying capacity
 - food supply issues, 11–12
 - per capita energy use, 12
 - population issue, 7–9
 - water issue, 9–11
- cathodes, 552
- cell analysis, photovoltaics, 406–416
- cell physics, 555
- cellulosic ethanol, 328–329
- cement manufacturing, 20
- Centre for Sustainable Transportation (Canada), 586
- centrifugal pumps, 425
- challenges, sustainability engineering, 7
- Chernobyl, Ukraine, 32, 236
- Chevrolet vehicles, 52, 596, 602
- Chicago (Illinois) public transit, 588
- Chicago Pile-1 (CP-1), 223
- Civic DX2012 vehicle, 603
- Clean Air Act Amendments, 6, 211, 212
- clear days, 383
- clearness number, 382
- climate change; *see also* Paris agreement
 - air pollution from combustion, 212–215
 - challenge, 18–22
- closed-cycle ocean thermal energy
 - conversion (CC-OTEC), 507–511, 514–515
- coal
 - production process, 84
 - resources and extraction, 195–198
 - societal and environmental costs, 71–72
- cocurrent gasifiers, 325
- coefficient of performance, 254–255
- cold-water pipe (CWP) and pumping
 - requirements, 506, 510, 515–516
- collectors and systems, *see* solar thermal collectors and systems
- collector-storage control, 575
- Columbia River Basin, 39
- combining HEVs/PHEVs with biofuels
 - carbon dioxide emissions, 600–602
 - overview, 598–599
 - petroleum requirement, 599–600
 - transportation, 598–602
- combustion, 337–339
- combustion and energy conversion technologies
 - electricity generation, 205–209
 - heat of combustion, 203
 - integrated gasification combined cycle, 209–210
 - natural gas, 208–209
 - pulverized coal, 205–208
 - use for heat, 204–205
- commercial buildings, energy efficiency
 - building envelope, 132
 - case studies, 135–137
 - heating and cooling equipment, 133–134
 - lighting, 133
 - National Renewable Energy Laboratory Research Support Facility, 136
 - Net-Zero Walgreens Store, 136–137
 - office computers and equipment office, 134–135
 - ventilation, 133
- commons, management of, 6
- Compact of Mayors, 146
- compressed air energy storage (CAES), 544, 549–550
- compressed air systems, 153
- compressed gases as transportation
 - fuel, 333
- compressed natural gas (CNG), 603–604
- computers, laptop, 139
- concentrating collector systems, 570
- concentrating solar collectors, 463–466
- concentrating solar power (CSP) plants, 35–36, 179, 492–493
- conduction bonds, 399
- conservation, 28–31, 107
- constant-speed, variable-pitch (VSVP), 278–279
- consumer price index (CPI), 60, 87, 320
- control schemes, wind energy, 278–279
- control strategies and hardware, 574–575
- conventional energy, 31–32
- conventional hydraulic turbines, 548
- conversion costs, biomass process economics, 318–320
- conversion factors, sustainable energy, 45
- conversion of biomass to gaseous fuels, 321–326
- cooking with biomass, 342–344
- cooling requirements, buildings, 121–125
- Copenhagen transport, 589
- COP21 Paris Agreement, 22
- copper indium diselenide (CIS) PV products, 425–426
- corn, energy content, 49; *see also* biomass
- corn ethanol
 - biomass to liquid fuels, 327–328
 - water issues, 11

costs; *see also* [economics](#); [levelized cost of energy](#)
 biomass conversion, [318–320](#)
 conserved energy, [109–110](#)
 energy production and development, [25–28](#)
 nuclear technologies, [238](#)
 “soft costs,” [434](#)
 wind and photovoltaics, [33](#)
 Coulomb properties, [555](#)
 countercurrent gasifiers, [325](#)
 covalent bonds, [399](#)
 Crescent Dunes plants, [493](#)
 critical mass, [229](#)
 cross-sector EROI, [94](#)
 cryogenic refrigeration systems, SMES, [551](#)
 cumulative distribution function, [267–268](#)
 current commercial power technologies, [534–536](#)
 current energy use, [17–18](#)
 current status, [238](#)
 cycle life, technology characterization, [544](#)
 cyanobacteria, *see* [aquatic microbial oxygenic photoautotrophs](#)
 Czocharski method, [416](#)

D

dams, *see* [hydroelectric generation](#); [hydropower](#)
 decarbonization, electricity system, [602](#)
 declination, [362](#), [369](#)
 dedicated energy crops, [310](#)
 Deepwater Horizon disaster, [202–203](#)
 deep water wave power, [523–526](#)
 deforestation, [213](#), [343](#), [344](#)
 degree-day method, [116–119](#)
 dehumidification, [480–481](#)
 demand response, [184–187](#)
 DePere Wind Project (DPWP), [99](#)
 depletion effects discussion, [49](#)
 depth of discharge (DOD), [543–544](#)
 desalination, [9](#)
 desiccant-based cooling systems, [133](#), [480](#)
 detectors for solar radiation instrumentation, [392–393](#)
 Detroit (Michigan) vehicle makers, [602](#)
 developing communities, use of biomass, [342–344](#)
 diatoms, *see* [aquatic microbial oxygenic photoautotrophs](#)
 diffuse radiation reflection, [447](#)
 direct beam radiation, [381](#)
 direct combustion, [336–338](#)

direct contact evaporation and condensation, [513–514](#)
 direct electrical technologies, [551](#)
 direct gain, passive solar heating systems, [478](#)
 direct methanol fuel cell (DMFC), [563](#)
 direct use, geothermal energy, [537](#)
 discounted cash flow analysis, [58](#)
 distributed grid technology, [542](#)
 distribution of wind, [259–261](#)
 domestic hot water, overnight storage for, [570](#), [572–576](#)
 downdraft gasifiers, [325](#)
 dye-sensitized cells, [431](#)

E

ECN Phyllis database, [316](#)
 EcoDistricts organization, [146](#)
 Economic Input–Output Life Cycle Assessment tool, [80](#)
 economics; *see also* [costs](#); [levelized cost of energy](#)
 fuel cells and hydrogen, [565–566](#)
 ocean thermal energy conversion, [516](#)
 radioactive wastes, [236](#)
 sustainable energy, [49](#)
 transition, other energy sources, [17–18](#)
 economics, energy generation and conservation systems
 capital recovery factor, [66–68](#)
 inflation, [59–60](#)
 internal rate of return, [63–66](#)
 levelized cost of energy, [68–71](#)
 payback period, [56](#)
 societal and environmental costs, [71–72](#)
 time value of money, [57–59](#)
 total life cycle costs, [60–63](#)
 unit cost of energy, [55–56](#)
 Edison, Thomas, [159](#), [162](#)
 Edison Electric Light Station, [159](#)
 Edwardsport IGCC station, [210](#)
 efficiency; *see also* [energy efficiency and conservation](#); [energy use and efficiency](#)
 and conservation, sustainability, [28–31](#)
 defined, [107](#)
 technology characterization, [542](#), [544](#)
 Einstein’s equation, [228](#)
 Elcogas IGCC plant, [210](#)
 Eldridge, F.R., [246](#)
 electrical transmission, [160–163](#)
 electric grid and electricity markets
 age, [160](#)
 electricity markets, [166–170](#)

- electricity supply systems, 163–170
 - overview, 163–166
 - rate structures, 166
- electricity generation
 - from natural gas, 208–209
 - from pulverized coal, 205–208
- electricity markets
 - ancillary services market, 169–170
 - capacity, 168
 - electric grid and electricity markets, 166–170
 - energy market, 167–168
 - overview, 166–167
- electricity pricing plans, 186
- electricity supply systems
 - demand response, 184–187
 - electrical transmission, 160–163
 - electric grid and electricity markets, 163–170
 - grid operations, 170–175
 - historical developments, 159–160
 - transactional controls, 184–187
 - variable renewable energy, integration into the grid, 175–184
- Electric Power Research Institute (EPRI), 596
- Electric Reliability Council of Texas (ERCOT), 163, 183
- electric transmission grid, virtual storage, 576–580
- electric vehicles, *see* vehicles
- electrochemical plating, 426–427
- electromagnetic force (EMF), 552, 555
- embedded energy, 87–92
- embodied energy, 87–92
- EMCORE cells, 428–430
- emittance, 448–449
- energy assessments, *see* energy return on investment (EROI)
- energy audits and management, 110–112
- energy budgeting, 96–99
- energy content, 49
- energy crisis, 3–5
- energy crops, 309–311
- energy density, 544
- energy economic efficiency, 23
- energy efficiency ratio (EER), 130
- energy end-use demand reduction, 29–30
- energy management, industry and manufacturing, 30–31
- energy market, 167–168
- Energy Plus, 292
- energy return on investment (EROI); *see also* payback period
 - biofuels, 592
 - calculation of, 95–96
 - cellulosic ethanol, 329
 - energy budgeting, 96–99
 - hydroelectric generation, 39
 - introduction, 92–94
 - Process Chain Analysis, 82
 - sustainability, 23–28
 - thin film PV, 427
 - wind energy system, 99–101
- energy scenarios, 18
- Energy Star program, 138–139, 481
- energy systems analysis methodologies
 - embedded energy, 87–92
 - energy return on energy invested, 92–101
 - greenhouse gas accounting, 101–103
 - input–output analysis, 83–87
 - life cycle approach, 77–80
 - process chain analysis, 81–83
- Energy Technology Perspectives: Towards Sustainable Urban Energy Systems*, 21
- energy transport, solar radiation, 351–352
- energy units and conversion factors, 45
- energy use, current, 17–18
- energy use, transportation, 586–589
- energy use and efficiency, buildings and industry
 - background, 107–110
 - buildings, 112–147
 - commercial buildings, energy efficiency, 130–137
 - cooling requirements, 121–125
 - energy audits and energy management, 110–112
 - equipment improvements, 151–153
 - evaporative cooling, 130
 - heating and hot water load calculations, 112–121
 - industrial energy efficiency, 148–153
 - processes improvement, 148–151
 - residential buildings, 137–146
 - vapor-compression cycle, 125–130
- energy use intensity (EUI), 130–131
- engine knock, 340
- enhanced geothermal systems (EGS), 38, 531
- entrained flow gasifiers, 325
- environmental impact, wind energy
 - bird and bat fatalities, 250–251
 - land use, 250
 - life cycle greenhouse gas emissions, 250
 - noise, 249
 - overview, 248
 - visual impact, 249
 - water use, 250

- equipment
 - flue gas desulfurization equipment, 206–207
 - heating and cooling, 133–134
 - improvements, 151–153
 - office computers and equipment office, 134–135
 - residential buildings, 138
- ERCOT, 183
- ethanol
 - cellulosic ethanol, 328–329
 - corn ethanol, 11, 327–328
 - energy return on investment, 98
 - production of, 38–39
 - water issues, 11
- evaporative cooling, 130; *see also* vapor-compression cycle
- experimental testing of collectors, 453–456
- exponential growth, mathematics of, 12–15
- externalities, 71
- extraterrestrial solar radiation, 377–380
- extrinsic semiconductors, 399
- Exxon Valdez disaster, 202
- F**
 - Fair Trade certification, 7
 - Faraday's constant, 555
 - fast food products, 150
 - Federal Mine Safety and Health Act, 197
 - Fermi, Enrico, 223
 - Fetch, 523
 - financial transmission rights (FTRs) market, 170
 - fine particulate air pollution, 211
 - Fischer–Tropsch liquids, 318, 330
 - fission mechanism, 225–229
 - flaming combustion, 337
 - “flash” evaporation, 513
 - floating moored plants, 506
 - flow batteries, 560–561
 - flue gas desulfurization equipment, 206–207
 - fluidized bed combustors, 339
 - fluidized bed gasifiers, 325, 326
 - flywheels, 544, 550
 - food supply issues, 11–12
 - forbidden gap, 399
 - forced-air systems, 575
 - forced-circulation systems, 464–476
 - forecasting solar energy, 181–182
 - “forward bias,” 407
 - fossil fuels
 - air pollution, 31, 210–217
 - biomass fuel properties, 340–341
 - carbon capture and sequestration, 215–217
 - climate change, 20–21, 212–215
 - coal, 195–198
 - combustion and energy conversion technologies, 203–210
 - conventional energy, 31
 - electricity generation, 205–209
 - energy development costs, 26
 - energy return on investment, 94, 95
 - food supply issues, 11
 - greenhouse gas emissions, 212–215
 - Hawaii situation, 184
 - heat of combustion, 203
 - integrated gasification combined cycle, 209–210
 - leaving it in the ground, 217
 - local and regional scale air pollution, 210–212
 - natural gas, 198–200, 208–209
 - overview, 31, 195
 - petroleum, 200–203
 - pulverized coal, 205–208
 - resources and extraction, 195–203
 - side effects, 1
 - sustainability issues, 4–5
 - use for heat, 204–205
 - fracking, 199
 - Francis turbines, 548
 - Freedom Car initiative, 603
 - freshwater, 9
 - Fresnel properties
 - linear collectors, 463
 - multilayer PV technology, 428
 - solar industrial process heat, 499
 - Frito-Lay plant, 501
 - fuel cell electric vehicles (FCEV), 591, 605
 - fuel cell physics, 555
 - fuel cells and hydrogen
 - economics, 565–566
 - hydrogen generation, 564–565
 - operation of cells, 562
 - storage and transport, 565
 - thermodynamics, 565–566
 - types of cells, 563–564
 - Fukushima, Japan, 32, 224, 237
 - future developments
 - all-electric transportation system, 602
 - new vehicle technology, 602
 - U.S. energy scenarios, 18
- G**
 - gallium-alloyed CIS (CIGS) PV products, 425–426

gasification, 321–326
 Gaussian distribution, 266
 Gemasolar plant, 493
 Generation IV International Forum (GIF), 240
 geometric correction factors (GCFs), 191
 geothermal energy and power, 531–537, 542
 Geothermal Energy Association (GEA),
 532, 537
 Geothermal Prospector, 532
 The Geysers, 533–534, 537
 GHG Protocol, 101–103
 Glenn Research Center, 246
 Global Alliance for Clean Cookstoves, 38, 342
 Global Energy Observatory, 533
 global warming potential (GWP), 102
 Grandpa's Knob (Vermont), 245
 Green Design Institute, 80, 85
 greenhouse gases
 accounting, 101–103
 emissions, 212–215
 GREET (Greenhouse Gases, Regulated
 Emissions, and Energy Use in
 Transportation) model, 590–591
 grid operations, 170–175
 gross national product (GNP), 60
 ground-level ozone, 211
 ground-source heat pumps, 537
 Grove, Sir William, 551
 growth, instability due to, 50
 gymnosperms, 311

H
 Haber process, 333
 Habitat for Humanity, 145–146
 hardwoods, 310–311
 Hawaii, 184, 476, 508
 heated floors or ceilings, water coils, 575
 heating and cooling equipment, 133–134
 heating and hot water load calculations
 buildings, 112–121
 degree-day method, 116–119
 heat loss calculations, 112–116
 internal heat sources, 116
 service hot water load calculation, 120–121
 heating systems, solar energy operation,
 572, 574
 heat loss calculations, 112–116
 heat of combustion, 203
 heavy water cooled and moderated reactor, 233
 heliostats, 464–466, 493
 herbaceous crops, 310
 heuristic approach, 422

hidden costs, 71
 highest heating value (HHV), 565
 high level nuclear waste (LLW), 234
 historical developments
 sustainability principles, 2–7
 U.S. electric power system, 159–160
 U.S. energy development, 15–17
 Honda vehicles, 603
 Hong Kong urban density, 588
 horizontal-axis wind turbine (HAWT), 245,
 254, 257
 Hottel-Whillier-Bliss equation, 453, 473
 hot water, overnight storage for domestic, 570,
 572–576
 hot water solar systems, 470–476
 hour angle, 362, 369
 household air pollution, 342–344
 Houston urban density, 588
 Human Development Index, 12
 Huntorf, Germany, 550
 hybrid electric vehicles (HEVs)
 storage applications, 542
 transportation, 594–595
 hydrocracking, 332
 hydroelectric generation
 energy return on investment, 94
 renewable energy, 39–40
 hydrogasification, 333
 hydrogen
 economics, 565–566
 energy return on investment, 98
 fuel cells, 562–566
 generation of, 564–565
 storage, 565
 sustainable energy, 40–42
 thermodynamics, 565–566
 transport and transportation, 333, 565,
 604–606
 vehicles, 42
 hydrogenation, 335
 hydronic heating systems, 574
 hydropower, 528–531
 hydrotreatment, 332
 hydro turbines, 548

I
 Idaho National Laboratory, 239
 improvements
 energy consumption, 108–109
 industrial equipment, 153
 indirect gain, passive solar heating
 systems, 478

industrial energy efficiency
 background, 148
 compressed air systems, 153
 energy use and efficiency, buildings and industry, 148–153
 improvements in industrial equipment, 151–153
 improving industrial processes, 148–151
 refrigeration systems, 153
 industrial process heat (IPH), 498–501
 inferred resources (IR), 230
 inflation, 59–60, 320
 input–output (I/O) analysis, 79, 83–87
 insolation, 377, 386, 388
 instability due to growth, 50
 instrumentation, solar radiation, 389–392
 integrated gasification combined cycle (IGCC), 209–210
 intensity of radiation, 357–360
 Intergovernmental Panel on Climate Change (IPCC), 21, 32, 102–103, 149, 213, 217
 intermediate level nuclear waste (LLW), 233–234
 intermittency issues, 284–285
 internal heat sources, heating/hot water load calculations, 116
 internal rate of return (IRR), 63–66; *see also* energy return on investment (EROI)
 International Energy Agency (IEA), 21, 107, 112, 213, 397
 International Energy Conservation Code (IECC), 140
 intrinsic semiconductors, 399
 ionic bonds, 399
 Ivanpah project, 492

J

jack pumps, 425
 Japan
 Fukushima Daiichi Nuclear Plant, 224, 237–238
 Nissan Motor Company, 602
 nuclear energy, 224
 nuclear power, 31, 32
 nuclear power plants, 224

K

Kaplan turbines, 548
 Keahole Point, Hawaii, 508
 Keeling, Charles David, 20

L

land use
 biomass production and, 307, 311–316
 energy development costs, 26–28
 greenhouse gas emissions and climate change, 213
 La Rance Tidal Power Plant, 518–519, 521–522
 latent heat, 567–568
 latitude angle, 362–363, 369
 law of diminishing returns, 572
 lead-acid batteries
 basics, 555–556
 electric vehicles, 558
 rechargeable batteries, 556–558
 Leadership in Energy and Environmental Design (LEED), 30
 LEAF vehicle, 602
 “leaving it in the ground,” 217
 Leontief approach, 85
 leveled cost of energy (LCOE); *see also* costs; economics
 annual energy production, 274
 economics, energy generation and conservation systems, 68–71
 energy production costs, 25
 energy return on investment, 98–99
 geothermal energy, 535
 grid operations, 170–175
 power towers, 493
 System Advisor Model, 44
 wind turbine, 279–283
 Lewis Research Center, 246
 life cycle approach/assessment (LCA), 77–80, 590
 life cycle greenhouse gas emissions
 hybrid electric vehicles, 594
 life cycle assessment, 79
 renewable energy, 33
 wind energy, 250
 Life Cycle Inventory (LCI) database, 80, 82
 light-emitting diode (LED) lighting, 133
 lighting, 133, 138
 Limpet, 527–528
 linear Fresnel collectors, 463
 line-focus concentrators
 concentrating solar collectors, 460–463
 linear Fresnel collectors, 463
 parabolic troughs, 460–463
 liquid-based solar heating systems for buildings, 476–477
 liquid fuels, biomass conversion

cellulosic ethanol, 328–329
 compressed gases as transportation fuel, 333
 corn ethanol, 327–328
 fermentation to alternative fuels, 329–330
 Fischer–Tropsch liquids, 330–331
 modern concepts, 333–336
 overview, 326
 pyrolysis oil to gasoline and diesel, 331–333
 lithium ion batteries, 559–560
 loads, estimation and profiles, 420–422
 local and regional scale air pollution, 210–212
 log law wind speed profile, 261–263
 low level nuclear waste (LLW), 233
 Luz Corporation, 482

M

Mammoth Lakes ski area, 534
 manufacture of solar cells and panels, 415–419
 Manufacturing Energy Consumption Survey (MECS), 87
 Maricopa installation, 464
 “market clearing price,” 168
 Marshall and Swift index, 320
 mathematics, exponential growth, 12–15
 Mayors’ Climate Protection Agreement, 146
 measurements, 388–393
 mechanical technologies
 compressed air energy storage, 549–550
 flywheels, 550
 pumped hydroelectric energy storage, 546–549
 turbines, 548–549
 mercury, 211
 Mesa Verde buildings (Colorado), 566
 methane, 198, 200, 333
 methanol, 334
 methylated furans, 336
 microalgae, 335
 micro hydro systems, 530
 miscellaneous electrical loads, 139
 Mitsubishi Motor Company, 602
 mixed oxide (MOX) fuel, 230–231
 Mohave Desert, 35
 molten carbonate fuel cell (MCFC), 563
 momentum theory, 270–274
 Montreal Protocol on Substances that Deplete the Ozone Layer, 6
 motors, improvements, 152–153
 mountaintop removal/mining/valley fill, 197
 multijunction solar cells, 411–412
 municipal solid wastes (MSWs), 308

N

nanoparticle printing, 427
 National Renewable Energy Laboratory (NREL), 42, 65, 80, 136, 140, 142, 150, 259, 279, 289, 329, 388, 459–460; *see also* Geothermal Prospector; System Advisor Model
 National Solar Radiation Database (NSRDB), 43, 393, 422
 National Western Center (Denver), 147
 natural circulation, solar systems, 464–470
 natural gas
 resources and extraction, 198–200
 as transportation fuel, 602–604
 natural gas combined cycle (NGCC), 208–209
 “negawatts,” 107
 Nelson, V., 246
 net metering, 435
 net present value (NPV), 63–64
 net-zero buildings
 commercial, 135–137
 residential, 145–146
 neutral cost point, 142
 Nevada Nuclear Test Site, 234
 Nevada Solar One, 36, 482
 New York City transport, 588–589
 next-generation nuclear technologies, 238–241
 nickel metal batteries, 558–559
 Nissan Motor Company, 602
 noise, wind energy, 249
 North American Electric Reliability Corporation (NERC), 163–164
 North Sea fields, 4
 nuclear energy
 available nuclear resources, 229–231
 boiling water reactors, 232
 cost of nuclear technologies, 238
 current status, 238
 fission mechanism, 225–229
 heavy water cooled and moderated reactor, 233
 introduction, 223–225
 next-generation nuclear technologies, 238–241
 nuclear power plant accidents, 237–238
 nuclear waste management and disposal, 233–236
 pressurized-water reactors, 231–232
 reactor types, 231–233
 spent fuel storage and reprocessing, 236
 nuclear generating systems, 95
 nuclear power, 31–32

nuclear power plant accidents, 237–238
 nuclear waste management and disposal,
 233–236
 NuScale SMR design, 239

O

Obama (Barack) administration, 214, 602
 ocean and geothermal renewable energy, 36–38
 ocean thermal energy conversion (OTEC)
 closed-cycle ocean thermal energy
 conversion, 507–511, 514–515
 cold-water pipe and pumping requirements,
 515–516
 direct contact evaporation and condensation,
 513–514
 economics, 516
 open-cycle ocean thermal energy
 conversion, 511–512, 514–515
 overview, 505–507
 octane number, 340
 ODEX index, 148
 office computers and equipment office, 134–135
 offshore wind energy, 287–291
 Ogallala aquifer, 9
 oil palm, 334–335
 oil production, EROI, 97–98
 oil supply, sustainability, 49
 open-cycle ocean thermal energy conversion
 (OC-OTEC), 511–512, 514–515
 OpenStudio software, 134, 143, 480
 operating reserves, 169
 organic Rankine cycle (ORC), 37, 204–205;
 see also Rankine cycle
 Organization of Petroleum Exporting
 Countries (OPEC), 4, 17, 93
 Orinoco oil belt, 202
 oscillating water column (OWC), 527
 Otto cycle, 340
Our Common Failure, 5
 overnight storage, 570, 572–576
 ozone air pollution, 211

P

packaging, 150
 parabolic trough-based power plants, 482–490
 parabolic troughs, line-focus concentrators,
 460–463
 Paris agreement, 22, 214; *see also* climate change
 passive solar heating systems, 477–480
 payback period (PP), 56, 93, 397, 417; *see also*
 energy return on investment (EROI)

“peaker plants,” 36, 172, 493
 “peak oil,” 31
 peak shaving, 185
 Pearl Street Station, 159
 Pelton wheels, 548
 per capita energy use, 12
 perovskite cells, 431
 personal transport, 588–589
 petroleum
 electric vehicles/biofuel combination,
 600–602
 resources and extraction, 200–203
 water issues, 11
 phase change heat storage, 567–568
 phosphoric acid fuel cell (PAFC), 563
 photons, 353
 photosynthesis conversion, 49
 photovoltaic cells analysis
 introduction, 406–411
 multijunction solar cells, 411–412
 photovoltaic system design, 412–415
 solar cells efficiency, 411
 photovoltaic detectors, 392
 photovoltaic effect, 402–406
 photovoltaics
 amorphous silicon PV technology, 425
 available solar radiation estimation, 422
 cadmium telluride modules, 425
 cell analysis, 406–416
 copper indium diselenide PV products,
 425–426
 current market, 434–435
 electrochemical plating, 426–427
 gallium-alloyed CIS PV products, 425–426
 integration, variable renewable energy into
 grid, 176, 180
 introduction, 397–398
 loads, estimation and profiles, 420–422
 manufacture of solar cells and panels,
 415–420
 multijunction solar cells, 411–412
 multilayer PV technology, 427–434
 nanoparticle printing, 427
 performance estimates, 436–441
 photovoltaic effect, 402–406
 p–*n* type junctions, 402
 polycrystalline cells, 415–419
 remote application design, 420–425
 renewable energy, 34–35
 semiconductors, 399–406
 single crystal cells, 415–419
 solar cells efficiency, 411
 sputtering, 426

storage applications, 542
 System Advisor Model analysis, 436–441
 system design, 412–415
 system sizing, 422–424
 thermal evaporation, 426
 thin-film PV technology, 425–427
 water pumping applications, 424–425
 physics, 351–352, 555
 pipe and pumping requirements, cold-water, 515–516
 Planck's constant and law, 353, 354, 403
 plate collectors, energy balance, 451–453
 plug-in hybrid electric vehicles (PHEVs)
 storage applications, 542
 transportation, 595–598
 plug loads, 139
 plutonium, 231
 p - n type junctions, 401–402, 417
 point-focus concentrators, 463–466
 Polk County, Florida, 210
 polycrystalline cells, 415–419
 polycrystalline thin films, 416
 population issues, 7–9
 Powder River Basin, 196
 power generation unit (PGU), 594
 power law wind speed profile, 263–264
 power load magnitude, 544
 power of wind, 252–254
 power quality, 542
 power towers, 490–498
 Prague public transit, 588
 present discounted money, 58
 pressurized-water reactors (PWRs), 224, 231–232
 price response, 185
 price signals, 186
 primary cells, 552
Principles of Heat Transfer, 112
 probability distribution function (PDF), 265–268
 process chain analysis (PCA), 79, 81–83
 process economics, 318–320
 processes improvement, 148–151
 producer gas, 321
 profile angle, 374
 proton exchange membrane fuel cell (PEMFC), 563
 proved reserves, 201
 proximated analysis, 316–317
 pulse-width modulated inverter, 415
 pulverized coal boilers, 338
 pumped hydroelectric energy storage (PHES), 544, 546–549
 PUREX, 236
 Putnam, Palmer C., 245

PVWatts, 65, 436
 pyranometers, 389–390
 pyrheliometers, 389, 391–392
 pyrolysis, 322, 331–333, 337

R

Raccoon Mountain installation, 546
 radiation function tables, 354, 356–357
 radiation properties of materials, 447–451
 radiation shape factor, 359
 radiation transmission through a medium, 360–361
 Rankine cycle; *see also* organic Rankine cycle
 biomass conversion to electricity, 336
 boiling water reactors, 232
 concentrating collector systems, 570
 electricity conversion from natural gas, 208
 nuclear energy, 223
 ocean thermal energy conversion, 36–37, 505, 507
 solar cooling systems, 480
 solar thermal power plants, 482
 water issues, 10
 rate structures, 166
 Rayleigh PDF, 266–268
 reactor-grade plutonium, 231
 reactor types
 boiling water reactors, 232
 heavy water cooled and moderated reactor, 233
 pressurized-water reactors, 231–232
 reasonably assured resources (RAR), 230
 rechargeable batteries
 flow batteries, 560–561
 lead-acid batteries, 556–558
 left-to-right/right-to-left, 557
 lithium ion batteries, 559–560
 nickel metal batteries, 558–559
 overview, 555–556
 Recife, Brazil, 508
 reflective surfaces, 449–451
 refrigeration systems, 125–130, 153
 Regional Transmission Organizations (RTOs), 166–170, 181
 regulation response, 186
 reliability response, 186
 remote photovoltaic application design
 available solar radiation estimation, 422
 introduction, 420
 loads, estimation and profiles, 420–422
 PV system sizing, 422–424
 water pumping applications, 424–425

- renewable energy (RE)
 - accommodating supply shortages, 180
 - biomass and biofuel, 38–39, 343
 - current energy use, 18
 - curtailment, 179
 - energy return on investment, 95, 98
 - geothermal energy, 534
 - hydroelectric generation, 39–40
 - ocean and geothermal energy, 36–38
 - overview, 32–33
 - societal and environmental costs, 72
 - solar photovoltaics, 34–35
 - solar thermal, 35–36
 - weather forecasts, 181–182
 - wind energy, 33–34
- residential buildings
 - appliances, 138
 - building envelope, 137–138
 - case study, 145–146
 - computers, laptop, 139
 - energy use and efficiency, 137–146
 - equipment, 138
 - lighting, 138
 - miscellaneous electrical loads, 139
 - net-zero Habitat for Humanity house, 145–146
 - plug loads, 139
 - thermostats, Smart, 139
 - WaterSense-labeled fixtures, 139
 - zero-energy urban districts, 146–147
- resources and extraction
 - coal, 195–198
 - natural gas, 198–200
 - petroleum, 200–203
- ReStock analysis, 140
- “reverse bias,” 407
- reversible chemical reactions, 568
- Reynolds number, 516
- Rhode Island, 288
- Roadster vehicle, 602
- round-trip energy analysis, 41–42
- Russia
 - nuclear power, 31
 - nuclear power plants, 224
 - uranium resources, 229
- S
 - Safe Drinking Water Act, 6
 - Sandia National Laboratories, 388, 464
 - Santa Barbara Channel oil blowout, 202
 - Scottish Administration’s Renewable Obligation Program, 528
 - seasonal storage, 566
 - secondary cells, 552, 554
 - security issues, energy crisis, 3–5
 - selective surfaces, 449
 - self-discharge time (SDT), 542–543
 - semiconductors
 - introduction, 399–401
 - photovoltaic effect, 402–406
 - p – n type junctions, 402
 - sensible heat, 566–567
 - service hot water load calculation, 120–121
 - Severn Estuary, Wales, 518
 - shadow-angle protractor, 374–376
 - “shadow flicker,” 249
 - shale
 - challenge of climate change, 21
 - conventional fossil fuels, 31
 - energy crisis, 4–5
 - EROI and energy budgets, 98
 - GHG emissions and climate change, 214–215
 - historical energy development, 17
 - natural gas, 199–200
 - peak of oil production, 585
 - petroleum, 201–202
 - shape factor, thermal radiation, 357–360
 - Shell Oil, 202
 - SHIP database, 499
 - Short–Diakov’s analysis, 577–580
 - short rotation woody crops (SRWCs), 310–311
 - single crystal cells, 415–419
 - sky diffuse radiation, 381
 - SkyFuel, 462
 - SkyTrough parabolic trough collector, 460, 462
 - Smart technology, 139
 - social responsibility, 7
 - societal and environmental costs, 71–72
 - “soft costs,” 434
 - softwoods, 310–311
 - Solana plant, 183, 482
 - solar altitude angle, 362
 - solar azimuth angle, 362
 - solar cells efficiency, 411
 - solar cooling systems, 480–481
 - solar domestic systems
 - forced-circulation hot water systems, 470–476
 - liquid-based solar heating systems for buildings, 476–477
 - passive solar heating systems, 477–480
 - solar cooling systems, 480–481
 - Solar Electric Generating Systems (SEGS), 35
 - solar energy flow rate, 49
 - Solar One plant, 482

- solar photovoltaics, [25](#), [34–35](#)
- solar radiation
 - atmospheric extinction of, [381–383](#)
 - black-body radiation, [353–354](#)
 - detectors for instrumentation, [392–393](#)
 - energy transport, [351–352](#)
 - estimation, photovoltaics, [422](#)
 - extraterrestrial solar radiation, [377–380](#)
 - instrumentation, [389–393](#)
 - intensity of radiation, [357–360](#)
 - measurement of, [388–393](#)
 - National Solar Radiation Database, [393](#)
 - overview, [376–377](#)
 - physics of the sun, [351–352](#)
 - radiation function tables, [354](#), [356–357](#)
 - radiation transmission through a medium, [360–361](#)
 - shadow-angle protractor, [374–376](#)
 - shape factor, [357–360](#)
 - solar time and angles, [364–369](#)
 - spectral solar radiation measurement, [393](#)
 - sun–earth geometric relationship, [361–376](#)
 - sun-path diagram, [369–374](#)
 - sunshine, instruments and measurement, [389–393](#)
 - terrestrial solar radiation estimation, [381–387](#)
 - thermal radiation, [352–361](#)
 - tilted surfaces, [384–387](#)
 - Typical Meteorological Year data set, [388](#)
- solar thermal collectors and systems
 - concentrating solar collectors, [460–466](#)
 - energy balance, flat plate collector, [451–453](#)
 - evacuated tube collectors, [456–457](#)
 - experimental testing of collectors, [453–456](#)
 - forced-circulation hot water systems, [470–476](#)
 - line-focus concentrators, [460–463](#)
 - liquid-based solar heating systems for buildings, [476–477](#)
 - overview, [447](#)
 - parabolic trough-based power plants, [482–490](#)
 - passive solar heating systems, [477–480](#)
 - point-focus concentrators, [463–466](#)
 - power towers, [490–498](#)
 - radiation properties of materials, [447–451](#)
 - reflective surfaces, [449–451](#)
 - selective surfaces, [449](#)
 - solar cooling systems, [480–481](#)
 - solar domestic systems, [466–481](#)
 - solar industrial process heat, [498–501](#)
 - solar thermal power plants, [482–498](#)
 - testing standard, [454–456](#)
 - thermosyphon water heating, [466–470](#)
 - transpired air collectors, [457–460](#)
- solar thermal power plants
 - parabolic trough-based power plants, [482–490](#)
 - power towers, [490–498](#)
- solar thermal renewable energy, [35–36](#)
- solar time and angles, [364–369](#)
- Solar Two plant, [493](#)
- solar zenith angle, [362](#)
- solid-fuel combustors, [338](#)
- solid oxide fuel cell (SCFC), [563](#), [564](#)
- Solucar Platform, [491](#)
- specific energy, [544](#)
- spectral solar radiation measurement, [393](#)
- specular radiation reflection, [447](#)
- spent fuel storage and reprocessing, [236](#)
- sputtering, [426](#)
- square-wave inverter, [415](#)
- standard of living, [12](#)
- standards
 - electrical transmission, [162](#)
 - energy audits and management, [111–112](#)
 - greenhouse gases, [101](#)
 - life cycle assessment, [79](#)
 - solar thermal collectors, [454–456](#)
- Stanley, William, [159](#)
- steel production process, [84–85](#)
- Stefan–Boltzmann properties, [354](#), [406](#), [491](#)
- storage and storage technologies
 - applications, [542](#), [570](#)
 - batteries and fuel cells, [551–555](#)
 - buildings, overnight storage for, [570](#), [572–576](#)
 - compressed air energy storage, [549–550](#)
 - concentrating collector systems, [570](#)
 - direct electrical technologies, [551](#)
 - domestic hot water, overnight storage for, [570](#), [572–576](#)
 - efficiency, [544](#)
 - energy density, [544](#)
 - flow batteries, [560–561](#)
 - flywheels, [550](#)
 - fuel cells, [562–566](#)
 - hot water, [570](#), [572–576](#)
 - hydrogen, [562–566](#)
 - lead-acid batteries, [556–558](#)
 - lithium ion batteries, [559–560](#)
 - mechanical technologies, [544–550](#)
 - nickel metal batteries, [558–559](#)
 - overnight storage, [570](#), [572–576](#)
 - overview, [541–544](#)
 - phase change heat storage, [567–568](#)

- storage and storage technologies (*Continued*)
 - pumped hydroelectric energy storage, 546–549
 - rechargeable batteries, 555–561
 - self-discharge time, 543
 - sensible heat, 566–567
 - size, 542, 544
 - specific energy, 544
 - spent nuclear fuel and reprocessing, 236
 - storage and transport, 565
 - superconducting magnetic energy storage, 551
 - technology characterization, 542–544
 - thermal energy storage, 566–576
 - thermochemical storage, 568–569
 - thermodynamics and economics, 565–566
 - turbines, 548–549
 - ultracapacitors, 551
 - virtual storage, electric transmission grid, 576–580
- sulfur oxides, 212
- sun, physics of, 351–352
- SunChips snack product, 501
- sun-earth geometric relationship
 - overview, 361–363
 - shadow-angle protractor, 374–376
 - solar time and angles, 364–369
- sun-path diagram, 369–374
- sunrise and sunset times, 366–367
- sunshine duration measurement, 393
- sunshine switch, 393
- Sun Valley Neighborhood (Denver), 147
- superconducting magnetic energy storage (SMES), 551
- Surface Mining Control and Reclamation Act, 197
- suspension burners, 338
- sustainability
 - climate change challenge, 18–22
 - costs of energy production and development, 25–28
 - energy economic efficiency, 23
 - energy return on investment, 23–28
- sustainable energy
 - biomass and biofuel, 38–39
 - carrying capacity, 7–15
 - challenges, sustainability engineering, 7
 - climate change challenge, 18–22
 - CO₂ emissions, 49–50
 - context/complex nature of, 15–18
 - conventional energy, 31–32
 - corn, 49
 - costs of energy, 25–28
 - critical issues for, 7–15
 - current energy use, 17–18
 - depletion effects discussion, 49
 - economics discussion, 49
 - efficiency and conservation, 28–31
 - energy content, 49
 - energy crisis, 3–5
 - energy economic efficiency, 23
 - energy efficiency and conservation, 28–31
 - energy return on investment, 23–28
 - energy units and conversion factors, 45
 - exponential growth, mathematics of, 12–15
 - food supply issues, 11–12
 - fossil fuels, 31
 - future U.S. energy scenarios, 18
 - growth, instability due to, 50
 - historical U.S. energy development, 15–17
 - hydroelectric generation, 39–40
 - hydrogen, 40–42
 - instability, due to growth, 50
 - NREL System Advisor Model, 42–45
 - nuclear power, 31–32
 - ocean and geothermal energy, 36–38
 - oil supply discussion, 49
 - online resources, 50–51
 - overview, 1–2
 - per capita energy use, 12
 - photosynthesis conversion, 49
 - population issue, 7–9
 - renewable energy, 32–40
 - security issues, 3–5
 - solar energy flow rate, 49
 - solar photovoltaics, 34–35
 - solar thermal, 35–36
 - sustainability, 2–7, 18–28, 48–49
 - sustainable development, 5–6
 - transportation, 49
 - water issue, 9–11
 - wind energy, 33–34
- “swamp cooler,” 130
- Swan, John, 159
- swimming pools, 453
- synthetic gas, 321, 333
- System Advisor Model (SAM)
 - overview, 2, 42–45
 - performance of solar energy systems, 393
 - PV performance estimates, 436–441
 - wind farm analysis, 292–298
- system sizing, 422–424
- system space, energy density, 544
- systems use, transportation, 586–589

T

- Tampa Electric IGCC, 210
- Tapchan concept, 526
- tar sands, Canada, 11, 98, 201–202, 217
- technology characterization, 542–544
- technology matrix, 85
- technology status, 536–537
- Tennessee Valley Authority (TVA), 166, 224, 530, 546
- terrestrial solar radiation estimation
 - atmospheric extinction of solar radiation, 381–383
 - fundamentals, 381–387
 - overview, 381
 - tilted surfaces, 384–387
- Tesla, Nikola, 159, 162
- Tesla Motors, Inc., 602
- testing standard, solar thermal collectors, 454–456
- thermal energy storage (TES)
 - applications, 541–542, 570
 - buildings, 570, 572–576
 - concentrating collector systems, 570
 - domestic hot water, 570, 572–576
 - overnight storage, 570, 572–576
 - phase change heat storage, 567–568
 - sensible heat, 566–567
 - thermochemical storage, 568–569
- thermal evaporation, 426
- thermal radiation
 - black-body radiation, 353–354
 - intensity of radiation, 357–360
 - overview, 352–353
 - radiation function tables, 354, 356–357
 - radiation transmission through a medium, 360–361
 - shape factor, 357–360
 - solar radiation fundamentals, 352–361
- thermal storage wall, passive solar heating systems, 478–479
- thermochemical storage, 568–569
- thermodynamics and economics, 565–566
- thermoelectric detectors, 392
- thermostats, smart, 139
- thermosyphon water heating, 466–470
- thin-film PV technology
 - amorphous silicon PV technology, 425
 - cadmium telluride modules, 425
 - copper indium diselenide PV products, 425–426
 - electrochemical plating, 426–427
 - gallium-alloyed CIS PV products, 425–426
 - nanoparticle printing, 427
 - thermal evaporation, 426
- Three Gorges Dam, 529
- Three Mile Island, Pennsylvania, 236, 239
- 3M programs, 31
- tidal energy, 516–522
- tilted surfaces, 384–387, 572
- time scale, 544
- time value of money, 57–59
- torrefaction/torrefied biomass, 326
- total annual energy requirement, buildings, 117–118
- total energy input, 100
- total life cycle costs (TLCC)
 - economics, energy generation and conservation systems, 60–63
 - levelized cost of energy, 68–71
- Toyota vehicles
 - Prius, 542, 594, 598
 - Prius Prime, 596
- transactional controls
 - electricity supply systems, 184–187
 - peak shaving, 185
 - price response, 185
 - regulation response, 186
 - reliability response, 186
- “transactional controls,” 186
- transesterification, 335
- transition, other energy sources, 17–18
- transpired air collectors, 457–460
- transport and transportation
 - biofuels, 592–593
 - carbon dioxide emissions, 600–602
 - combining HEVs/PHEVs with biofuels, 598–602
 - energy consumption by mode, 587–588
 - energy content, 49
 - fuel cells and hydrogen, 562–566
 - future all-electric system, 602
 - hybrid electric vehicles, 594–595
 - hydrogen, 565, 604–606
 - introduction, 585
 - natural gas as a transportation fuel, 602–604
 - petroleum requirement, 599–600
 - plug-in hybrid electric vehicles, 595–598
 - storage technology applications, 542
 - systems and energy use, 586–589
 - well-to-wheels analysis, 589–591
- transportation applications, 544
- triple bottom line accounting, 7
- true solar time, 373

Trump (Donald) administration, 22, 214

turbines

energy development costs, 26

levelized cost of energy, 279–283

levelized cost of wind energy, 279–283

performance, 269–279

pumped hydroelectric energy storage, 548–549

wind energy control schemes, 278–279

two-tank indirect system, 570

two-tank storage system, 570

Typical Meteorological Year (TMY) data set,
43, 388

U

Ukraine, 32, 197, 236

ultimate analysis, 317

ultracapacitors, 542, 551

U.N. District Energy Initiative, 147

unconfined aquifers, 9

uninterruptible power supply (UPS), 550

unit cost of energy, 55–56

United States

air pollution, 211–212

energy development, 15–17

energy economic efficiency, 23

energy efficiency and conservation, 29

energy end-use demand reduction,
buildings, 29

future energy scenarios, 18

geothermal energy and power, 533, 537

hydropower, 528

Life Cycle Inventory (LCI) database, 80, 82

natural gas, 199

nuclear power, 31, 32

nuclear power plants, 224

offshore wind energy, 289

per capita energy use, 12

personal transportation system, 30

PV installations, 35

shale oil, 201

units and conversion factors, 45

updraft gasifiers, 325

Upper Big Branch Mine-South, 197

uranium, 229–230

use for heat, 204–205

Utah Associated Municipal Power System, 239

utility shaping, 542

V

Vajont Dam, 531

valence bonds, 399

vanadium redox (VR) battery, 560–561

vapor-compression cycle, 125–130

variable renewable energy, integration into the
grid, 175–184

variable-speed, variable-pitch (VSVP), 278–279

vehicles

battery electric vehicles, 591

Bolt, 602

Chevrolet, 52, 596, 602

Civic DX2012, 603

Detroit (Michigan) vehicle makers, 602

electric vehicles, 558

electric vehicles/biofuel combination,
600–602

fuel cell electric vehicles, 591, 605

future developments, 602

Honda, 603

hybrid electric vehicles, 542, 594–595

hydrogen vehicles, 42

lead-acid batteries, electric vehicles, 558

LEAF, 602

petroleum, 600–602

plug-in hybrid electric vehicles, 542, 595–598

Prius, 542, 594, 598

Prius Prime, 596

Roadster, 602

storage applications, 542

Tesla, 602

Toyota vehicles, 542, 594, 596, 598

transportation, 594–598

Volt vehicle, 542, 596

zero-emission vehicles, 39, 602

Venezuela, 201–202

ventilation, 133

vertical-axis wind turbines (VAWT), 246,
254, 257

Virgil C. Summer Nuclear Generating
Station, 224

virtual storage, electric transmission grid,
576–580

visual impact, wind energy, 249

Vogtle Electric Generating Plant, 224

Volta, Alexander, 551

voltage control, 169–170

Volt vehicle, 542, 596

von Karman's constant, 261

W

Wabash River Coal Gasification Repowering
Project, 210

wake modeling, 286–287

Walgreens Store, 136–137

- waste management and disposal, 233–236
 - waste materials, 308–309
 - water issues
 - allocation systems, 6
 - carrying capacity, 9–11
 - wind energy, 250
 - water pumping applications, 424–425
 - WaterSense-labeled fixtures, 139
 - Watts Bar nuclear plant, 224
 - Wave Capture Systems, 526
 - wave energy
 - deep water wave power, 523–526
 - wave power devices, 526–528
 - weapons-grade plutonium, 231
 - weather forecasts, 181–182
 - Weibull PDF, 266–267
 - Wells turbine, 527–528
 - well-to-wheels analysis, 589–591, 603–605
 - Western Area Power Administration (WAPA), 166
 - Western Electricity Coordinating Council (WECC), 162
 - Westinghouse, George, 159, 162
 - Westinghouse concept, 512
 - West Village development, 147
 - wet-bulb temperature, 130
 - wholesale power markets, 166
 - wind characteristics
 - distribution of wind, 259–261
 - log law wind speed profile, 261–263
 - power law wind speed profile, 263–264
 - probabilities, given wind speed observation, 265–268
 - wind generation, 258–259
 - wind speed increasing with height, 261
 - wind energy
 - aerodynamics, 255–258
 - bird and bat fatalities, 250–251
 - coefficient of performance, 254–255
 - control schemes, 278–279
 - distribution of wind, 259–261
 - energy return on investment, 99–101
 - environmental impact, 248–251
 - integration, variable renewable energy into grid, 176
 - introduction, 245–248
 - land use, 250
 - life cycle greenhouse gas emissions, 250
 - log law wind speed profile, 261–263
 - noise, 249
 - offshore wind energy, 287–291
 - power and energy of wind, 252–254
 - power law wind speed profile, 263–264
 - probabilities, given wind speed observation, 265–268
 - renewable energy, 18, 33–34
 - study topics, 298–300
 - System Advisor Model, 292–298
 - turbine performance, 269–279
 - visual impact, 249
 - water use, 250
 - wind characteristics, 258–268
 - wind farm analysis, 292–298
 - wind farms, 284–287
 - wind generation, 258–259
 - wind speed increasing with height, 261
 - Wind Energy and Turbines*, 246
 - Wind Integration National Dataset (WIND) Toolkit, 43
 - Wind Machines*, 246
 - wind turbines, *see* turbines
 - World Agricultural Land Endowment, 11
 - World Commission on Environment and Development, 5
- Y**
- Yamani, Sheik Ahmed Zaki, 17
 - “yellow cake,” 229
 - Yucca Mountain, 234
- Z**
- zero-emission vehicles, 39, 602
 - Zero-Energy District Accelerator, 147
 - zero-energy urban districts, 146–147



Taylor & Francis Group
an informa business

Taylor & Francis eBooks

www.taylorfrancis.com

A single destination for eBooks from Taylor & Francis with increased functionality and an improved user experience to meet the needs of our customers.

90,000+ eBooks of award-winning academic content in Humanities, Social Science, Science, Technology, Engineering, and Medical written by a global network of editors and authors.

TAYLOR & FRANCIS EBOOKS OFFERS:

A streamlined experience for our library customers

A single point of discovery for all of our eBook content

Improved search and discovery of content at both book and chapter level

REQUEST A FREE TRIAL

support@taylorfrancis.com

 **Routledge**
Taylor & Francis Group

 **CRC Press**
Taylor & Francis Group